ORGANOMETALLICS

Volume 14, Number 9, September 1995

Communications

Kinetic Hydricity of Transition-Metal Hydrides toward Trityl Cation

Tan-Yun Cheng and R. Morris Bullock*

Chemistry Department, Brookhaven National Laboratory, Upton, New York 11973-5000

Received July 5, 1995[⊗]

Summary: The kinetics of hydride transfer from a series of metal hydrides (MH) to $Ph_3C^+BF_4^-$ (producing Ph_3CH and M- - -FBF_3) have been studied by stopped-flow methods in CH_2Cl_2 solution. Second-order rate constants at 25 °C span 5 orders of magnitude in kinetic hydricity, ranging from $k = 5.0 \times 10^1\ M^{-1}\ s^{-1}$ for $HMn(CO)_5$ to $k = 4.6 \times 10^6\ M^{-1}\ s^{-1}$ for trans-$HMo(CO)_2(PMe_3)Cp$.

Transition-metal hydrides are key reagents in many homogeneous catalytic reactions, and M–H bond cleavage is a requisite step in both catalytic and stoichiometric reactions of metal hydrides. A knowledge of the factors governing cleavage of the M–H bond may assist in the rational design of catalytic cycles employing metal hydrides. As might be expected due to their negative charge, anionic metal hydrides exhibit hydridic reactivity. Darensbourg and co-workers have reported extensive studies[1] demonstrating the utility of $HW(CO)_5^-$ and other anionic metal hydrides in the reduction of organic substrates. Neutral metal carbonyl hydrides such as $HW(CO)_3Cp$ ($Cp = \eta^5$-C_5H_5) undergo diverse reactivity patterns[2]—cleavage of the M–H bond can occur as a proton,[3] a hydrogen atom,[4] or a hydride.[5] In contrast to the detailed information available on the kinetics of *proton* transfer[3,6] and *hydrogen atom* transfer[4,7,8] reactions of these hydrides, little information is available on the kinetics of their *hydride* transfer reactions. The mechanism of ionic hydrogenation of olefins was shown to involve hydride transfer from metal hydrides to carbenium ions,[9] but a determination of the relative hydricity of the metal hydrides was not feasible from these reactions. We now report the kinetics of hydride transfer from a series of metal hydrides to a common carbenium ion, including kinetic hydricity data spanning 5 orders of magnitude.

The synthetic chemistry (eq 1) of organometallic complexes containing BF_4^- and other weakly coordinating ligands has been developed by Beck and others.[10]

$$Ph_3C^+\ BF_4^- + MH \xrightarrow{k_{H^-}} \begin{matrix} Ph_3C{-}H \\ + \\ M{\cdots}F{-}BF_3 \end{matrix} \quad (1)$$

We determined the kinetics of these hydride transfer

⊗ Abstract published in *Advance ACS Abstracts,* August 15, 1995.

(1) Darensbourg, M. Y.; Ash, C. E. *Adv. Organomet. Chem.* **1987**, *27*, 1–50.

(2) For a comparison of proton, hydrogen atom, and hydride transfer reactions of metal hydrides, see: Bullock, R. M. *Comments Inorg. Chem.* **1991**, *12*, 1–33.

(3) For a review of proton transfer reactions of metal hydrides, see: Kristjánsdóttir, S. S.; Norton, J. R. In *Transition Metal Hydrides*; Dedieu, A., Ed.; VCH: New York, 1992; Chapter 9.

(4) For a review of hydrogen atom transfer reactions of metal hydrides, see: Eisenberg, D. C.; Norton, J. R. *Isr. J. Chem.* **1991**, *31*, 55–66.

(5) For a review of nucleophilic reactivity of metal hydrides, see: Labinger, J. A. In *Transition Metal Hydrides*; Dedieu, A., Ed.; VCH: New York, 1992; Chapter 10.

(6) (a) Edidin, R. T.; Sullivan, J. M.; Norton, J. R. *J. Am. Chem. Soc.* **1987**, *109*, 3945–3953. (b) Kristjánsdóttir, S. S.; Norton, J. R. *J. Am. Chem. Soc.* **1991**, *113*, 4366–4367.

(7) Bullock, R. M.; Samsel, E. G. *J. Am. Chem. Soc.* **1990**, *112*, 6886–6898.

(8) Eisenberg, D. C.; Lawrie, C. J. C.; Moody, A. E.; Norton, J. R. *J. Am. Chem. Soc.* **1991**, *113*, 4888–4895.

(9) Bullock, R. M.; Song, J.-S. *J. Am. Chem. Soc.* **1994**, *116*, 8602–8612.

(10) Beck, W.; Sünkel, K. *Chem. Rev.* **1988**, *88*, 1405–1421.

0276-7333/95/2314-4031$09.00/0

Table 1. Rate Constants[a] for Hydride Transfer from Metal Hydrides to $Ph_3C^+BF_4^-$ (CH_2Cl_2, 25 °C)

metal hydride	k_{H^-} (M^{-1} s^{-1})	k_{MH}/k_{MD}
$HMn(CO)_5$	5.0×10^1	
$HCr(CO)_3Cp^*$	5.7×10^1	
$HW(CO)_3Cp$	7.6×10^1	
$HSiEt_3$	1.5×10^2	
cis-$HMn(CO)_4(PPh_3)$	2.3×10^2	
$HMo(CO)_3Cp$	3.8×10^2	1.8
$HW(CO)_3Cp^*$	1.9×10^3	1.7
$HRe(CO)_5$	2.0×10^3	
$HMo(CO)_3Cp^*$	6.5×10^3	1.7
cis-$HRe(CO)_4(PPh_3)$	1.2×10^4	
trans-$HMo(CO)_2(PCy_3)Cp$	4.3×10^5	1.7
trans-$HMo(CO)_2(PPh_3)Cp$	5.7×10^5	
trans-$HMo(CO)_2(PMe_3)Cp$	4.6×10^6	

[a] ±10% estimated uncertainty for all rate constants.

reactions (eq 1) using stopped-flow methods in CH_2Cl_2 solution.[11] Experiments carried out with an excess of metal hydride ($[MH]_0 \geq 10[Ph_3C^+BF_4^-]_0$) established the rate law: $-d[Ph_3C^+BF_4^-]/dt = k[Ph_3C^+BF_4^-][MH]$. Second-order rate constants are given in Table 1 and are listed in order of increasing kinetic hydricity.

Comparisons of these transition-metal hydrides with a main-group hydride donor[12,13] show that several transition-metal hydrides are much faster hydride donors than $HSiEt_3$, which is frequently used[14] as a hydride donor. Despite their higher homolytic bond dissociation energies,[15] third-row metal hydrides are faster hydride donors than their first-row analogs in these heterolytic reactions; e.g., $k_{HRe} > k_{HMn}$. Similarly, $HW(CO)_3Cp^*$ ($Cp^* = \eta^5$-C_5Me_5) is more hydridic than $HCr(CO)_3Cp^*$, but in this series of group 6 hydrides the second-row hydride $HMo(CO)_3Cp^*$ exhibits the fastest rate of hydride transfer of the three. For the Mo and W hydrides, the kinetics of hydride transfer are apparently influenced more strongly by electronic effects than by steric effects. For example, replacement of one CO in $HMo(CO)_3Cp$ by the electron-donating but sterically demanding PPh_3 ligand results in a rate enhancement of about 10^3.

An interpretation of the kinetics of hydride transfer from the phosphine-substituted hydrides $HMo(CO)_2(PR_3)Cp$ is complicated by the existence of cis and trans isomers.[16,17] The Mo hydride $HMo(CO)_2(PCy_3)Cp$ was found to exist as an 89:11 mixture of cis and trans isomers[18] in CD_2Cl_2. Activation parameters for the *cis*-$HMo(CO)_2(PCy_3)Cp \rightarrow$ *trans*-$HMo(CO)_2(PCy_3)Cp$ isomerization evaluated from NMR line-broadening experiments at seven temperatures between −45 and +11 °C in CD_2Cl_2 were $\Delta H^\ddagger = 11.3 \pm 0.3$ kcal mol^{-1}, $\Delta S^\ddagger = -7.0 \pm 1.2$ cal K^{-1} mol^{-1}, and $\Delta G^\ddagger(298\ K) = 13.4$ kcal mol^{-1}. As described above, second-order kinetics were deduced from experiments using excess $[HMo(CO)_2(PCy_3)Cp]$. In contrast, the kinetics of hydride transfer from $HMo(CO)_2(PCy_3)Cp$ at −55 °C using excess $[Ph_3C^+BF_4^-]$ (4.5−13 mM) showed an observed first-order rate constant (0.82 s^{-1}) that was *independent* of $[Ph_3C^+BF_4^-]$. This rate constant agrees with the rate constant of 0.67 s^{-1} for cis → trans isomerization of $HMo(CO)_2(PCy_3)Cp$ measured by NMR line broadening (and extrapolated to −55 °C). Following consumption of the first 11% of the hydride (the equilibrium amount of trans isomer), the rate-limiting step under these conditions is cis → trans hydride isomerization. From the observed rate constant at the highest $[Ph_3C^+BF_4^-]$, an upper limit of $k < 63$ M^{-1} s^{-1} (at −55 °C) can be determined for the rate constant for hydride transfer from *cis*-$HMo(CO)_2(PCy_3)Cp$.

These kinetics results in CH_2Cl_2 corroborate the conclusions reached by Tilset and co-workers from their studies of related reactions in MeCN.[19−21] They found that oxidation of $HMo(CO)_2(PPh_3)Cp$[20] in MeCN in the presence of a base led to *cis*-$[(MeCN)Mo(CO)_2(PPh_3)Cp]^+$. In contrast, hydride transfer to $(p\text{-}MeOC_6H_4)Ph_2C^+$ from $HMo(CO)_2(PPh_3)Cp$[20] in MeCN led to initial formation of *trans*-$[(MeCN)Mo(CO)_2(PPh_3)Cp]^+$, followed by a slow isomerization to the thermodynamically favored cis isomer. They concluded that *trans*-$HMo(CO)_2(PPh_3)Cp$ was more reactive than *cis*-$HMo(CO)_2(PPh_3)Cp$ as a hydride donor. We assume that the trans isomers are similarly much more reactive than cis isomers for $HMo(CO)_2(PMe_3)Cp$ and $HMo(CO)_2(PPh_3)Cp$ in our experiments as well. Accordingly, the second-order rate constants reported in Table 1 are the specific rate constants for hydride transfer from *trans*-$HMo(CO)_2(PR_3)Cp$. The activation parameters for hydride transfer from *trans*-$HMo(CO)_2(PCy_3)Cp$ to $Ph_3C^+BF_4^-$ determined from the temperature dependence of the rate constants at five temperatures between −20 and +25 °C are $\Delta H^\ddagger = 4.47 \pm 0.09$ kcal mol^{-1}, $\Delta S^\ddagger = -17.8 \pm 0.3$ cal K^{-1} mol^{-1}, and $\Delta G^\ddagger(298\ K) = 9.78$ kcal mol^{-1}. Extrapolation to −55 °C gives $k = 1.9 \times 10^4$ M^{-1} s^{-1} for hydride transfer from *trans*-$HMo(CO)_2(PCy_3)Cp$; comparison of this rate constant with the upper limit estimated above for *cis*-$HMo(CO)_2(PCy_3)Cp$ indicates that the trans isomer of $HMo(CO)_2(PCy_3)Cp$ is >300 times faster as a hydride donor than the cis isomer. The rate constant reported in Table 1 for *trans*-$HMo(CO)_2(PMe_3)Cp$ at 25 °C was extrapolated from an Eyring plot of the temperature dependence of the rate constants

(11) See the supporting information for experimental details.

(12) For thorough studies of the kinetics of hydride transfer from a series of hydrosilanes to carbenium ions, see: Mayr, H.; Basso, N.; Hagen, G. *J. Am. Chem. Soc.* **1992**, *114*, 3060−3066. Our value of $k(HSiEt_3) = 1.5 \times 10^2$ M^{-1} s^{-1} may be compared with a previously reported[13] value of 1.1×10^2 M^{-1} s^{-1} under the same conditions.

(13) Chojnowski, J.; Fortuniak, W.; Stańczyk, W. *J. Am. Chem. Soc.* **1987**, *109*, 7776−7781.

(14) Kursanov, D. N.; Parnes, Z. N.; Loim, N. M. *Synthesis* **1974**, 633−651.

(15) Tilset, M.; Parker, V. D. *J. Am. Chem. Soc.* **1989**, *111*, 6711−6717 (as modified in: *J. Am. Chem. Soc.* **1990**, *112*, 2843).

(16) Faller, J. W.; Anderson, A. S. *J. Am. Chem. Soc.* **1970**, *92*, 5852−5860.

(17) Kalck, P.; Pince, R.; Poilblanc, R.; Roussel, J. *J. Organomet. Chem.* **1970**, *24*, 445−452.

(18) A cis:trans ratio of 89:11 was measured by NMR for $HMo(CO)_2(PCy_3)Cp$ over the temperature range of −86 to −45 °C. There appears to be a very small temperature dependence of K_{eq}, since a ratio of 91:9 was estimated at 22 °C based on the observed J_{PH} coupling constant.[16] The temperature dependence of the equilibrium constant (K_{eq} = [cis]/[trans]) was measured for $HMo(CO)_2(PMe_3)Cp$ over the range −86 to −1 °C; $\Delta H^\circ = 0.34 \pm 0.02$ kcal mol^{-1}, $\Delta S^\circ = 1.4 \pm 0.1$ cal K^{-1} mol^{-1}, and $K_{eq}(298\ K) = 1.15$ (46% trans). Similar measurements for $HMo(CO)_2(PPh_3)Cp$ between −86 and −24 °C gave $\Delta H^\circ = 0.29 \pm 0.04$ kcal mol^{-1}, $\Delta S^\circ = 1.9 \pm 0.2$ cal K^{-1} mol^{-1}, and $K_{eq}(298\ K) = 1.62$ (38% trans).

(19) Ryan, O. B.; Tilset, M.; Parker, V. D. *J. Am. Chem. Soc.* **1990**, *112*, 2618−2626.

(20) Smith, K.-T.; Tilset, M. *J. Organomet. Chem.* **1992**, *431*, 55−64.

(21) In contrast to these similarities for the hydride transfer step, significant differences may exist in the kinetics of capture of the organometallic intermediates, leading to $Cp(CO)_2(PPh_3)MoFBF_3$ in CH_2Cl_2, compared to formation of $[(MeCN)Mo(CO)_2(PPh_3)Cp]^+BF_4^-$ in MeCN. NMR experiments indicated that *trans*-$Cp(CO)_2(PPh_3)MoFBF_3$ was the kinetic product resulting from hydride abstraction from $HMo(CO)_2(PPh_3)Cp$ at −78 °C; isomerization to *cis*-$Cp(CO)_2(PPh_3)MoFBF_3$ is ~95% complete within 1 h at −7 °C. Additional data and further discussion will be given in a full account of this work.

determined at four temperatures between −55 and −25 °C ($\Delta H^{\ddagger} = 2.95 \pm 0.01$ kcal mol^{-1}, $\Delta S^{\ddagger} = -18.1 \pm 0.1$ cal K^{-1} mol^{-1}, and $\Delta G^{\ddagger}$(298 K) = 8.36 kcal mol^{-1}).

While these reactions clearly involve overall hydride (H^-) transfer, the detailed mechanism might involve initial oxidation of the hydride by Ph_3C^+, followed by hydrogen atom transfer from the resultant radical cation of the metal hydride, as opposed to a single-step hydride transfer mechanism. Analogous questions have received intensive scrutiny in the context of hydride transfers related to NAD^+ models.[22] On the basis of electrochemical data, however, oxidation of $HMo(CO)_3Cp$ by Ph_3C^+ appears unlikely, since it is thermodynamically unfavorable by about 0.9 V ($\Delta G^{\circ} \approx 21$ kcal mol^{-1}).[19,23,24] Kinetic isotope effects ($k_{MH}/k_{MD} = 1.7-1.8$) found for some hydride/deuteride pairs are large enough to argue against rate-determining electron transfer. We interpret the data to indicate single-step hydride transfer.

A comprehensive understanding of the factors governing the kinetic hydricity of metal hydrides will require further study, but the data reported here provide some preliminary insights on the steric and electronic factors influencing the propensity of metal hydrides to function as hydride donors. Even in the absence of precise structural data on the octahedral $HMn(CO)_4(PPh_3)$ vs the four-legged piano stool geometry of the $HMo(CO)_2(PR_3)Cp$ compounds, some useful comparisons can be made. For the *trans*-$HMo(CO)_2(PR_3)Cp$ compounds, which probably have trans P−M−H angles >100°, the added steric bulk due to the phosphine has a relatively small effect on the hydride transfer kinetics. The threshold P−M−H angle below which steric effects have a substantial effect on the kinetics (steric hindrance from the PR_3 ligand offsetting the enhanced hydricity due to the electronic effect of the phosphine) is apparently reached by the time the P−M−H angles decrease to ~90° in the *cis*-$HM(CO)_4(PPh_3)$ complexes. This interpretation is congruent with the low reactivity of the *cis*-$HMo(CO)_2(PR_3)Cp$ complexes, since the expected P−M−H angles of ~80° or less in these cis isomers would entail substantial steric interference upon approach of Ph_3C^+.

Since data on the kinetics of proton transfer[3,6] and hydrogen atom transfer[4,7,8] reactions of several of the hydrides in Table 1 are already available for comparison, this series of metal carbonyl hydrides emerges as a group for which kinetic data are now available for all three modes of formal M−H bond cleavage (hydride, proton, and hydrogen atom).

Acknowledgment. This research was carried out at Brookhaven National Laboratory under Contract No. DE-AC02-76CH00016 with the U.S. Department of Energy and was supported by its Divison of Chemical Sciences, Office of Basic Energy Sciences. We thank Drs. Bruce Brunschwig, Mark Andrews, Carol Creutz, and Jerry Cook for helpful discussions.

Supporting Information Available: Text and figures giving details of the kinetics data and spectroscopic characterization of $M^+BF_4^-$ products (11 pages). This material is contained in many libraries on microfiche, immediately follows this article in the microfilm version of the journal, and can be ordered from the ACS; see any current masthead page for ordering information.

OM950513S

(22) For a review, see: Bunting, J. W. *Bioorg. Chem.* **1991**, *19*, 456–491. For recent results on hydride transfer from a ruthenium hydride to NAD^+ model compounds, see: Hembre, R. T.; McQueen, S. *J. Am. Chem. Soc.* **1994**, *116*, 2141–2142.

(23) The $E_{1/2}$ value for reduction of $Ph_3C^+ClO_4^-$ in MeCN was found from polarography[24] to be +0.27 V vs. SCE. Conversion of this value to a Cp_2Fe/Cp_2Fe^+ reference gives $E_{1/2} \approx -0.08$ V. The peak potential for oxidation of $HMo(CO)_3Cp$[19] is +0.800 V vs Cp_2Fe/Cp_2Fe^+, leading to an estimate of $\Delta E_0 \approx -0.88$ V for oxidation of $HMo(CO)_3Cp$ by Ph_3C^+ in MeCN.

(24) Volz, H.; Lotsch, W. *Tetrahedron Lett.* **1969**, *27*, 2275–2278.

Synthesis, Photophysics, Ion-Binding Studies, and Structural Characterization of Organometallic Rhenium(I) Crown Complexes

Vivian Wing-Wah Yam,* Keith Man-Chung Wong, Vicky Wing-Man Lee, Kenneth Kam-Wing Lo, and Kung-Kai Cheung

Department of Chemistry, The University of Hong Kong, Pokfulam Road, Hong Kong

Received May 9, 1995[⊗]

*Summary: A series of Re(I) complexes of [Re(L)(CO)$_3$Cl] (**1**, L = L$_1$ = N-(2-pyridinylmethylene)-2,3,5,6,8,9,11,-12-octahydro-1,4,7,10,13-benzopentaoxacyclononadecan-16-ylamine; **2**, L = L$_2$ = N-(2-pyridinylmethylene)-phenylamine) and [Re(phen)(CO)$_3$(L′)]$^+$ (**3**, L′ = L$_3$ = 1-(4-pyridinylformyl)aza-15-crown-5; **4**, L′ = L$_4$ = 4-(N,N-diethylformamido)pyridine) have been synthesized and their photophysical and cation binding properties studied. The X-ray crystal structure of **3** has also been determined.*

There has been a growing interest in the study of host−guest interactions, in particular a revival of interest in the crown ethers and related inclusion compounds owing to the recent developments in molecular recognition studies and the design of molecular switches and probes.[1,2] Although there have been numerous reports on the metal-to-ligand charge transfer (MLCT) excited state chemistry of rhenium(I) diimines,[3] their potential as metal ion probes, unlike the case for their ruthenium(II) analogues, has been relatively unexplored. Although there has been a report on the synthesis of rhenium(I) crown compounds,[4] there has been, to the best of our knowledge, no application of this class of compounds in ion-binding studies. In this communication, we report the synthesis, photophysics, and first cation-binding properties of a series of rhenium(I) crown complexes. The first crystal structure characterization of a rhenium(I) crown complex will also be described.

Reaction of Re(CO)$_5$Cl with L$_1$ in benzene at reflux under a nitrogen atmosphere followed by addition of petroleum ether produced [Re(L$_1$)(CO)$_3$Cl] (**1**) in high yield. Similar reaction with L$_2$ gave the non-crown analogue [Re(L$_2$)(CO)$_3$Cl] (**2**).[3g] On the other hand, reaction of [Re(phen)(CO)$_3$(MeCN)]OTf with L$_3$ in THF at reflux under a nitrogen atmosphere afforded [Re(phen)(CO)$_3$(L$_3$)]$^+$ (**3**), isolated as the PF_6^- salt. Similar reaction with L$_4$ gave the non-crown analogue [Re(phen)(CO)$_3$(L$_4$)]PF$_6$ (**4**). All newly synthesized complexes gave satisfactory elemental analyses and were characterized by ^{1}H NMR spectroscopy and positive FAB-MS.[5] The crystal structure of **3** has been determined by X-ray crystallography.[6]

Chart 1

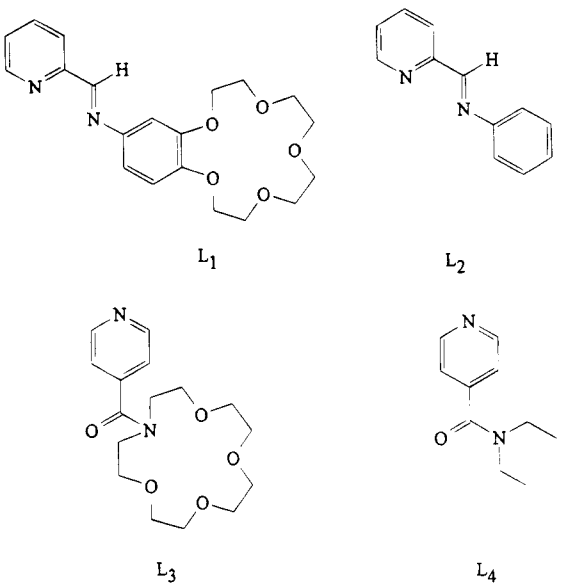

A perspective drawing of the cation of **3** with atomic numbering is depicted in Figure 1. The coordination geometry at the Re atom is a distorted octahedron with the three carbonyl ligands arranged in a facial fashion. The *trans* angles subtended by the Re atom and the two coordinated atoms *trans* to each other are in the range 172.0(9)−176(1)°, showing a slight deviation from an ideal octahedral geometry. The Re−C−O bond angles of 170(2)−177(2)° are slightly distorted from linearity. The N(1)−Re−N(2) bond angle (74.9(7)°), exceptionally smaller than 90°, is a consequence of the steric requirement of the chelating phen ligand. The Re−C(1) bond distance of 1.76(3) Å is shorter than the Re−C bonds (1.90(3) Å) *cis* to the pyridyl unit bearing the crown. This is also in line with the longer C(1)−O(1) bond distance (1.27(3) Å) relative to C(2)−O(2) and C(3)−O(3) (1.16(3) and 1.18(3) Å). This is understandable, given the poor π-accepting ability of the pyridine ligand *trans* to the C(1) atom, which would enhance the Re−C(1) metal to ligand π back-bonding. On the other hand, 1,10-phenanthroline is a better π-acceptor ligand. Similar observations have been reported in related Re(I) systems.[3f,7] The amido carbon atom C(21) is sp^2-

[⊗] Abstract published in *Advance ACS Abstracts,* August 15, 1995.

(1) See for example: (a) Cooper, S. R. *Crown Compounds: Toward Future Applications*; VCH: New York, 1992. (b) Gokel, G. Crown Ethers and Cryptands. In *Monographs in Supramolecular Chemistry*; Stoddart, J. F., Ed.; Royal Society of Chemistry: Cambridge, U.K., 1991. (c) Cram, D. J.; Cram, J. M. Container Molecules and Their Guests. In *Monographs in Supramolecular Chemistry*; Stoddart, J. F., Ed.; Royal Society of Chemistry: Cambridge, U.K., 1994. (d) Atwood, J. L.; Davies, J. E. D.; MacNicol, D. D. *Inclusion Compounds: Key Organic Host Systems*; Oxford University Press: New York, 1991; Vol. 4. (e) Vögtle, F. *Supramolecular Chemistry*; Wiley: Chichester, U.K., 1993.

(2) See for example: (a) Pullman, A. *Chem. Rev.* **1991**, *91*, 793. (b) de Silva, P. A.; de Silva, S. A. *J. Chem. Soc., Chem. Commun.* **1986**, 1709. (c) Beer, P. D. *Chem. Soc. Rev.* **1989**, *18*, 409. (d) Beer, P. D. *Adv. Inorg. Chem.* **1992**, *39*, 79. (e) Anson, C. E.; Creaser, C. S.; Stephenson, G. R. *J. Chem. Soc., Chem. Commun.* **1994**, 2175. (f) Yam, V. W.-W.; Lo, K. K.-W.; Cheung, K.-K. *Inorg. Chem.* **1995**, *34*, 4013. (g) Todd, M. D.; Dong, Y.; Horney, J.; Yoon, D. I.; Hupp, J. T. *Inorg. Chem.* **1993**, *32*, 2001.

(3) See for example: (a) Horváth, O.; Stevenson, K. L. *Charge Transfer Photochemistry of Coordination Compounds*; VCH: New York, 1993. (b) Balzani, V.; Scandola, F. *Supramolecular Photochemistry*; Ellis Horwood: Chichester, U.K., 1991. (c) Wrighton, M. S.; Morse, D. L. *J. Am. Chem. Soc.* **1974**, *96*, 998. (d) Tapolsky, G.; Duesing, R.; Meyer, T. J. *Inorg. Chem.* **1990**, *29*, 2285. (e) Shaw, J. R.; Schmehl, R. H. *J. Am. Chem. Soc.* **1991**, *113*, 389. (f) Lin, R.; Fu, Y.; Brock, C. P.; Guarr, T. F. *Inorg. Chem.* **1992**, *31*, 4346. (g) Dominey, R. N.; Hauser, B.; Hubbard, J.; Dunham, J. *Inorg. Chem.* **1991**, *30*, 4754.

(4) Yoon, D. I.; Berg-Brennan, C. A.; Lu, H.; Hupp, J. T. *Inorg. Chem.* **1992**, *31*, 3192.

0276-7333/95/2314-4034$09.00/0

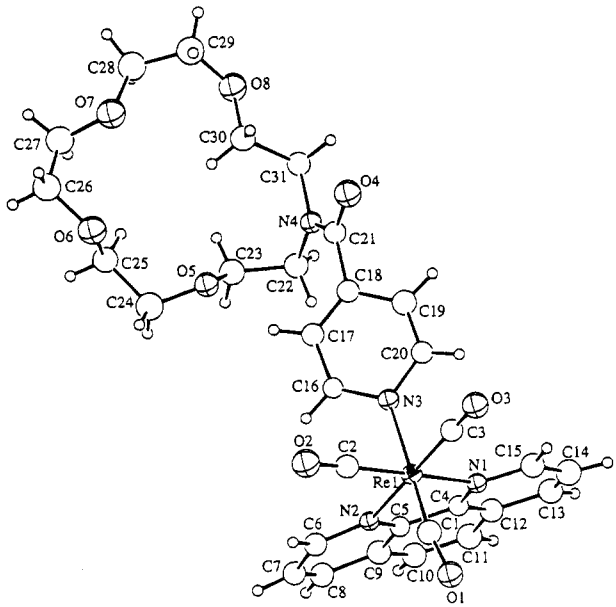

Figure 1. Perspective drawing of the complex cation of **3** with atomic numbering scheme. Thermal ellipsoids are shown at the 25% probability level. Selected bond lengths (Å) and angles (deg): Re(1)−N(1), 2.19(2); Re(1)−N(2), 2.18(2); Re(1)−N(3), 2.17(2); Re(1)−C(1), 1.76(3); Re(1)−C(2), 1.90(3); Re(1)−C(3), 1.90(3); C(1)−O(1), 1.27(3); C(2)−O(2), 1.16(3); C(3)−O(3), 1.18(3); C(21)−O(4), 1.25(3); N(1)−Re(1)−N(2), 74.9(7); N(1)−Re(1)−N(3), 82.4(7); N(1)−Re(1)−C(1), 100(1); N(1)−Re(1)−C(2), 172.0(9); N(1)−Re(1)−C(3), 101.2(9); N(2)−Re(1)−N(3), 84.5(7); N(2)−Re(1)−C(1), 98(1); N(2)−Re(1)−C(2), 98.1(9); N(2)−Re(1)−C(3), 175.5(9); N(3)−Re(1)−C(1), 176(1); N(3)−Re(1)−C(2), 93.2(9); N(3)−Re(1)−C(3), 92.9(9); C(1)−Re(1)−C(2), 84(1); C(1)−Re(1)−C(3), 84(1); C(2)−Re(1)−C(3), 85(1); Re(1)−C(1)−O(1), 170(2); Re(1)−C(2)−O(2), 176(2); Re(1)−C(3)−O(3), 177(2); O(4)−C(21)−N(4), 122(2); O(4)−C(21)−C(18), 116(2); N(4)−C(21)−C(18), 121(2).

hybridized with bond angles subtended at C(21) typical of sp^2 hybridization (116(2)−122(2)°). It is interesting to note that the C(1)−O(1) bond distance is similar to C(21)−O(4) (1.25(3) Å), approaching that for a C−O double bond. All other bond distances and angles have typical values.

(5) **1**: ^{1}H NMR (270 MHz, $CDCl_3$, 298 K, relative to TMS) δ 3.7−4.2 (m, 16H, $-OCH_2-$), 6.9 (d, 1H, aryl H *meta* to −N=CH), 7.1 (dd, 1H, aryl H *ortho* to −N=CH), 7.2 (d, 1H, aryl H *ortho* to $-OCH_2$ and −N=CH), 7.6 (m, 1H, pyridyl H), 8.0 (d, 1H, pyridyl H), 8.1 (td, 1H, pyridyl H), 8.8 (s, 1H, −CH=N), 9.0 (d, 1H, pyridyl H *ortho* to N); IR (Nujol mull, KBr, cm^{-1}) ν(C≡O) 2017 (s), 1913 (s), 1895 (s); positive FAB-MS ion clusters at *m/z* 677 $\{M\}^+$, 642 $\{M - Cl\}^+$; UV−vis (λ/nm (ϵ_{max}/dm^3 mol^{-1} cm^{-1})) MeOH, 274 (15 985) and 399 (9150), CH_2Cl_2, 275 (15 145) and 414 (8675). Anal. Found: C, 40.4; H, 3.8; N, 4.1. Calcd for **1**: C, 40.7; H, 3.5; N, 4.1. **2**: ^{1}H NMR (270 MHz, $CDCl_3$, 298 K, relative to TMS) δ 7.5 (m, 5H, aryl H's), 7.7−8.1 (m, 3H, pyridyl H's), 8.8 (s, 1H, −CH=N), 9.1 (m, 1H, pyridyl H *ortho* to N); IR (Nujol mull, KBr, cm^{-1}) ν(C≡O) 2023 (s), 1919 (s), 1884 (s); positive FAB-MS ion clusters at *m/z* 487 $\{M\}^+$, 459 $\{M - CO\}^+$, 452 $\{M - Cl\}^+$; UV−vis (λ/nm (ϵ_{max}/dm^3 mol^{-1} cm^{-1})) MeOH, 264 sh (9270), 313 (9050), and 410 (3715). Anal. Found: C, 37.3; H, 1.6; N, 6.1. Calcd for **2**: C, 36.9; H, 2.1; N, 5.7. **3**: ^{1}H NMR (270 MHz, acetone-d_6, 298 K, relative to TMS) δ 3.3−3.7 (m, 20H, crown protons), 7.4 (dd, 2H, pyridyl H's), 8.4 (m, 4H, phen H's), 8.7 (dd, 2H, pyridyl H's), 9.1 (dd, 2H, phen H's), 9.9 (dd, 2H, phen H's); IR (Nujol mull, KBr, cm^{-1}) ν(C≡O) 2028 (s), 1939 (s), and 1926 (s), ν(C=O) 1637 (s); positive FAB-MS ion clusters at *m/z* 774 $\{M\}^+$, 746 $\{M - CO\}^+$, 450 $\{M - L_3\}^+$, 422 $\{M - L_3 - CO\}^+$; UV−vis (λ/nm (ϵ_{max}/dm^3 mol^{-1} cm^{-1})) MeOH, 275 (28 210), 326 sh (7300), and 370 sh (3590). Anal. Found: C, 40.3; H, 3.3; N, 6.1. Calcd for **3**: C, 40.5; H, 3.5; N, 6.1. **4**: ^{1}H NMR (270 MHz, CD_2Cl_2, 298 K, relative to TMS) δ 1.0 (t, 3H, $-CH_3$), 1.1 (t, 3H, $-CH_3$), 3.0 (q, 2H, $-NCH_2$), 3.4 (q, 2H, $-NCH_2$), 7.2 (dd, 2H, pyridyl H's), 8.1 (dd, 2H, phen H's), 8.2 (dd, 2H, phen H's), 8.3 (dd, 2H, pyridyl H's), 8.8 (dd, 2H, phen H's), 9.6 (dd, 2H, phen H's); IR (Nujol mull, KBr, cm^{-1}) ν(C≡O) 2034 (s), 1928 (s), and 1909 (s), ν(C=O) 1641 (s); positive FAB-MS ion clusters at *m/z* 628 $\{M\}^+$, 600 $\{M - CO\}^+$, 450 $\{M - L_4\}^+$, 422 $\{M - L_4 - CO\}^+$; UV−vis (λ/nm (ϵ_{max}/dm^3 mol^{-1} cm^{-1})) MeOH, 275 (30 220), 327 sh (7345), and 369 sh (4005). Anal. Found: C, 39.0; H, 2.7; N, 6.9. Calcd for **4**: C, 38.8; H, 2.9; N, 7.2.

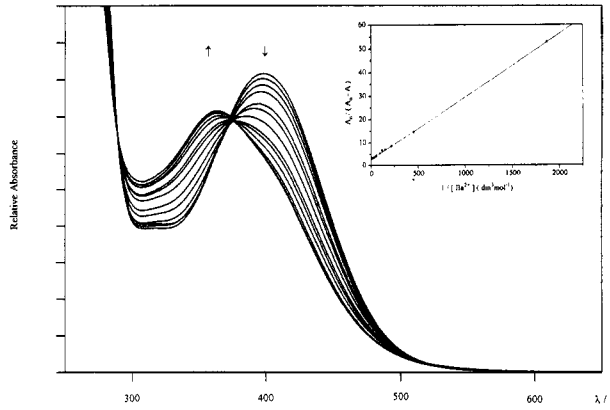

Figure 2. Electronic absorption spectrum of **1** in anhydrous methanol (106.8 μM) upon addition of $Ba(ClO_4)_2$. The insert shows a plot of $A_0/(A_0 - A)$ versus the reciprocal of $[Ba^{2+}]$. The absorbance was monitored at λ = 410 nm.

Table 1. Photophysical Data for Complexes 1−4

complex	medium (*T*/K)	λ_{em}/nm (τ_0/μs)
1	solid (298)	665
	solid (77)	633, 691
	CH_2Cl_2 (298)	717 (<0.1)
2	solid (298)	650
	solid (77)	625
	CH_2Cl_2 (298)	730 (<0.1)
3	solid (298)	513
	solid (77)	507
	MeOH (298)	549 (1.7 ± 0.1)
4	solid (298)	509
	solid (77)	498
	MeOH (298)	548 (1.8 ± 0.1)

The electronic absorption spectra of complexes **1**, **2** and **3**, **4** show low-energy absorption bands at *ca.* 400 and 370 nm in MeOH, respectively. With reference to previous spectroscopic work on Re(I) diimine systems,[3,4,7] they are tentatively assigned as a $d_\pi(Re) \rightarrow \pi^*(L_1/L_2)$ MLCT/$\pi(L_1/L_2) \rightarrow \pi^*$ (L_1/L_2) IL admixture and a pure $d_\pi(Re) \rightarrow \pi^*$(phen) MLCT transition, respectively. The slightly higher transition energy of the MLCT/IL band in **1** relative to that in **2** is in accordance with the higher π^* orbital energy of L_1 as a result of the electron-donating effect of the polyether substituents on the benzene ring. For complexes **3** and **4**, the $d_\pi(Re) \rightarrow \pi^*$(phen) MLCT transition energies are almost identical, since L_3 and L_4 have similar electronic effects. The photophysical data are summarized in Table 1. Addition of alkali-metal or alkaline-earth-metal ions to a methanolic solution of **1** results in a blue shift of the

(6) Crystal Data for **3**: $[C_{31}H_{32}N_4O_8Re^+PF_6^-]$, M_r = 919.79, crystal dimensions 0.10 × 0.07 × 0.25 mm, orthorhombic, space group *Pbca* (No. 61), *a* = 21.554(5) Å, *b* = 18.819(5) Å, *c* = 17.240(9) Å, *V* = 6994(9) Å^3, *Z* = 8, D_c = 1.747 g cm^{-3}, μ(Mo Kα) = 36.08 cm^{-1}, *F*(000) = 3632, *T* = 298 K, 215 parameters, 5080 data measured, 2281 data used in calculation ($I \geq 3\sigma(I)$), R = 0.074, R_w = 0.087, $w = 4F_o^2/\sigma^2(F_o^2)$, where $\sigma^2(F_o^2) = \sigma^2(I) + (0.018F_o^2)^2$. The maximum and minimum residues in the final ΔF synthesis were 1.32 e Å^{-3} around the Re atom (0.90 e Å^{-3} elsewhere) and −1.166 e Å^{-3}, respectively. Diffraction data were collected on a Rigaku AFC7R diffractometer with graphite-monochromatized Mo Kα radiation (λ = 0.710 73 Å) to $2\theta_{max}$ = 45°. Intensity data were corrected for decay, Lorentz, polarization, and absorption effects. The space group was determined from systematic absences, and the structure was solved by heavy-atom Patterson methods and expanded using Fourier techniques (PATTY and DIRDIF92: Beurskens, P. T.; Admiraal, G.; Beursken, G.; Bosman, W. P.; Garcia-Granda, S.; Gould, R. O.; Smits, J. M. M.; Smykalla, C. *The DIRDIF program system*; Technical Report of the Crystallography Laboratory; University of Nijmegen: Nijmegen, The Netherlands, 1992.) and refinement by full-matrix least squares using the MSC-Crystal Structure Package TEXSAN on a Silicon Graphics Indy computer. As the number of observed reflections was small, only the Re and P atoms were refined anisotropically; the other 49 non-hydrogen atoms were refined isotropically, and the 32 hydrogen atoms at calculated positions with thermal parameters equal to 1.3 times that of the attached C atoms were not refined.

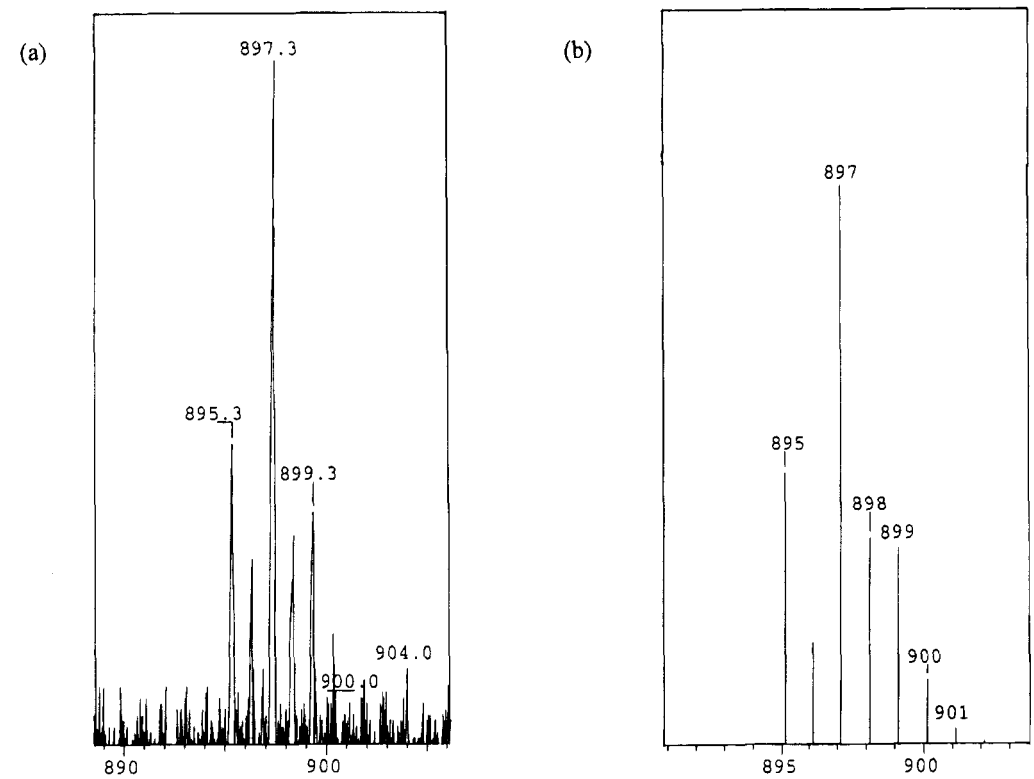

Figure 3. (a) Ion cluster at *m/z* 897, expanded from the positive-ion FAB mass spectrum of an acetonitrile solution of **3** and $NaClO_4$. (b) Simulated isotope pattern for the adduct $\{[\mathbf{3}\cdot Na](ClO_4)\}^+$.

MLCT/IL absorption band (Figure 2). These shifts were ascribed to the binding of the cations to the polyether cavity, as similar effects were absent for the uncrowned complex **2**. Similar findings have also been observed in the related Ru(II) and Cu(I) systems.[2f,8] Among the cations studied, sodium ion gives the largest stability constant with a log K value of 2.55, obtained from a plot[9] of $A_0/(A_0 - A)$ versus $1/[Na^+]$ in MeOH. The almost perfect linearity of the fit is supportive of a 1:1 stoichiometry, which is in accordance with the well-known binding mode of benzo-15-crown-5 for sodium ions with its appropriate cavity size.[10] With Ba^{2+}, a log K value of 2.01 and a stoichiometry of 1:1 were also obtained (Figure 2). For K^+, two complexes with stoichiometries of 1:2 (K^+:**1**) and 1:1 were formed, as indicated by the lack of well-defined isosbestic points in the UV–visible spectral trace and the absence of a satisfactory fit with $A_0/(A_0 - A)$ versus $1/[K^+]$ based on a 1:1 stoichiometry model. Similar 1:2 sandwich binding models have been reported in other K^+–(benzo-15-crown-5) systems.[11] In contrast, no spectral shifts were observable for complexes **3** and **4** upon addition of alkali-metal or alkaline-earth-metal ions. It is likely that any binding of cations into the cavity of L_3 is too remote to affect the $d_\pi(Re) \rightarrow \pi^*(phen)$ MLCT transition energy, given the indirect involvement of L_3 in the MLCT transition and the lack of conjugation and, hence, communication in the L_3 ligand to the Re metal center. Nevertheless, the uptake of alkali-metal/alkaline-earth-metal cations by the aza-crown moiety of **3** can be revealed by positive-ion FAB-MS. Figure 3a illustrates the ion cluster at *m/z* 897, expanded from the positive-ion FAB mass spectrum of an acetonitrile solution of **3** and $NaClO_4$. Figure 3b shows the simulated isotope pattern of the ion cluster attributable to the adduct $\{[\mathbf{3}\cdot Na](ClO_4)\}^+$. The presence of this soft–hard mixed-metal complex connected by a crown ether pendant ligand is directly observed, despite the fact that little information on the cation binding properties of **3** is provided by electronic absorption spectroscopy.

All complexes exhibit long-lived intense yellow-green to orange-red emission upon visible light excitation ($\lambda > 350$ nm) both in the solid state and in fluid solutions at 298 K (Table 1). It is likely that the emission is of MLCT triplet parentage, commonly observed in Re(I) diimine systems.[3,4,7] The lower emission energies of complexes **1** and **2** relative to those of **3** and **4** are consistent with the MLCT absorption spectral data. Extension of this work to other transition-metal centers is in progress.

Acknowledgment. V.W.-W.Y. acknowledges financial support from The Croucher Foundation and the Research Grants Council. V.W.-M.L. acknowledges the receipt of a postgraduate studentship and K.K.-W.L. the receipt of a postgraduate studentship and a Hung Hing Ying Postgraduate Scholarship, both administered by The University of Hong Kong.

Supporting Information Available: Text giving details of the crystal structure solution and crystal and structure determination data and tables giving fractional coordinates and thermal parameters, general displacement parameter expressions (U), and all bond distances and bond angles (11 pages). Ordering information is given on any current masthead page.

OM950338F

(7) See for example: (a) Yam, V. W.-W.; Lau, V. C.-Y.; Cheung, K.-K. *J. Chem. Soc., Chem. Commun.* **1995**, 259. (b) Yam, V. W.-W.; Lau, V. C.-Y.; Cheung, K.-K. *Organometallics* **1995**, *14*, 2749. (c) Horn, E.; Snow, M. R. *Aust. J. Chem.* **1980**, *33*, 2369. (d) Chen, P.; Curry, M.; Meyer, T. J. *Inorg. Chem.* **1989**, *28*, 2271. (e) Moya, S. A.; Guerrero, J.; Pastene, R.; Schmidt, R.; Sariego, R.; Sartori, R.; Sanz-Aparicio, J.; Fonseca, I.; Martinez-Ripoll, M. *Inorg. Chem.* **1994**, *33*, 2341.

(8) Beer, P. D.; Kocian, O.; Mortimer, R. J.; Ridgway, C. *J. Chem. Soc., Dalton Trans.* **1993**, 2629.

(9) (a) Fery-Forgues, S.; Le Bris, M. T.; Guetté, J. P.; Valeur, B. *J. Phys. Chem.* **1988**, *92*, 6233. (b) Bourson, J.; Valeur, B. *J. Phys. Chem.* **1989**, *93*, 3871.

(10) Izatt, R. M.; Pawlak, K.; Bradshaw, J. S.; Bruening, R. L. *Chem. Rev.* **1991**, *91*, 1721.

(11) (a) Mallinson, P. R.; Truter, M. R. *J. Chem. Soc., Perkin Trans. 2* **1972**, 1818. (b) Beer, P. D. *J. Chem. Soc., Chem. Commun.* **1986**, 1678.

Synthesis and Structure of $(\eta^5\text{-}C_5Me_5)_2Zr(Se)CO$, a Nonclassical d^0 Zirconium Carbonyl Complex

William A. Howard, Tina M. Trnka, and Gerard Parkin*

Department of Chemistry, Columbia University, New York, New York 10027

Received June 21, 1995[⊗]

Summary: $Cp^*_2Zr(Se)CO$ ($Cp^* = \eta^5\text{-}C_5Me_5$), an example of a nonclassical d^0 transition-metal carbonyl complex, has been synthesized by the reaction of $Cp^*_2Zr(CO)_2$ with elemental Se (ca. 1 equiv) at 50 °C. The CO ligand in $Cp^*_2Zr(Se)CO$ is labile and is rapidly displaced by pyridine to give $Cp^*_2Zr(Se)(NC_5H_5)$.

In contrast to the groups 5–8 transition metals, complexes of the group 4 transition metals (Ti, Zr, Hf) that exhibit metal–ligand multiple bonding are not common.[1] Accordingly, considerable effort has recently been directed toward the syntheses of such complexes. Indeed, in the case of zirconium, these efforts have been rewarded with the isolation of terminal benzylidene,[2] imido,[3] hydrazido,[4] phosphinidene,[5] and chalcogenido[6–9] derivatives. Interestingly, none of these multiply bonded derivatives possess CO as an ancillary ligand, even though CO is an otherwise ubiquitous ligand in organotransition-metal chemistry. The notable absence of such carbonyl derivatives is undoubtedly a consequence of the fact that the zirconium centers in all of these multiply bonded derivatives are formally d^0, Zr(IV), and are therefore ill-suited to partake in metal-to-ligand π-back-bonding, an important component of the metal–carbonyl interaction.[10] In this paper, we describe the synthesis and structure of $Cp^*_2Zr(Se)CO$, a unique example of a d^0 zirconium carbonyl complex which contains a metal–ligand multiple bond.

We have recently reported the syntheses of the terminal chalcogenido complexes $Cp^\dagger_2M(E)(NC_5H_5)$[11] (M = Zr,[7a] Hf;[12] E = S, Se, Te) by the reactions of $Cp^\dagger_2M(CO)_2$ with the elemental chalcogen in the presence of pyridine. In the absence of pyridine, $Cp^*_2Zr(CO)_2$ reacts with excess chalcogen to give the trichalcogenides $Cp^*_2Zr(\eta^2\text{-}E_3)$, while the η^2-dichalcogenido–carbonyl complexes $Cp^*_2Zr(\eta^2\text{-}E_2)(CO)$ may be obtained from the corresponding reactions with *ca.* 2 equiv of chalcogen.[13] More significantly, we now report that the terminal selenido–carbonyl complex $Cp^*_2Zr(Se)CO$ may be successfully isolated from the reaction of $Cp^*_2Zr(CO)_2$ with *ca.* 1 equiv of selenium (Scheme 1).[14] Notably, the isomeric η^2-carbonylselenide derivative $Cp^*_2Zr(\eta^2\text{-}SeCO)$, an alternative possible product derived by coupling of the carbonyl and selenide ligands,[15] is not obtained from this reaction.[16]

The molecular structure of $Cp^*_2Zr(Se)CO$ and, for purposes of comparison, the structures of the dichalcogenido–carbonyl derivatives $Cp^*_2Zr(\eta^2\text{-}E_2)CO$ (E = S, Se) have been determined by X-ray diffraction (Figures 1 and 2 and Table 1).[17] The Zr=Se bond length in $Cp^*_2Zr(Se)CO$ (2.478(2) Å) is comparable to that in $Cp^{Et*}_2Zr(Se)(NC_5H_5)$ (2.480(1) Å)[7a] but significantly shorter than the Zr–Se single bonds in $Cp^*_2Zr(\eta^2\text{-}Se_2)CO$ (2.715(2) and 2.688(2) Å).[18] These structural data clearly support the presence of a Zr=Se double bond in

[⊗] Abstract published in *Advance ACS Abstracts,* August 1, 1995.

(1) Nugent, W. A.; Mayer, J. M. *Metal-Ligand Multiple Bonds*; Wiley-Interscience: New York, 1988.

(2) Fryzuk, M. D.; Mao, S. S. H.; Zaworotko, M. J.; MacGillivray, L. R. *J. Am. Chem. Soc.* **1993**, *115*, 5336–5337.

(3) (a) Meyer, K. E.; Walsh, P. J.; Bergman, R. G. *J. Am. Chem. Soc.* **1995**, *117*, 974–985. (b) Walsh, P. J.; Hollander, F. J.; Bergman, R. G. *Organometallics* **1993**, *12*, 3705–3723. (c) Arney, D. J.; Bruck, M. A.; Huber, S. R.; Wigley, D. E. *Inorg. Chem.* **1992**, *31*, 3749–3755. (d) Bai, Y.; Roesky, H. W.; Noltemeyer, M.; Witt, M. *Chem. Ber.* **1992**, *125*, 825–831. (e) Cummins, C. C.; Van Duyne, G. D.; Schaller, C. P.; Wolczanski, P. T. *Organometallics* **1991**, *10*, 164–170. (f) Profilet, R. D.; Zambrano, C. H.; Fanwick, P. E.; Nash, J. J.; Rothwell, I. P. *Inorg. Chem.* **1990**, *29*, 4362–4364. (g) Walsh, P. J.; Hollander, F. J.; Bergman, R. G. *J. Am. Chem. Soc.* **1988**, *110*, 8729–8731. (h) Cummins, C. C.; Baxter, S. M.; Wolczanski, P. T. *J. Am. Chem. Soc.* **1988**, *110*, 8731–8733.

(4) (a) Walsh, P. J.; Carney, M. J.; Bergman, R. G. *J. Am. Chem. Soc.* **1991**, *113*, 6343–6345. (b) Walsh, P. J.; Hollander, F. J.; Bergman, R. G. *J. Organomet. Chem.* **1992**, *428*, 13–47.

(5) Hou, Z.; Breen, T. L.; Stephan, D. W. *Organometallics* **1993**, *12*, 3158–3167.

(6) Carney, M. J.; Walsh, P. J.; Hollander, F. J.; Bergman, R. G. *Organometallics* **1992**, *11*, 761–777.

(7) (a) Howard, W. A.; Parkin, G. *J. Am. Chem. Soc.* **1994**, *116*, 606–615. (b) Howard, W. A.; Waters, M.; Parkin, G. *J. Am. Chem. Soc.* **1993**, *115*, 4917–4918.

(8) (a) Jacoby, D.; Floriani, C.; Chiesi-Villa, A.; Rizzoli, C. *J. Am. Chem. Soc.* **1993**, *115*, 7025–7026. (b) Jacoby, D.; Isoz, S.; Floriani, C.; Chiesi-Villa, A.; Rizzoli, C. *J. Am. Chem. Soc.* **1995**, *117*, 2793–2804. (c) Jacoby, D.; Isoz, S.; Floriani, C.; Chiesi-Villa, A.; Rizzoli, C. *J. Am. Chem. Soc.* **1995**, *117*, 2805–2816.

(9) Christou, V.; Arnold, J. *J. Am. Chem. Soc.* **1992**, *114*, 6240–6242.

(10) (a) Mingos, D. M. P. In *Comprehensive Organometallic Chemistry*; Wilkinson, G., Stone, F. G. A., Abel, E. W., Eds.; Pergamon Press: Oxford, U.K., 1982; Vol. 3, Section 19.2. (b) Davidson, E. R.; Kunze, K. L.; Machado, F. B. C.; Chakravorty, S. J. *Acc. Chem. Res.* **1993**, *26*, 628–635.

(11) Abbreviations: $Cp^\dagger$ = Cp* or Cp^{Et*}; Cp* = $\eta^5\text{-}C_5Me_5$; Cp^{Et*} = $\eta^5\text{-}C_5Me_4Et$.

(12) Howard, W. A.; Parkin, G. *J. Organomet. Chem.* **1994**, *472*, C1-C4.

(13) Howard, W. A.; Parkin, G.; Rheingold, A. L. *Polyhedron* **1995**, *14*, 25–44.

(14) A mixture of $Cp^*_2Zr(CO)_2$ (0.5 g, 1.2 mmol) and Se powder (0.085 g, 1.1 mmol) in toluene (3 mL) was stirred at 50 °C for 1 day and then cooled to deposit a brown-orange precipitate from the dark orange solution. The mixture was filtered, and the precipitate was washed with pentane, giving $Cp^*_2Zr(Se)CO$ as a green crystalline solid which was dried *in vacuo* (0.17 g, 33%).

(15) Coupling of chalcogens and carbonyl ligands is precedented. For example, $(\eta^5\text{-}C_5H_4Me)_2Nb(CO)CH_2SiMe_3$ reacts with elemental sulfur to give the η^2-carbonylsulfide derivative $(\eta^5\text{-}C_5H_4Me)_2Nb(\eta^2\text{-}SCO)CH_2SiMe_3$. See: Fu, P.-F.; Khan, M. A.; Nicholas, K. M. *Organometallics* **1993**, *12*, 3790–3791.

(16) Moreover, coupling is also observed in the reaction of the terminal hydrazido intermediate $[Cp_2Zr(NNPh_2)]$ with CO to give the isocyanate derivative $Cp_2Zr(NCO)(NPh_2)$, rather than the d^0 carbonyl adduct $Cp_2Zr(NNPh_2)(CO)$.[4a]

(17) $Cp^*_2Zr(Se)CO$ is orthorhombic, $Pna2_1$ (No. 33), with a = 14.779(3) Å, b = 8.554(2) Å, c = 16.391(3) Å, V = 2072(1) Å^3, and Z = 4. $Cp^*_2Zr(\eta^2\text{-}S_2)(CO)$ is monoclinic, $P2_1/n$ (No. 14), with a = 8.601(2) Å, b = 14.925(3) Å, c = 17.308(2) Å, β = 104.16(2)°, V = 2115(1) Å^3, and Z = 4. $Cp^*_2Zr(\eta^2\text{-}Se_2)(CO)$ is monoclinic, $P2_1/n$ (No. 14), with a = 8.667(2) Å, b = 15.092(3) Å, c = 17.401(3) Å, β = 104.27(2)°, V = 2206(1) Å^3, and Z = 4.

(18) Zr–Se single bond lengths in permethylzirconocene complexes range from *ca.* 2.65 to 2.67 Å, *e.g.*, $Cp^*_2Zr(SeH)_2$ (d(Zr–Se) = 2.647(2) Å),[18a] $Cp^*_2Zr(OH)(SeH)$ (d(Zr–Se) = 2.665(1) Å),[18a] $Cp^*_2Zr(SePh)_2$ (d(Zr–Se) = 2.653(3), 2.648(4) Å),[18a] $Cp^*_2Zr(SeH)(\eta^1\text{-}OC(Ph)=CH_2)$ (d(Zr–Se) = 2.669(1) Å),[7a] and $Cp^*_2Zr(\eta^2\text{-}Se_3)$ (d(Zr–Se) = 2.653(3) Å).[13] (a) Howard, W. A.; Trnka, T. M.; Parkin, G. Manuscript in preparation.

0276-7333/95/2314-4037$09.00/0

Scheme 1

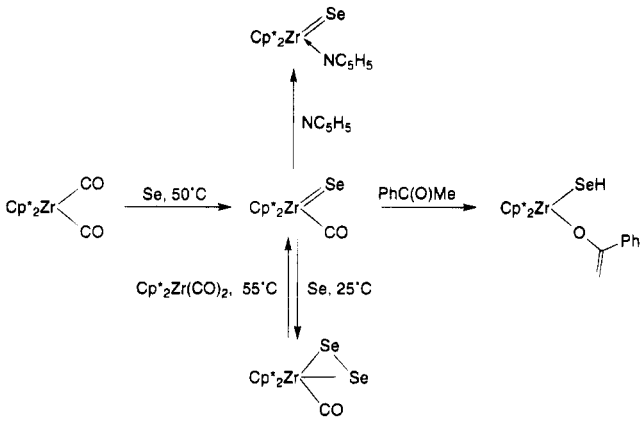

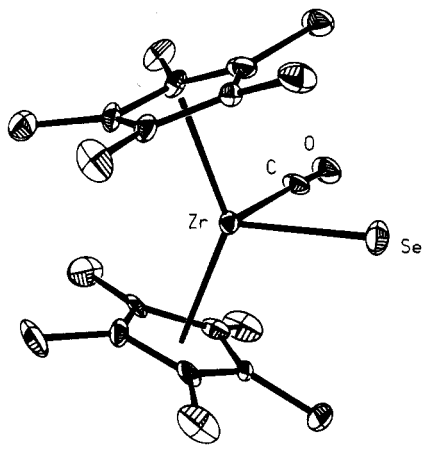

Figure 1. Molecular structure of $Cp^*_2Zr(Se)CO$.

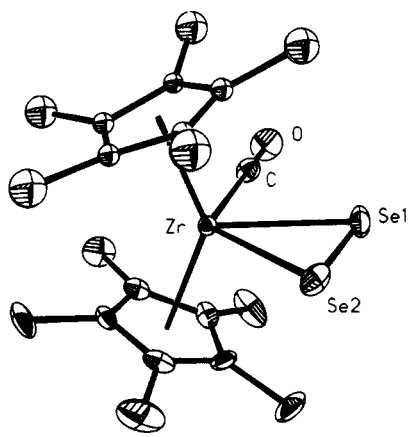

Figure 2. Molecular structure of $Cp^*_2Zr(\eta^2\text{-}Se_2)CO$.

Table 1. Metrical and IR Data for Structurally Characterized Neutral Permethylzirconocene Derivatives

	d(Zr–CO)/Å	d(C–O)/Å	ν(CO)/cm^{-1}	ref
$Cp^*_2Zr(Se)CO$	2.233(15)	1.116(19)	2037	*a*
$Cp^*_2Zr(\eta^2\text{-}S_2)CO$	2.261(6)	1.126(8)	2057	*a,b*
$Cp^*_2Zr(\eta^2\text{-}Se_2)CO$	2.253(13)	1.128(16)	2037	*a,b*
$Cp^*_2Zr(\eta^2\text{-}Te_2)CO$	2.241[7]	1.123[9]	2006	*b*
$Cp^*_2Zr(CO)_2$	2.145(9)	1.16(1)	1945, 1852	*c*

[a] This work. [b] Reference 13. [c] Reference 22.

$Cp^*_2Zr(Se)CO$ and are thereby in accord with its description as a d^0 Zr(IV) complex. As such, $Cp^*_2Zr(Se)CO$ provides an unusual example of a d^0 metal carbonyl complex that also contains a multiply bonded ligand.

In view of the d^0 nature of $Cp^*_2Zr(Se)CO$, π-back-bonding would not be expected to stabilize the Zr–CO interaction significantly, so that the bonding within $Cp^*_2Zr(Se)CO$ differs considerably from that in traditional metal carbonyl complexes. Accordingly, $Cp^*_2Zr(Se)CO$ may be regarded to be a nonclassical carbonyl complex.[19,20] The notion that $Cp^*_2Zr(Se)CO$ is a nonclassical carbonyl is supported by the observation that the Zr–CO and C–O bonds are marginally longer and shorter, respectively, than the corresponding values for the related d^2 derivative $Cp^*_2Zr(CO)_2$ (Table 1). Moreover, the reduced π-back-bonding is also manifested by the observation of a higher ν_{CO} stretching frequency for $Cp^*_2Zr(Se)CO$ (2037 cm^{-1})[21] compared to the corresponding values for $Cp^*_2Zr(CO)_2$ (1945 and 1852 cm^{-1}].[22] The ν_{CO} stretching frequency for $Cp^*_2Zr(Se)CO$ is, however, lower than that in CO (2143 cm^{-1}),[23] so that some degree of electron donation into the π^* CO orbital is evident. In view of the d^0 nature of the zirconium center, such donation may occur *via* interaction with the [Zr=Se] moiety.[24] Indeed, for $Cp^*_2ZrH_2(CO)$, the first spectroscopically characterized d^0 zirconium carbonyl complex, the lowering of the ν_{CO} stretching frequency (2044 cm^{-1}) with respect to that for carbon monoxide was proposed to arise from donation of electron density from a filled metal–hydride bonding orbital into an in-plane π^* CO orbital.[20b,25] More recently, Berry has identified that the direct donation of electron density from silicon to the CO π^* orbital is responsible for the anomalously low value (1797 cm^{-1}) for the CO stretching frequency in $Cp_2Zr(\eta^2\text{-}Me_2Si{=}NBu^t)CO$.[20f]

As would be expected for a d^0 carbonyl derivative, the CO ligand in $Cp^*_2Zr(Se)CO$ is labile.[26] For example, $Cp^*_2Zr(Se)CO$ reacts rapidly with pyridine at room temperature to afford $Cp^*_2Zr(Se)(NC_5H_5)$ (Scheme 1). $Cp^*_2Zr(Se)CO$ also reacts with selenium to give $Cp^*_2Zr(\eta^2\text{-}Se_2)(CO)$ and $Cp^*_2Zr(\eta^2\text{-}Se_3)$, sequentially. Interestingly, these chalcogen addition reactions may be reversed using $Cp^*_2Zr(CO)_2$ as a chalcogen trap. Thus,

(19) For leading recent references on nonclassical carbonyl complexes, see: (a) Hurlburt, P. K.; Rack, J. J.; Luck, J. S.; Dec, S. F.; Webb, J. D.; Anderson, O. P.; Strauss, S. H. *J. Am. Chem. Soc.* **1994**, *116*, 10003–10014. (b) Aubke, F.; Wang, C. *Coord. Chem. Rev.* **1994**, *137*, 483–524. (c) Weber, L. *Angew. Chem., Int. Ed. Engl.* **1994**, *33*, 1077–1078. (d) Willner, H.; Bodenbinder, M.; Wang, C.; Aubke, F. *J. Chem. Soc., Chem. Commun.* **1994**, 1189–1190.

(20) In addition to $Cp^*_2Zr(Se)CO$ and $Cp^*_2Zr(\eta^2\text{-}E_2)CO$ (E = S, Se, Te), other nonclassical carbonyl complexes of zirconium include $Cp^*_2ZrH_2(CO)$,[20a,b] $[Cp_2Zr\{\eta^2\text{-}CH(Me)(6\text{-ethylpyrid-2-yl})\text{-}C,N\}(CO)]^+$,[20c] $[Cp^*_2Zr(\eta^2\text{-}COCH_3)CO]^+$,[20d] $[Cp_2Zr(\eta^2\text{-}COCH_3)CO]^+$,[20d] $Cp^*_2Zr(\eta^3\text{-}C_3H_5)CO]^+$,[20e] and $Cp_2Zr(\eta^2\text{-}Me_2SiNBu^t)CO$.[20f] (a) Manriquez, J. M.; McAlister, D. R.; Sanner, R. D.; Bercaw, J. E. *J. Am. Chem. Soc.* **1978**, *100*, 2716–2724. (b) Marsella, J. A.; Curtis, C. J.; Bercaw, J. E.; Caulton, K. G. *J. Am. Chem. Soc.* **1980**, *102*, 7244–7246. (c) Guram, A. S.; Swenson, D. C.; Jordan, R. F. *J. Am. Chem. Soc.* **1992**, *114*, 8991–8996. (d) Guo, Z.; Swenson, D. C.; Guram, A. S.; Jordan, R. F. *Organometallics* **1994**, *13*, 766–773. (e) Antonelli, D. M.; Tjaden, E. B.; Stryker, J. M. *Organometallics* **1994**, *13*, 763–765. (f) Procopio, L. J.; Carroll, P. J.; Berry, D. H. *Polyhedron* **1995**, *14*, 45–55.

(21) $\nu(^{12}CO)/\nu(^{13}CO) = 1.023$.

(22) Sikora, D. J.; Rausch, M. D.; Rogers, R. D.; Atwood, J. L. *J. Am. Chem. Soc.* **1981**, *103*, 1265–1267.

(23) Elschenbroich, C.; Salzer, A. *Organometallics*, 2nd ed.; VCH: New York, 1992.

(24) The C···Se separation is 2.87 Å. For reference the sum of the covalent radii is 1.94 Å. See: Pauling, L. *The Nature of The Chemical Bond*, 3rd. ed.; Cornell University Press: Ithaca, NY, 1960.

(25) (a) Brintzinger, H. H. *J. Organomet. Chem.* **1979**, *171*, 337–344. (b) Strauss, S. H. *Chemtracts: Inorg. Chem.* **1994**, *6*, 157–162.

(26) In the absence of a suitable trapping ligand, however, $Cp^*_2Zr(Se)CO$ slowly decomposes. For example, removal of solvent from solutions of $Cp^*_2Zr(Se)CO$ under reduced pressure results in decomposition.

$Cp^*_2Zr(\eta^2\text{-}Se_3)$ reacts with $Cp^*_2Zr(CO)_2$ to give a mixture of $Cp^*_2Zr(\eta^2\text{-}Se_2)CO$ and $Cp^*_2Zr(Se)CO$. Finally, an additional mode of reactivity of the multiply bonded [Zr=Se] moiety in $Cp^*_2Zr(Se)CO$ is illustrated by its reaction with PhC(O)Me to give the enolate derivative $Cp^*_2Zr(SeH)[\eta^1\text{-}OC(Ph)=CH_2]$.[7a]

In summary, the nonclassical, d^0 carbonyl complex $Cp^*_2Zr(Se)CO$ may be isolated from the reaction of $Cp^*_2Zr(CO)_2$ with *ca.* 1 equiv of elemental selenium. The nonclassical nature of the metal–carbonyl interaction is manifested by longer Zr–CO bond lengths, shorter C–O bond lengths, and a higher ν_{CO} stretching frequency compared with those of the d^2 derivative $Cp^*_2Zr(CO)_2$.

Acknowledgment. We thank the U.S. Department of Energy, Office of Basic Energy Sciences (Contract No. DE-FG02-93ER14339), and the donors of the Petroleum Research Fund, administered by the American Chemical Society, for partial support of this research. G.P. is the recipient of a Camille and Henry Dreyfus Teacher-Scholar Award (1991–1996) and a Presidential Faculty Fellowship Award (1992–1997). T.M.T. acknowledges the Camille and Henry Dreyfus Foundation for the Jean Dreyfus Boissevain Undergraduate Scholarship in Chemistry (1994–1995).

Supporting Information Available: Tables of analytical and spectroscopic data for $Cp^*_2Zr(Se)CO$ and tables of crystal and intensity collection data, atomic coordinates, bond distances and angles, and anisotropic displacement parameters and additional ORTEP drawings for $Cp^*_2Zr(Se)CO$ and $Cp^*_2Zr(\eta^2\text{-}E_2)CO$ (E = S, Se) (40 pages). This material is contained in many libraries on microfiche, immediately follows this article in the microfilm version of the journal, and can be ordered from the ACS; see any current masthead page for ordering information.

OM950479H

Platinum-Mediated P=C Bond Cleavage in a Phosphaketene: Formation and Structure of the First Mononuclear Diphosphaureylene Complex

Marie-Anne David and David S. Glueck*

6128 Burke Laboratory, Department of Chemistry, Dartmouth College, Hanover, New Hampshire 03755

Glenn P. A. Yap and Arnold L. Rheingold

Department of Chemistry, University of Delaware, Newark, Delaware 19716

Received May 17, 1995[⊗]

*Summary: Reactions of Mes*P=C=O (**1**; Mes* = 2,4,6-(t-Bu)$_3$C$_6$H$_2$) with (PPh$_3$)$_2$Pt(C$_2$H$_4$) (**2**) and (PCy$_3$)$_2$Pt (**3**; Cy = cyclo-C$_6$H$_{11}$) give the diphosphaureylene carbonyl complexes (L)(CO)Pt(Mes*PCOPMes*) (**4**, L = PPh$_3$; **5**, L = PCy$_3$), respectively. The structure of **4** was determined by X-ray crystallography. Addition of dmpe (dmpe = Me$_2$P(CH$_2$)$_2$PMe$_2$) to **4** or **5** gives (dmpe)Pt(Mes*PCOPMes*) (**6**).*

The phosphaketene Mes*P=C=O[1] (**1**; Mes* = 2,4,6-(*t*-Bu)$_3$C$_6$H$_2$) is readily decarbonylated by metal complexes to give products derived from the phosphinidene Mes*P, which may bind to the metal center[2] or undergo intramolecular cyclization to form the phosphaindan 2,4-(t-Bu)$_2$C$_6$H$_2$(6-CMe$_2$CH$_2$PH).[3] We report here that the reactions of Pt(0) phosphine complexes with **1** give products containing carbonyl and diphosphaureylene [Mes*PC(O)PMes*]$^{2-}$ ligands, derived formally from decarbonylation of the phosphaketene and coupling of the resulting phosphinidene fragment with another equivalent of the cumulene.[4] The diphosphaureylene ligand was previously known only to bridge two metal centers.[5]

Reaction of (PPh$_3$)$_2$Pt(C$_2$H$_4$)[6] (**2**) or (PCy$_3$)$_2$Pt[7] (**3**; Cy = cyclo-C$_6$H$_{11}$) in THF with 2 equiv of **1** rapidly gives red solutions from which red crystals of the products (R$_3$P)Pt(CO)[Mes*PC(O)PMes*] (**4**, R = Ph; **5**, R = Cy) can be isolated by crystallization; the byproducts PPh$_3$ and PCy$_3$ are observed by ^{31}P NMR (Scheme 1).[8] When only 1 equiv of **1** is allowed to react with **2**, the products are **4**, Pt(PPh$_3$)$_3$, and a mixture of other unidentified Pt–P complexes.[9] However, a 1:1 ratio of **1** and **3** gives only complex **5**; free PCy$_3$ and unreacted starting material **3** are also observed by ^{31}P NMR.

Complexes **4** and **5** were identified by IR and by multinuclear NMR spectroscopy. Complex **4** shows carbonyl bands at 2059 and 1632 cm^{-1} assigned to Pt–CO and [Mes*PC(O)PMes*] groups, respectively. Signals due to these carbons appear in the ^{13}C NMR spectrum at δ 178.0 (ddd, $^1J_{Pt-C}$ = 1402 Hz, $^2J_{P-C}$ = 86 Hz, $^2J_{P-C}$ = 12 Hz, $^2J_{P-C}$ = 4 Hz) and δ 230.7 (ddd, $^1J_{P-C}$

[⊗] Abstract published in *Advance ACS Abstracts,* August 1, 1995.

(1) Appel, R.; Paulen, W. *Angew. Chem., Int. Ed. Engl.* **1983**, *22*, 785–786.

(2) Cowley, A. H.; Pellerin, B.; Atwood, J. L.; Bott, S. G. *J. Am. Chem. Soc.* **1990**, *112*, 6734–6735.

(3) (a) Champion, D. H.; Cowley, A. H. *Polyhedron* **1985**, *4*, 1791–1792. (b) David, M.-A.; Paisner, S. N.; Glueck, D. S. *Organometallics* **1995**, *14*, 17–19.

(4) The related chemistry of isocyanates is well known: (a) Beck, W.; Rieber, W.; Cenini, S.; Porta, F.; La Monica, G. *J. Chem. Soc., Dalton Trans.* **1974**, 298–304. For reviews, see: (b) Cenini, S.; La Monica, G. *Inorg. Chim. Acta* **1976**, *18*, 279–293. (c) Braunstein, P.; Nobel, D. *Chem. Rev.* **1989**, *89*, 1927–1945.

(5) For a review, see: King, R. B.; Wu, F.-J.; Holt, E. M. *J. Organomet. Chem.* **1990**, *383*, 295–305.

(6) Blake, D. M.; Roundhill, D. M. *Inorg. Synth.* **1978**, *18*, 120–122.

(7) Yoshida, T.; Otsuka, S. *Inorg. Synth.* **1979**, *19*, 101–107.

(8) **Synthesis of (PPh$_3$)(CO)Pt(Mes*PCOPMes*) (4).** To a solution of (PPh$_3$)$_2$Pt(C$_2$H$_4$) (**2**; 115 mg, 0.15 mmol) in THF (1 mL) was added Mes*PCO (1; 94 mg, 0.31 mmol) dissolved in THF (2 mL). The mixture became dark red immediately and was stirred at room temperature in the dark for a few hours. The solvent was removed under vacuum. The residue was washed with petroleum ether (bp 38–53 °C, 5 mL) to remove PPh$_3$. The red-orange residue was dissolved in a minimal amount of THF (ca. 1 mL). A layer of petroleum ether was added on top of the solution. Cooling of this mixture to −25 °C gave **4** as red crystals (127 mg, 77% yield). ^{1}H NMR (C$_6$D$_6$): δ 7.59 (d, $^4J_{P-H}$ = 2 Hz, 2H), 7.55 (d, $^4J_{P-H}$ = 2 Hz, 2H), 7.30–7.23 (m, 5H), 6.91–6.78 (m, 10H), 2.06 (18H), 1.73 (18H), 1.35 (9H), 1.21 (9H). ^{13}C{^{1}H} NMR (C$_6$D$_6$): δ 230.7 (ddd, $^1J_{P-C}$ = 126 Hz, $^1J_{P-C}$ = 92 Hz, $^3J_{P-C}$ = 17 Hz, quat, PCOP), 178.0 (ddd, $^1J_{Pt-C}$ = 1402 Hz, $^2J_{P-C}$ = 86 Hz, $^2J_{P-C}$ = 12 Hz, $^2J_{P-C}$ = 4 Hz, quat, CO), 159.7 (d, $^2J_{P-C}$ = 8 Hz, quat Ar), 158.4 (d, $^2J_{P-C}$ = 12 Hz, quat Ar), 151.3 (quat Ar), 150.7 (quat Ar), 139.4 (dm, $^1J_{P-C}$ = 99 Hz, Ar), 134.2 (d, J_{P-C} = 12 Hz, Ar), 132.6 (d, $^1J_{P-C}$ = 48 Hz, quat Ar), 131.2 (Ar), 130.3 (broad d, $^1J_{P-C}$ = 43 Hz, quat Ar), 129.1 (d, J_{P-C} = 10 Hz, Ar), 123.7 (d, $^3J_{P-C}$ = 7 Hz, Ar), 122.5 (d, $^3J_{P-C}$ = 5 Hz, Ar), 39.9 (d, $^3J_{P-C}$ = 3 Hz, quat), 39.6 (d, $^3J_{P-C}$ = 3 Hz, quat), 35.7 (quat), 35.3 (quat, overlaps with the next peak), 35.3 (broad, CH$_3$), 34.3 (broad, CH$_3$), 31.9 (CH$_3$); 31.8 (CH$_3$). ^{31}P{^{1}H} NMR (CD$_2$Cl$_2$): δ 58.7 (dd, $^1J_{Pt-P}$ = 681 Hz, $^2J_{P-P}$ = 177 Hz, $^2J_{P-P}$ = 124 Hz, P trans to PPh$_3$), 30.0 (dd, $^1J_{Pt-P}$ = 1830 Hz, $^2J_{P-P}$ = 177 Hz, $^2J_{P-P}$ = 15 Hz, P trans to CO), 23.1 (dd, $^1J_{Pt-P}$ = 2246 Hz, $^2J_{P-P}$ = 124 Hz, $^2J_{P-P}$ = 15 Hz, PPh$_3$). IR (KBr): 3056, 2912, 2059, 1632, 1592 (shoulder), 1529, 1478, 1434, 1390, 1359, 1228, 1210, 1182, 1120, 1097, 1027, 998, 921, 902, 879, 749, 740, 708, 692, 649, 590, 527, 511 cm^{-1}. Anal. Calcd for C$_{56}$H$_{73}$O$_2$P$_3$Pt: C, 63.08; H, 6.91. Found: C, 63.05; H, 7.13. **Synthesis of (PCy$_3$)(CO)Pt(Mes*PCOPMes*) (5).** To a solution of (PCy$_3$)$_2$Pt (**3**; 51 mg, 0.067 mmol) in THF (1 mL) was added Mes*PCO (41 mg, 0.135 mmol) dissolved in THF (1 mL). The mixture became dark red immediately and was stirred at room temperature in the dark for a few hours. CuCl (33 mg, 0.034 mmol) was added to complex free PCy$_3$ formed in the reaction. After 5 min of stirring, the solution was filtered, and the solvent was removed from the filtrate under vacuum. Complex **5** was recrystallized from petroleum ether at −25 °C (red needles) and was isolated in 45% yield (33 mg). ^{1}H NMR (C$_6$D$_6$): δ 7.67 (d, $^4J_{P-H}$ = 2 Hz, 2H), 7.65 (broad, 2H), 2.05 (18H), 2.01 (18H), 1.96–1.24 (m, 33H), 1.35 (9H), 1.34 (9H). ^{13}C{^{1}H} NMR (C$_6$D$_6$): δ 232.9–230.4 (m, PCOP), 180.0 (ddd, $^2J_{P-C}$ = 78 Hz, $^2J_{P-C}$ = 12 Hz, $^2J_{P-C}$ = 3 Hz, Pt satellites were not observed, quat, CO), 159.7 (d, $^2J_{P-C}$ = 10 Hz, quat Ar), 158.4 (d, $^2J_{P-C}$ = 11 Hz, quat Ar), 151.1 (quat Ar), 150.6 (quat Ar), 138.3 (dm, $^1J_{P-C}$ = 98 Hz, quat Ar), 131.3 (dm, $^1J_{P-C}$ = 71 Hz, quat Ar), 123.9 (d, $^3J_{P-C}$ = 7 Hz, Ar), 122.5 (d, $^3J_{P-C}$ = 5 Hz, Ar), 40.5 (d, $^3J_{P-C}$ = 3 Hz, quat), 39.6 (d, $^3J_{P-C}$ = 2 Hz, quat), 37.2 (d, $^1J_{P-C}$ = 23 Hz, CH), 35.6 (broad, overlapping quat and CH$_3$), 35.3 (broad, overlapping quat and CH$_3$), 31.9 (two overlapping CH$_3$), 30.4 (CH$_2$), 27.8 (d, $^3J_{P-C}$ = 10 Hz, CH$_2$), 26.6 (CH$_2$). ^{31}P{^{1}H} NMR (C$_6$D$_6$): δ 44.5 (dd, $^1J_{Pt-P}$ = 739 Hz, $^2J_{P-P}$ = 168 Hz, $^2J_{P-P}$ = 136 Hz, P trans to PCy$_3$), 37.1 (dd, $^1J_{Pt-P}$ = 2225 Hz, $^2J_{P-P}$ = 136 Hz, $^2J_{P-P}$ = 15 Hz, PCy$_3$), 23.2 (dd, $^1J_{Pt-P}$ = 1603 Hz, $^2J_{P-P}$ = 168 Hz, $^2J_{P-P}$ = 15 Hz, P trans to CO). IR (KBr): 2930, 2854 (shoulder), 2037, 1637, 1593 (shoulder), 1479, 1446, 1392, 1359, 1235, 1212, 1175, 1119, 1005, 874, 738, 591 cm^{-1}. Anal. Calcd for C$_{56}$H$_{91}$O$_2$P$_3$Pt: C, 62.02; H, 8.48. Found: C, 62.05; H, 8.77.

(9) **Reaction of (PPh$_3$)$_2$Pt(C$_2$H$_4$) with 1 equivalent of phosphaketene.** To a solution of (PPh$_3$)$_2$Pt(C$_2$H$_4$) (**2**; 200 mg, 0.27 mmol) in THF (1 mL) was added Mes*PCO (81 mg, 0.27 mmol) dissolved in THF (2 mL). The mixture became dark brown immediately and was stirred at room temperature in the dark overnight. The solvent was removed under vacuum. The brown residue was washed with petroleum ether (10 mL). Cooling the resulting petroleum ether solution to −25 °C gave **4** as a red-orange solid (75 mg, 26% yield). The remaining solid, sparingly soluble in petroleum ether, was dissolved in a minimal amount of THF (ca. 3 mL), and petroleum ether was added on top of the solution. Cooling of this mixture to −25 °C gave yellow crystals of Pt(PPh$_3$)$_3$ (64 mg, 32% yield), which was characterized by ^{31}P and ^{1}H NMR in C$_6$D$_6$ in comparison to the literature values (Tolman, C. A.; Seidel, W. C.; Gerlach, D. H. *J. Am. Chem. Soc.* **1972**, *94*, 2699–2676).

0276-7333/95/2314-4040$09.00/0

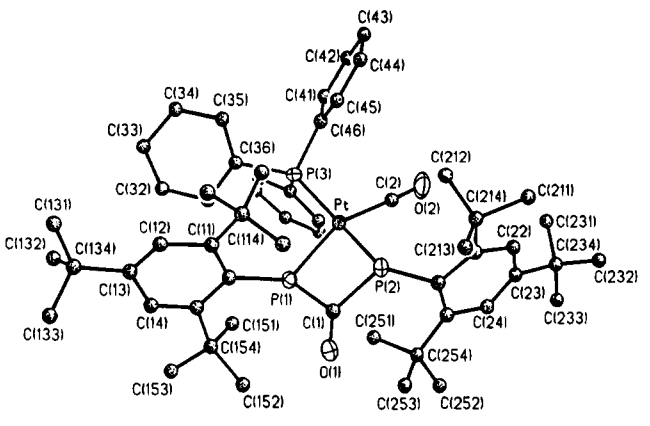

Figure 1. ORTEP diagram of **4**. Selected bond lengths (Å): Pt–P1, 2.321(7); Pt–P2, 2.337(7); Pt–P3, 2.350(7); Pt–C2, 1.887(27); P1–C1, 1.865(28); P2–C1, 1.849(27). Selected bond angles (deg): P1–Pt–P2, 73.3(2); P1–Pt–P3, 105.5(2); P2–Pt–P3, 170.4(3); P1–Pt–C2, 156.3(8); P2–Pt–C2, 89.5(8); P3–Pt–C2, 94.0(8); Pt–P1–C1, 94.8(9); Pt–P2–C1, 94.7(9); Pt–P1–C16, 132.7(9); C1–P1–C16, 115.2(12); Pt–P2–C26, 112.5(8); C1–P2–C26, 126.5(12); P1–C1–P2, 97.0(13); P1–C1–O1, 128.8 (20); P2–C1–O1, 134.2(20).

Scheme 1

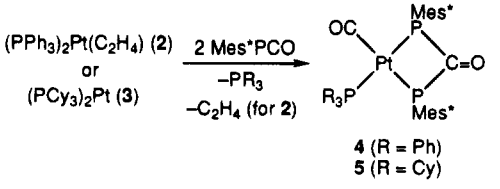

= 126 Hz, $^1J_{P-C}$ = 92 Hz, $^3J_{P-C}$ = 17 Hz). The $^{31}P\{^1H\}$ NMR spectrum shows peaks due to three different phosphorus nuclei. The phosphaureylene ^{31}P nuclei show small one-bond $^{195}Pt-^{31}P$ coupling constants characteristic of terminal phosphido (PR_2) ligands.[10] The different magnitudes of these couplings (681 Hz for the P trans to PPh_3 and 1830 Hz for the P trans to CO) reflect the trans influence.[11] The phosphaureylene P nuclei show a large cis coupling (177 Hz) and the expected large trans (124 Hz) and small cis (15 Hz) couplings to PPh_3. Spectroscopic data for **5** are similar.

The structure of **4** was confirmed by X-ray crystallography (Figure 1).[12] The coordination at Pt is distorted square planar, and the bite angle of the diphosphaureylene ligand (73.3(2)°) is significantly less than the idealized 90° angle. The platinum and the three coordinated P atoms lie on a plane (mean deviation 0.07 Å) with the metal carbonyl carbon 0.73 Å out of the plane. The chelating Pt–P distances (2.321(7) and 2.337(7) Å) are not significantly different, despite the different $^1J_{Pt-P}$ couplings observed in the ^{31}P NMR spectra. Coordination at these P atoms is pyramidal, indicating that Pt–P multiple bonding is not important. The diphosphaureylene ligand is planar (mean deviation

Scheme 2

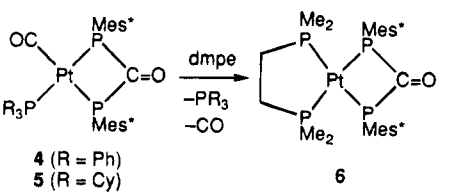

0.03 Å), and the P–C bond lengths (1.865(28) and 1.849(27) Å) and P–C–P bond angle (97.0(13)°) in it are quite similar to those in the related four-membered ring $[Mes^*PCO]_2$.[13] For comparison, in the previously reported diphosphaureylene $Fe_2(CO)_6$ complexes, which contain five-membered MPC(O)PM′ rings,[14] the P–C–P angle ranges from 84.4(4) to 88.3(2)°.

Related organic heterocycles containing diphosphaurea groups lose CO on photolysis,[15] but complex **4** survived irradiation (Hg lamp, THF) for 3.5 h. It decomposes on heating in THF to 50 °C for 12 h. Reaction of **4** or **5** with dmpe (dmpe = $Me_2P(CH_2)_2PMe_2$) in THF causes displacement of a tertiary phosphine and the carbonyl ligand to yield the orange, sparingly soluble (dmpe)Pt(Mes*PCOPMes*) (**6**) (Scheme 2).[16] This reaction proceeds quickly at ambient temperature for **4** but requires heating to 60 °C for 2 days for **5**. As expected, the IR spectrum of **6** shows only one CO stretch (1601 cm^{-1}), and the ^{31}P NMR spectrum is an AA′BB′ pattern. The diphosphaureylene P nuclei have a large cis coupling of 158 Hz, in contrast to the dmpe cis P–P coupling of 10 Hz, and a trans P–P coupling of 216.5 Hz. As in **4** and **5**, the $^{195}Pt-^{31}PR_2$ coupling is characteristically small (1103 Hz). Complex **6** remains unchanged on heating in CH_2Cl_2 at 40 °C for 3 days and in THF at 65 °C for 4 h. It decomposes on irradiation (Hg lamp, THF) for 6 h.

The formation of ureylene derivatives from metal-mediated isocyanate coupling may proceed via metal–imido complexes, and this step has been directly observed.[17] We are currently investigating the possibility

(10) (a) Schafer, H.; Binder, D. *Z. Anorg. Allg. Chem.* **1988**, *560*, 65–79. (b) Handler, A.; Peringer, P.; Muller, E. P. *J. Chem. Soc., Dalton Trans.* **1990**, 3725–3727.

(11) Appleton, T. G.; Bennett, M. A. *Inorg. Chem.* **1978**, *17*, 738–747.

(12) Crystal data for **4**: $C_{56}H_{73}O_2P_3Pt$, orthorhombic, $P2_12_12_1$, V = 5432(3) Å^3, Mo Kα (λ = 0.710 73 Å), d_{calc} = 1.304 g/cm^3, a = 15.944(5) Å, b = 17.037(5) Å, c = 19.998(7) Å, T = 230 K, Z = 4, $R(F)$ = 6.86%, $R(wF)$ = 8.05%. Details of the structure determination are provided as supporting information.

(13) Folling, P. Ph.D. Thesis, University of Bonn, 1988. For the orthorhombic form of this dimer of **1**, the P–C bond lengths are 1.838(16), 1.806(14), 1.814(15), and 1.809(15) Å, with P–C–P bond angles of 94.9(8) and 96.2(7)°. For the monoclinic form, the P–C bond lengths are 1.807(8) and 1.796(5) Å with a P–C–P bond angle of 98.3(3)°.

(14) (a) Weber, L.; Reizig, K.; Bungardt, D.; Boese, R. *Chem. Ber.* **1987**, *120*, 1421–1426. (b) De, R. L.; Wolters, D.; Vahrenkamp, H. *Z. Naturforsch., B* **1986**, *41*, 283–291. (c) King, R. B.; Wu, F.-J.; Sadanami, N. D.; Holt, E. M. *Inorg. Chem.* **1985**, *24*, 4449–4450.

(15) (a) Appel, R.; Paulen, W. *Chem. Ber.* **1983**, *116*, 2371–2373. (b) Appel, R.; Paulen, W. *Chem. Ber.* **1983**, *116*, 109–113.

(16) **Synthesis of (dmpe)Pt(Mes*PCOPMes*) (6).** To a solution of **4** (133 mg, 0.125 mmol) in THF (1 mL) was added dmpe (18.8 mg, 0.125 mmol) dissolved in THF (2 mL). The red mixture was stirred at room temperature and became orange after a few hours. The solvent was removed under vacuum. The orange residue was washed with petroleum ether (20 mL) and then recrystallized by diffusion of petroleum ether into THF at −25 °C to give 71 mg of orange crystals (61% yield). ^1H NMR (CD_2Cl_2): δ 7.34 (broad, 4H), 1.71 (36H), 1.55–1.43 (m, 4H), 1.28 (18H), 1.01–0.89 (m, 12H). $^{13}C\{^1H\}$ NMR (CD_2Cl_2): δ 237.2–233.8 (m, quat, PCOP), 158.7 (m, quat Ar), 149.5 (quat Ar), 137.2 (dm, $^1J_{P-C}$ = 75 Hz, quat Ar), 121.9 (Ar), 39.1 (quat), 35.0 (quat), 34.2 (CH_3), 31.6 (CH_3), 30.1–29.1 (m, CH_2), 15.6–14.6 (m, CH_3). $^{31}P\{^1H\}$ NMR (CD_2Cl_2): δ 32.0 ($^1J_{Pt-P}$ = 2435 Hz, dmpe), 14.0 ($^1J_{Pt-P}$ = 1103 Hz, Mes*P), AA′BB′ pattern, $^2J_{PP(trans)}$ = 216.5 Hz; $^2J_{PP(cis,Mes*P)}$ = 158 Hz; $^2J_{PP(cis,dmpe)}$ = 10 Hz, $^2J_{PP(cis,AB)}$ = −5.5 Hz. IR (KBr): 3068, 2957, 2907 (shoulder), 2861, 1601, 1477, 1434, 1417, 1389, 1358, 1296, 1286, 1237, 1211, 1123, 1026, 989, 952, 941, 899, 872, 839, 794, 743, 715, 696, 656, 589, 549, 510 cm^{-1}. Anal. Calcd for $C_{43}H_{74}OP_4Pt$: C, 55.76; H, 8.07. Found: C, 55.46; H, 8.19.

(17) (a) Michelman, R. I.; Bergman, R. G.; Andersen, R. A. *Organometallics* **1993**, *12*, 2741–2751. (b) Legzdins, P.; Phillips, E. C.; Rettig, S. J.; Trotter, J.; Veltheer, J. E.; Yee, V. C. *Organometallics* **1992**, *11*, 3104–3110.

that diphosphaureylene complexes **4** and **5** are formed from a related metal–phosphinidene species.

Acknowledgment. We thank Dartmouth College and the donors of the Petroleum Research Fund, administered by the American Chemical Society, for partial support of this work. We thank Johnson-Matthey/Alfa/Aesar for the loan of platinum salts and Dr. Jeffrey Lomprey for helpful discussions.

Supporting Information Available: Text giving details of the structure determination of **4** and tables of crystal data, positional and thermal parameters, and bond distances and angles (10 pages). This material is contained in many libraries on microfiche, immediately follows this article in the microfilm version of the journal, can be ordered from the ACS, and can be downloaded from the Internet; see any current masthead page for ordering information and Internet access instructions.

OM950358H

Zircona[1]metallocyclophanes: Synthesis, Properties, and Structure of $(t\text{Bu-}\eta^5\text{-}C_5H_4)_2Zr(\eta^1\text{-}1,\eta^1\text{-}1')(\eta^6\text{-}C_6H_5)_2V$ and Its Chromium Analog[1†]

Christoph Elschenbroich,* Eckhardt Schmidt, Bernhard Metz, and Klaus Harms

Fachbereich Chemie der Philipps-Universität, D-35032 Marburg, Germany

Received March 30, 1995[⊗]

Summary: The tilt caused by the one-atom interannular bridge in a zirconocene unit in **7** *imposed at bis(η^6-benzene)vanadium (***3**•*) is very small. As judged from EPR spectroscopy, the electronic structure of* **3**• *is virtually unaffected by zircona[1]vanadocyclophane formation. The novel binuclear complexes are very robust thermally but quite labile chemically. The latter property precludes a thorough electrochemical study of metal–metal interaction in* **7**•.

Organometallic chemistry abounds with structures featuring bent metallocene units.[2] In the class of bis(η^6-arene)metal complexes, however, precedent for bent sandwich units is much more limited. Typically, compounds of the composition $(\eta^6\text{-}C_6H_6)_2ML_n$ (L = halogen, H, alkyl, CO, phosphane, etc.) are scarce.[3] This divergence is even more pronounced in the class of sandwich complexes without ancillary ligands: numerous hetera[1]metallocenophanes containing Si,[4] Ge,[5] Zr,[6] P,[5,7] or As[7] as interannulary bridging atoms are parallelled by just two reports dealing with the homo[3.3]metallocyclophane (**1**)[8] and the hetera[1]metallocyclophane (**2**),[9] respectively.

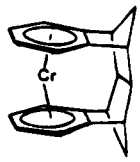

1

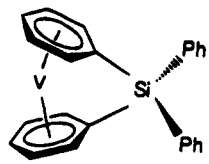

2

The example to be presented in this communication features $Cp_2Zr<$ as a bridging unit at bis(benzene)-vanadium and -chromium. This choice derives from the following reasons: (1) The small but well defined tilting angle to be expected from the large Zr atom serving as an interannular link is of interest with regard to the response of metal–ligand spin delocalization to structural distortion. (2) The reduction $Zr^{IV} \rightarrow Zr^{III}$ in the target molecule **7** could possibly lead to an organometallic biradical composed of two paramagnetic sandwich units at close proximity and in an orthogonal disposition. Obviously, the extent of spin–spin interaction would be the significant question here.

Reaction of the zirconocene dichlorides **5** and **6** with lithiated bis(η^6-benzene)vanadium (**3**) or -chromium (**4**) affords zircona[1]metallocyclophanes as highly air-sensitive black (**7**, **9**) or green (**8**) crystals[10] which are virtually insoluble in hydrocarbons and sparingly soluble in diethyl ether (Scheme 1). The compounds **7**–**9** are surprisingly stable against thermal degradation. Whereas diphenylzirconocene (**10**) in the solid state decomposes at 140 °C,[11] exchanges its phenyl substituents for aryl groups from the solvent at 70 °C, and upon photolysis at ambient temperature eliminates biphenyl,[12] the complexes **7**–**9** are thermally very robust: **7** may be sublimed at 240 °C/10^{-3} mbar, and

† Dedicated to Professor Henri Brunner on the occasion of his 60th birthday.

⊗ Abstract published in *Advance ACS Abstracts,* Junex 15, 1995.

(1) Metal π Complexes of Benzene Derivatives. 47. Part 46: Elschenbroich, Ch.; Isenburg, T.; Behrendt, A. *Inorg. Chem.* **1995**, *34*, 0000.

(2) Lauher, W. J.; Hoffmann, R. *J. Am. Chem. Soc.* **1976**, *98*, 1729.

(3) (a) Cloke, F. G. N.; Green, M. L. H.; Morris, G. E. *J. Chem. Soc., Chem. Commun.* **1978**, 72. (b) Cloke, F. N. G.; Green, M. L. H. *J. Chem. Soc., Chem. Commun.* **1979**, 127. (c) Green, M. L. H.; O'Hare, D.; Watkin, J. D. *J. Chem. Soc., Chem. Commun.* **1989**, 698. (d) Cloke, F. G. N.; Cox, P. K.; Green, M. L. H.; Bashkin, J.; Prout, K. *J. Chem. Soc., Chem. Commun.* **1981**, 117.

(4) Stoeckli-Evans, H.; Osborne, A. G.; Whiteley, R. H. *Helv. Chim. Acta* **1976**, *59*, 2402.

(5) Stoeckli-Evans, H.; Osborn, A. G.; Whiteley, R. H. *J. Organomet. Chem.* **1980**, *193*, 345; **1980**, *194*, 91.

(6) Broussier, R.; Da Rold, A.; Gautheron, B.; Dromzee, Y.; Jeannin, Y. *Inorg. Chem.* **1990**, *29*, 1817. Broussier, R.; Da Rold, A.; Kubicki, M.; Gautheron, B. *Bull. Soc. Chim. Fr.* **1994**, *131*, 951.

(7) Seyferth, D.; Withers, H. P., Jr. *Organometallics* **1982**, *1*, 1275.

(8) Elschenbroich, Ch.; Schneider, J.; Prinzbach, H.; Fessner, W.-D. *Organometallics* **1986**, *5*, 2091.

(9) Elschenbroich, Ch.; Hurley, J.; Metz, B.; Massa, W.; Baum, G. *Organometallics* **1990**, *9*, 889.

(10) Procedures are as follows. $[(\eta^6\text{-}C_6H_5)_2V]Zr(t\text{Bu-}\eta^5\text{-}C_5H_4)_2$ (**7**): To 1.14 g (5.5 mmol) of bis(η^6-benzene)vanadium (**3**), dissolved in 150 mL of cyclohexane, are added 8.25 mol of an 1.6 M solution of *n*-butyllithium (13.2 mmol) in hexane and 2.0 mL (13.28 mmol) of *N,N,N′,N′*-tetramethylethylenediamine. After being refluxed under N_2 for 1.5 h, the mixture is cooled to room temperature and decanted, and the residue is washed with petroleum ether and suspended in 120 mL of diethyl ether. To this is added at −40 °C during 1 h under vigorous stirring a solution of 2.2 g (2.5 mmol) of $(t\text{Bu-}\eta^5\text{-}C_5H_4)_2ZrCl_2$ (**6**) in 700 mL of diethyl ether. After 2 h of stirring at room temperature and filtration, the solid product is extracted with boiling toluene (≈250 mL) until the filtrate is colorless. From this solution at −25 °C **7** is obtained as black sparingly soluble crystals. Yield: 410 mg (0.76 mmol, 14%). The product may be sublimed at 240 °C/10^{-3} mbar. Anal. Calcd for $C_{30}H_{36}VZr$ (538.78): C, 66.88; H, 6.73. Found: C, 66.54; H, 6.74. MS (EI, 70 eV): *m/z* 537 (M^+, 100%), 51 (V^+, 34). EPR data: see text. $[(\eta^6\text{-}C_6H_5)_2Cr]Zr(t\text{Bu-}\eta^6\text{-}C_5H_4)_2$ (**8**) was prepared from bis(η^6-benzene)-chromium (**4**) (2 g, 0.7 mmol), *n*-butyllithium (23.2 mmol), *N,N,N′,N′*-tetramethylethylenediamine (3.44 mL, 23.2 mmol), and $(t\text{Bu-}\eta^5\text{-}C_5H_4)_2ZrCl_2$ (**6**) (3.9 g, 9.7 mmol) in 1.3 L of diethyl ether following the directions given for **7**. **8** precipitates at −25 °C as a green microcrystalline material. Yield: 650 mg (1.2 mmol, 12%). Anal. Calcd for $C_{30}H_{36}CrZr$ (539.84): C, 66.75; H, 6.72. Found: C, 66.79; H, 6.65. MS (EI, 70 eV): *m/z* 538 (M^+, 100%), 52 (Cr^+, 63). ^1H NMR (500 MHz, C_6D_6): δ 1.32 (s, 9 H; *t*Bu), 3.70 (t, J = 5.70 Hz, 4 H, *meta* Ar), 4.69 (d, J = 5.30 Hz, 4 H, *ortho* Ar), 4.81 (t, J = 5.75, 2 H, *para* Ar), 5.48 (t, J = 2.65 Hz, 4 H, *ortho* Cp), 5.98 (t, J = 2.65 Hz, 4 H, *meta* Cp). $^{13}C\{^1H\}$NMR (125 MHz, biphenyl-d_{12}, 120 °C): δ 30.7 (*ipso*, *t*Bu), 34.1 (CH_3, *t*Bu), 75.5 (*meta*, Ar), 78.2 (*para*, Ar), 93.3 (*ortho*, Ar) 106.3 (*meta*, Cp), 107.3 (*ortho*, Ar), 139.5 (*ipso*, Cp), 174.4 (*ipso*, Ar). $[(\eta^6\text{-}C_6H_5)_2Cr]Zr(\eta^5\text{-}C_5H_5)_2$ (**9**) was synthesized from 3.54 g (17 mmol) of **4**, lithiation, and subsequent reaction with $(\eta^5\text{-}C_5H_5)_2ZrCl_5$ (**5**) (5 g, 17 mmol) according to the procedure for **8** as a black, amorphous material which is highly insoluble in all common (and uncommon) solvents. Yield: 840 mg (11%). Anal. Calcd for $C_{22}H_{20}CrZr$ (427.66): C 61.79; H, 4.71. Found: C, 61.48; H, 5.13. MS (EI, 70 eV): *m/z* 426 (M^+, 100%), 348 ($M^+ - C_6H_5$, 30.6), 296 ($M^+ - C_6H_5Cr$, 93.3). 220 ($M^+ - (C_6H_5)_2Cr$, 84.0), 52 (Cr^+, 77.9). NMR data are unavailable for lack of solubility.

(11) Samuel, E.; Rausch, M. D. *J. Am. Chem. Soc.* **1973**, *95*, 6263.

(12) (a) Erker, G. *J. Organomet. Chem.* **1977**, *134*, 189. (b) Cardin, D. J.; Lappert, M. F.; Raston, C. L. *Chemistry of Organo-Zirconium and -Hafnium Compounds*; Ellis Horwood: Chichester, U.K., 1986; Chapter 9.

0276-7333/95/2314-4043$09.00/0

Scheme 1

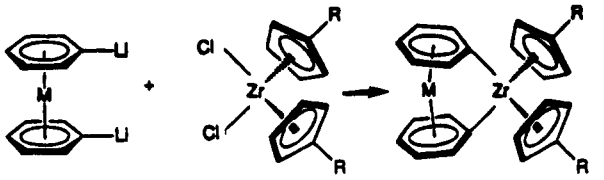

3 Li_2	M = V	5	R = H	7	M = V	R = *t*-Bu
4 Li_2	Cr	6	*t*-Bu	8	Cr	*t*-Bu
				9	Cr	H

the mass spectra exhibit the M^+ peak at 100% intensity. Furthermore, the lack of solubility required ^{13}C NMR spectra of **8** to be recorded at 120 °C, biphenyl-d_{10} serving as a solvent; after 3 h of signal accumulation at this temperature about 25% only of **8** had been cleaved as inferred from the parent bis(benzene)chromium.

Since the degree of tilting imposed by the $Cp_2Zr<$ bridge is the aspect of principal interest here, compound **7** was subjected to X-ray diffraction analysis;[13] a plot of the structure is presented in Figure 1, where important bond distances and bond angles are also given. Structural details of the zirconocene unit in **7** may be assessed by comparing them with the published data for dichlorobis(*tert*-butyl-η^5-cyclopentadienyl)zirconium (**6**)[14] and (1,1′-ferrocenediyl)di-*tert*-butylzirconocene **11**.[6] Our prime interest is, however, focused on the bis(η^6-arene)vanadium moiety. Concording with the larger atomic radius of Zr, the distortion in **7** is less severe than in the case of the $Ph_2Si<$ bridged complex **2**. Thus, the angle centroid−V−centroid of 176.3° signals very small bending of the sandwich axis. The deformation manifests itself more clearly if the η^6-arene ligands are considered; they are folded along the axes C(2)−C(6) and C(2′)−C(6′), respectively (5.1°), and the two planes C(2−6) and C(2′−6′) exhibit a dihedral angle of 8°. The deviation of the η^6-arene ligand plane and the C(ipso)−Zr bond from coplanarity is considerable (56.6°). The tilting of the two arenes causes the interannular distances of corresponding pairs of carbon atoms to differ: C(1)···C(1′) = 3.076, C(2)···C(2′) = 3.295, C(3)···C(3′) = 3.465, and C(4)···C(4′) = 3.507 Å. This gradation is reflected in the considerable spread of the chemical shifts in the NMR spectra of the chromium complexes **8** and **9**.[10]

A spectroscopic parameter which is very sensitive to bending of the sandwich structure is hyperfine coupling

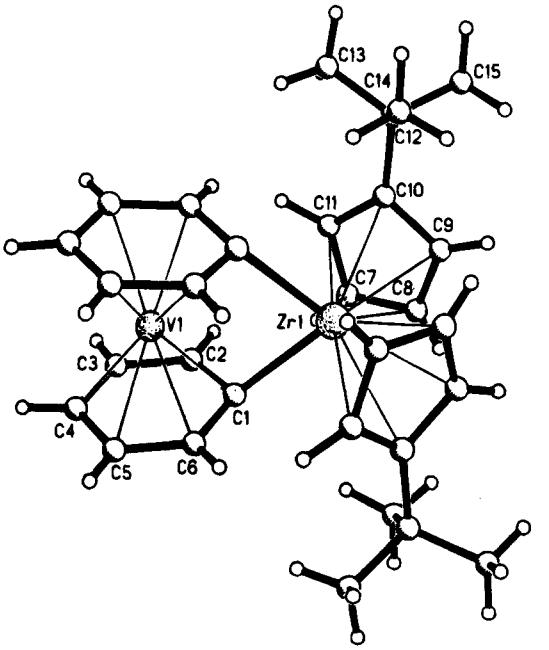

Figure 1. Molecular structure of **7** with atomic labeling scheme. Selected bond lengths (Å) and angles (deg): Zr(1)−C(1) = 2.317(5), V(1)−C(1) = 2.162(5), V(1)−C(2) = 2.179(5), V(1)−C(3) = 2.212(5), V(1)−C(4) = 2.230(5), V(1)−C(5) = 2.217(5), V(1)−C(6) = 2.174(5), Zr(1)−C(7) = 2.546(5), Zr(1)−C(8) = 2.518(5), Zr(1)−C(9) = 2.565(5), Zr(1)−C(10) = 2.645(5), Zr(1)−C(11) = 2.625(5), C(1)−C(2) = 1.437(8), C(2)−C(3) = 1.418(8), C(3)−C(4) = 1.404(8), C(4)−C(5) = 1.405(8), C(5)−C(6) = 1.422(8), C(1)−C(6) = 1.429(7), C(1)−Zr(1)−C(1′) = 83.1, C_5(centroid)−Zr(1)−C_5(centroid) = 123.1(2), C(1)Zr(1)C(1′)−C_5(centroid)Zr(1)C_5′(centroid) = 98.9(2). For additional parameters, see text.

present in the EPR spectra of bis(η^6-arene)metal(d^5) complexes, ligand as well as central metal magnetic nuclei being affected. In the case of the radical cation $\mathbf{1}^{+\bullet}$ (tilting angle = 18°), compared to undistorted (η^6-$C_6H_6)_2Cr^{+\bullet}$, a reduction of the coupling constant $a(^{53}$Cr) and inequivalence of the ortho- and meta-protons was observed.[8] For the neutral radical **2**• (tilting angle 14.4°), where proton hyperfine structure is only barely resolved, the reduction of $a(^{51}V)$ from 6.35 mT [(η^6-$C_6H_6)_2V^\bullet$, **3**•] to 5.63 mT (**2**•) is characteristic.[9] The EPR spectrum of **7**• in fluid and rigid solution is presented in Figure 2. The parameters $\langle g \rangle$, $g_{\parallel}$, $g_{\perp}$, and $a(^{51}V)$ for **7**• differ only marginally from those of the undistorted reference molecule **3**•.[9] There is, however, a strong dependence of line width on the nuclear spin quantum number $m_I(^{51}V)$. This effect, caused by restricted molecular tumbling motion, proves that in fact the spectrum of the bulky radical **7**• rather than that of a dezirconation product is recorded. The almost identical hyperfine couplings $a(^{51}V)$ for **3**• and **7**• accord with the very small tilt present in **7**•. They also strongly suggest that bending distortion with the attendant changes in metal → ligand overlap rather than an electronic effect caused by peripheral substitution is responsible for the modulation of metal → ligand spin delocalization. Bending deformation of a sandwich complex lowers its symmetry from axial to orthorhombic. Therefore, one would expect the rigid solution EPR spectrum to exhibit three values g_x, g_y, and g_z. However, as yet, resolution of $g_\perp$ into the components g_x and g_y has not been achieved for a tilted sandwich structure void of ancillary ligands. This also applies to **7**•. Interestingly, three *g*

(13) Crystal data for **7**: $C_{30}H_{36}VZr$, M_r = 538.75, monoclinic, space group *C*2/*c*, *a* = 16.404(1) Å, *b* = 19.308(1) Å, *c* = 7.530(1) Å, β = 98.00(1)°, *V* = 2361.8(4) Å^3, *Z* = 4, D_c = 1.515 g cm^{-3}, μ = 7.032 mm^{-1}, and *F*(000) = 1116. Data were collected on an Enraf-Nonius CAD4 diffractometer at 193(2) K using graphite-monochromated Cu Kα radiation (λ = 1.541 78 Å), 3737 measured reflections, 3.5° ≤ θ ≤ 60°, *h*(−18/18), *k*(−21/21), *l*(0/18), ω/2θ scans, and 3 intensity control reflections every 1 h. After the *Lp* correction and merging of equivalent reflections there were 1751 unique reflections (R_{int} = 0.11). The structure was solved by direct methods,[21] the non-hydrogen atoms were refined[22] anisotropically on F^2 with all unique data, and the hydrogen atoms were located and refined with common isotropic temperature factors for different groups. The extinction coefficient[21] was 0.00005(8), and the parameters for the weighting scheme were 0.0755 and 0.[21] The refinement of 178 parameters converged to w*R*2 = 0.1255 for all reflections (*R*1 = 0.050 for 1439 reflections with $I > 2\sigma(I)$). The data were corrected with DIFABS.[23]

(14) Howie, R. A.; McQuillan, G. P.; Thompson, D. W.; Lock, G. A. *J. Organomet. Chem.* **1986**, *303*, 213.

(15) In the presence of ancillary ligands paramagnetic bent metallocenes in rigid solution often display three components of the **g** tensor, for example, (CH_3-η^5-$C_5H_4)_2VCl_2$: Peterson, J. L.; Dahl, L. F. *J. Am. Chem. Soc.* **1975**, *97*, 6422.

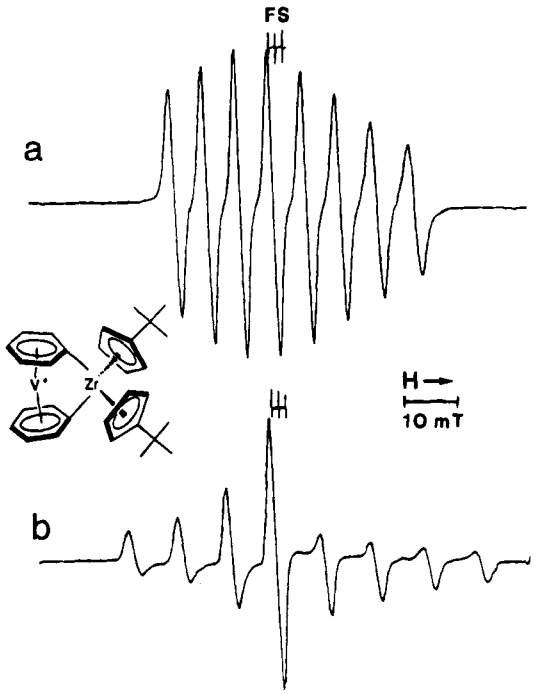

Figure 2. EPR spectra (X-band) of complex **7**• in toluene (FS = Frémy salt, $g = 2.0059$, $a(^{14}N) = 1.309$ mT): (a) Fluid solution, 300 K, $\langle g \rangle = 1.9863$, $a(^{51}V) = 6.23$ mT; (b) rigid solution, 130 K, $g_{\parallel} = 2.022$, $g_{\perp} = 1.969$, $A_{\parallel}(^{51}V) \approx 0$, $A_{\perp}(^{51}V) = 9.34$ mT.

values could be extracted from the spectra of half-open and open ferrocenium ions[16] and of (η^6-heteroarene)$_2$M-(d^5) complexes[17] possessing a linear axis centroid–metal–centroid. Thus for bis(η^6-arene)metal(d^5) complexes bending distortions have a pronounced influence on the hyperfine coupling pattern whereas electronic perturbations like the insertion of a heteroatom into the π-perimeter or even the elimination of a ring atom to form the "open" congeners strongly affect the **g** tensor.

Since X-ray diffraction failed to disclose significant sandwich slippage[18] in the bis(η^6-arene)vanadium moiety of **7**•, we set out to generate the biradical anion **7**$^{-\bullet\bullet}$ in order to search for exchange-coupling J which would point to V(d^5)···Zr(d^1) interaction. To this end, cyclovoltammetry was first performed on **7**• [19] (Figure 3). In the potential range $-3.0 < E < 0$ V four reversible waves are observed, two of which change in intensity with time: whereas, initially, the peak current of wave 3 exceeds that of wave 4, the former diminishes and has disappeared after 6 h. Wave 1 is caused by the couple

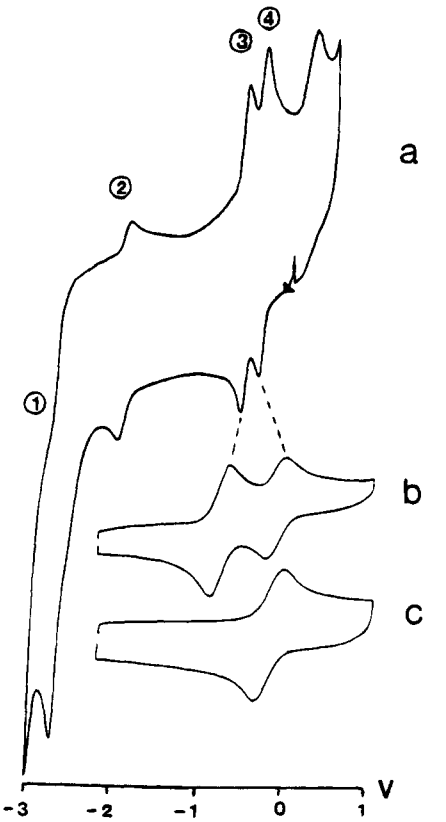

Figure 3. Cyclovoltammetry of complex **7** in DME/n-Bu$_4$NClO$_4$ (0.1 M) (−45 °C, at glassy carbon versus SCE, 200 mV s^{-1}): (a) $-3 < E < +0.5$ V; (b) expanded scale, limited range $-1 < E < 0$ V, immediately after sample preparation; (c) $-1 < E < 0$ V, after 6 h at −45 °C. Key: (1) $E_{pc} = -2.73$ V; (2) $E_{1/2} = -1.952$ V, $\Delta E_p = 92$ mV; (3): $E_{1/2} = -0.573$ V, $\Delta E_p = 54$ mV; (4) $E_{1/2} = -0.368$ V, $\Delta E_p = 64$ mV.

V$^{0/-I}$ of the bis(η^6-arene)vanadium unit,[20] wave 2 corresponds to the couple Zr$^{IV/III}$ in (tBu-η^5-C$_5$H$_4$)$_2$(η^1-C$_6$H$_5$)$_2$Zr (**12**) as proved by an independent measurement, and wave 4 is identical with that of the couple **2**$^{+/0}$.[20] Since **12** does not feature a redox process at potentials $E > -1.8$ V, wave 3 must represent the couple **7**$^{+/0}$, oxidation occurring at the bis(η^6-arene)vanadium moiety. The observation that this wave eventually vanishes to be replaced by wave 4 suggests cleavage of the single atom interannular bridge in **7**. Solvolytic lability of hetera[1]metallocyclophanes has been noted previously.[9] In the present case it precludes electrochemical generation of the biradical **7**$^{-\bullet\bullet}$ for EPR study.

Acknowledgment. The authors thank the Deutsche Forschungsgemeinschaft and the Fonds der Chemischen Industrie for support of this work. E.S. is indebted to the "Graduiertenkolleg Metallorganische Chemie" for the award of a scholarship.

Supporting Information Available: Additional crystallographic data for **7** including tables of atomic coordinates and equivalent isotropic displacement parameters (Å^2) (Table S1), bond lengths and angles (Table S2), torsion angles (Table S3), anisotropic displacement parameters (Table S4), and hydrogen coordinates and isotropic displacement parameters (Å^2) (Table S5) (11 pages). Ordering information is given on any current masthead page.

OM9502345

(16) Elschenbroich, Ch.; Bilger, E., Ernst, R. D.; Wilson, D. R.; Kralik, M. S. *Organometallics* **1985**, *4*, 2068.
(17) (a) Elschenbroich, Ch.; Nowotny, M.; Metz, B.; Massa, W.; Graulich, J. *Angew. Chem., Int. Ed. Engl.* **1991**, *30*, 547. (b) Elschenbroich, Ch.; Bär, F.; Bilger, E.; Mahrwald, D.; Nowotny, M.; Metz, B. *Organometallics* **1993**, *12*, 3373. (c) Nowotny, M.; Elschenbroich, Ch.; Behrendt, A.; Massa, W.; Wocadlo, S.; *Z. Naturforsch.* **1993**, *48b*, 1581.
(18) Sandwich slippage is defined as the distance between ring centroid and the perpendicular projection of the central metal atom on the ring plane.
(19) Lappert, M. F.; Pickett, C. J.; Riley, P. J.; Yarrow, P. J. W. *J. Chem. Soc., Dalton Trans.* **1981**, 805.
(20) Elschenbroich, Ch.; Bilger, E.; Metz, B. *Organometallics* **1991**, *10*, 2823.
(21) SHELXS-86: Sheldrick, G. M. Univ. of Göttingen, 1986.
(22) SHELXS-93: Sheldrick, G. M. Univ. of Göttingen, 1993.
(23) Walker, N.; Stuart, D. *Acta Crystallogr.* **1983**, *A39*, 158.

Synthesis and Structural Characterization of the *nido*-7-R-7,8,10-$C_3B_8H_{10}^-$ Tricarbollide Anion

Alexandra M. Shedlow, Patrick J. Carroll, and Larry G. Sneddon*

Department of Chemistry, University of Pennsylvania, Philadelphia, Pennsylvania 19104-6323

Received June 19, 1995[⊗]

*Summary: The reaction of the nido-6-R-5,6,9-$C_3B_7H_9^-$ anion with $BrBH_2{\cdot}SMe_2$, followed by deprotonation with Proton Sponge, yields the nido-7-R-7,8,10-$C_3B_8H_{10}^-$ isomer (where R = Bn (**1**$^-$) and R = Me (**2**$^-$)) of the tricarbollide anion. Ab initio/IGLO/NMR calculations and a single-crystal X-ray determination confirm that the anions adopt open nido-type structures based on an icosahedron missing one vertex, analogous to that observed for the isoelectronic dicarbollide anions.*

We recently reported the first general high-yield synthetic routes to tricarbaborane clusters, including *nido*-6-CH_3-5,6,9-$C_3B_7H_{10}$ and *arachno*-6-R-5,6,7-$C_3B_7H_{12}$ (where R = $NCCH_2$, $MeC(O)CH_2$).[1,2a] Furthermore, we showed that tricarbaboranyl monoanions, such as *nido*-6-CH_3-5,6,9-$C_3B_7H_9^-$, can bind to transition metals in both η^4 and η^6 fashions, serving as either three- or five-electron donors similar to the η^3-allyl or η^5-cyclopentadienyl ligand, respectively.[2] These results have prompted interest in designing new series of tricarbaboranyl anions with different types of open faces that might exhibit an even wider variety of metal-ligating properties.

Because of their close structural relationship to the dicarbollide anions 7,8-$C_2B_9H_{11}^{2-}$ and 7,9-$C_2B_9H_{11}^{2-}$, the 11-vertex tricarbollides $C_3B_8H_{11}^-$, are of particular interest as potential metal ligand systems. Štíbr and co-workers have, in fact, just reported the synthesis and NMR characterization of the 7,8,9-$C_3B_8H_{11}^-$ isomer of this cage system via the reaction of the *nido*-5,6-$C_2B_8H_{11}^-$ anion with isocyanides or cyanide, followed by deamination.[3] In this communication, we report the first synthesis and structural determination of a second tricarbollide isomer, *nido*-7-R-7,8,10-$C_3B_8H_{10}^-$.

As shown in eq 1, the *nido*-7-R-7,8,10-$C_3B_8H_{10}^-$ tricarbollides (where R = Bn (**1**$^-$) and R = Me (**2**$^-$)) were produced by a cage expansion route[4] involving the reaction of *nido*-6-R-5,6,9-$C_3B_7H_9^-$ with $BrBH_2{\cdot}SMe_2$, followed by deprotonation with Proton Sponge.

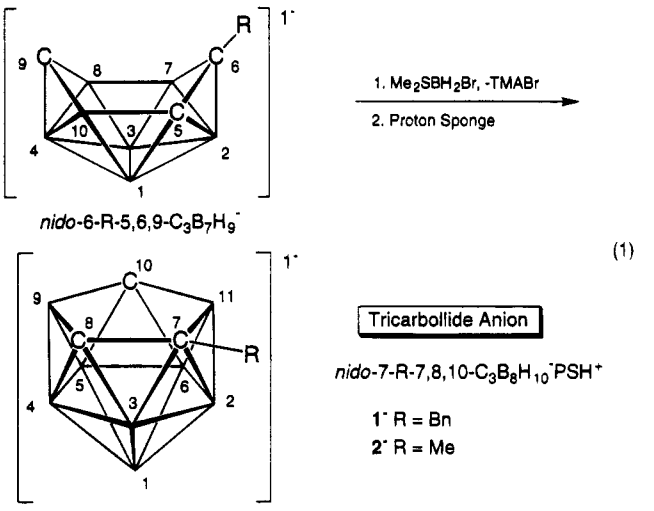

(1)

In a typical reaction, equivalent amounts (3.50 mmol) of $BrBH_2{\cdot}SMe_2$ and [*nido*-6-Bn-5,6,9-$C_3B_7H_9$]$^-TMA^+$ were reacted overnight in a stirred CH_2Cl_2 solution in the presence of Proton Sponge (PS, ≡1,8-$(Me_2N)_2C_{10}H_6$; 3.50 mmol). The solvent was then vacuum-evaporated and the residue recrystallized from a methylene chloride/diethyl ether/heptane solvent system to give 0.86 g (1.95 mmol) of PSH^+[*nido*-7-Bn-7,8,10-$C_3B_8H_{10}$]$^-$ (PSH^+**1**$^-$)[5] as a yellow solid in a 56% unoptimized yield. A similar reaction with [*nido*-6-Me-5,6,9-$C_3B_7H_9$]$^-Na^+$ gave PSH^+-[*nido*-7-Me-7,8,10-$C_3B_8H_{10}$]$^-$ (PSH^+**2**$^-$)[6] in 61% yield.

The X-ray-determined structure of **1**$^-$ (carried out on a PPN^+**1**$^-{\cdot}CH_2Cl_2$ crystal) is shown in the ORTEP view in Figure 1.[7] In agreement with the cluster's 26-skeletal-electron count, the anion adopts an open nido-type cage structure based on an icosahedron missing one vertex, analogous to that observed for the dicarbollide anions. The five-membered open face contains all three carbon atoms, but in contrast to Štíbr's 7,8,9-$C_3B_8H_{11}^-$ isomer, which contains three adjacent carbons, only two of the carbons are adjacent. Unfortu-

(1) (a) Kang, S. O.; Furst, G. T.; Sneddon, L. G. *Inorg. Chem.* **1989**, *28*, 2339–2347. (b) Su, K.; Barnum, B. A.; Carroll, P. J.; Sneddon, L. G. *J. Am. Chem. Soc.* **1992**, *114*, 2830–2731. (c) Su, K.; Carroll, P. J.; Sneddon, L. G. *J. Am. Chem. Soc.* **1993**, *115*, 10004–10017.

(2) (a) Plumb, C. A.; Carroll, P. J.; Sneddon, L. G. *Organometallics* **1992**, *11*, 1665–1671. (b) Plumb, C. A.; Carroll, P. J.; Sneddon, L. G. *Organometallics* **1992**, *11*, 1672–1680. (c) Plumb, C. A.; Sneddon, L. G. *Organometallics* **1992**, *11*, 1681–1685. (d) Weinmann, W.; Wolf, A.; Pritzkow, H.; Siebert, W.; Barnum, B. A.; Carroll, P. J.; Sneddon, L. G. *Organometallics* **1995**, *14*, 1911–1919. (e) Barnum, B. A.; Carroll, P. J.; Sneddon, L. G. to be submitted for publication.

(3) Štíbr, B.; Holub, J.; Teixidor, F.; Viñas, C. *J. Chem. Soc., Chem. Commun.* **1995**, 795–796.

(4) Gaines used a similar cage expansion reaction to produce the 7-$MeB_{11}H_{13}^-$ anion from the reaction of $ClBH_2{\cdot}SMe_2$ with $MeB_{10}H_{12}^-$ in the presence of Proton Sponge: Gaines, D. F.; Bridges, A. N.; Hayashi, R. K. *Inorg. Chem.* **1994**, *33*, 1243–1244.

(5) Anal. Calcd for PSH^+[7-Bn-7,8,10-$C_3B_8H_{10}$]$^-$ (**1**$^-$): C, 61.47; H, 7.84; N, 5.73. Found: C, 62.48; H, 7.72; N, 6.45.

(6) Anal. Calcd for PSH^+[7-Me-7,8,10-$C_3B_8H_{10}$]$^-$ (**2**$^-$): C, 59.57; H, 8.89; N, 7.72. Found: C, 57.60; H, 8.56; N, 7.91.

(7) PPN and CH_2Cl_2 were omitted from the figure for clarity. Single crystals of PPN^+**1**$^-{\cdot}CH_2Cl_2$ were grown at room temperature in a glass tube under slow evaporation of solvents by N_2. X-ray intensity data were collected at −40 °C on an MSC/RAXIS area detector employing graphite-monochromated Mo Kα radiation (λ = 0.7107 Å). The intensity data were corrected for Lorentz and polarization effects, but not for absorption. Structural data: space group $C2/c$ (No. 15), a = 36.3774(8) Å, b = 11.2090(4) Å, c = 26.5148(9) Å, β = 126.729(2)°, V = 8665.2(5) Å^3, Z = 8, and d_{calcd} = 1.30 g/cm^3. The structure was solved by direct methods (SIR92). Refinement was by full-matrix least-squares techniques based on F to minimize the quantity $\Sigma w(|F_o| - |F_c|)^2$ with $w = 1/\sigma^2(F)$. Non-hydrogen atoms were refined anisotropically; hydrogen atoms were included as constant contributions to the structure factors and were not refined. Due to problems with the refinement of the disordered solvent molecule, the structure could only be refined to R_1 = 0.095 and R_2 = 0.097.

0276-7333/95/2314-4046$09.00/0

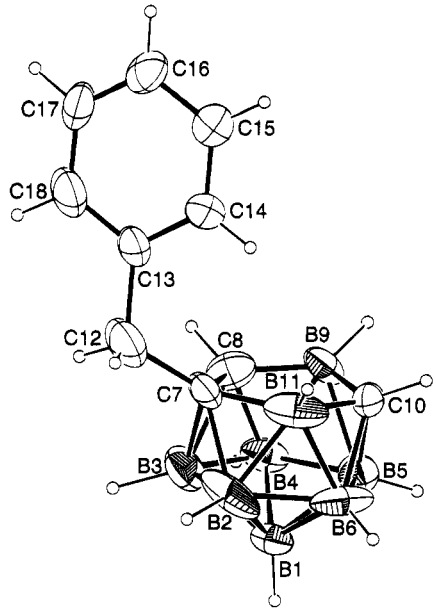

Figure 1. ORTEP drawing of the *nido*-7-Bn-7,8,10-$C_3B_8H_{10}^-$ ($\mathbf{1}^-$) tricarbollide anion.

nately, all crystals of $\mathbf{1}^-$ were found to contain a disordered methylene chloride solvent molecule that prevented refinement to a low *R* factor; therefore, while the gross cage geometry is clearly crystallographically established, it was necessary to carry out an ab initio/IGLO/NMR study to obtain conclusive structural confirmation and reliable values for the bond distances and angles.

Ab initio/IGLO/NMR calculations[8,9] carried out on $\mathbf{2}^-$ confirm both the gross cage geometry and the 7,8,10-carbon arrangement shown in Figure 1 with excellent agreement between the observed and calculated ^{11}B NMR chemical shifts: assignment (δ(obsd); δ(calcd)) B3 (−11.6; −12.7), B11 (−17.2; −17.3), B6 (−18.5; −18.1), B9 (−19.0; −18.9), B5,2 (−21.5 (overlapping); −19.9 and −24.7), B4 (−25.4; −27.6), B1 (−48.0; −50.2). The ab initio calculated intracage distances and angles for $\mathbf{2}^-$ fall in the normal ranges expected for carborane anions with the carbon−carbon (C7−C8, 1.551 Å) and boron−carbon (C8−B9, 1.601 Å; C10−B9, 1.626 Å; C10−B11, 1.627 Å; B11−C7, 1.604 Å) distances on the open face being similar to those crystallographically determined in the 7,8-$C_2B_9H_{12}^-$ and 7-MeC(O)-7,8-$C_2B_9H_{11}^-$ structures.[1c,10] The open face is slightly puckered, with the boron atoms (B9, B11) lying ~0.12−0.14 Å above the plane defined by the three carbon atoms (C7, C8, C10). The ab initio calculations also show that the *nido*-7-Me-7,8,10-$C_3B_8H_{10}^-$ tricarbollide anion is 21.7 kcal/mol lower in energy than the adjacent-carbon *nido*-7-Me-7,8,9-$C_3B_8H_{10}^-$ isomer. This leads to the prediction that the 7,8,9-$C_3B_8H_{11}^-$ anion isolated by Štíbr[3] should readily isomerize to the 7,8,10-$C_3B_8H_{11}^-$ isomer.

The 2D $^{11}B-^{11}B$ NMR COSY experiments carried out on $\mathbf{1}^-$ and $\mathbf{2}^-$ are also in complete agreement with the structure and assignments determined by the ab initio/IGLO/NMR and crystallographic studies.[11,12] The ^1H NMR spectra show, in addition to the peaks from the PSH^+ cation and benzyl ($\mathbf{1}^-$) and methyl ($\mathbf{2}^-$) groups, two C−H resonances in each spectrum (0.65 and 1.25 ppm, $\mathbf{1}^-$; 0.61 and 1.18 ppm, $\mathbf{2}^-$), attributed to the hydrogens bound to the cage carbons. In the ^{13}C NMR spectra the two hydrogen-substituted cage carbons appear as broad peaks at 27.65 and 33.36 ppm for $\mathbf{1}^-$ and at 27.66 and 35.80 ppm for $\mathbf{2}^-$.

Previous studies of the tricarbaboranyl complexes[2] have demonstrated that because of the strong electron-withdrawing properties of the tricarbaboranyl cages relative to cyclopentadienyl ligands, their metal complexes have properties, such as enhanced oxidative and thermal stabilities, that complement their organometallic counterparts. Unlike the *nido*-6-CH_3-5,6,9-$C_3B_7H_9^-$ anion, which has a puckered six-membered open face, the new 11-vertex tricarbollides have open pentagonal faces with dimensions similar to those for the cyclopentadienyl ligand. The efficient synthetic routes now available to both the 7,8,9- and 7,8,10-tricarbollides make these anions readily available for the construction of new series of metallocene-like complexes. Studies of the coordination properties of these new cage systems are ongoing.

Acknowledgment. We thank the National Science Foundation for support of this work. We also thank Dr. George Furst for help with the NMR experiments.

Supporting Information Available: Tables giving Cartesian coordinates, bond distances and angles, and least-squares planes of the optimized geometries at the HF/6-31G* level for *nido*-7-Me-7,8,10-$C_3B_8H_{10}^-$ and Cartesian coordinates of the optimized geometry at the HF/6-31G* level for *nido*-7-Me-7,8,9-$C_3B_8H_{10}^-$ and tables giving positional and thermal parameters and bond distances and angles for $\mathbf{1}^-$ (20 pages). Ordering information is given on any current masthead page.

OM9504718

(8) The procedures used for the ab initio/IGLO/NMR calculations are described in: Keller, W.; Barnum, B. A.; Bausch, J. W.; Sneddon, L. G. *Inorg. Chem.* **1993**, *32*, 5058−5066 and references therein.

(9) The ab initio geometries were optimized up to the HF/6-31G* level of theory and the NMR chemical shifts using the IGLO program employed the DZ basis set contracted as follows: B and C 7s3p {4111,21}; H 3s {21}.

(10) Buchanan, J.; Hamilton, E. J. M.; Reed, D.; Welch, A. J. *J. Chem. Soc., Dalton Trans.* **1990**, 677−680.

(11) Spectroscopic data for PSH^-[*nido*-7-Bn-7,8,10-$C_3B_8H_{10}$]$^-$ ($PSH^-\mathbf{1}^-$) are as follows. ^{11}B NMR (160.5 MHz, CD_2Cl_2): δ in ppm (mult, assgnt, J_{BH} in Hz) −11.8 (d, B3, 159), −17.7 (d, B11,6, 144), −18.7 (d, B9, 139), −20.9 (d, B5, 152), −21.9 (d, B2, 152), −25.0 (d, B4, 150), −48.1 (d, B1, 139). 2D $^{11}B-^{11}B$ NMR established the following connectivities: B1−B2, −B3, −B4, −B5, −B6; B2−B3, −B6; B3−B4; B4−B5, −B9; B5−B9. The expected connectivities for the following peaks were obscured by overlapping signals: B2−B11; B5−B6; B6−B11. ^1H NMR (500.1 MHz, CD_2Cl_2): δ in ppm (mult, assgnt, J_{HH} in Hz): 8.04−7.02 (m, 13H, Bn, PS), 3.17 (s, 12H, CH_3, PS), 2.79, 2.90 (d, CH_2, 15), 1.25 (s, CH), 0.65 (s, CH). ^{13}C NMR (125.7 MHz, CD_2Cl_2): δ in ppm (assgnt) 144.78 (s, C, PS), 144.21 (s, CH, Bn), 136.20 (s, C, PS), 130.41 (s, CH, PS), 129.60 (s, CH, Bn), 128.31 (s, CH, Bn), 127.84 (s, CH, PS), 125.76 (s, CH, Bn), 121.86 (s, CH, PS), 119.24 (s, C, PS), 47.26 (s, CH_3, PS), 44.60 (CH_2, Bn), 33.36 (CH), 27.65 (CH).

(12) Spectroscopic data for PSH^+[*nido*-7-Me-7,8,10-$C_3B_8H_{10}$]$^-$ ($PSH^+\mathbf{2}^-$) are as follows. ^{11}B NMR (160.5 MHz, CD_2Cl_2): δ in ppm (mult, assgnt, J_{BH} in Hz) −11.6 (d, B3, 158), −17.2 (d, B11, 132), −18.5 (d, B6, 138), −19.0 (d, B9, 132), −21.5 (d, B5,2, 140), −25.4 (d, B4, 144), −48.0 (d, B1, 144). 2D $^{11}B-^{11}B$ NMR established the following connectivities: B1−B3, −B4, −B5, −B6; B2−B3, −B6; B3−B4; B4−B9. The expected connectivities for the following peaks were obscured by overlapping signals: B1−B2; B2−B11; B4−B5; B5−B6, −B9; B6−B11. ^1H NMR (200.1 MHz, CD_2Cl_2): δ in ppm (mult, assgnt) 8.06−7.56 (m, 6H, PS), 3.25 (s, 12H, CH_3, PS), 1.36 (s, CH_3), 1.18 (s, CH), 0.61 (s, CH). ^{13}C NMR (125.7 MHz, CD_2Cl_2): δ in ppm (mult, assgnt) 144.08 (s, C, PS), 135.96 (s, C, PS), 130.13 (s, CH, PS), 127.59 (s, CH, PS), 121.69 (s, CH, PS), 119.05 (s, C, PS), 47.08 (s, CH_3, PS), 35.80 (s, CH), 27.66 (s, CH), 24.10 (s, CH_3).

Articles

A Simple Approach to 1-Phosphapentadienyl Chemistry

Ngoc Hoa Tran Huy, Louis Ricard, and François Mathey*

Laboratoire "Hétéroéléments et Coordination" URA 1499 CNRS, DCPH, Ecole Polytechnique, 91128 Palaiseau Cedex, France

Received April 28, 1995[⊗]

The metalation of a 2-vinylphosphirane P–$W(CO)_5$ complex (**1**) at C_3 leads to the corresponding 1-phosphapentadienide complex; this has been reacted with IMe and CpFe-$(CO)_2$I to give the corresponding derivatives at phosphorus. The structures of the iron derivatives show that the PC=CC=C chain has *E* stereochemistry at the central C=C double bond.

A fascinating parallel exists between cyclopentadienyl and phosphacyclopentadienyl (phospholyl) chemistry. Among the most noteworthy analogies are facile [1,5]-sigmatropic shifts around each ring[1] and a substantial series of isostructural η^5 complexes involving the two ring systems.[2] Recently, the chemistry of the open pentadienyl system has been developed and similar features have been found. In particular, an extensive series of η^5-pentadienyl complexes has been prepared.[3] As a logical extension of these earlier studies, we thought that an investigation of the properties of the 1-phosphapentadienyl system would be highly desirable. We describe hereafter an new and versatile approach to this system and a preliminary study of its properties. While we were already working on this project, Bleeke et al.[4] reported the parent (*E*)-1-phosphapentadienyl anion and one of its iridium complexes.

Our starting point was the easily accessible 2-vinylphosphirane system. The corresponding P→$W(CO)_5$ complexes are obtained via the [1 + 2] cheletropic cycloaddition of terminal phosphinidene complexes [RP→$W(CO)_5$] with conjugated dienes.[5–7] The complexing group confers a satisfactory stability, although these compounds rearrange at about 100 °C to the corresponding five-membered rings. In previous work, we observed that the highly basic and bulky lithium diisopropylamide (LDA) is able to selectively abstract one of the CH_2 ring protons of (1,2-diphenylphosphirane)-pentacarbonyltungsten to give the corresponding open lithium vinylphosphide.[8] Steric congestion plays a crucial role in that case, since less bulky amides attack the phosphirane at phosphorus. Our idea was to transpose this kind of chemistry onto 2-vinylphosphirane complexes. In line with expectation, the reaction of LDA with the representative 2-vinylphosphirane complex **1**[5] (as a mixture of its two isomers) gives the corresponding lithium 1-phosphapentadienide complex **2** (eq 1).

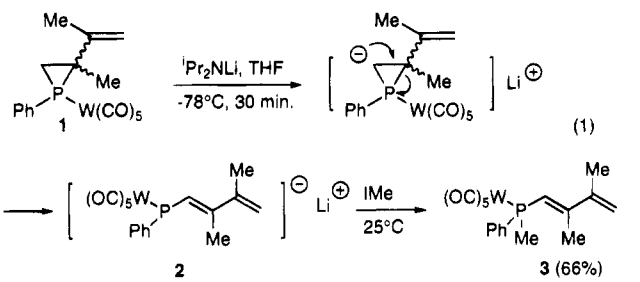

The formation of **2** can be monitored by ^{31}P NMR spectroscopy: $\delta(^{31}P)$(**2**) −87.8 (room temperature). The reaction of **2** with methyl iodide gives a single isomer of the P-methylated product **3**, but it proved impossible to assign a precise stereochemistry to the central C=C double bond from its NMR data. Thus, we also allowed **2** to react with (cyclopentadienyl)dicarbonyliron iodide. The reaction yields a mixture of two products (eq 2).

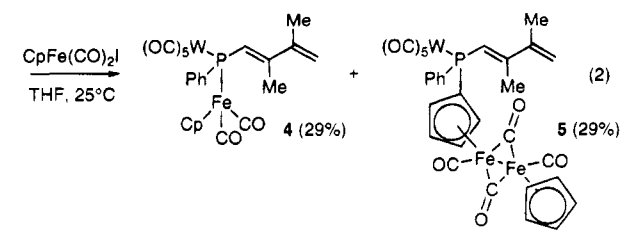

The attack of the very bulky nucleophile **2** at iron is partially blocked, and an *exo* attack at the cyclopenta-

[⊗] Abstract published in *Advance ACS Abstracts,* August 15, 1995.

(1) For example, the [1,5]-sigmatropic shifts of hydrogen around the phospholyl ring have been studied from both experimental and theoretical standpoints; see: Charrier, C.; Bonnard, H.; de Lauzon, G.; Mathey, F. *J. Am. Chem. Soc.* **1983**, *105*, 6871. Bachrach, S. M. *J. Org. Chem.* **1993**, *58*, 5414.

(2) For a recent review on η^5-phospholyl complexes, see: Mathey, F. *Coord. Chem. Rev.* **1994**, *137*, 1.

(3) Ernst, R. D. *Chem. Rev.* **1988**, *88*, 1255.

(4) (a) Bleeke, J. R.; Rohde, A. M.; Robinson, K. D. *Organometallics* **1994**, *13*, 401. (b) Bleeke, J. R.; Rohde, A. M.; Robinson, K. D. *Organometallics* **1995**, *14*, 1674.

(5) Marinetti, A.; Mathey, F. *Organometallics* **1984**, *3*, 456.

(6) Lammertsma, K.; Hung, J.-T.; Chand, P.; Gray, G. M. *J. Org. Chem.* **1992**, *57*, 6557.

(7) Hung, J.-T.; Lammertsma, K. *J. Org. Chem.* **1993**, *58*, 1800.

(8) Marinetti, A.; Mathey, F. *Tetrahedron* **1989**, *45*, 3061.

(9) Spek, A. L. University of Utrecht, Bijvoet Center for Biomolecular Research, The Netherlands.

0276-7333/95/2314-4048$09.00/0

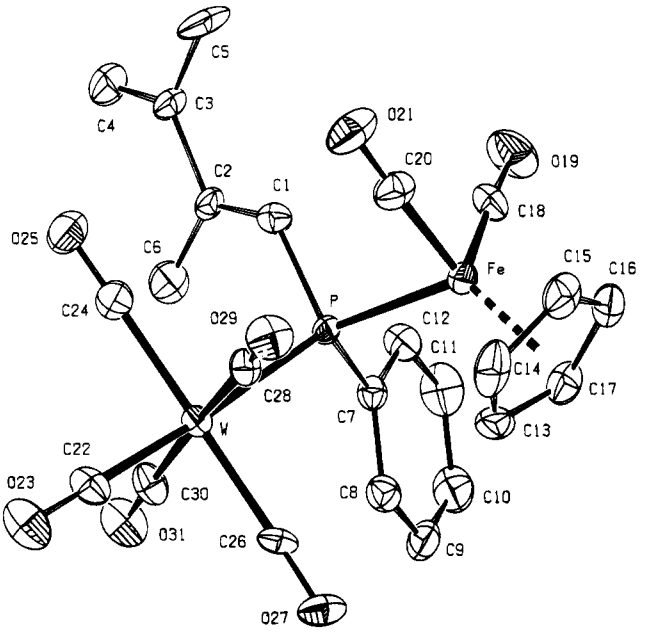

Figure 1. PLATON[9] drawing of complex **4**. Ellipsoids are scaled to enclose 50% of the electronic density. Hydrogen atoms are omitted for clarity. Selected bond lengths (Å) and angles (deg): P–W, 2.586(2); P–Fe, 2.319(2); P–C_1, 1.829(6); P–C_7, 1.841(6); C_1–C_2, 1.341(8); C_2–C_3, 1.496(8); C_2–C_6, 1.497(9); C_3–C_4, 1.33(1); C_3–C_5, 1.51(1); W–P–Fe, 118.95(7); W–P–C_1, 108.5(2); W–P–C_7, 115.6(2); Fe–P–C_1, 103.8(2); Fe–P–C_7, 104.1(2); C_1–P–C_7, 104.5(3); P–C_1–C_2, 130.9(5); C_1–C_2–C_3, 119.6(6); C_1–C_2–C_6, 124.0(6); C_2–C_3–C_4, 121.9(7); C_2–C_3–C_5, 117.8(6); C_1–C_2–C_3–C_4, torsion angle, 176.98(0.68).

dienyl ring is also observed. The structures of both **4** and **5** were established by X-ray analysis (Figures 1 and 2). The central C_1=C_2 bond displays *E* stereochemistry in both cases. The phosphapentadiene unit is quasiplanar and shows a transoid conformation. The C=C double bonds are well localized.

One question arises immediately. If, as in the cyclopropane case, the opening of the intermediate phosphirane anion is a concerted 4π-conrotatory process, then the two isomers of **1** must yield the two possible isomeric 1-phosphapentadienides **2**, having either *E* or *Z* stereochemistry at the central (P)C=C(Me) double bond (eq 3).

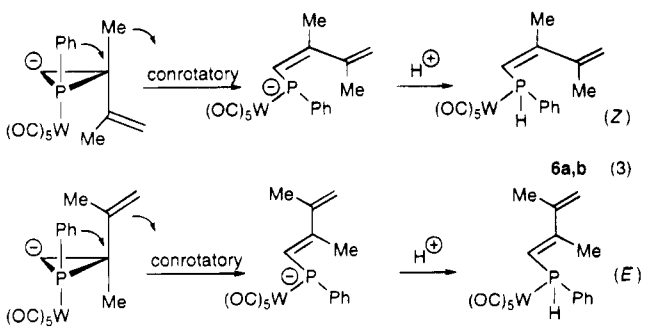

If we observe only the more stable *E* stereochemistry in the final products **3**–**5**, then it means that the *Z* → *E* transformation readily occurs in the pentadienide below room temperature. In order to check this hypothesis, we performed the protonation of **2** at low temperature. The two P–H products **6a,b** were obtained (eq 3), but we were unable to obtain them in the pure state.

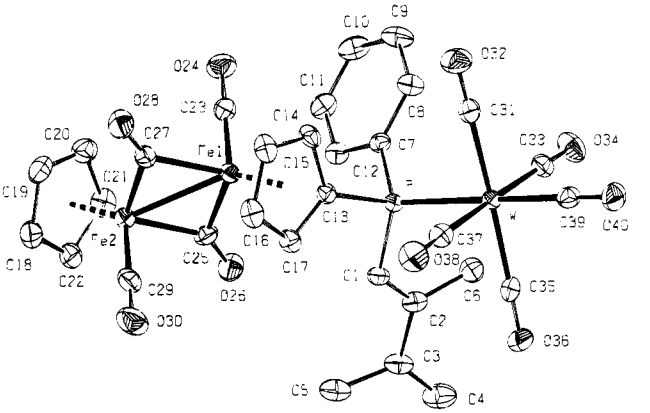

Figure 2. PLATON drawing of complex **5**. Ellipsoids are scaled to enclose 50% of the electronic density. Hydrogen atoms are omitted for clarity. Selected bond lengths (Å) and angles (deg): P–W, 2.5343(9); Fe_1–Fe_2, 2.5312(7); P–C_1, 1.811(4); P–C_7, 1.833(3); P–C_{13}, 1.817(3); C_1–C_2, 1.345(5); C_2–C_3, 1.477(5); C_2–C_6, 1.508(5); C_3–C_4, 1.350(6); C_3–C_5, 1.495(6); W–P–C_1, 115.9(1); W–P–C_7, 120.2(1); W–P–C_{13}, 108.3(1); C_1–P–C_7, 104.9(2); C_1–P–C_{13}, 103.0(2); C_7–P–C_{13}, 102.4(2); P–C_1–C_2, 125.2(3); C_1–C_2–C_3, 120.3(4); C_1–C_2–C_6, 123.0(3); C_2–C_3–C_4, 121.3(4); C_2–C_3–C_5, 118.4(4); C_4–C_3–C_5, 120.3(4).

That both contain the 1-phosphapentadiene unit is nevertheless quite clear from a study of the mixture by ^{1}H, ^{13}C, and ^{31}P NMR spectroscopy. These data are very similar to those recorded for **3** and establish the presence of the phosphapentadiene unit in both products. Apparently then, each isomer of **1** produces a different anion (*E*)-**2** or (*Z*)-**2**. We are presently studying this reaction in more depth in order to prepare the more interesting (*Z*)-1-phosphapentadienides in the pure state at low temperature.

Experimental Section

All reactions were carried out under argon, with silica gel (70–230 mesh) being used for chromatographic separations. For the preparation of **1**, see ref 5. The straightforward transformation of **1** into the isomeric five-membered phospholene must be noted. This phospholene complex appears as an impurity during the various reactions of **1**. It displays the following NMR characteristics: ^{31}P NMR ($CDCl_3$) δ −3.0; ^{1}H NMR ($CDCl_3$) δ 1.63 (s, Me), 3.01 (pseudo s, CH_2); ^{13}C NMR ($CDCl_3$) δ 16.33 (d, ^3J(C–P) = 7.5 Hz, Me), 44.57 (d, ^1J(C–P) = 27.5 Hz, CH_2–P).

[Phenylmethyl(2,3-dimethylbutadienyl)phosphine]-pentacarbonyltungsten (3). Phosphirane complex **1** (0.51 g, 1 × 10^{-3} mol) was added to a solution of LDA (1.2 × 10^{-3} mol) in THF (10 mL) at −78 °C with stirring. After 30 min, the solution was warmed to room temperature and methyl iodide (1.2 × 10^{-3} mol) was added. The crude product was purified by chromatography with hexane/CH_2Cl_2 (20:1) as the eluent. Yield of **3**: 0.35 g (66%). ^{31}P NMR ($CDCl_3$): δ −17.7, ^1J(^{31}P–^{183}W) = 232.3 Hz. ^{1}H NMR ($CDCl_3$): δ 1.67 (s, Me), 1.86 (d, ^2J(H–P) = 6.8 Hz, Me–P), 1.91 (s, Me), 5.00 (s, 1H, =CH_2), 5.12 (s, 1H, =CH_2), 5.95 (d, ^2J(H–P) = 17.4 Hz, =CH–P). ^{13}C NMR ($CDCl_3$): δ 18.84 (d, ^3J(C–P) = 10.6 Hz, Me), 20.98 (s, Me), 23.24 (d, ^1J(C–P) = 32.2 Hz, Me–P), 115.83 (s, =CH_2), 122.88 (d, ^1J(C–P) = 44.2 Hz, =CH–P), 143.57 (d, ^2J(C–P) = 12.1 Hz, Me–*C*=), 151.06 (d, ^3J(C–P) = 3 Hz, Me–*C*=), 197.27 (d, ^2J(C–P) = 6.2 Hz, *cis*-CO), 199.77 (d, ^2J(C–P) = 19.9 Hz, *trans*-CO). Mass spectrum (70 eV, ^{184}W): *m*/*z* 528 (M^+, 27%), 388 (M^+ − 5CO, 100%).

Synthesis of the Butadienylphosphide and -Phosphine Complexes 4 and 5. The same procedure as for the

synthesis of **3** was used, with $CpFe(CO)_2I$ (0.36 g, 1.2×10^{-3} mol) replacing methyl iodide. The final products **4** and **5** were separated by chromatography with hexane/CH_2Cl_2 as the eluent. Complex **4** was first isolated (4:1) as orange crystals (0.2 g, 29%). ^{31}P NMR ($CDCl_3$): δ −23.9, $^1J(^{31}P-^{183}W) = 212.3$ Hz. ^1H NMR ($CDCl_3$): δ 1.61 (s, Me), 2.01 (s, Me), 4.68 (d, $^3J(H-P) = 1.2$ Hz, Cp), 5.00 (s, 1H, $=CH_2$), 5.13 (s, 1H, $=CH_2$), 6.37 (d, $^2J(H-P) = 24.9$ Hz, $=CH-P$). ^{13}C NMR ($CDCl_3$): δ 18.62 (d, $^3J(C-P) = 6.0$ Hz, Me), 21.01 (s, Me), 87.79 (s, Cp), 114.25 (s, $=CH_2$). Anal. Calcd for $C_{24}H_{19}FeO_7PW$: C, 41.75; H, 2.75. Found: C, 41.53; H, 2.88.

Then, complex **5** was recovered with hexane/CH_2Cl_2 1:1 as the eluent (brown crystals, 0.25 g, 29%). ^{31}P NMR ($CDCl_3$): δ −7.54, $^1J(^{31}P-^{183}W) = 237.7$ Hz. ^1H NMR ($CDCl_3$): δ 1.84 (s, Me), 2.21 (s, Me), 4.19, 4.73, 5.02 (Cp), 5.17 (s, 1H, $=CH_2$), 5.31 (s, 1H, $=CH_2$), 6.74 (d, $^2J(H-P) = 14.7$ Hz, $=CH-P$). ^{13}C NMR ($CDCl_3$): δ 20.17 (d, $^3J(C-P) = 11.6$ Hz, Me), 21.17 (s, Me), 89.05 (s, C_5H_5), 101.16 (d, $^1J(C-P) = 38.8$ Hz, P−C(Cp)), 116.24 (s, $=CH_2$), 119.82 (d, $^1J(C-P) = 47.6$ Hz, $=CH-P$), 143.98 (d, $^2J(C-P) = 13.4$ Hz, Me−*C*=), 151.40 (d, $^3J(C-P) = 6.2$ Hz, Me−*C*=), 197.38 (d, $^2J(C-P) = 7.0$ Hz, *cis*-WCO), 199.57 (d, $^2J(C-P) = 21$ Hz, *trans*-WCO).

Protonation of the 1-Phosphapentadienide Anion. The same procedure as for the synthesis of **3** was used. The crude anion was protonated at −78 °C with 0.1 N HCl. The resulting products were purified by chromatography with hexane/CH_2Cl_2 (7:3) as the eluent. A mixture of **6a,b** and an unknown product ($\delta(^{31}P)$ −1.7, no $^1J(P-H)$ coupling) was obtained (0.3 g). **6a,b**: ^{31}P NMR ($CDCl_3$) δ −22.9 and −26.2, $^1J(P-H) = 340$ Hz; ^1H NMR ($CDCl_3$) δ 1.65 and 1.67 (2s, Me), 1.93 (s, Me), 5.52 (2dq, H−P), 5.04 (s, 1H, $=CH_2$), 5.15 (d, 1H, $=CH_2$), 6.02 (dd, $^3J(H-H) = 11.1$ Hz, $^2J(H-P) = 15.9$ Hz, $=CH-P$); ^{13}C NMR ($CDCl_3$) δ 115.88 (s, $=CH_2$), 120.78 (d, $^1J(C-P) = 47.6$ Hz, $=CH-P$), 120.83 (d, $^1J(C-P) = 42.6$ Hz, $=CH-P$), 143.36 (d, $^2J(C-P) = 12.2$ Hz, Me−*C*=), 150.85 (s, Me−*C*=).

Supporting Information Available: Tables of experimental details of the X-ray study, positional and thermal parameters, and bond distances and angles for **4** and **5** (16 pages). Ordering information is given on any current masthead page.

OM9503104

Mechanism of Alkyl Migration from Oxygen to Metal in Iron–Manganese Ethoxycarbyne Complexes. Induction of Postcleavage Intermolecular Ethyl Exchange by Hydride Bridging of Mononuclear Iron Species

Hamid Idmoumaz,[1a] Chien-Hsing Lin,[1b] and William H. Hersh*,[1a]

Department of Chemistry and Biochemistry, Queens College of the City University of New York, Flushing, New York 11367-1597, and Department of Chemistry and Biochemistry, University of California, Los Angeles, California 90024

Received May 11, 1995[⊗]

The iron–manganese ethoxycarbyne Cp(CO)Fe(μ-COCH$_2$CH$_3$)(μ-CO)Mn(CO)MeCp (**2a**) undergoes thermal decomposition at 65 °C to give MeCpMn(CO)$_3$ and, in the presence of PPh$_2$Me, CpFe(CO)(PPh$_2$Me)CH$_2$CH$_3$ (**4a**). The reaction is first order in carbyne and zero order in phosphine and exhibits a kinetic deuterium isotope effect $k_H/k_D = 2.0 \pm 0.1$. Crossover experiments between **2a** and its bis MeCp, CD$_2$CD$_3$ analog (**2b**-d_5) or between **2a**-d_5 and **2b** result in scrambling of the alkyl label between products **4a** and **4a**-d_5 and their MeCp analogs **4b** and **4b**-d_5. A crossover experiment between **2a** and **2b**-^{13}C labeled specifically at the ethoxy methylene carbon gave complete ^{13}C exchange in the methylene carbons of **4a,b** but no ^{13}C exchange in the starting materials after 50% conversion and no ^{13}C scrambling into the methyl position of **4a,b**. Ethylene does not affect the rate of decomposition of **2b** or **2b**-d_5, does not affect ethyl scrambling, and is not incorporated into **4b** during the decomposition of **2b**-d_5, ruling out ethylene rather than ethyl exchange. The course of the reaction between **2a** and **2b**-d_5 is not altered by the additives 2,6-di-*tert*-butyl-4-methoxyphenol, galvinoxyl, or thiophenol, ruling out involvement of radicals. "Control crossover" experiments between **2a**-d_5 and **4b** and between **2b**-d_5 and **4a** give no exchange. However, the iron hydride RC$_5$H$_4$Fe(CO)(PPh$_2$Me)H (R = H, **5a**; R = Me, **5b**) forms by β-elimination from RCpFe(CO)CH$_2$CH$_3$ followed by PPh$_2$Me displacement of ethylene, and alkyl exchange occurs when **2b** and **5a** are combined under the reaction conditions but not when **4b** and **5a** are combined. A mechanism for ethyl exchange is described in which catalytic amounts of **5a**, **5b**, and deuterated analogs **5a**-d_1 and **5b**-d_1 intercept the 16-electron carbyne decomposition intermediates CpFe(CO)CH$_2$CH$_3$, MeCpFe(CO)CH$_2$CH$_3$, and their C$_2$D$_5$ analogs to give hydride-bridged species. Concomitant migration of the ethyl group and the PPh$_2$Me ligand between the two iron atoms in these bridged species followed by cleavage to regenerate the hydride and 16-electron intermediate completes the exchange event. Slower trapping of the 16-electron intermediates by PPh$_2$Me irreversibly removes them from the catalytic cycle, giving products **4a,b**, **4a**-d_5, and **4b**-d_5.

Introduction

We have previously reported the syntheses of the first neutral heterodinuclear μ_2-alkoxycarbyne complexes Cp(CO)Fe(μ-COR)(μ-CO)Mn(CO)MeCp (**1**, R = CH$_3$; **2**, R = CH$_2$CH$_3$) and described the unprecedented oxygen-to-iron migration reaction of the carbyne alkyl group.[2,3] As shown in Scheme 1, the overall transformation involves not only alkyl migration but also metal–metal bond cleavage to give MeCpMn(CO)$_3$ and what could be the 16-electron fragment CpFe(CO)R (R = CH$_3$, CH$_2$CH$_3$) which is then trapped by phosphine to give CpFe(CO)(L)R (L = PPh$_3$, R = CH$_3$; L = PPh$_2$Me, R = CH$_2$CH$_3$). Determination of whether migration reactions are intramolecular or intermolecular is a necessary step in any mechanistic study and is particularly urgent here due to the fact that cluster cleavage occurs. Preliminary work reported for the methoxycarbyne case revealed the presence of intermolecular methyl exchange reactions,[2] and the 16-electron CpFe(CO)CH$_3$ fragment[4] seemed to be a reasonable candidate for mediation of the observed methyl scrambling. In order to test this hypothesis we sought to remove the CpFe(CO)CH$_3$ by trapping at a faster rate with increased amounts of PPh$_3$, but such efforts fail because **1** additionally undergoes S$_N$2 dealkylation by PPh$_3$ to give the MePPh$_3^+$ salt **3**,[3] a reaction that also occurs readily with a related iron–chromium methoxycarbyne.[5] Clearly the dealkylation reaction needed to be slowed down in order to implement faster trapping by using higher phosphine concentrations or even more nucleophilic phosphines. Since S$_N$2 reactions of *ethyl* electrophiles are known to be much slower than those of *methyl* electrophiles,[6] we chose to examine the *ethoxy*carbyne **2**. While the S$_N$2 reaction was in fact eliminated even

⊗ Abstract published in *Advance ACS Abstracts,* August 1, 1995.

(1) (a) Queens College. (b) University of California.

(2) Fong, R. H.; Hersh, W. H. *Organometallics* **1985,** *4,* 1468–1470.

(3) Fong, R. H.; Lin, C. H.; Idmoumaz, H.; Hersh, W. H. *Organometallics* **1993,** *12,* 503–516.

(4) Hersh, W. H.; Hunte, F.; Siegel, S. *Inorg. Chem.* **1993,** *32,* 2968–2971.

(5) Wang, B.; Hersh, W. H.; Rheingold, A. L. *Organometallics* **1993,** *12,* 1319–1330.

(6) March, J. *Advanced Organic Chemistry,* 4th ed.; Wiley-Interscience: New York, 1992; pp 228, 339.

0276-7333/95/2314-4051$09.00/0

Scheme 1. Thermal Decomposition of Alkoxycarbynes

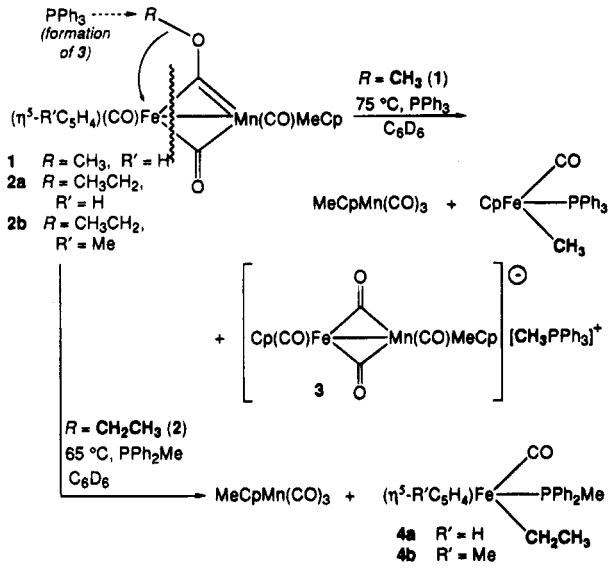

in the presence of the more nucleophilic PPh_2Me ligand, products form which are *still* due to *inter*molecular migration despite the presumed faster trapping of putative $CpFe(CO)CH_2CH_3$. In this paper we report details of these new crossover studies and show that scrambling of the ethyl label can occur *after* the initial migration from oxygen to metal via metal hydrides formed by β-hydride elimination from intermediate iron ethyl species.

Results

Kinetics of Thermal Decomposition. The major products of thermal decomposition of ethoxycarbynes **2a,b** are shown in Scheme 1. Characterizations of starting materials and products have been described previously[3] and so are only summarized here. In the absence of phosphines decomposition of **2a** or **2b** gives $MeCpMn(CO)_3$ in high yield but $CpFe(CO)_2CH_2CH_3$ or $MeCpFe(CO)_2CH_2CH_3$, respectively, in low yields. Alkyl cleavage also evidently occurs, with formation of ethane, ethylene, and $[CpFe(CO)_2]_2$; since CO is the limiting reagent, $[CpFe(CO)]_4$ forms[7] as the major iron-containing product, along with an uncharacterized precipitate. In the presence of PPh_2Me the stoichiometrically formed products are $MeCpMn(CO)_3$ and $CpFe(CO)(PPh_2Me)CH_2CH_3$ (**4a**) or $MeCpFe(CO)(PPh_2Me)CH_2CH_3$ (**4b**) from **2a** or **2b**, respectively. First-order decomposition of **2a** (Figure 1) was observed at 65 °C in C_6D_6 with virtually identical rate constants both in the absence and presence of PPh_2Me (Table 1, runs 1 and 2). Since the rate is completely independent of phosphine concentration, large excesses of PPh_2Me were not necessarily used in subsequent mechanistic runs. The bis MeCp analog **2b** decomposes at a slightly faster rate (run 6), while the CD_2CD_3 analogs **2a**-d_5 and **2b**-d_5 each decompose more slowly. Kinetic deuterium isotope effects were calculated by computing the weighted averages[8] of the rate constants for decomposition of each

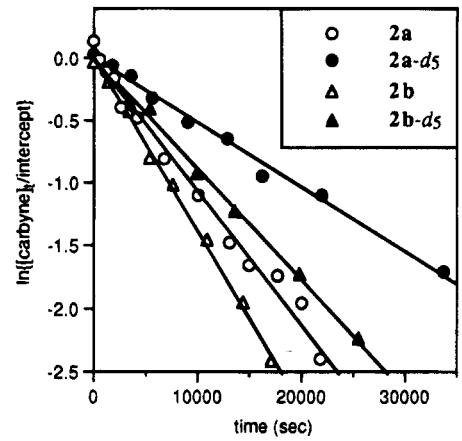

Figure 1. First-order plots of decomposition of ethoxycarbynes **2a** (Table 1, run 1), **2a**-d_5 (run 5), **2b** (run 6), and **2b**-d_5 (run 3). For readability the plots have been adjusted to give zero intercepts, rather than using the value of the first point by plotting $\ln([carbyne]_t/[carbyne]_{t=0})$ as usual, since the first points did not all fall on the least-squares fit lines.

Scheme 2. Ethyl Crossover Experiments

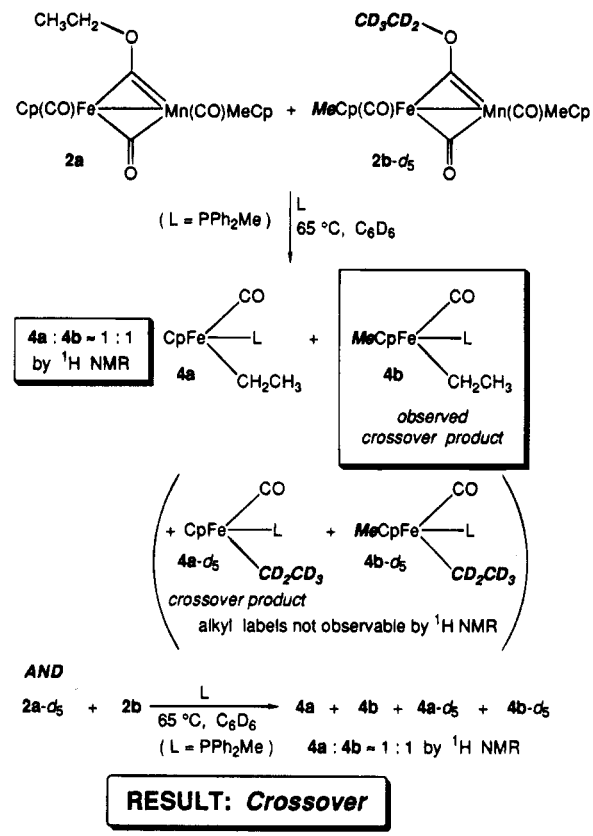

of the ethoxycarbyne analogs **2a**, **2a**-d_5, **2b**, and **2b**-d_5 using all of the data in Table 1; results are collected in Table 2.

Carbyne Crossover Experiments. Two crossover experiments were carried out for the ethoxycarbynes as shown in Scheme 2, one between **2a** and **2b**-d_5 and one between **2a**-d_5 and **2b** (runs 3 and 4). Both gave essentially complete scrambling of the ethyl label. Analysis of these reactions was complicated by the fact that the ethyl CH_3 signals of the products **4a,b** overlap with each other and with the phosphine methyl, as does the downfield member of the two diastereotopic CH_2 hydrogens in **4a**. However, the separation of the upfield

(7) Landon, S. J.; Rheingold, A. L. *Inorg. Chim. Acta* **1981**, *47*, 187–189.

(8) Hamilton, W. C. *Statistics in Physical Science*; The Ronald Press Co.: New York, 1964; pp 43, 78.

Table 1. Summary of Experimental Data: Rate Constants for Carbyne Decomposition and Carbyne and Product Crossover Results[a]

run	[carbyne] (M)	[L] (M)	[additive] (M)	10^4k (s^{-1})[a]	crossover[b]
1	[**2a**] = 0.042	[PPh_2Me] = 0		1.06 ± 0.04	
2	[**2a**] = 0.065	[PPh_2Me] = 0.675		0.986 ± 0.027	
3	[**2a**] = 0.048	[PPh_2Me] = 0.123	[**2b**-d_5] = 0.048	1.10 ± 0.028	yes
4	[**2a**-d_5] = 0.027	[PPh_2Me] = 0.081	[**2b**] = 0.023	0.568 ± 0.040	yes
5	[**2a**-d_5] = 0.027	[PPh_2Me] = 0.083	[**4b**] = 0.026	0.517 ± 0.017	no (**4a**-h_5 not detected after 9.4 h)
6	[**2b**] = 0.047	[PPh_2Me] = 0.093		1.38 ± 0.03	
4	[**2b**] = 0.023	[PPh_2Me] = 0.081	[**2a**-d_5] = 0.027	1.27 ± 0.05	yes (see run 4 above)
7	[**2b**] = 0.046	[PPh_2Me] = 0.100	[C_2H_4] = 0.16	1.12 ± 0.10	5% yield **5b**, 5% C_2H_6, 50% **4b**, 76% $MeCpMn(CO)_3$
8	[**2b**] = 0.016	[PPh_2Me] = 0.034	[C_2H_4] = 0.03	1.39 ± 0.06	10% yield **5b**, 5% C_2H_6, 53% **4b**, 94% $MeCpMn(CO)_3$
9[c]	[**2b**] = 0.019	[PPh_2Me] = 0.063	[**5a**] = 0.020	1.23 ± 0.11	yes; **5a**:**5b** ≈ 2:1 (65% exchange) after 23% conversion of **2b** and 1:1 (100% exchange) after 38% conversion of **2b**; 36% yield **5a** + **5b**, 41% **4a** + **4b**, 30% C_2H_6, 4% C_2H_4
10	[**2b**-^{13}C] = 0.030	[PPh_2Me] = 0.056		1.67 ± 0.21	no exchange of ^{13}C from CH_2 to CH_3 of ethyl group in **4b**-^{13}C; **5b** detected
11	[**2b**-^{13}C] = 0.022	[PPh_2Me] = 0.070	[**2a**] = 0.024		no exchange of ^{13}C from CH_2 of **2b**-^{13}C to CH_2 of **2a** after ~50% conversion (95 min); complete exchange of ^{13}C in CH_2 of **4a**-^{13}C and **4b**-^{13}C
3	[**2b**-d_5] = 0.048	[PPh_2Me] = 0.123	[**2a**] = 0.048	0.882 ± 0.019	yes (see run 3 above)
12	[**2b**-d_5] = 0.034	[PPh_2Me] = 0.095	[**4a**] = 0.034	0.96 ± 0.04	no (**4b**-h_5 not detected after 6.2 h)
13	[**2b**-d_5] = 0.026	[PPh_2Me] = 0.134	[C_2H_4] = 1.17	0.86 ± 0.02	no (**4b**-h_5 not detected after 9.4 h)
14	[**2b**-d_5] = 0.028	[PPh_2Me] = 0.079	[C_2H_4] = 0.19, [**2a**] = 0.027	0.72 ± 0.06	yes (same as without C_2H_4)
15	[**2b**-d_5] = 0.024	[PPh_2Me] = 0.076	[phenol][d] = 0.030, [**2a**] = 0.025	0.73 ± 0.09	yes (same as without phenol)
16	[**2b**-d_5] = 0.022	[PPh_2Me] = 0.067	[galv][e] = 0.011, [**2a**] = 0.022	0.97 ± 0.07	yes (same as without galvinoxyl)
17	[**2b**-d_5] = 0.022	[PPh_2Me] = 0.064	[PhSH] = 0.008, [**2a**] = 0.022	0.83 ± 0.04	yes (same as without PhSH; 1:1 **5a**:**5b** detected)
18	[**2b**-d_5] = 0.028	[PPh_2Me] = 0.087	[CCl_4] = 0.06, [**2a**] = 0.028	0.69 ± 0.08	yes (crossover of **4a** and **4b** same as without CCl_4; no **5a** or **5b** detected; yields are low)
19		[PPh_2Me] = 0.014	[**4b**] = 0.031, [**5a**] = 0.024		no (**4a** not detected after 22.5 h; **5a**:**5b** ≈ 92.8)

[a] All data collected in C_6D_6 solvent at 65 °C. [b] Crossover of alkyl label between **2a** and **2b**, except as noted. Ethyl exchange could not be quantified but by inspection was judged to be complete in all cases. [c] See Experimental Section for further details of this run. [d] Phenol = 2,6-di-*tert*-butyl-4-methoxyphenol. [e] galv = galvinoxyl.

Table 2. Weighted Average Rate Constants for Ethoxycarbyne Decomposition[a]

compd	10^4k (s^{-1})	k_H/k_D
2a	1.05 ± 0.02	
2a-d_5	0.52 ± 0.02	2.0 ± 0.1
2b	1.34 ± 0.02	
2b-d_5	0.87 ± 0.01	1.54 ± 0.03

[a] Data taken from runs 1–3 (**2a**; see Reaction section of Experimental Section), 4–5 (**2a**-d_5), 4, 6–9 (**2b**), and 3, 12–18 (**2b**-d_5).

member of the diastereotopic CH_2 hydrogens in **4a,b** is just great enough to carry out the analysis, despite its presence in each as a 16-line multiplet due to phosphorus and hydrogen coupling. However, since this signal overlapped that due to the ethane at δ 0.79 that formed in the reaction,[3] the samples were routinely stripped of solvent and volatiles and run through a short chromatography column before analysis. Acetone-d_6 was found to give slightly better separation than deuterated benzene, toluene, CD_2Cl_2, CD_3NO_2, and $C_6D_5NO_2$, and PPh_2Me was found to give slightly better separation and cleaner reactions than $PPhMe_2$ or PPh_3; PMe_3 apparently gave dealkylation as shown in Scheme 1 for **1** and PPh_3 to in this case give (presumably) [$Cp(CO)Fe(\mu$-$CO)_2Mn(CO)MeCp$][Me_4P]. At 500 MHz, the spectra could be analyzed directly (Figure 2a–d), while at 200 MHz the separation was marginal although on a qualitative basis the presence of ethyl scrambling was clear. Nevertheless, irradiation of the coincident CH_3 resonances of the products, and partial decoupling of the nearby remaining diastereotopic CH_2 proton, reduced the complex multiplet to a broad doublet for **4a** or **4b**, or a broad triplet for the 1:1 mixture, that could be simply and convincingly interpreted (Figure 2e–h).

Ethoxycarbyne Crossover Control Experiments. In order to look for ethyl exchange in the carbynes, a crossover reaction was run to partial completion and the carbyne composition analyzed by FAB mass spectrometry (Xe, *m*-nitrobenzyl alcohol matrix). No molecular ion peaks due to *any* carbynes were observed, perhaps due to decomposition in the presence of PPh_2Me. In order to avoid mass spectrometry, the experiment was conducted using **2b** labeled with ^{13}C (99% enrichment) in the CH_2 group of the ethoxycarbyne ligand (**2b**-^{13}C), allowing the starting materials **2a** and **2b**-^{13}C to be examined directly by ^{13}C NMR spectroscopy for scrambling of the $^{13}CH_2CH_3$ group (run 11, Scheme 3). The CH_2 resonances for each of the cis and trans isomers of **2a,b** are separated by about 0.2 ppm, and the DEPT-135 sequence was used to suppress the methylcyclopentadienyl methine signals since they have similar chemical shifts.[3] As can be seen in Figure 3, no exchange of the ethyl between **2b**-^{13}C and **2a** occurred after the reaction was 50% complete. However, complete exchange in the products **4a**-^{13}C and **4b**-^{13}C is clearly shown by the similar heights of the ^{13}C-labeled product

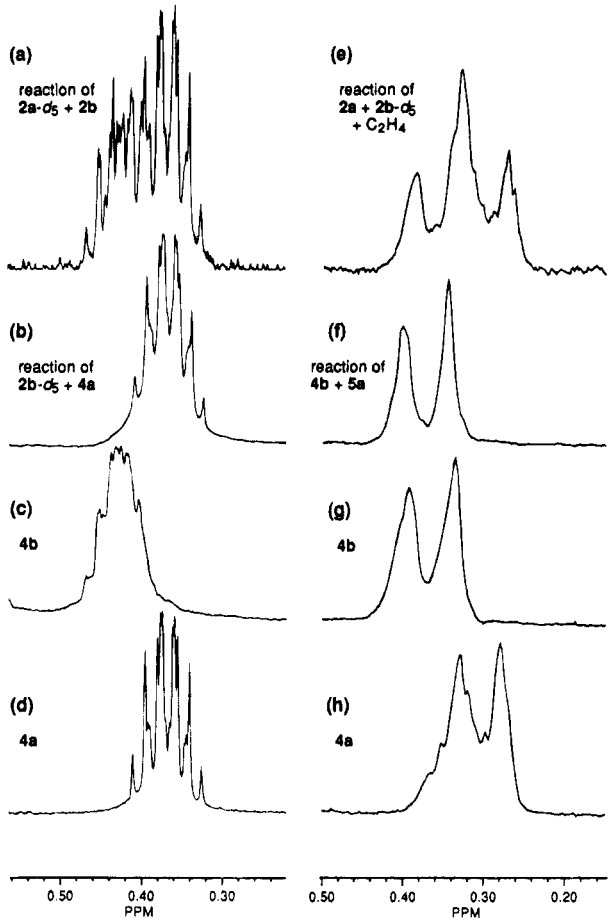

Figure 2. ^{1}H NMR spectra of representative final reaction mixtures showing the upfield FeC(H)*H*CH$_3$ multiplets of **4a,b**, **4a**-d_5, and **4b**-d_5 in acetone-d_6. Spectra (a)−(d) were taken at 500 MHz, and (e)−(h) at 200 MHz with homonuclear decoupling of the C(*H*)HC*H*$_3$ hydrogens (irradiation at δ 1.114). The difference in chemical shift between the two sets of spectra is due to the high decoupler power required for (e)−(h), since the irradiated hydrogens do not have coincident chemical shifts. Key: (a) Crossover reaction of **2a**-d_5 and **2b** (run 4) showing a mixture of **4a** and **4b**; (b) "control" crossover of **2b**-d_5 and **4a** showing only **4a** (run 12); (c) **4b**; (d) **4a**; (e) crossover reaction of **2a** and **2b**-d_5 in the presence of ethylene (run 14) showing mixture of **4a** and **4b**; (f) control reaction of **4b** and **5a** showing only **4b** (run 19); (g) **4b**; (h) **4a**.

peaks (which are doublets due to coupling to phosphorus) and so confirms the results previously obtained by ^{1}H NMR (Figure 2a,e). No other peaks from **2a**, **2b**, **4a**, or **4b** due to natural abundance ^{13}C were visible. Lastly, the "control" crossover between ethoxycarbyne **2a**−**d$_5$** and product **4b** (run 5, Scheme 4), as well as that between **2b**-d_5 and **4a** (run 12, Figure 2b), gave no crossover at all. It is interesting to note that no ethane was detected in these reactions, indicating that this product arises from the decomposing carbyne (and so would be C_2D_6 here), although some ethylene was still seen. Since in these cases no crossover was observed between the products **4a**-d_5 and **4b**, and between **4a** and **4b**-d_5, it was unnecessary to carry out a separate crossover reaction between the ethyl products **4a** and **4b**-d_5 (for instance) as a check on the source of exchange in the carbyne crossover experiment between (for instance) **2a** and **2b**-d_5.

Due to the presence of ethane and ethylene in the product mixtures upon ethoxycarbyne decomposition, a

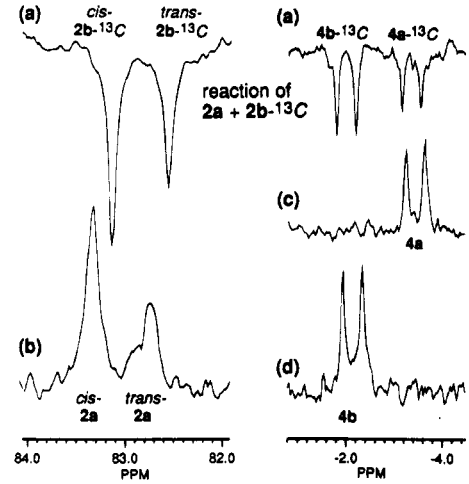

Figure 3. ^{13}C NMR spectra of **2b**-^{13}C, **2a**, and **4a,b** in C_6D_6 at 50 MHz showing the ethoxycarbyne methylene singlets near 83 ppm due to the cis and trans isomers[3] and the product Fe*C*H$_2$CH$_3$ doublets (due to phosphorus coupling) near −3 ppm: (a) DEPT-135 NMR (C_6D_6) of the crossover reaction of **2b**-^{13}C and **2a** run to 50% completion (run 11) showing only unreacted **2b**-^{13}C (with no formation of **2a**-^{13}C) but complete exchange of **4a**-^{13}C and **4b**-^{13}C; (b) broad-band decoupled spectrum of **2a**; (c) broad-band decoupled spectrum of **4a**; (d) broad-band decoupled spectrum of **4b**.

Scheme 3. ^{13}C Crossover Experiment: Products and Unreacted Starting Materials

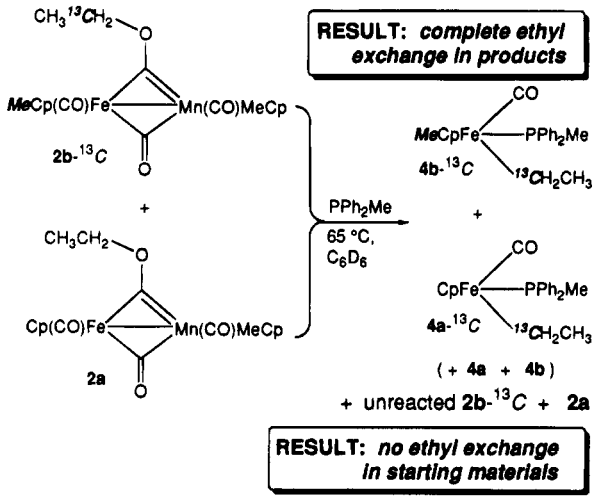

series of experiments was conducted to probe for the presence of radical species or the involvement of β-elimination reactions that might lead to crossover (Scheme 5). In all cases **2a** and **2b**-d_5 were used since they decompose at similar rates, compared to **2a**-d_5 and **2b** (Table 2). No changes in crossover or rate of decomposition were seen upon addition of 2,6-di-*tert*-butyl-4-methoxyphenol, galvinoxyl, or thiophenol (runs 15−17). For CCl_4 (run 18), decomposition (to unknown products) of the starting ethoxycarbynes commenced before heating and very low yields of **4a,b** were obtained, although crossover still occurred.

The β-elimination pathway, even more than the radical pathway, would provide an obvious intermolecular exchange mechanism. Given the complexity of the ^{1}H NMR signals, it was considered possible that *ethylene* exchange was occurring rather than *ethyl* exchange. Decomposition of **2b** in the presence of ethylene occurred at the same rate as in the absence of

Scheme 4. "Control" Crossover Experiment

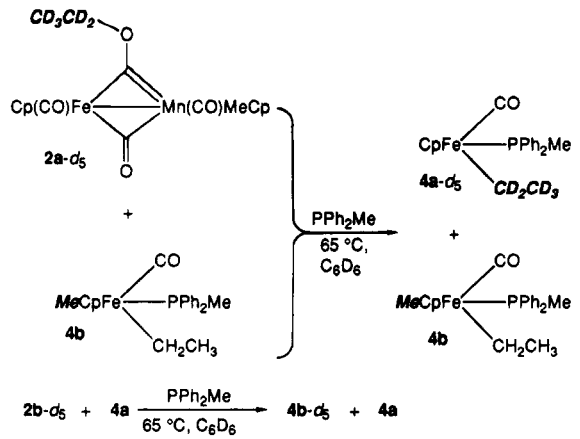

RESULTS: *no ethyl exchange between carbyne starting material and alkyl product*

Scheme 5. Radicals or Ethylene

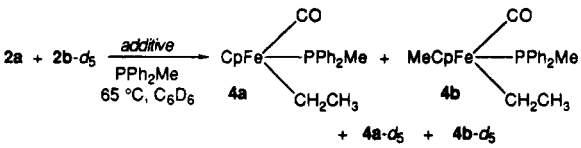

RESULTS: *no change in crossover or rate*

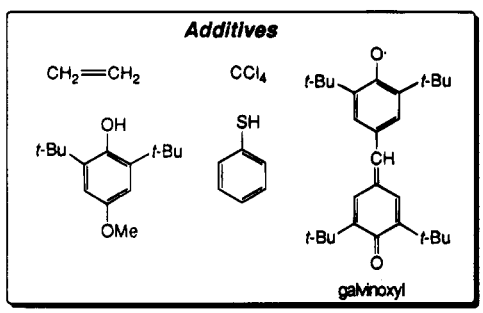

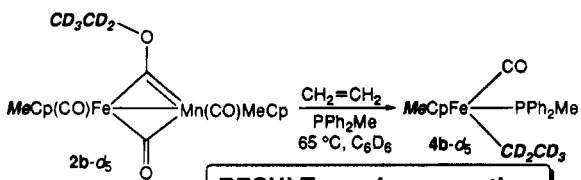

RESULT: *no incorporation of ethylene*

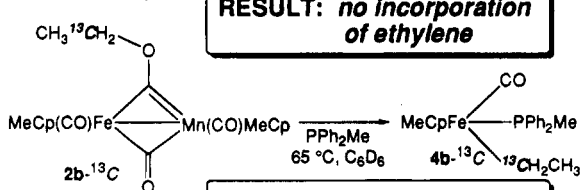

RESULT: *no exchange of ^{13}C label into CH_3*

ethylene (runs 7 and 8). More convincingly, reaction of **2b**-d_5 in the presence of 45 equiv of ethylene (run 13) did not result in the formation of any **4b**-h_4 or **4b**-h_5, and again the rate of reaction was unaffected. The crossover reaction between **2a** and **2b**-d_5 was also unaffected by ethylene (run 14). Lastly, decomposition of **2b**-^{13}C, where the ethyl group is selectively labeled at the CH_2 carbon, gave only **4b**-1-^{13}C, with no evidence from ^1H or ^{13}C NMR of scrambling of the label from the CH_2 carbon into the methyl carbon (run 10, Scheme 5). The ^{13}C crossover experiment described above (Scheme 3, Figure 3) confirms this result. All of these experiments clearly show that *reversible* ethylene exchange does not occur.

While β-elimination as a *stoichiometric* exchange pathway is precluded by the above results, the direct involvement of CpFe(CO)(PPh_2Me)H (**5a**), the presumed organometallic product of β-elimination from **2a** in the presence of PPh_2Me, was examined next since the PPh_3 and $PPhMe_2$ analogs are known stable compounds.[9–11] A search in the hydride region of the ^1H NMR spectra of a number of reactions (runs 7, 8, 17) indeed revealed the presence of hydride doublets (due to phosphorus coupling) due to authentic **5a** (−13.44 ppm) and/or (presumably) MeCp analog **5b** (−13.36 ppm; the hydride signal of MeCpFe(CO)$_2$H is 0.12 ppm downfield of that of CpFe(CO)$_2$H,[11] comparable to the 0.08 ppm difference here). The only experiment in which the NMR was searched *un*successfully for **5a**,**5b** was run 18 involving hydride scavenger CCl_4,[12–14] but the low product yields do not allow us to rule out sensitivity limitations as the cause. While the control crossover experiments between carbynes **2a**-d_5 or **2b**-d_5 and **4b** or **4a** had given no exchange, the substoichiometric formation of hydrides **5a**,**b** left open the possibility of a *catalytic* exchange process. The hydride crossover experiments shown in Scheme 6 therefore were carried out, and this time carbyne **2b** and hydride **5a** *gave complete scrambling of both the ethyl and hydride labels on the Cp and MeCp products **4a**,**b** and **5a**,**b*** (run 9). Since no exchange occurred between the products **4b** and **5a** (run 19), this hydride-induced ethyl exchange reaction provides a sufficient mechanism for carbyne crossover. A catalytic crossover mechanism consistent with these results is presented in the Discussion.

Discussion

Mechanism of Alkyl Migration. The decomposition of the ethoxycarbyne follows unimolecular kinetics, as evidenced by the linear first-order plots of decomposition. While it might be argued that NMR kinetics are not sufficiently precise to observe the curvature in a log plot that would be indicative of bimolecular kinetics, in fact similar rate constants have been observed in some runs where fairly different starting concentrations of the carbynes were used; for instance in run 2 [**2a**] is 1.5 times [**2a**] in run 1, in run 7 [**2b**] is 3 times [**2b**] in run 8, and in run 3 [**2b**-d_5] is 2 times [**2b**-d_5] in run 16. Moreover, bimolecular plots (i.e. 1/[**2a**] vs t rather than the first-order plot of ln [**2a**] vs t) give curved plots with a variety of rate "constants". Carbyne decomposition is zero-order in PPh_2Me, and no S_N2 dealkylation of the carbyne (to give $EtPPh_3^+$ salts) is observed. This result is particularly gratifying since it formed the basis for choosing to examine **2a** as described in the Introduction, but it is also somewhat surprising given the relative

(9) Kalck, P.; Poilblanc, P. *C. R. Acad. Sci., Ser. C* **1972**, *274*, 66–69.
(10) Reger, D. L.; Culbertson, E. C. *J. Am. Chem. Soc.* **1976**, *98*, 2789–2794.
(11) Shackleton, T. A.; Mackie, S. C.; Fergusson, S. B.; Johnston, L. J.; Baird, M. C. *Organometallics* **1990**, *9*, 2248–2253.
(12) Piper, T. S.; Wilkinson, G. *J. Inorg. Nucl. Chem.* **1956**, *3*, 104–124.
(13) Bainbridge, A.; Craig, P. J.; Green, M. *J. Chem. Soc. A* **1968**, 2715–2718.
(14) Green, M. L. H.; Knowles, P. J. *J. Chem. Soc., Perkin Trans. 1* **1973**, 989–991.

Scheme 6. Hydride Crossover Experiments

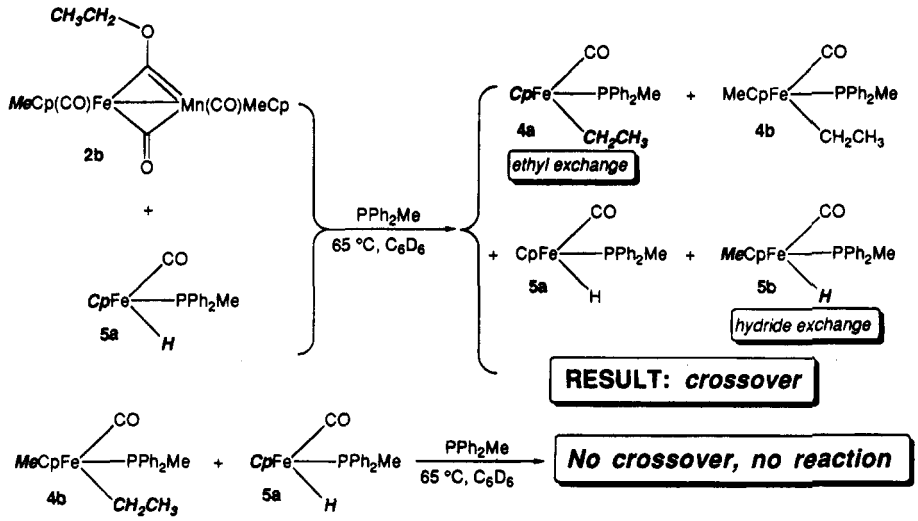

Scheme 7. A Proposed Mechanism of Ethoxycarbyne Decomposition

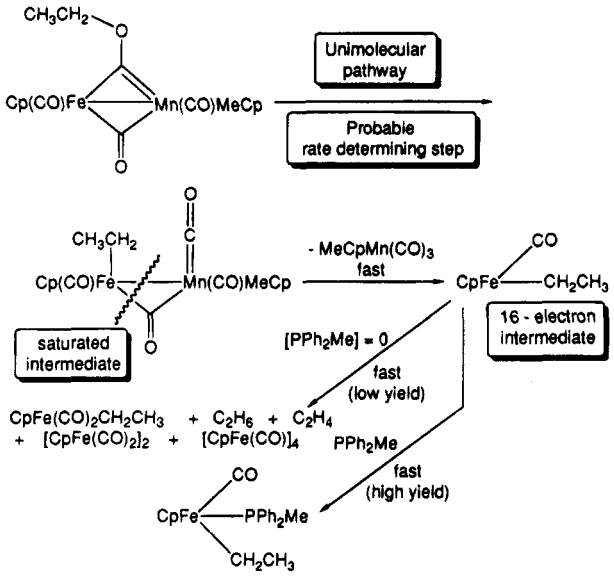

ease with which dealkylation of **1** by the less nucleophilic phosphine[15-17] PPh_3 occurs.

A proposed mechanism for the unimolecular decomposition reaction is shown in Scheme 7. The relevant data on which to base speculation are that there is a kinetic deuterium isotope effect for the ethoxycarbyne decomposition ($k_H/k_D = 2.0 \pm 0.1$ for **2a** and 1.54 ± 0.03 for **2b**), the methylcyclopentadienyl iron ethoxycarbynes decompose more rapidly than the cyclopentadienyl iron ethoxycarbynes ($k_{MeCp}/k_{Cp} = 1.5 \pm 0.2$), and ethyl migration is somewhat faster than methyl migration.[18] The deuterium isotope effect is a secondary kinetic isotope effect (SKIE) since C–D bond cleavage does not occur in this reaction and can be further classified as an α and/or β effect since there are deuterium atoms both α and β to the C–O bond that is cleaved. For both the α and β SKIE, observation of a normal deuterium isotope effect ($k_H/k_D > 1$) is associated with rehybridization at the cleavage site from sp^3 to sp^2.[6,19] While interpretation of secondary isotope effects is still an active area of research,[20-25] such a rehybridization would appear to be *inconsistent* with alkyl migration with its electron pair, a reaction that would be related formally to β-hydride elimination (Scheme 8).[26-28] Despite this, Gable[25] has recently argued that alkyl migration in a rhenium diolate system *is* consistent with observation of a normal SKIE, and as shown in Scheme 8, the rhenium system is a remarkably good analog of ours. The rate-determining step was proposed to be migration of the methylene carbon from oxygen to metal, although since no S_N1 character was proposed, a normal β secondary isotope effect due to hyperconju-

Scheme 8. "Nucleophilic" Migration Reactions

Migration with electron pair to electrophilic metal

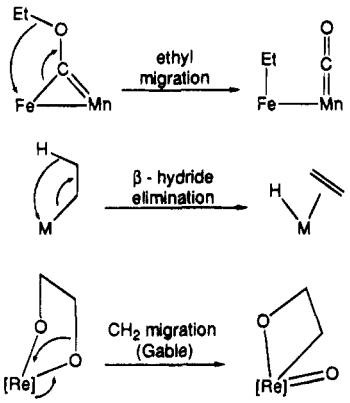

(15) Honeychuck, R. V.; Hersh, W. H. *Inorg. Chem.* **1987**, *26*, 1826–1828.
(16) Bush, R. C.; Angelici, R. J. *Inorg. Chem.* **1988**, *27*, 681–686.
(17) Rahman, M. M.; Liu, H.-Y.; Eriks, K.; Prock, A.; Giering, W. P. *Organometallics* **1989**, *8*, 1–7.
(18) Hersh, W. H.; Fong, R. H. Manuscript in preparation.
(19) Carey, F. A.; Sundberg, R. J. *Advanced Organic Chemistry, Part A: Structure and Mechanisms*, 3rd ed.; Plenum Press: New York, 1990; pp 218–220.
(20) Wolfe, S.; Kim, C. K. *J. Am. Chem. Soc.* **1991**, *113*, 8056–8061.
(21) Poirier, R. A.; Wang, Y. L.; Westaway, K. C. *J. Am. Chem. Soc.* **1994**, *116*, 2526–2533.
(22) Hostetler, M. J.; Bergman, R. G. *J. Am. Chem. Soc.* **1992**, *114*, 7629–7636.
(23) Abuhasanayn, F.; Kroghjespersen, K.; Goldman, A. S. *J. Am. Chem. Soc.* **1993**, *115*, 8019–8023.
(24) Gajewski, J. J.; Brichford, N. L. *J. Am. Chem. Soc.* **1994**, *116*, 3165–3166.
(25) Gable, K. P.; Phan, T. N. *J. Am. Chem. Soc.* **1994**, *116*, 833–839.
(26) Thorn, D. L.; Hoffmann, R. *J. Am. Chem. Soc.* **1978**, *100*, 2079–2090.
(27) Koga, N.; Obara, S.; Kitaura, K.; Morokuma, K. *J. Am. Chem. Soc.* **1985**, *107*, 7109–7116.
(28) Delbecq, F. *Organometallics* **1990**, *9*, 2223–2233.

Scheme 9. "Electrophilic" Ethyl Migration

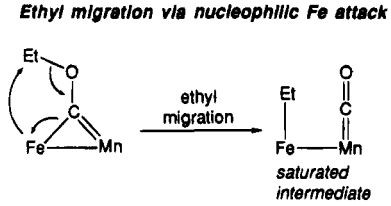

gation[6] was not considered. Hence only the two deuterium atoms in the α KIE were presumed to be involved, giving a reasonable SKIE of ~1.1 per deuterium atom. In **2a**, the SKIE assuming only an α SKIE of 1.4 per deuterium atom is high, but if comparable α and β effects were operative, the effect spread out over *five* deuterium atoms would be a more palatable 1.15 per atom. Unlike Gable's system, however, this would imply S_N1 character in the ethyl migration transition state.

If one accepts that the SKIE is indicative of S_N1 character in the migration, then the reactions in Scheme 8 that involve electron-pair migration to an electrophilic metal are *not* appropriate models for carbyne decomposition. Support for S_N1 character in the ethyl migration comes from the electrophilic character of the carbon bound to the carbyne oxygen, as seen for instance by the S_N2 dealkylation of **1** to give **3** (Scheme 1), the X-ray crystal structure of **2a** which shows the sp^2 hybridization of the carbyne oxygen atom[3] which presumably polarizes the C–O bond toward electrophilic cleavage, and the even higher degree of dealkylation of a related iron–chromium methoxycarbyne.[5] Rather than the β-hydride mode of alkyl migration, then, we instead picture the migration as shown in Scheme 9 proceeding via a nucleophilic attack *of iron* on the ethyl group. Molecular orbital calculations on isoelectronic [CpFe(CO)]$_2$(μ-CO)(μ-L) compounds[29] do not appear to support or reject either of the two directions of electron flow represented by Schemes 8 and 9. The HOMO is metal-based although not energetically isolated, so a number of orbitals might serve to attack the alkyl group, while the LUMO is M–M σ* antibonding in character and is located in the plane of the bridging ligands, and so could perhaps serve as an electrophilic site. The enhancement in rate for the MeCp ligand is in accord with the mechanism shown since the MeCp ligand is a better electron donor than the Cp ligand and would therefore make the iron more nucleophilic. The enhancement in rate for the ethoxycarbyne over the methoxycarbyne is in accord with this mechanism since to the extent that there is any S_N1 character to the reaction, positive charge buildup on the ethyl CH_2 carbon would be easier than on the methyl group of the methoxycarbyne. Clearly such detailed conclusions drawn on the basis of the combined α and β SKIE are speculative, but two more general conclusions are warranted: ethyl migration occurs in the rate-determining step and the kinetic isotope effect is large relative to those that have been reported. We would also suggest a third conclusion: the SKIE merits scrutiny in simpler but better understood migration reactions.

In addition to providing supporting evidence of nucleophilic attack of iron on the ethyl group, the MeCp

(29) Bursten, B. E.; Cayton, R. H. *J. Am. Chem. Soc.* **1986**, *108*, 8241–8249.

Scheme 10. Alternative Routes for Carbyne Decomposition

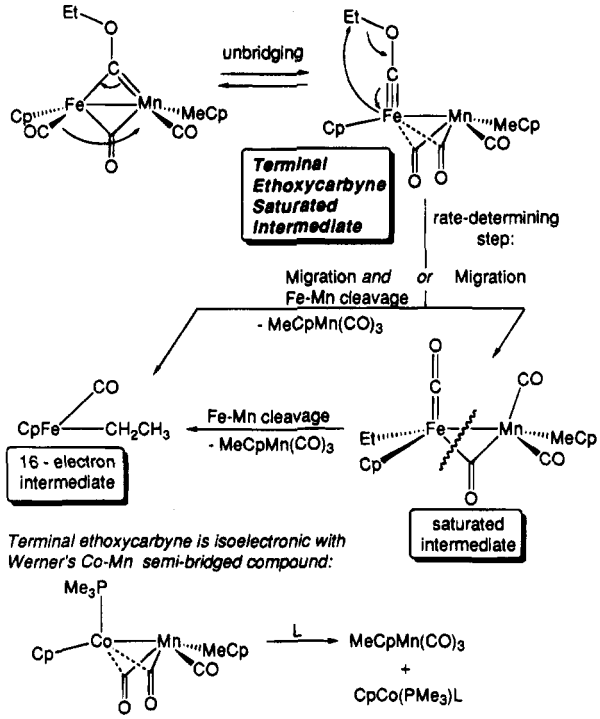

effect provides suggestive evidence that the migration occurs directly to iron rather than manganese, although we have not measured rates for any CpMn analogs for comparison. The proposed electronically saturated intermediate (Scheme 7) formed via the electrophilic or nucleophilic pathways would consist of MeCpMn(CO)$_3$ side-bound to the iron, and it is reasonable to suggest that this species will rapidly decompose via cleavage of the Fe–Mn and μ-CO bonds to give the 16-electron intermediate CpFe(CO)Et. In the absence of an external trapping ligand, decomposition of CpFe(CO)Et apparently occurs via β-hydride elimination to give ethane and ethylene, while scavenging of CO from more extensive decomposition leads to the low yields of CpFe(CO)$_2$Et. Loss of the ethyl group yields [CpFe(CO)$_2$]$_2$ upon CO scavenging and the tetrameric cluster [CpFe(CO)]$_4$ without any additional CO. In the presence of phosphines, the 16-electron species is trapped to give CpFe(CO)(PPh$_2$Me)Et.

We now consider an alternative saturated intermediate. Unbridging of the carbyne along with bridging of the Fe carbonyl ligand would give a terminal ethoxycarbyne complex with semibridging carbonyl ligands (Scheme 10). This mechanism has two attractive features. First, the structure of the intermediate is based on that of isoelectronic Co–Mn and Rh–Mn semibridged compounds such as Cp(PMe$_3$)Co(μ-CO)$_2$Mn(CO)MeCp, which further undergo ligand-induced Co–Mn cleavage with expulsion of MeCpMn(CO)$_3$ and formation of CpCo(PMe$_3$)L as shown.[30–32] Second, we have previously noted that carbyne unbridging must be involved in cis/trans isomerization of alkoxycarbynes,[3,5] and so this mechanism allows an attractive albeit unrequired con-

(30) Leonhard, K.; Werner, H. *Angew. Chem., Int. Ed. Engl.* **1977**, *16*, 649–650.
(31) Werner, H.; Juthani, B. *J. Organomet. Chem.* **1981**, *209*, 211–218.
(32) Werner, H. *Pure Appl. Chem.* **1982**, *54*, 177–188.

nection to that reaction channel. We note that carbyne migration to either metal is reasonable since the carbyne bridge is nearly symmetrical as seen from the X-ray crystal structure of **2a**,[3] despite the formal double bond to manganese. While the analogy between the cleavage of the terminal ethoxycarbyne and the Co–Mn model appears close since both yield $CpMn(CO)_3$ and ligand adducts of the remainder of the heterodinuclear species, the Co–Mn reaction is bimolecular while the carbyne reaction is not. However, this difference could arise readily from the differing stabilities of these species. Since the rate-determining step apparently involves ethyl migration rather than carbyne unbridging or cluster cleavage, decomposition of the semibridged intermediate would necessarily involve rate-determining ethyl migration either to give the previously proposed saturated intermediate with the single carbonyl bridge or to give CpFe(CO)Et directly as shown with concomitant cluster cleavage. The key difference between this mechanism and that in Scheme 9 is simply that the migration occurs from a terminal rather than a bridging ethoxycarbyne. Related migrations for proposed terminal hydroxy, stannoxy, and alkoxycarbyne intermediates or the reverse migration from metal to oxygen to give a terminal siloxycarbyne intermediate have been proposed,[33–37] and so it is possible that, in this cluster reaction as in others,[38–40] the "interesting" chemistry occurs at a single metal site.

Mechanism of Intermolecular Alkyl Exchange. While the crossover experiments between the doubly-labeled carbynes shown in Scheme 2 resulted in intermolecular ethyl exchange in the mononuclear products, they do not address the question of when or how the exchange occurs; in principle, exchange can occur at a number of testable points in the mechanism shown in Scheme 7, and these are now considered.

Alkyl exchange can in principle occur before carbyne decomposition occurs. The standard control experiment, in which a crossover reaction was run to partial conversion and then the unreacted starting carbynes examined for alkyl exchange, was carried out and analyzed by ^{13}C NMR on ^{13}C-labeled material (Scheme 3, run 11), but no crossover in the starting materials was observed. In principle, alkyl exchange among the carbynes could occur concomitant with carbyne decomposition, so that the unreacted carbynes would not exhibit crossover. However, such a scheme would give bimolecular decomposition kinetics, but as described above in detail (for this very reason), only unimolecular kinetics were observed.

Alkyl exchange also in principle can occur after carbyne decomposition occurs, that is, among the mononuclear products. This was not tested explicitly by reaction of (for instance) **4a** and **4b**-d_5, but since no exchange was observed in the "control" crossover reactions (Scheme 4) in which one ethyl product is generated in the presence of the other, no ethyl exchange can be occurring among the mononuclear iron ethyls **4a,b** and their deuterated analogs. The control crossover result stands in sharp contrast to the complete methyl crossover observed with *methoxy*carbyne **1** and $MeCpFe(CO)(PPh_3)CD_3$,[2,18] and so an explanation is required for the different methoxy and ethoxy control crossover results. We have shown that the 16-electron intermediate $CpFe(CO)CH_3$, presumed to form from **1** in the rate-determining step, also forms from $CpFe(CO)(PPh_3)CH_3$ by phosphine dissociation and at a comparable rate.[4] Since the methyl products, like their ethyl counterparts **4a,b**, do not undergo alkyl exchange by themselves during the carbyne decomposition, $CpFe(CO)CH_3$ *alone* cannot be responsible for alkyl exchange, although it may well participate in methyl exchange with a carbyne decomposition product. The absence of *ethyl* exchange in the control crossover experiment may perhaps be explained most simply by the presumed lower concentration of $CpFe(CO)CH_2CH_3$, if the 16-electron intermediates are involved somehow in the control crossover. Faster trapping of this intermediate by the more nucleophilic phosphine PPh_2Me compared to trapping of $CpFe(CO)CH_3$ by PPh_3 would lower the concentration of $CpFe(CO)CH_2CH_3$, as would rapid β-hydride elimination (see below). In complementary fashion, PPh_2Me is less labile than PPh_3; for instance PPh_2Me dissociation from $CpFe(CO)(PPh_2Me)CH_3$ is 36 times slower at 65 °C than is PPh_3 dissociation from $CpFe(CO)(PPh_3)CH_3$,[4] and we presume the ethyl analogs follow the same trend.

An alternative explanation for the different methyl and ethyl control crossover results arises by consideration of the relative ease of alkyl group bridging of two metal centers, which presumably must occur at some point in the crossover reaction. That is, while *methyl* bridges between two metal atoms are well-known,[41–44] *ethyl* bridges (which involve bridging by the CH_2 group[45]) are only well-known between electron-deficient centers such as lithium and aluminum,[46–50] and even for methyl-bridged compounds, most transition metal examples involve high-oxidation-state electron-deficient metals.[41,43,44] The best-studied cases are the aluminum alkyls, where two types of experiment show that methyl bridging is favored over ethyl bridging but not by a large amount: the "trialkyl" aluminum species R_3Al exist predominantly (typically >96%) as the dimers $R_2Al(\mu\text{-}R)_2AlR_2$ in solution (R = Me, Et, Pr, *n*-Bu, *n*-octyl), but the equilibrium shifts toward the monomer with increasing size of the alkyl group,[49,50] and in the mixed dimer $Et_3Me_3Al_2$ the methyl group is favored in the bridging site by a factor of 6.[48] Rare examples of μ-alkyl (other than μ-methyl) complexes involving metal carbonyl compounds include one having an ethyl-bridged

(33) Nicholas, K. M. *Organometallics* **1982**, *1*, 1713–1715.
(34) Schubert, U.; Hörnig, H. *J. Organomet. Chem.* **1987**, *336*, 307–315.
(35) Schubert, U. *J. Organomet. Chem.* **1988**, *358*, 215–228.
(36) Chatani, N.; Fukumoto, Y.; Murai, S. *J. Am. Chem. Soc.* **1993**, *115*, 11614–11615.
(37) Gibson, D. H.; Ye, M.; Sleadd, B. A.; Mehta, J. M.; Mbadike, O. P.; Richardson, J. F.; Mashuta, M. S. *Organometallics* **1995**, *14*, 1242–1255.
(38) Bergman, R. G. *Acc. Chem. Res.* **1980**, *13*, 113–120.
(39) Fyhr, C.; Garland, M. *Organometallics* **1993**, *12*, 1753–1764.
(40) Garland, M. *Organometallics* **1993**, *12*, 535–543.
(41) Holton, J.; Lappert, M. F.; Pearce, R.; Yarrow, P. I. W. *Chem. Rev.* **1983**, *83*, 135–201.
(42) Bursten, B. E.; Cayton, R. H. *Organometallics* **1986**, *5*, 1051–1053.
(43) Theopold, K. H. *Acc. Chem. Res.* **1990**, *23*, 263–270.
(44) Waymouth, R. W.; Potter, K. S.; Schaefer, W. P.; Grubbs, R. H. *Organometallics* **1990**, *9*, 2843–2846.
(45) Yamamoto, O. *Bull. Chem. Soc. Jpn.* **1964**, *37*, 1125–1128.
(46) Brown, T. L. *Adv. Organomet. Chem.* **1965**, *3*, 365–395.
(47) Oliver, J. P. *Adv. Organomet. Chem.* **1970**, *8*, 167–209.
(48) Yamamoto, O.; Hayamizu, K. *J. Phys. Chem.* **1968**, *72*, 822–828.
(49) Smith, M. B. *J. Organomet. Chem.* **1974**, *70*, 13–33.
(50) Oliver, J. P. *Adv. Organomet. Chem.* **1977**, *16*, 111–130.

Os–Os bond[51] and another having a *p*-methylbenzyl-bridged W–Re bond.[52] Thus, even if carbyne decomposition yields some intermediate that initiates *methyl* bridging from product $CpFe(CO)(PPh_3)CH_3$ and consequent methyl exchange in the control crossover reaction, the analogous *ethyl* bridging from product **4** might not occur and so preclude exchange in the ethyl control crossover reaction. *The fact that crossover nevertheless occurs between carbynes* ***2a*** *and* ***2b****-d*$_5$*, and between* ***2a****-d*$_5$ *and* ***2b*** *paradoxically requires that there be an alkyl exchange pathway in the ethyl case that need not be present in the methyl case.*

A radical exchange mechanism is one possibility that would be more likely for ethyl than methyl radicals.[53,54] However, the similarity in rates, and high reproducibility for the ethoxycarbyne kinetics in particular,[55] argue against the involvement of radicals in the rate-determining step. A number of additives (Scheme 5) were found to have no effect on either the rate or crossover reaction for the ethoxycarbynes, as well. Two of the additives, 2,6-di-*tert*-butyl-4-methoxyphenol and galvinoxyl, are used to initiate and/or quench radical reactions by forming and intercepting radical chain carriers.[11,53,56,57] Thiophenol was tried on the basis of its stabilization of $CpFe(CO)_2H$,[11] which was suggested to be due to trapping of adventitious 1-electron oxidizing reagents. Lastly, CCl_4 was tried since it too can trap organometallic radicals[58–60] as well as hydrides by donation of a chlorine atom, but as noted, it caused decomposition of the starting carbynes; only very low yields of product, which nevertheless exhibited crossover, were obtained.

With establishment that radicals are unlikely to be involved, the obvious pathway that could be available to the ethoxycarbyne but not the methoxycarbyne would involve β-elimination. Of particular interest is a result due to Reger[10] shown in Scheme 11. Thermal loss of PPh_3 gives the 16-electron intermediate shown which leads to deuterium scrambling in recovered starting material; even at early reaction time, the scrambling is extensive, requiring that the reversible β-elimination occurs many times before PPh_3 displaces the ethylene to give the hydride product. In the presence of PPh_3, no reaction occurs, so presumably the β-elimination step is not reached. A number of reactions established that reversible β-elimination was not occurring for the ethoxycarbyne. Free ethylene had no effect on the reaction and was not incorporated into the product (Scheme 5, runs 7, 8, 13, 14), and most convincingly use of ethoxycarbyne specifically ^{13}C-labeled at the methylene of the ethyl group gave rise to no scrambling of

Scheme 11

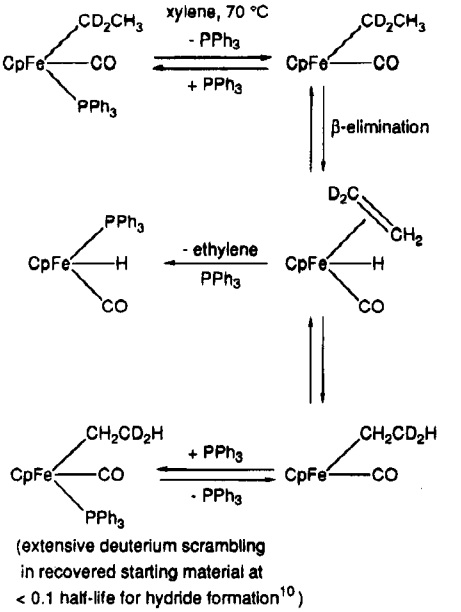

this label into the methyl position in the mononuclear products (Scheme 5, runs 10, 11). Since trapping of photochemically-generated $CpFe(CO)CH_2CH_3$ by PPh_3 is known to be faster than β-elimination,[61] it is not surprising that even if this 16-electron intermediate forms, it will be trapped by PPh_2Me faster than entry into the *reversible* ethylene manifold. But since ethylene is in fact a reaction product, displacement of ethylene by PPh_2Me must simply be faster than olefin insertion to give back the 16-electron intermediate, and the expected hydride would be a stable compound.[10,11] Small amounts were indeed found in the ethoxycarbyne decomposition reactions and prompted the crossover reaction between **2b** and **5a** (Scheme 6, run 9). In contrast to the control crossover, complete exchange of hydride and ethyl groups occurred between the iron centers of the Cp hydride **5a** and the MeCp carbyne decomposition product **4b**. This result could also occur by direct scrambling between the mononuclear alkyl and hydride products, but the control experiment between **4b** and **5a** shown in Scheme 6 (run 19) eliminated that mechanism and demonstrated the necessity of the carbyne for exchange.

The mechanism shown in Scheme 12 is proposed to take advantage of the presence of this hydride in order to generate the crossover results. The key facts that any ethyl exchange scheme must account for are that there is no reversible β-elimination, the ethyl group is exchanged intact without scrambling of the two carbons, *and there is no exchange once the iron alkyl products are formed.* This last point arises from the control crossover (Scheme 4), where the "other product" that is already present does *not* exchange with the carbyne-derived product. Thus, not only do the products not undergo exchange among themselves, the decomposing carbyne yields no products that *mediate* exchange among the existing products. As shown in Scheme 12, we propose that the 16-electron intermediate $CpFe(CO)CH_2CH_3$ formed in the rate-determining step from carbyne **2a** can (1) be trapped by PPh_2Me to give product

(51) Cree-Uchiyama, M.; Shapley, J. R.; St. George, G. M. *J. Am. Chem. Soc.* **1986**, *108*, 1316–1317.
(52) Jeffery, J. C.; Orpen, A. G.; Stone, F. G. A.; Went, M. J. *J. Chem. Soc., Dalton Trans.* **1986**, 173–186.
(53) Labinger, J. A.; Osborn, J. A.; Coville, N. J. *Inorg. Chem.* **1980**, *19*, 3236–3243.
(54) Hudson, A.; Lappert, M. F.; Lednor, P. W.; MacQuitty, J. J.; Nicholson, B. K. *J. Chem. Soc., Dalton Trans.* **1981**, 2159–2163.
(55) The ethoxycarbynes follow what we call "bicoastal kinetics"; that is, the same rate constants were obtained in Los Angeles and New York and by different workers using different equipment.
(56) Davies, A. G.; Roberts, B. P. In *Free Radicals*; Kochi, J. K., Ed.; Wiley-Interscience: New York, 1973; Vol. 1, pp 547–589.
(57) Hoffman, N. W.; Brown, T. L. *Inorg. Chem.* **1978**, *17*, 613–617.
(58) Laine, R. M.; Ford, P. C. *Inorg. Chem.* **1977**, *16*, 388–391.
(59) Meckstroth, W. K.; Walters, R. T.; Waltz, W. L.; Wojcicki, A.; Dorfman, L. M. *J. Am. Chem. Soc.* **1982**, *104*, 1842–1846.
(60) Tyler, D. R.; Schmidt, M. A.; Gray, H. B. *J. Am. Chem. Soc.* **1983**, *105*, 6018–6021.
(61) Kazlauskas, R. J.; Wrighton, M. S. *Organometallics* **1982**, *1*, 602–611.

Scheme 12. Iron-Hydride-Catalyzed Ethyl Exchange Mechanism

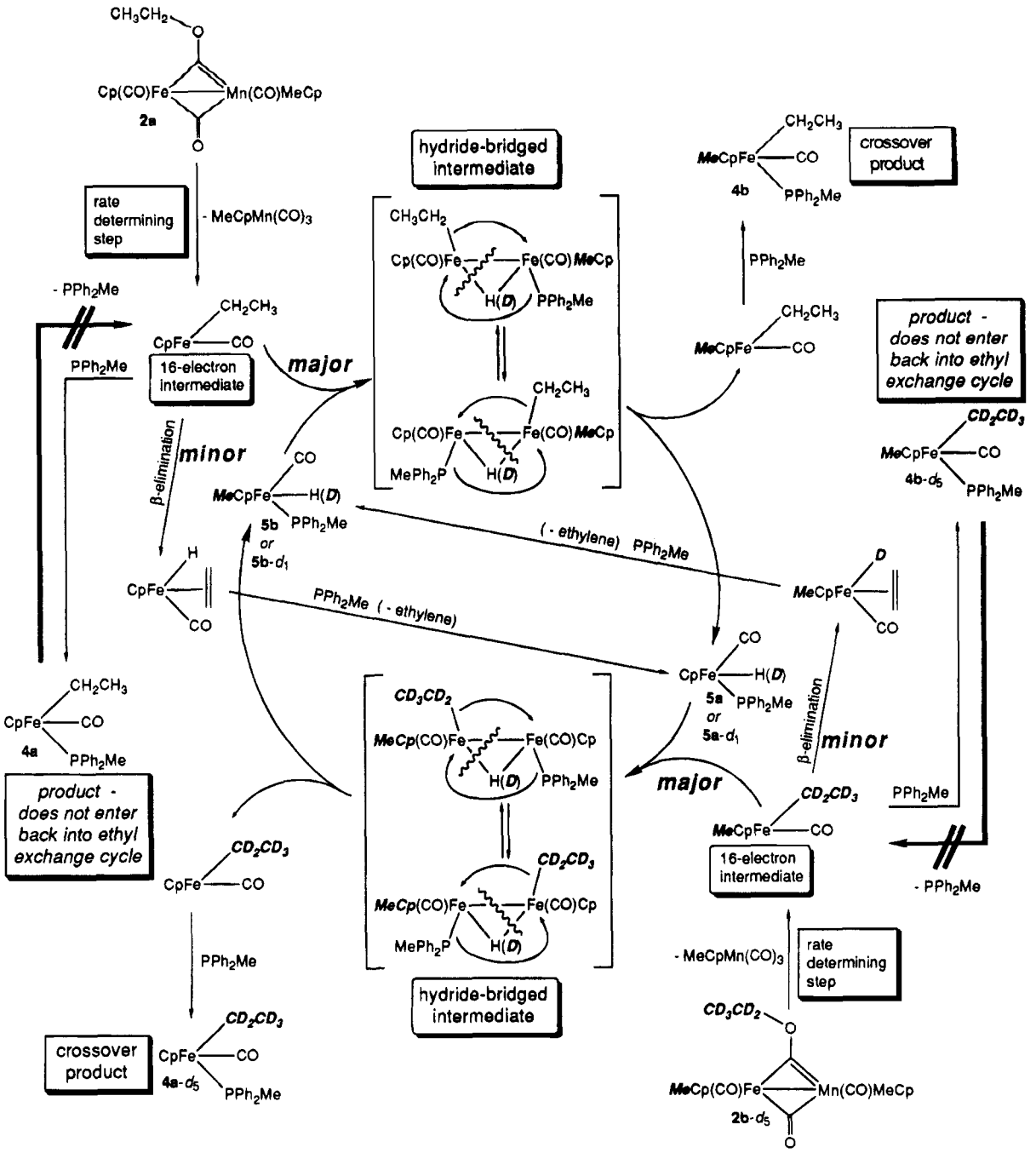

4a, (2) undergo β-elimination followed by substitution of ethylene with PPh_2Me to give hydride **5a**, or (3) undergo ethyl exchange via trapping by the saturated hydride **5b** (or **5b**-d_1). The first outcome, trapping to give **4a**, ends the involvement of the ethyl group; loss of phosphine to re-enter the exchange cycle does not occur, as shown by the control crossover where "preformed" **4b** does not exchange with product **4a**-d_5. The second outcome, β-elimination to give the ethylene hydride complex and from it **5a**, has precedent in the PPh_3 analog of **4a**[10] as seen above (Scheme 11). However, since no deuterium scrambling as well as no ^{13}C scrambling has been seen, ethylene insertion to give back an iron ethyl must not occur, so formation of the ethylene hydride must be followed immediately by phosphine displacement of ethylene. The relative amount of hydrides **5a**,**b** detected is quite small, however, so this pathway is a minor one. The third outcome leads to exchange as shown. If one starts at the point of entry into the catalytic cycle starting with **2a** going on to 16-electron intermediate $CpFe(CO)CH_2CH_3$, then trapping of this intermediate by **5b**-d_1 generated from **2b**-d_5 is proposed to give rise to an electronically saturated hydride-bridged dinuclear complex. While ethyl-bridged species are rare as described above, hydride bridging of metal–metal bonds obviously is not, and related mechanisms involving μ-hydrides have been proposed for a number of bimolecular reductive elimination reactions.[62-66] In addition, ethyl migration between

(62) Norton, J. R. *Acc. Chem. Res.* **1979**, *12*, 139–145.
(63) Janowicz, A. H.; Bergman, R. G. *J. Am. Chem. Soc.* **1981**, *103*, 2488–2489.
(64) Jones, W. D.; Huggins, J. M.; Bergman, R. G. *J. Am. Chem. Soc.* **1981**, *103*, 4415–4423.
(65) Nappa, M. J.; Santi, R.; Diefenbach, S. P.; Halpern, J. *J. Am. Chem. Soc.* **1982**, *104*, 619–621.
(66) Barborak, J. C.; Cann, K. *Organometallics* **1982**, *1*, 1726–1728.

transition metal centers bridged by another atom has also been proposed[67] and in at least two cases observed by dynamic NMR.[51,68] Here we propose that phosphine migration occurs concomitant with ethyl migration, and complete equilibration would make it equally likely that decomposition of this species occurs to give back the starting materials as well as the crossover hydride **5a**-d_1 and the 16-electron crossover intermediate $MeCpFe(CO)CH_2CH_3$. Trapping of this intermediate by phosphine would give the crossover product **4b**, which would then be out of the catalytic exchange cycle. Hydride **5a**-d_1 would remain in the cycle, however, and could trap $MeCpFe(CO)CD_2CD_3$ generated from carbyne **2b**-d_5 to give the hydride-bridged intermediate required to effect ethyl-d_5 exchange. Following equilibration and cleavage, $CpFe(CO)CD_2CD_3$ (and ultimately crossover product **4a**-d_5) along with hydride **5b**-d_1 would be generated. The catalytic cycle would then have come full-circle.

One feature of this mechanism is that any of the four hydrides **5a** or **5a**-d_1 and **5b** or **5b**-d_1 can carry the chain, since the bridging hydride or deuteride is never incorporated into the ethyl products. Hydride **5a** can form directly from **2a** as can **5b**-d_1 from **2b**-d_5, and the hydride crossover products would form in the cycle, **5b** from **5a** and **5a**-d_1 from **5b**-d_1. Hydride crossover likely also occurs without the carbynes, since it is known that $CpFe(CO)_2D$ and $MeCpFe(CO)_2H$ rapidly exchange,[11] and we observed complete equilibration of the Cp and MeCp hydrides well before the carbyne was consumed in the reaction of **2b** and **5a**. The isotopic identity of the bridging group as hydride or deuteride, as well as the number of reaction pathways for H/D exchange, is not proposed to have any effect on ethyl exchange.

The main problem with the ethyl exchange mechanism is the proposal that hydride **5b** (for instance) must trap the 16-electron intermediate $CpFe(CO)CH_2CH_3$ to give ethyl exchange at a rate comparable to that of trapping by PPh_2Me to give **4a**. That is, in considering the three reaction channels available to the 16-electron intermediate $CpFe(CO)CH_2CH_3$, we noted that the β-elimination pathway is relatively slow, but in order for complete ethyl exchange to occur, entry into the catalytic cycle must be faster than removal from the cycle by trapping by PPh_2Me. This must be the case since the alkyl products **4a** or **4a**-d_5 and **4b** or **4b**-d_5 *cannot re-enter the catalytic cycle* on the basis of the control crossover experiments between (for instance) **2a** and **4b**-d_5. The crossover experiments all occur in the presence of excess PPh_2Me, and so while it appears remarkable that this phosphine does not prevent formation of an ethyl exchange species by hydride bridging by **5**, at present we have no simpler explanation.

Conclusion

We have discovered the first example of a novel alkoxycarbyne "β-elimination" reaction, in which an alkyl group migrates from oxygen to iron. The observed secondary kinetic isotope effect shows that ethyl migration occurs in the rate-determining step and suggests an "electrophilic" migration mechanism by which a metal electron pair attacks the alkyl group. While we have been unable to prove that this reaction is intramolecular, the facts that the reaction is unimolecular and does not involve radicals eliminate any simple candidates for an intermolecular alkyl exchange mechanism. We have, on the other hand, demonstrated that exchange *can occur after alkyl migration and metal–metal bond cleavage*. While the "control crossover" experiment shows that exchange does not occur between the carbyne and the *final* ethyl products, the hydride crossover experiment shows that exchange nevertheless can be mediated by the observed β-elimination product $CpFe(CO)(PPh_2Me)H$. This isolable hydride is proposed to trap the unsaturated 16-electron species $CpFe(CO)CH_2CH_3$ and catalytically give ethyl exchange via a hydride-bridged intermediate. While we are uncomfortable with the counterintuitive proposal that $MeCpFe(CO)(PPh_2Me)H$ must trap the 16-electron species $CpFe(CO)CH_2CH_3$ competitively with PPh_2Me, as long as free ethyl radicals are not involved then *any* exchange mechanism will involve steps that at some point must pit an organometallic against PPh_2Me. Future work on these compounds must address the surprising requirement that the organometallic hydride in this case is at least as effective a kinetic trap as the donor phosphine.

Experimental Section

General Methods. All manipulations of air-sensitive compounds were carried out either in a Vacuum Atmospheres inert atmosphere drybox under recirculating nitrogen or by using standard Schlenk techniques. NMR spectra were recorded on Bruker WP-200, AM-360, and AM-500 and IBM/Bruker WP-200SY spectrometers; ^1H chemical shifts are reported relative to residual protons at δ 7.15 in C_6D_6 and δ 2.04 in acetone-d_6, ^{13}C relative to C_6D_6 at 128.0 ppm, and ^{31}P relative to external H_3PO_4 at 0 ppm. Infrared spectra were obtained on a Perkin-Elmer 237 spectrometer or Mattson 4020 Galaxy FT-IR with 0.1 mm NaCl solution cells. Elemental analyses were performed by Desert Analytics, Tucson, AZ. Mass spectra were obtained on an AEI-MS902 (EI) and an AEI-MS9 with FAB gun using xenon, at 5 kV in a matrix of NOBA (*m*-nitrobenzyl alcohol). Photolyses were carried out with a medium-pressure 450 W mercury Hanovia lamp.

All solvents were treated under nitrogen. Diethyl ether and tetrahydrofuran were distilled from sodium benzophenone ketyl. Hexane was purified by washing successively with 5% nitric acid in sulfuric acid, water, sodium bicarbonate solution, and water and then dried over calcium chloride and distilled from *n*-butyllithium in hexane. Acetone-d_6 was dried over molecular sieves and vacuum transferred prior to use, and benzene-d_6 was purified by vacuum transfer from sodium benzophenone ketyl. Compounds **2a**,**b** were prepared as we have previously described.[3] Triphenylphosphine was recrystallized from ethanol, Ph_3CH was recrystallized from hexane, and PPh_2Me (Pressure Chemical, Strem), galvinoxyl (Aldrich), and ethylene (Aldrich) were used as received. Iodomethane-d_3 (Aldrich), iodoethane-d_5 (Aldrich), iodoethane-1-^{13}C (Cambridge Isotope Laboratories), thiophenol, and TMS were vacuum transferred from CaH_2, and CCl_4 was vacuum transferred from P_2O_5.

$Cp(CO)Fe(\mu\text{-}COCD_2CD_3)(\mu\text{-}CO)Mn(CO)MeCp$ (2a-d_5). A solution of 229.9 mg (1.427 mmol) of CD_3CD_2I in 3 mL of benzene was added to a solution of 368.6 mg (1.434 mmol) of CF_3SO_3Ag in 2 mL of benzene, and the mixture was heated at 55 °C in a stopcock-sealed vessel for 12 h. The filtered solution was then added to 552.9 mg (1.417 mmol) of [Cp(CO)Fe(μ-

(67) Schore, N. E.; Ilenda, C. S.; White, M. A.; Bryndza, H. E.; Matturro, M. G.; Bergman, R. G. *J. Am. Chem. Soc.* **1984**, *106*, 7451–7461.

(68) Okeya, S.; Meanwell, N. J.; Taylor, B. F.; Isobe, K.; Vazquez de Miguel, A.; Maitlis, P. M. *J. Chem. Soc., Dalton Trans.* **1984**, 1453–1460.

$CO)_2Mn(CO)MeCp]^-Na^+$ in 25 mL of THF. After treatment as described for the protio compound,[3] 150 mg of a 1:1 mixture of the desired product and $[CpFe(CO)_2]_2$ was obtained from the benzene extraction. This was then subject to preparative TLC (Aldrich 20 × 20 cm silica plates, 250 μm thickness) in two portions. A 65 mg fraction was eluted a total of 10 times with 1:1 benzene/hexanes, each time allowing the plate to dry before rerunning, giving $[CpFe(CO)_2]_2$ as the higher R_f band and **2a**-d_5 as the lower R_f band. The lower band yielded 27 mg of a mixture that on the basis of ^1H NMR consisted of 9 mol % $[CpFe(CO)_2]_2$ and 91 mol % **2a**-d_5. The remaining 85 mg of the 1:1 mixture was eluted a total of three times with 1:4 ether/hexanes, again allowing the plate to dry before rerunning, giving $[CpFe(CO)_2]_2$ as the lower R_f band and **2a**-d_5 as the higher R_f band. This latter band yielded 33 mg of a mixture that on the basis of ^1H NMR consisted of 7.4 mol % $[CpFe(CO)_2]_2$ and 92.6 mol % **2a**-d_5. No signals appeared at ~4.7 ppm in the ^1H NMR spectrum (C_6D_6), indicating the absence of any CH_2 ethyl hydrogen atoms.

MeCp(CO)Fe(μ-CO)(μ-COCD$_2$CD$_3$)Mn(CO)MeCp (2b-d_5). This compound was conveniently prepared as previously described for **2b**,[3] using $CD_3CD_2SO_3CF_3$, prepared as described above for **2a**-d_5, and $[MeCp(CO)Fe(\mu\text{-}CO)_2Mn(CO)MeCp]^-Na^+$, giving material suitable for use without any further purification; a 2.5% residual CH_2 peak from the ethoxy group was visible by ^1H NMR spectroscopy.

MeCp(CO)Fe(μ-CO)(μ-CO^{13}CH$_2$CH$_3$)Mn(CO)MeCp (2b-^{13}C). This compound was prepared as described above for **2b**-d_5, using $CH_3{}^{13}CH_2SO_3CF_3$ prepared from iodoethane-1-^{13}C and silver triflate: ^1H NMR (C_6D_6): δ 4.73 (dq, J_{CH} = 149 Hz, J_{HH} = 7.2 Hz, $^{13}CH_2CH_3$), 4.37–3.89 (m, Me*Cp*), 1.91, 1.86, 1.84, 1.77 (s, cis, cis, trans, trans *Me*Cp, ~2:2:1:1), 1.725 (s, *Me*Cp of $[MeCpFe(CO)_2]_2$ impurity, 24% by weight), 1.265 (dt, $^2J_{CH}$ = 4.4 Hz, J_{HH} = 7.2 Hz, $^{13}CH_2CH_3$); ^{13}C NMR (C_6D_6) 83.17 (cis-$^{13}CH_2CH_3$), 82.59 (trans-$^{13}CH_2CH_3$) ppm; cis:trans ≈ 3:2.

CpFe(CO)(PPh$_2$Me)C$_2$H$_5$ (4a). To a solution[3] of 1.29 g (6.43 mmol) of $CpFe(CO)_2^-Na^+$ in 25 mL of THF was added 1.15 g (7.39 mmol) of CH_3CH_2I (purified by vacuum transfer from CaH_2). The mixture was stirred for 50 min and then concentrated in vacuo until it took on a gel-like consistency. Hexane was added to dissolve the product, the yellow solution was filtered through Celite, and the solvent was removed in vacuo to give 0.90 g (72.5% yield) of $CpFe(CO)_2C_2H_5$ as a yellow oil. A 0.775 g (3.76 mmol) sample of this material and 0.731 g (3.66 mmol) of PPh_2Me were dissolved in 20 mL of hexane and photolyzed for 3 h at room temperature under a slow nitrogen purge (1–2 bubbles/s of nitrogen from a syringe needle). The solvent was removed under vacuum and the product chromatographed on a silica column by elution with 1:1 pentane/chloroform. A red-orange band was collected which following solvent removal yielded an oil found by ^1H and ^{31}P NMR to contain ~40 mol % of the phosphine along with the desired product; no chromatographic method was found that allowed these two compounds to be separated. The oil was washed briefly with 1 mL of CH_3I in 3 mL of THF, and the white precipitate of $PPh_2Me_2{}^+I^-$ was filtered on Celite. Following solvent removal, 250 mg (18% yield) of product was obtained as an orange powder: IR (THF) 1888 (s) cm^{-1}; ^1H NMR (C_6D_6) δ 7.42–7.38 (m, 2H), 7.31–7.28 (m, 2H), 7.05–6.98 (m, 6H, Ph), 4.136 (d, J = 1.0 Hz, 5H, Cp), 1.59–1.52 (m, C*H*CH$_3$), 1.518 (t, J = 7.5 Hz, CH$_2$*CH$_3$*), 1.511 (d, J = 8.0 Hz, P*CH$_3$*, 7H for δ 1.59–1.51), 0.79–0.71 (m, 1H, C*H*CH$_3$); ^1H NMR (acetone-d_6, 500 MHz) δ 7.58–7.55 (m, 2H), 7.47–7.41 (m, 4H), 7.38–7.34 (m, 4H, Ph), 4.356 (d, J = 1.0 Hz, 5H, Cp), 1.879 (d, J = 8.3 Hz, 3H, P*CH$_3$*), 1.33–1.27 (m, 1H, C*H*CH$_3$), 1.110 (dt, J_{PH} = 2 Hz, J_{HH} = 7.4 Hz, 3H, CH$_2$*CH$_3$*), 0.40–0.33 (m, 1H, C*H*CH$_3$); ^{13}C NMR (C_6D_6) 222.47 (d, J_{CP} = 32.86 Hz, FeCO), 140.61, 139.79, 139.61, 138.90, 132.20, 132.00, 131.83, 131.65 (140.6–138.9, ipso carbons of Ph; 132.2–131.6, *o*, *m*-carbons of Ph; *p*-carbons obscured by solvent; chemical shifts and J_{CP} of the (presumed) doublets cannot be assigned), 84.05 (s, CpFe), 23.33 (d, J_{CP} = 4.0 Hz, CH$_2$*CH$_3$*), 16.90 (d, J_{CP} = 28.4 Hz, P*CH$_3$*), −3.48 (d, J_{CP} = 19.7 Hz, *CH$_2$*CH$_3$, assignment confirmed by DEPT-135 NMR) ppm; ^{31}P NMR (C_6D_6) 67.88 ppm. Anal. Calcd for $C_{21}H_{23}OPFe$: C, 66.69; H, 6.13. Found: C, 65.94; H, 6.15.

MeCpFe(CO)(PPh$_2$Me)C$_2$H$_5$ (4b). A mixture of PPh_2Me (1.128 g, 5.63 mmol) and $MeCpFe(CO)_2C_2H_5$ (1.247 g, 5.66 mmol; prepared as described above for $CpFe(CO)_2Et$, in 88% yield as a yellow oil) in 50 mL of hexane was photolyzed as described above for **4a**. The solvent was removed under vacuum and the dark oily product chromatographed on a silica column by elution with benzene to give a yellow, a deep orange, and last a green band. Solvent removal from the deep orange fraction yielded 1.61 g of a deep orange viscous oily residue (**4b** and PPh_2Me) which was treated with 1.5 mL of CH_3I in 5 mL of THF. The exothermic reaction was accompanied by a great deal of bubbling and gave a green solution with a white solid presumed to be $PPh_2Me_2{}^+I^-$. Filtration followed by solvent removal gave a green oily residue that was rechromatographed on silica with benzene. The second fraction (deep orange) was collected and the solvent removed, giving a deep orange viscous oil. The ^1H NMR spectrum in acetone-d_6 showed that the product was slightly contaminated (5% by weight) by $MeCpFe(CO)_2C_2H_5$ (the signals overlap in C_6D_6, but in acetone-d_6 the Me*Cp* signals of $MeCpFe(CO)_2C_2H_5$ at δ 4.75, 4.69 (m, 4H) are well separated from those of **4b**). The product was left under vacuum for 2 days in an only partially successful attempt to remove the $MeCpFe(CO)_2C_2H_5$, giving ~98% pure **4b** in 19% yield: IR (THF) 1890 (s) cm^{-1}; ^1H NMR (C_6D_6) δ 7.43–7.39 (m, 2H), 7.34–7.32 (m, 2H), 7.06–7.01 (m, 6H, Ph), 4.12 (m, 1H), 4.00 (m, 1H), 3.87 (m, 1H), 3.85 (m, 1H, Me*Cp*), 1.80 (s, 3H, *Me*Cp), 1.53 (d, J = 8.9 Hz, and overlapping m, 6H, P*Me* and CH$_2$*CH$_3$*), 1.46–1.42 (m, 1H, C*H*CH$_3$), 0.85–0.78 (m, 1H, C*H*CH$_3$); ^1H NMR (acetone-d_6, 500 MHz) δ 7.60–7.57 (m, 2H), 7.46–7.43 (m, 4H), 7.37–7.35 (m, 4H, Ph), 4.28, 4.22, 4.04, 4.03 (s, 1H each, Me*Cp*), 1.885 (d, J = 8.65 Hz, 3H, P*Me*), 1.876 (s, 3H, *Me*Cp), 1.15 (m, C*HCH$_3$*), 0.46–0.41 (m, C*H*CH$_3$); ^{13}C NMR (C_6D_6) 222.71 (d, J_{CP} = 31.4 Hz, FeCO), 140.98, 140.16, 139.31, 138.62 (ipso carbons of Ph; chemical shifts and J_{CP} of the (presumed) doublets cannot be assigned), 131.80 (d, J_{CP} = 19.6 Hz), 129.20 (d, J_{CP} = 4.3 Hz; *o*, *m*, or *p*-carbons of Ph; remainder of Ph obscured by solvent) 97.42 (s, ipso carbon of MeCp), 86.45 (s), 85.71 (s), 82.93 (s), 80.70 (s, Me*Cp*), 23.29 (s, *CH$_3$*CH$_2$), 17.11 (d, J_{CP} = 29.1 Hz, P*CH$_3$*), 13.07 (s, *Me*Cp), −2.19 (d, J_{CP} = 20.2 Hz, *CH$_2$*CH$_3$, confirmed by DEPT-135 NMR) ppm; ^{31}P NMR (C_6D_6) 67.59 ppm. Anal. Calcd for $C_{22}H_{25}OPFe$: C, 67.36; H, 6.42. Found: C, 65.94; H, 6.26.

CpFe(CO)(PPh$_2$Me)H (5a). In a manner analogous to that reported for the $PPhMe_2$ analog,[9,69] a solution of $CpFe(CO)_2I$ (0.714 g, 2.35 mmol) in 10 mL of ether was added dropwise at room temperature to a suspension of lithium aluminum hydride (1.00 g, 26.35 mmol) in 10 mL of ether. After 15 min, a solution of PPh_2Me (0.464 g, 2.32 mmol) in 2 mL of ether was added dropwise at −20 °C. The mixture was allowed to warm to room temperature after 20 min and then was hydrolyzed with degassed distilled water. The organic layer was dried ($MgSO_4$) and filtered, and the solvent was removed under vacuum at −5 °C, giving 0.513 g of an oily yellowish-green residue. Analysis by ^1H NMR (C_6D_6) showed that the desired product was contaminated by free phosphine. Addition of CH_3I in hexane as carried out for the purification of **4a**,**b** led only to product decomposition. A portion of the residue (184 mg) was subjected to preparative TLC using a mixture of benzene/hexane (3/1) as the eluting solvent, giving **5a** (115 mg) as a yellow oil. Analysis by ^1H NMR indicated the oil to consist only of **5a** and free PPh_2Me in a 1.655:1 molar ratio or 74.3% by weight **5a** (overall yield 29% based on $CpFe(CO)_2I$): ^1H NMR (C_6D_6) δ 7.57–7.32, 7.04 (m, 10 H, Ph), 4.21 (s, 5H, Cp), 1.63 (d, $^2J_{PH}$ = 8.65 Hz, 3H, Me), −13.44 (d,

(69) Davison, A.; McCleverty, J. A.; Wilkinson, G. *J. Chem. Soc.* **1963**, 1133–1138.

$^2J_{PH}$ = 77.0 Hz, 1H, FeH). Anal. Calcd for 74.32% $C_{19}H_{19}OPFe$ and 25.68% $C_{13}H_{13}P$: C, 68.46; H, 5.74. Found: C, 66.36; H, 5.58.

^{1}H NMR Reactions. General Method. In the glovebox, reactants were loaded into an NMR tube that had been sealed to a 14/20 ground glass joint. TMS was added (as an internal NMR integration standard) via microliter syringe, and C_6D_6 was added as the solvent used to transfer the weighed liquid PPh_2Me into the NMR tube. The tube was fitted with a vacuum stopcock, attached to a vacuum line, frozen, and evacuated. The tube was submitted to two freeze–pump–thaw cycles. For the ethylene experiments, a known volume and pressure of ethylene was added via vacuum transfer. The tube was then sealed with a torch. The sample was heated (inverted) in a thermostated constant-temperature water bath. The volume (in mL) used to calculate the concentrations was determined according to the formula $V = \pi(0.213)^2h$, where h is the height in cm of the solution measured immediately after removing the sample from the water bath. The NMR tube was cooled in water immediately after removing from the bath and centrifuged prior to recording each NMR spectrum. All data are collected in Table 1.

Reactions of 2a, 2a-d_5, 2b, 2b-d_5, 2b-^{13}C, 4a,b, and 5a. Kinetic runs of the decomposition of the ethoxycarbynes were analyzed by monitoring the disappearance of (1) the combined *Me*Cp singlets of the cis and trans isomers at δ 1.86 and 1.80 of **2a** (runs 1 and 2), (2) the CH_2 signal at δ 4.71 of **2a** (run 3, 500 MHz), the trans *Cp*Fe singlet at δ 4.49 of **2a**-d_5 (runs 4 and 5), and (3) the cis-*Me*Cp singlet at δ 1.91 of **2b** and **2b**-d_5 (runs 3, 4, 7–10, 12–18), each relative to the TMS resonance. Rate constants for decomposition of **2a** in the presence of **2b**-^{13}C or **2b**-d_5 could not be determined at 200 MHz (runs 11, 14–18) due to the absence of any suitably resolved peaks at this field strength. After the crossover reactions were complete, the NMR tubes were broken open in the glovebox, the solvent was removed under vacuum (in order to remove the ethane formed), and the mixture was chromatographed on a pipet column in benzene. The fast moving orange band (containing the mononuclear alkyls **4** contaminated by PPh_2Me) was collected, the solvent was again removed, and the sample was dissolved in acetone-d_6 for ^{1}H NMR analysis. The only reactions analyzed for **5a**,**b** (by examination of the hydride region of the ^{1}H NMR spectrum) were those conducted near the chronological end of this work; results are noted in Table 1. Chromatography of run 9 (**2b** and **5a**) gave a clean mixture of **4a**,**b**, **5a**,**b**, and PPh_2Me from which the ^{1}H NMR spectrum (C_6D_6) of **5b** could be extracted: δ 4.03 (m, 2H, Me*Cp*), 3.99 (m, 2H, Me*Cp*), 1.80 (s, 3H, *Me*Cp), 1.65 (d, J_{PH} = 8.6 Hz, 3H, PPh_2*Me*), −13.36 (d, J_{PH} = 77.0 Hz, Fe*H*).

Acknowledgment. Financial support for this work from the donors of the Petroleum Research Fund, administered by the American Chemical Society, and NSF Grant No. CHE-9096105 is gratefully acknowledged.

OM950342R

Oxadisilacyclopropane Reactivity with Stilbene Oxides

John E. Mangette,[†] Douglas R. Powell,[†] Joseph C. Calabrese,[‡] and Robert West*,[†]

Department of Chemistry, University of Wisconsin–Madison, Madison, Wisconsin 53706, and DuPont Science and Engineering Laboratory, Experimental Station, Wilmington, Delaware 19880

Received May 9, 1995[⊗]

The reaction of 1,1,2,2-tetramesityl-3-oxa-1,2-disilacyclopropane, **4**, with *cis*-stilbene oxide at 95 °C gave a mixture of products consisting of (a) the *cis/trans* six-membered rings, 1,1,3,3-tetramesityl-5,6-diphenyl-2,4-dioxa-1,3-disilacyclohexanes, **5**, (b) the siloxysilyl enol ether, (*E*)-1,2-diphenyl-1-[(1,1,3,3-tetramesityldisiloxanyl)oxy]ethylene, **E6**, and (c) the products of epoxide deoxygenation, stilbenes and 1,1,3,3-tetramesityl-2,4-dioxa-1,3-disilacyclobutane, **7**. The ratio of **5**:**6**:stilbenes was 9.2 (*trans* to *cis*, 11:1):1:2.1 (*trans* to *cis*, 4.6:1). Under similar conditions, *trans*-stilbene oxide reacted with **4** to give mainly *trans*-stilbene and **7** with comparatively low conversion. The structure of **E6** was supported by an independent synthesis. The five-membered rings, 1,1,3,3-tetramesityl-5-benzhydryl-2,4-dioxa-1,3-disilacyclopentane, **9a**, and 1,1,3,3-tetramesityl-5-benzyl-5-phenyl-2,4-dioxa-1,3-disilacyclopentane, **9b**, were synthesized by two different routes and ruled out as possible structures for ***cis*-5**. A mechanism is proposed to rationalize formation of **5** and **6**.

Introduction

Considering the intriguing reaction chemistry of disilenes,[1] and especially of tetramesityldisilene, **1**, one might expect the mono-oxidation product of **1**, 1,1,2,2-tetramesityl-3-oxa-1,2-disilacyclopropane, **4**,[2] to also show interesting reactivity. However, the only reactions of **4** to be thoroughly studied to date are its oxidation to the corresponding 2,4-dioxa-1,3-disilacyclobutane, **7**, with triplet oxygen[3] and its conversion to a mixture of **7** and a 2,4,5-tioxa-1,3-disilacyclopentane with singlet oxygen.[4]

In a recent publication on the reactions of stilbene oxides with **1** (eq 1), we briefly mentioned a secondary

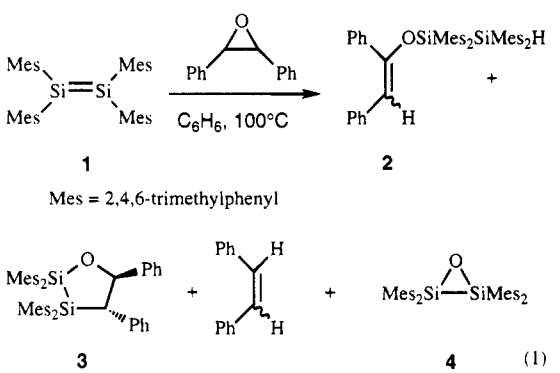

(1)

reaction between **4** and *cis*-stilbene oxide upon extended reaction times.[5] We have investigated this reaction in detail to learn more about the reactivity of **4** and to further illuminate the complex behavior of these silicon compounds toward epoxides. In the process of finding independent syntheses of products, we have also uncovered several new reactions of **4**. All reveal a propensity of the three-membered ring to cleave at the weakest bond of the system, the silicon–silicon single bond, giving products homologous to those from **1**.

Results and Discussion

Reaction of 4 with Stilbene Oxides. At elevated temperatures **4** reacted with *cis*-stilbene oxide to give a complex mixture of products (eq 2). Analogous to the

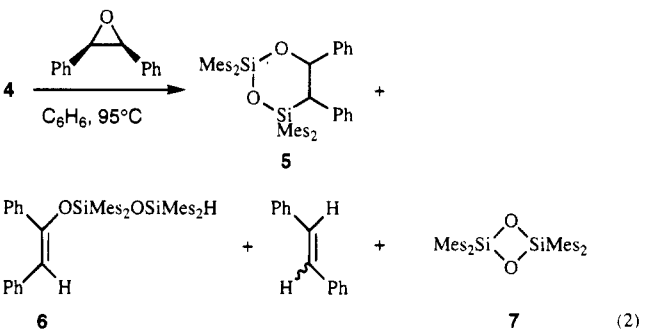

(2)

reaction of **1**, ring compounds, **5**, were produced along with an enol ether, **6**. Stilbenes and the known four-membered ring cyclodisiloxane, **7**,[3,6] were also formed, presumably via oxygen transfer from the epoxide to **4**.

[†] University of Wisconsin.
[‡] Du Pont.
[⊗] Abstract published in *Advance ACS Abstracts,* August 1, 1995.

(1) For reviews on disilene chemistry see: (a) West, R. *Angew. Chem., Int. Ed. Engl.* **1987**, *26*, 1201. (b) Raabe, G.; Michl, J. In *The Chemistry of Organosilicon Compounds*; Patai, S., Rappoport, Z., Eds.; Wiley: New York, 1989; Chapter 17, pp 1015–1044. (c) Weidenbruch, M. *Coord. Chem. Rev.* **1994**, *130*, 275.

(2) (a) Yokelson, H. B.; Millevolte, A. J.; Gillette, G. R.; West, R. *J. Am. Chem. Soc.* **1987**, *109*, 6865. (b) Boatz, J. A.; Gordon, M. S. *J. Phys. Chem.* **1989**, *93*, 3025.

(3) (a) Michalczyk, M. J.; West, R.; Michl, J. *J. Chem. Soc., Chem. Commun.* **1984**, 1525. (b) West, R.; Yokelson, H. B.; Gillette, G. R.; Millevolte, A. J. In *Silicon Chemistry*; Corey, J. Y., Corey, E. R., Gaspar, P. P., Eds.; Ellis Horwood: New York, 1988; Chapter 26, pp 269–281.

(4) (a) Ando, W.; Kako, M.; Akasaka, T.; Kabe, Y. *Tetrahedron Lett.* **1990**, *31*, 4177. (b) Akasaka, T.; Kako, M.; Nagase, S.; Yabe, A.; Ando, W. *J. Am. Chem. Soc.* **1990**, *112*, 7804. (c) Ando, W.; Kako, M.; Akasaka, T.; Nagase, S. *Organometallics* **1993**, *12*, 1514.

(5) Mangette, J. E.; Powell, D. R.; West, R. *Organometallics* **1994**, *13*, 4097.

(6) (a) Fink, M. J.; Haller, K. J.; West, R.; Michl, J. *J. Am. Chem. Soc.* **1984**, *106*, 822. (b) Michalczyk, M. J.; Fink, M. J.; Haller, K. J.; West, R.; Michl, J. *Organometallics* **1986**, *5*, 531. (c) Yokelson, H. B.; Millevolte, A. J.; Adams, B. R.; West, R. *J. Am. Chem. Soc.* **1987**, *109*, 4116.

0276-7333/95/2314-4064$09.00/0

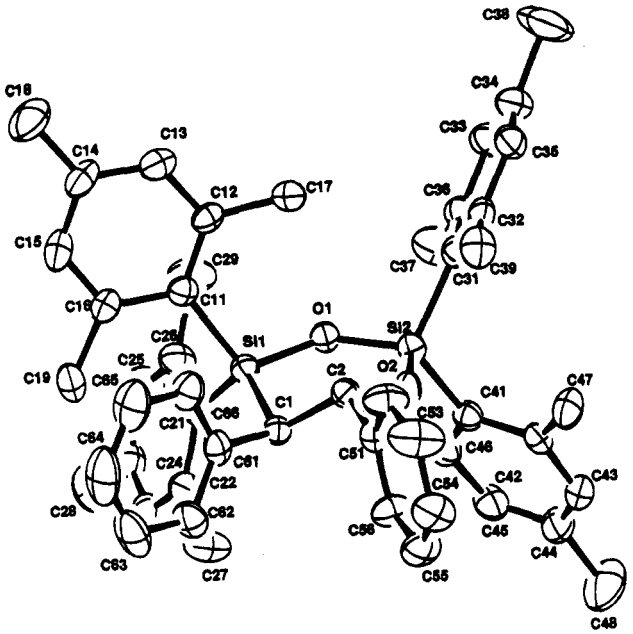

Figure 1. Thermal ellipsoid drawing of ***trans*-5** at the 50% probability level. Bond distances (Å) and angles (deg) of the central ring: Si(1)–O(1), 1.657; O(1)–Si(2), 1.643; Si(2)–O(2), 1.637; O(2)–C(2), 1.444; C(2)–C(1), 1.552; C(1)–Si(1), 1.936; C(1)–Si(1)–O(1), 103.1; Si(1)–O(1)–Si(2), 133.3; O(1)–Si(2)–O(2), 104.0; Si(2)–O(2)–C(2), 127.9; O(2)–C(2)–C(1), 110.7; C(2)–C(1)–Si(1), 109.4

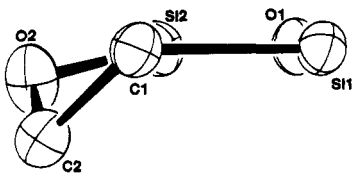

Figure 2. Side view of the central ring of ***trans*-5**.

Compound **7**, being sparingly soluble in benzene at room temperature, crystallized along with unreacted **4** as the original reaction mixture was cooled. The two were identified by ^{29}Si NMR in $CDCl_3$.[6c]

A mixture of **5** and **6** was isolated as the high molecular weight fraction from preparative gel permeation chromatography (GPC) of the crude reaction mixture. The major component, 1,1,3,3-tetramesityl-*trans*-5,6-diphenyl-2,4-dioxa-1,3-disilacyclohexane, ***trans*-5**, was isolated by crystallization from this mixture, and eventually X-ray-quality crystals were obtained. The structure, as shown in Figure 1, is similar to that of **3**.[5] The phenyl groups are *trans* to each other, occupying pseudoequatorial positions. The ring methine protons thus are in a 1,2 *trans* diaxial relationship. The ring has a slightly distorted envelope conformation (Figure 2) with O2 and C2 being 0.291 and 0.861 Å, respectively, to the same side of a plane defined by C1, Si1, O1, and Si2. See Tables 1 and 2.

This orientation is likely the dominant conformation in solution as well. The Karplus relationship[7] predicts a large vicinal coupling constant for a near 180° torsional angle between two protons. Experimental maximum values for $^3J_{trans}$ for various six-membered rings range from 10 to 13 Hz.[7a] The 10.4 Hz $^3J_{H-H}$ between the two methine protons of the central ring of ***trans*-5** (Table 3) is qualitatively consistent with this expectation. Note that the same can be said for ***trans*-3** with a $^3J_{H-H}$ of 11.8 Hz in solution and a torsional angle of 178.5° between the protons in the crystal.

Table 1. Summary of Crystal Data Collection for *trans*-5

empirical formula	$C_{50}H_{56}O_2Si_2$
fw	745.18
cryst syst	triclinic
space group	$P\bar{1}$
a, Å	12.380(1)
b, Å	15.788(1)
c, Å	12.215(1)
α, deg	92.234(5)
β, deg	107.010(4)
γ, deg	68.877(4)
V, Å^3	2123.7
Z	2
d(calcd), g/cm^3	1.163
cryst size, mm^3	0.082 × 0.082 × 0.44
abs coeff, cm^{-1}	1.16
F(000)	800
T, °C	−48
2θ range, deg	2.8–48.3
crystal to plate distance, mm	85.0
no. of frames	60 (two settings)
oscillation range, deg/frame	6.0
exposure, min/frame	4.0
no. of reflns collcd	18 450
no. of indep reflns	4092 (R_{int} = 4.0%)
final R indices (obs data), %	R = 4.5, R_w = 4.0
goodness of fit on F	1.11
largest Δ/σ	0.14
data-to-parameter ratio	5.72
largest diff, e Å^{-3}	0.23

A second compound, isolated in small quantities, was assigned as the *cis* isomer of **5**. It could be separated from ***trans*-5** and **6** by chromatography on silica gel, and the two ring compounds did not interconvert in solution, even at 90 °C. ^{29}Si shifts (Table 3) of −6.57 and −26.00 ppm are almost identical to those of the *trans* isomer at −6.46 and −28.40 ppm. The heterocyclic ^{13}C resonances are also very similar. The methine doublets are slightly shifted from those of ***trans*-5** with a coupling constant of only 1.6 Hz. In comparison to the analogous ^3J of ***trans*-5**, this small coupling constant supports the stereochemical assignment and suggests a torsional angle between the methine protons closer to 90°. This should be expected since, in contrast, a large $^3J_{cis}$ would correspond to a torsional angle approaching 0° between the protons, leading to eclipsing interactions between the *cis* phenyl groups.

The ratio of ***trans*-5** to ***cis*-5** was ca. 11:1 as determined by ^{1}H NMR of the crude reaction mixture.

A third compound, isolated on silica gel (in approximately a 1:1 ratio with ***cis*-5**), was assigned as (*E*)-1,2-diphenyl-1-[(1,1,3,3-tetramesityldisiloxanyl)oxy]ethylene, **E6**. Spectroscopic data (Table 4) indicate a structure similar to **2** with three main differences, all supporting the presence of oxygen between the two silicons: (1) a downfield shift of the Si–*H*, (2) an increase in the one-bond silicon–hydrogen coupling constant,[8] and (3) an increase in the Si–H stretching frequency.[9] In addition, Si(1) in **Z6** is upfield of Si(1)

(7) (a) Bothner-By, A. A. In *Advances in Magnetic Resonance*; Waugh, J. S., Ed.; Academic Press: New York, 1965; Vol. 1, pp 201–207. (b) Jackman, L. M.; Sternhell, S. *Applications of NMR Spectroscopy in Organic Chemistry*; Pergamon: Oxford, England, 1969; pp 280–301.

(8) Marsmann, H. In *NMR Basic Principles and Progress*; Diehl, P., Fluck, E., Kosfeld, R., Eds.; Springer-Verlag: Berlin, 1981; Vol. 17, pp 112–135.

(9) Smith, A. L.; Angelotti, N. C. *Spectrochim. Acta* **1959**, 412.

Table 2. Atomic Coordinates (×10⁴) and Isotropic Thermal Parameters for *trans*-5

atom	*x*	*y*	*z*	B_{iso},[a] Å²
Si(1)	3081.0(7)	3058.2(6)	7139.7(6)	2.1(1)
Si(2)	1461.5(7)	2034.9(6)	7259.6(7)	2.2(1)
O(1)	1791(2)	2920(1)	7039(1)	2.2(1)
O(2)	2737(2)	1170(1)	7427(2)	2.7(1)
C(1)	4288(2)	1852(2)	7654(2)	2.2(1)
C(2)	3770(2)	1130(2)	7075(2)	2.3(1)
C(11)	3171(2)	3405(2)	5708(2)	2.3(1)
C(12)	2407(3)	3309(2)	4625(2)	2.4(1)
C(13)	2497(3)	3619(2)	3623(3)	3.0(1)
C(14)	3344(3)	3997(2)	3609(3)	3.2(1)
C(15)	4112(3)	4061(2)	4654(3)	3.4(1)
C(16)	4040(3)	3791(2)	5696(2)	2.7(1)
C(17)	1493(3)	2863(3)	4507(3)	3.1(1)
C(18)	3432(6)	4315(4)	2499(4)	5.3(2)
C(19)	4928(4)	3918(3)	6779(3)	3.9(1)
C(21)	3005(3)	4052(2)	8071(2)	2.4(1)
C(22)	3749(3)	4027(2)	9209(2)	2.7(1)
C(23)	3578(3)	4816(2)	9793(3)	3.0(1)
C(24)	2687(3)	5637(2)	9334(3)	3.5(1)
C(25)	1940(3)	5665(2)	8234(3)	3.9(1)
C(26)	2080(3)	4899(2)	7599(3)	3.2(1)
C(27)	4708(4)	3161(3)	9832(3)	4.2(1)
C(28)	2489(5)	6462(4)	10035(5)	5.5(2)
C(29)	1163(4)	5034(3)	6416(4)	4.4(2)
C(31)	175(3)	2019(2)	5970(2)	2.5(1)
C(32)	−949(3)	2746(2)	5775(2)	3.0(1)
C(33)	−1919(3)	2811(3)	4801(3)	4.0(1)
C(34)	−1832(3)	2164(3)	4012(3)	4.1(1)
C(35)	−747(3)	1442(3)	4201(3)	3.5(1)
C(36)	267(3)	1352(2)	5159(2)	2.8(1)
C(37)	−1163(4)	3505(3)	6580(4)	4.3(2)
C(38)	−2903(5)	2240(6)	2956(5)	7.1(2)
C(39)	1412(3)	540(3)	5223(3)	3.5(1)
C(41)	1123(2)	1954(2)	8650(2)	2.4(1)
C(42)	1098(3)	1106(2)	8965(2)	2.6(1)
C(43)	944(3)	965(3)	10015(3)	3.4(1)
C(44)	783(3)	1628(3)	10779(3)	3.7(1)
C(45)	774(3)	2463(3)	10468(3)	3.4(1)
C(46)	943(3)	2648(2)	9430(2)	2.8(1)
C(47)	1292(4)	312(3)	8227(3)	3.5(1)
C(48)	645(8)	1433(5)	11926(4)	6.8(3)
C(49)	952(4)	3583(3)	9231(4)	4.0(2)
C(51)	4655(2)	157(2)	7395(2)	2.4(1)
C(52)	4886(3)	−439(2)	6568(3)	3.8(1)
C(53)	5632(4)	−1342(3)	6863(3)	5.0(1)
C(54)	6179(3)	−1656(3)	7991(3)	4.1(1)
C(55)	5977(3)	−1069(2)	8833(3)	3.9(1)
C(56)	5225(3)	−172(2)	8531(3)	3.3(1)
C(61)	5519(3)	1675(2)	7472(3)	2.6(1)
C(62)	6558(3)	1532(2)	8389(3)	3.5(1)
C(63)	7662(3)	1420(3)	8198(4)	4.9(2)
C(64)	7737(4)	1424(3)	7102(5)	5.6(2)
C(65)	6729(4)	1522(3)	6185(4)	4.7(2)
C(66)	5641(3)	1643(2)	6363(3)	3.3(1)

[a] $B_{iso} = (8\pi^2/3)\sum_i\sum_j U_{ij}a_i^*a_j^*\mathbf{a}_i\cdot\mathbf{a}_j$.

in **Z2**, and Si(2) in **Z6** is downfield of Si(2) in **Z2**, consistent with known ^{29}Si trends for increasing oxygen substitution on silicon.[10] The ^{13}C vinyl shifts are also consistent with the given structure.

The low molecular weight GPC fraction contained a mixture of stilbenes and stilbene oxides. ^{1}H NMR showed a 1:4.7 *cis* to *trans* ratio of alkenes.

The combined yield of **5** and **6** was 61.4%, and that of the alkenes was 19.1%. The overall product ratios were also estimated for reactions run in sealed NMR tubes and were found to be 22.8:2.1:2.7:4.6:1 for ***trans*-5**:***cis*-5**:**6**:*trans*-stilbene:*cis*-stilbene, respectively.

(10) Williams, E. A. In *The Chemistry of Organosilicon Compounds*; Patai, S., Rappoport, Z., Eds.; Wiley: New York, 1989; Chapter 8, pp 523–527.

Table 3. Selected NMR Data (ppm) on Five- and Six-Membered Rings

	^{1}H shifts of methylene or methine doublets[a] (^2J or ^3J, Hz)	^{13}C shifts of nonaromatic ring carbons[b]	^{29}Si shifts[a]
***trans*-3**[c]	4.41 (11.8)	50.28	−11.67
	5.81	82.32	1.88
***cis*-3**	4.05 (3.8)	48.25[a]	−0.53
	5.82	80.21	3.81
***trans*-5**	3.91 (10.4)	51.45	−28.40
	5.97	80.16	−6.46
***cis*-5**	3.80 (1.6)	49.73[a]	−26.00
	6.21	77.13	−6.57
9a	4.50 (11.4)	57.38	−14.96
	5.66	71.92	−3.00
9b	3.71 (16.6)	44.34	−15.31
	4.15	83.98	−1.18

[a] In C_6D_6. [b] In $CDCl_3$ except for ***cis*-3** and ***cis*-5**. [c] Reference 5.

Table 4. Comparison of Selected NMR (C_6D_6, ppm) and IR Data for Compounds 2[a] and 6

	vinyl and Si−*H* ^{1}H shifts ($^1J_{Si-H}$, Hz)[b]	vinyl ^{13}C shifts	^{29}Si shifts (*Si*−H in bold)[c]	ν_{Si-H} (cm^{-1})
E2	5.72	112.76	**−56.63**	2133
	5.74 (179.4)	152.40	−4.37	
Z2	5.76	114.60	**−49.29**	2144
	6.05 (181.3)	153.31	1.02	
E6	6.37	112.95	−35.93	2161
	6.47 (217.3)	151.80	**−29.82**	
Z6	5.87	113.38	−36.11	2181
	6.21 (219.7)	151.75	**−30.85**	

[a] Reference 5. [b] Si−*H* assignments made by observation of ^{29}Si satellites in the ^{1}H NMR. [c] *Si*−H assignments made using coupled ^{29}Si spectra.

Scheme 1

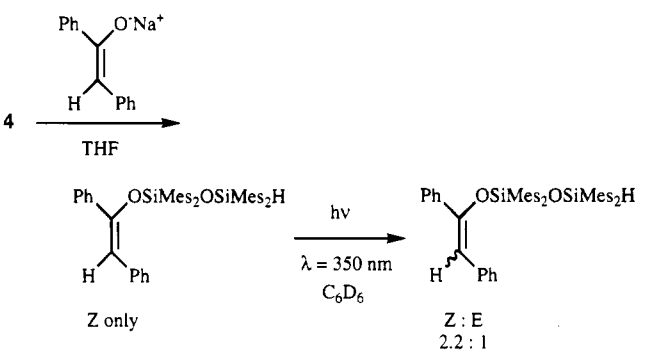

The reaction of **4** with *trans*-stilbene oxide was also studied. However, it was not as efficient or clean. After double the reaction time used for *cis*-stilbene oxide, reaction was, at most, 50% complete. A large amount of solid precipitated (ca. 40 mg, using 100 mg of starting material), mostly unreacted **4**. *Trans*-stilbene was isolated in 20% yield, the hydrolysis product of **4**, $HOSiMes_2OSiMes_2H$, in 18% yield, and ***trans*-5** in only 5% yield. Several small fractions (each ≤5 mg) gave very complex spectra that could not be interpreted as any of the other products from the *cis*-stilbene oxide reaction. A reaction run in a sealed NMR tube confirmed that the primary result was epoxide deoxygenation. The epoxide incorporation products, **5** and **6**, were not formed in detectable amounts.

Independent Synthesis of 6. To further support the assignment of **6**, **4** was treated with the sodium enolate of deoxybenzoin (Scheme 1) to give a compound assigned as **Z6**. The isolated yield was 44% based on **1** (assuming quantitative oxidation to **4**). This general

Scheme 2

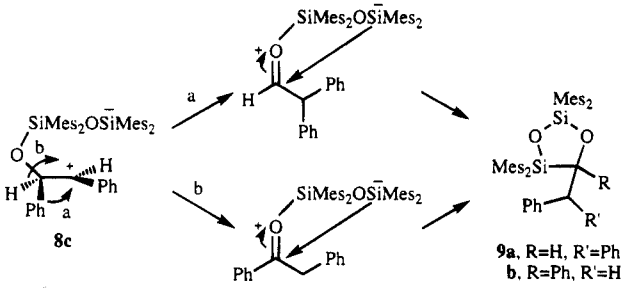

structure would be expected from enolate attack at silicon, followed by silicon–silicon bond cleavage and protonation of the resulting silyl anion.

A comparison of the spectroscopic data of **Z6** to either isomer of **2** paralleled the comparison of **E6** to **2** (Table 4). And, as should be expected for an isomeric pair of stilbene derivatives,[11] a mixture of **Z6** and **E6** was obtained by photolysis of **Z6** in benzene. The photostationary state Z:E ratio of 2.15:1 is similar to the 2.3:1 ratio obtained for the **Z2/E2** system,[5] and provides evidence of structure and stereochemistry of **6**.

Our stereochemical assignment is further supported by the results of Davis and co-workers, who found that the same enolate generated under either thermodynamic or kinetic conditions was quenched by trimethylsilyl chloride to give primarily the (*Z*)-trimethylsilyl enol ether.[12] We, likewise, have found that reaction of the enolate with **1** gave a 7:1 ratio of **Z2**:**E2**. Stereochemical confirmation, reported earlier,[5] was made by single-crystal X-ray analysis of **Z2** isolated from the photostationary state mixture of **2**.

The two isomers of **6** could be quantitatively separated by chromatography on silver nitrate-doped silica gel,[13] and an iterative process of photolysis and $AgNO_3/SiO_2$ chromatography was developed to give practical quantities of **E6**.

Synthesis of Dioxadisilacyclopentanes, 9. In the course of identifying the cyclic products, **5**, and especially the *cis* isomer, compounds **9** were considered as possible structures. These could result from an epoxide ring-opened intermediate with phenyl or hydride migration occurring before a final ring closure (see Scheme 2 and an overall mechanistic proposal in Scheme 4). Such a migration is known for reactions of epoxides with Lewis acids.[14]

A synthesis was accomplished by treatment of **4** with the appropriate carbonyl compound (Scheme 3, top sequence). Isolated yields, based on **1** (assuming quantitative oxidation to **4**), were 35% for **9a** and 52% for **9b**. Alternatively, addition of the carbonyl compound to **1** to give disilaoxetanes, **10**,[15] could be followed by

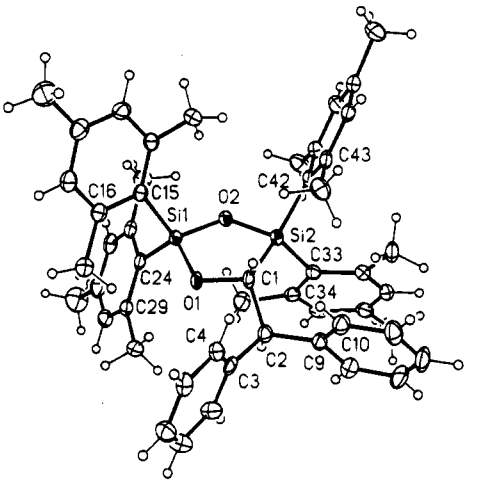

Figure 3. Thermal ellipsoid drawing of **9a** at the 50% probability level. Selected bond distances (Å) and angles (deg): Si(1)–O(2), 1.648; O(2)–Si(2), 1.661; Si(2)–C(1), 1.945; C(1)–O(1), 1.456; O(1)–Si(1), 1.647; C(1)–C(2), 1.533; O(1)–Si(1)–O(2), 99.73; Si(1)–O(2)–Si(2), 117.74; O(2)–Si(2)–C(1), 95.81; Si(2)–C(1)–O(1), 105.12; C(1)–O(1)–Si(1), 118.44.

Scheme 3

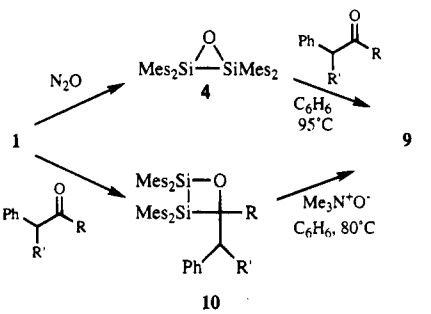

oxidation to **9** with trimethylamine-*N*-oxide (Scheme 3, bottom sequence). Isolated yields were 57% for **10a**, 66% for **10b**, 92% for **9a**, and 96% for **9b** (yields of **9** were based on **10**).

Confirmation of the general structure of **9** was made by single-crystal X-ray analysis of **9a** (Figure 3, Tables 5 and 6).

As can be seen from Table 3, ^1H NMR data eliminates both **9a** and **9b** as possible structures for ***cis*-5**. The methine doublets of **9a** are readily distinguishable from those of the proposed six-membered ring. The methylene protons in **9b** are diastereotopic by virtue of the asymmetric carbon of the central ring. They constitute an AB quartet, and hence the chemical shift difference between them is small compared to the differences between the methine protons in compounds **5** and **9a**.

Re-examination of the Reaction of 1 with Stilbene Oxides. The isolation of ***cis*-5** cast doubt on our previous results that ***trans*-3** was the only five-membered ring formed in the reaction of **1** with stilbene oxides. Reinvestigation has uncovered what we believe to be the *cis* isomer. It was formed only from *cis*-stilbene oxide in an estimated 4% yield. Our previous methods of isolation of compounds **2** and **3**, crystallization and multiple chromatographies, probably depleted and divided the quantities of ***cis*-3**, making detection difficult.

***Cis*-3**, unfortunately, could not be separated from the *trans* isomer. The assignment, therefore, is tentative but reasonable considering the present results. Table

(11) The photochemical behavior of **6** is consistent with known photochemical isomerizations of stilbenes and substituted stilbenes. For further reading see: (a) Saltiel, J.; D'Agostino, J.; Megarity, E. D.; Metts, L.; Neuberger, K. R.; Wrighton, M.; Zafiriou, O. C. In *Organic Photochemistry*; Chapman, O. L., Ed.; Marcel Dekker: New York, 1973; Vol. 3, pp 1–103. (b) Waldeck, D. H. *Chem. Rev.* **1991**, *91*, 415.

(12) Davis, F. A.; Sheppard, A. C.; Chen, B.-C.; Haque, M. S. *J. Am. Chem. Soc.* **1990**, *112*, 6679.

(13) (a) Padley, F. B. In *Thin Layer Chromatography*; Marini-Bettòlo, G. B., Ed.; Elsevier: Amsterdam, 1964; p 90. (b) Nano, G. M.; Martelli, A. *J. Chromatogr.* **1966**, *21*, 349.

(14) For a general overview of acid-catalyzed epoxide rearrangements see: Bartók, M.; Láng, K. L. In *Heterocyclic Compounds*; Hassner, A., Ed.; Wiley: New York, 1985; Vol. 42, Part 3, p 65.

(15) Fanta, A. D.; DeYoung, D. J.; Belzner, J.; West, R. *Organometallics* **1991**, *10*, 3466.

Table 5. Summary of Crystal Data Collection for 9a

empirical formula	$C_{50}H_{56}O_2Si_2$
fw	745.13
cryst syst	triclinic
space group	$P\bar{1}$
a, Å	12.269(2)
b, Å	12.3514(9)
c, Å	15.6528(13)
α, deg	68.132(9)
β, deg	77.155(10)
γ, deg	72.839(7)
V, Å^3	2086.3
Z	2
d(calcd), g/cm^3	1.186
cryst size, mm^3	0.30 × 0.20 × 0.20
abs coeff, mm^{-1}	1.062
F(000)	800
T, °C	−160
2θ range, deg	4.00−114.00
scan type	ω
scan speed, deg/min	variable, 2.00−40.00
scan range (ω), deg	1.00
index ranges	$0 \le h \le 13$, $-12 \le k \le 12$, $-16 \le l \le 17$
no. of reflns collcd	5780
no. of indep reflns	5464 (R_{int} = 2.06%)
final R indices (obsd data), %	R = 4.43, R_w = 11.35
goodness of fit on F^2	1.035
largest Δ/σ	0.006
data-to-parameter ratio	11.2
largest diff, e Å^{-3}	0.399

3 gives ^{1}H and ^{13}C NMR data. The downfield doublet of the minor isomer was obscured by that from ***trans*-3**, making detection of ***cis*-3** even more difficult. But homonuclear decoupling by irradiation of the upfield doublet of the major isomer allowed observation of this "missing" doublet. The vicinal coupling constant of 3.8 Hz again is indicative of a *cis* relationship between the phenyls, particularly when compared to the large coupling constant for the *trans* isomer.

Considering these current findings, the mechanistic conclusions on the reaction of **1** with stilbene oxides, based on our previous results, need only a minor reconsideration. Five-ring formation is still highly stereoselective for *trans* (6:1 *trans* to *cis* ratio), and, since no interconversion of the isomers was observed under the reaction conditions, ***trans*-3** is formed more quickly than ***cis*-3**. The steric interactions to which the rate difference was attributed, as discussed in detail below, are simply not as influential as previously thought.

Mechanistic Proposal. By analogy to the mechanism suggested for the reaction of **1** with stilbene oxides, the pathway shown in Scheme 4 is proposed to give **5** and **6**. Like the disilene **1**, **4** probably behaves as a Lewis acid toward the epoxide as a first step. Ring-opening to **8c** would provide a common intermediate to the observed products and explain the partial loss of the original epoxide stereochemistry. Simple ring-closure from **8** would give **5**, and deprotonation of **8c** would produce **E6**. Products **5** and **Z6** were configurationally stable under the reaction conditions. The observed ratios, therefore, are a reflection of a competition of rates of decay pathways and conformational changes of the intermediate zwitterion.

The high stereoselectivity of the formation of **5** and **6** is best rationalized by unfavorable steric interactions in the transition states leading to the less favored stereoisomers. Specifically, regarding **5**, transannular interactions between one phenyl forced to be pseudo-axial and two mesityl groups *cis* to it would inhibit attainment of the necessary transition state en route to the *cis* isomer. Alternatively, a steric interaction would occur between the two *cis* phenyl groups if, in the transition state, they were required to be nearly eclipsed.

A similar argument can explain the complete stereoselectivity in the generation of **6**. The transition state for deprotonation[16] would involve either a phenyl−phenyl interaction, as in A of Figure 4 to form **E6**, or

Table 6. Atomic Coordinates (×10^4) and Equivalent Isotropic Displacement Coefficients (×10^3) for 9a

atom	x	y	z	U(eq),[a] Å^2
Si(1)	2803(1)	3648(1)	2813(1)	18(1)
Si(2)	2921(1)	6080(1)	1934(1)	17(1)
O(1)	2578(1)	4334(1)	3581(1)	22(1)
O(2)	3126(1)	4724(1)	1861(1)	19(1)
C(1)	2359(2)	5639(2)	3252(2)	20(1)
C(2)	2914(2)	5942(2)	3894(2)	20(1)
C(3)	2524(2)	5308(2)	4915(2)	21(1)
C(4)	1372(2)	5357(2)	5262(2)	23(1)
C(5)	1041(2)	4812(2)	6197(2)	27(1)
C(6)	1862(2)	4198(2)	6800(2)	31(1)
C(7)	3006(2)	4128(3)	6456(2)	37(1)
C(8)	3331(2)	4683(2)	5523(2)	29(1)
C(9)	2725(2)	7281(2)	3707(2)	22(1)
C(10)	1639(2)	8039(2)	3742(2)	25(1)
C(11)	1503(3)	9251(2)	3575(2)	33(1)
C(12)	2454(3)	9720(2)	3388(2)	39(1)
C(13)	3540(3)	8973(2)	3380(2)	38(1)
C(14)	3676(2)	7761(2)	3535(2)	30(1)
C(15)	1424(2)	3221(2)	2891(2)	19(1)
C(16)	1037(2)	2461(2)	3776(2)	21(1)
C(17)	8(2)	2133(2)	3918(2)	25(1)
C(18)	−690(2)	2528(2)	3226(2)	27(1)
C(19)	−318(2)	3266(2)	2364(2)	26(1)
C(20)	717(2)	3618(2)	2179(2)	22(1)
C(21)	1701(2)	1998(2)	4594(2)	28(1)
C(22)	−1821(2)	2181(3)	3429(2)	43(1)
C(23)	1006(2)	4445(2)	1207(2)	31(1)
C(24)	4084(2)	2327(2)	2955(2)	20(1)
C(25)	4436(2)	1847(2)	2216(2)	22(1)
C(26)	5437(2)	954(2)	2214(2)	26(1)
C(27)	6105(2)	475(2)	2931(2)	29(1)
C(28)	5749(2)	923(2)	3658(2)	27(1)
C(29)	4769(2)	1838(2)	3689(2)	22(1)
C(30)	3753(2)	2289(2)	1408(2)	28(1)
C(31)	7184(3)	−509(3)	2908(2)	47(1)
C(32)	4525(2)	2268(2)	4511(2)	29(1)
C(33)	4288(2)	6628(2)	1659(2)	20(1)
C(34)	5380(2)	5828(2)	1752(2)	22(1)
C(35)	6370(2)	6255(2)	1405(2)	26(1)
C(36)	6337(2)	7468(2)	1008(2)	28(1)
C(37)	5267(2)	8258(2)	979(2)	27(1)
C(38)	4249(2)	7873(2)	1283(2)	23(1)
C(39)	5523(2)	4503(2)	2256(2)	29(1)
C(40)	7424(2)	7913(3)	644(2)	44(1)
C(41)	3135(2)	8828(2)	1212(2)	29(1)
C(42)	1954(2)	7051(2)	1008(2)	19(1)
C(43)	823(2)	7735(2)	1140(2)	21(1)
C(44)	200(2)	8375(2)	392(2)	24(1)
C(45)	639(2)	8360(2)	−501(2)	26(1)
C(46)	1752(2)	7693(2)	−629(2)	27(1)
C(47)	2412(2)	7041(2)	97(2)	22(1)
C(48)	245(2)	7802(2)	2081(2)	29(1)
C(49)	−75(3)	9023(2)	−1289(2)	37(1)
C(50)	3601(2)	6330(2)	−151(2)	30(1)

[a] U(eq) = $\frac{1}{3}\sum_i\sum_j U_{ij}\mathbf{a}_i^*\mathbf{a}_j^*\mathbf{a}_i\cdot\mathbf{a}_j$.

(16) Note that the breaking C−H bond is parallel to the empty p-orbital of the cation in the transition state model. This is a proposed alignment necessary for the deprotonation step of an E1 elimination. Kieboom, A. P. G.; Van Bekkum, H. *Recl. Trav. Chim. Pays-Bas* **1969**, *88*, 1424.

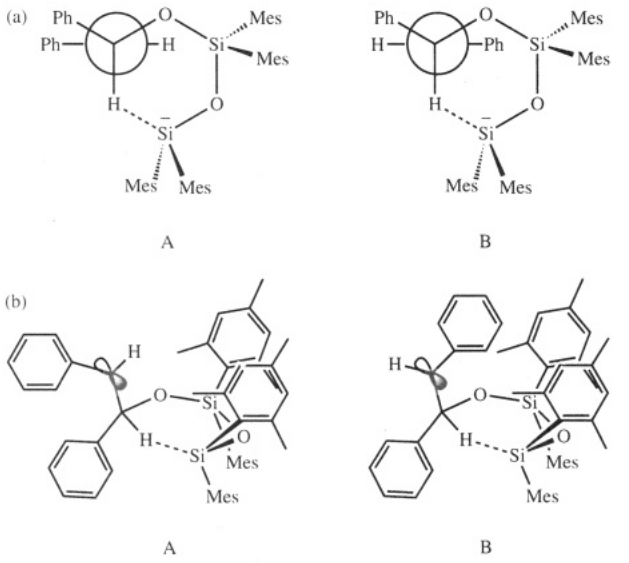

Figure 4. Transition state models for proton abstraction to give **6**: (a) Newman projection and (b) alternate view.

Scheme 4

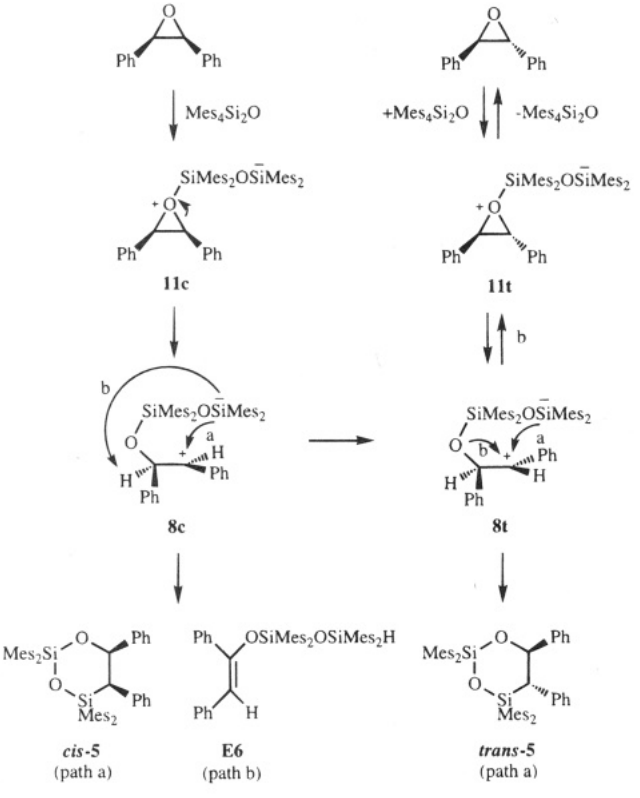

phenyl−mesityl interactions as in B en route to **Z6**. The alternate views (Figure 4b) strongly indicate B to be disfavored.

A comparison of the stereoselectivities of enol ether formation from **1** and **4** with *cis*-stilbene oxide shows a uniformity. The complete stereoselectivity observed for **6** is only a slight enhancement in comparison to **2** where the E isomer was formed with 95% selectivity. In fact, considering that *trans*-stilbene oxide was produced in the reaction mixture of **1**, the minute amount of **Z2** could have come from a parallel reaction of the *trans* epoxide. *Trans*-stilbene oxide was shown to give a mixture of **Z2** and **E2** (1:6 ratio) in its reaction with **1**. So it is possible that both **1** and **4** give enol ethers with complete stereoselectivity from *cis*-stilbene oxide.

As is evident from the reaction times and relative amounts of recovered **4**, *cis*-stilbene oxide reacted faster than *trans*-stilbene oxide. The same phenomenon was observed in the reactions of **1**; complete reaction took 2−3 days for *cis* and 10−14 days for *trans*. Related to this, Groves and co-workers noted a more rapid reaction of *cis* epoxides in their ruthenium(II) porphyrin-catalyzed *cis/trans* isomerizations.[17] They attributed the reactivity difference to an enhanced ability of the bulky porphyrin to coordinate to the epoxide oxygen of the *cis* epoxides which have one relatively unhindered face. They later supported this hypothesis with an X-ray structure of an adduct between styrene oxide and tetra(2,6-dichlorophenyl)porphyrinato(carbonyl)-ruthenium(II) which showed a side-on approach of the Lewis acid toward the epoxide with an anti orientation between the epoxide phenyl group and the porphyrin ring.[18] A similar coordination of **4** to the epoxide, as in **11**, could explain the enhanced reactivity of the *cis* isomer.

A pathway for deoxygenation was omitted from Scheme 4 because several complicating factors come into play. The first is a question of stereospecificity. The presence of *trans*-stilbene oxide in the *cis*-stilbene oxide reaction mixture makes it impossible to distinguish between two theoretically viable pathways: (1) a truly nonstereospecific mechanism such as silyl anion attack on oxygen of the ring-opened intermediate, **8**, or (2) a stereospecific deoxygenation with retention to give *cis*-stilbene from *cis*-stilbene oxide contaminated by *trans*-stilbene similarly generated from *trans*-stilbene oxide.

A second puzzling aspect is the disparity in the ratio of ***trans*-5** to *trans*-stilbene depending on the stereochemistry of the starting epoxide. Even considering the poor mass balance and the low relative reactivity of *trans*-stilbene oxide, we feel the qualitative comparison in the ratios is reliable. The same trend was noted in the reaction of the epoxides with **1** where material balance was much more acceptable. The simplest explanation, consistent with deoxygenation from **8**, is that conformational relaxation in the ring-opened intermediate is not complete before the final steps of the reaction. Under this condition, ***trans*-5** and *trans*-stilbene can still both come from **8**, but their ratio will be dependent on the origin of their common precursor. A second explanation is that ***trans*-5** and *trans*-stilbene do not come from a common intermediate. This allows multiple reasonable possibilities, including (a) a concerted deoxygenation without prior formation of **11** (via a transition state similar to those in alkene epoxidation

(17) Groves, J. T.; Ahn, K.-H.; Quinn, R. *J. Am. Chem. Soc.* **1988**, *110*, 4217.

(18) Groves, J. T.; Han, Y.; Van Engen, D. *J. Chem. Soc., Chem. Commun.* **1990**, 436.

(19) (a) Baumstark, A. L.; McCloskey, C. J. *Tetrahedron Lett.* **1987**, *28*, 3311. (b) Baumstark, A. L.; Vasquez, P. C. *J. Org. Chem.* **1988**, *53*, 3437. (c) Murray, R. W.; Shiang, D. L. *J. Chem. Soc., Perkin Trans. 2* **1990**, 349. (d) Bach, R. D.; Andrés, J. L.; Owensby, A. L.; Schlegel, H. B.; McDouall, J. J. W. *J. Am. Chem. Soc.* **1992**, *114*, 7207.

(20) (a) Davis, F. A.; Billmers, J. M.; Gosciniak, D. J.; Towson, J. C.; Bach, R. D. *J. Org. Chem.* **1986**, *51*, 4240. (b) Bach, R. D.; Wolber, G. J. *J. Am. Chem. Soc.* **1984**, *106*, 1410.

(21) Strictly speaking, such an analogy might seem more valid for a doubly bonded compound such as **1**. However, disilacyclopropane derivatives like **4** have been considered to exhibit double-bond character between the silicons based on structural and calculational results. See: (a) ref 2a. (b) West, R.; DeYoung, D. J.; Haller, K. J. *J. Am. Chem. Soc.* **1985**, *107*, 4942. (c) Grev, R. S.; Schaefer, H. F., III. *J. Am. Chem. Soc.* **1987**, *109*, 6577. (d) Cremer, D.; Gauss, J.; Cremer, E. *J. Mol. Struct. (THEOCHEM)* **1988**, *169*, 531.

with dioxiranes[19] or oxaziridines[20])[21] or (b) a reversal in the order of silyl anion attack on the oxygen and ring-opening from **11**.

Conclusions

Oxadisilacyclopropane, **4**, reacts much like disilene, **1**, giving analogous products, particularly in its reactions with epoxides, carbonyl compounds, and water. The similarity of reaction products with *cis*-stilbene oxide and the conclusions made regarding the reaction of **1** with both stilbene oxides support the proposed pathway for formation of **5** and **6**. However, more experimentation must be carried out to clarify mechanistic details of deoxygenation from **4** and, likewise, from **1** where complications arose regarding the origin of *trans*-stilbene from *cis*-stilbene oxide.

Experimental Section

General Procedures. All solvents for reactions of **4** were distilled from sodium benzophenone ketyl under nitrogen and degassed prior to use. Compound **4** was prepared by oxidation of tetramesityldisilene by the literature method[2a] using hexane as solvent (in place of benzene) and was recrystallized from benzene prior to use in the epoxide reactions. For all other reactions it was used crude. The epoxides were made as described earlier.[5] Chromatography on silica gel, unless otherwise stated, was performed on 20 × 20 cm commercial preparative plates (Whatman 60 Å, 1000 μm thickness). Reported melting points are uncorrected. ^{1}H and ^{13}C spectra were referenced to the residual solvent resonances which were calibrated against tetramethylsilane. All ^{29}Si NMR spectra were referenced to external tetramethylsilane. Data on ***trans*-5**, **10b**, and the *cis/trans* mixture of **3** were obtained by straight acquisition using inverse-gated decoupling in the presence of a relaxation agent, chromium(III) acetylacetonate (5×10^{-2} M).[22] All other ^{29}Si NMR spectra were obtained using INEPT pulse sequences.

Preparative-Scale Reaction of 1,1,2,2-Tetramesityl-3-oxa-1,2-disilacyclopropane, 4, with *cis*-Stilbene Oxide. A mixture of **4**·C_6H_6 (90 mg, 0.14 mmol) and *cis*-stilbene oxide (49 mg, 0.25 mmol, 1.8 eq) in 4 mL of benzene was sealed in a thick-walled glass ampule and heated to 95 °C for 3 days. The tube was cracked open, and 13.5 mg of precipitate was collected by filtration. ^{29}Si NMR ($CDCl_3$, 99.36 MHz) of the solid showed peaks at −3.05 and −26.88 ppm, corresponding to **7**[6c] and **4**,[2a] respectively. The filtrate was concentrated in vacuo, and the residue was separated into two fractions by preparative gel permeation chromatography (GPC). The lower molecular weight fraction (GPC frac 1) contained stilbenes in a *cis* to *trans* ratio of 1:4.7, along with stilbene oxides, while GPC fraction 2 contained ***trans*-5**, ***cis*-5**, and **6** in a ratio of 11:1:1. GPC fraction 1 was rechromatographed on silica gel with 3% diethyl ether in hexanes giving four fractions (from lowest to highest R_f): (1) *cis*-stilbene oxide, 12.6 mg, (2) *trans*-stilbene oxide, 4.9 mg, (3) *trans*-stilbene, 4.2 mg (16.7%), and (4) *cis*-stilbene, 0.6 mg (2.4%). GPC fraction 2 (64 mg, 61.4% combined **5** and **6**) yielded pure ***trans*-5** by crystallization from hexanes. Analytical data were as follows: ^{1}H NMR (C_6D_6, 300 MHz) δ 6.98−6.61 (aromatic multiplets), 6.52 (br s), 5.97 (d, 1 H, J = 10.4 Hz, −OPhC*H*PhCHSi−), 3.91 (d, 1 H, J = 10.4 Hz, −OPhCHPhC*H*Si−), 2.75 (s, 6 H, *o*-Me H), 2.58 (br s, Me H), 2.45 (s, 6 H, *o*-Me H), 2.11, 2.01 (2 s, 6 H each, *p*-Me H); ^{13}C ($CDCl_3$, 125.76 MHz) δ 145.04, 144.82, 144.74, 144.70, 140.01, 139.81, 139.65, 139.51, 139.34, 135.62, 132.70, 132.45, 131.73, 131.22, 129.74, 129.66, 129.36, 127.99, 127.88, 127,-13, 127.11, 125.66, 125.65 (aromatic C), 80.16 (−OPh*C*HPhCHSi−), 51.45 (−OPhCHPh*C*HSi−), 23.82, 23.62, 21.85, 21.81, 21.76, 21.73 (Me C); ^{29}Si NMR (C_6D_6, 99.36 MHz) δ −6.46, −28.40; exact mass for $C_{50}H_{56}O_2Si_2$ calcd *m/e* 744.3819, found 744.3817; mp 302−307 °C (decomp). Several crops of ***trans*-5** were taken, and the mother liquor was concentrated and combined with that from several other runs. Chromatography on silica gel with 1% diethyl ether in hexanes gave three fractions: (1) ***cis*-5**, (2) ***trans*-5**, and (3) **6**. ***Cis*-5** was purified by recrystallization from hexanes. Analytical data were as follows: ^{1}H NMR (C_6D_6, 300 MHz) δ 7.10−6.68 (aromatic multiplets), 6.54 (br s), 6.32 (br s), 6.21 (d, 1 H, J = 1.6 Hz, −OPhC*H*PhCHSi−), 3.80 (d, 1 H, J = 1.6 Hz, −OPhCHPhC*H*Si−), 2.99 (s, 6 H, *o*-Me H), 2.87 (br s, *o*-Me H), 2.60 (br s, *o*-Me H), 2.44 (s, 6 H, *o*-Me H), 2.18 (s, 9 H, Me H), 1.91 (s, 3 H, *p*-Me H), 1.79 (s, 3 H, *p*-Me H); ^{13}C (C_6D_6, 125.76 MHz) δ 146.05, 145.34, 144.38, 140.40, 140.24, 139.75, 138.96, 138.76, 135.47, 133.77, 132.82, 131.26, 130.45, 130.22, 129.70, 128.79, 128.61, 128.41, 127.25, 127.12, 126.28, 126.13 (aromatic C), 77.13 (−OPh*C*HPhCHSi−), 49.73 (−OPhCHPh*C*HSi−), 24.25, 23.78, 23.24, 21.71, 21.57, 21.40, 21.31 (Me C); ^{29}Si NMR (C_6D_6, 99.36 MHz) δ −6.57, −26.00; exact mass for $C_{50}H_{56}O_2Si_2$ calculated *m/e* 744.3819, found 744.3841. The ^{1}H NMR spectrum of **6** matched that from the independent synthesis (see details below).

Preparative-Scale Reaction of 4 with *trans*-Stilbene Oxide. A mixture of **4**·C_6H_6 (100 mg, 0.16 mmol) and *trans*-stilbene oxide (49 mg, 0.25 mmol, 1.56 equiv) in 4 mL of benzene was sealed in a thick-walled glass ampule and heated for 95 °C for 6 days. The tube was cracked open, and 27.4 mg of precipitate was collected by filtration. The tube was rinsed several times with benzene, and the rinsings were added to the original filtrate. Solid, adhered to the inside of the tube, was dissolved in chloroform. This solution was concentrated, and the resulting solid was added to the original precipitate for a total of 39.1 mg of a mixture of **7** and **4** (^{29}Si NMR). The filtrate was concentrated in vacuo, and a low molecular weight fraction (frac 1) containing *trans*-stilbene and *trans*-stilbene oxide was separated from several higher molecular weight products (frac 2) by preparative GPC. GPC fraction 1 was rechromatographed on silica gel with 3% diethyl ether in hexanes to give two fractions: (1) *trans*-stilbene oxide (lower R_f), 24.4 mg, and (2) *trans*-stilbene, 5.8 mg (20.2%). GPC fraction 2 was rechromatographed on silica gel with 3% diethyl ether in hexanes to give two identifiable fractions: (1) $HOSiMes_2OSiMes_2H$, 16.3 mg (18.0%), and (4) ***trans*-5**, 6.5 mg (5.4%). Fractions 2 (5.2 mg), 3 (3.4 mg), and 5 (3.7 mg) gave very complex ^{1}H NMR spectra that could not be interpreted. The ^{1}H NMR spectrum of the hydrolysis product of **4** matched that from an authentic sample (see hydrolysis of 4 described below).

NMR-Scale Reactions of 4 with Stilbene Oxides. A mixture of **4**·C_6H_6 (20 mg, 0.03 mmol) and epoxide (9.4 mg, 0.05 mmol, 1.7 equiv) in ca. 0.75 mL of d_6-benzene was sealed in an NMR tube and heated to 95 °C for 3 days. For the *cis*-stilbene oxide reaction the amounts of *cis*- and *trans*-stilbenes (relative to ***trans*-5**) were estimated by subtraction from their integrations of interfering peaks from **6**. The approximate ratio of ***trans*-5** to ***cis*-5** to **6** to *trans*-stilbene to *cis*-stilbene, averaged over three runs, was 22.8:2.1:2.7:4.6:1. For the *trans*-stilbene oxide reaction, besides comparatively complex mesityl (aromatic and methyl) regions, only *trans*-stilbene and $HOSiMes_2OSiMes_2H$ (Si−*H* peak at δ 6.32) were observed, in a ratio of 3:1.

Variable Temperature NMR of 5. A sealed NMR sample of each isomer of **5** in d_8-toluene was prepared. Spectra were taken at 25, 48, 72, and 93 °C. Neither sample showed contamination of the other isomer at any temperature. Both isomers showed sharpening (and coalescence for ***cis*-5**) of aromatic and methyl peaks which showed broadening at room temperature attributed to hindered rotation.

Synthesis of (*Z*)-1,2-Diphenyl-1-[(1,1,3,3-tetramesityldisiloxanyl)oxy]ethylene, Z6. A solution of deoxybenzoin

(22) Levy, G. C.; Cargioli, J. D.; Juliano, P. C.; Mitchell, T. D. *J. Am. Chem. Soc.* **1973**, *95*, 3445.

(130 mg, 0.66 mmol, 4 equiv) in 2 mL of tetrahydrofuran was added to sodium hydride (18 mg of a 60% dispersion in mineral oil, 10.8 mg, 0.45 mmol, 2.8 equiv) at 25 °C. After the solution had been stirred for 1 h, the clear yellow solution was added to **4** (from oxidation of 100 mg of **1**·THF, 0.16 mmol), and the mixture was stirred for 18 h. Concentration in vacuo gave a yellow-orange residue, which was chromatographed on silica gel with hexanes. The second of three major bands yielded 53 mg (44.5%) of **Z6**. Recrystallization from *n*-hexane gave pure **Z6** as white needles. Analytical data were as follows: ^{1}H NMR (C_6D_6, 500 MHz) δ 7.71 (d, J = 8 Hz, 2 H, *o*-H of α phenyl group), 7.38 (m, 2 H, *o*-H of β phenyl group), 7.05 (dd, J = 8 Hz, 7 Hz, 2 H, *m*-H of α phenyl group), 6.96 (t, J = 7 Hz, 1 H, *p*-H of α phenyl group), 6.88 (m, 3 H, *m*,*p*-H of β phenyl group), 6.66, 6.54 (2 s, 4 H each, Mes H), 6.21 (s, 1 H, Si−*H*), 5.87 (s, 1 H, vinyl H), 2.45, 2.32 (2 s, 12 H each, *o*-Me H), 2.08, 2.03 (2 s, 6 H each, *p*-Me H); ^{13}C (C_6D_6, 75.40 MHz) δ 151.75 (α vinyl C), 145.00, 144.78, 141.16, 139.92, 139.89, 137.11, 132.50, 131.54, 130.02, 129.90, 129.62, 128.06, 127.97, 127.83, 126.81 (aromatic C), 113.38 (β vinyl C), 24.87, 23.49 (*o*-Me C), 21.63, 21.53 (*p*-Me C); ^{29}Si (C_6D_6, 99.36 MHz) δ −30.85 ($^1J_{Si-H}$ = 219.7 Hz), −36.11; exact mass for $C_{50}H_{56}O_2Si_2$ calcd *m/e* 744.3819, found 744.3782; IR (cm^{-1}, Nujol) 2181.4 (Si−H), 1626.9, 1600.8; mp 168−169.5 °C. Anal. Calcd for $C_{50}H_{56}O_2Si_2$: C, 80.59; H, 7.57. Found: C, 80.52; H, 7.55.

Photolysis of Z6. An NMR sample of **Z6** (ca. 30 mg) in d_6-benzene (0.75 mL) was photolyzed, λ = 350 nm, at 25 °C, and the ratio of **Z6** to **E6** was monitred every 15 min by ^{1}H NMR. After 120 min, a photostationary state was reached with Z:E ratio of 2.15:1.

Preparative Photolysis of Z6 and Isolation of (*E*)-1,2-Diphenyl-1-[(1,1,3,3-tetramesityldisiloxyanyl)oxy]-ethylene, E6. A solution of **Z6** (110 mg, 0.15 mmol) in 3 mL of d_6-benzene was photolyzed, λ = 350 nm, in a 10 mm pyrex tube at 25 °C. Periodically, an aliquot was removed, and the Z:E ratio was determined by ^{1}H NMR. After 8 h, the Z:E ratio was 2.45:1. The solution was irradiated for an additional 2 h and was then concentrated in vacuo. Chromatography of the residue on a 10 × 20 cm preparative plate containing 10% w/w silver nitrate in silica gel (MN Kieselgel G/UV 254) gave quantitative separation of the two isomers (E with higher R_f) with 5% diethyl ether in hexanes. The Z isomer was recovered, and the photolysis/separation process was repeated twice to give 40 mg (36.4%) of **E6** as a glassy, noncrystalline solid. The product was further purified by preparative GPC. Analytical data were as follows: ^{1}H NMR (C_6D_6, 300 MHz) δ 7.32 (m, 2 H, phenyl H), 7.00−6.87 (3 m, 8 H, phenyl H), 6.66 (s, 8 H, Mes H), 6.47 (s, 1 H, Si−*H*), 6.37 (s, 1 H, vinyl H), 2.50, 2.45 (2 s, 12 H each, *o*-Me H), 2.07, 2.05 (2 s, 6 H each, *p*-Me H); ^{13}C (C_6D_6, 75.40 MHz) δ 151.80 (α vinyl C), 145.16, 144.95, 140.13, 140.06, 138.41, 137.65, 131.82, 131.24, 130.26, 129.90, 129.57, 128.72, 128.70, 126.26 (aromatic C), 112.95 (β vinyl C), 24.64, 23.34 (*o*-Me C), 21.59, 21.55 (*p*-Me C); ^{29}Si (C_6D_6, 99.36 MHz) δ −29.82 ($^1J_{Si-H}$ = 217.3 Hz), −35.93; exact mass for $C_{50}H_{56}O_2Si_2$ calcd *m/e* 744.3819, found 744.3818; IR (cm^{-1}, Nujol) 2161.1 (Si−H), 1636.5, 1605.6. Anal. Calcd for $C_{50}H_{56}O_2Si_2$: C, 80.59; H, 7.57. Found: C, 80.83; H, 7.90.

Synthesis of 1,2-Diphenyl-1-[(1,1,2,2-tetramesityl-1,2-disilanyl)oxy]Ethylene, 2. A solution of deoxybenzoin (130 mg, 0.66 mmol, 4 equiv) in 2 mL of tetrahydrofuran was added to sodium hydride (20 mg of a 60% dispersion in mineral oil, 12.0 mg, 0.50 mmol, 3.1 equiv) at 25 °C. After it had been stirred for 1 h, the clear yellow solution was added to **1**·THF (100 mg, 0.16 mmol) and the mixture was stirred for 4 h. Concentration in vacuo gave a yellow-orange residue, which was chromatographed on silica gel with 1% diethyl ether in hexanes. Two bands with R_f ca. 0.3 were taken: (1) **10b** (lower R_f) and (2) a mixture of **Z2**, **E2**, and **Z6** in a ratio of 11:1.6:1, 14.8 mg (estimated to contain 13 mg of **2**, 11%).

Hydrolysis of 4. A degassed solution of water (0.5 mL) in 25 mL of tetrahydrofuran was added to **4** (from oxidation of 400 mg of **1**·THF, 0.66 mmol) to give a thick suspension. After the suspension had been stirred for several hours, the resulting clear solution was concentrated in vacuo, and the residue recrystallized from diethyl ether at −25 °C. 1,1,3,3-Tetramesityl-1-hydroxydisiloxane, $HOSiMes_2OSiMes_2H$, was isolated as a white solid. Analytical data were as follows: ^{1}H NMR (C_6D_6, 300 MHz) δ 6.66 (s, 8 H, Mes H), 6.32 (s, 1 H, Si−*H*), 2.42, 2.41 (2 s, 24 H, *o*-Me H), 2.25 (s, 1 H, −O*H*), 2.08 (s, 12 H, *p*-Me H); ^{29}Si (C_6D_6, 99.36 MHz) δ −30.32, −31.36 ($^1J_{Si-H}$ = 214.8 Hz); exact mass for $C_{36}H_{46}O_2Si_2$ calcd *m/e* 566.3036, found 566.3052; IR (cm^{-1}, Nujol) 3675.1, 3608.6, 3409.9 (O−H), 2157.2 (Si−H). The crystals of $HOSiMes_2OSiMes_2H$ retained substantial amounts of solvent, so elemental analysis was not attempted.

Synthesis of 1,1,3,3-Tetramesityl-5-benzhydryl-2,4-dioxa-1,3-disilacyclopentane, 9a, from 4. A mixture of **4** (from oxidation of 200 mg of **1**·THF, 0.33 mmol) and diphenylacetaldehyde (98 mg, 0.50 mmol, 1.5 equiv) in 4 mL of benzene was sealed in a thick-walled glass ampule and heated to 90 °C for 3 days. The tube was cracked open, and the solution was concentrated in vacuo. The residue was chromatographed on silica gel with 1% diethyl ether in hexanes, giving three bands. That with the lowest R_f yielded 87.2 mg (35.5%) of **9a**, which was recrystallized from diethyl ether. Analytical data were as follows: ^{1}H NMR (C_6D_6, 300 MHz) δ 7.44 (m, 2 H, phenyl H), 7.07 (m, 1 H, phenyl H), 6.92−6.80 (m, 6 H, phenyl H), 6.70, 6.66, 6.61, 6.57 (4 s, 2 H each, Mes H), 5.66 (d, 1 H, J = 11.4 Hz, −OC*H*(CHPh$_2$)Si−), 4.50 (d, 1 H, J = 11.4 Hz, −OCH(C*H*Ph$_2$)Si−), 2.52, 2.42, 2.36 (3 s, 6 H each, *o*-Me H), 2.10, 2.08, 2.06 (3 s, 9 H, *p*-Me H), 1.98 (s, 3 H, *p*-Me H), 1.90 (br s, *o*-Me H); ^{13}C ($CDCl_3$, 125.76 MHz) δ 145.72, 145.42, 145.28, 144.88, 143.79, 142.45, 140.16, 139.77, 139.64, 134.71, 131.54, 131.47, 130.80, 130.14, 129.84, 129.63, 129.37, 129.34, 128.86, 128.38, 127.18, 126.19 (aromatic C), 71.92 (−O*C*H(CHPh$_2$)Si−), 57.38 (−OCH(*C*HPh$_2$)Si−), 25.40, 25.09, 23.82, 22.86 (*o*-Me C), 21.91, 21.87, 21.82, 21.80 (*p*-Me C); ^{29}Si (C_6D_6, 99.36 MHz) δ −3.00, −14.96; exact mass for $C_{50}H_{56}O_2Si_2$ calcd *m/e* 744.3819, found 744.3811; mp 280−282 °C.

Synthesis of 1,1,3,3-Tetramesityl-5-benzyl-5-phenyl-2,4-dioxa-1,3-disilacyclopentane, 9b, from 4. A mixture of **4** (from oxidation of 200 mg of **1**·THF, 0.33 mmol) and deoxybenzoin (97 mg, 0.50 mmol, 1.5 equiv) in 2 mL of benzene was sealed in a thick-walled glass ampule and heated to 100 °C for 3 days. The tube was cracked open, and the solution was concentrated in vacuo. The residue was chromatographed on silica gel with 2% diethyl ether in hexanes, giving several bands. That with the second highest R_f yielded 128 mg (52.1%) of **9b**. The product was recrystallized from *n*-hexane. Analytical data were as follows: ^{1}H NMR (C_6D_6, 300 MHz) δ 7.55 (m, 2 H, phenyl H), 7.01 (m, 2 H, phenyl H), 6.94−6.79, 6.76 (m, s, 8 H, phenyl H and Mes H), 6.68, 6.57, 6.46 (3 s, 2 H each, Mes H), 4.15, 3.71 (2 d, 1 H each, J = 16.6 Hz, −OCPh(C*H*$_2$Ph)Si−), 2.74, 2.60, 2.43 (3 s, 6 H each, *o*-Me H), 2.12, 2.11 (2 s, 9H, *p*-Me H and *o*-Me H), 2.05, 2.04 (2 s, 6 H, *p*-Me H), 1.94 (s, 3 H, *p*-Me H); ^{13}C ($CDCl_3$, 125.76 MHz) δ 146.00, 145.13, 144.66, 139.90, 139.83, 139.73, 139.35, 138.51, 133.28, 132.76, 131.97, 130.97, 130.03, 129.66, 129.44, 129.35, 128.18, 127.64, 125.97, 125.59 (aromatic C), 83.98 (−O*C*Ph(CH$_2$Ph)Si−), 44.34 (−OCPh(*C*H$_2$Ph)Si−), 26.29, 24.80, 24.00, 23.75 (*o*-Me C), 21.85, 21.80, 21.56 (*p*-Me C); ^{29}Si (C_6D_6, 99.36 MHz) δ −1.18, −15.31; exact mass for $C_{50}H_{56}O_2Si_2$ calcd *m/e* 744.3819, found 744.3827; mp 273−275 °C. Crystals of **9b** retained small amounts of solvent, so elemental analysis was not attempted.

Synthesis of 1,1,2,2-Tetramesityl-4-benzhydryl-3-oxa-1,2-disilacyclobutane, 10a. A degassed solution of diphenylacetaldehyde (189 mg, 0.96 mmol, 1.1 equiv) in 25 mL of hexanes was added to **1**·THF (530 mg, 0.88 mmol), and the mixture was stirred for 2 h. The resulting pale yellow solution was concentrated in vacuo. Recrystallization of the residue from diethyl ether gave 366 mg (57.1%) of **10a** as a white solid. The product was recrystallized a second time from *n*-hexane. Analytical data were as follows: ^{1}H NMR (C_6D_6, 300 MHz) δ 7.49 (m, 2 H, phenyl H), 7.20 (m, 2 H, phenyl H), 7.05 (m, 1

H, phenyl H), 6.86 (m, 5 H, phenyl H), 6.70, 6.65, 6.57, 6.50 (4 s, 2 H each, Mes H), 6.04 (d, 1 H, J = 12.1 Hz, $-OCH(CHPh_2)$-Si−), 4.46 (d, 1 H, J = 12.1 Hz, $-OCH(CHPh_2)Si-$), 2.58 (s, 6 H, *o*-Me H), 2.42 (br s, *o*-Me H), 2.27 (s, 6 H, *o*-Me H), 2.15 (s, 3 H, *p*-Me H), 2.06, 2.02 (2 s, 15 H, one *o*-Me group and three *p*-Me groups); ^{13}C ($CDCl_3$, 125.76 MHz) δ 146.08, 144.99, 144.59, 144.50, 142.76, 142.33, 139.78, 139.63, 139.10, 138.56, 134.80, 134.22, 133.55, 131.77, 129.83, 129.58, 129.38, 129.23, 129.19, 129.13, 128.80, 128.44, 127.09, 126.20 (aromatic C), 79.67 ($-OCH(CHPh_2)Si-$), 58.53 ($-OCH(CHPh_2)Si-$), 26.52, 25.97, 24.94, 23.22 (*o*-Me C), 21.93, 21.80, 21.69 (*p*-Me C); ^{29}-Si (C_6D_6, 99.36 MHz) δ 19.21, 18.42; exact mass for $C_{50}H_{56}OSi_2$ (M^+ − Mes) calcd *m/e* 609.3009, found 609.2999; mp 250−255 °C. Anal. Calcd for $C_{50}H_{56}OSi_2$: C, 82.36; H, 7.74. Found: C, 81.06; H, 7.82.

Synthesis of 1,1,2,2-Tetramesityl-4-benzyl-4-phenyl-3-oxa-1,2-disilacyclobutane, 10b. A degassed solution of deoxybenzoin (43 mg, 0.22 mmol, 1.8 equiv) in 15 mL of hexanes was added to **1**·THF (75 mg, 0.12 mmol). After 30 min, the solution was concentrated in vacuo, and the residue was chromatographed on silica gel in hexanes. The band with the highest R_f yielded 57.8 mg (66.1%) of **10b**. The product was recrystallized from *n*-hexane. Analytical data were as follows: ^1H NMR (C_6D_6, 300 MHz) δ 7.51 (br s, phenyl H), 7.02−6.76 (multiplets, phenyl H), 6.73, 6.67 (2 s, 6 H, Mes H), 6.52 (s 2 H, Mes H), 3.83 (AB quartet, 2 H, J = 16.8 Hz, $-OCPh(CH_2Ph)Si-$), 2.55, 2.36 (2 br s, Me H), 2.11, 2.08, 2.06, 2.01, 1.97 (5 s, Me H); ^{13}C ($CDCl_3$, 125.76 MHz) δ 148.46, 144.10, 139.98, 139.47, 139.44, 139.28, 138.94, 136.92, 136.80, 136.23, 135.64, 130.92, 129.21, 128.29, 127.86, 125.61, 125.32 (aromatic C), 93.73 ($-OCPh(CH_2Ph)Si-$), 48.21 ($-OCPh(CH_2$-Ph)Si−), 25.64, 21.82, 21.80, 21.56 (Me C); ^{29}Si (C_6D_6, 99.36 MHz) δ 32.17, 24.15; exact mass for $C_{50}H_{56}OSi_2$ calculated *m/e* 728.3870, found 728.3885; mp 261−264 °C. Anal. Calcd for $C_{50}H_{56}OSi_2$: C, 82.36; H, 7.74. Found: C, 81.57; H, 7.96.

Synthesis of 9a from 10a. A mixture of **10a** (142 mg, 0.195 mmol) and trimethylamine-*N*-oxide dihydrate (65 mg, 0.58 mmol, 3 equiv) was refluxed in 10 mL of benzene for 3 h. After the mixture had been cooled and concentrated in vacuo, ^1H NMR showed complete reaction. The residue was redissolved in benzene, and the organic layer was washed with water, dried over magnesium sulfate, filtered, and concentrated to give 133 mg (91.6%) of **9a**.

Synthesis of 9b from 10b. A mixture of **10b** (215 mg, 0.295 mmol) and trimethylamine-*N*-oxide dihydrate (98.2 mg, 0.88 mmol, 3 equiv) was refluxed in 10 mL of benzene for 6 h. After the mixture had been cooled and concentrated in vacuo, ^1H NMR showed the reaction to be ca. 50% complete. Trimethylamine-*N*-oxide dihydrate (50 mg) was again added along with 10 mL of benzene, and the mixture was again refluxed. After an additional 18 h, the reaction was complete. Aqueous workup gave 210 mg (95.6%) of **9b**.

Observation of *cis*-3. A mixture of **1**·THF (20 mg, 0.03 mmol) and *cis*-stilbene oxide (9.8 mg, 0.05 mmol, 1.7 equiv) in ca. 0.75 mL of d_6-benzene was sealed in an NMR tube and heated to 95 °C for 3 days. The ratio of ***trans*-3** to ***cis*-3** was found to be 6:1 by integration of their upfield doublets. A preparative-scale reaction was conducted,[5] and the product mixture was separated into two fractions by preparative GPC. The high molecular weight fraqction containing **2** and **3** was rechromatographed on silica gel with 3% diethyl ether in hexanes. The band with the third highest R_f gave **3** with a *trans* to *cis* ratio of 5:1. A mixture with a 4:1 *trans* to *cis* ratio (used in the isomerization study below) was obtained by removal of a portion of ***trans*-3** from the original mixture of **2** and **3** by recrystallization, followed by silica gel chromatography of the mother liquor. Aromatic and methyl regions of the ^1H and ^{13}C spectra of the mixtures of **3** were complex. Therefore, no assignments were made other than those given in Table 3.

Isomerization Studies. To rule out isomerization of ***cis*-5** and *cis*-stilbene[23] under the reaction conditions, a separate reaction was conducted in the presence of each product using α,α-dideuterio-*cis*-stilbene oxide. Under standard conditions 9.4 mg of epoxide (0.05 mmol, 1.7 equiv), 20 mg of **4**·C_6H_6 (0.03 mmol), 3−5 mg of product, and 2 mg of dimesitylsilane (an internal standard with the Si−*H* peak at 5.29 ppm) in 0.75 mL of d_6-benzene were heated in a sealed NMR tube for 48 h. The integrated ratio of product to dimesitylsilane was observed before and after reaction. Experimental error for ^1H NMR integration was assumed to be 10%. A control experiment showed no reaction between **4** and dimesitylsilane. The percent variation in the ratios were 4% for ***cis*-5** (no ***trans*-5** was observed), and 6% for *cis*-stilbene. An analogous experiment with ***trans*-5** gave a significant increase in the ratio upon reaction, attributed to a small amount of an observable impurity. A similar experiment conducted with α,α-dideuterio-*trans*-stilbene oxide (7-day reaction time) showed a variation in the ratio of dimesitylsilane to ***trans*-5** of 6% (no ***cis*-5** was observed). Samples of pure ***trans*-5**, ***cis*-5**, and **Z6** were also heated separately as d_6-benzene solutions at 95 °C for 2−3 days. All spectra remained unchanged. **Z6** was added to a standard reaction mixture (using nondeuteriated epoxide). Its ratio relative to $HOSiMes_2SiMes_2H$ (a minor impurity in **4**) changed during the course of the reaction by only 7%, again within experimental error.[24]

The reaction of α,α-dideuterio-*cis*-stilbene oxide (9.8 mg, 0.05 mmol, 1.7 equiv) with **1**·THF (20 mg, 0.03 mmol) was carried out in the presence of **3**. After 48 h, an initial 4:1 *trans* to *cis* mixture remained unchanged within experimental error (variation of 9%). A separate experiment showed no significant change of the initial 20:1 ratio of dimesitylsilane to ***cis*-3** with a variation of 9% (***trans*-3** to ***cis*-3** ratio of approx. 9:1).

X-ray Structure Determinations. Crystals of ***trans*-5** were obtained by slow evaporation of an *n*-hexane solution at room temperature. The X-ray crystallographic analysis was based on data collected on a Rigaku RU300 R-AXIS IIc image plate area detector using Mo Kα radiation (λ = 0.710 73 Å) with a graphite monochromator. Lattice constants and errors resulted from a least-squares analysis of the partiality ratios for all reflections. Due to the single rotation axis, data were collected along two settings to complete the Ewald sphere. At a crystal to plate distance of 85.0 mm, a total of 60 frames were collected with an oscillation range of 6.0°/frame and an exposure of 4.0 min/frame. A total of 18 450 data were collected from $2.8° \leq 2\theta \leq 48.3°$. After merging the 5346 duplicates (4.0% R-merge), 4092 unique reflections with $I \geq 3.0\sigma(I)$ remained for the analysis. The structure was solved by direct methods (MULTAN) and consists of one molecule in a general position. Hydrogen atoms were idealized from positions obtained from a difference map. The atom parameters were refined by full-matrix least-squares on F, with scattering factors from ref 28 including anomalous terms for silicon. All non-hydrogen atoms were successfully refined anisotropically, and all hydrogen atoms were refined isotropically, although several hydrogens showed high thermal motion. The final refinement cycle included 711 parameters, with a data/parameter ratio = 5.72, and resulted in R = 0.045 and R_w = 0.040 with an error of fit of 1.11. The max shift/error was 0.14, and the largest residual density on the final difference map was 0.23 e/Å^3, near C18.

X-ray crystallographic analysis on **9a** was performed on a Siemens P4 diffractometer equipped with a graphite crystal monochromator and a Cu X-ray tube (λ = 1.541 78 Å). Suitable crystals were grown by slow evaporation from diethyl ether at 25 °C. The orientation matrix and unit cell parameters were determined by the least-squares fitting of 37

(23) The catalyzed thermal equilibration of stilbene at 90 °C gave a *trans* to *cis* ratio of 250:1: Fischer, G.; Muszkat, K. A.; Fischer, E. *J. Chem. Soc. B* **1968**, 1156. It is therefore assumed that, if catalyzed isomerization were occurring under the present reaction conditions, only the *cis* to *trans* conversion would be observable by ^1H NMR.

(24) The stereospecific formation of **6** rules out an E to Z catalyzed isomerization under the reaction conditions.

centered reflections ($19° < \theta < 55°$). Intensities of three standard reflections were monitored every 100 reflections with a maximum variation of 0.07. A total of 5780 reflections were collected, of which 5464 were unique. The structure was solved using the SHELXS-86 program,[25] and the non-hydrogen atoms were refined anisotropically using the SHELXS-93 program[26] by full-matrix least-squares analysis on F^2. The applied weighting scheme was $w^{-1} = \sigma^2(F_o^2) + (0.0540P)^2 + 1.8300P$, where $P = (F_o^2 + 2F_c^2)/3$.[26] An extinction correction was applied with $F_c^* = kF_c[1 + 0.001\chi F_c^2\lambda^3/\sin(2\theta)]^{-1/4}$, where $\chi = 0.0030(2)$.[27] The positions of the hydrogen atoms were calculated by idealized geometry and refined using a riding model. The hydrogens on the *para*-methyl carbons were modeled with two sets of sites having equal occupancies. The final refinement cycle included 488 parameters, with a data/parameter ratio of 11.2, and resulted in $R = 0.0443$ and $R_w = 0.1135$ ($I > 2\sigma(I)$) with an error of fit of 1.035. The max shift/error was 0.006, and the largest residual density was 0.399 e/Å^3. Neutral atom scattering factors were taken from ref 28.

Acknowledgment. This research was supported by a grant from the National Science Foundation. Funding for X-ray instruments and computers was provided by the National Science Foundation (Grant No. CHE-9105497) and the University of Wisconson.

Supporting Information Available: Tables of all bond distances and angles, anisotropic displacement coefficients, and H atom coordinates and isotropic displacement coefficients (19 pages). This material is contained in many libraries on microfiche, immediately follows this article in the microfilm version of the journal, and can be ordered from the ACS; see any current masthead page for ordering information.

OM950334A

(25) Sheldrick, G. M. *Acta Crystallogr.* **1990**, *A46*, 467.
(26) Sheldrick, G. M. Manuscript in preparation.
(27) Larsen, A. C. In *Crystallographic Computing*; Ahmed, F. K., Ed.; Munksgaard: Copenhagen, 1970; pp 219–294.
(28) *International Tables for X-ray Crystallography*; Kynoch Press: Birmingham, England, 1992; Vol. C, Tables 6.1.1.4, 4.2.6.8, and 4.2.4.2 (present distributors Kluwer Academic Publishers: Boston).

Synthesis and Characterization of New Phosphine-Substituted (Fulvalene)dimolybdenum Carbonyl Hydrides and Halides

István Kovács† and Michael C. Baird*

Department of Chemistry, Queen's University, Kingston, Ontario, Canada K7L 3N6

Received February 10, 1995®

A number of (fulvalene)dimolybdenum carbonyl dihydrides and dihalides of the general formula $FvMo_2(CO)_4L_2X_2$ (X = H, L = CO (**1a**), PPh_3 (**1b**), PMe_3 (**1c**); X = Cl, L = CO (**2a**), PPh_3 (**2b**), PCy_3 (Cy = cyclohexyl; **2c**), PXy_3 (Xy = 3,5-dimethylphenyl; **2d**); X = Br, L = CO (**3a**), PPh_3 (**3b**), PCy_3 (**3c**), PXy_3 (**3d**), PMe_3 (**3e**); X = I, L = CO (**4a**), PPh_3 (**4b**)) have been synthesized and characterized by IR and ^1H, $^{13}C\{^1H\}$, and $^{31}P\{^1H\}$ NMR spectroscopy and, where possible, by elemental analyses. Spectroscopic data suggest that **2b–d** and **3b–e** exist solely as *cis,cis* isomers in solution. *cis,cis*-**4b** was also identified but was found to easily transform into a mixture of *cis,cis*, *cis,trans*, and *trans,trans* isomers. Such an interconversion of **1b** is fast on the NMR time scale at room temperature. The radical chain halogenation of **1a,b** by activated alkyl halides was found to take place in two distinct steps, involving the intermediate formation of $FvMo_2(CO)_4L_2HX$ (L = CO, X = Cl (**5a**), Br (**6a**), I (**7a**); L = PPh_3, X = Cl (**5b**), Br (**6b**), I (**7b**)). By stepwise addition of different alkyl halides, the hydrido–halo complexes **5a**, **6a**, and **7a** were transformed into the mixed dihalides $FvMo_2(CO)_6XY$ (X, Y = Cl, Br (**8**), Cl, I (**9**), and Br, I (**10**)). Mixed dihalides were formed alternatively in halide redistribution reactions between pairs of **2a**, **3a**, and **4a**.

Introduction

There is currently considerable interest in the preparation and characterization of 17-electron organotransition-metal compounds (metal-centered radicals).[1a,b] This class of compounds may be synthesized in a variety of ways[1] and may often be stabilized with respect to dimerization to the 18-electron metal–metal-bonded analogues by substitution of small ligands by more sterically demanding ligands (e.g. CO by tertiary phosphines, η^5-C_5H_5 by η^5-C_5Me_5 and η^5-C_5Ph_5). In general, it has been found that there is a correlation between the proclivity of an 18-electron dimer to undergo thermal homolysis to the corresponding 17-electron species and the length of the metal–metal bond. Thus, the chromium–chromium bond of $[(\eta^5\text{-}C_5H_5)Cr(CO)_3]_2$, which dissociates to the extent of a few percent in solution at room temperature,[1c,d] is much longer (3.281 Å)[1e] than the metal–metal bond of the analogous, much more homolytically stable molybdenum compound (3.235 Å)[1f] but much shorter than the chromium–chromium bonds of $[(\eta^5\text{-}C_5H_5)Cr(CO)_2P(OMe)_3]_2$ (3.343 Å)[1g] and $[(\eta^5\text{-}C_5Me_5)Cr(CO)_3]_2$ (3.311 Å),[1d] both of which dissociate much more extensively in solution.[1d,g] Consistent with the apparent role of steric effects on the extent of homolysis, the compounds $(\eta^5\text{-}C_5H_5)Cr(CO)_2PPh_3$[1h,i] and $(\eta^5\text{-}C_5Ph_5)Cr(CO)_3$[1j] are completely monomeric in solution and the solid state.

It was of considerable interest, therefore, to note that the metal–metal bonds of the fulvalene compounds (η^5:η^5-$C_{10}H_8$)$M_2(CO)_6$ (**A**; M = Cr, Mo, W)[2b] are extraordinarily long, *i.e.* 3.471, 3.371, and 3.347 Å,[2c,f,g,u] respectively, suggesting significant strain. In addition, each compound contains a fulvalene (Fv) ligand bent from planarity as in **A**, also suggestive of strain in these

† NATO Science Fellow; Research Group for Petrochemistry of the Hungarian Academy of Sciences, Veszprém, Hungary.

® Abstract published in *Advance ACS Abstracts,* August 1, 1995.

(1) (a) Baird, M. C. *Chem. Rev.* **1988**, *88*, 1217 and references therein. (b) Baird, M. C. In *Organometallic Radical Processes*; Trogler, W. C., Ed.; J. Organomet. Chem. Libr. 22; Elsevier: New York, 1990; p 49, and references therein. (c) McLain, S. J. *J. Am. Chem. Soc.* **1988**, *110*, 643. (d) Watkins, W. C.; Jaeger, T.; Kidd, C. E.; Fortier, S.; Baird, M. C.; Kiss, G.; Roper, G. C.; Hoff, C. D. *J. Am. Chem. Soc.* **1992**, *114*, 907. (e) Adams, R. D.; Collins, D. E.; Cotton, F. A. *J. Am. Chem. Soc.* **1974**, *96*, 749. (f) Adams, R. D.; Collins, D. E.; Cotton, F. A. *Inorg. Chem.* **1974**, *13*, 1086. (g) Goh, L.-Y.; D'Aniello, M. J.; Slater, S.; Muetterties, E. L.; Tavanaiepour, I.; Chang, M. I.; Frederich, M. F.; Day, V. W. *Inorg. Chem.* **1979**, *18*, 192. (h) Cooley, N. A.; Watson, K. A.; Fortier, S.; Baird, M. C. *Organometallics* **1986**, *5*, 2563. (i) Fortier, S.; Baird, M. C.; Preston, K. F.; Morton, J. R.; Ziegler, T.; Jaeger, T. J.; Watkins, W. C.; MacNeil, J. H.; Watson, K. A.; Hensel, K.; Le Page, Y.; Charland, J.-P.; Williams, A. J. *J. Am. Chem. Soc.* **1991**, *113*, 542. (j) Hoobler, R. J.; Hutton, M. A.; Dillard, M. M.; Castellani, M. P.; Rheingold, A. L.; Rieger, A. L.; Rieger, P. H.; Richards, T. C.; Geiger, W. E. *Organometallics* **1993**, *12*, 116.

(2) (a) Smart, J. C.; Curtis, C. J. *Inorg. Chem.* **1977**, *16*, 1788. (b) Vollhardt, K. P. C.; Weidman, T. W. *Organometallics* **1984**, *3*, 82. (c) Abrahamson, H. B.; Heeg, M. J. *Inorg. Chem.* **1984**, *23*, 2281. (d) Drage, J. S.; Tilset, M.; Vollhardt, K. P. C.; Weidman, T. W. *Organometallics* **1984**, *3*, 812. (e) Tilset, M.; Vollhardt, K. P. C. *Organometallics* **1985**, *4*, 2230. (f) Drage, J. S.; Vollhardt, K. P. C. *Organometallics* **1986**, *5*, 280. (g) Moulton, R.; Weidman, T. W.; Vollhardt, K. P. C.; Bard, A. J. *Inorg. Chem.* **1986**, *25*, 1846. (h) Meyerhoff, D. J.; Nunlist, R.; Tilset, M.; Vollhardt, K. P. C. *Magn. Reson. Chem.* **1986**, *24*, 709. (i) Huffman, M. A.; Newman, D. A.; Tilset, M.; Tolman, W. B.; Vollhardt, K. P. C. *Organometallics* **1986**, *5*, 1926. (j) Boese, R.; Myrabo, R. L.; Newman, D. A.; Vollhardt, K. P. C. *Angew. Chem., Int. Ed. Engl.* **1990**, *29*, 549. (k) Kahn, A. P.; Newman, D. A.; Vollhardt, K. P. C. *Synlett* **1990**, 141. (l) Boese, R.; Huffman, M. A.; Vollhardt, K. P. C. *Angew. Chem., Int. Ed. Engl.* **1991**, *30*, 1463. (m) Delville-Desbois, M.-H.; Brown, D. S.; Vollhardt, K. P. C.; Astruc, D. *J. Chem. Soc., Chem. Commun.* **1991**, 1355. (n) Brown, D.; Delville-Desbois, M.-H.; Vollhardt, K. P. C.; Astruc, D. *New J. Chem.* **1992**, *16*, 899. (o) El Amouri, H.; Vaissermann, J.; Besace, Y.; Vollhardt, K. P. C.; Ball, G. E. *Organometallics* **1993**, *12*, 605. (p) Kreiter, C. G.; Conrad, W.; Exner, R. *Z. Naturforsch.* **1993**, *48B*, 1635. (q) Kreiter, C. G.; Conrad, W. *Z. Naturforsch.* **1994**, *49B*, 383. (r) Brown, D. S.; Delville-Desbois, M.-H.; Boese, R.; Vollhardt, K. P. C.; Astruc, D. *Angew. Chem., Int. Ed. Engl.* **1994**, *33*, 661. (s) Kahn, A. P.; Boese, R.; Blümel, J.; Vollhardt, K. P. C. *J. Organomet. Chem.* **1994**, *472*, 149. (t) Tilset, M.; Vollhardt, K. P. C.; Boese, R. *Organometallics* **1994**, *13*, 3146. (u) The chemistry of (fulvalene)metal carbonyl complexes has also been reviewed recently: McGovern, P. A.; Vollhardt, K. P. C. *Synlett* **1990**, 493.

0276-7333/95/2314-4074$09.00/0

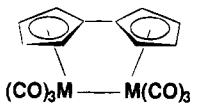

A

compounds. Interestingly, however, crystal structure data for the substituted derivative $FvMo_2(CO)_4(PMe_3)_2$ show that substitution by this relatively small phosphine, at least, results in a shorter and presumably stronger Mo–Mo bond than exists in $FvMo_2(CO)_6$ despite severe twisting and bending of the fulvalene ligand from planarity.[2t,3] Thus, the fulvalene system is much more complex than would be expected on the basis of the above-mentioned putative correlation between the extent of CO substitution and metal–metal bond lengths.

Nevertheless, although no evidence that this class of compounds can exist as isomers not containing metal–metal bonds (biradicals) has been reported,[2u] it seemed possible either that biradical species might be synthesized by alternative routes or that they might be detectable as reactive intermediates. It therefore seemed important to further probe the structures and chemistry of derivatives containing phosphines of greater steric demand and different electronic parameters, and in view of the relative abundance of available data on fulvalene compounds of the group VI metals,[2] particularly of molybdenum, we have begun with an investigation of derivatives of $FvMo_2(CO)_6$.

Unfortunately, direct substitutions of the carbonyl ligands of $FvMo_2(CO)_6$ with tertiary phosphines do not generally occur.[2f,t,u] Furthermore, with very few exceptions (none involving molybdenum), no fulvalene complexes are known with ligands larger than the relatively small PMe_3, suggesting that the preparation and study of compounds of the type $FvMo_2(CO)_4L_2$ (L = bulky ligand) might be difficult.

A potential route to biradicals, not heretofore attempted, could involve abstraction of hydrogen atoms from substituted hydrides of the type $FvMo_2(CO)_4L_2H_2$, as in eq 1. This approach has been extensively utilized

$$FvMo_2(CO)_4L_2H_2 + 2^{\bullet}CPh_3 \rightarrow FvMo_2(CO)_4L_2 + 2HCPh_3 \quad (1)$$

for the syntheses of simple 17-electron compounds[4] and has been shown to be of general utility. Furthermore, since the starting dihydride compounds would assume the *anti* conformation **B** established for several non-metal–metal-bonded fulvalene complexes by X-ray crystallography,[2i,r,s,t] the diradical products would presumably assume the same conformation initially and might well have difficulty coupling if L is a sufficiently bulky ligand.

Of course, utilization of the chemistry of eq 1 requires the availability of the substituted hydrides, $FvMo_2(CO)_4L_2H_2$; unfortunately, we find that direct substitution of $FvMo_2(CO)_6H_2$ is not possible with ligands larger than PPh_3. Halo compounds of the type $FvMo_2(CO)_4L_2X_2$ do undergo such substitutions, however, and these should be reducible, either directly to the desired $FvMo_2(CO)_4L_2$ or indirectly to the dianions $[FvMo_2(CO)_4L_2]^{2-}$, which should undergo protonation to the hydrides. We have therefore synthesized a series of dihydrides and dihalides of the type $FvMo_2(CO)_4L_2X_2$ (**C**: L = CO, PPh_3, PCy_3, PXy_3; X^1, X^2 = H, Cl, Br, I)

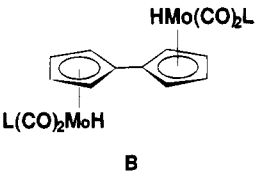

B

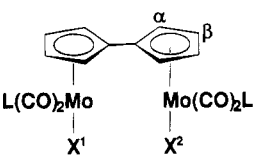

C

(Ph = phenyl, Cy = cyclohexyl, Xy = 3,5-dimethylphenyl), and we describe here the syntheses and properties of these compounds. Some have been reported previously but not fully characterized, but the vast majority are new. In a paper to follow,[5] we shall describe utilization of these compounds to form metal–metal-bonded analogues and our attempts to detect radical-like properties. The compounds discussed here are listed in Table 1.

Experimental Section

General Considerations. All manipulations were carried out under purified nitrogen by using standard Schlenk techniques and a Vacuum Atmospheres glovebox. All solvents were freshly distilled under nitrogen from sodium benzophenone ketyl (hexane, benzene, toluene, ether, and THF) or CaH_2 (CH_2Cl_2). Deuterated solvents were purchased from Isotec, Inc., and were degassed and stored in the glovebox. Tertiary phosphines (PMe_3 from Aldrich, PPh_3 from Strem, PCy_3 from Organometallics, Inc., PXy_3 from M&T) and other chemicals were used without further purification. Column chromatography was performed with a 1.5 × 20 cm column packed with silica gel 60 (70–230 mesh, EM Science) using hexane–CH_2Cl_2 mixtures and ultimately CH_2Cl_2 as eluant. IR spectra were recorded on a Bruker IFS-25 FT-IR spectrometer and NMR spectra on Bruker AC-200 (200.1 MHz, ^1H; 50.32 MHz, $^{13}C\{^1H\}$), CXP-200 (80.98 MHz, $^{31}P\{^1H\}$), and AM-400 (400.1 MHz, ^1H; 100.6 MHz, $^{13}C\{^1H\}$; 162.0 MHz, $^{31}P\{^1H\}$) NMR spectrometers. IR and ^1H, $^{13}C\{^1H\}$, and $^{31}P\{^1H\}$ NMR data are given in Tables 2–6. Elemental analyses were carried out by Canadian Microanalytical Services Ltd. (Delta, BC, Canada).

Preparation of $(NEt_4)_2[FvMo_2(CO)_6]$ and Hexane Solutions of $FvMo_2(CO)_6H_2$ (1a). The following procedure is a modification of that of Smart and Curtis.[2a] A solution of 5.4 g (30 mmol) of CpNa(DME)[2a] in 100 mL of THF, cooled to −78 °C, was treated dropwise with 20 mL of a THF solution of 3.8 g (30 mmol) I_2 over ~1.5 h. At this point, 15 mL of a 2.0 M hexane solution of BuLi (30 mmol) was added dropwise (~20 min) to give a pink reaction mixture, which was warmed to room temperature and then stirred for an additional 1 h, resulting in the formation of a fine, white solid. The mixture was transferred to a flask containing 7.9 g (30 mmol) of Mo-

(3) Kretchmar, S. A.; Cass, M. E.; Turowski, P. N. *Acta Crystallogr.* **1987**, *C43*, 435.

(4) (a) Ungváry, F.; Markó, L. *J. Organomet. Chem.* **1980**, *193*, 383. (b) Turaki, N. N.; Huggins, J. M. *Organometallics* **1986**, *5*, 1703. (c) Edidin, R. T.; Hennessy, K. M.; Moody, A. E.; Okrasinski, S. J.; Norton, J. R. *New J. Chem.* **1988**, *12*, 475. (d) Drake, P. R.; Baird, M. C. *J. Organomet. Chem.* **1989**, *363*, 131. (e) Eisenberg, D. C.; Lawrie, C. J. D.; Moody, A. E.; Norton, J. R. *J. Am. Chem. Soc.* **1991**, *113*, 4888. (f) Koeslag, M. D.; Baird, M. C. *Organometallics* **1994**, *13*, 11. (g) Kuksis, I.; Baird, M. C. *Organometallics* **1994**, *13*, 1551.

(5) Kovács, I.; Baird, M. C. *Organometallics* **1995**, *14*, 4084.

Table 1. Compounds of Type C Prepared in This Paper

compd	X^1	X^2	L	compd	X^1	X^2	L
1a	H	H	CO	**4a**	I	I	CO
1b	H	H	PPh_3	**4b**	I	I	PPh_3
1c	H	H	PMe_3	**5a**	H	Cl	CO
2a	Cl	Cl	CO	**5b**	H	Cl	PPh_3
2b	Cl	Cl	PPh_3	**6a**	H	Br	CO
2c	Cl	Cl	PCy_3	**6b**	H	Br	PPh_3
2d	Cl	Cl	PXy_3	**7a**	H	I	CO
3a	Br	Br	CO	**7b**	H	I	PPh_3
3b	Br	Br	PPh_3	**8**	Cl	Br	CO
3c	Br	Br	PCy_3	**9**	Cl	I	CO
3d	Br	Br	PXy_3	**10**	Br	I	CO
3e	Br	Br	PMe_3				

Table 2. Carbonyl Stretching Frequencies

compd	ν_{CO} (cm^{-1})[a]
$FvMo_2(CO)_6H_2$ (**1a**)	2027 (s), 1949 (vs)[b,c]
$FvMo_2(CO)_6Cl$ (**2a**)	2047 (s), 1976 (vs, br)[d]
$FvMo_2(CO)_6Br_2$ (**3a**)	2043 (s), 1970 (vs, br)[d]
$FvMo_2(CO)_6I_2$ (**4a**)	2035 (s), 1964 (vs, br)[d]
$FvMo_2(CO)_6HI$ (**7a**)	2034 (m), 2015 (m), 1962 (vs), 1930 (s)[d]
$FvMo_2(CO)_4(PPh_3)_2H_2$ (**1b**)	1936 (vs), 1858 (vs)
$FvMo_2(CO)_4(PMe_3)_2H_2$ (**1c**)	1928 (vs), 1846 (vs)[e]
cis,cis-$FvMo_2(CO)_4(PPh_3)_2Cl_2$ (**2b**)	1968 (vs), 1883 (m, br)
cis,cis-$FvMo_2(CO)_4(PCy_3)_2Cl_2$ (**2c**)	1951 (vs), 1871 (m)
cis,cis-$FvMo_2(CO)_4(PXy_3)_2Cl_2$ (**2d**)	1966 (vs), 1882 (m, br)
cis,cis-$FvMo_2(CO)_4(PPh_3)_2Br_2$ (**3b**)	1970 (vs), 1890 (m, br)
cis,cis-$FvMo_2(CO)_4(PCy_3)_2Br_2$ (**3c**)	1955 (vs), 1873 (m)
cis,cis-$FvMo_2(CO)_4(PXy_3)_2Br_2$ (**3d**)	1965 (vs), 1882 (m)
cis,cis-$FvMo_2(CO)_4(PMe_3)_2Br_2$ (**3e**)	1965 (vs), 1868 (m, br)
cis,cis-$FvMo_2(CO)_4(PPh_3)_2I_2$ (**4b**)	1965 (vs), 1887 (s)

[a] In CH_2Cl_2, unless denoted otherwise. [b] In hexane. [c] Lit.:[2f] 2020, 1929, 1902 cm^{-1} in THF. [d] In THF. [e] Lit.:[2t] 1922, 1840 cm^{-1} in THF.

Table 3. ^1H NMR Data for (Fulvalene)dimolybdenum Hexacarbonyl Complexes

compd	δ (ppm)[a] η^5:η^5-$C_{10}H_8$	δ (ppm)[a] Mo*H*
$FvMo_2(CO)_6H_2$ (**1a**)	4.50 ("t", 4 H), 4.85 ("t", 4 H)	−5.298 (s, 2 H)
$FvMo_2(CO)_6Cl_2$ (**2a**)	4.24 ("t", 4 H), 4.91 ("t", 4 H)	
$FvMo_2(CO)_6Br_2$ (**3a**)	4.27 ("t", 4 H), 4.86 ("t", 4 H)	
$FvMo_2(CO)_6I_2$ (**4a**)	4.32 ("t", 4 H), 4.80 ("t", 4 H)	
$FvMo_2(CO)_6HCl$ (**5a**)	4.24 ("t", 2 H), 4.61 ("t", 2 H), 4.82 ("t", 2 H), 4.93 ("t", 2 H)	−5.30 (s, 1 H)[b]
$FvMo_2(CO)_6HBr$ (**6a**)	4.28 ("t", 2 H), 4.58 ("t", 2 H), 4.73 ("t", 2 H), 4.89 ("t", 2 H)	−5.305 (s, 1 H)
$FvMo_2(CO)_6HI$ (**7a**)	4.36 ("t", 2 H), 4.55 ("t", 2 H), 4.69 ("t", 2 H), 4.88 ("t", 2 H)	−5.314 (s, 1 H)
$FvMo_2(CO)_6ClBr$ (**8**)	4.23 ("t", 2 H), 4.30 ("t", 2 H), 4.85 ("t", 2 H), 4.91 ("t", 2 H)	
$FvMo_2(CO)_6ClI$ (**9**)	4.19 ("t", 2 H), 4.37 ("t", 2 H), 4.81 ("t", 2 H), 4.90 ("t", 2 H)	
$FvMo_2(CO)_6BrI$ (**10**)	4.26 ("t", 2 H), 4.36 ("t", 2 H), 4.82 ("t", 2 H), 4.85 ("t", 2 H)	

[a] In toluene-d_8 (200 MHz). [b] Almost identical with **1a**.

$(CO)_6$ and 6.3 g (30 mmol) of Et_4NBr. The reaction mixture was refluxed for 5 h, after which gas evolution had ceased and IR spectra showed no further changes, although some unreacted $Mo(CO)_6$ was still present. After the mixture was cooled to room temperature, 100 mL of hexane was added to precipitate a solid mixed with a red oil. The solution was decanted, and the solid material was dried *in vacuo*. The resulting sticky substance was washed thoroughly with several 50 mL portions of ether until colorless washings were obtained. The remaining tan solid was then vacuum-dried again to give 14−19 g of impure, air-sensitive $(Et_4N)_2[FvMo_2(CO)_6]$. The salt was extracted with THF and reprecipitated with hexane to give a light yellow powder which was characterized on the basis of comparisons with spectroscopic data from the literature. IR (THF): ν_{CO} 1892 (vs), 1795 (vs), 1744 (m, br) cm^{-1}.

Table 4. $^{31}P\{^1H\}$ NMR Data for Phosphine-Substituted (Fulvalene)dimolybdenum Carbonyl Complexes

compd	δ (ppm)[a]
$FvMo_2(CO)_4(PPh_3)_2H_2$ (**1b**)	73.3 (br)
$FvMo_2(CO)_4(PPh_3)_2H_2$ (**1b**)[b]	71.90 (sh, *trans,trans*), 71.98 (*cis,trans*), 73.64 (*cis,cis*), 73.69 (sh, *cis,trans*)
cis,cis-$FvMo_2(CO)_4(PPh_3)_2Cl_2$ (**2b**)	50.34, 50.49
cis,cis-$FvMo_2(CO)_4(PPh_3)_2Cl_2$ (**2b**)[c]	49.9
cis,cis-$FvMo_2(CO)_4(PCy_3)_2Cl_2$ (**2c**)[c]	49.92, 50.02
cis,cis-$FvMo_2(CO)_4(PXy_3)_2Cl_2$ (**2d**)[c]	47.59, 47.84
cis,cis-$FvMo_2(CO)_4(PPh_3)_2Br_2$ (**3b**)[c]	47.8
cis,cis-$FvMo_2(CO)_4(PPh_3)_2Br_2$ (**3b**)[d]	47.90, 48.04
cis,cis-$FvMo_2(CO)_4(PCy_3)_2Br_2$ (**3c**)[c]	47.89, 48.00
cis,cis-$FvMo_2(CO)_4(PXy_3)_2Br_2$ (**3d**)[c]	45.68, 45.82
cis,cis-$FvMo_2(CO)_4(PPh_3)_2I_2$ (**4b**)	45.7, 45.8
cis,trans-**4b**	46.0 (*cis*), 67.0 (*trans*)
trans,trans-**4b**	67.3
$FvMo_2(CO)_4(PPh_3)_2HCl$ (**5b**)	50.5, 72.9 (br)
$FvMo_2(CO)_4(PPh_3)_2HBr$ (**6b**)	48.6, 72.9
$FvMo_2(CO)_4(PPh_3)_2HI$ (**7b**)	45.9 (*cis* iodide), 67.8 (*trans* iodide), 73.2 (br, hydride)

[a] In toluene-d_8 unless denoted otherwise. Relative to 85% H_3PO_4. [b] At −70 °C. [c] In $CDCl_3$. [d] At −23 °C.

^1H NMR (acetone-d_6): δ 1.37 (tt, J_1 = 7.2 Hz, J_2 = 1.8 Hz, 24H, Me), 3.45 (q, J = 7.2 Hz, 16H, CH_2N), 4.73 ("t", 4H, Fv), 5.22 ("t", 4H, Fv). $^{13}C\{^1H\}$ NMR (acetone-d_6): δ 84.5, 86.6 (Fv), 106.8 (Fv C-1), 237.2 (CO). The IR and ^1H NMR data well agree with those reported for $M_2[FvMo_2(CO)_6]$ (M = Li, Na).[2f] For the Li salt: IR (THF) ν_{CO} 1900, 1806, 1782, 1716 cm^{-1}; ^1H NMR (THF-d_8) δ 4.76 (m), 5.21 (m). For the Na salt: IR (THF) ν_{CO} 1890, 1790, 1740 cm^{-1}.

To synthesize the hydride, typically 2.0 g of the crude material were suspended in 80 mL of hexane and 0.5 mL of glacial acetic acid was injected at room temperature. After the mixture was stirred for 1 h, a red solid settled and the yellowish solution of **1a** was separated. The unstable hydride was not isolated but was characterized spectroscopically (see Tables 2 and 3 for IR and ^1H NMR data, respectively). $^{13}C\{^1H\}$ NMR (benzene-d_6): δ 88.2, 89.5 (Fv), 105.3 (Fv C-1), 227.0 (CO). On the basis of amounts of substituted (**1b,c**), halogenated (**2a, 3a, 4a**), and decomposition ($FvMo_2(CO)_6$) products, which were obtained during subsequent reactions of **1a**, **1a** was generally obtained in yields of ~50% based on $Mo(CO)_6$. Essentially the same result was obtained when trifluoroacetic acid was used for protonation.

$FvMo_2(CO)_4(PPh_3)_2H_2$ (1b). A solution of **1a** in 80 mL of hexane was added to 1.2 g (4.6 mmol) of PPh_3 dissolved in 10 mL of ether. A precipitate formed within a few minutes, but stirring was continued overnight at room temperature to complete the reaction. Solid **1b** separated, and the hexane solution, which contained no **1a** at this point (IR), was removed by syringe. The product was washed with 3 × 10 mL of hexane and dried *in vacuo*. Yield: 0.70 g (0.73 mmol, 47% based on $Mo(CO)_6$). Anal. Calcd for $C_{50}H_{40}Mo_2O_4P_2$: C, 62.64; H, 4.21. Found: C, 61.81; H, 4.21. ^1H NMR (CD_2Cl_2): δ −5.35 (d, J_{PH} = 48.4 Hz, 2H, Mo*H*), 4.93 ("t", 4H, Fv), 5.18 ("t", 4H, Fv), 7.35 (m, 30H, Ph). $^{13}C\{^1H\}$ NMR (CD_2Cl_2): δ 133.3 (d, J_{PC} = 11.3 Hz, *o*-Ph), 130.0 (d, J_{PC} = 2.3 Hz, *p*-Ph), 128.5 (d, J_{PC} = 9.6 Hz, *m*-Ph), 89.8 (s, Fv), 88.4 (s, Fv).

Complex **1b** is a light yellow, thermally stable powder, which is poorly soluble in aromatic hydrocarbons and $CHCl_3$ but soluble in THF and CH_2Cl_2. When it is heated to 110 °C in a toluene solution, it completely decomposes within 2 days to an unidentified carbonyl-containing product.

$FvMo_2(CO)_4(PMe_3)_2H_2$ (1c). Substitution of **1a** with PMe_3 was carried out as described for **1b**, in a modification of a recent published procedure.[2t] Into a 20 mL hexane solution of **1a** was injected 60 μL (0.58 mmol) of PMe_3, and the mixture

Table 5. Selected ^1H NMR Data for Phosphine-Substituted (Fulvalene)dimolybdenum Carbonyl Hydrides and Halides

compd	δ (ppm)[a] η^5:η^5-$C_{10}H_8$	Mo*H*
$FvMo_2(CO)_4(PPh_3)_2H_2$ (**1b**)	4.63 ("t", 4 H), 5.01 ("t", 4 H)	−5.03 (d, J_{PH} = 52 Hz, 2 H)
$FvMo_2(CO)_4(PPh_3)_2H_2$ (**1b**)[b]	4.24 (m), 4.35 (m), 4.40 (m), 4.45 (m), 4.56 (m), 4.61 (m), 4.68 (m), 4.75 (m), 4.91 (m), 4.98 (m), 5.07 (m), 5.15 (m)	−4.99 (d, J_{PH} = 65 Hz), −5.02 (d, J_{PH} = 21 Hz), −5.05 (d, J_{PH} = 21 Hz), −5.06 (d, J_{PH} = 65 Hz), −5.66 (s, br, 2 H)
$FvMo_2(CO)_4(PMe_3)_2H_2$ (**1c**)[c]	4.67 (s, br, 4 H), 5.03 (s, br, 4 H)	
cis,cis-$FvMo_2(CO)_4(PPh_3)_2Cl_2$ (**2b**)	4.40 (m, 2 H), 4.65 (m, 1 H), 4.77 (m, 1 H), 4.99 (m, 1 H), 5.14 (m, 1 H), 5.46 (m, 1 H), 5.54 (m, 1 H)	
cis,cis-$FvMo_2(CO)_4(PPh_3)_2Cl_2$ (**2b**)[d]	4.88 (m, 1 H), 4.96 (m, 1 H), 5.11 (m, 1 H), 5.17 (m, 1 H), 5.28 (m, 1 H), 5.32 (m, 1 H), 5.70 (m, 1 H), 5.75 (m, 1 H)	
cis,cis-$FvMo_2(CO)_4(PCy_3)_2Cl_2$ (**2c**)[d]	4.85 (m, 1 H), 4.95 (m, 1 H), 5.20 (m, 1 H), 5.28 (m, 1 H), 5.30 (m, 1 H), 5.34 (m, 1 H), 5.89 (m, 1 H), 5.94 (m, 1 H)	
cis,cis-$FvMo_2(CO)_4(PXy_3)_2Cl_2$ (**2d**)[d]	4.77 (m, 1 H), 4.88 (m, 1 H), 5.03 (m, 1 H), 5.13 (m, 1 H), 5.20 (m, 2 H), 5.63 (m, 1 H), 5.67 (m, 1 H)	
cis,cis-$FvMo_2(CO)_4(PPh_3)_2Br_2$ (**3b**)	4.36 (m, 2 H), 4.70 (m, 1 H), 4.81 (m, 1H), 4.87 (m, 1H), 5.12 (m, 1 H), 5.51 (m, 1 H), 5.64 (m, 1 H)	
cis,cis-$FvMo_2(CO)_4(PCy_3)_2Br_2$ (**3c**)	4.41 (m, 1 H), 4.45 (m, 1 H), 4.89 (m, 2 H), 5.05 (m, 1 H), 5.20 (m, 1 H), 5.69 (m, 1 H), 5.85 (m, 1 H)	
cis,cis-$FvMo_2(CO)_4(PXy_3)_2Br_2$ (**3d**)	4.49 (m, 1 H), 4.52 (m, 1 H), 4.93 (m, 1 H), 4.98 (m, 2 H), 5.14 (m, 1 H), 5.66 (m, 1 H), 5.77 (m, 1 H)	
cis,cis-$FvMo_2(CO)_4(PMe_3)_2Br_2$ (**3e**)	4.41 (m, 2 H), 4.58 (m, 1 H), 4.83 (m, 1 H), 4.95 (m, 1 H), 5.07 (m, 1 H), 5.18 (m, 1 H), 5.29 (m, 1 H)	
cis,cis-$FvMo_2(CO)_4(PPh_3)_2I_2$ (**4b**)	4.28 (m, 1 H), 4.33 (m, 1 H), 4.72 (m, 1 H), 4.81 (m, 1 H), 4.85 (m, 1 H), 5.06 (m, 1 H), 5.52 (m, 1 H), 5.79 (m, 1 H)	
$FvMo_2(CO)_4(PPh_3)_2HCl$ (**5b**)	4.40 (m, 2 H), 4.51 (m, 1 H), 4.71 (m, 1 H), 5.07 (m, 1 H), 5.13 (m, 2 H), 5.26 (m, 1 H)	−4.99 (d, J_{PH} = 52 Hz, 1 H)
$FvMo_2(CO)_4(PPh_3)_2HBr$ (**6b**)	4.41 (m, 1 H), 4.60 (m, 1 H), 4.64 (m, 1 H), 4.70 (m, 1 H), 4.94 (m, 1 H), 5.12 (m, 1 H), 5.21 (m, 1 H), 5.32 (m, 1 H)	−4.98 (d, J_{PH} = 52 Hz, 1 H)
$FvMo_2(CO)_4(PPh_3)_2HI$ (**7b**)		−4.99 (d, J_{PH} = 52 Hz), −5.01 (d, J_{PH} = 52 Hz)

[a] In toluene-d_8 and at 25 °C unless noted otherwise. [b] At −65 °C. [c] In C_6D_6. [d] In $CDCl_3$.

Table 6. $^{13}C\{^1H\}$ NMR Data for (Fulvalene)dimolybdenum Carbonyl Complexes in the Fulvalene Carbon Region

compd	δ (ppm)
$(Et_4N)_2[FvMo_2(CO)_6]$[a]	106.8 (C-1), 86.6, 84.5
$FvMo_2(CO)_6H_2$ (**1a**)[b]	105.3 (C-1), 89.5, 88.2
$FvMo_2(CO)_6Cl_2$ (**2a**)[a]	115.2 (C-1), 96.1, 91.7
$FvMo_2(CO)_6Br_2$ (**3a**)[a]	113.3 (C-1), 95.7, 92.1
$FvMo_2(CO)_6I_2$ (**4a**)[a]	110.7 (C-1), 94.8, 92.6
$FvMo_2(CO)_4(PPh_3)_2H_2$ (**1b**)[c]	89.8 (br), 88.4
cis,cis-$FvMo_2(CO)_4(PPh_3)_2Cl_2$ (**2b**)[d]	111.6 (C-1), 110.6 (C-1), 100.7, 98.6, 95.3, 93.4, 89.1, 87.3, 85.09, 85.06
cis,cis-$FvMo_2(CO)_4(PPh_3)_2Br_2$ (**3b**)[d]	109.9 (C-1), 108.6 (C-1), 100.4, 98.9, 95.7, 93.8, 88.7, 87.2, 84.50, 84.47
cis,cis-$FvMo_2(CO)_4(PCy_3)_2Cl_2$ (**2c**)[d]	112.3 (C-1), 111.5 (C-1), 101.7, 100.2, 94.1, 91.6, 86.1 (d, $J \approx 3$ Hz), 85.0 (d, $J \approx 3$ Hz), 83.7, 83.5
cis,cis-$FvMo_2(CO)_4(PCy_3)_2Br_2$ (**3c**)[d]	110.6 (C-1), 109.5 (C-1), 101.3, 100.0, 94.1, 91.8, 86.0 (d, $J \approx 3$ Hz), 84.9 (d, $J \approx 3$ Hz), 83.1 (d, $J \approx 5$ Hz), 82.9 (d, $J \approx 5$ Hz)
cis,cis-$FvMo_2(CO)_4(PXy_3)_2Br_2$ (**3d**)[d]	110.7 (C-1), 109.2 (C-1), 99.8, 98.9, 95.5, 93.8, 88.2, 87.0, 84.7, 84.3

[a] In acetone-d_6. [b] In C_6D_6. [c] In CD_2Cl_2; no C-1 (bridgehead) carbon resonance was observed. [d] In $CDCl_3$.

was stirred overnight at room temperature. A fine yellow precipitate settled from the solution, which did not contain unreacted **1a** by this time (IR). The solvent was decanted, and the solid was washed with 3 × 10 mL of hexane and dried *in vacuo*. Yield: 0.16 g (0.27 mmol, 33% based on $Mo(CO)_6$). The product was identified by IR and ^1H NMR spectroscopy.[2t] ^1H NMR (C_6D_6): δ −5.66 (br s, 2H, Mo*H*), 1.00 (d, J_{PH} = 9.0 Hz, 18H, PMe), 4.67 (br s, 4H, Fv), 5.05 (br s, 4H, Fv).

Complex **1c** is a light yellow, thermally stable powder which is soluble in many solvents. When heated to 110 °C in toluene, complete decomposition to a carbonyl-containing product occurred in 2 days, similar to the case for **1b**.

$FvMo_2(CO)_6X_2$ (X = Cl (2a), Br (3a), I (4a)). These compounds were obtained by hydrogen−halogen exchange reactions of **1a** with activated alkyl halides. In typical syntheses of **2a**, **3a**, or **4a**, a standard solution of **1a** (~0.78 mmol) in 80 mL of hexane was treated with 5 mL of CCl_4 (52 mmol), 4 mL of $CHBr_3$ (46 mmol), or 1 mL of ICH_2CO_2Et (8.5 mmol), respectively, at room temperature. Red, crystalline solids appeared within a few minutes, but stirring was continued overnight in each case. Since the products still contained some hydrido−halide intermediates (see below) at this point, spectroscopically pure samples were obtained by partially dissolving the crude products in 2 mL of CH_2Cl_2 and adding an extra 2 mL of CCl_4 or $CHBr_3$ or 1 mL of ICH_2CO_2-Et. After 1 day, products were precipitated by the addition of 5 mL of hexane, the solvents were decanted, and the remaining solids were washed with 3 × 5 mL of hexane and vacuum-dried. **2a**: yield 0.42 g (0.76 mmol, 49% based on $Mo(CO)_6$); ^1H NMR (acetone-d_6) δ 5.71 ("t", 4H, Fv), 6.29 ("t", 4H, Fv); $^{13}C\{^1H\}$ NMR (acetone-d_6) δ 242.5 (s, CO trans to Cl), 225.9 (s, CO cis to Cl), 115.2 (s, C-1 Fv), 96.1 (s, Fv), 91.7 (s, Fv). **3a**: yield 0.40 g (0.62 mmol, 40%); ^1H NMR (acetone-d_6) δ 5.76 ("t", 4H, Fv), 6.29 ("t", 4H, Fv); $^{13}C\{^1H\}$ NMR (acetone-d_6) δ 240.2 (s, CO trans to Br), 224.3 (s, CO cis to Br), 113.3 (s, C-1 Fv), 95.7 (s, Fv), 92.1 (s, Fv). **4a**: yield 0.54 g (0.72 mmol, 47%); ^1H NMR (acetone-d_6) δ 5.82 ("t", 4H, Fv), 6.31 ("t", 4H, Fv); $^{13}C\{^1H\}$ NMR (acetone-d_6) δ 237.7 (s, CO trans to I), 222.5 (s, CO cis to I), 110.7 (s, C-1 Fv), 94.8 (s, Fv), 92.6 (s, Fv). IR and further ^1H NMR spectroscopic data of **2a**, **3a**, and **4a** are compiled in Tables 2 and 3, respectively.

Complexes **2a** and **4a** are brick red, while **3a** is deep purple. All are poorly soluble in aromatic and chlorinated hydrocarbons but soluble in THF and acetone; solubilities decrease in the order **2a** > **3a** > **4a** (Cl > Br > I). All are air-sensitive in solution and in the solid state and readily decompose with gas evolution on heating in a toluene solution to 100 °C. None could be obtained analytically pure.

$FvMo_2(CO)_4L_2HX$ (L = CO, X = Cl (5a), Br (6a), I (7a); L = PPh_3, X = Cl (5b), Br (6b), I (7b)). These hydrido

halides were detected and characterized by ^{1}H NMR spectroscopy (Tables 3 and 5) as intermediates in hydrogen–halogen exchange reactions of **1a**,**b** with CCl_4, $CHBr_3$, and ICH_2CO_2Et in toluene-d_8 solutions. Attempts to isolate **5a**, **6a**, and **7a** resulted only in the formation of mixtures of the hydrido halides, the corresponding dihalide, and **1a** (^{1}H NMR). While the mixtures could not be separated by column chromatography because of hydride and/or halide ligand redistribution reactions, they could be enriched in the hydrido–halide complexes using the following process.

With hexane solutions of **1a** and CCl_4, $CHBr_3$, or ICH_2CO_2Et as starting materials, as described above for the synthesis of $FvMo_2(CO)_6X_2$, the initially formed red precipitates were separated after ~30 min by removing the supernatant liquid (which contained no **1a**). The solids were washed with 3 × 5 mL portions of hexane and dried *in vacuo*. When the crude products were dissolved in $CDCl_3$ or toluene-d_8 for NMR studies, it was found that most of the dihalo species were of low solubility and samples containing up to 80% pure **5a**, **6a**, or **7a** were obtained.

$FvMo_2(CO)_6XY$ (X, Y = Cl, Br (8), Cl, I (9), Br, I (10)). Method A. To the enriched toluene-d_8 solutions of **6a** and **7a**, prepared as described above, was added 10 μL of CCl_4 or $CHBr_3$ at room temperature. The reactions were monitored by ^{1}H NMR spectroscopy, and the consumption of the hydride halides as well as the formation of the corresponding mixed dihalides were unambiguously established after several hours. For spectroscopic data, see Table 3.

Method B. All three mixed dihalides were also identified by ^{1}H NMR spectroscopy as products of halide ligand redistribution reactions between pairs of the homodihalides; *e.g.*, complex **8** formed from **2a** and **3a** and **9** from **2a** and **4a**, as well as **10** from **3a** and **4a**. The reactions were carried out on NMR-scale samples in toluene-d_8 or acetone-d_6 at room temperature, and mixtures of the products and starting dihalides were obtained in 1 day.

$FvMo_2(CO)_4(PPh_3)_2X_2$ (X = Cl (2b), Br (3b), I (4b)). Method A. A slurry of **2a** (0.14 g, 0.25 mmol) and PPh_3 (0.13 g, 0.50 mmol) in 10 mL of toluene was heated in an oil bath at ~110 °C, resulting in dissolution of the solid, vigorous gas evolution, and a color change to deep red. Gas evolution stopped after ~10 min, and the solution was cooled to room temperature to give a red precipitate, which was a mixture of **2b** and $FvMo_2(CO)_6$ (IR, ^{1}H NMR). These two compounds exhibit considerably different solubilities in toluene, and analytically pure **2b** was obtained as the *cis,cis* isomer by extracting the $FvMo_2(CO)_6$ with 5 × 5 mL of toluene and subsequent vacuum drying. Yield: 0.13 g (0.13 mmol, 52%). Anal. Calcd for $C_{50}H_{38}Cl_2Mo_2O_4P_2$: C, 58.44; H, 3.73. Found: C, 58.18; H, 3.74. ^{1}H NMR ($CDCl_3$): δ 4.88 (m, 1H, Fv), 4.96 (m, 1H, Fv), 5.11 (m, 1H, Fv), 5.17 (m, 1H, Fv), 5.28 (m, 1H, Fv), 5.32 (m, 1H, Fv), 5.70 (m, 1H, Fv), 5.75 (m, 1H, Fv), 7.37 (m, 30H, Ph). $^{13}C\{^1H\}$ NMR ($CDCl_3$): δ 255.9 (d, J_{PC} = 28.7 Hz, CO trans to Cl), 255.8 (d, J_{PC} = 28.5 Hz, CO trans to Cl), 242.6 (d, J_{PC} = 5.1 Hz, CO cis to Cl), 242.5 (d, J_{PC} = 5.3 Hz, CO cis to Cl), 133.8 (d, J_{PC} = 10.4 Hz, *o*-Ph), 133.7 (d, J_{PC} ≈ 44 Hz, *ipso*-Ph), 130.3 (d, J_{PC} ≈ 2 Hz, *p*-Ph), 128.4 (d, J_{PC} = 9.8 Hz, *m*-Ph). The fulvalene carbon chemical shifts are given in Table 6.

The bromide *cis,cis*-**3b** was prepared similarly from **3a** (0.15 g, 0.23 mmol) and PPh_3 (0.12 g, 0.46 mmol) and was purified by column chromatography. Yield: 0.17 g (0.15 mmol, 66%). Anal. Calcd for $C_{50}H_{38}Br_2Mo_2O_4P_2$: C, 53.79; H, 3.43. Found: C, 52.94; H, 3.38. ^{1}H NMR ($CDCl_3$): δ 4.86 (m, 1H, Fv), 4.90 (m, 1H, Fv), 5.10 (m, 1H, Fv), 5.19 (m, 1H, Fv), 5.21 (m, 1H, Fv), 5.31 (m, 1H, Fv), 5.74 (m, 2H, Fv), 7.37 (m, 30H, Ph). $^{13}C\{^1H\}$ NMR ($CDCl_3$): δ 253.7 (d, J_{PC} = 28.1 Hz, CO trans to Br), 253.6 (d, J_{PC} = 28.6 Hz, CO trans to Br), 240.2 (d, J_{PC} = 5.1 Hz, CO cis to Br), 240.1 (d, J_{PC} = 4.9 Hz, CO cis to Br), 134.0 (d, J_{PC} = 43.1 Hz, *ipso*-Ph), 133.9 (d, J_{PC} = 10.3 Hz, *o*-Ph), 130.4 (d, J_{PC} = 2.5 Hz, *p*-Ph), 128.4 (d, J_{PC} = 9.9 Hz, *m*-Ph). The fulvalene carbon chemical shifts are given in Table 6.

The iodo complex **4b** was also obtained from 0.15 g of **4a** (0.20 mmol) and PPh_3 (0.11 g, 0.40 mmol) as described above. Yield: 0.13 g (0.11 mmol, 54%). Although no analytically pure material could be isolated by column chromatography, the product was thoroughly characterized by spectroscopic methods and appears to be a mixture of *cis,cis*, *cis,trans*, and *trans,trans* isomers. IR (toluene): ν_{CO} 1964 (vs), 1891 (vs) cm^{-1}. ^{1}H NMR (toluene-d_8): δ 4.28 (m), 4.30 (m), 4.33 (m), 4.36 (m), 4.72 (m), 4.81 (m), 4.82 (m), 4.85 (m), 4.97 (m), 5.06 (m), 5.07 (m), 5.21 (m), 5.24 (m), 5.52 (m), 5.76 (m), 5.79 (m) (all Fv resonances; see Table 5 for assignments for the major *cis,cis* isomer). $^{13}C\{^1H\}$ NMR ($CDCl_3$): δ 134 (d, br, J_{PC} = 10.4 Hz, *o*-Ph), 130.85 (d, J_{PC} = 3.1 Hz, *p*-Ph), 130.79 (d, J_{PC} = 3.1 Hz, *p*-Ph), 130.38 (d, J_{PC} = 2.9 Hz, *p*-Ph), 130.31 (d, J_{PC} = 3.1 Hz, *p*-Ph), 128.72 (d, J_{PC} = 9.8 Hz, *m*-Ph), 128.69 (d, J_{PC} = 10.6 Hz, *m*-Ph), 128.27 (d, J_{PC} = 9.8 Hz, *m*-Ph), 128.22 (d, J_{PC} = 10.5 Hz, *m*-Ph), 108.4–83.5 (Fv). The CO and *ipso*-Ph resonances were not identified.

cis,cis-**2b** is a purple powder, insoluble in toluene and acetone but soluble in chlorinated hydrocarbons and THF, giving orange solutions. It is air-sensitive but thermally stable both in solution and in the solid state under an inert atmosphere. *cis,cis*-**3b** is a purple solid of higher solubility with properties otherwise similar to those of **2b**; the isomeric mixture of **4b** is a brick red solid of higher solubility.

Method B. Into 0.6 mL of a toluene-d_8 solution of **1b** (ca. 5 mg, 5.2 × 10^{-3} mmol), 10 μL of CCl_4 (0.10 mmol), benzyl bromide (0.08 mmol), or ICH_2CO_2Et (0.08 mmol) was injected. After about 1 h, the ^{1}H and $^{31}P\{^1H\}$ NMR spectra of the reaction mixtures showed complete transformation of **1b** into *cis,cis*-**2b**, *cis,cis*-**3b**, and an isomeric mixture of **4b**, respectively.

Method C. Pure *cis,cis*-**4b** was obtained by titrating an NMR sample of **1b** in toluene-d_8 with iodine dissolved in a minimum amount of the same solvent. The reaction was instantaneous, complete consumption of **1b** being indicated by both ^{1}H and $^{31}P\{^1H\}$ NMR spectroscopy. *cis,cis*-**4b** transformed into the mixture of isomers obtained by method A on standing at room temperature overnight.

$FvMo_2(CO)_4(PCy_3)_2X_2$ (X = Cl (2c), Br (3c)). Compound **2c** (*cis,cis* isomer) was synthesized essentially as the PPh_3-substituted derivative from 0.20 g (0.36 mmol) of **2a** and 0.20 g (0.71 mmol) of PCy_3 in 15 mL of toluene. It was obtained reasonably pure by column chromatography, although several attempts to obtain an analytically pure sample failed. Yield: 0.24 g (0.22 mmol, 61%). ^{1}H NMR ($CDCl_3$): δ 1.23–1.45 (m, 30H, Cy), 1.69–1.82 (m, 30H, Cy), 2.28 (m, 6H, Cy), 4.85 (m, 1H, Fv), 4.95 (m, 1H, Fv), 5.20 (m, 1H, Fv), 5.28 (m, 1H, Fv), 5.30 (m, 1H, Fv), 5.34 (m, 1H, Fv), 5.89 (m, 1H, Fv), 5.94 (m, 1H, Fv). $^{13}C\{^1H\}$ NMR ($CDCl_3$): δ 258.4 (d, J_{PC} = 26.1 Hz, CO trans to Cl), 258.0 (d, J_{PC} = 25.8 Hz, CO trans to Cl), ~245.5 (two br s, CO cis to Cl), 35.5 (d, J_{PC} = 17.0 Hz, C-1 Cy), 30.5 (d, J_{PC} = 1.3 Hz, C-3 Cy), 29.6 (s, C-3, Cy), 28.0 (d, J_{PC} = 8.9 Hz, C-2 Cy), 27.8 (d, J_{PC} = 10.7 Hz, C-2 Cy), 26.5 (s, C-4 Cy). The fulvalene carbon chemical shifts are given in Table 6.

The dibromide *cis,cis*-**3c** was obtained similarly from 0.09 g (0.14 mmol) of **3a** and 0.08 g (0.28 mmol) of PCy_3 and purified by column chromatography. Yield: 0.13 g (0.11 mmol, 80%). Anal. Calcd for $C_{50}H_{74}Br_2Mo_2O_4P_2$: C, 52.10; H, 6.47. Found: C, 51.79; H, 6.46. ^{1}H NMR ($CDCl_3$): δ 1.24–1.40 (m, 30H, Cy), 1.70–1.79 (m, 30H, Cy), 2.30 (m, 6H, Cy), 4.86 (m, 1H, Fv), 4.97 (m, 1H, Fv), 5.09 (m, 1H, Fv), 5.25 (m, 1H, Fv), 5.34 (m, 1H, Fv), 5.38 (m, 1H, Fv), 5.86 (m, 1H, Fv), 5.90 (m, 1H, Fv). $^{13}C\{^1H\}$ NMR ($CDCl_3$): δ 256.2 (d, J_{PC} = 25.7 Hz, CO trans to Br), 255.8 (d, J_{PC} = 26.6 Hz, CO trans to Br), ~243.4 (two d, J_{PC} ≈ 3 Hz, CO cis to Br), 36.6 (d, J_{PC} = 17.6 Hz, C-1 Cy), 30.8 (d, J_{PC} = 4.6 Hz, C-3 Cy), 29.9 (s, C-3 Cy), 27.9 (d, J_{PC} = 9.0 Hz, C-2 Cy), 27.7 (d, J_{PC} = 11.1 Hz, C-2 Cy),

26.4 (s, C-4 Cy). The fulvalene carbon chemical shifts are given in Table 6. For IR and $^{31}P\{^1H\}$ NMR data for both *cis,cis*-**2c** and *cis,cis*-**3c**, see Tables 2 and 4, respectively.

The complex *cis,cis*-**2c** is a violet crystalline solid which is completely insoluble in hexane, toluene, and acetone but which gives cherry red solutions in chlorinated solvents and THF. The dibromide *cis,cis*-**3c** is a pink-red solid which exhibits solubility similar to that of **2c**. Both compounds are thermally stable in solution as well as in the solid state.

$FvMo_2(CO)_4(PXy_3)_2X_2$ (X = Cl (2d), Br (3d)). Compound **2d** was obtained as the *cis,cis* isomer from 0.22 g (0.39 mmol) of **2a** and 0.27 g (0.79 mmol) of PXy_3 in 20 mL of refluxing toluene in ~10 min. The deep red product was isolated in 75% yield (0.35 g, 0.29 mmol) and was identified by spectroscopic methods (Tables 2 and 4–6) by analogy with **3d** and analogues containing PPh_3 and PCy_3.

Similarly, *cis,cis*-**3d** was obtained by reacting 0.05 g (0.08 mmol) of **3a** with 0.06 g (0.16 mmol) of PXy_3 in 10 mL of toluene. In this particular case, however, ~2 h of refluxing was necessary to achieve complete transformation of **3a**, as monitored by IR spectroscopy. The product was isolated by column chromatography in 54% yield (0.06 g, 0.04 mmol) as a purple solid. Anal. Calcd for $C_{62}H_{62}Br_2Mo_2O_4P_2$: C, 57.96; H, 4.86. Found: C, 56.37; H, 4.11. ^1H NMR ($CDCl_3$): δ 2.245 (s, 18H, Me), 2.251 (s, 18H, Me), 4.75 (m, 1H, Fv), 4.83 (m, 1H, Fv), 5.02 (m, 1H, Fv), 5.12 (m, 1H, Fv), 5.14 (m, 1H, Fv), 5.17 (m, 1H, Fv), 5.65 (m, 2H, Fv), 6.97 (s, 6H, *p*-Xy), 7.00 (s, 12H, *o*-Xy). $^{13}C\{^1H\}$ NMR ($CDCl_3$): δ 254.5 (d, J_{PC} = 30.1 Hz, CO trans to Br), 241.4 (d, $J_{PC} \approx 6$ Hz, CO cis to Br), 137.5 (d, J_{PC} = 10.3 Hz, C-3 Xy), 133.9 (d, J_{PC} = 42 Hz, C-1 Xy), 133.8 (d, J_{PC} = 42 Hz, C-1 Xy), 132.0 (s, C-4 Xy), 131.6 (d, J_{PC} = 10.2 Hz, C-2 Xy), 21.6 (s, Me). The fulvalene carbon chemical shifts are given in Table 6. IR and $^{31}P\{^1H\}$ NMR data are listed in Tables 2 and 4, respectively.

$FvMo_2(CO)_4(PMe_3)_2Br_2$ (3e). This compound was observed *in situ* by IR and ^1H NMR spectroscopy as a red product of the reaction of **1c** (~10 mg, 1.7×10^{-2} mmol) with 10 μL of $CHBr_3$ in 0.6 mL of toluene-d_8. It was identified as the *cis,cis* isomer by analogy with the well-characterized derivatives containing other phosphines and halo groups (Tables 2 and 5). In addition to the fulvalene resonances, the ^1H NMR spectrum also exhibited two doublets of equal intensity at δ 1.13 (J_{PH} = 9.5 Hz, 9H) and 1.14 (J_{PH} = 9.5 Hz, 9H), attributed to two different PMe_3 ligands in the *meso* and *dl* forms.

$CpMo(CO)_2(PPh_3)I$. This compound was synthesized by a modification of the literature method.[6] A mixture of 0.20 g (0.54 mmol) of $CpMo(CO)_3I$ and 0.145 g (0.54 mmol) of PPh_3 was dissolved in 15 mL of toluene and refluxed for 1.5 h. Slow gas evolution was observed, and IR spectroscopic monitoring indicated nearly complete transformation into the substituted product. The solvent was removed under reduced pressure, and the resulting solid was washed with 3 × 5 mL of hexane to remove unreacted starting materials. After the solid was dried under vacuum, 0.21 g (0.35 mmol, 64% yield) of $CpMo(CO)_2(PPh_3)I$ was collected as spectroscopically pure orange crystals. IR (toluene): ν_{CO} 1968 (vs), 1891 (vs) cm^{-1}. ^1H NMR (toluene-d_8): δ 4.68 (d, J_{PH} = 1.9 Hz, Cp, *trans*) and 4.82 (s, Cp, *cis*), 5H altogether, 6.99 (m, 9H, *m,p*-Ph), 7.51 (m, 6H, *o*-Ph). $^{31}P\{^1H\}$ NMR (toluene-d_8): δ 45.4 (s, *cis*), 67.2 (s, *trans*). Both NMR spectra revealed a *cis*:*trans* = 60:40 ratio, in agreement with the literature.[6]

Results and Discussion

Preparation of Hexane Solutions of $FvMo_2(CO)_6H_2$ (1a). Much of our research has involved utilization of the known dihydride[2f] **1a** as starting material, and we required a facile procedure for its synthesis in good yields. The salt, $(NEt_4)_2[FvMo_2(CO)_6]$, was prepared by a modification of the procedure of Smart and Curtis for the synthesis of the corresponding Li salt.[2a] We routinely generate **1a** by protonation of $(NEt_4)_2[FvMo_2(CO)_6]$ with an excess of glacial acetic acid, in this way forming hexane solutions of ~0.01 M concentration. This method proved to be quite straightforward and reproducible.[2f] Furthermore, since the solid dianion can be synthesized free of hexane-soluble impurities, **1a** can be readily obtained pure by IR and ^1H NMR spectroscopy. The use of hexane as solvent is also an advantage since all products formed in subsequent reactions of **1a** are insoluble in hexane and can therefore be easily isolated.

Reaction of 1a with PPh_3: Synthesis and Characterization of $FvMo_2(CO)_4(PPh_3)_2H_2$ (1b). We find that **1a** reacts smoothly with PPh_3 at ambient temperature to give the light yellow product in quantitative yield. Its solution IR spectrum exhibits two strong bands at 1936 and 1858 cm^{-1}, while the $^{31}P\{^1H\}$ NMR spectrum exhibits a single, sharp resonance at δ 73.3, all data being comparable with those of the analogous Cp compound, $CpMo(CO)_2(PPh_3)H$.[7] The ^1H NMR spectrum of **1b** was not simple, however, exhibiting an unsymmetrical doublet at δ −5.03 (J_{PH} = 52 Hz), indicating nonequivalent hydride ligands (see below), and two poorly resolved fulvalene multiplets at δ 4.63 and 5.01. The $^{13}C\{^1H\}$ NMR spectrum revealed little additional information, one strong, sharp and one weak, broad resonance appearing at δ 88.4 and 89.8, respectively, attributable to fulvalene carbons, and three phenyl doublets, attributable to PPh_3; no quaternary carbon or carbonyl resonances could be observed.

The reactivity of **1a** toward phosphines has been recently reported,[2t] as has the isolation and spectroscopic characterization of the symmetrically substituted (fulvalene)dimolybdenum carbonyl dihydride, $FvMo_2(CO)_4(PMe_3)_2H_2$ (**1c**).[8] Interestingly, similar reactions with other phosphorus ligands have not been reported.[9] The smooth reaction of **1a** with PPh_3, in contrast to the behavior of both $FvCr_2(CO)_6H_2$[10] and $FvW_2(CO)_6H_2$,[2t] indicates much greater substitutional lability of (fulvalene)molybdenum complexes compared with the chromium and tungsten counterparts. As well, this reaction seems to represent the reactivity limit of **1a** with sterically demanding phosphines, since the relatively rapid thermal decomposition[2f] of **1a** prevented substitution with both PCy_3 and PXy_3. For comparison, $CpMo(CO)_3H$ reacts with these ligands in refluxing benzene to give $CpMo(CO)_2LH$.[7b] Nevertheless, **1b** is the first hydrido–fulvalene complex containing a phosphorus ligand as bulky as PPh_3.

Compounds of the type $FvMo_2(CO)_4L_2H_2$ may exist as four different geometrical isomers, *trans,trans*, *cis,trans* (*dl*), *cis,cis* (*meso*), and *cis,cis* (*dl*) (Figure 1),[2t]

(6) Manning, A. R. *J. Chem. Soc. A* **1967**, 1984.

(7) Data for $CpMo(CO)_2(PPh_3)H$ are as follows. (a) IR (C_6H_6): ν_{CO} 1940 vs, 1865 s cm^{-1}. ^1H NMR (C_6D_6): δ −5.12 (d, J_{PH} = 48 Hz, Mo*H*).[4d] (b) $^{31}P\{^1H\}$ NMR (C_6D_6/C_6H_6): δ 74.5 (s). Drake, P. R.; Baird, M. C. Queen's University at Kingston, unpublished results.

(8) $FvMo_2(CO)_5(PMe_3)H_2$ has also been reported[2t] but was obtained from the zwitterionic compound $FvMo_2(CO)_5(PMe_3)_2$ by reduction and protonation. It was not investigated whether this monosubstituted derivative was an intermediate in the reaction of **1a** with PMe_3.

(9) An unsuccessful attempt was made to substitute **1a** with dmpm: Tilset, M. Ph.D. Dissertation, University of California, Berkeley, 1986; *Diss. Abstr. Int. B* **1987**, *47*, 2924 (University Microfilms, Inc., Order No. AAC 8624962).

(10) $FvCr_2(CO)_6H_2$ shows reactivity in substitution reactions with phosphines similar to that of $FvW_2(CO)_6H_2$; that is, PMe_2Ph is the bulkiest ligand with which smooth reaction takes place at room temperature. Kovács, I.; Baird, M. C. To be submitted for publication.

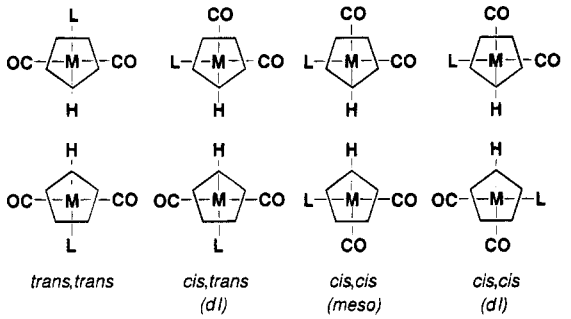

Figure 1. Stereoisomers possible for compounds of the type $FvMo_2(CO)_4L_2H_2$.

giving rise potentially to nine α- and nine β-hydrogen sites. Since several substituted cyclopentadienylmolybdenum carbonyl hydrides[11] and **1c**[2t] are fluxional, facile interconversion of the various *cis* and *trans* isomers of **1b** was also anticipated. It is noteworthy that, for **1c**, four doublets from both the hydridic and PMe_3 protons but only six multiplets from the ring protons were observed at −50 °C, consistent with a 55:45 *cis*:*trans* isomer ratio. In accord with more detailed studies on its tungsten counterpart,[2t] these resonances were assigned to *cis*,*cis* (both *meso* and *dl*), *cis*,*trans*, and *trans*,*trans* isomers. The $^{31}P\{^1H\}$ NMR spectrum of **1c** exhibited singlets at δ 21.8 (*trans*) and 25.5 (*cis*), also indicative of a mixture of *cis* and *trans* isomers.[2t]

When a toluene-d_8 solution of **1b** was cooled to −65 °C, we observed four hydride doublet resonances centered at δ −4.99 (J_{PH} = 65 Hz), −5.02 (J_{PH} = 21 Hz), −5.05 (J_{PH} = 21 Hz), and −5.06 (J_{PH} = 65 Hz) in the ^1H NMR spectrum. The P−H coupling constants may be utilized to infer stereochemistry of such compounds,[2t,11] the 65 and 21 Hz couplings respectively indicating that *cis* and *trans* isomers are present in a ratio of 65:35, reminiscent of the isomeric ratio (63:37) found for $CpMo(CO)_2(PPh_3)H$.[11] The ratio of *cis*,*cis*, *cis*,*trans*, and *trans*,*trans* isomers was found to be 4:2.5:1 on the basis of integrals.

In contrast to the case for **1c**, however, 12 individual fulvalene multiplet resonances were observed in the ^1H spectrum of **1b**, in addition to weaker, completely obscured resonances revealed by careful integrations. Although the spectrum of **1b** was too complex and poorly resolved for unambiguous assignments to be possible, detailed analyses of the similarly complicated spectra of the analogous substituted dihalo complexes were possible and are discussed below.

The $^{31}P\{^1H\}$ NMR spectrum of **1b** at room temperature exhibits only a broad singlet at δ 73.3, but the spectrum at −70 °C (Table 4) was consistent with the ^1H NMR spectrum. Four partially overlapped resonances were observed at δ 73.64 (*cis*,*cis*) and 71.90 (*trans*,*trans*), as well as at 73.69 and 71.98 (*cis* and *trans* halves, respectively, of the *cis*,*trans* isomer). Integrals of the upfield *trans* and downfield *cis* resonances suggested a *cis*:*trans* ratio of ~60:40.

Reactions of 1a with Activated Alkyl Halides: Synthesis and Characterization of the Complexes $FvMo_2(CO)_6X_2$ (X = Cl (2a), Br (3a), I (4a)) and $FvMo_2(CO)_6XY$ (X = Cl, Br, I; Y = H, Cl, Br, I) (5a, 6a, 7a, 8−10). Since our attempts to substitute **1a** with phosphines bulkier than PPh_3 failed, we turned our attention to the dihalides, $FvMo_2(CO)_6X_2$, to possibly provide access to (fulvalene)molybdenum(I) dimers or diradicals substituted with PCy_3 and PXy_3. If the more electrophilic dihalides would undergo ligand substitution with all three phosphines at elevated temperatures, the substituted $FvMo_2(CO)_4L_2X_2$ derivatives might be reduced either directly to $FvMo_2(CO)_4L_2$ or to dianions, $[FvMo_2(CO)_4L_2]^{2-}$, which could be either protonated to dihydrides or oxidized directly to radicals/dimers.

Surprisingly, of this series of compounds, only **4a** had previously been reported;[2g] it was prepared by the reaction of iodine with $FvMo_2(CO)_6$, no practical details or spectroscopic data being given. On attempting to employ this method for the synthesis of **3a** in CH_2Cl_2, we observed rapid CO evolution and precipitation of a brown solid, containing no carbonyl ligands; **3a** was formed only in minor amounts. However, the reaction of benzyl bromide or bromoform with **1a** gave **3a** in excellent yields.

Indeed, reaction of **1a** with the appropriate alkyl halides provided general access to all of the three dihalides, **2a**, **3a**, and **4a**, although all were sufficiently labile that none could be obtained analytically pure. Typically, **1a** was stirred with a large excess of CCl_4, $CHBr_3$, or ICH_2CO_2Et in hexane at ambient temperature; **2a**, **3a**, and **4a**, respectively, precipitated as red solids and were characterized by IR and ^1H and $^{13}C\{^1H\}$ NMR spectroscopy (Tables 2, 3, and 6). Each IR spectrum exhibits two strong carbonyl stretching bands, which are shifted to lower frequencies in the order **4a** > **3a** > **2a**, consistent with the relative electronegativities of the halogens and similar to behavior of the analogous Cp and indenyl complexes.[12] In addition, the ^1H NMR spectra each exhibited two well-resolved virtual "triplets" of equal intensity, characteristic of H_α and H_β fulvalene protons (AA'MM' spin systems).[2h] The $^{13}C\{^1H\}$ NMR spectra were also fully consistent with the formulations, exhibiting resonances attributable to the three types of fulvalene sites as well as the CO ligands. Indeed, separate CO resonances were observed for CO ligands *cis* and *trans* to X, as has been observed previously for the corresponding Cp compounds.[13]

During the syntheses of these compounds, additional weak bands were occasionally observed in both the IR and ^1H NMR spectra of the products. In an attempt to identify the minor species, we monitored an *in situ* reaction of **1a** with benzyl bromide in toluene-d_8 by ^1H NMR spectroscopy. Interestingly, during the first 20 min of the reaction, only four fulvalene "triplet" resonances at δ 4.28, 4.58, 4.73, and 4.89, all of equal intensity and corresponding to the above-mentioned weak resonances, could be observed. After this time, the two "triplet" resonances of **3a** slowly began to emerge at δ 4.27 and 4.86 and gradually became the dominant resonances, as those of **1a** (δ 4.52, 4.87) and, later, of the intermediate species diminished (~2 h). While both **1a** and the intermediate were present in the reaction mixture, two hydridic resonances, separated only by 0.007 ppm, also appeared at δ ~−5.30. This observation suggested the formation of the mixed hydrido bromide **6a**, and subsequently the corresponding hydrido−chloride and −iodide analogues were also

(11) Faller, J. W.; Anderson, A. S. *J. Am. Chem. Soc.* **1970**, *92*, 5852.

(12) Hart-Davis, A. J.; White, C.; Mawby, R. J. *Inorg. Chim. Acta* **1970**, *4*, 431.

(13) Todd, L. J.; Wilkinson, J. R.; Hickey, J. P. *J. Organomet. Chem.* **1978**, *154*, 151.

identified in the reactions of **1a** with CCl_4 and ICH_2CO_2Et, respectively. ^1H NMR data for these complexes are listed in Table 3.

The kinetic stabilities of the initially formed **5a**, **6a**, and **7a** in the presence of excess alkyl halides must be attributed to deactivation by the halo ligand on the metal center adjacent to that bearing the hydride ligand. Fortunately, our method of preparation of the dihalides provided a basis to obtain the hydrido halides in the solid state as mixtures with the corresponding dihalides, although the resulting mixtures could not be separated. As shown in eq 2 for **7a**, hydrido halides readily undergo

$$2FvMo_2(CO)_6HI \rightleftharpoons FvMo_2(CO)_6H_2 + FvMo_2(CO)_6I_2 \rightarrow FvMo_2(CO)_6I_2 + FvMo_2(CO)_6 + H_2 \quad (2)$$

redistribution reactions which prevent separation by chromatography. As a result of decomposition of **1a**, the final organometallic products from the hydrido halides are the corresponding dihalides and $FvMo_2(CO)_6$. On the other hand, since the three hydrido halides all react further with alkyl halides to form the corresponding dihalides, it seemed likely that treatment of these isolated compounds with a second alkyl halide would result in formation of the mixed dihalides. Indeed, we succeeded in the *in situ* preparation of mixed dihalides **8**, **9**, and **10**, which were characterized by ^1H NMR spectroscopy (Table 3).

Complexes **8**–**10** were also obtained by a second method, avoiding the use of alkyl halides. The facile nature of the redistribution reaction of the hydrido halides (eq 2) suggested that pairs of dihalides might also exchange halide ligands reversibly. Indeed, when the dihalides **2a**, **3a**, and **4a** were dissolved in pairs in toluene-d_8 or acetone-d_6, slow equilibration reactions leading to the formation of the corresponding mixed dihalides were observed by ^1H NMR spectroscopy (eq 3; X, Y = Cl, Br, I). Because of these ligand exchange

$$FvMo_2(CO)_6X_2 + FvMo_2(CO)_6Y_2 \rightleftharpoons 2FvMo_2(CO)_6XY \quad (3)$$

processes, the mixed-halogen compounds could not be obtained pure.

Synthesis and Characterization of the Complexes $FvMo_2(CO)_4L_2X_2$ (L = PPh_3, PCy_3, PXy_3; X = Cl, Br, I) (2b–d, 3b–d, 4b) and $FvMo_2(CO)_4(PPh_3)_2HX$ (X = Cl (5b), Br (6b), I (7b)). Phosphine-substituted (fulvalene)dimolybdenum carbonyl dihalo compounds containing PPh_3, PCy_3, and PXy_3 were readily prepared by direct substitution of a CO ligand at each Mo center of the parent dihalides **2a**, **3a**, and **4a**. These reactions were surprisingly facile, substitution with PPh_3 being complete in less than 1 day at room temperature (similarly to **1a**) and the bulkier ligands reacting with vigorous gas evolution in ~10 min to 2 h on heating to 110 °C. Interestingly, while a considerable amount (<40%) of the starting materials decomposed to $FvMo_2(CO)_6$ during these reactions, it was found that the thermal decomposition of **2a** in toluene at ~100 °C in the absence of added phosphine proceeds with gas evolution to yield an unidentified, insoluble precipitate and only traces of $FvMo_2(CO)_6$. In contrast, analogous Cp complexes require refluxing in benzene for at least several hours to produce $CpMo(CO)_2LX$ (L = PPh_3, PCy_3, PXy_3), and do not decompose to $[CpMo(CO)_3]_2$.[7b]

Complexes **2b–d**, **3b–d**, and **4b** were isolated as brick red, purple, or violet solids in good yields. The PPh_3-substituted products were identical with **2b**, **3b**, and **4b**, formed by the hydrogen–halogen exchange of **1b** with CCl_4, $PhCH_2Br$, and ICH_2CO_2Et, respectively. In addition, **4b** was obtained in solution by reacting **1b** with iodine. IR and multinuclear NMR techniques were used to characterize the products (Tables 2 and 4–6), all of which are new.

For all of the substituted dichlorides and dibromides, as well as for **4b** freshly prepared from **1b** and iodine, the IR spectra exhibited two carbonyl stretching bands (Table 2). However, while the $^{31}P\{^1H\}$ NMR spectra of **2b** and **3b** in $CDCl_3$ exhibited sharp singlets at δ 49.9 and 47.8, respectively, the $^{31}P\{^1H\}$ NMR spectra in toluene-d_8 each exhibited two resonances of equal intensity (Table 4). In addition, the $^{13}C\{^1H\}$ NMR spectra of both **2b** and **3b** ($CDCl_3$) exhibited two sets of five resonances in the fulvalene region (Table 6), while only a single set of PPh_3 phenyl $^{13}C\{^1H\}$ resonances was observed. In addition, four doublets appeared in the low-field region of coordinated CO ligands, arranged in two pairs (each pair having the same P–C coupling constants) due to the difference between ligands being in positions *cis* or *trans* to halogen (or phosphine).[13]

In contrast, the $^{31}P\{^1H\}$ NMR spectra of **2c,d** and **3c,d** all exhibited two singlets of equal intensity even in $CDCl_3$, the chemical shift difference between these resonances increasing with the bulk of phosphines, i.e. $PPh_3 < PCy_3 < PXy_3$.[14] Furthermore, the $^{13}C\{^1H\}$ NMR spectra of **2c** and **3c,d** exhibited five pairs of singlets in the fulvalene carbon region, similar to the PPh_3-substituted derivatives. Interestingly, the high-field resonances of **2c** and **3c**, which probably belong to the C_α carbons,[2h] appear as doublets, suggesting unusual coupling to phosphorus. The cyclohexyl carbon region of **2c** and **3c** also provided new information, there being two pairs of doublets, attributed to C-2 and C-3, and a doublet and a singlet, attributed to C-1 and C-4, respectively. For **3d**, only single resonances were found in the methyl and aromatic carbon region, except that the weak and broad C-1 Xy resonance appeared as two doublets. In contrast to the PPh_3- and PCy_3-substituted derivatives, only one pair of doublet CO carbon resonances was observed in the $^{13}C\{^1H\}$ NMR spectrum of **3d**.

The ^1H NMR spectra of all four compounds exhibited eight fulvalene multiplets of equal intensity, consistent with the $^{13}C\{^1H\}$ NMR spectra, although some spectra were complicated by an overlap of resonances (Table 5). Utilization of ^1H–^1H decoupling experiments made possible assignments of the resonances as belonging to identical or different rings. As an example, the ^1H NMR spectrum of **2b**, recorded in $CDCl_3$, exhibited a readily recognizable pattern of eight well-separated multiplets arranged into four pairs at δ 4.88 and 4.96, 5.11 and 5.17, 5.28 and 5.32, and 5.70 and 5.75 (Figure 2). These resonances were assigned as belonging to the two different ring systems as follows: H_β, $H_{\beta'}$, $H_{\alpha'}$, and H_α resonate at δ 4.88, 5.11, 5.32 and 5.75, respectively, in one ring, and at δ 4.96, 5.17, 5.28, and 5.70, respectively, in the other. As we show below, the two rings probably

(14) Tolman, C. A. *Chem. Rev.* **1977**, *77*, 313.

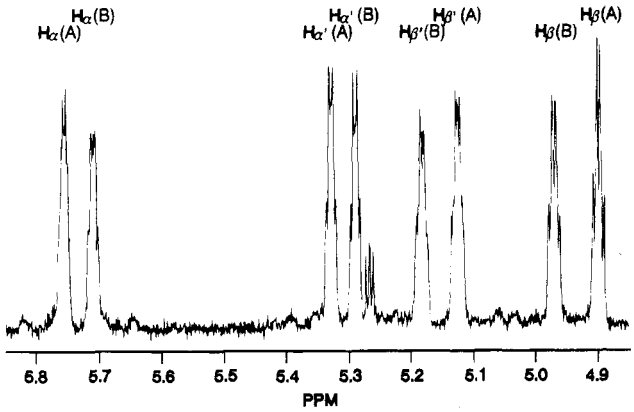

Figure 2. ^{1}H NMR spectrum (400 MHz) of *cis,cis*-$FvMo_2(CO)_4(PPh_3)_2Cl_2$ (**2b**) in the fulvalene proton region.

do not represent the two halves of a single fulvalene system but, rather, two different fulvalene systems in which the halves are spectroscopically identical.

The ^{1}H NMR spectrum of **2b** also exhibited a remarkable temperature dependence of the chemical shifts, gradual cooling of the solution to −70 °C resulting in a shifting of the eight resonances to δ 4.86, 5.04, 5.11, 5.24, 5.19, 5.38, 5.81, and 5.86, respectively. Furthermore, while heating a toluene-d_8 solution of **2b** resulted in pairs of resonances coalescing at 110 °C to give a four-resonance spectrum, the resulting H_α−$H_{\alpha'}$ and H_β−$H_{\beta'}$ pairs of resonances did not coalesce to give a two-resonance spectrum similar to that of **1b** at room temperature.

The ^{1}H NMR spectrum of a $CDCl_3$ solution of **2c** also exhibited eight separate multiplets in the fulvalene region (Table 5), and these were also readily differentiated into two groups of four on the basis of ^{1}H−^{1}H decoupling experiments as follows: H_β, $H_{\beta'}$, $H_{\alpha'}$, and H_α resonate at δ 4.85, 5.20, 5.30, and 5.94, respectively, in one ring and at δ 4.95, 5.28, 5.34, and 5.89, respectively, in the other. Surprisingly, when **2c** was freshly dissolved in CD_2Cl_2 and the spectrum recorded without delay, the first set of resonances were of approximately twice the intensity of the other. Within about 2 h, however, all of the resonances had became equal, indicating that a relatively slow equilibration process had taken place between two different species.

These results are consistent with structures containing the CO ligands in mutually *cis* arrangements and the pairs of α and β fulvalene protons and carbons being diastereotopic because of the chiral Mo centers. By analogy, while the compounds *cis*-$CpMo(CO)_2LX$ are chiral,[11,15] the chirality has only been confirmed by ^{1}H NMR investigations on derivatives where X = CH_2R or L = PMe_2Ph, in which the chiral center rendered the methylene or methyl protons diastereotopic. While examples with diastereotopic cyclopentadienyl nuclei are rare, we note that the chirality of the identyl complex (η^5-C_9H_7)$Mo(CO)_2(PPh_3)I$ results in nonequivalence of H_α and $H_{\alpha'}$ protons.[15] In the case of the fluorenylisopropyl-substituted complex (η^5-C_5H_4-$CMe_2C_{13}H_9$)$Mo(CO)_2(PMe_3)H$, nonequivalence of the cyclopentadienyl carbons was reported.[16]

As mentioned above, fulvalene compounds of the type *cis,cis*-$FvMo_2(CO)_4L_2X_2$ contain two chiral centers and can form *meso* and *dl* stereoisomers.[2t] The *meso* isomer has a plane of symmetry between the two rings, and thus only four Fv protons, five Fv carbons, and one phosphorus environment are expected. On the other hand, while the *dl* isomers contain no plane of symmetry, there is a C_2 axis perpendicular to the Fv plane (Figure 1), and again only four Fv protons, five Fv carbons, and one phosphorus environment are expected. On this basis, the spectral changes described above seem best interpreted in terms of *meso*−*dl* interconversion, presumably *via* intramolecular CO−phosphine exchange.

In view of the differences in the NMR spectra of **1b,c**, arising from substitution of the small PMe_3 with the larger bulky PPh_3, we decided to investigate the consequences of changing the halide ligands as well. First, **3e** was generated *in situ* by reacting **1c** with $PhCH_2Br$ and was found to exhibit the same IR and ^{1}H NMR characteristics as do most of the complexes of bulkier phosphines. That is, **3e** exists in solution as the *cis,cis* isomer, which gives rise to eight fulvalene proton resonances (two of them completely overlapping at δ 4.41) in the ^{1}H NMR spectrum. Thus, substitution of a small hydride ligand by a bulkier halide ligand results in the same effect on the appearance of the spectra as replacing a small phosphine with a sterically more demanding one.

Unlike the dichlorides and dibromides, *cis,cis*-**4b**, obtained *in situ* by reacting **1b** with iodine, was not stable in solution. While the IR spectrum of a sample which had remained in solution at room temperature for 1 day did not exhibit any new carbonyl stretching bands, the medium-intensity band of *cis,cis*-**4b** at 1887 cm^{-1} gained in relative intensity and became as strong and sharp as the band at 1965 cm^{-1}, suggesting the formation of one or more *trans* isomers.[11] In accordance with this, the $^{31}P\{^1H\}$ NMR spectrum exhibited three additional resonances at δ 45.9, 67.0, and 67.3, downfield from those of *cis,cis*-**4b** at δ 45.7 and 45.8. Those at δ 67.0 and 45.9 were of equal intensity and are tentatively assigned to the nonequivalent sites of the *cis,trans* isomer; by default, then, the resonance at δ 67.3 is tentatively assigned to the *trans,trans* isomer. The $^{13}C\{^1H\}$ NMR spectrum of the reaction mixture supported the $^{31}P\{^1H\}$ NMR spectroscopic interpretation. Altogether, four doublet resonances were observed for both the C-3 and C-4 carbon atoms of the coordinated PPh_3, suggesting four different phosphine environments. The doublets characteristic of both types of carbons were clearly arranged in two distinct pairs, suggesting that each pair contained resonances of two similar ligands, *i.e.* two *cis* and two *trans*, as in the $^{31}P\{^1H\}$ NMR spectrum.

The ^{1}H NMR spectrum of the mixture exhibited eight fulvalene multiplets at δ 4.30, 4.36, 4.82, 4.97, 5.07, 5.21, 5.24, and 5.76, in addition to those of *cis,cis*-**4b**. A mixture of *cis,trans* and *trans,trans* isomers of **4b** should exhibit 10 new resonances, but there is considerable overlap and a possibility of coincidence of some resonances of the *cis,trans* isomer. Thus, the spectrum is taken as being reasonably consistent with conversion to a mixture of *cis,trans* and *trans,trans* isomers of **4b**, established above on the basis of IR and ^{31}P NMR data.

(15) Faller, J. W.; Anderson, A. S.; Jakubowski, A. *J. Organomet. Chem.* **1971**, *27*, C47.
(16) Alt, H. G.; Maisel, H. E.; Han, J. S.; Wrackmeyer, B. *J. Organomet. Chem.* **1990**, *399*, 131.

When **4b** was prepared by direct substitution of **4a** with PPh_3, the same ^1H NMR spectrum was obtained. In fact, pure *cis,cis*-**4b** could not be prepared in this way, possibly because equilibration of the three isomers took place quickly at 110 °C or over 1 day at room temperature. Hydrogen–halogen exchange reactions of **1b** with ICH_2CO_2Et, ICH_2CN, or *t*-BuI gave varying ratios of the three isomers of **4b**.

Consistent with the above spectroscopic results, we note that while *cis*-$CpMo(CO)_2(PPh_3)I$ also readily isomerizes, the corresponding chloro and bromo compounds remain exclusively as the *cis* isomer.[11,17] The $^{31}P\{^1H\}$ NMR spectral data for *cis*- and *trans*-$CpMo(CO)_2(PPh_3)I$ have not been reported, but we find that the $^{31}P\{^1H\}$ NMR spectrum of an equilibrium mixture of the *cis* and *trans* isomers exhibits singlets at δ 45.4 and 67.2, respectively, supporting the above assignments.

The intermediate formation of hydrido–halide complexes in the reaction of **1a** with activated alkyl halides suggested that similar reactions of **1b** might proceed in the same way. Indeed, ^1H and $^{31}P\{^1H\}$ NMR monitoring of the reactions of **1b** with CCl_4, $PhCH_2Br$, and ICH_2CO_2Et or ICH_2CN unambiguously established the sole formation of **5b**, **6b**, and **7b**, respectively, early in the reactions. The hydridic doublet and fulvalene multiplet resonances of **5b** and **6b** could be readily assigned (Table 5), but overlapping of the various isomers of the iodo system rendered assignments of the fulvalene proton resonances of **7b** ambiguous. Nevertheless, two new hydridic doublets were observed at δ −4.99 and −5.01, attributed to hydrido–iodide compounds having both *cis* and *trans* iodide "halves", respectively. Consistent with this, new *cis* and *trans* $^{31}P\{^1H\}$ NMR resonances were also observed (Table 4).

The mechanism of hydrogen–halogen exchange in both substituted and unsubstituted dihydrides also merits comment. According to a recent review,[18] several mechanistic studies suggest that the reactions between alkyl halides and metal carbonyl hydrides may involve radical chain processes, as in eqs 4–6.

$$In^\bullet + HM(CO)_nL \rightarrow InH + {}^\bullet M(CO)_nL \quad (4)$$

$$^\bullet M(CO)_nL + RX \rightarrow XM(CO)_nL + R^\bullet \quad (5)$$

$$R^\bullet + HM(CO)_nL \rightarrow RH + {}^\bullet M(CO)_nL \quad (6)$$

$In^\bullet$ = unidentified radical initiator

The particular structure of fulvalene complexes, coupled with our experimental results and the known behavior of the analogous chromium-centered radical $CpCr(CO)_3$,[19] permit speculation on the involvement of

Scheme 1

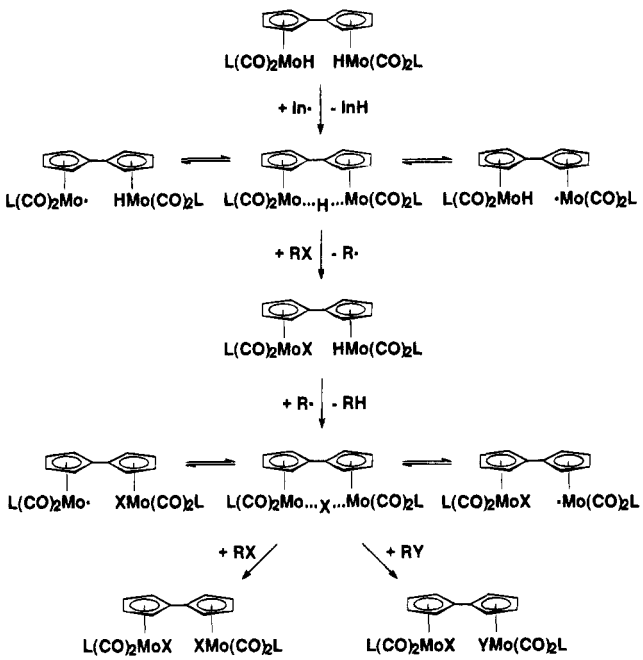

novel bimetallic radical intermediates. As shown in Scheme 1 for a fulvalene system of the type $FvMo_2(CO)_4L_2H_2$, hydrogen atom abstraction should result in two types of chain-propagating, metal-centered radicals: an initially formed radical hydride species and a subsequently formed halo radical species. In addition, the hydrogen or halogen atoms in the radical intermediates may also undergo rapid exchange processes involving the two metals, as occurs between $CpCr(CO)_3$ and the compounds $CpCr(CO)_3X$ (X = H, Br, I).[1h,19] The forced proximity of the metals in fulvalene complexes would increase the possibility of intramolecular atom exchange, but it is also reasonable to suppose that the radical intermediates may undergo intermolecular exchange processes of hydride and/or halide ligands, consistent with the reactions outlined in eqs 2 and 3. Note that the possible radical chain hydride and halide ligand redistributions in our fulvalene systems provide a novel mechanistic alternative. Such ligand redistributions have received considerable attention recently but were studied exclusively on coordinatively unsaturated complexes, and no other mechanisms were considered.[20]

Acknowledgment. We thank NATO for a Science Scholarship to I.K. (administered by the Natural Sciences and Engineering Research Council), the NSERC for a Research Grant to M.C.B., and the Hungarian Science Foundation for support provided by Grant No. OTKA F7419. Valuable discussions with Professor B. K. Hunter are also greatly appreciated.

OM950112C

(17) Beach, D. L.; Dattilo, M.; Barnett, K. W. *J. Organomet. Chem.* **1977**, *140*, 47.
(18) Brown, T. L. In *Organometallic Radical Processes*; Trogler, W. C., Ed.; J. Organomet. Chem. Libr. 22; Elsevier: New York, 1990; p 67, and references therein.
(19) McConnachie, C. A.; Nelson, J. M.; Baird, M. C. *Organometallics* **1992**, *11*, 2521.
(20) (a) Garrou, P. E. *Adv. Organomet. Chem.* **1984**, *23*, 95 and references therein. (b) Poulton, J. T.; Hauger, B. E.; Kuhlman, R. L.; Caulton, K. G. *Inorg. Chem.* **1994**, *33*, 3325.

Synthesis and Characterization of Mo–Mo-Bonded (Fulvalene)dimolybdenum Carbonyl Complexes Containing Sterically Demanding Phosphines

István Kovács[†] and Michael C. Baird*

Department of Chemistry, Queen's University, Kingston, Ontario, Canada K7L 3N6

Received February 10, 1995[⊗]

The new metal–metal-bonded (fulvalene)dimolybdenum carbonyl complexes $FvMo_2(CO)_4L_2$ (L = PPh_3, PCy_3, PXy_3; Xy = 3,5-dimethylphenyl) were synthesized via (a) hydride hydrogen atom abstraction from $FvMo_2(CO)_4L_2H_2$ (L = PPh_3, PXy_3) by trityl radicals, (b) sodium reduction of $FvMo_2(CO)_4L_2Cl_2$ (L = PPh_3, PCy_3, PXy_3), and (c) oxidation of the dianions $[FvMo_2(CO)_4L_2]^{2-}$ (L = PPh_3, PCy_3). The compounds were characterized by IR, UV–vis, and ^1H, $^{13}C\{^1H\}$, and $^{31}P\{^1H\}$ NMR spectroscopy, and the spectroscopic data are in all cases consistent with structures containing the phosphines in positions *trans* to the Mo–Mo bond. The UV–vis spectra of *trans*-$FvMo_2(CO)_4L_2$ (L = PPh_3, PCy_3, PXy_3) all exhibit a $\sigma \rightarrow \sigma^*$ transition at 374 nm, suggesting that the phosphines influence neither sterically nor electronically the Mo–Mo bond strength. Evidence for radical intermediates was found when $FvMo_2(CO)_4(PPh_3)_2$ was prepared from $FvMo_2(CO)_4(PPh_3)_2H_2$.

Introduction

There is currently considerable interest in the preparation and structural characterization of 17-electron organotransition-metal compounds (metal-centered radicals).[1] Investigations are also focusing on the kinetics of coupling reactions of metal-centered radicals to give the corresponding 18-electron metal–metal-bonded dimers[2] and the factors affecting the strengths of the metal–metal bonds thus formed.[1] In several cases, correlations have been noted between the bond strengths/lengths of metal–metal bonds of 18-electron dimers with the energies of the metal–metal σ–σ^* electronic transitions[3] and also with the proclivity of 18-electron dimers to undergo thermal homolysis to the corresponding 17-electron species.[4] Dimers with weaker metal–metal bonds commonly exhibit smaller σ–σ^* energy gaps and dissociate to a greater extent, although a caveat to the latter generalization must be noted.[4]

Thus, it is of considerable interest that the metal–metal bond of the fulvalene (Fv) compound (η^5:η^5-$C_{10}H_8$)-$Cr_2(CO)_6$ (**A**), which is believed not to undergo significant thermal dissociation to biradicals in solution,[5] is considerably longer (3.471 Å)[5,6c] than the metal–metal bonds of the analogous cyclopentadienyl compounds $[CpCr(CO)_3]_2$ (3.281 Å)[7] and $[Cp^*Cr(CO)_3]_2$ (3.3107 Å),[4] which readily undergo significant thermal dissociation in solution at ambient temperature.[4] The corresponding

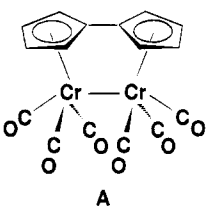

A

molybdenum and tungsten compounds $FvM_2(CO)_6$ (M = Mo, W) also contain seemingly very long metal–metal bonds (3.371 and 3.347 Å, respectively),[6a,b] without undergoing homolysis.[5] On the other hand, all three compounds contain fulvalene ligands bent from planarity as in **A**, suggestive of significant strain in the molecules.[5,6]

Equally intriguing, crystal structure data for $FvMo_2(CO)_4(PMe_3)_2$ show that substitution of two carbonyl groups by the sterically more demanding PMe_3 ligands results in a *shorter* and *presumably stronger* Mo–Mo bond than exists in $FvMo_2(CO)_6$,[8] again contrary to expectations based on the cyclopentadienyl–chromium system. Indeed, severe twisting and bending of the fulvalene ligand from planarity in this molecule are strongly suggestive of greatly enhanced steric strain,[8] and thus the fulvalene system stands in seemingly marked contrast with trends exhibited by other 18-electron metal–metal-bonded organometallic compounds.

[†] NATO Science Fellow; Research Group for Petrochemistry of the Hungarian Academy of Sciences, Veszprém, Hungary.

[⊗] Abstract published in *Advance ACS Abstracts,* August 1, 1995.

(1) For reviews, see: (a) Baird, M. C. *Chem. Rev.* **1988**, *88*, 1217. (b) Baird, M. C. In *Organometallic Radical Processes*; Trogler, W. C., Ed.; J. Organomet. Chem. Libr. 22; Elsevier: Amsterdam, 1990; p 49. (c) Connelly, N. G.; Geiger, W. E. *Adv. Organomet. Chem.* **1984**, *23*, 1. (d) Tyler, D. R. *Prog. Inorg. Chem.* **1988**, *36*, 125. (e) Kochi, J. K. *Organometallic Mechanisms and Catalysis*; Academic Press: New York, 1978.

(2) (a) Yao, Q.; Bakac, A.; Espenson, J. H. *Organometallics* **1993**, *12*, 2010. (b) Richards, T. C.; Geiger, W. E.; Baird, M. C. *Organometallics* **1994**, *13*, 4494. For reviews of earlier work, see: (c) Meyer, T. J.; Caspar, J. V. *Chem. Rev.* **1985**, *85*, 187. (d) Brown, T. L. In *Organometallic Radical Processes*; Trogler, W. C., Ed.; J. Organomet. Chem. Libr. 22; Elsevier: Amsterdam, 1990; p 67.

(3) (a) Madach, T.; Vahrenkamp, H. *Z. Naturforsch.* **1979**, *34B*, 573. (b) Jackson, R. A.; Poë, A. *Inorg. Chem.* **1978**, *17*, 997. (c) Poë, A.; Jackson, R. A. *Inorg. Chem.* **1978**, *17*, 2330.

(4) Watkins, W. C.; Jaeger, T.; Kidd, C. E.; Fortier, S.; Baird, M. C.; Kiss, G.; Roper, G. C.; Hoff, C. D. *J. Am. Chem. Soc.* **1992**, *114*, 907 and references therein.

(5) For a recent review of fulvalene complexes, see: McGovern, P. A.; Vollhardt, K. P. C. *Synlett* **1990**, 493.

(6) (a) Abrahamson, H. B.; Heeg, M. J. *Inorg. Chem.* **1984**, *23*, 2281. (b) Drage, J. S.; Vollhardt, K. P. C. *Organometallics* **1986**, *5*, 280. (c) Moulton, R.; Weidman, T. W.; Vollhardt, K. P. C.; Bard, A. J. *Inorg. Chem.* **1986**, *25*, 1846.

(7) Adams, R. D.; Collins, D. E.; Cotton, F. A. *J. Am. Chem. Soc.* **1974**, *96*, 749.

(8) (a) Kretchmar, S. A.; Cass, M. E.; Turowski, P. N. *Acta Crystallogr.* **1987**, *C43*, 435. (b) Tilset, M.; Vollhardt, K. P. C.; Boese, R. *Organometallics* **1994**, *13*, 3146.

0276-7333/95/2314-4084$09.00/0

Although no evidence that this class of compounds can exist as biradical isomers has been reported,[5] it nevertheless seemed important to investigate the structures and chemistry of derivatives containing phosphines of greater steric requirements. It is possible that biradical fulvalene species of the group VI metals might be synthesized by routes other than those utilized previously and that they might be stabilized with respect to coupling by bulky ligands. And even if stable metal–metal-bonded dimers are invariably formed, it is possible that radical species might be detectable as reactive intermediates.

Unfortunately, direct substitutions of the CO ligands of, *e.g.*, $FvMo_2(CO)_6$ with tertiary phosphines do not generally occur.[5,6b,8b] In addition, with very few exceptions, no fulvalene complexes are known with ligands larger than the relatively small PMe_3,[5] and therefore alternative routes to the compounds $FvMo_2(CO)_4L_2$ (L = *e.g.* PPh_3, PCy_3, and PXy_3, where Ph = phenyl, Cy = cyclohexyl, and Xy = 3,5-dimethylphenyl) are to be investigated. We have developed and describe herein the necessary chemistry.

As pointed out in the previous paper,[9] 17-electron compounds may often be synthesized by hydride hydrogen abstraction from transition-metal hydrides by trityl radicals, as in eq 1. This approach has been utilized

$$HML_n + {}^{\bullet}CPh_3 \rightarrow {}^{\bullet}ML_n + HCPh_3 \qquad (1)$$

extensively by ourselves and others for the preparation of a variety of 17-electron species[10] and has been shown to be of general utility for the synthesis of 17-electron compounds which are stabilized with respect to dimerization to the 18-electron, metal–metal-bonded analogues by substitution of small ligands by more sterically demanding ligands, *e.g.* of CO by tertiary phosphines.[2d]

We have therefore assessed the possible utility of reactions of the type shown in eq 1 as a potential route to fulvalene biradicals, using as starting points substituted hydrides of the type $FvMo_2(CO)_4L_2H_2$, as in eq 2.

$$FvMo_2(CO)_4L_2H_2 + 2{}^{\bullet}CPh_3 \rightarrow FvMo_2(CO)_4L_2 + 2HCPh_3 \qquad (2)$$

$$L = PPh_3, PCy_3, PXy_3$$

Since the starting dihydride compounds presumably assume the *anti* conformation shown by **B**, established

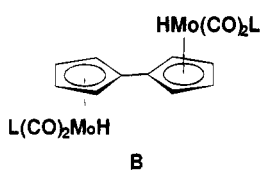

B

for several non-metal–metal-bonded fulvalene complexes by X-ray crystallography,[8b,11] any diradical products would probably assume the same conformation and might couple slowly or not at all to the corresponding 18-electron species $FvMo_2(CO)_4L_2$ if L is a sufficiently bulky ligand.

In the preceding paper,[9] we described the preparation and characterization of the new (fulvalene)dimolybdenum carbonyl dihydride $FvMo_2(CO)_4(PPh_3)_2H_2$. Since the hydrides containing PCy_3 and PXy_3 could not be synthesized in the same way, we also described the preparation and characterization of several new fulvalene halomolybdenum compounds of the type $FvMo_2(CO)_4L_2X_2$ (X = Cl, Br, I), which might be reducible directly to the desired products $FvMo_2(CO)_4L_2$ or to the corresponding dianions which, in turn, could give access to the missing hydrides. In this paper, we discuss applications of these synthetic methodologies to the preparation of the compounds $FvMo_2(CO)_4L_2$ (L = PPh_3, PCy_3, PXy_3), and describe experiments which imply the roles of radical and biradical (fulvalene)dimolydenum species as intermediates but which confirm the nonexistence of persistent biradical species. We also offer a tentative explanation for the apparently anomalous bond length correlations discussed above.

Experimental Section

General Considerations. All manipulations were carried out under purified nitrogen using standard Schlenk techniques and a Vacuum Atmospheres glovebox. All solvents were freshly distilled under nitrogen from sodium benzophenone ketyl (hexane, benzene, toluene, ether, and THF) or CaH_2 (CH_2Cl_2). Deuterated solvents were purchased from Isotec, Inc., and were degassed and stored in the glovebox. Tertiary phosphines (PMe_3 from Aldrich, PPh_3 from Strem, PCy_3 from Organometallics, Inc., PXy_3 from M&T) and other chemicals were used without further purification. Solutions of the trityl radical in benzene were prepared by the zinc reduction of Ph_3CCl,[10a] while $FvMo_2(CO)_6H_2$, $FvMo_2(CO)_4(PMe_3)_2H_2$, and $FvMo_2(CO)_4(PPh_3)_2H_2$ were prepared as previously described.[9]

UV–vis data were obtained on a Hewlett-Packard 8452A diode array spectrophotometer. IR spectra were recorded on a Bruker IFS-25 FT-IR spectrometer and NMR spectra on Bruker AC-200 (200.1 MHz, ^1H) and AM-400 (400.1 MHz, ^1H; 100.6 MHz, $^{13}C\{^1H\}$; 162.0 MHz, $^{31}P\{^1H\}$) NMR spectrometers. Relevant IR and ^1H NMR data are compiled in Tables 1 and 2, respectively. Elemental analyses were carried out by Canadian Microanalytical Services, Ltd., Delta, B.C., Canada.

Reaction of $FvMo_2(CO)_6H_2$ with Trityl Radicals. A 3-mL aliquot of a freshly prepared 0.01 M hexane solution of $FvMo_2(CO)_6H_2$ was mixed with 1 mL of a 0.1 M trityl solution in benzene at room temperature. A red precipitate formed instantly, and no CO-containing material could be detected in the solution by IR spectroscopy. The solvent was removed under reduced pressure, and the solid product was washed with 10 mL of hexane and dried *in vacuo*. Solutions in THF and acetone-d_6 exhibited IR and ^1H NMR spectra identical with those of an authentic sample of $FvMo_2(CO)_6$. IR: ν_{CO} 2015 (vs), 1962 (vs), 1929 (vs), 1911 (sh), 1885 (sh) cm^{-1}. ^1H NMR: δ 4.73 ("t", 4H, Fv), 5.57 ("t", 4H, Fv). When the experiment was repeated in 0.6 mL of toluene-d_8, equal amounts of both $FvMo_2(CO)_6$ (δ 3.38 ("t"), 4.30 ("t")) and Ph_3CH (δ 5.37 (s)) were identified.

Reaction of $FvMo_2(CO)_4(PMe_3)_2H_2$ with Trityl Radicals. To 0.03 g (0.05 mmol) of $FvMo_2(CO)_4(PMe_3)_2H_2$ was added 2 mL of a 0.05 M trityl solution in benzene. An IR

(9) Kovács, I.; Baird, M. C. *Organometallics* **1995**, *14*, 4074.

(10) (a) Drake, P. R.; Baird, M. C. *J. Organomet. Chem.* **1989**, 363, 131. (b) Koeslag, M. D.; Baird, M. C. *Organometallics* **1994**, *13*, 11. (c) Kuksis, I.; Baird, M. C. *Organometallics* **1994**, *13*, 1551. (d) Ungváry, F.; Markó, L. *J. Organomet. Chem.* **1980**, *193*, 383. (e) Turaki, N. N.; Huggins, J. M. *Organometallics* **1986**, *5*, 1703. (f) Edidin, R. T.; Hennessy, K. M.; Moody, A. E.; Okrasinski, S. J.; Norton, J. R. *New J. Chem.* **1988**, *12*, 475. (g) Eisenberg, D. C.; Lawrie, C. J. C.; Moody, A. E.; Norton, J. R. *J. Am. Chem. Soc.* **1991**, *113*, 4888.

(11) (a) Boese, R.; Myrabo, R. L.; Newman, D. A.; Vollhardt, K. P. C. *Angew. Chem., Int. Ed. Engl.* **1990**, *29*, 549. (b) Brown, D. S.; Delville-Desbois, M.-H.; Boese, R.; Vollhardt, K. P. C.; Astruc, D. *Angew. Chem., Int. Ed. Engl.* **1994**, *33*, 661. (c) Kahn, A. P.; Boese, R.; Blümel, J.; Vollhardt, K. P. C. *J. Organomet. Chem.* **1994**, *472*, 149.

Table 1. IR and UV–Vis Spectroscopic Data for the $FvMo_2(CO)_4L_2$ (L = CO, PMe_3, PPh_3, PCy_3, PXy_3) Complexes

compd	UV–vis $\lambda_{max}(\sigma \rightarrow \sigma^*)$ (nm)[a]	IR ν_{CO} (cm^{-1})[a]	lit.
$FvMo_2(CO)_6$	378	2010 (vs), 1960 (vs), 1925 (vs), 1905 (sh), 1880 (sh)	14a,c
trans-$FvMo_2(CO)_4(PMe_3)_2$	360	1903 (m), 1816 (vs)	8b, this work
trans-$FvMo_2(CO)_4(PMe_3)_2$	374	1932 (m), 1858 (vs)	this work
trans-$FvMo_2(CO)_4(PCy_3)_2$	374	1918 (m), 1841 (vs)	this work
trans-$FvMo_2(CO)_4(PXy_3)_2$	374	1931 (m), 1857 (vs)	this work

[a] In THF.

Table 2. Selected NMR Spectroscopic Data for the $FvMo_2(CO)_4L_2$ (L = CO, PMe_3, PPh_3, PCy_3, PXy_3) Complexes

	^1H NMR (Fv) δ (ppm)[a]		$^{13}C\{^1H\}$ NMR (Fv) δ (ppm)[a]				
compd	H_α	H_β	C-1	C-2	C-3	$^{31}P\{^1H\}$ NMR δ (ppm)[b]	lit.
$FvMo_2(CO)_6$	4.26 ("t")	5.25 ("t")	94.6	84.9	87.3[c]		this work, 14b
trans-$FvMo_2(CO)_4(PMe_3)_2$	4.20 ("t")	4.94 (m)[d]	90.5	82.6	85.4[c]	27.9[d]	8b, 14b
trans-$FvMo_2(CO)_4(PPh_3)_2$	4.45 ("t")	4.13 (m)	89.0	84.0	89.3	78.7	this work
trans-$FvMo_2(CO)_4(PCy_3)_2$	4.30 ("t")	5.01 (m)	88.5	83.2	85.4	69.7[a]	this work
trans-$FvMo_2(CO)_4(PXy_3)_2$	4.40 ("t")	4.08 (m)	89.0	83.8	89.2	78.0	this work

[a] In $CDCl_3$, unless noted otherwise. [b] In toluene-d_8, unless noted otherwise. [c] In THF-d_8. [d] In acetone-d_6.

spectrum was run and, after it was stirred for 1 h, the red solution was evaporated to dryness and the remaining red solid was dissolved in THF and benzene for IR analysis and in acetone-d_6 for ^1H NMR analysis. The initial and final IR spectra were identical, and the combination of IR and NMR spectroscopy showed that the solution contained $FvMo_2(CO)_6$, $FvMo_2(CO)_4(PMe_3)_2$, and $FvMo_2(CO)_5(PMe_3)$ (relative amounts ~1:1:0.75) and Ph_3CH.

Preparation of $FvMo_2(CO)_4(PPh_3)_2$ via Reaction of $FvMo_2(CO)_4(PPh_3)_2H_2$ with Trityl Radicals. A 4.2 mL aliquot of a 0.1 M trityl solution in benzene was added to a stirred solution of $FvMo_2(CO)_4(PPh_3)_2H_2$ (0.20 g, 0.21 mmol) in 80 mL of benzene, the solution turning deep red almost instantly. A sample was taken for IR analysis, and two new absorptions, tentatively attributable to $FvMo_2(CO)_4(PPh_3)_2$, were observed. The solvent was removed under reduced pressure to give a gray solid, which was purified by column chromatography using silica gel 60 (70–230 mesh, EM Scientific) and toluene and THF as eluants. The *purple* THF solution was evaporated to dryness, and the resulting *gray* solid was washed well with hexane and dried *in vacuo*. Yield: 0.09 g (0.09 mmol, 45%). Anal. Calcd for $C_{50}H_{38}Mo_2O_4P_2$: C, 62.77; H, 4.00. Found: C, 63.22; H, 4.66. The stoichiometry of this reaction was determined by ^1H and $^{31}P\{^1H\}$ NMR spectroscopic measurements of a reaction run in toluene-d_8. IR (THF): ν_{CO} 1932 (m), 1858 (vs) cm^{-1}. UV–vis (THF): λ_{max} 374 (vs), 564 (vw) nm. ^1H NMR ($CDCl_3$): δ 4.13 (m, 4H, Fv), 4.45 ("t", 4H, Fv), 7.37 (m, 18H, *m,p*-Ph), 7.57 (m, 12H, *o*-Ph). ^1H NMR (toluene-d_8): δ 4.16 (m, 4H, Fv), 4.40 ("t", 4H, Fv). ^1H NMR (acetone-d_6): δ 4.22 (m, 4H, Fv), 4.64 ("t", 4H, Fv). $^{13}C\{^1H\}$ NMR ($CDCl_3$): δ 236.7 (d, J_{PC} = 22.1 Hz, CO), 137.9 (d, J_{PC} = 42.8 Hz, *ipso*-Ph), 133.5 (d, J_{PC} = 11.1 Hz, *o*-Ph), 129.5 (d, J_{PC} = 2.5 Hz, *p*-Ph), 128.1 (d, J_{PC} = 10.0 Hz, *m*-Ph), 89.3 (Fv), 89.0 (C-1 Fv), 84.0 (Fv). $^{31}P\{^1H\}$ NMR (toluene-d_8): δ 78.7.

Decomposition of $FvMo_2(CO)_4(PPh_3)_2H_2$ in the Presence of $Co_2(CO)_8$. Approximately 10 mg of $FvMo_2(CO)_4(PPh_3)_2H_2$ and an excess of $Co_2(CO)_8$ were dissolved in 0.7 mL of toluene-d_8 in an NMR tube. A ^1H NMR spectrum was recorded and indicated the presence of approximately a 1:1 mixture of $FvMo_2(CO)_4(PPh_3)_2$ and unreacted $FvMo_2(CO)_4(PPh_3)_2H_2$. After ~2 h, all $FvMo_2(CO)_4(PPh_3)_2H_2$ had converted to $FvMo_2(CO)_4(PPh_3)_2$, as judged by a second ^1H NMR measurement. When $Co_2(CO)_8$ was used in greater excess, the transient formation of $Co(CO)_4H$ (δ 10.9) in low concentrations could also be detected by ^1H NMR spectroscopy.

Preparation of $FvMo_2(CO)_4(PPh_3)_2$ via Reduction of $FvMo_2(CO)_4(PPh_3)_2Cl_2$. A large excess of sodium dispersion in mineral oil (Aldrich) was placed in a Schlenk tube, washed with 3 × 10 mL of hexane, and dried *in vacuo*. The sodium was then stirred vigorously in 2 mL of THF, and 10 mL of a red-orange THF solution of $FvMo_2(CO)_4(PPh_3)_2Cl_2$ (0.10 g, 0.10 mmol) was added dropwise at room temperature, resulting in almost instant darkening. The reaction mixture was stirred for 1 h, the sodium was allowed to settle, and an IR spectrum was run, demonstrating complete consumption of the $FvMo_2(CO)_4(PPh_3)_2Cl_2$. The solution was filtered through activated carbon and evaporated to dryness, and the product was characterized by IR and ^1H NMR spectroscopy. It was found to be identical with the product of the reaction between $FvMo_2(CO)_4(PPh_3)_2H_2$ and trityl radicals, *i.e.* $FvMo_2(CO)_4(PPh_3)_2$.

Preparation of $FvMo_2(CO)_4(PPh_3)_2$ via Reduction of $FvMo_2(CO)_4(PPh_3)_2Br_2$ and Oxidation of the Resulting $Na_2[FvMo_2(CO)_4(PPh_3)_2]$. A red solution of $FvMo_2(CO)_4(PPh_3)_2Br_2$ (0.10 g, 0.09 mmol) in 10 mL of THF was added dropwise at ambient temperature to a slurry of finely dispersed sodium in 2 mL of THF, the color turning yellow instantly. Stirring was continued for 1 h, the sodium was allowed to settle, and an IR spectrum was recorded. Complete conversion to $Na_2[FvMo_2(CO)_4(PPh_3)_2]$ (ν_{CO} 1789 (vs, br), 1691 (s, br) cm^{-1}) was observed. The mixture was filtered through Celite into a Schlenk tube containing 2 molar equiv of Et_4NBr, and an IR spectrum of the resulting dark yellow solution was recorded (ν_{CO} 1786 (vs), 1702 (s) cm^{-1}). The solution was then divided into three equal portions. Excess glacial acetic acid was added to one portion of the solution, and complete conversion to $FvMo_2(CO)_4(PPh_3)_2H_2$ was observed (IR). About 0.5 mL of air was added to the second portion, resulting in complete oxidation of the dianion to $FvMo_2(CO)_4(PPh_3)_2$, identified by IR spectroscopy. The same result was obtained when 2 molar equiv of $[Cp_2Fe]PF_6$ was added to the third portion. ^1H NMR of the Na^+ salt (acetone-d_6): δ 4.39 ("t", 4H, Fv), 4.95 (m, 4H, Fv). $^{31}P\{^1H\}$ NMR (acetone-d_6): δ 27.8.

Preparation of $FvMo_2(CO)_4(PCy_3)_2$ via Reduction of $FvMo_2(CO)_4(PCy_3)_2Cl_2$. $FvMo_2(CO)_4(PCy_3)_2Cl_2$ (0.29 g, 0.27 mmol) was dissolved in 40 mL of THF and added dropwise to sodium suspended in 10 mL of THF at −78 °C. The reaction mixture was stirred and warmed to room temperature over ~1 h, and an IR spectrum of the dark solution showed that the absorptions of $FvMo_2(CO)_4(PCy_3)_2Cl_2$ had completely disappeared, giving rise to new bands attributable to $FvMo_2(CO)_4(PCy_3)_2$. The mixture was filtered through activated carbon, and the solution was evaporated to dryness. The residue was washed with 8 × 10 mL of toluene until colorless washings were obtained and dried *in vacuo* to give an analytically pure product. Yield: 0.15 g (0.15 mmol), 56%. Anal. Calcd for $C_{50}H_{74}Mo_2O_4P_2$: C, 60.48; H, 7.51. Found: C, 60.73; H, 7.53. IR (THF): ν_{CO} 1918 (m), 1841 (vs) cm^{-1}. UV–vis (THF): λ_{max} 374 (vs), 576 (vw) nm. ^1H NMR ($CDCl_3$): δ 1.30 (br m, 30H,

Cy), 1.71–2.10 (br m, 30H, Cy), 2.18 (m, 6H, Cy), 4.30 ("t", 4H, Fv), 5.01 (m, 4H, Fv). $^{13}C\{^1H\}$ NMR ($CDCl_3$): δ 242.4 (d, J_{PC} = 20.3 Hz, CO), 88.5 (s, C-1 Fv), 85.4 (Fv), 83.2 (Fv), 38.4 (d, J_{PC} = 18.1 Hz, C-1 Cy), 30.1 (s, C-3 Cy), 28.0 (d, J_{PC} = 9.9 Hz, C-2 Cy), 26.7 (s, C-4 Cy). $^{31}P\{^1H\}$ NMR ($CDCl_3$): δ 69.7.

$FvMo_2(CO)_4(PCy_3)_2$ is a thermally stable, light blue powder, which is insoluble in aromatic hydrocarbons and acetone but moderately soluble in THF and chlorinated hydrocarbons. Recrystallization from THF gave black microcrystals.

Preparation of $FvMo_2(CO)_4(PCy_3)_2$ via Reduction of $FvMo_2(CO)_4(PCy_3)_2Br_2$ and Oxidation of the Resulting $Na_2[FvMo_2(CO)_4(PCy_3)_2]$. A solution of $FvMo_2(CO)_4(PCy_3)_2Br_2$ (0.13 g, 0.11 mmol) in 10 mL of THF was added dropwise at ambient temperature to a slurry of finely dispersed sodium in 2 mL of THF. Stirring was continued for 1 h, the sodium was allowed to settle, and an IR spectrum exhibited absorptions characteristic of $[FvMo_2(CO)_4(PCy_3)_2]^{2-}$ (ν_{CO} 1769 (vs, br), 1670 (s, br) cm^{-1}). The mixture was filtered through Celite into a Schlenk tube containing 0.13 g of (PPN)Cl (0.11 mmol), and the resulting salt, $(PPN)_2[FvMo_2(CO)_4(PCy_3)_2]$, was characterized by IR and ^1H NMR spectroscopy. IR (THF): ν_{CO} 1770 (vs, br), 1689 (s, br) cm^{-1}. ^1H NMR (acetone-d_6): δ 4.56 ("t", 4H, Fv), 5.14 ("t", 4H, Fv).

A solution of $Na_2[FvMo_2(CO)_4(PCy_3)_2]$ was divided into three equal portions. Excess glacial acetic acid was added to one portion; $FvMo_2(CO)_4(PCy_3)_2H_2$ was formed and identified by IR spectroscopy (ν_{CO} 1926 (vs), 1850 (s) cm^{-1}) in comparison with the known PPh_3 and PMe_3 derivatives.[9] To the other portions were added 0.5 mL of air and 2 molar equiv of $[Cp_2Fe]PF_6$, respectively, resulting in the sole formation of $FvMo_2(CO)_4(PCy_3)_2$ (IR).

Preparation of $FvMo_2(CO)_4(PXy_3)_2$ via Reduction of $FvMo_2(CO)_4(PXy_3)_2Cl_2$. The reduction was carried out with sodium dispersion at 60 °C, as described above for $FvMo_2(CO)_4(PPh_3)_2Cl_2$, and the product, *trans*-$FvMo_2(CO)_4(PXy_3)_2$, was characterized spectroscopically. IR (THF): ν_{CO} 1931 (m), 1857 (vs) cm^{-1}. UV–vis (THF): λ_{max} 374 (vs), 526 (vw) nm. ^1H NMR ($CDCl_3$): δ 2.26 (m, 36H, Me), 4.08 (m, 4H, Fv), 4.40 ("t", 4H, Fv), 7.10 (s, 6H, *p*-Xy), 7.14 (s, 12H, *o*-Xy). ^1H NMR (toluene-d_8): δ 4.34 (m, 4H, Fv), 4.47 ("t", 4H, Fv). ^1H NMR (acetone-d_6): δ 4.14 (m, 4H, Fv), 4.55 ("t", 4H, Fv). $^{13}C\{^1H\}$ NMR ($CDCl_3$): δ 237.2 (d, J_{PC} = 21.4 Hz, *C*O), 89.2 (Fv), 89.0 (s, Fv C-1), 83.8 (Fv), 21.5 (Me). $^{31}P\{^1H\}$ NMR (toluene-d_8): δ 78.0. $^{31}P\{^1H\}$ NMR ($CDCl_3$): δ 76.8.

Preparation of $FvMo_2(CO)_4(PXy_3)_2H_2$ via Reduction of $FvMo_2(CO)_4(PXy_3)_2Br_2$. $FvMo_2(CO)_4(PXy_3)_2Br_2$ (2.30 g, 1.79 mmol) dissolved in 25 mL of THF was added dropwise to an excess of sodium dispersion (see reduction of $FvMo_2(CO)_4(PPh_3)_2Br_2$) in 10 mL of THF. A smooth reaction took place in ~1.5 h, resulting in a color change from deep red to yellow-brown. IR spectroscopy indicated complete conversion of the bromide to the salt $Na_2[FvMo_2(CO)_4(PXy_3)_2]$ (ν_{CO} 1762 (s, br), 1683 (s, br) cm^{-1}). The slurry was passed through Celite to remove sodium, and the resulting dark yellow solution was treated with 0.5 mL of glacial acetic acid and evaporated to dryness. The solids were extracted with benzene (20 mL), and the brown benzene solution was evaporated again to dryness. The remaining solid was washed with 50 mL of hexane and vacuum-dried to give a light yellow powder (1.80 g, 1.60 mmol, 89%) judged sufficiently pure for further use on the basis of NMR spectra. IR (C_6H_6): ν_{CO} 1934.5 (s), 1863 (vs) cm^{-1}. ^1H NMR (toluene-d_8): δ −4.85 (d, J_{PC} = 52 Hz, 2H, Mo*H*), 2.01 (s, 36H, Me), 4.75 (br "t", 4H, Fv), 5.16 (br "t", 4H, Fv), 6.69 (s, 6H, *p*-Xy), 7.31 (d, J_{PH} = 11 Hz, 12H, *o*-Xy). $^{31}P\{^1H\}$ NMR (toluene-d_8): δ 72.1 (br s, $\Delta\delta_{1/2}$ = 0.7 ppm).

Reaction of $FvMo_2(CO)_4(PXy_3)_2H_2$ with Trityl Radicals. Hydrogen atom abstraction reactions were performed on NMR sample scales using ca. 10 and 30 mg of the dihydride dissolved in 0.6 and 2.0 mL of toluene-d_8, respectively, for ^1H and $^{31}P\{^1H\}$ NMR experiments; for $^{13}C\{^1H\}$ and $^{31}P\{^1H\}$ NMR experiments, the 2 mL samples were evaporated to dryness and the residues were redissolved in $CDCl_3$. For IR studies, the reactions were repeated in benzene at room temperature.

The reactions resulted in the formation of mixtures containing *trans*-$FvMo_2(CO)_4(PXy_3)_2$ and an as yet unidentified compound. The IR and NMR spectra all exhibited two sets of peaks, those assigned above to *trans*-$FvMo_2(CO)_4(PXy_3)_2$ and those listed below for the unidentified compound. IR (C_6H_6): ν_{CO} 1919 (s), 1856 (m) cm^{-1}. ^1H NMR ($CDCl_3$): δ 2.31 (s, 36H, Me), 4.49 (m, 4H, Fv), 5.15 ("t", 4H, Fv). $^{13}C\{^1H\}$ NMR ($CDCl_3$): δ 94.8 (Fv), 92.4 (Fv C-1), 86.3 (Fv), 56.7 (Me). $^{31}P\{^1H\}$ NMR (toluene-d_8): δ 63.5. $^{31}P\{^1H\}$ NMR ($CDCl_3$): δ 61.90, 61.93.

Results and Discussion

The direct abstraction of hydride hydrogen atoms by trityl radicals (which exist in solution in equilibrium with the trityl dimer[12]) has proven to be very useful for the preparation of metal carbonyl radicals in recent years.[10] Unfortunately, $FvMo_2(CO)_6H_2$ cannot be used as a general starting point for the synthesis of derivatives by direct CO substitution because it is rather unstable thermally and reacts with bulky phosphines sufficiently slowly that decomposition is the major process. Thus, while $FvMo_2(CO)_4(PMe_3)_2H_2$ and $FvMo_2(CO)_4(PPh_3)_2H_2$ can be synthesized by direct substitution, $FvMo_2(CO)_4(PCy_3)_2H_2$ and $FvMo_2(CO)_4(PXy_3)_2H_2$ cannot and alternative routes to these compounds were sought.

In contrast to the case for $FvMo_2(CO)_6H_2$, the dihalide compounds $FvMo_2(CO)_6X_2$ (X = Cl, Br) are thermally relatively stable and readily undergo substitution reactions with all three bulky phosphines, PPh_3, PCy_3, and PXy_3, giving the compounds $FvMo_2(CO)_4L_2X_2$ (L = PPh_3, PCy_3, PXy_3; X = Cl, Br).[9] These compounds exist solely as *cis,cis* isomers in solution and are thermally quite robust.[9] Earlier reports[13] have demonstrated that Na/Hg reduction of the analogous Cp complexes $CpMo(CO)_2(PPh_3)X$ (X = Cl, I) results in formation of the anion $[CpMo(CO)_2(PPh_3)]^-$, and reduction of the dihalides $FvMo_2(CO)_4L_2X_2$ was expected to result in formation of the dianions $[FvMo_2(CO)_4L_2]^{2-}$, presumably via the possibly isolable intermediate compounds $FvMo_2(CO)_4L_2$. Alternatively, subsequent oxidation of the dianions might also lead to the neutral compounds $FvMo_2(CO)_4L_2$, while protonation of the dianions would also give those dihydrides $FvMo_2(CO)_4L_2H_2$ (L = PCy_3, PXy_3) not available by direct substitution of $FvMo_2(CO)_6H_2$, thus opening up the possibility of treating these with trityl also.

We discuss below the results of attempted preparations of the compounds $FvMo_2(CO)_4L_2$ (L = PPh_3, PCy_3, PXy_3) via (a) hydrogen atom abstraction reactions of $FvMo_2(CO)_4L_2H_2$ (L = PPh_3, PXy_3) with trityl radicals, (b) reduction of the halides $FvMo_2(CO)_4L_2X_2$ (L = PPh_3, PCy_3, PXy_3; X = Cl, Br), and (c) oxidation of the dianions $[FvMo_2(CO)_4L_2]^{2-}$ (L = PPh_3, PCy_3).

Hydrogen Atom Abstraction Reactions of $FvMo_2(CO)_4L_2H_2$ (L = CO, PMe_3, PPh_3): Synthesis and Characterization of $FvMo_2(CO)_4(PPh_3)_2$. We initially tested the reactivity of both $FvMo_2(CO)_6H_2$ and $FvMo_2(CO)_4(PMe_3)_2H_2$ with the trityl radical because the anticipated dimeric products, $FvMo_2(CO)_6$ and $FvMo_2$-

(12) Colle, T. H.; Glaspie, P. S.; Lewis, E. S. *J. Org. Chem.* **1978**, *43*, 2722.

(13) (a) Bolton, E. S.; Dekker, M.; Knox, G. R.; Robertson, C. G. *Chem. Ind.* **1969**, 327. (b) Manning, A. R. *J. Chem. Soc. A* **1968**, 651.

$(CO)_4(PMe_3)_2$, were already well characterized spectroscopically.[6b,8b] As shown in eq 3, Ph_3CH and $FvMo_2(CO)_6$ were formed quantitatively in a rapid reaction between $FvMo_2(CO)_6H_2$ and 2 molar equiv of trityl. This result parallels the behavior of $CpMo(CO)_3H$ in the same reaction,[10a] and the rapid, quantitative formation of $FvMo_2(CO)_6$ via the presumed biradical intermediate is in accord with the lack of the reverse process, homolytic dissociation of the Mo–Mo bond of $FvMo_2(CO)_6$.[6b]

$$FvMo_2(CO)_6H_2 + 2Ph_3C^{\bullet} \rightarrow FvMo_2(CO)_6 + 2Ph_3CH \quad (3)$$

A somewhat different product mixture was found in the reaction of $FvMo_2(CO)_4(PMe_3)_2H_2$ with trityl, as shown in eq 4. Beside Ph_3CH and $FvMo_2(CO)_4(PMe_3)_2$, anticipated on the basis of eqs 1–3, $FvMo_2(CO)_6$ and $FvMo_2(CO)_5(PMe_3)$ were also formed. The last two products were unambiguously identified by their ^1H NMR spectra,[6b,8b,14] although the IR spectrum of $FvMo_2(CO)_4(PMe_3)_2$ exhibited carbonyl stretching bands (1903 (m) and 1816 (vs) cm^{-1}) quite different from those reported previously (1926, 1850, 1805 cm^{-1}).[8b] Observation of $FvMo_2(CO)_6$ and $FvMo_2(CO)_5(PMe_3)$ suggests that rapid ligand scrambling, typical of radicals,[1] had occurred.

$$FvMo_2(CO)_4(PMe_3)_2H_2 + 2Ph_3C^{\bullet} \rightarrow FvMo_2(CO)_4(PMe_3)_2 + FvMo_2(CO)_5(PMe_3) + FvMo_2(CO)_6 + 2Ph_3CH \quad (4)$$

We then investigated the reaction of $FvMo_2(CO)_4(PPh_3)_2H_2$ with trityl; when stoichiometric amounts of the reactants were mixed in benzene or toluene (one trityl per MoH group), an instant color change from yellow to very dark red took place, followed by a gradual fading to a brownish color. Spectroscopic analyses of the reaction mixtures confirmed that Ph_3CH and a new fulvalene complex had formed, although the latter did not exhibit any of the properties normally characteristic of 17-electron species. Detailed investigations were carried out to establish the nature of this product, and we came to the conclusion (see below) that it is the new metal–metal-bonded compound $FvMo_2(CO)_4(PPh_3)_2$. Thus, hydrogen atom abstraction from $FvMo_2(CO)_4(PPh_3)_2H_2$ had indeed taken place, in agreement with eq 5 and in analogy to the reaction of $CpMo(CO)_2(PPh_3)H$.[10a]

$$FvMo_2(CO)_4(PPh_3)_2H_2 + 2Ph_3C^{\bullet} \rightarrow FvMo_2(CO)_4(PPh_3)_2 + 2Ph_3CH \quad (5)$$

The IR spectrum (Table 1) exhibited two strong carbonyl stretching bands at frequencies very similar to those of $FvMo_2(CO)_4(PPh_3)_2H_2$. The similarities in intensity patterns of the pairs of bands in the spectra of $FvMo_2(CO)_4(PMe_3)_2$ and $FvMo_2(CO)_4(PPh_3)_2$ suggest that the two compounds have the same symmetries, *i.e.* in which the phosphines occupy the *trans* positions relative to the Mo–Mo bonds, as in **C**, while the frequencies decrease, as anticipated, on going from PPh_3 to the more electron-releasing PMe_3. The ^1H, $^{13}C\{^1H\}$,

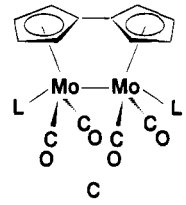

and $^{31}P\{^1H\}$ NMR spectra of $FvMo_2(CO)_4(PPh_3)_2$ are all consistent with its formulation as shown. The $^{31}P\{^1H\}$ NMR spectrum exhibits a single resonance at δ 78.7, to considerably lower field of the resonance of $FvMo_2(CO)_4(PPh_3)_2H_2$. As well, the $^{13}C\{^1H\}$ NMR spectrum of $FvMo_2(CO)_4(PPh_3)_2$ exhibits three fulvalene singlets, a doublet for CO ligands, and resonances of PPh_3, and thus both the $^{31}P\{^1H\}$ and $^{13}C\{^1H\}$ NMR spectroscopic results suggest that the halves of $FvMo_2(CO)_4(PPh_3)_2$ are identical and that the compound assumes the *trans* structure. The ^1H NMR spectrum exhibits virtual triplet and multiplet resonances at δ 4.45 and 4.13, respectively, in $CDCl_3$, also consistent with the AA′MM′XX′ spin system of structure **C**.

Two absorbances were observed in the UV–vis spectrum of $FvMo_2(CO)_4(PPh_3)_2$, at 374 and 564 nm, attributable to $d\sigma \rightarrow d\sigma^*$ and $d\pi \rightarrow d\sigma^*$ transitions, respectively, of the Mo–Mo bond.[5,8b] This conclusion is important because it provides not only direct evidence for the existence of a metal–metal bond in $FvMo_2(CO)_4(PPh_3)_2$ but also indicates that this bond should be as strong as that of $FvMo_2(CO)_6$ (378 and 558 nm),[5,8b,14c] contrary to the anticipated steric effects of PPh_3. It has been demonstrated that $\lambda_{max}(d\sigma \rightarrow d\sigma^*)$ absorption maxima correlate well with the Mo–Mo bond distances established by X-ray structure analyses for $FvMo_2(CO)_6$ and $FvMo_2(CO)_4(PMe_3)_2$.[5,6b,c,8]

We also carried out variable-temperature NMR experiments to investigate the nature and stability of the Mo–Mo bond of $FvMo_2(CO)_4(PPh_3)_2$. A variable-temperature ^1H NMR experiment in the range −65 to +105 °C demonstrated virtually no change in the ^1H NMR spectrum of a toluene-d_8 solution of $FvMo_2(CO)_4(PPh_3)_2$, suggesting very strongly that the Mo–Mo bond does not dissociate significantly over this temperature range. Dissociation of $[CpCr(CO)_3]_2$ to monomer to an extent of only a few percent results in very significant broadening and shifting of the Cp resonance,[4,15] and similar behavior by the fulvalene molybdenum system should be readily detectable. Furthermore, in a complementary experiment, no chemical reaction with benzyl bromide took place over this temperature range. Metal-centered radicals are generally very reactive with alkyl halides, abstracting a halogen atom to give 18-electron halometal products, as in eq 6.[2d,16] As with $[CpMo(CO)_3]_2$,[10a]

$$L_nM^{\bullet} + RX \rightarrow L_nMX + R^{\bullet} \quad (6)$$

however, exposure of $FvMo_2(CO)_4(PPh_3)_2$ to fluorescent room lighting does appear to result in homolysis. When it stands over several days in solution under room light, $FvMo_2(CO)_4(PPh_3)_2$ reacts with $CDCl_3$, $PhCH_2Br$, and MeI to give varying amounts of $FvMo_2(CO)_4(PPh_3)_2Cl_2$,

(14) (a) Smart, J. C.; Curtis, C. J. *Inorg. Chem.* **1977**, *16*, 1788. (b) Meyerhoff, D. J.; Nunlist, R.; Tilset, M.; Vollhardt, K. P. C. *Magn. Reson. Chem.* **1986**, *24*, 709. (c) Vollhardt, K. P. C.; Weidman, T. W. *Organometallics* **1984**, *3*, 82.

(15) Goh, L. Y.; Lim, Y. Y. *J. Organomet. Chem.* **1991**, *402*, 209.

(16) McConnachie, C. A.; Nelson, J. M.; Baird, M. C. *Organometallics* **1992**, *11*, 2521.

$FvMo_2(CO)_4(PPh_3)_2Br_2$, and $FvMo_2(CO)_4(PPh_3)_2I_2$, respectively, suggesting that the Mo–Mo bond is photochemically cleaved to the diradical isomer under these conditions. Conversion of $FvMo_2(CO)_4(PPh_3)_2$ to $FvMo_2(CO)_4(PPh_3)_2I_2$ was complete within 1 day in the presence of the highly reactive ICH_2CO_2Et. No other compounds were detected in the reaction mixtures.

Although $FvMo_2(CO)_4(PPh_3)_2$ was the only organometallic compound isolated from reaction of $FvMo_2(CO)_4(PPh_3)_2H_2$ with trityl, the identity of the bright red transient species intrigued us since hydrogen abstraction should be a stepwise process and the intermediacy of monohydride radical species such as $FvMo_2(CO)_4(PPh_3)_2H$ or $FvMo_2(CO)_4(PPh_3)_2(\mu\text{-H})$ seemed possible. Careful monitoring of the reaction (toluene-d_8) by ^1H NMR spectroscopy revealed the brief appearance of four broad resonances of equal intensity at δ 4.67, 4.74, 4.83, and 5.51. These were present as minor components relative to the resonances of $FvMo_2(CO)_4(PPh_3)_2$ and may well be attributed to the red intermediate species $FvMo_2(CO)_4(PPh_3)_2H$; the breadth of the resonances is consistent with the expected paramagnetism. Alternatively, as suggested by a reviewer, the red species may be the tetranuclear $\{HMo(CO)_2(PPh_3)FvMo(CO)_2(PPh_3)\}$-$\{Mo(CO)_2(PPh_3)FvMo(PPh_3)(CO)_2H\}$, arising from coupling of two molecules of $FvMo_2(CO)_4(PPh_3)_2H$. While this metal–metal-bonded formulation provides a possible rationale for the red color and the observation of four Fv ^1H resonances, it seems to us unlikely, since further hydrogen atom abstraction might be expected to result not in scission of the central Mo–Mo bond and the formation of the soluble dimer $FvMo_2(CO)_4(PPh_3)_2$ but rather of an insoluble polymeric isomer.

In any event, the formation of radical species was subsequently confirmed unambiguously by an experiment in which $FvMo_2(CO)_4(PPh_3)_2H_2$ was reacted with $Ph_3C^\bullet$ in the presence of excess $PhCH_2Br$. Addition of a trityl solution to a solution of a mixture of $FvMo_2(CO)_4(PPh_3)_2H_2$ and $PhCH_2Br$ resulted in the instant and complete formation of $FvMo_2(CO)_4(PPh_3)_2Br_2$ and Ph_3CH, suggesting that bromine atom abstraction succesfully competed with the intramolecular coupling of biradicals. In contrast, reaction of $FvMo_2(CO)_4(PPh_3)_2H_2$ and $PhCH_2Br$ in the absence of trityl required ~1 h to go to completion; $FvMo_2(CO)_4(PPh_3)_2HBr$[9] was the only new species observed for ~20 min, although $FvMo_2(CO)_4(PPh_3)_2Br_2$ was the eventual product.

It is also possible that the reaction of $FvMo_2(CO)_4(PPh_3)_2H_2$ with trityl involves disproportionation (eq 7)

$$2FvMo_2(CO)_4(PPh_3)_2H \rightarrow FvMo_2(CO)_4(PPh_3)_2 + FvMo_2(CO)_4(PPh_3)_2H_2 \quad (7)$$

rather than simple abstraction of the second hydrogen atom by trityl. This possibility is supported by observation that reaction of $FvMo_2(CO)_6HI$[9] with trityl proceeds as in eq 8. Here one of the hydride ligands has been

$$2FvMo_2(CO)_6HI + 2Ph_3C^\bullet \rightarrow FvMo_2(CO)_6I_2 + FvMo_2(CO)_6 + 2Ph_3CH \quad (8)$$

replaced by iodide, and therefore only a single hydrogen atom may be abstracted from each molecule. Reactions involving essentially the reverse of eq 6 will not occur, and thus the iodo ligands will not be abstracted by trityl. Assuming the intermediacy of $FvMo_2(CO)_6I$, the formation of $FvMo_2(CO)_6I_2$ and $FvMo_2(CO)_6$ seems to imply that a $FvMo_2(CO)_6I$ molecule can abstract an iodine atom from a second $FvMo_2(CO)_6I$ to form the organometallic products of eq 8. Note that the same type of radical species, containing either a hydride or a halide ligand, was previously proposed as an intermediate in the hydrogen–halogen exchange reactions of dihydrides with alkyl halides (eq 9).[9]

$$FvMo_2(CO)_4L_2H_2 + 2RX \rightarrow [FvMo_2(CO)_4L_2HX] \rightarrow FvMo_2(CO)_4L_2X_2 \quad (9)$$

We have pursued the possibility that Mo–Mo-bonded dimers might be prepared via radical-chain, possibly catalytic processes. Indeed, the spontaneous decomposition of $FvMo_2(CO)_6H_2$ to $FvMo_2(CO)_6$ and H_2 is quite likely a long-known but not fully recognized example; Tilset *et al.* earlier conducted a kinetic study of the analogous decomposition of $FvW_2(CO)_6H_2$, concluding that there was involvement of an as yet undefined radical chain process.[8b] We have found that addition of small amounts of $Co_2(CO)_8$, which is known to autocatalyze the decomposition of $Co(CO)_4H$ to $Co_2(CO)_8$ and H_2 via $Co(CO)_4$ radicals,[10d,17] results in much faster decomposition of $FvMo_2(CO)_6H_2$ to $FvMo_2(CO)_6$ than occurs in the absence of $Co_2(CO)_8$. A similar experiment was subsequently carried out with $FvMo_2(CO)_4(PPh_3)_2H_2$, which is otherwise thermally stable at ambient temperature but which readily gave $FvMo_2(CO)_4(PPh_3)_2$ in quantitative yield in the presence of $Co_2(CO)_8$.

These reactions provide examples in which the chemistry of (fulvalene)molybdenum complexes is quite different from that of the Cp analogs; reaction of $CpMo(CO)_3H$ with $Co_2(CO)_8$ results in a hydrogen atom transfer process leading to $CpMoCo(CO)_7$ and $HCo(CO)_4$,[18] while reaction of $CpMo(CO)_2(PPh_3)H$ with $Co_2(CO)_8$ results solely in exchange of PPh_3 and CO ligands, leading to $Co_2(CO)_7(PPh_3)$ and $CpMo(CO)_3H$.[19] A quite different mechanism was suggested for these reactions.[18]

Preparation of $FvMo_2(CO)_4(PCy_3)_2$ and $FvMo_2(CO)_4(PXy_3)_2$ by Reduction of the Dihalides $FvMo_2(CO)_4L_2X_2$ (L = PCy_3, PXy_3; X = Cl, Br). As pointed out above, phosphine-substituted (fulvalene)dimolybdenum dihydrides with phosphines bulkier than PPh_3 could not be synthesized via direct substitution reactions of $FvMo_2(CO)_6H_2$ with the phosphines. We therefore investigated reductions of the corresponding dihalides with a view either to generating the biradicals/dimers directly or, if reduction to the dianions occurred, to generating them by oxidations of the dianions.

To test the applicability of the idea, we initially attempted reductions of the PPh_3-substituted dihalides $FvMo_2(CO)_4(PPh_3)_2Cl_2$ and $FvMo_2(CO)_4(PPh_3)_2Br_2$ to demonstrate that the now well-characterized dimer $FvMo_2(CO)_4(PPh_3)_2$ could be prepared. Accordingly $FvMo_2(CO)_4(PPh_3)_2Cl_2$ was reduced by sodium dispersion to give good yields of $FvMo_2(CO)_4(PPh_3)_2$ (eq 10), while sodium dispersion reduction of $FvMo_2(CO)_4(PPh_3)_2Br_2$ resulted in the formation of good yields of

(17) Wegman, R. W.; Brown, T. L. *J. Am. Chem. Soc.* **1980**, *102*, 2494.
(18) Kovács, I.; Sisak, A.; Ungváry, F.; Markó, L. *Organometallics* **1989**, *8*, 1873.
(19) Kovács, I., unpublished results.

$[FvMo_2(CO)_4(PPh_3)_2]^{2-}$ (eq 11), characterized by IR and

$$FvMo_2(CO)_4(PPh_3)_2Cl_2 \xrightarrow{Na} FvMo_2(CO)_4(PPh_3)_2 \quad (10)$$

$$FvMo_2(CO)_4(PPh_3)_2Br_2 \xrightarrow{Na} [FvMo_2(CO)_4(PPh_3)_2]^{2-} \quad (11)$$

NMR spectroscopy of the Na^+ or Et_4N^+ salt. That $FvMo_2(CO)_4(PPh_3)_2$ obtained in eq 10 did not react further with sodium suggests that this compound is not an intermediate in the reduction of $FvMo_2(CO)_4(PPh_3)_2Br_2$.

Acidification of $[FvMo_2(CO)_4(PPh_3)_2]^{2-}$ with glacial acetic acid gave $FvMo_2(CO)_4(PPh_3)_2H_2$, while oxidation by $[Cp_2Fe]PF_6$ or air resulted in the formation of $FvMo_2(CO)_4(PPh_3)_2$, as anticipated, confirming the identity of the substituted dianion.

Repeating the above experiments with $FvMo_2(CO)_4(PCy_3)_2Cl_2$ and $FvMo_2(CO)_4(PCy_3)_2Br_2$ gave similar results. Reduction of the former by sodium dispersion produced $FvMo_2(CO)_4(PCy_3)_2$, isolated as a light blue powder. This new compound exhibits an IR spectrum very similar to that of $FvMo_2(CO)_4(PPh_3)_2$, but with both absorptions shifted to lower frequencies (Table 1). The $^{31}P\{^1H\}$ NMR spectrum exhibited one singlet at δ 69.7, considerably downfield from that of $FvMo_2(CO)_4(PCy_3)_2Cl_2$, while the ^1H NMR spectrum exhibited Fv resonances at δ 4.30 ("t") and 5.01 (m). The $^{13}C\{^1H\}$ NMR spectrum exhibited three fulvalene and one CO resonance, and thus the structure is presumably the same as that of $FvMo_2(CO)_4(PMe_3)_2$[8] and $FvMo_2(CO)_4(PPh_3)_2$ (see above). The UV–vis spectrum of $FvMo_2(CO)_4(PCy_3)_2$ featured a strong $\lambda_{max}(d\sigma \rightarrow d\sigma^*)$ absorption at 374 nm, similar to that of $FvMo_2(CO)_4(PPh_3)_2$ and indicating that increasing both the bulk and basicity of the phosphine ligands[20] do not alter the Mo–Mo bond strength significantly.

In contrast, $FvMo_2(CO)_4(PCy_3)_2Br_2$ readily underwent reduction to $[FvMo_2(CO)_4(PCy_3)_2]^{2-}$ with sodium dispersion at room temperature; this dianion was characterized by IR and ^1H NMR spectroscopy as the Na^+ and PPN^+ salts. It was found to be extremely air-sensitive in solution, smoothly transforming to $FvMo_2(CO)_4(PCy_3)_2$ on exposure to traces of oxygen. Addition of glacial acetic acid resulted in the formation of $FvMo_2(CO)_4(PCy_3)_2H_2$, which was identified by IR spectroscopy. Like $FvMo_2(CO)_4(PPh_3)_2H_2$,[9] this hydride exhibited absorptions at 1926 (vs) and 1850 (s) cm^{-1}, to lower frequency than those of $FvMo_2(CO)_4(PPh_3)_2H_2$.

Finally, the compounds $FvMo_2(CO)_4(PXy_3)_2Cl_2$ and $FvMo_2(CO)_4(PXy_3)_2Br_2$ were also reduced by sodium dispersion to the corresponding dimer, $FvMo_2(CO)_4(PXy_3)_2$, and dianion, $[FvMo_2(CO)_4(PXy_3)_2]^{2-}$, respectively. The former was not isolated analytically pure but was synthesized and characterized spectroscopically *in situ* (Tables 1 and 2). However, the close similarity to the spectral characteristics of $FvMo_2(CO)_4(PPh_3)_2$ suggests that $FvMo_2(CO)_4(PXy_3)_2$ formed in this way also exists as the *trans* isomer. It is noteworthy that the electronic spectrum of $FvMo_2(CO)_4(PXy_3)_2$ featured the same $\lambda_{max}(d\sigma \rightarrow d\sigma^*)$ transition at 374 nm as those of other new $FvMo_2(CO)_4L_2$ (L = PPh_3, PCy_3) derivatives, suggesting that even one of the bulkiest phosphines known (θ = 190°)[20] has little influence on the Mo–Mo bond strength in dimeric fulvalene complexes.

The ^1H NMR spectra of the three new (fulvalene)dimolybdenum dimers also merit comment. On the basis of heteronuclear NOE difference experiments, it has previously been shown that the fulvalene β-protons in the compounds $FvMo_2(CO)_4L_2$ (L = CO, PMe_3) are deshielded relative to the fulvalene α-protons, while the reverse ordering was found for non-metal–metal-bonded compounds.[14b] It was therefore suggested that the relative ordering of and the chemical shift differences between the α- and β-hydrogen resonances may possibly be utilized to differentiate between metal–metal-bonded and non-metal–metal-bonded compounds. While we have not carried out similar NOE difference studies, the assignments in Table 2 are reasonably posited on the assumption[14b] that the P–H spin–spin coupling decreases in the order $J(P-H_\beta) > J(P-H_\alpha)$. Thus, the ^1H NMR spectra of $FvMo_2(CO)_4L_2$ (L = PPh_3, PXy_3) imply that there is no correlation between the relative chemical shifts of H_β and H_α and the presence of a metal–metal bond.

The dianion $[FvMo_2(CO)_4(PXy_3)_2]^{2-}$ was characterized as the Na^+ salt in solution by IR spectroscopy and by comparison with $[FvMo_2(CO)_4(PPh_3)_2]^{2-}$. Similar to the analogous compounds containing PPh_3 and PCy_3, it could be protonated by glacial acetic acid to give $FvMo_2(CO)_4(PXy_3)_2H_2$, which was isolated in good yield and characterized by IR and ^1H and $^{31}P\{^1H\}$ NMR spectroscopy. The spectroscopic data were similar to those of $FvMo_2(CO)_4(PPh_3)_2H_2$[9] and serve to unambiguously identify this compound.

Hydrogen Atom Abstraction from $FvMo_2(CO)_4(PXy_3)_2H_2$ by Trityl Radicals. It seemed desirable to synthesize $FvMo_2(CO)_4(PXy_3)_2$ in an alternative way in order to confirm its formulation, and the hydrogen atom abstraction reaction of $FvMo_2(CO)_4(PXy_3)_2H_2$ with trityl radicals was utilized. While the expected product, *trans*-$FvMo_2(CO)_4(PXy_3)_2$, was obtained, formation of a second product was also indicated by the IR spectrum of the reaction mixture. In addition to carbonyl absorption bands at 1931 (m) and 1857 (vs) cm^{-1}, attributable to *trans*-$FvMo_2(CO)_4(PXy_3)_2$, there were also bands at 1919 (s) and 1856 (m) cm^{-1}. The relative intensities of the latter pair seemed to suggest an attribution to *cis*-$FvMo_2(CO)_4(PXy_3)_2$, a hypothesis strengthened by the $^{31}P\{^1H\}$ NMR spectrum ($CDCl_3$), which exhibited singlet resonances at δ 76.8 (attributed to *trans*-$FvMo_2(CO)_4(PXy_3)_2$), 61.93, and 61.90. A comparable difference between the ^{31}P resonances of *cis* and *trans* isomers of $CpMo(CO)_2(PPh_3)I$ and $FvMo_2(CO)_4(PPh_3)_2I_2$ has been observed previously,[9] and the closely spaced pair of ^{31}P resonances could be attributed to the *meso*- and *dl* stereoisomers of *cis*-$FvMo_2(CO)_4(PXy_3)_2$, as observed for *cis,cis*-$FvMo_2(CO)_4(PPh_3)_2I_2$.[9] However, the ^1H and $^{13}C\{^1H\}$ NMR spectra of the unidentified compound exhibit only two Fv proton and three fulvalene carbon resonances, respectively, and thus attribution to *cis*-$FvMo_2(CO)_4(PXy_3)_2$ is reasonable only if the compound is fluxional.

Molecular Mechanics Calculations on $FvMo_2(CO)_6$. Finally, we wish to offer a rationale for the

(20) (a) Tolman, C. A. *Chem. Rev.* **1977**, *77*, 313. (b) Dias, P. B.; Minas de Piedade, M. E.; Martinho Simões, J. A. *Coord. Chem. Rev.* **1994**, *135/136*, 737.

apparently anomalous observations, mentioned above, that the compounds $FvM_2(CO)_6$ (M = Cr, Mo, W) all contain extraordinarily long but intact metal–metal bonds and that substitution of CO by PMe_3 in $FvMo_2(CO)_6$ results in a *decrease* in the length of the Mo–Mo bond, in apparent contrast to other metal–metal-bonded systems. We have attempted to assess the major steric factors in $FvMo_2(CO)_6$ by carrying out molecular mechanics calculations on this compound. We have previously demonstrated the utility of the molecular modeling program PCMODEL[21] for determining minimum energy structures of a variety of flexible cyclopentadienyl and arene complexes, and we have successfully calculated, for instance, ligand rotation conformational energy profiles of a wide variety of alkyl, acyl, phosphine, olefin, and arene ligands.[22]

The molecule $FvMo_2(CO)_6$ was therefore constructed utilizing standard procedures,[22b,c,23] and the minimum energy structure was determined. Structures obtained computationally in this way reflect only steric, not electronic, influences on geometries[22b,f] and may differ from those found crystallographically when substantial electronic factors operate counter to steric factors.

The crystallographically determined structure of $FvMo_2(CO)_6$[6b] is as in **A**. Of relevance here, (i) the two fulvalene rings are almost coplanar, with a centroid–Mo–Mo–centroid angle of 4.9°, and (ii) the pairs of carbonyl ligands of each $Mo(CO)_3$ group "cis" to the Mo–Mo bond are eclipsed with those of the other $Mo(CO)_3$ group (OC–Mo–Mo–CO dihedral angles 3.7 and 5.4°) such that the CO – CO distances of neighboring CO ligands are 2.870 and 2.876 Å, considerably less than the sums of the van der Waals radii.[24] Therefore, in addition to ring strain arising from Mo–Mo bonding, which results in the observed fulvalene bending (θ = 15.3°),[5] there must be a great deal of steric strain arising from repulsions between the carbonyl ligands on one metal atom with those on the other. Indeed, while the two "trans" CO ligands are almost linear (Mo–C≡O bond angles 176.24 and 178.26°), the four "cis" carbonyl groups are bent (Mo–C≡O bond angles 170.72–172.26°) such that the oxygen atoms move away from each other. Similar observations have been made in the sterically very congested structures of $[CpCr(CO)_3]_2$ (3.281 Å)[7] and $[Cp^*Cr(CO)_3]_2$ (3.3107 Å).[4]

The crystallographically determined structure of $FvMo_2(CO)_4(PMe_3)_2$[8] is significantly different. The Mo–Mo bond, while still rather long (3.220 Å), is shorter than that of $FvMo_2(CO)_6$ and the fulvalene ligand is very significantly distorted from planarity (θ = 27.0°). Even more important, the five-membered rings are twisted such that the centroid–Mo–Mo–centroid angle is 24.2°, and thus the pairs of carbonyl ligands "cis" to the Mo–Mo bond are essentially staggered rather than eclipsed.

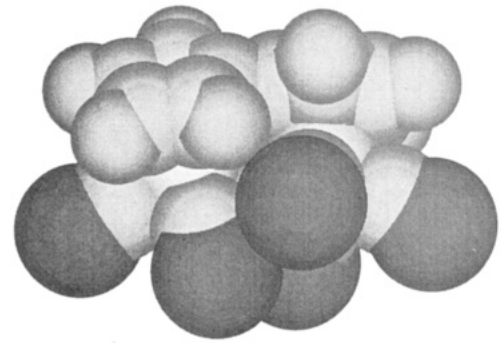

Figure 1. Optimized structure of $FvMo_2(CO)_6$.

Given the apparent steric disadvantages imposed by the eclipsed geometry of $FvMo_2(CO)_6$, the observed structure must arise from electronic factors which force the near-planarity of the fulvalene rings. If so, then the twisting away from this (presumably) electronically preferred, eclipsed structure in the case of $FvMo_2(CO)_4(PMe_3)_2$ may well be a result of significantly enhanced steric repulsions arising from coordination of the bulkier phosphine ligands. Coordination of PMe_3 would force the CO ligands closer together, resulting in even greater steric repulsions which could at least partially outweigh the electronically preferred structure and hence result in twisting of the molecule to the observed staggered structure. The molybdenum atoms could then approach each other more closely, offering a rationale for the shorter Mo–Mo bond distance.

Minimization of the steric effects[23] in $FvMo_2(CO)_6$ resulted in a structure in which the calculated Mo–Mo distance is a rather long 3.45 Å, the Mo–CO bond distances average 1.98 Å, in excellent agreement with the crystallographic data, and the Mo–Fv bond distances average 2.08 Å, ~0.25 Å shorter than those found experimentally. As anticipated on the basis of steric considerations, the halves of the molecule are twisted relative to each other (Figure 1), very much as in the crystal structure of $FvMo_2(CO)_4(PMe_3)_2$.[8] The centroid–Mo–Mo–centroid dihedral angle is 48°, and the "cis" OC–Mo–Mo–CO angles are staggered, with dihedral angles of 59 and 34°. Thus, it appears that a staggered structure is indeed preferred sterically for $FvMo_2(CO)_6$ and that $FvMo_2(CO)_4(PMe_3)_2$ may be at least tending toward the less crowded conformation which would be preferred by $FvMo_2(CO)_6$ in the absence of inter-ring conjugation or other electronic effects.

Acknowledgment. We thank NATO for a Science Scholarship to I.K. (administered by the Natural Sciences and Engineering Research Council), the NSERC for a Research Grant to M.C.B., and the Hungarian Science Foundation for support provided by Grant No. OTKA F7419. We also thank W. E. Geiger for drawing our attention to the fulvalene problem.

OM9501135

(21) Available as PCMODEL from Serena Software, Bloomington, IN. See: Gajewski, J. J.; Gilbert, K. E.; McKelvy, J. *Adv. Mol. Model.* **1990**, *2*, 65.

(22) (a) Mackie, S. C.; Park, Y.-S.; Shurvell, H. F.; Baird, M. C. *Organometallics* **1991**, *10*, 2993. (b) Mackie, S. C.; Baird, M. C. *Organometallics* **1992**, *11*, 3712. (c) Polowin, J.; Mackie, S. C.; Baird, M. C. *Organometallics* **1992**, *11*, 3724. (d) Britten, J.; Mu, Y.; Harrod, J. F.; Polowin, J.; Baird, M. C.; Samuel, E. *Organometallics* **1993**, *12*, 2672. (e) Polowin, J.; Baird, M. C. *J. Organomet. Chem.* **1994**, *478*, 45. (f) Polowin, J.; Baird, M. C. *Can. J. Chem.*, in press.

(23) Construction of $FvMo_2(CO)_6$ utilizing aromatic carbon atoms (type 40 of PCMODEL) resulted in the rings assuming a coplanar structure because the torsion parameters have a larger V2 term to ensure that the dihedral angles between the rings are either 0 or 180°. However, utilization of four olefinic (type 2) and one carbanionic (type 48) carbon atoms in each ring (all marked as π atoms), followed by a π calculation, resulted in a significant decrease in V2 such that the inter-ring steric factors outweighed the torsion term.

(24) Bondi, A. *J. Phys. Chem.* **1964**, *68*, 441.

Zirconium-Assisted Aldol Condensation Reactions of Amido Enolates: Structural and Kinetic Analysis of the Reaction of *N,N*-Diphenylacetamide and *N,N*-Diphenylpropionamide Enolates with Benzaldehyde and *p*-Substituted Acetophenones

Pier Giorgio Cozzi,† Patrick Veya, and Carlo Floriani*

Institut de Chimie Minérale et Analytique, BCH, Université de Lausanne, CH-1015 Lausanne, Switzerland

François P. Rotzinger

Institut de Chimie Physique, Ecole Polytechnique Fédérale, CH-1015 Lausanne, Switzerland

Angiola Chiesi-Villa and Corrado Rizzoli

Dipartimento di Chimica, Universitá di Parma, I-43100 Parma, Italy

Received June 27, 1995[⊗]

The deprotonation of *N,N*-diphenyl amides with LDA and subsequent reaction with $[(cp)_2ZrCl_2]$ (cp = η^5-C_5H_5) allowed the enolate complexes $[\{Ph_2NC(CH_2)O\}Zr(cp)_2(Cl)]$ (**5**) and $[\{Ph_2NC(CHCH_3)O\}Zr(cp)_2(Cl)]$ (**6**) to be isolated. The crystal structure of **6** is reported. Reaction of **5** with $[Cr(CO)_5]$·THF gave $[Ph_2NC\{CH_2Cr(CO)_5\}\{OZr(Cl)(cp)_2\}]$ (**7**), an O- and C-bonded dimetallic amido enolate. Reaction of **5** and **6** with benzaldehyde gave the corresponding aldol products **8** and **9**; according to previous reports, the conversion of **6** into **9** is *syn* selective. Reaction of **6** with acetophenone followed by addition of silver triflate gave the complex $[Ph_2NC(=O)CH(CH_3)C(Me)(Ph)OZr(cp)_2(Cl)(OSO_2CF_3)]$ (**11**) as a diastereoisomeric mixture in the ratio *anti:syn* = 65:35. The crystal structure of *syn*-**11** is reported. This cyclic complex mimics the postulated cyclic transition state of the aldol reaction mediated by zirconium amide enolates. A kinetic investigation of the reaction of **6** with acetophenone was performed and gave the following activation parameters: $\Delta H^{\ddagger} = 38.3 \pm 0.9$ kJ mol^{-1}; $\Delta S^{\ddagger} \geq -181 \pm 3$ J mol^{-1} K^{-1}; $\Delta G^{\ddagger}_{298} = 92.2 \pm 1.2$ kJ mol^{-1}. A similar study with 4-fluoroacetophenone gave $\Delta H^{\ddagger} = 43.5 \pm 1.3$ kJ mol^{-1}, $\Delta S^{\ddagger} \geq -167 \pm 4$ J mol^{-1} K^{-1}, and $\Delta G^{\ddagger}_{298} = 93.3 \pm 1.8$ kJ mol^{-1}. The reaction rate at 320 K determined with 4-chloro-, 4-methyl-, and 4-nitroacetophenone allowed the determination of a Hammett plot with $\varrho = 0.41$. This value is implicit of a carbon–carbon bond-forming, rate-limiting step.

Introduction

Amide enolates are of great synthetic importance, particularly with regard to highly selective carbon–carbon bond formation.[1] For example, their conversion into β-hydroxy carbonyls represents a convenient route to the building blocks of polypropionate- and polyacetate-derived natural products.[2] Despite such widespread use, however, structural information is sparse.[3] Although structural studies have been reported for some lithium amide enolates,[4] no previous study of transition-metal analogues has been published.[5]

Boron enolates have been subjected to *ab initio* calculations,[6] and a related force field study[7] has helped shed light on the aldolic reaction mediated by boron. However, the difficulties encountered in developing an *ab initio* approach for transition-metal complexes are well-known. Consequently, theoretical analysis of transition-metal amide enolates has only been performed at a primitive level.[8] For transition-metal enolate complexes, simple and facial stereoselection are currently interpreted by a hypothetical model derived from study-

* To whom correspondence should be addressed.
† Present address: Istituto di Chimica "G. Ciamician", Università di Bologna, I-40216 Bologna, Italy.
⊗ Abstract published in *Advance ACS Abstracts,* August 1, 1995.

(1) Heathcock, C. H. In *Comprehensive Organic Synthesis*; Heathcock, C. H., Ed.; Pergamon: Oxford, U.K., 1991; Vol. 2, p 181. Kim, M. B.; Williams, S. F.; Masamune, S. In *Comprehensive Organic Synthesis*; Heathcock, C. H., Ed.; Pergamon: Oxford, U.K., 1991; Vol. 2, p 239. Oare, D. A.; Heathcock, C. H. In *Topics in Stereochemistry*; Eliel, E. L., Wilen, S. H., Eds.; Wiley: New York, 1989; p 227.

(2) *Polyether Antibiotics*; Wesley, J. W., Ed.; Marcel Dekker: New York, 1982. *Macrolide Antibiotics*; Omura, S., Ed.; Academic: Orlando, FL, 1984. Paterson, I.; Mansury, M. M. *Tetrahedron* **1985**, *41*, 3569. Boeckman, R. H.; Goldstein, M. In *The Total Synthesis of Natural Products*; Wiley: New York, 1988. Tatsuta, K. In *Recent Progress in the Chemical Synthesis of Antibiotics*; Springer: Berlin, Germany, 1990. Nakata, M.; Tatsuta, K. In *Studies in Natural Product Chemistry*; Rahman, A. U., Ed.; Elsevier: Amsterdam, Holland, 1993; Vol. 12, part 4.

(3) Williard, P. G. In *Comprehensive Organic Synthesis*; Schreiber, S. L., Ed.; Pergamon: Oxford, England, 1991; Vol. 1, p 1. Seebach, D. *Angew. Chem., Int. Ed. Engl.* **1988**, *27*, 1624. Cieplak, A. S. In *Structure Correlation*; Bürgi, H.-B.; Dunitz, J. D., Eds.; VCH: New York, 1994; p 205.

(4) Laube, T.; Dunitz, J. D.; Seebach, D. *Helv. Chim. Acta* **1985**, *68*, 1373. Buaer, W.; Laube, T.; Seebach, D. *Chem. Ber.* **1985**, *118*, 764.

(5) Veya, P.; Floriani, C.; Chiesi-Villa, A.; Rizzoli, C. *J. Chem. Soc., Chem. Commun.* **1991**, 1166.

(6) Li, Y.; Paddon-Row, M. N.; Houk, K. N. *J. Am. Chem. Soc.* **1988**, *110*, 3684. Li, Y.; Paddon-Row, M. N.; Houk, K. N. *J. Org. Chem.* **1990**, *55*, 481. Bernardi, F.; Robb, M. A.; Suzzi-Valli, G.; Tagliavini, E.; Umani-Ronchi, A. *J. Org. Chem.* **1991**, *56*, 6472.

(7) Bernardi, A.; Capelli, A. M.; Gennari, C.; Goodman, J. M.; Paterson, I. *J. Org. Chem.* **1990**, *55*, 3576. Vulpetti, A.; Bernardi, A.; Gennari, C.; Goodman, J. M.; Paterson, I. *Tetrahedron* **1993**, *49*, 685.

0276-7333/95/2314-4092$09.00/0

Scheme 1

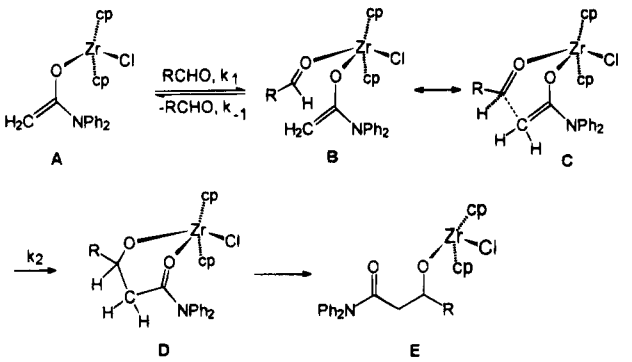

ing the scope of the reaction in connection with Hoffmann's analysis of the frontier orbitals available for a bent metallocene fragment.[9] It is therefore desirable to obtain accurate structural information for such complexes. The bond parameters observed should be of particular use in deciding the role of sterically bulky substituents in determining stereoselectivity. Moreover, although a detailed force field calculation is presently beyond us, the bond lengths and angles recorded may be of use for future studies in this area.

Therefore, we now report the synthesis and characterization of two zirconocene amido enolate complexes which we used in reactions with carbonyl compounds.[10] The X-ray structure determination of the starting zirconium enolate and a derivative of the final product allows us to support the mechanism accepted for transition-metal-mediated aldol reactions, as indicated in Scheme 1.

Furthermore, kinetic analysis of a stereogenic amido enolate reacting with a range of *p*-substituted acetophenones has allowed us to calculate activation parameters and derive a Hammett plot. These latter data have showed that the rate-determining step for the aldol reaction involves the formation of a carbon–carbon bond.

Results and Discussion

Deprotonation of *N,N*-diphenylacetamide (**1**) and *N,N*-diphenylpropionamide (**2**) was carried out according to Scheme 2. As shown by the ^{1}H NMR spectrum, the lithium enolate **3** possesses two molecules of THF bound to the alkali-metal center and we therefore propose a dimeric structure with tetracoordinate lithium atoms. The ^{1}H NMR spectrum of **3** includes singlets at 3.42 and 3.63 ppm, which are assigned to the enolic protons: these chemical shifts fall within the range of previously reported data for unsolvated enolates.[11]

The *in situ* generation of **3** and **4** was followed by transmetalation with $(cp)_2ZrCl_2$ at low temperature. Slow warming to room temperature and appropriate workup procedures led to the isolation of **5** and **6** (Scheme 2). The corresponding reaction with $(cp)_2TiCl_2$ gave products which could not be isolated without decomposition.[12] Nonetheless, although they are highly

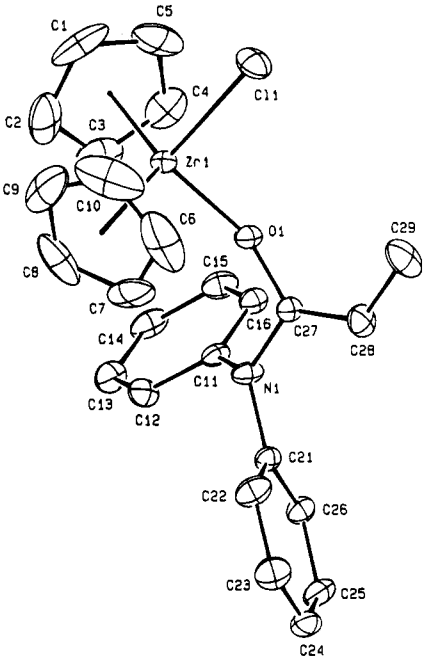

Figure 1. ORTEP drawing for complex **6** (30% ellipsoids).

Scheme 2

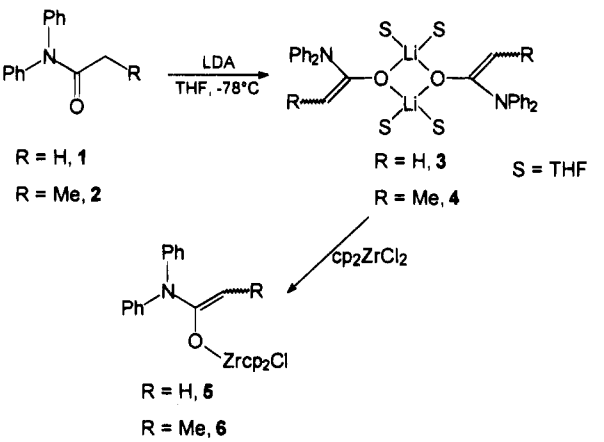

susceptible to moisture, both **5** and **6** are yellow solids stable at room temperature under an inert atmosphere.

Isolation of **6** directly from the reaction mixture gave a 65:35 mixture of diastereoisomers; attempts to separate these by recrystallization failed, with the original ratio unchanged. Structural analysis on an X-ray-quality crystal of **6** allowed us to determine the bond connectivity and parameters of the *Z* isomer. The structure of **6** is shown in Figure 1, while a selection of bond distances and angles is given in Table 2. Complex **6** is a monomer, with a geometry very close to the structure of nonstereogenic *N,N*-diphenyl amido enolates previously characterized.[5] Some differences are observed in the torsion angles, as indicated by the values reported in Table 2.

The dihedral angles of the C11···C16 and C21···C26 phenyl planes with respect to the enolato O1,N1,C27,-C28 plane are very close in both complexes (111.5(1) and 104.7(1)°, respectively, for **6**; 112.5(1) and 109.5(2)° for **5**). The main feature of both structures is the disposition of the enolate carbon *syn* to Cl. One of the phenyls is *syn* to zirconium. The dihedral angle between C11–

(8) Paterson, I. In *Comprehensive Organic Synthesis*; Heathcock, C. H., Ed.; Pergamon: Oxford, U.K., 1991; Vol. 2, p 301.
(9) Evans, D. A.; McGee, R. *Tetrahedron Lett.* **1980**, *21*, 3975. Evans, D. A.; McGee, R. *J. Am. Chem. Soc.* **1981**, *103*, 2876.
(10) For previous study by our laboratory in this area: (a) Berno, P.; Floriani, C.; Chiesi-Villa, A.; Rizzoli, C. *Organometallics* **1990**, *9*, 1995. (b) Veya, P.; Cozzi, P. G.; Rotzinger, F.; Floriani, C.; Chiesi-Villa, A.; Rizzoli, C. *Organometallics* **1995**, *14*, 4101.
(11) Veya, P. Thèse de doctorat, University of Lausanne, Lausanne, Switzerland, 1993.
(12) Titanium enolates prepared *in situ* from pyrrolidinopropionamide react with aldehydes, giving *anti* products: Murphy, P. J.; Procter, G.; Russel, A. T. *Tetrahedron Lett.* **1987**, *28*, 2037.

Table 1. Experimental Data for the X-ray Diffraction Studies on Crystalline Compounds 6, 7, and 11

	6	7	11
formula	$C_{25}H_{24}ClNOZr$	$C_{29}H_{22}ClCrNO_6Zr$	$C_{34}H_{32}F_3NO_5SZr \cdot C_4H_8O$ (2/1)
a (Å)	10.636(1)	9.870(1)	18.368(5)
b (Å)	12.029(1)	23.237(2)	14.115(4)
c (Å)	9.405(1)	13.338(1)	14.398(4)
α (deg)	70.45(1)	90	90
β (deg)	77.97(1)	105.94(1)	109.08(4)
γ (deg)	76.37(1)	90	90
V (Å^3)	1093.6(2)	2941.4(5)	3527.8(19)
Z	2	4	4
fw	481.1	659.2	751.0
space group	$P\bar{1}$ (No. 2)	Cc (No. 9)	$P2_1/n$ (No. 14)
t (°C)	22	22	22
λ (Å)	0.71069	0.71069	0.71069
ϱ_{calc} (g cm^{-3})	1.461	1.489	1.414
μ (cm^{-1})	6.41	8.55	4.19
transmission coeff	0.985–1.00	0.937–1.000	0.952–1.000
R^a	0.026	0.026 [0.027][c]	0.058
$R_G{}^b$		0.028 [0.029]	

[a] $R = \Sigma||\Delta F|/\Sigma|F_o|$. [b] $R_G = [\Sigma w|\Delta F|^2/\Sigma w|F_o|^2]^{1/2}$. [c] Values in brackets refer to the "inverted" structure.

Zr–O1 and O1–C27–C28 varies from 30.0(1)° in **6** to 33.8(3)° in **5**. The angles Zr–O–C11 (19.2(3)°) and Cl1–Zr–C11 (−179.4(2)°) show the *Z* configuration of the enolate in **6**. The C27–C28 bond distances in **5**[5] and **6** confirm the presence of a localized double bond.

However, despite a full characterization of **6**, assignment of configuration to the major and minor components of the diastereoisomeric mixture was not directly possible. A ^{1}H NMR NOESY experiment suggested that the major component has a *Z* configuration, but this was no conclusive. Nevertheless, indirect evidence firmly supports the *Z* isomer as the most abundant diastereoisomer. First, it is well-established that hindered amides favor the formation of *Z* enolates.[1] Furthermore, the ^{1}H NMR chemical shift of the most intense methyl signal correlates closely with related *Z* enolates reported previously.[9]

The reaction of **5** and **6** with carbonyl compounds probably proceeds according to the pathway in Scheme 1, where the metal plays the role of templating agent. We envisaged, however, a number of reactions where the zirconium-nonassisted nucleophilic reactivity of the enolate can lead to novel organometallic bifunctional species. This is exemplified in the reaction of **5** with the soft electrophile [Cr(CO)$_5$(THF)].

The reaction in Scheme 3 exemplifies the preliminary attack of the enolate nucleophile at an electrophilic center, and this is not followed by an evolution of the nucleophile–electrophile adduct. Such a reaction was successful only with the most strongly nucleophilic enolates, such as the amido enolates, while it was not observed with the ketone enolates. The strong electronic influence of the [Cr(CO)$_5$] fragment affects the chemical shifts of the methylene group. The proposed bonding scheme of compound **7** is supported by the structural data in Table 2, which were obtained from a single crystal X-ray analysis.

In complex **7** the enolato fragment has a geometry close (see Figure 2) to that observed in complexes **5** and **6**. Also in this case the nucleophilic CH_2 is *syn* to N1 and *trans* with respect to the Cl1 ligand at zirconium, as indicated by the value of the torsional angles Cl1–Zr···C27–N1 and Cl1–Zr···C27–C28 (Table 2). The orientation of the phenyl rings is similar to that observed in complex **6**, the dihedral angles of the C11···C16 and C21···C26 phenyl planes with respect to the enolato O1,N1,C27,C28 plane being 109.8(1) and 101.9(1)°. The binding of [Cr(CO)$_5$] induces a specific rotation around the Zr–O bond, as indicated by the values of the Cl1–Zr–O1–C27, Zr–O1–C27–C28, and Zr–O1–C27–N1 torsional angles. The CH_2 nucleophile binds Cr at a normal distance for a Cr–C σ bond (2.328(5)°). The CO *trans* to it takes care of the major amount of the charge transferred by the enolate to the metal, the Cr–C33 (1.814(5) Å) and C33–O33 (1.66(7) Å) being significantly shorter and longer, respectively, than those found for the other four Cr–CO groups (mean values: Cr–C, 1.898(8) Å; C–O, 1.139(10) Å). Lengthening of the C27–C28 and Zr–O1 bonds and shortening of the C27–O1 and N1–C27 bonds were observed on moving from complexes **6** and **5** to **7** (see Table 2). This is in agreement with a partial electronic transfer at the intermediate stage by nucleophilic attack at an electrophile, before further reaction. The choice of metal carbonyls in the reaction with nucleophilic metal enolates was made because they contain two different electrophilic sites, namely the metal center in the case of coordinatively unsaturated metal carbonyls and the CO ligands in the case of coordinatively saturated metal carbonyls. The former reaction leads, as in the present case, to the formation of a O- and C-bonded dimetallic enolate, the chemistry of which is under investigation. In the latter case the attack by the enolate at the metal-bonded CO led to a novel class of dimetallocarbene.[13]

We were unable to identify any interesting reactivity behavior of **7**. Enolates **5** and **6** react cleanly with benzaldehyde to give extremely soluble oily products which we have not been able to crystallize. The reaction can be conveniently monitored using ^{1}H NMR in a sealed tube, and spectroscopic data for **8** and **9** (Scheme 4) are reported in the Experimental Section. In both products zirconium is now bonded to the oxygen derived from the carbonyl substrate.

Complex **8** displays characteristic ABX methylene signals at 2.42, 2.93, and 5.90 ppm (respective coupling constants of 3.5, 9.2, and 15.35 Hz). It is reassuring to note that these coupling constants are very close to those we found for cationic aldolato complexes with the metallacycle structure reported below, which we believe to be structural models for the aldol reaction transition state.[10] The aldol product **9** was found to be a mixture of diastereoisomers in an 81:19 ratio. Hydrolysis showed that the *syn* isomer is the most abundant one.[9]

(13) Veya, P.; Floriani, C.; Chiesi-Villa, A.; Rizzoli, C. *Organometallics* **1994**, *13*, 214.

Table 2. Selected Bond Distances (Å) and Angles (deg)

Complexes **6**, **7**, and **11**

	6	**7**	**11**
Within the Zirconium Coordination Sphere[a]			
Zr1–X	2.475(1)	2.415(2)	1.947(7)
Zr1–O1	1.981(2)	2.046(3)	2.239(7)
Zr1–cp1	2.230(4)	2.202(5)	2.259(16)
Zr1–cp2	2.215(7)	2.206(6)	2.267(15)
cp1–Zr1–cp2	129.2(2)	130.2(3)	123.9(5)
cp1–Zr1–X	106.5(1)	106.2(1)	118.4(4)
cp1–Zr1–O1	106.2(1)	108.2(2)	94.8(4)
cp2–Zr1–X	105.1(2)	106.8(2)	117.7(4)
cp2–Zr1–O1	106.8(2)	103.4(2)	97.5(4)
X–Zr1–O1	99.0(1)	97.3(1)	75.4(3)
Within the Ligands			
O1–C27	1.346(3)	1.310(5)	1.258(13)
N1–C27	1.424(3)	1.361(6)	1.337(13)
N1–C11	1.429(4)	1.423(5)	1.431(9)
N1–C21	1.438(3)	1.427(5)	1.432(10)
C27–C28	1.335(4)	1.385(7)	1.500(14)
C28–C29	1.487(5)		1.486(16)
X–C29			1.431(13)
Zr1–O1–C27	151.0(2)	141.1(3)	134.2(7)
Zr1–X–C29			145.8(7)
C27–N1–C11	117.9(2)	122.1(4)	119.8(8)
C27–N1–C21	118.9(2)	120.6(4)	123.4(8)
C11–N1–C21	117.2(2)	117.2(3)	116.7(8)
O1–C27–N1	112.4(2)	114.2(4)	118.1(10)
O1–C27–C28	124.1(3)	122.1(4)	122.6(10)
N1–C27–C28	123.4(3)	123.7(5)	119.2(10)
C27–C28–C29	124.9(3)		113.8(10)

Complex **7**

In the Coordination Sphere			
Cr1–C28	2.328(5)	O29–C29	1.146(7)
Cr1–C29	1.895(5)	O30–C30	1.131(11)
Cr1–C30	1.895(8)	O31–C31	1.135(11)
Cr1–C31	1.896(8)	O32–C32	1.144(12)
Cr1–C32	1.907(9)	O33–C33	1.166(7)
Cr1–C33	1.814(5)		
C28–Cr1–C33	173.6(2)	C31–Cr1–C32	93.2(3)
C29–Cr1–C31	175.5(3)	Cr1–C29–O29	172.7(5)
C30–Cr1–C32	174.5(3)	Cr1–C30–O30	174.5(7)
C29–Cr1–C30	84.4(3)	Cr1–C31–O31	176.5(8)
C29–Cr1–C32	90.1(3)	Cr1–C32–O32	176.1(6)
C30–Cr1–C31	92.2(4)	Cr1–C33–O33	177.6(5)

Torsional Angles for the Metal Enolate Fragment in **5**–**7**

	5	**6**	**7**
Cl1–Zr··C27–N1	176.7(3)	179.4(2)	181.7(4)
Cl1–Zr··C27–C28	18.4(4)	19.2(3)	23.1(3)
Zr–O1–C27–C28	−87.4(7)	−95.4(4)	−61.3(7)
Zr–O1–C27–N1	90.6(6)	83.1(4)	119.3(4)
Cl1–Zr–O1–C27	95.9(5)	104.9(4)	76.2(5)

[a] X = Cl1 for complexes **6** and **7**; X = O2 for complex **11**. Cp1 and Cp2 refer to the centroids of the cyclopentadienyl rings C1–C5 and C6–C10, respectively.

Applying the Karplus equation[14] to the NMR data for complex **8** (*i.e.* correlating coupling constants to dihedral angles between H_A, H_B, and H_X) allowed us to derive the following Newman projection to represent the favored solution conformation:

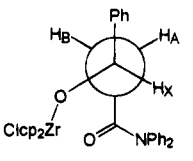

8

We believe that this is probably similar to the solid-state situation, because the bulky nature of the amide nitrogen substituents will hinder rotation around the newly formed carbon–carbon bond.[10] The steric encumbrance also serves to place the two oxygen atoms in a synclinal position. Although this orientation can be explained on steric grounds, it is worthy noting that this conformation can be derived from a cyclic transition state.[15]

The high rate of reaction of **5** with benzaldehyde and with acetophenone precluded a kinetic analysis of the

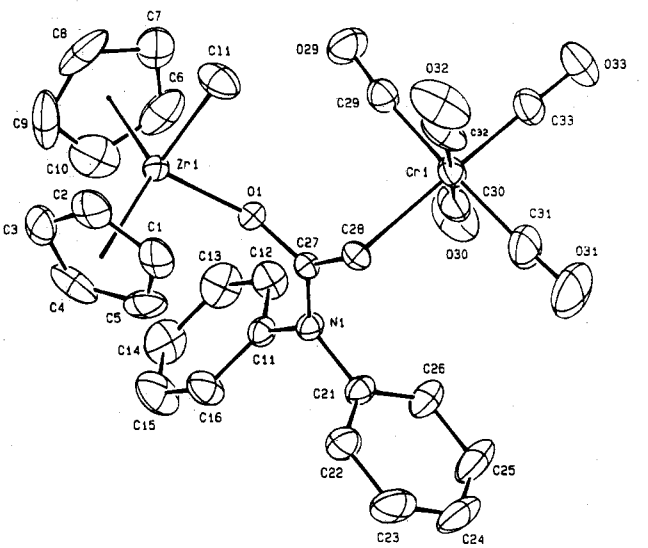

Figure 2. ORTEP drawing for complex **7** (30% ellipsoids).

Scheme 3

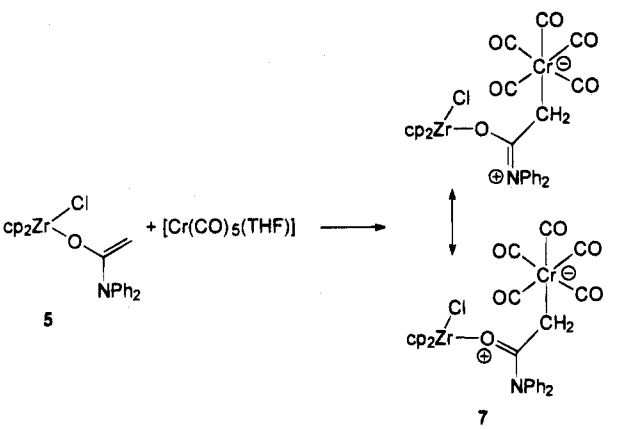

Scheme 4

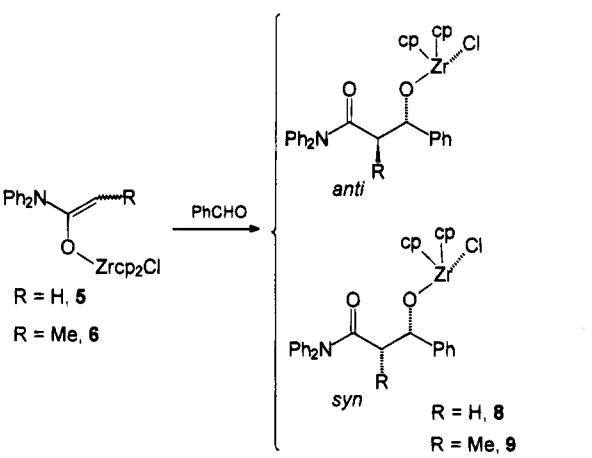

(14) (a) Pretsch, E.; Seibl, J.; Simon, W.; Clerc, T. *Tables of Spectral Data for Structure Determination of Organic Compounds*; Springer: Berlin, Germany, 1983. (b) Fleming, I.; Williams, D. H. *Spectroscopic Methods in Organic Chemistry*, 3rd ed.; McGraw-Hill: New York, 1980; p 100.

(15) Zimmerman, H. E.; Traxler, M. D. *J. Am. Chem. Soc.* **1957**, *79*, 1920.

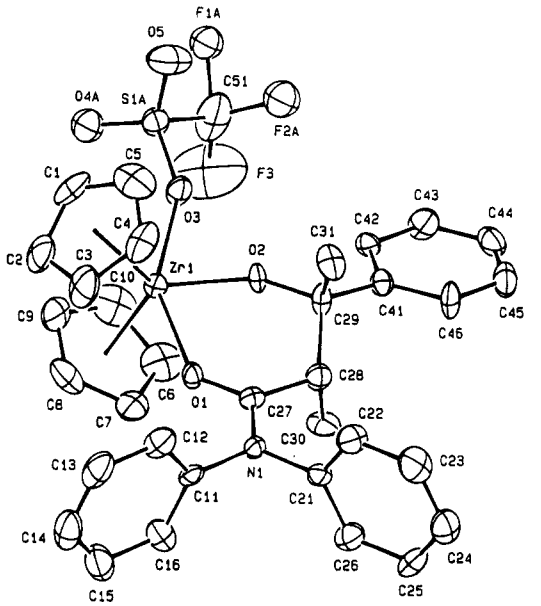

Figure 3. ORTEP drawing for complex **11** (30% ellipsoids). Only the A positions are given for the disordered S1, O4, F1, and F2 atoms.

Scheme 5

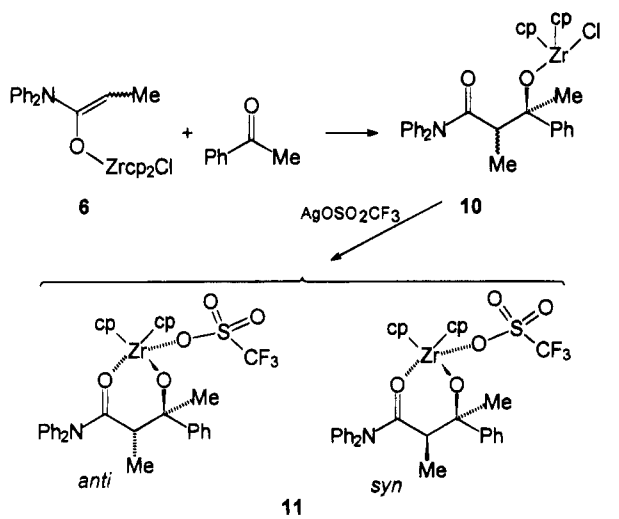

aldolic reaction. However, the reaction of **6** with acetophenone (to give **10** as a 65:35 diastereoisomeric mixture) proceeds more slowly at a rate amenable to a kinetic study by ^{1}H NMR (Scheme 5). Complex **10** is an oil but can be converted to the solid aldol product **11** by reaction with silver(I) triflate (Scheme 5).

Complex **11** also exists as a diastereoisomeric mixture (ratio 65:35). Given the similar nature of the diastereoisomer ratios of **10** and **11**, we believe it is reasonable to assume that the reaction with silver triflate does not affect the configuration of the stereogenic centers. The diastereoisomers of **11** may be separated by recrystallization. An X-ray analysis on a crystal so obtained showed the presence of a *syn* configuration. However, the ^{1}H NMR spectrum of this sample corresponded to the minor component of the product mixture: i.e., **10** is a diastereoisomeric ratio of 65% *anti*, 35% *syn*.

In the structure of **11** the cationic aldolato metallacycle has a rather long distance interaction between the metal and the counteranion (Zr1–O3, 2.290(7) Å). The Zr1,O1,O2,O3 plane is perpendicular to the cp1–Zr–cp2 plane (dihedral angle 88.0(4)°). The narrow O1–Zr–O2 angle (75.4(3)°) allows the binding of the fifth ligand by the metal. This ligand slightly affects the structural parameters of the $(cp)_2Zr$ group, the Zr–cp bond distances being significantly longer (2.259(16), 2.267(15) Å) and the cp1–Zr–cp2 angle narrower (123.9-(5)°) than in **6** and **7**. The bidentate O,O′ ligand gives rise to a six-membered metallacycle with a half-chair conformation, the C28 carbon being 0.464(11) Å out of the plane containing Zr,O1,O2,C27,C29 (maximum displacement 0.114(12) Å for C29). The structural parameters of the metallacycle are essentially in agreement with the proposed bonding scheme, though the C27–O1 and C27–N1 bond distances, along with the planarity of the O1,N1,C27,C28 fragment, suggest some delocalization over the O1–C27–N1 moiety. The C30 and C31 methyl carbons assume an *anti* conformation, the C31–C29–C28–C30 torsion angle being −169.4(9)°. It is worth mentioning at this stage the relevance of **11** with respect to the transition state of the aldol reaction.

An important difference between the ^{1}H NMR spectra of **10** and **11** is the inversion in chemical shifts of the α-methyl protons. Although we cannot explain this peculiar effect, it is intriguing to note that a similar phenomenon is not observed for the methine proton (see Experimental Section). We suggest that in the syn isomer the α-methyl substituent lies in a position subjected to a shielding effect associated with one of the amide nitrogen phenyl rings (C21–C26). However, in the anti configuration, the methyl group lies outside any such electronic influence.

By examining the ratio of the starting enolate and the aldol products in the reaction of **6** with acetophenone, we assume that the *Z* enolate gives the *anti* product, while the *E* enolate gives the *syn* aldol adduct.[16]

This relationship between the starting enolate and the final product requires a boatlike transition structure.[17] Although some reports indicated that it is possible to obtain the *anti* aldol product in reactions of the zirconium enolate of esters with aldehydes,[18] this fact was interpreted on the basis of a chair transition state. To the best of our knowledge, no report has appeared on the reactions of amide stereogenic zirconium enolates with ketones.

Previously Evans and McGee[9] have proposed that the *Z* $(cp)_2ZrCl_2$ enolates react with aldehydes *via* a chair-like transition state, whereas *E* enolates prefer to react *via* a boatlike transition state, with both the *E* and *Z* enolates affording *syn* aldol products. The isolation and structural characterization of **11** are our starting points for the discussion of the possible transition state involved in the reaction of **6** with acetophenone.

We assume that the reaction proceeds first *via* ketone complexation to the zirconium (we will see later in this article that the coordination of the carbonyl substrate to the zirconium is not the rate-determining step in this aldol condensation). We also assume that ketone complexation to the zirconium center is not linear, as shown

(16) Heathcock, C. H. In *Asymmetric Synthesis*; Morrison, D. J., Ed.; Academic: New York, 1984; Vol. 3, Chapter 2. Evans, D. A.; Nelson, J. V.; Taber, T. R. In *Topics in Stereochemistry*; Eliel, E. L., Wilen, S. H., Eds.; Wiley: New York, 1983; Vol. 13, p 1. Denmark, S. E.; Henke, B. R. *J. Am. Chem. Soc.* **1991**, *113*, 2177.

(17) Nakamura, E.; Kuwajima, I. *Tetrahedron Lett.* **1983**, 3343. Hoffmann, R. W.; Ditrich, K.; Froech, S. *Tetrahedron* **1985**, *41*, 5517. Nakamura, E.; Kuwajima, I. *Acc. Chem. Res.* **1985**, *18*, 181. Gennari, C.; Todeschini, R.; Beretta, M. G.; Favini, G.; Scolastico, C. *J. Org. Chem.* **1986**, *51*, 612.

(18) Sacha, H.; Waldmüller, D.; Braun, M. *Chem. Ber.* **1994**, *127*, 1959.

by spectroscopic,[19] computational,[19] and crystallographic[19,20] studies. In the case of aldehydes, theoretical calculations have shown that complexation of the Lewis acid *syn* to the aldehyde hydrogen atom is energetically favored.[19] In the case of ketones, spectroscopic studies[21] and calculations[19,22] have shown that complexation of the Lewis acid *syn* to the less sterically hindered group is less favored. The crystallographically observed conformation for **11** is half-chair. A force field calculation method recently developed[23] was able to generate structures of $(cp)_2MCl_2$ complexes (M = Ti, Zr) which are almost identical with those found by X-ray diffraction. However, the force field calculations have shown that clusters of energetically closely spaced conformations can exist which could accommodate reacting substrates. The isolated structure of **11** does not necessarily have the same conformation as that proposed for the transition state.[9] This notwithstanding, **11** does show some similarity with the transition structure, where the enolate, the carbonyl substrate, and the other zirconium substituents are in the same plane. This implies a rather acute O–Zr–O bond angle (75.4° in complex **11**). In a "normal" aldol reaction, the preferred chairlike structure for the idealized Zimmerman–Traxler cyclic transition state avoids vicinal nonbonding interactions. When an important steric interaction dominates, as in the case of the zirconium enolate for the presence of the bulky cp ring, the unfavorable eclipsing interactions in the boat transition structure are not energetically unfavorable. From this point of view, the cp zirconium enolate resembles the case of Denmark's recently calculated transition structure for five-coordinate silicon enolates.[24] The assumption that the aldolate product comes from the cyclic transition state is completely justified on the basis of our kinetic study (*vide infra*). In the case of the reaction of the *E* enolate **6** with acetophenone, we propose two possible transition structures, shown in Scheme 6.

Other conformations are surely possible and should be considered. The only way to distinguish the two transition structures is to calculate the energy difference between **A** and **B**. Steric interactions of the carbonyl substituents with the cp ring show that the twist-boat transition structure is favored, as also calculated by Denmark.[24] This naive view, however, does not consider the role of the bulky substituent groups on nitrogen and their interaction with the cp rings and the carbonyl substituent.

We have started to examine the possibility of an *ab initio* calculation on transition-metal enolates[25] and hope to address the question in the near future.

Mechanism of the Aldol Reaction. The structural characterization of cyclic **11** is, however, not enough to show that a cyclic transition state is encountered during this reaction. To address this question and to find the rate-determining step for the condensation, we undertook a kinetic study of complex **6** with acetophenone and *p*-substituted acetophenones.

Scheme 6

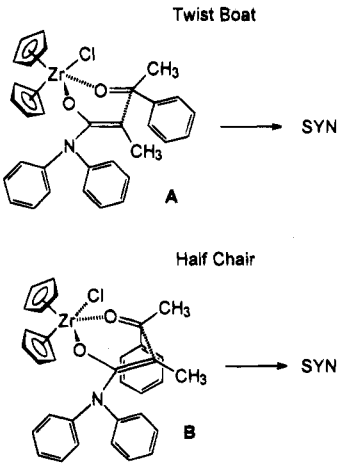

Table 3. Rate Constants from 300 to 340 K for the Reaction of 6 with Acetophenone in C_6D_6[a]

T (K)	k (M^{-1} h^{-1})	T (K)	k (M^{-1} h^{-1})
340	11.81 ± 0.07	310	3.05 ± 0.04
330	7.47 ± 0.08	300	1.66 ± 0.02
320	5.03 ± 0.06		

[a] $c_{10} = 2c_{20}$; $c_{20} = 0.1000$ M in all cases.

A kinetic study on the aldolic reaction promoted by silyl ketene acetals derived from amides was recently published,[26] and the authors reported activation parameters for the second-order reaction. The reaction is accelerated by electron-withdrawing groups, and a Hammett plot revealed that the rate-determining step is carbon–carbon bond formation. To the best of our knowledge, only one kinetic study on the aldolic reaction with a metal enolate has been performed previously, and this was conducted by our group on the aldolic condensation of acetophenone with $[\{(cp)_2Fe)CH(CH_2)O\}Zr(cp)_2Cl]$.[10b] However, the metal enolate used in this study, although useful for modeling purposes, does not find use in organic synthesis, unlike zirconium amide enolates.

The stereogenic zirconium enolate **6** was therefore allowed to react with acetophenone at five different temperatures, and the results are listed in Table 3.

On the basis of our previous explorations, we assume that the *Z* enolate gives rise to *anti* products, while *syn* compounds are formed from *E* enolates. Although we cannot exclude the possibility of cross-product (*i.e. Z* enolate giving *syn* product), it seems unlikely, given the constant mixture ratio observed during the course of the reactions. The reaction was monitored by recording the ratio of the integrals of the methyl peaks of **6** to those of **10**. The temperatures investigated were chosen so as to avoid overlap of the signals in question. The kinetic parameters derived for the conversion of the *Z* form of **6** into the *anti* diastereoisomer of **10**, and those for (*E*)-**6** into *syn*-**10**, were measured independently and found to be the same. An Eyring analysis of the reaction as a function of temperature gave the following results: $\Delta H^{\ddagger} = 38.3 \pm 0.9$ kJ mol^{-1}; $\Delta S^{\ddagger} \geq -181 \pm 3$ J

(19) Shambayati, S.; Crowe, W. E.; Schreiber, S. L. *Angew. Chem., Int. Ed. Engl.* **1990**, *29*, 256. Shambayati, S.; Schreiber, S. L. In *Comprehensive Organic Synthesis*; Schreiber, S. L., Ed.; Pergamon: Oxford, U.K., 1991; Vol. 1, p 283–324.
(20) Cozzi, P. G.; Floriani, C. Manuscript in preparation.
(21) Hartman, J. S.; Stilbs, P.; Forsens, S. *Tetrahedron Lett.* **1975**, *16*, 3497. Fratiello, A.; Stoner, C. S. *J. Org. Chem.* **1975**, *40*, 1244. Fratiello, A.; Kubo, R.; Chow, S. *J. Chem. Soc., Perkin Trans. 2* **1976**, 1205. Torri, J.; Azzaro, M. *Bull. Soc. Chim. Fr.* **1978**, 283.
(22) Goodman, J. M. *Tetrahedron Lett.* **1992**, *33*, 7219. Rauk, A.; Hunt, I. R.; Keay, B. A. *J. Org. Chem.* **1994**, *59*, 6808 and references therein.
(23) Doman, T. N.; Hollis, K. T.; Bosnich, B. *J. Am. Chem. Soc.* **1995**, *117*, 1352.
(24) Denmark, S. E.; Griedel, B. D.; Coe, D. M.; Schnute, M. E. *J. Am. Chem. Soc.* **1994**, *116*, 7026.
(25) Nottoli, R.; Sgamellotti, A.; Floriani, C. Unpublished results.
(26) Myers, A. G.; Kephart, S. E.; Chen, H. *J. Am. Chem. Soc.* **1992**, *114*, 7922. Myers, A. G.; Widdowson, K. L.; Kukkola, P. J. *J. Am. Chem. Soc.* **1992**, *114*, 2765.

Scheme 7

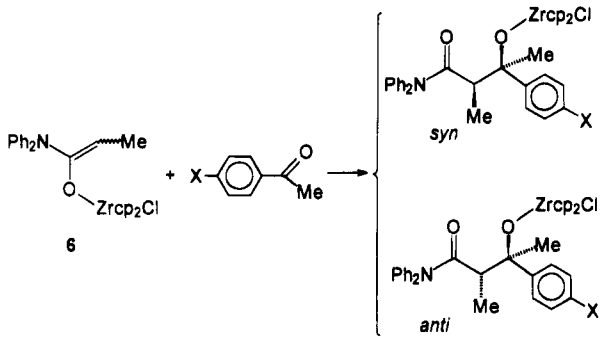

X = H, **10**
X = Me, **12a**
X = F, **12b**
X = Cl, **12c**
X = NO_2, **12d**

Table 4. Rate Constants from 300 to 340 K for the Reaction of 6 with *p*-Fluoroacetophenone in C_6D_6

T (K)	c_{20} (M)[a]	k (M^{-1} h^{-1})
340	0.0933	9.62 ± 0.30
330	0.0933	6.18 ± 0.10
330	0.0933[b]	5.74 ± 0.10
320	0.0933	3.75 ± 0.08
320	0.0933	3.52 ± 0.05
310	0.0933	2.19 ± 0.05
300	0.0933	1.08 ± 0.02

[a] $c_{10} = 2c_{20}$. [b] $c_{10} = 0.176$ M.

mol^{-1} K^{-1}; $\Delta G^{\ddagger}_{298} = 92.2 \pm 1.2$ kJ mol^{-1}. The entropy value is of the same order of magnitude as that reported by Myers and shows an ordered transition state, while the enthalpy of activation is lower than that of the aldol reaction of a silyl ketene acetal; in this latter example the coordination around the silicon must be disrupted in order to allow the binding to the electrophile. In our reaction the zirconium has an empty orbital available for the carbonyl substrate to bind to in the same plane as the amido enolate ligand, and any strain needed to accomplish the necessary geometry of the transition state is minimal.

As previously noted for acetophenone, **6** also reacts with a variety of *p*-substituted acetophenones to give mixtures of diastereoisomers (Scheme 7). In all cases significant deviations from the originally recorded ratio of 65:35 were not observed.

With 4-fluoroacetophenone the kinetic measurement was repeated at four different temperatures; results are collected in Table 4. A least-squares fit according to the Eyring equation gave the following activation parameters: $\Delta H^{\ddagger} = 43.5 \pm 1.3$ kJ mol^{-1}; $\Delta S^{\ddagger} \geq -167 \pm 4$ J mol^{-1} K^{-1}; $\Delta G^{\ddagger}_{298} = 93.3 \pm 1.8$ kJ mol^{-1}.

A kinetic study using other *p*-substituted acetophenones was carried out (Table 5). From the rates derived, we constructed a Hammett plot, which gave a positive ϱ value of 0.41. This is consistent with carbon–carbon bond formation as the rate-determining step and also confirms that, in general, electron-withdrawing substituents accelerate the rate. The point for *p*-nitroacetophenone does not correlate with the other points, presumably due to the complexation of the ketone as a process competing with the rate-determining steps as originally observed by Myers.[26]

In conclusion, our study, focusing on a widely used enolate for simple selection, represents the first complete presentation of the isolation and structural characterization of a zirconium amide enolate. It is hoped that the structural parameters can be used as a starting point to develop a theoretical model for the aldol reaction mediated by early transition metals. In addition, we have presented the first measurement of activation parameters for the aldolic reaction of a stereogenic enolate. The results obtained are consistent with the previously proposed cyclic transition state mechanism outlined at the beginning of this paper (Scheme 1).

Table 5. Rate Constants for the Reaction of 7 with Substituted *p*-Acetophenones in C_6D_6 at 320 K

c_{20} (M)[a]	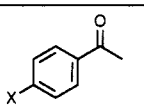	k (M^{-1} h^{-1})
0.0540	X = Me	2.37 ± 0.06
0.0933[b]	X = F	3.52 ± 0.05
0.0540	X = Cl	3.73 ± 0.09
0.0540	X = NO_2	9.37 ± 0.15
0.100[b]	X = H	5.03 ± 0.06

[a] $c_{10} = 3c_{20}$. [b] $c_{10} = 2c_{20}$.

Experimental Section

General Procedure. All reactions were carried out under an atmosphere of purified nitrogen. Solvents were dried and distilled before use by standard methods. Infrared spectra were recorded with a Perkin-Elmer 883 spectrophotometer, ^{1}H NMR spectra were measured on a 200-AC Bruker instrument.

Synthesis of *N,N*-Diphenylacetamide (1). Diphenylamine (23.82 g, 140 mmol) and acetyl chloride (5.53 g, 70 mmol) were dissolved in Et_2O (200 mL) and refluxed overnight. Diphenylamine hydrochloride was filtered off and the solution concentrated to 100 mL. The solution was left at 0 °C for a few days, and the crystallized amide was collected and used without further purification (85%). IR (Nujol): ν(C=O) 1671 cm^{-1}. Anal. Calcd for $C_{14}H_{13}NO$: C, 79.59; H, 6.20; N, 6.63. Found: C, 80.01; H, 6.34; N, 6.56. ^{1}H NMR (CD_2Cl_2): δ 2.03 (s, 3H, COMe), 7.3–7.5 (m, 10H, Ph).

Synthesis of *N,N*-Diphenylpropionamide (2). Diphenylamine (38.8 g, 288 mmol) and propionyl chloride (10 mL, 114 mmol) were dissolved in Et_2O (350 mL) and refluxed overnight. Diphenylamine hydrochloride was filtered off and the solvent evaporated to dryness, affording a white oil which crystallized after several days. The solid was washed with cyclohexane (50 mL), dried, and used without further purification (80%). IR (Nujol): ν(C=O) 1671 cm^{-1}. Anal. Calcd for $C_{15}H_{15}NO$: C, 79.97; H, 6.71; N, 6.22. Found: C, 80.34; H, 6.71; N, 6.48. ^{1}H NMR (CD_2Cl_2): δ 1.09 (t, 3H, J = 6.9 Hz, Me), 2.24 (q, 2H, J = 6.9 Hz, $COCH_2$), 7.2–7.5 (m, 10H, Ph).

Synthesis of 3. To an Et_2O (100 mL) solution of Pr^i_2NH (1.62 g, 160 mmol) was added a solution of BuLi in *n*-hexane (10 mL, 1.6 M, 16.0 mmol) at 0 °C. The solution was stirred for 20 min and then was cooled to −78 °C. To this ether solution of LDA was added a solution of **1** (3.38 g, 16.0 mmol) in THF (10 mL) over 1 h. After the addition the solution was warmed to room temperature, stirred for 1 h, and then stored at −20 °C. After a few days a white crystalline solid was formed, which was collected and dried under vacuum (81%). ^{1}H NMR (C_6D_6): δ 1.40 (m, 8H, THF), 3.42 (s, 1H, =CH_2), 3.63 (m, 9H, =CH_2, THF), 6.85–6.90 (m, 2H, Ph), 7.1–7.3 (m, 8H, Ph).

Synthesis of 5. To a solution of Pr^i_2NH (3.36 g, 32.3 mmol) in THF (150 mL) was added a solution of BuLi in *n*-hexane (20 mL, 32.0 mmol) at 0 °C, and the solution was stirred at the same temperature for 20 min. The LDA solution was cooled to −50 °C, and a solution of **1** (6.80 g, 32.2 mmol) in THF (50 mL) was slowly added over 1 h and stirred for another 30 min. To the clear solution was added $(cp)_2ZrCl_2$ (8.94 g,

30.6 mmol) in one portion. The yellow solution was stirred for 5–6 h and warmed to room temperature. The solvent was pumped off and the yellow solid collected with Et_2O. The solid was charged on a Soxhlet and extracted with mother liquor to afford, after 2 days, a yellow crystalline solid, which was filtered and collected (75%). Crystals suitable for X-ray analysis were obtained by extraction with Et_2O. Anal. Calcd for $C_{24}H_{22}ClNOZr$: C, 61.71; H, 4.75; N, 3.00. Found: C, 62.19, H, 4.75; N, 3.01. ^1H NMR (CD_2Cl_2): δ 3.64 (s, 2H, $=CH_2$), 6.22 (s, 10H, $Zr(cp)_2$), 7.0–7.4 (m, 10H, Ph). ^{13}C NMR (CD_2Cl_2): δ 78.1 ($=CH_2$), 115.1 ($Zr(cp)_2$), 123.5, 123.82, 125.15, 125.27, 129.54, 129.67 (Ph), 147.07 (Ph), 163.9 (COZr).

Synthesis of 6. To a solution of LDA (28.8 mmol) in THF (150 mL) at −60 °C was slowly added a solution of **2** (6.50 g, 28.85 mmol) in THF (50 mL), and this mixture was stirred at the same temperature for 1 h. To the clear solution was added $(cp)_2ZrCl_2$ (8.01 g, 27.4 mmol), and the mixture was warmed to room temperature with stirring over 6 h. The solvent was pumped off and the yellow solid collected with diethyl ether (60 mL). The solid was charged on a Soxhlet and extracted for 2 days with freshly distilled Et_2O. The yellow solid was collected and dried under vacuum (71%). X-ray-quality crystals were obtained by extraction with Et_2O. Anal. Calcd for $C_{25}H_{24}ClNOZr$: C, 62.41; H, 5.03; N, 2.91. Found: C, 62.35; H, 5.18; N, 2.83. ^1H NMR (CD_2Cl_2; two isomers, *Z*:*E* = 65:35): *Z*, δ 1.67 (d, 3H, J = 6.9 Hz, Me), 4.27 (q, 1H, J = 6.9 Hz, $=CHCH_3$), 6.14 (s, 10H, $(cp)_2Zr$), 7.0–7.4 (m, 10H, Ph); *E*, δ 1.43 (d, 3H, J = 6.8 Hz, Me), 4.56 (q, 2H, J = 6.8 Hz, $=CHCH_3$), 6.14 (s, $(cp)_2Zr$, 10H), 7.0–7.4 (m, 10H, Ph).

Synthesis of 7. A $[Cr(CO)_5(THF)]$ solution prepared in situ by photolysis of $Cr(CO)_6$ (0.88 g, 4.0 mmol) in THF (250 mL) was added dropwise to a stirred solution of the complex **5** (1.64 g, 3.5 mmol) in THF (50 mL) at room temperature. The red solution was stirred for 5 h, and then the solvent was evaporated to dryness. To the oily residue was added Et_2O (80 mL), yielding a yellow crystalline solid, which was collected and dried (43%). Crystals suitable for X-ray analysis were obtained by extraction with Et_2O. IR (Nujol): ν(Cr(CO)) 2051 (w), 1938 (s), 1916 (s), 1840 (m) cm^{-1}. Anal. Calcd for $C_{29}H_{22}ClCrNO_6Zr$: C, 52.84; H, 3.36; N, 2.12. Found: C, 52.42; H, 3.14; N, 1.96. ^1H NMR (CD_2Cl_2): δ 1.72 (AB, 2H, J = 2.50 Hz, CH_2Cr), 6.28 (s, 5H, cp), 6.31 (s, 5H, cp), 7.3–7.5 (m, 10H, Ph). ^{13}C NMR (C_6D_6): δ 13.8 (CH_2Cr), 114.6 ($(cp)_2Zr$), 110–130 (Ph), 163.9 (NC–O), 191.3 (C–O), 219.8 (CrCO), 225.2 (CrCO).

Reaction of 5 with Benzaldehyde in a Sealed Tube. Synthesis of 8. Complex **5** (0.057 g, 0.12 mmol) and distilled benzaldehyde (0.012 mL, 0.12 mmol) were added to C_6D_6 in a NMR tube under nitrogen; then the solution was frozen and the tube sealed. After 2 h a ^1H NMR spectrum was recorded. ^1H NMR (C_6D_6): δ 2.42–2.93 (AB part of ABX, 2H, J_{AX} = 3.50 Hz, J_{BX} = 9.20 Hz, J_{AB} = 15.35 Hz, CH_2CO), 5.86 (s, 5H, $(cp)_2Zr$), 5.90 (X part of ABX, 1H, J_{AX} = 3.50 Hz, J_{BX} = 9.20 Hz, CHOZr), 6.18 (s, 5H, $(cp)_2Zr$), 6.8–7.3 (m, 15H, Ph).

Reaction of 5 with Acetophenone in a Sealed Tube. Synthesis of 10. Complex **5** (0.052 g, 0.11 mmol) and distilled acetophenone (0.013 mL, 0.11 mmol) were added to an NMR tube containing C_6D_6 under nitrogen; then the solution was frozen and the tube sealed. After 24 h a ^1H NMR spectrum was recorded. ^1H NMR (C_6D_6): δ 1.92 (s, 3H, Me), 2.79 (s, 2H, CH_2), 5.91 (s, 5H, $(cp)_2Zr$), 6.02 (s, 5H, $(cp)_2Zr$), 6.8–7.5 (m, 15H, Ph).

Reaction of 6 with Benzaldehyde in a Sealed Tube. Synthesis of 9. Complex **6** (0.054 g, 0.11 mmol) and distilled benzaldehyde (0.011 mL, 0.11 mmol) were added to an NMR tube containing CD_2Cl_2; then the solution was frozen and the tube sealed. After 24 h a ^1H NMR spectrum was recorded. ^1H NMR (CD_2Cl_2); two diastereoisomers, *syn*:*anti* = 81:19): *syn*, δ 1.38 (d, 3H, J = 6.7 Hz, Me), 2.70 (m, 1H, CHMe), 5.12 (d, 1H, J = 9.1 Hz, CH–O), 6.11 (s, 5H, cp), 6.28 (s, 5H, cp), 6.7–7.5 (m, 15H, Ph); *anti*, δ 0.76 (d, 3H, J = 6.9 Hz), 2.92 (m, 1H, CHMe), 5.20 (d, 1H, J = 9.0 Hz, CH–O), 6.01 (s, 5H, cp), 6.35 (s, 5H, cp), 6.75–7.5 (m, 15H, Ph).

Reaction of 6 with Acetophenone in a Sealed Tube. Synthesis of 10. Complex **6** (0.046 g, 0.09 mmol) and distilled acetophenone (0.011 mL, 0.09 mmol) were added to an NMR tube containing C_6D_6; then the solution was frozen and the tube sealed. After 24 h a ^1H NMR spectrum was recorded. ^1H NMR (C_6D_6; two diastereoisomers, *syn*:*anti* = 37:67): *syn*, δ 1.51 (d, 3H, J = 6.91 Hz, Me), 1.97 (s, 3H, Me), 3.05 (q, 2H, J = 6.91 Hz, CH_2), 5.81 (s, 5H, $(cp)_2Zr$), 6.16 (s, 5H, $(cp)_2Zr$), 6.8–7.5 (m, 15H, Ph); *anti*, δ 0.93 (d, 3H, J = 7.07 Hz), 1.88 (s, 3H), 3.21 (q, 1H, J = 7.07 Hz), 5.86 (s, 10H, $(cp)_2Zr$), 6.8–7.5 (m, 15H, Ph). IR (Nujol): ν(CO) 1664 cm^{-1}.

Synthesis of 11. The zirconium enolate **6** (1.61 g, 3.35 mmol) was added to a solution of distilled acetophenone (0.41 g, 3.40 mmol) in CH_2Cl_2 (50 mL), and the yellow solution was stirred overnight. To the resulting pale yellow solution was added dropwise a solution of silver triflate (0.88 g, 3.40 mmol) in CH_3CN (20 mL). The solution turned colorless, and AgCl was filtered off after 30 min of stirring. The solvent was pumped off, and to the resulting oil was added Et_2O (50 mL). The mixture was stirred, yielding a white crystalline solid, which was filtered and dried. Crystals suitable for X-ray analysis were obtained from an extraction with 5:1 Et_2O/dimethoxyethane. Anal. Calcd for $C_{34}H_{32}FNO_5SZr$: C, 57.12; H, 4.51; N, 1.96. Found: C, 57.17; H, 4.78; N, 2.26. ^1H NMR (CH_2Cl_2); two isomers, *syn*:*anti* = 35:65): *syn*, δ 0.90 (d, 3H, J = 7.12 Hz, Me), 1.68 (s, 3H, Me), 3.00 (q, 1H, J = 7.12 Hz, CH), 6.12 (s, 10H, $(cp)_2Zr$), 7.15–7.60 (m, 15H, Ph); *anti*, δ 1.35 (s, 3H, Me), 1.48 (d, 3H, J = 6.97 Hz), 3.18 (q, 1H, J = 6.97 Hz), 5.95 (s, 10H, $(cp)_2Zr$), 7.15–7.60 (m, 15H, Ph). IR (Nujol): ν(CO) 1590 cm^{-1}.

X-ray Crystallography for Complexes 6, 7, and 11. The crystals selected for study were mounted in glass capillaries and sealed under nitrogen. The reduced cells were obtained with use of TRACER.[27] Crystal data and details associated with data collection are given in Tables 1 and S1 (Table S1 is in the supporting information). Data were collected at room temperature (295 K) on a single-crystal diffractometer. For intensities and background the profile measurement technique was used.[28] The structure amplitudes were obtained after the usual Lorentz and polarization corrections,[29] and the absolute scale was established by the Wilson method.[30] The crystal quality was tested by ψ scans, showing that crystal absorption effects could not be neglected. Data were then corrected for absorption using the program ABSORB.[31] The function minimized during the least-squares refinement was $\sum w|\Delta F|^2$. Unit weights were used for all complexes, since these gave a satisfactory analysis of variance and the best agreement factors.[29] Anomalous scattering corrections were included in all structure factor calculations.[32b] Scattering factors for neutral atoms were taken from ref 32a for non-hydrogen atoms and from ref 33 for H atoms. Solution and refinement were based on the observed reflections.

Complex 6. The structure was solved using SHELX86.[34] Refinement was first done isotropically, and then anisotropically for non-hydrogen atoms, by full-matrix least squares. The hydrogen atoms were located from difference Fourier maps and introduced in the subsequent refinements as fixed-atom contributions with isotropic U's fixed at 0.10 Å^2. During the

(27) Lawton, S. L.; Jacobson, R. A. TRACER (a Cell Reduction Program); Ames Laboratory, Iowa State University of Science and Technology: Ames, IA, 1965.
(28) Lehmann, M. S.; Larsen, F. K. *Acta Crystallogr., Sect. A: Cryst. Phys. Diffr., Theor. Gen. Crystallogr.* **1974**, *A30*, 580.
(29) Data reduction, structure solution, and refinement were carried out on an IBM AT personal computer equipped with an INMOS T800 transputer using: Sheldrick, G. SHELX-76: System of Crystallographic Computer Programs; University of Cambridge: Cambridge, England, 1976.
(30) Wilson, A. J. C. *Nature* **1942**, *150*, 151.
(31) Ugozzoli, F. *Comput. Chem.* **1987**, *11*, 109.
(32) (a) *International Tables for X-ray Crystallography*; Kynoch Press: Birmingham, England, 1974; Vol. IV, p 99. (b) *Ibid.*, p 149.
(33) Stewart, R. F.; Davidson, E. R.; Simpson, W. T. *J. Chem. Phys.* **1965**, *42*, 3175.
(34) Sheldrick, G. SHELX-86: Program for the Solution of Crystal Structures; University of Göttingen, Göttingen, Germany, 1986.

refinement the phenyl and cyclopentadienyl rings were constrained to be regular hexagons (C–C = 1.395 Å) and pentagons (C–C = 1.42 Å), respectively. Since the space group is polar, the crystal chirality was tested by inverting all the coordinates ($x, y, z \rightarrow -x, -y, -z$) and refining to convergence once again. The resulting R values ($R = 0.026$, $R_G = 0.028$ *vs* $R = 0.027$, $R_G = 0.029$) indicated that the original choice should be considered the correct one.

Complex 7. The structure was solved by the heavy-atom method starting from a three-dimensional Patterson map. Refinement was first done isotropically, and then anisotropically for non-hydrogen atoms, by full-matrix least squares. The hydrogen atoms were located from difference Fourier maps and introduced in the subsequent refinements as fixed-atom contributions with isotropic U's fixed at 0.12 Å^2 for those associated to the cyclopentadienyl rings and C29 methyl and 0.06 Å^2 for the remainders.

Complex 11. The structure was solved by the heavy-atom method starting from a three-dimensional Patterson map. Refinement was done by full-matrix least squares first isotropically, and then anisotropically for non-hydrogen atoms, except for the S1N, F1A, F1B, F2A, and O4A, and O4B atoms of the $CF_3SO_3^-$ anion and for the THF solvent molecule. The $CF_3SO_3^-$ anion was found to be affected by a severe disorder. The best fit was obtained by considering the S1, O4, F1, and F2 atoms distributed over two positions (A and B) with the site occupation factors given in Table S4 (supporting information). Attempts to split the F3 fluorine atom in two positions were unsuccessful. The THF solvent molecule (O6, C61–C64) was found to be statistically distributed over two positions around an inversion center. The hydrogen atoms were put in geometrically calculated positions and introduced in the last stage of refinement as fixed-atom contributions with isotropic U's fixed at 0.10 Å^2. The H atoms associated with the disordered THF molecule were ignored. During the refinement the phenyl and cyclopentadienyl rings were constrained to be regular hexagons (C–C = 1.395 Å) and pentagons (C–C = 1.42 Å), respectively. Some constraints were also applied to distances within the THF molecule.

The final difference maps showed no unusual features, with no significant peak above the general background. Final atomic coordinates are listed in Tables S2–S4 for non-hydrogen atoms and in Tables S5–S7 for hydrogens (supporting information). Thermal parameters are given in Tables S8–S10 and bond distances and angles in Tables S11–S13 (supporting information).[35]

Kinetics. Kinetic measurements were obtained by ^{1}H NMR in deuterated benzene at 300, 310, 320, 330, and 340 K. Measurements at 310 K have been made twice with the same concentration and once with a lower concentration. Values of rate constants are reproducible to within 5% error. Relative concentrations of starting and final products are measured with the integration of the doublet of the methyne proton for the couple *Z–anti* in **6** and **10** at 1.67 and 0.93 ppm, respectively, and for the couple *E–syn* at 1.43 and 1.51 ppm, respectively. Integrations of both peak couples give very accurate values with a general difference of 1–2%.

Reaction 1 has been carried out by mixing **6** and acetophenone in the NMR tube at low temperature (~220 K).

$$\mathbf{6} + \text{acetophenone} \xrightarrow{k} \mathbf{10}\ (\text{or}\ \mathbf{12}) \qquad (1)$$

The reaction was started by heating the sample up to the desired temperature. Since this heating process in the NMR spectrometer does not proceed like a unit step function, the time at which $t = 0$ cannot be determined precisely. For this reason, unequal initial concentrations of the reactants were chosen, *viz.* c_{10} (=[acetophenone]) = $2c_{20}$ (=2[**6**]), and the time at the estimated $t = 0$ was set to t_0, a parameter that will be optimized by the least-squares fitting procedure. This ensures that the evaluation of the rate constant k does not depend on the more or less arbitrarily chosen time scale. Integration of the differential equations describing reaction 1 yields eq 2.

$$[\mathbf{10}]\ (\text{or}\ [\mathbf{12}]) = c_{20} - \frac{c_{10} - c_{20}}{\frac{c_{10}}{c_{20}} e^{(c_{10}-c_{20})k(t-t_0)} - 1} \qquad (2)$$

The parameters c_{10}, c_{20}, and t_0 are defined above, t is the time in hours, and k is the second-order rate constant in M^{-1} h^{-1}. Since the relative concentration of **10** (or **12**) in percent (percentage of **10** or of **12**) is available with a minimum error, k and t_0 were evaluated *via* a least-squares analysis according to eq 3.

$$\%\ \mathbf{10}\ (\text{or}\ \%\ \mathbf{12}) = 100\left[1 - \frac{c_{10} - c_{20}}{c_{10} e^{(c_{10}-c_{20})k(t-t_0)} - c_{20}}\right] \qquad (3)$$

The rate constants at various temperatures are given in Tables 3 and 4. The concentration of acetophenone, c_{10}, is (2–3)c_{20}.

Activation parameters are calculated by a $1/\sigma^2$ weighted least-squares fit according to the transition state theory (eq 4), where $\kappa = 1$ if the probability is 100% that the transition state does not give the starting materials, k_B is the Boltzmann constant and is 1.38×10^{-23} J K^{-1}, h is Planck's constant and is 6.63×10^{-34} J Hz^{-1}, and $R = 8.314$ J mol^{-1} K^{-1}. The

$$k = \kappa k_B \frac{T}{h} \exp\left\{\frac{-\Delta H^{\ddagger}}{RT}\right\} \exp\left\{\frac{\Delta S^{\ddagger}}{R}\right\} \qquad (4)$$

following parameters were obtained: $\Delta S^{\ddagger} \geq -181 \pm 3$ J mol^{-1} K^{-1}, $\Delta H^{\ddagger} = 38.3 \pm 0.9$ kJ mol^{-1}, $\Delta G^{\ddagger}_{298} = 92.2 \pm 1.2$ kJ mol^{-1} and $\Delta S^{\ddagger} \geq -167 \pm 4$ J mol^{-1} K^{-1}, $\Delta H^{\ddagger} = 43.5 \pm 1.3$ kJ mol^{-1}, $\Delta G^{\ddagger}_{298} = 93.3 \pm 1.8$ kJ mol^{-1} for the reaction of **6** with acetophenone or *p*-fluoroacetophenone, respectively (see Tables 3 and 4).

Acknowledgment. We thank the "Fonds National Suisse de la Recherche Scientifique" (Grant No. 20-40268.94) and Ciba-Geigy (Basel, Switzerland) for financial support.

Supporting Information Available: Tables giving crystal data and details of the structure determination, fractional atomic coordinates, anisotropic thermal parameters, bond lengths, and bond angles for complexes **6**, **7**, and **11** (14 pages). Ordering information is given on any current masthead page.

OM9505017

(35) See paragraph at the end of the paper regarding supporting information.

Titanium and Zirconium Ferrocene-Substituted Enolates and Their Reaction Products with Benzaldehyde and Acetophenone: Structural and Kinetic Studies of the Aldol Condensation Pathway

Patrick Veya, Pier Giorgio Cozzi,† and Carlo Floriani*

Institut de Chimie Minérale et Analytique, BCH, Université de Lausanne, CH-1015 Lausanne, Switzerland

François P. Rotzinger

Institut de Chimie Physique, Ecole Polytechnique Fédérale, CH-1015 Lausanne, Switzerland

Angiola Chiesi-Villa and Corrado Rizzoli

Dipartimento di Chimica, Università di Parma, I-43100 Parma, Italy

Received June 27, 1995[⊗]

The reaction of acetyl- and propionylferrocene, [(RCOcp)(cp)Fe] (R = Me (**1**), Et (**2**)), with KH led to the isolation of the corresponding ion-pair enolates **3** and **4** in the solid state. When the deprotonation of **1** is carried out in the presence of 18-crown-6, the naked enolate **5**, $[(CH_2COcp)(cp)Fe]^-K(18\text{-crown-6})^+$], was isolated. The potassium enolate **3** has been converted into the corresponding titanium and zirconium enolates *via* the reaction with $(cp)_2MCl_2$ (M = Ti, Zr), while only **4** was converted into the analogous zirconium enolate. The following metal enolates have been isolated in good yield and as crystalline solids: [(cp)-Fe(cpC(CH_2)O)M$(cp)_2$(Cl)] (M = Ti (**6**), Zr (**7**)) and [(cp)Fe(cpC(CHMe)O)Zr$(cp)_2$(Cl)] (**8**). Compounds **6** and **7** have been characterized by ^{1}H and ^{13}C NMR, and an X-ray crystal structure of **7** was obtained; compound **8** was characterized by ^{1}H NMR. The aldol reaction of **6** and **7** with benzaldehyde led to the corresponding metal aldol derivatives [(cp)Fe(cpC-(O)CH_2C(H)(Ph)O)M$(cp)_2$(Cl)] (M = Ti (**9**), Zr (**10**)). For compound **9** the solid-state structure and solution data are reported. Complex **9** undergoes a facile Ti–Cl ionization, leading to the cationic complex [(cp)Fe(cpC(O)CH_2C(H)(Ph)O)Ti$(cp)_2$]$^+BPh_4^-$ (**11**). In complex **11**, the aldol fragment forms a metallacycle where both oxygens are bonded to titanium. This structure mimics the bond connectivity of the generally proposed "transition state" of aldol reactions. The isolation of structurally well-defined titanium and zirconium enolates allowed us to carry out a kinetic investigation into the reaction of **7** with acetophenone. The reaction was carried out in C_6D_6 at temperatures from 283 to 340 K. The reaction is second order (first order in each reactant), and the following activation parameters have been obtained: $\Delta H^{\ddagger} = 44.4 \pm 1.7$ kJ mol^{-1}, $\Delta S^{\ddagger} \geq -150 \pm 6$ J mol^{-1} K^{-1}, and $\Delta G^{\ddagger}_{298} = 89.0 \pm 2.4$ kJ mol^{-1}. A similar study with 4-fluoroacetophenone gave $\Delta H^{\ddagger} = 33.0 \pm 4.6$ kJ mol^{-1}, $\Delta S^{\ddagger} \geq -189 \pm 15$ J mol^{-1} K^{-1}, and $\Delta G^{\ddagger}_{298} = 89.2 \pm 6.4$ kJ mol^{-1}. The reaction rate at 320 K determined with 4-chloro-, 4-methyl-, and 4-nitroacetophenone allowed the determination of a Hammett plot with $\varrho = 0.42 \pm 0.9$. This value is implicit for a carbon–carbon bond-forming, rate-limiting step. Complexes **7** and **9** have been characterized by X-ray analysis.

The employment of early transition metals to influence the reactivity of enolates is a commonly used method of organic synthesis.[1] In particular, transition metals have been successfully used *in situ* to improve the regioselectivity[2] and the diastereoselectivity[3] in aldolic additions. Although mediation by titanium(IV)[4] and, in some cases, zirconium(IV)[5] is commonly encountered,[6] a structural characterization of titanium and zirconium enolates or their reaction products has never been carried out.[7] This fact mainly originates from the intrinsic difficulty in using $TiCl_4$[8] and $ClTi(OR)_3$[9] which are kinetically labile and coordinatively unsaturated. We therefore decided to examine the structure of the starting enolates (**A**) and their reaction products with representative carbonyl substrates, such as benzaldehyde and acetophenone, using the assistance of titanocene and zirconocene dichloride.[10] In addition, we tried to mimic the structure of the proposed transition state by converting the aldol product **E** into compound **F** (see Scheme 1).

* To whom correspondence should be addressed.
† Present address: Istituto di Chimica "G. Ciamician", Università di Bologna, I-40216 Bologna, Italy.
⊗ Abstract published in *Advance ACS Abstracts,* August 15, 1995.
(1) Paterson, I. In *Comprehensive Organic Synthesis*; Heathcock, C. H., Ed.; Pergamon: Oxford, U.K., 1991; Vol. 2, p 301.
(2) Bernardi, A.; Dotti, P.; Poli, G.; Scolastico, C. *Tetrahedron* **1992,** *48,* 5597. Comins, D. L.; Brown, J. D. *Tetrahedron Lett.* **1984,** 3292.
(3) Reetz, M. T.; Kesseler, K. *J. Chem. Soc., Chem. Commun.* **1984,** 1079. Reetz, M. T.; Hüllmann, M. *J. Chem. Soc., Chem. Commun.* **1986,** 1600. Reetz, M. T.; Steinbach, R.; Westermann, J.; Urz, R.; Wenderoth, B.; Peter, R. *Angew. Chem., Int. Ed. Engl.* **1982,** *21,* 135. D'Angelo, J.; Pecquet-Dumas, F. *Tetrahedron Lett.* **1983,** *24,* 1403. Reetz, M. T. *Angew. Chem., Int. Ed. Engl.* **1984,** *23,* 556. Chen, X.; Hortelano, E. R.; Eliel, E. L.; Frye, S. V. *J. Am. Chem. Soc.* **1992,** *114,* 1778 and references therein.

0276-7333/95/2314-4101$09.00/0

Scheme 1

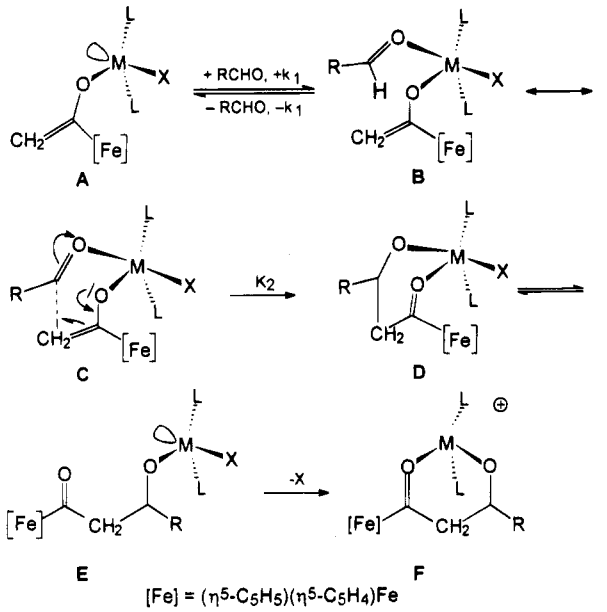

Scheme 2

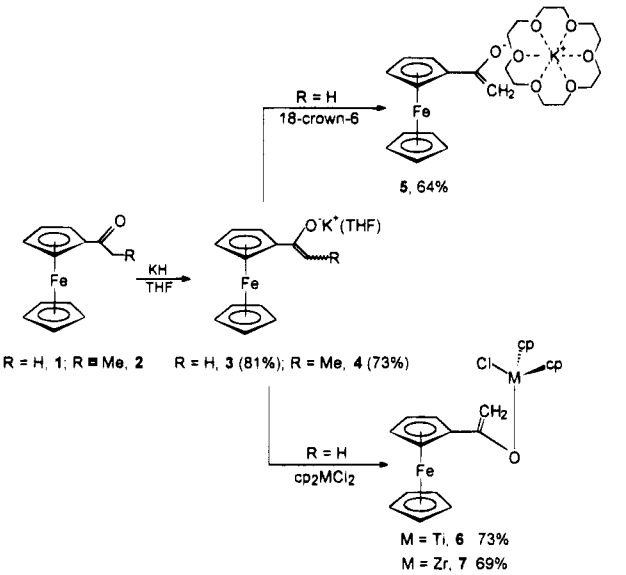

We also report a kinetic and mechanistic investigation[11] into the reaction of a cyclopentadienylzirconium enolate with acetophenone, leading to the determination of the energetic parameters of this general reaction.[12]

Results and Discussion

The acetylferrocene **1** is commercially available, while **2** is easily prepared by acylation of ferrocene with propionic anhydride. Both were deprotonated by using potassium hydride in THF, and the enolates **3** and **4** were precipitated in either THF or diethyl ether. A THF molecule remains bonded to potassium, as shown by elemental analysis.

The enolate **3** was obtained in 81% yield in THF, in which it is weakly soluble, and **4** in 73% yield from diethyl ether. Both are orange microcrystalline solids which were used without further purification.

The addition of 18-crown-6 led to isolation of the naked form of the enolate as orange needles:[13] the ^{1}H NMR spectrum of **5** in C_6D_6 showed two diastereotopic protons as doublets at 3.76 and 4.25 ppm (J_{HH} = 2.2 Hz).

The low solubility of **3** in THF allowed us to control its transmetalation reaction with $(cp)_2MCl_2$ (M = Ti, Zr),[10] with a single chloride ligand being replaced in the final compound. These reactions led to the formation of **6** and **7** as crystalline red solids in very good yields.

The metalation of **3** using typical oxophilic metals such as titanium and zirconium is expected to yield η^1-(O)-bonded enolato species.[10] However, complexes **6** and **7** are also rare examples of monomeric metal enolates.[10] Owing to the purpose of our study, the subsequent

(4) Reetz, M. T. In *Organometallics in Synthesis*; Schlosser, M., Ed.; Wiley: London, 1994; p 195. Duthaler, R. O.; Hafner, A. *Chem. Rev.* **1992**, *92*, 807.

(5) Cardin, D. J.; Lappert, M. F.; Raston, C. L. *Chemistry of Organo-zirconium and -hafnium Compounds*; Ellis Horwood: Chichester, U.K., 1986.

(6) Masamune, S.; Imperiali, B.; Garvey, D. S. *J. Am. Chem. Soc.* **1982**, *104*, 5528. Brenet, B.; Bishop, P. M.; Caron, M.; Kawamato, T.; Roy, B. L.; Ruest, L.; Sauvé, G.; Souly, P.; Deslongchamps, P. *Can. J. Chem.* **1985**, *63*, 2810. Oertkle, K.; Beyler, H.; Duthaler, R. O.; Lottenbach, W.; Riediker, M.; Steiner, E. *Helv. Chim. Acta* **1990**, *73*, 353. Evans, D. A.; Clark, J. S.; Metternich, R.; Novack, V. J.; Sheppard, G. S. *J. Am. Chem. Soc.* **1990**, *112*, 866. Evans, D. A.; Gage, J. R.; Leighton, J. L. *J. Am. Chem. Soc.* **1992**, *114*, 9434. Evans, D. A.; Dow, R. L.; Shih, T. L.; Takacs, J. M.; Zahler, R. *J. Am. Chem. Soc.* **1990**, *112*, 5290. Evans, D. A.; Gage, J. R. *J. Org. Chem.* **1992**, *57*, 1958. Evans, D. A.; Gage, J. R.; Leighton, J. L.; Kim, S. A. *J. Org. Chem.* **1992**, *57*, 1961. Paterson, I.; Bower, S.; Tillyer, R. *Tetrahedron Lett.* **1993**, *34*, 4393. Oppolzer, W.; Rodriguez, I. *Helv. Chim. Acta* **1993**, *76*, 1282. Paterson, I.; Perkins, M. W. *Tetrahedron Lett.* **1992**, *33*, 801. Evans, D. A.; Miller, S. J.; Ennis, M. D. *J. Org. Chem.* **1993**, *58*, 471. Evans, D. A.; Ng, H. P.; Rieger, D. L. *J. Am. Chem. Soc.* **1993**, *115*, 11446. White, J. D.; Porter, W. J.; Tiller, T. *Synlett* **1993**, 535.

(7) Only very limited structural characterizations for the enolates were reported: (a) Hortmann, K.; Diebold, J.; Brintzinger, H. H. *J. Organomet. Chem.* **1993**, *445*, 107. (b) Curtis, M. D.; Thanedar, S.; Butler, W. M. *Organometallics* **1984**, *3*, 1855. (c) Veya, P.; Floriani, C.; Chiesi-Villa, A.; Rizzoli, C. *Organometallics* **1994**, *13*, 208, 4839. (d) Cozzi, P. G.; Floriani, C. Unpublished results.

(8) Harrison, C. R. *Tetrahedron Lett.* **1987**, *28*, 4135. Brocchini, S. G.; Eberle, M.; Lawton, R. G. *J. Am. Chem. Soc.* **1988**, *110*, 5211. Evans, D. A.; Urpi, F.; Somers, T. C.; Clark, J. S.; Bilodeau, M. T. *J. Am. Chem. Soc.* **1990**, *112*, 8215. Evans, D. A.; Bilodeau, M. T.; Somers, T. C.; Clardy, J.; Cherry, D.; Kato, J. *J. Org. Chem.* **1991**, *56*, 5750. Evans, D. A.; Rieger, D. L.; Bilodeau, M. T.; Urpi, F. *J. Am. Chem. Soc.* **1991**, *113*, 1047. Annunziata, R.; Cinquini, M.; Cozzi, F.; Cozzi, P. G.; Consolandi, E. *Tetrahedron* **1991**, *47*, 7897. Xiang, Y.; Olivier, E.; Ouimet, N. *Tetrahedron Lett.* **1992**, *33*, 457. Mukai, C.; Kim, I. J.; Hanaoka, M. *Tetrahedron: Asymmetry* **1992**, *3*, 1007. Annunziata, R.; Cinquini, M.; Cozzi, F.; Lombardi-Borgia, A. *J. Org. Chem.* **1992**, *57*, 6339. Yan, T.-H.; Tan, C.-W.; Lee, H.-C.; Lo, H.-C.; Huang, T.-Y. *J. Am. Chem. Soc.* **1993**, *115*, 2613.

(9) Reetz, M. T.; Peter, R. *Tetrahedron Lett.* **1981**, *22*, 4691. Reetz, M. T.; Steinbach, R.; Kesseler, K. *Angew. Chem., Int. Ed. Engl.* **1982**, *21*, 864. Nerz-Stormes, M.; Thornton, E. R. *Tetrahedron Lett.* **1986**, *27*, 697. Siegel, C.; Thornton, E. R. *J. Am. Chem. Soc.* **1989**, *111*, 5722. Bonner, M. P.; Thornton, E. R. *J. Am. Chem. Soc.* **1991**, *113*, 1299. Van Draanen, N. A.; Arseniyadis, S.; Crimmins, M. T.; Heathcock, C. H. *J. Org. Chem.* **1991**, *56*, 2499. Fujisawa, T.; Ukaji, Y.; Noro, T.; Date, K.; Shimizu, M. *Tetrahedron* **1992**, *48*, 5629. Choudhury, A.; Thornton, E. R. *Tetrahedron* **1992**, *48*, 5701. Hafner, A.; Duthaler, R. O.; Marti, R.; Rihs, G.; Rothe-Streit, P.; Schwarzenbach, F. *J. Am. Chem. Soc.* **1992**, *114*, 2321.

(10) $(cp)_2TiCl_2$ enolates: Nakamura, E.; Kuwajima, I. *Tetrahedron Lett.* **1983**, *24*, 3343. Stille, J. R.; Grubbs, R. H. *J. Am. Chem. Soc.* **1983**, *105*, 1664. Devant, R.; Brown, M. *Chem. Ber.* **1986**, *119*, 8191. Murphy, P. J.; Procter, G.; Russel, T. A. *Tetrahedron Lett.* **1987**, *28*, 2037. Duthaler, R. O.; Herold, P.; Wyler-Helfer, S.; Riediker, M. *Helv. Chim. Acta* **1990**, *73*, 659. $(cp)_2ZrCl_2$ enolates: Evans, D. A.; McGee, L. *Tetrahedron Lett.* **1980**, *21*, 3975. Yamamoto, Y.; Muruyama, K. *Tetrahedron Lett.* **1980**, *21*, 4607. Evans, D. A.; McGee, L. *J. Am. Chem. Soc.* **1981**, *103*, 2876. Katsuki, T.; Yamaguchi, M. *Tetrahedron Lett.* **1985**, *26*, 5807. Panek, J. S.; Bula, O. A. *Tetrahedron Lett.* **1988**, *29*, 1661. Shibasaki, M.; Ishida, Y.; Okabe, N. *Tetrahedron Lett.* **1985**, *26*, 2217. Mikami, K.; Takahashi, O.; Kasuga, T.; Nakai, T. *Chem. Lett.* **1985**, 1729. Pearson, W. H.; Cheng, M.-C. *J. Org. Chem.* **1987**, *52*, 3178.

(11) Previous mechanistic studies on the aldol reaction: Berno, P.; Floriani, C.; Chiesi-Villa, A.; Rizzoli, C. *Organometallics* **1990**, *9*, 1995.

(12) Guthrie, J. P. *J. Am. Chem. Soc.* **1991**, *113*, 7249 and references therein.

(13) Veya, P.; Floriani, C.; Chiesi-Villa, A.; Rizzoli, C. *Organometallics* **1991**, *10*, 1652; **1994**, *13*, 214.

reactions of **6** and **7** were carried out with the typical prostereogenic substrate PhCHO with the objective of structurally identifying the steps leading to the aldol addition.[11,14]

The ^1H and ^{13}C NMR spectra of enolates **6** and **7** are very similar. In the ^1H NMR spectrum, the unsubstituted iron cp gives one singlet at 4.24 (**6**) and 4.22 (**7**) ppm. The substituted iron cp gives two multiplets (AA'BB') at 4.17 and 4.33 ppm (**6**) and 4.18 and 4.38 ppm (**7**). The two vinylic protons show two singlets at 3.82 and 4.24 ppm (**6**) and 3.84 and 4.22 ppm (**7**). The zirconium–cp gives one singlet at 6.43 ppm. The NMR results agree with those in the literature: ketone enolates[10] usually show two singlets at 3.85 and 3.96 ppm, while the aldehyde enolates[7b] show two doublets at 3.99 and 4.11 ppm. ^{13}C NMR spectra of **6** and **7** show a signal for the methylene carbon at 85.5 ppm for **6** and at 84.7 ppm for **7**, instead of 87.4 ppm, reported in the literature for ketone enolates. Recently elucidated stereogenic cp titanium enolates show an analogous ^{13}C NMR signal at 96.9 ppm.[15]

The stereogenic zirconium enolate **8** was prepared by following the usual procedure:

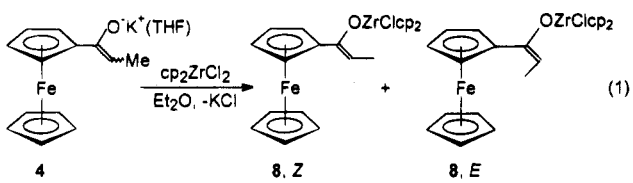

8 was isolated as a mixture of two diastereoisomers, *E* and *Z*, in a 1:9 ratio. From the ^1H NMR data and in comparison to the elucidated structure of a titanium propiophenone enolate,[15] we assigned the *Z* configuration to the most abundant diastereoisomer. In addition, the *Z* isomer is generally obtained from the deprotonation of hindered ketones.[16]

The reactions of **6** and **7** with benzaldehyde are clean, complete in about 45 min, as followed by ^1H NMR. Reaction 2 can also be performed on a preparative scale and gave a good yield (see the Experimental Section) of **9** (73%) and **10** (55%).

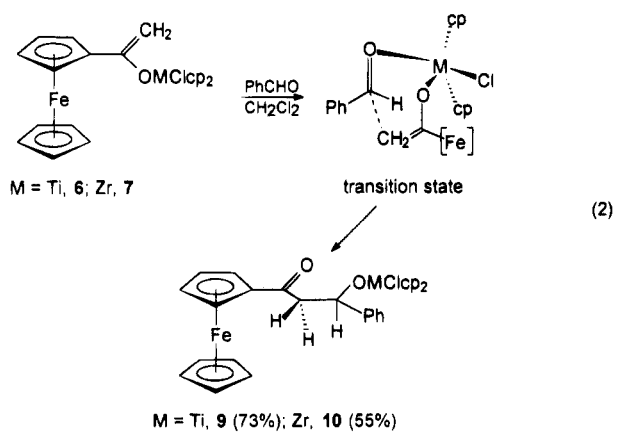

The ^1H NMR spectra of the aldol products **9** and **10** are similar. Both show an ABX system of three quadruplets at 2.92, 3.22, and 6.08 ppm for **9** and at 2.92, 3.10, and 5.64 ppm for **10**.

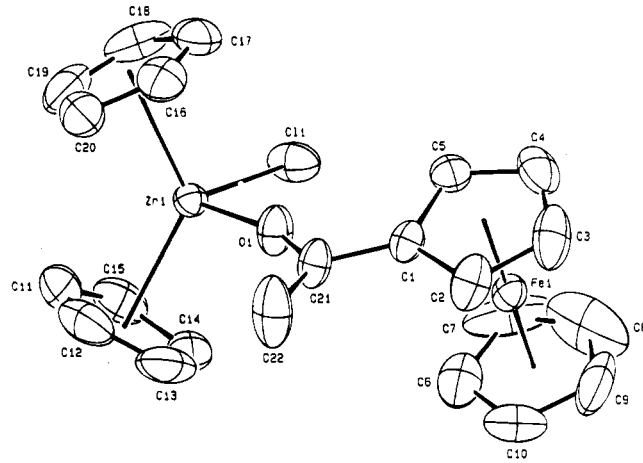

Figure 1. ORTEP view of complex **7** (30% probability ellipsoids).

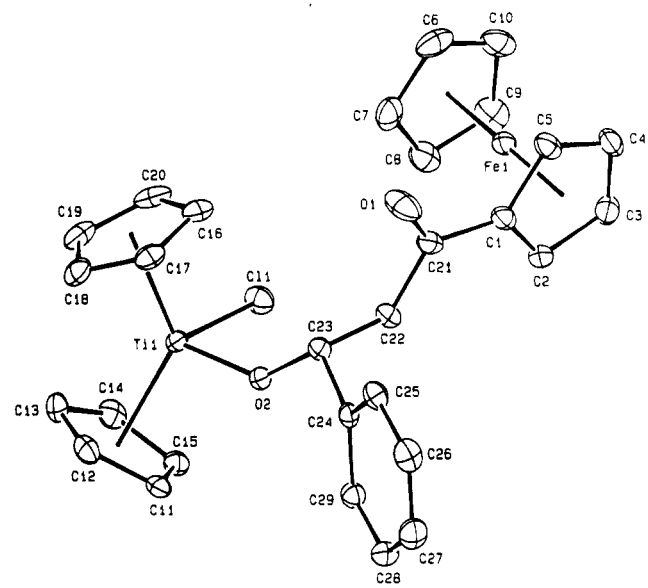

Figure 2. ORTEP view of complex **9** (30% probability ellipsoids).

Complexes **9** and **10** were isolated as crystalline solids. They have been spectroscopically characterized, including an X-ray analysis of **9**. The most relevant structural characteristics of **7**, shown in Figure 1, are related to the enolate functionality and to the overall conformation of the molecule. The nucleophilic "CH_2" is *anti* to the Cl at zirconium, the Cl–Zr···C(21)–C(22) torsional angle being −161.1(7)°. The zirconium is almost coplanar, with the enolato group being just 0.006(1) Å out of the C(1),C(21),C(22),O(1) plane. The enolato plane C(22),C(21),O(1) forms a dihedral angle of 18.6(7)° with the Cl,Zr,O(1) equatorial plane of the $(cp)_2ZrX_2$ group. The cp plane C(1)···C(5) of ferrocene is only slightly twisted (16.6(3)°) with respect to the enolato plane C(1),C(21),C(22),O(1). The C–C and C–O bond lengths within the enolato functionality (Table 6) are almost identical, both with a significant double-bond character.

The addition of benzaldehyde to **6** causes major changes on the fragment bridging the $(cp)_2Fe$ and $(cp)_2Ti$ moieties in **9** (see Figure 2). C(21)–C(22) becomes a single bond, while C(21)–O(1) is restored as a double bond. All the other bond distances support the bonding

(14) Weinstock, I.; Floriani, C.; Chiesi-Villa, A.; Guastini, C. *J. Am. Chem. Soc.* **1986**, *108*, 8298.

(15) Adam, W.; Mueller, M.; Prechtl, F. *J. Org. Chem.* **1994**, *59*, 2358.

scheme proposed. O(1) does not interact with titanium in **9**, a rotation, at least in the solid state, of −35.0° around C(21)−C(22) being necessary for an appropriate possible matching with the metal.

D is related to the final compound by a M−O bond-breaking step. The conformation of **9** and **10**, however, cannot be strictly related to the cyclic transition state **C** (Scheme 1), because only in particular cases of titanium and zirconium $(cp)_2MX_2$ compounds (i.e., where the complex is cationic) does the interaction with a carbonyl oxygen occur. Therefore (Figure 2), the two metals are in an *anti* arrangement with respect to the formed C−C bond, at least in the solid state.

A simulation of the bond connectivity in **C** and **D** was achieved by removing the Cl ligand around titanium in complex **9** using $NaBPh_4$ (see eq 3). The resulting

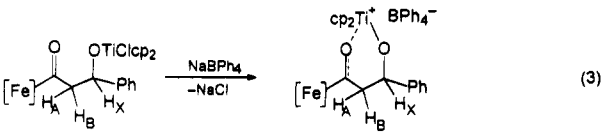

(3)

unsaturation at the metal center forces the oxygen to coordinate to it, as clearly shown by the disappearance of the IR band at 1663 cm^{-1} in **11**. Complex **12**, derived from the reaction of benzaldehyde with $[(cp)Fe(CO)(PPh_3)C(CH_2)OTiCl(cp)_2]$, which was equally ionized to **13** (see eq 3), has been previously described.[11] The coordination of the carbonyl group to $[(cp)_2TiCl]^+$ introduces a frozen conformation in **11** and **13**. The structure of **13** represents our first attempt to simulate the bond connectivity in the transition state of the aldol reaction.[11]

Complexes **11** and **13** have very similar ^1H NMR spectra, thus supporting related structures. When the carbonyl is coordinated to the titanocene in complex **11**, the ^1H NMR spectrum shows an AMX splitting pattern composed of three well-separated quadruplets at 2.63, 3.5, and 5.8 ppm. We were not able to crystallize the complex **11**, but, from the analysis of the coupling constants, we propose a structure for this complex. From the structure of **9**, dihedral angles between H_A, H_B, and H_X can be measured in the solid state. In addition, coupling constants can be measured from the NMR spectra for **9** and **11**, and dihedral angles can be easily calculated from the Karplus equation.[17]

In order to clarify the discussion, the dihedral angles are reported in Table 1 and shown as Newman projections (Chart 1) along the C−C bond for the related pairs of compounds **9** and **12**, and **11** and **13**.

While in complex **9** there is no correlation between the solid-state structure and the favored conformation in solution (probably due to free rotation) in complex **12**, the value of the dihedral angles obtained from the coupling constants measured in solution are very close

Table 1. Chemical Shifts and Coupling Constants Related to Dihedral Angles in Complexes 9−13

	δ_A, (ppm)	J_{AX} (Hz)	dihedral angle (deg)	δ_B (ppm)	J_{BX} (Hz)	dihedral angle (deg)
9, soln	2.92	6.7	30 (150)	3.22	6.0	145 (35)
9, solid		0.3	98.3		7.0	153.4
12, soln	3.13	9.8	180 (0)	3.58	3.2	55 (125)
12, solid		9.0	167.0		1.0	69.4
11, soln	2.64	10.6	180 (0)	3.51	2.2	60 (120)
13, soln	2.58	10.5	180 (0)	4.09	2.2	60 (120)
13, solid		9.5	175.9		3.0	54.8

Chart 1

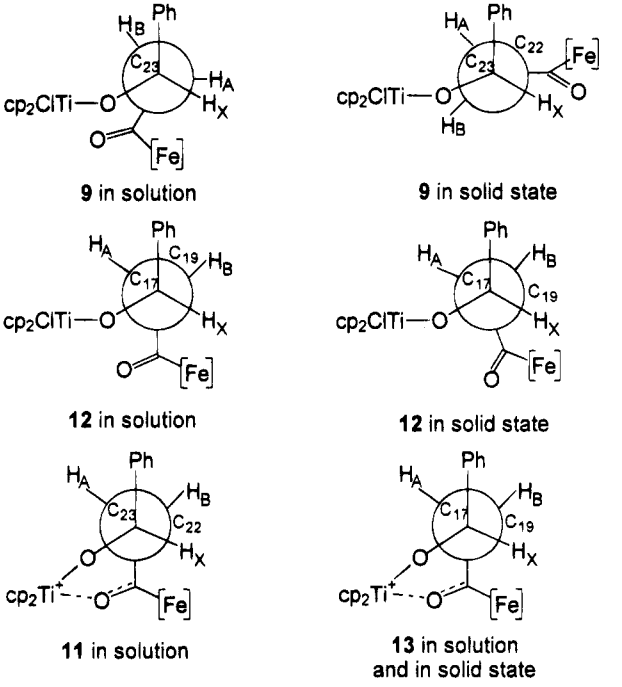

to the structure characterized in the solid state. In complex **13** the accord is rather close, due to the introduction of additional constraints, specifically the chelation with the titanocene.

The good agreement between solid-state and solution conformations for complex **13** (Table 1) allows a confident assignment of the structure of **11** from the ^1H NMR in solution.

The hypothetical structure **C** proposed for the transition state of the aldol reaction promoted by the metallocene fragment, imitated by the isolated cationic complex **11**, is a chair transition state.[18] However, zirconium metallocene stereogenic enolates show stereoconvergence for *syn*[19] type products in aldol reactions,[1] and most of the authors interpreted this behavior as suggesting other transition-state structures, including boat or twist-boat conformations[20] according to the starting enolate configuration. Reaction pathways different from those assuming the chair transition-state configuration

(16) Dubois, J.-E.; Felmann, P. *Tetrahedron Lett.* **1975**, 1225. Heathcock, C. H.; Buse, C. T.; Kleschick, W. A.; Pirrung, M. C.; Sohn, J. E.; Lampe, J. *J. Org. Chem.* **1980**, *45*, 1066. Masamune, S.; Ellingboe, J. W.; Choy, W. *J. Am. Chem. Soc.* **1982**, *104*, 5526. Seebach, D.; Ertas, M.; Locker, M.; Schweizer, W. B. *Helv. Chim. Acta* **1985**, *68*, 264.

(17) (a) Pretsch, E.; Seibl, J.; Simon, W.; Clerc, T. *Tables of Spectral Data for Structure Determination of Organic Compounds*; Springer: Berlin, Germany, 1983. (b) Fleming, I.; Williams, D. H. *Spectroscopic Methods in Organic Chemistry*, 3rd ed.; McGraw-Hill: New York, 1980; p 100.

(18) Zimmerman, H. E.; Traxler, M. D. *J. Am. Chem. Soc.* **1957**, *79*, 1920. Evans, D. A.; Nelson, J. V.; Vogel, E.; Taber, T. R. *J. Am. Chem. Soc.* **1981**, *103*, 3099. Heathcock, C. H. In *Asymmetric Synthesis*; Morrison, D. J., Ed.; Academic: New York, 1984; Vol. 3, Chapter 2. Evans, D. A.; Nelson, J. V.; Taber, T. R. In *Topics in Stereochemistry*; Eliel, E. L., Wilen, S. H., Eds.; Wiley: New York, 1983; Vol. 13, p 1. Denmark, S. E.; Henke, B. R. *J. Am. Chem. Soc.* **1991**, *113*, 2177 and references therein.

(19) For *anti*-selective aldol addition with $(cp)_2ZrCl_2$ enolates, see: Sacha, H.; Waldmüller, D.; Braun, M. *Chem. Ber.* **1994**, *127*, 1959.

(20) Hoffmann, R. W.; Ditrich, K.; Froech, S. *Tetrahedron* **1985**, *41*, 5517. Nakamura, E.; Kuwajima, I. *Acc. Chem. Res.* **1985**, *18*, 181. Gennari, C.; Todeschini, R.; Beretta, M. G.; Favini, G.; Scolastico, C. *J. Org. Chem.* **1986**, *51*, 612.

have been recently considered in boron-mediated aldol reactions[21] and in some recent *ab initio* calculations on transition states for aldol reactions.[22] We do not make a distinction between different transition states, but our results provide structural and spectroscopic information on the starting and final products of a metal-mediated aldol reaction along with some dihedral angles for a compound model of the transition state. These data should enable development of an appropriate force field model for a metal-assisted aldol reaction.[23] This is particularly important for understanding the effective role played by different transition states and evaluating the diastereoselectivity with transition-metal enolates currently employed in organic synthesis.

The well-defined monomeric nature of **7** allowed us to tackle kinetic and mechanistic studies without the complication derived from the usual aggregate forms.[24] A thermochemical analysis has been recently reported on the lithium enolate aldol reaction,[25] though a kinetic study was, probably, prevented by the number of aggregates present in solution having different molecular complexities.

Kinetic and Mechanistic Studies of the Aldol Reaction. The reaction of **7** with acetophenone and substituted acetophenones seemed particularly appropriate for a kinetic study because of the reasonably slow speed of the reaction.

Table 2. Rate Constants from 283 to 340 K for the Reaction of 7 with Acetophenone in C_6D_6

T (K)	c_{20} (M)[a]	k (M^{-1} h^{-1})	T (K)	c_{20} (M)[a]	k (M^{-1} h^{-1})
283	0.1443	2.03 ± 0.03	310	0.0577	12.98 ± 0.40
294	0.1443	4.33 ± 0.04	320	0.0577	20.92 ± 0.67
310	0.1443	11.84 ± 0.20	330	0.0577	28.21 ± 1.78
310	0.1443	14.76 ± 0.49	340	0.0577	38.81 ± 3.90

[a] $c_{10} = 2c_{20}$.

Table 3. Rate Constants for the Reaction of 7 with *p*-Substituted Acetophenones in C_6D_6 at 320 K

c_{20} (M)[a]	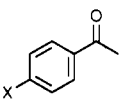	k (M^{-1} h^{-1})
0.0500	X = Me	11.96 ± 0.22
0.0500	X = F	12.94 ± 0.44
0.0500	X = Cl	19.48 ± 0.29
0.0500	X = NO_2	87.11 ± 1.32
0.0577	X = H	20.92 ± 0.67

[a] $c_{10} = 2c_{20}$.

Table 4. Rate Constants for the Reaction of 7 with *p*-Fluoroacetophenone from 330 to 300 K in C_6D_6[a]

T (K)	k (M^{-1} h^{-1})	T (K)	k (M^{-1} h^{-1})
330	19.33 ± 0.60	310	9.97 ± 0.19
320	12.94 ± 0.44	300	5.24 ± 0.11

[a] $c_{10} = 2c_{20}$; c_{20} is 0.0500 M in all cases.

The kinetic measurements were carried out in C_6D_6 at different temperatures (see the Experimental Section). In the case of acetophenone the data have been collected at six different temperatures, and the corresponding rate constants are listed in Table 2. The reaction is significantly enhanced by *ca.* 30% (k = 18.2 M^{-1} h^{-1} at 310 K) in a solvent such as CD_2Cl_2 having a poor σ-donating ability, while it is almost completely suppressed in THF. The latter observation emphasizes the relevance of precoordination to zirconium (**B**; Scheme 1).

The reaction rate in the case of acetophenone is second order (first order in each reactant), and the following activation parameters, according to the Eyring theory, have been obtained: $\Delta H^{\ddagger} = 44.4 \pm 1.7$ kJ mol^{-1}, $\Delta S^{\ddagger} \geq -150 \pm 6$ J mol^{-1} K^{-1}, and $\Delta G^{\ddagger}_{298} = 89.0 \pm 2.4$ kJ mol^{-1}. The reaction rates along with the large activation entropy are consistent with an associative mechanism requiring the precoordination of acetophenone to zirconium. The activation parameters are rather close to those reported for the reaction between the silylketene acetal of amides and aldehydes.[26] In the latter case, it has been shown by a Hammett plot that the rate-determining step is the C–C bond formation rather than the precoordination. In order to discriminate between the two steps, we used the same argument. The Hammett correlation has been determined by studying four *p*-substituted acetophenones, and in the case of *p*-fluoroacetophenone the kinetic study has been extended over four temperatures. The results are summarized in Tables 3 and 4, respectively. The correlation does not hold well for *p*-nitroacetophenone.

(21) Bernardi, A.; Capelli, A. M.; Gennari, C.; Goodman, J. M.; Paterson, I. *J. Org. Chem.* **1990**, *55*, 3576. Bernardi, F.; Robb, M. A.; Suzzi-Valli, G.; Tagliavini, E.; Trombini, C.; Umani-Ronchi, A. *J. Org. Chem.* **1991**, *56*, 6472. Gennari, C.; Hewkin, C. T.; Molinari, F.; Bernardi, A.; Comotti, A.; Goodman, J. M.; Paterson, I. *J. Org. Chem.* **1992**, *57*, 5173.

(22) Li, Y.; Paddon-Row, M. N.; Houk, K. N. *J. Org. Chem.* **1990**, *55*, 481. Goodman, J. M.; Kahn, S. D.; Paterson, I. *J. Org. Chem.* **1990**, *55*, 3295.

(23) For transition-state modeling, see: Houk, K. N.; Paddon-Row, M. N.; Rondan, N. G.; Wu, Y.-D.; Brown, F. K.; Spellmeyer, D. C.; Metz, J. T.; Li, Y.; Longharich, J. *Science* **1986**, 1108. Houk, K. N.; Tucker, J. A.; Dorigo, A. E. *Acc. Chem. Res.* **1990**, *23*, 107. Brocker, J. L.; Houk, K. N.; Giese, B. *J. Am. Chem. Soc.* **1991**, *113*, 5006. Wu, Y.-D.; Houk, K. N.; Florez, J.; Trost, B. M. *J. Org. Chem.* **1991**, *56*, 3656. Wu, Y.-D.; Wang, Y.; Houk, K. N. *J. Org. Chem.* **1992**, *57*, 1362. Gonzales, J.; Taylor, E. C.; Houk, K. N. *J. Org. Chem.* **1992**, *57*, 3753. Wu, Y.-D.; Houk, K. N.; Valentine, J. S.; Nam, W. *Inorg. Chem.* **1992**, *31*, 718. For a force field for transition metals, see: Rappé, A. K.; Casewit, C. J.; Colwell, K. S.; Goddard, W. A., III; Skiff, W. M. *J. Am. Chem. Soc.* **1992**, *114*, 10024. Allured, V. S.; Kelly, C. M.; Landis, C. R. *J. Am. Chem. Soc.* **1991**, *113*, 1. Gajewski, J. J.; Gilbert, K. E.; McKelvey, J. In *Advances in Molecular Modeling*; Liotta, D., Ed.; JAI: Greenwich, CT, 1990; Vol. 2, p 65. For a force field for cp–metal complexes: Menger, F. M.; Sherrod, M. J. *J. Am. Chem. Soc.* **1988**, *110*, 8606. Thiem, H.-J.; Brandl, M.; Breslow, R. *J. Am. Chem. Soc.* **1988**, *110*, 8612. Du Plooy, K. E.; Marais, C. F.; Carlton, L.; Hunter, R.; Boeyens, J. C. A.; Coville, N. J. *Inorg. Chem.* **1989**, *28*, 3855. Lin, Z.; Marks, T. J. *J. Am. Chem. Soc.* **1990**, *112*, 5515. Davies, S. G.; Derome, A. E.; McNally, J. P. *J. Am. Chem. Soc.* **1991**, *113*, 2854. Bogdan, P. L.; Irwin, J. J.; Bosnich, B. *Organometallics* **1989**, *8*, 1450. Doman, T. N.; Landis, C. R.; Bosnich, B. *J. Am. Chem. Soc.* **1992**, *114*, 7264. For a recent application of the force field approach to metal-promoted reactions: Gugelchuck, M. M.; Houk, K. N. *J. Am. Chem. Soc.* **1994**, *116*, 330. For recent *ab initio* calculations on early-transition-metal complexes: Jonas, V.; Frenking, G.; Reetz, M. T. *Organometallics* **1993**, *12*, 2111. Voldkamp, A.; Frenking, G. *J. Am. Chem. Soc.* **1994**, *116*, 4937. Re, N.; Sgamellotti, A.; Persson, J.; Roos, B.; Floriani, C. *Organometallics* **1995**, *14*, 63. Gleiter, R.; Hyla-Kryspin, I. H.; Niu, S.; Erker, G. *Organometallics* **1993**, *12*, 3822. Kundari, T. R. *Organometallics* **1993**, *12*, 4971. Reetz, M. T. *Acc. Chem. Res.* **1993**, *26*, 462 and references therein.

(24) Jackman, L. A.; Lange, B. C. *J. Am. Chem. Soc.* **1981**, *103*, 4494. Jackman, L. A.; Dunne, T. S. *J. Am. Chem. Soc.* **1985**, *107*, 2805. Jackman, L. A.; Smith, B. D. *J. Am. Chem. Soc.* **1988**, *110*, 3829. Jackman, L. A.; Lange, B. C. *Tetrahedron* **1977**, *33*, 2737. Seebach, D. *Angew. Chem., Int. Ed. Engl.* **1988**, *27*, 1624. Arnett, E. M.; Moe, K. D. *J. Am. Chem. Soc.* **1991**, *113*, 7288. Galiano-Roth, A. S.; Kim, Y.-J.; Gilchrist, J. H.; Harrison, A. T.; Fuller, D. J.; Collum, D. S. *J. Am. Chem. Soc.* **1991**, *113*, 5053. Hall, P.; Gilchrist, J. H.; Harrison, A. T.; Fuller, D. J.; Collum, D. S. *J. Am. Chem. Soc.* **1991**, *113*, 9575. Williard, P. G.; Hintze, M. J. *J. Am. Chem. Soc.* **1987**, *109*, 5539; **1990**, *112*, 8602.

(25) Arnett, E. M.; Fisher, F. J.; Nichols, M. A.; Ribeiro, A. A. *J. Am. Chem. Soc.* **1989**, *111*, 748; **1990**, *112*, 801.

(26) Myers, A. G.; Kephart, S. E.; Chen, H. *J. Am. Chem. Soc.* **1992**, *114*, 7922. Myers, A. G.; Widdowson, K. L.; Kukkola, P. J. *J. Am. Chem. Soc.* **1992**, *114*, 2765.

Scheme 3

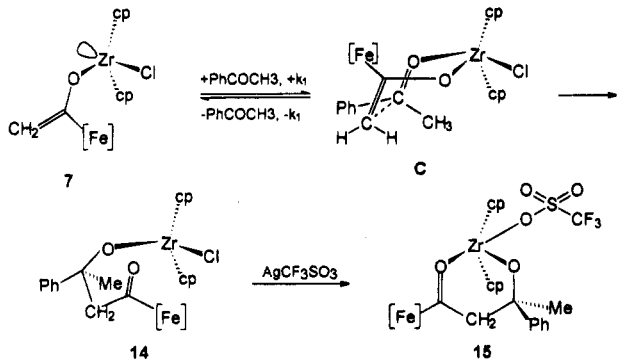

This is due, as previously pointed out,[26] to the fact that the C−C formation process is competitive with precoordination of the metal to the electrophile. The positive value $\varrho = 0.42 \pm 0.9$ provides strong evidence that the more basic ketone reacts more slowly. This leads to the conclusion, in our case, that C−C bond formation is probably the rate-determining step. On the other hand, in some recent studies on boron enolates, the precoordination of the carbonyl compound seems to have some influence on the rate-determining step of the reaction.[27] In the case of *p*-fluoroacetophenone the activation parameters are $\Delta H^{\ddagger} = 33.0 \pm 4.6$ kJ mol^{-1}, $\Delta S^{\ddagger} \geq -189 \pm 15$ J mol^{-1} K^{-1}, and $\Delta G^{\ddagger}_{298} = 89.2 \pm 6.4$ kJ mol^{-1}.

The strong negative value of the entropy agrees well with an ordered transition state. The variation of energy and entropy compared to those for the unsubstituted acetophenone should be considered carefully because of the strong correlation of the two parameters. We wish to mention that **14**, the product between **7** and acetophenone (Scheme 3) has been converted by the addition of silver triflate to **15**, which mimics the bond connectivity of the transition state. The structure of an analogous ion-pair form will be reported in a following paper.[28]

Conclusions

We have fully characterized cyclopentadienylzirconium enolates, prepared from acetylferrocene, and their corresponding aldol products, derived from reaction with benzaldehyde and acetophenone. The X-ray crystal structures of both the isolated complexes **7** and **9** gave bond distances and bond angles for the starting complex and for the product of an aldol condensation mediated by early transition metals. In addition, bond angles for complex **11**, which imitates the connectivity of the transition state, can be deduced from the NMR data in solution.

This information could provide a useful basis for comparisons with future *ab initio* or density functional calculations of transition-state structures for aldolic reactions mediated by transition metals and eventually help us understand the role played by the metal and the different transition states in determining stereoselectivity. The monomeric, well-characterized zirconium enolate **7** was used for undertaking a kinetic study on the aldolic reaction. We measured activation parameters for its aldol reaction and studied the rate-determining step with a Hammett plot. The present study represents the first clear measurement of activation parameters in aldol reactions.

Experimental Section

All the reactions described were carried out under an atmosphere of purified nitrogen. Solvents were purified by standard methods. Acetylferrocene is commercially available, and benzaldehyde was distilled before use. Propionylferrocene was prepared according to the literature.[29] IR spectra were recorded with a Perkin-Elmer 883 spectrophotometer. ^{1}H NMR and ^{13}C NMR spectra were obtained with a Bruker (200 MHz) apparatus.

Preparation of 3. KH (4.0 g, 100 mmol) and acetylferrocene (**1**; 20.0 g) were stirred in THF (250 mL) for 4 h. The orange fluffy solution was refluxed for 1 h and then cooled. The raw product was extracted with THF (250 mL) and then filtered and dried under vacuum (81%). Anal. Calcd for [(cp)Fe(cp)C(CH$_2$)OK(THF)], $C_{16}H_{19}FeKO_2$: C, 56.81; H, 5.66. Found: C, 56.89; H, 4.93.

Preparation of 4. KH (1.11 g, 27.8 mmol) and propionylferrocene (**2**; 6.54 g, 27.0 mmol) were stirred in THF (150 mL) for 4 h. The solvent was removed and the red oil treated with diethyl ether (100 mL). An orange solid was obtained, which was filtered and dried under vacuum (73%). Anal. Calcd for [(cp)Fe(cp)C(CHCH$_3$)OK(THF)], $C_{17}H_{21}FeKO_2$: C, 57.96; H, 6.01. Found: C, 57.75; H, 6.17.

Preparation of 5. KH (0.4 g, 11.0 mmol) and acetylferrocene (**1**; 2.40 g, 10.5 mmol) were stirred overnight in THF (50 mL). 18-crown-6 (2.78 g, 10.5 mmol) was added and the solution heated and filtered while hot. Orange needles formed upon cooling to 0 °C (64%). Anal. Calcd for $C_{24}H_{35}FeKO_7 \cdot C_4H_8O$: C, 55.81; H, 7.19. Found: C, 55.60; H, 7.06. ^{1}H NMR (C_6D_6): δ 3.30 (s, OCH$_2$, 24H), 3.76 (d, =CH$_2$, 1H, J = 2.2 Hz), 4.21 (m, (cp)Fe, 2H), 4.25 (d, =CH$_2$, 1H, J = 2.2 Hz), 4.39 (s, (cp)Fe, 5H), 5.04 (m, (cp)Fe, 2H).

Preparation of 6. Potassium enolate **3** (4.69 g, 17.6 mmol) and titanocene dichloride (4.30 g, 17.3 mmol) were stirred overnight in THF (50 mL). The dark red solution was filtered and the solvent removed. Toluene (50 mL) was added and the solution concentrated very slowly (to let crystallization start). The red-brown microcrystalline solid was then collected with diethyl ether (50 mL), filtered, and dried under vacuum (73%). When heated, the enolate can decompose to give oxo complexes, for example ((cp)$_2$TiCl)$_2$O, as a major impurity. Anal. Calcd for $C_{22}H_{21}ClOFeTi$: C, 59.97; H, 4.80; Cl, 8.05. Found: C, 59.87; H, 4.93; Cl, 7.98. ^{1}H NMR (CD_2Cl_2): δ 3.82 (s, =CH$_2$, 1H), 4.14 (s, (cp)Fe, 5H), 4.17 (t, (cp)Fe, 2H), 4.24 (s, =CH$_2$, 1H), 4.33 (t, (cp)Fe, 2H), 6.43 (s, (cp)$_2$Ti, 10H). ^{13}C NMR (CD_2Cl_2): δ 67.0, 69.2, 70.1 (3s, (cp)Fe), 84.5 (s, =CH$_2$), 119.0 (s, (cp)Ti), 171.2 (s, =COTi).

Preparation of 7. Potassium enolate **3** (5.96 g, 22.4 mmol) and zirconocene dichloride (6.48 g, 22.2 mmol) were stirred overnight in THF (50 mL). The red solution was filtered and the solvent removed. Toluene (50 mL) was added, and the mixture was warmed until the solid had completely dissolved and then cooled until the solid began to crystallize. The solution was then concentrated very slowly to obtain an orange microcrystalline solid. This solid was extracted with 50 mL of diethyl ether, the extracts were filtered and dried in vacuo, and the residue was collected (69%). X-ray-quality crystals were grown slowly by recrystallizing 1.0 g of solid from 10 mL of warm toluene. Anal. Calcd for $C_{22}H_{21}ClFeOZr$: C, 54.60; H, 4.37; Cl, 7.33. Found: C, 54.36; H, 4.36; Cl, 7.22. ^{1}H NMR (CD_2Cl_2): δ 3.84 (s, =CH$_2$, 1H), 4.16 (s, (cp)Fe, 5H), 4.18 (t, (cp)Fe, 2H), 4.22 (s, =CH$_2$, 1H), 4.38 (t, (cp)Fe, 2H), 6.44 (s, (cp)Zr, 10H). ^{1}H NMR (C_6D_6): δ 3.88 (s, =CH$_2$, 1H), 4.07 (t, (cp)Fe, 2H), 4.17 (s, (cp)Fe, 5H), 4.33 (s, =CH$_2$, 1H), 6.04 (s,

(27) Bernardi, A.; Comotti, A.; Gennari, C.; Hewkin, C. T.; Goodman, J. M.; Schlapsach, A.; Paterson, I. *Tetrahedron* **1994**, *50*, 1227. See also: Goodman, J. M.; Paterson, I. *Tetrahedron Lett.* **1992**, *33*, 7223.

(28) Cozzi, P. G.; Veya, P.; Floriani, C.; Rotzinger, F.; Chiesi-Villa, A.; Rizzoli, C. *Organometallics* **1995**, *14*, 4092.

(29) Graham, P. J.; Lindsey, R. V.; Parshall, G. W.; Peterson, M. L. *J. Am. Chem. Soc.* **1957**, *79*, 3416.

(cp)Zr, 10H). ^{13}C NMR (CD_2Cl_2): δ 66.9, 69.3, 70.1 (3s, (cp)-Fe), 84.7 (s, $=CH_2$), 114.8 (s, (cp)Zr), 166.1 (s, =COZr).

Preparation of 8. Potassium enolate **4** (3.04 g, 8.62 mmol) and zirconocene dichloride (2.40 g, 8.2 mmol) were stirred overnight in diethyl ether (80 mL). The orange solution was filtered, concentrated to 20 mL, and then cooled to 0 °C. An orange microcrystalline solid formed, which was filtered and dried (43%). Anal. Calcd for $C_{23}H_{23}ClFeOZr$: C, 55.48; H, 4.66. Found: C, 56.06; H, 4.96. ^1H NMR (CD_2Cl_2; two isomers, Z/E = 9/1) *Z* δ 1.62 (d, Me, 3H, *J* = 6.75 Hz), 4.13 (t, (cp)Fe, 2H), 4.14 (s, (cp)Fe, 5H), 4.37 (t, (cp)Fe, 2H), 4.72 (q, =CH, 1H, *J* = 6.75 Hz), 6.41 (s, (cp)Zr, 10H); *E*, δ 1.73 (d, Me, 3H, *J* = 6.9 Hz), 4.16 (s, (cp)Fe, 5H), 4.18 (m, (cp)Fe, 2H), 4.41 (m, (cp)Fe, 2H), 4.85 (q, =CH, 1H, *J* = 6.9 Hz), 6.36 (s, (cp)Zr, 10H).

Preparation of 9. A toluene solution (20 mL) of titanium enolate **6** (1.13 g, 2.56 mmol) was reacted for 1 h with neat benzaldehyde (0.28 g, 2.64 mmol) at room temperature. An orange solid precipitated after 45 min, which was filtered off and dried (73%). It was recrystallized in dichloromethane (40 mL) and diethyl ether (20 mL), giving red crystals suitable for X-ray analysis. Anal. Calcd for $C_{29}H_{27}ClFeO_2Ti$: C, 63.71; H, 4.98; Cl, 6.48. Found: C, 63.53; H, 5.09; Cl, 6.28. ^1H NMR (CD_2Cl_2): δ 2.92 and 3.22 (AB part of a ABX system, $COCH_2$, 2H, J_{AX} = 6.70 Hz, J_{BX} = 6.00 Hz, J_{AB} = 15.85 Hz), 4.03 (s, (cp)Fe, 5H); 4.50 (m, (cp)Fe, 2H), 4.73 (m, (cp)Fe, 2H), 6.08 (X part of a ABX system, *J* = 6.70, 6.00 Hz, CHOTi, 1H), 6.23 and 6.28 (2s, (cp)Ti, 10H), 7.20–7.40 (m, Ph, 5H). IR (Nujol): ν(C=O) 1663 cm^{-1}.

Preparation of 10. A dichloromethane solution (10 mL) of zirconium enolate **7** (2.32 g, 4.80 mmol) was reacted with neat benzaldehyde (0.51 g, 4.80 mmol) over 1 h. Addition of diethyl ether (10 mL) caused red crystals to form (55%). Anal. Calcd for $C_{29}H_{27}ClFeO_2Zr$: C, 59.03; H, 4.61; Cl, 6.01. Found: C, 58.75; H, 4.74; Cl, 6.06. IR (Nujol): ν(C=O) 1667 (m) cm^{-1}. ^1H NMR (CD_2Cl_2): δ 2.92 and 3.10 (AB part of a ABX system, $COCH_2$, 2H, J_{AX} = 5.00 Hz, J_{BX} = 8.05 Hz, J_{AB} = 15.70 Hz), 4.11 (s, (cp)Fe, 5H), 4.54 (m, (cp)Fe, 2H), 4.80 (m, (cp)Fe, 2H), 5.64 (X part of a ABX system, CHOZr, 1H, *J* = 5.00, 8.05 Hz), 6.15 and 6.31 (2s, (cp)Zr, 10H), 7.30–7.40 (m, Ph, 5H).

Preparation of 11. A dichloromethane solution (30 mL) of **9** (1.00 g, 1.83 mmol) and $NaBPh_4$ (0.63 g, 1.83 mmol) was stirred for 4 h. The red solution changed to deep violet, and NaCl was removed by filtration. After addition of diethyl ether (35 mL), a violet microcrystalline solid was obtained (83%). Anal. Calcd for $C_{53}H_{47}BFeO_2Ti$: C, 76.65; H, 5.70; Ti, 5.77. Found: C, 76.45; H, 5.59; Ti, 5.87. IR (Nujol): the band at 1663 cm^{-1} disappeared. ^1H NMR (CD_2Cl_2): δ 2.64 and 3.51 (AB part of a ABX system, $COCH_2$, 2H, J_{AX} = 10.60 Hz, J_{BX} = 2.20 Hz, J_{AB} = 17.95 Hz), 4.44 (s, (cp)Fe, 5H), 4.90 (m, (cp)Fe, 2H), 5.11 (m, (cp)Fe, 2H), 5.90 (X part of a ABX system, CHOTi, 1H, *J* = 10.60, 2.20 Hz), 6.33 and 6.48 (2s, (cp)Ti, 10H), 6.90–7.50 (m, Ph, 25H).

Preparation of 14. A dichloromethane solution (10 mL) of **7** (0.57 g, 1.18 mmol) was reacted with neat acetophenone (0.15 g, 1.25 mmol) over a period of 1 day. An orange solution was obtained, which was concentrated to a red oil. No crystals were obtained. ^1H NMR (CD_2Cl_2): δ 1.80 (s, Me, 3H), 3.14 (AB system, $COCH_2$, 2H, *J* = 13.5 Hz), 4.12 (s, (cp)Fe, 5H), 4.50–4.74 (m, (cp)Fe, 4H), 6.12 (s, (cp)Zr, 10H), 6.22 (s, (cp)-Zr), 7.50 (m, Ph, 3H), 7.95 (m, Ph, 2H). ^1H NMR (C_6D_6): δ 1.85 (s, Me, 3H), 3.13 (AB system, CH_2, 2H, *J* = 13.6 Hz), 3.82 (s, (cp)Fe, 5H), 4.10 (m, (cp)Fe, 2H), 4.69 (m, (cp)Fe, 2H), 5.88 and 6.00 (s, (cp)Zr, 10H), 7.00–7.30 and 7.70 (m, Ph, 5H). IR: ν(CO) 1653 cm^{-1}.

Preparation of 15. To a CH_2Cl_2 (50 mL) solution of **7** (2.59 g, 5.35 mmol) was added acetophenone (0.75 g, 6.25 mmol), and the mixture was stirred for 24 h. Then a THF (20 mL) solution of $AgCF_3SO_3$ (1.37 g, 5.35 mmol) was added, the mixture was stirred for 30 min, and the AgCl produced was filtered off. A dark red solution was obtained, which was concentrated to dryness, giving a red product. Recrystallizing from CH_2Cl_2/Et_2O (10 mL/50 mL) gave red crystals (78%). Anal. Calcd for $C_{31}H_{29}F_3FeO_5SZr$: C, 51.90; H, 4.05. Found: C, 51.35; H, 4.20. ^1H NMR (CD_2Cl_2): δ 1.51 (s, Me, 3H), 3.12 (AB system, CH_2, 2H, *J* = 14.5 Hz), 4.30 (s, (cp)Fe, 5H), 4.93 (m, (cp)Fe, 4H), 6.24 (s, (cp)Zr, 10H), 7.2–7.6 (m, Ph, 5H). IR: ν(CO) 1587 cm^{-1}.

Table 5. Experimental Data for the X-ray Diffraction Studies on Crystalline Compounds 7 and 9

	7	**9**
chem formula	$C_{22}H_{21}ClFeOZr$	$C_{29}H_{27}ClFeO_2Ti$
a (Å)	13.989(1)	10.456(1)
b (Å)	14.380(1)	13.119(1)
c (Å)	19.764(1)	8.844(1)
α (deg)	90	99.31(1)
β (deg)	90	90.95(1)
γ (deg)	90	98.77(1)
V (Å^3)	3975.8(4)	1182.1(2)
Z	8	2
fw	483.9	456.7
space group	*Pbca* (No. 61)	*P*$\bar{1}$ (No. 2)
t (°C)	23	23
λ (Å)	0.71069	0.71069
ϱ_{calc} (g cm^{-3})	1.617	1.536
μ (cm^{-1})	13.89	10.86
transmission coeff	0.747–1.000	0.908–1.000
R^a	0.034	0.027
$R_w{}^b$	0.037	0.029

^{a} $R = \Sigma|\Delta F|/\Sigma|F_o|$. ^{b} $R_w = \Sigma w^{1/2}|\Delta F|/\Sigma w^{1/2}|F_o|$.

X-ray Crystallography. The compounds **7** and **9** were mounted in glass capillaries and sealed under nitrogen. The reduced cells were obtained with the use of TRACER.[30] Crystal data and details associated with data collection are given in Table 5. Data were collected at room temperature (295 K) on a single-crystal diffractometer (Nonius CAD4 and Siemens AED for **7** and **9**, respectively). For intensities and background individual profiles were analyzed.[31] The structure amplitudes were obtained after the usual Lorentz and polarization corrections, and the absolute scale was established by the Wilson method.[32] The crystal quality was tested by ψ scans, showing that crystal absorption effects could not be neglected for complex **7**. The data for complex **7** were then corrected for absorption using ABSORB.[33] The function minimized during the least-squares refinement was $\Sigma w|\Delta F|^2$. A weighting scheme ($w = k/\sigma^2(F_o) + g|F_o|^2$), based on counting statistics, was applied.[34] Anomalous scattering corrections were included in all structure factor calculations.[35b] Scattering factors for neutral atoms were taken from ref 35a for non-hydrogen atoms and from ref 36 for H. Among the low-angle reflections no correction for secondary extinction was deemed necessary. All calculations were carried out on a IBM-AT personal computer using SHELX-76.[34]

Solution and refinement were based on the observed reflections. The structures were solved by the heavy-atom method starting from a three-dimensional Patterson map. Refinement was first done isotropically, then anisotropically for non-hydrogen atoms, by full-matrix least squares. All the hydrogen atoms were located from difference Fourier maps and introduced in the final refinement as fixed-atom contributions (isotropic *U*'s fixed at 0.10 and 0.05 Å^2 for **7** and **9**, respectively). The final difference maps showed no unusual features, with no significant peak above the general background. Final

(30) Lawton, S. L.; Jacobson, R. A. TRACER (a Cell Reduction Program); Ames Laboratory, Iowa State University of Science and Technology: Ames, IA, 1965.
(31) Lehmann, M. S.; Larsen, F. K. *Acta Crystallogr., Sect. A: Cryst. Phys., Diffr., Theor. Gen. Crystallogr.* **1974**, *A30*, 580.
(32) Wilson, A. J. C. *Nature* **1942**, *150*, 151.
(33) Ugozzoli, F. *Comput. Chem.* **1987**, *11*, 109.
(34) Sheldrick, G. M. SHELX-76: System of Crystallographic Computer Programs; University of Cambridge: Cambridge, England, 1976.
(35) (a) *International Tables for X-ray Crystallography*; Kynoch Press: Birmingham, U.K., 1974; Vol. IV, p 99. (b) *Ibid.*, p 149.
(36) Stewart, R. F.; Davidson, E. R.; Simpson, W. T. *J. Chem. Phys.* **1965**, *42*, 3175.

Table 6. Selected Bond Distances (Å) and Angles (deg) for Complex 7[a]

Zr1–C11	2.493(7)	Fe1–C1	2.026(5)
Zr1–C12	2.470(9)	Fe1–C2	2.010(6)
Zr1–C13	2.507(9)	Fe1–C3	2.022(9)
Zr1–C14	2.519(10)	Fe1–C4	2.026(7)
Zr1–C15	2.507(8)	Fe1–C5	2.019(6)
Zr1–C16	2.507(8)	Fe1–C6	2.012(8)
Zr1–C17	2.514(7)	Fe1–C7	2.012(13)
Zr1–C18	2.523(9)	Fe1–C8	1.954(15)
Zr1–C19	2.500(9)	Fe1–C9	1.966(13)
Zr1–C20	2.472(9)	Fe1–C10	1.998(10)
Zr1–cp3	2.213(7)	Fe1–cp1	1.624(7)
Zr1–cp4	2.217(9)	Fe1–cp2	1.631(12)
Zr1–Cl1	2.462(2)	O1–C21	1.345(7)
Zr1–O1	1.935(4)	C21–C22	1.335(10)
		C1–C21	1.446(9)
cp3–Zr1–cp4	128.0(4)	Zr1–O1–C21	164.0(4)
O1–Zr1–cp3	107.2(3)	C5–C1–C21	125.4(5)
O1–Zr1–cp4	105.7(3)	C2–C1–C21	127.2(5)
Cl1–Zr1–cp3	107.4(3)	C2–C1–C5	107.5(5)
Cl1–Zr1–cp4	106.3(2)	O1–C21–C1	114.2(5)
Cl1–Zr1–O1	98.4(1)	C1–C21–C22	123.1(6)
cp1–Fe1–cp2	179.3(5)	O1–C21–C22	122.7(6)

[a] cp1, cp2, cp3, and cp4 refer to the centroids of the cyclopentadienyl rings C1···C5, C6···C10, C11···C15, and C16···C20, respectively.

Table 7. Selected Bond Distances (Å) and Angles (deg) for Complex 9[a]

Ti1–C11	2.418(2)	Fe1–C1	2.030(2)
Ti1–C12	2.381(3)	Fe1–C2	2.028(2)
Ti1–C13	2.419(3)	Fe1–C3	2.049(2)
Ti1–C14	2.403(2)	Fe1–C4	2.051(2)
Ti1–C15	2.396(2)	Fe1–C5	2.041(2)
Ti1–C16	2.417(2)	Fe1–C6	2.040(2)
Ti1–C17	2.394(2)	Fe1–C7	2.040(2)
Ti1–C18	2.374(3)	Fe1–C8	2.033(2)
Ti1–C19	2.382(2)	Fe1–C9	2.026(3)
Ti1–C20	2.418(2)	Fe1–C10	2.040(2)
Ti1–cp3	2.088(3)	Fe1–cp1	1.645(2)
Ti1–cp4	2.079(2)	Fe1–cp2	1.646(2)
Ti1–Cl1	2.407(1)	C21–C22	1.507(4)
Ti1–O2	1.856(1)	O2–C23	1.414(3)
O1–C21	1.211(3)	C22–C23	1.529(3)
C1–C21	1.470(4)	C23–C24	1.522(3)
cp3–Ti1–cp4	130.4(1)	Ti1–O2–C23	140.2(1)
O2–Ti1–cp4	109.0(1)	O1–C21–C1	122.1(2)
O2–Ti1–cp3	106.1(1)	C1–C21–C22	116.1(2)
Cl1–Ti1–cp4	105.4(1)	O1–C21–C22	121.8(2)
Cl1–Ti1–cp3	104.5(1)	C21–C22–C23	116.0(2)
Cl1–Ti1–O2	96.0(1)	O2–C23–C22	109.1(2)
cp1–Fe1–cp2	177.9(1)	C22–C23–C24	110.7(2)
		O2–C23–C24	110.6(2)

[a] cp1, cp2, cp3, and cp4 refer to the centroids of the cyclopentadienyl rings C1···C5, C6···C10, C11···C15, and C16···C20, respectively.

atomic coordinates are listed in Tables S2 and S3 for nonhydrogen atoms and in Tables S4 and S5 for hydrogens (supporting information). Thermal parameters are given in Tables S6 and S7 and selected bond distances and angles in Tables 6 and 7.[37]

Kinetics. Kinetic measurements were obtained using NMR spectroscopy in deuterated benzene at 283, 294, 310, 320, 330, and 340 K. Measurements at 310 K were made twice with the same concentration and once with a lower concentration. Values of rate constants are reproducible within 5% error. Relative concentrations of starting and final product were measured by integrating the cp and/or methylene peaks: the cp of **7** is a singlet at 6.04 ppm, whereas **14** gives two singlets at 5.88 and 6.00 ppm. Enolate peaks of **7** give two singlets at 3.88 and 4.33 ppm, whereas those of **14** give a quadruplet AB pattern at 3.13 ppm. Integrations of both peak groups produce very accurate values with a general difference of 2%.

Reaction 4 was carried out by mixing **7** and acetophenone in the NMR tube at low temperature (~220 K).

$$\mathbf{7} + \text{acetophenone} \xrightarrow{k} \mathbf{14} \tag{4}$$

The reaction was started by heating the sample up to the desired temperature. Since this heating process in the NMR spectrometer does not proceed like a unit step function, the time at which $t = 0$ cannot be determined precisely. For this reason, unequal initial concentrations of the reactants were chosen, *viz.* c_{10} (=[acetophenone]) = $2c_{20}$ (=2[**7**]), and the time at the estimated $t = 0$ is set to t_0, a parameter that will be optimized by the least-squares fitting procedure. This ensures that the evaluation of the rate constant k does not depend on the more or less arbitrarily chosen time scale. Integration of the differential equations describing reaction 4 yields eq 5.

$$[\mathbf{14}] = c_{20} - \frac{c_{10} - c_{20}}{\frac{c_{10}}{c_{20}} e^{(c_{10}-c_{20})k(t-t_0)} - 1} \tag{5}$$

The parameters c_{10}, c_{20}, and t_0 are defined above, t is the time in hours, and k is the second-order rate constant in M^{-1} h^{-1}. Since the relative concentration of **14** in percent (percentage of **14**) is available with a minimum error, k and t_0 were evaluated *via* a least-squares analysis according to eq 6. The

$$\%\ \mathbf{14} = 100\left[1 - \frac{c_{10} - c_{20}}{c_{10}\, e^{(c_{10}-c_{20})k(t-t_0)} - c_{20}}\right] \tag{6}$$

rate constants at various temperatures are given in Tables 2 and 4. A measurement at 310 K in deuterated methylene chloride gives a rate constant of $k = 18.24 \pm 0.31$ M^{-1} h^{-1}, which is 30% higher than rate constants obtained in deuterated benzene. This effect is due to the higher polarity of methylene chloride.

Activation parameters are calculated by a $1/\sigma^2$ weighted least-squares fit according to the transition-state theory (eq 7),

$$k = \kappa \cdot k_B \cdot \frac{T}{h} \cdot \exp\left\{\frac{-\Delta H^{\ddagger}}{RT}\right\} \cdot \exp\left\{\frac{\Delta S^{\ddagger}}{R}\right\} \tag{7}$$

where $\kappa = 1$ if the probability is 100% that the transition state does not restore the starting materials, k_B is Boltzmann's constant and is 1.38×10^{-23} J K^{-1}, h is Planck's constant and is 6.63×10^{-34} J Hz^{-1}, and $R = 8.314$ J mol^{-1} K^{-1}. The following parameters were obtained: $\Delta S^{\ddagger} \geq -150 \pm 6$ J mol^{-1} K^{-1}, $\Delta H^{\ddagger} = 44.4 \pm 1.7$ kJ mol^{-1}, and $\Delta G^{\ddagger}_{298} = 89.0 \pm 2.4$ kJ mol^{-1} and $\Delta S^{\ddagger} \geq -189 \pm 15$ J mol^{-1} K^{-1}, $\Delta H^{\ddagger} = 33.0 \pm 4.6$ kJ mol^{-1}, and $\Delta G^{\ddagger}_{298} = 89.2 \pm 6.4$ kJ mol^{-1} for the reactions of **7** with acetophenone and *p*-fluoroacetophenone, respectively (see Tables 2 and 4).

Acknowledgment. We thank the Fonds National Suisse de la Recherche Scientifique (Grant No. 20-40268.94) and Ciba-Geigy (Basel, Switzerland) for financial support.

Supporting Information Available: For complexes **7** and **9**, tables giving experimental details associated with data collection and structure refinement, fractional atomic coordinates, thermal parameters, and bond distances and angles (13 pages). Ordering information is given on any current masthead page.

OM950502Z

(37) See paragraph at the end of the paper regarding supporting information.

Silylation of *gem*-Dichlorobicyclo[*n*.1.0]alkanes and Alkenes with Me_3SiCl/Li/THF Reagent: The Dramatic Influence of Lithium Quality†

Marie-Catherine Grelier-Marly and Micheline Grignon-Dubois*

Laboratoire de Chimie Organique et Organométallique, Université Bordeaux I, 351, cours de la Libération, 33405 Talence-Cedex, France

Received April 28, 1995®

The silylation of *gem*-dichlorobicyclo[*n*.1.0]alkanes and alkenes with Me_3SiCl/Li/THF reagent was studied under various experimental conditions. The disilylated derivatives were systematically isolated as the major product when using Li containing 1% of Na, while the chlorosilylated derivatives were isolated when using Li containing only 0.01% of Na. These results show the dramatic influence of lithium quality upon the reaction outcome.

Introduction

Cyclopropylsilanes are of interest due to their original reactivity.[1] In this context, silylcyclopropane moieties included in a polycyclic structure constitute useful tools to access to functional polycylic derivatives, so it is important to have an efficient preparation of these synthons. We have previously proposed a synthesis of *gem*-bis(trimethylsilyl)bicyclo[*n*.1.0]alkanes and alkenes ($n = 4$ or 6) by silylation of the dichloro derivatives using Me_3SiCl/Li/THF reagent.[2] The disilylation product was obtained in 60%–65% yield with the saturated series, and in 40%–45% yield along with the chlorosilylated derivatives (10%–15% yield) with the unsaturated series. For this work, we used lithium ingot from Prolabo, which was granulated in mineral oil prior to use. More recently, when these compounds were needed for synthetic applications, we reproduced these experiments using metal from Aldrich. This change surprisingly resulted in the chlorosilylated derivatives as the major products. This prompted us to reinvestigate this reaction in relation to the experimental conditions and especially the lithium used.

Results and Discussion

Silylation of 7,7-dichlorobicyclo[4.1.0]hept-2-ene, **1**, and 9,9-dichlorobicyclo[6.1.0]non-2-ene, **2**, with lithium and trimethylchlorosilane (TMSCl) in THF medium was studied under various conditions. The experiments were conducted using three kinds of lithium, which contained 0.01%,[3a] 0.1%,[3b] and 1% of Na, respectively.[3c] The influence of the reagent ratio, which was expected to have an influence on the course of the reaction, was also systematically studied, especially in the case of compound **2**, which was chosen as a model for defining the optimum conditions for the respective production of the chlorosilylated or disilylated compounds. The reaction mixtures were analyzed by gas chromatography, and the results are reported in Table 1. They show the dramatic influence of the percentage of sodium contained in lithium upon the reaction outcome. Indeed, using optimum conditions to perform disilylation, we isolated as the major product the disilylated derivatives **B** with Li ("1% Na"), while the chlorosilylated derivatives **A** were isolated with Li ("0.01% Na") (Scheme 1, Table 1, entries 1, 5, 6, and 14). Lithium at 0.1% Na content led to intermediate behavior (Table 1, entries 3, 4, 12, and 13). In each case, **A** or **B** was the major product, along with small amounts of unreacted starting material and monochloro (**C**) or monosilyl compounds (**D**). Each of them was isolated by fractional distillation as previously reported.[2] The possible reaction pathways for all these products are depicted in Scheme 2. They involve electron transfer from the metal onto the substrate, leading to radical anions and then to radicals[4] (**a** or **b**) by losing Cl^-. Capture of an electron by **a** or **b** followed by the silylation of the corresponding anion give, respectively, **A** or **B**. Hydrogen trapping from the solvent leads to the byproducts **C** and **D**. Theoretically, obtaining **A** requires only 1 equiv of TMSCl for 2 equiv of Li, while **B** requires 2 equiv of TMSCl for 4 equiv of Li. As expected, examination of Table 1 shows that the ratio of reactants was also very significant:

(i) An increase in the quantity of metal and/or TMSCl leads to an increase in the amount of disilylated compounds **B** obtained, but it is worth noting that 3 equiv of TMSCl (instead of the 2 equiv theoretically required) are necessary to obtain **B** in good yields (see Table 1, entries 5, 14, and 15).

(ii) An excess of TMSCl is always necessary to limit side-reactions with the solvent and to make all of the substrate react.

(iii) An excess of lithium is necessary to obtain the chlorosilylated derivatives **A** (see Table 1, entries 8 and 10). Using 2 or 3 equiv led to the same ratio of **B**, but the ratio of **A** is weaker with 2 equiv, due to an important part of the substrate which was recovered unreacted.

From these results, it appears that the optimum experimental conditions are as follows:

† Dedicated to Professor Raymond Calas on the occasion of his 80th birthday.

® Abstract published in *Advance ACS Abstracts,* August 1, 1995.

(1) For a review see: Paquette, L. A. *Chem. Rev.* **1986**, *86*, 733.

(2) Laguerre, M.; Grignon-Dubois, M.; Dunoguès, J. *Tetrahedron* **1981**, *37*, 1161. Grignon-Dubois, M.; Dunoguès, J.; Ahra, M. *Recl. Trav. Chim. Pays-Bas* **1988**, *107*, 216.

(3) (a) Lithium wire, 0.01% sodium content, Aldrich (ref. 22,091-4). (b) Granulated lithium, 0.1% sodium content, from Prolabo (ref. Z 4996.150). (c) Lithium wire, 1% sodium content, from Aldrich (ref. 27,832-7).

(4) See, for example: Calas, R. *J. Organomet. Chem.* **1980**, *200*, 11.

0276-7333/95/2314-4109$09.00/0

Table 1. Reductive Silylation of 1–5

			reactant ratio (equiv)		product ratio (%),[a] R,R' [b]				
entry no.	substrate	% Na	Li	TMSCl	H,Cl	Cl,Cl	H,Si	Cl,Si (*anti*/*syn*)[c]	Si,Si
1	**1**	0.01	4	3	3	11		64 (85/15)	22
2			3	1.5		9		77 (80/20)	14
3		0.1	4	3	2	3	7	20 (90/10)	68
4			3	1.5	5	2	9	44 (85/15)	40
5		1	4	3			5	13 (90/10)	82
6	**2**	0.01	4	3	2	2		73 (80/20)	23
7			4	2	5	3	4	69 (85/15)	19
8			3	1.5	1	7		86 (85/15)	6
9			3	1	5	24		65 (85/15)	6
10			2	1.5	5	28		59 (80/20)	8
11			2	1	7	31		59 (85/15)	3
12		0.1	4	3	2	2	8	19 (90/10)	69
13			3	1.5	2	5	4	31 (90/10)	57
14		1	4	3					100
15			4	2			8	7 (90/10)	85
16	**3**[d]	0.01	3	1.5	2	7	8	59 (60/40)	12
17		1	4	3			5	10 (53/47)	95
18	**4**	0.01	3	1.5	3	4	7	71 (55/45)	15
19		1	4	3			3	11 (51/49)	96
20	**5**	0.01	3	1.5		5	10	77 (55/45)	8
21		1	4	3					100

[a] Product ratios were determined by GC and NMR. [b] R and R' are cyclopropyl substituents. [c] *Anti*/*syn* stereochemistry is related to the trimethylsilyl group position with respect to the polymethylene bridge. [d] 7-(2'-Tetrahydrofuranyl)norcarane was also characterized in the reaction mixture.

Scheme 1

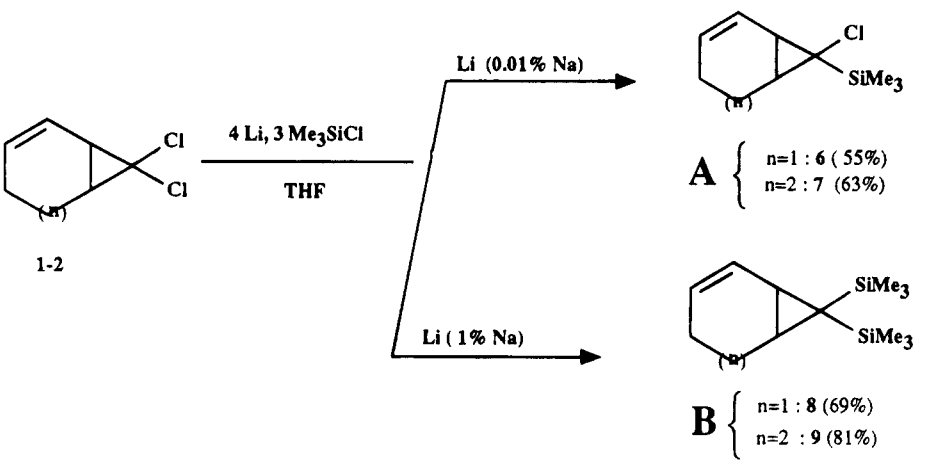

(i) 3 equiv of Li ("0.01% Na") and 1.5 equiv of TMSCl are required to obtain the chlorosilylated compounds **A** (Table 2).

(ii) 4 equiv of Li ("1% Na") and 3 equiv of TMSCl are required to obtain the disilylated compounds **B** (Table 3).

Under these conditions, the saturated substrates **3–5** (Scheme 3, Tables 1–3) respectively led to **10–12** using Li at "0.01% Na" (3 equiv) and **13–15** using Li at "1% Na" (4 equiv). Compared to our previous results,[1] all the product yields have been increased of about 20%. These results confirm the dramatic influence of lithium quality on the silylation outcome. It is well-known that lithium, due to its manufacturing process,[5] always contains small amounts of sodium, which was said to play a role in its efficiency in the silylation processes. However, to the best of our knowledge, this is the first time a systematic study of this factor and such an important effect related to a relatively small variation in sodium amount are reported. Moreover, it is worth noting that lithium contains other metallic impurities, which can be as abundant as sodium (see Experimental Section).

The chlorosilylated compounds were isolated as an *anti*/*syn*[6] isomeric mixture, which was separated by distillation. Their stereochemistry has been unambiguously attributed using ^{29}Si NMR on the basis of the ^{3}J(^{29}Si,^{1}H) coupling constant values.[7] It is worth noting that the *anti*/*syn* ratio is always close to 85/15 from **1–2**, but 55/45–60/40 from **3–5**. The larger predominance of the *anti* isomer with unsaturated substrate shows the effect of the double bond on the stereochemistry and will be discussed below.

Replacement of a halogen of *gem*-dihalocyclopropanes by a trimethylsilyl group had been previously accomplished. Compound **10** was obtained as an *anti*/

(5) Guntz, M. *C. R. Acad. Sci.* **1983**, *117C*, 732. Ruff, O.; Johannsen, O. *Z. Electrochem.* **1906**, *12*, 186.

(6) The *anti*/*syn* stereochemistry is related to the trimethylsilyl group or the negative charge position with respect to the polymethylene bridge.

(7) Grignon-Dubois, M.; Ahra, M.; Laguerre, M.; Barbe, B.; Pétraud, M. *Spectrochim. Acta* **1989**, *45A*, 911.

Scheme 2

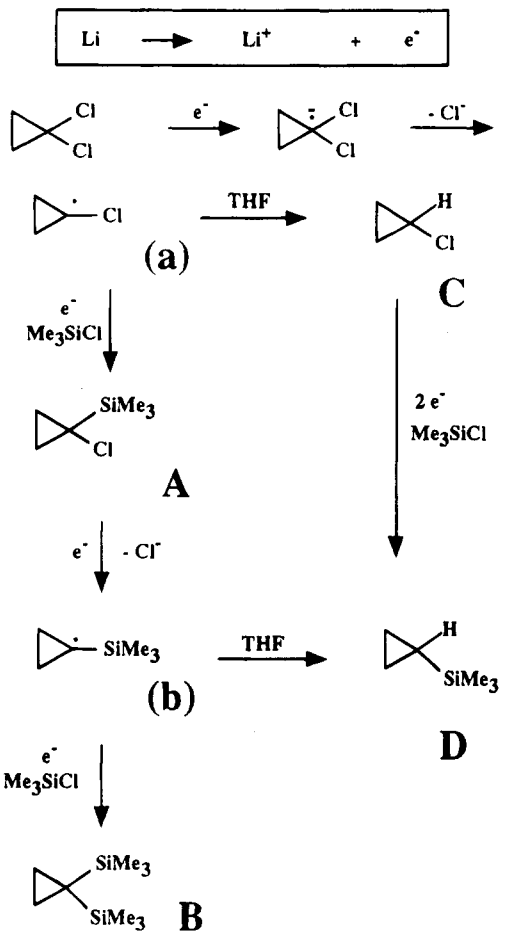

Scheme 3

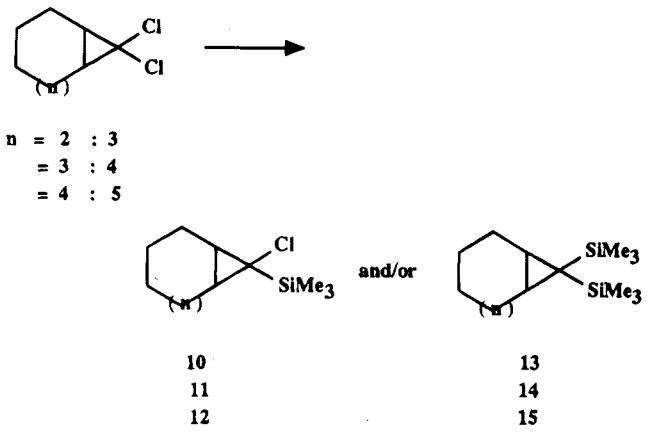

syn mixture (60/40; 70% yield) by reacting 7-chloro-7-bromonorcarane with BuLi and TMSCL[8a] and as the single *anti* isomer (24% yield) by reacting cyclohexene with bis(trimethylsilyldichloromethyl)mercury at 120 °C for 6 days.[8b] Using TMSCl/Mg/THF reagent with dibromonorcarane only led to the disilylated compound,[8c] whereas TMSCl/Mg/HMPA led to the bromosilylated derivative (68% yield, *anti/syn* 28:72).[8d] In order to determine which of the metal or the solvent was responsible for the stereoselectivity in this last case, we

(8) (a) Seyferth, D.; Lambert, R. L., Jr.; Massol, M. *J. Organomet. Chem.* **1975**, *88*, 255. (b) Seyferth, D.; Hanson, E. M. *J. Organomet. Chem.* **1971**, *27*, 19. (c) Seyferth, D.; Lambert, R. L., Jr. *J. Organomet. Chem.* **1975**, *88*, 287. (d) Shimizu, N.; Tsuno, Y. *Mem. Fac. Sci. Kyushu Univ., Ser. C* **1979**, *12*, 95; *Chem. Abstr.* **1980**, *92*, 110576z.

Table 2. Reductive Silylation of 1–5 Using 3 Equiv of Li (0.01% Na) and 1.5 Equiv of TMSCl

	product ratio (%),[a] R,R'[b]					
substrate	H,Cl	Cl,Cl	H,Si	Cl,Si (*anti/syn*)[c]	Si,Si	Cl,Si yield (%)
1		9		77 (80/20)	14	55
2	1	7		86 (85/15)	6	63
3	2	7	8	59 (60/40)	12	45
4	3	4	7	71 (55/45)	15	51
5		5	10	77 (55/45)	8	56

[a] Product ratios were determined by GC and NMR. [b] R and R' are cyclopropyl substituents. [c] *Anti/syn* stereochemistry is related to the trimethylsilyl group position with respect to the polymethylene bridge.

Table 3. Reductive Silylation of 1–5 Using 4 Equiv of Li (1% Na) and 3 Equiv of TMSCl

	product ratio (%),[a] R,R'[b]					
substrate	H,Cl	Cl,Cl	H,Si	Cl,Si (*anti/syn*)[c]	Si,Si	Si,Si yield (%)
1			5	13 (90/10)	82	69
2					100	81
3			5	10 (53/47)	95	78
4			3	11 (51/49)	96	80
5					100	83

[a] Product ratios were determined by GC and NMR. [b] R and R' are cyclopropyl substituents. [c] *Anti/syn* stereochemistry is related to the trimethylsilyl group position with respect to the polymethylene bridge.

investigated the silylation of **3–5** using Mg in THF medium under reflux.[9] Our results (Table 4) show that a significant amount of starting material was almost systematically recovered, and the selectivity was not as good as with Li. Moreover, the reactivity decreased when the size of the bicycloalkanes increased. Without an activating agent (Table 4, entries 1 and 2), no silylation occurred. Adding 2 equiv of HMPA[10] only led to a small amount of chlorosilylated products in a 1:1 ratio. In the case of quinoline and isoquinoline derivatives, silylation yields were improved and the reaction times shortened by adding small amounts of Zn to the TMSCl/Mg/THF reagent.[11] Indeed, examination of entries 5 and 6 (Table 4) shows that the addition of 0.3 equiv of Zn increases the silylation power, but 51% of **4** was still recovered unreacted, confirming the weaker reactivity of the larger ring. Using 0.3 equiv of Zn associated to 0.06 equiv of CuCl (Table 4, entries 8–11) led to better results. During these reactions, the mixture turned a brick color after some hours of heating, which could indicate the formation of metallic copper. The same phenomenon was observed during the methylenation of olefins by the Simmons–Smith procedure,[12a] especially when using the Zn/CuCl reagent.[12b] More precise investigation into the CuCl effect is necessary to conclude, but it could play the same role as the impurities contained in lithium. Concerning the stereochemistry of the monosilylation process, examination

(9) We also studied silylation of **1–5** with TMSCl/Mg/HMPA, but only small amounts of silylated products were detected, even after 72 h at 80 °C.

(10) (a) Biran, C. Ph.D. Thesis, Université Bordeaux I, France, 1972. (b) Calas, R.; Duffaut, N.; Biran, C.; Bourgeois, P.; Pisciotti, F. *C. R. Acad. Sci.* **1968**, *267C*, 322.

(11) Grignon-Dubois, M.; Fialeix, M.; Léger, J. M. *Can. J. Chem.* **1993**, *71*, 754. Grignon-Dubois, M.; Gauffre, J. C. Results to be published.

(12) (a) Simmons, H. E.; Smith, R. D. *J. Am. Chem. Soc.* **1958**, *80*, 5323. *Ibid.* **1959**, *81*, 4256. (b) Rawson, R. J.; Harrison, I. T. *J. Org. Chem.* **1970**, *35*, 2057.

Table 4. Reductive Silylation of 3–5 Using TMSCl/Mg/THF Reagent Activated by HMPA, Zn, and CuCl

		reagent ratio (equiv) product		production ratio (%),[a] R,R′			
entry no	substrate	Mg	activating agent	Cl,Cl	H,Si	Cl,Si (*anti*/*syn*)[c]	Si,Si
1	**3**	2		88	traces	traces	
2	**4**	2		90			
3	**3**	2	2 HMPA	80		20 (50/50)	traces
4	**4**	2	2 HMPA	86	traces	14 (60/40)	traces
5	**3**	3	0.3 Zn		25	15 (*anti*)	30
6	**4**	3	0.3 Zn	51		49 (50/50)	
7	**3**	3	0.3 Zn +0.03 CuCl	20	22	8 (*anti*)	47
8	**4**	3	0.3 Zn +0.03 CuCl	31		69 (55/45)	
9	**5**	3	0.3 Zn +0.03 CuCl	28	8	60 (65/35)	3

[a] Product ratios were determined by GC and NMR. [b] R and R′ are cyclopropyl substituents. [c] *Anti*/*syn* stereochemistry is related to the trimethylsilyl group position with respect to the polymethylene bridge.

Scheme 4

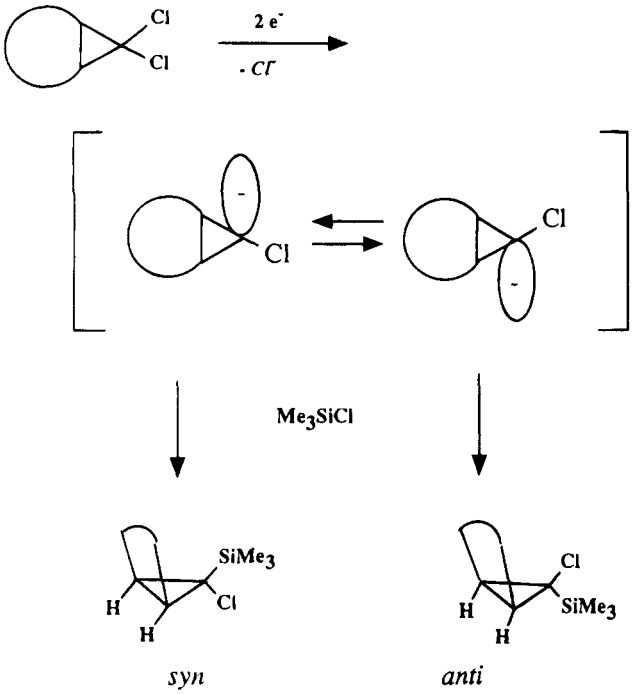

of Table 4 shows that the *anti*/*syn* ratio remains almost the same as with Li, despite the difference in the reaction temperature.

The stereoselectivity of the monosilylation step can have several origins. First, the intermediate anion may be configurationally unstable and isomerize to the thermodynamically favorable isomer (Scheme 4).[13] We have previously shown that silylation of the monochlorinated derivatives with TMSCl/Li/THF was not stereoselective but led to a 50:50 *anti*/*syn* mixture from a single isomer.[14] The systematic predominance of the *anti* isomer could also mean that the replacement of a chlorine atom occurs preferentially at the outer side of **1–5**, which is the less sterically hindered, or is a result of thermodynamical control.

In an attempt to better understand the stereochemistry of the silylation, molecular mechanics calculations have been performed for all the chlorosilylated and disilylated products. For this purpose, we used the PC-MODEL program[15] on a PC-compatible computer.) Energy minimization was performed in the program using the MMX force field, which is a modification of Allinger's MM2 and MMP1 programs.[16] The minimum MMX energies are reported in Table 5 and Figure 1. They show that the steric energies of the disilylated products are always lower than those of their chlorosilylated homologues (compound **13** expected, for which we found a 0.4 kcal/mol difference in energies between **13** and the *anti* isomer of **10**). The lowest energies are observed for the disilyl unsaturated compounds **8** and **9**. Examination of the energy summary (see Table 6 and Experimental Section) shows that the greater torsion and bending contributions in all the disilyl products compared to the *syn*/*anti* chlorosilyl isomers are counterbalanced by stabilizing van der Waals and electrostatic contributions. It is interesting to note that the most important effects are observed with the unsaturated compounds **8** (−3.5 kcal/mol for each contribution) and **9** (−2.1 to −3.7 kcal/mol). With the saturated disilyl compounds **13–15**, we observed a

Table 5. MMX Steric Energies (kcal/mol) for Chlorosilylated and Disilylated Derivatives

	Cl,Si[a]			
substrate	*anti*	*syn*	substrate	Si,Si
6	16.5	18.9	**8**	8.2
7	20.8	23.8	**9**	13.6
10	19.8	26.0	**13**	20.2
11	19.8	24.2	**14**	18.4
12	22.2	26.0	**15**	19.9

[a] *Anti*/*syn* stereochemistry is related to the trimethylsilyl group position with respect to the polymethylene bridge.

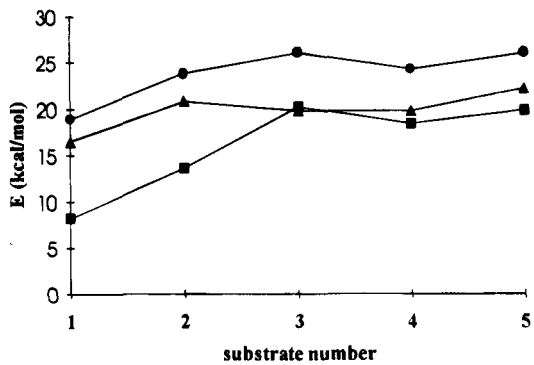

Figure 1. MMX steric energies for compounds **6–15**: (■), Si,Si; (▲), Cl,Si *anti*; (●), Cl,Si *syn*.

(13) α-Bromocyclopropyl anions have been reported to exist in equilibrium. See, for example, ref 8a.

(14) Ahra, M.; Grignon-Dubois, M.; Dunoguès, J. *Organomet. Chem.* **1984**, *271*, 15. The calculated strain energies (see ref 15) of the two 9-trimethylsilylbicyclo[6.1.0]nonane isomers (18.7 kcal/mol for the *anti* and 24.1 kcal/mol for the *syn*) show the greatest stability of the *anti* form.

(15) Program: PCMODEL, Version 4.1; Serena Software: P.O. Box 3076, Bloomington, IN 47402-3076.

(16) (a) Allinger, N. L. *J. Am. Chem. Soc.* **1977**, *99*, 8127. (b) Allinger, N. L.; Sprague, J. T. *J. Am. Chem. Soc.* **1973**, *95*, 3893.

Table 6. Summary of the Contributions to the MMX Energy

product	total E (kcal/mol)	energy contributions[a] (kcal/mol) STR	BND	S−B	TOR	vdW	QQ
6 *anti*	16.5	0.6	6.3	−0.2	6.5	−0.2	3.5
syn	18.9	0.7	6.9	−0.2	8.3	−0.4	3.6
7 *anti*	20.8	0.9	6.3	−0.1	9.3	0.8	3.6
syn	23.8	0.9	8.9	−0.1	9.6	1.0	3.5
10 *anti*	19.8	0.8	6.0	−0.2	10.3	0.5	2.4
syn	26.0	1.1	9.9	−0.3	10.5	2.2	2.6
11 *anti*	19.8	0.9	6.8	−0.1	8.7	1.1	2.4
syn	24.2	1.0	10.5	−0.1	8.7	1.5	2.6
12 *anti*	22.2	1.0	7.8	0	9.5	1.5	2.4
syn	26.0	1.2	11.0	0	9.4	1.8	2.6
8	8.2	1.1	8.1	−0.2	8.4	−3.5	−5.7
9	13.6	1.4	10.3	−0.1	9.7	−2.0	−5.7
13	20.2	1.6	11.7	−0.2	10.5	−0.8	−2.6
14	18.4	1.6	12.2	−0.1	8.8	−1.5	−2.6
15	19.9	1.7	12.5	0.1	9.5	−1.3	−2.6

[a] For the definition of the different contributions, see Experimental Section.

weaker van der Waals contribution (−0.8 to 1.5 kcal/mol) and a comparable electrostatic one (2.6 kcal/mol). The smaller energy values of disilylated products compared to the chlorosilylated ones are in good agreement with the lower selectivity of the silylation process (mono/di) with Mg at reflux than with Li at 0 °C. For the chlorosilylated compounds, the *anti* isomer is always more stable than the *syn* isomer. This difference in energy is essentially due to the greater torsion and bending contributions in all the *syn* isomers, which can be attributed to the steric hindrance of the silyl group. It is interesting to note that the larger the *syn* − *anti* difference in energy, the smaller the *syn*/*anti* ratio. This shows that silylation with lithium is not thermodynamically controlled or, if so, only in part, the regiochemistry being rather governed by the equilibrium rate of the anion stereoisomers. In the case of the unsaturated compounds, a repulsive interaction between the π electrons of the double bond and the cyclopropyl charge could destabilize the *syn* anion. Unfortunately, the MMX force field does not allow calculations for cyclopropyl anions.

Experimental Section

Materials. THF (SDS purex) was distilled from sodium benzophenone ketyl and degassed before use by an ultrasonic cleaning bath. Trimethylchlorosilane was distilled from magnesium powder prior to use. All *gem*-dichlorobicycloalkanes and alkenes were prepared using phase transfer reactions.[1] Lithium wire from Aldrich was cut into small pieces and then washed with THF just prior to use. On request, Aldrich Chemical Co. provided us with the following product information, which shows that lithium contains many more metallic impurities than sodium. In fact, the product that contains 0.01% of Na actually contains a greater amount of silicon impurity:

(i) Lithium wire, 0.01% sodium content from Aldrich (ref. 22,091−4) (ppm): Si, 280; Na, 230; Ca, 210; Cs, 190; K, 55; Al, 30; Fe, 20; Sn, 20; Mg, 10; Ba, 4; Cu, 3.

(ii) Lithium wire, 1% sodium content from Aldrich (ref. 27,832−7) (ppm): Na, 5100; Ca, 340; Si, 190; K, 90; Fe, 85; Mg, 20; Ag, 15; Ba, 15.

Granulated lithium (0.1% Na) from Prolabo was used as received. Despite our repeated requests, it was impossible to obtain detailed product information from this company.

Silylation: Typical Procedures. All the reactions were carried out under an argon atmosphere by employing vacuum line techniques. The ratios of reactants are given in Tables 1 and 4.

TMSCl/Li/THF. To a vigorously stirred suspension of lithium in THF (200 mL) and *gem*-dichlorobicycloalkane (0.1 mol) was added TMSCl dissolved in THF (10 mL) dropwise over a period of 0.5 h. During the addition, the temperature was maintained at 0 °C. The mixture was then stirred for 5 h at this temperature. Most of the THF and unreacted TMSCl were evaporated, and then cyclohexane (50 mL) was added, leading to precipitation of LiCl, which was filtered off. After evaporation of the solvent, this procedure was repeated twice. The solvent was distilled off *in vacuo*, and the crude product was analyzed by GC, using a Perkin-Elmer IGC 15 apparatus (Silicon OV-101 (5%) on Chromosorb P). The resulting ratios of products thus determined have been corrected for detector response, using weighed samples of pure authentic sample. The constituents of the mixture were isolated by distillation under reduced pressure using a spinning band apparatus. All the products isolated were identical to the sample previously described.[1,5,6,17]

TMSCl/Mg/THF. The reactions were conducted as described above, but replacing Li by Mg, alone or associated with Zn, Zn, and CuCl or HMPA (Table 4). During the addition of TMSCl, the temperature was kept at reflux of THF. The mixture was stirred for 72 h at this temperature, and then the workup was carried out as described above.

Molecular Modeling. Calculations were performed on a 486 PC-compatible running the program PC-Model, Version 4.1.[15] The dielectric constant used throughout the calculations was 1.5. Each calculated total energy reported in Table 5 consisted of stretching (STR), bending (BND), stretching−bending (S−B), torsional (TOR), van der Waals (vdW), and electrostatic (QQ) contributions (Table 6).

OM950313G

(17) Marchand, A.; Gerval, P.; Ahra, M.; Grignon-Dubois, M. *Spectrochim. Acta* **1987**, *43A*, 539. *Ibid.* **1988**, *44A*, 263.

Preparation, Structure, and Reactivity of New Bis(acetylide) and Acetylide–Vinylidene Ruthenium(II) Complexes Stabilized by Phosphite Ligands

Gabriele Albertin,*[†] Stefano Antoniutti,[†] Emilio Bordignon,[†] Franco Cazzaro,[†] Sandra Ianelli,[‡] and Giancarlo Pelizzi[‡]

Dipartimento di Chimica, Università di Venezia, Dorsoduro 2137, 30123 Venezia, Italy, and Dipartimento di Chimica Generale ed Inorganica, Centro CNR di Strutturistica Diffrattometrica, Università di Parma, Viale delle Scienze, 43100 Parma, Italy

Received December 8, 1994[⊗]

Bis(alkynyl) complexes $Ru(C{\equiv}CR)_2P_4$ (**1**–**3**) (R = Ph, *p*-tolyl, ^{t}Bu; P = $P(OMe)_3$ (**1**), $P(OEt)_3$ (**2**), $PPh(OEt)_2$ (**3**)) were prepared by reacting $RuCl_2P_4$ with excess Li^+ $RC{\equiv}C^-$, and a *trans* geometry was established both in solids (X-ray) and in solution. The reaction of these alkynyls (**1**–**3**) with electrophilic reagent depends on the nature of the phosphite ligand. Vinylidene–acetylide derivatives $[Ru(C{\equiv}CR)\{{=}C{=}C(R_1)R\}P_4]^+$ (R_1 = H (**4**, **5**), CH_3 (**7**, **8**), ArN=N (**10**), I (**12**), 2,3-$(NO_2)_2C_6H_3S$ (**14**)) were prepared with $P(OMe)_3$ and $P(OEt)_3$ ligand by treatment of **1** and **2** with HBF_4, CF_3SO_3Me, $ArN_2^+BF_4^-$, I_2, and 2,3-$(NO_2)_2C_6H_3SCl$, respectively. Instead, only the diazo- and iodovinylidenes $[Ru(C{\equiv}CR)\{{=}C{=}C(R_1)R\}P_4]^+$ (R_1 = *p*-tolN=N (**11**), I (**13**)) were obtained with the $PPh(OEt)_2$ phosphite ligand. These vinylidene compounds were fully characterized by IR, ^{1}H, ^{31}P, and ^{13}C NMR spectra, and a single-crystal X-ray structure determination of complex $[Ru(C{\equiv}CPh)\{{=}C{=}C(Me)Ph\}\{P(OEt)_3\}_4]CF_3SO_3$ (**8a**) is reported. The alkynyl–vinylidene $[Ru(C{\equiv}CR)\{{=}C{=}C(H)R\}P_4]^+$ cations (**4**, **5**) rearrange in solution to enynyl $[Ru(\eta^3\text{-}RC_3CHR)P_4]^+$ derivatives, and the reaction is inhibited by the presence of free alkyne. Kinetic data support a mechanism involving a pentacoordinate intermediate formed by loss of the vinylidene ligand. Substitution of the =C=C(H)R ligand by phosphite, isocyanide, and nitrile is easy in **4** and **5** and leads to $[Ru(C{\equiv}CPh)\{P(OMe)_3\}P_4]^+$ (**17**), $[Ru(C{\equiv}CPh)(p\text{-tolNC})P_4]^+$ (**18**), and $[Ru(p\text{-tolCN})_2P_4]^{2+}$ (**19**) (P = $P(OEt)_3$), derivatives. Deprotonation with a base of the vinylidene ligand in **4** and **5**, giving $Ru(C{\equiv}CR)_2P_4$, was also detected.

Introduction

A large number of studies on the chemistry of transition-metal vinylidene complexes has been reported during the last decade,[1–3] and it now seems certain that the properties of vinylidene ligands are a function of the nature of the $C{=}CRR_1$ substituents, the central metal, and its ancillary ligands. Interest in these studies arises not only from the unique and diverse reactivity modes and structural properties that complexes containing the metal–carbon double bond exhibit,[1–3] but also because vinylidene species seem to play an important role in Fischer–Tropsch chemistry,[4] in alkyne polymerization,[5] and in C–C bond formation in the condensation of alkynes with other substrates.[6] Closely related to vinylidene complexes are transition-metal alkynyl derivatives which are common precursors to, and reaction products of, $C{=}CRR_1$ vinylidene derivatives.[7] These compounds are also of interest as precur-

[†] Università di Venezia.

[‡] Università di Parma.

[⊗] Abstract published in *Advance ACS Abstracts*, July 1, 1995.

(1) (a) Bruce, M. I. *Chem. Rev.* **1991**, *91*, 197. (b) Werner, H. *Angew. Chem., Int. Ed. Engl.* **1990**, *29*, 1077.

(2) (a) Terry, M. R.; Mercando, L. A.; Kelley, C.; Geoffroy, G. L.; Nombel, P.; Lugan, N.; Mathieu, R.; Ostrander, R. L.; Owens-Waltermire, B. E.; Rheingold, A. L. *Organometallics* **1994**, *13*, 843. (b) Werner, H.; Baum, M.; Schneider, D.; Windmüller, B. *Organometallics* **1994**, *13*, 1089. (c) Touchard, D.; Haquette, P.; Pirio, N.; Toupet, L.; Dixneuf, P. H. *Organometallics* **1993**, *12*, 3132. (d) Hughes, D. L.; Leigh, G. J.; Jimenez-Tenorio, M.; Rowley, A. T. *J. Chem. Soc., Dalton Trans.* **1993**, 75. (e) Xiao, J.; Cowie, M. *Organometallics* **1993**, *12*, 463. (f) Lomprey, J. R.; Selegue, J. P. *J. Am. Chem. Soc.* **1992**, *114*, 5518. (g) Field, L. D.; George, A. V.; Purches, G. R.; Slip, I. H. M. *Organometallics* **1992**, *11*, 3019. (h) Miller, D. C.; Angelici, R. J. *Organometallics* **1991**, *10*, 79. (i) Wakatsuki, Y.; Yamazaki, H.; Kumegawa, N.; Satoh, T.; Satoh, J. Y. *J. Am. Chem. Soc.* **1991**, *113*, 9604. (j) Selnau, H. E.; Merola, J. S. *J. Am. Chem. Soc.* **1991**, *113*, 4008. (k) Bianchini, C.; Peruzzini, M.; Vacca, A.; Zanobini, F. *Organometallics* **1991**, *10*, 3697. (l) Seyferth, D.; Ruschke, D. P.; Davis, W. M.; Cowie, M.; Hunter, A. D. *Organometallics* **1989**, *8*, 836. (m) Bullock, R. M. *J. Chem. Soc., Chem. Commun.* **1989**, 165.

(3) (a) Senn, D. R.; Wong, A.; Patton, A. T.; Marsi, M.; Strouse, C. E.; Gladysz, J. A. *J. Am. Chem. Soc.* **1988**, *110*, 6096. (b) Consiglio, G.; Schwab, R.; Morandini, F. *J. Chem. Soc., Chem. Commun.* **1988**, 25. (c) van Asselt, A.; Burger, B. J.; Gibson, V. C.; Bercaw, J. E. *J. Am. Chem. Soc.* **1986**, *108*, 5347. (d) Collman, J. P.; Brothers, P. J.; McElwee-White, L.; Rose, E. *J. Am. Chem. Soc.* **1985**, *107*, 6110. (e) Birdwhitstell, K. R.; Tonker, T. L.; Templeton, J. L. *J. Am. Chem. soc.* **1985**, *107*, 4474. (f) Beevor, R. G.; Freeman, M. J.; Green, M.; Morton, C. E.; Orpen, A. G. *J. Chem. Soc., Chem. Commun.* **1985**, 68. (g) Mayr, A.; Schaefer, K. C.; Huang, E. Y. *J. Am. Chem. Soc.* **1984**, *106*, 1517. (h) Reger, D. L.; Swift, C. A. *Organometallics* **1984**, *3*, 876. (i) Antonova, A. B.; Kovalenko, S. V.; Korniyets, E. D.; Johansson, A. A.; Struchkov, Y. T.; Ahmedov, A. I.; Yanovsky, A. I. *J. Organomet. Chem.* **1983**, *244*, 35. (j) Abbot, S.; Davies, S. G.; Warner, P. *J. Organomet. Chem.* **1983**, *246*, C65. (k) Berke, H.; Huttner, G.; von Seyerl, J. *J. Organomet. Chem.* **1981**, *218*, 193. (l) Roper, W. R.; Waters, J. M.; Wright, L. J.; van Meuers, F. *J. Organomet. Chem.* **1980**, *201*, C27.

(4) Gibson, V. C.; Parkin, G.; Bercaw, J. E. *Organometallics* **1991**, *10*, 220. Hoel, E. L. *Organometallics* **1986**, *5*, 587. McCandlish, L. E. *J. Catal.* **1983**, *83*, 362.

(5) Nombel, P.; Lugan, N.; Mulla, F.; Lavigne, G. *Organometallics* **1994**, *13*, 4673. Alt, H. G.; Engelhardt, H. E.; Rausch, M. D.; Kool, L. B. *J. Organomet. Chem.* **1987**, *329*, 61. Landon, S. J.; Shulman, P. M.; Geoffroy, G. L. *J. Am. Chem. Soc.* **1985**, *107*, 6739.

(6) Trost, B. M.; Dyker, G.; Kulawiec, R. J. *J. Am. Chem. Soc.* **1990**, *112*, 7809.

0276-7333/95/2314-4114$09.00/0

sors of molecules containing a linear array and delocalizable π-systems[7f,8] or polymeric materials[8] in the search for π-interactions through the metal center and new properties.[9]

Despite the large number of vinylidene complexes with cyclopentadienyl and arene rings and mono-, bi-, and polydentate phosphines as supporting ligands,[1-3] very few of them are reported with phosphite ($P(OR)_3$, $PPh(OR)_2$) ligands,[1,10] although it may be expected[11] that the steric and electronic properties of these ligands will reveal new properties of vinylidene and acetylide derivatives.

In this paper we report the synthesis of a series of bis(acetylide) and acetylide–vinylidene ruthenium(II) complexes containing phosphite ligands of the type $Ru(C{\equiv}CR)_2P_4$ and $[Ru(C{\equiv}CR)(=C=CRR_1)P_4]^+$ together with some studies on the reactivity of the new vinylidene derivatives and an X-ray crystal-structure determination.

Experimental Section

All synthetic work was carried out under an inert atmosphere using standard Schlenk techniques or a Vacuum Atmosphere drybox. Once isolated, the complexes turned out to be quite air-stable and were stored at −20 °C. All solvents used were dried over appropriate drying agents, degassed on a vacuum line, and distilled into vacuum-tight storage flasks. Trimethyl and triethyl phosphite were Aldrich products purified by distillation under nitrogen; diethoxyphenyl phosphine was prepared by the method of Rabinowitz and Pellon.[12] Alkynes were Aldrich products, used without any further purification. Lithium acetylides $Li^+RC{\equiv}C^-$ (R = Ph or *p*-tol) were prepared by reacting a slight excess of the appropriate acetylene (40 mmol) with lithium (35 mmol, 0.24 g) in 10 mL of THF. *tert*-Butylacetylide $Li^+{}^tBuC{\equiv}C^-$ was prepared by adding a solution of Li^nBu 2.5 *M* in hexane (8 mmol, 3.2 mL) to a solution of $^tBuC{\equiv}CH$ (10 mmol, 1.23 mL) in 10 mL of THF cooled to −80 °C. The reaction mixture was stirred for 20–30 min at −80 °C and was then used. Diazonium salts were obtained in the usual way described in the literature.[13] The labeled diazonium salt $PhN{\equiv}{}^{15}N^+BF_4^-$ was prepared from $Na^{15}NO_2$ (99% enriched, CIL) and aryl amine. *p*-Tolyl isocyanide was obtained by the phosgene method of Ugi *et al.*[14] Other reagents were purchased from commercial sources in the highest available purity and used as received. Infrared spectra were recorded on Perkin-Elmer Model 683 or Digilab BioRad FTS-40 spectrophotometers. NMR spectra (^1H, ^{13}C, ^{31}P) were obtained on a Bruker AC200 spectrometer at temperatures varying between −90 and +30 °C, unless otherwise noted. ^1H and ^{13}C spectra are referenced to internal tetramethylsilane, while $^{31}P\{^1H\}$ chemical shifts are reported with respect to 85% H_3PO_4, with downfield shifts considered positive. IR and NMR data are collected in Table 1. The conductivity of 10^{-3} M solutions of the complexes in CH_3NO_2 at 25 °C was measured with a Radiometer CDM 83 instrument.

Synthesis of Complexes. The dichlorotetrakis(triethyl phosphite)ruthenium(II) complex was prepared as previously reported.[15] The related $RuCl_2[P(OMe)_3]_4$ and $RuCl_2[PPh(OEt)_2]_4$ were also prepared as follows by slight modification of this method.

$RuCl_2[P(OMe)_3]_4$ was prepared by adding an excess of $P(OMe)_3$ (0.15 mol, 19 mL) to ruthenium trichloride trihydrate (0.01 mol, 2.6 g). The mixture was stirred for 1 h at room temperature, and then $NaBH_4$ (0.026 mol, 1 g) was added. After 30 min of stirring, a yellow suspension formed, which was cooled to −20 °C and then filtered. The solid obtained was dissolved in 20 mL of CH_2Cl_2, filtered, and evaporated at reduced pressure. The resulting yellow solid was crystallized by slowly cooling to −30 °C its saturated solution in CH_3OH prepared at 20 °C; yield: ≥45%. Anal. Calcd: C, 21.57; H, 5.43. Found: C, 21.42; H, 5.50. ^1H NMR ($CDCl_3$), δ: 3.85 (m, 36H, CH_3). $^{31}P\{^1H\}$ NMR ($CDCl_3$), δ: 129.9 s.

$RuCl_2[PPh(OEt)_2]_4$ was obtained by adding an excess of $PPh(OEt)_2$ (0.15 mol, 30 mL) to solid $RuCl_3{\cdot}3H_2O$ (0.01 mol, 2.6 g) and heating the mixture under vigorous stirring until a reaction took place, giving a yellow suspension (about 1 h at 70–80 °C). After the mixture was cooled to 20 °C, 1 g (0.026 mol) of $NaBH_4$ was added and the suspension was stirred for about 5 h. The solid that formed was filtered, washed with ethanol, and dissolved in CH_2Cl_2. The resulting solution was filtered, and removal of the solvent gave an oil, which was treated with ethanol, affording the $RuCl_2[PPh(OEt)_2]_4$ complex as a yellow microcrystalline solid; yield: ≥75%. Anal. Calcd: C, 49.80; H, 6.27. Found: C, 49.96; H, 6.19. ^1H NMR (CD_2Cl_2), δ: 7.77–7.05 (m, 20H, Ph); 3.99, 3.63 (m, 16H, CH_2); 1.15 (t, 24H, CH_3). $^{31}P\{^1H\}$ NMR (CD_2Cl_2), δ: 146.4 s.

$Ru(C{\equiv}CR)_2P_4$ (1–3) [R = Ph (a), *p*-Tol (b), ^{t}Bu (c); P = $P(OMe)_3$ (1), $P(OEt)_3$ (2), $PPh(OEt)_2$ (3)]. To a solution of $RuCl_2P_4$ (1.0 mmol) in 10 mL of THF was added an excess of the appropriate $Li^+RC{\equiv}C^-$ in THF solution (4 mmol), and the resulting mixture was refluxed for about 15 min. Removal of the solvent at reduced pressure gave a brown oil, which was triturated with methanol or ethanol (15 mL). The resulting solution was stirred until a yellow solid separated out, which was filtered and crystallized by slowly cooling at −20 °C its saturated solution in ethanol/hexane (10/25 mL); yield: ≥35%. Anal. Calcd for **1a**: C, 42.06; H, 5.80. Found: C, 41.93; H, 5.82. Mp: 122 °C decomp. Calcd for **1b**: C, 43.53; H, 6.09. Found: C, 43.40; H, 5.98. Mp: 131 °C decomp. Calcd for **1c**: C, 37.94; H, 7.17. Found: C, 37.72; H, 7.02. Mp: 106 °C decomp. Calcd for **2a**: C, 49.63; H, 7.29. Found: C, 49.45; H, 7.45. Mp: 152 °C decomp. Calcd for **2b**: C, 50.65; H, 7.49. Found: C, 50.71; H, 7.40. Mp: 142 °C decomp. Calcd for **2c**: C, 46.59; H, 8.47. Found: C, 46.45; H, 8.65. Mp: 175–177 °C decomp. Calcd for **3a**: C, 61.36; H, 6.44. Found: C, 61.19; H, 6.53. Mp: 93–95 °C decomp. Calcd for **3b**: C, 61.97; H, 6.64. Found: C, 61.79; H, 6.53. Mp: 110 °C decomp. Calcd for **3c**: C, 59.13; H, 7.44. Found: C, 59.22; H, 7.38. Mp: 123–126 °C decomp.

(7) Many of the papers cited in refs 1–3 deal with alkynyl complexes. See also: (a) Rappert, T.; Yamamoto, A. *Organometallics* **1994**, *13*, 4984. (b) Bianchini, C.; Frediani, P.; Masi, D.; Peruzzini, M.; Zanobini, F. *Organometallics* **1994**, *13*, 4616. (c) Alcock, N. W.; Hill, A. F.; Melling, R. P.; Thompsett, A. R. *Organometallics* **1993**, *12*, 641. (d) Espuelas, J.; Esteruelas, M. A.; Lahoz, F. J.; Oro, L. A.; Valero, C. *Organometallics* **1993**, *12*, 663. (e) Santos, A.; Lopez, J.; Matas, L.; Ros, J.; Galan, A.; Echavarren, A. M. *Organometallics* **1993**, *12*, 4215. (f) Sun, Y.; Taylor, N. J.; Carty, A. J. *Organometallics* **1992**, *11*, 4293. (g) Bruce, M. I.; Hambley, T. W.; Liddell, M. J.; Snow, M. R.; Swincer, A. G.; Tiekink, E. R. T. *Organometallics* **1990**, *9*, 96. (h) Stang, P. J.; Crittell, C. *Organometallics* **1990**, *9*, 3191.

(8) See, for example: (a) Prasad, P. N.; Ulrich, D. R., Eds. *Nonlinear Optical and Electron Active Polymers*; Plenum Press: New York, 1988. (b) Ferraro, J. R.; Williams, J. M. *Introduction to Synthetic Electrical Conductors*; Academic Press: Orlando, FL, 1987; Chapter 3. (c) Takahashi, S.; Morimoto, H.; Murata, E.; Kataoka, S.; Sonogashira, K.; Hagihara, N. *J. Polym. Sci., Polym. Chem. Ed.* **1982**, *20*, 565.

(9) Fyfe, H. B.; Mlebuz, M.; Zargarian, D.; Taylor, J.-J.; Marder, T. B. *J. Chem. Soc., Chem. Commun.* **1991**, 188 and references therein.

(10) Löwe, C.; Hund, H. U.; Berke, H. *J. Organomet. Chem.* **1989**, *372*, 295. Shubert, U.; Grönen, J. *Chem. Ber.* **1989**, *122*, 1237. Bruce, M. I.; Cifuentes, M. P.; Snow, M. R.; Tiekink, E. R. T. *J. Organomet. Chem.* **1989**, *359*, 379.

(11) (a) Albertin, G.; Antoniutti, S.; Bordignon, E. *J. Am. Chem. Soc.* **1989**, *111*, 2072. (b) Amendola, P.; Antoniutti, S.; Albertin, G.; Bordignon, E. *Inorg. Chem.* **1990**, *29*, 318. (c) Albertin, G.; Amendola, P.; Antoniutti, S.; Ianelli, S.; Pelizzi, G.; Bordignon, E. *Organometallics* **1991**, *10*, 2876. (d) Albertin, G.; Antoniutti, S.; Del Ministro, E.; Bordignon, E. *J. Chem. Soc., Dalton Trans.* **1992**, 3203.

(12) Rabinowitz, R.; Pellon, J. *J. Org. Chem.* **1961**, *26*, 4623.

(13) Vogel, A. I. *Practical Organic Chemistry*, 3rd ed.; Longmans, Green and Co.: New York, 1956; p 609.

(14) Ugi, I.; Fetzer, U.; Eholzer, W.; Knupfer, H.; Offermann, K. *Angew. Chem., Int. Ed. Engl.* **1965**, *4*, 472.

(15) Peet, W. G.; Gerlach, D. H. *Inorg. Synth.* **1974**, *15*, 38.

Table 1. Infrared and NMR Data for Ruthenium Complexes

compd	IR[a,b] (cm^{-1})	^1H NMR[c,d] (δ)	^{13}C NMR[c,d] (δ)	spin system	$^{31}P\{^1H\}$ NMR[c,e] (δ)
1a	$\nu_{C\equiv C}$ 2078 (s)[b]	3.85 (m, CH_3)	114.8 (qi, $^3J_{CP}$ = 1.6, ≡C−Ph) 114.4 (qi, $^2J_{CP}$ = 20, ≡C−Ru) 52.9 (qm, CH_3)	A_4	140.1 (s)
1b	$\nu_{C\equiv C}$ 2081 (s)[b]	3.91 (m, CH_3 phos)[f] 2.16 (s, CH_3 *p*-tol)		A_4[f]	141.1 (s)
1c	$\nu_{C\equiv C}$ 2088 (s)[b]	3.88 (m, CH_3 phos)[f] 1.24 (s, CH_3 ^{t}Bu)		A_4[f]	142.9 (s)
2a	$\nu_{C\equiv C}$ 2076 (s)[b]	4.52 (m, CH_2)[f] 1.28 (t, CH_3)	117.2 (qi, $^2J_{CP}$ = 20, ≡C−Ru) 113.8 (qi, $^3J_{CP}$ = 1.6, ≡C−Ph) 61.3 (t, CH_2) 16.6 (q, CH_3)	A_4	138.1 (s)
2b	$\nu_{C\equiv C}$ 2077 (s)[b]	4.54 (m, CH_2)[f] 2.14 (s, CH_3 *p*-tol) 1.30 (t, CH_3 phos)	114.8 (qi, $^2J_{CP}$ = 20, ≡C−Ru) 113.4 (qi, $^3J_{CP}$ = 1.6, ≡C−Ph) 61.2 (t, CH_2) 21.2 (q, CH_3 *p*-tol) 16.6 (q, CH_3 phos)	A_4[f]	138.3 (s)
2c	$\nu_{C\equiv C}$ 2085 (s)[b]	4.54 (m, CH_2) 1.21 (t, CH_3 phos) 1.04 (s, CH_3 ^{t}Bu)	117.8 (qi, br, ≡C−Ph) 88.2 (qi, $^2J_{CP}$ = 20, ≡C−Ru) 61.0 (t, CH_2) 32.9 (q, CH_3 ^{t}Bu) 29.9 (s, C−$(CH_3)_3$) 16.5 (q, CH_3 phos)	A_4	138.7 (s)
3a	$\nu_{C\equiv C}$ 2069 (s)[b]	4.28, 3.77 (m, CH_2) 1.12 (t, CH_3)	125.0 (qi, $^2J_{CP}$ = 18, ≡C−Ru) 115.6 (qi, br, ≡C−Ph) 62.1 (t, CH_2) 16.5 (q, CH_3)	A_4[f]	153.0 (s)
3b	$\nu_{C\equiv C}$ 2077 (s)[b]	4.35, 3.83 (m, CH_2)[f] 2.77 (s, CH_3 *p*-tol) 1.19 (t, CH_3 phos)		A_4[f]	153.0 (s)
3c	$\nu_{C\equiv C}$ 2076 (s)[b]	4.19, 3.65 (m, CH_2) 1.09 (t, CH_3 phos) 1.09 (s, CH_3 ^{t}Bu)		A_4	151.7 (s)
4a[i]	$\nu_{C\equiv C}$ 2100 (s) $\nu_{C=C}$ 1668 (s), 1633 (m)	5.98 (qi, J_{PH} = 1.5, CH vinyl) 3.95 (m, CH_3 phos)	379.8 (qi, $^2J_{CP}$ = 17, Ru=C=) 125.5 (br, ≡C−Ph) 112.9 (dm, $^1J_{CH}$ = 150, =C(H)Ph) 97.1 (qi, $^2J_{CP}$ = 25, ≡C−Ru) 54.5 (q, CH_3)	A_4	124.5 (s)
5a[i]	$\nu_{C\equiv C}$ 2102 (s) $\nu_{C=C}$ 1666 (s), 1634 (w)	5.32 (qi, br, CH vinyl) 4.23 (m, CH_2) 1.27 (t, CH_3)	377.4 (qi, $^2J_{CP}$ = 17, Ru=C=) 112.6 (dm, $^1J_{CH}$ = 150, =C(H)Ph) 120.3 (qi, $^3J_{CP}$ = 2.0, ≡C−Ph) 99.5 (qi, $^2J_{CP}$ = 25, ≡C−Ru) 62.7 (t, CH_2) 15.9 (q, CH_3)	A_4 A_2B_2[h]	118.6 (s) δ_A = 124.1; δ_B = 115.4; J_{AB} = 57.6
5a$_1$[i]	$\nu_{C\equiv C}$ 2097 (s) $\nu_{C=C}$ 1662 (s), 1630 (m)	5.29 (qi, br, CH vinyl) 4.25 (m, CH_2) 1.29 (t, CH_3)		A_4	119.1 (s)
5b[i]	$\nu_{C\equiv C}$ 2101 (s) $\nu_{C=C}$ 1664 (s)	5.25 (qi, $^1J_{CH}$ = 1.6, CH vinyl) 4.24 (m, CH_2) 2.34, 2.36 (s, CH_3 *p*-tol) 1.28 (t, CH_3 phos)		A_4	119.2 (s)
5c[i]	$\nu_{C\equiv C}$ 2097 (m) $\nu_{C=C}$ 1685 (s), 1652 (w)	5.37 (qi, br, CH vinyl) 4.22 (m, CH_2) 1.14, 1.09 (s, CH_3 ^{t}Bu) 1.28 (t, CH_3 phos)	367.8 (qi, $^2J_{CP}$ = 17, Ru=C=) 117.6 (dm, $^1J_{CH}$ = 150, =C(H)^{t}Bu) 78.4 (qi, $^2J_{CP}$ = 25, ≡C−Ru) 62.4 (t, CH_2) 33.3, 32.6 (s, br, C−$(CH_3)_3$) 31.9, 31.7 (q, CH_3 ^{t}Bu) 15.8 (q, CH_3 phos)	A_4	119.3 (s)
7a	$\nu_{C\equiv C}$ 2095 (m) $\nu_{C=C}$ 1648 (s)	3.83 (m, CH_3 phos) 2.15 (s, CH_3 vinyl)	383.1 (qi of q, $^2J_{CP}$ = 17, $^3J_{CH}$ = 4, Ru=C=) 119.8 (br, ≡C−Ph) 118.2 (br, =C(Me)Ph) 97.8 (qi, $^2J_{CP}$ = 25, ≡C−Ru) 53.8 (q, CH_3 phos) 8.0 (q, CH_3 vinyl)	A_4	123.1 (s)
8a	$\nu_{C\equiv C}$ 2096 (s) $\nu_{C=C}$ 1671 (s), 1645 (m)	4.22 (m, CH_2) 2.20 (s, CH_3 vinyl) 1.26 (t, CH_3 phos)	379.4 (qi of q, $^2J_{CP}$ = 17, $^3J_{CH}$ = 4.5, Ru=C=) 124.2 (qi, $^3J_{CP}$ = 2.5, ≡C−Ph) 119.6 (qi, $^3J_{CP}$ = 2.5, =C(Me)Ph) 100.4 (qi, $^2J_{CP}$ = 25, ≡C−Ru) 62.9 (t, CH_2) 16.0 (q, CH_3 phos) 8.68 (q, CH_3 vinyl)	A_4 A_2B_2[h]	118.9 (s) δ_A = 125.0; δ_B = 116.4; J_{AB} = 58.4

Table 1 (Continued)

compd	IR[a,b] (cm^{-1})	^1H NMR[c,d] (δ)	^{13}C NMR[c,d] (δ)	spin system	$^{31}P\{^1H\}$ NMR[c,e] (δ)
8b	$\nu_{C\equiv C}$ 2099 (s)	4.22 (m, CH_2)	380.5 (qi of q, $^2J_{CP}$ = 17, $^3J_{CH}$ = 4.5, Ru=C=)	A_4	119.2 (s)
	$\nu_{C=C}$ 1672 (s), 1648 (s)	2.34, 2.30 (s, CH_3 *p*-tol) 2.17 (s, CH_3 vinyl) 1.26 (t, CH_3 phos)	124.5 (qi, $^3J_{CP}$ = 2.5, ≡C−Ph) 119.8 (qi, $^3J_{CP}$ = 2.5, =C(Me)*p*-tol 99.0 (qi, $^2J_{CP}$ = 25, ≡C−Ru) 63.3 (tm, CH_2) 21.3, 21.1 (q, CH_3 *p*-tol) 16.4 (q, CH_3 phos) 9.1 (q, CH_3 vinyl)	A_2B_2[h]	δ_A = 125.2; δ_B = 116.5; J_{AB} = 58.1
8c	$\nu_{C\equiv C}$ 2096 (s)	4.20 (m, CH_2)		A_4	119.2 (s)
	$\nu_{C=C}$ 1671 (s)	1.76 (qi, J_{PH} = 1.1, CH_3 vinyl) 1.29 (t, CH_3 phos) 1.12 (s, CH_3 ^{t}Bu)		A_2B_2[h]	δ_A = 122.5; δ_B = 118.7; J_{AB} = 57.0
10aa	$\nu_{C\equiv C}$ 2104 (s)	4.18 (m, CH_2)	382.2 (qi, $^2J_{CP}$ = 17, Ru=C=)	A_4	115.3 (s)
	$\nu_{C=C}$ 1593 (s)	1.23 (t, CH_3 phos)	126.7 (qi, $^3J_{CP}$ = 3.0, ≡C−Ph)	A_2B_2[h]	δ_A = 120.2; δ_B = 114.1; J_{AB} = 57.0
	$\nu_{N=N}$ 1574 (m)		98.8 (qi, $^2J_{CP}$ = 26, ≡C−Ru) 63.6 (t, CH_2) 16.2 (q, CH_3)		
10ab	$\nu_{C\equiv C}$ 2107 (s)	4.18 (m, CH_2)		A_4	115.5 (s)
	$\nu_{C=C}$ 1595 (s)	2.38 (s, CH_3 *p*-tol)			
	$\nu_{N=N}$ 1573 (m)	1.30 (t, CH_3 phos)			
10ac	$\nu_{C\equiv C}$ 2104 (s)	4.18 (m, CH_2)	382.2 (qi of d, $^2J_{CP}$ = 17, $^2J_{C^{15}N}$ = 7, Ru=C=)	A_4	115.3 (s)
	$\nu_{C=C}$ 1592 (s)	1.22 (t, CH_3)	126.7 (qi, $^3J_{CP}$ = 3.0, ≡C−Ph) 98.8 (qi, $^2J_{CP}$ = 26, ≡C−Ru) 63.6 (t, CH_2) 16.2 (q, CH_3)		
10ad	$\nu_{C\equiv C}$ 2103 (s)	4.18 (m, CH_2)	381.9 (qi of d, $^2J_{CP}$ = 17, $^2J_{C^{15}N}$ = 7, Ru=C=)	A_4	115.2 (s)
	$\nu_{C=C}$ 1593 (s)	1.22 (t, CH_3)	126.7 (qi, $^3J_{CP}$ = 3.0, ≡C−Ph) 98.9 (qi, $^2J_{CP}$ = 25, ≡C−Ru) 63.6 (t, CH_2) 16.2 (q, CH_3)		
11ab	$\nu_{C\equiv C}$ 2096 (s)	3.82 (m, CH_2)[g]		A_4[g]	142.6 (s)
	$\nu_{C=C}$ 1582 (s)	2.40 (s, CH_3 *p*-tol)			
	$\nu_{N=N}$ 1565 (m)	1.20 (t, CH_3 phos)			
12a	$\nu_{C\equiv C}$ 2104 (s)	4.22 (m, CH_2)	336.1 (qi, $^2J_{CP}$ = 17, Ru=C=)	A_4	117.1 (s)
	$\nu_{C=C}$ 1673 (m), 1626 (m)	1.16 (t, CH_3)	124.3 (br, ≡C−Ph) 100.2 (qi, $^2J_{CP}$ = 25, ≡C−Ru) 91.3 (br, =C(I)Ph) 62.8 (t, CH_2) 16.0 (q, CH_3)		
13a	$\nu_{C\equiv C}$ 2083 (s)	3.71 (m, CH_2)[g]		A_4[g]	141.6 (s)
	$\nu_{C=C}$ 1658 (m), 1633 (m)	1.18 (t, CH_3)			
14a	$\nu_{C\equiv C}$ 2101 (s)	4.36 (m, CH_2)[g]	349.6 (qi, $^2J_{CP}$ = 17, Ru=C=)	A_4[g]	116.2 (s)
	$\nu_{C=C}$ 1620 (s)	1.31 (t, CH_3)	116.5 (qi, br, ≡C−Ph) 109.4 (br, =C(SR_1)Ph) 99.4 (qi, $^2J_{CP}$ = 25, ≡C−Ru) 64.0 (t, CH_2) 16.5 (q, CH_3)		
16		6.37 (dm, CH vinyl)[g]		ABC_2[g]	δ_A = 142.5; δ_B = 137.3; δ_C = 124.0
		4.25, 3.90 (m, CH_2) 1.28 (t, CH_3 ^{t}Bu) 1.42, 1.31, 1.13 (t, CH_3 phos)			J_{AB} = 47.3; J_{AC} = 55.7; J_{BC} = 65.7
17	$\nu_{C\equiv C}$ 2105 (s)[b]	4.28 (m, CH_2 of $P(OEt)_3$)[g] 3.77 (d, CH_3 of $P(OMe)_3$) 1.28 (t, CH_3 of $P(OEt)_3$)		AB_4[g]	δ_A = 134.3; δ_B = 127.4; J_{AB} = 53.6
18	ν_{CN} 2134 (s)[b]	4.22 (m, CH_2)		A_4	127.3 (s)
	$\nu_{C\equiv C}$ 2100 (s)	2.38 (s, CH_3 *p*-tol) 1.27 (t, CH_3 phos)			
19	ν_{CN} 2262 (w)[b]	4.34 (m, CH_2)[g] 2.45 (s, CH_3 *p*-tol) 1.39, 1.35 (t, CH_3 phos)		A_2B_2[g]	δ_A = 126.6; δ_B = 118.5; J_{AB} = 60.0

[a] In Nujol mull. [b] In KBr pellets. [c] At 25 °C in CD_2Cl_2, coupling constants in Hz. [d] Phenyl group signals are omitted. [e] Positive shift downfield from 85% H_3PO_4. [f] In C_6D_6. [g] In $(CD_3)_2CO$. [h] At −100 °C. [i] NMR data obtained at −30 °C.

[Ru(C≡CR){=C=C(H)R}P_4]BF_4 (4,5) [R = Ph (a), *p*-Tol (b), ^{t}Bu (c); P = P(OMe)$_3$ (4), P(OEt)$_3$ (5)]. To a solution of the appropriate Ru(C≡CR)$_2P_4$ complex (0.25 mmol) in 10 mL of Et_2O cooled to −80 °C was added HBF_4·Et_2O (0.25 mmol, 36 μL of 54% solution), and the reaction mixture was brought to 20 °C under stirring. A pink solid separated out, which was filtered and dried under vacuum; yield: ≥80%. Anal. Calcd for **4a**: C, 37.89; H, 5.34. Found: C, 37.72; H, 5.28. Λ_M = 89.4 Ω^{-1} mol^{-1} cm^2. Calcd for **5a**: C, 45.50; H, 6.78. Found: C, 45.38; H, 6.72. Mp: 137 °C decomp. Λ_M = 92.3 Ω^{-1} mol^{-1}

cm². Calcd for **5b**: C, 46.54; H, 6.98. Found: C, 46.65; H, 6.83. Mp: 106 °C decomp. Λ_M = 88.6 Ω^{-1} mol^{-1} cm². Calcd for **5c**: C, 42.57; H, 7.84. Found: C, 42.44; H, 7.77. Mp: 143–145 °C decomp. Λ_M = 90.3 Ω^{-1} mol^{-1} cm².

[Ru(C≡CPh){=C=C(H)Ph}{P(OEt)$_3$}$_4$]CF$_3$SO$_3$ (5a$_1$). Triflic acid (CF_3SO_3H; 0.25 mmol, 22 μL) was added to a solution of Ru(C≡CPh)$_2${P(OEt)$_3$}$_4$ (0.25 mmol, 0.24 g) in 15 mL of diethyl ether cooled to −80 °C. The reaction mixture was brought to 20 °C under stirring, and, as the temperature increased, a pink solid began to separate out, which, after 1 h, was filtered and dried under vacuum; yield: ≥70%. Anal. Calcd: C, 44.04; H, 6.40. Found: C, 43.89; H, 6.29. Mp: 112–115 °C decomp. Λ_M = 76.1 Ω^{-1} mol^{-1} cm².

[Ru(η³-RC$_3$CHPh){PPh(OEt)$_2$}$_4$]BF$_4$ (6a). This compound was obtained following a procedure similar to that used for the synthesis of **4** and **5** by reacting the bis(acetylide) [Ru(C≡CPh)$_2${PPh(OEt)$_2$}$_4$] (0.25 mmol, 0.27 g) with HBF$_4$·Et$_2$O (0.25 mmol, 36 μL of a 54% solution) in 10 mL of diethyl ether cooled to −80 °C. The reaction mixture was brought to 20 °C while stirring, and, as the temperature increased, an oil separated out, which slowly gave a yellow solid by addition of 1–2 mL of ethanol. After filtration, the product was crystallized from CH_2Cl_2 (5 mL)/diethyl ether (10 mL); yield: ≥90%. Anal. Calcd: C, 56.81; H, 6.04. Found: C, 56.72; H, 6.11.

[Ru(C≡CR){=C=C(Me)R}P$_4$]CF$_3$SO$_3$ (7,8) [R = Ph (a), *p*-Tol (b), ^{t}Bu (c); P = P(OMe)$_3$ (7), P(OEt)$_3$ (8)]. Methyl triflate (CF_3SO_3Me) was added to a solution of the appropriate bis(acetylide) Ru(C≡CR)$_2$P$_4$ (0.25 mmol) in 10 mL of Et_2O previously cooled to −80 °C. The mixture was brought to room temperature and was stirred until a purple solid separated out, which was filtered and dried under vacuum; yield: ≥80%. Anal. Calcd for **7a**: C, 37.39; H, 5.12. Found: C, 37.26; H, 5.04. Mp: 114–116 °C decomp. Λ_M = 77.8 Ω^{-1} mol^{-1} cm². Calcd for **8a**: C, 44.56; H, 6.50. Found: C, 44.64; H, 6.49. Mp: 122 °C decomp. Λ_M = 82.8 Ω^{-1} mol^{-1} cm². Calcd for **8b**: C, 45.55; H, 6.69. Found: C, 45.63; H, 6.55. Mp: 116 °C decomp. Λ_M = 73.9 Ω^{-1} mol^{-1} cm². Calcd for **8c**: C, 41.79; H, 7.48. Found: C, 41.66; H, 7.51. Mp: 127 °C decomp. Λ_M = 72.9 Ω^{-1} mol^{-1} cm².

[Ru(C≡CPh){=C=C(N=NR)Ph}{P(OEt)$_3$}$_4$]BPh$_4$ (10) [R = Ph, (aa); *p*-tol, (ab)]. A solid sample of the acetylide Ru(C≡CPh)$_2${P(OEt)$_3$}$_4$ (0.25 mmol, 0.24 g) and solid arenediazonium tetrafluoroborate $RN_2^+BF_4^-$ (0.25 mmol) were mixed together and cooled to about −196 °C. Dichloromethane (10 mL) was added, and the resulting mixture was slowly brought to room temperature and stirred for 1 h. Removal of the solvent at reduced pressure gave an oil, which was treated with ethanol (10 mL) containing an excess of $NaBPh_4$ (0.5 mmol, 0.17 g). The resulting solution slowly yielded a green solid, which was filtered and crystallized from CH_2Cl_2/ethanol (5/15 mL); yield: ≥80%. Anal. Calcd for **10aa**: C, 60.38; H, 6.88; N, 2.01. Found: C, 60.23; H, 6.94; N, 1.97. Λ_M = 50.9 Ω^{-1} mol^{-1} cm². Calcd for **10ab**: C, 60.64; H, 6.95; N, 1.99. Found: C, 60.43; H, 6.98; N, 1.96. Mp: 125–127 °C decomp. Λ_M = 53.4 Ω^{-1} mol^{-1} cm².

[Ru(C≡CPh){=C=C(¹⁵N=NPh)Ph}{P(OEt)$_3$}$_4$]BPh$_4$ (10ac). The complex was prepared exactly as **10aa** using the labeled $PhN{\equiv}^{15}N^+BF_4^-$ arenediazonium salt; yield: ≥80%. Anal. Calcd: C, 60.34; H, 6.87; N, 2.08. Found: C, 60.19; H, 6.80; N, 1.99. Λ_M = 49.7 Ω^{-1} mol^{-1} cm².

[Ru(C≡CPh){=C=C(¹⁵N=NPh)Ph}{P(OEt)$_3$}$_4$]BF$_4$ (10ad). This complex, too, was prepared like **10aa** by mixing together solid samples of Ru(C≡CPh)$_2$[P(OEt)$_3$]$_4$ (0.15 mmol, 0.145 g) and $PhN{\equiv}^{15}N^+BF_4^-$ (0.15 mmol, 0.031 g), cooling to about −196 °C, and adding 10 mL of CH_2Cl_2. After the reaction mixture had reached room temperature, it was stirred for 1 h and the solvent was removed at reduced pressure. The oil obtained was triturated with Et_2O (10 mL) and THF (2 mL), giving, after 3–4 h of stirring, a green solid which was crystallized from CH_2Cl_2 and Et_2O (3/10 mL); yield: ≥80%. Anal. Calcd: C, 47.59; H, 6.51; N, 2.50. Found: C, 47.38; H, 6.64; N, 2.42. Λ_M = 91.4 Ω^{-1} mol^{-1} cm².

[Ru(C≡CPh){=C=(N=N-*p*-tol)Ph}{PPh(OEt)$_2$}]BPh$_4$ (11ab). This compound was prepared exactly like the related **10** by reacting Ru(C≡CPh)$_2${PPh(OEt)$_2$}$_4$ with *p*-toluenediazonium tetrafluoroborate at −196 °C in CH_2Cl_2; yield ≥70%. Anal. Calcd: C, 68.09; H, 6.37; N, 1.83. Found: C, 67.88; H, 6.22; N, 1.90. Mp: 73–75 °C. Λ_M = 52.6 Ω^{-1} mol^{-1} cm².

[Ru(C≡CPh){=C=C(I)Ph}{P(OEt)$_3$}$_4$]I$_3$ (12a) and [Ru(C≡CPh){=C=C(I)Ph}{PPh(OEt)$_2$}$_4$]I$_3$ (13a). An excess of I_2 (0.5 mmol, 4.17 mL of a 0.12 M solution in Et_2O) was added to a solution of the appropriate Ru(C≡CPh)$_2$P$_4$ acetylide (0.2 mmol) in 10 mL of diethyl ether, and the reaction mixture was stirred at room temperature for 2 h. The brown solid that formed was filtered and dried under vacuum; yield: ≥60%. Anal. Calcd for **12a**: C, 32.56; H, 4.78; I, 34.40. Found: C, 32.39; H, 4.50; I, 33.20. Mp: 92 °C decomp. Λ_M = 69.1 Ω^{-1} mol^{-1} cm². Calcd for **13a**: C, 41.94; H, 4.40; I, 31.65. Found: C, 41.72; H, 4.47; I, 30.50. Mp: 81 °C decomp. Λ_M = 64.6 Ω^{-1} mol^{-1} cm².

[Ru(C≡CPh)[=C=C{2,4-(NO$_2$)$_2$C$_6$H$_3$S}Ph]{P(OEt)$_3$}$_4$]Cl (14a). A solution of 2,4-$(NO_2)_2C_6H_3SCl$ (0.20 mmol, 0.047 g) in 3 mL of Et_2O was added via syringe to a solution of Ru(C≡CPh)$_2$[P(OEt)$_3$]$_4$ (0.20 mmol, 0.19 g) in 10 mL of Et_2O cooled to −80 °C, and the reaction mixture was brought to room temperature. A purple oil began to separate out after 10 min of stirring, which slowly gave a microcrystalline solid in about 2 h. After filtration, the sample was dried under vacuum; yield: ≥55%. Anal. Calcd: C, 45.94; H, 6.12; N, 2.33. Found: C, 45.70; H, 5.97; N, 2.51. Mp: 98 °C decomp. Λ_M = 65.2 Ω^{-1} mol^{-1} cm².

[Ru(η³-PhC$_3$CHPh){P(OEt)$_3$}$_4$]BF$_4$ (15). A solid sample of [Ru(C≡CPh){=C=C(H)Ph}{P(OEt)$_3$}$_4$]BF$_4$ (0.25 g, 0.24 mmol) was placed in a 25-mL three-necked flask, and 10 mL of CH_2Cl_2 was added. The solution was vigorously stirred for 2 h, and then the solvent was removed under reduced pressure. The oil obtained was triturated with 10 mL of diethyl ether containing 2 mL of ethanol until a white solid separated out. By crystallization from ethanol (2 mL)/diethyl ether (10 mL) white microcrystals of the complex were obtained. Yield: ≥85%. Anal. Calcd: C, 45.50; H, 6.78. Found: C, 45.39; H, 6.82.

The related BPh_4^- salt can easily be obtained using $NaBPh_4$ (0.16 g; 0.48 mmol) as a precipitating agent and crystallizing the product from ethanol. Anal. Calcd for [Ru(η³-PhC$_3$CHPh){P(OEt)$_3$}$_4$]BPh$_4$: C, 59.67; H, 7.12. Found: C, 59.43; H, 6.97.

[Ru{η³-(Ph)C$_3$C(H)^{t}Bu}{P(OEt)$_3$}$_4$]BF$_4$ (16). A solid sample of [Ru(C≡CPh){=C=C(H)Ph}{P(OEt)$_3$}$_4$]BF$_4$ (0.20 mmol, 0.21 g) was added to a CH_2Cl_2 solution containing an excess of ^{t}BuC≡CH (2 mmol, 0.25 mL) cooled to −20 °C. The reaction mixture was first brought to 0 °C and stirred for 1 h and then to room temperature and stirred again for 30 min. Removal of solvent gave a white solid, which was triturated with Et_2O and filtered. Crystallization from CH_2Cl_2/Et_2O (1/10 mL) gave white microcrystals of the product; yield: ≥80%. Anal. Calcd: C, 44.06; H, 7.30. Found: C, 43.82; H, 7.38. Mp: 187 °C decomp. Λ_M = 89.3 Ω^{-1} mol^{-1} cm².

[Ru(C≡CPh){P(OMe)$_3$}{P(OEt)$_3$}$_4$]BF$_4$ (17). A dichloromethane solution (10 mL) containing an excess of P(OMe)$_3$ (2 mmol, 0.25 mL) was cooled to −20 °C, and solid [Ru(C≡CPh){=C=C(H)Ph}{P(OEt)$_3$}$_4$]BF$_4$ (0.20 mmol, 0.21 g) was added. The reaction mixture was brought to 0 °C in about 10 min and was stirred for 2 h. Removal of the solvent under reduced pressure gave an oil, which was triturated with diethyl ether. A pale yellow solid was obtained after vigorous stirring, which was filtered and crystallized from CH_2Cl_2/Et_2O (1/10 mL); yield: ≥70%. Anal. Calcd: C, 39.01; H, 6.92. Found: C, 38.88; H, 6.98. Mp: 197–199 °C decomp. Λ_M = 89.9 Ω^{-1} mol^{-1} cm².

[Ru(C≡CPh)(*p*-tolNC){P(OEt)$_3$}$_4$]BPh$_4$ (18). A solid sample of [Ru(C≡CPh){=C=C(H)Ph}{P(OEt)$_3$}$_4$]BF$_4$ (0.21 g, 0.20 mmol) was placed in a three-necked flask cooled to −20 °C and treated with 10 mL of CH_2Cl_2. An excess of *p*-tolyl isocyanide (2 mmol, 0.23 mL) was added to the resulting

Table 2. Crystallographic Data for [Ru(C≡CPh){=C=C(Me)Ph}{P(OEt)$_3$}$_4$]CF$_3$SO$_3$ (8a)

formula	$C_{42}H_{73}F_3O_{15}P_4RuS$
fw	1132.05
cryst syst	orthorhombic
space group	$P2_12_12_1$
a, Å	23.362(8)
b, Å	12.072(4)
c, Å	20.350(6)
V, Å^3	5739(3)
Z	4
D_{calcd}, g/cm^3	1.310
temp, °C	22
2θ range, deg	6–54
μ, cm^{-1}	4.9
no. of unique data collcd	12491
no. params refined	514
R1 (on F)	0.0717 (6604 4σ data), 0.1559 (12 491 data)
wR2 (on F^2)	0.2284 (12 491 data)

solution, and the reaction mixture was slowly brought to 0 °C and was stirred for 1 h. The solvent was removed under reduced pressure, giving an oil, which was treated with ethanol (5 mL) containing an excess of $NaBPh_4$ (0.4 mmol, 0.14 g). When the resulting solution, cooled to 0 °C, was stirred vigorously, a yellow solid separated out, which was filtered and crystallized from ethanol; yield: ≥70%. Anal. Calcd: C, 58.98; H, 7.12; N, 1.08; Found: C, 59.12; H, 7.00; N, 1.12. Mp: 197 °C decomp. Λ_M = 49.7 Ω^{-1} mol^{-1} cm^2.

[Ru(*p*-tolCN)$_2${P(OEt)$_3$}$_4$](BPh$_4$)$_2$ (19). A dichloromethane solution (10 mL) containing an excess of *p*-toluonitrile (2 mmol, 0.24 mL) was cooled to −20 °C, and solid [Ru(C≡CPh){=C=C(H)Ph}{P(OEt)$_3$}$_4$]BF$_4$ (0.2 mmol, 0.21 g) was added. The reaction mixture was slowly brought to 0 °C, was stirred for 2 h, and was then evaporated to dryness. The oil obtained was treated with 5 mL of ethanol containing an excess of $NaBPh_4$ (0.4 mmol, 0.14 g), and the resulting solution was cooled to −25 °C. After 1–2 days, yellow microcrystals separated out, which were filtered and dried under vacuum. Yield: ≥70%. Anal. Calcd: C, 64.51; H, 7.01; N, 1.71. Found: C, 64.32; H, 6.88; N, 1.85. Mp: 178 °C decomp. Λ_M = 118.4 Ω^{-1} mol^{-1} cm^2.

Reactions with Cl$^-$ and Br$^-$. A solution containing an excess of the appropriate lithium halogenide (2 mmol) in ethanol/dichloromethane (7:3 mL) was cooled to −20 °C, and solid [Ru(C≡CPh){=C=C(H)Ph}{P(OEt)$_3$}$_4$]BF$_4$ (0.2 mmol, 0.21 g) was added. The reaction mixture was slowly brought to 0 °C and then to room temperature. After 1 h of stirring, the solvent was removed under reduced pressure to give an oil, which was treated with 3 mL of ethanol. When the resulting solution was stirred vigorously, a little amount of a yellow solid separated out, which was filtered and identified as the bis(acetylide) complex Ru(C≡CPh)$_2$[P(OEt)$_3$]$_4$ (**2a**) by IR and NMR. The yield was about 20%. The bis(acetylide) compound was also obtained (in low yield) by treatment of [Ru(C≡CPh){=C=C(H)Ph}{P(OMe)$_3$}$_4$]BF$_4$ with an excess of LiCl in ethanol/dichloromethane solution.

X-ray Structure Determination of [Ru(C≡CPh){=C=C(Me)Ph}{P(OEt)$_3$}$_4$]CF$_3$SO$_3$ (8a). X-ray work was carried out with a Philips PW 1100 diffractometer using Mo Kα (λ = 0.710 69 Å) radiation. The crystallographic data are summarized in Table 2. No loss of intensity of standard reflections was detected during data collection. Data were processed with the peak profile analysis procedure and corrected for Lorentz, polarization, and absorption effects.

The structure was solved by automated Patterson and difference Fourier techniques. Full-matrix least-squares refinement on F^2 was used with anisotropic thermal parameters for all non-hydrogen atoms, with the exception of most terminal methyl groups and anion atoms. The hydrogen atoms were refined isotropically in their calculated riding positions. Complex neutral-atom scattering factors were used, and anomalous dispersion corrections were applied to all non-hydrogen atoms. Calculations were carried out on GOULD POWERNODE 6040 and ENCORE 91 computers using SHELXS86[16] and SHELXL92[17] programs. Other crystallographic programs used have been cited elsewhere.[18] Fractional atomic coordinates are listed in Table 3, and selected bond distances and angles are given in Table 4.

Kinetic Measurements. The kinetics of the reaction of vinylidene [Ru(C≡CPh){=C=C(H)Ph}{P(OEt)$_3$}$_4$]BF$_4$ (**5a**) to enynyl [Ru(η^3-PhC$_3$CHPh){P(OEt)$_3$}$_4$]BF$_4$ (**15**) derivative was studied by $^{31}P\{^1H\}$ NMR, monitoring the intensity decrease of the signal of compound **5a**. No significant signals other than those of **5a** (sharp singlet near 118 ppm) and **15** (ABC_2 multiplet: δ_A 137.9 ppm, δ_B 136.0 ppm, δ_C 121.1 ppm, J_{AB} = 49.0 Hz, J_{AC} = 57.9 Hz, J_{BC} = 63.1 Hz) could be observed during the course of reaction. In typical kinetic runs, the initial concentration of **5a** was 2.0 × 10^{-2} mol/L in $CDCl_3$, and the NMR tube was thermostated to 15 °C; the [PhC≡CH]:[**5a**] ratio varied from 0 to about 15. Preliminary measurements were made at different initial concentrations of **5a** and/or temperatures to establish both the kinetic order of the reaction and the best $t_{1/2}$ conditions for following the reaction. First-order rate constants (s^{-1}) were obtained by a linear least-squares fitting of ln[**5a**] plotted against time using standard computer software.

Results and Discussion

Preparation of Bis(acetylide) Complexes. Dichloro complexes $RuCl_2P_4$ (P = P(OMe)$_3$, P(OEt)$_3$, and PPh(OEt)$_2$) quickly reacted with excess lithium acetylides Li$^+$RC≡C$^-$ (R = Ph, *p*-tol, ^{t}Bu) in THF to give the bis(alkynyl) derivatives Ru(C≡CR)$_2$P$_4$ (**1–3**) as yellow powders in 30–40% yield (eq 1). Subsequent crystal-

$$RuCl_2P_4 \xrightarrow[THF]{RC\equiv C^-,\ excess} \underset{(\mathbf{1-3})}{Ru(C\equiv CR)_2P_4} \qquad (1)$$

P = P(OMe)$_3$, **1**; P(OEt)$_3$, **2**, PPh(OEt)$_2$, **3**

R = Ph, **a**; *p*-tolyl, **b**; ^{t}Bu, **c**

lization afforded analytically pure, air-stable crystals of the complexes, which were characterized by IR, ^{1}H, ^{31}P, and ^{13}C NMR data (Table 1). The reaction between $RuCl_2\{P(OEt)_3\}_4$ and phenyl acetylide at room temperature was also followed by IR spectra in the 2200–2000 cm^{-1} region. A $\nu_{C\equiv C}$ band at 2040 cm^{-1} initially appeared which was predominant for the low Ru:PhC≡C$^-$ ratio (1:1) and was reasonably attributed to the mono(acetylide) RuCl(C≡CPh)P$_4$ complex. As the reaction proceeded in excess Li$^+$PhC≡C$^-$, the band at 2040 cm^{-1} was substituted by two bands at 2073 and 2051 cm^{-1}, which were of comparable intensity and always present for all Ru:RC≡C$^-$ ratios. From this solution only the bisacetylide complex **2** with a $\nu_{C\equiv C}$ band at 2073 cm^{-1} (THF) was isolated as a solid, and therefore no formulation of the other acetylide species with $\nu_{C\equiv C}$ at 2051 cm^{-1} could be proposed.

The infrared spectra of alkynyl complexes **1–3** showed only one $\nu_{C\equiv C}$ band at 2088–2069 cm^{-1}, suggesting a mutually *trans* arrangement of the two acetylide ligands. This geometry was confirmed by $^{31}P\{^1H\}$ NMR spectra, which gave a sharp singlet between +30 and −90 °C.

(16) Sheldrick, G. M. *SHELXS86, A Program for Crystal Structure Determination*; University of Göttingen: Göttingen, Germany, 1986.
(17) Sheldrick, G. M. *SHELXL92, A Program for Structure Refinement*; University of Göttingen: Göttingen, Germany, 1992.
(18) Bacchi, A.; Ferranti, F.; Pelizzi, G. *Acta Crystallogr.* **1993**, *1163*, C49.

Table 3. Atomic Coordinates (×10⁴) and Equivalent Isotropic Displacement Parameters (Å × 10⁴) (One-Third Trace of the Diagonalized Matrix) for Non-Hydrogen Atoms

atom	*x/a*	*y/b*	*z/c*	U_{eq}
Ru	9155.7(2)	3858.7(5)	94.4(3)	513(2)
P1	9907(1)	4725(2)	−468(1)	636(7)
P2	8569(1)	2628(2)	675(1)	740(8)
P3	9421(1)	4685(2)	1090(1)	736(8)
P4	8810(1)	3119(2)	−897(1)	634(7)
O1	10451(2)	4842(5)	−4(3)	853(22)
O2	9764(3)	5940(5)	−718(4)	911(26)
O3	10141(3)	4230(6)	−1135(3)	822(23)
O4	7929(3)	3067(7)	771(4)	1019(29)
O5	8519(4)	1483(7)	301(4)	1109(32)
O6	8731(4)	2322(7)	1394(3)	984(29)
O7	9718(4)	5870(7)	1110(4)	994(30)
O8	9831(3)	4070(7)	1583(3)	956(28)
O9	8856(3)	4830(6)	1533(3)	939(27)
O10	8154(3)	2737(6)	−933(4)	891(26)
O11	9144(3)	2089(6)	−1177(3)	943(26)
O12	8868(3)	4025(6)	−1458(3)	790(22)
C1	8612(3)	5016(6)	2(4)	614(26)
C2	8208(4)	5785(8)	−17(4)	748(31)
C3	7816(5)	5866(10)	548(6)	1115(50)
C4	8098(4)	6571(7)	−574(5)	776(34)
C5	7695(6)	7385(10)	−523(7)	1166(54)
C6	7623(8)	8048(14)	−1095(12)	1664(95)
C7	7874(7)	7906(14)	−1679(10)	1445(75)
C8	8283(8)	7219(12)	−1667(7)	1402(71)
C9	8406(6)	6519(11)	−1149(7)	1148(52)
C10	9752(3)	2553(6)	199(4)	620(26)
C11	10091(3)	1802(7)	256(4)	665(29)
C12	10475(4)	862(7)	256(5)	709(31)
C13	10667(5)	296(12)	−332(7)	1147(52)
C14	11034(7)	−508(11)	−309(7)	1245(64)
C15	11241(7)	−897(12)	247(10)	1337(70)
C16	11077(8)	−431(16)	830(11)	1660(90)
C17	10683(7)	472(11)	828(7)	1282(63)
C18	10980(5)	5368(15)	−191(7)	1395(63)
C19	11431(10)	5061(21)	197(13)	2294(104)
C20	10039(8)	6464(12)	−1273(9)	1515(78)
C21	9954(11)	7601(24)	−1312(13)	2263(102)
C22	10469(5)	3193(11)	−1197(5)	1002(44)
C23	10607(7)	3030(17)	−1870(8)	1597(82)
C24	7516(7)	2694(21)	1189(13)	2381(136)
C25	6997(11)	3168(23)	1091(13)	2150(101)
C26	8223(8)	566(16)	530(11)	1833(103)
C27	8574(10)	−550(21)	352(12)	2011(90)
C28	9138(9)	1579(16)	1629(7)	1563(80)
C29	9025(10)	1563(20)	2375(11)	1993(89)
C30	9453(7)	6809(11)	838(8)	1374(68)
C31	9715(12)	7880(28)	1036(17)	2580(132)
C32	10422(7)	3877(14)	1493(6)	1209(57)
C33	10623(10)	3442(20)	2134(12)	2454(136)
C34	8897(7)	5318(15)	2200(6)	1409(71)
C35	8341(11)	5305(22)	2461(12)	2068(91)
C36	7665(5)	3386(12)	−865(8)	1144(55)
C37	7185(6)	2794(17)	−934(11)	1674(94)
C38	8945(12)	1071(13)	−1341(9)	2175(136)
C39	9313(8)	366(14)	−1718(10)	1790(96)
C40	8713(8)	3736(15)	−2154(5)	1433(71)
C41	8958(7)	4566(15)	−2547(9)	1517(56)
C42	2528(10)	6201(21)	7868(11)	1874(73)
F1	2383(9)	6054(19)	7271(11)	2985(49)
F2	2788(8)	5238(19)	7851(10)	2985(49)
F3	3037(9)	6350(19)	8123(10)	2985(49)
S	1974(2)	6251(5)	8434(3)	1564(15)
O13	2185(7)	6320(17)	9093(9)	2271(66)
O14	1434(6)	6426(12)	8159(7)	1838(47)
O15	1999(12)	4997(23)	8301(12)	3085(106)

Furthermore, in the $^{13}C\{^1H\}$ spectra, the C_α and C_β signals of the two equivalent acetylides were present as quintets: at δ 125.0−88.2 ppm the C_α had an appreciable $^2J_{CP}$ of about 20 Hz, while the C_β at δ 113.4−117.8 ppm had a $^3J_{CP}$ of about 1.6 Hz. A similar *trans* geometry[19] was observed in the recently reported

Table 4. Selected Bond Distances (Å) and Angles (deg) with Esd's in Parentheses

	Bond Distances		
Ru−P1	2.342(2)	P3−O7	1.590(8)
Ru−P2	2.342(3)	P3−O8	1.573(8)
Ru−P3	2.341(3)	P3−O9	1.608(8)
Ru−P4	2.350(2)	P4−O10	1.602(7)
Ru−C1	1.898(7)	P4−O11	1.575(8)
Ru−C10	2.114(8)	P4−O12	1.586(7)
P1−O1	1.590(6)	C1−C2	1.323(11)
P1−O2	1.587(7)	C2−C3	1.473(15)
P1−O3	1.580(7)	C2−C4	1.502(14)
P2−O4	1.598(8)	C10−C11	1.209(11)
P2−O5	1.582(9)	C11−C12	1.446(12)
P2−O6	1.557(7)		
	Angles		
C1−Ru−C10	179.2(3)	Ru−P1−O1	110.4(2)
P4−Ru−C10	91.7(2)	Ru−P2−O6	118.8(3)
P4−Ru−C1	88.0(2)	Ru−P2−O5	110.7(3)
P3−Ru−C10	93.2(2)	Ru−P2−O4	113.6(3)
P3−Ru−C1	87.1(2)	Ru−P3−O9	108.3(3)
P3−Ru−P4	174.8(1)	Ru−P3−O8	120.8(3)
P2−Ru−C10	82.1(2)	Ru−P3−O7	121.4(3)
P2−Ru−C1	97.2(2)	Ru−P4−O12	109.0(2)
P2−Ru−P4	89.5(1)	Ru−P4−O11	116.1(3)
P2−Ru−P3	89.4(1)	Ru−P4−O10	118.5(3)
P1−Ru−C10	83.6(2)	Ru−C1−C2	174.9(7)
P1−Ru−C1	97.2(2)	C1−C2−C4	126.0(8)
P1−Ru−P4	90.4(1)	C1−C2−C3	117.8(8)
P1−Ru−P3	91.9(1)	C3−C2−C4	116.2(9)
P1−Ru−P2	165.7(1)	Ru−C10−C11	179.6(7)
Ru−P1−O3	120.7(3)	C10−C11−C12	173.8(9)
Ru−P1−O2	114.2(3)		

Ru(II) bis(acetylide) complexes of the type $Ru(C{\equiv}CR)_2(PMe_3)_4$,[7a] $Ru(CO)_2(PEt_3)_2[(C{\equiv}C)_nR]_2$ (n = 1, 2),[7f] and $Ru(dppm)_2[(C{\equiv}C{-}C{\equiv}CCPh_2(OSiMe_3)]_2$[20] (dppm = $Ph_2PCH_2PPh_2$), whose $\nu_{C\equiv C}$ frequencies fitted those of our (**1**−**3**) derivatives very well.

The solid-state structure of $Ru(C{\equiv}CPh)_2\{P(OEt)_3\}_4$ (**2a**) was investigated by the X-ray diffraction technique, an experiment that was only partially successful. The compound crystallized in the tetragonal space group $I4_1/acd$, with a = 20.332(8) Å, c = 24.071(9) Å, and Z = 8. After many unsuccessful attempts, the structure was solved by application of direct methods and was refined by the full-matrix least-squares procedures to an R value of 0.07. In spite of this quite satisfactory value, structure analysis was greatly hampered by disorder problems involving the phosphite ligands. Because the space group has 32 general positions, the eight molecules per unit cell have to be constrained at special positions.

Although the disorder does not allow a detailed description, there is no doubt that the basic structure is correct and that the complex is monomeric, with the ruthenium atom surrounded by four phosphite molecules and two acetylide groups in a distorted *trans* octahedral geometry (**I**).

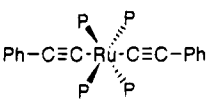

(I)

Protonation and Methylation of $Ru(C{\equiv}CR)_2P_4$. Complexes **1** and **2**, containing $P(OMe)_3$ and $P(OEt)_3$

(19) Examples of *cis*-bis(acetylide) Ru(II) complexes that also catalyze the dimerization of alkynes have also recently been reported (refs 7a,b).

(20) Pirio, N.; Touchard, D.; Dixneuf, P. H.; Fettouhi, M.; Ouahab, L. *Angew. Chem., Int. Ed. Engl.* **1992**, *31*, 651.

Scheme 1[a]

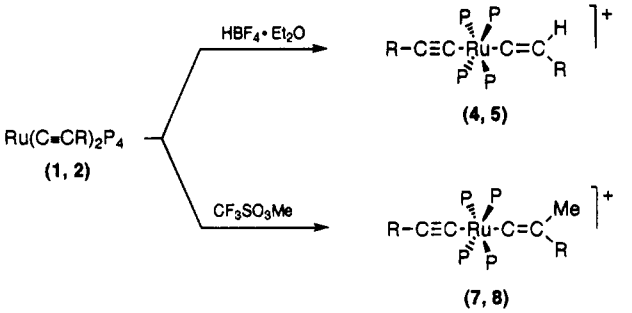

[a] Legend: P = $P(OMe)_3$ (**1**, **4**, **7**), and $P(OEt)_3$ (**2**, **5**, **8**); R = Ph (**a**), *p*-tolyl (**b**), ^{t}Bu (**c**).

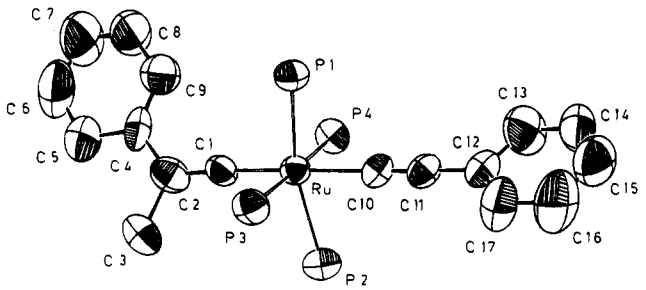

Figure 1. ORTEP diagram and numbering scheme for $[Ru(C{\equiv}CPh)\{{=}C{=}C(Me)Ph\}\{P(OEt)_3\}_4]^+$ (cation of **8a**). OEt moieties and H atoms have been omitted for clarity; thermal ellipsoids are drawn at 50% probability level.

ligands, reacted with $HBF_4{\cdot}Et_2O$ and CF_3SO_3Me in diethyl ether to afford the vinylidene–acetylide[21,22] derivatives $[Ru(C{\equiv}CR)\{{=}C{=}C(R_1)R\}P_4]^+$ (**4**, **5**, **7**, **8**) (Scheme 1) as stable pink or purple solids.

In contrast, the protonation reaction of related $PPh(OEt)_2$ derivatives **3** did not afford vinyldene complexes but rather an oily product which, after solidification, turned out to be the already known[11c] $[Ru\{\eta^3\text{-}RC_3C(H)R\}\{PPh(OEt)_2\}_4]^+$ (**6**) derivative (eq 2). Methylation

$$Ru(C{\equiv}CR)_2[PPh(OEt)_2]_4 \xrightarrow{HBF_4{\cdot}Et_2O} \underset{(\mathbf{3})}{} [Ru\{\eta^3\text{-}RC_3C(H)R\}\{PPh(OEt)_2\}_4]^+ \quad (2)$$
$$(\mathbf{6})$$

of **3** with CF_3SO_3Me also did not afford vinylidene species, only an intractable oil whose NMR spectra excluded the presence of enynyl derivativers such as those forming in the protonation reaction.

While vinylidene complexes **4** and **5** were unstable in solution (see below), related methyl–vinylidene derivatives **7** and **8** did yield suitable crystals for X-ray analysis from their solutions. The X-ray analysis carried out on $[Ru(C{\equiv}CPh)\{{=}C{=}C(Me)Ph\}\{P(OEt)_3\}_4]CF_3SO_3$ (**8a**) showed the structure to consist of discrete, clearly separated cations and anions. In the cation, which is shown in the ORTEP diagram of Figure 1, the ruthenium atom lies in a six-coordinated environment comprising four phosphorus atoms from the phosphite molecules and two carbon atoms from the vinylidene and acetylide groups. The donor atoms adopt a distorted octahedral arrangement with the two carbon-donor ligands *trans* to each other. Both of these ligands coordinate to ruthenium in an essentially linear mode, thus giving rise to a somewhat unusual nearly linear array of six atoms, C2–C1–Ru–C10–C11–C12, in which the bond angles range from 173.8 to 179.6°, the greatest deviations from linearity occurring at the two ends. This linkage is nearly orthogonal to the best plane through the four P atoms (88.1°). The distorted octahedral nature is also seen in the least-squares planes drawn through the three sets of donor atoms forming the coordination planes of the octahedron. While the two planes of the RuP_2C_2 sets indicate an almost planar arrangement, the plane for the RuP_4 set shows a marked deviation from planarity, describing a flattened tetrahedron.

Another parameter also characterizing departure from regular octahedral geometry is the P1–Ru–P2 angle of 165.7(1)°, which should be 180°. The four Ru–P bond distances are nearly equal, and the average value of 2.344(2) Å is somewhat shorter than the single Ru–P value of 2.43 Å calculated from Pauling's covalent radii, but it is almost identical to the value of 2.35(1) Å found in *trans*-bis(acetone hydrazone)tetrakis(trimethyl phosphite)ruthenium(II) bis(tetraphenylborate),[23] the only structurally characterized ruthenium complex containing a pair of mutually *trans* phosphite ligands. The Ru–C1 bond distance to the vinylidene ligand is 1.898(7) Å, only slightly longer than the corresponding bond in related compounds (see below), while the C1–C2 distance of 1.32(1) Å is typical for a vinylidene bond. As pointed out in a recent review[1a] on the organometallic chemistry of vinylidene and related unsaturated carbenes, the metal–carbon bond in mononuclear vinylidene complexes is consistent with a bond order of about 2 and the C=C bond corresponds to an order between 2 and 3, as predicted by theory.

Concerning ruthenium derivatives, the Ru–C and C=C bond distances in the complexes characterized so far range from 1.82 to 1.88 Å and from 1.22 to 1.34 Å, respectively.[1a,2c,f] An Ru–C (vinylidene) bond as short as 1.749(5) Å has also been reported.[24] Like most vinylidene complexes, the ligand is nearly linear, with an Ru–C1–C2 angle of 174.9(7)°. The orientation of the vinylidene ligand with respect to the phosphite moieties can be defined by the angles its least-squares plane forms with the four Ru–P bonds, *i.e.*, −36.3(2)° (P1), 37.1(2)° (P2), −51.6(2)° (P3), and 53.4(2)° (P4). The Ru–C10 bond to the acetylide ligand of 2.114(8) Å is consistent with a single bond from ruthenium(II) to an sp carbon. This value as well as that of the C10–C11 triple bond, 1.21(1) Å, falls at the long end of the range observed for phenylethynyl ruthenium derivatives:[25] Ru–C, 2.01–2.12 Å; C≡C, 1.17–1.21 Å. The Ru–C≡C–C linkage is almost exactly linear at C10

(21) For theoretical studies on protonation and methylation of vinylidene complexes see: Kostic, N. M.; Fenske, R. F. *Organometallics* **1982**, *1*, 974.

(22) The first alkynyl–vinylidene complex has recently been reported for rhodium: Schäfer, M.; Mahr, N.; Wolf, J.; Werner, H. *Angew. Chem., Int. Ed. Engl.* **1993**, *32*, 1315.

(23) Nolte, M. J.; Singleton, E. *J. Chem. Soc., Dalton Trans.* **1974**, 2406.

(24) Werner, H.; Stark, A.; Schulz, M.; Wolf, J. *Organometallics* **1992**, *11*, 1126.

(25) (a) Consiglio, G.; Morandini, F.; Sironi, A. *J. Organomet. Chem.* **1986**, *306*, C45. (b) Bruce, M. I.; Humphrey, M. G.; Snow, M. R.; Tiekink, E. R. T. *J. Organomet. Chem.* **1986**, *314*, 213. (c) Jia, G.; Gallucci, J. C.; Rheingold, A. L.; Haggerty, B. S.; Meek, D. W. *Organometallics* **1991**, *10*, 3459. (d) Sun, Y.; Taylor, N. J.; Carty, A. J. *J. Organomet. Chem.* **1992**, *423*, C43. (e) Montoya, J.; Santos, A.; Lopez, J.; Echavarren, A. M.; Ros, J.; Romero, A. *J. Organomet. Chem.* **1992**, *426*, 383.

(179.6(7)°) and only slightly bent at C11 (173.8(9)°). Atoms C10–C17 are coplanar to within 0.02 Å, and their mean plane makes angles of 116.2(4) and 26.0(4)° with the two RuP2C2 coordination planes.

In the absence of chiral elements in the molecule, the chirality of the crystal structure (the space group $P2_12_12_1$ is free of reflective elements) must be ascribed to the spatial arrangement of the molecules. Packing is determined mainly by van der Waals interactions, with normal intermolecular distances. The shortest contact between non-hydrogen atoms is C19···O13 ($x + 1, y, z - 1$), 3.23(3) Å.

The spectroscopic properties of the methyl–vinylidene complexes **7** and **8** are reported in Table 1 and suggest a geometry in solution like that in the solid state. Characteristic features of IR spectra are the $\nu_{C\equiv C}$ band of the alkynyl ligand at 2099–2095 cm^{-1} and those due to $\nu_{C=C}$ of the vinylidene ligand[1-3] at 1672–1645 cm^{-1}. In the ^1H NMR spectra, vinylidenes **7** and **8** show the signal of the =C=C(Me)R methyl group as a sharp singlet at δ 2.15–2.20 ppm for the Ph and *p*-tol complexes. The ^{t}Bu derivative **8c** shows a sharp quintet with a small coupling constant of 1.1 Hz at δ 1.76 ppm, probably due to coupling with the four phosphorus atoms.

The ^{13}C spectra of **7** and **8** display the characteristic highly deshielded Ru=*C* carbene carbon resonance at δ 383.1–379.4 ppm as a quintet of quartets, due to coupling with all of the four phosphorus atoms ($^2J_{CP}$ of 17 Hz) and the three methyl protons of the Me substituent ($^3J_{CH}$ near 4 Hz), and the vinylic =*C*(Me)R carbon resonance in the δ 120–118 ppm region as a sharp quintet, with a smaller $^3J_{CP}$ coupling constant of 2.5 Hz. Note that both vinylidene carbon atoms Ru=C_α=C_β should be coupled with the methyl protons of the Me substituent, but coupling is only observed with the carbene Ru=C_α= with a $^3J_{CH}$ value of 4.0–4.5 Hz, while in the vinylic carbon atom, =C_β(Me)R, the $^2J_{CH}$ is probably too small to be detected.

The ethynyl carbons of the RC≡C ligand also appear in the ^{13}C spectra as quintets due to ^{31}P coupling at δ 97.8–100.4 ppm with J_{CP} of 25 Hz for C_α and at δ 119.8–124.5 ppm with a smaller $^3J_{CP}$ of about 2.5 Hz for C_β. In the proton-coupled ^{13}C spectra, the methyl substituent of the vinylidene ligand =C=C(Me)R is also present as a quartet at δ 8.0–9.1 ppm with a typical $^1J_{CH}$ of 132 Hz.

In the temperature range from +30 to −70 °C, the $^{31}P\{^1H\}$ NMR spectra of vinylidenes **7** and **8** appear as sharp singlets at δ 123.1–118.9 ppm, but at temperatures below −70 °C, the singlet broadens and at −90 °C resolves into two triplets, indicating that each of the two pairs of phosphorous atoms are magnetically equivalent. The spectra can also be simulated using an A_2B_2 model with the parameters reported in Table 1. These results may be interpreted on the basis of the existence of a *trans* octahedral geometry in which the inequivalence of the phosphorus atoms at low temperature may be due to a restricted vinylidene rotation which makes each of the two pairs of P atoms magnetically equivalent.

The spectroscopic properties of vinylidenes **4** and **5** were measured in solution, kept below −20 °C to avoid the formation of new species, and are reported in Table 1. These data confirm the formulation proposed for the

Scheme 2[a]

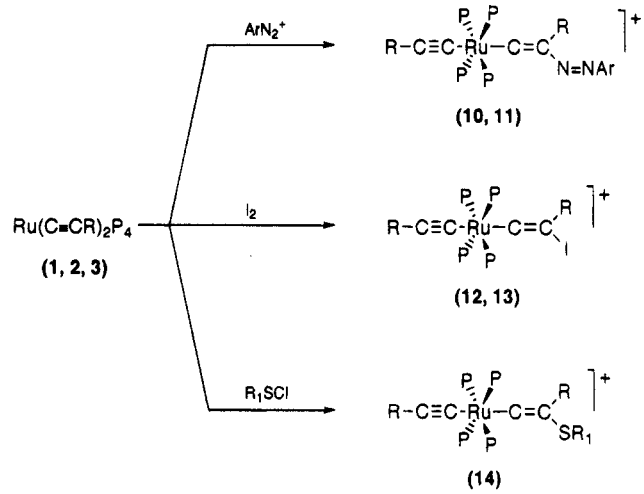

[a] Legend: P = $P(OEt)_3$ (**10**, **12**, **14**) and $PPh(OEt)_2$ (**11**, **13**); R = Ph (**a**); Ar = Ph, *p*-tol; R_1 = 2,4-$(NO_2)_2C_6H_3$.

complexes, showing the $\nu_{C\equiv C}$ of the alkynyl at 2102–2097 cm^{-1} and the $\nu_{C=C}$ of the vinylidene ligand at 1685–1633 cm^{-1} in the infrared spectra. In the ^1H NMR spectra, the vinylic proton [Ru=C=C(*H*)R] is present at δ 5.98–5.25 ppm as a quintet due to coupling with the four P atoms (J_{PH} about 1.5 Hz), while in the ^{13}C spectra the characteristic C_α of the vinylidene ligand is observed as a quintet at δ 379.8 ppm (**4a**) and at δ 377.4 ppm (**5a**) with $^2J_{CP}$ = 17 Hz. The vinylic carbon atom =C=C_β(H)R is also observed as a CH resonance at δ 112.6–117.6 ppm ($^1J_{CH}$ = 150 Hz), while the C_α and C_β of the alkynyl ligand RuC≡CR appear as quintets near δ 78–100 and δ 120–125 ppm, with J_{CP} coupling constants of 25 and 2 Hz, respectively. Finally, the ^{31}P spectra for **4** and **5** suggest a *trans* geometry in solution like that proposed for related methyl–vinylidene derivatives **7** and **8**. In fact, the sharp singlet observed from +30 to −70 °C begins to broaden as the temperature is further lowered and appears at −100 °C as an A_2B_2 multiplet, in agreement with a slight distortion of *trans* geometry at low temperatures.

Reactions with Other Electrophiles. The reactions of bis(acetylide) $Ru(C\equiv CR)_2P_4$ with other electrophilic reagents were studied. Results are summarized in Scheme 2. Aryldiazonium cations react with **2** and **3** in CH_2Cl_2 to give diazo–vinylidene $[Ru(C\equiv CR)\{=C=C(N=NAr)R\}P_4]^+$ cations **10** and **11**, which can be isolated as BPh_4^- or BF_4^- salts.[26] The compounds are stable both in solid state and in solution of polar organic solvents, where they behave as 1:1 electrolytes. Their spectroscopic properties, reported in Table 1, confirm the formulation proposed. The IR spectra show the $\nu_{C\equiv C}$ of the alkynyl groups at 2104–2096 cm^{-1}, while the two bands at 1593–1582 and 1574–1565 cm^{-1} are reasonably assigned to the $\nu_{C=C}$ and $\nu_{N=N}$ modes of the =C=C(N=NAr)R ligand.[27,28] Diagnostic for the pres-

(26) $P(OMe)_3$ derivative **1** also reacted with aryldiazonium cations to give diazo–vinylidene, but the oily nature of the product prevented its complete characterization.

(27) Bruce, M. I.; Humphrey, M. G.; Liddell, M. J. *J. Organomet. Chem.* **1987**, *321*, 91.

(28) In the labeled compound **10ad** the $\nu_{^{15}N=N}$ band cannot be unambiguously assigned owing to the presence in the expected region (1500–1550 cm^{-1}) of other intense absorptions, and comparison with the IR spectrum of **10aa** shows only the disappearance of a medium intensity band at 1574 cm^{-1} attributed to $\nu_{N=N}$.

Scheme 3

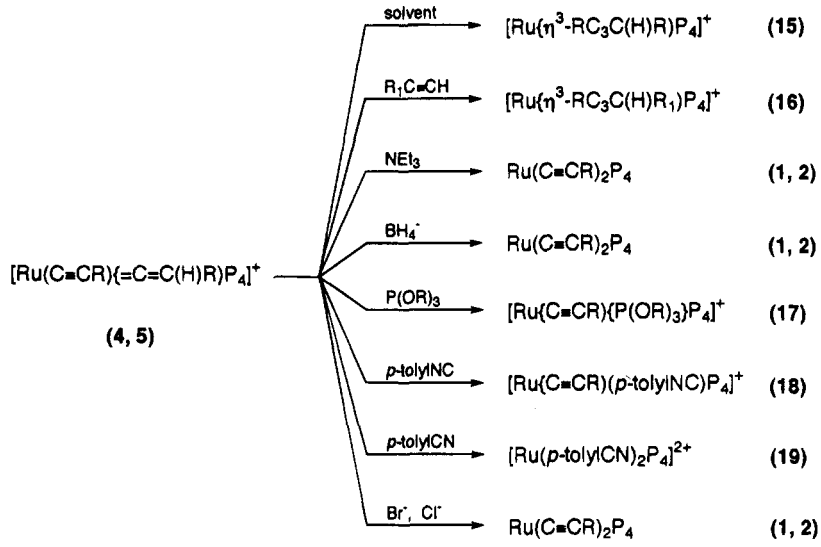

ence of diazo–vinylidene was the highly deshielded quintet of carbene carbon resonances C_α near δ 382 ppm, with $^2J_{CP}$ of 17 Hz, which is split into a quintet of doublets by coupling with ^{15}N ($^2J_{C^{15}N}$ = 7 Hz) in the labeled [Ru(C≡CPh){=C=C(^{15}N=NPh)Ph}{P(OEt$_3$}$_4$]-BF_4 (**10ac**) derivative. The C_β vinylic =*C*(N=NAr)R resonances could not be assigned, even in BF_4^- compound **10ac**, probably because they were masked by the phenyl carbon signals. Instead, the C_α and C_β of the alkynyl RC≡C ligand appear as quintets at δ 98.8 and δ 126.7 ppm (**10**), with J_{CP} of 26 and 3 Hz, respectively. The $^{31}P\{^1H\}$ NMR spectra of the diazo–vinylidene complexes **10** and **11** show a behavior similar to that of the other vinylidenes, showing a sharp singlet up to −70 °C which then broadens and resolves into an A_2B_2 multiplet at −90 °C. On this basis, a *trans* geometry with inequivalent P *nuclei* at low temperature can reasonably be proposed for these complexes.

Iodine reacts in diethyl ether with the bis(acetylide) complexes **2** and **3**, affording iodo–vinylidenes **12a** and **13a**, which separate out as I_3^- salts. 2,4-Dinitrobenzenesulfenyl chloride also reacts with Ru(C≡CR)$_2$P$_4$, giving the thio–vinylidene derivative [Ru(PhC≡C)-{=C=C(SR$_1$)Ph}P$_4$]$^+$Cl$^-$, **14a**, which is obtained as a solid only with the P(OEt)$_3$ ligand. The spectroscopic properties of these compounds also confirm their formulation as vinylidene–acetylide derivatives, the IR spectra showing the $\nu_{C\equiv C}$ of the alkynyl groups at 2104–2083 cm^{-1} and the $\nu_{C=C}$ of the vinylidene at 1673–1620 cm^{-1}, respectively.

In the ^{13}C spectra, the characteristic carbene carbon atom resonance appears as a quintet at δ 336.1 ppm ($^2J_{CP}$ = 17 Hz) for iodo–vinylidene **12a** and at δ 349.6 ppm for thio–vinylidene **14a**. The C_β vinylic carbon atom is also observed at δ 91.3 (**12a**) and δ 109.4 ppm (**14a**), as well as the C_α and C_β carbon signals of the alkynyl ligand. Finally a *trans* geometry can be proposed in solution for the complexes on the basis of the sharp singlet[29] that appears in the ^{31}P spectra between +30 and −80 °C. It is worth noting that diazo–vinylidene[27] and iodo–vinylidene[30] complexes are rare and that the only thio–vinylidene reported[2h] was obtained starting from thio–acetylide complexes, so that 2,4-(NO$_2$)$_2$C$_6$H$_3$SCl is a new electrophilic reagent for alkynyl derivatives giving thio–vinylidene complexes.

Reactions of Vinylidene Derivatives. Whereas methyl– (**7**, **8**), diazo– (**10**, **11**), and iodo– (**12**, **13**) vinylidenes are robust complexes that are quite inert toward ligand substitution, the related H–vinylidenes **4** and **5** quickly react in solution. The results are summarized in Scheme 3.

Acetylide–vinylidene complexes **4** and **5** react in solutions of CH_2Cl_2, ethanol, *etc.* to give enynyl derivatives [Ru{η^3-RC$_3$CHR}P$_4$]$^+$ [11c] which can be isolated and characterized. The reaction occurs slowly enough to be measured by following the disappearance of the ^{31}P signal of the vinylidene complexes. Kinetic measurements[31] of the reaction of **5a** (eq 3) show that the

$$[Ru(C{\equiv}CPh)\{{=}C{=}C(H)Ph\}\{P(OEt)_3\}_4]^+ \rightarrow \underset{(\mathbf{5a})}{}$$

$$[Ru\{\eta^3\text{-}PhC_3C(H)Ph\}\{P(OEt)_3\}_4]^+ \quad (3)$$
$$(\mathbf{15})$$

reaction rate is first-order in vinylidene (**5a**) and that it is inhibited by the presence of free acetylene PhC≡CH in the reaction mixture, thus ruling out an intramolecular mechanism. The plot of the reciprocal of k_{obs} for the reaction of disappearance of vinylidene **5a** (Table 5) versus [PhC≡CH] gives a good straight line, as shown in Figure 2.

Chemical studies also showed (Scheme 3) that the vinylidene ligand is so labile in **4** and **5** that it is readily replaced by P(OMe)$_3$, *p*-tolNC and *p*-tolCN ligands. Furthermore, the mixed-enynyl complex [Ru{η^3-PhC$_3$C-(H)^{t}Bu}{P(OEt)$_3$}$_4$]BF$_4$ (**16**) was isolated in pure form and almost quantitative yield by reacting [Ru(C≡CPh)-{=C=C(H)Ph}{P(OEt)$_3$}$_4$]BF$_4$ with an excess of ^{t}Bu-C≡CH.

(29) In contrast with the other vinylidene complexes, only slight broadening of the signal was observed in the temperature range between −70 and −100 °C and no A_2B_2 multiplet appeared, even at the lowest temperature attained.

(30) Bruce, M. I.; Koutsantonis, G. A.; Liddell, M. J.; Nicholson, B. K. *J. Organomet. Chem.* **1987**, *320*, 217.

(31) Preliminary measurements show that the kinetic behavior of all vinylidene complexes **4** and **5** is strictly similar to that of **5a**, only values for k_{obs} being different.

Table 5. Observed Rate Constants for Reaction of Vinylidene 5a To Give Enynyl Complex 15 at 15 °C in $CDCl_3$

[PhC≡CH], mol/L	k_{obs}, s^{-1}
0.00×10^{-2}	1.29×10^{-3}
4.89×10^{-2}	4.92×10^{-4}
6.98×10^{-2}	2.96×10^{-4}
1.00×10^{-1}	2.18×10^{-4}
1.52×10^{-1}	1.49×10^{-4}
2.05×10^{-1}	1.33×10^{-4}
3.05×10^{-1}	9.50×10^{-5}

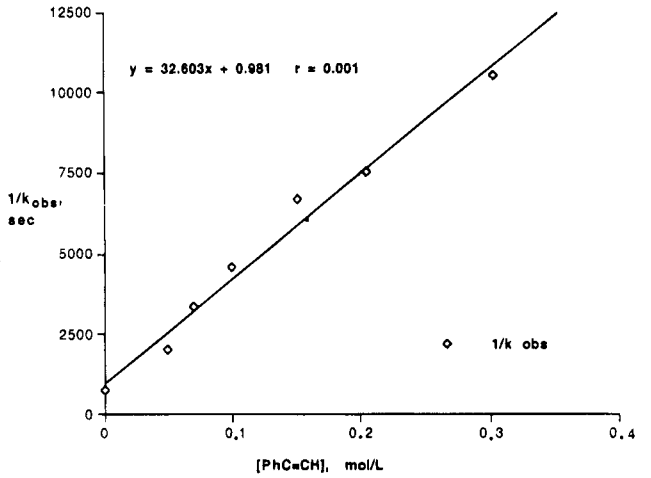

Figure 2. Plot of [PhC≡CH] vs $1/k_{obs}$, the reciprocal of the observed rate constant obtained at 15 °C in $CDCl_3$ for the reaction $[Ru(C{\equiv}CPh)\{{=}C{=}C(H)Ph\}\{P(OEt)_3\}_4]^+ \rightarrow [Ru\{\eta^3\text{-}PhC_3C(H)Ph\}\{P(OEt)_3\}_4]^+$.

Scheme 4[a]

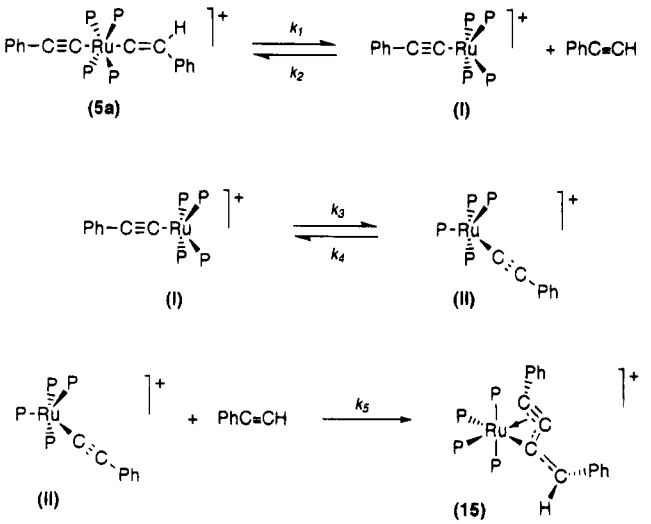

[a] Legend: P = $P(OEt)_3$.

These results suggest the mechanism of Scheme 4 for the reaction of formation of enynyl complexes from alkynyl–vinylidene derivatives. Steady-state treatment gives the following expression for the rate:

$$-d[\mathbf{5a}]/dt = [\mathbf{5a}]k_1k_3k_5/\{k_2k_4 + k_3k_5 + k_2k_5[PhC{\equiv}CH]\}$$

which leads to $k_{obs} = k_1k_3k_5/\{k_2k_4 + k_3k_5 + k_2k_5[PhC{\equiv}CH]\}$ for the observed rate constant. This equation gives $1/k_{obs}$ = constant + $k_2[PhC{\equiv}CH]/k_1k_3$ as experimentally observed, in a plot of $1/k_{obs}$ versus [PhC≡CH] (Figure 2), in agreement with the proposed mechanism.

The dissociation of the vinylidene ligand (Scheme 4) to give free alkyne and the pentacoordinate intermediate **I** may first involve a η^2-PhC≡CH complex of the type $[Ru(C{\equiv}CPh)(\eta^2\text{-}PhC{\equiv}CH)P_4]^+$ (**I***) in equilibrium with **5a** through a 1,2 H-shift on PhC≡CH (**5a** ⇄ **I***). The dissociation of the alkyne ligand from this η^2-complex (**I***) may give the pentacoordinate **I**. However, no spectroscopic (IR and NMR) evidence of the formation of a η^2-RC≡CH complex was detected from our acetylide–vinylidene compounds **4** and **5**, and, although examples of η^2-RC≡CH complexes are known[32] and in two cases the rearrangement[33] to a vinylidene derivative is reported,[2f,m] the dissociation of **5a** into **I** and RC≡CH may also take place without any η^2-alkyne intermediate. In the same way, the reaction of intermediate **II** with PhC≡CH to give enynyl **15** may involve a series of other intermediate compounds such as the *cis*-η^2-RC≡CH complex, which rearranges to *cis*-$[Ru(C{\equiv}CPh)\{{=}C{=}C(H)Ph\}P_4]^+$ and gives the final product **15** through a C–C coupling reaction.

Our chemical and kinetic results do not allow us to clarify the nature of these debated intermediates.[34] However, they do exclude an intramolecular mechanism and are consistent with a pathway, similar to that found in *cis–trans* octahedral isomerization,[35] which involves a pentacoordinate acetylide intermediate. This should be present in the two isomers **I** and **II**, which can be assumed to have square-pyramidal geometries (or geometries distorted toward trigonal bipyramidal) with the acetylide ligand in the apical and in the equatorial position, respectively, in the two isomers, as proposed in Scheme 4.

Enynyl complexes have been reported for the Fe,[2g,36] Ru,[2i,11b,25c,37] Os[38] families and for W,[32b] their study stimulated by the fact that these η^3-ligands may be key intermediates in alkyne dimerization/oligomerization processes catalyzed by transition-metal complexes. The alkynyl–vinylidene coupling reaction had been proposed for the formation of enynyl compounds and $[Fe(C{\equiv}CR)\{{=}C{=}C(H)R\}(P{-}P)_2]^+$ (P–P = $Me_2PCH_2CH_2PMe_2$) complexes[2g,36] have recently been reported to give enynyls as well as $[W\{{=}C{=}C(Me)^tBu\}(\eta^2\text{-}HC{\equiv}C^tBu)(CO)Cp^*]^+$ after deprotonation.[32b] Our complexes **4** and **5** represent new examples of such a reaction that also allows kinetic information to be obtained.

(32) (a) Caldarelli, J. L.; White, P. S.; Templeton, J. L. *J. Am. Chem. Soc.* **1992**, *114*, 10097. (b) McMullen, A. K.; Selegue, J. P.; Wang, J. *Organometallics* **1991**, *10*, 3421. (c) Schneider, D.; Werner, H. *Angew. Chem., Int. Ed. Engl.* **1991**, *30*, 700. (d) Kowalczyk, J. J.; Arif, A. M.; Gladysz, J. A. *Organometallics* **1991**, *10*, 1079.

(33) For the rearrangement of 1-alkynes in vinylidenes see ref 21 and the following: Silvestre, J.; Hoffmann, R. *Helv. Chim. Acta* **1985**, *68*, 1461. Albiez, T.; Bernhardt, W.; von Schnering, C.; Roland, E.; Bantel, H.; Vahrenkamp, H. *Chem. Ber.* **1987**, *120*, 141.

(34) It may be noted that a mechanism also involving η^2-PhC≡CH complexes as additional intermediates in equilibrium with vinylidene tautomers, after a steady-state treatment, gives an expression for the rate that shows linear dependence of $1/k_{obs}$ on [PhC≡CH], as for the simpler proposed mechanism.

(35) Basolo, F.; Pearson, R. G. *Mechanism of Inorganic Reactions*; Wiley-Interscience: New York, 1967. Wright, G.; Glyde, R. W.; Mawby, R. J. *J. Chem. Soc., Dalton Trans.* **1973**, 220.

(36) Hughes, D. L.; Jimenez-Tenorio, M.; Leigh, G. J.; Rowley, A. T. *J. Chem. Soc., Dalton Trans.* **1993**, 3151.

(37) Bianchini, C.; Peruzzini, M.; Zanobini, F.; Frediani, P.; Albinati, A. *J. Am. Chem. Soc.* **1991**, *113*, 5453.

(38) Gotzig, J.; Otto, H.; Werner, H. J. *J. Organomet. Chem.* **1985**, *287*, 247.

Results of the $P(OMe)_3$ and $P(OEt)_3$ derivatives can also explain the behavior of $Ru(C{\equiv}CR)_2\{PPh(OEt)_2\}_4$ complexes **3**, which do not allow vinylidene cations $[Ru(C{\equiv}CR)\{{=}C{=}C(H)R\}P_4]^+$ to be isolated by protonation, only η^3-enynyl derivatives **6**. In this case, too, protonation probably affords a $=C=C(H)R$ complex that rearranges very quickly to the final product, preventing isolation of the vinylidene intermediate.

The vinylidene ligand in complexes **4** and **5** can be easily deprotonated with bases such as NEt_3 or LiOH to give bis(acetylide) compounds (**1** and **2**) in almost quantitative yields (Scheme 3). Complexes **1** and **2** can also be obtained by treating vinylidenes **4** and **5** with $NaBH_4$ which in this case does not reduce the $=C=C(H)R$ group[39] to vinyl $-CH=C(H)R$ but acts as a base, affording the acetylide derivatives. Furthermore, the $=C=C(H)R$ ligand in these derivatives (**4** and **5**) is shown to be a good leaving group[40] and can easily be substituted by several ligands operating at low temperature (−20 °C) to prevent rearrangement to enynyl derivatives. As a result, the new mono(acetylide) $[Ru(C{\equiv}CPh)\{P(OMe)_3\}\{P(OEt)_3\}_4]^+$ (**17**) and $[Ru(C{\equiv}CPh)(p\text{-tolNC})\{P(OEt)_3\}_4]^+$ (**18**) derivatives can be prepared and characterized. Both complexes show *trans* geometry (**II**) in solution, as indicated by the $^{31}P\{^1H\}$ NMR spectra, appearing as an AB_4 multiplet for **17** and as a sharp singlet for the isocyanide complex **18**, in agreement with structure (**II**).

p-Toluonitrile also substitutes the acetylide ligand in **5a** giving the bis(nitrile) complex $[Ru(p\text{-tolCN})_2\{P(OEt)_3\}_4](BPh_4)_2$ (**19**) which shows an A_2B_2 multiplet in the ^{31}P spectra, in agreement with a *cis* geometry. Finally, the lability of the $=C=C(H)R$ ligand in **4** and **5** prompted us to attempt the preparation of halogen–acetylide complexes $RuX(C{\equiv}CR)P_4$ (X = Cl, Br) by substitution reaction with Cl^- or Br^-. The reaction proceeded easily with substitution of the vinylidene ligand and formation of a new species with only one $\nu_{C\equiv C}$ band at 2035–2040 cm^{-1} reasonably attributed to the $RuX(C{\equiv}CR)P_4$ complex. However, these compounds were found to be rather instable; every attempt to isolate them failed, and the only products isolable from the reaction mixture were the already known bis(acetylide) $Ru(C{\equiv}CR)_2P_4$ derivatives.

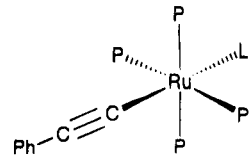

(II)

P = $P(OEt)_3$

L = $P(OMe)_3$, *p*-tolNC

Conclusions

A series of bis(alkynyl) derivatives $Ru(C{\equiv}CR)_2P_4$ can easily be prepared using monodentate phosphite as an ancillary ligand. Reactions with electrophilic reagents of these acetylides allow new alkynyl–vinylidene $[Ru(C{\equiv}CR)\{{=}C{=}C(R_1)R\}P_4]^+$ (R_1 = H, Me, PhN=N, *p*-tolyl-N=N, I, 2,4-$(NO_2)_2C_6H_3S$; R = Ph, *p*-tol, ^{t}Bu) derivatives to be obtained. The simple H–vinylidene $[Ru(C{\equiv}CR)\{{=}C{=}C(H)R\}P_4]^+$ compounds show some novel properties, including easy replacement of the vinylidene ligand and rearrangement of the complexes in solution to give enynyl $[Ru(\eta^3\text{-}RC_3CHR)P_4]^+$ derivatives according to a proposed mechanism.

Acknowledgment. The financial support of MURST and CNR (Progetto Finalizzato Chimica Fine II), Rome, is gratefully acknowledged. We thank Daniela Baldan for her valuable technical assistance.

Supporting Information Available: Details of the structural determination are available for the complex $[Ru(C{\equiv}CPh)\{{=}C{=}C(Me)Ph\}\{P(OEt_3\}_4]CF_3SO_3$ including listings of atomic coordinates for hydrogen, anisotropic and isotropic displacement parameters, and complete listings of bond distances and angles (13 pages). Ordering information is given on any current masthead page.

OM9409377

(39) Davison, A.; Selegue, J. P. *J. Am. Chem. Soc.* **1980**, *102*, 2455.

(40) One example of substitution of the vinylidene ligand on protonation with the NH_4PF_6 salt of the $Ru(C{\equiv}CR)_2(dppe)_2$ complex has been shown: Touchard, D.; Morice, C.; Cadierno, V.; Haquette, P.; Toupet, L.; Dixneuf, P. H. *J. Chem. Soc., Chem. Commun.* **1994**, 859.

Synthesis and New Reactions of Alkynylcobalt Complexes: Preparation and Structure of $[Co\{\eta^2:\eta^1\text{-}C_6H_4P(OEt)_2C(H)C(H)Ph\}(CO)\{PPh(OEt)_2\}_2]BPh_4$

Gabriele Albertin,*[1a] Stefano Antoniutti,[1a] Alessia Bacchi,[1b] Emilio Bordignon,[1a] and Giancarlo Pelizzi[1b]

Dipartimento di Chimica, Università di Venezia, Dorsoduro, 2137, 30123 Venezia, Italy, and Dipartimento di Chimica Generale ed Inorganica, Centro CNR di Strutturistica Diffrattometrica, 43100 Parma, Italy

Received March 7, 1995[⊗]

The alkynylcobalt complexes $Co(C{\equiv}CR)(CO)\{PPh(OEt)_2\}_3$ (**1**) (R = Ph, *p*-tol) were prepared. Protonation reaction with $HBF_4{\cdot}Et_2O$ or CF_3SO_3H allowed the synthesis of $[Co\{\eta^2:\eta^1\text{-}C_6H_4P(OEt)_2C(H){=}C(H)R\}(CO)\{PPh(OEt)_2\}_2]BPh_4$ (**2**) derivatives, which were characterized crystallographically and spectroscopically. Oxidation of **1** with I_2 affording $CoI_2(C{\equiv}CR)(CO)\{PPh(OEt)_2\}_2$ was also tested.

Introduction

A number of studies on the synthesis and reactivity of metal σ-acetylide complexes have been reported in recent years.[2-4] This interest is due to different factors, including the strict relation with vinylidene complexes,[2-4] the possibility of giving cycloaddition reactions with organic substrates,[2b,5] and the implications of alkynyl complexes in catalysis[6] and in the preparation of new materials.[7]

Among the metal centers used to bind a C≡CR unit, cobalt has not received much attention, resulting in rather few known alkynyl compounds for this metal.[8]

We have begun a study on the synthesis and reactivity of acetylide complexes containing phosphite ligands,[9] and in this paper we report the preparation of new alkynyl cobalt complexes and a novel reaction shown by these derivatives which affords the first example, to the best of our knowledge, of a metal complex containing the phenylphosphorane $\eta^2:\eta^1\text{-}C_6H_4P(OEt)_2C(H){=}C(H)R$ as a ligand.

Results and Discussion

The cobalt(I) acetylide complexes $Co(C{\equiv}CR)(CO)\{PPh(OEt)_2\}_3$ (**1**) (R = Ph, **a**; *p*-tol, **b**) were prepared by treating the monocarbonyl compound[10] $[Co(CO)\{PPh(OEt)_2\}_4]BPh_4$ with an excess of lithium acetylide in THF, as shown in eq 1.

$$[Co(CO)\{PPh(OEt)_2\}_4]^+ \xrightarrow[THF]{\text{exc. } Li^+[C{\equiv}CR]^-} Co(C{\equiv}CR)(CO)\{PPh(OEt)_2\}_3 \quad (1)$$

1

(R = Ph, **a**; *p*-tol, **b**)

Compounds **1** are air-stable, diamagnetic, orange microcrystalline solids. Their IR spectra exhibit $\nu_{C\equiv C}$ bands at 2088 (**1a**) and 2089 (**1b**) cm^{-1} and ν_{CO} at 1956 and at 1955 cm^{-1}, respectively. The formulation is confirmed by their NMR spectra. The ^{13}C NMR spectrum of **1a** shows the CO carbon signal as a quartet at δ 213.5, and the C_α and C_β atoms of the acetylide ligand appear as two quartets at δ 109.1 for C_α, which has a

[⊗] Abstract published in *Advance ACS Abstracts,* July 15, 1995.

(1) (a) Università di Venezia. (b) Università di Parma.

(2) Reviews: (a) Nast, R. *Coord. Chem. Rev.* **1982,** *47,* 89. (b) Bruce, M. I. *Chem. Rev.* **1991,** *91,* 197.

(3) (a) Rappert, T.; Yamamoto, A. *Organometallics* **1994,** *13,* 4984. (b) Terry, M. R.; Mercando, L. A.; Kelley, C.; Geoffroy, G. L.; Nombel, P.; Lugan, N.; Mathieu, R.; Ostrander, R. L., Owens-Waltermire, B. E.; Rheingold, A. L. *Ibid.* **1994,** *13,* 843. (c) Werner, H.; Baum, M.; Schneider, D.; Windmüller, B. *Ibid.* **1994,** *13,* 1089. (d) Santos, A.; Lopez, J.; Matas, L.; Ros, J.; Galan, A.; Echavarren, A. M. *Ibid.* **1993,** *12,* 4215. (e) Espuelas, J.; Esteruelas, M. A.; Lahoz, F. J.; Oro, L. A.; Valero, C. *Ibid.* **1993,** *12,* 663. (f) Touchard, D.; Haquette, P.; Pirio, N.; Toupet, L.; Dixneuf, P. H. *Ibid.* **1993,** *12,* 3132. (g) Hughes, D. L.; Jimenez-Tenorio, M.; Leigh, G. J.; Rowley, A. T. *J. Chem. Soc., Dalton Trans.* **1993,** 3151. (h) Lomprey, J. R.; Selegue, J. P. *J. Am. Chem. Soc.* **1992,** *114,* 5518. (i) Kelley, C.; Lugan, N.; Terry, M. R.; Geoffroy, G. L.; Haggerty, B. S.; Rheingold, A. L. *Ibid.* **1992,** *114,* 6735. (j) Werner, H.; Stark, A.; Schulz, M.; Wolf, J. *Organometallics* **1992,** *11,* 1126. (k) Sun, Y.; Taylor, N. J.; Carty, A. J. *Ibid.* **1992,** *11,* 4293. (l) Miller, D. C.; Angelici, R. J. *Ibid.* **1991,** *10,* 79. (m) Bianchini, C.; Peruzzini, M.; Vacca, A.; Zanobini, F. *Ibid.* **1991,** *10,* 3697. (n) Selnau, H. E.; Merola, J. S. *J. Am. Chem. Soc.* **1991,** *113,* 4008. (o) Field, L. D.; George, A. V.; Malouf, E. Y.; Slip, I. H.; Hambley, T. W. *Organometallics* **1991,** *10,* 3842. (p) Wakatsuki, Y.; Yamazaki, H.; Kumegewa, H.; Satoh, T.; Satoh, J. Y. *J. Am. Chem. Soc.* **1991,** *113,* 9604. (q) Stang, P. J.; Crittell, C. M. *Organometallics* **1990,** *9,* 3191. (r) Seyferth, D.; Ruschke, D. P.; Davis, W. M.; Cowie, M.; Hunter, A. D. *Ibid.* **1989,** *8,* 836. (s) Bullock, R. M. *J. Chem. Soc., Chem. Commun.* **1989,** 165. (t) Schubert, U.; Grönen, *J. Chem. Ber.* **1989,** *122,* 1237.

(4) (a) Senn, D. R.; Wong, A.; Patton, A. T.; Marsi, M.; Strouse, C. E.; Gladysz, J. *A. J. Am. Chem. Soc.* **1988,** *100,* 6096. (b) Consiglio, G.; Schwab, R.; Morandini, F. *J. Chem. Soc., Chem. Commun.* **1988,** *25.* (c) Adams, J. S.; Bitcon, C.; Brown, J. R.; Collison, D.; Cunningham, M.; Whiteley, M. W. *J. Chem. Soc., Dalton Trans.* **1987,** 3049. (d) van Asselt, A.; Burger, B. J.; Gibson, V. C.; Bercaw, J. E. *J. Am. Chem. Soc.* **1986,** *108,* 5347. (e) Collman, J. P.; Brothers, P. J.; McElwee-White, L.; Rose, E. *Ibid.* **1985,** *107,* 6110. (f) Birdwhistell, K. R.; Tonker, T. L.; Templeton, J. L. *Ibid.* **1985,** *107,* 4474. (g) Mayr, A.; Schaefer, K. C.; Huang, E. Y. *Ibid.* **1984,** *106,* 1517. (h) Reger, D. L.; Swift, C. A. *Organometallics* **1984,** *3,* 876. (i) Chan, Y. W.; Renner, M. W.; Balch, A. L. *Ibid.* **1983,** *2,* 1888. (j) Abbott, S.; Davies, S. G.; Warner, P. *J. Organomet. Chem.* **1983,** *246,* C65. (k) Beevor, R. G.; Freeman, M. J.; Green, M.; Morton, C. E.; Orpen, A. G. *J. Chem. Soc., Chem. Commun.* **1985,** *68.* (l) Berke, H.; Huttner, G.; von Seyerl, J. *J. Organomet. Chem.* **1981,** *218,* 193. (m) Roper, W. R.; Waters, J. M.; Wright, L. J.; van Meuers, F. *Ibid.* **1980,** *201,* C27.

(5) (a) Barrett, A. G. M.; Carpenter, N. E.; Mortoir, J.; Sabat, M. *Organometallics* **1990,** *9,* 151 and references therein. (b) Bruce, M. I.; Hambley, T. W.; Liddell, M. J.; Swincer, A. G.; Tiekink, E. R. T. *Ibid.* **1990,** *9,* 2886.

(6) (a) Bianchini, C.; Frediani, P.; Masi, D.; Peruzzini, M.; Zanobini, F. *Organometallics* **1994,** *13,* 4616. (b) Berry, D. H.; Eisenberg, R. *Ibid.* **1987,** *6,* 1976 and references therein.

(7) (a) Fyfe, H. B.; Mlekuz, M.; Zargarian, D.; Taylor, N. J.; Marder, T. B. *J. Chem. Soc., Chem. Commun.* **1991,** 188 and references therein. (b) Takahashi, S.; Takai, Y.; Morimoto, H.; Sonogashira, K. *Ibid.* **1984,** 3.

0276-7333/95/2314-4126$09.00/0

large $^2J_{CP}$ of 48.4 Hz, and at δ 115.2 for C_β, which has a small $^3J_{CP}$ of 4 Hz.

The $^{31}P\{^1H\}$ NMR spectra of **1** over the temperature range 173–298 K show one sharp singlet near δ 169.4, suggesting the magnetic equivalence of the three phosphites, as in an equatorial plane of TBP geometry. Previously known cobalt(I) acetylides are those having bi- and polydentate phosphine ligands of the type Co(dpe)$_2$(C≡CR) (dpe = 1,2-bis(diphenylphosphino)ethane)[8k] and Co(PP$_3$)(C≡CR)[PP$_3$=P(CH$_2$CH$_2$PPh$_2$)$_3$].[8c] The $\nu_{C\equiv C}$ of these acetylides are comparable with our compounds (**1a,b**). Only with PPh(OEt)$_2$ as the ligand can new acetylide **1** be isolated as a crystalline solid, the other related P(OEt)$_3$ and P(OMe)$_3$ complexes being formed as oils.

Protonation of **1** with HBF$_4$·Et$_2$O or CF$_3$SO$_3$H afforded a deep purple solution, which turned yellow after stirring and yielded, after workup, [Co{η^2:η^1-C$_6$H$_4$P(OEt)$_2$C(H)=C(H)R}(CO){PPh(OEt)$_2$}$_2$]BPh$_4$ (**2**) (R = Ph, **a**; *p*-tol, **b**) derivatives in about 75% yield. These compounds are air-stable yellow solids, diamagnetic and 1:1 electrolytes in solution. The structure of one of them (**2a**) was determined using X-ray crystallography and is shown in Figure 1, with selected bonding parameters listed in Table 1. Considering the ethylene group as occupying one coordination site, the coordination around the cobalt atom is approximately that of a trigonal bipyramid and involves the two phosphonite ligands, the carbonyl group, and the bidentate ortho-metalating ligand through the ethylene and phenyl carbon atoms. The bond angles at cobalt in the trigonal plane range from 109.2(1) to 131.2(1)°, thus showing a considerable deviation from the ideal 120°. The axial-to-axial angle is 175.84(8)°.

The Co–P distances of 2.217(1) and 2.229(1) Å and the Co–C (carbonyl) distance of 1.755(4) Å are in excellent agreement with those reported for the corresponding bonds in the related five-coordinate Co(I) compounds,[11–15] whereas a comparison of Co–C (phenyl) distances is rather difficult owing to the lack of data in the literature. However, the value found here, 2.010(3) Å, is only slightly longer than the 1.997 Å value found in Co(η^2-C$_2$H$_4$)(Ph)(PMe$_3$)$_3$.[16]

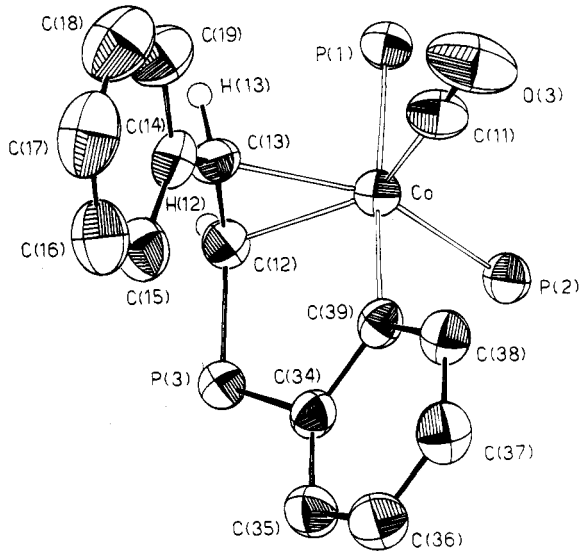

Figure 1. ORTEP view of [CO{η^2:η^1-C$_6$H$_4$P(OEt)$_2$C(H)C(H)Ph}(CO){PPh(OEt)$_2$}$_2$]$^+$ (cation of **2a**) with thermal ellipsoids enclosing 50% of the electron probability distribution. All of the ethoxy groups, the phenyl rings bonded to P1 and P2, and the hydrogen atoms, except for the ethylene hydrogens, have been omitted for clarity.

The coordination of the diethoxy((*z*)-2-phenylethene)-(2-phenyl)phosphorane ligand to the cobalt atom results in the formation of a puckered five-membered chelate ring constituted by the metal, two phenyl carbons, the ylid phosphorus, and the P-bound ethylenic carbon. The conformation of the ring is defined by the parameters[17] q_2 = 0.370(2) Å and ϕ_2 = 22.5(4)°, which are the puckering amplitude and the phase angle, respectively, and by the presence of a pseudo 2-fold axis passing through C34 and bisecting the opposite Co–C12 bond.

Few examples of structural investigation on ortho-metalated compounds comparable with **2a** are reported,[18–23] whose ring members of the metallacycle are, as here, one metal, one P, and three C atoms. Features common among these compounds and **2a** are a significant difference (0.06–0.13 Å) between the M–C (ylid) and the M–C (phenyl) bonds, a formal positive charge associated with the P atom, and the puckered nature of the metallacycle.

As regards the P–C–C–metal system, some P–C multiple bonding together with a significant zwitterionic

(8) (a) Khan, M. S.; Pasha, N. A.; Kakkar, A. K.; Raithby, P. R.; Lewis, J.; Fuhrmann, K.; Friend, R. H. *J. Mater. Chem.* **1992**, *2*, 759. (b) Giese, B.; Zehnder, M.; Neuburger, M.; Trach, F. *J. Organomet. Chem.* **1991**, *412*, 415. (c) Bianchini, C.; Innocenti, P.; Meli, A.; Peruzzini, M.; Zanobini, F.; Zanello, P. *Organometallics* **1990**, *9*, 2514. (d) Kergoat, R.; Gomesole Lima, L. C.; Jégat, C.; Le Berre, N.; Kubiki, M. M.; Guercais, J. E.; L'Haridon, P. *J. Organomet. Chem.* **1990**, *389*, 71. (e) Habadie, N.; Dartiguenave, M.; Dartiguenave, Y.; Britten, J. F.; Beauchamp, A. *Organometallics* **1989**, *8*, 2564. (f) Van den Bergen, A. M.; Elliot, R. L.; Lyons, C. J.; Mackinnon, K. P.; West, B. O. *J. Organomet. Chem.* **1985**, *297*, 361. (g) Rojas, E.; Santos, A.; Moreno, V.; del Pinto, C. *Ibid.* **1979**, *181*, 365. (h) Taube, R.; Drevs, H.; Marx, G. *Z. Anorg. Allg. Chem.* **1977**, *436*, 5. (i) Nast, R.; Fock, K. *Chem. Ber.* **1977**, *110*, 280. (j) Nast, R.; Fock, K. *Chem. Ber.* **1976**, *109*, 455. (k) Ikariya, T.; Yamamoto, A. *J. Organomet. Chem.* **1976**, *116*, 231.

(9) (a) Albertin, G.; Amendola, P.; Antoniutti, S.; Ianelli, S.; Pelizzi, G.; Bordignon, E. *Organometallics*, **1991**, *10*, 2876. (b) Albertin, G.; Antoniutti, S.; Del Ministro, E.; Bordignon, E. *J. Chem. Soc., Dalton Trans.* **1992**, 2203. (c) Albertin, G.; Antoniutti, S.; Bordignon, E.; Cazzaro, F.; Ianelli, S.; Pelizzi, G. *Organometallics*, in press.

(10) Albertin, G.; Bordignon, E.; Orio, A. A.; Rizzardi, G. *Inorg. Chem.* **1975**, *14*, 944.

(11) For example: Co–P, 2.143(2), 2.167(2), 2.175(2); Co–C, 1.729(6) Å in CoH(CO)(PPh$_3$)$_3$;[12] Co–P, 2.189(1), 2.200(1), 2.203(1); Co–C, 1.739(4), 1.780(4) Å in [Co$_2$(CO)$_4$(eHTP)]$^{2+}$;[13] Co–P, 2.209(2), 2.211(2), 2.246(2); Co–C, 1.740(6), 1.766(5) Å in [Co(CO)$_2$(PMe$_3$)$_3$]$^+$;[14] Co–P, 2.128(4), 2.174(4), 2.179(3); Co–C, 1.741(9) Å in [Co(dppep)(SPh)(CO)].[15]

(12) Moody, D. C.; Ryan, R. R. *Cryst. Struct. Commun.* **1981**, *10*, 129.

(13) Askham, F. R.; Stanley, G. G.; Marques, E. C. *J. Am. Chem. Soc.* **1985**, *107*, 7423.

(14) Peres, Y.; Kerkeni, A.; Dartiguenave, M.; Dartiguenave, Y.; Belanger-Gariepy, F.; Beauchamp, A. L. *J. Organomet. Chem.* **1987**, *323*, 397.

(15) Wei, G.; Huang, Z.; Lei, X.; Cao, R.; Jiang, F.; Hong, M.; Liu, H. *Acta Crystallogr.* **1992**, *C48*, 2130.

(16) Klein, H. F.; Gross, J.; Hammer, R.; Schubert, U. *Chem. Ber.* **1983**, *116*, 1441.

(17) Cremer, D.; Pople, J. A. *J. Am. Chem. Soc.* **1975**, *97*, 1354.

(18) See, for example, the six compounds: Fe$_2$(CO)$_6$[C(CHO)P(Ph$_2$C$_6$H$_4$)],[19] [Pt(μ-Cl)CH$_3$COCHP(C$_6$H$_4$)Ph$_2$]·2CDCl$_3$,[20] Ir(CH$_2$PPh$_2$-C$_6$H$_4$)HI(CO)(PPh$_3$),[21] Fe(Cp)(CO)[HC$_2$H$_5$CP(C$_6$H$_4$)Ph$_2$],[22] Fe(CO)$_2$-[C$_6$H$_4$C(Ph)(η^3-C$_5$H$_5$)P(C$_6$H$_4$)Ph],[22] and Os$_3$(μ-H)$_2$(μ$_3$-C$_6$H$_4$PPh$_2$CCHO)(CO)$_8$.[23]

(19) Churchill, M. R.; Rotella, F. J. *Inorg. Chem.* **1978**, *17*, 2614.

(20) Illingsworth, M. L.; Teagle, J. A.; Burmeister, J. L.; Fultz, W. C.; Rheingold, A. L. *Organometallics* **1983**, *2*, 1364.

(21) Clark, G. R.; Roper, W. R.; Wright, A. H. *J. Organomet. Chem.* **1984**, *273*, C17.

(22) Caballero, C.; Chàvez, J. A.; Göknur, Ö.; Löchel, I.; Nuber, B.; Pfisterer, H.; Ziegler, M. L.; Alburquerque, P.; Eguren, L.; Korswagen, R. P. *J. Organomet. Chem.* **1989**, *371*, 329.

(23) Deeming, A. J.; Nuel, D.; Powell, N. I.; Whittaker, C. *J. Chem. Soc., Dalton Trans.* **1992**, 757.

Table 1. Selected Bond Distances (Å) and Angles (deg) for 2a

	Bond Distances		
Co–P1	2.229(1)	P3–C12	1.729(2)
Co–P2	2.217(1)	P3–C34	1.745(3)
Co–C11	1.755(4)	O3–C11	1.139(4)
Co–C12	2.047(3)	C12–C13	1.422(5)
Co–C13	2.073(3)	C12–H12	0.890(27)
Co–C39	2.010(3)	C13–C14	1.479(5)
P1–O1	1.595(2)	C13–H13	0.886(20)
P1–O2	1.593(2)	C34–C35	1.395(4)
P1–C5	1.808(3)	C34–C39	1.398(4)
P2–O4	1.597(3)	C35–C36	1.372(5)
P2–O5	1.595(2)	C36–C37	1.388(5)
P2–C24	1.818(3)	C37–C38	1.383(4)
P3–O6	1.573(2)	C38–C39	1.396(4)
P3–O7	1.566(3)		
	Bond Angles		
C13–Co–C39	92.8(1)	O7–P3–C34	116.6(1)
C12–Co–C39	87.4(1)	O7–P3–C12	104.7(1)
C12–Co–C13	40.4(1)	O6–P3–C34	104.9(1)
C11–Co–C39	88.9(1)	O6–P3–C12	118.0(1)
C11–Co–C13	99.6(1)	O6–P3–O7	106.8(1)
C11–Co–C12	139.4(1)	Co–C11–O3	177.1(3)
P2–Co–C39	87.1(1)	Co–C12–P3	106.6(2)
P2–Co–C13	151.2(1)	P3–C12–C13	127.1(2)
P2–Co–C12	110.9(1)	Co–C12–C13	70.8(2)
P2–Co–C11	109.2(1)	P3–C12–H12	111.8(16)
P1–Co–C39	175.8(1)	Co–C12–H12	115.2(16)
P1–Co–C13	90.7(1)	C13–C12–H12	116.7(16)
P1–Co–C12	96.7(1)	Co–C13–C12	68.9(2)
P1–Co–C11	88.3(1)	C12–C13–C14	133.9(3)
P1–Co–P2	91.0(1)	Co–C13–C14	120.2(2)
Co–P1–C5	121.8(1)	C12–C13–H13	113.8(17)
Co–P1–O2	116.9(1)	Co–C13–H13	107.7(17)
Co–P1–O1	108.2(1)	C14–C13–H13	105.9(16)
O2–P1–C5	98.2(1)	P3–C34–C39	112.2(2)
O1–P1–C5	103.9(1)	P3–C34–C35	123.8(2)
O1–P1–O2	106.2(1)	C35–C34–C39	123.6(3)
Co–P2–C24	116.8(1)	C34–C35–C36	119.7(3)
Co–P2–O5	113.2(1)	C35–C36–C37	118.5(3)
Co–P2–O4	117.5(1)	C36–C37–C38	120.9(3)
O5–P2–C24	103.3(1)	C37–C38–C39	122.6(3)
O4–P2–C24	99.3(1)	C34–C39–C38	114.6(3)
O4–P2–O5	104.7(1)	Co–C39–C38	126.8(2)
C12–P3–C34	106.4(1)	Co–C39–C34	118.6(2)

character is sometimes observed. The P3–C34 bond length (1.745(3) Å) found in the title compound is shorter than the corresponding values found in the above compounds[18] (1.77–1.79 Å) and indicates a partial delocalization on the P–C–C–Co system of the positive charge formally located on P. A certain degree of multiple-bond resonance on the metallacycle could also be responsible for the slight elongation of the bond distances at C34 and C39 (1.395–1.398 Å) and for the corresponding shortening of the remaining three (1.372–1.388 Å) in the metal-coordinated phenyl ring. The ring is planar within 0.01 Å, thus indicating no other appreciable distortion. As expected for an ipso-carbon atom, the angle C34–C39–C38 (114.6(3)°) is narrowed at the expense of the adjacent C35–C34–C39 (123.7(3)°) and C37–C38–C39 (122.7(3)°) angles.

The bonding parameters found in our compound are comparable to those of the compounds[24] containing the Co(η^2-C=C–P) fragment, the average values being

(24) Zolk, R.; Werner, H. *J. Organomet. Chem.* **1987**, *331*, 95. Werner, H.; Zolk., R. *Chem. Ber.* **1987**, *120*, 1003. Regragui, R.; Dixneuf, P. H.; Taylor, N. J.; Carty, A. J. *Organometallics* **1990**, *9*, 2234. Lang, H.; Zsolnai, L. *Chem. Ber.* **1991**, *124*, 259. Caffyn, A. J. M.; Mays, M. J.; Solan, G. A.; Braga, D.; Sabatino, P.; Conole, G.; McPartlin, M.; Powell, H. R. *J. Chem. Soc., Dalton Trans.* **1991**, 3103. Edwards, A. J.; Martin, A.; Mays, M. J.; Raithby, P. R.; Solan, G. A. *J. Chem. Soc., Chem. Commun.* **1992**, 1416.

Scheme 1

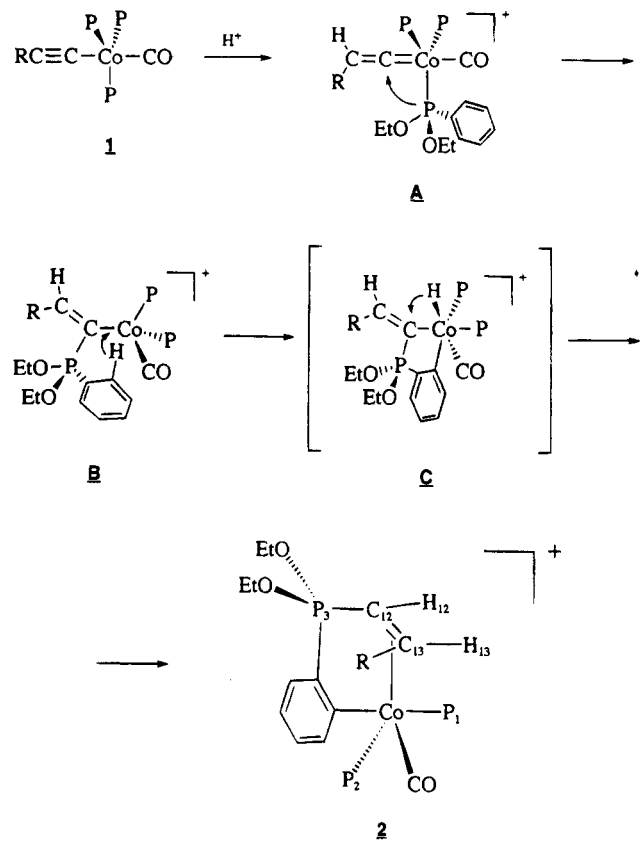

Co–C, 2.004 Å; C=C, 1.402 Å; C–P, 1.797 Å; C–Co–C, 40.95°; Co–C–C, 69.53°.

The spectroscopic properties of the chelate complexes **2** are diagnostic for their formulation and seem to suggest in solution the same geometry as the solid state. The IR spectra show the ν_{CO} as a strong band at 1998 (**2a**) and 1997 (**2b**) cm^{-1}, whereas in the ^1H NMR spectra the two olefinic protons H12 and H13 appear as two multiplets at δ 3.65–3.13. The $^{31}P\{^1H\}$ NMR spectra are temperature-dependent and at −90 °C display three doublets of doublets for both the complexes. The high-field signal near 70 ppm is attributed to the P3 phosphonium atom coupled to the two phosphorus *nuclei*, P1 and P2, of the phosphonite ligands. The other two resonances at δ 166.5 and a δ 159.5–159.3, due to the nonequivalent phosphonite ligands, are broadened, probably by the cobalt nuclear quadrupole, and fine structures are not resolved even at −90 °C, thus preventing the determination of the P–P coupling constant. The proton-coupled and -decoupled ^{13}C NMR spectra for **2a** allow clear assignment of the characteristic carbon atoms in the molecule. Thus, the carbonyl appears as a multiplet at δ 207.7, the metalate C–Co at δ 168.4, and the two olefinic C13 and C12 as CH resonances at δ 63.8 ($^2J_{CP}$ = 21.8 Hz and $^1J_{CH}$ = 151 Hz) and at δ 32.1 ($^1J_{CP}$ = 127 Hz and $^1J_{CH}$ = 160 Hz), respectively.

Spectroscopic investigations on the reaction course **1** → **2** allow us to propose the reaction path reported in Scheme 1.

Protonation of **1** gives the vinylidene complexes **A**, as confirmed by the highly deshielded[2–4] C_α signal observed at δ 382.8 (starting from **1a**) in the ^{13}C spectrum of the solution recorded at −80 °C immediately after protonation. Attempts to isolate **A** gave a deep purple

oil, whose IR spectrum exhibited ν_{CO} at 1993 cm^{-1} and two medium intensity bands at 1690 and 1639 cm^{-1} characteristic of $\nu_{C=C}$ of vinylidene ligands.[3,4,25] Increase in temperature does not cause a color change but does cause spectral variation, involving the appearance in the ^{31}P spectra, beside the signal of phosphonites at about 150−170 ppm, of a new high-field signal at 61.0 ppm. Furthermore, the ^{13}C NMR spectrum obtained 30−60 min into the reaction shows the presence of a new broad doublet at δ 237.6 (in CD_2Cl_2 at 243 K) with a J_{CP} of 24 Hz which may be attributed to the C_α atom of a vinyl phosphonium complex of type **B** formed by intramolecular attack of one phosphonite on C_α of the vinylidene ligand. The type **B** complex cannot be isolated as a solid, but the reaction has some good precedents.[26] ^{13}C and ^{31}P NMR and the nature of final product **2**, which contains a P−C bond, suggest to us that compounds of type **B** are formed as intermediates. These coordinatively unsaturated cobalt complexes **B** can then undergo an aryl C−H metalation reaction followed by a vinyl C−H reductive elimination, affording the final complexes **2**.

The octahedral cobalt(III) complex **C** may also be proposed as an intermediate in the ortho metalation reaction proceeding *via* an oxidative addition mechanism[27] on an unsaturated Co(I) complex. The reductive elimination of a small molecule that often follows the reaction may result, in this case, in moving a proton from the cobalt atom to the C_α carbon of the vinyl phosphonium ligand giving the olefin moiety that rearranges to a π-bond as in **2**. Vinyl phosphonium derivatives are known[26] also with phosphite ligands, and in one case, the formation of a η^2-phosphatoethylene ligand at a manganese center[28] has been described. No example, however, of a metalation reaction and a hydrogen shift giving a η^2,η^1-phosphorane has been reported for a vinyl phosphonium $-C(PR_3)=C<$ fragment, resulting in $C_6H_4P(OEt)_2CH=C(H)R$, a completely new ligand.

The alkynyls $Co(C{\equiv}CR)(CO)\{PPh(OEt)_2\}_3$ were rather inert to the substitution of ligands with CO and RNC but quickly reacted with equimolar amounts of I_2 to give $CoI_2(C{\equiv}CPh)(CO)\{PPh(OEt)_2\}_2$ (**3a**) as a brown solid in about 60% yield (eq 2).

$$\underset{\textbf{2a}}{Co(C{\equiv}CR)(CO)\{PPh(OEt)_2\}_3} \xrightarrow{I_2} \underset{\textbf{3a}}{CoI_2(C{\equiv}CPh)(CO)\{PPh(OEt)_2\}_2} \quad (2)$$

The complex is air-stable, diamagnetic, and moderately soluble in polar organic solvents, in which it behaves as a nonelectrolyte. The infrared spectrum shows a medium intensity band at 2117 cm^{-1} (CH_2Cl_2) attributed to $\nu_{C\equiv C}$ and a strong absorption at 2070 cm^{-1} (CH_2Cl_2) due to the stretch of the CO ligand. The ^1H NMR spectrum shows the characteristic signals of the phosphonite ligands, whereas the ^{31}P NMR spectrum between +30 and −90 °C shows a sharp singlet at δ 145. These data together with the elemental analysis support the formulation of **3a** as a proposed Co(III) alkynyl complex. However in the absence of X-ray data we cannot propose a geometry.

Experimental Section

All synthetic work was carried out under an inert atmosphere using standard Schlenk techniques or a Vacuum Atmospheres drybox. Once isolated, the complexes turned out to be quite air-stable and were stored at −20 °C. All solvents used were dried over appropriate drying agents, degassed on a vacuum line, and distilled into vacuum-tight storage flasks. Diethoxyphenyl phosphine was prepared by the method of Rabinowitz and Pellon.[29] Alkynes were Aldrich products, used without any further purification. Lithium acetylides $Li^+RC{\equiv}C^-$ (R = Ph or *p*-tol) were prepared by reacting a slight excess of the appropriate acetylene (40 mmol) with lithium (35 mmol, 0.24 g) in 10 mL of THF. Other reagents were purchased from commercial sources in the highest available purity and used as received. Infrared spectra were recorded on Digilab BioRad FTS-40 spectrophotometers. NMR spectra (^1H, ^{13}C, ^{31}P) were obtained on a Bruker AC200 spectrometer at temperatures varying between −90 and +30 °C, unless otherwise noted. ^1H and ^{13}C spectra are referenced to internal tetramethylsilane, while $^{31}P\{^1H\}$ chemical shifts are reported with respect to 85% H_3PO_4, with downfield shifts considered positive. The conductivity of 10^{-3} M solutions of the complexes in CH_3NO_2 at 25 °C was measured with a Radiometer CDM 83 instrument.

Synthesis of Complexes. The monocarbonyl $[Co(CO)(PPh(OEt)_2\}_4]BPh_4$ compound was prepared as previously reported.[10]

$Co(C{\equiv}CR)(CO)\{PPh(OEt)_2\}_3$ (1) (R = Ph, a; *p*-tol, b). An excess (6 mmol) of lithium acetylide $Li^+C{\equiv}Cr^-$ (R = Ph, *p*-tol) was added to a solution of 2.4 g (2 mmol) of $[Co(CO)\{PPh(OEt)_2\}_4]BPh_4$ in 30 mL of THF, and the reaction mixture was stirred at room temperature for 2 h. Evaporation of the solvent under reduced pressure gave a brown oil, which was treated with 15 mL of ethanol. The resulting solution was stirred vigorously at 0 °C until an orange solid separated out (from 3 to 7 h), which was collected by filtration and crystallized from ethanol; yield ≥70%. Anal. Calcd for $C_{39}H_{50}O_7P_3Co$ (**1a**): C, 59.85; H, 6.44. Found: C, 59.63; H, 6.45. Mp 91−94 °C decomp. IR (KBr and CH_2Cl_2): 2086 m (2088 m), $\nu_{C\equiv C}$; 1951 s (1956 s), ν_{CO} cm^{-1}. ^1H NMR ($(CD_3)_2CO$, 25 °C): δ 7.65−6.80 (m, 20H, Ph), 3.82, 3.54 (m, 12H, CH_2), 1.10 (t, 18H, CH_3). $^{31}P\{^1H\}$ NMR ($(CD_3)_2CO$, −90 °C): δ 169.4 s. ^{13}C NMR ($(CD_3)_2CO$, 25 °C): δ 213.5 (q, $^2J_{CP}$ = 25 Hz, CO), 142−124 (m, Ph), 115.2 (q, $^3J_{CP}$ = 4 Hz, C≡*C* Ph), 109.1 (q, $^2J_{CP}$ = 48.4, *C*≡CPh), 61.8 (t, CH_2), 16.7 (q, CH_3). Calcd for $C_{40}H_{52}O_7P_3Co$ (**1b**): C, 60.30; H, 6.58. Found: C, 60.34; H, 6.61. Mp 70−72 °C dec. IR (KBr and CH_2Cl_2): 2090 m (2089 m), $\nu_{C\equiv C}$; 1954 s (1955 s), ν_{CO} cm^{-1}. ^1H NMR ($(CD_3)_2CO$, 25 °C): δ 7.70−6.77 (m, 19H, Ph), 3.80, 3.51 (m, 12H, CH_2), 2.21 (s, 3H, CH_3 *p*-tol), 1.08 (t, 18H, CH_3). $^{31}P\{^1H\}$ NMR ($(CD_3)_2CO$ −90 °C): δ 169.4 s; (25 °C): δ 167.9 s.

$[Co\{\eta^2{:}\eta^1\text{-}C_6H_4P(OEt)_2C(H){=}C(H)R\}(CO)\{PPh(OEt)_2\}_2]BPh_4$ (2) (R = Ph, a; *p*-tol, b). To a solution of $Co(C{\equiv}CR)(CO)\{PPh(OEt)_2\}_3$ (2 mmol) in 15 mL of ethanol cooled to −80 °C was added an equimolar amount of $HBF_4{\cdot}Et_2O$ (2 mmol, 0.29 mL of 54% solution in Et_2O), and the reaction mixture was brought to room temperature. The deep purple solution obtained was gently warmed to 50−60 °C while stirring until

(25) Although few examples of cobalt complexes containing vinylidene ligands have been described, their spectroscopic properties are well comparable with those of **A**. See refs. 3m, 8c, and the following: Albiez, T.; Vahrenkamp, H. *Angew. Chem., Int. Ed. Engl.* **1987**, *26*, 572. Jacobsen, E. N.; Bergman, R. G. *J. Am. Chem. Soc.* **1985**, *107*, 2023. Seyferth, D. *Adv. Organomet. Chem.* **1976**, *14*, 97 and references therein.

(26) See ref 4a and the following: Boland-Lussier, B. E.; Churchill, M. R.; Hughes, R. P.; Rheingold, A. L. *Organometallics* **1982**, *1*, 628. Kolobova, N. E.; Ivanov, L. L.; Zhvanko, O. S.; Khitrova, O. M.; Batsanov, A. S.; Struchkov, Y. T. *J. Organomet. Chem.* **1984**, *265*, 271. Bianchini, C.; Meli, A.; Peruzzini, M.; Zanobini, F.; Zanello, P. *Organometallics* **1990**, *9*, 241.

(27) Bruce, M. I. *Angew. Chem., Int. Ed. Engl.* **1977**, *16*, 73.

(28) Antonova, A. B.; Kovalenko, S. V.; Korniyets, E. D.; Johansson, A. A.; Struchkov, Y. T.; Ahmedov, A. I.; Yanovsky, A. I. *J. Organomet. Chem.* **1983**, *244*, 35.

(29) Rabinowitz, R.; Pellon, J. *J. Org. Chem.* **1961**, *26*, 4623.

a yellow-orange color appeared (about 30–40 min). The addition of $NaBPh_4$ (2 mmol, 0.69 g) in 5 mL of ethanol caused the precipitation of a yellow solid, which was collected by filtration and crystallized from ethanol; yield ≥75%. The preparation of **2** can also be carried out using CF_3SO_3H instead of $HBF_4{\cdot}Et_2O$ or operating at room temperature by stirring the protonated solution until a color change from purple to yellow takes place (10–15 h). Also the reaction can occur in a different solvent such as CH_2Cl_2, but the yield was lower than 75%. Anal. Calcd for $C_{63}H_{71}BO_7P_3Co$ (**2a**): C, 68.61; H, 6.49. Found: C, 68.52; H, 6.48. Mp 128 °C. Λ_M (CH_3NO_2, 25 °C): 49.3 Ω^{-1} mol^{-1} cm^2. IR (KBr and CH_2Cl_2): 2001 s (1998 s), ν_{CO} cm^{-1}. ^{1}H NMR ($(CD_3)_2CO$, 25 °C): δ 7.60–6.70 (m, 39H, Ph), 4.58, 3.98 (m, 12H, CH_2), 3.65, 3.13 (m, 2H, CH), 1.48, 1.45, 1.38, 1.36, 1.15, 1.05 (t, 18H, CH_3). $^{31}P\{^1H\}$ NMR ($(CD_3)_2CO$, −90 °C): δ 166.5, 159.3, 70.4 dd. ^{13}C NMR (CD_2Cl_2, 25 °C): δ 207.7 (m, CO), 168.4 (m, C–Co), 166–120 (m, Ph), 67–59 (t of m, CH_2), 63.8 (q of m, $^2J_{CP}$ = 21.8 Hz, $^1J_{CH}$ = 151 Hz, C_{13}), 32.1 (q of m, $^1J_{CP}$ = 127 Hz, $^1J_{CH}$ = 160 Hz, C_{12}), 21–12 (m of qi, CH_3). Calcd for $C_{64}H_{73}BO_7P_3Co$ (**2b**): C, 68.82; H, 6.59. Found: C, 68.69; H, 6.66. Mp 68–70 °C decomp. Λ_M (CH_3NO_2, 25 °C): 52.4 Ω^{-1} mol^{-1} cm^2. IR (KBr and CH_2Cl_2): 1991 s (1997 s), ν_{CO} cm^{-1}. ^{1}H NMR ($(CD_3)_2CO$, 25 °C): δ 7.70–6.62 (m, 38H, Ph), 4.55, 3.92 (m, 12H, CH_2), 3.63, 3.13 (m, 2H, CH), 2.02 (s, 3H, CH_3 *p*-tol), 1.49, 1.45, 1.38, 1.36, 1.17, 1.04 (t, 18H, CH_3). $^{31}P\{^1H\}$ NMR ($(CD_3)_2CO$, −60 °C): δ 166.5, 159.5, 70.4 dd.

$CoI_2(C{\equiv}CPh)(CO)\{PPh(OEt)_2$ (3a). A solution of I_2 in diethyl ether (1 mmol, 2.5 mL of 0.4 M solution) was added to a solution of $Co(C{\equiv}CPh)(CO)\{PPh(OEt)_2\}_3$ (1 mmol, 0.8 g) in 10 mL of diethyl ether cooled to −80 °C, and the reaction mixture was brought to room temperature. A brown solid began to separate out after a few minutes, which was collected after 1 h and dried under vacuum; yield ≥60%. In the case of the synthesis of the related compound $CoI_2\{C{\equiv}C(p\text{-tol})\}(CO)\{PPh(OEt)_2$ (**3b**), only a brown oil separated out, which decomposed in an attempt to crystallize it. Anal. Calcd for $C_{29}H_{35}I_2O_5P_2Co$ (**3a**): C, 41.55; H, 4.21. Found: C, 41.45; H, 4.20. Mp 94–96 °C decomp. IR (KBr and CH_2Cl_2): 2123 m (2117 m), $\nu_{C{\equiv}C}$; 2068 s (2070 s), ν_{CO} cm^{-1}. ^{1}H NMR (CD_2Cl_2, 25 °C): δ 8.10–6.90 (m, 15H, Ph), 4.55, 4.30 (m, 8H, CH_2), 1.39 (t, 12H, CH_3). $^{31}P\{^1H\}$ NMR (CD_2Cl_2, −85 °C): δ 145.8 s; (0 °C) 145.0 s.

X-ray Structure Determination of Compound $[Co\{Co\{\eta^2{:}\eta^1\text{-}C_6H_4P(OEt)_2C(H){=}C(H)Ph\}(CO)\{PPh(OEt)_2\}_2]BPh_4$ (2a). A yellow crystal (0.20 × 0.39 × 0.60 mm^3) was mounted on an Enraf-Nonius CAD4 diffractometer, used to measure cell dimensions and diffraction intensities by means of graphite-monochromatized Mo Kα radiation. Automatic routines to search for, center, and index reflections gave a primitive triclinic cell. The intensity statistics suggested that the crystal was centric, and a successful model was found with space group *P*1. Crystal data: M = 1102.91; a = 12.554(2), b = 12.685(2), c = 19.901(6) Å; α = 108.32(2)°, β = 104.20(2)°, γ = 89.88(1)°; V = 2907(**1**) Å^3, Z = 2, D_c = 1.260 g cm^{-3}; Mo Kα radiation (λ = 0.710 69 Å), μ(Mo Kα) = 4.3 cm^{-1}. A total of 10 164 unique reflections were measured by the θ–2θ scan technique over a range of 6–50° in 2θ, with an ω scan range of (0.80 + 0.35 tan θ)° centered about the calculated Mo Kα peak position. The scan area was actually extended at each side by 25% for background determination. The net count was then calculated as NC = P − 2(BG1 − BG2), where P is the integrated peak intensity. No correction for crystal decomposition or loss of alignment was required. Intensities were corrected for Lorentz and polarization factors. Correction for absorption effects was also applied according to the method of Walker and Stuart.[30]

The structure was solved by automated Patterson (SHELXS-86)[31] and difference Fourier techniques and refined by full-matrix least-squares procedures based on F^2. Thermal pa-

(30) Walker, N.; Stuart, D. *Acta Crystallogr.* **1983**, *A39*, 158.

Table 2. Atomic Coordinates (×10^4) and Equivalent Isotropic Displacement Parameters (Å^2 × 10^4) (One-Third of the Trace of the Diagonalized Matrix) for 2a

atom	*x/a*	*y/b*	*z/c*	U_{eq}
Co	626.0(3)	4510.3(2)	2130.1(2)	358(2)
P1	1340.5(6)	5383.9(6)	3322.0(4)	403(3)
P2	−992.7(6)	4206.0(6)	2325.9(4)	391(3)
P3	723.2(6)	2054.1(6)	1344.5(4)	390(3)
O1	2414(2)	6140(2)	3414(1)	517(9)
O2	578(2)	6189(2)	3751(1)	537(9)
O3	749(2)	6626(2)	1876(1)	847(13)
O4	−988(2)	3911(2)	3050(1)	513(9)
O5	−1764(2)	3223(2)	1675(1)	486(9)
O6	1336(2)	1168(2)	857(1)	477(8)
O7	113(2)	1419(2)	1719(1)	486(9)
C1	3066(3)	6858(3)	4123(2)	746(17)
C2	4213(3)	6969(3)	4102(2)	887(20)
C3	318(3)	7263(3)	3693(2)	736(19)
C4	256(4)	8014(3)	4397(2)	1046(25)
C5	1796(2)	4629(2)	3961(2)	419(12)
C6	2752(3)	4072(3)	3954(2)	546(14)
C7	3095(3)	3469(3)	4427(2)	716(17)
C8	2492(4)	3413(3)	4905(2)	737(19)
C9	1563(3)	3967(3)	4925(2)	732(19)
C10	1211(3)	4566(3)	4456(2)	566(15)
C11	684(3)	5804(3)	1989(2)	485(13)
C12	1512(2)	3141(2)	2060(2)	383(12)
C13	2161(2)	4015(2)	2008(2)	408(12)
C14	2580(2)	4183(2)	1413(2)	445(13)
C15	2342(3)	3498(3)	688(2)	551(15)
C16	2834(3)	3715(3)	188(2)	687(18)
C17	3576(3)	4627(4)	404(3)	808(23)
C18	3823(3)	5316(4)	1116(3)	814(22)
C19	3333(3)	5100(3)	1615(2)	621(16)
C20	−807(4)	2842(3)	3113(2)	958(23)
C21	−1259(4)	2636(3)	3662(2)	971(24)
C22	−2904(3)	2963(3)	1640(2)	877(21)
C23	−3612(4)	2925(6)	983(3)	2078(51)
C24	−1867(2)	5360(2)	2442(2)	435(12)
C25	−2355(3)	5717(3)	3015(2)	606(16)
C26	−3047(3)	6568(3)	3056(2)	751(19)
C27	−3252(3)	7081(3)	2543(2)	734(19)
C28	−2786(3)	6746(3)	1972(2)	889(22)
C29	−2089(3)	5884(3)	1924(2)	750(19)
C30	2352(3)	727(3)	1180(2)	591(15)
C31	3025(3)	446(3)	644(2)	881(21)
C32	−739(3)	515(3)	1269(2)	722(17)
C33	−751(4)	−304(3)	1649(3)	1112(26)
C34	−105(2)	2654(2)	744(2)	381(11)
C35	−616(2)	2070(3)	12(2)	503(13)
C36	−1153(3)	2635(3)	−439(2)	574(15)
C37	−1147(3)	3785(3)	−154(2)	532(14)
C38	−636(2)	4348(2)	573(2)	442(13)
C39	−96(2)	3808(2)	1056(1)	362(11)
B	4911(3)	−435(3)	7033(2)	462(15)
C40	4769(3)	242(2)	7861(2)	500(13)
C41	5384(3)	1227(3)	8322(2)	645(16)
C42	5223(4)	1800(3)	9007(2)	786(19)
C43	4447(4)	1393(4)	9261(2)	827(21)
C44	3839(3)	425(4)	8831(2)	848(21)
C45	3993(3)	−124(3)	8145(2)	710(17)
C46	3977(3)	−68(2)	6419(2)	519(14)
C47	2902(3)	51(3)	6480(2)	690(17)
C48	2078(3)	282(4)	5941(3)	920(23)
C49	2318(4)	423(3)	5339(2)	853(22)
C50	3357(4)	293(3)	5260(2)	879(22)
C51	4170(3)	49(3)	5796(2)	757(19)
C52	6144(3)	−153(2)	6974(2)	473(13)
C53	6486(3)	904(3)	6988(2)	645(16)
C54	7527(3)	1177(3)	6957(2)	798(20)
C55	8283(3)	397(4)	6892(2)	874(23)
C56	7987(3)	−659(4)	6861(2)	771(20)
C57	6937(3)	−918(3)	6907(2)	553(15)
C58	4693(2)	−1791(2)	6856(2)	448(13)
C59	5044(3)	−2307(3)	7387(2)	594(16)
C60	4913(3)	−3460(3)	7228(2)	680(19)
C61	4416(3)	−4123(3)	6531(3)	729(20)
C62	4071(3)	−3658(3)	5997(2)	806(20)
C63	4209(3)	−2511(3)	6161(2)	600(15)

rameters were refined anisotropically for non-hydrogen atoms and isotropically for hydrogen atoms, which were all introduced at their calculated positions and refined riding on their carrier atoms, except for the ethylene hydrogens which were located from a difference Fourier map. At convergence: $R_1 = 0.0357$ for 689 parameters and 5475 observed reflections ($F_o > 4\sigma(F_o)$) and $wR_2 = 0.0807$ for all data, with $w = [\sigma^2(F_o^2)]^{-1}$. The final difference map was essentially featureless. Neutral scattering factors were employed and anomalous dispersion terms were included in F_c. Calculations were performed on GOULD POWERNODE 6040 and ENCORE91 computers using the programs SHELXL92,[32] PARST,[33] and ORTEP.[34] Atomic coordinates for non-hydrogen atoms are given in Table 2.

(31) Sheldrick, G. M. *SHELX86, A Program for Structure Determination*; University of Göttingen: Göttingen, FRG, 1986.
(32) Sheldrick, G. M. *SHELXL92, A Program for Structure Refinement*; University of Göttingen: Göttingen, FRG, 1992.
(33) Nardelli, M. *Comput. Chem.* **1983**, *7*, 95.
(34) Johnson, C. K. ORTEP. Report ORNL-3794; Oak Ridge National Laboratory: Oak Ridge, TN, 1965.

Acknowledgment. The financial support of MURST and CNR, Rome, is gratefully acknowledged. Extensive use of the Cambridge Structural Database was made. We thank Daniela Baldan for technical assistance.

Supporting Information Available: Details of the structural determination for complex **2a**, including tables of atomic coordinates, anisotropic displacement parameters, and bond distances and angles (6 pages). Ordering information is given on any current masthead page.

OM950176N

Synthesis, Characterization, and Configurational Lability of (η^3-Allyl)dicarbonyl[hydrotris(1-pyrazolyl)borato]molybdenum Complexes Bearing Substituents at the Termini: Thermodynamic Preference for the *Anti* Stereoisomer

Yancey D. Ward, Lawrence A. Villanueva, Gary D. Allred, Sonha C. Payne, Mark A. Semones, and Lanny S. Liebeskind*

Sanford S. Atwood Chemistry Center, Emory University, 1515 Pierce Drive, Atlanta, Georgia 30322

Received April 18, 1995[⊗]

1-, 1,3-, 1,1,3- and 1,2,3-substituted dicarbonyl[hydrotris(1-pyrazolyl)borato](η^3-allyl)-molybdenum complexes were prepared and characterized by IR and ^{1}H and ^{13}C NMR spectroscopy and, in some cases, by X-ray crystallography. From the (*E*)-stereoisomers of 1° allylic acetates, *syn*-monosubstituted 1-ethyl- and 1-phenylallylic complexes were generated in high yield. The isomeric 1,3-transposed 2° allylic acetates, CH_2=CHCHR(OAc), gave *syn*/*anti* mixtures for R = Et, *i*-Pr, and cyclohexyl, but only *syn*-products were formed when R = aryl. The corresponding *anti* isomers of the 1-ethyl- and 1-phenylallyl complexes were efficiently generated from the (*Z*)-stereoisomers of 2-pentenyl acetate and cinnamyl acetate, respectively, demonstrating the importance of double bond stereochemistry in establishing the allyl substituent kinetic stereochemistry. Monosubstituted allyls bearing alkyl, aryl, methoxy, acetoxy, and carbomethoxy substituents were configurationally stable at room temperature. However, at elevated temperature (110–125 °C) both *syn* and *anti* isomers of monosubstituted allyls equilibrated to mixtures in which the *anti* isomer predominated when the substituent was an alkyl, acetoxy, or carbomethoxy group. The *syn* isomer of 1-aryl- and 1-methoxy substituted allyls was strongly favored at equilibrium. 1,3-Di-, 1,1,3-tri-, and 1,2,3-trisubstituted complexes equilibrated in solution at room temperature to mixtures in which the *syn*/*anti* isomer predominated over the *syn*/*syn* isomer for all cases studied except the 1,3-diphenyl-substituted allyl. Again, aryl groups showed a strong preference for the *syn* configuration. Eight of the complexes were characterized by X-ray crystallography.

Introduction and Background

(η^3-Allyl)metal complexes are of great use in organic synthesis, as both nucleophilic and electrophilic partners in synthetic transformations.[1-31] π-Allyl complexes of palladium play an important role in reactions that proceed catalytically in metal,[1,2,32-39] while π-allyl com-

[⊗] Abstract published in *Advance ACS Abstracts,* August 1, 1995.

(1) Trost, B. M. *Angew. Chem., Int. Ed. Engl.* **1995**, *34*, 259.
(2) Trost, B. M. *Angew. Chem., Int. Ed. Engl.* **1989**, *28*, 1173.
(3) Semmelhack, M. F. *Org. React.* **1972**, *19*, 115.
(4) Baker, R. *Chem. Rev.* **1973**, *73*, 487.
(5) Billington, D. C. *Chem. Soc. Rev.* **1985**, *14*, 93.
(6) Faller, J. W.; Ma, Y. N. *Organometallics* **1993**, *12*, 1927.
(7) Faller, J. W.; Nguyen, J. T.; Ellis, W.; Mazzieri, M. R. *Organometallics* **1993**, *12*, 1434.
(8) Faller, J. W.; Lambert, C.; Mazzieri, M. R. *J. Organomet. Chem.* **1990**, *383*, 161.
(9) Faller, J. W.; Linebarrier, D. *Organometallics* **1988**, *7*, 1670.
(10) Faller, J. W.; Lambert, C. *Tetrahedron* **1985**, *41*, 5755.
(11) Faller, J. W.; Chao, K.-H. *Organometallics* **1984**, *3*, 927.
(12) Faller, J. W.; Chao, K. H.; Murray, H. H. *Organometallics* **1984**, *3*, 1231.
(13) Faller, J. W.; Murray, H. H.; White, D. L.; Chao, K. H. *Organometallics* **1983**, *2*, 400.
(14) Faller, J. W.; Chao, K.-H. *J. Am. Chem. Soc.* **1983**, *105*, 3893.
(15) Pearson, A. J.; Mallik, S.; Pinkerton, A. A.; Adams, J. P.; Zheng, S. *J. Org. Chem.* **1992**, *57*, 2910.
(16) Pearson, A. J.; Mallik, S.; Mortezaei, R.; Perry, M. W. D.; Shively, R. J., Jr.; Youngs, W. J. *J. Am. Chem. Soc.* **1990**, *1132*, 8034.
(17) Pearson, A. J.; Khetani, V. D. *J. Am. Chem. Soc.* **1989**, *111*, 6778.
(18) Pearson, A. J.; Blystone, S. L.; Nar, H.; Pinkerton, A. A.; Roden, B. A.; Yoon, J. *J. Am. Chem. Soc.* **1989**, *111*, 134.
(19) Pearson, A. J. In *Advances in Metal–Organic Chemistry*; Liebeskind, L. S., Ed.; JAI Press: Greenwich, CT, 1989; Vol. I; pp 1.
(20) Pearson, A. J. *Phil. Trans. R. Soc. Lond. A* **1988**, *326*, 525.
(21) Yu, R. H.; McCallum, J. S.; Liebeskind, L. S. *Organometallics* **1994**, *13*, 1476.
(22) McCallum, J. S.; Sterbenz, J. T.; Liebeskind, L. S. *Organometallics* **1993**, *12*, 927.
(23) Rubio, A.; Liebeskind, L. S. *J. Am. Chem. Soc.* **1993**, *115*, 891.
(24) Liebeskind, L. S.; Bombrun, A. *J. Am. Chem. Soc.* **1991**, *113*, 8736.
(25) Hansson, S.; Miller, J. F.; Liebeskind, L. S. *J. Am. Chem. Soc.* **1990**, *112*, 9660.
(26) Su, G. M.; Lee, G. H.; Peng, S. M.; Liu, R. S. *J. Chem. Soc., Chem. Commun.* **1992**, 215.
(27) Lin, S. H.; Peng, S. M.; Liu, R. S. *J. Chem. Soc., Chem. Commun.* **1992**, 615.
(28) Yang, G. M.; Su, G. M.; Liu, R. S. *Organometallics* **1992**, *11*, 3444.
(29) Lin, S.-H.; Yang, Y.-J.; Liu, R.-S. *J. Chem. Soc., Chem. Commun.* **1991**, 1004.
(30) Yang, G.-M.; Lee, G.-H.; Peng, S.-M.; Liu, R.-S. *Organometallics* **1991**, *10*, 2531.
(31) Vong, W.-J.; Peng, S.-M.; Lin, S.-H.; Lin, W.-J.; Liu, R.-S. *J. Am. Chem. Soc.* **1991**, *113*, 573.
(32) Trost, B. M. *Pure Appl. Chem.* **1992**, *64*, 315.
(33) Backvall, J. E.; Gatti, R.; Schink, H. E. *Synthesis* **1993**, 343.
(34) Backvall, J. E. *Pure Appl. Chem.* **1992**, *64*, 429.
(35) Backvall, J. E.; Andersson, P. G. *J. Am. Chem. Soc.* **1992**, *114*, 6374.
(36) Takahara, J. P.; Masuyama, Y.; Kurusu, Y. *J. Am. Chem. Soc.* **1992**, *114*, 2577.

0276-7333/95/2314-4132$09.00/0

plexes of molybdenum, in particular those based on the η^5-CpMo(CO)$_2$ fragment, have proven very useful in stoichiometric processes.[6-31]

One limitation to the broad use of η^5-CpMo(CO)$_2$(η^3-allyl) complexes in organic synthesis is the cyclopentadienyl ligand itself. It is most common to introduce the η^5-cyclopentadienyl ligand by treating a precursor complex such as (η^3-allyl)MoX(CH$_3$CN)$_2$(CO)$_2$ with a source of cyclopentadienyl anion. Though perfectly suitable for simple unfunctionalized π-allylic systems, the cyclopentadienyl anion is both too basic and too nucleophilic for use with π-allylic substrates bearing sensitive functionality. These limitations were overcome by the use of a nonbasic and nonnucleophilic substitute for the cyclopentadienyl ligand.

The search for a cyclopentadienyl replacement in (π-allyl)molybdenum complex chemistry led to consideration of hydrotris(1-pyrazolyl)borate (Tp), a member of the poly(pyrazolyl)borate family of ligands introduced by Trofimenko in the late 1960's.[40-42] Hydrotris(1-pyrazolyl)borate is isoelectronic with the η^5-cyclopentadienyl ligand, both being uninegative six-electron donors. K$^+$Tp$^-$ is trivial to prepare in high yield on large scale (1 mol of K$^+$Tp$^-$ may be prepared by heating excess pyrazole (4 mol) with 1 mol of potassium borohydride to an internal temperature of 190–210 °C for 2.5–4.0 h). It appears and handles much like potassium acetate, being an air-stable, free-flowing white solid that can be stored indefinitely.[43] On the other hand, the cyclopentadienyl anion must be prepared through the tedious cracking of dicyclopentadiene followed by deprotonation with a strong base. The resulting carbanion, being easily oxidized and protonated, must be stored and utilized under anaerobic and anhydrous conditions.

With the exception of a brief earlier study by Ipaktschi,[44,45] little is known about the synthetic potential of TpMo(CO)$_2$(η^3-allyl) complexes, although simple molybdenum allyls of the TpMo(CO)$_2$ system have been known for many years.[46] TpMo(CO)$_2$(η^3-allyl) complexes should participate in the rich, stereospecific π-complex functionalization chemistry already defined for the η^5-CpMo(CO)$_2$ system, yet be preparable in good yield from a more varied range of allylic precursors than the cyclopentadienyl-based complexes. Therefore, a general investigation was initiated to explore the scope and synthetic potential of (1) the synthesis of a diverse array of TpMo(CO)$_2$(η^3-allyl) complexes, (2) the conversion of those η^3-allyls into cationic η^4-diene complexes and their stereospecific functionalization, and (3) the conversion of the neutral TpMo(CO)$_2$(η^3-allyl) complexes into cationic TpMo(CO)(NO)(η^3-allyl)$^+$ complexes and their reaction with nucleophiles.

During the course of the first stage of the investigation an unexpectedly facile *syn–anti* equilibration of substituted acyclic TpMo(CO)$_2$(η^3-allyl) complexes was discovered (Figure 1). Furthermore, an unusual thermodynamic preference for the *anti* stereoisomer was observed in the solution spectra. *Syn–anti* isomerization of substituents at the allylic termini has been well-studied in the case of palladium,[47-49] where isomerization of acyclic complexes occurs through a π–σ–π process that places sterically demanding substituents at a *syn* rather than an *anti* position in order to minimize allylic strain between substituents at the ends of the allyl. To overcome the preference for *syn* geometry at equilibrium, one must introduce destabilizing steric interactions between the *syn* substituents and the central substituent[47,48] or between the *syn* substituents and other ligands on the metal. The latter strategy was used successfully by Åkermark and co-workers in palladium-catalyzed allylation reactions influenced by 2,9-disubstituted phenanthroline ligands.[50,51]

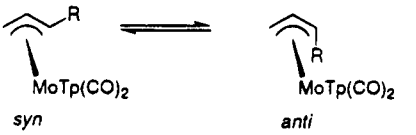

Figure 1. *Syn* and *anti* isomers of (π-allyl)molybdenum complexes.

Both the unexpectedly facile *syn–anti* equilibration of substituted acyclic TpMo(CO)$_2$(η^3-allyl) complexes and the strong thermodynamic preference for the *anti* stereoisomer were surprising, since η^5-CpMo(CO)$_2$(η^3-allyl) complexes are configurationally stable at ambient temperature, and in one documented case of *syn–anti* isomerization in π-allyl complexes based on the η^5-CpMo(CO)$_2$ auxiliary, equilibration to a pure *syn* isomer occurred at 100 °C.[52] Given this background, a full study of the *syn–anti* isomerization process in acyclic TpMo(CO)$_2$(η^3-allyl) complexes was undertaken. Complete details of that study are reported herein. A related brief study of substituted allylmolybdenum complexes bearing the hydrotris(3,5-dimethylpyrazolyl)borato ligand was recently described by Sarkar and co-workers.[53]

Results and Discussion

Synthesis of TpMo(CO)$_2$(η^3-allyl) Complexes. Traditionally, (π-allyl)molybdenum complexes have been prepared by the treatment of allylic halides with Mo(CO)$_3$(CH$_3$CN)$_3$ in CH$_3$CN at room temperature or by the treatment of allylic acetates with Mo(CO)$_3$(CH$_3$CN)$_3$ in CH$_3$CN at reflux. On addition of a cyclopentadienyl anion or potassium hydrotris(pyrazolyl)borate, the oxidative addition intermediates are transformed into η^5-CpMo(CO)$_2$(allyl) or TpMo(CO)$_2$(allyl) complexes, respectively. Although other allylic moieties have been studied as precursors to η^5-CpMo(CO)$_2$(η^3-allyl) complexes,[22] allylic acetates represent the best potential precursors to (π-allyl)molybdenum complexes, particu-

(37) Larsson, E. M.; Akermark, B. *Tetrahedron Lett.* **1993**, *34*, 2523.
(38) Tsuji, J. *Pure Appl. Chem.* **1981**, *53*, 2371.
(39) Consiglio, G.; Waymouth, R. M. *Chem. Rev.* **1989**, *89*, 257.
(40) Trofimenko, S. *Chem. Rev.* **1993**, *93*, 943.
(41) Trofimenko, S. *Chem. Rev.* **1972**, *72*, 497.
(42) Trofimenko, S. *Acc. Chem. Res.* **1971**, *4*, 17.
(43) Trofimenko, S. *J. Am. Chem. Soc.* **1967**, *89*, 3170.
(44) Ipaktschi, J.; Hartmann, A.; Boese, R. *J. Organomet. Chem.* **1992**, *434*, 303.
(45) Ipaktschi, J.; Hartmann, A. *J. Organomet. Chem.* **1992**, *431*, 303.
(46) Trofimenko, S. *J. Am. Chem. Soc.* **1969**, *91*, 588.
(47) Faller, J. W.; Thomsen, M. E.; Mattina, J. J. *J. Am. Chem. Soc.* **1971**, *93*, 2642.
(48) Lukas, J.; Ramakers-Blom, J. E.; Hewitt, T. G.; De Boer, J. J. *J. Organomet. Chem.* **1972**, *46*, 167.
(49) Åkermark, B.; Vitagliano, A. *Organometallics* **1985**, *4*, 1275.
(50) Åkermark, B.; Hansson, S.; Vitagliano, A. *J. Am. Chem. Soc.* **1990**, *112*, 4587.
(51) Sjogren, M.; Hansson, S.; Norrby, P. O.; Akermark, B.; Cucciolito, M. E.; Vitagliano, A. *Organometallics* **1992**, *11*, 3954.
(52) Mérour, J. Y.; Charrier, C.; Benaïm, J.; Roustan, J. L.; Commereuc, O. *J. Organomet. Chem.* **1972**, *39*, 321.
(53) Joshi, V. S.; Sathe, K. M.; Nandi, M.; Chakrabarti, P.; Sarkar, A. *J. Organomet. Chem.* **1995**, *485*, C1.

Table 1. Synthesis of (Tris(pyrazolyl)borato)allylmolybdenum Dicarbonyl Complexes Bearing Alkyl, Aryl, and Carbomethoxy Substituents

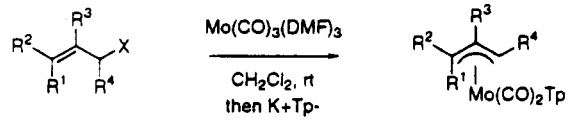

allylic substrate	(π-allyl)molybdenum complex R¹	R²	R³	R⁴	cpd no.	yield (%)
allyl acetate	H	H	H	H	**1**	77
(*E*)- and (*Z*)-1-bromo-2-butene	H	Me	H	H	**2a**	38
	Me	H	H	H	**2b**	19
(*E*)-1-acetoxy-2-pentene	H	Et	H	H	**3a**	75
(*Z*)-1-acetoxy-2-pentene	Et	H	H	H	**3b**	71
3-acetoxy-4-methyl-1-pentene	H	*i*-Pr	H	H	**4a**	87
	i-Pr	H	H	H	**4b**	5
3-acetoxy-4,4-dimethyl-1-pentene	H	*t*-Bu	H	H	**5a**	46
3-acetoxy-3-cyclohexyl-1-propene	H	C_6H_{11}	H	H	**6a**	74
	C_6H_{11}	H	H	H	**6b**	7
(*E*)-cinnamyl acetate	H	Ph	H	H	**7a**	91
(*Z*)-cinnamyl acetate	Ph	H	H	H	**7b**	49
3-acetoxy-3-(4-methoxyphenyl)-1-propene	H	*p*-MeOPh	H	H	**8a**	92
3-acetoxy-3-(4-(trifluoromethyl)phenyl)-1-propene	H	*p*-CF_3Ph	H	H	**9a**	86
(*E*)-4-acetoxy-2-pentene	Me	H	H	Me	**10a**	66
	H	Me	H	Me	**10b**	6
(*E*)-4-acetoxy-4-phenyl-2-butene	H	Me	H	Ph	**11a**	62
	Me	H	H	Ph	**11b**	19
(*E*)-3-acetoxy-1,3-diphenyl-1-propene	H	Ph	H	Ph	**12a**	51
	Ph	H	H	Ph	**12b**	26
(*E*)-5-acetoxy-2,2,6,6-tetramethyl-3-heptene	H	*t*-Bu	H	*t*-Bu	**13a**	4
	t-Bu	H	H	*t*-Bu	**13b**	9
(*E*)-3-acetoxy-4,4-dimethyl-1-phenyl-1-pentene	H	*t*-Bu	H	Ph	**14a**	81
4-acetoxy-2-methyl-2-pentene	Me	Me	H	Me	**15a**	70
mixture of (*E*)- and (*Z*)-4-acetoxy-3-methyl-2-pentene	H	Me	Me	Me	**16a**	3
	Me	H	Me	Me	**16b**	48
methyl (*Z*)-4-bromo-2-butenoate	H	CO_2Me	H	H	**17a**	61

larly if functionally rich and enantiomerically pure π-complexes are desired. However, using the published reaction conditions [prolonged refluxing with $Mo(CO)_3(CH_3CN)_3$ in CH_3CN] only simple allylic acetates are effective precursors to (π-allyl)molybdenum complexes. For the present study, the simple expedient of using CH_2Cl_2, a noncoordinating solvent, and $Mo(CO)_3(DMF)_3$,[54] an easy-to-prepare source of zerovalent molybdenum, allowed conversion of a wide range of allylic acetates to (π-allyl)molybdenum complexes under very mild conditions. These conditions have also proven of use in the synthesis of more elaborate and enantiomerically pure (π-allyl)molybdenum complexes, and these latter details will be provided in a future publication.[55]

Using the new protocol, the parent complex **1**, $TpMo(CO)_2$(allyl), and (π-allyl)molybdenum complexes **2**–**17** bearing alkyl, aryl, and carbomethoxy substituents were prepared by the rapid dropwise addition of 1.0 to 1.5 equiv of an allylic acetate precursor (in two cases a readily available allylic bromide was used) to a room-temperature dichloromethane solution of 1 equiv of $Mo(CO)_3(DMF)_3$. After 0.25–24 h (the more substituted substrates required longer reaction times), addition of 1 equiv of solid potassium hydrotris(1-pyrazolyl)borate produced a bright yellow-green solution from which the $TpMo(CO)_2(\eta^3$-allyl) complexes depicted in Table 1 were obtained by flash chromatography and/or recrystallization. With the exception of the more highly substituted and sterically congested allylic complexes **5** and **13**–**16**, which decomposed as solids or on standing in solution, the $TpMo(CO)_2$(allyl) complexes were robust yellow to yellow-orange solids preparable in good to excellent yields. The complexes were stable in solution and decomposed only slowly on standing exposed to air.

Synthesis of Alkyl- and Aryl-Monosubstituted $TpMo(CO)_2(\eta^3$-allyl) Complexes. A 2.2 to 1.0 mixture of the *syn* and *anti* methyl complexes **2a** and **2b** was prepared by treatment of a CH_2Cl_2 solution of $Mo(CO)_3(DMF)_3$ with the commercially available mixture of (*E*)-1-bromo-2-butene, (*Z*)-1-bromo-2-butene, and 3-bromo-1-butene (80:10:10). *Syn*-Et and *syn*-Ph complexes **3a** and **7a** were formed stereospecifically without contamination from the *anti*-isomers by treatment of a CH_2Cl_2 solution of $Mo(CO)_3(DMF)_3$ with the corresponding (*E*)-disubstituted 1° allylic acetates. The isomeric *anti*-Et and *anti*-Ph complexes **3b** and **7b** were formed stereospecifically in the same manner from the corresponding (*Z*)-disubstituted 1° allylic acetates, thus demonstrating the kinetic retention of olefin geometry in the oxidative addition to disubstituted allylic acetates. All other alkyl- and aryl-monosubstituted complexes (**4**–**6**, **8**, and **9**) were prepared, as above, from the 1,3-transposed 2° allylic acetates. Varying mixtures of the *syn*- (**a**) and *anti*- (**b**) isomers were generated in which the *syn*-isomer was kinetically favored with ratios ranging from 7.8 to 1.0 in the case of the cyclohexyl complex **6** to >20 to 1 for the *t*-Bu **5** and aryl complexes **8** and **9**.

Pure *syn*- and *anti*-isomers of all monosubstituted allyls were configurationally stable in solution at room

(54) Pasquali, M.; Leoni, P.; Sabatino, P.; Braga, D. *Gazz. Chim. Ital.* **1992**, *122*, 275.
(55) Ward, Y. D.; Villanueva, L. A.; Liebeskind, L. S. Unpublished results.

temperature. That the η^3-allyl substituent kinetic stereochemistry is established in the oxidative addition of Mo(0) to the allylic acetates and not on addition of potassium trispyrazoylborate to the Mo allyl intermediate may be inferred from the stereospecific preparation of complexes **3a,b** and **7a,b**. In addition, none of the *syn*-Et isomer **3a** is formed from (*Z*)-2-pentenyl acetate, even when the addition of KTp is delayed 24 h after treatment of (*Z*)-2-pentenyl acetate in CH_2Cl_2 with Mo(CO)$_3$(DMF)$_3$. None of the *anti*-Et isomer **3b** is formed from (*E*)-2-pentenyl acetate under the same conditions, thus demonstrating that the Tp allyl precursor [(η^3-R-C_3H_4)Mo(OAc)(DMF)$_2$(CO)$_2$] does not equilibrate rapidly to *syn*/*anti* mixtures before addition of KTp.

Synthesis of Functionalized 1-Substituted Complexes (OMe, OAc, and COOMe). TpMo(CO)$_2$(allyl) complexes bearing an electron-withdrawing (COOMe, **17a**) and electron-donating (OMe, **18a**; OAc, **19a**) substituents were prepared in order to probe the effect of electronic parameters on the *syn*−*anti* isomerization. The methoxy- and acetoxy-substituted complexes were generated by a new procedure shown in eq 1,[56] while

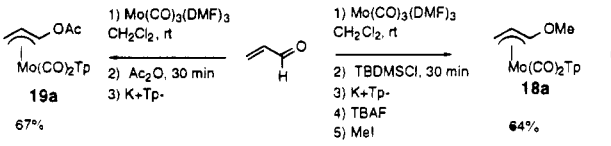

(1)

the general protocol used for the examples in Table 1 was suitable for the preparation of the carbomethoxy-substituted analog from methyl (*E*)-4-bromo-2-butenoate. All three new complexes were generated kinetically as their respective *syn* isomers.

Synthesis of Disubstituted Acyclic TpMo(CO)$_2$(η^3-allyl) Complexes. 1,3-Disubstituted (π-allyl)molybdenum complexes **10**−**14** bearing alkyl and aryl substituents were obtained uneventfully from allylic acetate precursors. However, unlike the 1-monosubstituted allyls, the 1,3-disubstituted allyls were configurationally unstable in solution at room temperature and were usually isolated after flash chromatography as thermodynamic mixtures of *syn*/*syn* (**a**) and *syn*/*anti* (**b**) isomers. An exception was the preparation of complex **12** from (*E*)-1-acetoxy-1-phenyl-2-butene which gave, after flash chromatography, an initial 3 to 1 mixture of *syn*/*syn* (**12a**) vs *syn*-Ph/*anti*-Me (**12b**) isomers (kinetic retention of olefin geometry in the allyl product), but the complex did equilibrate on standing in solution (see below). Complexes **10**−**12** were stable indefinitely as solids exposed to air and decomposed only slowly (over months) in solution at ambient temperature. Complexes **13a,b** which bear bulky *t*-Bu substituents decomposed rapidly both in solution and as solids even in the absence of O_2. Complex **14a** which bears a Ph and a *t*-Bu substituent decomposed rapidly in solution but was stable in the solid state.

Synthesis of Trimethyl-Substituted TpMo(CO)$_2$(η^3-allyl) Complexes. Syntheses of the 1,1,3- and 1,2,3-trimethylallyls were carried out with the standard protocol using Mo(CO)$_3$(DMF)$_3$ and the corresponding allylic acetates. The complexes were somewhat unstable both in solution and as solids. The 1,1,3-trimethyl complex was isolated as a single isomer in which the C(3) methyl group occupied the *syn* position (**15a**), while the 1,2,3-trimethyl complex was isolated as an equilibrium mixture of the *syn*/*syn* (**16a**) and *syn*/*anti* (**16b**) isomers in a 1.0 to 18.0 ratio.

Equilibration Studies. General Comments. Monosubstituted allyls were equilibrated by heating a sealed-tube ^{1}H NMR sample in C_6D_6 in an oil bath maintained at 120−125 °C. Heating was continued until no further changes in the *syn*/*anti* ratios were observed by ^{1}H NMR. Complexes bearing substituents at both ends of the allyl equilibrated at room temperature in $CDCl_3$. *Syn*- and *anti*-isomer assignments were made on the basis of ^{1}H NMR coupling constants and chemical shifts trends. The assignments were corroborated with X-ray crystallographic studies of the *syn*-ethyl complex **3a**, *anti*-methyl complex **2b**, *syn*/*anti*-1,3-dimethyl complex **10b**, *syn*-phenyl/*anti*-methyl complex **11b**, *syn*/*syn*-diphenyl complex **12a**, *syn*-carbomethoxy complex **17a**, and *syn*-methoxy complex **18a**. Relevant ^{1}H NMR data are listed in Tables 2 and 3. The ^{1}H NMR chemical shift and coupling constant trends for allyl protons on unsubstituted or on alkyl or aryl bearing terminal positions (trends for oxygen bearing substituted allyls are described below in the pertinent section) are summarized as follows:

Protons occupying *anti* positions exhibited significantly larger coupling constants (8.7−12.2 Hz) to the central proton than did *syn* protons (5.4−8.1 Hz). Other trends in the magnitude of the coupling constants are described below.

Protons occupying *anti* positions resonated 1.5−2.0 ppm upfield from protons occupying *syn* postions when the allyl carbons bear similar substituents. *Anti* protons resonated in the range 1.04−3.85 ppm in alkyl-bearing allyls and between 3.31 and 4.52 ppm for aryl-bearing allyls. *Syn* protons of alkyl-bearing allyl carbons appeared between 3.41 and 4.36 ppm, while *syn* protons on aryl-bearing allyl carbons resonated between 5.41 and 5.50 ppm.

Equilibration of Deuterium-Substituted Allyl 1. Complex **1**, enriched in deuterium in the *anti* position, was prepared by the standard method from (*Z*)-3-acetoxy-1-deuterio-1-propene. Unlike *E* and *Z* alkyl- and aryl-substituted allyl acetates, the deuterium was not cleanly retained in the *anti* position during the oxidative addition; for reasons that are not currently understood, the labeled complex was generated with 61% of the deuterium in the *anti* position and 39% in the *syn* position as shown by ^{2}H NMR. The complex did not equilibrate over a 1 week period while dissolved in C_6H_6; however, on heating of the sample to 120 °C for 2 h, the label was completely scrambled between the *syn* and *anti* positions.

Equilibration of Monoalkyl-Substituted Allyls. Both *syn*- and *anti*-isomers of complexes **2**−**6** were configurationally stable in C_6D_6 at room temperature over a period of 2 weeks. In addition, *syn*-*i*-Pr complex **4a** did not equilibrate after 4 h at 60 °C; however, on heating to 120 °C in a sealed NMR tube all complexes equilibrated to mixtures of *syn*- and *anti*-allyl isomers within 2 h. The *syn*-Me and *syn*-Et substituted complexes **2a** and **3a** gave mixtures in which the *anti* isomer

(56) Ward, Y. D.; Villanueva, L. A.; Allred, G. D.; Liebeskind, L. S. Unpublished results.

Table 2. ^{1}H NMR Characterization of 1-Monosubstituted (Tris(pyrazolyl)borato)allylmolybdenum Dicarbonyl Complexes

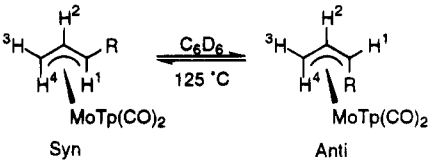

allyl complex (no.)	*anti* to *syn* ratio	chem shifts of terminal allyl protons (ppm) H^1	H^3	H^4	coupling const of terminal protons to central proton (Hz) H^1	H^3	H^4
allyl, R = H (**1**)		1.51	3.63		10.0	6.0	
syn-Me (**2a**)	3.8	2.33	3.41	1.25	8.7	5.4	9.9
anti-Me (**2b**)		4.36	3.65	2.29	6.5	7.2	10.5
syn-Et (**3a**)	4.1	2.31	3.42	1.24	9.5	6.8	9.5
anti-Et (**3b**)		4.33	3.62	2.22	7.6	7.6	10.4
syn-*i*-Pr (**4a**)	1.3	2.32	3.43	1.11	10.8	6.6	8.7
anti-*i*-Pr (**4b**)		4.27	3.70	1.84	7.1	obscd[a]	9.9
syn-*t*-Bu (**5a**)	1.3	2.64	3.36	1.04	11.7	6.6	8.4
anti-*t*-Bu (**5b**)		4.54	3.57	2.48	8.1	obscd[a]	9.9
syn-*c*-Hex (**6a**)	1.1	2.29	3.41	1.08	10.8	6.6	8.7
anti-*c*-Hex (**6b**)		4.26	3.70	2.55	8.1	obscd[a]	10.2
syn-Ph (**7a**)	all *syn*	3.31	3.61	1.41	10.8	6.9	9.0
anti-Ph (**7b**)		5.50	3.86	2.62	8.1	7.2	10.8
syn-*p*-MeOC$_6$H$_4$ (**8a**)	all *syn*	3.40	3.58	1.38	10.5	6.6	9.0
syn-*p*-CF$_3$C$_6$H$_4$ (**9a**)	all *syn*	3.21	3.66	1.45	10.5	6.6	9.0
syn-CO$_2$Me (**17a**)	3.7	2.49	3.65	1.42	9.5	6.5	9.5
anti-CO$_2$Me (**17b**)		4.47	3.90	3.12	6.9	7.5	10.5
syn-OMe (**18a**)	all *syn*	4.59	3.31	1.27	8.1	7.2	9.0
syn-OAc (**19a**)	3.3	5.43	3.39	1.49	7.2	7.5	9.3
anti-OAc (**19b**)		7.75	3.80	2.38	4.8	6.9	10.2

[a] Obscd = obscured.

Table 3. ^{1}H NMR Characterization of 1,3-Disubstituted (Tris(pyrazolyl)borato)allylmolybdenum Dicarbonyl Complexes

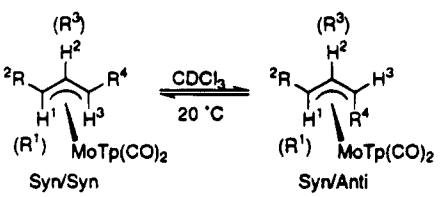

cpd no.	*syn*/*anti* to *syn*/*syn* ratio	configuration of allyl substituents R^1	R^2	R^3	R^4	chem shifts of terminal protons H^1	H^3	coupling const to central proton H^1	H^3
syn/*syn* **10a**	12.5	H	Me	H	Me	=H^3	2.21	=H^3	10.2
syn/*anti* **10b**		H	Me	H	Me	3.20	4.09	11.9	6.5
syn/*anti* **16b**	18.0	H	Me	Me	Me	2.62	4.09	none	none
3-*syn* **15a**	all R^4 *syn*	Me	Me	H	Me	none	3.16	none	12.2
syn/*syn* **13a**	2.5	H	*t*-Bu	H	*t*-Bu	=H^3	2.61	=H^3	10.5
syn/*anti* **13b**		H	*t*-Bu	H	*t*-Bu	3.85	4.00	11.4	obscd
syn/*syn* **11a**	4.7	H	Ph	H	Me	3.48	1.90	9.9	9.9
syn/*anti* **11b**		H	Ph	H	Me	4.05	4.29	11.1	6.8
syn/*syn* **14a**	0.0	H	Ph	H	*t*-Bu	3.68	2.64	10.2	10.8
syn/*syn* **12a**	0.5	H	Ph	H	Ph	=H^3	3.49	=H^3	10.2
syn/*anti* **12b**		H	Ph	H	Ph	4.52	5.41	11.7	8.4

predominated over the *syn* isomer (3.8 to 1.0 and 4.1 to 1.0, respectively). Confirmation of equilibration was achieved by thermolysis of the pure *anti*-Et complex **3b** to an identical 4.1 to 1.0 mixture of *anti*:*syn* complexes. Sterically more demanding alkyl substituents gave diminished proportions of the *anti* isomer at equilibrium (*anti*/*syn*: *t*-Bu, 1.3 to 1.0; isopropyl, 1.3 to 1.0; cyclohexyl, 1.1 to 1.0).

Anti-Me complex **2b** and *syn*-Et complex **3a** were both characterized by X-ray crystallography (Figures 6 and 7 and Tables 7−10); thus their ^{1}H NMR spectra serve as specific examples of how other isomers in this and the subsequent sections were identified. For *syn*-Et complex **3a** the protons absorbing at 2.31 ppm (ddd) and 1.24 ppm (dd) are readily assigned the *anti* configuration by the magnitude of their coupling to the central proton (9.5 Hz apiece); the *syn* proton in this complex resonates at 3.42 ppm (dd) with a coupling to the central proton of 6.8 Hz. In *anti*-Me complex **2b** the *anti* proton resonates at 2.29 ppm (dd) with a coupling to the central proton of 10.5 Hz; the two *syn* protons in this complex are found at 4.36 ppm (dq) and 3.65 ppm (dd) with couplings to the central proton of 6.5 and 7.2 Hz, respectively (Table 2).

Equilibration of Monoaryl-Substituted Allyls. The *syn*-Ph complex **7a** did not equilibrate to the *anti*

isomer at temperatures up to 145 °C, at which point the complex slowly decomposed. In order to verify the equilibrium position of the phenyl-substituted derivative, the *anti*-Ph complex **7b** was stereospecifically prepared from (*Z*)-cinnamyl acetate. This complex equilibrated rapidly at 120 °C to give the pure *syn*-Ph complex **7a**. *Syn*-*p*-MeOC$_6$H$_4$ and *syn*-*p*-CF$_3$C$_6$H$_4$ complexes **8a** and **9a** showed no evidence of equilibration to their *anti* isomers after prolonged heating at 120 °C, and at temperatures exceeding 150 °C these complexes decomposed. The *anti* isomers of these complexes were not prepared and studied.

Aryl-substituted complexes **8a** and **9a** were assigned the *syn* configuration by comparison of the ^{1}H NMR spectrum of each to the spectrum of the stereospecifically prepared *syn*- and *anti*-substituted isomeric pair **7a,b** and by comparison to the spectra of the X-ray crystallographically characterized complexes **11b** (*syn*-Ph/*anti*-Me) and **12a** (*syn*/*syn*-diphenyl). The general trends observed in the ^{1}H NMR spectra of all the allyls analyzed in this study are fully consistent with this assignment. The presence of an aryl substituent at the 1-position of the allyl induces an approximate 1−2 ppm downfield shift of the geminal allyl proton relative to such a proton on an alkyl-substituted allyl carbon.

Equilibration of Mono-Substituted Allyls Bearing Electron-Donating and Electron-Withdrawing Groups. *Syn*-CO$_2$Me complex **17a**, *syn*-MeO complex **18a**, and *syn*-AcO complex **19a** were configurationally stable in solution at ambient temperature. Equilibration of **17a** to a 3.7 to 1.0 mixture of **17b/17a** (*anti*/*syn*) was accomplished by heating a C$_6$D$_6$ solution in a sealed tube to 125 °C for 2 h. Despite the different electronic nature of carbomethoxy and alkyl groups, complexes **17a** and **17b** showed equilibrium ratios and ^{1}H chemical shift and coupling constant data that were very similar to those of monomethyl and -ethyl complexes **2** and **3** in the monoalkyl-substituted series (Table 3).

Heating *syn*-MeO complex **18a** to temperatures exceeding 150 °C (the complex began to decompose at this temperature) produced no measurable amount of the *anti* isomer. However, *syn*-AcO complex **19a** readily equilibrated at 120 °C in C$_6$D$_6$ to a 3.3 to 1.0 mixture of **19b/19a** (*anti*/*syn*). The reason for the divergent behavior of the methoxy- and acetoxy-substituted complexes is discussed below. The ^{1}H chemical shift and coupling constant data for the *syn* and *anti* protons on the unsubstituted end of the allyl are very similar to those in the alkyl series; however, the proton on the oxygen-bearing allyl carbon experiences a downfield shift of approximately 3 ppm in both the *syn* and *anti* configurations when compared to the monoalkyl series. In addition, the coupling to the central proton is approximately 2 Hz less in both configurations when compared to the constants of the monoalkyl series; both of these effects are attributable to the greater electronegativity of the heteroatom substituent.[57]

Equilibration of Dialkyl- and Trialkyl-Substituted Allyls. 1,3-Disubstituted allyls were fluxional in solution at room temperature. Immediately after its preparation from (*E*)-4-acetoxy-2-pentene, ^{1}H NMR analysis of an aliquot of complex **10** revealed a 2 to 1 ratio of the *syn*/*anti* (**10b**) to the *syn*/*syn* (**10a**) isomers. However, within 2 h at room temperature, the ratio increased to a final value of 12.5 to 1.0. The 1,2,3-trimethylated complex **16** showed similar behavior; however, the steric effect of the central methyl substituent increased the final *syn*/*anti* to *syn*/*syn* ratio to 18.0 to 1.0. In order to probe the possibility of placing two subsituents in an *anti* position, 1,1,3-trimethylated complex **15a** was prepared; however, this allyl existed exclusively as the 3-*syn* isomer. As was seen in the monosubstituted series, sterically demanding substituents at the allylic termini diminished the preference for the *syn*/*anti* isomer; the 1,3-di-*tert*-butyl complex **13** equilibrated to a 2.5 to 1.0 mixture favoring the *syn*/*anti* isomer **13b**.

Structure assignments for the dialkyl- and trialkyl-substituted complexes were based on the same ^{1}H NMR trends in chemical shifts and coupling constants delineated above for the monosubstituted series, in addition to the X-ray structure determination of *syn*/*anti*-1,3-diMe complex **10b** described below. Furthermore, the symmetry differences between the minor *syn*/*syn* isomers and the major *syn*/*anti* isomers for complexes **10**, **13**, and **16** (1,3-di-Me, 1,3-di-*t*-Bu, and 1,2,3-tri-Me) allowed easy assignment by ^{1}H NMR.

Equilibration of Disubstituted Allyls Possessing Aryl Substituents. The π-allyl complex bearing both a methyl and a phenyl substituent at the allylic termini existed as a mixture of two isomers in a 4.7 to 1.0 ratio at equilibrium. The minor isomer was assigned the configuration *syn*-Ph/*syn*-Me **11a** on the basis of the 9.9 Hz coupling constant between each terminal allyl proton and the central proton. The major isomer was assigned the *syn*-Ph/*anti*-Me configuration **11b** based on (1) the presence of an apparent pentet at 4.29 ppm with a coupling constant of 6.8 Hz to the central proton, both typical of a *syn* hydrogen substituent, and (2) the presence of a doublet at 4.05 ppm with a coupling constant of 11.1 Hz to the central allyl proton, the latter typical for an *anti* hydrogen substituent geminal to an aryl group. This analysis was confirmed by the X-ray crystallographic analysis of *syn*-Ph/*anti*-Me complex **11b** described below.

On the basis of ^{1}H NMR coupling constants to the central allyl proton, the π-allyl complex bearing a *tert*-butyl and a phenyl substituent at the allylic termini was assigned the *syn*/*syn* configuration **14a**, exclusively. However, on heating or prolonged standing in solution at ambient temperature, this complex decomposed before any evidence of equilibration to a second isomer could be obtained.

The 1,3-diphenylallylic complex **12** existed as a 2 to 1 mixture of *syn*/*syn* (**12a**) to *syn*/*anti* (**12b**) isomers in solution at room temperature. The major isomer was easily assigned the *syn*/*syn* configuration on the basis of the symmetry reduction of signals in both the ^{1}H and ^{13}C NMR. Further confirmation of the structure was achieved by X-ray crystallography as described below.

Origin of the Thermodynamic Preference for the *Anti* Configuration: X-ray Crystallographic Studies. General Comments. In order to understand the structural features underlying the stability of *syn* and *anti* isomers of Tp-ligated molybdenum allyls, solid state structures of the following complexes were determined by X-ray crystallography: unsubstituted allyl **1** (Figure 5, Tables 5 and 6), *anti*-Me **2b** (Figure 6, Tables

(57) Schaefer, T. *Can. J. Chem.* **1962**, *40*, 14.

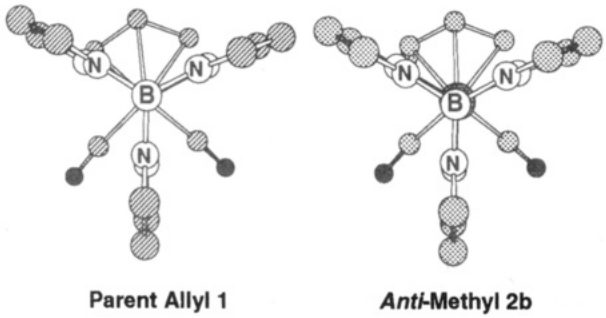

Figure 2. View of complexes **1** and **2b** down the B−Mo axis.

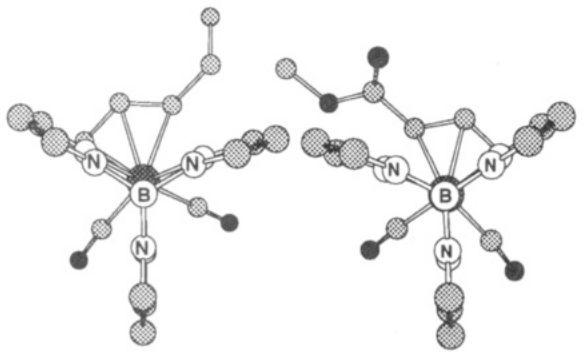

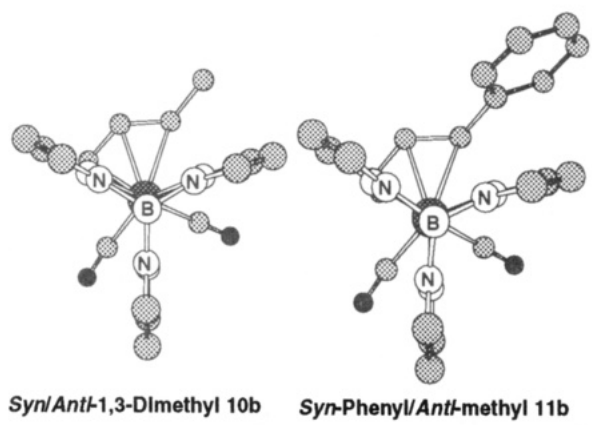

Figure 3. View of complexes **3a**, **17a**, **10b**, and **11b** down the B−Mo axis.

7 and 8), *syn*-Et **3a** (Figure 7, Tables 9 and 10), *syn*/*anti*-1,3-diMe **10b** (Figure 9, Tables 17 and 18), *syn*-Ph/*anti*-Me **11b** (Figure 10, Tables 11 and 12), *syn*/*syn*-1,3-diPh **12a** (Figure 11, Tables 13 and 14), *syn*-CO_2Me **17a** (Figure 8, Tables 15 and 16), *syn*-methoxy **18a** (Figure 12, Tables 19 and 20).

In order to clarify the following discussion of the individual structures, it is helpful to visually inspect the significant and general geometric features of the structurally characterized complexes. Unsubstituted complex **1** and *anti*-Me complex **2b** display a nearly symmetrical arrangement of the carbonyl, allyl, and Tp ligands, while complexes that bear at least one *syn* substituent display significant distortion in the arrangement of ligands; these features are most easily seen when viewing a 3D model along the boron−molybdenum axis using the Tp ligand's 3-fold axis of symmetry as a reference point (Figures 2 and 3).

In every case, with the exception of the *syn*-MeO complex **18a** which is discussed below, the complexes

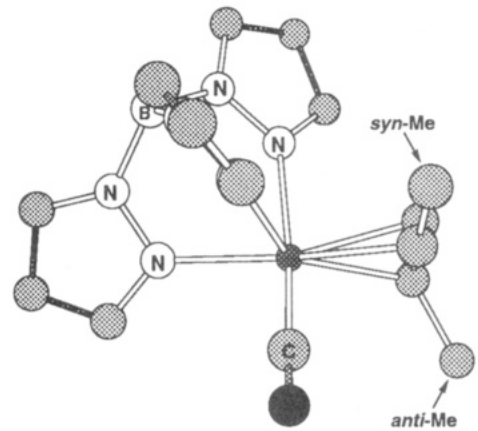

Figure 4. View of **10b** with carbonyl ligands eclipsed.

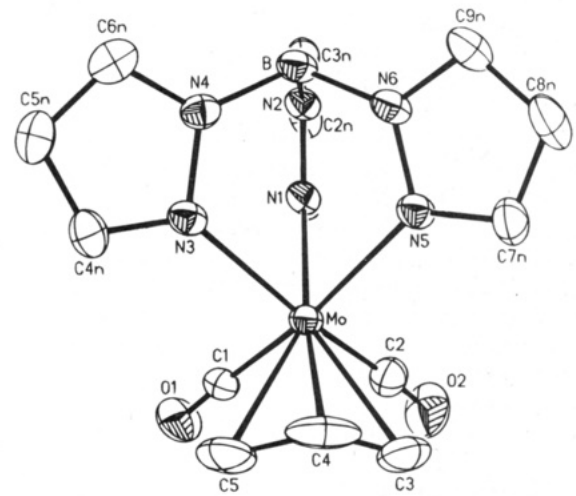

Figure 5. ORTEP of complex **1**.

orient themselves such that a *syn* substituent is rotated into the uncongested cleft between two pyrazole rings. Two other general features are obvious: (1) *syn* substituents lie in the plane defined by the three allyl carbons, while *anti* substituents are significantly distorted out of the allyl plane (this feature has several consequences which are described below), and (2) the plane defined by the three allyl carbons is nearly periplanar with that defined by the $Mo(CO)_2$ fragment (Figure 4).

Unsubstituted Complex 1. The crystal structure of parent allyl **1** (Tables 5 and 6 and Figure 5) serves as a useful reference point for the discussion of substituted allyl complexes that follows. When considering the allyl ligand as a single substituent, the complex possesses a six coordinate octahedral geometry, which defines the Tp pyrazole unit *trans* to the allyl as unique. The other two coordinated pyrazole nitrogens adopt identical *cis* positions in a plane defined by the metal and the two *cis* carbonyl ligands—for clarity in the discussion below this is referred to as the equatorial plane and the unique pyrazole will be referred to as the *trans* pyrazole. As mentioned above, the plane defined by the allyl ligand is nearly periplanar to that defined by the metal center and the carbonyl carbons. In addition, the allyl adopts an *exo* conformation with respect to the $Mo(CO)_2$ unit in which the terminal carbon atoms of the allyl (C(3), C(5)) eclipse the carbonyl carbon atoms (C(1) and C(2)) and the central carbon of the allyl (C(4)) eclipses the Mo. Rotation by 180° about

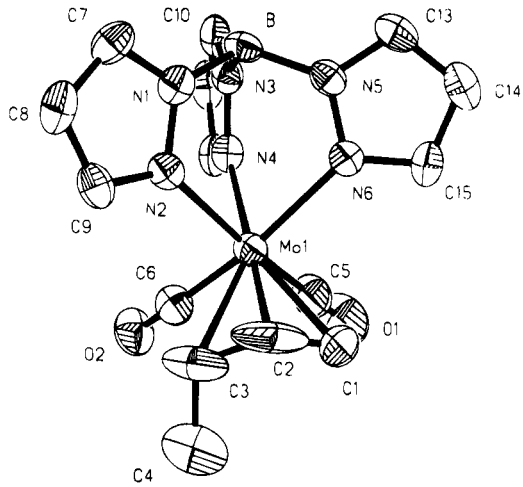

Figure 6. ORTEP of *anti*-methyl complex **2b**.

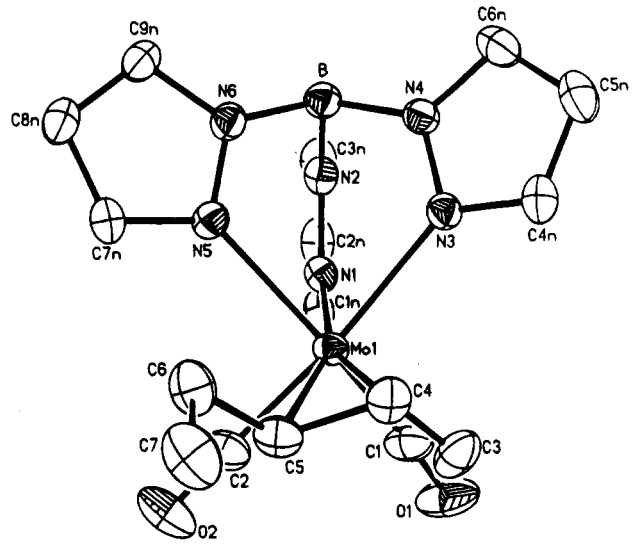

Figure 7. ORTEP of *syn*-ethyl complex **3a**.

the Mo–allyl centroid axis would produce the *endo* conformer. In solution the ^{1}H NMR spectrum of complex **1** demonstrates symmetry reduction of signals, an observation corroborated in the solid state where the allyl adopts a nearly symmetrical arrangement with respect to the TpMo(CO)$_2$ fragment. The allyl central proton is projected into the cleft defined by the two identical equatorial plane pyrazole ligands. Inspection of this structure indicates two types of close contacts: between the two *anti* protons and, most importantly, between the *syn* protons and the C(4N) and C(7N) protons of the equatorial pyrazole ligands. As shown below, it is the latter nonbonded interaction that destabilizes the *syn* configuration with respect to the *anti*.

***Anti*-Methyl Complex 2b.** Inspection of the structure of *anti*-Me complex **2b** (Tables 7 and 8 and Figure 6) reveals that, other than the presence of the methyl group, **2b** possesses bond lengths and a symmetrical orientation with respect to the TpMo(CO)$_2$ fragment that are similar to those of the unsubstituted allyl **1**. Distortion of the methyl group 47° out of the plane of the allyl minimizes nonbonded steric repulsion between the methyl group and the carbonyl group *cis* to it.

***Syn*-Ethyl Complex 3a.** In comparison to the *anti*-Me complex **2b**, *syn*-Et complex **3a** (Tables 9 and 10 and Figure 7) shows three distinct types of distortion: (1) the three carbon allyl fragment is rotated slightly away from a full eclipse with the Mo(CO)$_2$, (2) the Tp ligand has rotated about the B–Mo axis to move one equatorial plane pyrazole ligand away from the adjacent *syn*-Et substituent, and (3) the two ends of the allyl have significantly different bond distances to the metal center. The three effects are complementary in that all serve to decrease the nonbonded interaction between the *syn* ethyl group and the proximal C(7N) pyrazole hydrogen.

The extent of allyl rotation with respect to the Mo(CO)$_2$ fragment (quantified by the dihedral angle defined by the centroid of the allyl fragment, the central allyl carbon, the molybdenum atom, and the centroid of the Mo(CO)$_2$ unit) in a perfectly symmetrical arrangement would be equal to 0°, and in the nearly symmetrical complexes **1** and **2b** the rotation is 6 and 4°, respectively. In *syn*-Et complex **3a** it increases to 10°. In addition, the Tp ligand is rotated with respect to the Mo(CO)$_2$ fragment in the opposite direction; the magnitude of this rotation may be approximated by $^1/_2$ the difference of the two dihedral angles N(2)–B–Mo–C(2) and N(2)–B–Mo–C(1); this rotation would be equal to 0° in a symmetrical arrangement and is 5 and 3° for nearly symmetrical complexes **1** and **2b** but is 11° for *syn*-Et complex **3a**. As is found in all *syn* substituents in the structures below, the methylene of the Et group is nearly coplanar with the allyl (C(6)–C(5)–C(4)–C(3) dihedral angle = 175°); however, the methyl group is nearly perpendicular to the allyl plane and projected away from the metal center (C(7)–C(6)–C(5)–C(4) dihedral angle = 87°). Rotation of the ligands in allyl complex **3a** decreases the steric interaction of the Et substituent with the proximal pyrazole proton by bringing the Et group into the relatively uncongested cleft of the equatorial plane pyrazole ligands. In addition, the bond between the Mo and the substituted end of the allyl is 0.13 Å longer than the bond to the unsubstituted end of the allyl, and the Mo to central carbon bond distance is about 0.05 Å longer than in the unsubstituted complex **1** or *anti*-Me complex **2b**. These factors contribute to a noticeable distortion of the allyl from η^3 toward η^1. It is clear from these distortions that it is the steric repulsion between the ethyl group and the proximal pyrazole hydrogen that destabilizes the *syn* configuration relative to the *anti* to the extent that the *anti* isomer predominates at equilibrium.

***Syn*-Carbomethoxy Complex 17a.** The structure of *syn*-CO$_2$Me complex **17a** (Tables 15 and 16 and Figure 8) is similar to that of the *syn*-Et complex, a result not unexpected given their similar *syn*:*anti* ratios at equilibrium. The allyl is rotated with respect to the Mo(CO)$_2$ fragment by 9° while the Tp ligand is rotated with respect to the Mo(CO)$_2$ fragment in the opposite direction by 8°. The substituted allyl terminus is farther from the metal center than the unsubstituted terminus by 0.04 Å.

One additional feature of this structure should be noted: the carbomethoxy substituent is nearly coplanar (O(1)–C(1)–C(2)–C(3) dihedral angle = 7°) with the allyl ligand, a structural feature most likely representing some resonance delocalization between the two π-systems. One might have expected that such resonance would have stabilized the *syn* isomer with respect

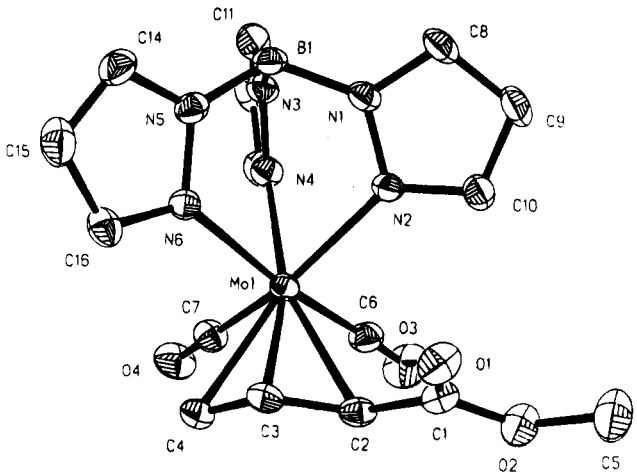

Figure 8. ORTEP of *syn*-carbomethoxy complex **17a**.

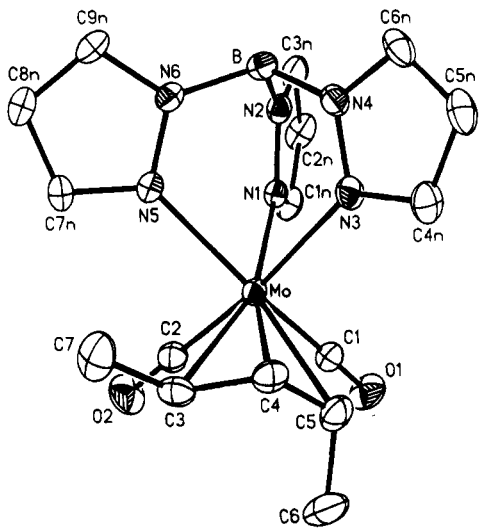

Figure 9. ORTEP of *syn*/*anti*-1,3-dimethyl complex **10b**.

to the *anti* isomer since the *syn* orientation allows greater coplanarity of the two π systems; however, the *anti*:*syn* equilibrium ratio of 3.7 to 1.0 suggests that resonance stabilization is not very significant in this case or, in part, is compensated for by increased steric interaction between the in-plane methoxy group and the proximal pyrazole hydrogen (compare to *syn*-**3a** and *syn*-**18a**).

***Syn*/*Anti*-Dimethyl Complex 10b.** Because of the presence of one *syn*-substituent, the structure of the *syn*/*anti*-1,3-dimethylated complex **10b** (Tables 17 and 18 and Figure 9) mimics that of the *syn*-Et complex. The *anti*-methyl group is deflected out of the allyl plane by 43° while the *syn*-methyl is in the allyl plane. The allyl is rotated with respect to the $Mo(CO)_2$ fragment by 13° and the Tp ligand is rotated in the opposite direction with respect to the $Mo(CO)_2$ fragment by 15° bringing the *syn* methyl group into the open cleft of the equatorial pyrazole ligands. Also, the *syn*-substituted end of the allyl is 0.10 Å farther from the metal than the *anti*-substituted end which results in allyl rehybridization where the bond length of the *syn*-substituted end to central carbon is 0.04 Å shorter than that of the *anti*-substituted end to central carbon.

Why does complex **10** show a much greater preference for the *anti* configuration than either methyl-substituted

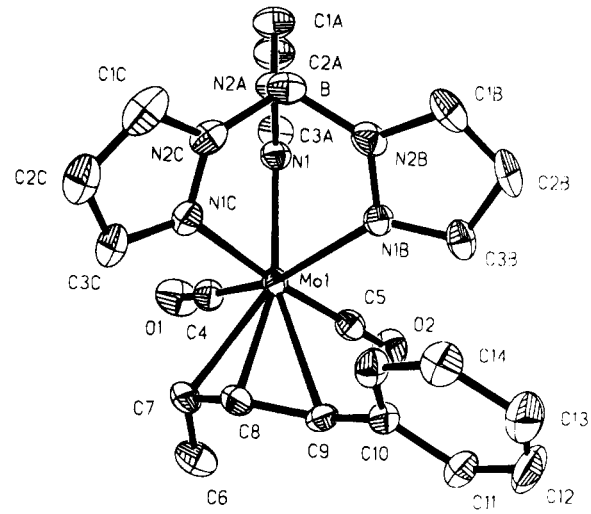

Figure 10. ORTEP of *syn*-phenyl/*anti*-methyl complex **11b**.

complex **2** or ethyl-substituted complex **3** (12.0:1.0 vs 4.1:1.0)? Bearing only a single substituent, *syn*-Et complex **3a** can rotate the ethyl group into the uncongested cleft of the equatorial pyrazoles thus minimizing steric repulsion between the substituent and the proximal pyrazole proton. This same rotation brings the *syn* proton on the *unsubstituted* end of the allyl closer to its proximal pyrazole proton. Therefore, allyl rotation of the *syn*/*syn*-isomer of the 1,3-dimethylated complex would bring one *syn* methyl substituent into the cleft defined by the two equatorial plane pyrazoles (stabilizing) but necessarily force the *syn* methyl substituent at the other end of the allyl into close contact with the proximal pyrazole proton (see Figure 3). This destabilizing effect contributes to the greater preference for an *anti* configuration in the 1,3-dimethylated allyl **10** compared to the related monosubstituted complexes, **2** and **3**.

***Syn*-Phenyl/*Anti*-Methyl Complex 11b.** The structure of the *syn*-Ph/*anti*-Me complex **11b** (Tables 11 and 12 and Figure 10) is quite similar to that of the 1,3-dimethylated structure **10b** described above. The allyl is rotated with respect to the $Mo(CO)_2$ fragment by 19°, and the Tp ligand is rotated in the opposite direction with respect to the $Mo(CO)_2$ fragment by 16° bringing the *syn* phenyl group into the pyrazole cleft. The *anti* methyl is bent out of the allyl plane away from the CO ligands by 38°. The *syn*-substituted end of the allyl is 0.09 Å farther from the metal than the *anti*-substituted end resulting in a slight rehybridization of the allyl toward η^1 at the methyl substituted end; however, the Mo to allyl bond lengths are nearly identical to those of the *syn*/*anti*-dimethyl complex **10b**.

Why do aryl substituents exclusively adopt the *syn* position at equilibrium in the monosubstituted series (complexes **7**–**9**) and in the disubstituted complex **11**? Two factors together probably contribute to the *syn*-preference for aryl substituents: (1) the planar phenyl group can rotate into a conformation that minimizes nonbonded steric interactions with the proximal pyrazole ligand, and (2) in contrast to *anti* substituents that are deflected out of the plane of the allyl by angles greater than 35°, the nearly in-plane *syn* configuration allows more efficient resonance overlap of the aryl π-bonds with those of the allyl moiety. It is also feasible

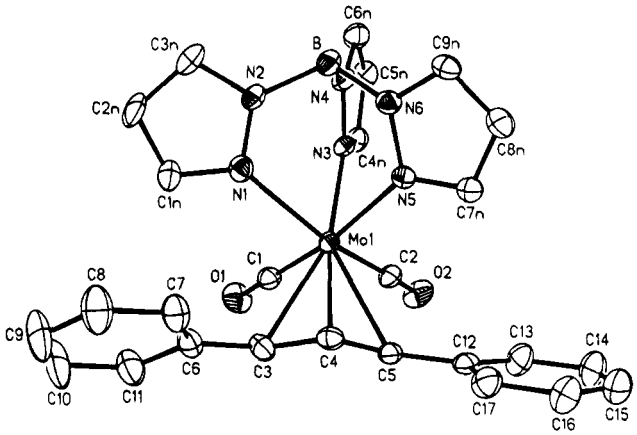

Figure 11. ORTEP of *syn*/*syn*-1,3-diphenyl complex **12a**.

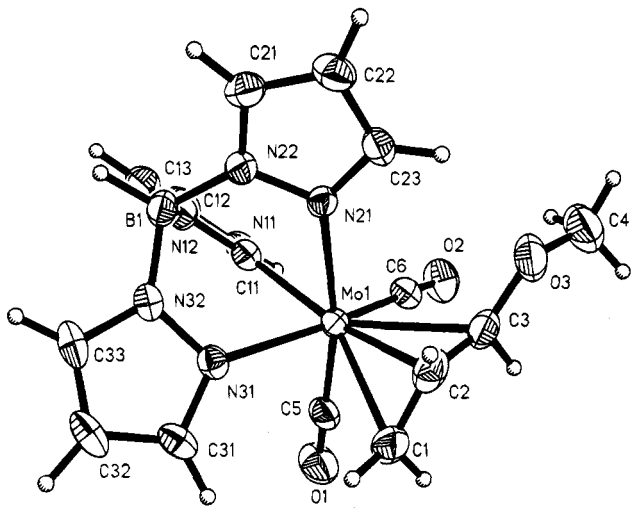

Figure 12. ORTEP of *syn*-methoxy complex **18a**.

that arene–pyrazole π-stacking plays a role in stabilizing the *syn*-configuration for monoaryl-substituted complexes.[58,59]

***Syn/Syn*-Diphenyl Complex 12a.** *Syn*/*anti*-diphenyl complex **12b** is the only complex that provides any *anti* phenyl group at equilibrium; however, it is still the *syn*/*syn* isomer **12a** that predominates at equilibrium (2.0 to 1.0), and the *syn*/*syn* isomer selectively crystallized allowing determination of its molecular structure (Tables 13 and 14, Figure 11). The unit cell consists of two slightly different molecules (for clarity only one of the molecules is shown in the ORTEP) whose major features are very similar. The allyl is rotated with respect to the $Mo(CO)_2$ fragment by 9°, and the Tp ligand is rotated with respect to the $Mo(CO)_2$ fragment in the opposite direction by 12° bringing one phenyl substituent into the cleft while the other is brought nearer the proximal pyrazole proton. The axis of the cleft phenyl is bent out of the allyl plane only 7°, a number similar to every other *syn* substituent determined in this study. However, the axis of the noncleft phenyl is bent out of plane by 18°, a distortion most likely due to a steric interaction with the proximal pyrazole proton. In addition, the cleft phenyl is more nearly coplanar with the allyl, being rotated approximately 20°, whereas the noncleft phenyl is rotated approximately 30°. Another feature of this structure is the longer bond length from Mo to the cleft-phenyl end of the allyl than to the allyl terminus bearing the non-cleft phenyl by approximately 0.07 Å, even though it is the noncleft end of the allyl that sterically interacts with its proximal pyrazole to a greater degree. The different bond lengths to Mo are probably a manifestation of better π-orbital overlap of the cleft-end phenyl with the allyl which favors an η^1-distortion at the allyl terminus bearing the noncleft phenyl.

***Syn*-Methoxy Complex 18a.** Of the eight complexes whose structures were determined in this study, the *syn*-methoxy complex **18a** (Tables 19 and 20 and Figure 12) possessed unique features. The allyl is rotated with respect to the $Mo(CO)_2$ fragment by 6°, and the Tp ligand is rotated in the opposite direction with respect to the $Mo(CO)_2$ fragment by 11°; however, the *syn* methoxy substituent is rotated *out* of the cleft of the equatorial pyrazoles. Comparison of **18a** with the *syn*-Et complex **3a** is informative. In the structure of **3a**, the allyl moiety has rotated to place the ethyl group in the cleft of the equatorial plane pyrazole ligands. Although the methylene of the ethyl substituent lies in the plane of the allyl, the methyl group is nearly perpendicular to the plane pointing out away from the rest of the complex (dihedral angle = 86°). If the methyl group remained in plane with the allyl, it would come into close contact with either the proximal pyrazole proton (dihedral angle = 180°) or the central proton of the allyl (dihedral angle = 0°), either of which would produce a destabilizing steric interaction. In contrast, the methoxy substituent of complex **18a** is found in plane with the allyl (C(4)–O(3)–C(3)–C(2) dihedral angle = 175°, < 5° deflection; an *s-trans* conformation). If the allyl rotated to place the methoxy group in the equatorial plane pyrazole cleft, the methyl group would be brought into close contact with the proximal pyrazole proton. In order to minimize steric interactions, the allyl rotates to place the methoxy group out of the cleft. The closest contact to a pyrazole proton in this arrangement is the oxygen atom itself.

The planar arrangement of the allyl–OMe fragment in **18a** is due to overlap of an oxygen lone pair of electrons with the allyl π-orbitals which allows significant double bond character between the oxygen and the allyl carbon. The O–allyl bond length in **18a** is 1.37 Å which is intermediate between that of a carbon–oxygen double bond and single bond. Resonance overlap of the oxygen nonbonded electron pair with the allyl π-system is most efficient when the oxygen occupies a *syn* position where the oxygen atom would be coplanar with the allyl. Therefore, the *syn* configuration of this complex is stabilized relative to the *anti* orientation to a degree that the *anti* isomer is not seen in solution spectra at equilibrium. This analysis dovetails nicely with the behavior of the acetoxy analogue **19** which shows *syn*/*anti* equilibrium numbers similar to the monoalkyl-substituted allyls. Resonance delocalization of a nonbonded electron pair of the acetoxy group sp^3-oxygen with the allyl π-system is diminished due to competing delocalization of the sp^3-oxygen lone pair with the acetyl π-system, and the sterically-based thermodynamic preference for the *anti* isomer is reestablished.

(58) Hunter, C. A. *Angew. Chem., Int. Ed. Engl.* **1993**, *32*, 1584.
(59) Hunter, C. A.; Sanders, J. K. M. *J. Am. Chem. Soc.* **1990**, *112*, 5525.

Correlation of Solid State Structures with Solution Spectra. IR Spectroscopy. With structural data in hand, a correlation of the partial rehybridization ($\eta^3 \rightarrow \eta^1$) of the allyls bearing *syn* substituents with the ^{1}H, ^{13}C, and IR spectra was sought. It has been suggested that the Tp ligand is a better electron donor than Cp.[46,60,61] Indeed, the ν_{CO} frequencies of **1** are 5−15 cm^{-1} lower than CpMo(CO)$_2$(η^3-C$_3$H$_5$).[62] In the monoalkyl-substituted series, if rehybridization of the *syn*-substituted allyls increases proportionally to the size of the substituent, then the *syn*-substituted end of the allyl becomes increasingly alkene-like in the series *syn*-H < -Me < -Et < -*i*-Pr < -*t*-Bu. As rehybridization toward η^1 increases, filled metal d-orbital to allyl back-bonding decreases allowing an increase in back-bonding from the metal to the carbonyl ligands. This may be reflected in the small but regular decrease in the CO stretching frequency down the series *syn*-H (1944, 1851 cm^{-1}), *syn*-Me (1934, 1842 cm^{-1}), *syn*-Et (1932, 1840 cm^{-1}), *syn*-*i*-Pr (1932, 1839 cm^{-1}), and *syn*-*t*-Bu (1926, 1835 cm^{-1}). Additionally, if the *anti* isomers experience little or no rehybridization, as the structure of *anti*-Me complex **2b** indicates, the carbonyl stretches in this series should and do show almost no regular variation from one complex to the next (*anti*-Me = 1937, 1845 cm^{-1}, *anti*-Et = 1938, 1847 cm^{-1}, *anti*-*i*-Pr = 1935, 1843 cm^{-1}, and *anti*-*t*-Bu = 1936, 1841 cm^{-1}). Trends in the disubstituted series were difficult to determine because IR spectra of most of the minor isomers were not obtainable. Burdett has reported the use of ν_{CO} frequencies to determine OC−M−CO bond angles.[63] Although a wide range of ν_{CO} frequencies were observed in the current study, the OC−Mo−CO bond angles for the eight structures reported are between 78 and 81°. Extended Hückel molecular orbital calculations were recently used in order to establish the relationship between the OC−W−CO bond angle and a variety of π-donor ligands.[64]

^{1}H NMR Spectroscopy. A regular increase in the coupling constant between the *anti* proton on the substituted allyl terminus and the central proton is observed for *syn*-alkyl-substituted allyls **2a**−**5a** (*syn*-Me = 8.7 Hz, *syn*-Et = 9.5 Hz, *syn*-*i*-Pr = 10.8 Hz, and *syn*-*t*-Bu = 11.7 Hz). This possibly reflects an increasing $\eta^3 \rightarrow \eta^1$ distortion with a concomitant drift toward a pure sp^2 hybrid at the *syn*-substituted end of the allyl. However, it should be noted that the coupling of the *anti* protons in the *unsubstituted* complex **1** is 10.0 Hz.

If $\eta^3 \rightarrow \eta^1$ distortion of the *syn*-alkyl-substituted allyls increases down the series H to *t*-Bu, then rehybridization of the unsubstituted end of the allyl toward sp^3 should increase accordingly. This trend should reveal itself in the magnitude of the coupling constants of the *syn* and *anti* protons on the unsubstituted end to the central proton. As the unsubstituted terminal allyl carbon moves toward sp^3 hybridization, the dihedral angle between the attached *anti* proton and the central proton should decrease toward 109.5°. A regular decrease in the *anti* proton to central proton coupling constant is observed (parent complex **1** = 10.0 Hz, *syn*-Me = 9.9 Hz, *syn*-Et = 9.0 Hz, *syn*-*i*-Pr = 8.7 Hz, *syn*-*t*-Bu = 8.4 Hz). However, an analogous regular decrease in the coupling of the *syn* proton to the central proton as the dihedral angle between them increases from near 0° is not seen (parent complex **1** = 6.0 Hz, *syn*-Me = 5.4 Hz, *syn*-Et = 6.8 Hz, *syn*-*i*-Pr = 6.6 Hz, *syn*-*t*-Bu = 6.6 Hz).

Scheme 1. *Syn/Anti* Isomerization by a $\pi-\sigma-\pi$ Mechanism

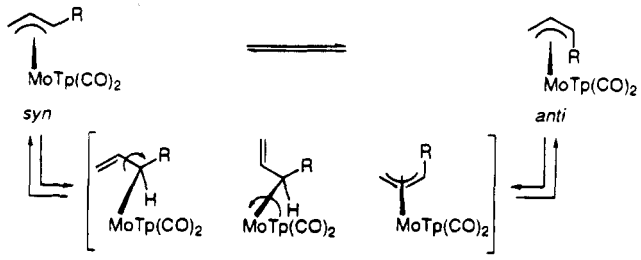

^{13}C NMR Spectroscopy. In the ^{13}C NMR spectra of the monoalkyl-substituted series, the *anti*-substituted allyl carbon absorbs 4−13 ppm upfield relative to the same carbon atom of the *syn*-substituted complex, while the unsubstituted carbons of the *anti* complexes absorb 3−11 ppm downfield from those of the corresponding *syn* complexes. This correlates with the previously described $\eta^3 \rightarrow \eta^1$ distortion of the *syn*-substituted allyls where, relative to the *anti*-substituted isomers, the substituted terminus becomes more alkene-like and the unsubstituted terminus less alkene-like.

Mechanism of *Syn/Anti* Isomerization. The most likely mechanism for *syn*/*anti* isomerization is a $\pi-\sigma-\pi$ mechanism (Scheme 1) where an η^3 to η^1 conversion allows rotation about the Mo−C(1) and C(1)−C(2) bonds; rotation about the allyl C(1)−C(2) bond and reformation of the η^3 allyl (in an *endo* conformation) effects *syn*−*anti* interconversion of the substituents attached to the C(1) carbon. Rotation about the Mo−allyl centroid would reestablish the *exo* conformation. The complete scrambling of deuterium between *syn* and *anti* positions of complex **1** enriched in deuterium in the *anti* position (mentioned above) is fully consistent with this scenario. Nonbonded steric effects between the equatorial plane pyrazole ligands and the substituents at the allyl termini must induce geometric distortions that lower the barrier to η^3 to η^1 conversion, because 1,3-disubstituted allyls undergo *syn*/*anti* equilibration at a lower temperature than monosubstituted allyls. Because a library of *syn*- and *anti*-substituted η^5-CpMo(CO)$_2$(η^3-allyls) analogous to the TpMo(CO)$_2$-based complexes prepared in this study is not currently available, comparison of the two systems is not feasible.

Miscellaneous. Fluxionality of the Tp Ligand in Solution. An additional feature in the ^{1}H and ^{13}C NMR spectra is the appearance of the Tp ligand resonances. In an allyl with a plane of symmetry, such as parent complex **1**, six signals should be observed for the nine protons and the nine carbons of the pyrazoles *if* the Tp does not rapidly exchange pyrazole environments on the NMR time scale—three signals from the unique *trans* pyrazole and three signals from the identical equatorial pyrazoles. The Tp signals in the ^{1}H NMR are somewhat broad and overlapped, but four resolved regions are

(60) Curtis, M. D.; Shiu, K.-B. *Inorg. Chem.* **1985**, *24*, 1213.
(61) Caffyn, A. J. M.; Feng, S. G.; Dierdorf, A.; Gamble, A. S.; Eldredge, P. A.; Vossen, M. R.; White, P. S.; Templeton, J. L. *Organometallics* **1991**, *10*, 2842.
(62) Faller, J. W.; Chen, C.-C.; Mattina, M. J.; Jakubowski, A. *J. Organomet. Chem.* **1973**, *52*, 361.
(63) Burdett, J. K. *Inorg. Chem.* **1981**, *20*, 2607.
(64) Templeton, J. L.; Caldarelli, J. L.; Feng, S.; Philipp, C. C.; Wells, M. B.; Woodworth, B. E.; White, P. S. *J. Organomet. Chem.* **1994**, *478*, 103.

observed; however, only three very broad ^{13}C singlets are seen, indicating interconversion of pyrazole environments on the ^{13}C NMR time scale. Trofimenko and coworkers studied the fluxionality of the simple allyl, the 2-methylallyl, and the 2-bromoallyl bearing both the tris- and tetrakis(pyrazolyl)borate ligand using variable-temperature NMR. Both 2-substituted complexes averaged pyrazole environments more rapidly than the unsubstituted complex, and the uncomplexed pyrazole unit of the tetrakis(pyrazolyl)borate ligand remained unique in the high-temperature ^{1}H NMR spectra. A simple rapid rotation about the B–Mo axis, analogous to the rotation of a Cp ligand, which averages the signals due to the coordinated pyrazole rings was invoked to explain these observations.

The complexes prepared in this study can be roughly divided into four groups on the basis of the rate of Tp ligand rotation as judged by the appearance of the Tp signals in the room-temperature ^{1}H NMR spectra: (1) *no Tp rotation on the NMR time scale*—those complexes that exhibit more than three pyrazole resonances in the ^{1}H NMR spectra, in which all Tp signals are sharp doublets and triplets—this group including *syn*-Ph/*anti*-Me complex **11b** and all *anti* monosubstituted complexes except the *i*-Pr (**4b**) and cyclohexyl (**6b**) complexes which are slightly broadened; (2) *slow Tp rotation on the NMR time scale*—those complexes that exhibit more than three pyrazole resonances in the ^{1}H NMR spectra, in which one or more peaks are broadened into singlets—this group including the aforementioned *anti*-*i*-Pr and Cy complexes **4b** and **6b**, all *syn* monoaryl-substituted complexes **7a–9a**, *syn*-MeO and -AcO complexes **18a** and **19a**, *syn*/*anti*-1,3-di-Me and *syn*/*anti*-1,2,3-tri-Me complexes **10b** and **16b**, and *syn*/*anti*-di-Ph complex **12b**; (3) *moderate rotation on the NMR time scale*—those complexes that exhibit only three pyrazole resonances in the ^{1}H NMR spectra, in which one or more of the signals is broadened into a singlet—this group including all *syn* monoalkyl-substituted allyls except *t*-Bu complex **5a** (which shows three sharp coupled resonances), *syn*-CO_2Me complex **17a**, 3-*syn*-1,1,3-triMe complex **15**, and *syn*-Ph/*syn*-Me complex **11a**; (4) *rapid rotation of Tp on the NMR time scale*—those complexes that show two sharp doublets and one sharp triplet for the Tp protons—this group including the aforementioned *syn*-*t*-Bu complex **5a**, both the *syn*/*syn* and *syn*/*anti* isomers of the 1,3-di-*t*-Bu complexes (**13a,b**), and *syn*/*syn*-phenyl-*tert*-butyl complex **14a**. Two trends are quite apparent: (1) the presence of *syn* substituents increases the rate of Tp rotation, and (2) the larger (compare complex **5a** with other *syn* monoalkylallyls) or more numerous (compare complexes **10b** and **15**) the *syn* substituents, the more rapidly the Tp ligand rotates. Nonbonded interactions of *syn* substituents with the equatorial pyrazole rings presumably play a role in raising the ground state energy of the complex thus lowering the barrier to rotation.

***Exo* to *Endo* Isomerism.** Both *exo* and *endo* rotamers of η^3-allyls based on the η^5-CpMo(CO)$_2$ fragment have been characterized and their interconversion studied by temperature-dependent NMR.[62] In the *exo* isomer the allylic termini eclipse the carbonyl carbons, while the allyl is rotated 180° with respect to the Mo(CO)$_2$ fragment in the *endo* rotamer. Every crystallographically characterized TpMo(CO)$_2$-based allyl complex in this study and those found in the Cambridge Database exist in the *exo* conformation. No evidence of *exo*–*endo* isomerism in solution was found.

Conclusions

An unexpectedly facile *syn*–*anti* equilibration of substituted (π-allyl)molybdenum complexes based on the TpMo(CO)$_2$ moiety has been discovered, where the *anti* stereoisomer is favored at equilibrium for 1°, 2°, and 3° alkyl, COOMe, and OAc substituents. A difference is noted for aryl and OMe substituents both of which show a strong preference for *syn* stereochemistry at equilibrium. Analysis of the molecular structure of eight different complexes by X-ray crystallography highlights the importance of nonbonded steric effects between *syn*-substituents and two of the pyrazole ligands which destabilize the *syn* configuration in favor of *anti*. However, it is only the *syn* configuration, which lies nearly in the plane of the π-allyl, and not the *anti* configuration, which is distorted significantly away from the plane of the allyl ligand, that allows stabilization of aryl and OMe substituents by resonance delocalization, thus accounting for the strong *syn* preference of these two substituents. (π-Allyl)molybdenum complexes monosubstituted at a terminal position undergo *syn* to *anti* equilibration within 2 h above 100 °C; those complexes at higher levels of substitution equilibrate at lower temperatures. The results of this study form a foundation for understanding all subsequent investigations of transformations of TpMo(CO)$_2$(η^3-allyl) complexes.

Experimental Section

General Methods. Dichloromethane was distilled from calcium hydride or dried with 4 Å molecular sieves prior to use. Anhydrous *N*,*N*-dimethylformamide and anhydrous toluene were purchased from Aldrich Chemical Co. and sparged with dry argon or nitrogen for at least 5 min prior to use. Tetrahydrofuran and diethyl ether were distilled from sodium/benzophenone prior to use. Molybdenum hexacarbonyl, $CeCl_3 \cdot 7H_2O$, 4-(*N*,*N*-dimethylamino)pyridine, 2-propenal, (*E*)-2-pentenal, (*E*)-2-butenal, allyl acetate, (*E*)-cinnamyl acetate, crotyl bromide, (*E*)-3-penten-2-ol, (*Z*)-2-penten-1-ol, and 3-phenyl-2-propyn-1-ol were purchased from Aldrich Chemical Co. and used as received. Potassium hydrotris(1-pyrazolyl)borate was prepared by the method of Trofimenko.[43] (DMF)$_3$Mo(CO)$_3$ was prepared according to a literature procedure.[54] (*Z*)-3-phenyl-2-propen-1-ol was prepared by Lindlar reduction of 3-phenyl-2-propyn-1-ol.[65] (*E*)-2,2,6,6-tetramethyl-4-hepten-3-one was prepared by the method of House.[66,67] All reactions were performed under a positive pressure of dry argon or nitrogen. Analytical TLC was performed on glass plates precoated with Merck F_{254} silica gel 60 and visualized by UV light. Column chromatography of the (π-allyl)molybdenum complexes was performed with mixtures of hexane and ethyl acetate on Merck silica gel 60 under a positive pressure of air.

Synthesis of Allylic Acetates. (*Z*)-3-Acetoxy-1-deuterio-1-propene. A solution of $LiAlH_4$ (2.32 g, 61.1 mmol, 1.20 equiv) in dry THF (50 mL) was cooled in an ice-bath under nitrogen. Propargyl alcohol (2.86 g, 51.0 mmol, 1.00 equiv) was added via syringe over 10 min. The solution was warmed

(65) Pelter, A.; Ward, R. S.; Little, G. M. *J. Chem. Soc., Perkin Trans. 1* **1990**, 2775.
(66) House, H. O.; Crumrine, D. S.; Teranishi, A. Y.; Olmstead, H. D. *J. Am. Chem. Soc.* **1973**, *95*, 3310.
(67) House, H. O.; Weeks, P. D. *J. Am. Chem. Soc.* **1975**, *97*, 2770.

to room temperature and stirred for 24 h. The solution was again cooled in an ice bath, and the reaction was quenched with 2 mL of D_2O. An additional 50 mL of ether was added and the solution filtered and dried with $MgSO_4$. Solvent was removed by distillation at atmospheric pressure affording the D-labeled alcohol. Further purification was not attempted, and the alcohol was used as is.[68] The allyl alcohol was dissolved in 30 mL of dry ether, and then DMAP (6.86 g, 56.2 mmol, 1.10 equiv) and acetic anhydride (5.73 g, 56.13 mmol, 1.10 equiv) were added via syringe. The solution was stirred at room temperature for 18 h, then an additional 20 mL of ether was added, and the solution was filtered. The organic layer was washed with 3% HCl (3 × 50 mL), saturated $NaHCO_3$ (3 × 50 mL), and then brine (50 mL). The organic layer was dried with $MgSO_4$ and decanted, and most of the solvent was removed by distillation at atmospheric pressure. The concentration of the allyl acetate (0.58 g, 5.74 mmol, 11%) in residual solvent was determined by ^1H NMR spectroscopy: ^1H NMR ($CDCl_3$, 300 MHz) δ 5.85 (m, 1 H), 5.15 (d, J = 10.4 Hz, 1 H), 4.51 (d, J = 5.8 Hz, 2 H), 2.02 (s, 3 H); ^{13}C NMR ($CDCl_3$, 75.5 MHz) δ 170.5, 132.0, 117.7 (t, J = 23.1 Hz), 64.9, 20.7; IR (CH_2Cl_2, KCl, cm^{-1}) 2950, 2872, 1738, 1372, 1228.

(*E*)-1-Acetoxy-2-pentene. To a stirring solution of (*E*)-2-pentenal (10.6 g, 126.0 mmol, 1.00 equiv) in MeOH (150 mL) was added cerium trichloride heptahydrate (51.6 g, 138.5 mmol, 1.10 equiv) producing a white suspension. Solid $NaBH_4$ (7.15 g, 189.0 mmol, 1.50 equiv) was added in small portions very slowly over a period of 30 min, and then the reaction mixture was stirred at ambient temperature for 12 h. The crude reaction mixture was poured into 200 mL of water, and the product was extracted with 3 × 100 mL of Et_2O. The organic phases were combined, dried with sodium sulfate, and concentrated to a colorless oil. The oil was dissolved in 100 mL of Et_2O and treated with DMAP (18.5 g, 151.4 mmol, 1.20 equiv) and acetic anhydride (15.4 g, 151.4 mmol, 1.20 equiv) and stirred for 4 h. The reaction mixture was washed with 100 mL of water, 3 × 100 mL of 10% HCl, and 3 × 100 mL of saturated aqueous $NaHCO_3$. Drying with sodium sulfate and concentration provided (*E*)-1-acetoxy-2-pentene (12.1 g, 94.4 mmol, 75%) as a clear colorless oil that was used without further purification: ^1H NMR ($CDCl_3$, 300 MHz) δ 5.81 (dt, J = 15.6, 6.3 Hz, 1 H), 5.55 (m, 1 H), 4.50 (d, J = 6.6 Hz, 2 H), 2.06 (m, 2 H), 2.05 (s, 3 H), 1.00 (t, J = 7.2 Hz, 3 H); ^{13}C NMR ($CDCl_3$, 75.5 MHz) δ 170.8, 138.0, 122.7, 60.3, 25.2, 20.8, 13.0.

(*Z*)-1-Acetoxy-2-pentene. To a diethyl ether solution (25 mL) of commercially available (*Z*)-2-penten-1-ol (2.00 g, 23.22 mmol, 1.00 equiv) and DMAP (3.40 g, 27.83 mmol, 1.20 equiv) was added acetic anhydride (2.85 g, 27.92 mmol, 1.20 equiv) dropwise over a 10 min period. A white precipitate formed rapidly, and the reaction mixture warmed slightly. The reaction mixture was stirred for 2 h and then diluted with 50 mL of Et_2O and washed successively with 50 mL of H_2O, 3 × 50 mL of 10% HCl, and 3 × 50 mL of saturated $NaHCO_3$. The organic layer was dried over Na_2SO_4 and concentrated to a colorless oil (2.1 g, 16.38 mmol, 71%) that was used without further purification: ^1H NMR ($CDCl_3$, 300 MHz) δ 5.68–5.58 (m, 1 H), 5.53–5.45 (m, 1 H), 4.61 (d, J = 6.9 Hz, 2 H), 2.14 (m, 2 H), 2.05 (dq, J = 7.4, 7.4 Hz, 3 H), 0.99 (t, J = 7.4 Hz, 3 H); ^{13}C NMR ($CDCl_3$, 75.5 MHz) δ 170.8, 136.9, 122.6, 60.2, 20.9, 20.8, 14.0.

3-Acetoxy-4-methyl-1-pentene. A 250 mL Schlenk tube equipped with a magnetic stirring bar was flushed with argon and charged with 100 mL of a diethyl ether solution of isopropylmagnesium chloride (100 mL, 2.00 M, 200.0 mmol, 0.95 equiv) which was then cooled to 0 °C. 2-Propenal (14 mL, 209 mmol, 1.00 equiv) was added dropwise to the Grignard solution over a period of 20 min at which time the ice bath was removed and the reaction mixture was warmed to ambient temperature. The reaction was quenched by dropwise addition of 50 mL of 5% H_2SO_4. The layers were separated, and the ether layer was washed with 50 mL of saturated K_2CO_3 and dried over Na_2SO_4. After decantation, DMAP (31.70 g, 259.4 mmol, 1.24 equiv) was added followed by acetic anhydride (26.50 g, 259.57 mmol, 1.24 equiv) dropwise over a 10 min period. After being stirred for 4 h, the reaction mixture was washed successively with 100 mL of H_2O, 3 × 100 mL of 10% HCl, and 3 × 100 mL of saturated $NaHCO_3$. Drying with sodium sulfate and concentration provided the desired product (21.6 g, 151.9 mmol, 72%) as a clear colorless oil that was used without further purification: ^1H NMR ($CDCl_3$, 300 MHz) δ 5.75 (ddd, J = 17.1, 10.5, 6.6 Hz, 1 H), 5.25–5.18 (m, 2 H), 5.04 (app t, J = 6.0 Hz, 1 H), 2.07 (s, 3 H), 1.86 (dsept, J = 6.7, 6.7 Hz, 1 H), 0.91 (d, J = 6.7 Hz, 3 H), 0.90 (d, J = 6.7 Hz, 3 H); ^{13}C NMR ($CDCl_3$, 75.5 MHz) δ 170.3, 134.7, 117.4, 79.3, 31.7, 21.1, 17.9, 17.8.

3-Acetoxy-4,4-dimethyl-1-pentene. To a stirring pentane solution of *tert*-butyllithium (30.00 mL, 1.70 M, 51.00 mmol, 1.00 equiv) at 0 °C was added 2-propenal (3.4 mL, 50.9 mmol, 1.0 equiv) dropwise over a 10 min period. The reaction mixture was stirred for 1 h and carefully quenched by the dropwise addition of 5 mL of H_2O. The mixture was diluted with 80 mL of Et_2O and washed with 50 mL of 5% H_2SO_4 and 50 mL of saturated K_2CO_3 and then dried with sodium sulfate and concentrated. The colorless oil was dissolved in 50 mL of Et_2O and treated with DMAP (7.18 g, 58.77 mmol, 1.16 equiv). Acetic anhydride was added dropwise over a 10 min period, and the mixture was stirred for 12 h and then washed successively with 50 mL H_2O, 3 × 50 mL of 10% HCl, and 3 × 50 mL of saturated $NaHCO_3$. Drying with sodium sulfate and concentration provided 3-acetoxy-4,4-dimethyl-1-pentene (2.7 g, 17.280 mmol, 34%) as a clear colorless oil that was used without further purification: ^1H NMR ($CDCl_3$, 300 MHz) δ 5.79 (ddd, J = 17.4, 10.2, 6.9 Hz, 1 H), 5.24–5.18 (m, 2 H), 4.98 (d, J = 6.9 Hz, 1 H), 2.08 (s, 3 H), 0.91 (s, 9 H); ^{13}C NMR ($CDCl_3$, 75.5 MHz) δ 170.3, 133.6, 118.0, 81.8, 34.1, 25.7, 21.1.

3-Acetoxy-3-cyclohexyl-1-propene. Cyclohexylmagnesium chloride was prepared under argon by the dropwise addition over a 15 min period of cyclohexyl chloride (5.00 g, 42.15 mmol, 0.91 equiv) to a slurry of crushed magnesium turnings (1.54 g, 63.35 mmol, 1.37 equiv) in 100 mL of dry Et_2O. After an additional 1.5 h, the flask was immersed in an ice bath and 2-propenal (3.1 mL, 46.4 mmol, 1.0 equiv) was added dropwise over a 10 min period. The reaction mixture was stirred for 1 h, and then it was quenched with 5 mL of H_2O, washed with 50 mL of 5% H_2SO_4 and 50 mL of saturated K_2CO_3, and dried over Na_2SO_4. After decantation, the solution of the crude alcohol was poured into a round-bottomed flask equipped with a magnetic stirring bar and containing DMAP (6.70 g, 54.8 mmol, 1.18 equiv). Acetic anhydride (5.60 g, 54.8 mmol, 1.18 equiv) was added dropwise over a 10 min period, and the resulting mixture was stirred for 4 h at which time it was washed successively with 50 mL of H_2O, 3 × 50 mL of 10% HCl, and 3 × 50 mL of saturated $NaHCO_3$. Drying and concentration provided 3-acetoxy-3-cyclohexyl-1-propene (5.2 g, 28.5 mmol, 62%) as a clear colorless oil that was used without further purification: ^1H NMR ($CDCl_3$, 300 MHz) δ 5.75 (ddd, J = 17.4, 10.5, 7.2 Hz, 1 H), 5.23–5.17 (m, 2 H), 5.04 (app t, J = 6.6 Hz, 1 H), 2.10–2.00 (m, 1 H), 2.07 (s, 3 H), 1.76–0.93 (m, 10 H); ^{13}C NMR ($CDCl_3$, 75.5 MHz) δ 170.3, 135.1, 117.3, 78.9, 41.5, 28.5, 28.4, 26.3, 25.9 (s, 2 C), 21.1.

(*Z*)-Cinnamyl Acetate. (*Z*)-Cinnamyl alcohol (9.40 g, 70.1 mmol, 1.00 equiv) was dissolved in a solution of Et_2O (100 mL) and DMAP (10.30 g, 84.3 mmol, 1.20 equiv). Acetic anhydride (8.60 g, 84.2 mmol, 1.20 equiv) was added dropwise over a 10 min period. Stirring of the mixture was continued for 4 h, and then it was washed successively with 100 mL of water, 3 × 50 mL of 10% HCl, and 3 × 100 mL of saturated $NaHCO_3$. Drying and concentration provide (*Z*)-cinnamyl acetate (10.3 g, 58.4 mmol, 83%) as a clear colorless oil that was used without further purification: ^1H NMR ($CDCl_3$, 300 MHz) δ 7.39–7.21 (m, 5 H), 6.67 (d, J = 11.7 Hz, 1 H), 5.82 (dt, J =

(68) Baldwin, J. E.; Black, K. A. *J. Org. Chem.* **1983**, *48*, 2778.

11.7, 6.6 Hz, 1 H), 4.85 (dd, J = 6.6, 0.9 Hz, 2 H), 2.09 (s, 3 H); ^{13}C NMR ($CDCl_3$, 75.5 MHz) δ 170.8, 136.0, 133.0, 128.7, 128.4, 127.5, 125.8, 61.5, 20.9.

3-Acetoxy-3-(4-methoxyphenyl)-1-propene. *p*-Anisaldehyde (8.00 g, 58.76 mmol, 1.00 equiv) was added dropwise to a THF solution of vinylmagnesium bromide (100.0 mL, 1.00 M, 100.0 mmol, 1.70 equiv) cooled to 0 °C. The reaction mixture was then stirred at ambient temperature for 1 h, quenched with 5 mL of water, diluted with 150 mL of Et_2O, and washed with 50 mL of 5% H_2SO_4 and 50 mL of saturated K_2CO_3. After drying over Na_2SO_4 and decanting, DMAP (7.90 g, 64.6 mmol, 1.10 equiv) was added followed by the dropwise addition of acetic anhydride (6.60 g, 64.6 mmol, 1.10 equiv). The mixture was stirred for 4 h and then washed successively with 50 mL of water, 3 × 50 mL of 10% HCl, and 3 × 50 mL of saturated $NaHCO_3$. Drying with sodium sulfate and concentration provided 3-acetoxy-3-(4-methoxyphenyl)-1-propene (9.8 g, 47.5 mmol, 81%) as a clear colorless oil: ^{1}H NMR ($CDCl_3$, 300 MHz) δ 7.29 (d, J = 8.4 Hz, 2 H), 6.89 (d, J = 8.4 Hz, 2 H), 6.23 (d, J = 5.7 Hz, 1 H), 6.01 (ddd, J = 16.5, 10.5, 5.7 Hz, 1 H), 5.30–5.21 (m, 2 H), 3.80 (s, 3 H), 2.09 (s, 3 H); ^{13}C NMR ($CDCl_3$, 75.5 MHz) δ 169.9, 159.4, 136.3, 130.9, 128.6, 116.4, 113.9, 75.7, 55.2, 21.2.

3-Acetoxy-3-(4-(trifluoromethyl)phenyl)-1-propene. *p*-(Trifluoromethyl)phenylmagnesium bromide was prepared by the dropwise addition of *p*-bromo(trifluoromethyl)benzene (Aldrich) (10.0 g, 44.4 mmol, 1.00 equiv) to a diethyl ether (100 mL) slurry of crushed magnesium turnings (1.40 g, 57.6 mmol, 1.30 equiv). After the addition the reaction mixture was stirred for 1 h to give a red solution. 2-Propenal (2.74 g, 48.9 mmol, 1.10 equiv) was added dropwise to the Grignard solution over a period of 10 min, and the mixture was stirred for an additional 30 min and then carefully quenched by the addtion of 50 mL of 5% sulfuric acid. Layers were separated, and the organic phase was washed with 50 mL of saturated K_2CO_3. The red solution was dried with sodium sulfate, decanted, then treated with DMAP (5.98 g, 49.0 mmol, 1.10 equiv) and acetic anhydride (5.00 g, 49.0 mmol, 1.10 equiv) and stirred for 4 h, and then washed with 50 mL of water, 3 × 50 mL of 10% HCl, and 3 × 50 mL of saturated $NaHCO_3$. Drying with sodium sulfate and concentration provided 3-acetoxy-3-(4-(trifluoromethyl)phenyl)-1-propene (7.1 g, 29.1 mmol, 65%) as a clear red oil which was used without further purification: ^{1}H NMR ($CDCl_3$, 300 MHz) δ 7.62 (d, J = 8.4 Hz, 2 H), 7.47 (d, J = 8.4 Hz, 2 H), 6.29 (d, J = 6.0 Hz, 1 H), 5.98 (ddd, J = 16.8, 10.5, 6.3 Hz, 1 H), 5.34–5.27 (m, 2 H), 2.13 (s, 3 H); ^{13}C NMR ($CDCl_3$, 75.5 MHz) δ 169.7, 142.9, 135.5, 130.3 (q, J = 32.5 Hz, CCF_3), 127.3, 125.5 (q, J = 3.9 Hz), 124.0 (q, J = 272.0 Hz, CF_3), 117.7, 75.4, 21.0.

(*E*)-4-Acetoxy-2-pentene. (*E*)-3-penten-2-ol (2.00 g, 23.2 mmol, 1.00 equiv) was dissolved in 50 mL of Et_2O and treated with DMAP (3.40 g, 27.8 mmol, 1.20 equiv) and acetic anhydride (2.85 g, 27.9 mmol, 1.20 equiv). After being stirred for 4 h, the reaction mixture was washed successively with 50 mL water, 3 × 50 mL of 10% HCl, and 3 × 50 mL of saturated $NaHCO_3$. Drying with sodium sulfate and concentration provided (*E*)-4-acetoxy-2-pentene (2.1 g, 16.4 mmol, 70%) as a colorless oil which was used without further purification: ^{1}H NMR ($CDCl_3$, 300 MHz) δ 5.72 (dq, J = 15.6, 6.9 Hz, 1 H), 5.47 (ddq, J = 15.6, 7.2, 1.4 Hz, 1 H), 5.29 (app pent, J = 6.5 Hz, 1 H), 2.03 (s, 3H), 1.69 (d, J = 6.0 Hz, 3 H), 1.28 (d, J = 6.6 Hz, 3 H); ^{13}C NMR ($CDCl_3$, 75.5 MHz) δ 170.3, 130.7, 128.0, 71.1, 21.3, 20.2, 17.6.

(*E*)-1-Acetoxy-1-phenyl-2-butene. A solution of phenylmagnesium bromide was prepared by the reaction of magnesium turnings (1.86 g, 76.5 mmol, 1.20 equiv) with bromobenzene (10.0 g, 63.7 mmol, 1.00 equiv) in 100 mL of dry Et_2O for 1 h. (*E*)-2-butenal (4.46 g, 63.6 mmol, 1.00 equiv) was added dropwise to the Grignard reagent over a 10 min period followed by stirring at ambient temperature for an additional 10 min. The reaction was carefully quenched with 74 mL of 5% sulfuric acid, the layers were separated, and the organic phase was washed with 100 mL of saturated K_2CO_3. After drying over Na_2SO_4, the solution was decanted and treated with DMAP (9.57 g, 78.4 mmol, 1.23 equiv) and acetic anhydride (8.00 g, 78.4 mmol, 1.23 equiv) and stirred for 4 h. The mixture was washed with 100 mL of water, 3 × 100 mL of 10% HCl, and 3 × 100 mL saturated $NaHCO_3$. Drying with sodium sulfate and concentration provided (*E*)-1-acetoxy-1-phenyl-2-butene (8.1 g, 42.6 mmol, 67%) as a clear colorless oil that was used without further purification: ^{1}H NMR ($CDCl_3$, 300 MHz) δ 7.35–7.31 (m, 5 H), 6.22 (d, J = 6.4 Hz, 1 H), 5.82–5.63 (m, 2 H), 2.10 (s, 3 H), 1.72 (d, J = 6.0 Hz, 3 H); ^{13}C NMR ($CDCl_3$, 75.5 MHz) δ 169.9, 139.7, 129.5, 129.5, 128.4, 127.8, 126.8, 76.2, 21.3, 17.7.

(*E*)-5-Acetoxy-2,2,6,6-tetramethyl-3-heptene. (*E*)-2,2,6,6-tetramethyl-4-hepten-3-one (4.28 g, 25.4 mmol, 1.00 equiv) was dissolved in a mixture of cerium trichloride heptahydrate (10.4 g, 28.0 mmol, 1.1 equiv) and methanol (50 mL). Solid potassium borohydride (2.06 g, 38.1 mmol, 1.5 equiv) was added very slowly in small portions over a period of 20 min to produce a very vigorous reaction; the reaction mixture was stirred at ambient temperature for 1 h and then carefully poured into 200 mL of water. The reaction mixture was extracted with 3 × 100 mL of Et_2O, and the combined organic phases were dried over Na_2SO_4, decanted, and concentrated under high vacuum. The residue was redissolved in 50 mL of dry Et_2O and treated with DMAP (3.72 g, 30.5 mmol, 1.2 equiv) and acetic anhydride (3.11 g, 30.5 mmol, 1.2 equiv) with stirring for 12 h at which time the reaction mixture was washed with 100 mL of water, 3 × 100 mL of 10% HCl, and 3 × 100 mL of saturated $NaHCO_3$. Drying with sodium sulfate and concentration provided (*E*)-5-acetoxy-2,2,6,6,-tretramethyl-3-heptene (4.88 g, 90%) as a clear colorless oil which was used without further purification: ^{1}H NMR ($CDCl_3$, 300 MHz) δ 5.68 (d, J = 15.9 Hz, 1 H), 5.28 (dd, J = 15.9, 7.8 Hz, 1 H), 4.95 (d, J = 7.8 Hz, 1 H), 2.04 (s, 3 H), 0.99 (s, 9 H), 0.87 (s, 9 H); ^{13}C NMR ($CDCl_3$, 75.5 MHz) δ 170.3, 146.2, 120.1, 82.0, 34.4, 33.0, 29.4, 25.8, 21.3.

(*E*)-3-Acetoxy-4,4-dimethyl-1-phenyl-1-pentene. To a stirring pentane solution of *tert*-butyllithium (80.00 mL, 1.70 M, 136.0 mmol, 1.33 equiv) under argon was added (*E*)-cinnamaldehyde (12.9 mL, 102.3 mmol, 1.00 equiv) dropwise over a 20 min period. The reaction mixture was stirred for 1 h and then quenched with 100 mL of 5% H_2SO_4 and diluted with 100 mL of Et_2O. The layers were separated, and the organic phase was washed with 100 mL of saturated K_2CO_3 and then dried with sodium sulfate, concentrated, and distilled (bp = 93–97 °C, 1.4 Torr) providing (*E*)-2,2-dimethyl-5-phenyl-4-penten-3-ol (10.2 g) as a colorless oil. The alcohol was dissolved in 100 mL of dry Et_2O, and the solution was treated with DMAP (7.86 g, 64.3 mmol, 0.63 equiv) and acetic anhydride (6.57 g, 64.4 mmol, 0.63 equiv) and stirred at ambient temperature for 12 h. The reaction mixture was washed with 100 mL of water, 3 × 100 mL of 10% HCl, and 3 x 100 mL of saturated $NaHCO_3$. Drying with sodium sulfate and concentration provided (*E*)-3-acetoxy-4,4-dimethyl-1-phenyl-1-pentene (11.3 g, 48.6 mmol, 48%) as a clear colorless oil that was used without further purification: ^{1}H NMR ($CDCl_3$, 300 MHz) δ 7.41–7.25 (m, 5 H), 6.60 (d, J = 15.9 Hz, 1 H), 6.17 (dd, J = 15.9, 7.5 Hz, 1 H), 5.18 (d, J = 7.5 Hz, 1 H), 2.10 (s, 3 H), 0.98 (s, 9 H); ^{13}C NMR ($CDCl_3$, 75.5 MHz) δ 170.3, 136.5, 133.8, 128.5, 127.8, 126.5, 125.0, 81.7, 34.7, 25.9, 21.2.

4-Acetoxy-2-methyl-2-pentene. 4-Methyl-3-penten-2-one (10.0 g, 101.9 mmol, 1.00 equiv) was dissolved in a solution of cerium trichloride heptahydrate (41.8 g, 112.2 mmol, 1.10 equiv) in 200 mL of MeOH. Sodium borohydride (5.78 g, 152.8 mmol, 1.50 equiv) was added in small portions over a 20 min period resulting in considerable warming and gas evolution. The reaction mixture was stirred at ambient temperature for 2 h and then poured into 200 mL of water and extracted with 2 × 200 mL of Et_2O. The organic layers were combined and dried over $MgSO_4$, decanted, and concentrated to a colorless oil. The oil was redissolved in 100 mL of dry Et_2O and treated

with DMAP (15.0 g, 122.4 mmol, 1.21 equiv) and acetic anhydride (12.5 g, 122.4 mmol, 1.20 equiv). The resulting mixture was stirred for 2 h and then washed with 100 mL of water, 3 × 100 mL of 10% HCl, and 3 × 100 mL of saturated $NaHCO_3$. Drying with sodium sulfate and concentration provided 4-acetoxy-2-methyl-2-pentene (11.9 g, 83.7 mmol, 82%) as a clear colorless oil that was used without further purification: ^{1}H NMR ($CDCl_3$, 300 MHz) δ 5.58 (dq, J = 8.7, 6.5 Hz, 1 H), 5.16 (d, J = 8.7 Hz, 1 H), 2.02 (s, 3 H), 1.72 (s, 3 H), 1.71 (s, 3 H), 1.25 (d, J = 6.5 Hz, 3 H); ^{13}C NMR ($CDCl_3$, 75.5 MHz) δ 170.4, 136.2, 124.9, 68.2, 25.6, 21.4, 20.9, 18.2.

(*E*)-4-Acetoxy-3-methyl-2-pentene. (*E*)-3-Methyl-2-butenal (10.0 g, 118.9 mmol, 1.00 equiv) was added dropwise over a 20 min period to a Et_2O solution of methylmagnesium bromide (59.4 mL, 3.00 M, 178.2 mmol, 1.50 equiv). The reaction mixture was stirred at ambient temperature for 1 h and then quenched with 100 mL of 5% sulfuric acid, extracted with 100 mL of Et_2O, and washed with 100 mL of saturated K_2CO_3. After drying of the organic phase over $MgSO_4$, the decanted solution was treated with DMAP (17.5 g, 143.2 mmol, 1.20 equiv) and acetic anhydride (14.6 g, 143.0 mmol, 1.20 equiv). After being stirred for 2 h, the reaction mixture was washed with 100 mL of water, 3 × 100 mL of 10% HCl, and 3 × 100 mL of saturated $NaHCO_3$. Drying with sodium sulfate and concentration provided (*E*)-4-acetoxy-3-methyl-2-pentene as a colorless oil that was used without further purification: ^{1}H NMR ($CDCl_3$, 300 MHz) δ 5.53 (q, J = 6.0 Hz, 1 H), 5.26 (q, J = 6.3 Hz, 1 H), 2.03 (s, 3 H), 1.61 (s, 3 H), 1.60 (d, J = 6.0 Hz, 3 H), 1.28 (d, J = 6.3 Hz, 3 H); ^{13}C NMR ($CDCl_3$, 75.5 MHz) δ 170.4, 135.0, 121.5, 75.5, 21.4, 19.0, 13.0, 11.6.

Synthesis of (π-Allyl)molybdenum Complexes. General Procedure for the Preparation of Tp(CO)$_2$Mo(η^3-allyl) Complexes from Allylic Acetates. A solution of $(DMF)_3Mo(CO)_3$ was prepared in a Schlenk flask under argon using dry, deoxygenated dichloromethane as the solvent (approximately 12 mL/g of metal complex). To the stirring dark green solution was added the neat acetate (1.0−1.5 equiv) from a preweighed syringe. As the oxidative addition proceeded, the color changed to bright orange-yellow. Stirring was continued from 0.25 to 24 h at which time solid potassium hydrotris(1-pyrazolyl)borate (1 equiv) was added. The color changed again turning bright yellow-green. The reaction mixture was stirred for 15 min and concentrated to a paste which was purified by flash chromatography on SiO_2. Some of the complexes were purified by recrystallization. The complexes were somewhat air or moisture sensitive and were best stored under inert atmosphere. Sterically congested complexes **5**, **6**, **13**, **14**, and **16** decomposed at room temperature in air in a matter of hours to weeks.

Dicarbonyl[hydrotris(1-pyrazolyl)borato][η-(1,2,3)-2-propen-1-yl]molybdenum (Parent Complex 1).[46] $(DMF)_3Mo(CO)_3$ (1000 mg, 2.50 mmol, 1.00 equiv) was dissolved in 15 mL of dry, deoxygenated dichloromethane in a Schlenk flask under argon. To this was added allyl acetate (0.297 mL, 2.75 mmol, 1.10 equiv). The color immediately changed from green to dark orange, and CO gas was evolved. Stirring was continued for 1.5 h, and then solid potassium hydrotris(1-pyrazolyl)borate (631 mg, 2.50 mmol, 1.00 equiv) was added and the reaction mixture concentrated to a yellow paste which was purified by flash silica gel chromatography (hexane/EtOAc, 5/1) to afford complex **1** (783 mg, 1.93 mmol, 77%) as a yellow solid: ^{1}H NMR ($CDCl_3$, 300 MHz) δ 8.57 (br s, 1 H), 7.81 (br s, 2 H), 7.55 (br s, 3 H), 6.19 (br s, 3 H), 3.78 (m, 1 H), 3.63 (d, J = 6.0 Hz, 2 H), 1.51 (d, J = 10.0 Hz, 2 H); ^{13}C NMR ($CDCl_3$, 75.5 MHz) δ 227.5, 141.8 (br s, 3 C), 135.8 (br s, 3 C), 105.3 (br s, 3 C), 73.9, 58.7; IR (CH_2Cl_2, KCl, cm^{-1}) 1944 (s), 1851 (s).

Deuterated Dicarbonyl[hydrotris(1-pyrazolyl)borato]-[η-(1,2,3)-2-propen-1-yl]molybdenum (Deuterated Parent Complex 1). In a Schlenk tube under nitrogen, $Mo(DMF)_3(CO)_3$ (963 mg, 2.41 mmol, 1.00 equiv) was dissolved in 10 mL of dry, degassed CH_2Cl_2. To this solution was added via syringe the deuterated allyl acetate (in residual THF from preparation) (372 mg, 3.68 mmol, 1.53 equiv). The solution color changed immediately to dark orange brown. After the solution was stirred for 4 h at room temperature, solid KTp (669 mg, 2.65 mmol, 1.10 equiv) was added. The solution was stirred for 1 h, and then solvent was removed and purification by the procedure used for **1** afforded the deuterated allyl complex as a yellow brown solid. ^{1}H and ^{2}H NMR revealed that the label was partially scrambled between both the *syn* and *anti* positions (61% in *anti*, and 39% in *syn*): ^{2}H NMR (C_6H_6, 92.1 MHz) δ 3.30 (br s, 0.39 D, *syn*-deuterio), 1.38 (br s, 0.61 D, *anti*-deuterio).

Dicarbonyl[hydrotris(1-pyrazolyl)borato][η-(1,2,3)-(±)-(2*R*,3*R*)-2-buten-1-yl]molybdenum (*Syn*-Methyl Complex 2a). $(DMF)_3Mo(CO)_3$ (820 mg, 2.05 mmol, 1.00 equiv) was dissolved in 15 mL of dry, deoxygenated dichloromethane in a Schlenk flask under argon. To this was added an isomeric mixture of (*E*)- and (*Z*)-crotyl bromides and 3-bromo-1-butene (80:10:10) (317 mL, 3.02 mmol, 1.50 equiv). The color immediately changed from green to dark orange, and CO gas was evolved. Stirring was continued for 1.5 h at which time solid potassium hydrotris(1-pyrazolyl)borate (518 mg, 2.05 mmol, 1.00 equiv) was added and the reaction mixture concentrated to an orange paste which was purified by flash silica gel chromatography (hexane/EtOAc, 5/1) to afford complex **2a/b** (490 mg, 1.17 mmol, 57%) as a yellow solid. ^{1}H NMR analysis revealed a kinetic mixture of *syn* and *anti* isomers **2a** and **2b** in a 2 to 1 ratio. Data for *syn*-methyl complex **2a**: ^{1}H NMR ($CDCl_3$, 300 MHz) δ 8.01 (br s, 3 H), 7.55 (d, J = 1.8 Hz, 3 H), 6.20 (app t, J = 1.8 Hz, 3 H), 3.81 (dt, J = 8.1, 5.4 Hz, 1 H), 3.41 (dd, J = 5.4, 2.7 Hz, 1 H), 2.33 (dq, J = 8.7, 5.4 Hz, 1 H), 2.01 (d, J = 5.4 Hz, 3 H), 1.25 (dd, J = 9.9, 2.7 Hz, 1 H); ^{13}C NMR ($CDCl_3$, 75.5 MHz) δ 228.8, 226.5, 143.6 (br s, 3 C), 135.1 (s, 3 C), 104.5 (s, 3 C), 80.6, 79.5, 49.3, 18.0; IR (CH_2Cl_2, cm^{-1}) 2486 (w), 1934 (s), 1842 (s); TLC R_f 0.24 (hexanes/EtOAc, 5/1).

Dicarbonyl[hydrotris(1-pyrazolyl)borato][η-(1,2,3)-(±)-(2*R*,3*S*)-2-buten-1-yl]molybdenum (*Anti*-Methyl Complex 2b). *Syn*-Me complex **2a** (contaminated with about 30% of the *anti* isomer) was equilibrated to a mixture of *syn* and *anti* isomers by heating a solution in C_6D_6 in a sealed NMR tube to a temperature of 125 °C for 2 h, during which time periodic ^{1}H NMR spectra were obtained. A *syn* to *anti* equilibrium ratio of 1.0 to 3.8 was determined from the ^{1}H NMR integrals. Data for *anti*-Me complex **2b**: ^{1}H ($CDCl_3$, 300 MHz) δ 8.57 (d, J = 1.2 Hz, 1 H), 7.89 (d, J = 1.2 Hz, 1 H), 7.74 (d, J = 1.2 Hz, 1 H), 7.56 (d, J = 1.8 Hz, 2 H), 7.50 (d, J = 1.8 Hz, 1 H), 6.28 (app t, J = 1.8 Hz, 1 H), 6.18 (app t, J = 2.1 Hz, 1 H), 6.17 (app t, J = 1.5 Hz, 1 H), 4.36 (dq, J = 6.5, 6.5 Hz, 1 H), 3.90 (dt, J = 10.5, 7.4 Hz, 1 H), 3.65 (dt, J = 7.2, 1.5 Hz, 1 H), 2.29 (dd, J = 10.5, 1.1 Hz, 1 H), 1.25 (d, J = 6.6 Hz, 3 H); ^{13}C NMR ($CDCl_3$, 75.5 MHz) δ 231.2, 227.8, 146.7, 141.7, 140.7, 135.1, 134.7, 133.6, 105.1, 104.6, 104.5, 75.4, 69.2, 56.2, 14.9; IR (CH_2Cl_2, cm^{-1}) 2485 (w), 1937 (s), 1845 (s).

Dicarbonyl[hydrotris(1-pyrazolyl)borato][η-(1,2,3)-(±)-(2*R*,3*R*)-2-penten-1-yl]molybdenum (*Syn*-Ethyl Complex 3a). The complex was prepared from $(DMF)_3Mo(CO)_3$ (270 mg, 0.68 mmol, 1.00 equiv), (*E*)-1-acetoxy-2-pentene (86 mg, 0.74 mmol, 1.09 equiv), and potassium hydrotris(1-pyrazolyl)borate (170 mg, 0.67 mmol, 0.99 equiv) according to the general procedure in which the reaction mixture was stirred for 30 min before the addition of KTp. Flash silica gel chromatography (hexanes/EtOAc, 5/1) and recrystallization (hexanes/dichloromethane, 20/1) provided pure *syn*-Et complex **3a** (217 mg, 0.50 mmol, 74%) as a microcrystalline yellow solid: mp = 166−167 °C; ^{1}H NMR ($CDCl_3$, 360 MHz) δ 8.00 (br s, 3 H), 7.54 (d, J = 2.2 Hz, 3 H), 6.20 (app t, J = 2.2 Hz, 3 H), 3.80 (ddd, J = 9.5, 9.5, 6.8 Hz, 1 H), 3.42 (dd, J = 6.8, 2.9 Hz, 1 H), 2.40 (m, 1 H), 2.31 (m, 1 H), 1.90 (m, 1 H), 1.28 (app t, J = 7.2 Hz, 3 H), 1.24 (dd, J = 9.5, 2.9 Hz, 1 H); ^{13}C NMR ($CDCl_3$, 75.5 MHz) δ 232.2, 228.5, 144.2 (br s, 3 C), 135.4 (s, 3 C), 105.3 (s, 3 C), 88.7, 79.1, 50.2, 26.9, 17.9; IR (CH_2Cl_2, KCl, cm^{-1}) 2485 (w), 1932 (s), 1840 (s); TLC R_f 0.42 (hexanes/EtOAc, 5/1).

Anal. Calcd for $C_{16}H_{19}BMoN_6O_2$: C, 44.27; H, 4.41. Found: C, 44.37; H, 4.42.

Dicarbonyl[hydrotris(1-pyrazolyl)borato][η-(1,2,3)-(±)-(2*R*,3*S*)-2-penten-1-yl]molybdenum (*Anti*-Ethyl Complex 3b). The complex was prepared from $(DMF)_3Mo(CO)_3$ (260 mg, 0.65 mmol, 1.00 equiv), (*Z*)-1-acetoxy-2-pentene (83 mg, 0.71 mmol, 1.09 equiv), and potassium hydrotris(1-pyrazolyl)borate (164 mg, 0.65 mmol, 1.00 equiv) according to the general procedure in which the reaction mixture was stirred for 30 min before the addition of KTp. Flash silica gel chromatography (hexanes/EtOAc, 5/1) and recrystallization (hexanes/CH_2Cl_2, 20/1) provided pure *anti*-Et complex **3b** (200 mg, 0.46 mmol, 71%) as a yellow solid: mp = 175−177 °C; ^{1}H NMR ($CDCl_3$, 360 MHz) δ 8.55 (d, J = 1.8 Hz, 1 H), 7.87 (d, J = 2.2 Hz, 1 H), 7.77 (d, J = 1.8 Hz, 1 H), 7.55 (d, J = 2.5 Hz, 2 H), 7.49 (d, J = 2.2 Hz, 1 H), 6.27 (app t, J = 2.2 Hz, 1 H), 6.17 (m, 2 H), 4.33 (m, 1 H), 3.81 (ddd, J = 10.4, 7.6, 7.6 Hz, 1 H), 3.62 (ddd, J = 7.6, 1.6, 1.6 Hz, 1 H), 2.22 (dd, J = 10.4, 1.6 Hz, 1 H), 2.06 (ddq, J = 14.4, 7.2, 4.0 Hz, 1 H), 1.08 (app t, J = 7.2 Hz, 3 H), 0.42 (m, 1 H); ^{13}C NMR (acetone-d_6, 75.5 MHz) δ 230.3, 228.4, 148.1, 143.5, 143.0, 137.1 (s, 2 C), 135.6, 106.9, 106.3 (s, 2 C), 78.4, 75.2, 57.2, 25.0, 19.3; IR (CH_2Cl_2, KCl, cm^{-1}) 2486 (w), 1938 (s), 1847 (s); TLC R_f 0.36 (hexanes/EtOAc, 5/1). Anal. Calcd for $C_{16}H_{19}BMoN_6O_2$: C, 44.27; H, 4.41. Found: C, 44.29; H, 4.46.

Dicarbonyl[hydrotris(1-pyrazolyl)borato][η-(1,2,3)-(±)-(2*R*,3*R*)-4-methyl-2-penten-1-yl]molybdenum (*Syn*-*i*-Pr Complex 4a). The complex was prepared from $(DMF)_3Mo(CO)_3$ (1.5 g, 3.76 mmol, 1.10 equiv), 3-acetoxy-4-methyl-1-pentene (0.588 g, 4.14 mmol, 1.10 equiv), and potassium hydrotris(1-pyrazolyl)borate (0.947 g, 3.76 mmol, 1.00 equiv) according to the general procedure in which the reaction mixture was stirred for 1.5 h before the addition of KTp. Flash silica gel chromatography (hexanes/EtOAc, 5/1) and recrystallization (hexane) provided nearly pure (contaminated by approximately 5% of the *anti* isomer) *syn*-*i*-Pr complex **4a** (1.54 g, 3.44 mmol, 91%) as a yellow-orange solid: mp = 149−150 °C; ^{1}H NMR ($CDCl_3$, 300 MHz) δ 8.00 (br s, 3 H), 7.55 (d, J = 2.1 Hz, 3 H), 6.20 (t, J = 2.1 Hz, 3 H), 3.83 (m, 1 H), 3.43 (dd, J = 6.6, 3.0 Hz, 1 H), 2.51 (m, 1 H), 2.32 (dd, J = 10.8, 6.3 Hz, 1 H), 1.39 (d, J = 6.6 Hz, 3 H), 1.11 (dd, J = 8.7, 3.0 Hz, 1 H), 1.01 (d, J = 6.6 Hz, 3 H); ^{13}C NMR ($CDCl_3$, 75.5 MHz) δ 232.9, 228.3, 143.8 (s, 3 C), 135.4 (s, 3 C), 105.3 (s, 3 C), 97.1, 76.9, 48.7, 29.6, 24.7, 24.2; IR (CH_2Cl_2, KCl, cm^{-1}) 2964 (m), 2485 (m), 1932 (s), 1839 (s); TLC R_f 0.47 (hexanes/EtOAc, 5/1). Anal. Calcd for $C_{17}H_{21}BMoN_6O_2$: C, 45.56; H, 4.72. Found: C, 45.66; H, 4.66.

Dicarbonyl[hydrotris(1-pyrazolyl)borato][η-(1,2,3)-(±)-(2*R*,3*S*)-4-methyl-2-penten-1-yl]molybdenum (*Anti*-*i*-Pr Complex 4b). *Syn*-*i*-Pr complex **4a** was equilibrated to a mixture of *syn* and *anti* isomers by heating a solution in a sealed NMR of C_6D_6 tube to a temperature of 125 °C for 2 h, during which time periodic ^{1}H NMR spectra were obtained. An equilibrium ratio of *syn* to *anti* of 1.0 to 1.3 was determined from the ^{1}H NMR integrals. Data for *anti*-*i*-Pr complex **4b**: ^{1}H NMR ($CDCl_3$, 300 MHz) δ 8.57 (br s, 1 H), 7.98 (br s, 1 H), 7.71 (br s, 1 H), 7.56 (obscured, 2 H), 7.50 (br s, 1 H), 6.29 (br s, 1 H), 6.22 (obscured, 1 H), 6.19 (app t, J = 1.5 Hz, 1 H), 4.27 (app t, J = 7.1 Hz, 1 H), 3.80−3.67 (m, 2 H), 1.84 (dd, J = 9.9, 1.5 Hz, 1 H), 1.41 (d, J = 5.4 Hz, 3 H), 1.33 (m, 1 H), 1.03 (d, J = 6.3 Hz, 3 H); ^{13}C NMR ($CDCl_3$, 75.5 MHz) δ 230.9, 227.6, 147.3, 144.1, 139.9, 135.8, 135.6, 134.2, 105.8, 105.2, 105.2, 93.4, 76.1, 51.5, 31.2, 29.3, 23.1; IR (CH_2Cl_2, KCl, cm^{-1}) 2485 (w), 1935 (s), 1843 (s).

Dicarbonyl[hydrotris(1-pyrazolyl)borato][η-(1,2,3)-(±)-(2*R*,3*R*)-4,4-dimethyl-2-penten-1-yl]molybdenum (*Syn*-*t*-Bu Complex 5a). The complex was prepared from $(DMF)_3Mo(CO)_3$ (700 mg, 1.75 mmol, 1.00 equiv), 3-acetoxy-4,4-dimethyl-1-pentene (301 mg, 1.93 mmol, 1.10 equiv), and potassium hydrotris(1-pyrazolyl)borate (442 mg, 1.75 mmol, 1.00 equiv) according to the general procedure in which the reaction mixture was stirred for 4 h before the addition of KTp. Flash silica gel chromatography (hexanes/EtOAc, 5/1) and recrystallization (hexane) provided pure *syn*-*t*-Bu complex **5a** (371 mg, 0.8 mmol, 46%) as a yellow solid: mp = 95 °C with decomp; ^{1}H NMR ($CDCl_3$, 300 MHz) δ 8.11 (d, J = 1.8 Hz, 3 H), 7.54 (d, J = 2.1 Hz, 3 H), 6.19 (app t, J = 2.1 Hz, 3 H), 3.97 (ddd, J = 11.7, 8.7, 6.6 Hz, 1 H), 3.36 (dd, J = 6.6, 3.6 Hz, 1 H), 2.64 (d, J = 11.7 Hz, 1 H), 1.16 (s, 9 H), 1.04 (dd, J = 8.4, 3.3 Hz, 1 H); ^{13}C NMR ($CDCl_3$, 75.5 MHz) δ 236.0, 228.8, 144.4 (s, 3 C), 135.5 (s, 3 C), 108.4, 105.1 (s, 3 C), 77.8, 45.0, 34.6, 31.1; IR (CH_2Cl_2, KCl, cm^{-1}) 2485 (w), 1926 (s), 1835 (s); TLC R_f 0.46 (hexanes/EtOAc, 5/1). Anal. Calcd for $C_{18}H_{23}BMoN_6O_2$: C, 46.78, 5.02. Found: C, 46.95; H, 5.05.

Dicarbonyl[hydrotris(1-pyrazolyl)borato][η-(1,2,3)-(±)-(2*R*,3*S*)-4,4-dimethyl-2-penten-1-yl]molybdenum (*Anti*-*t*-Bu Complex 5b). *Syn*-*t*-Bu complex **5a** was equilibrated to a mixture of *syn* and *anti* isomers by heating a solution in a sealed NMR tube of C_6D_6 tube to a temperature of 125 °C for 1.3 h, during which time periodic ^{1}H NMR spectra were obtained. An equilibrium ratio of *syn* to *anti* of 1.0 to 1.3 was determined from the ^{1}H NMR integrals. Data for *anti*-*t*-Bu complex **5b**: ^{1}H NMR ($CDCl_3$, 300 MHz) δ 8.58 (d, J = 1.8 Hz, 1 H), 7.99 (d, J = 1.2 Hz, 1 H), 7.76 (d, J = 1.5 Hz, 1 H), 7.57−7.54 (obscured, 2 H), 7.49 (d, J = 2.1 Hz, 1 H), 6.27 (app t, J = 2.1 Hz, 1 H), 6.19 (obscured, 1 H), 6.17 (app t, J = 1.8 Hz, 1 H), 4.54 (dd, J = 8.1, 2.4 Hz, 1 H), 3.66−3.55 (m, 2 H), 2.48 (d, J = 9.9 Hz, 1 H), 1.16 (s, 9 H); ^{13}C NMR ($CDCl_3$, 75.5 MHz) δ 230.5, 230.0, 147.0, 143.2, 140.5, 135.9, 135.8, 134.2, 105.8, 105.2, 105.1, 95.4, 74.7, 56.2, 37.4, 32.9; IR (CH_2Cl_2, KCl, cm^{-1}) 2486 (w), 1936 (s), 1841 (s).

Dicarbonyl[hydrotris(1-pyrazolyl)borato][η-(1,2,3)-(±)-(1*R*,2*R*)-1-cyclohexyl-2-propen-1-yl]molybdenum (*Syn*-Cyclohexyl Complex 6a). The complex was prepared from $(DMF)_3Mo(CO)_3$ (1.06 g, 2.65 mmol, 1.00 equiv), 3-acetoxy-3-cyclohexyl-1-propene (532 mg, 2.90 mmol, 1.10 equiv), and potassium hydrotris(1-pyrazolyl)borate (669 mg, 2.65 mmol, 1.00 equiv) according to the general procedure in which the reaction mixture was stirred for 0.5 h before the addition of KTp. Flash silica gel chromatography (hexanes/EtOAc, 5/1) and recrystallization (hexane) provided nearly pure (contaminated by approximately 9% of the *anti* isomer) *syn*-cyclohexyl complex **6a** (1.05 g, 2.15 mmol, 81%) as a yellow solid: mp = 146−148 °C; ^{1}H NMR ($CDCl_3$, 300 MHz) δ 7.98 (br s, 3 H), 7.55 (d, J = 2.1 Hz, 3 H), 6.20 (app t, J = 2.1 Hz, 3 H), 3.83 (ddd, J = 10.8, 8.7, 6.6 Hz, 1 H), 3.41 (dd, J = 6.6, 3.0 Hz, 1 H), 2.29 (dd, J = 10.8, 6.6 Hz, 1 H), 2.15−1.12 (m, 11 H), 1.08 (dd, J = 8.7, 3.0 Hz, 1 H); ^{13}C NMR ($CDCl_3$, 75.5 MHz) δ 232.8, 228.5, 143.9, 135.4, 105.3, 95.9, 76.8, 48.8, 39.3, 35.7, 34.9, 26.4, 26.1 (s, 2 C); IR (CH_2Cl_2, KCl, cm^{-1}) 2485 (m), 1931 (s), 1839 (s); TLC R_f 0.44 (hexanes/EtOAc, 5/1). Anal. Calcd for $C_{20}H_{25}BMoN_6O_2$: C, 49.20; H, 5.16. Found: C, 49.46; H, 5.26.

Dicarbonyl[hydrotris(1-pyrazolyl)borato][η-(1,2,3)-(±)-(1*S*,2*R*)-1-cyclohexyl-2-propen-1-yl]molybdenum (*Anti*-Cyclohexyl Complex 6b). *Syn*-cyclohexyl complex **6a** was equilibrated to a mixture of *syn* and *anti* isomers by heating a solution in a sealed NMR tube of C_6D_6 to a temperature of 125 °C for 1.5 h, during which time periodic proton spectra were obtained. An equilibrium ratio of *syn* to *anti* of 1.0 to 1.1 was determined from the ^{1}H NMR integrals. Data for *anti*-cyclohexyl complex **6b**: ^{1}H NMR ($CDCl_3$, 300 MHz) δ 8.55 (br s, 1 H), 7.99 (br s, 1 H), 7.68 (d, J = 0.9 Hz, 1 H), 7.56 (br s, 2 H), 7.49 (d, J = 1.8 Hz, 1 H), 6.27 (br t, J = 1.8 Hz, 1 H), 6.21 (br s, 1 H), 6.17 (br s, 1 H), 4.26 (dt, J = 8.1, 1.8 Hz, 1 H), 3.77−3.65 (m, 2 H), 2.55 (br d, J = 10.2 Hz, 1 H), 2.00−0.87 (m, 11 H); ^{13}C NMR ($CDCl_3$, 75.5 MHz) δ 147.2, 144.4, 139.6, 135.7, 135.5, 134.2, 105.8, 105.2, 105.1, 92.6, 76.1, 51.0, 40.7, 39.9, 34.0, 26.6, 26.1 (s, 2 C); IR (CH_2Cl_2, KCl, cm^{-1}) 1933 (s), 1841.

Dicarbonyl[hydrotris(1-pyrazolyl)borato][η-(1,2,3)-(±)-(1*R*,2*R*)-1-phenyl-2-propen-1-yl]molybdenum (*Syn*-Phenyl Complex 7a). The complex was prepared from $(DMF)_3Mo(CO)_3$ (980 mg, 2.45 mmol, 1.00 equiv), (*E*)-cinnamyl acetate (432 mg, 2.45 mmol, 1.00 equiv), and potassium hydrotris(1-

pyrazolyl)borate (618 mg, 2.45 mmol, 1.00 equiv) according to the general procedure in which the reaction mixture was stirred for 30 min before the addition of KTp. Flash silica gel chromatography (hexanes/EtOAc, 5/1) and recrystallization (acetonitrile) provided pure *syn*-Ph complex **7a** (1077 mg, 2.23 mmol, 91%) as a red solid: mp = 194–195 °C; ^{1}H NMR ($CDCl_3$, 300 MHz) δ 8.45 (br s, 1 H), 7.75 (br s, 1 H), 7.47 (br s, 3 H), 7.20–7.09 (m, 5 H), 6.20 (br s, 2 H), 6.10 (br s, 1 H), 5.65 (br s, 1 H), 4.43 (ddd, J = 10.8, 9.0, 6.9 Hz, 1 H), 3.61 (dd, J = 6.9, 3.3 Hz, 1 H), 3.31 (d, J = 10.8 Hz, 1 H), 1.41 (dd, J = 9.0, 3.3 Hz, 1 H); ^{13}C NMR ($CDCl_3$, 75.5 MHz) δ 233.7, 227.6, 148.0–144.0 (br s, 2 C), 142.0–138.0 (br s, 1 C), 138.5, 137.0–133.0 (br s, 3 C), 128.6, 127.8, 127.2, 106.0–104.0 (br s, 3 C), 85.8, 76.5, 47.4; IR (CH_2Cl_2, KCl, cm^{-1}) 2485 (w), 1934 (s), 1845 (s); TLC R_f 0.38 (hexanes/EtOAc, 5/1). Anal. Calcd for $C_{20}H_{19}BMoN_6O_2$: C, 49.82; H, 3.97. Found: C, 49.69; H, 3.88.

Dicarbonyl[hydrotris(1-pyrazolyl)borato][η-(1,2,3)-(±)-(1*S*,2*R*)-1-phenyl-2-propen-1-yl]molybdenum (*Anti*-Phenyl Complex 7b). The complex was prepared from $(DMF)_3Mo(CO)_3$ (870 mg, 2.18 mmol, 1.00 equiv), (*Z*)-cinnamyl acetate (422 mg, 2.40 mmol, 1.10 equiv), and potassium hydrotris(1-pyrazolyl)borate (354 mg, 1.40 mmol, 1.00 equiv) according to the general procedure in which the reaction mixture was stirred for 30 min before the addition of KTp. Flash silica gel chromatography (hexanes/EtOAc, 5/1) and recrystallization (hexane) provided pure *anti*-Ph complex **7b** (511 mg, 1.06 mmol, 49%) as an orange solid: mp = 91–95 °C; ^{1}H NMR ($CDCl_3$, 300 MHz) δ 8.55 (d, J = 1.5 Hz, 1 H), 8.14 (d, J = 1.2 Hz, 1 H), 7.84 (d, J = 1.2 Hz, 1 H), 7.62 (d, J = 2.1 Hz, 1 H), 7.59 (d, J = 1.8 Hz, 1 H), 7.51 (d, J = 2.1 Hz, 1 H), 7.28–7.08 (m, 5 H), 6.28–6.26 (m, 2 H), 6.22 (app t, J = 1.8 Hz, 1 H), 5.50 (dt, J = 8.1 Hz, 1 H), 4.06 (dt, J = 10.8, 7.7 Hz, 1 H), 3.86 (dt, J = 7.2, 2.1 Hz, 1 H), 2.62 (d, J = 10.8 Hz, 1 H); ^{13}C NMR ($CDCl_3$, 75.5 MHz) δ 229.9, 226.6, 147.5, 143.2, 140.7, 140.4, 136.1, 135.8, 134.3, 128.6, 128.1, 125.9, 105.9, 105.4, 105.3, 81.9, 75.3, 54.5; IR (CH_2Cl_2, KCl, cm^{-1}) 2486 (s), 1945 (s), 1856 (s); TLC R_f 0.31 (hexanes/EtOAc, 5/1). Anal. Calcd for $C_{20}H_{19}BMoN_6O_2$: C, 49.82; H, 3.97. Found: C, 49.97; H, 3.96.

Dicarbonyl[hydrotris(1-pyrazolyl)borato][η-(1,2,3)-(±)-(1*R*,2*R*)-1-(4-methoxyphenyl)-2-propen-1-yl]molybdenum (*Syn*-*p*-MeOPh Complex 8a). The complex was prepared from $(DMF)_3Mo(CO)_3$ (560 mg, 1.40 mmol, 1.00 equiv), 3-acetoxy-3-(4-methoxyphenyl)-1-propene (318 mg, 1.54 mmol, 1.10 equiv), and potassium hydrotris(1-pyrazolyl)borate (354 mg, 1.40 mmol, 1.00 equiv) according to the general procedure in which the reaction mixture was stirred for 30 min before the addition of KTp. Flash silica gel chromatography (hexanes/EtOAc, 5/1) and recrystallization (hexane) provided pure *syn*-*p*-MeOPh complex **8a** (660 mg, 1.29 mmol, 92%) as an orange solid: mp = 191–193 °C; ^{1}H NMR ($CDCl_3$, 300 MHz) δ 8.44 (br s, 1 H), 7.74 (br s, 1 H), 7.46 (br, J = Hz, 3 H), 7.04 (d, J = 8.4 Hz, 2 H), 6.72 (d, J = 8.4 Hz, 2 H), 6.36–6.05 (br, J = Hz, 3 H), 5.69 (br s, 1 H), 4.31 (ddd, J = 10.5, 9.0, 6.6 Hz, 1 H), 3.79 (s, 3 H), 3.58 (dd, J = 6.6, 3.3 Hz, 1 H), 3.40 (d, J = 10.5 Hz, 1 H), 1.38 (dd, J = 9.0, 3.3 Hz, 1 H); ^{13}C NMR ($CDCl_3$, 75.5 MHz) δ 233.6, 227.9, 159.3, 147–145 (br s, 2 C), 140–139 (br s, 1 C), 135.7 (br s, 2 C), 135–134 (br s, 1 C), 130.6, 129.1, 114.2, 105.2 (s, 3 C), 87.7, 75.5, 55.4, 47.3; IR (CH_2Cl_2, KCl, cm^{-1}) 2485 (m), 1930 (s), 1841 (s); TLC R_f 0.26 (hexanes/EtOAc, 5/1). Anal. Calcd for $C_{21}H_{21}BMoN_6O_3$: C, 49.25; H, 4.13. Found: C, 49.09; H, 4.19.

Dicarbonyl[hydrotris(1-pyrazolyl)borato][η-(1,2,3)-(±)-(1*R*,2*R*)-1-(4-(trifluoromethyl)phenyl)-2-propen-1-yl]molybdenum (*Syn*-*p*-CF_3Ph Complex 9a). The complex was prepared from $(DMF)_3Mo(CO)_3$ (590 mg, 1.48 mmol, 1.00 equiv), 3-acetoxy-3-(4-(trifluoromethyl)phenyl)-1-propene (397 mg, 1.63 mmol, 1.10 equiv), and potassium hydrotris(1-pyrazolyl)borate (373 mg, 1.48 mmol, 1.00 equiv) according to the general procedure in which the reaction mixture was stirred for 30 min before the addition of KTp. Flash silica gel chromatography (hexanes/EtOAc, 5/1) and recrystallization (hexane) provided pure *syn*-*p*-CF_3Ph complex **9a** (700 mg, 1.27 mmol, 86%) as an orange solid: mp = 179–180 °C; ^{1}H NMR ($CDCl_3$, 300 MHz) δ 8.70–8.00 (br s, 2 H), 7.49 (br s, 4 H), 7.37 (d, J = 8.1 Hz, 2 H), 7.11 (d, J = 8.1 Hz, 2 H), 6.20 (br s, 2 H), 5.72 (br s, 1 H), 4.47 (m, 1 H), 3.66 (dd, J = 6.6, 3.3 Hz, 1 H), 3.21 (d, J = 10.5 Hz, 1 H), 1.45 (dd, J = 9.0, 3.3 Hz, 1 H); ^{13}C NMR ($CDCl_3$, 75.5 MHz) δ 233.7, 227.0, 147–146 (br s, 2 C), 143.2, 141–139 (br s, 1 C), 137–135 (br s, 3 C), 128.6 (q, J = 32.4 Hz), 127.7, 125.4 (q, J = 3.9 Hz), 124.2 (q, J = 272.0 Hz), 105.1 (br s, 3 C), 82.0, 78.7, 47.3; IR (CH_2Cl_2, KCl, cm^{-1}) 2486 (m), 1939 (s), 1852 (s); TLC R_f 0.36 (hexanes/EtOAc, 5/1). Anal. Calcd for $C_{21}H_{19}BF_3MoN_6O_2$: C, 45.85; H, 3.30. Found: C, 45.99; H, 3.31.

Dicarbonyl[hydrotris(1-pyrazolyl)borato][η-(2,3,4)-(±)-(2*R*,4*R*)-3-penten-2-yl]molybdenum (*Syn*/*Anti*-1,3-Dimethyl Complex 10b). The complex was prepared from $(DMF)_3Mo(CO)_3$ (360 mg, 0.902 mmol, 1.00 equiv), (*E*)-4-acetoxy-2-pentene (136 mg, 1.171 mmol, 1.30 equiv), and potassium hydrotris(1-pyrazolyl)borate (227 mg, 0.900 mmol, 1.00 equiv) according to the general procedure in which the reaction mixture was stirred for 2 h before the addition of KTp. Flash silica gel chromatography (hexanes/EtOAc, 5/1) and recrystallization (hexanes/CH_2Cl_2, 12/1) provided nearly pure (contaminated by the equilibrium amount of the *syn*/*syn* isomer—about 8%) *syn*/*anti*-1,3-di-Me complex **10b** (280 mg, 0.645 mmol, 72%) as a yellow solid: mp 212–214 °C; ^{1}H NMR ($CDCl_3$, 360 MHz) δ 8.50 (br s, 1 H), 7.85 (br s, 1 H), 7.58 (br s, 3 H), 7.49 (br s, 1 H), 6.20 (br s, 3 H), 4.10 (dq, J = 6.8, 6.8 Hz, 1 H), 3.98 (dd, J = 10.8, 7.9 Hz, 1 H), 3.22 (dq, J = 12.2, 6.1 Hz, 1 H), 1.90 (d, J = 6.5 Hz, 3 H), 1.28 (d, J = 6.1 Hz, 3 H); ^{13}C NMR ($CDCl_3$, 75.5 MHz) δ 234.2, 228.2, 147–145 (br s, 2 C), 140.5–139.5 (br s, 1 C), 136.5–135 (br s, 2 C), 134.5–133.5 (br s, 1 C), 105.6–104.9 (br m, 3 C), 86.2, 78.2, 59.4, 19.1, 17.0; IR (CH_2Cl_2, KCl, cm^{-1}) 2485 (w), 1927 (s), 1834 (s); TLC R_f 0.41 (hexanes/EtOAc, 5/1). Anal. Calcd for $C_{16}H_{19}BMoN_6O_2$: C, 44.27; H, 4.41. Found: C, 44.32; H, 4.38.

Dicarbonyl[hydrotris(1-pyrazolyl)borato][η-(2,3,4)-(±)-(2*R*,4*R*)-3-penten-2-yl]molybdenum (*Syn*/*Syn*-Dimethyl Complex 10a). The complex was obtained in the preceding reaction. Data for *syn*/*syn*-diMe complex **10a**: ^{1}H NMR ($CDCl_3$, 300 MHz) δ 2.21 (dq, J = 10.2, 6.3 Hz, 2 H, $-CHCH_3$), 1.98 (d, J = 6.3 Hz, 6 H, $-CHCH_3$), the rest of the peaks are obscured by those of the major isomer; ^{13}C NMR ($CDCl_3$, 75.5 MHz) δ 145.6, 135.3, 69.9, 17.9, the rest of the resonances were not found due to overlap with the resonances of the major isomer and due to the low equilibrium concentration of the minor isomer.

Dicarbonyl[hydrotris(1-pyrazolyl)borato][η-(1,2,3)-(±)-(1*R*,2*R*,3*S*)-1-phenyl-2-buten-1-yl]molybdenum (*Syn*/*Syn*-1-Phenyl-3-Methyl Complex 11a). The complex was prepared from $(DMF)_3Mo(CO)_3$ (1.62 g, 4.06 mmol, 1.00 equiv), (*E*)-1-acetoxy-1-phenyl-2-butene (849 mg, 4.46 mmol, 1.10 equiv), and potassium hydrotris(1-pyrazolyl)borate (1.02 g, 4.05 mmol, 1.00 equiv) according to the general procedure in which the reaction mixture was stirred for 30 min before the addition of KTp. Flash silica gel chromatography (hexanes/EtOAc, 5/1) and recrystallization from hexane provided pure complex **11a/b** (1.64 g, 3.31 mmol, 82%) as a 3 to 1 mixture of all-*syn* **11a** to *syn*-Ph/*anti*-Me **11b** as determined by ^{1}H NMR. Data for the orange product *syn*/*syn*-**11a**: mp = 174–175 °C (mp on 3 to 1 mixture of isomers); ^{1}H NMR ($CDCl_3$, 300 MHz) δ 7.69 (br s, 3 H), 7.50 (d, J = 2.1 Hz, 3 H), 6.99–6.95 (m, 3 H), 6.75–6.72 (m, 2 H), 6.03 (br s, 3 H), 4.70 (app t, J = 10.1 Hz, 1 H), 3.48 (d, J = 9.9 Hz, 1 H), 2.40 (d, J = 6.6 Hz, 3 H), 1.90 (dq, J = 9.9, 6.6 Hz, 1 H); ^{13}C NMR ($CDCl_3$, 75.5 MHz) δ 239.6, 227.5, 145.3 (s, 3 C), 140.1, 135.1 (s, 3 C), 128.2, 127.6, 126.0, 105.0 (s, 3 C), 88.6, 80.7, 62.1, 16.8; IR (CH_2Cl_2, KCl, cm^{-1}, obtained on the 3 to 1 *syn*/*syn* to *syn*/*anti* mixture) 2485 (m), 1925 (s), 1837 (s); TLC R_f 0.44 (hexanes/EtOAc, 5/1, obtained on the 3 to 1 *syn*/*syn* to *syn*/*anti* mixture). Anal. Calcd for $C_{21}H_{21}BMoN_6O_2$: C, 50.83; H, 4.27. Found: C, 50.72; H, 4.22.

Dicarbonyl[hydrotris(1-pyrazolyl)borato][η-(1,2,3)-(±)-(1*R*,2*R*,3*R*)-1-phenyl-2-buten-1-yl]molybdenum (*Syn*-Phenyl/*Anti*-Methyl Complex 11b). While in solution at room temperature in $CDCl_3$, the 3 to 1 mixture of *syn*/*syn* to *syn*/*anti* isomers obtained in the above reaction equilibrated within 24 h to a 1 to 4.7 mixture of *syn*/*syn* and *syn*-Ph/*anti*-Me isomers. NMR data for *syn*-Ph/*anti*-Me complex **11b**: ^{1}H NMR ($CDCl_3$, 300 MHz) δ 8.46 (d, J = 1.2 Hz, 1 H), 7.67 (d, J = 0.9 Hz, 1 H), 7.62 (d, J = 1.8 Hz, 1 H), 7.43 (d, J = 1.8 Hz, 1 H), 7.39 (d, J = 1.8 Hz, 1 H), 7.12–6.97 (m, 5 H), 6.32 (d, J = 1.2 Hz, 1 H), 6.25 (app t, J = 1.8 Hz, 1 H), 6.20 (app t, J = 1.8 Hz, 1 H), 5.60 (app t, J = 1.5 Hz, 1 H), 4.63 (dd, J = 11.4, 8.1 Hz, 1 H), 4.30 (dq, J = 6.8, 6.8 Hz, 1 H), 4.05 (d, J = 11.4 Hz, 1 H), 1.42 (d, J = 6.6 Hz, 3 H); ^{13}C NMR ($CDCl_3$, 75.5 MHz) δ 235.8, 227.5, 146.8, 145.8, 139.4, 138.9, 135.7, 135.5, 134.2, 128.4, 127.9, 126.9, 83.2, 81.8, 57.3, 17.0. The equilibrated mixture gave an IR spectrum identical to that described above for the 3 to 1 mixture of *syn*/*syn* to *syn*/*anti* isomers.

Dicarbonyl[hydrotris(1-pyrazolyl)borato][η-(1,2,3)-(1*R*,3*S*)-1,3-diphenyl-2-propen-1-yl]molybdenum (*Syn*/*Syn*-Diphenyl Complex 12a). The complex was prepared from $(DMF)_3Mo(CO)_3$ (456 mg, 1.14 mmol, 1.00 equiv), (*E*)-3-acetoxy-1,3-diphenyl-1-propene (288 mg, 1.14 mmol, 1.00 equiv), and potassium hydrotris(1-pyrazolyl)borate (288 mg, 1.14 mmol, 1.00 equiv) according to the general procedure in which the reaction mixture was stirred for 1 h before the addition of KTp. Flash silica gel chromatography (hexanes/EtOAc, 5/1) gave an equilibrium mixture of the *syn*/*syn* to *syn*/*anti* isomers while recrystallization (acetonitrile) provided pure *syn*/*syn*-di-Ph complex **12a** (491 mg, 0.88 mmol, 77%) as an orange solid: mp = 188–190 °C; ^{1}H NMR ($CDCl_3$, 300 MHz) δ 7.48–7.45 (m, 6 H), 7.26–7.24 (m, 10 H), 5.91 (app t, J = 2.1 Hz, 3 H), 5.16 (t, J = 10.1 Hz, 1 H), 3.49 (d, J = 10.2 Hz, 2 H); ^{13}C NMR ($CDCl_3$, 75.5 MHz) δ 234.7, 145.4 (br s, 3 C), 139.7, 135.2 (br s, 3 C), 129.1, 128.6, 127.2, 104.9 (br s, 3 C), 82.8, 76.4; IR (CH_2Cl_2, KCl, cm^{-1}, obtained on the pure *syn*/*syn* isomer) 2485 (w), 1928 (s), 1841 (s); TLC R_f 0.45 (hexanes/EtOAc, 5/1). Anal. Calcd for $C_{26}H_{23}BMoN_6O_2$: C, 55.94; H, 4.15. Found: C, 55.89; H, 4.24.

Dicarbonyl[hydrotris(1-pyrazolyl)borato][η-(1,2,3)-(±)-(1*R*,3*R*)-1,3-diphenyl-2-propen-1-yl]molybdenum (*Syn*/*Anti*-Diphenyl Complex 12b). Complex **12a** was obtained after recrystallization of the mixture obtained in the preceding reaction. Equilibrium was established either at ambient temperature in approximately 24 h or more rapidly at 100 °C. At equilibrium the *syn*/*syn* isomer predominated by 2 to 1. Data for *syn*/*anti*-diPh complex **12b**: ^{1}H NMR ($CDCl_3$, 300 MHz) δ 8.48 (br s, 1 H), 7.99 (br s, 1 H), 7.66 (br s, 1 H), 7.50–7.00 (m, 12 H), 6.50–6.10 (br, J = Hz, 3 H), 5.61 (br s, 1 H), 5.40 (d, J = 8.4 Hz, 1 H), 4.86 (dd, J = 11.7, 8.4 Hz, 1 H), 4.52 (d, J = 11.7 Hz, 1 H).

Dicarbonyl[hydrotris(1-pyrazolyl)borato][η-(3,4,5)-(3*R*,5*R*)-2,2,6,6-tetramethyl-4-hepten-3-yl]molybdenum (*Syn*/*Anti*-Di-*t*-Bu Complex 13b). The complex was prepared from $(DMF)_3Mo(CO)_3$ (1.25 g, 3.130 mmol, 1.00 equiv), (*E*)-5-acetoxy-2,2,6,6-tetramethyl-3-heptene (665 mg, 3.132 mmol, 1.00 equiv), and potassium hydrotris(1-pyrazolyl)borate (789 mg, 3.129 mmol, 1.00 equiv) according to the general procedure in which the reaction mixture was stirred for 24 h before the addition of KTp. Very rapid flash silica gel chromatography (hexanes/EtOAc, 83/17) and washing with hexane provided *syn*/*anti*-di-*t*-Bu complex **13b**, contaminated with approximately 33% of the *syn*/*syn* isomer (212 mg, 0.409 mmol, 13%) as an *extremely* sensitive brown glass: ^{1}H NMR ($CDCl_3$, 300 MHz) δ 8.12 (d, J = 1.8 Hz, 3 H), 7.54 (d, J = 2.1 Hz, 3 H), 6.18 (app t, J = 2.1 Hz, 3 H), 4.10–4.00 (m, 2 H), 3.85 (d, J = 11.4 Hz, 1 H), 1.17 (s, 9 H), 1.01 (s, 9 H); TLC R_f 0.62 (hexanes/EtOAc, 5/1, obtained on the 2.5 to 1 *syn*/*anti* to *syn*/*syn* mixture). The extreme sensitivity of this complex precluded further characterization.

Dicarbonyl[hydrotris(1-pyrazolyl)borato][η-(3,4,5)-2,2,6,6-tetramethyl-4-hepten-3-yl]molybdenum (*Syn*/*Syn*-Di-*t*-Bu Complex 13a). This complex was prepared as in the reaction described above. ^{1}H NMR data for *syn*/*syn*-di-*t*-Bu complex **13a**: ^{1}H NMR ($CDCl_3$, 300 MHz) δ 7.95 (d, J = 1.8 Hz, 3 H), 7.63 (d, J = 2.4 Hz, 3 H), 6.18–6.17 (obscured, 3 H), 4.72 (t, J = 10.8 Hz, 1 H), 2.62 (d, J = 10.5 Hz, 2 H), 1.10 (s, 18 H).

Dicarbonyl[hydrotris(1-pyrazolyl)borato][η-(1,2,3)-(±)-(1*R*,2*R*,3*S*)-1-phenyl-4,4-dimethyl-2-penten-1-yl]molybdenum (*Syn*-Phenyl/*Syn*-*t*-Bu Complex 14a). The complex was prepared from $(DMF)_3Mo(CO)_3$ (1.66 g, 4.16 mmol, 1.00 equiv), (*E*)-3-acetoxy-4,4-dimethyl-1-phenyl-1-pentene (966 mg, 4.16 mmol, 1.00 equiv), and potassium hydrotris(1-pyrazolyl)borate (1.05 g, 4.16 mmol, 1.00 equiv) according to the general procedure in which the reaction mixture was stirred for 3 h before the addition of KTp. Flash silica gel chromatography (hexanes/EtOAc, 5/1) and recrystallization (hexane) provided pure *syn*-Ph/*syn*-*t*-Bu complex **14a** (1.71 mg, 3.18 mmol, 76%) as an orange solid that decomposed in solution before giving any evidence of a second isomer: mp = 139–141 °C; ^{1}H NMR ($CDCl_3$, 300 MHz) δ 7.61 (d, J = 1.5 Hz, 3 H), 7.56 (d, J = 2.1 Hz, 3 H), 7.06–7.04 (m, 3 H), 6.84–6.31 (m, 2 H), 6.04 (app t, J = 2.0 Hz, 3 H), 5.13 (app t, J = 10.5 Hz, 1 H), 3.68 (d, J = 10.2 Hz, 1 H), 2.64 (d, J = 10.8 Hz, 1 H), 1.49 (s, 9 H); ^{13}C NMR ($CDCl_3$, 75.5 MHz) δ 237.6, 236.4, 144.9 (s, 3 C), 140.6, 135.5 (s, 3 C), 128.3, 127.4, 126.2, 105.1 (s, 3 C), 92.6, 86.2, 84.4, 33.4, 32.7; IR (CH_2Cl_2, KCl, cm^{-1}) 2963 (w), 2486 (w), 1921 (s), 1831 (s); TLC R_f 0.45 (hexanes/EtOAc, 5/1). Anal. Calcd for $C_{24}H_{27}BMoN_6O_2$: C, 53.55; H, 5.06. Found: C, 53.80; H, 5.19.

Dicarbonyl[hydrotris(1-pyrazolyl)borato][η-(1,2,3)-(±)-(3*R*,4*S*)-2-methyl-3-penten-2-yl]molybdenum (3-*Syn*-1,1,3-Trimethyl Complex 15a). The complex was prepared from $(DMF)_3Mo(CO)_3$ (1.35 g, 3.38 mmol, 1.00 equiv), 4-acetoxy-2-methyl-2-pentene (479 mg, 3.37 mmol, 1.00 equiv), and potassium hydrotris(1-pyrazolyl)borate (852 mg, 3.38 mmol, 1.00 equiv) according to the general procedure in which the reaction mixture was stirred for 2 h before the addition of KTp. Flash silica gel chromatography (hexanes/EtOAc, 5/1) and recrystallization (hexane) provided pure 3-*syn*-1,1,3-tri-Me complex **15a** (1.06 g, 2.37 mmol, 70%) as an orange-yellow microcrystalline solid: mp = 230 °C with decomp; ^{1}H NMR ($CDCl_3$, 360 MHz) δ 8.02 (br s, 3 H), 7.56 (d, J = 2.5 Hz, 3 H), 6.20 (app t, J = 2.2 Hz, 3 H), 4.33 (d, J = 10.8 Hz, 1 H), 3.16 (dq, J = 12.2, 6.1 Hz, 1 H), 1.99 (s, 3 H), 1.84 (d, J = 6.1 Hz, 3 H), 1.39 (s, 3 H); ^{13}C NMR ($CDCl_3$, 75.5 MHz) δ 236.9, 232.9, 145.1, 135.3, 105.2, 96.9, 84.8, 68.6, 27.8, 25.2, 18.4; IR (CH_2Cl_2, KCl, cm^{-1}) 2485 (w), 1916 (s), 1823 (s); TLC R_f 0.44 (hexanes/EtOAc, 5/1). Anal. Calcd for $C_{17}H_{21}BMoN_6O_2$: C, 45.56; H, 4.72. Found: C, 45.69; H, 4.71.

Dicarbonyl[hydrotris(1-pyrazolyl)borato][η-(2,3,4)-(±)-(2*R*,4*R*)-3-methyl-3-penten-2-yl]molybdenum (*Syn*/*Anti*-1,2,3-Trimethyl Complex 16b). The complex was prepared from $(DMF)_3Mo(CO)_3$ (280 mg, 0.70 mmol, 1.00 equiv), (*E*)-4-acetoxy-3-methyl-2-pentene (150 mg, 1.05 mmol, 1.50 equiv), and potassium hydrotris(1-pyrazolyl)borate (177 mg, 0.70 mmol, 1.00 equiv) according to the general procedure in which the reaction mixture was stirred for 7 h before the addition of KTp. Flash silica gel chromatography (hexanes/EtOAc, 5/1) and recrystallization (hexanes) provided *syn*/*anti*-1,2,3-tri-Me complex **16b**, contaminated by the equilibrium amount of the *syn*/*syn* isomer (about 5%) (160 mg, 0.36 mmol, 51%) as an orange microcrystalline solid: mp = 170 °C with decomp; ^{1}H NMR ($CDCl_3$, 300 MHz) δ 8.39 (br s, 1 H), 7.91 (br s, 1 H), 7.85 (br s, 1 H), 7.60 (br s, 2 H), 7.36 (d, J = 1.8 Hz, 1 H), 6.19 (t, J = 1.5 Hz, 1 H), 6.15 (br s, 2 H), 4.09 (q, J = 6.5 Hz, 1 H), 2.62 (q, J = 6.7 Hz, 1 H), 2.09 (d, J = 6.7 Hz, 3 H), 1.58 (s, 3 H), 1.28 (d, J = 6.5 Hz, 3 H); ^{13}C NMR ($CDCl_3$, 75.5 MHz) δ 230.2, 229.1, 146.8, 145.5, 142.4, 136.8, 136.3, 133.7, 105.2, 104.9, 104.9, 85.7, 73.4, 66.1, 17.3, 17.0, 16.6; IR (CH_2Cl_2, KCl, cm^{-1}) 2985 (w), 2482 (m), 1930 (s), 1836 (s); TLC R_f 0.46 (hexanes/EtOAc, 5/1). Anal. Calcd for $C_{17}H_{21}BMoN_6O_2$: C, 45.56; H, 4.72. Found: C, 45.81; H, 4.67.

Dicarbonyl[hydrotris(1-pyrazolyl)borato][η-(1,2,3)-(±)-(1*S*,2*S*)-1-carbomethoxy-2-propen-1-yl]molybdenum (*Syn*-Carbomethoxy Complex 17a). A Schlenk flask equipped with a stir bar and flushed with dry Ar was charged with $(DMF)_3Mo(CO)_3$ (299 mg, 0.75 mmol, 1.00 equiv) and 10 mL of dry deoxygenated CH_2Cl_2 to give a light green solution. Neat methyl (*E*)-4-bromo-2-butenoate (147 mg, 0.82 mmol, 1.10 equiv) was added to produce a yellow brown solution; stirring was continued for 2 h at which time solid potassium hydrotris-(1-pyrazolyl)borate (207 mg, 0.82 mmol, 1.10 equiv) was added and the reaction mixture was stirred an additional 1 h. The product was isolated by a combination of flash silica gel chromatography (hexanes/EtOAc, 1/1) and recrystallization from pentane and Et_2O to give *syn*-carbomethoxy complex **17a** (217 mg, 0.457 mmol, 61%) as a yellow solid: mp 140–142 °C; ^1H NMR ($CDCl_3$, 500 MHz) δ 7.93 (br s, 3 H), 7.53 (d, J = 2.0 Hz, 3 H), 6.20 (app t, J = 2.3 Hz, 3 H), 4.83 (ddd, J = 9.5, 9.5, 6.5 Hz, 1 H), 3.65 (dd, J = 6.5, 2.8 Hz, 1 H), 3.55 (s, 3 H), 2.49 (d, J = 9.5 Hz, 1 H), 1.42 (dd, J = 9.5, 2.8 Hz, 1 H); ^{13}C NMR ($CDCl_3$, 75.5 MHz) δ 234.6, 224.9, 172.0, 143.7 (br s, 3 C), 135.5 (s, 3 C), 105.5 (s, 3 C), 85.6, 66.9, 51.5, 48.0; IR (CH_2Cl_2, KCl, cm^{-1}) 1954 (s), 1866 (s), 1712 (s); TLC R_f 0.19 (hexanes/EtOAc, 5/1). Anal. Calcd for $C_{16}H_{17}BMoN_6O_4$: C, 41.41; H, 3.69. Found: C, 41.27, 3.75.

Dicarbonyl[hydrotris(1-pyrazolyl)borato][η-(1,2,3)-(±)-(1*R*,2*S*)-1-carbomethoxy-2-propen-1-yl]molybdenum (*Anti*-Carbomethoxy Complex 17b). *Syn*-carbomethoxy complex **17a** was equilibrated at 125 °C in C_6D_6 to a mixture of *syn*-**17a** and *anti*-carbomethoxy **17b** in which the *anti* isomer predominated; the final ratio was 3.7 to 1.0. Data for *anti*-carbomethoxy complex **17b**: ^1H NMR ($CDCl_3$, 300 MHz) δ 8.58 (d, J = 1.2 Hz, 1 H), 8.14 (d, J = 0.9 Hz, 1 H), 7.67 (d, J = 1.2 Hz, 1 H), 7.58 (d, J = 1.5 Hz, 1 H), 7.57 (d, J = 2.1 Hz, 1 H), 7.50 (d, J = 1.8 Hz, 1 H), 6.29 (app t, J = 1.8 Hz, 1 H), 6.23 (app t, J = 1.5 Hz, 1 H), 6.20 (app t, J = 1.8 Hz, 1 H), 4.47 (d, J = 6.9 Hz, 1 H), 4.30 (ddd, J = 10.8, 7.5, 7.5 Hz, 1 H), 3.90 (d, J = 7.5 Hz, 1 H), 3.70 (s, 3 H), 3.13 (dd, J = 10.5, 1.2 Hz, 1 H); ^{13}C NMR ($CDCl_3$, 75.5 MHz) δ 230.5, 225.0, 175.1, 147.6, 144.8, 139.3, 135.9 (s, 2 C), 134.4, 106.1, 105.6, 105.5, 82.8, 69.1, 53.0, 51.0; IR (CH_2Cl_2, KCl, cm^{-1}) 2489 (w), 1958 (s), 1870 (s), 1709 (s).

Dicarbonyl[hydrotris(1-pyrazolyl)borato][η-(1,2,3)-(±)-(1*R*,2*S*)-1-methoxy-2-propen-1-yl]molybdenum (*Syn*-Methoxy Complex 18a). Under Ar in a Schlenk tube equipped with a magnetic stirring bar was combined, in order, Mo-$(DMF)_3(CO)_3$ (1.46 g, 3.65 mmol, 1.00 equiv), CH_2Cl_2 (20 mL), 2-propenal (225 mg, 4.01 mmol, 1.10 equiv), and TBDMSCl (660 mg, 4.38 mmol, 1.20 equiv); the resulting dark red solution was stirred at ambient temperature for 1 h during which time the color slowly lightened to orange. Potassium hydrotris(1-pyrazolyl)borate (1.01 g, 4.01 mmol, 1.10 equiv) was added in one portion, and stirring was continued for 15 min. A THF solution of tetra-*n*-butylammonium fluoride (9.13 mL, 1.00 M, 4.01 mmol, 2.50 equiv) was added, and after 15 min methyl iodide (10.4 g, 73.0 mmol, 20.0 equiv) was added. After being stirred for 48 h, the reaction mixture was concentrated to a dark red oil which was flash chromatographed on silica gel (hexanes/EtOAc, 1/1) to give an orange-red solid that was recrystallized (hexanes/CH_2Cl_2, 4/1) to yield pure *syn*-MeO complex **18a** (1.01 g, 2.32 mmol, 64%) as a high-melting yellow solid: mp 161–163 °C with decomp; ^1H NMR ($CDCl_3$, 300 MHz) δ 8.50 (br s, 1 H), 8.11 (br s, 1 H), 7.81 (br s, 1 H), 7.58 (br s, 2 H), 7.54 (br s, 1 H), 6.27 (br s, 1 H), 6.17 (br s, 2 H), 4.59 (d, J = 8.0 Hz, 1 H), 3.81 (m, 1 H), 3.85 (s, 3 H), 3.31 (dd, J = 7.0, 4.0 Hz, 1 H), 1.26 (dd, J = 9.0, 3.0 Hz, 1 H); ^{13}C NMR ($CDCl_3$, 75.5 MHz) δ 232.6, 227.8, 147.1, 144.4, 141.8, 135.7 (s, 2 C), 134.2, 120.4, 105.1, 104.9 (2 C), 61.7, 59.8, 47.5; IR (CH_2Cl_2, KCl, cm^{-1}) 1930 (s), 1832 (s); TLC R_f 0.43 (hexanes/EtOAc). Anal. Calcd for $C_{15}H_{17}BMoN_6O_3$: C, 41.31; H, 3.93; N, 19.27. Found: C, 41.27; H, 3.97; N, 19.19.

Dicarbonyl[hydrotris(1-pyrazolyl)borato][η-(1,2,3)-(±)-(1*R*,2*S*)-1-acetoxy-2-propen-1-yl]molybdenum (*Syn*-Acetoxy Complex 19a). A Schlenk flask equipped with a magnetic stirring bar was charged with $(DMF)_3Mo(CO)_3$ (780 mg, 1.95 mmol, 1.00 equiv) and 12 mL of dry deoxygenated CH_2Cl_2 to give a green solution. 2-Propenal (0.131 mL, 1.95 mmol, 1.00 equiv) was added producing a dark red solution to which acetic anhydride (0.203 mL, 2.15 mmol, 1.1 equiv) was added, and the reaction mixture was stirred at ambient temperature for 1 h during which time the color slowly lightened to dark yellow-orange. Solid potassium hydrotris-(1-pyrazolyl)borate (493 mg, 1.95 mmol, 1.00 equiv) was added, and the reaction mixture was stirred an additional 15 min and then concentrated to a yellow paste that was flash chromatographed on silica gel (hexanes/EtOAc, 15/10) and recrystallized (hexanes/CH_2Cl_2, 7/1) to give the *syn*-acetoxy complex **19a** (605 mg, 1.30 mmol, 67%): mp 170–171 °C; ^1H NMR ($CDCl_3$, 360 MHz) δ 8.70–8.10 (br s, 1 H), 8.30–7.70 (br s, 2 H), 7.57 (br s, 3 H), 6.22 (br s, 3 H), 5.42 (d, J = 7.2 Hz, 1 H), 4.05 (ddd, J = 9.0, 7.4, 7.4 Hz, 1 H), 3.38 (dd, J = 7.2, 2.5 Hz, 1 H), 2.23 (s, 3 H), 1.49 (dd, J = 9.4, 2.3 Hz, 1 H); ^{13}C NMR ($CDCl_3$, 75.5 MHz) δ 228.7, 227.5, 169.0, 147–143 (br s, 3 C), 136–135 (br s, 3 C), 105.4 (br s, 3 C), 97.9, 66.6, 48.2, 21.2; IR (CH_2Cl_2, KCl, cm^{-1}) 2486 (w), 1949 (s), 1859 (s), 1753 (s); TLC R_f 0.23 (hexanes/EtOAc, 5/1). Anal. Calcd for $C_{16}H_{17}BMoN_6O_4$: C, 41.41; H, 3.69. Found: C, 41.34; H, 3.68.

Dicarbonyl[hydrotris(1-pyrazolyl)borato][η-(1,2,3)-(±)-(1*S*,2*S*)-1-acetoxy-2-propen-1-yl]molybdenum (*Anti*-Acetoxy Complex 19b). *Syn*-acetoxy complex **19a** was equilibrated to a 3.3 to 1.0 mixture of *anti* to *syn* isomers by heating a C_6D_6 solution in a sealed NMR tube at 125 °C until no further changes were observed in the ^1H NMR. Data for *anti*-acetoxy complex **19b**: ^1H NMR ($CDCl_3$, 300 MHz) δ 8.53 (d, J = 0.9 Hz, 1 H), 8.49 (d, J = 0.9 Hz, 1 H), 7.75 (dd, J = 4.8, 1.2 Hz, 1 H, C*H*OAc), 7.67 (d, J = 0.9 Hz, 1 H), 7.57 (m, 2 H, overlapping with the minor isomer absorptions), 6.30–6.19 (m, 3 H), 3.80 (d, J = 6.9 Hz, 1 H), 3.52 (ddd, J = 10.2, 6.9, 4.8 Hz, 1 H), 2.38 (dd, J = 10.2, 1.4 Hz, 1 H), 2.08 (s, 3 H); ^{13}C NMR ($CDCl_3$, 75.5 MHz) δ 228.4, 222.7, 170.4, 147.2, 145.1, 139.2, 135.8, 135.6, 134.3, 108.3, 105.8, 105.6, 105.2, 63.6, 50.6, 20.8; IR (CH_2Cl_2, KCl, cm^{-1}) 1951 (s), 1862 (s), 1735 (s).

X-ray Crystallography. X-ray Structure Methods, Collection, and Reduction for 1, 2b, 3a, 10b, 11b, 12a, 17a, and 18a. All 8 compounds were mounted on a glass fiber with super glue and placed on a Siemens P4 automated diffractometer for data collection. Semi-empirical corrections for absorption, using azimuthal ψ scans, were applied to **1**, **2b**, **10b**, **11b**, **12a**, and **17a**, and all data were corrected for *Lp* effects. The structures were solved by direct methods or Patterson interpretation, and refinement was carried out by the full-matrix least-squares program on F^2 with SHELXTL-93. The scattering factors for all atoms, the anomalous-dispersion corrections, and the linear absorption coefficients are from the *International Tables for X-ray Crystallography*, Vol. C.

Parent Allyl Complex 1 Structure Solution and Refinement. X-ray crystallographic quality crystals of **1** were obtained through slow evaporation from acetonitrile, by allowing the solution to sit undisturbed at 25 °C for a few days. A yellow crystal of dimensions 0.20 × 0.52 × 0.36 was selected, mounted, and placed on a Siemens P4 diffractometer for data collection. The orientation matrices and unit cell parameters were determined by least-squares treatment of 39 centered reflections between 10 and 25° in 2θ. The intensities of three reflections (301, 240, and 54$\bar{3}$), measured every 100 reflections at approximately 1 h intervals, exhibited little decay.

The structure was solved by direct methods and refined by full-matrix least-squares on F^2 using the program SHELXTL-93. All non-hydrogen atoms were refined with anisotropic thermal parameters. The maximum shift/esd for the final cycle of refinement was 0.001, and the maximum and minimum peaks in the difference electron density map were 0.649 and −0.451 e/Å^3. Least-squares refinement converged to the R factors provided in Table 4. Final non-hydrogen atom positional parameters are given in Table 5, and selected

Table 4. Crystal and Structure Refinement Data for Complexes 1, 2b, 3a, 10b, 11b, 12a, 17a, and 18a

	1	*anti*-Me **2b**	*syn*-Et **3a**	*syn*-CO_2Me **17a**	*syn*-MeO **18a**	*syn*/*anti* **10b**	*syn*/*anti* **11b**	*syn*/*syn* **12a**
empirical formula	$C_{14}H_{15}BMoN_6O_2$	$C_{15}H_{17}BMoN_6O_2$	$C_{16}H_{19}BMoN_6O_2$	$C_{17}H_{17}BCl_2MoN_6O_4$	$C_{15}H_{17}BMoN_6O_3$	$C_{16}H_{19}BMoN_6O_2$	$C_{21}H_{21}BMoN_6O_2$	$C_{52}H_{46}B_2Mo_2N_{12}O_4$
fw	406.07	420.10	434.12	547.02	436.10	434.12	496.19	1116.51
cryst size (mm)	0.20 × 0.52 × 0.36	0.20 × 0.20 × 0.40	not obtained	0.20 × 0.40 × 0.50	0.33 × 0.30 × 0.18	0.56 × 0.22 × 0.16	0.20 × 0.20 × 0.50	0.23 × 0.3 × 0.48
temp (K)	298	298	298	298	298	294(2)	296(2)	294(2)
wavelength (Å)	0.717 03	0.710 73	0.710 73	0.710 73	0.710 73	0.710 73	0.710 73	0.710 73
cryst system	monoclinic	orthorhombic	orthorhombic	orthorhombic	monoclinic	monoclinic	monoclinic	triclinic
space group	$P2_1/n$	*Pbca*	*Pbcn*	*Pbca*	$P2_1/n$	$P2_1/n$	*C*2/*c*	$P\bar{1}$
unit cell dimens	a = 9.1700(10) Å b = 14.996(3) Å c = 12.953(4) Å β = 109.79°	a = 14.151(3) Å b = 13.119(2) Å c = 19.423(7) Å α = 90° β = 90° γ = 90°	a = 28.683(6) Å b = 9.205(2) c = 14.062(3)	a = 10.5244(7) Å b = 20.757(3) Å c = 20.992(2) Å α = 90° β = 90° γ = 90°	a = 13.1890(10) Å b = 9.3730(10) Å c = 15.2750(10) Å α = 90.0(0)° β = 103.550(10)° γ = 90.00(0)°	a = 9.775(2) Å b = 12.754(3) Å c = 14.764(3) Å β = 102.92(3)°	a = 10.3670(10) Å b = 16.946(2) Å c = 24.789(4) Å α = 90° β = 93.23° γ = 90°	a = 9.32(2) Å b = 15.70(3) Å c = 17.70(4) Å α = 86.71(3)° β = 83.63(3)° γ = 80.01(3)°
V (Å^3)	1663.7(6)	3602(2)	3712.7(14)	4585.8(8)	1835.7(3)	1794.0(7)	4348.0(10)	2533.2(9)
Z	4	8	8	8	4	4	8	2
D(calcd) (Mg/m^3)	1.621	1.548	1.550	1.783	1.578	1.607	1.516	1.464
abs coeff (mm^{-1})	0.808	0.748	0.729	0.945	0.742	0.755	0.634	0.553
F(000)	816	1696	1752	2466	880	880	2016	1136
θ range for data (deg)	2−45	2.10−22.50	2−45	1.94−24.00	2−45	2−45	1.65−22.50	2−45
index ranges	$-1 \le h \le 9$, $-1 \le k \le 16$, $-13 \le l \le 13$	$-1 \le h \le 15$, $-1 \le k \le 14$, $-20 \le l \le 1$	$-1 \le h \le 30$, $-1 \le k \le 9$, $-1 \le l \le 15$	$-1 \le h \le 12$, $-1 \le k \le 23$, $-1 \le l \le 24$	$-1 \le h \le 14$, $-1 \le k \le 10$, $-16 \le l \le 16$	$-1 \le h \le 10$, $-1 \le k \le 13$, $-15 \le l \le 15$	$-1 \le h \le 11$, $-1 \le k \le 18$, $-26 \le l \le 26$	$-1 \le h \le 8$, $-16 \le k \le 16$, $-19 \le l \le 19$
reflcns coll	2860	3036	3176	4507	3067	3123	3699	7792
independent reflcns coll	2140 [R(int) = 0.0456]	2362 [R(int) = 0.0419]	2426 [R(int) = 0.0200]	3588 [R(int) = 0.0362]	2328 [R(int) = 0.0241]	2333 [R(int) = 0.0418]	2848 [R(int) = 0.1092]	6325 [R(int) = 0.0477]
refinement method	full-matrix least-squares on F^2	full-matrix least-squares on F^2	full-matrix least-squares on F^2	full-matrix least-squares on F^2	full-matrix least-squares on F^2	full-matrix least-squares on F^2	full-matrix least-squares on F^2	full-matrix least-squares on F^2
data/ restraints/ params	2140/0/217	2362/0/230	2426/0/236	3588/0/284	2328/0/235	2333/0/235	2848/0/280	6325/0/649
goodness-of- fit on F^2	1.014	1.027	0.903	1.038	1.068	1.043	1.137	1.111
final R indices [$I > 2\sigma(I)$]	$R1$ = 0.0318, w$R2$ = 0.0878	$R1$ = 0.0578, w$R2$ = 0.1420	$R1$ = 0.0296, w$R2$ = 0.0792	$R1$ = 0.0503, w$R2$ = 0.1142	$R1$ = 0.0362, w$R2$ = 0.0929	$R1$ = 0.0300, w$R2$ = 0.0828	$R1$ = 0.0496, w$R2$ = 0.1595	$R1$ = 0.0470, w$R2$ = 0.1213
R indices (all data)	$R1$ = 0.0355, w$R2$ = 0.0896	$R1$ = 0.0958, w$R2$ = 0.1663	$R1$ = 0.0386, w$R2$ = 0.0981	$R1$ = 0.0841, w$R2$ = 0.1328	$R1$ = 0.0441, w$R2$ = 0.0983	$R1$ = 0.0339, w$R2$ = 0.0846	$R1$ = 0.0687, w$R2$ = 0.2147	$R1$ = 0.0571, w$R2$ = 0.1317
largest diff peak and hole (e/Å^3)	0.649 and −0.451	0.651 and −0.481	0.287 and −0.604	0.740 and −0.497	0.405 and −0.445	0.442 and −0.414	0.783 and −1.081	0.852 and −1.359

Table 5. Atomic Coordinates ($\times 10^4$) and Equivalent Isotropic Displacement Parameters (Å^2 $\times 10^3$) for Unsubstituted Complex 1

atom	x	y	z	U(eq)
Mo	471(1)	1628(1)	2442(1)	37(1)
O(1)	1002(4)	−423(2)	2392(3)	79(1)
O(2)	1387(5)	1294(3)	377(3)	96(1)
N(1)	−1926(3)	1425(2)	1344(2)	40(1)
N(2)	−3146(3)	1900(2)	1427(2)	42(1)
N(3)	−800(3)	1611(2)	3672(3)	41(1)
N(4)	−2185(3)	2057(2)	3459(2)	41(1)
N(5)	−365(3)	3097(2)	2217(2)	42(1)
N(6)	−1782(3)	3306(2)	2279(3)	43(1)
B	−2905(5)	2575(3)	2379(4)	45(1)
C(1N)	2499(4)	878(2)	475(3)	50(1)
C(2N)	−4085(5)	1003(2)	7(3)	55(1)
C(3N)	−4450(4)	1647(2)	633(3)	48(1)
C(4N)	−593(5)	1164(2)	4608(3)	50(1)
C(5N)	−1803(5)	1299(3)	4998(3)	57(1)
C(6N)	−2792(5)	1878(3)	4235(3)	53(1)
C(7N)	249(5)	3884(3)	2065(4)	55(1)
C(8N)	−736(5)	4583(3)	2029(4)	65(1)
C(9N)	−2023(5)	4199(2)	2160(3)	53(1)
C(1)	810(4)	340(3)	2450(3)	49(1)
C(2)	1056(5)	1466(3)	1140(4)	58(1)
C(3)	2883(5)	2248(3)	2634(5)	83(2)
C(4)	2660(5)	2158(4)	3643(5)	83(2)
C(5)	2613(5)	1274(4)	3998(4)	84(2)

Table 6. Selected Bond Lengths (Å) and Angles (deg) for Unsubstituted Complex 1

Mo−C(1)	1.941(4)	O(1)−C(1)	1.155(5)
Mo−C(2)	1.950(5)	O(2)−C(2)	1.156(6)
Mo−N(1)	2.197(3)	N(2)−B	1.547(5)
Mo−C(4)	2.227(4)	N(4)−B	1.537(5)
Mo−N(3)	2.271(3)	N(6)−B	1.534(5)
Mo−N(5)	2.303(3)	C(3)−C(4)	1.395(8)
Mo−C(3)	2.331(4)	C(4)−C(5)	1.400(8)
Mo−C(5)	2.349(4)		
C(1)−Mo−C(2)	78.0(2)	N(6)−B−N(2)	108.2(3)
C(1)−Mo−N(1)	89.51(13)	N(4)−B−N(2)	107.5(3)
C(2)−Mo−N(1)	86.1(2)	N(6)−B−N(4)	109.8(3)
C(1)−Mo−C(4)	104.0(2)	O(1)−C(1)−Mo	176.1(4)
C(2)−Mo−C(4)	101.6(2)	O(2)−C(2)−Mo	174.2(4)
N(1)−Mo−C(4)	165.55(14)	C(4)−C(3)−Mo	68.2(3)
C(1)−Mo−N(3)	96.02(13)	C(5)−C(4)−C(3)	115.3(4)
C(2)−Mo−N(3)	164.3(2)	C(5)−C(4)−Mo	77.0(3)
C(1)−Mo−N(5)	169.80(13)	C(3)−C(4)−Mo	76.3(3)
C(2)−Mo−N(5)	100.68(14)	C(4)−C(5)−Mo	67.5(2)

interatomic distances are provided in Table 6. A full listing of bond lengths and angles, non-hydrogen thermal parameters, and hydrogen fixed positional and final thermal parameters are given in Tables S1, S2, and S3, respectively (supporting information).

***Anti*-Methylallyl Complex 2b. Structure Solution and Refinement.** X-ray crystallographic quality crystals were obtained through recrystallization of **2b** from hexane/methylene chloride, by allowing the solution to sit undisturbed at 25 °C for a few days. A yellow crystal of dimensions 0.20 × 0.20 × 0.40 was selected, mounted, and placed on a Siemens P4 diffractometer for data collection. The orientation matrices and unit cell parameters were determined by least-squares treatment of 40 centered reflections between 10 and 18° in 2θ. The intensities of three reflections (405, 322, and 205), measured every 100 reflections at approximately 1 h intervals, exhibited little decay.

The structure was solved by Patterson interpretation and refined by full-matrix least-squares on F^2 using the program SHELXTL-93. All hydrogen atoms were included but not refined in calculated positions (C−H 0.96 Å) with isotropic thermal parameters set at 0.08× that of the parent carbon. All non-hydrogen atoms were refined with anisotropic thermal parameters. The maximum shift/esd for the final cycle of refinement was 0.000, and the maximum and minimum peaks in the difference electron density map were 0.651 and −0.481 e/Å^3. Least-squares refinement converged to the R factors provided in Table 4. Final non-hydrogen atom positional parameters are given in Table 7, and selected interatomic distances are provided in Table 8. A full listing of bond lengths and angles, non-hydrogen thermal parameters, and hydrogen fixed positional and final thermal parameters are given in Tables S4, S5, and S6, respectively (supporting information).

Table 7. Atomic Coordinates ($\times 10^4$) and Equivalent Isotropic Displacement Parameters (Å^2 $\times 10^3$) for *Anti*-Methyl Complex 2b

atom	x	y	z	U(eq)
Mo(1)	8299(1)	1576(1)	6455(1)	58(1)
N(3)	8147(5)	3215(5)	5268(4)	61(2)
N(6)	6804(5)	2012(5)	6114(4)	55(2)
O(2)	10417(5)	1702(6)	6826(4)	102(3)
N(1)	7961(5)	1451(5)	4831(4)	57(2)
N(5)	6625(5)	2293(5)	5466(4)	58(2)
C(15)	5979(7)	2063(7)	6442(5)	68(3)
N(2)	8384(5)	936(5)	5359(4)	57(2)
N(4)	8579(5)	2982(5)	5879(4)	60(2)
C(6)	9633(8)	1588(7)	6686(5)	73(3)
O(1)	8317(8)	2825(10)	7784(5)	183(5)
C(14)	5262(7)	2353(7)	5998(6)	76(3)
C(5)	8282(9)	2340(10)	7300(6)	104(4)
C(10)	8442(7)	4143(6)	5057(6)	72(3)
C(3)	8849(14)	−60(9)	6765(6)	122(5)
C(7)	8131(7)	963(7)	4220(5)	69(3)
C(9)	8811(6)	133(7)	5070(5)	67(2)
C(8)	8662(7)	123(8)	4366(5)	78(3)
C(2)	7890(13)	40(12)	6803(9)	140(8)
C(12)	9143(7)	3777(7)	6024(5)	71(3)
C(13)	5706(7)	2496(7)	5394(5)	69(3)
B	7435(8)	2457(8)	4959(6)	59(3)
C(11)	9069(7)	4517(7)	5519(6)	84(3)
C(1)	7491(10)	644(13)	7289(9)	166(9)
C(4)	9366(11)	−265(11)	7440(8)	163(6)

Table 8. Selected Bond Lengths (Å) and Angles (deg) for *Anti*-Methyl Complex 2b

Mo(1)−C(5)	1.922(12)	N(3)−B	1.537(13)
Mo(1)−C(6)	1.940(11)	O(2)−C(6)	1.151(11)
Mo(1)−N(4)	2.193(7)	N(1)−B	1.535(12)
Mo(1)−C(2)	2.204(12)	N(5)−B	1.528(13)
Mo(1)−N(6)	2.289(7)	O(1)−C(5)	1.136(12)
Mo(1)−N(2)	2.291(7)	C(3)−C(2)	1.37(2)
Mo(1)−C(1)	2.329(12)	C(3)−C(4)	1.52(2)
Mo(1)−C(3)	2.362(11)	C(2)−C(1)	1.36(2)
C(5)−Mo(1)−C(6)	79.1(4)	C(2)−C(3)−C(4)	117(2)
C(5)−Mo(1)−N(4)	90.0(4)	C(3)−C(2)−C(1)	121(2)
C(6)−Mo(1)−N(4)	86.3(4)	N(5)−B−N(1)	110.3(8)
C(5)−Mo(1)−N(2)	169.9(4)	N(5)−B−N(3)	109.3(8)
C(6)−Mo(1)−N(2)	99.6(3)	N(1)−B−N(3)	107.6(7)
O(1)−C(5)−Mo(1)	175.8(14)		

***Syn*-Ethylallyl Complex 3a. Structure Solution and Refinement.** X-ray crystallographic quality crystals of **3a** were obtained through slow evaporation from acetonitrile, by allowing the solution to sit undisturbed at 25 °C for a few days. A yellow crystal was selected, mounted, and placed on a Siemens P4 diffractometer for data collection. The orientation matrices and unit cell parameters were determined by least-squares treatment of 40 centered reflections between 10 and 26° in 2θ. The intensities of three reflections (0,2,10, 185, and 4,0,12), measured every 100 reflections at approximately 1 h intervals, exhibited little decay.

The structure was solved by direct methods and refined by full-matrix least-squares on F^2 using the program SHELXTL-93. All non-hydrogen atoms were refined with anisotropic thermal parameters. The maximum shift/esd for the final cycle of refinement was 0.001, and the maximum and minimum peaks in the difference electron density map were 0.287 and −0.604 e/Å^3. Least-squares refinement converged to the R factors provided in Table 4. Final non-hydrogen atom positional parameters are given in Table 9, and selected

Table 9. Atomic Coordinates ($\times 10^4$) and Equivalent Isotropic Displacement Parameters (Å^2 $\times$ 10^3) for *Syn*-Ethyl Complex 3a

atom	*x*	*y*	*z*	*U*(eq)
Mo(1)	1291(1)	−30(1)	1841(1)	34(1)
C(1)	809(1)	−1459(4)	1584(3)	57(1)
O(1)	518(1)	−2326(3)	1492(2)	86(1)
C(2)	1512(1)	−1589(4)	2649(2)	52(1)
O(2)	1640(1)	−2544(3)	3123(2)	84(1)
C(3)	1313(1)	−1118(4)	349(3)	62(1)
C(4)	1726(1)	−320(4)	526(2)	46(1)
C(5)	2041(1)	−863(3)	1199(2)	46(1)
C(6)	2499(1)	−154(3)	1378(3)	55(1)
C(7)	2872(1)	−692(5)	697(2)	67(1)
N(1)	749(1)	760(2)	2847(2)	37(1)
N(2)	679(1)	2200(3)	3024(2)	40(1)
N(3)	1050(1)	1989(2)	1013(2)	37(1)
N(4)	945(1)	3238(2)	1484(2)	39(1)
N(5)	1686(1)	1650(2)	2692(2)	37(1)
N(6)	1499(1)	2990(3)	2864(2)	40(1)
C(1N)	422(1)	48(3)	3355(2)	47(1)
C(2N)	151(1)	1012(4)	3847(2)	55(1)
C(3N)	320(1)	2353(4)	3635(2)	52(1)
C(4N)	973(1)	2274(4)	99(2)	50(1)
C(5N)	814(1)	3669(4)	−28(2)	60(1)
C(6N)	801(1)	4254(4)	865(2)	53(1)
C(7N)	2078(1)	1592(4)	3213(2)	45(1)
C(8N)	2146(1)	2870(4)	3708(2)	50(1)
C(9N)	1770(1)	3727(3)	3477(2)	45(1)
B	994(1)	3348(4)	2567(3)	43(1)

Table 10. Selected Bond Lengths (Å) and Angles (deg) for *Syn*-Ethyl Complex 3a

Mo(1)−C(2)	1.937(4)	Mo(1)−C(5)	2.455(3)
Mo(1)−C(1)	1.941(4)	C(1)−O(1)	1.163(4)
Mo(1)−N(1)	2.225(2)	C(2)−O(2)	1.163(4)
Mo(1)−C(4)	2.247(3)	C(3)−C(4)	1.416(4)
Mo(1)−N(5)	2.261(2)	C(4)−C(5)	1.398(4)
Mo(1)−N(3)	2.300(2)	C(5)−C(6)	1.489(4)
Mo(1)−C(3)	2.326(3)	C(6)−C(7)	1.519(5)
C(2)−Mo(1)−C(1)	80.81(14)	O(1)−C(1)−Mo(1)	175.6(3)
C(2)−Mo(1)−N(1)	95.63(11)	O(2)−C(2)−Mo(1)	178.7(3)
C(1)−Mo(1)−N(1)	80.97(11)	C(5)−C(4)−C(3)	118.3(3)
C(2)−Mo(1)−N(5)	91.84(12)	C(5)−C(4)−Mo(1)	81.1(2)
C(1)−Mo(1)−N(5)	156.81(12)	C(3)−C(4)−Mo(1)	75.0(2)
N(1)−Mo(1)−N(5)	77.89(8)	C(4)−C(5)−C(6)	121.8(3)
C(2)−Mo(1)−N(3)	173.81(11)	C(4)−C(5)−Mo(1)	64.7(2)
C(1)−Mo(1)−N(3)	103.84(12)	C(6)−C(5)−Mo(1)	125.0(2)
N(1)−Mo(1)−N(3)	81.23(8)	C(5)−C(6)−C(7)	111.9(3)
N(5)−Mo(1)−N(3)	82.30(8)		

interatomic distances are provided in Table 10. A full listing of bond lengths and angles, non-hydrogen thermal parameters, and hydrogen fixed positional and final thermal parameters are given in Tables S7, S8, and S9, respectively (supporting information).

***Syn/anti*-1,3-Dimethyl 10b. Structure Solution and Refinement.** X-ray crystallographic quality crystals of **10b** were obtained through slow evaporation from acetonitrile, by allowing the solution to sit undisturbed at 25 °C for a few days. An orange crystal of dimensions 0.56 × 0.22 × 0.16 was selected, mounted, and placed on a Siemens P4 diffractometer for data collection. The orientation matrices and unit cell parameters were determined by least-squares treatment of 35 centered reflections between 10 and 25° in 2θ. The intensities of three reflections, measured every 100 reflections at approximately 1 h intervals, exhibited no decay.

The structure was solved by direct methods and refined by full-matrix least-squares on F^2 using the program SHELXTL-93. All hydrogen atoms were included but not refined in calculated positions (C−H 0.96 Å) with isotropic thermal parameters set at 0.08× that of the parent carbon. All non-hydrogen atoms were refined with anisotropic thermal parameters. The maximum shift/esd for the final cycle of refinement was 0.003, and the maximum and minimum peaks in the difference electron density map were 0.442 and −0.414 e/Å^3. Least-squares refinement converged to the *R* factors provided in Table 4. Final non-hydrogen atom positional parameters are given in Table 11, and selected interatomic distances are provided in Table 12. A full listing of bond lengths and angles, non-hydrogen thermal parameters, and hydrogen fixed positional and final thermal parameters are given in Tables S10, S11, and S12, respectively (supporting information).

Table 11. Atomic Coordinates ($\times 10^4$) and Equivalent Isotropic Displacement Parameters (Å^2 $\times$ 10^3) for *Syn/Anti*-Dimethyl Complex 10b

atom	*x*	*y*	*z*	*U*(eq)
Mo	31(1)	2161(1)	1877(1)	26(1)
C(1)	473(4)	693(3)	1708(2)	39(1)
O(1)	785(3)	−175(2)	1668(2)	58(1)
C(2)	1920(4)	2113(3)	2650(3)	39(1)
O(2)	3055(3)	2080(2)	3106(2)	65(1)
N(1)	−2275(3)	2319(2)	1095(2)	35(1)
N(2)	−3241(3)	2684(2)	1547(2)	34(1)
N(3)	−1036(3)	1461(2)	2917(2)	28(1)
N(4)	−2244(3)	1866(2)	3085(2)	32(1)
N5)	−432(3)	3569(2)	2671(2)	31(1)
N(6)	−1728(3)	3731(2)	2841(2)	31(1)
C3)	1395(4)	3376(3)	1127(3)	42(1)
C(4)	351(4)	2827(3)	527(2)	40(1)
C(5)	482(4)	1726(3)	417(2)	45(1)
C(6)	1317(5)	4552(3)	1210(3)	60(1)
C(7)	1861(5)	1257(4)	337(3)	67(1)
B	−2867(5)	2888(3)	2597(3)	35(1)
C(1N)	−2970(4)	2175(3)	208(3)	44(1)
C(2N)	−4364(4)	2460(3)	84(3)	47(1)
C(3N)	−4496(4)	2775(3)	956(3)	43(1)
C(4N)	−751(4)	602(3)	3456(2)	40(1)
C(5N)	−1768(4)	455(3)	3966(3)	49(1)
C(6N)	−2691(4)	1264(3)	3710(2)	44(1)
C(7N)	402(4)	4323(3)	3132(2)	37(1)
C(8N)	−355(4)	4974(3)	3586(3)	43(1)
C(9N)	−1693(4)	4585(2)	3383(2)	37(1)

Table 12. Selected Bond Lengths (Å) and Angles (deg) for *Syn/Anti*-Dimethyl Complex 10b

Mo−C(2)	1.942(4)	C(2)−O(2)	1.163(5)
Mo−C(1)	1.950(4)	N(2)−B	1.533(5)
Mo−N(3)	2.226(3)	N(4)−B	1.547(5)
Mo−N(5)	2.244(3)	N(6)−B	1.531(5)
Mo−C(4)	2.251(3)	C(3)−C(4)	1.383(5)
Mo−N(1)	2.300(3)	C(3)−C(6)	1.508(5)
Mo−C(5)	2.362(4)	C(4)−C(5)	1.423(5)
Mo−C(3)	2.464(4)	C(5)−C(7)	1.503(6)
C(1)−O(1)	1.154(4)		
C(1)−Mo−C(3)	112.85(14)	N(5)−Mo−N(1)	84.44(10)
N(3)−Mo−C(3)	161.20(11)	C(4)−Mo−N(1)	80.62(13)
N(5)−Mo−C(3)	85.65(12)	C(2)−Mo−C(5)	100.5(2)
C(4)−Mo−C(3)	33.73(13)	C(1)−Mo−C(5)	64.22(14)
N(1)−Mo−C(3)	106.70(12)	N(3)−Mo−C(5)	138.31(12)
C(5)−Mo−C(3)	60.46(13)	N(5)−Mo−C(5)	139.94(12)
O(1)−C(1)−Mo	175.5(3)	C(4)−Mo−C(5)	35.82(13)
O(2)−C(2)−Mo	179.5(4)	N(1)−Mo−C(5)	85.65(13)
C(2)−Mo−C(1)	80.54(14)	C(2)−Mo−C(3)	75.23(14)
C(2)−Mo−N(3)	96.49(13)	C(7N)−N(5)−Mo	131.9(2)
C(1)−Mo−N(3)	81.65(12)	N(6)−N(5)−Mo	121.5(2)
C(2)−Mo−N(5)	89.71(13)	C(4)−C(3)−C(6)	120.9(4)
C(1)−Mo−N(5)	155.67(12)	C(4)−C(3)−Mo	64.7(2)
N(3)−Mo−N(5)	77.35(10)	C(6)−C(3)−Mo	123.1(3)
C(2)−Mo−C(4)	103.3(2)	C(3)−C(4)−C(5)	120.1(4)
C(1)−Mo−C(4)	99.76(14)	C(3)−C(4)−Mo	81.6(2)
N(3)−Mo−C(4)	160.15(13)	C(5)−C(4)−Mo	76.3(2)
N(5)−Mo−C(4)	104.17(11)	C(4)−C(5)−C(7)	120.5(4)
C(2)−Mo−N(1)	173.65(13)	C(4)−C(5)−Mo	67.9(2)
C(1)−Mo−N(1)	103.89(13)	C(7)−C(5)−Mo	121.3(3)

***Syn*-Ph/*anti*-Me Allyl Complex 11b. Structure Solution and Refinement.** X-ray crystallographic quality crystals were obtained through recrystallization of **11b** from hexane/methylene chloride, by allowing the solution to sit undisturbed at −30 °C for a few days. An orange crystal of dimensions 0.20 × 0.20 × 0.40 was selected, mounted, and placed on a

Table 13. Atomic Coordinates ($\times 10^4$) and Equivalent Isotropic Displacement Parameters ($Å^2 \times 10^3$) for *Syn*-Phenyl/*Anti*-Methyl Complex 11b

atom	x	y	z	U(eq)
Mo(1)	1968(1)	1058(1)	1335(1)	35(1)
N(1)	2376(6)	−32(4)	1819(3)	46(2)
N(1C)	2530(6)	225(4)	655(2)	46(2)
O(2)	1417(6)	2167(4)	2289(3)	76(2)
N(2A)	3359(6)	−533(4)	1692(3)	50(2)
N(2B)	4884(6)	488(4)	1450(3)	51(2)
N(1B)	4096(6)	1125(3)	1524(3)	44(2)
N(2C)	3590(6)	−246(4)	733(3)	46(2)
O(1)	−806(5)	552(4)	1597(3)	77(2)
C(1B)	6111(8)	675(6)	1636(4)	65(2)
C(7)	302(8)	1558(5)	728(4)	57(2)
C(11)	3885(9)	3431(5)	1065(4)	68(3)
C(3A)	1820(8)	−339(5)	2234(3)	53(2)
C(10)	3497(7)	2690(4)	858(3)	45(2)
C(3C)	2107(8)	141(5)	133(3)	55(2)
C(8)	1549(8)	1858(5)	619(3)	48(2)
C(9)	2176(8)	2401(4)	960(4)	53(2)
C(2C)	2910(10)	−388(6)	−126(4)	68(3)
C(15)	4386(8)	2261(4)	575(3)	47(2)
C(1C)	3822(9)	−620(5)	253(4)	65(3)
C(5)	1659(7)	1757(5)	1929(3)	45(2)
C(2B)	6122(8)	1411(7)	1835(3)	63(2)
C(2A)	2381(11)	−1039(5)	2397(4)	72(3)
C(3B)	4841(8)	1681(5)	1770(3)	49(2)
C(14)	5599(9)	2537(6)	539(4)	62(2)
C(1A)	3349(10)	−1151(5)	2058(4)	63(2)
C(4)	218(8)	751(5)	1458(3)	47(2)
B	4331(9)	−312(5)	1285(4)	48(2)
C(6)	−732(9)	2092(6)	930(4)	70(3)
C(13)	6025(10)	3259(6)	721(5)	79(3)
C(12)	5113(12)	3693(6)	998(4)	79(3)

Table 14. Selected Bond Lengths (Å) and Angles (deg) for *Syn*-Phenyl/*Anti*-Methyl Complex 11b

Mo(1)−C(4)	1.928(8)	C(7)−C(8)	1.430(11)
Mo(1)−C(5)	1.931(8)	C(7)−C(6)	1.510(13)
Mo(1)−N(1)	2.230(6)	C(10)−C(9)	1.489(11)
Mo(1)−N(1B)	2.232(6)	C(8)−C(9)	1.386(11)
Mo(1)−C(8)	2.256(7)	O(1)−C(4)	1.184(9)
Mo(1)−N(1C)	2.299(6)	O(2)−C(5)	1.168(9)
Mo(1)−C(7)	2.382(7)	C(10)−C(9)	1.489(11)
Mo(1)−C(9)	2.474(7)		
C(4)−Mo(1)−C(5)	81.2(3)	C(4)−Mo(1)−N(1C)	103.3(3)
C(4)−Mo(1)−N(1)	81.0(3)	C(5)−Mo(1)−N(1C)	174.8(3)
C(5)−Mo(1)−N(1)	97.6(3)	C(8)−C(7)−C(6)	121.1(8)
C(4)−Mo(1)−N(1B)	155.3(3)	C(9)−C(8)−C(7)	121.3(8)
C(5)−Mo(1)−N(1B)	90.7(3)	C(8)−C(9)−C(10)	121.3(8)

Siemens P4 diffractometer for data collection. The orientation matrices and unit cell parameters were determined by least-squares treatment of 49 centered reflections between 10 and 25° in 2θ. The intensities of three reflections (402, 17$\bar{4}$, and 467), measured every 100 reflections at approximately 1 h intervals, exhibited no decay.

The structure was solved by Patterson interpretation and refined by full-matrix least-squares on F^2 using the program SHELXTL-93. All hydrogen atoms were included but not refined in calculated positions (C−H 0.96 Å) with isotropic thermal parameters set at 0.08× that of the parent carbon. All non-hydrogen atoms were refined with anisotropic thermal parameters. The maximum shift/esd for the final cycle of refinement was 0.002, and the maximum and minimum peaks in the difference electron density map were 0.783 and −1.081 e/Å^3. Least-squares refinement converged to the R factors provided in Table 4. Final non-hydrogen atom positional parameters are given in Table 13, and selected interatomic distances are provided in Table 14. A full listing of bond lengths and angles, non-hydrogen thermal parameters, and hydrogen fixed positional and final thermal parameters are given in Tables S13, S14, and S15, respectively (supporting information).

***Syn/syn*-1,3-Diphenyl Complex 12a. Structure Solution and Refinement.** X-ray crystallographic quality crystals of **12a** were obtained through slow evaporation from acetonitrile, by allowing the solution to sit undisturbed at 25 °C for a few days. An orange crystal of dimensions 0.24 × 0.30 × 0.48 was selected, mounted, and placed on a Siemens P4 diffractometer for data collection. The orientation matrices and unit cell parameters were determined by least-squares treatment of 40 centered reflections between 10 and 24° in 2θ. The intensities of three reflections (053, 2$\bar{3}\bar{3}$, and 2$\bar{3}$1), measured every 100 reflections at approximately 1 h intervals, exhibited no decay

The structure was solved by direct methods and refined by full-matrix least-squares on F^2 using the program SHELXTL-93. All hydrogen atoms were included but not refined in calculated positions (C−H 0.96 Å) with isotropic thermal parameters set at 0.05× that of the parent carbon. All non-hydrogen atoms were refined with anisotropic thermal parameters. The maximum shift/esd for the final cycle of refinement was 0.184, and the maximum and minimum peaks in the difference electron density map were 0.852 and −1.359 e/Å^3. Least-squares refinement converged to the R factors provided in Table 4. Final non-hydrogen atom positional parameters are given in Table 15, and selected interatomic distances are provided in Table 16. A full listing of bond lengths and angles, non-hydrogen thermal parameters, and hydrogen fixed positional and final thermal parameters are given in Tables S16, S17, and S18, respectively (supporting information).

***Syn*-COOMe Allyl Complex 17a. Structure Solution and Refinement.** X-ray crystallographic quality crystals were obtained through recrystallization of **17a** from hexane/methylene chloride, by allowing the solution to sit undisturbed at 25 °C for a few days. A red crystal of dimensions 0.20 × 0.40 × 0.50 was selected, mounted, and placed on a Siemens P4 diffractometer for data collection. The orientation matrices and unit cell parameters were determined by least-squares treatment of 42 centered reflections between 10 and 24° in 2θ. The intensities of three reflections (066, 006, and 224), measured every 100 reflections at approximately 1 h intervals, exhibited little decay.

The structure was solved by direct methods and refined by full-matrix least-squares on F^2 using the program SHELXTL-93. All hydrogen atoms were included but not refined in calculated positions (C−H 0.96 Å) with isotropic thermal parameters set at 0.05× that of the parent carbon. All non-hydrogen atoms were refined with anisotropic thermal parameters. The crystal retained one molecule of methylene chloride per each molybdenum complex. The solvent molecule was refined anisotropically. The maximum shift/esd for the final cycle of refinement was 0.008, and the maximum and minimum peaks in the difference electron density map were 0.740 and −0.497 e/Å^3. Least-squares refinement converged to the R factors provided in Table 4. Final non-hydrogen atom positional parameters are given in Table 17, and selected interatomic distances are provided in Table 18. A full listing of bond lengths and angles, non-hydrogen thermal parameters, and hydrogen fixed positional and final thermal parameters are given in Tables S19, S20, and S21, respectively (supporting information).

***Syn*-Methoxyallyl Complex 18a. Structure Solution and Refinement.** X-ray crystallographic quality crystals were obtained of syn-MeO complex **18a** through slow evaporation of methylene chloride from a solution, by allowing the solution to sit undisturbed at 25 °C for a few days. A yellow crystal of dimensions 0.33 × 0.30 × 0.18 was selected, mounted, and placed on a Siemens P4 diffractometer for data collection. The orientation matrices and unit cell parameters were determined by least-squares treatment of 40 centered reflections between 10 and 24° in 2θ. The intensities of three reflections (025, 303, and 11$\bar{4}$), measured every 100 reflections at approximately 1 h intervals, exhibited no decay.

Table 15. Atomic Coordinates (×10^4) and Equivalent Isotropic Displacement Parameters (Å^2 × 10^3) *for Syn/Syn*-Diphenyl Complex 12a

atom	*x*	*y*	*z*	*U*(eq)	atom	*x*	*y*	*z*	*U*(eq)
Mo(1)	1905(1)	2247(1)	377(1)	28(1)	Mo(2)	177(1)	7487(1)	4017(1)	39(1)
C(1)	179(6)	2768(3)	1012(3)	39(1)	C(18)	1172(7)	8210(4)	4550(4)	58(2)
O(1)	−881(4)	3081(3)	1373(2)	59(1)	O(18)	1759(6)	8710(3)	4805(3)	91(2)
C(2)	431(6)	2428(3)	−329(3)	39(1)	C(19)	1163(8)	8078(4)	3188(4)	62(2)
O(2)	−539(4)	2611(2)	−708(2)	57(1)	O(19)	1719(7)	8470(4)	2696(3)	106(2)
C(3)	1260(6)	1176(3)	1388(3)	41(1)	C(20)	2246(6)	6711(4)	4620(3)	48(1)
C(4)	1978(6)	814(3)	712(3)	35(1)	C(21)	1720(6)	6189(3)	4109(3)	43(1)
C(5)	1164(6)	909(3)	68(3)	35(1)	C(22)	2007(6)	6377(4)	3333(3)	48(1)
C(6)	1822(6)	1073(3)	2131(3)	43(1)	C(23)	2396(6)	6408(4)	5433(3)	50(2)
C(7)	3273(7)	731(4)	2235(3)	54(2)	C(24)	2323(7)	6982(5)	6019(4)	69(2)
C(8)	3745(9)	649(5)	2968(4)	76(2)	C(25)	2593(8)	6661(6)	6736(4)	81(2)
C(9)	2785(10)	910(5)	3576(4)	91(3)	C(26)	2958(9)	5822(6)	6900(4)	87(2)
C(10)	1346(9)	1260(6)	3487(4)	86(2)	C(27)	3042(10)	5256(5)	6346(4)	91(3)
C(11)	866(7)	1332(4)	2770(3)	63(2)	C(28)	2754(8)	5552(5)	5614(4)	73(2)
C(12)	1631(6)	400(3)	−627(3)	39(1)	C(29)	1695(6)	5858(3)	2730(3)	39(1)
C(13)	1026(7)	649(4)	−1307(3)	55(2)	C(30)	697(7)	5291(3)	2842(3)	48(1)
C(14)	1470(8)	163(4)	−1955(4)	66(2)	C(31)	536(7)	4760(4)	2274(3)	54(2)
C(15)	2485(8)	−583(4)	−1921(4)	65(2)	C(32)	1307(7)	4800(4)	1576(3)	55(2)
C(16)	3048(7)	−853(4)	−1257(4)	60(2)	C(33)	2256(7)	5371(4)	1439(3)	58(2)
C(17)	2637(7)	−368(3)	−609(3)	51(2)	C(34)	2473(7)	5904(4)	2005(3)	51(2)
N(1)	3392(5)	2646(2)	1182(2)	38(1)	N(7)	−1353(5)	6867(3)	4918(2)	42(1)
N(2)	4649(5)	2941(3)	912(2)	38(1)	N(8)	−2818(5)	7009(3)	4861(3)	47(1)
N(3)	2340(4)	3516(2)	−140(2)	31(1)	N(9)	−1401(5)	7188(3)	3225(2)	46(1)
N(4)	3698(5)	3744(2)	−227(2)	36(1)	N(10)	−2859(5)	7255(3)	3448(3)	48(1)
N(5)	4071(4)	1837(2)	−395(2)	34(1)	N(11)	−1648(6)	8587(3)	4180(2)	50(1)
N(6)	5197(4)	2292(2)	−389(2)	35(1)	N(12)	−3086(5)	8495(3)	4257(2)	47(1)
C(1N)	3247(6)	2745(3)	1935(3)	46(1)	C(35)	−1170(7)	6380(4)	5564(3)	51(2)
C(2N)	4384(7)	3096(4)	2148(3)	54(2)	C(36)	−2500(7)	6209(4)	5915(3)	59(2)
C(3N)	5256(7)	3216(3)	1487(3)	49(2)	C(37)	−3510(7)	6623(4)	5455(3)	52(2)
C(4N)	1449(6)	4175(3)	−438(3)	39(1)	C(38)	−1241(7)	7098(4)	2465(3)	55(2)
C(5N)	2202(6)	4823(3)	−720(3)	46(1)	C(39)	−2577(8)	7089(4)	2204(4)	69(2)
C(6N)	3623(7)	4530(3)	−578(3)	46(1)	C(40)	−3565(8)	7200(4)	2827(4)	65(2)
C(7N)	4507(6)	1286(3)	−951(3)	45(1)	C(41)	−1641(8)	9443(4)	4176(3)	61(2)
C(8N)	5884(6)	1370(3)	−1301(3)	49(2)	C(42)	−3054(9)	9899(4)	4232(4)	70(2)
C(9N)	6281(6)	2010(3)	−930(3)	40(1)	C(43)	−3932(8)	9280(4)	4287(3)	62(2)
B	5023(7)	3129(4)	48(3)	37(1)	B(2)	−3507(8)	7594(4)	4224(4)	52(2)

Table 16. Selected Bond Lengths (Å) and Angles (deg) for *Syn/Syn*-Diphenyl Complex 12a

Mo(1)−C(2)	1.933(6)	Mo(2)−C(19)	1.923(7)
Mo(1)−C(1)	1.942(6)	Mo(2)−C(18)	1.929(7)
Mo(1)−N(3)	2.227(4)	Mo(2)−N(11)	2.211(5)
Mo(1)−N(1)	2.277(4)	Mo(2)−N(9)	2.263(5)
Mo(1)−C(4)	2.285(4)	Mo(2)−C(21)	2.291(5)
Mo(1)−N(5)	2.322(4)	Mo(2)−N(7)	2.307(4)
Mo(1)−C(5)	2.431(5)	Mo(2)−C(20)	2.415(6)
Mo(1)−C(3)	2.481(5)	Mo(2)−C(22)	2.482(5)
C(1)−O(1)	1.163(6)	C(18)−O(18)	1.168(7)
C(2)−O(2)	1.171(6)	C(19)−O(19)	1.163(7)
C(3)−C(4)	1.404(7)	C(20)−C(21)	1.432(8)
C(3)−C(6)	1.460(7)	C(20)−C(23)	1.502(8)
C(4)−C(5)	1.425(7)	C(21)−C(22)	1.395(7)
C(5)−C(12)	1.486(7)	C(22)−C(29)	1.463(7)
C(2)−Mo(1)−C(1)	78.0(2)	C(19)−Mo(2)−C(18)	78.3(3)
C(2)−Mo(1)−N(3)	81.7(2)	C(19)−Mo(2)−N(11)	92.8(2)
C(1)−Mo(1)−N(3)	93.3(2)	C(18)−Mo(2)−N(11)	82.4(2)
C(2)−Mo(1)−N(1)	155.9(2)	C(19)−Mo(2)−N(9)	89.7(2)
C(1)−Mo(1)−N(1)	90.9(2)	C(18)−Mo(2)−N(9)	156.4(2)
C(2)−Mo(1)−N(5)	103.5(2)	C(19)−Mo(2)−N(7)	170.5(2)
C(1)−Mo(1)−N(5)	171.0(2)	C(18)−Mo(2)−N(7)	106.9(2)
O(1)−C(1)−Mo(1)	177.9(5)	O(18)−C(18)−Mo(2)	172.5(6)
O(2)−C(2)−Mo(1)	172.6(5)	O(19)−C(19)−Mo(2)	176.9(6)
C(4)−C(3)−C(6)	126.0(5)	C(21)−C(20)−C(23)	120.5(5)
C(3)−C(4)−C(5)	116.9(5)	C(22)−C(21)−C(20)	116.8(5)
C(4)−C(5)−C(12)	123.1(5)	C(21)−C(22)−C(29)	124.4(5)

The structure was solved by direct methods and refined by full-matrix least-squares on F^2 using the program SHELXTL-93. All hydrogen atoms were included but not refined in calculated positions (C−H 0.96 Å) with isotropic thermal parameters set at 0.08× that of the parent carbon. All non-hydrogen atoms were refined with anisotropic thermal parameters. The maximum shift/esd for the final cycle of refinement was 0.004, and the maximum and minimum peaks in the difference electron density map were 0.405 and −0.445 e/Å^3. Least-squares refinement converged to the *R* factors provided in Table 4. Final non-hydrogen atom positional

Table 17. Atomic Coordinates (×10^4) and Equivalent Isotropic Displacement Parameters (Å^2 × 10^3) for *Syn*-COOMe Complex 17a

atom	*x*	*y*	*z*	*U*(eq)
Mo(1)	4043(1)	1739(1)	4243(1)	32(1)
N(4)	3994(5)	679(2)	4309(2)	41(1)
N(6)	3366(4)	1643(2)	5280(2)	33(1)
C(3)	4039(6)	2784(3)	4510(3)	40(2)
C(10)	1167(6)	1697(3)	3584(3)	42(2)
O(4)	6938(5)	1471(3)	4281(3)	67(1)
N(2)	1979(5)	1522(2)	4044(2)	36(1)
N(5)	2543(5)	1166(2)	5446(2)	39(1)
O(1)	1592(5)	3141(2)	4043(2)	51(1)
C(14)	2322(6)	1188(4)	6074(3)	51(2)
C(15)	2995(7)	1686(4)	6328(3)	59(2)
N(1)	1305(4)	1115(2)	4433(2)	38(1)
O(2)	2338(4)	3099(2)	3046(2)	54(1)
O(3)	4849(7)	1734(3)	2824(2)	90(2)
C(7)	5870(6)	1584(3)	4295(3)	45(2)
N(3)	3068(5)	351(2)	4618(3)	43(1)
C(8)	111(6)	1060(3)	4215(3)	49(2)
C(5)	1115(7)	3328(4)	2823(4)	72(2)
C(6)	4511(7)	1735(3)	3344(3)	49(2)
C(16)	3626(6)	1957(3)	5822(3)	43(2)
C(1)	2438(7)	3031(3)	3685(3)	42(2)
C(13)	4773(7)	238(3)	4068(3)	52(2)
C(12)	4383(7)	−374(3)	4222(4)	64(2)
C(4)	5286(6)	2575(3)	4653(3)	45(2)
C(2)	3717(6)	2810(3)	3865(3)	40(2)
C(11)	3299(8)	−288(3)	4570(4)	58(2)
B(1)	1980(7)	719(4)	4946(4)	41(2)
C(9)	−9(6)	1426(3)	3674(3)	51(2)
Cl(1)	6000(5)	−488(2)	1979(4)	273(4)
Cl(2)	7619(5)	308(3)	2730(2)	221(2)
C(17)	6756(16)	141(7)	2059(7)	177(6)

Table 18. Selected Bond Lengths (Å) and Angles (deg) for *Syn*-COOMe Complex 17a

Mo(1)–C(6)	1.949(7)	C(3)–C(2)	1.395(9)
Mo(1)–C(7)	1.952(7)	C(3)–C(4)	1.415(9)
Mo(1)–N(4)	2.205(5)	C(1)–C(2)	1.472(9)
Mo(1)–C(3)	2.239(6)	O(4)–C(7)	1.149(7)
Mo(1)–N(2)	2.258(5)	O(1)–C(1)	1.187(7)
Mo(1)–N(6)	2.300(5)	O(2)–C(1)	1.354(7)
Mo(1)–C(4)	2.337(6)	O(2)–C(5)	1.451(8)
Mo(1)–C(2)	2.384(6)	O(3)–C(6)	1.148(8)
C(6)–Mo(1)–C(7)	78.8(3)	N(2)–Mo(1)–N(6)	81.9(2)
C(6)–Mo(1)–N(4)	93.6(2)	O(1)–C(1)–C(2)	125.7(6)
C(7)–Mo(1)–N(4)	81.7(2)	C(4)–C(3)–C(2)	125.7(6)
C(6)–Mo(1)–N(2)	93.6(2)	C(3)–C(2)–C(1)	118.8(6)
C(7)–Mo(1)–N(2)	157.7(2)	C(2)–C(1)–O(1)	125.7(6)
N(4)–Mo(1)–N(2)	77.9(2)	O(1)–C(1)–O(2)	123.4(6)
C(6)–Mo(1)–N(6)	173.7(2)	C(1)–O(2)–C(5)	115.0(5)
C(7)–Mo(1)–N(6)	103.7(2)	O(4)–C(7)–Mo(1)	174.7(6)
N(4)–Mo(1)–N(6)	81.2(2)	O(3)–C(6)–Mo(1)	176.6(7)

Table 19. Atomic Coordinates ($\times 10^4$) and Equivalent Isotropic Displacement Parameters (Å^2 $\times 10^3$) for *Syn*-Methoxy Complex 18a

atom	*x*	*y*	*z*	*U*(eq)
Mo(1)	706(1)	493(1)	2754(1)	40(1)
B(1)	−392(4)	−2533(6)	1754(3)	51(1)
C(1)	2343(4)	1341(8)	2736(4)	84(2)
C(2)	2379(4)	503(7)	3487(4)	69(2)
C(3)	1965(4)	1080(6)	4163(3)	62(1)
O(1)	423(4)	3352(4)	1716(3)	92(1)
C(4)	1663(7)	1021(8)	5619(4)	106(2)
N(11)	−940(3)	−85(4)	2149(2)	46(1)
N(12)	−1225(3)	−1382(4)	1780(2)	50(1)
C(11)	−1825(4)	685(6)	2042(3)	57(1)
C(12)	−2652(5)	−114(8)	1621(4)	73(2)
C(13)	−2258(4)	−1416(7)	1453(3)	68(2)
N(21)	676(3)	−1786(4)	3293(2)	41(1)
N(22)	190(3)	−2833(4)	2728(2)	45(1)
C(21)	269(4)	−4075(5)	3167(3)	55(1)
C(22)	821(5)	−3858(5)	4033(3)	63(1)
C(23)	1055(4)	−2421(5)	4087(3)	54(1)
N(31)	901(3)	−693(4)	1502(2)	43(1)
N(32)	355(3)	−1911(4)	1225(2)	46(1)
C(31)	1347(4)	−329(6)	834(3)	55(1)
C(32)	1105(4)	−1301(6)	143(3)	63(2)
C(33)	480(4)	−2277(6)	407(3)	59(1)
O(2)	−268(3)	2460(4)	3966(2)	76(1)
C(5)	537(4)	2284(6)	2100(3)	59(1)
O(3)	2021(4)	329(4)	4941(2)	79(1)
C(6)	131(4)	1662(5)	3556(3)	52(1)

parameters are given in Table 19, and selected interatomic distances are provided in Table 20. A full listing of bond lengths and angles, non-hydrogen thermal parameters, and hydrogen fixed positional and final thermal parameters are given in Tables S22, S23, and S24, respectively (supporting information).

Table 20. Selected Bond Lengths (Å) and Angles (deg) for *Syn*-Methoxy Complex 18a

Mo(1)–C(6)	1.926(5)	Mo(1)–C(3)	2.453(5)
Mo(1)–C(5)	1.940(5)	C(1)–C(2)	1.382(8)
Mo(1)–N(11)	2.217(4)	C(2)–C(3)	1.387(7)
Mo(1)–C(2)	2.228(5)	C(3)–O(3)	1.369(6)
Mo(1)–N(31)	2.279(3)	O(1)–C(5)	1.152(6)
Mo(1)–N(21)	2.292(3)	C(4)–O(3)	1.394(7)
Mo(1)–C(1)	2.308(5)	O(2)–C(6)	1.176(5)
C(6)–Mo(1)–C(5)	79.7(2)	N(11)–Mo(1)–N(21)	79.92(13)
C(6)–Mo(1)–N(11)	84.9(2)	N(31)–Mo(1)–N(21)	82.04(12)
C(5)–Mo(1)–N(11)	90.8(2)	N(32)–B(1)–N(22)	110.2(4)
C(6)–Mo(1)–C(2)	99.7(2)	N(32)–B(1)–N(12)	107.3(4)
C(5)–Mo(1)–C(2)	103.6(2)	N(22)–B(1)–N(12)	107.5(4)
C(6)–Mo(1)–N(31)	161.8(2)	C(1)–C(2)–C(3)	117.0(6)
C(5)–Mo(1)–N(31)	90.7(2)	O(3)–C(3)–C(2)	119.7(5)
N(11)–Mo(1)–N(31)	79.81(13)	O(1)–C(5)–Mo(1)	178.9(5)
C(6)–Mo(1)–N(21)	105.0(2)	C(3)–O(3)–C(4)	116.5(5)
C(5)–Mo(1)–N(21)	169.1(2)	O(2)–C(6)–Mo(1)	172.8(4)

Acknowledgment. This investigation was supported by Grant No. GM43107, awarded by the National Institute of General Medical Sciences, DHHS. We acknowledge the use of a VG 70-S mass spectrometer purchased through funding from the National Institutes of Health, Grant S10-RR-02478, and a 300 MHz NMR and 360 MHz NMR purchased through funding from the National Science Foundation, Grants NSF CHE-85-16614 and NSF CHE-8206103, respectively. We thank Dr. Amitabha Sarkar of National Chemical Laboratory, Pune, India, Håkan Frisell of the Royal Institute of Technology, Stockholm, Sweden, and Professor Paul Pregosin of ETH, Zürich, Switzerland, for reading and critiquing this manuscript prior to submission. We also thank Dr. Sarkar for sharing his results with us prior to publication.

Supporting Information Available: Listings of bond lengths and angles and non-hydrogen thermal parameters, as well as hydrogen fixed positional and final thermal parameters (20 pages). This material is contained in many libraries on microfiche, immediately follows this article in the microfilm version of the journal, can be ordered from the ACS; and can be downloaded from the Internet; see any current masthead page for ordering information and Internet access instructions.

OM9502796

Hydroboration with Haloborane/Trialkylsilane Mixtures[1]

Raman Soundararajan and Donald S. Matteson*

Department of Chemistry, Washington State University, Pullman, Washington 99164-4630

Received May 8, 1995[⊗]

Trialkylsilanes or dialkylsilanes react rapidly with boron trichloride in the absence of ethereal solvents or other nucleophiles to form unsolvated dichloroborane. If no substrate is present, dichloroborane disproportionates to trichloroborane and two geometric isomers of chloroborane dimer, which in turn yield monochlorodiborane and, slowly but irreversibly, diborane. All of the B–H compounds in the mixture except diborane are highly active hydroborating agents. With alkenes in the presence of sufficient boron trichloride, the products are alkyldichloroboranes. These are free from detectable contamination by dialkylchloroboranes unless more than 1 mol of hydride is present. Similar hydroboration of terminal acetylenes can be controlled to yield either (*E*)-1-(dichloroboryl)alkenes or 1,1-bis(dichloroboryl)alkanes, each free from significant contamination by the other. Alkyldichloroboranes with trialkylsilanes at 25 °C produce alkylmonochloroboranes, detected by ^{11}B NMR. 1,1-Bis(dichloroboryl)alkanes similarly yield 1,1-diborylalkane dimers. An alkylmonochloroborane can hydroborate a second alkene to form a dialkylchloroborane. For this purpose, differing alkyl groups may be introduced in either order, regardless of their relative steric properties. With 2 mol of trialkylsilane, alkyldichloroboranes are converted to alkylborane dimers. Boron tribromide and its bromoborane derivatives behave similarly to the chloro compounds in the examples tested.

Introduction

Dihaloboranes have been known to be hydroborating agents for some time. Dichloroborane was reported to be generated from hydrogen and trichloroborane over magnesium at 400–450 °C, to be trapped at −135 °C, and to react "readily and energetically with olefinic and acetylenic hydrocarbons" at 10–30 °C in 1959.[2] Later patents indicated best results at temperatures between 550 and 1000 °C with rapid quenching and that the dichloroborane disproportionates slowly to form diborane.[3] Disproportionation of dichloroborane to monochlorodiborane (ClB_2H_5) and boron trichloride was reported to have a half-life of 8–12 h at −4 °C,[4] and it was previously known that pure monochlorodiborane disproportionates slowly to boron trichloride and diborane.[5]

There have been a few reports that silanes reduce trihaloboranes, but diborane was the only borane product noted.[6] In a study of mechanisms of nucleophilic displacement at silicon, methylnaphthylphenylsilane with boron trichloride yielded the halosilane with retention of configuration at silicon, plus diborane.[7]

The information published by 1966,[2,6,7] had it ever been considered together, would have strongly suggested that trialkylsilanes with boron halides should produce useful ether-free hydroborating agents. However, chemists may have been diverted by the knowledge that in the absence of ethers the reaction of diborane with alkenes requires temperatures above 100 °C in order to proceed at any appreciable rate and is not synthetically useful.[8] Dichloroborane and dibromoborane were first developed as useful hydroborating agents in the form of their etherate or dimethyl sulfide complexes.[9] Dissociation of the monomeric haloboranes from these complexes, the rate-limiting step in the general mechanism of hydroborations,[10] has turned out to be slow. Hydroborations with dichloroborane etherate require boron trichloride to capture the ether and generally require several hours to complete.[9]

Our work evolved from an exploratory study of boron halides with tributyltin hydride, which transferred alkyl and hydride indiscriminately, and a silane was tried instead.

⊗ Abstract published in *Advance ACS Abstracts,* August 1, 1995.

(1) A preliminary account of part this work has appeared: Soundararajan, R.; Matteson, D. S. *J. Org. Chem.* **1990**, *55*, 2274–2275.

(2) Lynds, L.; Stern, D. R. *J. Am. Chem. Soc.* **1959**, *81*, 5006. Most of the hydroborations were normal, but isobutylene yielded *tert*-butyl alcohol, which we would reinterpret as an artifact, perhaps derived via *tert*-butyl chloride from hydrogen chloride produced in the BCl_3/H_2 reaction.

(3) (a) Pearson, R. K. U.S. Patent 3,323,867, June 6, 1967. (b) Hunt, C. D'A.; Kerrigan, J. V.; Leffler, A. J.; Martin, W. W. U.S. Patent 3,328,135, June 27, 1967.

(4) Cooper, H. B. H. U.S. Patent 3,684,462, August 15, 1972.

(5) (a) Schlesinger, H. I.; Burg, A. B. *J. Am. Chem. Soc.* **1931**, *53*, 4321. (b) Myers, H. W.; Putnam, R. F. *Inorg. Chem.* **1963**, *2*, 655–657. (c) Cueilleron, J.; Bouix, J. *Bull. Soc. Chim. Fr.* **1967**, 2945–2949.

(6) (b) Van Dyke, C. H.; MacDiarmid, A. G. *J. Inorg. Nucl. Chem.* **1963**, *25*, 1503–1506. (c) Drake, J. E.; Goddard, N. *Inorg. Nucl. Chem. Lett.* **1968**, *4*, 385–388. (a) Vanderwielen, A. J.; Ring, M. A. *Inorg. Nucl. Chem. Lett.* **1972**, *8*, 421–422.

(7) Attridge, C. J.; Haszeldine, R. N.; Newlands, M. J. *J. Chem. Soc., Chem. Commun.* **1966**, 911.

(8) (a) Hurd, D. T. *J. Am. Chem. Soc.* **1948**, *70*, 2053. (b) Whatley, A. T.; Pease, R. N. *J. Am. Chem. Soc.* **1954**, *76*, 835. (c) Brown, H. C. *Boranes in Organic Chemistry*; Cornell University Press: Ithaca, NY, 1972; pp 256–261

(9) (a) Brown, H. C.; Ravindran, N. *J. Am. Chem. Soc.* **1976**, *98*, 1798–1806. (b) Brown, H. C.; Ravindran, N. *Inorg. Chem.* **1977**, *16*, 2938–2940. (c) Brown, H. C.; Ravindran, N. *J. Org. Chem.* **1977**, *42*, 2533–2534. (d) Brown, H. C.; Chandrasekharan, J. *Organometallics* **1983**, *2*, 1261–1263. (e) Brown, H. C.; Chandrasekharan, J. *J. Org. Chem.* **1988**, *53*, 4811–4814.

(10) (a) Brown, H. C.; Scouten, C. G.; Wang, K. K. *J. Org. Chem.* **1979**, *44*, 2589–2591. (b) Wang, K. K.; Brown, H. C. *J. Org. Chem.* **1980**, *45*, 5303–5306. (c) Nelson, D. J.; Brown, H. C. *J. Am. Chem. Soc.* **1982**, *104*, 4907–4912. (d) Nelson, D. J.; Blue, C. D.; Brown, H. C. *J. Am. Chem. Soc.* **1982**, *104*, 4913–4917. (e) Wang, K. K.; Brown, H. C. *J. Am. Chem. Soc.* **1982**, *104*, 7148–7155.

0276-7333/95/2314-4157$09.00/0

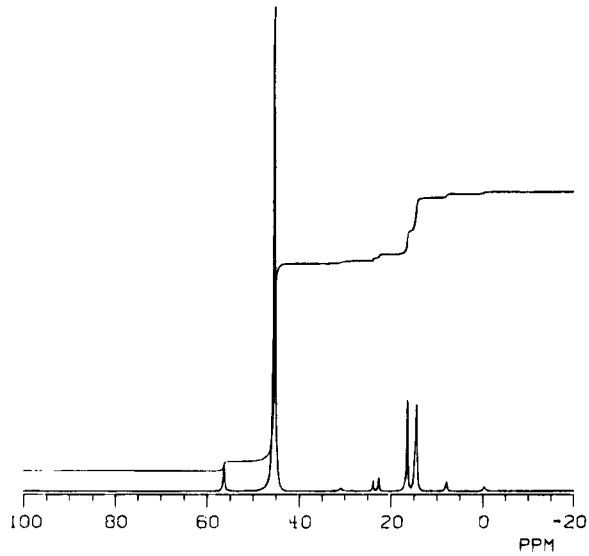

Figure 1. 64 MHz ^{1}H-decoupled ^{11}B NMR spectrum of an equimolar mixture of boron trichloride and diethylsilane taken after ~1 h at −40 °C.

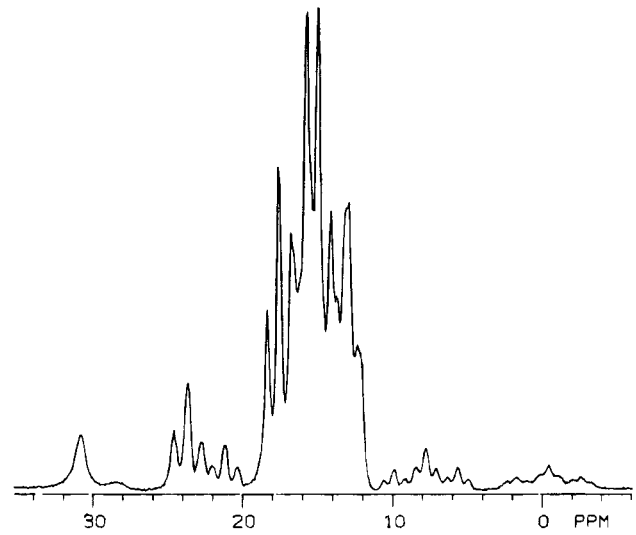

Figure 2. Portion of a 64 MHz ^{1}H-coupled ^{11}B NMR spectrum of an equimolar mixture of boron trichloride and diethylsilane taken after ~1 h at −40 °C.

Results

Dichloroborane and Chloroborane Formation. Addition of diethylsilane or a trialkylsilane to an approximately equimolar amount of boron trichloride in an NMR tube at −78 to −40 °C produced a mixture that showed prominent absorptions in the ^{11}B NMR spectrum at δ 46 (boron trichloride) and two overlapping sets of doublets of triplets at δ 14.3 and 16.2 in the ^{11}B NMR spectrum, attributed to *cis*- and *trans*-1,2-dichlorodiborane **1** and **2**. Also present was monochlorodiborane, $ClHB[H_2]BH_2$, δ 7.7 (t of t's) and 22.5 (d of t's), which matched the known ^{11}B NMR spectrum,[11] a small triplet of triplets at δ −0.6, and a peak with an equal integral at δ 23.7, which in the ^{1}H-coupled spectrum appeared to be a triplet coincident with one-half of the monochlorodiborane peak. This is the expected splitting pattern, though with unexpectedly upfield chemical shifts, for the third possible isomer **3** of dichlorodiborane. A small doublet at δ 56.1, d, J_{BH} = 204 Hz, might be due to dichloroborane ($HBCl_2$), though the only certainties are that dichloroborane is not present at more than a few mol % concentration as monomer and that no detectable amount of hydrogen bridged dimer, $B_2H_2Cl_4$, is present. The ~70:25 ratio of BCl_3 to the BH_2Cl dimers is consistent within experimental error to transfer only one hydrogen of diethylsilane to boron under these conditions. The ^{1}H-coupled and ^{1}H-decoupled 64-MHz ^{11}B NMR spectra are illustrated in Figures 1 and 2.

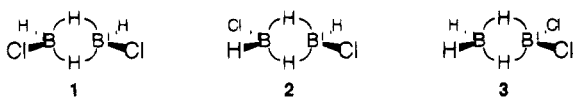

1 **2** **3**

When the mixture was warmed to −20 °C, the multiplet centered at δ 16.2 attributed to **1** or **2** decreased in intensity, the monochlorodiborane peaks increased substantially, a small amount of diborane appeared at δ 17, and the δ 56, 23.7, and −0.6 peaks increased slightly. Boron trichloride and the multiplet centered at δ 14.3 (**2** or **1**) remained constant within experimental error, and a slight splitting (~15 Hz) appeared in some of the peaks of the δ 14.3 multiplet, conceivably an H−B−B long-range coupling. A spectrum of a similar sample prepared from triethylsilane and boron trichloride taken at room temperature showed only the peaks attributed to boron trichloride, monochlorodiborane, and diborane.

Hydroboration with Preformed Chloroboranes. Mixtures containing either 1,2-dichlorodiborane or monochlorodiborane and boron trichloride readily hydroborated either cyclohexene or 1-hexene to alkyldichloroborane, as shown by the prompt appearance of the characteristic alkyldihaloborane peak[12] in the range δ 61−64 in the ^{11}B NMR spectrum. However, in accord with the previously reported inert character of diborane,[8] solutions of diborane in boron trichloride, with or without added chlorotrimethylsilane, failed to hydroborate 1-hexene in a few hours at temperatures below the boiling point of the mixture.

Hydroboration of 1-hexene with premixed trimethylsilane and boron trichloride followed by oxidation yielded 1-hexanol containing 0.8% 2-hexanol, twice the proportion of 2-hexanol found when the hydroboration was carried out under the improved conditions described below.

The foregoing hydroborations were carried out by first adding the trialkylsilane to boron trichloride, neat or in pentane, while being cooled with a −78 °C bath, then adding the alkene dropwise to the cold, stirred borane mixture. For synthetic purposes, it could be hazardous to prepare large batches of unstable haloboranes that gradually liberate gaseous, spontaneously flammable diborane above −40 °C. Therefore, we tested other conditions for mixing the reagents.

Addition of Silanes to Alkene/Boron Trichloride Mixtures. Conditions tested first involved adding an equimolar amount of an alkene to neat boron trichloride stirred at −78 °C, followed by introduction of an equimolar amount of trimethylsilane via cannula. After

(11) Eaton, G. R.; Lipscomb, W. N. *NMR Studies of Boron Hydrides and Related Compounds*; W. A. Benjamin, Inc.: New York, 1969; pp 9−23.

(12) Brown, H. C.; Sikorski, J. A. *Organometallics* **1982**, *1*, 28−37.

5–10 min at −78 °C, the mixture was warmed to room temperature. In this manner, 1-hexene was converted to 1-hexyldichloroborane (**4a**) and cyclohexene to cyclo-

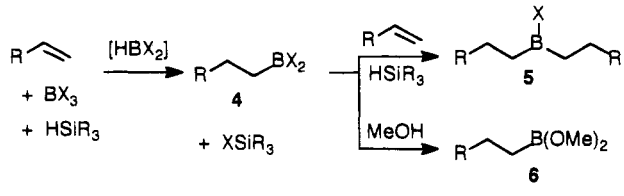

a, R = $CH_3(CH_2)_3$, X = Cl; **b**, R = $CH_3(CH_2)_3$, X = Br; **c**, R = H, X = Cl

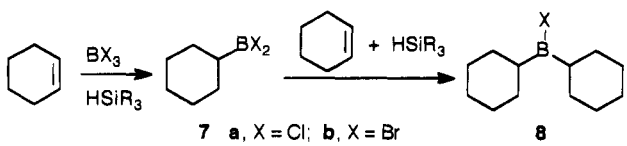

7 **a**, X = Cl; **b**, X = Br **8**

hexyldichloroborane (**7a**), and the products were separated from the trimethylsilyl chloride byproduct by simple distillation. Contamination of **4a** by dihexylchloroborane (**5a**) or of **7a** by dicyclohexylchloroborane (**8a**) was not detectable (≤1%) by ^{11}B NMR. Oxidation of **4a** with alkaline hydrogen peroxide yielded 1-hexanol containing only 0.4% 2-hexanol by GC analysis.

The rate of the reaction is remarkable. Diethylsilane was layered on top of 1-hexene/boron trichloride in a 5-mm NMR tube encased in a 14-mm tube at −98 °C. After 5 min the reactants remained unmixed, BCl_3 δ 47, but after one inversion of the tube and a return to the −98 °C bath in 2–3 s, the ^{11}B NMR within 1 min showed only **4a**, δ 62. In another experiment, a mixture of diethylsilane and 1-hexene was added dropwise to stirred boron trichloride in pentane at approximately −100 °C. After 1 h, methanol was added in order to destroy all haloboranes and thus stop the hydroboration before the bath was warmed above −100 °C.[13] Dimethyl hexylboronate was isolated by distillation (60%).

Ethylene Hydroboration. Because ethylene is not condensed at −78 °C at atmospheric pressure, a different experimental technique was tested for laboratory use. Passage of ethylene through boron trichloride at −78 °C while slowly adding triethylsilane resulted in formation of ethyldichloroborane (**4c**), together with a significant amount of diethylchloroborane (**5c**). After being warmed to room temperature (though not at −78 °C) the crude reaction mixture proved pyrophoric. Addition of just enough methanol to convert the boron halides to methoxyboranes resulted in a mixture of trimethyl borate, dimethyl ethylboronate (**6c**), and methyl diethylborinate [$CH_3OB(CH_2CH_3)_2$], which were incompletely separated by fractional distillation through an efficient packed column, plus recoverable trimethylchlorosilane.

When the boron trichloride was diluted to ~3 M with mixed xylenes and a similar hydroboration procedure was followed, the resulting solution of ethyldichloroborane and some diethylchloroborane was not pyrophoric, but when the chloroboranes were separated from most of the xylenes and triethylchlorosilane by simple distillation, pyrophoricity returned. Placed on filter paper, the crude ethyldichloroborane ignited spontaneously but burned off with only slight darkening of the paper. The distilled crude ethyldichloroborane was treated with methanol, and after simple distillation dimethyl ethylboronate was obtained in ~70% yield (after correcting for the ~80% purity), with about 9% trimethyl borate and the remainder divided between methyl diethylborinate, xylenes, and triethylchlorosilane.

Dichloromethane has been used elsewhere as the solvent for hydroboration with trialkylsilane and boron trichloride.[14] When the ethylene hydroboration was repeated in this solvent, the unchanged boron trichloride could be removed completely by distillation, and the mixture of dichloromethane, ethyldichloroborane (**4c**), and diethylchloroborane (**5c**) that distilled from the unchanged triethylchlorosilane was not pyrophoric. Treatment with methanol then yielded dimethyl ethylboronate containing an insignificant amount of trimethyl borate (<1%), but the proportion of methyl diethylborinate in the product was ~11%. Inasmuch as the boiling points of ethyldichloroborane and diethylchloroborane have been reported to differ by 25 °C at 100 Torr,[15] it would appear that the pure monoethylated boron species could be most easily purified as ethyldichloroborane, provided the equipment can accommodate pyrophoric substances safely.

Addition of Silane/Alkene Mixtures to Boron Trihalides. It is expected that acid-sensitive alkenes will be rearranged or destroyed by mixing with boron trichloride, even at low temperatures. Therefore an alternative set of reaction conditions was tested, in which the alkene and an equimolar amount of a trialkylsilane were mixed at room temperature and then added dropwise to stirred boron trichloride, either as the neat liquid or diluted with pentane, at any temperature from −78 °C to the boiling point of boron trichloride (12 °C). For example, an equimolar mixture of triethylsilane and 1-hexene added dropwise to stirred, refluxing boron trichloride cleanly yielded **4a**. Boron tribromide behaved similarly, and addition of an equimolar mixture of cyclohexene and triethylsilane to boron tribromide maintained at 20 °C in a bath readily yielded cyclohexyldibromoborane (**7b**), as indicated by the ^{11}B NMR peak at δ 65.

Addition of an equimolar mixture of allyl chloride or bromide with trimethylsilane (or triethylsilane) to boron trichloride at −78 °C yielded (3-halopropyl)dichloroborane (**9**). Trimethylsilyl chloride was removed from **6**

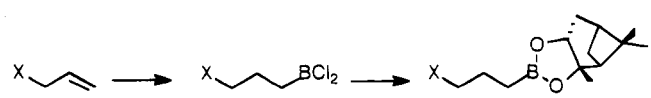

9 **a**, X = Cl; **b**, X = Br **10**

under reduced pressure, and **6** was then converted to the known[16] pinanediol esters **10** for characterization. There was no visible evidence of chlorine–bromine exchange in the ^1H NMR spectrum of pinanediol (3-bromopropyl)boronate (**10b**).

Dialkylhaloborane Formation. Alkyldihaloboranes, RBX_2, react readily with trialkylsilanes to form alkylmonohaloboranes, RBHX, which also hydroborate

(13) We thank Professor H. C. Brown for suggesting this experiment.

(14) Hawkins, J. M.; Loren, S.; Nambu, M. *J. Am. Chem. Soc.* **1994**, *116*, 1657–1660.

(15) Buls, V. W.; Davis, O. L.; Thomas, R. I. *J. Am. Chem. Soc.* **1957**, *79*, 337–339.

(16) Matteson, D. S.; Jesthi, P. K.; Sadhu, K. M. *Organometallics* **1984**, *3*, 1284–1288.

alkenes in situ. In the absence of alkene, 1-hexylchloroborane, $C_6H_{13}BHCl$, disproportionated to dihexylchloroborane (**5a**) (^{11}B δ 78.3) and dealkylated chlorodiboranes, including B_2H_5Cl. Symmetrical dialkylchloroboranes **5a** and **7a** were efficiently prepared from the corresponding alkene, triethylsilane, and boron trichloride in the theoretical 2:2:1 molar ratio. Disproportionation of hexylchloroborane is slow compared to its reaction with 1-hexene, as addition of an equimolar mixture of cyclohexene and triethylsilane to hexyldichloroborane (**4a**) yielded (cyclohexyl)(1-hexyl)chloroborane (**11**) which contained no **5a** or **8a** at the ~5% limit of detectability in the ^{13}C NMR.

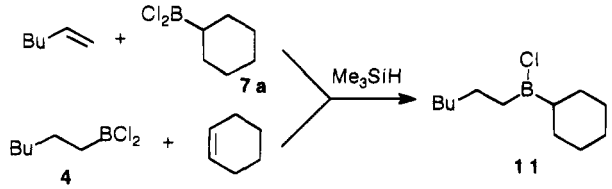

Addition of an equimolar mixture of (+)-α-pinene and trimethylsilane to boron trichloride at −78 °C yielded isopinocampheyldichloroborane (**12**), which was char-

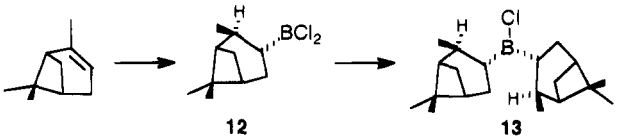

acterized by ^{11}B NMR and oxidation to isopinocampheol (95% gc). Treatment of **12** with a second mole of boron trichloride and trimethylsilane, or addition of a mixture of 2 mol of (+)-α-pinene with 2 mol of trimethylsilane to 1 mol of boron trichloride yielded diisopinocampheylchloroborane (**13**), which was also converted to isopinocampheol (88% GC) for characterization.

Reduction of cyclohexyldichloroborane (**7a**) with 2 mol of trialkylsilane yielded 1,2-dicyclohexyldiborane (cyclohexylborane dimer): ^{11}B NMR δ 23.7 [lit.[17] $(RBH_2)_2$ δ 22−24]; ^1H-coupled, broad d (J = 105 Hz), bridge H couplings not resolved.

Alkyne Hydroboration. Addition of an equimolar mixture of trimethylsilane and 1-hexyne to boron trichloride yielded 1-hexenyldichloroborane (**14**), which was

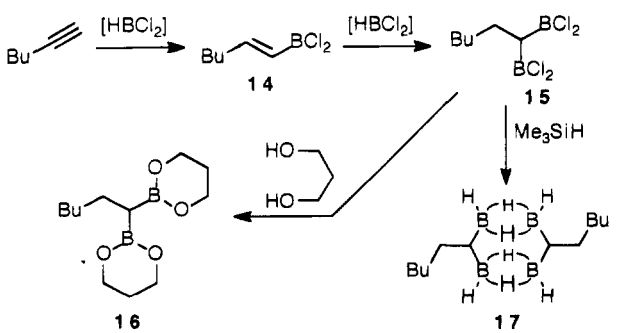

found by ^{11}B NMR to contain no more than 2% of the disubstitution product 1,1-bis(dichloroboryl)hexane (**15**). Addition of triethylsilane and 1-hexyne in a 2:1 molar ratio to sufficient boron trichloride efficiently yielded 1,1-bis(dichloroboryl)hexane (**15**), which was characterized first by NMR and finally by conversion to the known[18] 1,3-propanediol ester (**16**). Treatment of **15** with trimethylsilane yielded 1,1-bis(diborylhexane) dimer (**17**), which was characterized by ^{11}B NMR and mass spectrometry.

Other Silanes. The use of diethylsilane has been noted above. Only one of the two silicon-bound hydrides reacts under the conditions used. The reaction of the inexpensive reagent dimethylchlorosilane, $(CH_3)_2SiHCl$, with boron trichloride and cyclohexene in pentane was shown by ^{11}B NMR to yield cyclohexyldichloroborane (**7a**) slowly, requiring several hours at room temperature to complete the reaction. Attempts were made to use trichlorosilane as a hydride source, but no evidence of hydride transfer was detected by ^{11}B NMR.

Tributylsilane behaved similarly to triethylsilane, though hydroboration of 1-hexene in pentane was relatively slow. Triphenylsilane and boron tribromide in pentane hydroborated 1-hexene over a period of several hours at room temperature. Triphenylsilyl bromide precipitated and could be removed by filtration.

Discussion

Caution. Volatile alkyldichloroboranes ignite spontaneously in air. Butyldichloroborane has been reported as pyrophoric,[15] but appears to be at about the upper molecular weight limit for primary alkyldichloroborane pyrophoricity.[19] Secondary alkyl groups confer greater oxygen sensitivity, and cyclohexyldichloroborane (**7a**) has been reported to be pyrophoric.[19] We observed no flames when **7a** was handled in ordinary glassware under a blanket of argon, but the pyrophoric behavior of the more volatile ethyldichloroborane has been noted in the Results section.

The use of preformed chloroborane mixtures is not recommended for multigram synthetic purposes. Diborane is an inevitable byproduct in such mixtures. In one instance where boron trichloride and triethylsilane were mixed first at −78 °C, 1-hexene was added subsequently; as the solution was warmed to 20 °C, the septum cap was expelled from the container and the vapors ignited. Similarly, a boron trihalide should never be added to a trialkylsilane or a mixture containing trialkylsilane, as excess trialkylsilane will reduce the boron trihalide all the way to diborane.

Based on standard heats of formation,[20] for the reaction $SiH_4 + CH_3Cl \rightarrow CH_4 + SiH_3Cl$ (gas phase), $\Delta H° = -40.0$ kcal mol^{-1}. Assuming similar bond energies, the stoichiometric mixture of triethylsilane with allyl chloride described in this work could conceivably liberate ~200 cal/g if accidental catalysis of halide/hydride exchange should occur. We have never seen any evidence of reaction of silanes with alkyl halides, but the safety of indefinite scaleup has not been proved. Dilution with an inert (hydrocarbon) solvent would be a straightforward precaution.

A stoichiometric mixture of diethylsilane with dichloromethane theoretically could liberate ~450 cal/g, but dichloromethane is safe with boron trichloride, and the

(17) Cole, T. E.; Bakshi, R. K.; Srebnik, M.; Singaram, B.; Brown, H. C. *Organometallics* **1986**, *5*, 2303−2307.

(18) Matteson, D. S.; Moody, R. J. *Organometallics* **1982**, *1*, 20−28.

(19) McCusker, P. A.; Ashby, E. C.; Makowski, H. S. *J. Am. Chem. Soc.* **1957**, *79*, 5182−5184.

(20) (a) Chase, M. W., Jr.; Davies, C. A.; Downey, J. R., Jr.; Frurip, D. J.; McDonald, R. A.; Syverud, A. N. JANAF Thermochemical Tables. *J. Phys. Chem. Ref. Data* **1985**, *14* (Suppl. 1).

silicon and boron hydrides are consumed as quickly as an alkene/silane mixture is added to boron trichloride. Dichloromethane provides better protection than hydrocarbon solvents against the spontaneous flammability of low molecular weight alkylhaloboranes.

Mechanism. The first step, hydride exchange between the silane and boron halide, is rapid unless hindered by steric or electronic effects. The reaction $SiH_4 + {}^1/_3BCl_3 \rightarrow {}^1/_3BH_3 + SiH_3Cl$ has $\Delta H° = -2.68$ kcal mol^{-1}, based on a high level quantum mechanical calculation of $\Delta H_f°$ for BH_3,[21] or $\Delta H° = -1.49$ kcal mol^{-1} if the rather uncertain experimental value[20] is assumed. The analogous reaction $SiHCl_3 + {}^1/_3BCl_3 \rightarrow {}^1/_3BH_3 + SiCl_4$ has $\Delta H°$ from -0.4 to $+0.9$ kcal mol^{-1}, insufficiently different to explain the unreactivity of trichlorosilane or the sluggish reactivity of dimethylchlorosilane, which must instead be related to activation energies. The nearly complete reduction of boron trichloride by silanes to chloroborane dimers and chlorosilanes is driven thermodynamically by the heat of dimerization.

Monomeric boranes are the active intermediates in hydroborations.[10] Our observations are consistent with the hypotheses that dichlorodiboranes (**1**–**3**) and monochlorodiborane dissociate readily, eqs 1 and 2 but diborane does not, and that only the monomeric boranes undergo hydride/halide exchange.

$$B_2H_4Cl_2 \rightarrow 2H_2BCl \quad (1)$$

$$B_2H_5Cl \rightarrow H_2BCl + BH_3 \quad (2)$$

The observed disappearance of one of the isomers **1** or **2** while the other remains constant (or perhaps increases slightly) implies that the initial ratio of **1**:**2** is kinetically controlled and that one of the dimers, possibly the *trans*-isomer **2**, is thermodynamically more stable than the other.

Because halide/hydride exchange among trigonal borane species is rapid, it makes little practical difference whether the actual hydroborating agent is dichloroborane or monochloroborane. Any alkylchloroborane, RBHCl, formed would undergo hydride–chloride exchange with boron trichloride to yield alkyldichloroborane, $RBCl_2$. The observation that hydroboration of 1-hexene with preformed chloroboranes resulted in more attack of boron at the 2-carbon (0.8%) than did addition of the 1-hexene/trialkylsilane mixture to boron trichloride (0.4%) suggests the possibility that dichloroborane may be a bit more regioselective than monochloroborane, which in turn is known to be measurably more selective than borane–THF.[22] Thus, in addition to safety considerations, the addition of a mixture of the trialkylsilane and the alkene to the boron trichloride appears to yield the best chemical result.

Alternative Hydroborating Agents.[23] Etherates of dichloroborane[9a] and chloroborane[24] have been known as hydroborating agents for some time. Dichloroborane etherate[9a] and dichloroborane dimethyl sulfide[9c] are very slow hydroborating agents unless an equivalent amount of boron trichloride is added in order to free the dichloroborane monomer. Dibromoborane dimethylsulfide complex is more reactive and gives good hydroboration rates with a catalytic amount of boron tribromide.[9e] Chloroborane etherate[22] and chloroborane dimethyl sulfide[9c] or haloborane dimethyl sulfide complexes[25] work well for making dialkylhaloboranes.

Dimethyl sulfide complexes strongly with alkyldihaloboranes.[9] Alkyldichloroborane dimethyl sulfide complexes dissociate sufficiently that the liberated dimethyl sulfide inhibits dissociation of the dichloroborane dimethyl sulfide complex and thus inhibits the hydroboration process.[9e] The trialkylsilane boron trichloride system was chosen in preference to the dimethylsulfide boranes for preparing free alkyldichloroboranes or their crystalline complexes with chiral ketones.[14]

Where boronic esters are the synthetic objectives, hydroboration with catecholborane is an alternative.[22,26] However, these reactions are slow and require heating. The recently reported pinacolborane reacts faster, though excess reagent is required.[27]

The use of less expensive silanes in our process appears feasible. Our data indicate that dimethylchlorosilane would efficiently generate dichloroborane from boron trichloride at slightly elevated temperatures in a pressurized reactor.

Limitations. A major limitation on the synthetic use of hydroboration with haloboranes is their tendency to complex strongly with oxygen functions. Functionalized alkenes other than allyl halides have not been explored in the present investigation. Reagents such as catecholborane can be expected to work in the presence of acid-sensitive functionality that is incompatible with boron trihalides.

Unexpectedly, 3-hexyne did not yield much of the corresponding alkenyldichloroborane when it was mixed with triethylsilane and added to boron trichloride.[28]

Conclusions. (1) Trialkylsilanes or dialkylsilanes with boron trichloride or boron tribromide provide a convenient source of unsolvated dichloroborane or dibromoborane, and these are very rapid in situ hydroborating agents for alkenes and 1-alkynes. (2) The best general procedure for carrying out these hydroborations is to add a mixture of equivalent amounts of the silane and alkene slowly to the stirred boron trihalide, neat or in a solvent. Any convenient temperature between -78 °C and the boiling point of boron trichloride (+12 °C) or, for boron tribromide, room temperature, is generally satisfactory. (3) Taking into account rapidity of reaction, ease of use, cost, availability and storability of reagents, efficiency, and ease of product purification, no other means of hydroborating alkenes with dihaloboranes is competitive overall with the new technique. (4) For conversion of hydrocarbon substrates to boronic

(21) Sana, M.; Leroy, G.; Wilante, C. *Organometallics* **1991**, *10*, 264–270.

(22) Brown, H. C.; Ravindran, N. *J. Am. Chem. Soc.* **1976**, *98*, 1785–1798.

(23) For a more extensive review, see: Matteson, D. S. In *The Chemistry of the Metal–Carbon Bond*; Hartley, F., Patai, S., Eds.; John Wiley and Sons: New York, **1987**; Vol. 4, pp 307–409.

(24) (a) Zweifel, G. *J. Organomet. Chem.* **1967**, *9*, 215–221. (b) Pasto, D. J.; Balasubramaniyan, P. *J. Am. Chem. Soc.* **1967**, *89*, 295–300.

(25) (a) Brown, H. C.; Ravindran, N. *Synthesis* **1977**, 695–697. (b) Brown, H. C.; Ravindran, N.; Kulkarni, S. U. *J. Org. Chem.* **1979**, *44*, 2417–2425.

(26) Brown, H. C.; Gupta, S. K. *J. Am. Chem. Soc.* **1971**, *93*, 1816–1818.

(27) Tucker, C. E.; Davidson, J.; Knochel, P. *J. Org. Chem.* **1992**, *57*, 3482–3485.

(28) We thank W. Hiscox and B. Schafman for the initial observation. Work in progress with B. Schafman indicates that this problem can be overcome by proper choice of reagents and conditions, to be published later.

esters, there is no known technique that is superior to the use of the new method followed by alcoholysis of the alkylboron dihalide. (5) Hydroboration of an alkyne by the new technique can efficiently provide either the (*E*)-alkenyldichloroborane or the 1,1-bis(dichloroboryl)alkane in a fully controlled manner. (6) Reduction of an alkyldihaloborane with a trialkylsilane to an alkylmonohaloborane in the presence of an alkene provides a superior general route to dialkylhaloboranes having two different alkyl groups. The order of introduction of the two alkyl groups can be independent of their relative steric requirements. (7) Reduction of an alkyldihaloborane with 2 equiv of a trialkylsilane yields an alkylborane dimer.

Experimental Section

General Procedures. Silanes, boron trichloride, and alkenes were purchased and used without further purification. *Caution*! Because alkylboranes, diborane, and other boron hydrides are rapidly oxidized by air and are in some cases spontaneously flammable and because haloboranes are easily hydrolyzed by atmospheric moisture, all reactions were carried out under an inert atmosphere of argon. An external boron trifluoride etherate reference was used for ^{11}B NMR spectra.

Dichloroborane and Chloroborane Formation. Diethylsilane was added to an approximately equimolar amount of boron trichloride in an NMR tube cooled with a −78 °C bath, then kept ~1 h at −40 °C and analyzed by 64 MHz ^{11}B NMR. In addition to BCl_3 (δ 46, 71 g-atom %, s), the major products appeared to be *cis*- and *trans*-1,2-dichlorodiborane, ClHB[H_2]BHCl, as indicated by ^1H-coupled and ^1H-decoupled 64 MHz ^{11}B NMR data, δ 14.3 (12 g-atom %, d, $J \approx 178$ Hz, of t's, $J \approx 50$ Hz) and 16.2 (8 g-atom %, d, $J \approx 170$ Hz, of t's, $J \approx 50$ Hz). The ^1H-coupled spectra overlapped so that only approximate estimates of coupling constants were possible. Other peaks included δ 56.1 (3 g-atom %, d, $J_{BH} = 204$ Hz), attributed tentatively to dichloroborane ($HBCl_2$); a set of multiplets characteristic of known[11] monochlorodiborane (B_2H_5Cl), δ 7.7 (1.1%, t of t's, $J = 45$ Hz and $J = 137$ Hz) and 22.5 (1.1%, d, $J = 162$ Hz, of t's, $J = 54$ Hz); small peaks at δ −0.6 (0.9%, t of t's, $J = 141$ Hz, $J = 41$ Hz) and 23.7 (0.9%, t, $J \approx 58$ Hz, coincident with one t of B_2H_5Cl), which is the expected splitting pattern, though unexpected chemical shifts, for Cl_2B-[H_2]BH_2; δ 30.8 (1.4%, s, $(RO)_3B$?). After ~1 h at −20 °C, the proportions of BCl_3 and the $B_2H_4Cl_2$ isomer centered at δ 14.3 were unchanged, but the $B_2H_4Cl_2$ isomer at δ 16.2 decreased to 2.8%; each peak at δ −0.6 and 23.7 (B_2H_5Cl) increased to 2.1%; the unknown peaks at δ −0.6 and 23.7 both increased to 1.4%, the δ 56 peak increased to 4.6%, and diborane appeared at δ 17 (1%). In a separate experiment, a similar mixture was prepared from boron trichloride and triethylsilane and the 64 MHz ^{11}B NMR spectrum was taken at room temperature. The only BH species present were monochlorodiborane (B_2H_5Cl), δ 9.0 (t of t's, $J = 45$ Hz and $J = 137$ Hz) and 24.2 (d, $J = 162$ Hz, of t's, $J = 54$ Hz) [lit.[11] similar], and diborane (B_2H_6), δ 18.4 (t of t's, $J = 46$ Hz, $J = 138$ Hz).

Dichlorohexylborane (4a). (a) From Triethylsilane and Boron Trichloride at ≥12 °C. Boron trichloride (1.60 g, 13.7 mmol) was placed in a flask under a solid carbon dioxide cooled condenser and stirred under reflux during the dropwise addition of a mixture of 1-hexene (0.78 g, 9.36 mmol) and triethylsilane (1.09 g, 9.36 mmol) from a syringe. The ^{11}B NMR spectrum showed the strong peak at δ 60.3 attributed to dichlorohexylborane, with no additional peak at δ 75.6−78.3, the region characteristic of dialkylchloroboranes.[29] Complete consumption of the 1-hexene was indicated by the ^1H NMR spectrum, which showed no evidence of olefinic hydrogen in the region near δ 5.

Dichlorohexylborane (4a) from Tributylsilane at −78 °C. A solution of 1.91 g (16.25 mmol) of boron trichloride and 1.37 g (2.03 mL, 16.25 mmol) of 1-hexene in 5 mL of pentane at −78 °C was stirred under argon during the dropwise addition of 3.26 g (4.2 mL, 16.25 mmol) of tributylsilane. The ^{11}B NMR spectrum showed the only major peak at δ 63.1, characteristic of alkyldichloroboranes. Distillation yielded 2.4 g (88%) of dichlorohexylborane, bp 89−90 °C (19 Torr).

Dimethyl 1-Hexylboronate (6a) via 4a from Diethylsilane at −100 °C. A solution of boron trichloride (9.8 g, 0.084 mol) in pentane (50 mL) was chilled in a −100 °C bath (95% ethanol partially frozen with liquid nitrogen) and stirred during the addition of a mixture of 1-hexene (7.58 g, 0.090 mol) and diethylsilane (7.46 g, 0.085 mol) dropwise down the chilled side of the flask over a period of 10 min. Stirring in the −100 °C bath was maintained over a period of 1 h. (In preliminary tests monitored by ^{11}B NMR and not recorded in full detail, hydroboration was ~40% complete in 5 min and ~85% complete in 15 min at −100 °C.) Methanol (9.0 g, 0.281 mol) was added dropwise down the side of the flask to the chilled, stirred solution over a period of 5 min. The magnetic stirrer froze, but was released and resumed turning well before the bath warmed past −78 °C, at which point dry ice lumps in the bath resumed gas evolution. Stirring was continued, and the bath was warmed to 25 °C overnight, with the argon source arranged to sweep evolved hydrogen chloride into a gas trap. A dense phase (methanol) was separated (~5 mL), and the pentane solution was distilled. After foreruns at mainly 49−52 °C and 72−83 °C but continuous up to 152 °C, dimethyl hexylboronate was distilled in the range 152−170 °C, mostly at 163−168 °C (~700 Torr) [lit.[30] bp 69−70 °C (16 Torr)]; 8.16 g (60%); 300 MHz ^1H NMR ($CDCl_3$) δ 0.76 (t, 2), 0.88 (t, 3), [1.0 (m, ~0.4, impurity)], 1.27−1.43 (m, 8), 3.53 (s, 6); 75 MHz ^{13}C NMR ($CDCl_3$) δ 14.1, 22.7, 23.9, 31.8, 32.4, 51.3 (B*C* not observed); HRMS found 158.1482 for $C_8H_{19}BO_2$ calcd 158.1478. It appeared that **6a** partially decomposed during GC−mass spectral analysis, yielding a large number of impurity peaks. The last significant component to elute and the second most abundant was tentatively identified as tri-*B*-hexylboroxine, M^+ obsd 336 ($C_{18}H_{39}B_3O_3$), easily rationalized as a hydrolysis product of **6a**. The liquid distillation residue (1.2 g) was not characterized.

Dibromohexylborane (4b) from Triphenylsilane and Boron Tribromide at Room Temperature in Pentane. Boron tribromide (3.3 g, 13.15 mmol), 1-hexene (1.11 g, 13.15 mmol), and a solution of triphenylsilane (3.42 g, 13.15 mmol) in a minimal amount of pentane were stirred together at room temperature.

(29) Brown, H. C.; Srebnik, M; Ramachandran, P. V. *J. Org. Chem.* **1989**, *54*, 1577−1583.
(30) Brown, H. C.; Bhat, N. G.; Somayaji, V. *Organometallics* **1983**, *2*, 1311−1316.

After 15 min, the conversion to dibromo(1-hexyl)borane, ^{11}B NMR δ 64.9, was 50%. After 4.5 h the reaction was complete as shown by the absence of any ^{11}B signal for boron tribromide and any olefinic ^{1}H signal. Bromotriphenylsilane precipitated as a crystalline solid from the reaction mixture, making isolation of the (dibromo)-(1-hexyl)borane very simple.

Dimethyl Ethylboronate (6c). (a) In Dichloromethane. A 500-mL three-neck flask was equipped with an efficient magnetic stirrer, a gas inlet tube that would reach below the surface of 200 mL of liquid, a glass stopper in the center neck, and an adapter tube for connection to an argon supply, which was vented via a T-tube to a good gas trap for acidic vapors. The detached apparatus was tared and then connected, filled with argon, and cooled with a −78 °C bath while boron trichloride was admitted through the gas inlet tube until approximately the right volume (80−85 mL) had condensed (wt obsd: 113.6 g, 0.97 mol). The glass stopper was replaced by a pressure-equalized addition funnel (≥125 mL), and a dry ice cooled condenser was inserted between the flask and the argon supply. Dichloromethane (200 mL) was added. The mixture was stirrred while a slow stream of ethylene was passed through, and triethylsilane (96.33 g, 0.828 mol) was added dropwise (~80 drops/min) over a period of 1 h. During this time a slow stream of argon was maintained so that vented ethylene was diluted, except that the argon flow was interrupted occasionally to be sure that a slight excess of ethylene was passing through the system. Ethylene was introduced for an additional 20 min, at which time it appeared that saturation had been reached. The resulting solution was not pyrophoric on paper. The flask was equipped with a distillation head having a reflux condenser and a stopcock to regulate take-off rate, the gas inlet and outlet were replaced by stoppers, and the argon supply and exit gas trap were connected to the still head. The solution was warmed slowly (boron trichloride evolved) and distilled, first fraction up to 35 °C (10.7 g, discarded; reacted violently with water), second fraction mostly 35−60 °C [ethyldichloroborane, lit.[19] bp 50.8 °C (745 Torr)], some to 136 °C [diethylchloroborane, lit.[15] bp 25 °C (100 Torr), compared with ethyldichloroborane, bp 1 °C (100 Torr)], residue mainly triethylchlorosilane (116.7 g). The second fraction was redistilled in part through a 30-cm vacuum-jacketed column packed with glass helices, bp to 35 °C (30 g, violently reactive to water), 35−38.5 °C (46 g, moderately reactive to water), residue not pyrophoric on filter paper. The flask containing the residue was fitted with an adapter having a side arm for connection to the argon supply and trap system and a pressure-equalized addition funnel above, then cooled under argon in a −78 °C bath. Methanol (53.5 g, 1.67 mol) was added dropwise over a period of 15 min. Not much gas was evolved until the material was warmed to near 0 °C, at which time the flask was reattached to the fractionating column and hydrogen chloride began to escape at a rapid rate through the argon delivery system and into the gas trap. Careful fractionation separated dichloromethane (35−38 °C, plus intermediate cut to 50 °C), then yielded an apparent methanol azeotrope (mostly 58 °C, included 50−78 °C, ~35 g), leaving the major product in the first residue, which was stored under argon. The methanol azeotrope was combined with pentane (80 mL) and refractionated until azeotrope (28 °C) and pentane (36 °C) distillation ceased. The second residue was then purified by simple distillation (bp 79−84 °C), and the first residue (bp 81−85 °C, a little to 89 °C) was distilled into the same flask, total 50.0 g, estimated by ^{1}H NMR analysis to contain dimethyl ethylboronate[31] (86%−88%; yield 51%−52%), methyl diethylborinate[31] (11%−13%; yield 7%−8%), trimethyl borate (0.7%), and triethylsilane (0.8%).

(b) In Xylenes. A similar procedure to that in the foregoing paragraph was followed, using a solution of boron trichloride (129 g, 1.1 mol) in mixed xylene isomers (300 mL) and adding triethylsilane (117.2 g, 1.008 mol) over a period of 2 h. The solution was warmed to room temperature, resulting in considerable gas evolution (presumably ethylene). A sample was taken for 96 MHz ^{11}B NMR and showed peaks at δ 63.69 [dichloroethylborane], δ 46.15 (boron trichloride), and δ 78.36 (diethylchloroborane) in the ratios 1.00/0.11/0.06, respectively. When the mixture was heated above room temperature, distillation began, and the first distillate was pyrophoric. Simple distillation was continued fairly rapidly, without separating any fractions, at atmospheric pressure under argon until the bp reached 128 °C (xylenes, bp 139 °C; chlorotriethylsilane, bp 144 °C); 144 g collected. When this flask was separated from the distillation apparatus, the vapors ignited immediately though not vigorously at the mouth of the flask, which was restoppered uneventfully within 1−2 s and stored in a dry ice filled dewar. Treatment with methanol (90 mL, 2.2 mol) was followed by slow simple distillation, with a distillation head allowing partial or total reflux; methanol/methyl borate azeotrope and methyl borate, bp 55−78 °C; impure (83%) dimethyl ethylboronate, bp 79−89 °C, 75.6 g (estimated by NMR analysis to contain 11% trimethyl borate, 3% xylenes, and 3% triethylchlorosilane); impure (~75%) dimethyl ethylboronate, 13.7 g; total dimethyl ethylboronate in both fractions, 73 g (72%).

(c) Without Solvent. Boron trichloride (113 g, 0.96 mol) was condensed and stirred under argon while a slow stream of ethylene was passed through, with a dry ice condenser to retain boron trichloride, and triethylsilane (110.4 g, 0.9496 mol) was added dropwise over a period of 1.7 h. Ethylene was introduced for an additional 25 min, at which time it appeared that saturation had been reached. Methanol (62.1 g) was added dropwise, and the evolved hydrogen chloride was allowed to exit into a stream of argon leading to an aqueous trap. Simple distillation using a good distillation head yielded 1.8 g of forerun up to 86 °C, then 105.3 g at 86−131 °C. NMR analysis indicated the presence of trimethyl borate (~24.2 g), dimethyl ethylboronate (~49.4 g), methyl diethylborinate (~15.2 g), and triethylsilyl chloride (~16.4 g). Fractionation through a 30-cm column packed with stainless steel helices yielded fractions at 67−73 °C, 20.9 g, estimated by NMR analysis to contain trimethyl borate (15.2 g) and dimethyl ethylboronate (5.7 g); 73−78 °C, 10.3 g, estimated by NMR to contain trimethyl borate (1.6 g), dimethyl ethylboronate (8.1 g), and methyl diethylbori-

(31) (a) Dimethyl ethylboronate, δ 0.69, 0.89, 3.50; methyl diethylborinate, δ 0.83, 0.85, 3.65: Nöth, H.; Vahrenkamp, H. *J. Organomet. Chem.* **1968**, *12*, 23−36. (b) Methyl diethylborinate, δ 0.87, 3.62: Köster, R.; Fenzl, W.; Seidel, G. *Justus Liebigs Ann. Chem.* **1975**, 352−372.

nate (0.6 g); 78–82 °C, 43.1 g, estimated to contain dimethyl ethylboronate (35.1 g) and methyl diethylborinate (8.0 g); 82–95 °C, 9.7 g, estimated to contain dimethyl ethylboronate (2.6 g) and methyl diethylborinate (7.1 g); total contained dimethyl ethylboronate estimated 51.5 g (53%).

(Dichloro)(cyclohexyl)borane (7a) from Tributylsilane and Boron Trichloride at −78 °C. Condensed boron trichloride (4.68 g, 40 mmol) was weighed in a 50-mL flask under argon, then stirred at −78 °C (acetone–solid carbon dioxide bath). Pentane (5 mL) was added as a diluent, followed by 3.28 g (40 mmol) of cyclohexene. Tributylsilane (8 g) was added dropwise from a syringe. The mixture was stirred for 5 min at −78 °C. A small portion of the mixture was transferred to an NMR tube via cannula with the aid of argon pressure. The ^{11}B NMR spectrum showed a strong peak at δ 63.0 (external $BF_3{\cdot}Et_2O$ reference), which is characteristic of alkyldichloroboranes.[12] There was also a small peak (~3%) at δ 45.5 (boron trichloride) and a small impurity peak at δ 30.9 attributed to accidental hydrolysis of the boron halides during transfer to the NMR tube. Simple distillation of the major portion of the mixture yielded dichlorocyclohexylborane (6.2 g), bp 95 °C (30 Torr) containing ~10% tributylsilyl chloride as a contaminant as indicated by ^{1}H and ^{13}C NMR spectra. Allowing for the impurity, the corrected yield of dichlorocyclohexylborane was 85%.

Dichlorocyclohexylborane (7a) from Premixed Triethylsilane and Boron Trichloride. To a 3.94-g (33.5-mmol) sample of boron trichloride stirred at −78 °C under argon was added 5 mL of pentane followed by 3.89 g (33.5 mmol) of triethylsilane dropwise at a rate slow enough to avoid boiling of the solution. The ^{11}B NMR spectrum of this mixture indicated unchanged boron trichloride at δ 46.8, diborane at δ 18.55 (triplet of triplets, J = 47 Hz and J = 138 Hz), and monochlorodiborane at δ 9.07 (^{1}H-coupled: triplet of triplets, J = 45 Hz and J = 138 Hz) and 24.89 (doublet, J = 164 Hz, of triplets, J = 55 Hz). Addition of 33.5 mmol of cyclohexene to this solution at −78 °C resulted in rapid reaction, and the resulting solution showed the ^{11}B NMR peak at δ 63.3 characteristic of (dichloro)(cyclohexyl)borane with only minor impurities at δ 31 and 34.

Dichlorocyclohexylborane (7a) from Diethylsilane and Boron Trichloride. A mixture of boron trichloride (25.5 mmol) and cyclohexene (25.5 mmol) in pentane at −78 °C was stirred during the dropwise addition of diethylsilane (12.75 mmol). The ^{11}B NMR spectrum taken after 5 min showed complete conversion of the boron trichloride to dichlorocyclohexylborane, δ 63.3.

Dichlorocyclohexylborane (7a) from Dimethylchlorosilane and Boron Trichloride. A mixture of boron trichloride (2.0 g, 17.0 mmol) and cyclohexene (1.39 g, 17.0 mmol) in pentane at −78 °C was stirred during the dropwise addition of dimethylchlorosilane (1.61 g, 17 mmol). The ^{11}B NMR spectrum taken after 10 min showed only 4% conversion to dichlorocyclohexylborane. After 1.1 h at room temperature in the NMR tube sealed with a rubber septum, the conversion had reached ~57%, and after 4.5 h complete conversion of the boron trichloride to (dichloro)(cyclohexyl)borane, δ 63.3, was observed.

1,2-Dicyclohexyldiborane (Cyclohexylborane Dimer). The solution of dichlorocyclohexylborane (33.5 mmol) prepared from premixed triethylsilane and boron trichloride was treated with 67 mmol (2 additional equiv) of triethylsilane. Analysis by ^{11}B NMR indicated slow reaction, but after remaining overnight at room temperature the strong peak at δ 23.7 (^{1}H-coupled; broad doublet, J = 105 Hz, bridge B–H couplings not resolved) indicated complete conversion to 1,2-dicyclohexyldiborane, the dimer of cyclohexylborane. In another test, dichlorocyclohexylborane was treated with triethylsilane in the absence of solvent, and ^{1}H NMR indicated rapid conversion to 1,2-(dicyclohexyl)diborane.

Dibromocyclohexylborane (7b) from Triethylsilane and Boron Tribromide. Boron tribromide (3.19 g, 12.7 mmol) was stirred at 20 °C (maintained with a water bath) during the dropwise addition of a mixture of cyclohexene (1.04 g, 12.7 mmol) and triethylsilane (1.50 g, 12.7 mmol) from a syringe. The ^{11}B NMR spectrum consisted of a peak at δ 65 characteristic of (alkyl)(dibromo)boranes; hence, dibromocyclohexylborane is present.[30]

Dichloro(3-chloropropyl)borane (9a) and (*S*)-Pinanediol (3-Chloropropyl)boronate (10a). Trimethylsilane (1.73 g, 23.3 mmol) was condensed under argon at −78 °C and mixed with allyl chloride (1.81 g, 23.3 mmol), and this mixture was added via cannula to boron trichloride (2.74 g, 23.3 mmol) stirred at −78 °C under argon. On completion of the addition the formation of $Cl(CH_2)_3BCl_2$ was indicated by the typical alkyldichloroborane peak[29] at δ 62.6 in the ^{11}B NMR spectrum. (In a parallel experiment with triethylsilane in place of trimethylsilane, small amounts of R_2BCl at δ 76.7 and BCl_3 at δ 46 were also observed, perhaps because the addition of the mixture of triethylsilane and allyl chloride was carried out too rapidly.) Volatile byproducts were removed at 25 °C (100 Torr) for 1 h. The residue was cooled in an ice bath, and a solution of (*S*)-pinanediol[32] (3.97 g, 23.3 mmol) in diethyl ether (15 mL) was added. After being stirred for 10 min, the mixture was distilled. The yield of (*S*)-pinanediol (3-chloropropyl)boronate, bp 130 °C (0.5 Torr), was 5.7 g (92% after correction for minor impurities detected by ^{1}H NMR analysis). The ^{1}H NMR spectrum was similar to that previously reported.[16]

Dichloro(3-bromopropyl)borane (9b) and (*S*)-Pinanediol (3-Bromopropyl)boronate (10b). The procedure was the same as that described in the preceding paragraph for dichloro(3-chloropropyl)borane and (*S*)-pinanediol (3-chloropropyl)boronate except that allyl bromide was used in place of allyl chloride. (*S*)-Pinanediol (3-bromopropyl)boronate distilled at 145 °C (0.25 Torr), yield 80%, ^{1}H NMR similar to that reported previously.[16] It is noteworthy that the 200 MHz ^{1}H NMR spectrum clearly indicated that only the bromopropyl group was present, and that chloride–bromide exchange to produce (3-chloropropyl)boronic ester as a byproduct had not occurred.

Chlorodihexylborane (8a) from Tributylsilane, 1-Hexene, and Dichlorohexylborane. A solution of 0.5 g (3 mmol) of dichlorohexylborane and 0.252 g (0.38 mL, 3 mmol) of 1-hexene in 5 mL of pentane was stirred

(32) Chemical Abstracts name: [1*S*-(1α,2β,3β,5α)]-2,6,6-trimethylbicyclo[3.1.1]heptane-2,3-diol. This compound was purchased from the Aldrich Chemical Company.

under argon at room temperature during the dropwise addition of 0.60 g (0.77 mL, 3 mmol) of tributylsilane. Analysis by ^{11}B NMR indicated that the reaction required some time to complete, but after 4 h the peak at δ 63 characteristic of (dichloro)(hexyl)borane had disappeared and had been replaced by a peak at δ 77.3 characteristic of chlorodihexylborane.

Chlorodihexylborane (5a) from Diethylsilane, 1-Hexene, and Boron Trichloride. A mixture of 1-hexene (25.5 mmol) and diethylsilane (12.75 mmol) was added dropwise to boron trichloride (8.5 mmol) at a rate slow enough to avoid any appearance of boiling in the flask, which was cooled in a −78 °C bath. The ^{11}B NMR spectrum taken at room temperature shortly after mixing showed mostly dichlorohexylborane at δ 62.8 and chlorodihexylborane at δ 78.0 in an approximately 1:1 ratio, with a small proportion of unchanged boron trichloride at δ 46.8. After 4 h at room temperature, the peaks due to boron trichloride and dichlorohexylborane had disappeared and the only peak was that of chlorodihexylborane at δ 78. Distilled material: *m/e* calcd 216.1816, found 216.1810; ^{13}C NMR ($CDCl_3$) δ 14.1, 22.7, 24.6, 29.4 (broad, B*C*), 31.9, 32.0

Dichlorohexylborane (4a) and Chlorodihexylborane (5a) from 1-Hexene and Trimethylsilane. Boron trichloride (2.0 g, 17 mmol) and 1-hexene (1.26 g, 17 mmol) were placed in a flask under a solid carbon dioxide cooled condenser and were stirred under reflux during the dropwise addition of condensed trimethylsilane (1.42 g, 17 mmol) via cannula. The ^{11}B NMR spectrum immediately showed the strong peak at δ 60.3 attributed to dichlorohexylborane. A second 17 mmol of 1-hexene was added, followed by a second 17 mmol of trimethylsilane. At the end of the addition the ^{11}B NMR spectrum consisted of a single peak at δ 77.3 characteristic of a dialkylchloroborane.[29]

Stepwise Preparation of Dichlorohexylborane (4a) and Chlorodihexylborane (5a) from Trimethylsilane, 1-Hexene, and Boron Trichloride at Reflux Temperature. Boron trichloride (17.0 mmol) was condensed at −78 °C in a flask equipped with a dry ice cooled reflux condenser, then allowed to come to reflux temperature (approximately 12 °C). Trimethylsilane (17.0 mmol) was condensed separately and mixed with 1-hexene (17.0 mmol), and the mixture was added dropwise to the refluxing boron trichloride. The ^{11}B NMR spectrum was taken immediately and indicated the presence of dichloro(1-hexyl)borane at δ 63 with ≤2% chlorobis-1-hexyl)borane at δ 78.4. Treatment of this product mixture with additional trimethylsilane (17 mmol) and 1-hexene (17 mmol) resulted in complete conversion of the (dichloro)(1-hexyl)borane to chlorobis-(1-hexyl)borane within 2 h at room temperature, as indicated by the ^{11}B NMR signal at δ 78.4. Addition of a third equivalent of trimethylsilane (17 mmol) and 1-hexene (17 mmol) resulted in no measurable conversion of the chlorobis(1-hexyl)borane to trihexylborane in 2 h at room temperature.

Bromodicyclohexylborane (8b) from Cyclohexene, Triethylsilane, and Dibromocyclohexylborane. The (dibromo)(cyclohexyl)borane from the preceding experiment was treated with a mixture of 12.7 mmol of cyclohexene and 12.7 mmol of triethylsilane. The ^{11}B NMR spectrum immediately showed only a peak at δ 80.1, characteristic of bromodicyclohexylborane. Dialkylbromoboranes characteristically absorb at δ 78–83.[30]

Chlorocyclohexylhexylborane (11). (a) Via Dichlorohexylborane (4a) and Cyclohexene. A mixture of 1-hexene (30 mmol) and triethylsilane (30 mmol) was added to boron trichloride (30 mmol) at −78 °C in the usual manner. The ^{11}B NMR spectrum indicated complete conversion of the boron trichloride to dichloro-(1-hexyl)borane, and the ^{1}H NMR indicated complete consumption of the 1-hexene. This product mixture was treated at room temperature with a mixture of triethylsilane (30 mmol) and cyclohexene (30 mmol). The ^{11}B NMR signal at δ 63.0 ($RBCl_2$) disappeared gradually over the course of 30 min, and was replaced by the signal at δ 78 characteristic of chlorocyclohexyl(1-hexyl)-borane. The ^{1}H NMR indicated no olefinic protons remained; 50 MHz ^{13}C NMR δ 14.1, 22.7, 24.6, 26.8, 27.4, 28.1, ~28 (broad, obscured by sharp peaks, B*C*), 31.8, 32.1, 37.7 (broad, B*C'*)]. Possible impurities not detected: ≤5% bis(*n*-hexyl)chloroborane [δ 14.1, 22.7, 24.6, 29.4 (broad, B*C*), 31.9, 32.0] and ≤5% dicyclohexylchloroborane [δ 26.7, 27.2, 27.8, 36.4 (broad, B*C*)].

(b) Via Dichlorocyclohexylborane (7a) and 1-Hexene. The procedure described in the preceding paragraph was followed, except that cyclohexene was used in place of 1-hexene in the first step. The resulting solution of dichlorocyclohexylborane was treated with triethylsilane and 1-hexene at room temperature and after 4.5 h showed disappearance of the ^{11}B NMR $RBCl_2$ signal at δ 63 and complete conversion to chlorocyclohexyl(1-hexyl)borane, δ 78, as well as disappearance of olefinic protons in the ^{1}H NMR.

Dichloroisopinocampheylborane (12) and Chlorodiisopinocampheylborane (13). (+)-α-Pinene (98% ee) (2.92 g, 21.4 mmol) and triethylsilane (2.49 g, 21.4 mmol) were mixed and added dropwise to boron trichloride (2.51 g, 21.4 mmol), stirred, and cooled with a −78 °C bath. The rate of addition was kept slow enough to avoid any boiling of the boron trichloride. After 5 min, the ^{11}B NMR spectrum showed only a typical $RBCl_2$ peak at δ 62.4 and no remaining boron trichloride. The ^{1}H NMR indicated that no olefinic protons remained; ^{13}C NMR in accord with the assigned structure; *m/e* calcd 218.0800, found 218.0779. This crude dichloroisopinocampheylborane was stirred and cooled with a 0 °C bath during dropwise addition of a mixture of (+)-α-pinene (2.92 g, 21.4 mmol) and triethylsilane (2.49 g, 21.4 mmol). The mixture was then stirred at room temperature overnight. After 16 h, the ^{11}B NMR spectrum indicated complete conversion to chlorodiisopinocampheylborane, which showed a broad peak at δ 76.0; ^{13}C NMR in accord with the assigned structure; *m/e* calcd 320.2442, found 320.2440, which with hydrogen peroxide yielded isopinocampheol, mp 54–56 °C, $[\alpha]^{23}D$ −32.5° (*c* 10, benzene) (lit.[33] mp 57 °C, $[\alpha]^{20}D$ −32.0°; lit.[34] $[\alpha]^{27}D$ −35.79°).

Dichloro(1-hexenyl)borane (14) and 1,1-Bis(dichloroboryl)hexane (15). A 4.3-g (36.6 mmol) portion

(33) Shin-Piaw, C. *C. R. Hebd. Seances Acad. Sci.* **1936**, *202*, 127.
(34) Brown, H. C.; Mandal, A. K.; Yoon, N. M.; Singaram, B.; Schwier, J. R., Jadhav, P. K. *J. Org. Chem.* **1982**, *47*, 5069–5074. We thank a referee for calling our attention to this reference. Both the melting point and rotation (92.7% of theoretical) indicate that our sample contained some impurity. The 200 MHz NMR spectra available when this work was done were inadequate to reveal the nature of the impurity.

of boron trichloride was stirred at −78 °C under argon during the dropwise addition of a mixture of 2.13 g (18.3 mmol) of triethylsilane and 1.50 g (18.3 mmol) of 1-hexyne from a syringe. The ^{11}B NMR spectrum of this mixture showed major peaks in the ratio 1:1 at δ 53.15 corresponding to dichloro(1-hexenyl)borane and δ 46.9 corresponding to the unconsumed boron trichloride. Addition of a second 2.13-g portion of triethylsilane resulted in disappearance of the peak at δ 53.15 and appearance of a new peak at δ 60.83 characteristic of 1,1-bis(dichloroboryl)hexane, with only ~2%−3% remaining BCl_3 at δ 45.9. Distillation yielded 3.8 g (83%) of 1,1-bis(dichloroboryl)hexane, bp 76−77 °C (3 Torr). The structure was supported by ^1H and ^{13}C NMR spectra.

1,1-Bis(dichloroboryl)hexane (15). A 2.2-g (18.72 mmol) portion of boron trichloride was stirred at −78 °C under argon during the dropwise addition of a mixture of 2.18 g (18.72 mmol) of triethylsilane and 0.76 g (9.36 mmol) of 1-hexyne from a syringe. The ^{11}B NMR spectrum of this mixture showed a peak at δ 60.3 characteristic of 1,1-bis(dichloroboryl)hexane, with some remaining BCl_3 at δ 46. No (dichloro)(1-hexenyl)-borane was detected at δ 53. The ^1H NMR spectrum indicated complete conversion of the hexyne to saturated product.

1,1-Bis[2-(1,2,3-dioxaborinyl)]hexane (16). Treatment of 1,1-bis(dichloroboryl)hexane (550 mg, 2.2 mmol) with 1,3-propanediol (338 mg, 4.4 mmol) yielded 1,1-bis[2-(1,2,3-dioxaborinyl)]hexane (360 mg, 91%) as shown by bp 141 °C (0.5 Torr) and by ^1H NMR spectral data in good agreement with the literature values.[18]

1,1-Diborylhexane Dimer [1,2-bis(hexylidene)-bis(diborane)] (17). 1-Hexyne (0.84 g, 10.2 mmol) was mixed with trimethylsilane (1.51 g, 20.4 mmol) at −78 °C and added via cannula to 2.4 g (20.4 mmol) of boron trichloride stirred at −78 °C. When the addition was complete, the ^{11}B NMR spectrum showed a broad singlet at δ 60.8 and less than 2% unreacted boron trichloride (δ 45.5). The mixture was allowed to warm to room temperature and the trimethylsilyl chloride was evaporated for 2 h at approximately 100 Torr. The resulting 1,1-bis(dichloroboryl)hexane was stirred at −78 °C during the addition of 3.02 g (40.8 mmol) of trimethylsilane. After 10 min, the ^{11}B NMR spectrum showed less than 2% 1,1-bis(dichloroboryl)hexane (δ 60.8) and a new peak at δ 25.8. When the spectrum was proton decoupled, this peak was a broad singlet, and when it was proton coupled, the absorption became broader but was not resolved. The mass spectrum (CI, CH_4) showed m/e 220.2827 for $C_{12}H_{32}B_4$ (calcd, 220.2876).

Acknowledgment. We thank the National Science Foundation for Grant Nos. CHE-8618762 and CHE-9303074 and for support of the Washington State University NMR center (Bruker 300 MHz NMR spectrometer, Grant No. CHE-9115282) and the Boeing Corporation for part of the cost of the Nicolet NT-200 NMR instrument.

OM9503297

Carbon–Carbon Bond Cleavage by Osmium Clusters. Ring Opening of a Cyclobutenyl Ligand by a Triosmium Cluster

Richard D. Adams* and Xiaosu Qu

Department of Chemistry and Biochemistry, University of South Carolina, Columbia, South Carolina 29208

Received May 1, 1995[⊗]

The reaction of 1-iodo-2-methylcyclobutene with the triosmium cluster complex $Os_3(CO)_{10}(NCMe)_2$ has yielded four new osmium cluster compounds: $Os_2(CO)_6(\mu\text{-I})[\mu\text{-}\overline{CC(Me)CH_2CH_2}]$, **1** (5% yield), $Os_3(CO)_9(\mu\text{-I})[\mu_3\text{-}CC(Me)CH_2CH_2]$, **2** (8% yield), $Os_3(CO)_9(\mu\text{-I})[\mu_3\text{-}CC(Me)CH_2CH_2]$, **3** (16% yield), and $Os_3(CO)_{10}(\mu\text{-I})[\mu\text{-}\overline{CC(Me)CH_2CH_2}]$, **4** (33% yield). Compounds **1**–**3** were characterized by single-crystal X-ray diffraction analysis. Compounds **1** and **4** contain a σ,π-coordinated 2-methylcyclobutenyl ligand. Compounds **2** and **3** are isomers. Both contain open triosmium clusters with a metalated acyclic σ,π-coordinated bridging alkenylidene ligand formed by the cleavage of one of the carbon–carbon bonds of the cyclobutenyl ring. An iodo ligand bridges one of the two metal–metal bonds in **2** and the nonbonded Os–Os pair of metal atoms in **3**. Compound **2** is an intermediate to **3** and is converted to **3** in 90% yield in solution at 25 °C in 48 h. From the structure of **2** it can be inferred that the C–C bond cleavage process involves a direct oxidative addition of the $C-CH_2$ carbon–carbon σ-bond of the σ,π-coordinated bridging cyclobutenyl ligand in **4** adjacent to the π-coordinated C–C double bond and occurs at the same metal atom. Crystal data for **1**: space group = $P2_1/n$, a = 8.376(2) Å, b = 13.925(2) Å, c = 13.138(3) Å, β = 102.32(1)°, Z = 4, 1719 reflections, R = 0.033. For **2**: space group = $P\bar{1}$, a = 9.146(2) Å, b = 14.618(3) Å, c = 8.528(2) Å, α = 94.49(2)°, β = 116.38(1)°, γ = 81.94(2)°, Z = 2, 2246 reflections, R = 0.025. For **3**: space group = $P\bar{1}$, a = 13.900(3) Å, b = 18.022(6) Å, c = 12.896(2) Å, α = 94.82(2)°, β = 109.44(1)°, γ = 90.17(2)°, Z = 6, 3941 reflections, R = 0.045.

Introduction

The cleavage of carbon–carbon σ-bonds by metal atoms is of great interest.[1–3] The most common examples involve strained ring hydrocarbons.[2,3] In our recent studies of the transformations of cyclobutenyl groupings into cyclobutyne ligands,[4–6] we have observed a competitive ring-opening transformation involving the cleavage of one of the carbon–carbon bonds of a σ,π-coordinated cyclobutenyl ring in the complex $Os_3(CO)_{10}(\mu\text{-Br})(\mu\text{-}\overline{CCHCH_2CH_2})$ (Scheme 1).[7]

To study this ring-opening transformation further, we have now investigated the reaction of 1-iodo-2-methylcyclobutene with $Os_3(CO)_{10}(NCMe)_2$. The principal

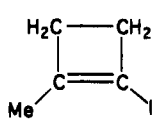

1-iodo-2-methylcyclobutene

product is $Os_3(CO)_{10}(\mu\text{-I})[\mu\text{-}\overline{CC(Me)CH_2CH_2}]$, **4**, which contains an iodo ligand and a cyclobutenyl ligand formed by the displacement of the two NCMe ligands in the cluster and the addition of one molecule of 1-iodo-2-methylcyclobutene with cleavage of the carbon–iodine bond. A minor diosmium product $Os_2(CO)_6(\mu\text{-I})[\mu\text{-}\overline{CC(Me)CH_2CH_2}]$, **1**, containing an iodo ligand and a cyclobutenyl ligand was formed, and two triosmium isomers $Os_3(CO)_9(\mu\text{-I})[\mu_3\text{-}CC(Me)CH_2CH_2]$, **2**, and $Os_3(CO)_9(\mu\text{-I})[\mu_3\text{-}CC(Me)CH_2CH_2]$, **3**, were formed by the addition and opening of the cyclobutenyl ring. The results of this study, which includes a new mechanism for the opening of cyclobutenyl rings, are reported here.

Experimental Section

General Procedures. All reactions were performed under a dry nitrogen atmosphere. Reagent grade solvents were purified by distillation under nitrogen from the appropriate drying agents (sodium/benzophenone for THF, CaH_2 for CH_2Cl_2 and hexane), stored over molecular sieves, and deoxygenated by purging with nitrogen prior to use. $Os_3(CO)_{10}(NCMe)_2$[8]

⊗ Abstract published in *Advance ACS Abstracts,* August 1, 1995.

(1) Crabtree, R. H. *Chem. Rev.* **1985**, *85*, 245.

(2) (a) Puddephatt, R. J. *Coord. Chem. Rev.* **1980**, *33*, 149. (b) Al-Essa, R. J.; Puddephatt, R. J.; Tipper, C. F. H.; Thompson, P. J. *J. Am. Chem. Soc.* **1980**, *102*, 7546. (c) Parsons, E. J.; Larsen, R. D.; Jennings, P. W. *J. Am. Chem. Soc.* **1985**, *107*, 1793. (d) Miyashita, A.; Takahashi, M.; Takaya, H. *J. Am. Chem. Soc.* **1981**, *103*, 6257. (e) Green, M.; Orpen, A. G.; Schaverien, C. J. *J. Chem. Soc., Chem. Commun.* **1984**, 37. (f) Binger, P.; Langhauser, F.; Gabor, B.; Mynott, R.; Herrmann, A. T.; Krüger, C. *J. Chem. Soc., Chem. Commun.* **1992**, 505.

(3) (a) Bishop, K. C., III. *Chem. Rev.* **1976**, *76*, 461. (b) Eisch, J. J.; Piotrowski, A. M.; Han, K. I.; Krüger, C.; Tsay, Y. H. *Organometallics* **1985**, *4*, 224. (c) Flood, T. C.; Statler, J. A. *Organometallics* **1984**, *3*, 1795.

(4) (a) Adams, R. D.; Chen, G.; Qu, X.; Wu, W.; Yamamoto, J. H. *Organometallics* **1993**, *12*, 3029. (b) Adams, R. D.; Chen, G.; Qu, X.; Wu, W.; Yamamoto, J. H. *J. Am. Chem Soc.* **1992**, *114*, 10977.

(5) Adams, R. D.; Qu, X.; Wu, W. *Organometallics* **1993**, *12*, 4117.

(6) Adams, R. D.; Qu, X.; Wu, W. *Organometallics* **1994**, *13*, 1272.

(7) Adams, R. D.; Chen, L.; Qu, X. *Organometallics* **1994**, *13*, 1992.

0276-7333/95/2314-4167$09.00/0

Scheme 1

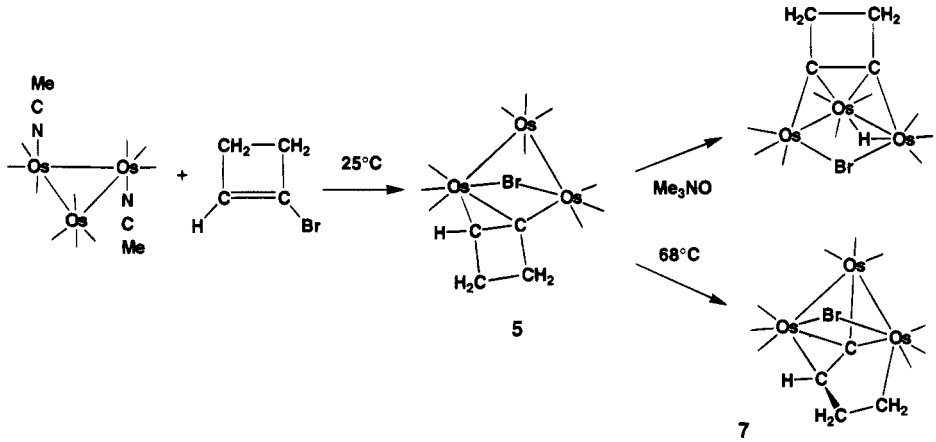

and 1-iodo-2-methylcyclobutene[9] were prepared according to the published procedures. IR spectra were recorded on a Nicolet 5DXB FT-IR spectrophotometer. ^{1}H NMR spectra were recorded on either a Bruker AM-300 or a Bruker AM-500 FT-NMR spectrometer. Mass spectra were recorded on a VG model 70SQ mass spectrometer. Elemental microanalyses were performed by Desert Analytics Organic Microanalysis, Tucson, AZ. TLC separations were performed in air by using silica gel (60 Å, F_{254}) on plates (Analtech, 0.25 mm).

Reaction of $Os_3(CO)_{10}(NCMe)_2$ with 1-Iodo-2-methylcyclobutene. A solution consisting of $Os_3(CO)_{10}(NCMe)_2$ (110.0 mg, 0.118 mmol) and 1-iodo-2-methylcyclobutene (45.0 mg, 0.232 mmol) in dichloromethane (25 mL) was stirred for 48 h at 25 °C. During this time, the color slowly changed from yellow to red. The solvent was removed under vacuum, and the residue was separated by TLC on silica gel with hexane. This yielded four products in the following order of elution: 4.5 mg of a pale yellow band, $Os_2(CO)_6(\mu\text{-I})[\mu\text{-}\overline{CC(Me)CH_2CH_2}]$, **1** (5%), 9.6 mg of a yellow band, $Os_3(CO)_9(\mu\text{-I})[\mu_3\text{-}CC(Me)CH_2\text{-}CH_2]$, **2** (8%), 19.3 mg of an orange band, $Os_3(CO)_9(\mu\text{-I})[\mu_3\text{-}CC(Me)CH_2CH_2]$, **3** (16%), and 40.5 mg of a red band, $Os_3(CO)_{10}(\mu\text{-I})[\mu\text{-}\overline{CC(Me)CH_2CH_2}]$, **4** (33%). Spectroscopic data for the products are as follows for **1**: IR (ν_{CO} in hexane, cm^{-1}) 2089 (m), 2060 (vs), 2016 (s), 2000 (s), 1993 (s), 1985 (w); ^{1}H NMR (δ in $CDCl_3$) 3.04 (broad, s, 2H), 2.96 (broad, s, 2H), 2.63 (s, 3H). Anal. Calcd (found): C, 17.79 (17.74); H, 0.94 (0.97). For **2**: IR (ν_{CO} in hexane, cm^{-1}) 2093 (w), 2069 (vs), 2058 (vs), 2021 (m), 2010 (s), 1999 (s), 1992 (m); ^{1}H NMR (δ in $CDCl_3$) 4.41 (ddd, 1H, $^2J_{HH}$ = 15 Hz, $^3J_{HH}$ = 10 Hz, $^3J_{HH}$ = 3 Hz), 3.16 (ddd, 1H, $^2J_{HH}$ = 15 Hz, $^3J_{HH}$ = 11 Hz, $^3J_{HH}$ = 7 Hz), 2.42 (s, 3H), 0.30 (ddd, 1H, $^2J_{HH}$ = 11 Hz, $^3J_{HH}$ = 11 Hz, $^3J_{HH}$ = 3 Hz), 0.08 (ddd, 1H, $^2J_{HH}$ = 11 Hz, $^3J_{HH}$ = 10 Hz, $^3J_{HH}$ = 7 Hz). Anal. Calcd (found): C, 16.52 (16.82); H, 0.69 (0.69). For **3**: IR (ν_{CO} in hexane, cm^{-1}) 2097 (m), 2077 (s), 2052 (s), 2025 (m), 2015 (s), 2041 (s), 1997 (m), 1983 (m), 1971 (m); ^{1}H NMR (δ in $CDCl_3$) 5.33 (ddd, 1H, $^2J_{HH}$ = 16 Hz, $^3J_{HH}$ = 8 Hz, $^3J_{HH}$ = 8 Hz), 5.15 (ddd, 1H, $^2J_{HH}$ = 16 Hz, $^3J_{HH}$ = 9 Hz, $^3J_{HH}$ = 5 Hz), 3.21 (ddd, 1H, $^2J_{HH}$ = 12 Hz, $^3J_{HH}$ = 9 Hz, $^3J_{HH}$ = 8 Hz), 2.82 (ddd, 1H, $^2J_{HH}$ = 12 Hz, $^3J_{HH}$ = 8 Hz, $^3J_{HH}$ = 5 Hz), 2.53 (s, 3H). Anal. Calcd (found): C, 16.52 (16.71); H, 0.69 (0.58). For **4**: IR (ν_{CO} in hexane, cm^{-1}) 2102 (m), 2062 (s), 2052 (m), 2018 (s), 2012 (m), 1995 (m), 1982 (w), 1977 (w); ^{1}H NMR (δ in $CDCl_3$) 3.17–3.14 (m, 2H), 2.61 (s, 3H), 2.58–2.53 (m, 2H). Anal. Calcd (found): C, 17.23 (17.45); H, 0.67 (0.81). The mass spectrum of compound **4** showed the parent ion ($^{192}Os_{76}$) m/e = 1050 and the ions corresponding to the loss of each of the 10 carbonyl ligands.

Pyrolysis of Compound 4 at 68 °C. A solution of compound **4** (35.0 mg, 0.0335 mmol) in hexane (25 mL) was heated to reflux for 1 h. The solvent was then removed under vacuum, and the residue was separated by TLC on silica gel using hexane solvent. This yielded two products in the following order of elution: 3.5 mg of a pale yellow band of compound **1** (10%) and 15.7 mg of compound **3** (46%).

Conversion of Compound 2 to 3. A solution of compound **2** (10.0 mg, 0.010 mmol) in CH_2Cl_2 (10 mL) was stirred for 40 h at 25 °C. During this time, the color changed slowly from yellow to orange. The solvent was then removed under vacuum, and the residue was separated by TLC on silica gel with hexane. This yielded only one product, 9.0 mg of compound **3** (90%).

Attempted Pyrolysis of Compound 3 at 68 °C in Refluxing Hexane. A solution of compound **3** (10.0 mg, 0.010 mmol) in hexane (10 mL) was heated to reflux for 3 h. At the end of this period, the IR spectrum of the solution showed no changes. The solvent was then removed under vacuum, and the residue was separated by TLC on silica gel with hexane solvent. Only 9.5 mg of an orange band of compound **3** (95%) was found.

Crystallographic Analyses. Crystals of compound **1** suitable for X-ray diffraction analysis were grown from a solution of a solvent mixture of dichloromethane and hexane by slow evaporation of the solvent at −14 °C. Crystals of compound **2** were grown from a solution of a solvent mixture of dichloromethane and hexane by slow evaporation of the solvent at −14 °C. Crystals of compound **3** were grown from a solution of a solvent mixture of dichloromethane and methanol by slow evaporation of the solvent at 25 °C. All crystals used in data collection were mounted in thin-walled glass capillaries. Diffraction measurements were made on a Rigaku AFC6S automatic diffractometer by using graphite-monochromated Mo Kα radiation. The unit cells were determined from 15 randomly selected reflections obtained by using the AFC6 automatic search, center, index, and least-squares routines. Crystal data, data collection parameters, and results of the refinements are listed in Table 1. All data processing was performed on a Digital Equipment Corp. VAXstation 3520 computer by using the TEXSAN structure-solving program library obtained from the Molecular Structure Corp., The Woodlands, TX. Lorentz–polarization (Lp) corrections were applied to the data in each analysis. An empirical absorption correction based on three azimuthal ψ-scans was applied to the data in each analysis. Neutral atom scattering factors were calculated by the standard procedures.[10a] Anomalous dispersion corrections were applied to all non-hydrogen atoms.[10b] All structures were solved by a combination of direct methods (MITHRIL) and difference Fourier syntheses. Full-matrix least-squares refinements minimized the function $\sum_{hkl} w(|F_o| - |F_c|)^2$, where $w = 1/\sigma(F)^2$, $\sigma(F) = \sigma(F_o^2)/2F_o$, and $\sigma(F_o^2) = [\sigma(I_{raw})^2 + (0.02I_{net})^2]^{1/2}/\mathrm{Lp}$.

(8) Aime, S.; Deeming, A. J. *J. Chem. Soc. Dalton Trans.* **1983**, 1807.
(9) (a) Boardman, L. D.; Bagheri, V.; Sawada, H.; Nigishi, E. *J. Am. Chem. Soc.* **1984**, *106*, 6105. (b) Boardman, L. D. Ph.D. Thesis, Purdue University, West Lafayette, IN, 1985, 99–100.

(10) (a) *International Tables for X-ray Crystallography*; Kynoch Press: Birmingham, England, 1975; Vol. IV, Table 2.2B, pp 99–101. (b) *Ibid.*, Table 2.3.1, pp 149–150.

Table 1. Crystal Data for Compounds 1–3

compd	1	2	3
formula	$Os_2IO_6C_{11}H_7$	$Os_3IO_9C_{14}H_7$	$Os_9I_3O_{27}C_{42}H_{21}$
fw	742.48	1016.71	3035.13
cryst syst	monoclinic	triclinic	triclinic
lattice params			
a (Å)	8.376(2)	9.146(2)	13.900(3)
b (Å)	13.925(2)	14.618(3)	18.022(6)
c (Å)	13.138(3)	8.528(2)	12.896(2)
α (deg)	90	94.49(2)	94.82(2)
β (deg)	102.32(1)	116.38(1)	109.44(1)
γ (deg)	90	81.94(2)	90.17(2)
V (Å^3)	1497.0(4)	1011.2(8)	3034(1)
space group	$P2_1/n$ (No. 14)	$P\bar{1}$ (No. 2)	$P\bar{1}$ (No. 2)
Z value	4	2	6
ϱ_{calcd} (g/cm^3)	3.29	3.34	3.34
μ(Mo Kα) (cm^{-1})	190.30	203.75	203.56
temp (°C)	20	20	20
$2\theta_{max}$ (deg)	45.0	45.0	40.0
no. of obsd ($I > 3\sigma$)	1719	2246	3941
goodness of fit	2.49	1.56	1.97
residuals:[a] R; R_w	0.033; 0.040	0.025; 0.028	0.045; 0.042
abs cor	empirical	empirical	empirical
largest peak in final diff. map	1.54	1.22	1.86

[a] $R = \sum_{hkl}(||F_{obsd}| - |F_{calcd}||/\sum_{hkl}|F_{obsd}|$; $R_w = [\sum_{hkl}w(|F_{obsd}| - |F_{calcd}|^2)/\sum_{hkl}wF_{obsd}^2]^{1/2}$, $w = 1/\sigma^2(F_{obsd})$; GOF $= [\sum_{hkl}(|F_{obsd}| - |F_{calcd}|/\sigma(F_{obsd})]/(n_{data} - n_{vari})$.

For all three structural analyses, the positions of hydrogen atoms were calculated by assuming idealized geometries at the attached carbon atoms. The scattering contributions of all hydrogen atoms were added to the structure factor calculations, but their positions were not refined.

Compound **1** crystallized in the monoclinic crystal system. The space group $P2_1/n$ was identified by the patterns of systematic absences observed in the data. All of the non-hydrogen atoms were refined with anisotropic thermal parameters.

Compound **2** crystallized in the triclinic crystal system. The space group $P\bar{1}$ was assumed and confirmed by the successful solution and refinement of the structure. All of the non-hydrogen atoms of the complex were refined with anisotropic thermal parameters.

Compound **3** crystallized in the triclinic crystal system. The space group $P\bar{1}$ was assumed and confirmed by the successful solution and refinement of the structure. The crystal contains three complete symmetry independent molecules in the asymmetric crystal unit. As a result of the large size of the analysis, only the atoms heavier than carbon were refined with anisotropic thermal parameters. The carbon atoms were refined isotropically.

Results and Discussion

Four new osmium cluster complexes were obtained from the reaction of 1-iodo-2-methylcyclobutene with the lightly stabilized triosmium cluster complex $Os_3(CO)_{10}(NCMe)_2$ at 25 °C for 48 h. These have been identified as $Os_2(CO)_6(\mu\text{-I})[\mu\text{-}\overline{CC(Me)CH_2CH_2}]$, **1** (5% yield), $Os_3(CO)_9(\mu\text{-I})[\mu_3\text{-CC(Me)CH}_2\text{CH}_2]$, **2** (8% yield), $Os_3(CO)_9(\mu\text{-I})[\mu_3\text{-CC(Me)CH}_2\text{CH}_2]$, **3** (16% yield), and $Os_3(CO)_{10}(\mu\text{-I})[\mu\text{-}\overline{CC(Me)CH_2CH_2}]$, **4** (33% yield). All compounds were characterized by a combination of IR, ^{1}H NMR, and elemental analyses. Compounds **1**–**3** were further characterized by single-crystal X-ray diffraction analyses.

These products appear to be formed in a series, and compound **4** appears to be the first of these. For example, compounds **1** and **3** can be obtained directly from **4** by pyrolysis. It appears that compound **2** is an intermediate en route to **3** since it is converted to **3** in high yield when its solutions stand at room temperature for extended periods, (e.g., 90% yield in 40 h at 25 °C). It was not observed in the pyrolysis of **4** because of the more forcing conditions that were used.

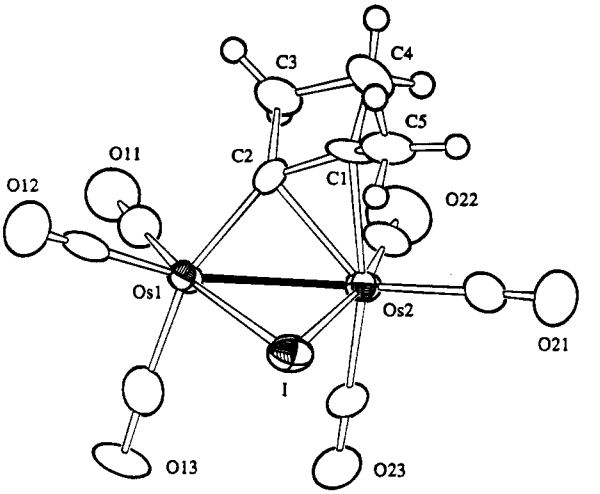

Figure 1. ORTEP diagram of $Os_2(CO)_6(\mu\text{-I})[\mu\text{-}\overline{CC(Me)CH_2CH_2}]$, **1**, showing 50% probability thermal ellipsoids.

Crystals of compound **4** suitable for X-ray diffraction analyses could not be obtained. However, on the basis of its IR, ^{1}H NMR, and mass spectra, we can be fairly certain that this compound is structurally analogous to the compound $Os_3(CO)_{10}(\mu\text{-Br})(\mu\text{-}\overline{CCHCH_2CH_2})$, **5**, that we obtained from the reaction of 1-bromocyclobutene with $Os_3(CO)_{10}(NCMe)_2$ and structurally characterized.[7]

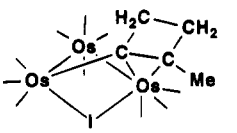

4

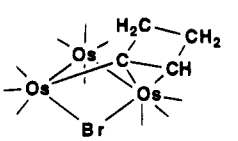

5

An ORTEP diagram of the molecular structure of **1** is shown in Figure 1. Final atomic positional parameters are listed in Table 2, and selected interatomic distances and angles are listed in Table 3. The molecule contains only two osmium atoms which are mutually bonded, Os(1)–Os(2) = 2.7589(9) Å. There is a bridging iodo ligand and a bridging σ,π-coordinated 2-methylcyclobutenyl ligand, and there are six linear terminal carbonyl ligands arranged in the classic "sawhorse" structure. The structure is very similar to that of the compound $Os_2(CO)_6(\mu\text{-SPh})(\mu\text{-}\overline{CCHCH_2CH_2})$, **6**, that was obtained from the reaction of 1-phenylthiocyclobutene with $Os_3(CO)_{10}(NCMe)_2$.[4a]

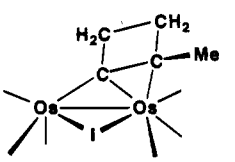

1

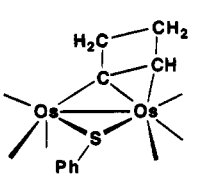

6

Table 2. Positional Parameters and *B*(eq) Values (Å²) for 1

atom	x	y	z	*B*(eq)
Os(1)	0.61855(7)	0.13435(4)	0.20025(4)	2.19(3)
Os(2)	0.36355(7)	0.25204(4)	0.10800(4)	2.23(3)
I	0.6833(1)	0.30942(7)	0.11955(8)	2.99(4)
O(11)	0.460(2)	−0.0452(9)	0.261(1)	5.1(6)
O(12)	0.941(2)	0.101(1)	0.357(1)	5.1(6)
O(13)	0.713(2)	0.0334(8)	0.011(1)	4.1(6)
O(21)	0.199(2)	0.443(1)	0.036(1)	6.4(8)
O(22)	0.050(2)	0.143(1)	0.105(1)	6.1(7)
O(23)	0.384(1)	0.1644(8)	−0.1019(9)	4.2(6)
C(1)	0.404(2)	0.304(1)	0.283(1)	2.9(7)
C(2)	0.469(2)	0.209(1)	0.276(1)	2.2(6)
C(3)	0.335(2)	0.168(1)	0.336(1)	3.6(7)
C(4)	0.264(2)	0.272(1)	0.333(1)	3.9(8)
C(5)	0.475(2)	0.402(1)	0.304(1)	3.4(7)
C(11)	0.522(2)	0.022(1)	0.237(1)	3.4(7)
C(12)	0.820(2)	0.113(1)	0.298(1)	3.1(7)
C(13)	0.681(2)	0.070(1)	0.083(1)	3.4(7)
C(21)	0.256(2)	0.372(1)	0.063(1)	3.7(8)
C(22)	0.169(2)	0.187(1)	0.109(1)	3.6(8)
C(23)	0.375(2)	0.197(1)	−0.024(1)	2.8(7)

Table 3. Selected Interatomic Distances and Angles for 1

(a) Intramolecular Distances[a]

Os(1)−Os(2)	2.7589(9)	C(1)−C(4)	1.53(2)
Os(1)−I	2.758(1)	C(1)−C(5)	1.49(2)
Os(1)−C(2)	2.05(1)	C(2)−C(3)	1.61(2)
Os(2)−I	2.768(1)	C(3)−C(4)	1.56(2)
Os(2)−C(1)	2.37(1)	Os−C(av)	1.91(2)
Os(2)−C(2)	2.27(1)	C−O(av)	1.14(2)
C(1)−C(2)	1.43(2)		

(b) Intramolecular Bond Angles[b]

Os(2)−Os(1)−C(2)	54.0(4)	C(4)−C(1)−C(5)	120(1)
Os(1)−Os(2)−C(1)	79.3(4)	C(1)−C(2)−C(3)	89(1)
Os(1)−Os(2)−C(2)	46.8(4)	C(2)−C(3)−C(4)	88(1)
Os(1)−I−Os(2)	59.90(3)	C(1)−C(4)−C(3)	87(1)
C(2)−C(1)−C(4)	96(1)	Os−C(av)−O	178(2)
C(2)−C(1)−C(5)	135(1)		

[a] Distances are in angstroms. Estimated standard deviations in the least significant figure are given in parentheses. [b] Angles are in degrees. Estimated standard deviations in the least significant figure are given in parentheses.

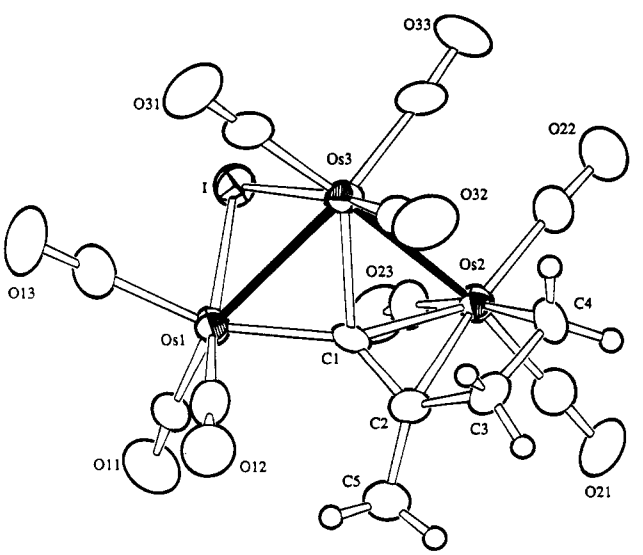

Figure 2. ORTEP diagram of $Os_3(CO)_9(\mu\text{-}I)[\mu_3\text{-}CC(Me)CH_2\text{-}CH_2]$, **2**, showing 50% probability thermal ellipsoids.

An ORTEP diagram of the molecular structure of **2** is shown in Figure 2. Final atomic positional parameters are listed in Table 4, and selected interatomic distances and angles are listed in Tables 5 and 6. This

Table 4. Positional Parameters and *B*(eq) Values (Å²) for 2

atom	x	y	z	*B*(eq)
Os(1)	0.93217(5)	0.23435(4)	0.63539(6)	2.90(2)
Os(2)	1.27889(5)	0.31986(3)	1.09121(6)	2.77(2)
Os(3)	1.17631(5)	0.14120(3)	0.92321(6)	2.75(2)
I	0.86684(9)	0.19744(6)	0.9069(1)	3.59(4)
O(11)	0.708(1)	0.4142(8)	0.517(1)	6.8(6)
O(12)	1.065(1)	0.2400(8)	0.372(1)	6.2(6)
O(13)	0.698(1)	0.0909(8)	0.412(1)	6.5(6)
O(21)	1.404(1)	0.5070(8)	1.181(2)	7.0(6)
O(22)	1.432(1)	0.2646(8)	1.472(1)	6.0(6)
O(23)	0.958(1)	0.4160(7)	1.096(2)	6.1(5)
O(31)	1.034(1)	−0.0356(8)	0.738(2)	6.6(6)
O(32)	1.472(1)	0.0701(7)	0.860(2)	6.3(6)
O(33)	1.324(1)	0.0696(7)	1.298(1)	5.4(5)
C(1)	1.154(1)	0.2724(8)	0.815(1)	2.6(5)
C(2)	1.261(1)	0.3288(8)	0.811(1)	2.8(5)
C(3)	1.448(1)	0.296(1)	0.880(2)	3.6(6)
C(4)	1.510(1)	0.275(1)	1.074(1)	4.0(6)
C(5)	1.199(1)	0.414(1)	0.702(2)	3.8(6)
C(11)	0.787(2)	0.344(1)	0.557(2)	3.8(6)
C(12)	1.013(2)	0.239(1)	0.473(2)	4.5(7)
C(13)	0.781(2)	0.144(1)	0.496(2)	4.3(7)
C(21)	1.355(2)	0.435(1)	1.148(2)	4.4(7)
C(22)	1.373(1)	0.283(1)	1.324(2)	3.8(6)
C(23)	1.069(2)	0.373(1)	1.089(2)	3.9(6)
C(31)	1.085(2)	0.030(1)	0.807(2)	3.8(6)
C(32)	1.360(1)	0.1012(9)	0.886(2)	3.6(6)
C(33)	1.272(1)	0.100(1)	1.161(2)	3.9(6)

Table 5. Intramolecular Distances for 2[a]

Os(1)−Os(3)	2.769(1)	C(1)−C(2)	1.38(2)
Os(1)−I	2.743(1)	C(2)−C(3)	1.56(2)
Os(1)−C(1)	2.05(1)	C(2)−C(5)	1.50(2)
Os(2)−Os(3)	2.943(1)	C(3)−C(4)	1.53(2)
Os(2)−C(1)	2.22(1)	Os−C(av)	1.90(2)
Os(2)−C(2)	2.33(1)	C−O(av)	1.15(2)
Os(2)−C(4)	2.18(1)	Os(1)···Os(2)	4.016(1)
Os(3)−I	2.779(1)	C(1)···C(4)	3.02(1)
Os(3)−C(1)	2.14(1)		

[a] Distances are in angstroms. Estimated standard deviations in the least significant figure are given in parentheses.

Table 6. Intramolecular Bond Angles for 2[a]

Os(1)−Os(3)−Os(2)	89.29(3)
Os(1)−I−Os(3)	60.19(3)
Os(1)−C(1)−Os(2)	140.8(5)
Os(1)−C(1)−Os(3)	82.8(4)
Os(2)−C(1)−Os(3)	85.0(4)
C(1)−C(2)−C(3)	122(1)
C(1)−C(2)−C(5)	121(1)
C(3)−C(2)−C(5)	115(1)
C(2)−C(3)−C(4)	106(1)

[a] Angles are in degrees. Estimated standard deviations in the least significant figure are given in parentheses.

molecule consists of a triosmium cluster with only two metal−metal bonds, Os(1)−Os(3) = 2.769(1) Å and Os(2)−Os(3) = 2.943(1) Å. The Os(1)−Os(2) distance, 4.016(1) Å, is clearly indicative of a nonbonding interaction. The iodo ligand bridges the Os(1)−Os(3) bond. A metalated alkenyl ligand, C(1)−C(2)−C(3)−C(4), with a methyl group on C(2), bridges the three metal atoms via the carbon C(1). The C(1)−C(2) link is formally a C−C double bond, C(1)−C(2) = 1.38(2) Å, which is π-bonded to Os(2), such that Os(2)−C(1) = 2.22(1) Å and Os(2)−C(2) = 2.33(1) Å. The methylene group C(4) is σ-bonded to Os(2), Os(2)−C(4) = 2.18(1) Å, and each metal atom has three linear terminal carbonyl ligands. The ^{1}H NMR spectrum shows four resonances for the four inequivalent methylene protons with all as doublets of doublets of doublets as expected for this structure

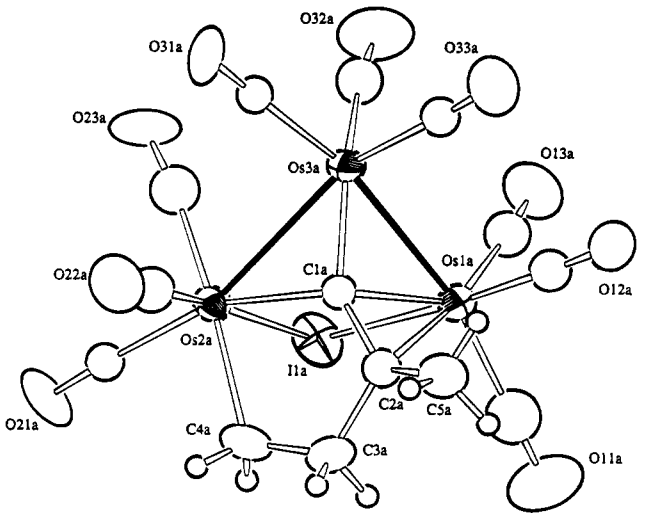

Figure 3. ORTEP diagram of $Os_3(CO)_9(\mu\text{-I})[\mu_3\text{-CC(Me)CH}_2\text{-CH}_2]$, **3**, showing 50% probability thermal ellipsoids.

{4.41 (ddd, 1H, $^2J_{HH}$ = 15 Hz, $^3J_{HH}$ = 10 Hz, $^3J_{HH}$ = 3 Hz), 3.16 (ddd, 1H, $^2J_{HH}$ = 15 Hz, $^3J_{HH}$ = 11 Hz, $^3J_{HH}$ = 7 Hz), 0.30 ppm (ddd, 1H, $^2J_{HH}$ = 11 Hz, $^3J_{HH}$ = 11 Hz, $^3J_{HH}$ = 3 Hz) and 0.08 (ddd, 1H, $^2J_{HH}$ = 11 Hz, $^3J_{HH}$ = 10 Hz, $^3J_{HH}$ = 7 Hz)} and a singlet at 2.42 ppm for the methyl group. This indicates that the molecule is stereochemically rigid on the NMR time scale at 25 °C.

Compound **3** crystallizes with three independent molecules in the asymmetric crystal unit. All three molecules are structurally similar, and an ORTEP diagram of the molecular structure of one of the three molecules is shown in Figure 3. Final atomic positional parameters are listed in Table 7, and selected interatomic distances and angles are listed in Tables 8 and 9. The structure of **3** is very similar to that of the compound $Os_3(CO)_9(\mu\text{-Br})(\mu_3\text{-CCHCH}_2\text{CH}_2)$, **7**, that was obtained from the reaction of $Os_3(CO)_{10}(NCMe)_2$ with 1-bromocyclobutene.[7]

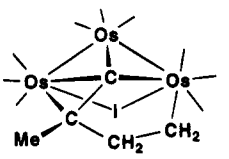

3

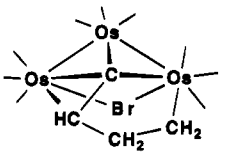

7

Compound **3** is an isomer of **2** with only two metal–metal bonds, Os(1)–Os(3) = 2.838(2) Å [2.829(2) and 2.825(2) Å] and Os(2)–Os(3) = 2.934(2) Å [2.942(2) and 2.936(2) Å]. The values in brackets are for the two other molecules. The corresponding values in **7** are 2.845(1) and 2.932(1) Å. The nonbonding Os(1)···Os(2) distance, 3.659(2) Å [3.603(2) and 3.605(2) Å] is much shorter than that in **2** because the iodo ligand bridges the two nonbonded metal atoms in this compound and pulls them together. There is also a metalated alkenyl ligand in this molecule, C(1)–C(2)–C(3)–C(4) with a methyl

Table 7. Positional Parameters and *B*(eq) Values (Å²) for 3

atom	*x*	*y*	*z*	*B*(eq)	atom	*x*	*y*	*z*	*B*(eq)
Os(1)	0.6929(1)	0.37432(8)	0.2264(1)	3.63(6)	C(1b)	0.372(2)	0.074(2)	0.618(2)	4.3(7)
Os(1a)	0.9787(1)	0.19142(8)	1.0357(1)	3.82(6)	C(2)	0.584(2)	0.472(2)	0.233(2)	3.4(7)
Os(1b)	0.4579(1)	0.1261(1)	0.7932(1)	5.17(7)	C(2a)	1.155(2)	0.182(2)	1.053(2)	3.5(7)
Os(2a)	1.1388(1)	0.35122(8)	1.04537(9)	3.33(6)	C(2b)	0.446(3)	0.129(2)	0.604(3)	6(1)
Os(2b)	0.2190(1)	0.09540(8)	0.5697(1)	4.50(7)	C(3a)	1.232(3)	0.211(2)	1.163(3)	6(2)
Os(2)	0.7543(1)	0.52210(8)	0.4531(1)	3.39(6)	C(3b)	0.388(3)	0.195(3)	0.544(3)	8(2)
Os(3a)	0.9995(1)	0.25988(8)	0.85438(9)	3.44(6)	C(3)	0.615(3)	0.549(2)	0.216(2)	5(2)
Os(3b)	0.3633(1)	−0.01212(8)	0.6891(1)	4.88(7)	C(4)	0.676(2)	0.593(2)	0.319(3)	5(2)
Os(3)	0.6674(1)	0.37114(8)	0.4355(1)	3.37(6)	C(4b)	0.285(4)	0.191(2)	0.519(3)	6(2)
I(1a)	0.9991(2)	0.3329(2)	1.1505(2)	5.7(1)	C(4a)	1.239(3)	0.291(2)	1.180(2)	6(2)
I(1)	0.8663(2)	0.4665(1)	0.3254(2)	4.8(1)	C(5)	0.469(2)	0.452(2)	0.170(2)	5(2)
I(1b)	0.2638(2)	0.1775(2)	0.7704(2)	5.8(1)	C(5b)	0.547(3)	0.108(3)	0.590(4)	10(3)
O(11a)	1.022(2)	0.118(2)	1.250(2)	10(2)	C(5a)	1.182(3)	0.105(2)	1.016(3)	6(2)
O(11)	0.705(2)	0.421(2)	0.007(2)	9(2)	C(11b)	0.501(3)	0.225(3)	0.827(3)	7(1)
O(11b)	0.537(2)	0.285(2)	0.846(2)	10(2)	C(11a)	1.009(3)	0.143(2)	1.169(3)	7(1)
O(12a)	0.932(2)	0.044(1)	0.899(2)	6(1)	C(11)	0.698(3)	0.398(3)	0.084(3)	8(1)
O(12b)	0.668(2)	0.065(2)	0.843(2)	9(2)	C(12a)	0.955(2)	0.100(2)	0.954(2)	4.1(7)
O(12)	0.830(2)	0.241(2)	0.271(2)	7(1)	C(12)	0.778(3)	0.289(2)	0.254(3)	4.6(9)
O(13)	0.512(2)	0.269(2)	0.109(2)	9(2)	C(12b)	0.584(4)	0.092(2)	0.825(3)	7(1)
O(13b)	0.457(3)	0.087(2)	1.017(2)	11(2)	C(13)	0.579(3)	0.308(2)	0.154(3)	6(1)0
O(13a)	0.750(2)	0.219(2)	0.979(2)	8(1)	C(13a)	0.837(3)	0.204(2)	1.000(3)	5.0(8)
O(21)	0.900(2)	0.660(1)	0.535(2)	6(1)	C(13b)	0.467(3)	0.104(2)	0.938(3)	7(1)
O(21a)	1.238(2)	0.487(1)	1.208(2)	7(1)	C(21b)	0.214(3)	0.040(3)	0.421(4)	8(1)
O(21b)	0.211(2)	0.014(2)	0.347(2)	10(2)	C(21)	0.844(2)	0.608(2)	0.506(2)	3.8(7)
O(22b)	0.020(2)	0.182(2)	0.480(2)	8(1)	C(21a)	1.201(2)	0.440(2)	1.149(2)	3.4(7)
O(22)	0.614(2)	0.583(2)	0.572(2)	8(2)	C(22)	0.668(3)	0.564(2)	0.529(2)	4.2(8)
O(22a)	1.306(2)	0.348(1)	0.942(2)	7(1)	C(22a)	1.243(3)	0.350(2)	0.979(3)	5.0(8)
O(23)	0.893(2)	0.445(1)	0.650(2)	5(1)	C(22b)	0.092(3)	0.150(2)	0.513(3)	7(1)
O(23b)	0.092(2)	−0.019(2)	0.626(2)	9(2)	C(23)	0.835(2)	0.469(2)	0.571(2)	3.3(7)
O(23a)	1.002(2)	0.457(1)	0.891(2)	8(1)	C(23b)	0.160(3)	0.029(2)	0.617(3)	7(1)
O(31)	0.585(2)	0.402(2)	0.627(2)	7(1)	C(23a)	1.050(3)	0.414(2)	0.943(3)	5.8(9)
O(31a)	1.082(2)	0.331(1)	0.690(2)	6(1)	C(31b)	0.300(3)	−0.096(2)	0.579(3)	5.5(9)
O(31b)	0.268(2)	−0.142(2)	0.510(2)	10(2)	C(31)	0.621(2)	0.392(2)	0.560(2)	3.5(7)
O(32a)	0.786(2)	0.322(2)	0.781(2)	10(2)	C(31a)	1.051(2)	0.307(2)	0.749(2)	3.0(6)
O(32b)	0.291(3)	−0.063(2)	0.870(2)	10(2)	C(32b)	0.321(4)	−0.046(3)	0.800(4)	9(1)
O(32)	0.512(2)	0.244(2)	0.348(2)	7(1)	C(32a)	0.867(3)	0.303(2)	0.805(3)	5.0(8)
O(33b)	0.570(2)	−0.086(2)	0.752(2)	9(2)	C(32)	0.571(3)	0.292(2)	0.380(2)	4.0(7)
O(33)	0.851(2)	0.276(1)	0.538(2)	6(1)	C(33a)	0.964(2)	0.171(2)	0.754(2)	3.5(7)
O(33a)	0.944(2)	0.121(2)	0.693(2)	9(2)	C(33b)	0.493(4)	−0.059(3)	0.735(3)	7(1)
C(1)	0.628(2)	0.451(1)	0.337(2)	2.0(5)	C(33)	0.779(3)	0.307(2)	0.504(2)	3.5(7)
C(1a)	1.108(2)	0.235(2)	0.985(2)	2.9(6)					

Table 8. Intramolecular Distances for 3[a]

Os(1)–Os(3)	2.838(2)	Os(3)–C(1)	1.95(2)
Os(1)–I(1)	2.788(3)	C(1)–C(2)	1.37(3)
Os(1)–C(1)	2.30(3)	C(1a)–C(2a)	1.37(4)
Os(1)–C(2)	2.33(3)	C(1b)–C(2b)	1.49(4)
Os(1a)–Os(3a)	2.829(2)	C(2)–C(3)	1.51(4)
Os(1a)–I(1a)	2.804(3)	C(2)–C(5)	1.55(4)
Os(1a)–C(1a)	2.27(3)	C(2a)–C(3a)	1.51(4)
Os(1a)–C(2a)	2.40(3)	C(2a)–C(5a)	1.52(5)
Os(1b)–Os(3b)	2.825(2)	C(2b)–C(3b)	1.56(5)
Os(1b)–I(1b)	2.785(3)	C(2b)–C(5b)	1.51(5)
Os(1b)–C(1b)	2.30(3)	C(3a)–C(4a)	1.44(5)
Os(1b)–C(2b)	2.39(3)	C(3b)–C(4b)	1.35(5)
Os(2a)–Os(3a)	2.942(2)	C(3)–C(4)	1.47(4)
Os(2a)–I(1a)	2.746(3)	Os–C(av)	1.93(4)
Os(2a)–C(1a)	2.16(3)	Os(a)–C(av)	1.91(4)
Os(2a)–C(4a)	2.20(3)	Os(b)–C(av)	1.90(5)
Os(2b)–Os(3b)	2.936(2)	C–O(av)	1.14(4)
Os(2b)–I(1b)	2.748(3)	C(a)–O(av)	1.13(4)
Os(2b)–C(1b)	2.06(3)	C(b)–O(av)	1.14(4)
Os(2b)–C(4b)	2.19(4)	Os(1)–Os(2)	3.659(2)
Os(2)–Os(3)	2.934(2)	Os(1a)–Os(2a)	3.603(2)
Os(2)–I(1)	2.753(3)	Os(1b)–Os(2b)	3.605(2)
Os(2)–C(1)	2.21(2)	C(1)–C(4)	2.70(4)
Os(2)–C(4)	2.23(3)	C(1a)–C(4a)	2.68(4)
Os(3a)–C(1a)	1.93(3)	C(1b)–C(4b)	2.64(5)
Os(3b)–C(1b)	1.88(3)		

[a] Distances are in angstroms. Estimated standard deviations in the least significant figure are given in parentheses.

Table 9. Intramolecular Bond Angles for 3[a]

Os(3)–Os(1)–I(1)	89.19(6)	C(1)–C(2)–C(5)	119(2)
Os(3a)–Os(1a)–I(1a)	88.63(7)	C(1a)–C(2a)–C(3a)	115(3)
Os(3b)–Os(1b)–I(1b)	87.60(8)	C(1a)–C(2a)–C(5a)	126(3)
Os(3a)–Os(2a)–I(1a)	87.50(7)	C(1b)–C(2b)–C(3b)	109(3)
Os(3b)–Os(2b)–I(1b)	86.13(7)	C(1b)–C(2b)–C(5b)	124(4)
Os(3)–Os(2)–I(1)	87.94(7)	C(2a)–C(3a)–C(4a)	114(3)
Os(1a)–Os(3a)–Os(2a)	77.24(5)	C(2b)–C(3b)–C(4b)	116(4)
Os(1b)–Os(3b)–Os(2b)	77.45(6)	C(2)–C(3)–C(4)	115(3)
Os(1)–Os(3)–Os(2)	78.65(5)	Os–C(av)–O	175(4)
Os(1a)–I(1a)–Os(2a)	80.95(8)	Os(2a)–C(av)–O	176(4)
Os(1)–I(1)–Os(2)	82.65(7)	Os(b)–C(av)–O	173(5)
Os(1b)–I(1b)–Os(2b)	81.31(8)	C(1)–C(2)–C(3)	114(2)

[a] Angles are in degrees. Estimated standard deviations in the least significant figure are given in parentheses.

group on C(2). It also bridges the three metal atoms via the carbon C(1), but in this compound the C(1)–C(2) double bond, 1.37(3) Å [1.37(4) and 1.49(4) Å], is π-bonded to Os(1) while the methylene group C(4) is σ-bonded to the neighboring metal atom Os(2), Os(2)–C(4) = 2.23(3) Å [2.20(3) and 2.19(4) Å]. The C–C distance of the coordinated double bond is 1.40(2) Å, and Os–C distance to the σ-bonded methylene group is 2.20(2) Å. As in **2** and **7**, each metal atom has three linear terminal carbonyl ligands. The ^{1}H NMR spectrum of **3** shows four independent resonances for the four inequivalent methylene protons {5.33 (ddd, 1H, $^2J_{HH}$ = 16 Hz, $^3J_{HH}$ = 8 Hz, $^3J_{HH}$ = 8 Hz), 5.15 (ddd, 1H, $^2J_{HH}$ = 16 Hz, $^3J_{HH}$ = 9 Hz, $^3J_{HH}$ = 5 Hz), 3.21 (ddd, 1H, $^2J_{HH}$ = 12 Hz, $^3J_{HH}$ = 9 Hz, $^3J_{HH}$ = 8 Hz), 2.82 (ddd, 1H, $^2J_{HH}$ = 12 Hz, $^3J_{HH}$ = 8 Hz, $^3J_{HH}$ = 5 Hz)} and a singlet for the methyl group at 2.53 ppm.

A summary of the results of these studies is shown in Scheme 2. On the assumption that compound **2** is an intermediate in the formation of **3**, this study provides valuable new information about the mechanism of the C–C bond cleavage step in the opening of the cyclobutenyl ring in the transformation of **4** to **2**. The C–C bond that is cleaved is the one between the bridging carbon atom and the CH_2 group that is bonded

Scheme 2

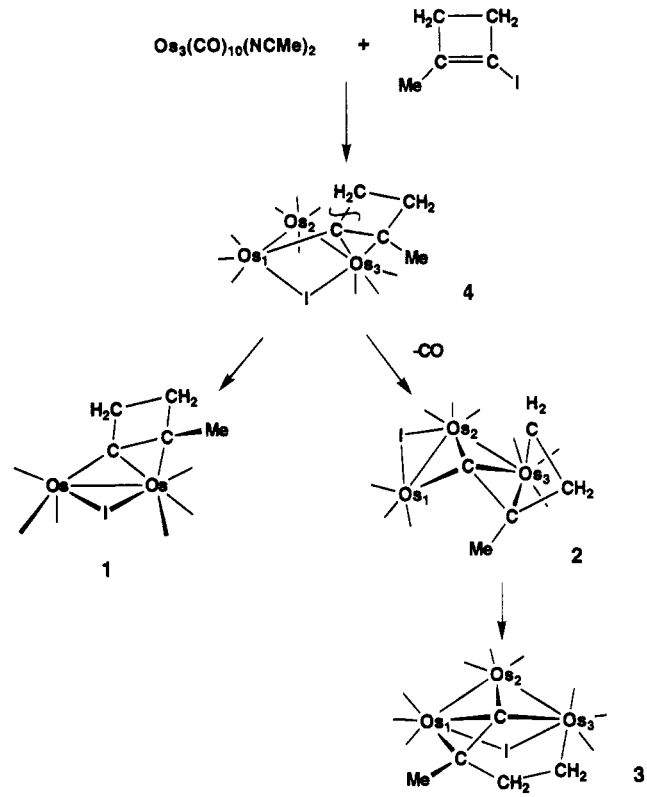

to it. This bond is indicated by the wavy line on the structure of **4** shown in Scheme 2. It seems likely that the **4** to **2** transformation is initiated by the loss of CO from **4**. This probably occurs at the CO-rich $Os(CO)_4$ group. The vacant site produced at that osmium atom could induce the shift of the iodo ligand to a bridging position across the Os(1)–Os(3) bond. This would move the vacant site to the atom Os(2) where a direct oxidative addition of the C–CH_2 carbon–carbon bond could then occur. The subsequent isomerization to **3** is readily accomplished by a suprafacial exchange of the metal atoms Os(1) and Os(2) over the face of the C(1)–C(2) π-bond. This repositioning of the C(1)–C(2) bond would then induce the shift of the iodo ligand back to a bridging position between the nonbonded pair of metal atoms. Note: this mechanism differs from the one proposed for the transformation of **5** to **7** which was proposed in the absence of the observation of any intermediates.[7] At this time we believe that the transformation of **5** to **7** is probably mechanistically similar to that of **4** to **3** via the intermediate **2**. Compound **1** is a spurious side product formed by fragmentation of the cluster of **4** and clearly has no bearing on the ring-opening process since its C_4 ring is still intact.

Acknowledgment. These studies were supported by the Division of Chemical Sciences of the Office of Basic Energy Sciences of the U.S. Department of Energy.

Supporting Information Available: Tables of positional parameters for the hydrogen atoms and anisotropic thermal parameters for all of the structural analyses (8 pages). Ordering information is given on any current masthead page.

OM9503151

Cationic Phosphenium Complexes of Group 6 Transition Metals: Reactivity, Isomerization, and X-ray Structures

Hiroshi Nakazawa,*,† Yoshitaka Yamaguchi,† Tsutomu Mizuta,† and Katsuhiko Miyoshi*,‡

Coordination Chemistry Laboratories, Institute for Molecular Science, Myodaiji, Okazaki 444, Japan, and Department of Chemistry, Faculty of Science, Hiroshima University, Higashi-Hiroshima 739, Japan

Received April 19, 1995®

The reaction of cationic diamino-substituted phosphenium complexes of group 6 transition metals *mer*-[(bpy)(CO)$_3$M{PN(Me)CH$_2$CH$_2$NMe}]$^+$ (M = Cr, Mo, W) with L (L = PN(Me)CH$_2$CH$_2$NMe(OR) (R = Me, Et), PPh$_3$) proceeds with substitution of L for CO to produce [(bpy)(CO)$_2$LM{PN(Me)CH$_2$CH$_2$NMe}]$^+$. During the reaction, the phosphenium ligand remains intact. The product consists of *trans* (two phosphorus ligands are mutually *trans*) and *cis* isomers, and they equilibrate. The *cis* form is electronically and the *trans* form is sterically favored. A similar reaction takes place when cationic monoamino-substituted phosphenium complexes are treated. Complexes *trans*-[(bpy)(CO)$_2$\{PN(Me)CH$_2$CH$_2$NMe(OMe)\}Mo\{PN(Me)CH$_2$CH$_2$NMe\}]·OTf (*trans*-**2a**·OTf) (OTf = SO$_3$CF$_3$) and *trans*-[(phen)(CO)$_2$\{PN(t-Bu)CH$_2$CH$_2$O(OMe)\}Mo\{PN(t-Bu)CH$_2$CH$_2$O\}]·OTf·CH$_2$Cl$_2$ (*trans*-**2j**·OTf·CH$_2$Cl$_2$) have been characterized by X-ray diffraction. The bond distance of Mo–P(phosphenium) is significantly shorter than that of Mo–P(phosphite) for both complexes: for *trans*-**2a**, 2.254 Å vs 2.495 Å and, for *trans*-**2j**, 2.238 Å vs 2.529 Å, indicating a significant double bond character between Mo and P(phosphenium). For both complexes, the P–N bond distances in phosphenium and in phosphite ligands are almost equal, indicating that there is no significant N → P(phosphenium) π donation. The role of the amino groups on the phosphenium phosphorus is probably to protect the approach of a nucleophile to phosphenium phosphorus by high pπ lone pair density flanking the phosphenium center.

Introduction

Since the first discovery of cationic transition-metal phosphenium complexes in 1978 by Parry et al.,[1] some such complexes have been prepared for several kinds of transition metals.[2–7] Phosphenium phosphorus in

Phosphenium

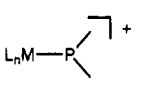

Cationic transition-metal phosphenium complex

these complexes takes sp^2 hybridization, so that it has lone pair electrons coordinating to a transition metal and a vacant p orbital accepting some electron density from a transition-metal d orbital. The phosphenium phosphorus can be thus considered to have the same electronic configuration as a carbene carbon or a silylene silicon in their transition-metal complexes. It is known that a carbene carbon and a silylene silicon in transition-metal complexes are very electrophilic and these complexes are stabilized by adduct formation with a Lewis base.[8,9] We here report the reactions of cationic phosphenium complexes of group 6 transition metals formulated as [(bpy)(CO)$_3$M{PN(Me)CH$_2$CH$_2$NMe}]$^+$ (bpy = 2,2′-bipyridine; M = Cr, Mo, W) with a trivalent phosphorus compound as a Lewis base and also report the geometrical isomerization and the crystal structures of the products.

† Institute for Molecular Science.
‡ Hiroshima University.
® Abstract published in *Advance ACS Abstracts,* August 1, 1995.

(1) Montemayor, R. G.; Sauer, D. T.; Fleming, S.; Bennett, D. W.; Thomas, M. G.; Parry, R. W. *J. Am. Chem. Soc.* **1978**, *100*, 2231. (b) Bennett, D. W.; Parry, R. W. *J. Am. Chem. Soc.* **1979**, *101*, 755.
(2) Cowley, A. H.; Kemp, R. A. *Chem. Rev.* **1985**, *85*, 367.
(3) Sanchez, M.; Mazieres, M. R.; Lamande, L.; Wolf, R. In *Multiple Bonds and Low Coordination in Phosphorus Chemistry*; Regitz, M., Scherer, O. J., Eds.; Thieme: New York, 1990; Chapter D1.
(4) (a) Day, V. W.; Tavanaiepour, I.; Abdel-meguid, S. S.; Kirner, J. F.; Goh, L.-Y.; Muetterties, E. L. *Inorg. Chem.* **1982**, *21*, 657. (b) Choi, H. W.; Gavin, R. M.; Muetterties, E. L. *J. Chem. Soc., Chem. Commun.* **1979**, 1085. (c) Muetterties, E. L.; Kirner, J. F.; Evans, W. J.; Watson, P. L.; Abdel-meguid, S. S.; Tavanaiepour, I.; Day, V. W. *Proc. Natl. Acad. Sci. U.S.A.* **1978**, *75*, 1056.
(5) (a) Cowley, A. H.; Kemp, R. A.; Ebsworth, E. A. V.; Rankin, D. W. H.; Walkinshaw, M. D. *J. Organomet. Chem.* **1984**, *265*, C19. (b) Cowley, A. H.; Kemp, R. A.; Wilburn, J. C. *Inorg. Chem.* **1981**, *20*, 4289.
(6) (a) Nakazawa, H.; Ohta, M.; Yoneda, H. *Inorg. Chem.* **1988**, *27*, 973. (b) Nakazawa, H.; Ohta, M.; Miyoshi, K.; Yoneda, H. *Organometallics* **1989**, *8*, 638. (c) Nakazawa, H.; Yamaguchi, Y.; Miyoshi, K. *J. Organomet. Chem.* **1994**, *465*, 193. (d) Nakazawa, H.; Yamaguchi, Y.; Mizuta, T.; Ichimura, S.; Miyoshi, K. *Organometallics*, in press.
(7) Electrically neutral transition-metal complexes described as [L$_n$MPR$_2$] can be considered as phosphenium complexes if one thinks that they consist of L$_n$M$^-$ and $^+$PR$_2$. However, in this paper we focus on electrically cationic transition–metal complexes described as [L$_n$MPR$_2$]$^+$.
(8) For carbene complexes see: Fischer, H. In *The Chemistry of the Metal-carbon Bond*; Hartley, F. R., Patai, S., Eds.; John Wiley & Sons: New York, 1982; p 207, Vol. 1.

0276-7333/95/2314-4173$09.00/0

Results and Discussion

Formation of $[(bpy)(CO)_2LM\{PN\text{-}N\}]^+$ (L = Trivalent Phosphorus Compound). Recently we reported a preparative method for cationic phosphenium complexes of group 6 transition metals as shown in eq 1,[6b,c]

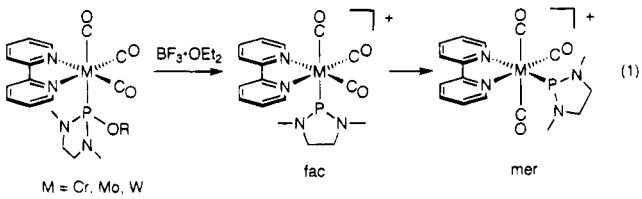

(1)

where an alkoxy group on the coordinating phosphite is abstracted as an anion by $BF_3{\cdot}OEt_2$. The facial and meridional isomers of the product are the kinetic and thermodynamic products, respectively.[6c] Although the reactions are very clean and the products are stable in the solution unless exposed to air, these phosphenium complexes have not been isolated so far due to the high reactivity. Therefore, $[(bpy)(CO)_3M\{\overline{PN(Me)CH_2CH_2NMe}\}]^+$ prepared in situ was used as a starting complex in the reaction with trivalent phosphorus compounds.

A CH_2Cl_2 solution containing a starting cationic phosphenium complex prepared according to eq 1 was cooled to −78 °C, an equimolar amount of a trivalent phosphorus compound (L) was added, and then the solution was allowed to warm to room temperature. The results are shown in eq 2, and the ^{31}P NMR data are summarized in Table 1.

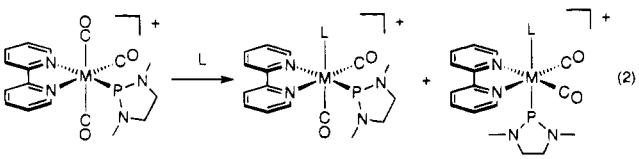

(2)

1a : M = Mo
cis-2a : M = Mo, L = P(N-N)(OMe)
trans-2a : M = Mo, L = P(N-N)(OMe)
cis-2b : M = Mo, L = P(N-N)(OEt)
trans-2b : M = Mo, L = P(N-N)(OEt)
cis-2c : M = Mo, L = PPh_3
trans-2c : M = Mo, L = PPh_3
1d : M = Cr
trans-2d : M = Cr, L = P(N-N)(OMe)
1e : M = W
cis-2e : M = W, L = P(N-N)(OMe)
trans-2e : M = W, L = P(N-N)(OMe)

N-N = $N(Me)CH_2CH_2NMe$

In the case of reaction of **1a** with $\overline{PN(Me)CH_2CH_2NMe(OMe)}$, the reaction mixture showed two absorption bands at 1912 and 1834 cm^{-1} (relatively broad compared with the absorption bands for **1a**) in the ν_{CO} region in the IR spectrum, indicating that one carbonyl ligand in **1a** is replaced by L. The ^{31}P NMR spectrum showed four doublets, 257.71 (d, J = 42.7 Hz), 242.18 (d, J = 274.7 Hz), 135.00 (d, J = 42.7 Hz), and 130.15 (d, J = 274.7 Hz). The first and third doublets were relatively weaker than the other two in intensity (The ratio was 24/76 (see Table 2)). The first two chemical shifts are in the region due to phosphenium ligands, and the last two ones are in that due to coordinating phosphites.[6b,c] This observation suggests that two geometrical isomers are formed and both of them have one phosphenium ligand ($\overline{PN(Me)CH_2CH_2NMe}^+$) and one diamino-substituted phosphite ligand ($\overline{PN(Me)CH_2CH_2NMe(OMe)}$). The coupling constants observed here indicate that in one isomer two phosphorus ligands are mutually *cis* (*cis* isomer) and in the other isomer they are *trans* (*trans* isomer). The *trans* isomer can be depicted uniquely as shown in eq 2, whereas there are three possible structures (**A**–**C**) for the *cis* isomer.

Table 1. ^{31}P NMR Data[a]

x	1x	*cis*-2x	*trans*-2x
a	269.39 (s)	135.00 (d, J = 42.7 Hz)	130.15 (d, J = 274.7 Hz)
		257.71 (d, J = 42.7 Hz)	242.18 (d, J = 274.7 Hz)
b		131.32 (d, J = 42.7 Hz)	126.52 (d, J = 274.6 Hz)
		256.74 (d, J = 42.7 Hz)	241.88 (d, J = 274.6 Hz)
c		34.15 (d, J = 27.5 Hz)	35.84 (d, J = 180.1 Hz)
		257.64 (d, J = 27.5 Hz)	246.93 (d, J = 180.1 Hz)
d	277.32 (s)		149.22 (d, J = 91.6 Hz)
			248.56 (d, J = 91.6 Hz)
e	242.72 (s) (J_{PW} = 561.1 Hz)	126.09 (d, J = 27.5 Hz; (J_{PW} = 329.6 Hz)	119.56 (d, J = 268.6 Hz; (J_{PW} = 271.6 Hz)
		234.02 (d, J = 27.5 Hz; (J_{PW} = 589.0 Hz)	222.16 (d, J = 268.6 Hz; (J_{PW} = 518.8 Hz)
f	253.84 (s)	149.61 (d, J = 54.9 Hz)	144.28 (d, J = 326.6 Hz)
		149.73 (d, J = 54.9 Hz)	235.57 (d, J = 326.6 Hz)
		241.94 (d, J = 54.9 Hz)	
		242.36 (d, J = 54.9 Hz)	
g			139.89 (d, J = 320.5 Hz)
			227.52 (d, J = 320.5 Hz)
h		157.15 (d, J = 58.0 Hz)	152.70 (d, J = 369.2 Hz)
		214.93 (d, J = 58.0 Hz)	224.47 (d, J = 369.2 Hz)
i	269.04 (s)	134.04 (d, J = 42.8 Hz)	130.12 (d, J = 271.6 Hz)
		258.43 (d, J = 42.8 Hz)	242.29 (d, J = 271.6 Hz)
j			140.41 (d, J = 317.4 Hz)
			228.10 (d, J = 317.4 Hz)

[a] In CH_2Cl_2.

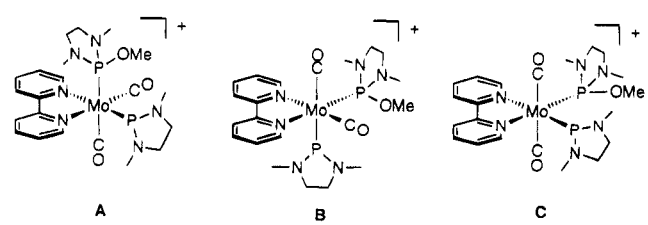

In order to determine the structure of the *cis* form, the ^{13}C NMR spectrum of the reaction mixture was measured. The resonance pattern in the CO region gave us the clue. The apparent triplet observed at 224.39 ppm with J_{CP} = 18.2 Hz as a main peak can be assigned to the *trans* isomer. In addition, two doublet of doublets were observed at 226.05 ppm with J_{CP} = 18.2 Hz and 11.8 Hz and at 213.89 ppm with J_{CP} = 57.0 Hz and 16.1 Hz. Therefore, the possibility of **C** can be ruled out,

(9) For leading references of silylene complexes see: (a) Zybill, C.; Müller, G. *Angew. Chem., Int. Ed. Engl.* **1987**, *26*, 669. (b) Zybill, C.; Wilkinson, D. L.; Leis, C.; Müller, G. *Angew. Chem., Int. Ed. Engl.* **1989**, *28*, 203. (c) Probst, R.; Leis, C.; Gamper, S.; Herdtweck, E.; Zybill, C.; Auner, N. *Angew. Chem., Int. Ed. Engl.* **1991**, *30*, 1132. (d) Leis, C.; Wilkinson, D. L.; Handwerker, H.; Zybill, C.; Müller, G. *Organometallics* **1992**, *11*, 514. (e) Straus, D. A.; Tilley, T. D.; Rheingold, A. L.; Geib, S. J. *J. Am. Chem. Soc.* **1987**, *109*, 5872. (f) Straus, D. A.; Zhang, C.; Quimbita, G. E.; Grumbine, S. D.; Heyn, R. H.; Tilley, T. D.; Rheingold, A. L.; Geib, S. J. *J. Am. Chem. Soc.* **1990**, *112*, 2673. (g) Grumbine, S. D.; Chadha, R. K.; Tilley, T. D. *J. Am. Chem. Soc.* **1992**, *114*, 1518. (h) Grumbine, S. D.; Tilley, T. D.; Arnold, F. P.; Rheingold, A. L. *J. Am. Chem. Soc.* **1993**, *115*, 7884. (i) Ueno, K.; Tobita, H.; Shimoi, M.; Ogino, H. *J. Am. Chem. Soc.* **1988**, *110*, 4092. (j) Tobita, H.; Ueno, K.; Shimoi, M.; Ogino, H. *J. Am. Chem. Soc.* **1990**, *112*, 3415. (k) Takeuchi, T.; Tobita, H.; Ogino, H. *Organometallics* **1991**, *10*, 835. (l) Corriu, R.; Lanneau, G.; Priou, C. *Angew. Chem., Int. Ed. Engl.* **1991**, *30*, 1130. (m) Woo, L. K.; Smith, D. A.; Young, V. G., Jr. *Organometallics* **1991**, *10*, 3977. (n) Lee, K. E.; Arif, A. M.; Gladysz, J. A. *Chem. Ber.* **1991**, *124*, 309. (o) Jutzi, P.; Möhrke, A. *Angew. Chem., Int. Ed. Engl.* **1990**, *29*, 893.

Scheme 1

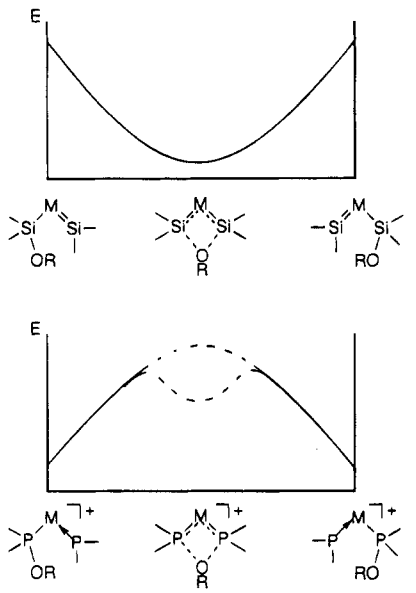

because the two CO ligands in **C** are magnetically equal. Since it has been demonstrated that the phosphenium ligand $\overline{PN(Me)CH_2CH_2NMe}^+$ is a stronger π-acceptor than a CO ligand,[1b,6c] the phosphenium ligand is highly likely to prefer situating *trans* to bpy to *trans* to CO. Therefore, we propose that the *cis* isomer formed in the reaction has a structure **A** rather than **B**.

Recently, Ogino and his co-workers reported the preparative methods and the X-ray structures of donor-stabilized bis(silylene)complexes for Fe[9i,j] and Mn.[9k] They proposed that these complexes are formed from an alkoxy-substituted silyl (silylene) complex, which is not detected because of the coordination of the alkoxy oxygen to the silylene silicon.

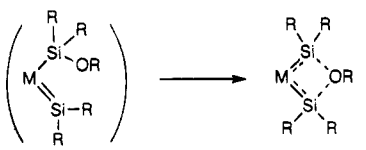

In the case of *cis*-**2a**, the ^{31}P NMR resonances are diagnostic of a phosphite (phosphenium) structure. The cyclization product (which may be referred to as a bis(phosphenium) complex) is not observed.

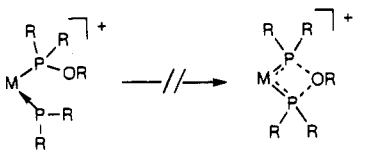

Muetterties also reported the X-ray structure of $[Mo\{P(OMe)_3\}_5\{P(OMe)_2\}]PF_6$, which does not take a cyclization form but has a discrete phosphenium ligand.[4a] Therefore, a phosphenium ligand seems to have inherently less tendency to take a base-stabilized form, but a silylene ligand has the tendency, even though phosphenium and silylene ligands are isoelectronic. In other words, as shown in Scheme 1, the middle point between the two silicon ligands for alkoxy-substituted silyl (silylene) complexes is the energy minimum position for the OR group, whereas the middle point between the two phosphorus ligands for phosphite (phosphenium) complexes is not.

The reactions of **1a** with $\overline{PN(Me)CH_2CH_2NMe}(OEt)$ and PPh_3, and the reactions of Cr complex **1d** and W complex **1e** with $\overline{PN(Me)CH_2CH_2NMe}(OMe)$, showed basically similar results to those of the reaction of **1a** with $\overline{PN(Me)CH_2CH_2NMe}(OMe)$; i.e., the phosphenium ligand remains intact and CO/L exchange reaction takes place resulting in the *cis* and *trans* isomer formation (shown in eq 2). In the case of the Cr complex, only the *trans* isomer was detected. The reason will be discussed later.

The starting phosphenium complex of W (**1e**) exists mainly as the *fac* form. However monitoring the reaction with L by the ^{31}P NMR spectra revealed that the isomerization from *fac* to *mer* forms was immediately completed by the addition of L, and then the CO/L exchange reaction took place gradually. So, it can be said that, even in the case of the W complex, the reaction of the *mer* isomer with L eventually takes place. The promotion of the *fac*−*mer* isomerization by the addition of $\overline{PN(Me)CH_2CH_2NMe}(OMe)$, HOEt, or OTf^- was observed. The details will be reported elsewhere.

Although every reaction shown in eq 2 takes place cleanly to give only *cis*-**2** and *trans*-**2** (in the Cr case, only *trans*-**2d**), several attempts to isolate these products in the solid state were unsuccessful presumably due to their high reactivity. However, it was found that only *trans*-**2a** could be isolated as a $SO_3CF_3^-$ (OTf^-) salt when **1a** prepared from *fac*-$[(bpy)(CO)_3Mo\{\overline{PN(Me)CH_2CH_2NMe}(OMe)\}]$ and $Me_3SiSO_3CF_3$ (TMS·OTf) in place of $BF_3{\cdot}OEt_2$ was treated with $\overline{PN(Me)CH_2CH_2NMe}(OMe)$. The reaction mixture contains *cis*-**2a** and *trans*-**2a**, but after workup only *trans*-**2a**·OTf was obtained as reddish orange crystals. The X-ray structure will be shown below.

Formation of $[(bpy)(CO)_2LM\{PN\text{-}O\}]^+$ and $[(bpy)(CO)_2LM\{PO\text{-}O\}]^+$. Next we examined the reaction of cationic complexes containing monoamino-substituted phosphenium ligand with monoamino phosphite. **1f** prepared from *fac*-$[(bpy)(CO)_3Mo\{\overline{PN(Me)CH_2CH_2O}\}(OMe)]$ with $BF_3{\cdot}OEt_2$ reacted with $\overline{PN(Me)CH_2CH_2O}(OMe)$ to give *cis*-**2f** and *trans*-**2f** (eq 3).

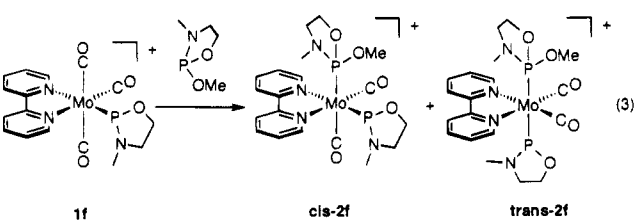

1f **cis-2f** **trans-2f** (3)

In the reaction of **3g** with $BF_3{\cdot}OEt_2$ or TMS·OTf, the corresponding phosphenium complex $[(bpy)(CO)_3Mo\{\overline{PN(t\text{-}Bu)CH_2CH_2O}\}]^+$ was formed, but some other Mo complexes were also formed. So the resulting solution could not be used for the next reaction. However, the treatment of **3g** with TMS·OTf in the presence of an

equimolar amount of PN(t-Bu)CH_2CH_2O(OMe) showed a clean reaction to give *trans*-**2g** without the *cis* isomer (eq 4).

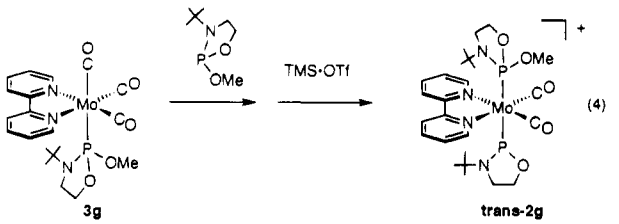

(4)

In order to examine the reaction of cationic phosphenium complex having no amino substituent with phosphite, we attempted the preparation of [(bpy)$(CO)_3$Mo{POCMe$_2$CMe$_2$O}]$^+$ in the reaction of *fac*-[(bpy)$(CO)_3$Mo{POCMe$_2$CMe$_2$O(OMe)}] with BF_3·OEt_2. However, the product in this reaction was not the cationic phosphenium complex but a fluorinated complex, *fac*-[(bpy)$(CO)_3$Mo{POCMe$_2$CMe$_2$O(F)}]. Thus, we sought another preparative method and found that a diphosphite complex, **4h**, reacts with TMS·OTf to give *cis*-**2h** and *trans*-**2h** (eq 5). The resonance pattern in the CO region

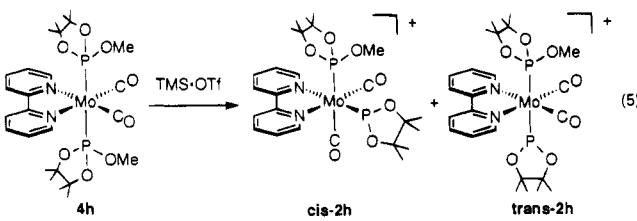

(5)

in the ^{13}C NMR spectrum of the reaction mixture is consistent with the formation of *trans*-**2h** and *cis*-**2h** which corresponds to structure A type (vide supra): 221.78 ppm (t, J_{CP} = 18.4 Hz) due to *trans*-**2h** and 220.15 ppm (dd, J_{CP} = 25.7, 21.9 Hz) and 209.28 ppm (dd, J_{CP} = 69.6, 19.5 Hz) due to *cis*-**2h**.

Formation of [(phen)$(CO)_2$LM{PN-N}]$^+$ and [(phen)$(CO)_2$LM{PN-O}]$^+$. phen analogues of *trans*-**2a** (diamino-substituted) and *trans*-**2g** (monoamino-substituted) were prepared according to eqs 6 and 7,

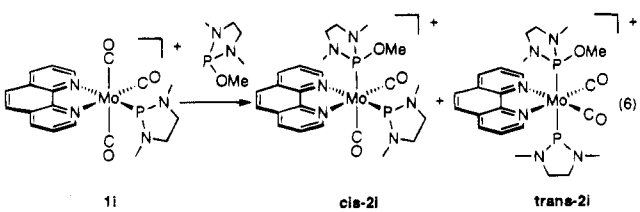

(6)

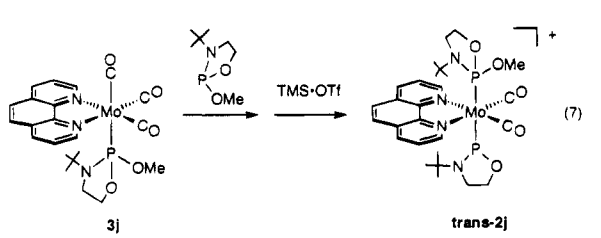

(7)

respectively. Changing bpy to phen (*trans*-**2a** → *trans*-**2i** and *trans*-**2g** → *trans*-**2j**) exerted no significant effect

Table 2. *Cis*–*Trans* Isomer Ratio of [(bpy)$(CO)_2$LM(phosphenium)]$^+$

x	*cis*-**2x**	*trans*-**2x**
a	24	76
b	28	72
c	7	93
d	0	100
e	22	78
f	69	31
g	0	100
h	63	37
i	23	77
j	0	100

Scheme 2

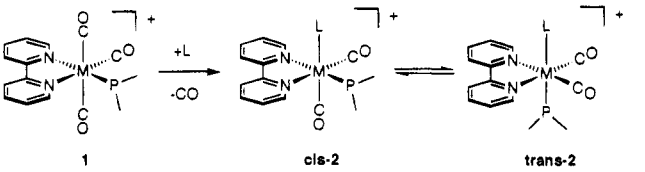

on the ^{31}P NMR data (chemical shifts and coupling constants). A single crystal of *trans*-**2j** was obtained; thus, it was subjected to X-ray analysis (vide infra).

***Cis* and *Trans* Isomers of [(bpy)$(CO)_2$LM(phosphenium)]$^+$.** As mentioned above, a meridional isomer of [(bpy)$(CO)_3$M(phosphenium)]$^+$ reacts with a trivalent phosphorus compound (L) to give [(bpy)$(CO)_2$LM(phosphenium)]$^+$ by CO/L exchange reaction. The product consists of the *cis* and *trans* isomers, and their ratio depends on the kind of M, the substituent on the phosphenium phosphorus, and L. Table 2 shows the isomer ratios.

Before looking at the ratios, it is pertinent to check whether the two isomers are at equilibrium or not. The isolated *trans*-**2a** was redissolved in CH_2Cl_2, and the intensity change of resonances in the ^{31}P NMR spectra was monitored. Immediately after the dissolution, *trans*-**2a** was the main component, but a small amount of *cis*-**2a** was already present; the *cis*-**2a**/*trans*-**2a** ratio was 6/94. The amount of *cis*-**2a** increased gradually with time at the cost of the amount of *trans*-**2a**, and after 48 h the apparent change ceased. The final ratio was 24/76. Therefore, it was confirmed that the *trans* isomer is in equilibrium with the *cis* isomer.

Although *cis*-**2** and *trans*-**2** are in equilibrium, *cis*-**2** may be formed first in the reaction of **1** with L (Scheme 2); a phosphenium ligand is a strong π acceptor, so three CO ligands in **1**, especially two CO ligands mutually *trans*, are activated by it. Thus, one of the two CO ligands is readily replaced by L to give *cis*-**2**, which then isomerizes to *trans*-**2** to reach the equilibrium. It should be noted here that a non-phosphenium complex, [(bpy)$(CO)_3$Mo{PN(Me)CH_2CH_2NMe(OMe)}], does not undergo CO/L exchange reaction at room temperature.

Now, let us consider the isomer ratios shown in Table 2. First, we compare the ratios for **2a**, **2d**, and **2e** to elucidate the effect of a central metal on the equilibrium. The ratios for Mo (24/76) and for W (22/78) are almost equal, whereas the *cis* isomer for Cr was not detected. It is suggested that Cr, having a smaller radius than Mo or W (Cr = 1.25 Å, Mo = 1.36 Å, and W = 1.37 Å), is too small to accept the two large ligands in the *cis* configuration. The P–P coupling constant for the Cr complex (*trans*-**2d**) is 91.6 Hz, whereas those for the Mo

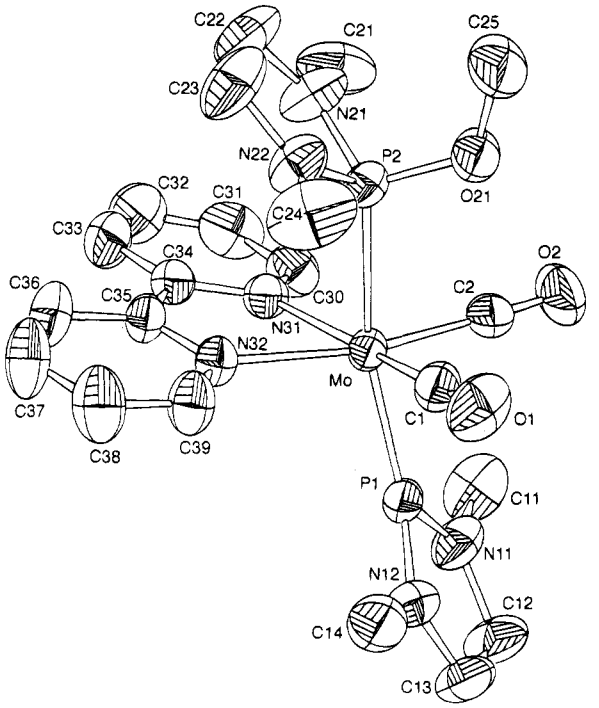

Figure 1. ORTEP drawing of *trans*-**2a** (50% probability ellipsoids) showing the numbering system. All hydrogen atoms are omitted for clarity.

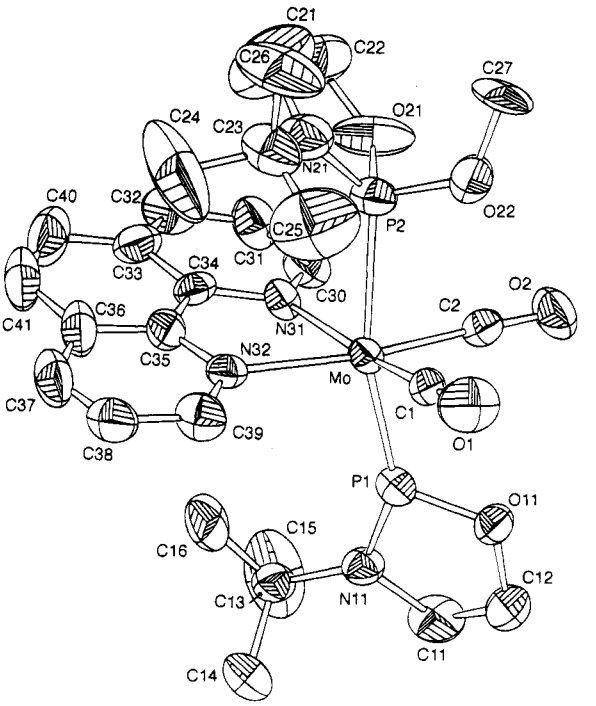

Figure 2. ORTEP drawing of *trans*-**2j** (50% probability ellipsoids) showing the numbering system. All hydrogen atoms are omitted for clarity.

and W complexes (*trans*-**2a** and *trans*-**2e**) are 274.7 and 268.6 Hz, respectively. It is suggested that the phosphite and/or the phosphenium may not closely approach the small Cr to make a sufficient bond due to the steric repulsion with the other ligands (bpy and two CO ligands) on the Cr. The ratio of 7/93 for **2c** can be rationalized also by steric effects, if PPh_3 is assumed to be bulkier than $\overline{PN(Me)CH_2CH_2N}Me(OMe)$.

bpy and phosphite ligands serve as σ-donors and also a weak π-acceptors, and the π-acidity is weaker for bpy than for phosphite.[6c,10] Therefore, the *cis* form of **2**, where a phosphenium ligand being a strong π acid is *trans* to bpy, is electronically favored over the *trans* form, where a phosphenium ligand is *trans* to phosphite. This is embodied by the J_{PW} values of **2e**. J_{PW} is 518.8 Hz for *trans*-**2e** but is 589.0 Hz for *cis*-**2e**, indicating that the phosphenium ligand is bonded more strongly to W for the *cis* form than for the *trans* form.

π-Acidity of a phosphenium ligand seems stronger for **2f** than for **2a**, so it is expected that the *cis*/*trans* ratio is greater for **2f** than **2a**. Actually the equilibrium of **2f** is shifted toward the *cis* form. **2g** has the phosphenium ligand electronically similar to that of **2f**, but *cis*-**2g** has not been detected. This may come from the bulkiness of a t-Bu group. *cis*-**2j** has also not been detected presumably for the same reason. The equilibrium is on a critical balance, but basically it can be said that the *cis* form is electronically and the *trans* form is sterically favored.

Crystal Structures of *trans*-2a·OTf and *trans*-2j·OTf·CH_2Cl_2. X-ray structure analyses of *trans*-**2a**·OTf and *trans*-**2j**·OTf·CH_2Cl_2 were undertaken. The ORTEP drawings of *trans*-**2a** and *trans*-**2j** are displayed in Figures 1 and 2, respectively. The crystal data and

Table 3. Summary of Crystal Data for *trans*-2a·OTf and *trans*-2j·OTf·CH_2Cl_2

	trans-**2a**·OTf	*trans*-**2j**·OTf·CH_2Cl_2
formula	$C_{22}H_{31}F_3MoN_6O_6P_2S$	$C_{29}H_{39}Cl_2F_3MoN_4O_8P_2S$
fw	722.50	889.53
cryst syst	monoclinic	triclinic
space group	$P2/n$	$P\bar{1}$
cell consts		
a, Å	19.155(2)	10.230(3)
b, Å	13.604(2)	11.299(4)
c, Å	11.798(2)	17.043(4)
α, deg		96.25(2)
β, deg	98.22(1)	99.82(2)
γ, deg		91.83(3)
V, Å^3	3042.6(7)	1927(1)
Z	4	2
D_{calcd}, g cm^{-3}	1.58	1.39
μ, cm^{-1}	5.89	5.25
cryst size, mm	0.66 × 0.40 × 0.12	0.55 × 0.26 × 0.05
radiation (λ, Å)	Mo Kα (0.710 73)	Mo Kα (0.710 73)
scan technique	$\omega-2\theta$	$\omega-2\theta$
scan range, deg	$3 < 3\theta < 55$	$3 < 2\theta < 55$
scan rate, deg min^{-1}	6.0	6.0
no. of unique data	6993	6783
no. of unique data with $F_o > 3\sigma(F_o)$	4601	3373
R	0.050	0.099
R_w	0.059	0.062

the selected bond distances and angles for *trans*-**2a**·OTf and *trans*-**2j**·OTf·CH_2Cl_2 are listed in Tables 3–5. The final atomic coordinates for non-hydrogen atoms are presented in Tables 6 and 7.

Both complexes have pseudooctahedral geometries around the Mo atom, and two phosphorus atoms are coordinated to the Mo in mutually *trans* positions. The most interesting structural feature is that the bond distance of Mo–P(phosphenium) is significantly shorter than that of Mo–P(phosphite) for both complexes: for *trans*-**2a**, Mo–P(phosphenium) = 2.254 Å, Mo–P(phosphite) = 2.495 Å; for *trans*-**2j**, Mo–P(phosphenium) =

(10) Chisholm, M. H.; Connor, J. A.; Huffman, J. C.; Kober, E. M.; Overton, C. *Inorg. Chem.* **1984**, *23*, 2298.

Table 4. Intramolecular Distances (Å) and Angles (deg) with Esd's in Parentheses for *trans*-2a·OTf

Bond Distances			
Mo–C1	1.953(6)	O2–C2	1.148(7)
Mo–C2	1.966(6)	O21–C25	1.44(1)
Mo–N32	2.244(4)	N11–C12	1.449(8)
Mo–P1	2.254(1)	N11–C11	1.46(1)
Mo–N31	2.255(4)	N12–C14	1.43(1)
Mo–P2	2.495(1)	N12–C13	1.453(8)
P1–N11	1.642(5)	N21–C22	1.44(1)
P1–N12	1.644(5)	N21–C21	1.46(1)
P2–O21	1.611(4)	N22–C24	1.44(1)
P2–N21	1.648(5)	N22–C23	1.44(1)
P2–N22	1.662(5)	C12–C13	1.50(1)
O1–C1	1.158(7)	C22–C23	1.49(1)
Bond Angles			
C1–Mo–C2	90.1(2)	N21–P2–Mo	120.6(2)
C1–Mo–N32	98.9(2)	N22–P2–Mo	118.7(2)
C1–Mo–P1	84.2(2)	C25–O21–P2	121.1(4)
C1–Mo–N31	169.3(2)	C12–N11–C11	118.3(6)
C1–Mo–P2	85.3(2)	C12–N11–P1	116.3(4)
C2–Mo–N32	168.2(2)	C11–N11–P1	125.2(4)
C2–Mo–P1	84.1(2)	C14–N12–C13	118.6(5)
C2–Mo–N31	98.3(2)	C14–N12–P1	125.4(4)
C2–Mo–P2	88.0(2)	C13–N12–P1	115.9(4)
N32–Mo–P1	104.3(1)	C22–N21–C21	119.2(6)
N32–Mo–N31	71.9(2)	C22–N21–P2	117.1(5)
N32–Mo–P2	85.2(1)	C21–N21–P2	123.6(5)
P1–Mo–N31	103.1(1)	C24–N22–C23	120.0(6)
P1–Mo–P2	166.85(5)	C24–N22–P2	122.9(5)
N31–Mo–P2	88.4(1)	C23–N22–P2	116.4(5)
N11–P1–N12	92.6(2)	O1–C1–Mo	179.1(4)
N11–P1–Mo	132.7(2)	O2–C2–Mo	178.3(5)
N12–P1–Mo	132.7(2)	N11–C12–C13	107.3(6)
O21–P2–N21	109.5(3)	N12–C13–C12	107.6(5)
O21–P2–N22	107.6(2)	N21–C22–C23	107.3(6)
N21–P2–N22	90.9(3)	N22–C23–C22	107.8(7)
O21–P2–Mo	108.2(2)		

2.238 Å, Mo–P(phosphite) = 2.529 Å. Normal Mo–P dative bond distances are reported to fall in the range 2.40–2.57 Å.[2] The observation that the Mo–P(phosphenium) bond is about 10% shorter than the Mo–P dative bond is consistent with double bond character in the phosphenium complex.

Another structural feature of interest is concerned with the P–N bond distance. For both *trans*-**2a** and *trans*-**2j**, the P–N bond distances (Å) in phosphenium and in phosphite ligands are almost equal: 1.642 (P1–N11), 1.644 (P1–N12), 1.648 (P2–N21), and 1.662 (P2–N22) for *trans*-**2a** and 1.65 (P1–N11) and 1.63 (P2–N21) for *trans*-**2j**. This observation gives an insight into the role of an amino group on a phosphenium phosphorus (vide infra).

Although the geometry around the coordinating phosphite phosphorus is pseudotetrahedral, the geometry around the phosphenium phosphorus is planar: the sum of angles at the phosphorus is 358.0° for *trans*-**2a** and 359.1° for *trans*-**2j**. For nitrogen atoms both in phosphenium and in phosphite ligands, the trigonal-planar geometry is indicated: the sum of angles is 359.8° (N11), 359.9° (N12), 359.9° (N21), and 359.3° (N22) for *trans*-**2a** and 359.2° (N11) and 359.0° (N21) for *trans*-**2j**.

The orientation of the phosphenium ligand is interesting. With *trans*-**2a** the Mo–P1–N11–N12 least-squares mean plane bisects the C1–Mo–N32 and C2–Mo–N31 angles, making a bisect angle of 47.07° with the N31–Mo–C1 vector, and with *trans*-**2j** the Mo–P1–N11–O11 least-squares mean plane bisects the C1–Mo–C2 and N31–Mo–N32 angles, making a bisect angle of 38.85° with the N31–Mo–C1 vector.

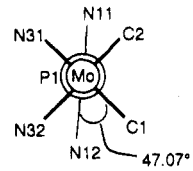

trans-2a

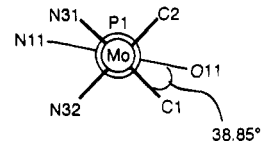

trans-2j

Two cationic phosphenium complexes of transition metals have been characterized by X-ray diffraction so far.[4a,5a] One of them is a Mo complex, $[Mo\{P(OMe)_3\}_5\{P(OMe)_2\}]PF_6$[4a] in which the phosphenium ligand is oriented in the similar way; the least-squares mean plane makes a dihedral angle of 23.80° with that determined by Mo and four phosphorus atoms involving the phosphenium phosphorus. Muetterties mentioned that the phosphenium is oriented in such a way as to minimize repulsion with the trimethyl phosphite ligands.[4a] In the case of *trans*-**2a** and *trans*-**2j**, no significant steric repulsion exists between the phosphenium ligand and equatorial ligands (bpy (phen) and 2 CO ligands). So the phosphenium orientation found here seems to be inherent.

The X-ray structure of *trans*-**2j** implies intramolecular CH-π interaction. The distance between C16 and the least-squares mean plane of the phen ring is 3.133 Å, which is significantly shorter than the sum of the C–H bond distance (1.09 Å), the van der Waals radius of H (1.20 Å), and that of an aromatic ring (1.7 Å).[11] The CH-π interaction may be the reason for the different orientation (about 90°) of the phosphenium ligands in *trans*-**2a** and in *trans*-**2j**.

Double-Bond Character between a Transition Metal and a Phosphenium Phosphorus. A cationic phosphenium complex has been described in the resonance forms shown in Scheme 3. **R2** corresponds to a transition-metal phosphenium complex where a plus charge is located on the phosphorus and a phosphenium cation coordinates to a transition metal through its lone pair. The bond between M and P in **R2** can be seen as a dative bond. If a sufficient electron density flows from the filled d orbital of a transition metal into the vacant p orbital on the phosphorus, the plus charge would be located on a transition metal and the M–P bond would become a double bond (**R1**). The π-electron donation to the empty p orbital of the phosphorus may occur not only from M but also from the two other substituents on the phosphorus (X and Y). These features are depicted in **R3** and **R4**.

In relation to this study, it is useful to note that Arduengo and co-workers recently reported the preparation of the first isolable crystalline carbene (imidazol-2-ylidene) and claimed that there is no convincing

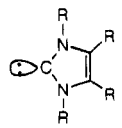

imidazol-2-ylidene

evidence that π-delocalization is an important feature of the carbene; that is, the nitrogen lone pairs do not

(11) The van der Waals distance between two parallel benzene nuclei is usually at least 3.4 Å. (a) Fessner, W.-D.; Sedelmeier, G.; Spurr, P. R.; Rihs, G.; Prinzbach, H. *J. Am. Chem. Soc.* **1987**, *109*, 4626. (b) Vögtle, F.; Neumann, P. *Top. Curr. Chem.* **1974**, *48*, 67.

Table 5. Intramolecular Distances (Å) and Angles (deg) with Esd's in Parentheses for *trans*-2j·OTf·CH_2Cl_2

	Bond Distances		
Mo–C1	1.88(1)	O1–C1	1.21(2)
Mo–C2	1.94(1)	O2–C2	1.18(1)
Mo–P1	2.238(4)	O11–C12	1.44(2)
Mo–N31	2.240(9)	O21–C22	1.42(2)
Mo–N32	2.256(9)	O22–C27	1.40(2)
Mo–P2	2.529(4)	N11–C11	1.46(2)
P1–O11	1.602(7)	N11–C13	1.50(1)
P1–N11	1.65(1)	N21–C23	1.49(2)
P2–O21	1.59(1)	N21–C21	1.51(2)
P2–O22	1.627(9)	C11–C12	1.48(2)
P2–N21	1.63(1)	C21–C22	1.42(2)
	Bond Angles		
C1–Mo–C2	84.1(5)	O22–P2–N21	107.2(6)
C1–Mo–P1	89.8(4)	O21–P2–Mo	109.7(4)
C1–Mo–N31	169.4(5)	O22–P2–Mo	107.2(4)
C1–Mo–N32	100.8(4)	N21–P2–Mo	130.8(5)
C1–Mo–P2	90.0(4)	C12–O11–P1	115.0(7)
C2–Mo–P1	82.5(4)	C22–O21–P2	115.8(9)
C2–Mo–N31	100.8(4)	C27–O22–P2	123.0(8)
C2–Mo–N32	172.7(4)	C11–N11–C13	118(1)
C2–Mo–P2	81.5(4)	C11–N11–P1	112.7(8)
P1–Mo–N31	100.1(3)	C13–N11–P1	128.5(8)
P1–Mo–N32	102.9(3)	C23–N21–C21	119(1)
P1–Mo–P2	163.9(1)	C23–N21–P2	129(1)
N31–Mo–N32	73.6(3)	C21–N21–P2	111(1)
N31–Mo–P2	81.5(3)	N11–C11–C12	105(1)
N32–Mo–P2	93.0(3)	O11–C12–C11	107(1)
O11–P1–N11	93.4(4)	C22–C21–N21	108(1)
O11–P1–Mo	118.8(3)	C21–C22–O21	109(1)
N11–P1–Mo	146.9(3)	O1–C1–Mo	178(1)
O21–P2–O22	103.4(5)	O2–C2–Mo	176(1)
O21–P2–N21	95.0(6)		

Table 6. Positional Parameters and Equivalent Isotropic Thermal Parameters (Å²) with Esd's in Parentheses for *trans*-2a·OTf

atom	*x*	*y*	*z*	*B*(eq)
Mo	0.13274(2)	−0.05071(3)	−0.27855(3)	2.76(1)
P1	0.11571(7)	−0.1403(1)	−0.4408(1)	3.30(3)
P2	0.13113(7)	0.07390(9)	−0.1238(1)	3.32(3)
O1	0.1161(3)	0.1290(3)	−0.4433(4)	6.5(2)
O2	−0.0303(2)	−0.0663(4)	−0.2905(4)	6.4(2)
O21	0.0616(2)	0.1407(3)	−0.1550(4)	5.0(1)
N11	0.0590(3)	−0.2269(4)	−0.4869(4)	4.5(1)
N12	0.1383(3)	−0.1233(4)	−0.5687(4)	4.7(1)
N21	0.1385(3)	0.0398(4)	0.0114(4)	5.5(2)
N22	0.1996(3)	0.1493(4)	−0.0942(4)	5.1(1)
N31	0.1625(2)	−0.1649(3)	−0.1416(3)	3.3(1)
N32	0.2503(2)	−0.0473(3)	−0.2299(3)	3.5(1)
C1	0.1222(3)	0.0616(4)	−0.3828(5)	4.0(1)
C2	0.0297(3)	−0.0598(4)	−0.2877(4)	4.1(1)
C11	0.0160(4)	−0.2814(6)	−0.4161(7)	6.0(2)
C12	0.0480(4)	−0.2444(6)	−0.6093(6)	6.0(2)
C13	0.0994(4)	−0.1806(6)	−0.6608(5)	5.6(2)
C14	0.1898(4)	−0.0547(6)	−0.5960(6)	6.1(2)
C21	0.0935(5)	−0.0344(6)	0.0538(7)	6.8(3)
C22	0.1897(5)	0.0909(7)	0.0916(6)	7.1(3)
C23	0.2305(6)	0.1560(7)	0.0241(8)	7.3(3)
C24	0.2214(6)	0.2160(7)	−0.1771(9)	8.2(3)
C25	0.0485(5)	0.2234(6)	−0.0852(9)	7.4(3)
C30	0.1171(3)	−0.2299(4)	−0.1048(5)	4.3(2)
C31	0.1353(4)	−0.2918(5)	−0.0144(6)	5.4(2)
C32	0.2024(4)	−0.2891(5)	0.0436(6)	5.7(2)
C33	0.2498(4)	−0.2259(5)	0.0068(5)	5.0(2)
C34	0.2293(3)	−0.1642(4)	−0.0866(4)	3.7(1)
C35	0.2780(3)	−0.0983(4)	−0.1362(4)	3.6(1)
C36	0.3499(3)	−0.0934(5)	−0.0938(6)	5.3(2)
C37	0.3938(3)	−0.0389(6)	−0.1505(7)	6.5(2)
C38	0.3661(3)	0.0110(6)	−0.2473(7)	6.3(2)
C39	0.2949(3)	0.0070(5)	−0.2830(6)	4.8(2)
S1	−0.1174	−0.4856	−0.2692	5.6(1)
S1′	−0.0930	−0.5127	−0.2447	6.0(1)
F1	−0.0328	−0.3647	−0.1440	14.2(3)
F2	−0.1120	−0.4326	−0.0572	12.9(3)
F3	−0.0156	−0.5204	−0.1070	16.3(8)
F3′	−0.1396	−0.3421	−0.2288	15.5(7)
O41	−0.1523	−0.5653	−0.2376	12.3(3)
O42	−0.0688	−0.4829	−0.3464	8.7(2)
O43	−0.1727	−0.4143	−0.3030	12.5(6)
O44	−0.0447	−0.5699	−0.1713	10.6(5)
C40	−0.0655	−0.4553	−0.1337	7.6(6)
C40′	−0.0972	−0.4019	−0.1716	8.5(7)

Scheme 3

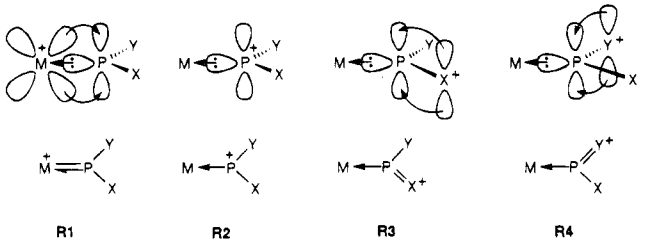

show significant delocalization into either the carbon–carbon double bond or the carbene center.[12] The reason for the stability of the carbene is ascribed to the high electron density on the nitrogen flanking the carbene center to repel nucleophiles that might otherwise react with the carbenic carbon.

Let us consider the role of amino groups in cationic phosphenium complexes. Studies on amino-substituted phosphorus compounds reveal that at least one nitrogen atom bonded to a phosphorus atom is sp^2-hybridized for trivalent tricoordinated (**D**),[13] trivalent tetracoordinated

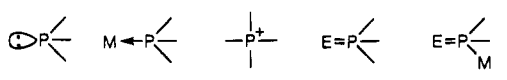

(**E**[14] and **F**),[15] and pentavalent tetracoordinated (**G**[16] and **H**)[17] phosphorus. Therefore, it can be said that a nitrogen on a phosphorus shows N → P π-donation (from a filled p orbital on N to an empty d or a σ^* orbital on P) to some extent irrespective of the valency and coordination number of the phosphorus atom or the existence of a bond between the phosphorus atom and a transition metal. If we say the π-donation is a "back-ground π-donation", there may be back-ground π-donation, in *trans*-**2a** and *trans*-**2j**, from N to phosphenium

(12) (a) Arduengo, A. J., III; Harlow, R. L.; Kline, M. *J. Am. Chem. Soc.* **1991**, *113*, 361. (b) Arduengo, J. A., III; Rasika Dias, H. V.; Dixson, D. A.; Harlow, R. L.; Klooster, W. T.; Koetzle, T. F. *J. Am. Chem. Soc.* **1994**, *116*, 6812 and references cited therein.

(13) (a) Morris, E. D., Jr.; Nordman, C. E. *Inorg. Chem.* **1969**, *8*, 1673. (b) Cowley, A. H.; Dewar, M. J. S.; Jackson, W. R.; Jennings, W. B. *J. Am. Chem. Soc.* **1970**, *92*, 1085. (c) Cowley, A. H.; Dewar, M. J. S.; Jackson, W. R.; Jennings, W. B. *J. Am. Chem. Soc.* **1970**, *92*, 5206. (d) Csizmadia, I. G.; Cowley, A. H.; Taylor, M. W.; Wolfe, S. *J. Chem. Soc., Chem. Commun.* **1974**, 432. (e) Rømming, C.; Songstad, J. *Acta Chem. Scand.* **1978**, *A32*, 689. (f) Cowley, A. H.; Mitchell, D. J.; Whangbo, M.-H.; Wolfe, S. *J. Am. Chem. Soc.* **1979**, *101*, 5224. (g) Rømming, C.; Songstad, J. *Acta Chem. Scand.* **1982**, *A36*, 665.

(14) Cowley, A. H.; Davis, R. E.; Remadna, K. *Inorg. Chem.* **1981**, *20*, 2146.

(15) (a) Rømming, C.; Songstad, J. *Acta Chem. Scand.* **1980**, *A34*, 631. (b) Nevstad, G. O.; Maartmann-Moe, K.; Rømming, C.; Songstad, J. *Acta Chem. Scand.* **1985**, *A39*, 523.

(16) (a) Rømming, C.; Songstad, J. *Acta Chem. Scand.* **1979**, *A33*, 187. (b) Rømming, C.; Iversen, A. J.; Songstad, J. *Acta Chem. Scand.* **1980**, *A34*, 333. (c) Maartmann-Moe, K.; Rømming, C.; Songstad, J. *Acta Chem. Scand.* **1982**, *A36*, 757. (d) Romming, C.; Maartmann-Moe, K.; Songstad, J. *Acta Chem. Scand.* **1984**, *A38*, 349. (e) Nevstad, G. O.; Rømming, C.; Songstad, J. *Acta Chem. Scand.* **1985**, *A39*, 691.

(17) (a) Nakazawa, H.; Kadoi, Y.; Mizuta, T.; Miyoshi, K.; Yoneda, H. *J. Organomet. Chem.* **1989**, *366*, 333. (b) Nakazawa, H.; Kadoi, Y.; Itoh, T.; Mizuta, T.; Miyoshi, K. *Organometallics* **1991**, *10*, 766.

Table 7. Positional Parameters and Equivalent Isotropic Thermal Parameters (Å²) with Esd's in Parentheses for *trans*-2j·OTf·CH_2Cl_2

atom	x	y	z	B(eq)
Mo	0.0271(1)	−0.2342(1)	0.09393(7)	2.62(4)
P1	0.1035(3)	−0.2602(3)	−0.0219(2)	3.2(1)
P2	−0.0947(3)	−0.2595(3)	0.2088(2)	3.8(1)
O1	−0.2094(9)	−0.1022(8)	0.0128(6)	6.4(4)
O2	−0.1539(8)	−0.4572(7)	0.0156(5)	5.4(3)
O11	0.0010(7)	−0.3034(7)	−0.1028(4)	4.0(3)
O21	−0.050(1)	−0.3769(8)	0.2479(6)	7.5(4)
O22	−0.2504(8)	−0.2902(9)	0.1704(5)	6.3(3)
N11	0.2348(9)	−0.2740(8)	−0.0662(5)	3.3(3)
N21	−0.090(1)	−0.177(1)	0.2942(7)	5.7(4)
N31	0.1885(8)	−0.3146(8)	0.1742(6)	3.0(3)
N32	0.1588(9)	−0.0807(8)	0.1636(6)	3.3(3)
C1	−0.115(1)	−0.152(1)	0.0443(7)	3.7(4)
C2	−0.083(1)	−0.375(1)	0.0467(7)	3.0(4)
C11	0.203(1)	−0.338(1)	−0.1472(8)	5.2(5)
C12	0.060(1)	−0.322(1)	−0.1741(8)	4.8(5)
C13	0.378(1)	−0.245(1)	−0.0307(7)	3.9(4)
C14	0.431(1)	−0.156(1)	−0.0826(9)	7.3(6)
C15	0.456(1)	−0.354(1)	−0.031(1)	8.6(7)
C16	0.391(1)	−0.178(1)	0.0528(9)	6.3(5)
C21	−0.040(2)	−0.246(2)	0.364(1)	10.5(9)
C22	−0.024(2)	−0.365(2)	0.333(1)	7.6(6)
C23	−0.121(2)	−0.050(1)	0.310(1)	6.0(6)
C24	0.006(2)	0.020(2)	0.347(1)	15(1)
C25	−0.172(2)	−0.002(2)	0.234(1)	11.7(9)
C26	−0.212(2)	−0.035(1)	0.366(1)	10.7(8)
C27	−0.344(1)	−0.325(1)	0.2152(9)	7.5(6)
C30	0.208(1)	−0.429(1)	0.1793(8)	4.1(4)
C31	0.298(1)	−0.474(1)	0.2362(9)	4.8(5)
C32	0.370(1)	−0.394(1)	0.2946(9)	5.3(5)
C33	0.358(1)	−0.272(1)	0.2932(8)	4.5(5)
C34	0.265(1)	−0.234(1)	0.2325(6)	3.1(4)
C35	0.251(1)	−0.111(1)	0.2239(8)	3.6(4)
C36	0.334(1)	−0.024(1)	0.2752(9)	4.7(5)
C37	0.326(1)	0.094(1)	0.2584(9)	5.2(5)
C38	0.237(2)	0.122(1)	0.1983(9)	5.1(5)
C39	0.152(1)	0.033(1)	0.1494(8)	4.4(4)
C40	0.434(1)	−0.181(2)	0.3506(9)	5.9(6)
C41	0.422(1)	−0.064(1)	0.3393(9)	5.5(5)
S	−0.3532(5)	0.3647(5)	0.3573(3)	6.0(2)
F1	−0.382(2)	0.378(1)	0.5029(7)	15.1(7)
F2	−0.195(1)	0.329(2)	0.482(1)	21(1)
F3	−0.358(1)	0.207(1)	0.4523(6)	12.9(6)
O31	−0.274(2)	0.297(2)	0.3191(9)	19.4(9)
O32	−0.483(1)	0.344(1)	0.3328(9)	13.2(6)
O33	−0.318(1)	0.485(1)	0.3695(6)	10.9(5)
C50	−0.310(3)	0.327(2)	0.452(2)	12(1)
Cl1	0.2899(5)	0.1956(5)	0.4696(3)	11.0(2)
Cl2	0.1130(8)	0.3533(6)	0.3972(5)	19.4(4)
C51	0.262(2)	0.341(1)	0.450(1)	11.3(9)

phosphorus as well as to phosphite phosphorus. However, from the X-ray structures of *trans*-**2a** and *trans*-**2j**, extra π-donation like in **R3** and **R4** may not exist. The P−N bond lengths observed in our system are obviously longer than those of $[P(N\text{-}i\text{-}Pr_2)_2][AlCl_4]$ (1.613 Å); transition-metal-free phosphenium has been proposed to involve extra π-donation.[18] The role of the amino groups on the phosphenium phosphorus may be, as is proposed for the imidazol-2-ylidene system, to protect the approach of a nucleophile to phosphenium phosphorus by high pπ lone pair density flanking the phosphenium center.

The substituents on the phosphenium phosphorus affect the M−P(phosphenium) double-bond character. For example, the Mo−P bond distances become shorter in the order 2.254 Å (*trans*-**2a**), 2.238 Å (*trans*-**2j**), and 2.229 Å ($[Mo\{(P(OMe)_3\}_5\{P(OMe)_2\}]^+$), which corresponds to the replacement of the substituent atoms on the phosphenium phosphorus from N to O. And the P−P coupling constants become greater on going from **2a** to **2f** and to **2h** for both the *cis* and *trans* isomers, *cis*-**2a** (42.7 Hz) → *cis*-**2f** (54.9 Hz) → *cis*-**2h** (58.0 Hz), and *trans*-**2a** (274.7 Hz) → *trans*-**2f** (326.6 Hz) → *trans*-**2h** (369.2 Hz). These tendencies indicate that an O-substituent rather than an N-substituent makes an M−P(phosphenium) double bond stronger. The reason may come from the greater electronegativity of O than that of N. That is, the σ-interaction, not π-interaction, between phosphenium phosphorus and its substituents (X and Y in Scheme 3) may affect the M−P double-bond character to some extent.

Experimental Section

General Remarks. All reactions were carried out under an atmosphere of dry nitrogen by using Schlenk tube techniques. All solvents were purified by distillation: toluene, p-xylene, and hexane were distilled from sodium metal, and CH_2Cl_2 and CH_3CN were distilled from P_2O_5. All solvents were stored under a nitrogen atmosphere. $BF_3{\cdot}OEt_2$ and TMS·OTf were distilled prior to use. Complexes **1a**,[6b,c] **1d**,[6c] **1e**,[6c] and **1i**,[6b] were prepared by the literature methods.

IR spectra (cm^{-1}) were recorded on a Shimadzu FTIR-8100 spectrometer. JEOL PMX-60, EX-270, and EX-400 instruments were used to obtain ^1H, ^{13}C, and ^{31}P NMR spectra. ^1H and ^{13}C NMR data were referenced to $(CH_3)_4Si$, and ^{31}P NMR data were referenced to 85% H_3PO_4.

Preparation of the 2a−e and 2i Complexes. A solution of the phosphenium complex (**1a**, **1d**, **1e**, **1i**) in CH_2Cl_2 (10 mL) was cooled to −78 °C, and an equimolar amount of the corresponding phosphite or phosphine was added. The solution was then allowed to warm to room temperature. The resulting solution was subjected to spectroscopic measurements. IR (ν_{CO}, in CH_2Cl_2): 1912, 1834 for **2a**; 1912, 1835 for **2b**; 1909, 1831 for **2c**; 1904, 1827 for **2d**, 1906, 1825 for **2e**; 1913, 1836 for **2i**.

Isolation of *trans*-2a. A solution of *fac*-[Mo(bpy)(CO)$_3${PN(Me)CH_2CH_2NMe(OMe)}] (210 mg, 0.43 mmol) in CH_2Cl_2 (10 mL) was cooled to −78 °C, and TMS·OTf (78 μL, 96 mg, 0.43 mmol) was added. After being warmed to room temperature, the solution was again cooled to −78 °C, and then PN(Me)CH_2CH_2NMe(OMe) (65 μL, 66 mg, 0.44 mmol) was added. After the solution was allowed to warm to room temperature, hexane (16 mL) was added. Keeping the solution in a refrigerator resulted in the formation of reddish orange crystals, which were collected by filtration, washed with hexane, and dried in vacuo to give *trans*-**2a**·OTf (214 mg, 0.30 mmol, 68%). Anal. Calcd for $C_{22}H_{31}F_3MoN_6O_6P_2S$: C, 36.58; H, 4.32; N, 11.63. Found: C, 36.12; H, 4.63; N, 11.68. IR (ν_{CO}, in CH_2Cl_2): 1912, 1834. ^{31}P NMR (δ, in CH_2Cl_2): 130.10 (d, J_{PP} = 274.7 Hz, PN(Me)CH_2CH_2NMe(OMe)), 242.16 (d, J_{PP} = 274.7 Hz, PN(Me)CH_2CH_2NMe). ^1H NMR (δ, in CD_2Cl_2): 2.32 (d, J = 11.7 Hz, 6H, PN(CH_3)CH_2CH_2N(CH_3)(OMe)), 2.82 (d, J = 11.7 Hz, 6H, PN(CH_3)CH_2CH_2N(CH_3)), 2.87 (m, 2H, PN(Me)CH_2CH_2NMe(OMe)), 3.10 (d, J = 10.7 Hz, 3H, OCH_3), 3.17 (m, 2H, PN(Me)CH_2CH_2NMe(OMe)), 3.53 (d, J = 6.4 Hz, 4H, PN(Me)CH_2CH_2NMe), 7.49−9.10 (m, 8H, bpy). ^{13}C NMR (δ,

(18) (a) Thomas, M. G.; Schultz, C. W.; Parry, R. W. *Inorg. Chem.* **1977**, *16*, 994. (b) Cowley, A. H.; Cushner, M. C.; Szobota, J. S. *J. Am. Chem. Soc.* **1978**, *100*, 7784. (c) Cowley, A. H.; Cushner, M. C.; Lattman, M.; Mckee, M. L.; Szobota, J. S.; Wilburn, J. C. *Pure Appl. Chem.* **1980**, *52*, 789. (d) Trinquler, G.; Marre, M.-R. *J. Phys. Chem.* **1983**, *87*, 1903.

in CD_2Cl_2): 32.50 (d, J = 12.8 Hz, $\overline{PN(CH_3)CH_2CH_2N(CH_3)(OMe)}$), 33.85 (d, J = 17.2 Hz, $\overline{PN(CH_3)CH_2CH_2N(CH_3)}$), 51.57 (d, J = 4.0 Hz, OCH_3), 52.64 (m, NCH_2), 123.62 (s, bpy), 125.78 (s, bpy), 139.18 (s, bpy), 153.38 (s, bpy), 155.30 (s, bpy), 224.39 (t, J = 18.2 Hz, CO).

Preparation of 1f and 2f. A solution of $Mo(bpy)(CO)_4$ (1000 mg, 2.75 mmol) and $\overline{PN(Me)CH_2CH_2O(OMe)}$ (0.48 mL, 520 mg, 3.86 mmol) in toluene (35 mL) was refluxed for 1 h. Standing the reaction mixture for 1 night at room temperature yielded a reddish purple powder, which was collected by filtration, washed with hexane, and then dried in vacuo to give *fac*-$[Mo(bpy)(CO)_3\{\overline{PN(Me)CH_2CH_2O(OMe)}\}]$ (730 mg, 1.55 mmol, 56%). Anal. Calcd for $C_{17}H_{18}MoN_3O_5P$: C, 43.33; H, 3.85; N, 8.92. Found: C, 43.24; H, 4.07; N, 8.94. IR (ν_{CO}, in CH_2Cl_2): 1924, 1827, 1794. ^{31}P NMR (δ, in CH_2Cl_2): 157.00 (s). ^1H NMR (δ, in acetone-d_6): 2.53 (d, J = 10.6 Hz, 3H, NCH_3), 2.72–3.50 (m, 2H, NCH_2), 3.21 (d, J = 10.4 Hz, 3H, OCH_3), 3.51–4.56 (m, 2H, OCH_2), 7.34–9.26 (m, 8H, bpy).

Procedures similar to those for **1a** and **2a** were applied to obtain **1f** from *fac*-$[Mo(bpy)(CO)_3\{\overline{PN(Me)CH_2CH_2O(OMe)}\}]$ and $BF_3{\cdot}OEt_2$, and to obtain **2f** from **1f** and $\overline{PN(Me)CH_2CH_2O(OMe)}$. IR ($\nu_{CO}$, in CH_2Cl_2): 1915, 1839 for **2f**.

Preparation of 3g and 2g. A solution of $Mo(bpy)(CO)_4$ (2014 mg, 5.53 mmol) in CH_3CN (120 mL) was refluxed for 5 h to give $Mo(bpy)(CO)_3(NCCH_3)$ (IR (ν_{CO}): 1909, 1789). The solvent was removed under reduced pressure. The residue was dissolved in THF (70 mL), and $\overline{PN(t\text{-}Bu)CH_2CH_2O(OMe)}$ (1.23 mL, 1280 mg, 7.21 mmol) was added to the solution. After being refluxed for 1 h, the solution was concentrated to ca. 30 mL. Addition of hexane (80 mL) resulted in the formation of a reddish purple powder, which was washed with hexane several times and dried in vacuo to give **3g** (2763 mg, 5.37 mmol, 97%). Anal. Calcd for $C_{20}H_{24}MoN_3O_5P$: C, 46.79; H, 4.68; N, 8.19. Found: C, 47.12; H, 4.72; N, 7.81. IR (ν_{CO}, in CH_2Cl_2): 1920, 1819, 1793. ^{31}P NMR (δ, in CH_2Cl_2): 149.24 (s). ^1H NMR (δ, in acetone-d_6): 1.17 (s, 9H, t-Bu), 2.82 (m, 1H, NCH_2), 3.18 (m, 1H, NCH_2), 3.21 (d, J = 10.7 Hz, 3H, OCH_3), 3.35 (m, 1H, OCH_2), 3.94 (m, 1H, OCH_2), 7.50–9.15 (m, 8H, bpy). ^{13}C NMR (δ, in CD_2Cl_2): 29.11 (d, J = 4.9 Hz, $NC(CH_3)_3$), 44.24 (s, $NC(CH_3)_3$), 50.02 (d, J = 8.5 Hz, OCH_3), 51.93 (d, J = 7.3 Hz, NCH_2), 66.97 (d, J = 9.8 Hz, OCH_2), 121.63 (s, bpy), 121.87 (s, bpy), 124.62 (s, bpy), 124.74 (s, bpy), 136.55 (s, bpy), 136.60 (s, bpy), 153.04 (s, bpy), 153.15 (s, bpy), 155.04 (s, bpy), 155.15 (s, bpy), 217.24 (d, J = 62.2 Hz, CO *trans* to P), 228.42 (d, J = 13.4 Hz, CO *cis* to P), 228.48 (d, J = 12.2 Hz, CO *cis* to P). Due to the chirality of the phosphorus atom, bpy carbons and two CO carbons *cis* to P are diastereotopically observed.

A solution of **3g** (307 mg, 0.60 mmol) and $\overline{PN(t\text{-}Bu)CH_2CH_2O(OMe)}$ (100 μL, 104 mg, 0.59 mmol) in CH_2Cl_2 (10 mL) was cooled to −78 °C, and TMS·OTf (110 μL, 135 mg, 0.61 mmol) was added. The solution was then allowed to warm to room temperature. Addition of hexane (5 mL) and toluene (8 mL) and cooling the solution resulted in the formation of reddish purple crystals, which was washed with hexane several times and dried in vacuo to give *trans*-**2g**·OTf·$2CH_2Cl_2$ (388 mg, 0.41 mmol, 68%). Anal. Calcd for $C_{28}H_{41}Cl_4F_3MoN_4O_8P_2S$: C, 35.39; H, 4.35; N, 5.90. Found: C, 35.02; H, 4.44; N, 6.41. IR (ν_{CO}, in CH_2Cl_2): 1932, 1853. ^{31}P NMR (δ, in CH_2Cl_2): 139.89 (d, J_{PP} = 320.5 Hz, $\overline{PN(t\text{-}Bu)CH_2CH_2O(OMe)}$), 227.52 (d, J_{PP} = 320.5 Hz, $\overline{PN(t\text{-}Bu)CH_2CH_2O}$). ^1H NMR (δ, in CD_2Cl_2): 1.15 (s, 9H, $\overline{PN\{C(CH_3)_3\}CH_2CH_2O(OMe)}$), 1.19 (s, 9H, $\overline{PN\{C(CH_3)_3\}CH_2CH_2O}$), 2.89 (m, 1H, $\overline{PN(t\text{-}Bu)CH_2CH_2O(OMe)}$), 3.21 (d, J = 11.2 Hz, 3H, $POCH_3$), 3.23 (m, 1H, $\overline{PN(t\text{-}Bu)CH_2CH_2O(OMe)}$), 3.62 (m, 1H, $\overline{PN(t\text{-}Bu)CH_2CH_2O(OMe)}$), 3.66 (quart, J = 7.3 Hz, 2H, $\overline{PN(t\text{-}Bu)CH_2CH_2O}$), 4.06 (m, 1H, $\overline{PN(t\text{-}Bu)CH_2CH_2O(OMe)}$), 4.41 (tdd, J = 7.3, 7.3, 2.3 Hz, 2H, $\overline{PN(t\text{-}Bu)CH_2CH_2O}$), 7.47–8.97 (m, 8H, bpy). ^{13}C NMR (δ, in CD_2Cl_2): 28.56 (d, J = 3.7 Hz, $\overline{PN\{C(CH_3)_3\}CH_2CH_2O(OMe)}$), 29.63 (d, J = 4.9 Hz, $\overline{PN\{C(CH_3)_3\}CH_2CH_2O}$), 43.95 (s, $\overline{PN\{C(CH_3)_3\}CH_2CH_2O(OMe)}$), 46.77 (s, $\overline{PN\{C(CH_3)_3\}CH_2CH_2O}$), 50.30 (d, J = 12.2 Hz, OCH_3), 52.04 (d, J = 7.4 Hz, $\overline{PN\{C(CH_3)_3\}CH_2CH_2O(OMe)}$), 55.93 (d, J = 6.1 Hz, $\overline{PN\{C(CH_3)_3\}CH_2CH_2O}$), 67.04 (d, J = 9.8 Hz, $\overline{PN\{C(CH_3)_3\}CH_2CH_2O(OMe)}$), 68.04 (d, J = 8.5 Hz, $\overline{PN\{C(CH_3)_3\}CH_2CH_2O}$), 123.27 (s, bpy), 123.47 (s, bpy), 125.37 (s, bpy), 125.50 (s, bpy), 139.21 (s, bpy), 153.04 (s, bpy), 153.12 (s, bpy), 154.72 (s, bpy), 154.86 (s, bpy), 223.63 (t, J = 18.3 Hz, CO), 223.97 (t, J = 18.3 Hz, CO). Due to the chirality of the phosphorus atom, bpy carbons (a resonance at 139.21 ppm is not separated cleanly) and two CO carbons are diastereotopically observed.

Preparation of 4h and 2h. A solution of $Mo(bpy)(CO)_4$ (2103 mg, 5.78 mmol) and $\overline{POCMe_2CMe_2O(OMe)}$ (2.95 mL, 3080 mg, 17.30 mmol) in p-xylene (120 mL) was refluxed for 14.5 h. After the solvent was removed under reduced pressure, the residue was washed with hexane several times to give **4h** as a bluish purple powder (2104 mg, 3.17 mmol, 55%). Anal. Calcd for $C_{26}H_{38}MoN_2O_8P_2$: C, 47.00; H, 5.76; N, 4.22. Found: C, 47.10; H, 5.82; N, 4.08. IR (ν_{CO}, in CH_2Cl_2): 1842, 1761. ^{31}P NMR (δ, in CH_2Cl_2): 176.11 (s). ^1H NMR (δ, in acetone-d_6): 0.68 (s, 12H, CH_3), 1.17 (s, 12H, CH_3), 3.54 (t, J = 5.7 Hz, 6H, OCH_3), 7.39–9.15 (m, 8H, bpy). ^{13}C NMR (δ, in acetone-d_6): 25.48 (s, $C(CH_3)_2$), 25.70 (s, $C(CH_3)_2$), 51.32 (s, OCH_3), 84.73 (t, J = 3.7 Hz, $C(CH_3)_2$), 122.68 (s, bpy), 124.85 (s, bpy), 135.94 (s, bpy), 153.04 (s, bpy), 155.65 (s, bpy), 231.12 (t, J = 15.3 Hz, CO).

A solution of **4h** (261 mg, 0.39 mmol) in CH_2Cl_2 (10 mL) was cooled to −78 °C, and TMS·OTf (70 μL, 86 mg, 0.39 mmol) was added; then the solution was allowed to warm to room temperature. The resulting solution was subjected to IR and ^{31}P NMR measurements, showing the formation of *trans*-**2h**. IR (ν_{CO}, in CH_2Cl_2): 1958, 1887.

Preparation of 3j and 2j. A solution of $Mo(phen)(CO)_4$ (1384 mg, 3.57 mmol) in CH_3CN (100 mL) was refluxed for 4 h to give $Mo(phen)(CO)_3(NCCH_3)$ (IR (ν_{CO}): 1909, 1789 cm^{-1}). The solvent was removed under reduced pressure. The residue was dissolved in THF (70 mL), and $\overline{PN(t\text{-}Bu)CH_2CH_2O(OMe)}$ (760 μL, 790 mg, 4.46 mmol) was added to the solution. After being refluxed for 1 h, the solution was concentrated to ca. 35 mL. Addition of hexane (100 mL) resulted in the formation of a reddish purple powder, which was washed with hexane several times and dried in vacuo to give **3j** (1824 mg, 3.39 mmol, 95%). Anal. Calcd for $C_{22}H_{24}MoN_3O_5P$: C, 49.17; H, 4.50; N, 7.82. Found: C, 49.24; H, 4.36; N, 7.75. IR (ν_{CO}, in CH_2Cl_2): 1920, 1820, 1793. ^{31}P NMR (δ, in CH_2Cl_2): 149.46 (s). ^1H NMR (δ, in acetone-d_6): 1.02 (s, 9H, t-Bu), 2.58 (m, 2H, NCH_2), 3.10 (d, J = 10.3 Hz, 3H, OCH_3), 3.88 (m, 2H, OCH_2), 7.88–9.52 (m, 8H, phen). ^{13}C NMR (δ, in CD_2Cl_2): 29.02 (d, J = 4.9 Hz, $NC(CH_3)_3$), 44.19 (s, $NC(CH_3)_3$), 50.50 (d, J = 8.6 Hz, OCH_3), 51.84 (d, J = 7.3 Hz, NCH_2), 66.94 (d, J = 9.7 Hz, OCH_2), 123.95 (s, phen), 124.10 (s, phen), 127.06 (s, phen), 127.13 (s, phen), 129.88 (s, phen), 130.04 (s, phen), 135.60 (s, phen), 146.65 (s, phen), 146.70 (s, phen), 152.75 (d, J = 2.4 Hz, phen), 152.90 (d, J = 2.4 Hz, phen), 217.26 (d, J = 62.3 Hz, CO *trans* to P), 228.36 (d, J = 13.4 Hz, CO *cis* to P), 228.47 (d, J = 13.5 Hz, CO *cis* to P). Due to the chirality of the phosphorus atom, phen carbons (a resonance at 135.60 ppm is not separated cleanly) and two CO carbons *cis* to P are diastereotopically observed.

A solution of **3j** (178 mg, 0.33 mmol) and PN(t-Bu)CH_2CH_2O(OMe) (56 μL, 58 mg, 0.33 mmol) in CH_2Cl_2 (10 mL) was cooled to −78 °C, and TMS·OTf (60 μL, 74 mg, 0.33 mmol) was added. After the solution was allowed to warm to room temperature, hexane (16 mL) was added. Keeping the solution in a refrigerator resulted in the formation of reddish orange crystals, which were collected by filtration, washed with hexane, and dried in vacuo to give *trans*-**2j**·OTf·CH_2Cl_2 (251 mg, 0.28 mmol, 86%). Anal. Calcd for $C_{29}H_{39}Cl_2F_3MoN_4O_8P_2S$: C, 39.16; H, 4.42; N, 6.30. Found: C, 39.20; H, 4.28; N, 6.76. IR (ν_{CO}, in CH_2Cl_2): 1933, 1855. ^{31}P NMR (δ, in CH_2Cl_2): 140.41 (d, J_{PP} = 317.4 Hz, PN(t-Bu)CH_2CH_2O(OMe)), 228.10 (d, J_{PP} = 317.4 Hz, PN(t-Bu)CH_2CH_2O). ^1H NMR (δ, in CD_2Cl_2): 1.00 (s, 9H, PN{C(CH_3)$_3$}CH_2CH_2O(OMe)), 1.12 (s, 9H, PN{C(CH_3)$_3$}CH_2CH_2O), 2.65 (m, 1H, PN(t-Bu)CH_2CH_2O(OMe)), 3.09 (d, J = 11.2 Hz, 3H, OCH_3), 3.12 (m, 1H, PN(t-Bu)CH_2CH_2O(OMe)), 3.50 (m, 1H, PN(t-Bu)CH_2CH_2O(OMe)), 3.66 (quart, J = 7.3 Hz, 2H, PN(t-Bu)CH_2CH_2O), 3.98 (m, 1H, PN(t-Bu)CH_2CH_2O(OMe)), 4.42 (quint, J = 7.1 Hz, 2H, PN(t-Bu)CH_2CH_2O), 7.87−9.35 (m, 8H, phen). ^{13}C NMR (δ, in CD_2Cl_2): 28.18 (s, PN{C(CH_3)$_3$}CH_2CH_2O(OMe)), 29.39 (s, PN{C(CH_3)$_3$}CH_2CH_2O), 43.63 (s, PN{C(CH_3)$_3$}CH_2CH_2O(OMe)), 46.58 (s, PN{C(CH_3)$_3$}CH_2CH_2O), 50.12 (d, J = 12.2 Hz, OCH_3), 51.62 (d, J = 6.1 Hz, PN{CCH_3)$_3$}CH_2CH_2O(OMe)), 55.67 (d, J = 4.9 Hz, PN{C(CH_3)$_3$}CH_2CH_2O), 66.83 (d, J = 9.8 Hz, PN{C(CH_3)$_3$}CH_2CH_2O(OMe)), 67.99 (d, J = 8.5 Hz, PN{C(CH_3)$_3$}CH_2CH_2O), 124.33 (s, phen), 124.51 (s, phen), 127.15 (s, phen), 127.24 (s, phen), 129.79 (s, phen), 130.03 (s, phen), 138.09 (s, phen), 145.23 (s, phen), 145.42 (s, phen), 153.13 (s, phen), 223.46 (t, J = 22.0 Hz, CO), 223.79 (t, J = 22.0 Hz, CO). Due to the chirality of the phosphorus atom, phen carbons (two resonances at 138.09 and 153.13 ppm are not separated cleanly) and two CO carbons are diastereotopically observed.

X-ray Structure Determination for *trans*-2a·OTf and *trans*-2j·OTf·CH_2Cl_2. Single crystals of *trans*-**2a**·OTf and *trans*-**2j**·OTf·CH_2Cl_2 were individually sealed under N_2 in a thin-walled glass capillary, mounted on a Mac Science MXC3 diffractometer, and irradiated with graphite-monochromated Mo Kα radiation (λ = 0.710 73 Å). Unit-cell dimensions were obtained by least squares from the angular setting of 30 accurately centered reflections with 10° < 2θ < 25°. Reflection intensities were collected in the usual manner at 25 °C, and three check reflections measured after every 100 reflections showed no decrease in intensity. $P2_1/n$ and $P\bar{1}$ were selected as space groups for *trans*-**2a**·OTf and *trans*-**2j**·OTf·CH_2Cl_2, respectively, which led to successful refinements.

The structures were solved by direct methods with the program Monte Carlo-Multan.[19] For *trans*-**2a**·OTf, the OTf was disordered in very close positions. Even if the OTf was located in the two positions in a certain probability, they were fused after refinement. Therefore, the OTf was fixed in the two positions estimated from difference Fourier maps with a respective weight of 0.5. The positions of hydrogen atoms for *trans*-**2a**·OTf were determined from subsequent difference Fourier maps, and those for *trans*-**2j**·OTf·CH_2Cl_2 were calculated by assuming idealized geometries. Absorption and extinction corrections were then applied,[20,21] and several cycles of a full-matrix least-squares refinement with anisotropic temperature factors for non-hydrogen atoms led to final R_w values of 0.059 and 0.062 for *trans*-**2a**·OTf and *trans*-**2j**·OTf·CH_2Cl_2, respectively. All calculations were performed on a Titan 750 computer using the program system Crystan-G.[19]

Acknowledgment. This work was supported by the Grant-in-Aid for Scientific Research on Priority Area of Reactive Organometallics No. 06227250 from the Ministry of Education, Science, and Culture of Japan.

Supporting Information Available: Additional structural data for complexes *trans*-**2a**·OTf and *trans*-**2j**·OTf·CH_2Cl_2, including tables of thermal parameters and distances and angles (7 pages). Ordering information is given on any current masthead page.

OM950287M

(19) Furusaki, A. *Acta Crystallogr., Sect. A* **1979**, *A35*, 220.
(20) Katayama, C. *Acta Crystallogr., Sect. A* **1986**, *A42*, 19.
(21) Coppens, P.; Hamilton, W. C. *Acta Crystallogr., Sect. A* **1970**, *A26*, 71.

Models for Bimetallic Catalysis: Selectivity in Ligand Addition to a Coordinatively Unsaturated Pt_3Re Cluster Cation

Jianliang Xiao, Leijun Hao, and Richard J. Puddephatt*

Department of Chemistry, University of Western Ontario, London, Canada N6A 5B7

Ljubica Manojlović-Muir,* Kenneth W. Muir, and Ali Ashgar Torabi

Department of Chemistry, University of Glasgow, Glasgow, Scotland G12 8QQ

Received April 19, 1995[⊗]

The coordinatively unsaturated, 54-electron Pt_3Re cluster cation $[Pt_3\{Re(CO)_3\}(\mu\text{-dppm})_3]^+$, **2**, dppm = $Ph_2PCH_2PPh_2$, reacts with ligands L = $P(OR)_3$, CO, RNC, RSH or RC≡CH to give the 56-electron cluster cations $[Pt_3\{Re(CO)_3L\}(\mu\text{-dppm})_3]^+$ by selective addition to the rhenium center, in contrast to the known addition of these ligands to the Pt_3 center in $[Pt_3(\mu_3\text{-}CO)(\mu\text{-dppm})_3]^{2+}$. The reaction with CO is easily reversible. The complex with L = $P(OPh)_3$ has been characterized by an X-ray structure determination {$[Pt_3\{Re(CO)_3L\}(\mu\text{-dppm})_3]$-$[PF_6]$·EtOH; triclinic, $P\bar{1}$, a = 13.993(1) Å, b = 17.868(1) Å, c = 19.753(2) Å, α = 88.198(7)°, β = 87.766(7)°, γ = 72.394(4)°, V = 4702.9(7) Å^3, Z = 2, R = 0.0405, R_w = 0.0429 for 14 765 unique reflections with $I > 3\sigma(I)$}. The structure contains a distorted tetrahedral Pt_3Re core with the Pt_3 triangle edge-bridged by three μ-dppm ligands, the two PtRe edges weakly semibridged by CO ligands, and the phosphite ligand bound to rhenium [Pt–Pt = 2.603(1)–2.677(1) Å, Pt–Re = 2.762(1)–2.942(1) Å]. NMR studies indicate that several of the adducts are fluxional, by rotation of the $Re(CO)_3L$ fragment about the Pt_3 triangle, such that they appear to have C_3 symmetry. Phosphite ligands displace CO or HCCH from $[Pt_3\{Re(CO)_4\}(\mu\text{-dppm})_3]^+$ or $[Pt_3\{Re(CO)_3(HCCH)\}(\mu\text{-dppm})_3]^+$, respectively, to give $[Pt_3\{Re(CO)_3P(OR)_3\}(\mu\text{-dppm})_3]^+$. The clusters are considered to be formed by donation of electron pairs from the Pt–Pt bonding orbitals of a $Pt_3(\mu\text{-dppm})_3$ fragment to acceptor orbitals of the $Re(CO)_3$ or $Re(CO)_3L$ unit; Pt–Re bonding is therefore weaker in the 56-electron clusters. An analogy is noted between the donor orbitals of the $Pt_3(\mu\text{-dppm})_3$ fragment and of $C_5H_5^-$, which is useful in interpreting the chemistry. The observation of selective reactivity at rhenium is relevant to the mode of action of heterogeneous Pt/Re catalysts.

Introduction

Heteronuclear transition metal cluster complexes have fascinating properties and are of particular interest as models for heterogeneous bimetallic alloy catalysts.[1,2] One of the most important of such catalysts is the $Pt/Re/Al_2O_3$ system used in catalytic reforming of petroleum.[3] As a result of this interest, several binuclear and cluster complexes containing Pt–Re bonds have been synthesized and structurally characterized and can serve as models for the metal–metal-bonded units which may be present in the bimetallic catalysts.[4] However, there have been few studies of the chemical reactivity of Pt–Re-bonded complexes.[1,4,5] In order to model the reactivity of a bimetallic catalyst compared to a simple platinum catalyst, it would be useful to study the reactivity of a coordinatively unsaturated Pt–Re cluster compared to a simple Pt cluster. This is now possible with clusters based on the $Pt_3(\mu\text{-dppm})_3$ triangle, dppm = $Ph_2PCH_2PPh_2$, since both cluster cations $[Pt_3(\mu_3\text{-}CO)(\mu\text{-dppm})_3]^{2+}$, **1**,[6] and $[Pt_3\{\mu_3\text{-}Re(CO)_3\}(\mu\text{-dppm})_3]^+$, **2**,[5] are now known. The complex cations **1** and **2** have 42- and 54-electron configurations, respec-

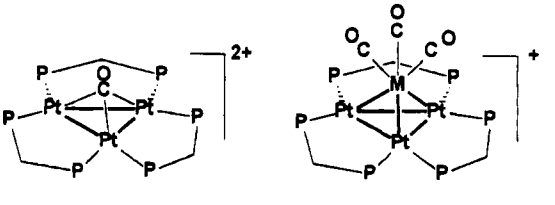

1 **2, M = Re; 3, M = Mn**

[⊗] Abstract published in *Advance ACS Abstracts,* August 1, 1995.

(1) (a) Adams, R. D.; Wu, W. *Organometallics* **1993**, *12*, 1238; 1248. (b) Churchill, M. R.; Lake, C. H.; Safarowic, F. J.; Parfitt, D. S.; Nevinger, L. R.; Keister, J. B. *Organometallics* **1993**, *12*, 671. (c) Song, L. C.; Shen, J. Y.; Hu, Q. M.; Wang, R. J.; Wang, H. G. *Organometallics* **1993**, *12*, 408. (d) Adams, R. D.; Li, Z.; Swepston, P.; Wu, W.; Yamamoto, J. *J. Am. Chem. Soc.* **1992**, *114*, 10657. (e) Farrugia, L. J. *Adv. Organomet. Chem.* **1990**, *31*, 301.

(2) Adams, R. D.; Herrmann, W. A. *Polyhedron* **1988**, *7*, 2255–2464.

(3) Biswas, J.; Bickle, G. M.; Gray, P. G.; Do, D. D.; Barbier, J. *Catal. Rev. Sci. Eng.* **1988**, *30*, 161.

(4) (a) Xiao, J.; Vittal, J. J.; Puddephatt, R. J. *J. Chem. Soc., Chem. Commun.* **1993**, 167. (b) Beringhelli, T.; Ceriotti, A.; Ciani, G.; D'Alfonso, G.; Garlaschelli, L.; Pergola, R. D.; Moret, M.; Sironi, A. *J. Chem. Soc., Dalton Trans.* **1993**, 199. (c) Antognazza, P.; Beringhelli, T.; D'Alfonso, G.; Minoja, A.; Ciani, G.; Moret, M.; Sironi,A. *Organometallics* **1992**, *11*, 1777. (d) Powell, J.; Brewer, J. C.; Gulia, G.; Sawyer, J. F. *J. Chem. Soc., Dalton Trans.* **1992**, 2503. (e) Beringhelli, T.; D'Alfonso, G.; Minoja, A. P. *Organometallics* **1991**, *10*, 394. (f) Ciani, G.; Moret, M.; Sironi, A.; Antognazza, P.; Beringhelli, T.; D'Alfonso, G.; Pergola, R. D.; Minoja, A. *J. Chem. Soc., Chem. Commun.* **1991**, 1255. (g) Ciani, G.; Moret, M.; Sironi, A.; Beringhelli, T.; D'Alfonso, G.; Pergola, R. D. *J. Chem. Soc., Chem. Commun.* **1990**, 1668. (h) Beringhelli, T.; Ceriotti, A.; D'Alfonso, G.; Pergola, R. D. *Organometallics* **1990**, *9*, 1053. (i) Carr, S. W.; Fontaine, X. L. R.; Shaw, B. L.; Thornton-Pett, M. *J. Chem. Soc., Dalton Trans.* **1988**, 769.

0276-7333/95/2314-4183$09.00/0

tively, and so each is coordinatively unsaturated (the common electron counts for trinuclear and tetranuclear clusters are 48 and 60, respectively).[7] In heteronuclear clusters containing platinum, the coordinative unsaturation is normally localized at the platinum, which commonly has a 16-electron configuration in mononuclear, binuclear, and cluster complexes.[7] Of course, the complex cation **1** can only react at platinum, but previous work on mixed platinum/main group metal clusters, such as those containing $Pt_3(\mu_3\text{-}SnX_3)$ or $Pt_3(\mu_3\text{-}Hg)$ units, has shown that ligands add selectively to platinum as expected, sometimes with displacement of the main group metal.[8,9] It is therefore particularly interesting that neutral donor ligands react with complex **2** at rhenium and not at one or more of the platinum centers,[10] while anionic ligands such as I^- add to the Pt_3 triangle.[11] This article reports details of the neutral ligand addition reactions to **2** and, to a lesser extent, to the corresponding manganese cluster $[Pt_3\{\mu_3\text{-}Mn(CO)_3\}(\mu\text{-dppm})_3]^+$, **3**, using the reagents CO, RNC, $P(OR)_3$, RSH, and RC≡CH. Previous communications have reported the synthesis of **2** and **3** and the unique reactions of **2** with oxygen and sulfur donors.[5]

Results

It will be seen that the ligand addition reactions are much better defined with the rhenium cluster **2** than with the manganese analog **3**. The reactions with phosphite ligands, carbon monoxide, and alkynes will be described in that order.

Reactions with Phosphite Ligands. Phosphite ligands reacted rapidly with cluster **2** to give the adducts $[Pt_3\{Re(CO)_3L\}(\mu\text{-dppm})_3]^+$, [**4**, L = $P(OMe)_3$; **5**, L = $P(OPh)_3$] according to eq 1. These complexes, as the

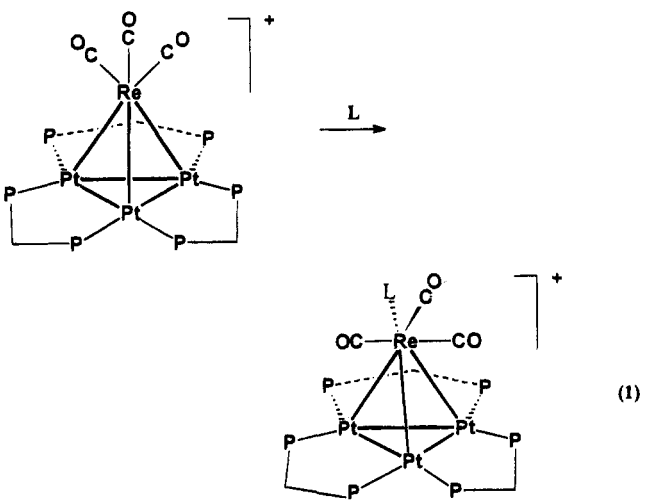

(1)

4, L = $P(OMe)_3$ **10**, L = XyNC
5, L = $P(OPh)_3$ **11**, L = EtSH
6, L = CO **12**, L = *t*-BuSH
7, L = MeNC **13**, L = 3-MeC_6H_4SH
8, L = *t*-BuNC **14**, L = HCCH
9, L = CyNC **15**, L = PhCCH

$[PF_6]^-$ salts, are dark brown solids; they are stable to air at room temperature, and they do not easily undergo ligand dissociation of either a carbonyl or the phosphite ligand. It is important to note that **1** reacts with these ligands in a completely different way, namely by addition to platinum as shown in eq 2.[8,12]

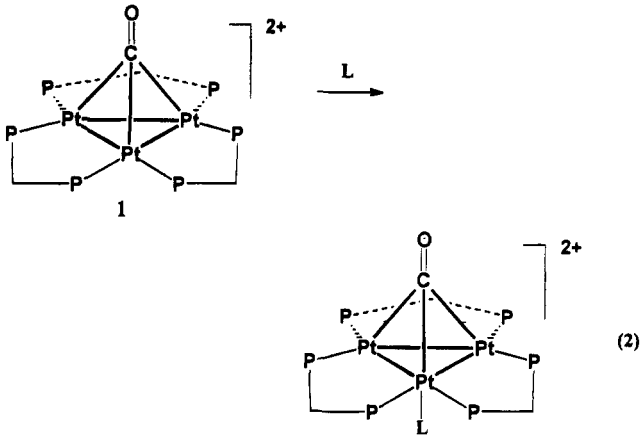

1

(2)

Complex **5** was characterized by an X-ray structure analysis of **5**$[PF_6]$·EtOH. Selected bond lengths and angles are listed in Table 1. The molecular structure of **5**, presented in Figure 1, shows that addition of the phosphite ligand to **2** occurs selectively at the rhenium center.

The structure is built of $Re(CO)_3\{P(OPh)_3\}^+$ and $Pt_3(\mu\text{-dppm})_3$ fragments. The Pt_3 triangle is capped by the $Re(CO)_3\{P(OPh)_3\}^+$ fragment to form a distorted tetrahedral Pt_3Re cluster with two edges, Pt(1)–Re and Pt(2)–Re, weakly semibridged by carbonyl ligands [Re–C = 1.969(9), 1.998(9) Å; Pt–C = 2.428(9), 2.550(9) Å; Re–C–O = 171.4(8), 170.6(8)°]. The $Pt_3Re(CO)_3(PO_3)(\mu\text{-PCP})_3$ core approximates C_s symmetry (Figure 2), with the mirror plane passing through the Pt(3), Re, P(7), C(1), and C(4) atoms and bisecting the Pt(1)–Pt(2) bond. Distorted octahedral geometry about the Re atom in the $Re(CO)_3\{P(OPh)_3\}^+$ unit, evident from the bond angles shown in Table 1, is completed by the Pt(3) atom and the midpoint of the Pt(1)–Pt(2) bond.

In **5**, the Pt–Pt bonds show small variations [2.603(1), 2.635(1), 2.677(1) Å]. Variations in the Pt–Re distances are larger [2.762(1), 2.825(1), 2.942(1) Å], but all three distances lie within the accepted range of 2.65–3.00 Å.[4,5,10,11] The average Pt–Pt (2.60 Å in **2**, 2.64 Å in **5**) and Pt–Re (2.67 Å in **2**, 2.84 Å in **5**) distances indicate that the phosphite addition occurs at the expense of metal–metal bonding, with the Pt–Re bonds weakened more than the Pt–Pt bonds.

(5) (a) Xiao, J.; Vittal, J. J.; Puddephatt, R. J.; Manojlović-Muir, Lj.; Muir, K. W. *J. Am. Chem. Soc.* **1993**, *115*, 7882. (b) Hao, L.; Xiao, J.; Vittal, J. J.; Puddephatt, R. J. *J. Chem. Soc., Chem. Commun.* **1994**, 2183.

(6) Ferguson, G.; Lloyd, B. R.; Puddephatt, R. J. *Organometallics* **1986**, *5*, 344.

(7) Mingos, D. M. P.; May, A. S. In *The Chemistry of Metal Cluster Complexes*: Shriver, D. F., Kaesz, H. D., Adams, R. D., Eds.; VCH: New York, 1990. The most common electron count for tetrahedral clusters is 60, such as in $[Ir_4(CO)_{12}]$.

(8) Puddephatt, R. J.; Manojlović-Muir, Lj.; Muir, K. W. *Polyhedron* **1990**, *9*, 2767.

(9) (a) Jennings, M. C.; Schoettel, G.; Roy, S.; Puddephatt, R. J.; Douglas, G.; Manojlović-Muir, Lj.; Muir, K. W. *Organometallics* **1991**, *10*, 580. (b) Schoettel, G.; Vittal, J. J.; Puddephatt, R. J. *J. Am. Chem. Soc.* **1990**, *112*, 6400. (c) Payne, N. C.; Ramachandran, R.; Schoettel, G.; Vittal, J. J.; Puddephatt, R. J. *Inorg. Chem.* **1991**, *30*, 4048.

(10) Xiao, J.; Hao, L.; Puddephatt, R. J.; Manojlović-Muir, Lj.; Muir, K. W.; Torabi, A. A. *J. Chem. Soc., Chem. Commun.* **1994**, 2221.

(11) Xiao, J.; Hao, L.; Puddephatt, R. J.; Manojlović-Muir, Lj.; Muir, K. W.; Torabi, A. A. *Organometallics*, **1995**, *14*, 2194.

(12) (a) Bradford, A. M.; Douglas, G.; Manojlović-Muir, Lj.; Muir, K. W.; Puddephatt, R. J. *Organometallics* **1990**, *9*, 409. (b) Bradford, A. M.; Kristof, E.; Rashidi, M.; Yang, D.-S.; Payne, N. C.; Puddephatt, R. J. *Inorg. Chem.* **1994**, *33*, 2355. (c) Jennings, M. C.; Payne, N. C.; Puddephatt, R. J. *Inorg. Chem.* **1987**, *26*, 3776.

Table 1. Selected Interatomic Distances (Å) and Angles (deg)

Pt(1)–Pt(2)	2.677(1)	Pt(1)–Pt(3)	2.635(1)	P(1)–C(1)	1.851(8)	P(2)–C(1)	1.863(8)
Pt(1)–Re	2.825(1)	Pt(1)–P(2)	2.298(2)	P(3)–C(2)	1.869(8)	P(4)–C(2)	1.840(8)
Pt(1)–P(5)	2.253(3)	Pt(1)–C(6)	2.550(9)	P(5)–C(3)	1.858(9)	P(6)–C(3)	1.846(8)
Pt(2)–Pt(3)	2.603(1)	Pt(2)–Re	2.762(1)	P(7)–O(1)	1.598(6)	P(7)–O(2)	1.623(6)
Pt(2)–P(1)	2.268(3)	Pt(2)–P(4)	2.289(3)	P(7)–O(3)	1.625(6)	O(1)–C(G1)	1.410(11)
Pt(2)–C(5)	2.428(9)	Pt(3)–Re	2.942(1)	O(2)–C(H1)	1.373(10)	O(3)–C(I1)	1.388(9)
Pt(3)–P(3)	2.307(2)	Pt(3)–P(6)	2.281(3)	O(4)–C(4)	1.149(12)	O(5)–C(5)	1.150(11)
Re–P(7)	2.255(3)	Re–C(4)	1.885(10)	O(6)–C(6)	1.147(11)		
Re–C(5)	1.998(9)	Re–C(6)	1.969(9)				
Pt(2)–Pt(1)–Pt(3)	58.7(1)	Pt(2)–Pt(1)–Re	60.2(1)	C(4)–Re–C(5)	90.5(4)	C(4)–Re–C(6)	89.9(4)
Pt(2)–Pt(1)–P(2)	96.6(1)	Pt(2)–Pt(1)–P(5)	142.0(1)	C(5)–Re–C(6)	175.5(4)	Pt(2)–P(1)–C(1)	111.1(3)
Pt(2)–Pt(1)–C(6)	102.7(2)	Pt(3)–Pt(1)–Re	65.1(1)	Pt(2)–P(1)–C(E1)	111.7(4)	Pt(2)–P(1)–C(F1)	121.0(3)
Pt(3)–Pt(1)–P(2)	155.1(1)	Pt(3)–Pt(1)–P(5)	91.9(1)	C(1)–P(1)–C(E1)	106.7(5)	C(1)–P(1)–C(F1)	98.2(5)
Pt(3)–Pt(1)–C(6)	88.1(2)	Re–Pt(1)–P(2)	107.3(1)	C(E1)–P(1)–C(F1)	106.6(5)	Pt(1)–P(2)–C(1)	108.8(3)
Re–Pt(1)–P(5)	132.2(1)	Re–Pt(1)–C(6)	42.6(2)	Pt(1)–P(2)–C(C1)	122.2(3)	Pt(1)–P(2)–C(D1)	115.7(3)
P(2)–Pt(1)–P(5)	108.6(1)	P(2)–Pt(1)–C(6)	101.8(3)	C(1)–P(2)–C(C1)	101.9(4)	C(1)–P(2)–C(D1)	103.2(4)
P(5)–Pt(1)–C(6)	99.4(3)	Pt(1)–Pt(2)–Pt(3)	59.8(1)	C(C1)–P(2)–C(D1)	102.8(5)	Pt(3)–P(3)–C(2)	113.5(3)
Pt(1)–Pt(2)–Re	62.6(1)	Pt(1)–Pt(2)–P(1)	93.5(1)	Pt(3)–P(3)–C(K1)	118.1(4)	Pt(3)–P(3)–C(M1)	115.9(3)
Pt(1)–Pt(2)–P(4)	139.0(1)	Pt(1)–Pt(2)–C(5)	107.0(3)	C(2)–P(3)–C(K1)	104.5(5)	C(2)–P(3)–C(M1)	101.2(4)
Pt(3)–Pt(2)–Re	66.4(1)	Pt(3)–Pt(2)–P(1)	152.3(1)	C(K1)–P(3)–C(M1)	101.4(4)	Pt(2)–P(4)–C(2)	109.1(3)
Pt(3)–Pt(2)–P(4)	92.0(1)	Pt(3)–Pt(2)–C(5)	83.6(3)	Pt(2)–P(4)–C(J1)	115.6(4)	Pt(2)–P(4)–C(L1)	120.0(4)
Re–Pt(2)–P(1)	109.7(1)	Re–Pt(2)–P(4)	136.3(1)	C(2)–P(4)–C(J1)	103.0(4)	C(2)–P(4)–C(L1)	101.7(4)
Re–Pt(2)–C(5)	44.7(3)	P(1)–Pt(2)–P(4)	106.1(1)	C(J1)–P(4)–C(L1)	105.2(5)	Pt(1)–P(5)–C(3)	108.0(3)
P(1)–Pt(2)–C(5)	113.5(3)	P(4)–Pt(2)–C(5)	97.8(3)	Pt(1)–P(5)–C(N1)	119.4(4)	Pt(1)–P(5)–C(O1)	118.7(4)
Pt(1)–Pt(3)–Pt(2)	61.5(1)	Pt(1)–Pt(3)–Re	60.6(1)	C(3)–P(5)–C(N1)	103.7(4)	C(3)–P(5)–C(O1)	102.8(4)
Pt(1)–Pt(3)–P(3)	155.1(1)	Pt(1)–Pt(3)–P(6)	94.8(1)	C(N1)–P(5)–C(O1)	102.2(5)	Pt(3)–P(6)–C(3)	112.2(3)
Pt(2)–Pt(3)–Re	59.4(1)	Pt(2)–Pt(3)–P(3)	93.8(1)	Pt(3)–P(6)–C(A1)	120.8(4)	Pt(3)(–P(6)–C(B1)	113.1(3)
P5(2)–Pt(3)–P(6)	155.6(1)	Re–Pt(3)–P(3)	110.2(1)	C(3)–P(6)–C(A1)	101.6(5)	C(3)–P(6)–C(B1)	101.3(4)
Re–Pt(3)–P(6)	115.6(1)	P(3)–Pt(3)–P(6)	109.6(1)	C(A1)–P(6)–C(B1)	105.7(4)	Re–P(7)–O(1)	113.9(3)
Pt(1)–Re–Pt(2)	57.2(1)	Pt(1)–Re–Pt(3)	54.3(1)	Re–P(7)–O(2)	120.1(3)	Re–P(7)–O(3)	122.4(3)
Pt(1)–Re–P(7)	126.6(1)	Pt(1)–Re–C(4)	133.2(3)	O(1)–P(7)–O(2)	98.4(4)	O(1)–P(7)–O(3)	101.9(3)
Pt(1)–Re–C(5)	115.6(3)	Pt(1)–Re–C(6)	61.2(3)	P(2)–P(7)–O(3)	95.9(3)	P(7)–O(1)–C(G1)	129.9(6)
Pt(2)–Re–Pt(3)	54.2(1)	Pt(2)–Re–P(7)	124.0(1)	P(7)–O(2)–C(H1)	126.3(5)	P(7)–O(3)–C(I1)	123.9(6)
Pt(2)–Re–C(4)	136.0(3)	Pt(2)–Re–C(5)	58.7(3)	P(1)–C(1)–P(2)	112.2(4)	P(3)–C(2)–P(4)	111.4(4)
Pt(2)–Re–C(6)	118.4(3)	Pt(3)–Re–P(7)	177.6(1)	P(5)–C(3)–P(6)	108.2(4)	Re–C(4)–O(4)	178.1(9)
Pt(3)–Re–C(4)	94.9(3)	Pt(3)–Re–C(5)	83.2(3)	Pt(2)–C(5)–Re	76.5(3)	Pt(2)–C(5)–O(5)	111.9(6)
Pt(3)–Re–C(6)	92.3(3)	P(7)–Re–C(4)	85.8(3)	Re–C(5)–O(5)	171.4(8)	Pt(1)–C(6)–Re	76.2(3)
P(7)–Re–C(5)	94.5(3)	P(7)–Re–C(6)	90.0(3)	Pt(1)–C(6)–O(6)	112.9(6)	Re–C(6)–O(6)	170.6(8)

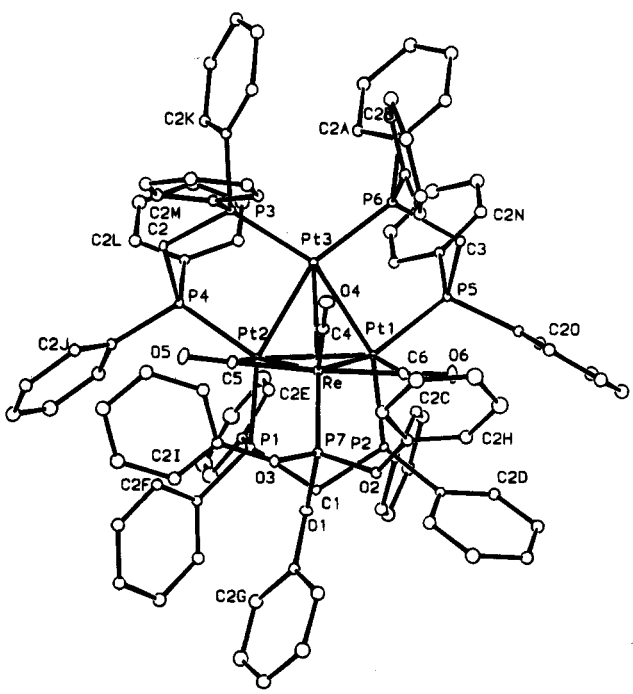

Figure 1. View of the molecular structure of **5**, with atoms represented by spheres of arbitrary size. In the phenyl rings, atoms are numbered in sequences C(n1)...C(n6), where n = A – L and the C(n1) atom is P- or O-bonded. The H atoms are omitted for clarity.

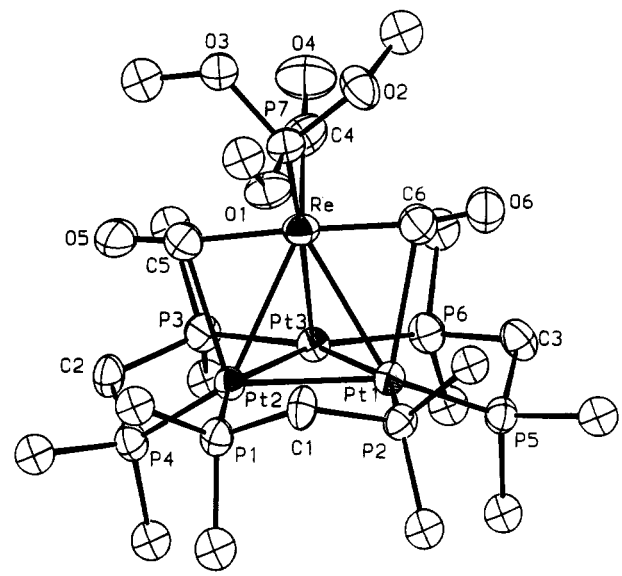

Figure 2. View of the inner core of **5**, using 50% probability ellipsoids. Only the *ipso* carbon atoms of the phenyl groups are shown.

In the $Pt_3(\mu\text{-dppm})_3$ fragment, the Pt_3P_6 skeleton is severely distorted from the ideal latitudinal geometry (Figure 2). All Pt–P bonds are bent out of the Pt_3 plane and away from the bulky $Re(CO)_3\{P(OPh)_3\}^+$ fragment. The out-of-plane displacement of the phosphorus atoms [0.088(2)–1.195(2) Å] is particularly large for the P(4) and P(5) atoms [1.195(2) and 0.969(2) Å], evidently to create space for the semibridging carbonyl ligands. The conformation of the $Pt_3P_6C_3$ unit differs from that in **2**, where the Pt_3P_6 skeleton is essentially planar and all three Pt_2P_2C rings show envelope conformations with carbon at the flap.[5] In **5** the three rings also adopt

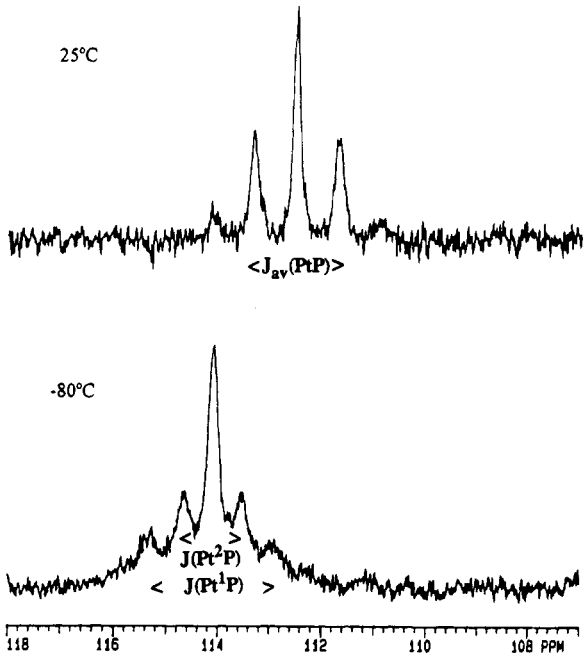

Figure 3. ^{31}P NMR spectra of complex **5** in the region of the P(OPh)$_3$ ligand. Upper, spectrum at 25 °C showing the apparent 1:4:7:4:1 quintet due to equal coupling to all platinum atoms in the fast fluxionality region. Lower, spectrum at −80 °C showing the 1:4:1 triplet of 1:8:18:8:1 quintets due to coupling to Pt^2 and 2 × Pt^1, respectively, in the slow rotation region.

envelope conformations, but with carbon at the flap only in the Pt(1)Pt(2)P(1)C(1)P(2) ring; in the other two rings the flaps are occupied by phosphorus atoms, P(4) and P(5) (Figure 2).

The spectroscopic data give further insight into the nature of the cluster cations **4** and **5**. The IR spectra of both **4** and **5** displayed three bands due to terminal carbonyls, as expected for the structure of Figure 1. The stretching frequencies were decreased slightly compared to **2**,[5] indicating that the phosphites are net donors to rhenium. The room temperature ^{31}P NMR spectra contained a singlet resonance due to the dppm phosphorus atoms and a 1:4:7:4:1 quintet for the phosphite ligand. The quintet resonance is characteristic of a nucleus with equal coupling to three platinum atoms and, together with the singlet dppm resonance, suggests that the clusters have C_3 symmetry on the NMR time scale.[8-10] Since the actual symmetry is lower (Figure 1), the clusters must be fluxional. The average coupling between platinum and the phosphite phosphorus, J(PtP), is 157 and 194 Hz for **4** and **5**, respectively. Such small couplings cannot be due to ^1J(PtP)[5,8-10] but are consistent with a longer range ^2J(PtReP) coupling, as expected if P(OR)$_3$ adds to the rhenium atom of **2**.

The apparent fluxionality of **4** and **5** was studied by low-temperature ^{31}P NMR spectroscopy. At −80 °C, the singlet dppm phosphorus resonance observed at room temperature for **5** split to give three resolved resonances. This is expected for the structure shown in eq 1, which possesses a plane of symmetry containing the atoms LRe(C^{1}O)Pt^2 (note that the atom labeling is different from that in Figure 1). Analysis of the resonance due to the phosphite ligand of **5** was also informative. At ambient temperature, this resonance appeared as a 1:4:7:4:1 quintet with ^2J(PtP) = 194 Hz (Figure 3). At −80 °C, this signal was broader and two

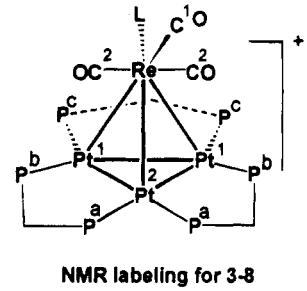

NMR labeling for 3-8

different couplings ^2J(PtP) were observed. Thus the resonance was interpreted as a 1:4:1 triplet [due to coupling to one platinum atom with ^2J(Pt^{2}P) = 300 Hz] of 1:8:18:8:1 quintets [due to coupling to two equivalent platinum atoms with ^2J(Pt^{1}P) = 135 Hz].[10] The average coupling is therefore expected to be $^1/_3$(2 × 135 + 300) = 190 Hz, in good agreement with the observed value of 194 Hz. The mechanism of fluxionality is proposed to be that shown in eq 3. It involves rotation of the

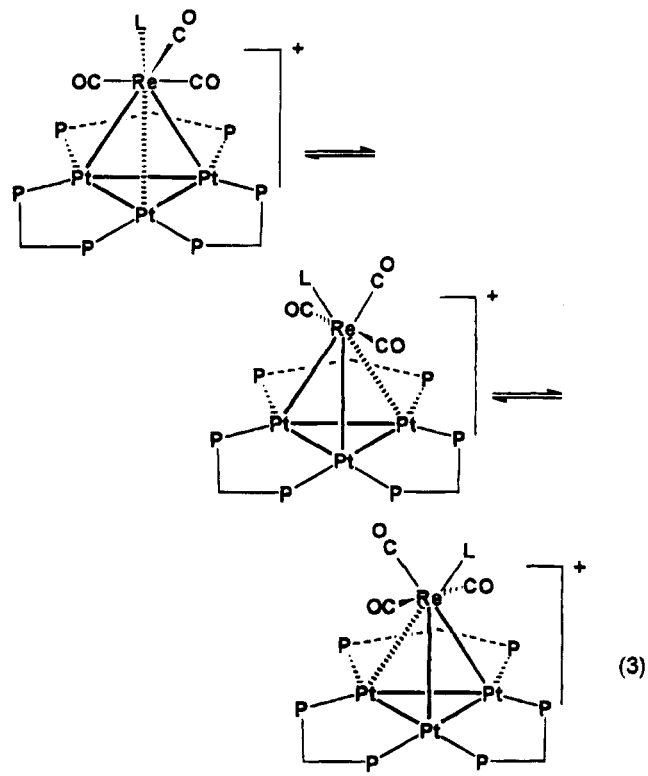

(3)

Re(CO)$_3$L unit about the Pt$_3$ triangle, with each stable structure having an approximately linear L−Re−Pt unit [P(7)−Re−Pt(3) = 177.6(1)° in Figure 1]. This naturally leads to apparent 3-fold symmetry at the limit of rapid rotation. The activation energy for rotation of the Re(CO)$_3$L unit of **4** appears to be lower than for **5**. Thus, at −80 °C, the ^{31}P resonance due to the dppm phosphorus atoms had split into three broad unresolved resonances, indicating that the fluxionality was not completely frozen out. The difference is most readily interpreted in terms of steric hindrance involving the phosphite ligand leading to slower rotation of the Re(CO)$_3$L unit when L = P(OPh)$_3$ than with the smaller L = P(OMe)$_3$.

The reaction of P(OMe)$_3$ with **3** gave a complex mixture of products, which were not identified, while P(OPh)$_3$ failed to react with **3** at room temperature.

Reactions with CO. Solutions of the tricarbonyl

Scheme 1

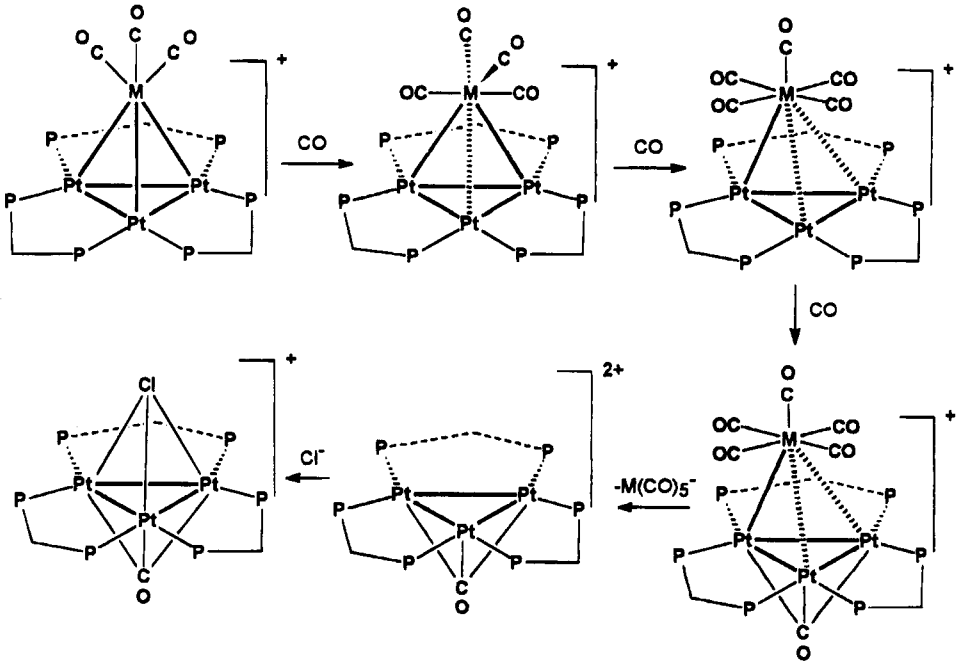

cluster cation **2** in acetone or dichloromethane reacted rapidly with CO to give the tetracarbonyl cluster $[Pt_3\{\mu_3\text{-}Re(CO)_4\}(\mu\text{-dppm})_3]^+$, **6** (eq 1). The reaction was reversible, and bubbling nitrogen through the solution containing **6** led to loss of one carbonyl ligand with formation of **2**. This reversibility gives an easy route for enrichment of the cluster with ^{13}CO and clearly indicates how ligand substitution reactions may occur at the rhenium center of **2**. Redissolution of solid samples containing **6** also gave solutions containing mixtures of **2** and **6**, so that pure samples of **6** were obtained with some difficulty. These reactions were readily monitored by NMR or IR spectroscopy. Both **2** and **6** are deep red in color, but **6** is slightly darker in color than **2**. Complex **6** was stable to excess CO in acetone solution but unstable in dichloromethane, in which further reaction occurred to give cluster fragmentation and formation of the known cluster $[Pt_3(\mu_3\text{-}Cl)(\mu_3\text{-}CO)(\mu\text{-dppm})_3]^+$;[8,13] the rhenium-containing product was not identified. Interestingly, as monitored by ^{31}P NMR spectroscopy, the fragmentation appeared to proceed via an intermediate cluster, which showed a singlet at $\delta(^{31}P)$ −23.3. The concentration of this complex grew in the early stages of reaction and then decreased as the final products were formed, so it could not be isolated. It is possible that this complex is formed by addition of a second carbonyl ligand to give $[Pt_3\{Re(CO)_5\}(\mu\text{-dppm})_3]^+$.

The reaction of the Pt_3Mn cluster **3** with CO did not give an identifiable carbonyl adduct. When the reaction was carried out in dichloromethane, the platinum cluster $[Pt_3(\mu_3\text{-}Cl)(\mu_3\text{-}CO)(\mu\text{-dppm})_3]^+$ was formed but no intermediates could be detected.[8,10] Again, the formation of this chloro complex is due to the involvement of the solvent used. However, in contrast to the reaction of **2**, when complex **3** was treated with CO in acetone, fragmentation of the cluster took place, yielding the known cluster cation $[Pt_3(\mu_3\text{-}CO)(CO)(\mu\text{-dppm})_3]^{2+}$. This is known to be formed reversibly by reaction of $[Pt_3(\mu_3\text{-}CO)(\mu\text{-dppm})_3]^{2+}$ with CO,[14] and flushing the acetone solution of $[Pt_3(\mu_3\text{-}CO)(CO)(\mu\text{-dppm})_3]^{2+}$ with dinitrogen gave rise to $[Pt_3(\mu_3\text{-}CO)(\mu\text{-dppm})_3]^{2+}$. The easier fragmentation of the Pt_3Mn cluster is indicative of a weaker Pt−Mn bond in comparison with the corresponding Pt−Re bond.

Both reactions of **2** and **3** can be understood in terms of Scheme 1. Sequential CO additions at rhenium or manganese give the tetracarbonyl and pentacarbonyl clusters, and the next addition occurs at platinum with displacement of $[M(CO)_5]^-$, M = Mn or Re. The cluster $[Pt_3(\mu_3\text{-}CO)(\mu\text{-dppm})_3]^{2+}$ is stable in dichloromethane, so the formation of $[Pt_3(\mu_3\text{-}Cl)(\mu_3\text{-}CO)(\mu\text{-dppm})_3]^+$ is probably initiated by reaction of $[M(CO)_5]^-$ with CH_2Cl_2 with generation of Cl^-. It should be clear that the reactions shown in Scheme 1 are just the reverse of those which are presumably involved in the formation of **2** or **3** from **1** and $[M(CO)_5]^-$.[5]

The new complex **6** was characterized spectroscopically. The IR spectrum contained two terminal carbonyl bands [ν(CO) = 1995, 1889 cm^{-1}], shifted to higher frequency compared to **2** [ν(CO) = 1981, 1882, 1871 cm^{-1}],[5] and no bridging carbonyl bands. The room temperature ^{31}P NMR spectrum of **6** showed a singlet, with complex satellites arising from coupling to ^{195}Pt that are typical of complexes with metal−metal-bonded $Pt_3(dppm)_3$ triangles with apparent C_3 symmetry.[6,8] The ^{13}C NMR spectrum of **6***, prepared by using ^{13}CO, was more informative. It displayed two carbonyl resonances in a 1:1 ratio, a singlet at δ 196 and a more complex resonance at δ 217. The latter resonance appears as an apparent quintet with 1:4:7:4:1 intensities, typical of a group coupled to three equivalent platinum atoms. The observed coupling constant, J(PtC) = 160 Hz, is much too low for a ^1J(PtC) coupling but is consistent with a ^2J(PtReC) coupling.[14] Clearly then, all four carbonyls are bound to rhenium but are in two different

(13) Manojlović-Muir, Lj.; Muir, K. W.; Lloyd, B. R.; Puddephatt, R. J. *J. Chem. Soc., Chem. Commun.* **1985**, 536.

(14) Lloyd, B. R.; Bradford, A. M; Puddephatt, R. J. *Organometallics* **1987**, *6*, 424.

chemical environments, with two showing long-range coupling to platinum and two not coupled to platinum. These data are mostly consistent with the proposed structure shown in eq 1 with L = CO except, of course, that such a $Re(CO)_4$ unit cannot have C_3 symmetry whereas the spectra suggest that this symmetry element is present. The problem is overcome if the cluster is fluxional, undergoing rapid rotation of the $Re(CO)_4$ group with respect to the Pt_3 triangle. To test for this, low-temperature ^{31}P and ^{13}C NMR spectra were recorded. The ^{31}P NMR spectrum of **6** at −80 °C was far broader than at room temperature, but it did not split into separate resonances. The ^{13}C NMR spectrum did not change significantly at −80 °C except that the quintet broadened and $J(PtC) = 77$ Hz was somewhat decreased. These data indicate that rotation of the $Re(CO)_4$ unit was still fairly rapid at −80 °C. The rate of rotation of the $Re(CO)_3L$ units in **4**−**6** appears to follow the sequence L = $P(OPh)_3$ < L = $P(OMe)_3$ < L = CO, as expected if the main barrier to rotation is steric hindrance.

Reactions with Isocyanides RNC (R = Me, t-Bu, Cy (cyclohexyl), Xy (2,6-$Me_2C_6H_3$)). The reactions of isocyanide ligands RNC with **2** gave the adducts $[Pt_3\{Re(CO)_3(CNR)\}(\mu\text{-dppm})_3]^+$, **7** (R = Me), **8** (R = t-Bu), **9**, (R = Cy), and **10** (R = Xy) by addition to the rhenium center. In contrast, these ligands react with equal molar amounts of the cluster $[Pt(\mu_3\text{-CO})(\mu\text{-dppm})_3]^{2+}$ to form the adducts $[Pt_3(CNR)(\mu_3\text{-CO})(\mu\text{-dppm})_3]^{2+}$ by addition at platinum.[12] The reaction of **2** with RNC took about 1/2 h (R = Me, t-Bu, Cy) or 1 h (R = Xy) to reach completion as monitored by NMR spectroscopy. The isocyanide adducts are stable in solution under a N_2 atmosphere.

The IR spectrum of **10** displayed two terminal carbonyl bands at $\nu(CO)$ = 1981 and 1874 cm^{-1} and a terminal isocyanide absorption at $\nu(NC)$ = 2088 cm^{-1}. Note that the value of $\nu(NC)$ is lower than in free XyN≡C (2115 cm^{-1}), whereas the value of $\nu(NC)$ in $[Pt_3(\mu_3\text{-CO})(XyN{\equiv}C)(\mu\text{-dppm})_3]^{2+}$ = 2165 cm^{-1} is higher, indicating stronger back-bonding to the isocyanide ligand when coordinated to rhenium. The room temperature ^{31}P NMR spectrum of **10** gave a sharp singlet resonance, but, at −90 °C, this split to give three broad resonances at δ 3.1, −3.0, and −13.1, respectively. The ^{31}P NMR spectrum coalesced at −50 °C. These data are fully consistent with fluxionality as shown in eq 3.

The spectroscopic properties of **7**−**9** are similar, and details are given in the Experimental Section. In all cases the values of $\nu(NC)$ were lower than in the free ligands (2144, 2102, and 2120 cm^{-1} for **7**−**9**, respectively, compared to 2167, 2140, and 2145 cm^{-1} for free MeNC, t-BuNC, and CyNC in CH_2Cl_2 solution, respectively), indicative of coordination to the rhenium center in all cases.

Reactions with Thiols RSH (R = Et, t-Bu or 3-MeC_6H_4). The thiol ligands RSH reacted with cluster **2** to give the adducts **11**−**13**, R = Et, t-Bu, or 3−MeC_6H_4, respectively (eq 1). The reaction rates followed the sequence R = Et (seconds to complete) > t-Bu (minutes) > 4-MeC_6H_4 (1 h), as monitored by ^{31}P NMR spectroscopy. In contrast, the thiol ligands RSH (R = Et and Ph) react with $[Pt(\mu_3\text{-CO})(\mu\text{-dppm})_3]^{2+}$ to form $[Pt_3(SHR)(\mu_3\text{-CO})(\mu\text{-dppm})_3]^{2+}$, which then readily transforms to the stable $[Pt_3H(\mu_3\text{-SR})(\mu_3\text{-CO})(\mu\text{-dppm})_3]^{2+}$.[8,12]

The IR spectrum of **13** contained three terminal carbonyl bands at $\nu(CO)$ = 1997, 1897, and 1883 cm^{-1}. The room temperature ^{31}P NMR spectrum of **13** showed a sharp singlet resonance due to the dppm ligands, with satellites due to coupling to ^{195}Pt, indicating 3-fold symmetry on the NMR time scale. The resonance broadened but did not split at −90 °C indicating a low barrier to rotation of the $Re(CO)_3(RSH)$ unit. The magnitude of coupling, $^1J(PtP)$ = 3028 Hz, is similar to those of isocyanide adducts.

Reactions with Alkynes. The reactions of alkynes also occur rapidly according to eq 1 to give the new alkyne clusters $[Pt_3\{Re(CO)_3L\}(\mu\text{-dppm})_3]^+$ (**14**, L = HC≡CH; **15**, L = PhC≡CH). These were thermally stable complexes. For example, **14** could be heated under reflux in benzene without decomposition by either CO or HC≡CH loss. The disubstituted alkynes RC≡CR, R = Me, Ph, CF_3, or CO_2Me, failed to react with **2**, presumably due to steric hindrance. The alkyne complexes failed to give X-ray quality crystals, so spectroscopic characterization was necessary. There are two possible complications with alkyne ligands. The first is that rearrangement of Re(HC≡CR) to the vinylidene Re=C=CHR is possible,[15] and the second is that two orientations of the alkyne are possible, either *in* the plane of symmetry, **A**, or *perpendicular to* the plane of symmetry of the cluster, **B**. The ^{13}C NMR spectrum of

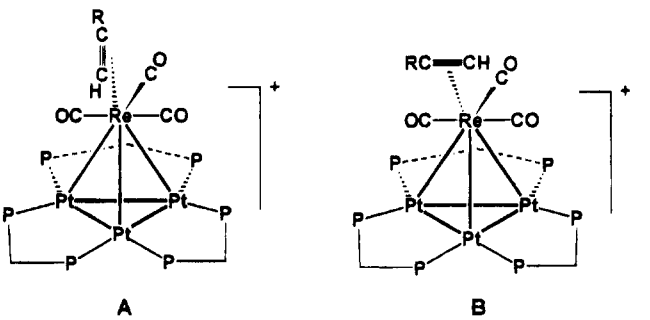

A B

14*, prepared using ^{13}C-enriched acetylene, contained only a broad singlet, with no resolved $^{13}C-^{195}Pt$ coupling, for the coordinated acetylene at either room temperature or at −80 °C. The broadening of the peak is probably due to quadrupolar relaxation by the rhenium nucleus (^{185}Re and ^{187}Re each have $I = 5/2$). The absence of $J(PtC)$ coupling shows immediately that the alkyne is bound to rhenium and not platinum, and the presence of only one resonance at δ 85.2 immediately rules out the vinylidene structure which would give two ^{13}C resonances, of which the α-carbon resonance would be expected in the range δ 250−380.[15b] It is less certain if the conformation is **A** or **B**; only **B** should give a single ^{13}C resonance and so this is the more likely structure. However, the possibility that the structure is **A** with a rapidly rotating acetylene ligand cannot be eliminated by the data. The ^{31}P NMR spectrum of **14** contained three resonances for the dppm phosphorus atoms, and these resonances showed no significant change at temperatures from 25 to −80 °C. Hence this cluster is not fluxional and the $Re(CO)_3(HCCH)$ group cannot easily rotate with respect to the Pt_3 triangle. The ^{31}P NMR spectrum of **15** contained six resonances, showing that all six phosphorus atoms are inequivalent. In structure

(15) (a) Caulton, K. G. *Coord. Chem. Rev.* **1981**, *38*, 1. (b) Bruce, M. I. *Chem. Rev.* **1991**, *91*, 197.

A the plane of symmetry remains even with an unsymmetrical alkyne and so this should give only three ^{31}P resonances. The observation of six resonances is therefore strong evidence for structure **B**.

It is noted that alkynes react with complex **1** at the Pt_3 triangle and so give rise to very different products containing triply bridging alkyne ligands.[8,16] The reactions of HCCH and PhCCH with **3** gave an unidentified mixture of products.

Ligand Exchange Reactions. The cluster **6** can undergo ligand for carbonyl exchange according to Scheme 2 (L = CO) on reaction with ligands L′ (L′ = $P(OMe)_3$, $P(OPh)_3$, HCCH, HCCPh) by substitution at rhenium while reactions with halide (X = Cl, Br, I) lead to displacement of L = CO from rhenium with addition of X^- at platinum. These substitution reactions are all substantially slower than the analogous addition reactions to cluster **2**. Similarly, the cluster $[Pt_3\{Re(CO)_3(HCCH)\}(\mu\text{-dppm})_3]^+$, **14**, reacted slowly (ca. 14 and 24 h to completion when R = Me or Ph respectively) with $P(OR)_3$ (R = Me and Ph) by displacement of acetylene to give **4** or **5** respectively. The rates followed the sequence **2** ≫ **6** ≫ **14** in reactions with the phosphite ligands. The reactions with **14** are presumed to be associative since **14** is stable to dissociation of acetylene. Carbon monoxide did not displace acetylene from **14**.

Discussion

The cations **2** and **3** are coordinatively unsaturated 54-electron clusters.[7] The bonding in **2** has been interpreted in terms of the three filled M−M bonding orbitals of the $Pt_3(\mu\text{-dppm})_3$ fragment (a_1 + e symmetry) acting as donors to the three vacant acceptor orbitals of the $Re(CO)_3$+ fragment (also a_1 + e symmetry) as shown in **C**.[5] In this way, each Pt atom shares 16 and

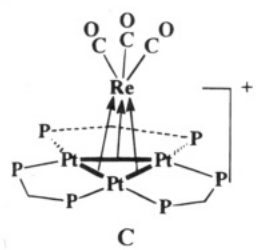

C

the Re atom shares 18 valence electrons.[5] It might be expected that ligands would therefore add selectively to platinum in much the same way as has been observed in trinuclear complexes such as $[Pt_3(\mu_3\text{-CO})(\mu\text{-dppm})_3]^{2+}$.[8] However, all the ligands studied in this work add selectively at rhenium (eq 1). It is interesting to ask why.

Consider first the bonding in the products, all of which probably have a 56-electron count (the possibility of the alkyne acting as a 4-electron donor has not been disproved). Complex **6** is the simplest example. The bonding may still be considered in terms of the $Pt_3(\mu\text{-dppm})_3$ fragment acting as a donor to the $Re(CO)_4$+ fragment, but this has only two acceptor orbitals so only

(16) Manojlović-Muir, Lj.; Muir, K. W.; Rashidi, M.; Schoettel, G.; Puddephatt, R. J. *Organometallics* **1991**, *10*, 1719.

Scheme 2

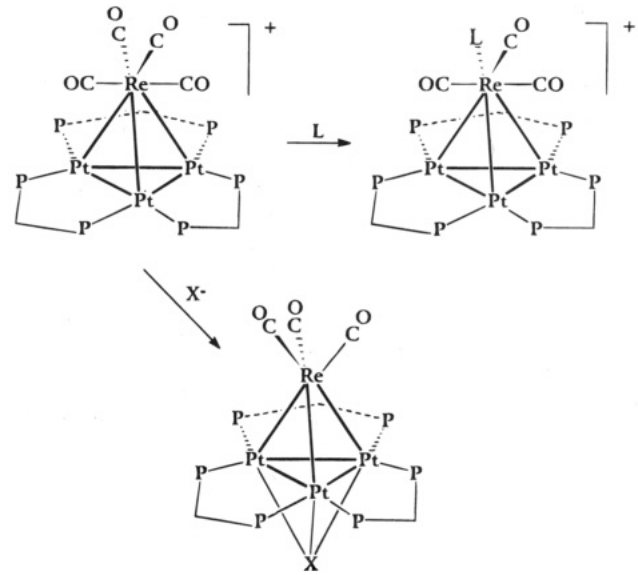

[a] L = $P(OR)_3$ or HCCH; X = Cl, Br, or I.

two donor−acceptor bonds are possible as shown in **D**.[17] Hence, weaker Pt−Re bonding is expected in **6** than in

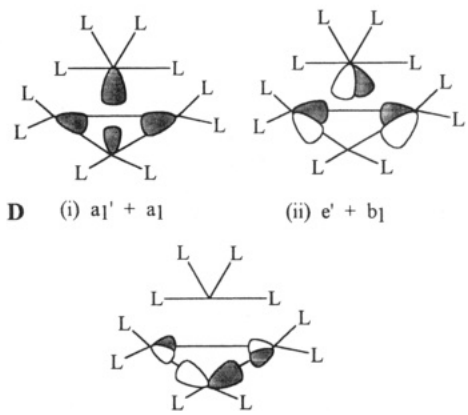

D (i) $a_1' + a_1$ (ii) $e' + b_1$ (iii) e′

2, consistent with the observed increase in Pt−Re bond distances in **5** compared to **2**. This interpretation also rationalizes the slippage of the rhenium from the center of the Pt_3 triangle in **5**. Another way of looking at this is to consider that the LUMO in **2** is a cluster antibonding orbital of e symmetry and considerable Re character. Donation of two electrons into such an orbital will naturally weaken the cluster bonding.[7] It should be pointed out that if the ligand did add below the Pt_3 plane it could donate electron density into one or more of the empty p-orbitals on platinum and this need not weaken the cluster bonding; this is what happens when ligands add to the Pt_3 cluster **1**.[8]

There is another useful analogy to this chemistry. The proposed donor orbitals of the $Pt_3(\mu\text{-dppm})_3$ fragment have a_1 + e symmetry and so do the donor orbitals of $C_5H_5^-$ or C_6H_6.[15] Hence, in the limit, it could be argued that the cluster **2** is isolobal to $[CpRe(CO)_3]$. This

(17) For previous theoretical work on Pt_3L_6 clusters and on $M(CO)_n$ fragments, see: (a) Evans, D. G. *J. Organomet. Chem.* **1988**, *352*, 397. (b) Mealli, C. *J. Am. Chem. Soc.* **1985**, *107*, 2245. (c) Albright, T. A.; Burdett, J. K.; Whangbo, M.-H. *Orbital Interactions in Chemistry*; Wiley: New York, 1985; Chapter 20.

complex is inert to ligand addition but the related complex [CpRe(CO)(NO)R] is known to add ligands at rhenium with slippage of the η^5-C_5H_5 ligand to η^3 and then η^1.[18] The ligand addition to **2** could be considered analogous to this chemistry. Hence, the addition of one or two ligands to **2** might lead to slippage of the $Re(CO)_3L_n$ unit from η^3 ($n = 0$) to η^2 ($n = 1$) and η^1 ($n = 2$) with respect to the Pt_3 triangle. The Pt_3Mn complex **3** appears to have weaker metal–metal bonding, and ligand addition appears to occur with cleavage of the manganese fragment from the cluster.

In an additional analogy, rotation of η^5-C_5H_5 ligands about the Cp–metal axis is known to occur with a very low activation energy so it might be predicted that the $Pt_3(\mu$-dppm$)_3$ "ligand" should rotate easily about the Re–Pt_3 centroid axis in **2**. There is no easy way to study this reaction which, of course, is equivalent to rotation of the $Re(CO)_3$ unit about the Pt_3 triangle. A somewhat higher activation energy might be expected for rotation of the $Re(CO)_3L$ units in **4**–**8**, since the analogy here is to η^3-Cp ligands. Nevertheless, the complexes **4**–**6** are all fluxional and only the alkyne complexes **7** and **8** are not. A related fluxionality has been observed previously for the clusters $[Pt_4(\mu\text{-H})(\mu\text{-CO})_2(\mu\text{-dppm})_3L]^+$, in which the $Pt(CO)_2L$ group migrates from edge to edge of the dppm-bridged Pt_3 triangle.[19]

The above arguments, based on analogies only, are supported by EHMO calculations on the model cluster $[Pt_3(CO)_6\{\mu\text{-Re}(CO)_4\}]^+$, substituting two carbonyl ligands for each μ-dppm ligand in **6** and with initial geometry **E**. An energy correlation diagram is shown as Figure

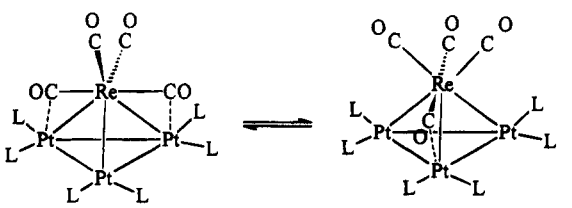

E **F**

4. The $2a_1$ acceptor orbital of the $[Re(CO)_4]^+$ fragment[17] overlaps with the $1a_1'$ donor orbital of the $[Pt_3(CO)_6]$ fragment[17] to give the bonding orbital 3a′, which is the HOMO. The $1b_1$ acceptor orbital of the $[Re(CO)_4]^+$ fragment overlaps with one of the 1e′ donor orbitals of the $[Pt_3(CO)_6]$ fragment to give the bonding orbital 2a′. Both of these effects contribute to Pt–Re bonding, and it is the $1b_1$–1e′ overlap which leads to asymmetry in the Pt–Re bonding. The other e′ donor orbital is destabilized by a four-electron interaction with one of the filled "t_{2g}-like" orbitals of the d^6 $[Re(CO)_4]^+$ fragment (note that the net repulsive interaction is also reduced by slippage of the $Re(CO)_4$ group). Rotation of the $[Re(CO)_4]^+$ fragment is calculated to have a low activation barrier, since, as overlap of $1b_1$ with one of the 1e′ donors decreases, overlap with the other increases, and the energies of the frontier orbitals change only slightly

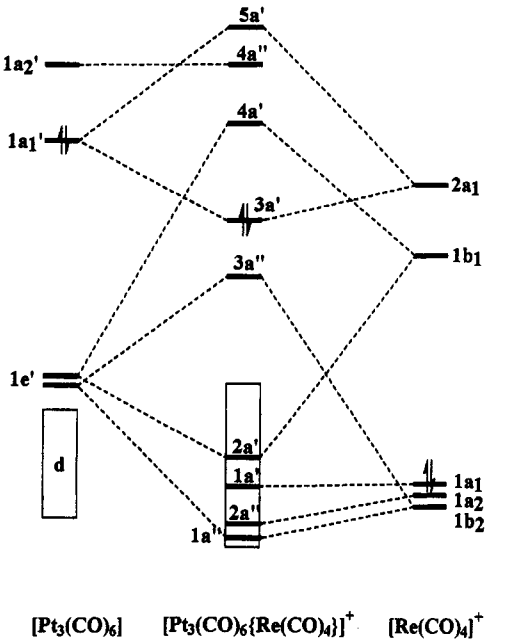

Figure 4. Energy correlation diagram for interaction of D_{3h} $[Pt_3(CO)_6]$ and C_{2v} $[Re(CO)_4]^+$ fragments to give C_s $[Pt_3(CO)_6\{Re(CO)_4\}]^+$. For frontier orbitals, see **D**.

during the rotation between limiting structures **E** and **F**. Note, however, that the rhenium is expected to move during the rotation to remain away from the center of the Pt_3 triangle. The preferred orientation may be determined by steric effects, by the semibridging carbonyl effects or by changes in energy due to slippage of the Re atom with respect to the Pt_3 triangle. The EHMO method is not well suited to geometry optimization so these effects have not been pursued, though it should be clear from the 1e′–b_1 overlap shown in **D** why the slippage of rhenium toward an edge of the Pt_3 triangle is favored.

The observation that Pt_3Re cluster **2** is reactive at the rhenium center was unexpected. It is not known what role each metal plays in the heterogeneous Pt/Re catalysts, but, on the basis of the model complex **2**, an active role for the rhenium atoms may be envisaged.[20]

Experimental Section

The compounds $[Pt_3\{M(CO)_3\}(\mu\text{-dppm})_3]^+$ (M = Re, **2**; Mn, **3**) were prepared by the previously reported procedure.[5] IR spectra were recorded by using a Perkin-Elmer 2000 spectrometer, and the NMR spectra were recorded in CD_2Cl_2 solution at ambient temperature, unless otherwise indicated, with a Varian Gemini-300 spectrometer; chemical shifts are referenced to TMS (^{1}H) and 85% H_3PO_4 (^{31}P{^{1}H}). Elemental analyses were performed by Galbraith Laboratories, Inc.

$[Pt_3\{Re(CO)_3(P(OMe)_3)\}(\mu\text{-dppm})_3][PF_6]\cdot 2CH_2Cl_2$. To a solution of **2** (30 mg) in CH_2Cl_2 (10 mL) was syringed $P(OMe)_3$ (0.1 mL). The solution immediately darkened slightly. The mixture was stirred for 15 min, the solution was concentrated, and the product was precipitated as a deep brown solid by addition of pentane and then washed with pentane and dried under vacuum. It was recrystallized from CH_2Cl_2/hexane. Yield: 70%. Anal. Calcd for $C_{83}H_{79}O_6F_6P_7Cl_2RePt_3$: C, 40.7; H, 3.2. Found: C, 40.8; H, 3.4. IR (Nujol): ν(CO)/cm^{-1} = 1943 s, 1877 m, 1856 vs. NMR in CD_2Cl_2: δ(^{1}H) 6.40 [m, H_2CP_2]; 4.72 [m, H_2CP_2]; 3.10 [d, ^3J(PH) = 17 Hz, P(OCH_3)$_3$]; δ(^{31}P) 130.5 [quin, ^2J(PtP) = 157 Hz, $P(OMe)_3$]; −5.6 [s, ^1J(PtP) =

(18) (a) Casey, C. P.; O'Connor, J. M.; Jones, W. D.; Haller, K. J. *Organometallics* **1983**, *2*, 535. (b) Bang, H.; Lynch, T. J.; Basolo, F. *Organometallics* **1992**, *11*, 40. (c) Biagioni, R. N.; Lorkovic, I. M.; Skelton, J.; Hartung, J. B. *Organometallics* **1990**, *9*, 547. (d) O'Connor, J. M.; Casey, C. P. *Chem. Rev.* **1987**, *87*, 307.

(19) Douglas, G.; Manojlović-Muir, Lj.; Muir, K. W.; Jennings, M. C.; Lloyd, B. R.; Rashidi, M.; Schoettel, G.; Puddephatt, R. J. *Organometallics* **1991**, *10*, 3927.

(20) Bond, G. C. *Chem. Soc. Rev.* **1991**, *20*, 441.

3028 Hz, ^3J(PP) = 186 Hz, dppm]; δ(^{31}P, −80 °C) 132.2 [m, ^2J(PtP) = 156 Hz]; 1.1, −2.4, −15.6 [br, dppm].

[Pt$_3${Re(CO)$_3$(P(OPh)$_3$)}(μ-dppm)$_3$][PF$_6$]. Complex **5**[PF$_6$] was prepared in a similar way except that the reagent P(OPh)$_3$ was used. It was recrystallized from CH_2Cl_2/diethyl ether. Yield: 85%. Anal. Calcd for $C_{96}H_{81}O_6F_6P_7RePt_3$: C, 48.8; H, 3.3. Found: C, 48.5; H, 3.7. IR (Nujol): ν(CO)/cm^{-1} = 1955 m, 1899 m, 1868 s. NMR in CD_2Cl_2: δ(^{1}H) 6.45 [m, H_2CP_2]; 4.75 [m, H_2CP_2]; δ(^{31}P) 111.8 [quin, ^2J(PtP) = 194 Hz, P(OPh)$_3$]; −5.5 [s, ^1J(PtP) = 3007 Hz, ^3J(PP) = 195 Hz, dppm]; δ(^{31}P, −80 °C) 114.1 [tquin, ^2J(PtP) = 300 Hz, 135 Hz, P(OPh)$_3$]; 1.3 [s, br, ^1J(PtP) = 3577 Hz, dppm], −3.7 [m, ^1J(PtP) = 2833 Hz, dppm], −16.7 [m, ^1J(PtP) = 2688 Hz, dppm].

[Pt$_3${Re(CO)$_4$}(μ-dppm)$_3$][PF$_6$]. CO was bubbled through a solution of **2** (15 mg, 0.007 mmol) in CD_2Cl_2 (0.5 mL) in an NMR tube for 1 min. The solution became slightly darker in color. NMR spectra (^{1}H and ^{31}P{^{1}H}) indicated the immediate disappearance of **1** and the quantitative formation of **6**. This reaction was reversible, as evidenced by the fact that, in the absence of CO, complex **2** was slowly regenerated at the expense of **6** in the solution. IR (CH_2Cl_2): ν(CO)/cm^{-1} = 1995 s, 1889 vs. NMR: δ(^{1}H) 6.35 [m, H_2CP_2]; 4.60 [m, H_2CP_2]; δ(^{31}P) −2.6 [s, ^1J(PtP) = 3000 Hz, ^3J(PP) = 194 Hz, dppm]; δ(^{13}C) 216.5 [quin, ^2J(PtC) = 81 Hz, C^{1}O], 195.6 [s, C^{2}O]; δ(^{31}P, −80 °C) −2.8 [br, ^1J(PtP) = 3120 Hz, dppm]; δ(^{13}C, −80 °C) 217.3 [m, ^2J(PtC) = 77 Hz, C^{1}O], 196.8 [s, C^{2}O].

Addition of CO to the CD_2Cl_2 solution of **6** for a longer period led to the complete conversion to the previously characterized complex, [Pt$_3$(μ_3-Cl)(μ_3-CO)(μ-dppm)$_3$]$^+$, within 15 min.[14]

The reaction of complex **3** with CO was carried out similarly. When the reaction was conducted in CD_2Cl_2 in an NMR tube, the formation of [Pt$_3$(μ_3-Cl)(μ_3-CO)(μ-dppm)$_3$]$^+$ was occurred rapidly and in almost quantitative yield, as monitored by NMR. When this reaction was carried out using an acetone solution, the product was [Pt$_3$(μ_3-CO)(CO)(μ-dppm)$_3$]$^{2+}$ which, upon flushing with dinitrogen, was converted to [Pt$_3$(μ_3-CO)(μ-dppm)$_3$]$^{2+}$. Both compounds are known and they were identified by their ^{1}H and ^{31}P NMR spectra.[14]

[Pt$_3${Re(CO)$_3$(MeNC)}(μ-dppm)$_3$][PF$_6$]. To a solution of **2** (36 mg, 0.017 mmol) in acetone (15 mL) was added MeNC (0.8 μL, 0.017 mmol) via microsyringe. The color of the red solution darkened immediately. After 0.5 h of being stirred, the solution was concentrated to ca. 1 mL under vacuum. Hexane was added to precipitate the product, which was further washed with diethyl ether followed by vacuum drying to give the product as an orange-yellow powder in 87% yield. Anal. Calcd for $C_{80}H_{69}F_6NO_3P_7Pt_3Re$: C, 43.78; H, 3.17. Found: C, 43.65; H, 3.16. IR (Nujol): ν(CO)/cm^{-1} = 1981 s, 1879 vs, br; ν(NC)/cm^{-1} = 2144 s. NMR in $(CD_3)_2CO$: δ(^{1}H) 6.64 [br, 3H, H^aCP_2], 4.58 [br, 3H, H^bCP_2], 2.60 [s, 3H, CH_3]; δ(^{31}P{^{1}H}) −2.5 [s, 6P, ^1J(PtP) = 2940, ^2J(PtP) = 255, ^{3}J(PP) = 189 Hz, dppm].

[Pt$_3${Re(CO)$_3$(t-BuNC)}(μ-dppm)$_3$][PF$_6$]. The same procedure as above was followed with the use of t-BuNC instead of MeNC. The product was obtained was orange-yellow powder. Yield: 80%. Anal. Calcd for $C_{83}H_{75}F_6NO_3P_7Pt_3Re$: C, 44.57; H, 3.38. Found: C, 44.30; H, 3.25. IR (Nujol): ν(CO)/cm^{-1} = 1983 s, 1869 vs, br; ν(NC)/cm^{-1} = 2102 s. NMR in $(CD_3)_2CO$: ^{1}H, δ = 6.63 [br, 3H, H^aCP_2], 4.61 [br, 3H, H^bCP_2], 0.91 [s, 9H, C(CH_3)$_3$]; δ(^{31}P{^{1}H}) −2.1 [s, 6P, ^1J(PtP) = 2975, ^2J(PtP) = 235, ^3J(PP) = 206 Hz, dppm].

[Pt$_3${Re(CO)$_3$(CyNC)}(μ-dppm)$_3$][PF$_6$]. This was prepared similarly and isolated as an orange-yellow powder. Yield: 76%. Anal. Calcd for $C_{85}H_{77}F_6NO_3P_7Pt_3Re$: C, 45.12; H, 3.43. Found: C, 44.9; H, 3.2. IR (Nujol): ν(CO)/cm^{-1} = 1980 s, 1876 s, sh, 1869 s; ν(NC)/cm^{-1} = 2192 s. NMR in $(CD_3)_2$-CO: δ(^{1}H) 6.30 [br, 3H, H^aCP_2], 4.63 [br, 3H, H^bCP_2], 1.60–0.80 [m, 11H, C_6H_{11}]; δ(^{31}P{^{1}H}) −2.3 [s, 6P, ^1J(PtP) = 2981, ^2J(PtP) = 255, ^3J(PP) = 187 Hz, dppm].

[Pt$_3${Re(CO)$_3$(2,6-Me$_2$C$_6$H$_3$NC)}(μ-dppm)$_3$][PF$_6$]. This was prepared in a similar way except that 2,6-xylyl isocyanide was used. Yield: 82%. Anal. Calcd for $C_{87}H_{75}F_6NO_3P_7Pt_3Re$: C, 45.73; H, 3.31. Found: C, 45.68; H, 3.46. IR (Nujol): ν(CO)/cm^{-1} = 1981 s, 1874 vs, br; ν(NC)/cm^{-1} = 2088 s. NMR in $(CD_3)_2CO$: δ(^{1}H) 6.30 [m, 3H, H^aCP_2], 4.73 [m, 3H, H^bCP_2], 2.60 [s, 6H, $(CH_3)_2C_6H_3NC$]; δ(^{31}P{^{1}H}), −2.5 [s, 6P, ^1J(PtP) = 3026, ^2J(PtP) = 227, ^3J(PP) = 182, dppm]; δ(^{1}H, −90 °C) 6.09 [br, 2H, H^aCP_2], 5.31 [br, 1H, $H^{a'}CP_2$], 4.84 [m, 2H, H^bCP_2], 4.55 [br, 1H, $H^{b'}CP_2$]; δ(^{31}P{^{1}H}, −90 °C) 3.1 [br, 2P, dppm], −3.0 [br, 2P, dppm], 13.1 [br, 2P, dppm]; ^{31}P{^{1}H} NMR spectrum coalesced at −50 °C, δ = −2.9 [br, 6P, ^1J(PtP) = 2992 Hz, dppm].

[Pt$_3${Re(CO)$_3$(3-MeC$_6$H$_4$SH)}(μ-dppm)$_3$][PF$_6$]. To a solution of **1** (34 mg, 0.016 mmol) in acetone (15 mL) was added 3-toluenethiol (1.9 μL, 0.016 mmol) via microsyringe. The color of the red solution became more intense immediately. After 0.5 h of being stirred, the solution was concentrated to ca. 1 mL under vacuum. Hexane was added to precipitate the product, which was further washed with diethyl ether followed by vacuum drying to give the product as an orange-red powder in 85% yield. Anal. Calcd for $C_{85}H_{74}F_6O_3P_7Pt_3ReS$: C, 44.82; H, 3.27. Found: C, 45.11; H, 3.10. IR (Nujol): ν(CO)/cm^{-1} = 1997 s, 1897 s, sh, 1883 s; NMR in $(CD_3)_2CO$: δ(^{1}H) 6.28 [m, 3H, ^2J(PH) = 54, H^aCP_2], 4.67 [m, 3H, H^bCP_2]; δ(^{31}P{^{1}H}) −1.9 [s, 6P, ^1J(PtP) = 3028, ^2J(PtP) = 213, ^3J(PP) = 171, dppm]; δ(^{1}H, −90 °C 6.22 [br, 3H, H^aCP_2], 4.55 [br, 3H, H^bCP_2]; δ(^{31}P{^{1}H}, −90 °C) −2.2 [br, 6P, ^1J(PtP) = 3080 Hz, dppm].

[Pt$_3${Re(CO)$_3$(C$_2$H$_5$SH)}(μ-dppm)$_3$][PF$_6$]. This was prepared similarly. Anal. Calcd for $C_{80}H_{72}F_6O_3P_7Pt_3ReS$: C, 43.36; H, 3.28. Found: C, 43.16; H, 3.12. IR (Nujol): ν(CO)/cm^{-1} = 1979 s, 1869 s, br; NMR in $(CD_3)_2CO$: δ(^{1}H), 5.81 [m, 3H, H^aCP_2], 5.44 [m, 3H, H^bCP_2], 1.86 [quar, 2H, ^3J(HH) = 7.3, CH_2 of C_2H_5], 1.11 [t, 3H, ^3J(HH) = 7.3, CH_3 of C_2H_5]; δ(^{31}P{^{1}H}) −1.9 [s, 6P, ^1J(PtP) = 2948, ^2J(PtP) = 187, ^3J(PP) = 199, dppm].

[Pt$_3${Re(CO)$_3$(t-BuSH)}(μ-dppm)$_3$][PF$_6$]. This was prepared similarly. Anal. Calcd for $C_{80}H_{72}F_6O_3P_7Pt_3ReS$: C, 43.89; H, 3.41. Found: C, 44.17; H, 3.58. IR (Nujol): ν(CO)/cm^{-1} = 1983 s, 1876 s, br; NMR in $(CD_3)_2CO$: δ(^{1}H) 6.32 [br, 3H, H^aCP_2], 4.69 [m, 3H, H^bCP_2], 1.39 [s, 9H, CH_3]; δ(^{31}P{^{1}H}) −1.9 [s, 6P, ^1J(PtP) = 3026, ^2J(PtP) = 198, ^3J(PP) = 176 Hz, dppm].

[Pt$_3${Re(CO)$_3$(HC≡CH)}(μ-dppm)$_3$][PF$_6$]. Acetylene was bubbled through a solution of **2** (30 mg) in CH_2Cl_2 (10 mL) for 1 min, immediately causing a color change to dark brown. The mixture was stirred for 15 min, the volume was reduced to

Table 2. Crystallographic Data for [Pt$_3${Re(CO)$_3$P(OPh)$_3$}(μ-dppm)$_3$][PF6]·C$_2$H$_5$(OH), 1[PF$_6$]·C$_2$H$_5$(OH)

empirical formula	$C_{98}H_{87}F_6O_7P_8Pt_3Re$
fw	2510.0
space group	$P\bar{1}$
a, Å	13.993(1)
b, Å	17.868(1)
c, Å	19.753(2)
α, deg	88.198(7)
β, deg	87.766(7)
γ, deg	72.394(4)
V, Å^3	4702.9(7)
Z	2
F(000)	2428
D_{calcd}, g cm^{-3}	1.772
cryst dimens, mm^3	0.33 × 0.25 × 0.15
temp, °C	23
radiation	Mo Kα
wavelength, Å	0.719 73
μ(Mo Kα), cm^{-1}	59.93
abs corr factors on F	0.75 to 1.20
data collcn range, θ (deg)	2.4 to 30.5
no. of reflns in refinement [$I > 3\sigma(I)$]	14765
no. of params refined	464
R	0.0405
R_w	0.0429
observation of unit wt	1.53
largest shift/esd ratio	0.10
final difference synthesis, e Å^{-3}	−0.94 to 1.19

Table 3. Atomic Fractional Coordinates and Displacement Parameters (Å²) for Atoms in the Phenyl Groups and Solvent Molecule [C(A)–C(O6), C(1S), C(2S), and O(S)]

atom	*x*	*y*	*z*	*U*	atom	*x*	*y*	*z*	*U*
Pt(1)	0.09857(2)	0.22934(2)	0.17596(1)	0.031	C(E6)	0.0350(7)	0.0325(7)	0.4021(7)	0.095(4)
Pt(2)	0.16111(2)	0.22307(2)	0.30296(1)	0.031	C(F1)	0.2617(4)	0.0273(6)	0.3687(5)	0.044(2)
Pt(3)	0.11056(2)	0.35599(2)	0.23544(1)	0.031	C(F2)	0.3285(6)	0.0566(3)	0.4005(4)	0.050(2)
Re	0.29575(2)	0.23129(2)	0.19908(2)	0.037	C(F3)	0.4077(6)	0.0062(5)	0.4344(3)	0.066(3)
P(1)	0.16276(16)	0.09659(12)	0.32031(10)	0.037	C(F4)	0.4200(4)	−0.0734(5)	0.4366(4)	0.060(2)
P(2)	0.10266(14)	0.10006(11)	0.17144(10)	0.035	C(F5)	0.3532(6)	−0.1027(3)	0.4048(3)	0.072(3)
P(3)	0.13759(15)	0.42667(11)	0.32465(10)	0.039	C(F6)	0.2740(6)	−0.0523(6)	0.3709(3)	0.060(2)
P(4)	0.10885(15)	0.28435(13)	0.40379(11)	0.038	C(G1)	0.5118(7)	−0.0230(5)	0.2006(7)	0.051(2)
P(5)	−0.02023(15)	0.30118(12)	0.10641(1)	0.037	C(G2)	0.5040(8)	−0.0738(3)	0.2531(6)	0.078(3)
P(6)	0.03969(15)	0.43991(12)	0.14921(10)	0.040	C(G3)	0.5779(5)	−0.1446(4)	0.2611(3)	0.094(4)
P(7)	0.43879(15)	0.13469(12)	0.17581(10)	0.042	C(G4)	0.6597(6)	−0.1646(5)	0.2166(6)	0.086(3)
P(8)	0.4465(2)	0.3500(2)	0.5820(2)	0.073	C(G5)	0.6676(7)	−0.1137(3)	0.1641(5)	0.096(4)
F(1)	0.3567(7)	0.3761(6)	0.5342(5)	0.163	C(G6)	0.5937(4)	−0.0429(5)	0.1561(4)	0.074(3)
F(2)	0.3749(9)	0.3201(7)	0.6307(5)	0.192	C(H1)	0.4980(4)	0.1704(4)	0.0518(4)	0.053(2)
F(3)	0.4800(7)	0.2682(5)	0.5491(6)	0.178	C(H2)	0.4569(7)	0.1750(6)	−0.0112(3)	0.074(3)
F(4)	0.4089(8)	0.4290(6)	0.6187(6)	0.181	C(H3)	0.4746(8)	0.2265(7)	−0.0601(4)	0.112(4)
(F5)	0.5068(10)	0.3835(9)	0.5346(7)	0.253	C(H4)	0.5333(4)	0.2734(4)	−0.0461(3)	0.116(5)
F(6)	0.5314(9)	0.3269(7)	0.6283(8)	0.257	C(H5)	0.5744(7)	0.2688(7)	0.0169(3)	0.102(4)
O(1)	0.4342(4)	0.0488(3)	0.1972(3)	0.051	C(H6)	0.5568(8)	0.2173(8)	0.0658(4)	0.072(3)
O(2)	0.4785(4)	0.1174(3)	0.0979(3)	0.050	C(I1)	0.5587(9)	0.1564(7)	0.2697(2)	0.050(2)
O(3)	0.5462(4)	0.1339(3)	0.2048(3)	0.048	C(I2)	0.5710(8)	0.1028(5)	0.3230(4)	0.069(3)
O(4)	0.4107(5)	0.3448(4)	0.1554(4)	0.075	C(I3)	0.5863(4)	0.1244(4)	0.3872(4)	0.088(3)
O(5)	0.3555(4)	0.2470(4)	0.3484(3)	0.069	C(I4)	0.5894(7)	0.1995(6)	0.3981(2)	0.084(3)
O(6)	0.2423(5)	0.2316(5)	0.0479(3)	0.080	C(I5)	0.5771(7)	0.2531(4)	0.3448(4)	0.076(3)
O(S)	0.8429(14)	0.2216(11)	0.6671(10)	0.256(8)	C(I6)	0.5618(5)	0.2315(6)	0.2806(4)	0.064(3)
C(1S)[b]	0.786(2)	0.221(1)	0.730(1)	0.21(1)	C(J1)	0.1605(5)	0.2278(6)	0.4794(5)	0.045(2)
C(2S)	0.7022(14)	0.2167(11)	0.7784(9)	0.152(6)	C(J2)	0.2510(4)	0.2291(3)	0.5039(2)	0.055(2)
C(1)	0.1840(6)	0.0432(4)	0.2396(4)	0.041	C(J3)	0.2921(5)	0.1811(6)	0.5580(4)	0.064(3)
C(2)	0.1537(6)	0.3709(5)	0.4072(4)	0.043	C(J4)	0.2428(5)	0.1317(5)	0.5878(4)	0.085(3)
C(3)	0.0179(6)	0.3874(5)	0.0751(4)	0.045	C(J5)	0.1523(4)	0.1304(4)	0.5633(3)	0.097(4)
C(4)	0.3687(7)	0.3009(6)	0.1722(5)	0.056	C(J6)	0.1111(6)	0.1784(7)	0.5092(5)	0.072(3)
C(5)	0.3273(6)	0.2394(5)	0.2959(4)	0.052	C(K1)	0.0431(7)	0.5211(4)	0.3436(3)	0.044(2)
C(6)	0.2546(6)	0.2298(5)	0.1050(4)	0.051	C(K2)	−0.0386(4)	0.5251(3)	0.3864(4)	0.052(2)
C(A1)	−0.0818(6)	0.5131(5)	0.1614(6)	0.046(2)	C(K3)	−0.1159(5)	0.5944(3)	0.3915(4)	0.065(3)
C(A2)	−0.1334(4)	0.5129(6)	0.2223(5)	0.051(2)	C(K4)	−0.1116(6)	0.6598(3)	0.3539(5)	0.066(3)
C(A3)	−0.2280(6)	0.5650(4)	0.2322(3)	0.069(3)	C(K5)	−0.0299(3)	0.6558(3)	0.3112(3)	0.075(3)
C(A4)	−0.2711(6)	0.6174(4)	0.1811(5)	0.077(3)	C(K6)	0.0474(6)	0.5865(3)	0.3060(5)	0.060(2)
C(A5)	−0.2195(4)	0.6176(5)	0.1201(4)	0.074(3)	C(L1)	−0.0248(6)	0.3267(5)	0.4235(6)	0.043(2)
C(A6)	−0.1248(7)	0.5655(3)	0.1103(4)	0.065(3)	C(L2)	−0.0587(5)	0.3443(7)	0.4894(5)	0.063(3)
C(B1)	0.1234(4)	0.4936(5)	0.1115(3)	0.049(2)	C(L3)	−0.1580(7)	0.3854(5)	0.5027(3)	0.081(3)
C(B2)	0.1088(7)	0.5713(3)	0.1262(6)	0.065(3)	C(L4)	−0.2234(6)	0.4089(4)	0.4501(5)	0.084(3)
C(B3)	0.1809(7)	0.6068(4)	0.1070(4)	0.084(3)	C(L5)	−0.1894(6)	0.3914(6)	0.3843(4)	0.078(3)
C(B4)	0.2676(4)	0.5645(4)	0.0731(3)	0.082(3)	C(L6)	−0.0902(8)	0.3503(4)	0.3710(4)	0.057(2)
C(B5)	0.2822(7)	0.4868(3)	0.0584(5)	0.076(3)	C(M1)	0.2536(4)	0.4554(5)	0.3185(4)	0.044(2)
C(B6)	0.2101(8)	0.4513(4)	0.0776(4)	0.063(3)	C(M2)	0.3021(5)	0.4653(3)	0.3755(3)	0.060(2)
C(C1)	−0.0110(4)	0.0692(5)	0.1845(4)	0.042(2)	C(M3)	0.3848(6)	0.4921(6)	0.3691(3)	0.071(3)
C(C2)	−0.1030(5)	0.1244(3)	0.1753(3)	0.055(2)	C(M4)	0.4191(4)	0.5089(4)	0.3057(3)	0.073(3)
C(C3)	−0.1900(5)	0.1045(5)	0.1878(5)	0.070(3)	C(M5)	0.3706(5)	0.4990(4)	0.2487(2)	0.067(3)
C(C4)	−0.1850(4)	0.0293(4)	0.2096(3)	0.069(3)	C(M6)	0.2878(7)	0.4722(7)	0.2551(3)	0.053(2)
C(C5)	−0.0930(5)	−0.0260(3)	0.2188(4)	0.077(3)	C(N1)	−0.1482(6)	0.3447(4)	0.1399(6)	0.041(2)
C(C6)	−0.0060(5)	−0.0060(5)	0.2063(6)	0.064(3)	C(N2)	−0.2180(6)	0.3973(4)	0.1004(3)	0.062(2)
C(D1)	0.1604(8)	0.0488(4)	0.0943(4)	0.040(2)	C(N3)	−0.3161(4)	0.4267(6)	0.1238(5)	0.080(3)
C(D2)	0.1007(6)	0.0428(5)	0.0421(6)	0.055(2)	C(N4)	−0.3445(5)	0.4035(4)	0.1868(5)	0.085(3)
C(D3)	0.1440(6)	0.0067(6)	−0.0171(4)	0.067(3)	C(N5)	−0.2747(5)	0.3509(4)	0.2263(3)	0.080(3)
C(D4)	0.2469(7)	−0.0234(4)	−0.0240(4)	0.064(3)	C(N6)	−0.1766(5)	0.3215(6)	0.2029(6)	0.051(2)
C(D5)	0.3067(5)	−0.0173(5)	0.0282(5)	0.087(3)	C(O1)	−0.0414(9)	0.2569(6)	0.0270(3)	0.045(2)
C(D6)	0.2634(7)	0.0188(7)	0.0874(3)	0.071(3)	C(O2)	−0.1236(7)	0.2303(3)	0.0213(4)	0.057(2)
C(E1)	0.0442(6)	0.0903(5)	0.3566(6)	0.049(2)	C(O3)	−0.1340(5)	0.1918(5)	−0.0361(3)	0.074(3)
C(E2)	−0.0397(4)	0.1500(4)	0.3380(3)	0.062(3)	C(O4)	−0.0622(7)	0.1798(5)	−0.0879(3)	0.077(3)
C(E3)	−0.1329(6)	0.1519(6)	0.3648(6)	0.095(4)	C(O5)	0.0200(6)	0.2064(3)	−0.0822(4)	0.074(3)
C(E4)	−0.1422(6)	0.0941(5)	0.4103(5)	0.108(4)	C(O6)	0.0304(6)	0.2449(6)	−0.0248(3)	0.058(2)
C(E5)	−0.0583(5)	0.0344(5)	0.4289(4)	0.114(5)					

[a] *U* is the isotropic displacement parameter, and for other atoms $U = {}^1/_3 \sum_{i=1}^{3}\sum_{j=1}^{3} U_{ij} a_i^* a_j^* (\vec{a}_i \cdot \vec{a}_j)$. [b] Atoms in the solvent molecule are labeled by S.

about 2 mL, followed by precipitation of the product as a dark brown solid using pentane. It was washed with pentane, dried under vacuum, and recrystallized from CH_2Cl_2/diethyl ether. Yield: 90%. Anal. Calcd for $C_{80}H_{68}O_3F_6P_7RePt_3$: C, 44.1; H, 3.2. Found: C, 43.9; H, 2.8. IR (Nujol): ν(CO)/cm^{-1} = 1979 s, 1886 s, 1867 s. NMR in CD_2Cl_2: δ(^{1}H) 6.00 [br, 2H, H_2C_2]; 5.87 [br, H_2CP_2]; 4.95 [br, H_2CP_2]; 3.92 [m, H_2CP_2]; δ(^{31}P) 25.2 [m, ^1J(PtP) = 3073 Hz, dppm], −1.1 [m, ^1J(PtP) = 2462 Hz, dppm], −15.3 [m, ^1J(PtP) = 4567 Hz, dppm]; δ(^{13}C) 85.2 (br, H_2C_2).

[Pt$_3${Re(CO)$_3$(PhC≡CH)}(μ-dppm)$_3$][PF$_6$]·CH$_2$Cl$_2$. This was prepared in a similar way except that the reagent phenylacetylene (0.2 mL) was used. The complex was recrystallized from CH_2Cl_2/diethyl ether. Yield: 70%. Anal. Calcd for $C_{87}H_{74}O_3F_6P_7Cl_2RePt_3$: C, 44.6; H, 3.1. Found: C, 44.9; H, 3.2%. IR (Nujol): ν(CO)/cm^{-1} = 1977 vs, 1882 s, 1863 s. NMR in CD_2Cl_2: δ(^{1}H) 5.50 [br, 1H, PhC$_2$*H*]; 5.18 [m, 2H, H_2CP_2]; 4.31 [m, 2H, H_2CP_2]; 3.88 [m, 2H, H_2CP_2]; δ(^{31}P) 21.3 [m, ^1J(PtP) = 3037 Hz, dppm], 13.9 [m, ^1J(PtP) = 3100 Hz, dppm], −0.4 [m, ^1J(PtP) = 2575 Hz, dppm]; −6.3 [m, ^1J(PtP)

= 2502 Hz, dppm], −16.9 [m, ^1J(PtP) = 4494 Hz, dppm], −20.5 [m, ^1J(PtP) = 4494 Hz, dppm].

Reactions of [Pt$_3${Re(CO)$_4$}(μ-dppm)$_3$][PF$_6$]. To a solution of **6** (28 mg, 0.013 mmol) in acetone (0.5 mL) was added Et_4NBr (2.7 mg, 0.013 mmol). A brown precipitate formed immediately with the evolution of CO. This precipitate was further washed with acetone (0.5 mL) to give [Pt$_3$(μ_3-Br){Re(CO)$_3$}(μ-dppm)$_3$] as a red brown powder, identified by its NMR and IR spectra. Yield: 70%. Similar reactions of **6** with Et_4NCl and Bu_4NI give complexes [Pt$_3$(μ_3-Cl){Re(CO)$_3$}(μ-dppm)$_3$] in 55% yield and [Pt$_3$(μ_3-I){Re(CO)$_3$}(μ-dppm)$_3$] in 80% yield, respectively.

Similarly, reaction of **6** (35 mg, 0.016 mmol) in acetone (15 mL) with P(OMe)$_3$ (1.9 μL, 0.016 mmol) gave [Pt$_3${Re(CO)$_3$(P(OMe)$_3$)}(μ-dppm)$_3$][PF$_6$] in 88% yield. The product was characterized by its NMR and IR spectra. Similar reactions with P(OPh)$_3$, HCCH and PhCCH afforded [Pt$_3${Re(CO)$_3$(P(OPh)$_3$)}(μ-dppm)$_3$][PF$_6$] in 85% yield, [Pt$_3${Re(CO)$_3$(HCCH)}(μ-dppm)$_3$][PF$_6$] in 90% yield and [Pt$_3${Re(CO)$_3$(PhCCH)}(μ-dppm)$_3$][PF$_6$] in 87% yield, respectively. Reactions of [Pt$_3${Re(CO)$_3$(HCCH)}(μ-dppm)$_3$][PF$_6$] with P(OMe)$_3$ or P(OPh)$_3$ to give [Pt$_3${Re(CO)$_3$(P(OMe)$_3$)}(μ-dppm)$_3$][PF$_6$] or [Pt$_3${Re(CO)$_3$(P(OPh)$_3$)}(μ-dppm)$_3$][PF$_6$] were carried out in a similar way.

X-ray Crystal Structure Analysis of 5[PF$_6$]·EtOH. The crystal was a red chunk of approximate dimensions 0.33 × 0.25 × 0.15 mm^3. The X-ray crystallographic measurements were made at 23 °C, with graphite-monochromated Mo K_α radiation and an Enraf-Nonius CAD4 diffractometer.

The unit cell constants (Table 2) were determined by a least-squares treatment of 25 reflections with Bragg angles 20.8 < θ < 22.9°. The intensities of diffracted beams were measured by continuous $\theta/2\theta$ scans of width (0.99 + 0.59 tan θ)° in θ. The scan speeds were adjusted to give $\sigma(I)/I$ < 0.03, subject to a time limit of 30 s. Intensities of three reflections, remeasured every 2 h, decreased by 21% of their mean initial value during the data collection. The intensities of all reflections, derived in the usual manner (q = 0.03),[21] were corrected for Lorentz, polarization, and crystal decomposition effects. The absorption correction was made at the end of isotropic refinement, using the empirical correction of Walker and Stuart.[22] The 6187 symmetry-related reflections were averaged to obtain 2999 independent ones and R(merge) = 0.031. Of 28 429 unique reflections measured, only 14 765 with $I > 3\sigma(I)$ were used in the structure analysis.

The positions of the platinum and rhenium atoms were determined from a Patterson function and those of the remaining non-hydrogen atoms from the subsequent difference Fourier syntheses. Hydrogen atoms were included in the structural model in calculated positions, and their displacement parameters were fixed at U(H) = 1.2 U(C), where U(C) is the equivalent isotropic displacement parameter of the carbon atom to which the hydrogen is bonded. No allowance was made for scattering of the hydrogen atoms of the solvent molecule. The structure was refined by full-matrix least-squares, minimizing the function $\Sigma w(|F_o| - |F_c|)^2$, where $w = \sigma|F_o|^{-2}$. The carbon and hydrogen atoms of each phenyl group were treated as a rigid body with D_{6h} symmetry, C−C = 1.38 Å and C−H = 0.96 Å. The carbon and oxygen atoms of the phenyl groups and solvent molecule were refined with isotropic displacement parameters, and the remaining non-hydrogen atoms with anisotropic displacement parameters. The atomic scattering factors and anomalous dispersion corrections were taken from the *International Tables for X-ray Crystallography*.[23] The refinement of the structure, involving 464 variables and 14 765 reflections with $I > 3\sigma(I)$, converged at R = 0.0405 and R_w = 0.0429. The residual electron density showed no chemically significant features. The final atomic coordinates and atomic displacement parameters are listed in Table 3. All calculations were performed using the GX program package.[24]

EHMO Calculations. These were carried out using the program CACAO. The geometry used was based on a planar D_{3h} [Pt$_3$(CO)$_6$] unit with d(Pt−Pt) = 2.6 Å and d(Pt−C) = 2.0 Å. The [Re(CO)$_4$]$^+$ unit was based on an octahedral fragment with d(Pt−Re) = 2.7 Å and d(Re−C) = 2.0 Å.

Acknowledgment. We thank the NSERC (Canada) for financial support, SERC (U.K.) for an equipment grant, and the Iranian government for a studentship (to A.A.T.).

Supporting Information Available: Tables giving H atom coordinates, anisotropic displacement parameters, and bond lengths and angles (6 pages). Ordering information is given on any current masthead page.

OM9502852

(21) Manojlović-Muir, Lj.; Muir, K. W. *J. Chem. Soc., Dalton Trans.* **1974**, 2427.
(22) Walker, N.; Stuart, D. *Acta Crystallogr.* **1983**, *A39*, 158.
(23) *International Tables for X-ray Crystallography*; Kynoch Press: Birmingham, U.K., **1974**; Vol. IV.
(24) Mallinson, P. R.; Muir, K. W. *J. Appl. Crystallogr.* **1985**, *18*, 51.

Synthesis and Structural Characterization of the Luminescent Gold(I) Complex $[(MeTPA)_3AuI]I_3$. Use of $NaBPh_4$ as a Phenyl-Transfer Reagent To Form $[(MeTPA)AuPh](BPh_4)$ and (TPA)AuPh

Jennifer M. Forward, John P. Fackler, Jr.,* and Richard J. Staples

Department of Chemistry and Laboratory of Molecular Structure and Bonding, Texas A&M University, College Station, Texas 77843-3255

Received April 5, 1995[⊗]

The luminescent gold(I) complex $[(MeTPA)_3AuI]I_3 \cdot 2H_2O$ (**1**) has been synthesized and structurally characterized, where [MeTPA]I is 1-methyl-1-azonia-3,5-diaza-7-phosphaadamantane iodide. This complex shows an interesting temperature-dependent emission spectrum in the solid state. It gives a yellow emission (598 nm) at 77 K and an orange emission (686 nm) at 140 K. Compound **1** is soluble in water and undergoes an unusual phenyl-transfer reaction in aqueous solution with $NaBPh_4$ to form $[(MeTPA)AuPh](BPh_4)$ (**2**). The closely related complex $[(TPA)_3Au]Cl$, containing the 1,3,5-triaza-7-phosphaadamantane ligand (TPA), also undergoes a similar reaction with $NaBPh_4$ to form (TPA)AuPh (**3**). Compounds **2** and **3** both have been crystallographically characterized.

Introduction

Although the usual coordination observed for Au(I) is linear two-coordination, there are examples of both trigonal-planar and tetrahedral gold complexes that have been structurally characterized.[1] Three-coordinate gold(I) complexes are of special interest, due to the luminescent properties that appear to be associated with gold(I) centers in a trigonal-planar environment. Fackler and co-workers have demonstrated that while the $[(Ph_3P)_3Au]^+$ species shows a strong emission in acetonitrile solutions at 512 nm, the bis- and tetrakis(phosphine) complexes $[(Ph_3P)_2Au]^+$ and $[(Ph_3P)_4Au]^+$ show no emission.[2] Several other three-coordinate gold(I) complexes have been structurally characterized, mainly utilizing polydentate phosphines. Gray has synthesized the complex $[(dcpe)_3Au_2](PF_6)$ with the bidentate phosphine complex dcpe (dcpe = 1,2-bis(dicyclohexylphosphino)ethane), which contains two well-separated P_3Au units.[3] This complex luminesces both in acetonitrile solution (508 nm) and in the solid state (501 nm) with a lifetime in solution of 21 ms. The tridentate phosphine np_3 (np_3 = tris(2-(diphenylphosphino)ethyl)amine) has also been used to form the mononuclear and dinuclear three-coordinate gold(I) complexes $[(np_3)Au](PF_6)$ and $[(np_3)_2Au_2](BPh_4)_2$ which show luminescence in the solid state but not in solution.[4] However, only a few three-coordinate species have been structurally characterized with monodentate phosphines. Two examples are the triphenylphosphine complexes $[(Ph_3P)_3Au](BPh_4)$[5] and $[(Ph_3P)_3Au](B_9H_{12}S)$.[6] Alkylphosphines such as PMe_3 and PEt_3 form three- and four-coordinate species in solution, as shown by $^{31}P\{^1H\}$ NMR studies, but crystallize as the bis(phosphines) $[(R_3P)_2Au]^+$, even in the presence of excess ligand.[1]

The 1,3,5-triaza-7-phosphaadamantane ligand (TPA) has been of special interest to us due to several of its unique features. It has a very small cone angle (102°), it is water-soluble, and it is air- and water-stable. Several gold(I) complexes have been synthesized and structurally characterized with this ligand, including (TPA)AuCl,[7] $(TPA)_2AuCl$,[8] and $[(HTPA)_3(TPA)Au]Cl_4$.[9] The four-coordinate complex has three of the ligands protonated on a nitrogen center and forms a well-ordered hydrogen-bonded network in the solid state. The three-coordinate complex $[(TPA)_3Au]Cl$ has been synthesized, but unfortunately no single crystals have been formed. This complex is water-soluble and is luminescent both in aqueous solution (547 nm) and in the solid state (533 nm).[10] Repeated attempts to crystallize this species formed the tetrahedral four-coordinate species, which appears to be strongly favored by its hydrogen-bonding network. Coordinating an alkyl group such as methyl to one of the nitrogen centers to form [MeTPA]I is expected to reduce the sites for hydrogen bonding and hence the propensity of the system to form four-coordinate species. Fortunately, this proved to be the case and single crystals of $[(MeTPA)_3AuI]I_3$ (**1**) can be synthesized in relatively high yields. These single crystals are water-soluble and show interesting luminescence properties in the solid state. Surprisingly, both **1** and $[(TPA)_3Au]Cl$ react with $NaBPh_4$ in water

* To whom correspondence should be addressed.

⊗ Abstract published in *Advance ACS Abstracts,* August 1, 1995.

(1) Puddephatt, R. H. In *Comprehensive Coordination Chemistry;* Wilkinson, G., Ed.; Pergamon Press: Oxford, U.K., 1987; Vol. 5, pp 869–886.

(2) King, C.; Khan, M. N. I.; Staples, R. J.; Fackler, J. P., Jr. *Inorg. Chem.* **1992**, *31*, 3236.

(3) McCleskey, T. M.; Gray, H. B. *Inorg. Chem.* **1992**, *31*, 1734.

(4) (a) Khan, M. N. I.; Staples, R. J.; King, C.; Fackler, J. P., Jr.; Winpenny, R. E. P. *Inorg. Chem.* **1993**, *32*, 5800. (b) Forward, J. M.; Fackler, J. P., Jr.; Staples, R. J. Manuscript in preparation.

(5) Jones, P. J. *Acta Crystallogr.* **1980**, *B36*, 3105.

(6) Guggenberger, L. J. *J. Organomet. Chem.* **1974**, *81*, 271.

(7) Assefa, Z.; McBurnett, B. G.; Fackler, J. P., Jr.; Staples, R. J.; Assmann, B.; Angermaier, K.; Schmidbaur, H. *Inorg. Chem.* **1995**, *34*, 75.

(8) Assefa, Z.; Staples, R. J.; Fackler, J. P., Jr. *Acta. Crystallogr.*, submitted for publication.

(9) Forward, J. M.; Assefa, Z.; Staples, R. J.; Fackler, J. P., Jr. Manuscript in preparation.

(10) Forward, J. M.; Assefa, Z.; Fackler, J. P., Jr. Manuscript in preparation.

0276-7333/95/2314-4194$09.00/0

Table 1. Crystallographic Data

	[(MeTPA)$_3$AuI]I$_3$·2H$_2$O (**1**)	[(MeTPA)AuPh](BPh$_4$) (**2**)	(TPA)AuPh (**3**)
chem formula	$C_{21}H_{49}N_3P_3I_4AuO_2$	$C_{37}H_{40}AuBN_3P$	$C_{12}H_{17}AuN_3P$
mol wt	1257.2	765.5	431.2
cryst size, mm	0.4 × 0.3 × 0.1	0.2 × 0.2 × 0.04	0.16 × 0.04 × 0.04
cryst syst	orthorhombic	monoclinic	monoclinic
space group	*Pnma* (No. 62)	$P2_1/n$ (No. 14)	$P2_1/n$ (No. 14)
a, Å	14.034(3)	11.181(3)	6.142(2)
b, Å	17.864(2)	18.782(9)	17.754(6)
c, Å	15.205(3)	16.106(3)	11.892(3)
β, deg		107.57(2)	103.02(2)
V, Å^3	3792(1)	3224(2)	1263.4(7)
Z	4	4	4
μ, mm^{-1}	7.22	4.64	11.75
D_c, g cm^{-3}	2.19	1.58	2.27
temp, K	298	298	298
radiation (λ, Å)		graphite-monochromated Mo Kα (0.710 73)	
transmissn factors: min, max	0.5060, 0.9990	0.9782, 1.0237	0.488, 0.978
R,[a] R_w[b]	0.0415, 0.0546	0.0678, 0.0885	0.0531, 0.0813

[a] $R = \Sigma||F_o| - |F_c||\Sigma|F_o|$. [b] $R_w = [\Sigma w^{1/2}(|F_o| - |F_c|)]/\Sigma w|F_o|$.

to form Au(I) phenyl phosphine products, which are described here.

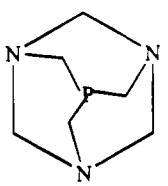

TPA

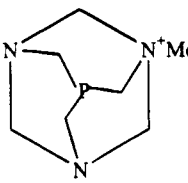

[MeTPA]I

Experimental Section

All experiments were routinely carried out under pure dry nitrogen using a standard Schlenk line apparatus. The organic solvents were rigorously dried before use. The TPA[11] and [MeTPA]I[12] ligands and (Me$_2$S)AuCl[13] and [(TPA)$_3$Au]Cl[10] were synthesized as reported in the literature. NaBPh$_4$ was purchased from Aldrich and used without further purification.

X-ray structural analysis was performed on a Nicolet R3m/E diffractometer employing SHELXS and a Micro-Vax II computer. The $^{31}P\{^1H\}$ NMR spectra were collected on a Varian XL-200E spectrometer operating at 81 MHz, in 10 mm tubes. Chemical shifts, in ppm, were referenced to an external standard of 80% H_3PO_4. ^1H NMR spectra were recorded on a Varian XL-200 spectrometer. Emission and excitation spectra were measured at 77 K with a SLM/AMINCO Model 8100 spectrofluorometer using a xenon lamp. Spectra were corrected for instrumental response.

Synthesis. [(MeTPA)$_3$AuI]I$_3$ (1). (Me$_2$S)AuCl (0.07 g, 2.38 × 10^{-4} mol) was stirred in 10 mL of CH_2Cl_2/H_2O (1:1). Three equivalents of [MeTPA] (0.213 g, 7.13 × 10^{-4} mol) were added in one portion, and the reaction mixture was stirred vigorously in a foil-wrapped Schlenk flask for 1 h. After separation of the aqueous layer 1 equiv of KI was added (0.039 g, 2.38 × 10^{-4} mol) causing the precipitation of a white solid. The solution was filtered off, and the precipitate was washed with cold ethanol (3 × 5 mL). Recrystallization of this precipitate from H_2O gave a white crystalline precipitate of [(MeTPA)$_3$AuI]I$_3$ (yield 62%). $^{31}P\{^1H\}$ NMR (D_2O/H_2O, H_3PO_4): −54.4 ppm.

[(MeTPA)AuPh](BPh$_4$) (2). [(MeTPA)$_3$AuI]I$_3$ (0.132 g, 1.08 × 10^{-4} mol) was stirred in 15 mL of H_2O. Five equivalents of NaBPh$_4$ (0.184 g, 5.40 × 10^{-4} mol) were added, causing the precipitation of a white solid. After the reaction mixture was stirred for 1 h, the solution was filtered off and the precipitate was washed with 3 × 5 mL of H_2O. Recrystallization from acetone/water gave a white crystalline solid of [(MeTPA)AuPh](BPh$_4$) (yield 69%). $^{31}P\{^1H\}$ NMR (D_2O/H_2O, H_3PO_4): −82.8 ppm (broad). ^1H NMR (acetone-d_6): 6.8−7.0 (m, 5H), 3.9−5.2 (m, 12H), 2.8 ppm (s, 3H).

[(MeTPA)$_3$AuI](PF$_6$)$_3$. [(MeTPA)$_3$AuI]I$_3$ (0.1 g, 8.17 × 10^{-5} mol) was dissolved in water, and 4 equiv of $NaPF_6$ was added (0.055 g, 3.27 × 10^{-4} mol). A white solid precipitated, and after the reaction mixture was stirred for 1 h, the solution was filtered and the solid washed with 3 × 5 mL of cold water. Recrystallization from hot water gave the white microcrystalline solid [(MeTPA)$_3$AuI](PF$_6$)$_3$ (yield 61%). $^{31}P\{^1H\}$ NMR (D_2O/H_2O, H_3PO_4): −59.4, 79.0 ppm (sept, PF_6).

(TPA)AuPh (3). The same reaction was repeated using [(TPA)$_3$Au]Cl (0.060 g, 8.53 × 10^{-5} mol) and NaBPh$_4$ (0.1458 g, 4.26 × 10^{-4} mol). The white product, (TPA)AuPh, was moderately soluble in acetone and soluble in acetonitrile. Recrystallization from acetonitrile/diethyl ether yielded 41% of the product. ^1H NMR (CD_3CN): 6.8−7.0 (m, 5H), 4.5 (d, 6H), 4.2 ppm (s, 6H).

X-ray Structural Characterization

Compound **1** was crystallized from H_2O, compound **2** was crystallized from acetone/H_2O, and compound **3** was crystallized from CH_3CN/Et_2O. Single crystals of each compound were mounted on glass fibers with epoxy resin, and data were collected. The details of the data collection and the refinement have been published.[14] No decay was observed for the chosen standard reflections. Crystallographic data are contained in Table 1. The data have been corrected for decay and for Lorentz and polarization effects. Heavy-atom positions were determined from direct methods and used as the initial phasing model for difference Fourier synthesis. All nonhydrogen atoms were refined anisotropically. Hydrogen atoms were fixed to the carbon atoms in idealized positions at a distance of 0.96 Å.

The structure of **1** is shown in Figure 1. Atomic coordinates are given in Table 2 and selected bond angles and distances are given in Table 3. The coordination environment of the three monodentate phosphines around the gold(I) center is approximately trigonal planar, where the gold lies out of the plane formed by the three phosphorus atoms by 0.375 Å toward the iodide. The iodide is weakly coordinated to the gold atom perpendicular to the P_3Au plane at a

(11) Daigle, D. J.; Pepperman, A. B. *J. Heterocycl. Chem.* **1975**, *12*, 579.
(12) Daigle, D. J.; Pepperman, A. B., Jr.; Vail, S. L. *J. Heterocycl. Chem.* **1974**, *11*, 407.
(13) Tamaki, A.; Kochi, J. K. *J. Organomet. Chem.* **1974**, *64*, 411.
(14) Porter, L. C.; Khan, M. N. I.; King, C.; Fackler, J. P., Jr. *Acta Crystallogr.* **1989**, *C45*, 947.

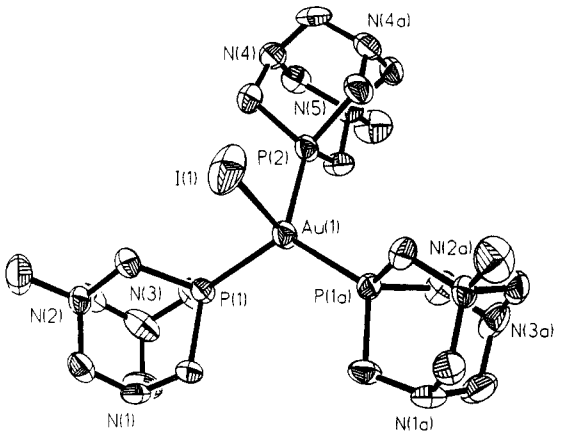

Figure 1. Drawing of $[(MeTPA)_3AuI]I_3 \cdot 2H_2O$ (**1**) (50% probability ellipsoids). The iodides and water molecules have been omitted for clarity.

Table 2. Atomic Coordinates ($\times 10^4$) and Equivalent Isotropic Displacement Parameters ($Å^2 \times 10^3$) for $[(MeTPA)_3AuI]I_3 \cdot 2H_2O$ (1)

	x	*y*	*z*	*U*(eq)[a,b]
Au(1)	1027(1)	2500	1998(1)	38(1)
I(1)	3104(1)	2500	2229(1)	84(1)
I(2)	4633(1)	2500	−1005(1)	75(1)
I(3)	8395(1)	482(1)	−247(1)	67(1)
P(1)	640(2)	3635(1)	2676(2)	32(1)
P(2)	1022(3)	2500	457(2)	37(1)
N(1)	96(6)	4462(5)	4111(5)	42(3)
N(2)	1284(6)	5048(4)	3164(5)	38(3)
N(3)	−386(7)	4946(5)	2677(6)	55(3)
N(4)	1415(7)	3181(5)	−1116(5)	51(3)
N(5)	−88(9)	2500	−1039(7)	41(4)
C(1)	282(8)	3680(5)	3839(6)	43(3)
C(2)	1591(7)	4330(5)	2732(6)	39(3)
C(3)	−270(8)	4231(6)	2192(6)	47(4)
C(4)	918(8)	4915(6)	4099(6)	45(3)
C(5)	459(9)	5401(6)	2640(6)	48(4)
C(6)	−674(9)	4811(8)	3589(7)	60(4)
C(7)	−161(12)	2500	−43(10)	50(5)
C(8)	1561(9)	3266(6)	−178(7)	51(4)
C(9)	441(8)	3201(6)	−1362(6)	47(4)
C(10)	1859(12)	2500	−1458(10)	54(6)
C(21)	2103(9)	5582(7)	3181(8)	66(5)
C(51)	−1072(12)	2500	−1409(12)	71(7)
O(1)	6712(17)	1577(12)	−1476(13)	46(4)

[a] Equivalent isotropic *U*, defined as one-third of the trace of the orthogonalized $\mathbf{U}_{ij}$ tensor. [b] Estimated standard deviations are given in parentheses.

Table 3. Selected Interatomic Distances (Å) and Angles (deg) for $[(MeTPA)_3AuI]I_3 \cdot 2H_2O$ (1)

Au(1)−I(1)	2.936(1)	N(2)−C(21)	1.49(1)
Au(1)−P(1)	2.339(2)	N(5)−C(51)	1.49(2)
Au(1)−P(2)	2.343(3)		
I(1)−Au(1)−P(1)	100.3(1)	P(1)−Au(1)−P(2)	116.1(1)
I(1)−Au(1)−P(2)	97.0(1)	P(1)−Au(1)−P(1a)	120.2(1)

distance of 2.936(1) Å. The Au−P distances of 2.343(3) and 2.339(2) Å are similar to values observed for related complexes, and the P−Au−P angles are close to 120° (116.1(1) and 120.2(1)°). Each of the phosphine ligands are methylated on only one of the nitrogen centers, where the methyl carbon to TPA nitrogen bond distances are 1.49(1) and 1.49(2) Å. The three iodide anions associated with the methyl groups are not coordinated directly to the complex but hydrogen bond to the two water molecules that crystallize in the lattice. There are no short gold−gold interactions in the solid-state structure, and the closest Au−Au distance is 7.181 Å.

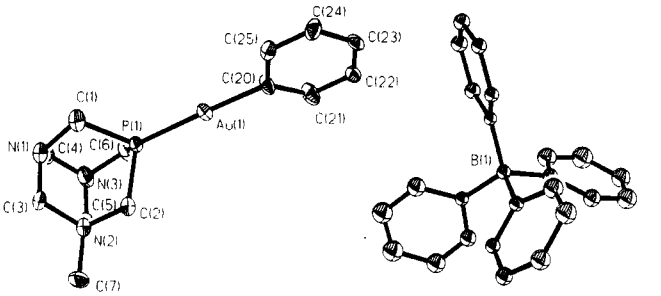

Figure 2. Drawing of $[(MeTPA)AuPh](BPh_4)$ (**2**) (50% probability ellipsoids).

Table 4. Atomic Coordinates ($\times 10^4$) and Equivalent Isotropic Displacement Parameters ($Å^2 \times 10^3$) for [(MeTPA)AuPh][BPh_4] (2)

	x	*y*	*z*	*U*(eq)[a]
Au(1)	608(1)	6170(1)	58(1)	46(1)
P(1)	2246(3)	5981(2)	1280(2)	41(1)
N(1)	3330(11)	5967(7)	3052(6)	54(2)
N(2)	4574(10)	6523(7)	2216(6)	46(2)
N(3)	4296(12)	5220(7)	2221(7)	60(2)
C(1)	2062(12)	6017(9)	2382(7)	62(3)
C(2)	3504(11)	6629(8)	1408(7)	44(3)
C(3)	4141(13)	6563(8)	3025(7)	46(3)
C(4)	3886(14)	5306(8)	2987(8)	60(3)
C(5)	5129(14)	5783(8)	2172(9)	55(3)
C(6)	3181(14)	5180(8)	1441(8)	62(3)
C(7)	5593(13)	7056(8)	2275(9)	61(5)
C(20)	−836(12)	6403(8)	−1032(8)	47(5)
C(21)	−866(13)	6251(9)	−1872(8)	59(5)
C(22)	−1864(13)	6404(7)	−2590(8)	43(5)
C(23)	−2909(12)	6721(8)	−2506(8)	39(4)
C(24)	−2967(13)	6883(8)	−1695(8)	50(5)
C(25)	−1946(13)	6719(7)	−961(8)	41(4)
B(1)	−927(13)	6835(9)	−5649(9)	29(4)
C(101)	−1074(12)	6583(8)	−6686(8)	33(4)
C(102)	−1078(13)	5853(9)	−6881(9)	55(5)
C(103)	−1258(14)	5607(10)	−7732(10)	72(5)
C(104)	−1351(12)	6068(9)	−8390(9)	55(4)
C(105)	−1286(13)	6780(9)	−8218(9)	58(5)
C(106)	−1157(11)	7036(8)	−7382(8)	42(4)
C(107)	−840(11)	7737(7)	−5626(7)	28(3)
C(108)	−1856(13)	8159(8)	−6073(8)	50(4)
C(109)	−1846(12)	8869(10)	−6054(8)	54(4)
C(110)	−725(12)	9215(8)	−5601(8)	46(4)
C(111)	310(11)	8832(8)	−5168(6)	38(3)
C(112)	217(11)	8091(7)	−5167(7)	29(3)
C(113)	412(11)	6537(6)	−5019(8)	28(3)
C(114)	603(12)	6394(7)	−4131(8)	50(4)
C(115)	1795(12)	6215(10)	−3579(8)	63(4)
C(116)	2825(13)	6214(10)	−3888(8)	67(4)
C(117)	2673(13)	6354(8)	−4757(8)	56(4)
C(118)	1509(11)	6502(7)	−5278(8)	40(4)
C(119)	−2069(11)	6550(7)	−5333(7)	23(3)
C(120)	−2197(12)	5804(8)	−5177(8)	37(4)
C(121)	−3200(12)	5531(8)	−4879(8)	41(4)
C(122)	−4029(11)	5976(7)	−4716(7)	38(4)
C(123)	−3950(11)	6712(7)	−4854(7)	31(4)
C(124)	−2971(11)	6985(7)	−5126(7)	27(3)

[a] *U*(eq) is defined as one-third of the trace of the orthogonalized $\mathbf{U}_{ij}$ tensor.

The structure of **2** is shown in Figure 2. Atomic coordinates are given in Table 4, and selected bond angles and distances are given in Table 5. The compound **2** crystallizes in the monoclinic space group $P2_1/n$ with one anion and one cation well-separated in the asymmetric unit. The BPh_4^- anion shows typical bond distances and bond angles. The $[(MeTPA)AuPh]^+$ cation shows an approximately linear coordination about the gold(I) center (P(1)−Au(1)−C(20) = 176.5(5)°). As in

Table 5. Selected Interatomic Distances (Å) and Angles (deg) for [(MeTPA)AuPh](BPh$_4$) (2)

Au(1)–P(1)	2.274(3)	N(2)–C(2)	1.49(1)
Au(1)–C(20)	2.04(1)	N(2)–C(3)	1.52(2)
N(2)–C(7)	1.50(2)	N(2)–C(5)	1.53(2)
N(1)–C(1)	1.50(1)	N(3)–C(4)	1.45(2)
N(1)–C(3)	1.45(2)	N(3)–C(5)	1.43(2)
N(1)–C(4)	1.40(2)	N(3)–C(6)	1.48(1)
P(1)–Au(1)–C(20)	176.5(5)		

Table 6. Atomic Coordinates (×10^4) and Equivalent Isotropic Displacement Parameters (Å^2 × 10^3) for (TPA)AuPh (3)

atom	x	y	z	U(eq)[a]
Au(1)	704(1)	5835(1)	4167(1)	33(1)
P(1)	−693(8)	6710(3)	5232(4)	32(1)
N(1)	−4034(22)	7465(8)	5933(13)	35(3)
N(2)	−1073(24)	8241(9)	5420(13)	43(4)
N(3)	−312(25)	7510(10)	7230(12)	40(4)
C(1)	−3618(27)	6778(9)	5321(16)	37(4)
C(2)	−272(28)	7670(11)	4732(14)	39(5)
C(3)	636(30)	6840(11)	6779(13)	40(4)
C(4)	−3496(30)	8151(10)	5426(17)	45(5)
C(5)	−2716(31)	7445(11)	7137(15)	46(5)
C(6)	170(30)	8198(11)	6676(15)	40(5)
C(7)	2217(31)	5208(10)	3119(16)	38(3)
C(8)	1179(30)	4977(9)	1972(16)	38(3)
C(9)	2330(31)	4663(10)	1235(17)	39(3)
C(10)	4579(31)	4509(10)	1588(16)	41(3)
C(11)	5676(31)	4750(9)	2677(16)	39(3)
C(12)	4541(29)	5083(9)	3440(16)	37(3)

[a] U(eq) is defined as one-third of the trace of the orthogonalized U_{ij} tensor.

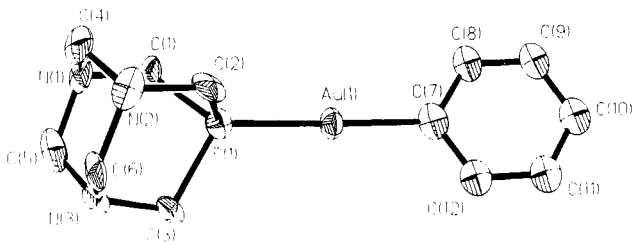

Figure 3. Drawing of (TPA)AuPh (**3**) (50% probability ellipsoids).

compound **1**, the TPA ligand has a methyl group coordinated to one of the nitrogen centers at a distance of 1.50(2) Å. The distances from this methylated nitrogen to the carbon atoms of the TPA are significantly longer than the other C–N bond distances in the ligand (average 1.51 Å compared to 1.45 Å). This has been observed previously for these alkylated TPA ligands and also the protonated TPA ligand, HCl·TPA.[15] There are no close intermolecular gold–gold interactions, and the shortest gold–gold distance is 4.581 Å.

The structure of **3** is shown in Figure 3. Atomic coordinates are given in Table 6, and selected bond distances and angles are given in Table 7. The structure of **3** is similar to that of the cation of compound **2**, but the molecule is neutral and the TPA ligand has only tertiary amine nitrogen sites. The Au(1)–C(7) distance is 2.04(2) Å, almost identical with the distance found for compound **2** (2.04(1) Å), and is within the range expected for related compounds. The coordination of the gold center shows some deviation from linearity (P(1)–Au(1)–C(7) = 170.1(5)°), and this can be seen in Figure 4, the packing diagram viewed along the *c* axis. The

(15) Reibenspies, J. H. Manuscript in preparation.

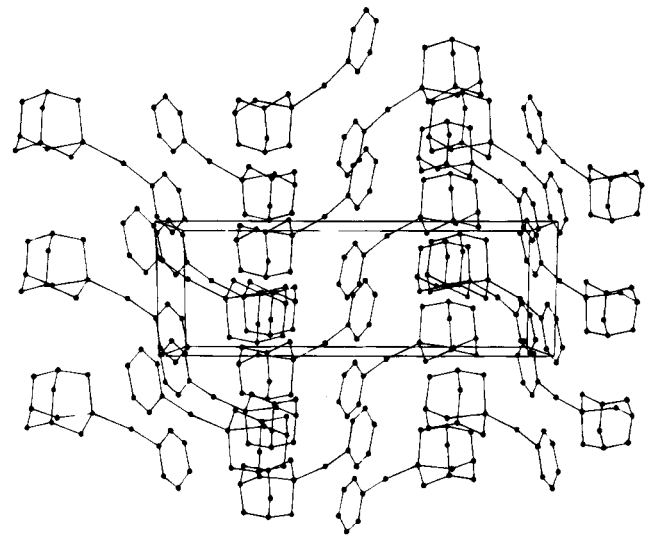

Figure 4. Packing diagram for **3**, viewed along the *c* axis.

Table 7. Selected Interatomic Distances (Å) and Angles (deg) for (TPA)AuPh (3)

Au(1)–P(1)	2.289(5)	N(2)–C(4)	1.50(2)
Au(1)–C(7)	2.040(2)	N(2)–C(6)	1.52(2)
N(1)–C(1)	1.47(2)	N(3)–C(3)	1.48(2)
N(1)–C(4)	1.43(2)	N(3)–C(6)	1.46(2)
N(1)–C(5)	1.48(2)	N(3)–C(6)	1.45(2)
N(2)–C(2)	1.45(2)		
P(1)–Au(1)–C(7)	170.1(5)		

distance between the closest gold centers is 3.774 Å, too long for any significant interaction to be invoked, but the two gold centers appear to be deviating slightly from linear coordination toward each other.

Discussion

Single crystals of compound **1** are readily formed from the slow evaporation of an aqueous solution of the product. The three phosphorus ligands surround the gold in a trigonal-planar arrangement with the gold sitting out of the plane by only 0.375 Å. This compares with a displacement of 0.020 Å for the [(Ph$_3$P)$_3$Au](BPh$_4$) complex,[5] where there is no interaction between the anion and cation. The small distortion toward tetrahedral geometry indicates that the gold–iodide interaction must be relatively weak. In addition, the Au(1)–I(1) distance of 2.936(1) Å is long compared with previously characterized gold(I) iodide complexes, which show distances in the range 2.5–2.6Å. This three-coordinate complex does luminesce in the solid state and shows an interesting temperature-dependent emission (Figure 5). It shows a yellow emission (598 nm) at 77 K (spectrum a) and an orange emission (686 nm) at 140 K (spectrum c) and above. When the emission is monitored over time as the sample is slowly warmed it can be seen that, at a temperature between 77 and 140 K (spectrum b), emission is observed at both 598 and 686 nm. The origin of this behavior, which has not been completely evaluated, probably involves both ligand to metal charge transfer between the iodide and the gold center and metal-centered transitions, results similar to observations made with other gold(I) halide species.[7] The triphenylphosphine complex [(Ph$_3$P)$_3$Au](BPh$_4$) and related complexes containing three-coordinate gold in a trigonal-planar arrangement all show emissions that

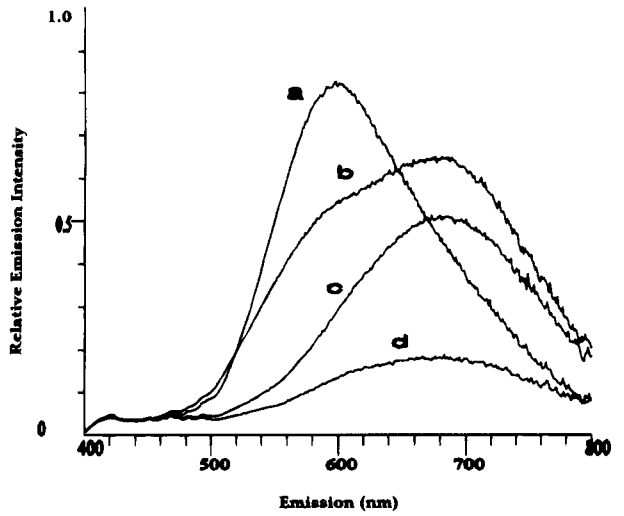

Figure 5. Luminescence of $[(MeTPA)_3AuI]I_3 \cdot 2H_2O$: (a) 77 K; (b) 77–140 K; (c) 140 K; (d) 175 K.

have been assigned as $a_2''(p_z) \rightarrow e'(d_{x^2-y^2},d_{xy})$ metal-centered transitions.[16] However, none of these complexes have a fourth interaction at the gold center. Attempts to replace this iodide with noncoordinating anions have not been successful to date. Reaction of **1** with $NaPF_6$ gives a compound that has been characterized as $[(MeTPA)_3AuI](PF_6)_3$ from $^{31}P\{^1H\}$ NMR and X-ray analysis. Unfortunately, the preliminary data set showed considerable disorder in the structure, mainly with the PF_6 groups. However, it was clear that the gold was trigonal planar with the iodide still coordinated perpendicular to this plane as found in compound **1** and the added $NaPF_6$ had only replaced the three iodides that were associated with the methyl groups on the TPA ligand. The PF_6 complex showed a temperature-dependent emission spectrum similar to the one observed for compound **1**. At 77 K two emission bands were observed, centered at 590 and 680 nm, while at temperatures above 140 K only the band at 680 nm was observed. Neither of these two gold(I) complexes show luminescence in solution.

An exchange reaction similar to the above with $NaPF_6$ was tried with $NaBPh_4$. Interestingly, reaction of **1** with $NaBPh_4$ in aqueous solution caused the rapid precipitation of a white solid which was characterized as [(MeTPA)AuPh](BPh_4) (**2**). The product is formed in high yield and is air- and water-stable. The only source of the phenyl group is $NaBPh_4$. The $[BPh_4]^-$ anion is well-known for participating in phenyl transfer reactions with other transition metals,[17] although this appears to be one of the first reported examples of phenyl transfer to a gold center and the first in water as a solvent. Schmidbaur also has recently observed[18] a similar type of reaction where phenyl(tri-*tert*-butylphosphine)gold(I) is formed from the slow reaction of $[((t\text{-}Bu)_3PAu)_3O](BF_4)$ with sodium tetraphenylborate in ethanol. The only other unsubstituted phenyl gold(I) compound that has been structurally characterized was reported in the literature recently. It was made from the well-established reaction of Ph_3PAuCl with PhLi to form Ph_3PAuPh.[19] Attempts to prepare compound **2** via this route failed, giving decomposition to Au^0.

Compound **3** also was formed from a phenyl-transfer reaction using $NaBPh_4$ and the unsubstituted TPA complex $[(TPA)_3Au]Cl$. This phenyl compound is formed in high yield and is air- and water-stable. As expected, both compounds **2** and **3** show an approximately linear coordination at the gold(I) center. Commonly, linear gold(I) complexes crystallize to form dinuclear species.[20,21] For example, (TPA)AuCl and (TPA)AuBr both show[7] structures wherein two molecules are crossed at approximately 90° to each other with Au–Au distances of 3.092(1) and 3.107(2) Å, respectively. The TPA ligands do not hinder the close approach of two molecules; thus, the lack of Au–Au interactions in **2** and **3** must not be steric in origin.

Pyykkö[22] calculated the strength of the expected interaction between two gold centers in the model system $(XAuPH_3)_2$, where the two $XAuPH_3$ molecules are crossed perpendicular to one another, and correlated the strength of the interaction with the softness of the ligand X. According to these calculations, the phenyl group is expected to lead to a relatively weak gold–gold interaction, weaker than that found with X = Cl. Therefore, the lack of close gold–gold contacts in **2** and **3** and the $(Ph_3P)AuPh$ and $PhAuP(t\text{-}Bu)_3$ complexes observed by Che[19] and Schmidbaur[18] can be explained by considering the electronic effects of the phenyl group. However, the possibility of close-packing forces such as phenyl–phenyl attractions being the reason for the absence of interactions in these complexes has not been completely ruled out.

Linear L_2Au species that do show[7] close Au–Au contacts have interesting luminescence properties which arise from gold-centered transitions that are influenced by the gold–gold distance. As expected, compounds **2** and **3**, which have no significant interactions between the gold centers, show no strong emission, even at 77 K. The weak blue emission centered at 473 nm with excitation at 330 nm, which is observed at liquid-N_2 temperatures for compound **2**, has been assigned as transitions associated with the phenyl groups on the tetraphenylborate anion and the phenol ligand similar to that observed for the PPh_3 ligand.[23]

Acknowledgment. The National Science Foundation (Grant No. CHE9300107) and the Robert Welch Foundation have generously supported these studies.

Supporting Information Available: ORTEP drawings giving additional views and tables giving crystal data and data collection and refinement details, atomic coordinates, thermal parameters, and bond distances and angles for **1**–**3** (25 pages). Ordering information is given on any current masthead page.

OM950246Q

(16) King, C.; Khan, M. N. I.; Staples, R. J.; Fackler, J. P., Jr. *Inorg. Chem.* **1992**, *31*, 3236.
(17) Strauss, S. H., *Chem. Rev.* **1993**, *93*, 927 and references therein.
(18) Sladek, A.; Hofreiter, S.; Paul, M.; Schmidbaur, H. *J. Organomet. Chem.*, in press.
(19) Hong, X.; Cheung, K. K.; Guo, C. X.; Che, C. M. *J. Chem. Soc., Dalton Trans.* **1994**, 1867.
(20) Schmidbaur, H.; Wohlleben, A.; Wagner, F.; Orama, O.; Huttner, G. *Chem. Ber.* **1977**, *110*, 1748.
(21) Bates, P. A.; Waters, J. M. *Inorg. Chim. Acta* **1985**, *98*, 125.
(22) Pyykko, P.; Li, J.; Runeberg, N. *Chem. Phys. Lett.* **1994**, *218*, 133.
(23) Segers, D. P.; DeArmond, M. K.; Grutsch, P. A.; Kutal, C. *Inorg. Chem.* **1984**, *23*, 2874.

Synthesis and Characterization of Fulvene Derivatives of the Ruthenium Carbido Cluster $[Ru_6C(CO)_{17}]$

Alexander J. Blake, Paul J. Dyson, Brian F. G. Johnson,* Simon Parsons, David Reed, and Douglas S. Shephard

Department of Chemistry, The University of Edinburgh, West Mains Road, Edinburgh EH9 3JJ, U.K.

Received March 13, 1995[⊗]

Oxidative removal of two carbonyl ligands using trimethylamine *N*-oxide from the parent cluster, $[Ru_6C(CO)_{17}]$ (**1**), in the presence of 6,6-diphenylfulvene (dpf) affords $[Ru_6C(CO)_{14}(\mu\text{-}\eta^2\text{:}\eta^2\text{-}C_5H_4CPh_2)]$ (**2**). Similarly removal of three carbonyl ligands using trimethylamine *N*-oxide from the parent cluster, $[Ru_6C(CO)_{17}]$ (**1**), in the presence of 6,6-diphenylfulvene (dpf) or 6,6-dimethylfulvene (dmf) affords $[Ru_6C(CO)_{14}(\mu_3\text{-}\sigma\text{:}\eta^2\text{:}\eta^3\text{-}C_5H_4CPh_2)]$ (**3**) and $[Ru_6C(CO)_{14}(\mu_3\text{-}\sigma\text{:}\eta^2\text{:}\eta^3\text{-}C_5H_4CMe_2)]$ (**4**), respectively. In a similar reaction employing cyclopentadiene, the compound $[Ru_6C(CO)_{14}(\mu\text{-}\eta^5\text{:}\eta^1\text{-}C_5H_4CH_2]$ (**6**) has been isolated as a byproduct. Heating **4** in acetonitrile yields $[Ru_6C(CO)_{13}(\mu\text{-}\eta^5\text{:}\eta^3\text{-}C_5H_4C\{CH_2\}_2)]$ (**5**). Further oxidative removal of two carbonyl ligands from **4** in the presence of 6,6-dimethylfulvene and water yields $[Ru_6C(CO)_{12}(\eta^5\text{-}C_5H_4CMe_2H)(\eta^5\text{-}C_5H_4CMe_2OH)]$ (**7**). The solid-state molecular structures of **2**, **3**, and **5**–**7** have been confirmed by single-crystal X-ray structure determinations. All these clusters are based on a *closo*-hexaruthenium carbido cage; in **3** the fulvene ring is bound to a metal face, in **2**, **5**, and **6** the ligand bridges a metal vertex, and in **7** two rings are η^5 bonded to *cis*-ruthenium atoms of the cluster core. A variable-temperature ^1H NMR spectroscopic study of **3** and **4** reveals that a high degree of stereochemically nonrigid behavior occurs in solution.

Introduction

We have developed synthetic routes to a wide variety of compounds containing unsaturated carbocycles bound to a variety of transition metal clusters. These studies have yielded many different modes of coordination of the hydrocarbon, many of which involve bonding of the carbocycle to more than one metal center.[1–6] Structure analysis of these cluster derivatives has provided valuable insight into the surface chemistry of such chemisorbed organic molecules.[7] The redox-active nature of clusters such as $[Ru_6C(CO)_{17}]$[8] has led to interest in the possibility of synthesizing polymeric systems incorporating the active metal sites.

The fulvene ligand has been shown to bond to transition metals in several different modes. Examples of this varied coordination chemistry are best observed within the platinum group metals. Bonding through one of the ring double bonds[9,10] or through the exocyclic double bond[10,11] has been established. Further coordination in an η^4 manner through the two cyclic double bonds[12–17] or alternatively *via* a $\mu\text{-}\eta^2\text{:}\eta^2$ mode through the two cyclic double bonds has also been observed.[13] More commonly, the fulvene ligand acts as a six electron donor,[6,14–24,35] but there are also examples of arylfulvenes acting as eight electron donors.[15,25–27,33–35] A representation of the varied bonding modes of the fulvene ligand is given in Figure 1. However, structural and spectroscopic data on these complexes have shown that interesting and subtle variations in the nature of the bonded fulvene can occur according to the nature of the fulvene and the bonding requirements of the metal coordination site.

[⊗] Abstract published in *Advance ACS Abstracts,* August 1, 1995.

(1) Gomez-Sal, M. P.; Johnson, B. F. G.; Lewis, J.; Raithby, P. R.; Wright, A. H. *J. Chem. Soc., Chem. Commun.* **1985**, 1682.
(2) Braga, D.; Grepioni, F.; Parisini, E.; Dyson, P. J.; Blake, A. J.; Johnson, B. F. G. *J. Chem. Soc., Dalton Trans.* **1993**, 2951.
(3) Dyson, P. J.; Johnson, B. F. G.; Lewis, J.; Martinelli, M.; Braga, D.; Grepioni, F. *J. Am. Chem. Soc.* **1993**, *115*, 9062.
(4) Braga, D.; Grepioni, F.; Sabatino, P.; Dyson, P. J.; Johnson, B. F. G.; Lewis, J.; Raithby, P. R.; Stalke, D. *J. Chem. Soc., Dalton Trans.* **1993**, 2951.
(5) Braga, D.; Grepioni, F.; Parisini, E.; Dyson, P. J.; Johnson, B. F. G.; Reed, D.; Shephard, D. S.; Bailey, P. J.; Lewis, J. *J. Organomet. Chem.* **1993**, *462*, 301.
(6) Blake, A. J.; Dyson, P. J.; Johnson, B. F. G.; Reed, D.; Shephard, D. S. *J. Chem. Soc., Chem. Commun.* **1994**, 1347.
(7) Johnson, B. F. G.; Gallop, M.; Roberts, Y. V. *J. Mol. Catal.* **1994**, *86*, 51.
(8) Johnson, B. F. G.; Drake, S.; Lewis, J. *J. Chem. Soc., Dalton Tran.s* **1991**, 2447.
(9) Jens, K. J.; Edelmann, F.; Behrens, U. *Chem. Ber.* **1978**, *111*, 2895.
(10) Christofides, A.; Howard, J. A. K.; Spencer, J. L.; Stone, F. G. A. *J. Organomet. Chem.* **1982**, *232*, 279.
(11) Altmann, J.; Wilkinson, G. *J. Chem. Soc.* **1964**, 5654.
(12) Weiss, E.; Merényi, R.; Hübel, W. *Chem. Ber.* **1962**, *95*, 1155.
(13) Weiss, E.; Hübel, W. *Chem. Ber.* **1962**, *95*, 1186.
(14) Lubke, B.; Edelmann, F.; Behrens, U. *Chem. Ber.* **1982**, *115*, 1325.
(15) Behrens, U.; Weiss, E. *J. Organomet. Chem.* **1975**, *96*, 399.
(16) Wadepohl, H.; Pritzkow, H. *Acta Crystallogr.* **1991**, *C47*, 2061.
(17) Behrens, U.; Rau, D. *J. Organomet. Chem.* **1990**, *387*, 219.
(18) Behrens, U.; Edelmann, F. *J. Organomet. Chem.* **1977**, *134*, 31.
(19) Bandy, J. A.; Mtetwa, V. S. B.; Prout, K.; Green, J. C.; Davies, C. E.; Green, M. L. H.; Hazel, N. J.; Izquierdo, A.; Martin-Polo, J. J. *J. Chem. Soc., Dalton Trans.* **1985**, 2037.
(20) Andrianov, V. G.; Struchkov, Y. T.; Setkina, V. N.; Zdanovich, V. I.; Zhakaeva, A'Zh.; Kursanov, N. *J. Chem. Soc., Chem. Commun.* **1975**, 117.
(21) Lubke, B.; Edelmann, F.; Behrens, U. *Chem. Ber.* **1983**, *116*, 11.
(22) Drews, R.; Behrens, U. *Chem. Ber.* **1985**, *118*, 888.
(23) Kock, O.; Edelmann, F.; Behrens, U. *Chem. Ber.* **1982**, *115*, 1313.
(24) van Meerssche, M.; Piret, P.; Meunier-Piret, J.; Debgrève, Y. *Bull. Soc. Chim. Belg.* **1964**, *73*, 824.
(25) Behrens, U.; Weiss, E. *J. Organomet. Chem.* **1975**, *96*, 435.
(26) Kock, O.; Behrens, U. *Chem. Ber.* **1978**, *111*, 1998.
(27) Töfke, S.; Haupt, E. T. K.; Behrens, U. *Chem. Ber.* **1986**, *119*, 96.

0276-7333/95/2314-4199$09.00/0

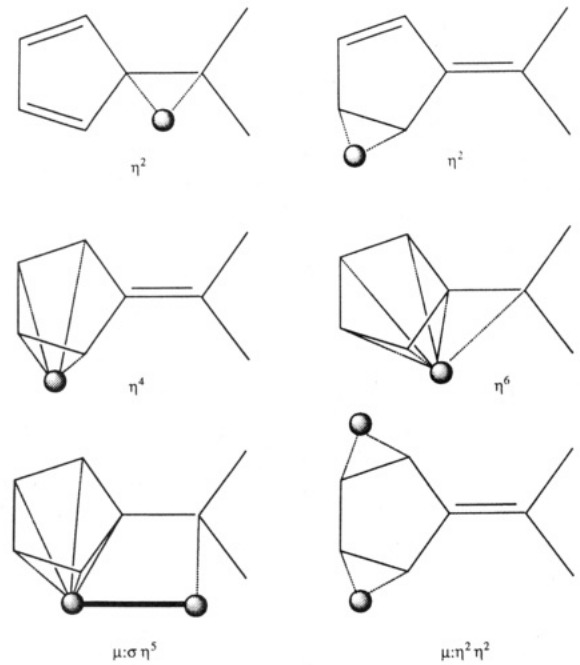

Figure 1. Previously observed bonding modes of fulvenes.

The chemical reactivity of fulvene derivatives is exceedingly interesting:[19,28–30,36] the unusual template reaction in which $[Rh(dpf)_2]^+$ (dpf = 6,6-diphenylfulvene) traps O_2 across the exocyclic α-carbons points to potentially useful applications,[31,32] and the reaction of tricarbonyl(fulvene)chromium with tertiary phosphines and methylenetriphenylphosphorane to give zwitterionic addition products has significant synthetic potential.[22,29] The possible resonance forms of fulvenes are given in Figure 2.

Results and Discussion

The syntheses of the compounds (**2**–**7**) described in this paper are shown in Scheme 1. Comprehensive spectroscopic data for these compounds are given in the Experimental Section.

$[Ru_6C(CO)_{15}(\mu\text{-}\eta^2\text{:}\eta^2\text{-}C_5H_4CPh_2)]$ (2). The dropwise addition of a solution of 2 molar equiv of Me_3NO in dichloromethane to a solution of the octahedral carbido-cluster $[Ru_6C(CO)_{17}]$ (**1**), also in dichloromethane and containing an excess of 6,6-diphenylfulvene (dpf), afforded compound **2**, as the major product, and some $[Ru_6C(CO)_{14}(\mu_3\text{-}\sigma\text{:}\eta^2\text{:}\eta^3\text{-}C_5H_4CPh_2)]$ **3**. Isolation was achieved by column chromatography using 25% dichloromethane–hexane as eluent. The positive FAB mass spectrum of **2** gave parent peaks centered at 1268 (calc 1268) amu. Following the parent ion successive carbonyl elimination typical of such systems is observed. The ^1H NMR spectrum of **2** in $CDCl_3$ obtained at room temperature shows a shift to lower frequency for the protons attached to the C_5 carbocycle, compared to the spectrum of the free hydrocarbon.[40] A similar effect has been observed for arenes bound to cluster species.[1] Interestingly, protons in the 2,5 and 3,4 positions appear to be equivalent on the NMR time scale. This is clearly not the case in the solid-state structure (*vide infra*): in solution, however, carbonyl scrambling and libration or rotation of the C_5 carbocycle presumably take place at ambient temperature.

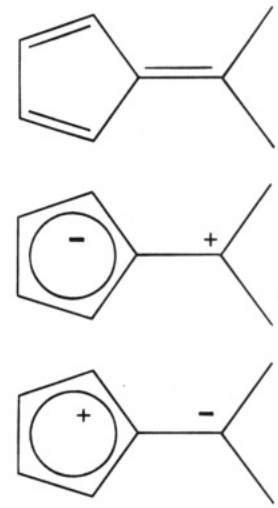

Figure 2. Possible resonance forms of the fulvene moiety.

The molecular structure of **2**, as determined by single-crystal X-ray diffraction, is shown in Figure 3. Crystals were grown from a solution of dichloromethane by slow evaporation of the solvent. The metal framework consists of an octahedral arrangement of six ruthenium atoms with an interstitial carbon atom occupying the central cavity. Of primary importance is the coordination of the fulvene ligand along a Ru–Ru vertex, formally replacing two adjacent terminal CO ligands. The four cluster coordinated carbon atoms [C(2z), C(3z), C(4z), C(5z)] produce a butadiene "short–long–short" type arrangement. Metal–carbon bond distances are within the normal range, the longest being Ru(1)–C(4z) 2.340(9) Å and the shortest being Ru(3)–C(3z) 2.228(9) Å. The C_5 ring deviates from planarity, by way of a fold across the C(2z)–C(5z) axis, indicating the localized nature of the cluster–fulvene bonding in this mode. The *exo*-cyclic double bond [C(1z)–C(1) 1.356(10) Å] appears to have essentially olefinic character. The remaining coordination sphere of the cluster is satisfied by fifteen carbonyl ligands; three are in a bridging mode, and the remaining twelve are terminal. Compound **2** is a precursor to **3** and may be converted, by oxidative removal of a third CO by 1 equiv of Me_3NO, in good yield.

$[Ru_6C(CO)_{14}(\mu_3\text{-}\sigma\text{:}\eta^2\text{:}\eta^3\text{-}C_5H_4CPh_2)]$ 3 and $[Ru_6C(CO)_{14}(\mu_3\text{-}\sigma\text{:}\eta^2\text{:}\eta^3\text{-}C_5H_4CMe_2)]$ (4). The dropwise addition of a solution of 3 molar equiv of Me_3NO in dichloromethane to a solution of **1** also in dichloro-

(28) Mtetwa, V. S. B.; Prout, K.; Green, M. L. H.; Hazel, N. J.; Izquierdo, A.; Martin-Polo, J. J. *J. Chem., Soc., Chem. Commun.* **1983**, 538.
(29) Kock, O.; Edelmann, F.; Behrens, U. *Chem. Ber.* **1982**, *115*, 1305.
(30) Turpeinen, U.; Kreindlin, A. Z.; Petroskii, P. V.; Rybinskya, M. I. *J. Organomet. Chem.* **1992**, *441*, 109.
(31) Jeffery, J.; Mawby, R. J.; Hursthouse, M. B.; Walker, N. P. C. *J. Chem. Soc., Chem. Commun.* **1982**, 1411.
(32) Dauter, Z.; Hansen, L. K.; Mawby, R. J.; Probitts, E. J.; Reynolds, C. D. *Acta Crystallogr.* **1985**, *C41*, 850.
(33) Edwards, J. D.; Knox, S. A. R.; Stone, F. G. A. *J. Chem. Soc., Dalton Trans.* **1976**, 1813.
(34) Behrens, U.; Karnatz, D.; Weiss, E. *J. Organomet. Chem.* **1976**, *117*, 171.
(35) Kock, O.; Edelmann, F.; Lubke, B.; Behrens, U. *Chem. Ber.* **1982**, *115*, 3049.
(36) Müller, J.; Stock, R.; Pickardt, J. *Z. Naturforsch.* **1981**, *36b*, 1219.
(37) Cosier, J.; Glazer, A. M. *J. Appl. Crystallogr.* **1986**, *19*, 105.
(38) SHELXS-86, Sheldrick, G. M. *Acta Crystallogr.* **1990**, *A46*, 467.
(39) SHELXL-92, Sheldrick, G. M. University of Göttingen, Germany, 1992.
(40) Aldrich Library of ^1H NMR Spectra.
(41) Walker, N.; Stuart, D. *Acta Cryst., Sect. A*, **1983**, *39*, 158.
(42) North, A. C. T.; Phillips, D. C.; Mathews, F. S. *Acta Crystallogr., Sect. A*, **1968**, *24*, 351.

Scheme 1. Synthetic Routes to Compounds 2–7[a]

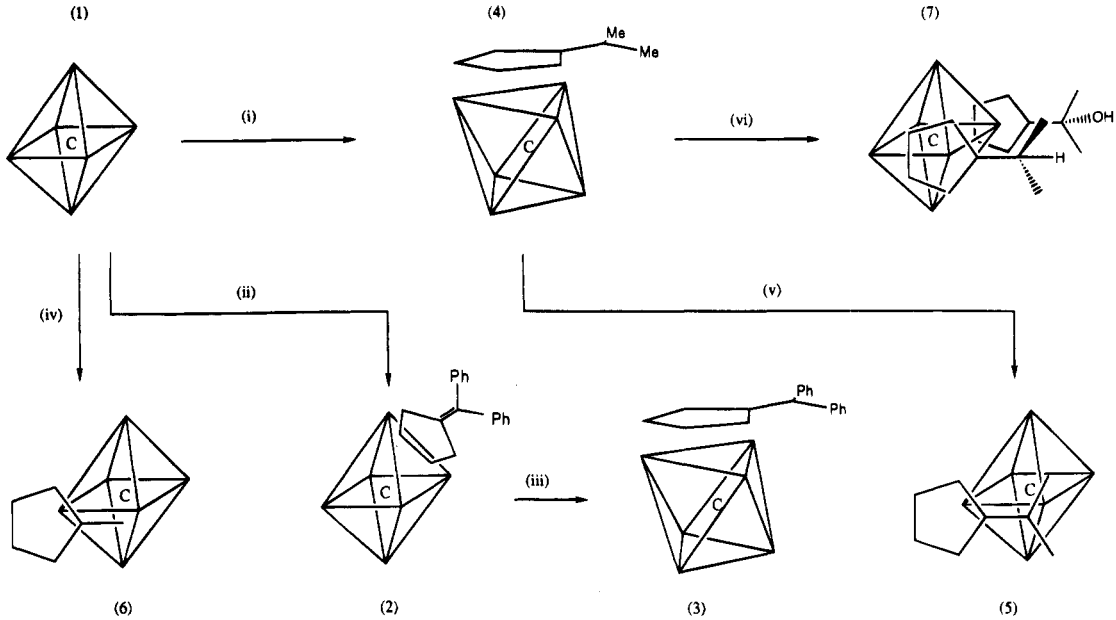

[a] Key: (i) 3 equiv of Me_3NO/CH_2Cl_2/dmf/195 K; (ii) 2 equiv of Me_3NO/CH_2Cl_2/dpf/195 K; (iii) 1 equiv of Me_3NO/CH_2Cl_2/195 K; (iv) 2.5 equiv of Me_3NO/CH_2Cl_2/Cp/195 K; (v) reflux in CH_2Cl_2/MeCN; (vi) 2 equiv of $Me_3NO/CH_2Cl_2/H_2O$/dmf/195 K.

Table 1. Crystal Data and Details of Structural Analyses for 2, 3, and 5–7[a]

	2	**3**	**5**	**6**	**7**
empirical formula	$C_{34}H_{14}O_{15}Ru_6$	$C_{33}H_{14}O_{14}Ru_6$	$C_{23}H_{10}Cl_2O_{13}Ru_6$	$C_{21}H_6O_{14}Ru_6$	$C_{29}H_{22}O_{13}Ru_6$
fw	1268.87	1240.90	1171.63	1104.68	1184.89
cryst system	monoclinic	monoclinic	monoclinic	orthorhombic	monoclinic
space group	$P2_1/a$	$C2/c$	$P2_1/n$	$Pcab$	$C2/c$
unit cell dimens					
a (Å)	18.663(3)	26.046(3)	17.468(6)	14.276(4)	19.072(3)
b (Å)	9.7381(15)	18.674(3)	10.384(5)	15.688(5)	11.872(2)
c (Å)	19.790(4)	17.016(2)	17.447(6)	23.015(7)	29.772(7)
β (deg)	92.84(3)	121.2(7)	111.45(2)	–	107.99(2)
V (Å^3)	3592(1)	7079(2)	2946(2)	5155(3)	6412(2)
Z	4	8	4	8	8
D(calc) (g cm^{-3})	2.346	2.328	2.642	2.847	2.455
μ (mm^{-1})	2.531	2.512	3.244	3.503	2.821
F(000)	2408	4704	2200	4128	4512
cryst size (mm)	0.47 × 0.11 × 0.08	0.08 × 0.29 × 0.31	0.25 × 0.25 × 0.09	0.60 × 0.60 × 0.01	0.25 × 0.25 × 0.25
θ range for data collcn (deg)	2.55 to 25.03	2.59 to 22.47	2.51 to 22.54	2.60 to 22.52	2.70 to 22.48
index ranges	$-22 \le h \le 22$, $0 \le k \le 11$, $0 \le l \le 23$	$-27 \le h \le 23$, $0 \le k \le 20$, $0 \le l \le 16$	$-18 \le h \le 17$, $0 \le k \le 11$, $0 \le l \le 16$	$-1 \le h \le 15$, $-1 \le k \le 16$, $-1 \le l \le 16$	$-1 \le h \le 15$, $-1 \le k \le 16$, $-1 \le l \le 31$
reflcns collcd	7618	3778	3057	6072	4148
indepdt reflcns	6248	3778	3043	3205	4148
ψ scans[42] [T_{max}, T_{min}]	0.558, 0.495	0.981, 0.722		0.958, 0.425	0.849, 0.685
data/restraints/params	6248/0/493	3778/198/478	3027/0/282	3192/156/388	4106/0/423
goodness-of-fit F^2	1.089	1.021	0.984	1.116	1.153
final R indices					
R [$F > 4\sigma(F)$]	0.0398	0.0529	0.0370	0.0365	0.0455
wR (all data)	0.0899	0.1390	0.1092	0.0863	0.1358
largest diff peak and hole (e Å^{-3})	1.155, −0.916	1.124, −1.036	0.726, −0.926	0.996, −0.877	1.056, −1.122

[a] Common parameters: wavelength 0.710 73 Å (Mo Kα); T = 150.0(2) K. Structure solution: direct methods.[38] Refinement method: full-matrix least squares.[39]

methane and containing an excess of 6,6-diphenylfulvene (dpf) or 6,6-dimethylfulvene (dmf) afforded compound **3** or **4**, respectively, as the major product. Isolation was achieved by column chromatography using 25% dichloromethane–hexane as eluent. The positive ion FAB mass spectra of **3** and **4** gave parent peaks centered at 1240 (calc 1240) amu and at 1117 (calc 1117) amu, respectively. Following these parent ions a carbonyl regression typical of such systems is observed. The IR spectra of **3** and **4** in dichloromethane are similar, displaying the same profiles in the carbonyl region.

Crystals of **4** were grown by diffusion of pentane vapor into a solution in dichloromethane, but repeated attempts to collect data on **4** were unsuccessful since the crystals deteriorated rapidly in the X-ray beam, even at 150 K. Crystals of **3** were grown from a solution of chloroform by slow evaporation of the solvent under ambient conditions. The molecular structure of **3**, as determined by single-crystal X-ray diffraction, is shown in Figure 5. The metal framework consists of an octahedral arrangement of six ruthenium atoms encapsulating a carbon atom. The fulvene ligand is *facially* bonded, formally replacing three adjacent terminal CO ligands.

On close inspection, the fulvene is seen to bond *via* three different modes of coordination to the three

Table 2. Bond Lengths (Å) with Esd's for 2

Ru(1)–C(12)	1.899(8)	Ru(5)–C(41)	2.084(8)
Ru(1)–C(11)	1.911(9)	Ru(5)–C	2.100(7)
Ru(1)–C	2.011(8)	Ru(5)–C(32)	2.519(9)
Ru(1)–C(5z)	2.275(8)	Ru(5)–Ru(6)	2.8890(11)
Ru(1)–C(4z)	2.340(9)	Ru(6)–C(62)	1.901(10)
Ru(1)–Ru(3)	2.8135(11)	Ru(6)–C(52)	1.909(11)
Ru(1)–Ru(4)	2.8386(10)	Ru(6)–C(61)	1.909(9)
Ru(1)–Ru(2)	2.9093(10)	Ru(6)–C	2.060(8)
Ru(1)–Ru(5)	2.9697(10)	C(1z)–C(1)	1.356(10)
Ru(2)–C(21)	1.888(10)	C(1z)–C(5z)	1.495(10)
Ru(2)–C(22)	1.904(10)	C(1z)–C(2z)	1.495(10)
Ru(2)–C(23)	1.971(9)	C(2z)–C(3z)	1.411(11)
Ru(2)–C	2.035(7)	C(3z)–C(4z)	1.443(11)
Ru(2)–Ru(6)	2.8371(11)	C(4z)–C(5z)	1.407(10)
Ru(2)–Ru(4)	2.8812(10)	C(1y)–C(1)	1.479(11)
Ru(2)–Ru(3)	3.0579(12)	C(1y)–C(1)	1.517(10)
Ru(3)–C(31)	1.879(8)	C(11)–O(11)	1.141(10)
Ru(3)–C(32)	1.900(9)	C(12)–O(12)	1.140(9)
Ru(3)–C	2.005(8)	C(21)–O(21)	1.139(11)
Ru(3)–C(3z)	2.228(9)	C(22)–O(22)	1.144(11)
Ru(3)–C(2z)	2.290(8)	C(23)–O(23)	1.143(10)
Ru(3)–Ru(5)	2.8781(10)	C(31)–O(31)	1.145(10)
Ru(4)–C(43)	1.875(8)	C(32)–O(32)	1.168(10)
Ru(4)–C(42)	1.906(10)	C(41)–O(41)	1.170(9)
Ru(4)–C	2.085(8)	C(42)–O(42)	1.150(11)
Ru(4)–C(41)	2.084(8)	C(43)–O(43)	1.136(10)
Ru(4)–C(23)	2.413(9)	C(51)–O(51)	1.146(10)
Ru(4)–Ru(5)	2.8292(11)	C(52)–O(52)	1.152(12)
Ru(4)–Ru(6)	3.0132(12)	C(53)–O(53)	1.135(10)
Ru(5)–C(53)	1.878(8)	C(61)–O(61)	1.147(11)
Ru(5)–C(51)	1.880(8)	C(62)–O(62)	1.131(11)

ruthenium atoms constituting the triangular metal face. First, there is a σ-type (η^1) mode, producing the Ru(4)–C(3z) bond. Second, there is a π-type (η^2) mode giving the Ru(1)–C(4z) and Ru(1)–C(5z) bonds. Third, there is a π-allyl (η^3) mode produced by coordination of C(1), C(1z), and C(2z) to Ru(3). The coordinated moiety is planar to within estimated error. Atom C(1) occupies a distorted tetrahedral environment in the α-position and constitutes a rather unusual arrangement for what is essentially an α-carbocation. The C–C bond lengths vary considerably (Figure 4) and are typical of single and double bonds. The two pendant phenyl groups are in distinctly nonequivalent environments. One is in a sterically constrained position with respect to rotation about the C(1)–Ph axis, and the other less so. This concurs with ^{1}H NMR spectroscopic data for the compound. The ^{1}H NMR spectrum of **3** in $CDCl_3$ obtained at room temperature comprises three sets of signals at *ca.* δ 7.2, 5.0, and 2.8 ppm. The simplicity of this spectrum is consistent with some kind of fluxional process, and this has been confirmed by recording spectra over a range of temperatures, the results of which are presented in Figure 6.

These observations may be explained in terms of the observed solid-state structure (Figure 5) and from a consideration of the ligand movements indicated in Figure 7. The coalescence of the signals A/B and C/D, due to the protons H(2z)/H(5z) and H(3z)/H(4z), respectively, on the five-membered ring, can be explained by the swiveling movement of this ring relative to a face of the Ru_6 octahedron, as indicated in Figure 7. At lower temperatures, the rate of this process is reduced, and as a consequence, the equivalence of the two phenyl groups is lost. Additionally, one of the phenyl groups will experience restricted rotation due to its proximity to and consequent steric hindrance by the cluster carbonyls, resulting in the detection of two distinct signals from the *ortho* protons of this ring at low temperature (coalescence at *ca.* δ 7.7 ppm at 221 K, with signals G and H resolving out clearly at 208 K).

The ^{1}H NMR spectrum of the isostructural compound **4** (the proposed structure of which is shown in Figure 8) in $CDCl_3$ at 298 K comprises three sets of signals at *ca.* δ 5.2, 3.1, and 2.0 ppm. The two signals at higher frequency are very broad. The appearance of this spectrum is also consistent with a fluxional process similar to that described above for **3**. A variable-temperature NMR experiment was undertaken, and on cooling of the sample the two high-frequency signals coalesced at 283 K. Further cooling of the sample to 223 K yielded six separate resonances, δ 5.72, 4.22, 3.71, and 1.99 ppm of equal intensity due to the ring protons together with singlet resonances at δ 2.34 and 1.78 ppm (3H each) for the methyl protons. These observations may also be explained by consideration of the ligand movements indicated in Figure 7. The coalescence of the high-frequency signals and subsequent formation of the six independent signals at 223 K can be explained by the swiveling movement of the five-membered ring relative to a face of the Ru_6 octahedron.

It is interesting to compare the transition state free energy ($\Delta G^{\ddagger}$) for the swivel process as derived from the coalescence temperature (T_c) of equivalent signals for **3** and **4**. Compound **4** gives a value of *ca.* 52 kJ/mol while compound **3** gives a value of *ca.* 47 kJ/mol. This observation is perhaps surprising in the light of the more bulky phenyl substituents in **3**. We tentatively suggest that it is the ability of the R-group to stabilize the α-C carbocation that is dominant in this case. While the +I effect of the methyl groups will contribute to this in **4**, greater stabilization is produced by the phenyl groups in **3**, with concomitant lowering of the transition state free energy. There are two possible pathways by which this process occurs: first through a sequence in which the α-C atom eclipses a ruthenium metal atom and second where it does not. The former seems most likely to be the lowest energy process since the α-C atom would remain further stabilized by the metal interaction throughout the transition. However, the experiment is unable to distinguish between these two pathways and we conclude that the fluxionality observed is probably an admixture of them.

$[Ru_6C(CO)_{13}(\mu\text{-}\eta^5\text{:}\eta^3\text{-}C_5H_4C\{CH_2\}_2]$ (5) and $[Ru_6C(CO)_{14}(\mu\text{-}\sigma\text{:}\eta^5\text{-}C_5H_4CH_2)]$ (6). Compound $[Ru_6C(CO)_{14}(\mu_3\text{-}\sigma\text{:}\eta^2\text{:}\eta^3\text{-}C_5H_4CMe_2)]$ (**4**) undergoes conversion to $[Ru_6C(CO)_{13}(\mu\text{-}\eta^5\text{:}\eta^3\text{-}C_5H_4C\{CH_2\}_2)]$ (**5**) under ambient conditions in chloroform over a period of about 1 week. The rate of this process can be greatly increased using slightly more aggressive conditions, *viz.* warming in acetonitrile, which results in its quantitative conversion to **5** in about 20 min. The reaction of the parent cluster **1** with 2.5 molar equiv of Me_3NO in the presence of cyclopentadiene (C_5H_6) results in the formation of a number of products including $[Ru_6C(CO)_{12}(\eta^5\text{-}C_5H_5)_2]$ and $[Ru_5C(CO)_{10}(\eta^5\text{-}C_5H_5)_2]$, both reported previously,[43] and the new complex $[Ru_6C(CO)_{14}(\mu\text{-}\eta^5\text{:}\eta^1\text{-}C_5H_4CH_2)]$ (**6**), which is isolated as a minor side product. Isolation of compounds **5** and **6** was achieved chromatographically on silica eluting with 25% dichloromethane–hexane. Both compounds have been characterized by spectroscopy and by single-crystal X-ray diffraction. The mass spectrum of **5** exhibits a parent peak at 1087 (calc 1088) amu and peaks corresponding to the successive loss of several CO groups. The ^{1}H NMR spectrum of **5** com-

(43) Blake, A. J.; Dyson, P. J.; Gash, R. C.; Johnson, B. F. G.; Trickey, P. *J. Chem. Soc., Dalton Trans.* **1994**, 1105.

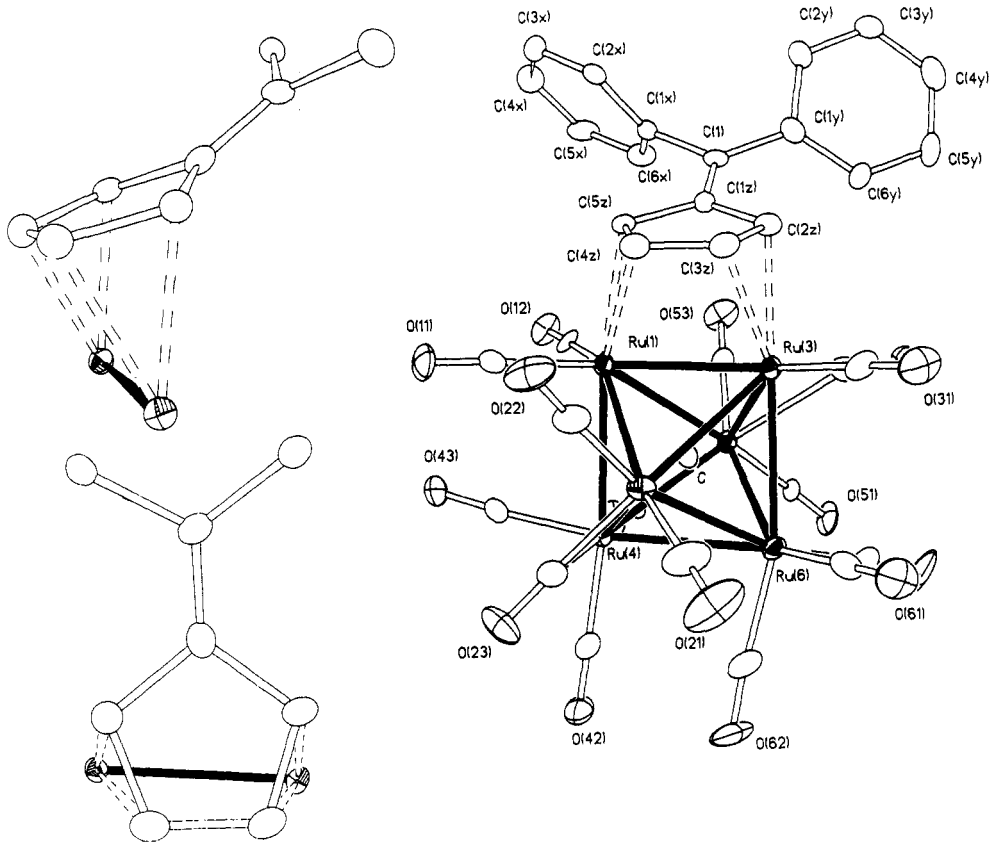

Figure 3. Solid-state molecular structure of **2** with insets emphasizing the bonding mode.

Table 3. Bond Lengths (Å) with Esd's for 3

Ru(1)–C(12)	1.91(2)	Ru(5)–C(51)	1.87(2)
Ru(1)–C(11)	1.91(2)	Ru(5)–C(52)	1.90(2)
Ru(1)–C	2.007(13)	Ru(5)–C(63)	2.02(2)
Ru(1)–C(5z)	2.238(12)	Ru(5)–C	2.06(2)
Ru(1)–C(4z)	2.370(14)	Ru(5)–Ru(6)	2.810(2)
Ru(1)–Ru(4)	2.834(2)	Ru(6)–C(61)	1.87(2)
Ru(1)–Ru(3)	2.897(2)	Ru(6)–C(62)	1.91(2)
Ru(1)–Ru(5)	2.908(2)	Ru(6)–C(63)	2.07(2)
Ru(1)–Ru(6)	2.924(2)	Ru(6)–C	2.067(13)
Ru(2)–C(13)	1.89(2)	C(1z)–C(1)	1.43(2)
Ru(2)–C(22)	1.89(2)	C(1z)–C(2z)	1.46(2)
Ru(2)–C(21)	1.90(2)	C(1z)–C(5z)	1.48(2)
Ru(2)–C	2.056(13)	C(2z)–C(3z)	1.40(2)
Ru(2)–Ru(3)	2.849(2)	C(3z)–C(4z)	1.43(2)
Ru(2)–Ru(6)	2.862(2)	C(4z)–C(5z)	1.41(2)
Ru(2)–Ru(4)	2.915(2)	C(1)–C(1x)	1.50(2)
Ru(2)–Ru(5)	2.966(2)	C(1)–C(1y)	1.52(2)
Ru(3)–C(31)	1.89(2)	C(11)–O(11)	1.14(2)
Ru(3)–C(32)	1.90(2)	C(12)–O(12)	1.12(2)
Ru(3)–C	2.09(2)	C(13)–O(13)	1.12(2)
Ru(3)–C(1z)	2.201(12)	C(21)–O(21)	1.13(2)
Ru(3)–C(1)	2.364(12)	C(22)–O(22)	1.14(2)
Ru(3)–C(2z)	2.466(14)	C(31)–O(31)	1.15(2)
Ru(3)–Ru(6)	2.949(2)	C(32)–O(32)	1.16(2)
Ru(3)–Ru(4)	2.972(2)	C(41)–O(41)	1.15(2)
Ru(4)–C(41)	1.83(2)	C(42)–O(42)	1.16(2)
Ru(4)–C(42)	1.89(2)	C(51)–O(51)	1.13(2)
Ru(4)–C	2.025(13)	C(52)–O(52)	1.12(2)
Ru(4)–C(3z)	2.165(14)	C(61)–O(61)	1.14(2)
Ru(4)–C(2z)	2.549(14)	C(62)–O(62)	1.11(2)
Ru(4)–Ru(5)	2.927(2)	C(63)–O(63)	1.15(2)

prises of four multiplets at δ 5.51, 3.79, 3.15, and 1.49 ppm with equal relative intensities. These signals may be readily assigned to the four pairs of inequivalent protons, four attached to the ring, and two pairs of *endo* and *exo* protons on the allyl fragment. Similarly, the mass spectrum of **6** contains a strong parent ion at 1089 (calc 1089) amu together with a sequence of peaks corresponding to the successive loss of 14 carbonyl ligands. The ^{1}H NMR spectrumconsists ofthree signals of equal relative intensity at δ 5.61, 3.72, and 2.35 ppm. The former two signals are multiplets and may be attributed to the ring protons; the signal at δ 2.35 ppm is a singlet resonance and can be assigned to the protons of the CH_2 fragment.

Definitive characterization of **5** and **6** was achieved in the solid state by X-ray diffraction methods on crystals grown from dichloromethane–hexane solutions at 248 K. The molecular structures of **5** and **6** are depicted in Figures 9 and 10, and principal bond parameters are found in Tables 4 and 5, respectively. Since the molecular structures are closely related, they will be discussed together.

The six ruthenium atoms form an octahedron which encapsulates a carbide atom. The Ru–Ru bonds range from 2.785(2) to 2.956(2) Å in **5** and from 2.8052(13) to 2.9703(13) Å in **6**. In both clusters the shortest Ru–Ru bond corresponds to the organo-bridged edge, Ru(3)–Ru(5) 2.785(2) Å in **5** and Ru(1)–Ru(5) 2.8052(13) Å in **6**. The Ru–C(carbide) distances average 2.03(3) and 2.04(2) Å in **5** and **6**, respectively, these values being typical of those found in related derivatives of $[Ru_6C(CO)_{17}]$. In **5** there are a total of thirteen carbonyl ligands, one of which bridges the Ru(3)–Ru(6) vector, the remainder exhibiting essentially terminal coordination. In **5** there are fourteen CO ligands, two of which adopt bridging modes along the Ru(1)–Ru(3) and Ru(1)–Ru(4) edges.

The most interesting feature of these molecules is the presence of the organic moiety and its method of bonding to the cluster. In **5** the organo ligand displays a unique η^5–η^3 (cyclopentadienyl–allylic) coordination to two adjacent metal atoms and formally donates a total of eight electrons to the cluster framework. Metal–carbon distances show little variation and lie in the range 2.16(2)–2.21(2) Å. The C–C bond distances in

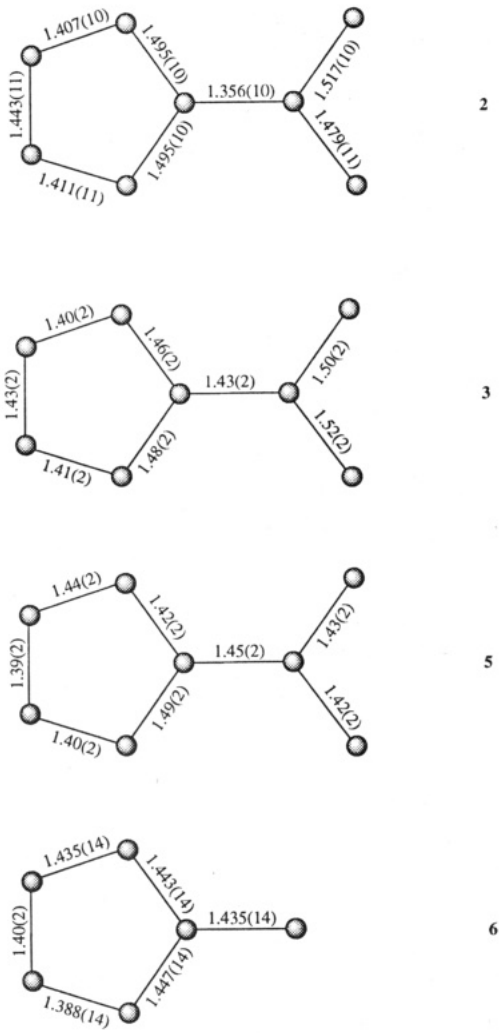

Figure 4. Representation of the cluster-coordinated carbon frameworks of **2**, **3**, **5**, and **6**.

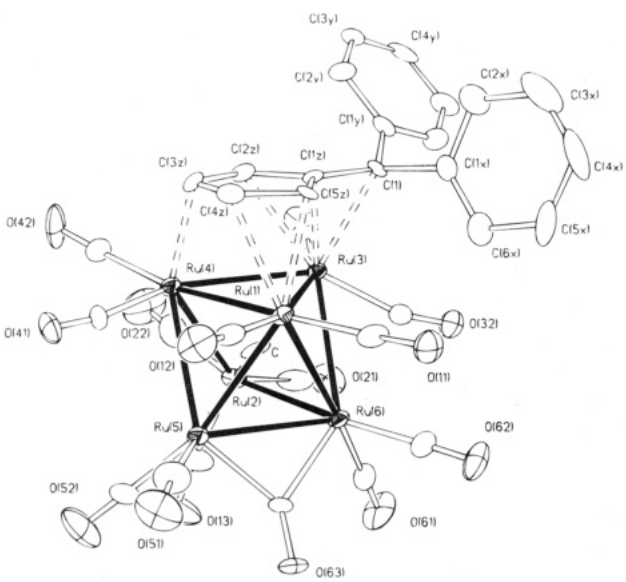

Figure 5. Solid-state molecular structure of **3**.

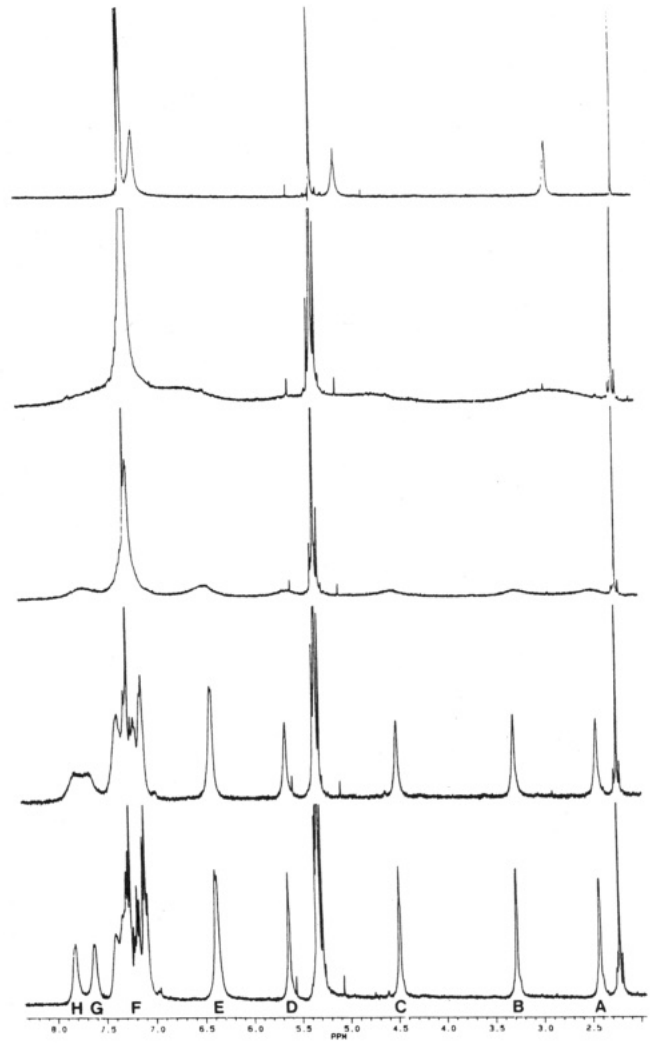

Figure 6. 360 MHz ^{1}H NMR spectra of **3** recorded over a range of temperatures, these being from top to bottom 298, 254, 233, 221, and 208 K. The coalescence of signals C and D at 245 K gives $\Delta G^{\ddagger}$ 47.43 kJ mol^{-1} for the ligand swivel process.

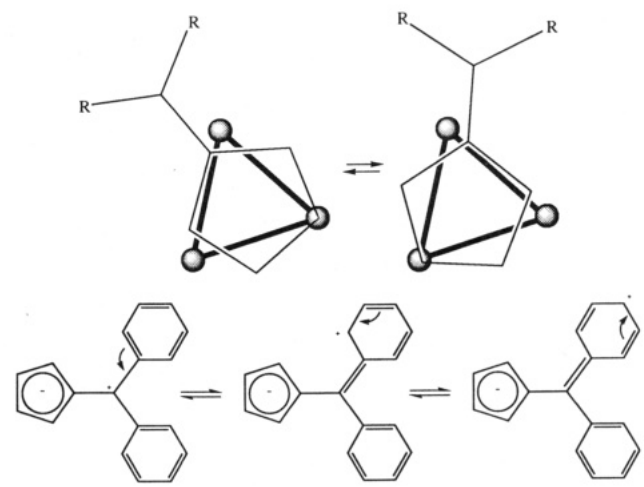

Figure 7. Possible mechanism for the exchange process in **3** and **4** (see text).

the cluster-bound ligand are shown in Figure 4. The similarity of these bond lengths [mean 1.43(4) Å] is indicative of delocalization around the system and the *in extenso* nature of bonding in **5**, rather than being partitioned between individual ruthenium atoms. Their mean value corresponds to a bond intermediate between that of a single and double bond. A similar bonding description applies to the organo-ligand system in **6**, except that it displays a $\eta^5-\sigma$ (cyclopentadienyl$-\sigma$) coordination bridging two adjacent ruthenium atoms, formally donating a total of six electrons to the cluster framework. The Ru−C(ring) orientation (see Table 5) is such that the Ru(1)−C(1) distance is longer than the

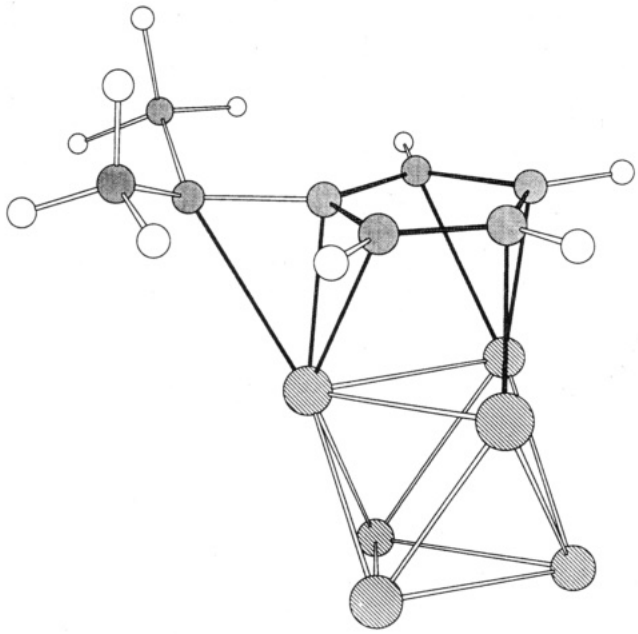

Figure 8. Computer-generated representation of **4**.

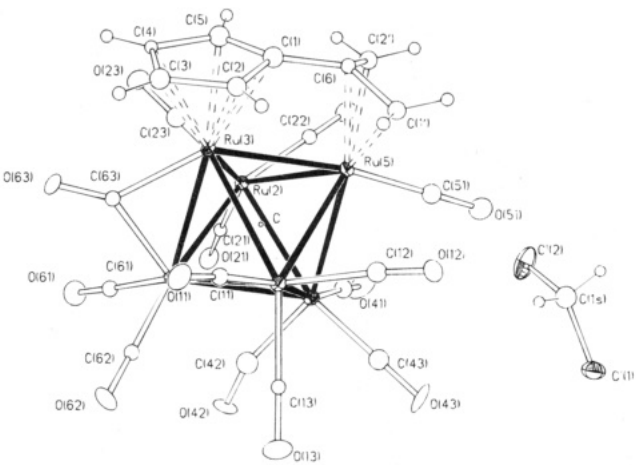

Figure 9. Solid-state molecular structure of **5** along with dichloromethane of crystallization.

other four distances. The CH_2 moiety is closely bonded to Ru(5), 2.204(10) Å. The C−C bond distances [mean = 1.42(4) Å] are shown in Figure 4, and it can be appreciated by comparison that the two organo systems in **5** and **6** are similar. As in **5**, the entire moiety in **6** can be viewed as a completely delocalized system.

The bonding arrangement observed in **6** is similar to that encountered in the six-membered ring system in $[HRu_6(\eta^2\text{-}\mu_4\text{-}CO)(CO)_{13}(\mu_2\text{-}\eta^1\text{:}\eta^6\text{-}C_6H_3Me_2CH_2)]$ which has been isolated as a byproduct from the thermolysis of $Ru_3(CO)_{12}$ with mesitylene. A similar arrangement has also been identified in a mononuclear complex, $[Cr(CO)_3(\eta^5\text{:}\eta^1\text{-}C_5H_4CPh_2)]$, wherein both the C_5 ring and the α-carbon atom bond to the metal the Cr−C bond lengths are very similar to those observed in **6**.

The conversion of **4** to **5** is relatively straightforward to rationalize. The transformation requires the loss of two H atoms from the fulvene and one carbonyl from the cluster core. Since the reaction proceeds more rapidly in the presence of a donor solvent, it might reasonably be assumed that a CO group is initially replaced by MeCN, which is relatively labile, and this, coupled with the driving force for the organic moiety to become delocalized, results in the expulsion of two H atoms, thereby affording the allylic unit in **5**.

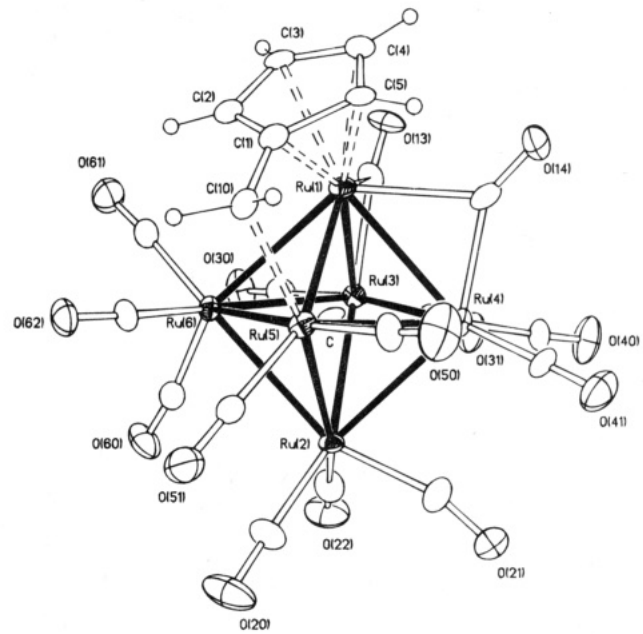

Figure 10. Solid-state molecular structure of **6**.

Table 4. Bond Lengths (Å) with Esd's for 5

Ru(1)−C(13)	1.89(2)	Ru(5)−C(51)	1.88(2)
Ru(1)−C(11)	1.93(2)	Ru(5)−C	2.017(14)
Ru(1)−C(12)	1.96(2)	Ru(5)−C(6)	2.17(2)
Ru(1)−C	2.066(13)	Ru(5)−C(2′)	2.19(2)
Ru(1)−Ru(6)	2.825(2)	Ru(5)−C(1′)	2.21(2)
Ru(1)−Ru(4)	2.839(2)	Ru(6)−C(62)	1.89(2)
Ru(1)−Ru(5)	2.928(2)	Ru(6)−C(61)	1.92(2)
Ru(1)−Ru(3)	2.928(2)	Ru(6)−C(63)	2.04(2)
Ru(2)−C(21)	1.91(2)	Ru(6)−C	2.055(14)
Ru(2)−C(22)	1.92(2)	C(1)−C(5)	1.42(2)
Ru(2)−C(23)	1.92(2)	C(1)−C(6)	1.45(2)
Ru(2)−C	2.035(13)	C(1)−C(2)	1.49(2)
Ru(2)−Ru(4)	2.838(2)	C(2)−C(3)	1.40(2)
Ru(2)−Ru(6)	2.854(2)	C(3)−C(4)	1.39(2)
Ru(2)−Ru(3)	2.888(2)	C(4)−C(5)	1.44(2)
Ru(2)−Ru(5)	2.956(2)	C(6)−C(1′)	1.42(2)
Ru(3)−C	1.982(14)	C(6)−C(2′)	1.43(2)
Ru(3)−C(63)	2.07(2)	C(11)−O(11)	1.13(2)
Ru(3)−C(5)	2.16(2)	C(12)−O(12)	1.12(2)
Ru(3)−C(1)	2.19(2)	C(13)−O(13)	1.15(2)
Ru(3)−C(4)	2.191(14)	C(21)−O(21)	1.12(2)
Ru(3)−C(3)	2.20(2)	C(22)−O(22)	1.14(2)
Ru(3)−C(2)	2.20(2)	C(23)−O(23)	1.12(2)
Ru(3)−Ru(5)	2.785(2)	C(41)−O(41)	1.15(2)
Ru(3)−Ru(6)	2.809(2)	C(42)−O(42)	1.11(2)
Ru(4)−C(434)	1.89(2)	C(43)−O(43)	1.14(2)
Ru(4)−C(41)	1.89(2)	C(51)−O(51)	1.12(2)
Ru(4)−C(42)	1.94(2)	C(61)−O(61)	1.12(2)
Ru(4)−C	2.047(14)	C(62)−O(62)	1.15(2)
Ru(4)−Ru(5)	2.923(2)	C(63)−O(63)	1.17(2)
Ru(4)−Ru(6)	2.940(2)		

In **6** the formation of the $C_5H_4CH_2$ moiety is somewhat more complicated. We find from a separate experiment that this compound is not produced from the reaction with dicyclopentadiene (DCp), the original source of CpH, indicating that it is not formed directly from DCp or from an impurity in the DCp employed. Further evidence that **6** is not formed from an impurity (*e.g.* $C_5H_4CH_3$ or another organic system which could undergo reaction to yield $C_5H_4CH_2$) is that no other product identified from the chemical activation reaction contains methyl−Cp groups.

An alternative possibility is that the CH_2 unit is derived from a coordinated CO ligand. We have previously developed a systematic method for the substitution of tricarbonyl units by benzene using chemical activation and cyclohexa-1,3-diene.[3] For example, with

Table 5. Bond Lengths (Å) with Esd's for 6

Ru(1)–C	2.024(9)	Ru(5)–C(50)	1.865(11)
Ru(1)–C(5)	2.170(10)	Ru(5)–C(51)	1.877(11)
Ru(1)–C(13)	2.173(11)	Ru(5)–C	2.047(9)
Ru(1)–C(2)	2.215(9)	Ru(5)–C(10)	2.204(10)
Ru(1)–C(4)	2.216(10)	Ru(5)–Ru(6)	2.9092(14)
Ru(1)–C(3)	2.223(9)	Ru(6)–C(60)	1.881(12)
Ru(1)–C(1)	2.254(9)	Ru(6)–C(62)	1.894(10)
Ru(1)–C(14)	2.266(11)	Ru(6)–C(61)	1.927(11)
Ru(1)–Ru(5)	2.8052(13)	Ru(6)–C	2.025(9)
Ru(1)–Ru(4)	2.8212(12)	C(1)–C(10)	1.435(14)
Ru(1)–Ru(3)	2.8254(13)	C(1)–C(5)	1.443(14)
Ru(1)–u(6)	2.9448(13)	C(1)–C(2)	1.447(14)
Ru(2)–C(22)	1.894(11)	C(2)–C(3)	1.388(14)
Ru(2)–C(20)	1.896(11)	C(3)–C(4)	1.40(2)
Ru(2)–C(21)	1.912(11)	C(4)–C(5)	1.435(14)
Ru(2)–C	2.028(9)	C(13)–O(13)	1.172(12)
Ru(2)–Ru(4)	2.8443(13)	C(14)–O(14)	1.138(12)
Ru(2)–Ru(6)	2.9074(12)	C(20)–O(20)	1.143(12)
Ru(2)–Ru(3)	2.9505(13)	C(21)–O(21)	1.140(12)
Ru(2)–Ru(5)	2.9510(13)	C(22)–O(22)	1.135(12)
Ru(3)–C(30)	1.877(11)	C(30)–O(30)	1.144(12)
Ru(3)–C(31)	1.892(10)	C(31)–O(31)	1.145(11)
Ru(3)–C(13)	1.998(11)	C(40)–O(40)	1.138(12)
Ru(3)–C	2.055(9)	C(41)–O(41)	1.155(11)
Ru(3)–Ru(6)	2.8132(12)	C(50)–O(50)	1.132(12)
Ru(3)–Ru(4)	2.9011(14)	C(51)–O(51)	1.141(12)
Ru(4)–C(40)	1.875(11)	C(60)–O(60)	1.156(12)
Ru(4)–C(41)	1.897(10)	C(61)–O(61)	1.130(12)
Ru(4)–C(14)	2.000(11)	C(62)–O(62)	1.154(11)
Ru(4)–C	2.071(9)		
Ru(4)–Ru(5)	2.9703(13)		

$[Ru_6C(CO)_{17}]$ two carbonyls may be replaced by a bridging C_6H_8 ring by addition of Me_3NO. Subsequent reaction of this species with further Me_3NO results in the formation of $[Ru_6C(CO)_{14}(\eta^6\text{-}C_6H_6)]$, and the dehydrogenation process is thought to occur *via* the intermediacy of a hexadienyl–hydrido cluster, $[HRu_6C(CO)_{14}(C_6H_7)]$. We have attempted to mimic this behavior by employing the five-membered diene ring C_5H_6, but at no stage have we observed the formation of $[HRu_6C(CO)_{14}(C_5H_5)]$[43] which one would anticipate if the same mechanism operated. Instead, *bis*(C_5H_5) complexes are produced, possibly indicating that a different mechanism of deprotonation occurs in this system. It is conceivable that the $C_5H_5^-$ anion formed by deprotonation under the reaction conditions undergoes nucleophilic addition to a coordinated carbonyl group followed by a sequence of H^+/H^- transfer reactions to generate coordinated $C_5H_4CH_2$ and CO_2. We have been able to isolate **6** only in low yields which has ruled out the possibility of ^{13}C labeling experiments at this stage.

$[Ru_6C(CO)_{12}(\eta^5\text{-}C_5H_4CMe_2H)(\eta^5\text{-}C_5H_4CMe_2OH)]$ (7). Compound **4** undergoes further reaction with 2 molar equiv of Me_3NO in the presence of dimethylfulvene and water, to yield $[Ru_6C(CO)_{12}(\eta^5\text{-}C_5H_4CMe_2H)(\eta^5\text{-}C_5H_4CMe_2OH)]$ (**7**). Extraction of **7** from the crude reaction mixture was performed by thin-layer chromatography using 20% dichloromethane–80% hexane as the eluent. The mass spectrum of **7** exhibits a strong molecular ion at 1196 (calc 1196) amu together with peaks which correspond to the sequential loss of 12 CO groups. The ^1H NMR spectrum contains resonances at δ 5.39, 5.24, 5.11, 2.93, 2.73, 1.48, and 1.17 ppm with relative intensities of 2:2:4:1:1:6:6. Multiplets at δ 5.39, 5.24, and 5.11 ppm correspond to the cyclopentadienyl protons. The isopropyl group shows typical signals at δ 2.73 (septet) and 1.17 (d, J = 7 Hz). A slightly broadened signal at δ 2.93 corresponds to the hydroxyl proton and the remaining resonance at δ 1.48 (s) is due to the six methyl protons.

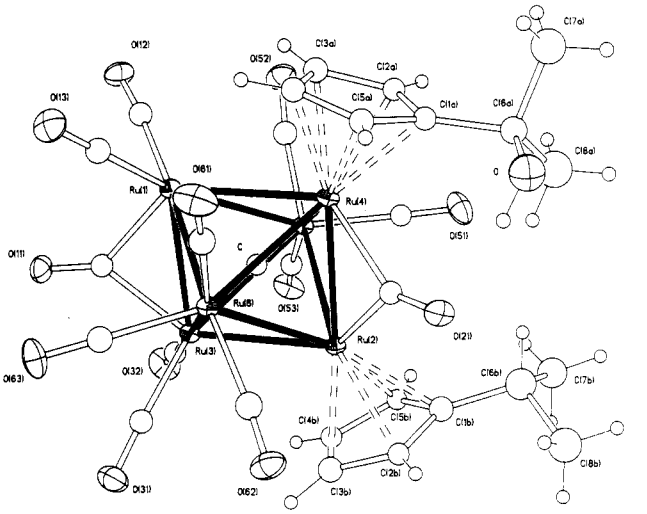

Figure 11. Solid-state molecular structure of **7**.

Table 6. Bond Lengths (Å) with Esd's for 7

Ru(1)–C(13)	1.88(2)	C(1A)–C(5A)	1.41(2)
Ru(1)–C(12)	1.895(14)	C(1A)–C(2A)	1.42(2)
Ru(1)–C(11)	2.047(13)	C(1A)–C(6A)	1.54(2)
Ru(1)–C	2.071(12)	Ru(6)–C(63)	1.900(14)
Ru(1)–Ru(3)	2.803(2)	Ru(6)–C(61)	1.911(14)
Ru(1)–Ru(6)	2.8724(14)	Ru(6)–C(62)	1.94(2)
Ru(1)–Ru(5)	2.962(2)	Ru(6)–C	2.077(12)
Ru(1)–Ru(4)	3.062(2)	C(2A)–C(3A)	1.43(2)
Ru(2)–C	2.027(12)	C(3A)–C(4A)	1.41(2)
Ru(2)–C(21)	2.071(13)	C(4A)–C(5A)	1.40(2)
Ru(2)–C(3B)	2.198(13)	C(6A)–O	1.45(2)
Ru(2)–C(4B)	2.221(13)	C(6A)–C(8A)	1.47(2)
Ru(2)–C(5B)	2.225(12)	C(6A)–C(7A)	1.50(2)
Ru(2)–C(2B)	2.225(12)	C(1B)–C(5B)	1.44(2)
Ru(2)–C(1B)	2.264(14)	C(1B)–C(2B)	1.44(2)
Ru(2)–Ru(4)	2.7832(14)	C(1B)–C(6B)	1.52(2)
Ru(2)–Ru(5)	2.8449(14)	C(2B)–C(3B)	1.41(2)
Ru(2)–Ru(6)	2.901(2)	C(3B)–C(4B)	1.40(2)
Ru(2)–Ru(3)	2.927(2)	C(4B)–C(4B)	1.43(2)
Ru(3)–C(31)	1.853(14)	C(6B)–C(7B)	1.494(10)
Ru(3)–C(32)	1.861(14)	C(6B)–C(7B′)	1.497(10)
Ru(3)–C(11)	2.050(13)	C(6B)–C(8B)	1.499(10)
Ru(3)–C	2.075(12)	C(6B)–C(8B′)	1.510(10)
Ru(3)–Ru(6)	2.917(2)	C(11)–O(11)	1.17(2)
Ru(3)–Ru(5)	2.9769(14)	C(12)–O(12)	1.13(2)
Ru(4)–C(21)	2.106(13)	C(13)–O(13)	1.14(2)
Ru(4)–C	2.021(12)	C(21)–O(21)	1.17(2)
Ru(4)–C(4A)	2.186(13)	C(31)–O(31)	1.16(2)
Ru(4)–C(5A)	2.211(13)	C(32)–O(32)	1.15(2)
Ru(4)–C(3A)	2.223(13)	C(51)–O(51)	1.15(2)
Ru(4)–C(2A)	2.249(12)	C(52)–O(52)	1.15(2)
Ru(4)–C(1A)	2.287(13)	C(53)–O(53)	1.11(2)
Ru(4)–Ru(5)	2.814(2)	C(61)–O(61)	1.15(2)
Ru(4)–Ru(6)	2.8649(14)	C(62)–O(62)	1.10(2)
Ru(5)–C(51)	1.880(13)	C(63)–O(63)	1.14(2)
Ru(5)–C(52)	1.884(14)		
Ru(5)–C(53)	1.940(14)		
Ru(5)–C	2.011(12)		

The molecular structure of **7** has been established by a single-crystal X-ray diffraction study on a crystal obtained from a dichloromethane–pentane solution by vapor diffusion at *ca.* 253 K. It is illustrated in Figure 11, and relevant bond parameters are listed in Table 6. In a similar manner to the other compounds described (**2**–**6**) the metal core constitutes an octahedron encapsulating a carbon atom. The Ru–Ru bond lengths range from 2.784(2) to 3.062(2) Å [mean 2.89(6) Å]. The C(carbide) occupies the center of the octahedral cavity with a mean distance of 2.05 Å for the Ru–C bond lengths.

The two cyclopentadienyl rings donate a total of ten electrons, with each ring displaying η^5 coordination to

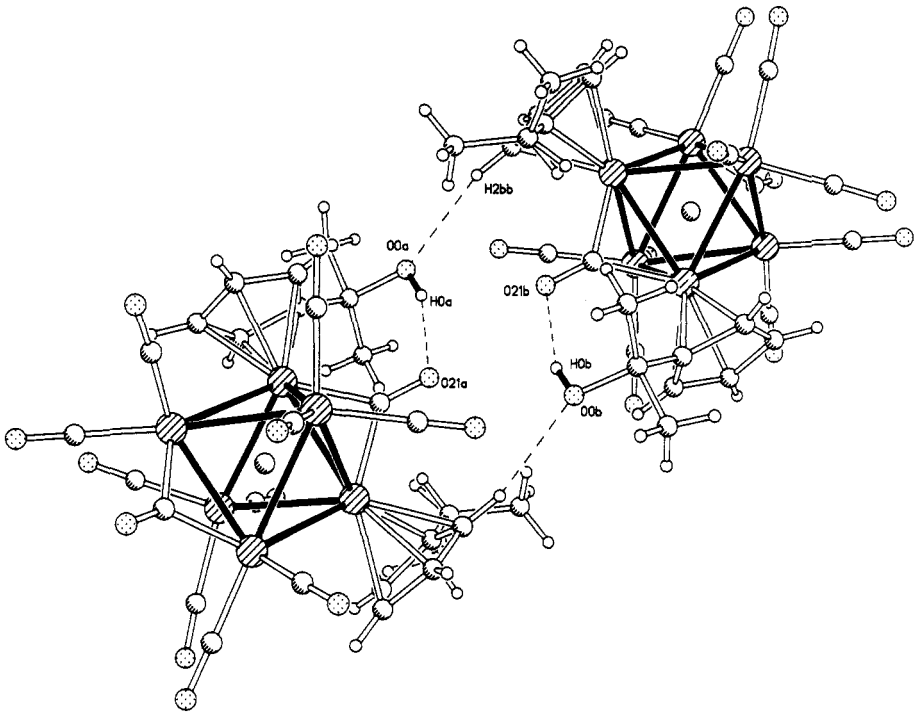

Figure 12. Solid-state packing interactions of **7**.

Scheme 2. Proposed Mechanism for the Formation of 7

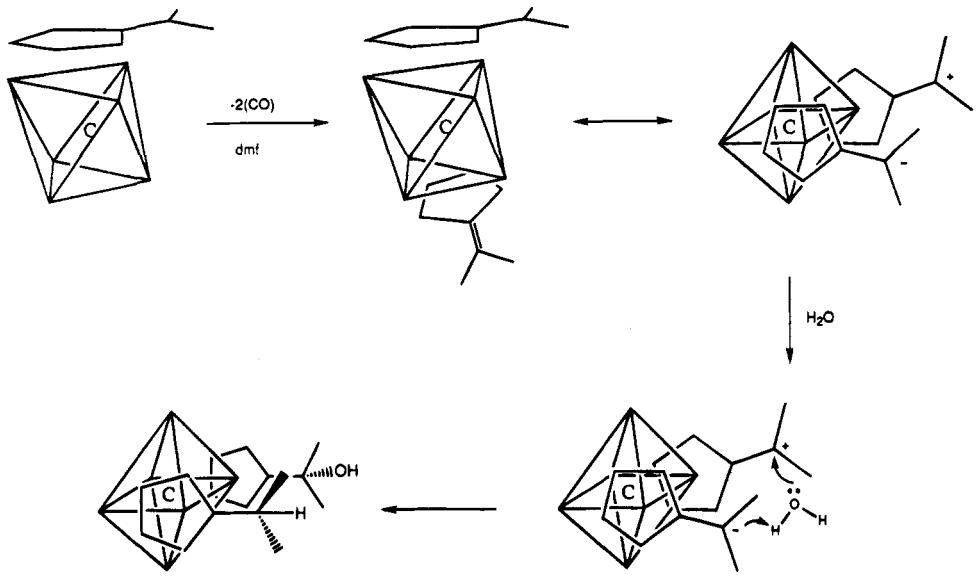

two adjacent metal atoms; this edge [Ru(2)–Ru(4)] is also bridged by a carbonyl ligand and is the shortest. There is one other bridging CO group, the others being essentially terminal. This structural form involving the *cis*-C_5 rings is similar to that observed in [$Ru_6C(CO)_{12}$-(η^5-C_5H_5)$_2$].[43] The R-group of one ring constitutes that of an isopropyl group; the other contains an OH group attached to the α-carbon atom. The isopropyl group shows a small degree of rotational disorder about the C(1b),C(6b) axis producing two close-lying [*ca.* 0.5 Å] and equally occupied positions for each methyl. The Ru–C(ring) distances average 2.22(2) and 2.23(2) Å for the two systems, and *intra*-ring C–C bonds average 1.42(2) Å for both moieties. The C–C bond spanning the ring and R-group are clearly of single character, being 1.53(2) Å in both cases.

The crystal structure of **7** is composed of pairs of molecules related by a center of inversion (Figure 12). *Inter*molecular hydrogen bonding occurs between the hydroxyl oxygen atom and the weakly acidic hydrogens attached to the cyclopentadienyl group located on Ru-(2) [O···H(2b) 2.47 Å]. A much shorter *intra*molecular hydrogen bonding occurs between the oxygen of the carbonyl bridging Ru(2) and Ru(4) and the hydroxyl hydrogen [O(21)···H(0) 2.04 Å]. The latter dipoles are aligned *anti*parallel such that they may also be instrumental in the molecular pairing of **7** in the solid state.

The proposed mechanism by which **7** is produced from **4** is illustrated in Scheme 2. The first step may be taken to involve the removal of two carbonyl ligands by Me_3NO. This intermediate compound, in which the dimethylfulvene ligands are formally coordinated as a diene ring (*cf.* **2**) and in a face bonding mode (*cf.* **3**) may resonate, alternately generating positive and negative charges at the 6-positions. Insertion of water between the 6-positions of the two fulvenes followed by O–H bond cleavage gives **7**.

Experimental Section

All reactions were carried out with the exclusion of air using solvents distilled under an atmosphere of nitrogen. Subsequent workup of products was achieved without precautions to exclude air. IR spectra were recorded on a Perkin-Elmer 1710 series FTIR instrument in CH_2Cl_2 using NaCl cells (0.5 mm path length). Positive ion fast atom bombardment mass spectra were obtained using a Kratos MS50TC spectrometer, using CsI as calibrant. ^1H NMR spectra were recorded in $CDCl_3$ using a Bruker AM360 instrument, referenced to internal TMS. Separation of products was accomplished by thin-layer chromatography (TLC) using plates supplied by Merck, 0.25 mm layer of Kieselgel 60 F_{254}. The cluster $[Ru_6C(CO)_{17}]$ was prepared by the standard literature procedure. Diphenylfulvene (dpf) and dimethylfulvene (dmf) were purchased from Aldrich and used without further purification. Dicyclopentadiene was cracked into monomer units prior to use, and trimethylamine *N*-oxide was sublimed before use.

Reaction of $[Ru_6C(CO)_{17}]$ (1) with Trimethylamine *N*-Oxide in the Presence of dpf. Synthesis of Compound 2. To a solution of **1** (500 mg) in dichloromethane (50 mL), and dpf (500 mg), cooled to −78 °C, a solution of Me_3NO (84 mg, 2.1 mol equivalent) in dichloromethane (15 mL) was added dropwise over a period of 10 min. The solution was brought to room temperature with stirring. IR spectroscopy indicated complete consumption of starting material. The solvent was removed *in vacuo* and the residue purified by column chromatography on silica (60 mesh). Elution with hexane gave a yellow-orange band of unreacted dpf. Further elution with dichloromethane−hexane (1:4, v/v) yielded a bright red band, which was characterized as $[Ru_6C(CO)_{14}(\mu\text{-}\eta^2\text{:}\eta^2\text{-}C_5H_4CPh_2)]$ (**2**) (42%) a dark red solid. (Anal. Found: C, 31.9; H, 1.21. Calc for $C_{23}H_{10}O_{14}Ru_6$ (**2**): C, 32.2; H, 1.11).

Spectroscopic data for **2**: IR (CH_2Cl_2) ν(CO) 2081 (m), 2046 (vs), 2035 (vs), 1837 (w br) cm^{-1}; ^1H NMR ($CDCl_3$, 298 K) δ 7.32 (m, 6H), δ 7.14 (m, 4H), δ 5.54 (m, 2H), δ 4.55 (m, 2H); MS M^+ = 1268 (calc 1268) amu.

Reaction of $[Ru_6C(CO)_{17}]$ (1) with Trimethylamine *N*-Oxide in the Presence of dmf or dpf. Synthesis of Compounds 3 and 4. To a solution of **1** (500 mg) in dichloromethane (50 mL), and dmf (2 mL) or dpf (500 mg), cooled to −78 °C, a solution of Me_3NO (124 mg, 3.1 mol equiv) in dichloromethane (15 mL) was added dropwise over a period of 10 min. The solution was brought to room temperature with stirring. IR spectroscopy indicated complete consumption of starting material. The solvent was removed *in vacuo* and the residue purified by column chromatography on silica (60 mesh). Elution with hexane gave a yellow-orange band of unreacted dmf/dpf. Further elution with dichloromethane−hexane (1:4, v/v) yielded a bright red band, which was characterized as $[Ru_6C(CO)_{14}(\mu_3\text{-}\sigma\text{:}\eta^2\text{:}\eta^3\text{-}C_5H_4CPh_2)]$ (**3**) (71%) or $[Ru_6C(CO)_{14}(\mu_3\text{-}\sigma\text{:}\eta^2\text{:}\eta^3\text{-}C_5H_4CMe_2)]$ (**4**) (24%) both dark red solids. Spectroscopic data for **3**: IR (CH_2Cl_2) ν(CO) 2077 (m), 2041 (s), 2025 (vs), 1815 (w br) cm^{-1}; ^1H NMR ($CDCl_3$, 298 K) δ 7.24 (m, 6H), δ 7.11 (s, 4H), δ 5.04 (s, 2H), δ 2.86 (s, 2H); MS M^+ = 1240 (calc 1240) amu.

Spectroscopic data for **4**: IR (CH_2Cl_2) ν(CO) 2078 (m), 2040 (s), 2024 (vs) and 1810 (w, br) cm^{-1}; ^1H NMR ($CDCl_3$, 223 K) δ 5.72 (m, 1H), 4.22 (m, 1H), 3.71 (m, 1H), 2.34 (s, 3H), 1.99 (m, 1H), 1.78 (s, 3H) ppm; Ms M^+ = 1117 (calc = 1117) amu. Anal. Found: C, 24.9; H, 0.88. Calc for $C_{23}H_{10}O_{14}Ru_6$ (**4**): C, 24.74; H, 0.91.

Thermolysis of 4 in Dichloromethane−Acetonitrile. Synthesis of Compound 5. A solution of **4** (50 mg) in dichloromethane (50 mL) and acetonitrile (1.0 mL) was warmed to near reflux for 20 min. IR spectroscopy indicated a large degree of conversion. The solvent was removed *in vacuo* and the residue purified by thin-layer chromatography on silica plates. Elution with dichloromethane−hexane (1:3, v/v) gave a brown band and a faint red band due to unconverted starting material. The brown band was extracted by washing with dichloromethane and subsequently evaporated to dryness *in vacuo* to give $[Ru_6C(CO)_{13}\mu\text{-}\eta^3\text{:}\eta^5C_5H_4C(CH_2)_2CH_2Cl_2]$ (**4**), a very dark brown solid (45 mg, 91%).

Spectroscopic data for **5**: IR (CH_2Cl_2) ν(CO) 2072 (m), 2048 (s), 2039 (vs), 2026 (m), 2010 (vs), 1999 (vs), and 1815 (w) cm^{-1}; ^1H NMR ($CDCl_3$) δ 5.51 (m, 2H), 3.79 (m, 2H), 3.15 (m, 2H), 1.49 (m, 2H) ppm; MS M^+ = 1087 (calc = 1087) amu.

Reaction of $[Ru_6C(CO)_{17}]$ (1) with Trimethylamine *N*-Oxide in the Presence of Cyclopentadiene. Synthesis of Compound 6. To a solution of $[Ru_6C(CO)_{17}]$ (**1**) (100 mg) in dichloromethane (20 mL) containing cyclopentadiene (1.0 mL), cooled to 195 K, a solution of Me_3NO (36 mg, 2.5 mol equiv) also in dichloromethane (2 mL) was added dropwise. Allowing the solution to warm slowly to room temperature over a period of about 40 min results in a darkening of the solution to a deep brown color. Chromatographic separation of the products on silica, eluting with dichloromethane−hexane (1:4, v/v), results in the isolation of several products, including $[Ru_6C(CO)_{14}(\mu_2\text{-}\eta^5\text{:}\eta^1\text{-}C_5H_4CH_2)]$ (**6**) (brown, 7%).

Spectroscopic data for **6**: IR (CH_2Cl_2) ν(CO) 2077 (m), 2046 (vs), 2022 (s), 2004 (m, sh), 1971 (m), 1830 (w, br) cm^{-1}; ^1H NMR ($CDCl_3$) δ 5.61 (m, 2H), 3.72 (m, 2H), 2.35 (m, 2H) ppm; MS M^+ = 1089 (calc = 1089) amu.

Reaction of $[Ru_6C(CO)_{14}(\mu_3\text{-}\sigma\text{:}\eta^2\text{:}\eta^3\text{-}C_5H_4C\{CH_3\}_2)]$ (4) with dmf and Me_3NO. Synthesis of Compound 7. To a solution of **4** (50 mg) in dichloromethane (50 mL) was added water (1 μL) and dmf (0.25 mL), and the solution was cooled to 195 K. A solution of Me_3NO (8.1 mg, 2 mol equiv) in dichloromethane (15 mL) was added dropwise over a period of 10 min. The solution was brought to room temperature over 30 min with stirring. IR spectroscopy indicated complete consumption of starting material. The solvent was removed *in vacuo* and the residue purified by column chromatography on silica (60 mesh). Elution with hexane gave a yellow band of unreacted dmf. Further elution with dichloromethane−hexane (1:4, v/v) then gave a bright green band, which was evaporated to dryness *in vacuo* to give $[Ru_6C(CO)_{12}(\eta^5\text{-}CHMe_2)(\eta^5\text{-}C_5H_4CMe_2OH)]$ (**7**), a dark green solid (7 mg, 13%).

Spectroscopic data for **7**: IR (CH_2Cl_2) ν(CO) 2056 (m), 2032 (vs), 2004 (vs) cm^{-1}; MS. ^1H NMR ($CDCl_3$) δ 5.39 (m, 2H), 5.24 (m, 2H), 5.11 (m, 4H), 2.93 (s, 1H), 2.73 (sep, 1H, J = 7 Hz), 1.48 (s, 6H), 1.17 (d, 6H, J = 7 Hz) ppm; MS M^+ = 1185 (calc = 1185) amu.

Crystal Structure Determination of Compounds 2, 3, and 5−7. Diffraction intensities for **2**, **3**, and **5−7** were collected on a Stoë Stadi-4 four-circle diffractometer equipped with an Oxford Cryosystems low-temperature device.[37] Crystallographic information and details of measurements are summarized in Table 1. H atoms in **2**, **5**, and **7** were placed in calculated positions and allowed to refine "riding" on their respective C atoms. H atoms in **6** were located in ΔF maps and allowed to refine subject to the restraint that all $C(sp^2)-H$ and $C(sp^3)-H$ distances were respectively equal and that $U_{iso}(H) = 1.2U_{eq}(C)$: H atoms in **3** were placed in fixed calculated positions. All non-H atoms were refined with anisotropic displacement parameters in **2**, **3**, and **6**. Ru and O atoms were refined with anisotropic displacement parameters in **5** and **6**. At isotropic convergence corrections (maximum 1.368, minimum 0.631) for absorption were applied to **3** using DIFABS.[41]

Acknowledgment. We thank The University of Edinburgh and the EPSRC for financial support.

Supporting Information Available: Tables of crystal data, atomic coordinates, isotropic and anisotropic thermal parameters, and bond distances and angles (48 pages). Ordering information is given on any current masthead page.

OM950191S

Hydrogenation of Imines Catalyzed by a Zwitterionic Rhodium Complex

Zhongxin Zhou,† Brian R. James,*,‡ and Howard Alper*,†

Departments of Chemistry, University of Ottawa, 10 Marie Curie, Ottawa, Ontario, Canada K1N 6N5, and University of British Columbia, Vancouver, British Columbia, Canada V6T 1Z1

Received March 21, 1995®

The hydrogenation of both aldimines and ketimines catalyzed by the zwitterionic rhodium complex, (η^6-PhBPh$_3$)$^-$Rh$^+$(1,5-COD), **1**, was achieved in excellent yield with 9/1 (v/v) THF and methanol as the solvent under 200–600 psi of H_2 at 40 °C and the addition of 1 equiv of 1,4-bis(diphenylphosphino)butane (DPPB). The extent of imine conversion is sensitive to the substrate structure and solvent employed.

Introduction

Previous studies from one of our laboratories have demonstrated that the zwitterionic rhodium complex **1**[1]

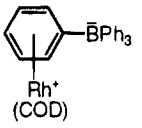

1

is a useful catalyst for a variety of carbonylation reactions.[2–8] This complex, either alone or in the presence of 1,4-bis(diphenylphosphino)butane (DPPB), has been found to be a highly regioselective catalyst for the hydroformylation of aryl and 1,1-disubstituted alkenes,[2,3] allyl acetates,[6] vinyl ethers,[2] vinyl silanes,[8] vinyl sulfones and sulfoxides,[7] as well as α,β-unsaturated esters.[4] Complex **1** is also an excellent catalyst for the inter- and intramolecular silylhydroformylation of alkynes.[9,10] Moderate diastereoselectivity resulted from the hydroformylation of phenyl vinyl sulfoxide[7] and the hydrosilylation of prochiral ketones[11] using **1** and a chiral ligand. Finally, an interesting example has been reported for the application of the zwitterionic complex **1** to the stereoregular polymerization of phenylacetylene.[12]

The catalytic hydrogenation of imines to amines (cf. eq 1)[13–17] has attracted considerable interest in recent

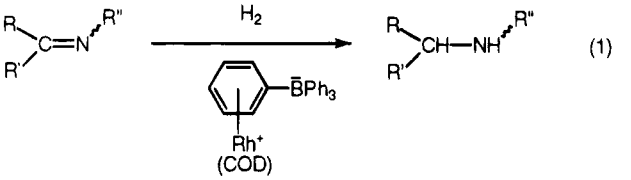

years, especially in the asymmetric hydrogenation of prochiral imines.[18–42] Both early (Ti) and late (Ir, Rh, Ru) transition metal complexes have been applied as the catalyst precursors, with neutral and cationic rho-

† University of Ottawa.
‡ University of British Columbia.
® Abstract published in *Advance ACS Abstracts,* July 1, 1995.

(1) Schrock, R. R.; Osborn, J. A. *Inorg. Chem.* **1970**, *9*, 2339.
(2) Amer, I.; Alper, H. *J. Am. Chem. Soc.* **1990**, *112*, 3674.
(3) Zhou, J. Q.; Alper, H. *J. Chem. Soc., Chem. Commun.* **1991**, 233.
(4) Alper, H.; Zhou, J. Q. *J. Org. Chem.* **1992**, *57*, 3729.
(5) Zhou, J. Q.; Alper, H. *J. Org. Chem.* **1992**, *57*, 3328.
(6) Alper, H.; Zhou, J. Q. *J. Chem. Soc., Chem. Commun.* **1993**, 316.
(7) Totland, K.; Alper, H. *J. Org. Chem.* **1993**, *58*, 3326.
(8) Crudden, C. M.; Alper, H. *J. Org. Chem.* **1994**, *59*, 3091.
(9) Zhou, J. Q.; Alper, H. *Organometallics* **1994**, *13*, 1586.
(10) Monteil, F.; Matsuda, I.; Alper, H. *J. Am. Chem. Soc.* **1995**, *117*, 4419.
(11) Goldberg, Y.; Alper, H. *Tetrahedron: Asymmetry* **1992**, *3*, 1055.
(12) Goldberg, Y.; Alper, H. *J. Chem. Soc., Chem. Commun.* **1994**, 1209.
(13) Fogg, D. E.; James, B. R.; Kilner, M. *Inorg. Chim. Acta* **1994**, *222*, 85.
(14) Longley, C. J.; Goodwin, T. J.; Wilkinson, G. *Polyhedron* **1986**, *5*, 1625.
(15) Brune, H. A.; Unsin, J.; Hemmer, R.; Reichhardt, M. *J. Organomet. Chem.* **1989**, *369*, 335.
(16) Bhaduri, S.; Sapre, N.; Sharma, K.; Jones, P. G.; Carpenter, G. *J. Chem. Soc., Dalton Trans.* **1990**, 1305.
(17) Basu, A.; Bhaduri, S.; Sharma, K.; Jones, P. G. *J. Chem. Soc., Chem. Commun.* **1987**, 1126.
(18) James, B. R. *Chem. Ind.* **1995**, *62*, 167.
(19) Bolm, C. *Angew. Chem., Int. Ed. Engl.* **1993**, *32*, 232.
(20) Willoughby, C. A.; Buchwald, S. L. *J. Am. Chem. Soc.* **1992**, *114*, 7562.
(21) Willoughby, C. A.; Buchwald, S. L. *J. Org. Chem.* **1993**, *58*, 7627.
(22) Willoughby, C. A.; Buchwald, S. L. *J. Am. Chem. Soc.* **1994**, *116*, 8952.
(23) Willoughby, C. A.; Buchwald, S. L. *J. Am. Chem. Soc.* **1994**, *116*, 11703.
(24) Burk, M. J.; Feaster, J. E. *J. Am. Chem. Soc.* **1992**, *114*, 6266.
(25) Burk, M. J.; Martinez, J. P.; Feaster, J. E.; Cosford, N. *Tetrahedron* **1994**, *50*, 4399.
(26) Kang, Guo-J.; Cullen, W. R.; Fryzuk, M. D.; James, B. R.; Kutney, J. P. *J. Chem. Soc., Chem. Commun.* **1988**, 1466.
(27) Cullen, W. R.; Fryzuk, M. D.; James, B. R.; Kutney, J. P.; Kang, Guo-J.; Herb, G.; Thorburn, I. S.; Spogliarich, R. *J. Mol. Catal.* **1990**, *62*, 243.
(28) Becalski, A. G.; Cullen, W. R.; Fryzuk, M. D.; James, B. R.; Kang, Guo-J.; Rettig, S. J. *Inorg. Chem.* **1991**, *30*, 5002.
(29) Ball, G. E.; Cullen, W. R.; Fryzuk, M. D.; Henderson, W. J.; James, B. R.; MacFarlane, K. S. *Inorg. Chem.* **1994**, *33*, 1464.
(30) Spindler, F.; Pugin, B.; Blaser, H.-U. *Angew. Chem., Int. Ed. Engl.* **1990**, *29*, 558.
(31) Chan, Y. N. C.; Osborn, J. A. *J. Am. Chem. Soc.* **1990**, *112*, 9400.
(32) Chan, Y. N. C.; Meyer, D.; Osborn, J. A. *J. Chem. Soc., Chem. Commun.* **1990**, 869.
(33) Levi, A.; Modena, G.; Scorrano, G. *J. Chem. Soc., Chem. Commun.* **1975**, 6.
(34) Vastag, S.; Bakos, J.; Tórös,, S.; Takach, N. E.; King, R. B.; Heil, B.; Markó, L. *J. Mol. Catal.* **1984**, *22*, 283.
(35) Kagan, H. B.; Langlois, N.; Dang, T. P. *J. Organomet. Chem.* **1975**, *90*, 353.
(36) Bakos, J.; Tóth, I.; Heil, B.; Markó, L. *J. Organomet. Chem.* **1985**, *279*, 23.
(37) Bakos, J.; Tóth, I.; Heil, B.; Szalontai, G.; Párkányi, L.; Fülöp, V. *J. Organomet. Chem.* **1989**, *370*, 263.
(38) Lensink, C.; de Vries, J. *Tetrahedron: Asymmetry* **1992**, *3*, 235.
(39) Brunner, H.; Huber, C. *Chem. Ber.* **1992**, *125*, 2085.
(40) Lensink, C.; de Vries, J. G. *Tetrahedron: Asymmetry* **1993**, *4*, 215.

0276-7333/95/2314-4209$09.00/0

Table 1. Solvent Effects on the Hydrogenation of *N*-Benzylidenemethylamine by 1[a]

entry no.	solvent	$P(H_2)$ (psi)	conversion (%)[b]
1	MeOH	300	<1
2	CH_2Cl_2	300	8
3	CH_2Cl_2/MeOH (v/v 5/5)	100	57[c]
		300	79
		600	>99 (84[d])
4	DME[e]	300	8
5	benzene	300	3
6	THF[e]	100	78
		200	94
		300	97 (90[d])
7	THF/MeOH (v/v 9/1)	200	>99 (94[d])
8	THF/MeOH (v/v 5/5)	200	8
9	THF/MeOH (v/v 9/1)[f]	200	55

[a] Reaction conditions: substrate, 3.4 mmol; (η^6-$PhBPh_3$)$^-$$Rh^+$(1,5-COD), 1.2 mol %; mol of Rh/mol of DPPB, 1/1; temperature, 40 °C; solvent, 10 mL. Unless otherwise described reaction times are 24.5 ± 0.5 h. [b] Determined by ^1H NMR with dibenzyl ether as the internal reference, *N*-benzylmethylamine was the only product. [c] Time, 50 h. [d] Isolated yield. [e] DME = 1,2-dimethoxyethane; THF = tetrahydrofuran. [f] Mol of Rh/mol of DPPB, 1/2.

dium(I) complexes being the most numerous. To our knowledge, there are no publications or patents on the use of zwitterionic rhodium complexes for the reduction of imines. We now wish to report that the zwitterionic complex **1** is an excellent catalyst for converting imines to amines.

Results and Discussion

It is well-known[43] that homogeneous hydrogenation is very sensitive to the solvent used in the reaction. Thus, solvent effects in the hydrogenation of *N*-benzylidenemethylamine (Table 1) were examined using H_2 (300 psi), a catalytic amount of **1** (1.2 mol %), and DPPB (Rh/DPPB 1/1) at 40 °C for 24.5 h. The conversion of *N*-benzylidenemethylamine to *N*-benzylmethylamine was very low when methanol, dichloromethane, dimethoxyethane (DME), or benzene was used as the only solvent (Table 1, entries 1, 2, 4, and 5). The low conversions in methanol and DME were possibly due to the lack of solubility of the zwitterionic rhodium complex **1** in these solvents. The reaction conversion increased dramatically when methanol and dichloromethane were combined as the solvent for the hydrogenation reaction. Although tetrahydrofuran was not considered to be a good solvent for rhodium(I) complex-catalyzed hydrogenation of imines,[14,24,26-28,34,35] THF was an excellent solvent for the zwitterionic rhodium-catalyzed hydrogenation of *N*-benzylidenemethylamine (cf. Table 1, entry 6), giving *N*-benzylmethylamine in 97% conversion (90% isolated yield). Addition of a small amount of methanol (9/1 THF/MeOH) to the reaction mixture resulted in a slight increase in imine conversion (>99% versus 94% at $P(H_2)$ = 200 psi; Table 1, entries 6 and 7), which was confirmed by time dependent experiments. The conversion on *N*-benzylidenemethylamine, however, decreased to less than 10% when THF/MeOH (v/v 5/5) was used as the solvent, presumably due to decreased solubility of **1**. Therefore, THF/MeOH (v/v 9/1) was chosen as the solvent system for this investigation.

In the absence of an added phosphine ligand, rhodium black was formed during the reaction and the aromatic ring in the produced amine was further hydrogenated to give the saturated amine. The latter process could be inhibited by addition of 1 equiv of DPPB. Note that addition of 2 equiv of DPPB significantly reduced the conversion of imine to amine (55% in 24.5 h under the same conditions shown in Table 1, entry 9).

The hydrogenation of imines, catalyzed by **1** and added DPPB (100/1/1 ratio of imine/**1**/DPPB) in 9/1 THF/MeOH, is sensitive to both electronic and steric effects, and the results of reactions of a variety of aldimines and ketimines are presented in Table 2. Reaction of *N*-benzylidene-*n*-butylamine at 40 °C and 400 psi of H_2 for 26 h afforded *N*-benzyl-*n*-butylamine in 98% conversion and 95% isolated yield (Table 2, entry 2). The reactivity of imines, and the yield of amines, decreased with an increase in the effective bulk of the *N*-substituent from *n*-butyl to *sec*-butyl to *tert*-butyl (Table 2, entries 2–4). Substitution of a hydrogen atom of the methyl group by phenyl (Ph–CH=N–CH_2–Ph; Table 2, entry 5) resulted in a lower yield at 200 psi of H_2, but dibenzylamine was isolated in 84% yield using 400 psi of H_2. Under identical conditions, the methoxypropylimine (Table 2, entry 6) was also hydrogenated in high yield. *N*-Benzylideneaniline, containing an *N*-Ph group, was much less active than the *N*-Me analog, and reasonable yield of amine was only realized at higher H_2 pressure (600 psi; Table 2, entries 7 and 8). Alkyl aldimines and ketimines were hydrogenated in good to quantitative yield (Table 2, entries 9–13). The aryl alkyl ketimine $PhC(CH_3)=NC_4N_9$ gave the amine in 47% isolated yield using 600 psi of H_2, and use of 1500 psi of H_2 increased the yield by 19% (Table 2, entry 14).

It was reported that $RhCl(PPh_3)_3$ and $[Rh(PPh_3)_2(NBD)]PF_6$ could hydrogenate aldimines at 25 °C and 1 atm of H_2 in *neat* alcohol as the solvent.[14] No examples were presented, however, for the use of these catalysts in the hydrogenation of ketimines under the same conditions. Of note, the alcohol solvent was essential for activity in these Rh-based systems[14] and for other effective imine hydrogenation catalysts;[18] a possible chemical role for a coordinated alcohol, in providing H-bonded stabilization of a putative, coordinated η^2-imine moiety, has been suggested,[14,18] but clearly the data of Table 1 show that systems can be effective in the absence of alcohol. The zwitterionic rhodium complex **1**–DPPB system shows comparable reactivity toward the hydrogenation of aromatic ketimines as rhodium(I) catalysts reported previously, such as $[Rh(diene)Cl]_2$–P–P (P–P = chelating phosphines)[26,28,34,36,38,42] and $[Rh(NBD)(BDPP)]^+$ (BDPP = 2,4-bis(diphenylphosphino)pentane).[37] However, the **1**–DPPB catalyst system possesses higher reactivity for the hydrogenation of alkyl ketimines than the *in situ* produced cationic $[Rh(diene)Cl]_2$–P–P catalysts.[26,28]

In conclusion, the zwitterionic rhodium complex **1** is an excellent catalyst for the hydrogenation of both aldimines and ketimines. The reaction is simple in execution and workup.

(41) Oppolzer, W.; Wills, M.; Starkemann, C.; Bernardinelli, G. *Tetrahedron Lett.* **1990**, *31*, 4117.
(42) Bakos, J.; Orosz, A.; Heil, B.; Laghmari, M.; Lhoste, P.; Sinou, D. *J. Chem. Soc., Chem. Commun.* **1991**, 1684.
(43) James, B. R. In *Homogeneous Hydrogenation*; John Wiley & Sons: New York, 1973.

Table 2. (η^6-PhBPh$_3$)$^-$Rh$^+$(1,5-COD)-Catalyzed Hydrogenation of Imines[a]

entry no.	substrate	product[b]	$P(H_2)$ (psi)	time (h)	conversion (yield, %)[c]
1	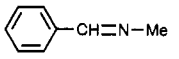	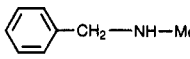	200	25	>99 (94)
2	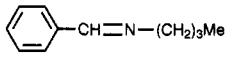	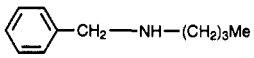	200 400	25 26	92 (71) 98 (95)
3	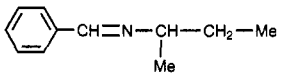	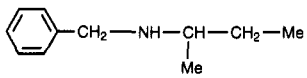	400	48	87 (79)
4	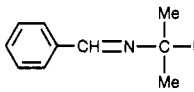	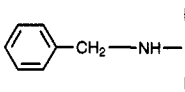	400	76	30 (27)
5	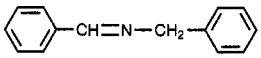	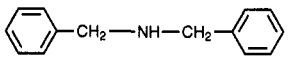	200 400	25 27	68 92 (84)
6	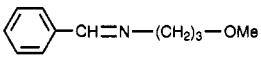	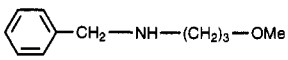	400	25	94 (86)
7	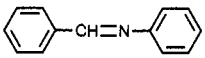	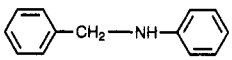	200 600	49 25	17 47 (40)
8	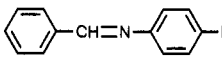	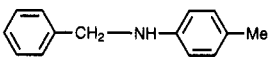	600	96	66 (53)
9	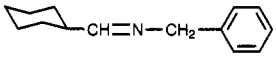	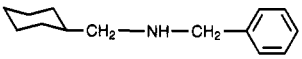	400	25	87 (78)
10	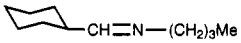	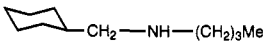	400	18	>99 (93)
11	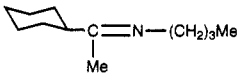	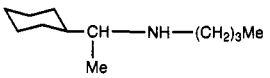	600	68	96 (86)
12	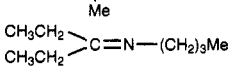	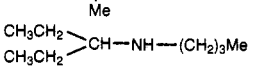	600	20	>99 (94)
13	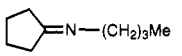	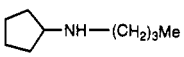	600	25	>99 (89)[d]
14	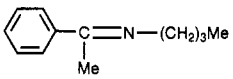	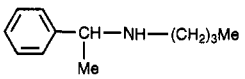	600 1500	96 48	53 (47) 70 (66)

[a] Reaction conditions: substrate, 4.0 ± 0.2 mmol; catalyst, 1.0 mol %; DPPB, 1.0 mol %; THF/MeOH (v/v 9/1, 10 mL); temperature, 40 °C. [b] Products were characterized by comparison of spectral data (IR, NMR (^{1}H, ^{13}C), MS) with literature results. [c] Conversions were determined by ^{1}H NMR with dibenzyl ether or triphenylmethane as the internal reference; yields were isolated yields of purified products. [d] Use of [Rh(COD)$_2$]$^+$OTf$^-$ instead of the zwitterionic complex, under otherwise *identical* conditions, afforded the hydrogenation product in 3% yield. Also, use of [(DPPB)Rh(COD)]$^+$BF$_4^-$ or [(DPPB)Rh(COD)]$^+$BPh$_4^-$ as a substitute for the zwitterionic complex and DPPB, under otherwise *identical* conditions, gave the reduction products in 20% and 23% yield, respectively.

Experimental Section

General Considerations. All ^{1}H and ^{13}C NMR spectra were recorded on a Varian 200 MHz Gemini spectrometer using $CDCl_3$ as the solvent. Mass spectra were obtained on a VG 7070 E mass spectrometer. Infrared spectra were run on a Bomem MB-100 FT-IR spectrometer. Solvents were dried and purified by standard methods. Column chromatography was performed with Merck Silica gel 60 (70–230 or 230–400 mesh) using solvent combinations determined via initial TLC analysis with Merck Silica gel 60 F_{254} plates (precoated).

N-Benzylidenemethylamine was purchased from Aldrich and used as received. All other chemicals used for making imines and catalyst were purchased from Aldrich, Lancaster, or Strem chemical companies and used as received. All imines, prepared at ambient temperature (aldimines) or at 70 °C (ketimines) using procedures described previously[44] and purified by Kugelrohr (bulb to bulb) distillation under reduced pressure, were characterized by NMR (^{1}H, ^{13}C), IR, and MS methods and compared with literature data, except for *N*-(1-cyclohexylethylidene)-*n*-butylamine (Cy(Me)C=N–C_4H_9). ^{1}H NMR ($CDCl_3$, δ(TMS) 0.00 ppm): major isomer, 3.22 (t, 2H, N–CH_2), 2.15 (m, 1H, C*H*), 1.74 (s, 3H, CH_3–C=N), 1.85–1.50 (m, 7H), 1.45–1.10 (m, 7H), 0.93 (t, 3H, CH_2CH_3); minor isomer, 3.29 (t, 2H, N–CH_2), 1.91 (s, 3H, CH_3–C=N), all other resonances are obscured by those of the major isomer. ^{13}C NMR ($CDCl_3$, $\delta(CDCl_3)$ 77.00 ppm, major isomer): 173.19 (*C*=N), 50.88 (N–CH_2), 50.69 (*C*H), 33.01 (CH_2), 30.14 ($2CH_2$), 26.11 ($2CH_2$), 26.01 (CH_2), 20.69 (CH_2), 14.72 (CH_3), 14.01 (CH_3). IR ν(C=N) 1656 cm^{-1} (neat). MS: M$^+$, 181 (4). Bp (Kugelrohr distillation): 60 °C/0.5 mmHg. Anal. Calcd for $C_{12}H_{23}N$: C, 79.49; H, 12.78; N, 7.72. Found: C, 79.23; H, 12.65; N, 7.81. (η^6-PhBPh$_3$)$^-$Rh$^+$(1,5-COD) was synthesized according to the literature procedure.[1]

General Procedure for the Hydrogenation Reactions. To a 45-mL Parr autoclave fitted with a glass liner and stirring bar was added (η^6-PhBPh$_3$)$^-$Rh$^+$(1,5-COD) (0.04 mmol), substrate (4.0 mmol), 1,4-bis(diphenylphosphino)butane (DPPB) (0.04 mmol), dry THF (9 mL), and methanol (1 mL). The H_2 line was flushed three times with H_2, the autoclave was fill–vented three times with H_2 to displace the air, and subsequently the pressure was increased to the desired level with H_2. The mixture was stirred in the autoclave at 40 °C (oil bath temperature, see Table 2 for reaction time). The excess H_2 was released, the system was disassembled, and the solvent was removed from the reaction mixture by rotary evaporation. The residues were analyzed by ^{1}H NMR. In those cases where reactions were incomplete, an internal reference (either dibenzyl ether or triphenylmethane) was added and the percent

(44) Taguchi, K.; Westheimer, F. H. *J. Org. Chem.* **1971**, *36*, 1570.

conversion was determined by ^1H NMR. The reaction mixture was separated by silica gel column chromatography using 4/1 (v/v) *n*-pentane/ether as the eluant followed by ether and then acetone. The product was purified further by Kugelrohr distillation under reduced pressure. All products were characterized spectroscopically (NMR (^1H, ^{13}C), IR, and MS) and compared with literature data, except for *N*-butyl-(1-cyclohexylethyl)amine (Cy(Me)CH−NH−C_4H_9). ^1H NMR ($CDCl_3$, δ(TMS) 0.00 ppm): 2.72−2.42 (m, 3H, C*H*−N−C*H*$_2$), 1.82−1.55 (m, 5H), 1.53−1.00 (m, 11H), 0.97 (d, 3H, C*H*$_3$−CH), 0.95 (t, 3H, CH_2CH_3). ^{13}C NMR ($CDCl_3$, $\delta(CDCl_3)$ 77.00 ppm): 57.82 (*C*H−N), 47.32 (N−*C*H$_2$), 42.82 (*C*H), 32.56 (*C*H$_2$), 29.96 (*C*H$_2$), 27.86 (*C*H$_2$), 26.74 (*C*H$_2$), 26.63 (*C*H$_2$), 26.47 (*C*H$_2$), 20.55 (*C*H$_2$), 16.72 (*C*H$_3$), 13.99 (*C*H$_3$). IR, ν(NH) 3312 cm^{-1} (neat). MS: $(M + H)^+$, 184 (100). Bp (Kugelrohr distillation): 65 °C/0.5 mmHg. Anal. Calcd for $C_{12}H_{25}N$: C, 78.62; H, 13.74; N, 7.64. Found: C, 78.90; H, 13.85; N, 7.97.

Acknowledgment. We are indebted to the Natural Sciences and Engineering Research Council of Canada for the award of a collaborative project grant in support of this research. We thank Johnson Matthey for a loan of some $RhCl_3 \cdot 3H_2O$.

OM9502087

Organolead Derivatives of Coordinatively Saturated Platinum(II) Olefin Complexes. Molecular Structure of [PtCl(PbPh$_2$Cl)(2,9-dimethyl-1,10-phenanthroline)(dimethyl maleate)] and Its Deplumbation Product [PtCl(Ph)(2,9-dimethyl-1,10-phenanthroline)(dimethyl maleate)]

Vincenzo G. Albano,* Carlo Castellari, and Magda Monari

Dipartimento di Chimica "G. Ciamician", Università di Bologna, via F. Selmi 2, I-40126, Bologna, Italy

Vincenzo De Felice

Facoltà di Agraria, Università del Molise, via Tiberio 21/A, I-86100, Campobasso, Italy

Maria L. Ferrara and Francesco Ruffo*

Dipartimento di Chimica, Università di Napoli "Federico II", via Mezzocannone 4, I-80134, Napoli, Italy

Received April 3, 1995[⊗]

The stabilization of Pt(II)–PbR$_2$Cl linkages (R = Me, Ph) is reported. The compounds of general formula [PtCl(PbR$_2$Cl)(N–N)(olefin)] (N–N = 2,9-dimethyl-1,10-phenanthroline (dmphen) and 6-methylpyridine-2-phenylimine (pimpy)) have been obtained through the oxidative addition of PbMe$_2$Cl$_2$ and PbPh$_2$Cl$_2$ to three-coordinate Pt(0) complexes [Pt(N–N)(olefin)]. In the presence of less hindered N–N ligands (e.g., 2-methyl-1,10-phenanthroline) the addition leads only to the isolation of the mononuclear Pt(II) complexes [PtCl(R)(N–N)]. The molecular structure of [PtCl(PbPh$_2$Cl)(dmphen)(dimethyl maleate)] has shown that the Pt–Pb bond is stabilized by an additional interaction of a carboxylate oxygen to the lead atom. The deplumbation product [PtCl(Ph)(dmphen)(dimethyl maleate)] has also been characterized by X-ray crystallography.

Introduction

The behavior of group 14 organometal fragments in the coordination environments of transition ions is the object of extensive investigations.[1] In the case of the d^8 ions the interest has been mainly addressed to tin compounds, also in view of their useful applications.[2,3] However, lead derivatives have been investigated to a very limited extent.[1] To our knowledge, no examples of organolead fragments linked to a metal of the platinum group in a coordinatively saturated environment have yet been reported,[4] and only very few four-coordinate 16e complexes are known.[5–7]

On the other hand, recent results have prompted a feasible route to the attainment of coordinatively saturated platinum olefin complexes with Pt–Sn[8] and Pt–Hg[9] bonds, prepared through oxidative addition of organometal halides to three-coordinate Pt(0) species (eq 1):

$$[Pt(N–N)(olefin)] + MR_xCl_{y+1} \rightarrow [PtCl(MR_xCl_y)(N–N)(olefin)] \quad (1)$$

$$M = Sn, Hg$$

Aiming to understand the behavior of organolead halides in similar processes, we have extended the addition reaction to PbR$_n$Cl$_{4-n}$ derivatives.[10] Thus, we report here the synthesis of stable coordinatively saturated species of general formula [PtCl(PbR$_2$Cl)(N–N)(olefin)] (N–N = chelate ligand) and their characterization and the molecular structures of [PtCl(PbPh$_2$Cl)(dmphen)(dimethyl maleate)] and its deplumbation product [PtCl(Ph)(dmphen)(dimethyl maleate)].

Results

Products from Three-Coordinate Pt(0) Species and PbR$_2$X$_2$. The three-coordinate substrates (type **I**)

[⊗] Abstract published in *Advance ACS Abstracts,* July 15, 1995.

(1) Mackay, K. M.; Nicholson, B. K. In *Comprehensive Organometallic Chemistry*; Pergamon Press: New York, 1982; Vol. 2, 650.

(2) Kumar Das, V. G.; Chu, C. In *The Chemistry of the Metal-Carbon Bond*; Hartley, F. R., Patai, S., Eds.; J. Wiley and Sons: New York, 1985; Vol. 3, 1.

(3) Holt, M. S.; Wilson, W. L. *Chem. Rev.* **1989**, *89*, 11.

(4) A remarkable exception consists in a recently reported trinuclear cluster containing a bicoordinate lead in the axial position of the square-pyramidal coordination spheres of two Pt(II) atoms: Usòn, R.; Forniés, J.; Falvello, L. R.; Usòn, M. A.; Usòn, I. *Inorg. Chem.* **1992**, *31*, 3697.

(5) Deganello, G.; Carturan, G.; Belluco, U. *J. Chem. Soc. A* **1968**, 2873.

(6) Crociani, B.; Nicolini, M.; Clemente, D. A.; Bandoli, G. *J. Organomet. Chem.* **1973**, *49*, 249.

(7) Al-Allaf, T. A. K.; Butler, G.; Eaborn, C.; Pidcock, A. *J. Organomet. Chem.* **1980**, *188*, 335.

(8) Albano, V. G.; Castellari, C.; De Felice, V.; Panunzi, A.; Ruffo, F. *J. Organomet. Chem.* **1992**, *425*, 177.

(9) Cucciolito, M. E.; De Felice, V.; Giordano, F.; Panunzi, A.; Ruffo, F. *J. Chem. Soc., Dalton Trans.* **1993**, 3421.

(10) A preliminary account of this work has been previously given: Albano, V. G.; Castellazi, C.; Panunzi, A.; Ruffo, F.; Sanchez, A. Latin-American Inorganic Chemistry Meeting, Santiago De Compostela, Spain, September, 1993; Abstracts, p 205.

0276-7333/95/2314-4213$09.00/0

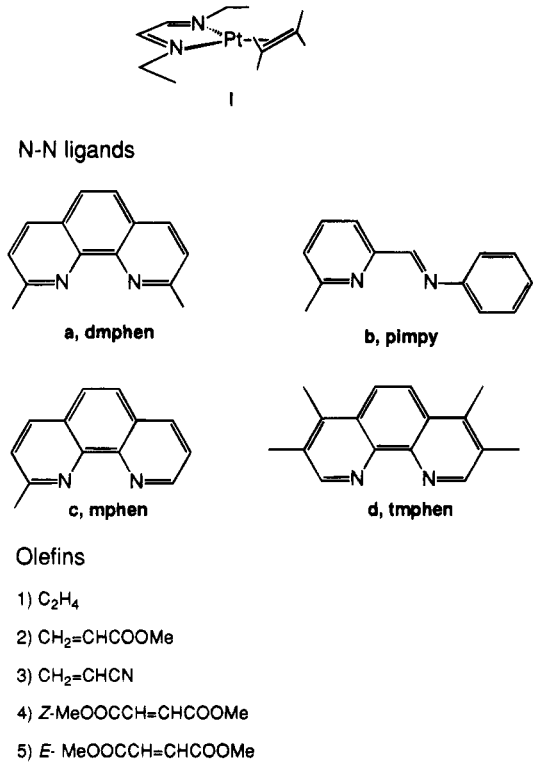

Figure 1.

Scheme 1

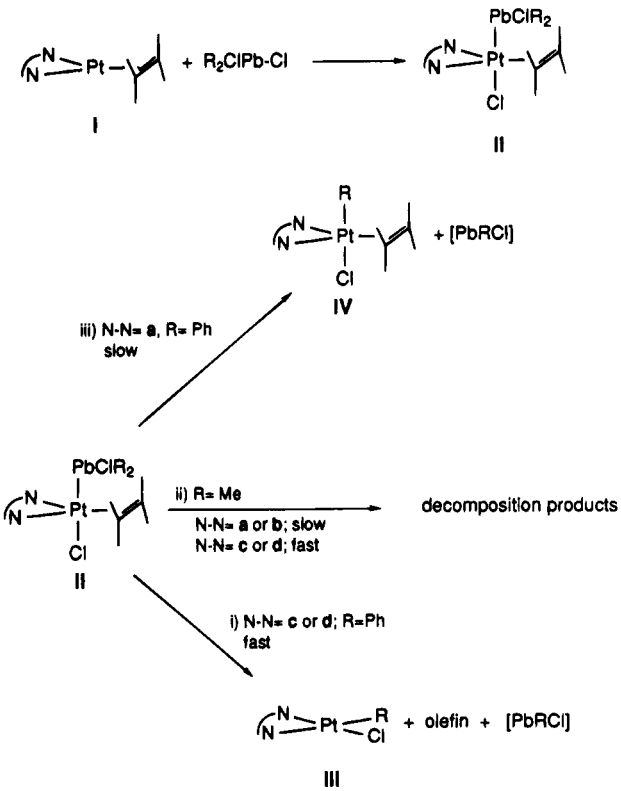

are denoted by a label in which a lower-case letter and a subscript number represent the chelate and the olefin ligand, respectively (Figure 1).

Owing to their polynuclear structure, $PbMe_2Cl_2$ and $PbPh_2Cl_2$ are nearly insoluble in the common organic solvents, and so the reactions have been performed in a heterogeneous phase. Chloroform or methylene chloride, which are good solvents for the platinum(0) species, have been used as reaction media.

The nature of the isolated product depends on the features of the N–N chelate, the olefin, and the R group (see Scheme 1).

The five-coordinate type **II** products are isolated when N–N is **a** or **b**. The completion of the reaction is indicated by the total dissolution of the plumbane. The products are obtained as yellow-orange crystalline precipitates from the reaction solution by addition of diethyl ether.

The type **II** complexes can undergo additional reactions (processes i–iii) but are not isolated if these are fast (see Discussion).

When the reaction produced a type **III** complex, its progression was monitored through measurements of the ^{1}H NMR spectrum of the crude soluble material recovered by solvent removal from filtered aliquots of the reaction mixture. The isolation of type **III** products (namely, [PtCl(Ph)(mphen)] (**IIIc**) and [PtCl(Ph)-(tmphen)] (**IIId**)) was carried out by removing the solvent under vacuum after filtration of the insoluble material.

The characterization of the complexes was performed through elemental analyses and spectroscopic NMR measurements. Tables 1–3 list type **II** complexes and their characterization data. The notation for the complexes includes a prime which refers to the R group on Pb: single prime for phenyl and double prime for methyl.

Particularly, ^{1}H NMR spectra allow the unequivocal structural assignment **II** only for the products arising from the addition of $PbMe_2Cl_2$. On the other hand, owing to the complexity of the phenyl patterns, no clearcut conclusion can be reached by inspecting the ^{1}H NMR spectra of the products derived from $PbPh_2Cl_2$, and the alternative reaction pathway involving the cleavage of the Pb–Ph bond can not be ruled out. In

Table 1. Elemental Analysis for the Type II Five-Coordinate Complexes

no.	complex	formula	Anal. found (calcd) C	H	N
IIa′$_1$	[PtCl($PbPh_2Cl$)(dmphen)(C_2H_4)]	$C_{28}H_{26}Cl_2N_2PbPt$	39.01 (38.94)	3.11 (3.03)	3.28 (3.24)
IIa′$_2$	[PtCl($PbPh_2Cl$)(dmphen)(CH_2=CHCOOMe)]	$C_{30}H_{28}Cl_2N_2O_2PbPt$	39.20 (39.09)	3.18 (3.06)	3.02 (3.04)
IIa′$_3$	[PtCl($PbPh_2Cl$)(dmphen)(CH_2=CHCN)]	$C_{29}H_{25}Cl_2N_3PbPt$	39.12 (39.19)	2.69 (2.84)	4.81 (4.73)
IIa′$_4$	[PtCl($PbPh_2Cl$)(dmphen)(*Z*-MeOOCCH=CHCOOMe)]	$C_{32}H_{30}Cl_2N_2O_4PbPt$	39.46 (39.23)	3.14 (3.09)	2.77 (2.86)
IIa′$_5$	[PtCl($PbPh_2Cl$)(dmphen)(*E*-MeOOCCH=CHCOOMe)]	$C_{32}H_{30}Cl_2N_2O_4PbPt$	39.35 (39.23)	3.02 (3.09)	2.83 (2.86)
IIa″$_2$	[PtCl($PbMe_2Cl$)(dmphen)(CH_2=CHCOOMe)]	$C_{20}H_{24}Cl_2N_2O_2PbPt$	30.42 (30.12)	2.95 (3.03)	3.51 (3.51)
IIa″$_4$	[PtCl($PbMe_2Cl$)(dmphen)(*Z*-MeOOCCH=CHCOOMe)]	$C_{22}H_{26}Cl_2N_2O_4PbPt$	30.64 (30.88)	3.15 (3.06)	3.40 (3.27)
IIa‴$_4$	[PtCl($PbPhCl_2$)(dmphen)(*Z*-MeOOCCH=CHCOOMe)]	$C_{26}H_{25}Cl_3N_2O_4PbPt$	33.67 (33.29)	2.85 (2.69)	3.05 (2.99)
IIb′$_4$	[PtCl($PbPh_2Cl$)(pimpy)(*Z*-MeOOCCH=CHCOOMe)]	$C_{31}H_{30}Cl_2N_2O_4PbPt$	38.11 (38.47)	3.12 (3.12)	2.82 (2.89)
IIb′$_5$	[PtCl($PbPh_2Cl$)(pimpy)(*E*-MeOOCCH=CHCOOMe)]	$C_{31}H_{30}Cl_2N_2O_4PbPt$	38.51 (38.47)	3.19 (3.12)	2.96 (2.89)
IIb″$_4$	[PtCl($PbMe_2Cl$)(pimpy)(*Z*-MeOOCCH=CHCOOMe)]	$C_{21}H_{26}Cl_2N_2O_4PbPt$	30.01 (29.90)	3.04 (3.11)	3.38 (3.32)

Table 2. Selected ^{1}H NMR[a] (δ(ppm) and J(Hz)) for Type II Five-Coordinate Complexes

no.	$PbMe_2Cl$[b]	olefin−H[c]	Me−C(het)	others
IIa′$_1$		3.57 (60, app d, 2H)	3.44 (6H)	
		3.28 (78, app d, 2H)		
IIa′$_2$		3.91 (81, dd, 1H)	3.34 (3H)	3.75 (OMe, 3H)
		3.51 (43, dd, 1H)	2.87 (3H)	
		3.42 (*d*, dd, 1H)		
IIa′$_3$ (more stable isomer, see text)		3.54 (*d*, d, 1H)	3.40 (3H)	
	3.32 (*d*, dd, 1H)	3.19 (3H)		
		1H[e]		
IIa′$_3$ (other isomer)		3.94 (*d*, dd, 1H)	3.45 (3H)	
		2H[e]	3.34 (3H)	
IIa′$_4$		4.45 (78, 2H)	3.20 (6H)	3.50 (OMe, 6H)
IIa′$_5$		4.76 (74, d, 1H)	3.53 (3H)	3.80 (OMe, 3H)
		4.44 (69, d, 1H)	2.78 (3H)	3.71 (OMe, 3H)
IIa″$_2$	1.63 (57, 3H)	3.86 (74, dd, 1H)	3.43 (3H)	3.79 (OMe, 3H)
	1.03 (54, 3H)	3.18 (40, dd, 1H)	3.27 (3H)	
		1H[e]		
IIa″$_4$	1.13 (57, 6H)	4.38 (78, 2H)	3.45 (6H)	3.83 (OMe, 6H)
IIb′$_4$		4.71 (78, d, 1H)	2.69 (3H)	9.13 (49,[f] CH=N, 1H)
		3.87 (72, d, 1H)		3.75 (OMe, 3H)
				2.67 (OMe, 3H)
IIb′$_5$ (isomer, 80% abundance)		4.44 (72, ABq, 2H)	2.64 (3H)	9.10 (50,[f] CH=N, 1H)
				3.67 (OMe, 3H)
IIb″$_4$	1.27 (59, 6H)	4.45 (76, d, 1H)	3.15 (3H)	9.07 (48,[f] CH=N, 1H)
		4.00 (76, d, 1H)		3.79 (OMe, 3H)
				3.41 (OMe, 3H)
IIa‴$_4$		4.46 (68, 4,[g] 2H)	3.39 (6H)	3.95 (OMe, 6H)

[a] 270 or 200 MHz, $CDCl_3$ as solvent and $CHCl_3$ (δ 7.26 ppm) as internal standard. Abbreviations: d, doublet; q, quartet; app, apparent; no attribute, singlet. [b] $^2J_{Pb-H}$ in parentheses. [c] $^2J_{Pt-H}$ in parentheses. [d] $^2J_{Pt-H}$ not measurable. [e] Signals partially or totally overlapped by other signals. [f] $^3J_{Pt-H}$. [g] $^3J_{Pb-H}$.

Table 3. Selected ^{13}C NMR[a] (δ(ppm) and J(Hz)) for Some Type II Five-Coordinate Complexes

no.	Pb−C−C[b]	olefin[c]	Me−C(het)	OMe
IIa′$_2$	135.9 (76, 2C)	34.8 (*d*, 1C)	30.9 (1C)	53.0 (1C)
	135.5 (76, 2C)	26.9 (*d*, 1C)	30.0 (1C)	
IIa′$_3$[e]	136.1 (79, 2C)	25.6 (406, 1C)	30.9 (1C)	
	135.4 (76, 2C)	7.05 (342, 1C)	29.0 (1C)	
IIa′$_4$	135.2 (83, 4C)	33.7 (375, 2C)	29.7 (2C)	52.8 (2C)
IIa′$_5$	135.7 (82, 2C)	33.4 (359, 1C)	31.2 (1C)	53.4 (1C)
	135.4 (78, 2C)	29.3 (367, 1C)	29.3 (1C)	51.3 (1C)
IIb′$_4$	135.7 (81, 2C)	35.6 (374, 1C)	29.7 (1C)	53.7 (1C)
	135.6 (76, 2C)	35.2 (374, 1C)		51.4 (1C)

[a] 67.9 or 50.3 MHz, $CDCl_3$ as solvent and $CHCl_3$ (δ 77.0 ppm) as internal standard. [b] $^2J_{Pb-C}$ in parentheses. [c] $^1J_{Pt-C}$ in parentheses. [d] $^1J_{Pt-C}$ not measurable. [e] More stable isomer, see text.

these cases ^{13}C NMR spectra are necessary to confirm the type **II** structure.

Some aspects of the NMR spectroscopic results appear to be worthy of comment. These are mainly concerned with stereoisomerism, which in type **IIa** complexes is related only to the symmetry of the olefin ligand:

(i) Ethylene (D_{4h} symmetry) can only afford a single isomer. The olefin proton signals of **IIa′$_1$** are two apparent doublets (AA′XX′ system), owing to the unequality of the two axial groups.

(ii) The symmetry of dimethyl maleate (C_{2v}) is consistent with the possible attainment of two diastereomers. However, the addition is stereoselective and only one isomer is actually observed. For example, in complex **IIa″$_4$** the olefin protons give rise to a singlet (δ 4.38 ppm, $^2J_{Pt-H}$ = 78 Hz), and another singlet at δ 1.13 ppm is observed for the methyl protons of the $-PbMe_2Cl$ fragment.

The proton spectrum of **IIa′$_4$** presents a complex pattern for the $-PbPh_2Cl$ group, while the ^{13}C spectrum supports the equivalence of the two aromatic rings. In fact, a single signal is observed for the two pairs of carbon atoms adjacent to the Pb−C_{ipso} bond (δ 135.2 ppm, $^2J_{Pb-C}$ = 83 Hz).[11]

(iii) The coordination of a prochiral olefin, such as dimethyl fumarate (symmetry C_{2h}) in **IIa′$_5$**, affords two enantiomers, obviously not distinguishable via NMR. The nonequivalent olefin protons signals are doublets, with coupling to ^{195}Pt.

The two Ph groups on the lead atom are diastereotopic, and the corresponding signals are resolved in both ^{1}H and ^{13}C NMR spectra. The latter also indicate that the two groups are both on Pb, accounting for the presence of two nearly coincident signals for the two diasterotopic carbon pairs adjacent to the Pb−C_{ipso} bond (δ 135.7 and 135.4 ppm, $^2J_{Pb-C}$ = 82 and 78 Hz, respectively).

(iv) The coordination of olefins with lower symmetry, such as acrylonitrile and methyl acrylate, makes possible in principle the existence of two diastereomeric pairs. A freshly prepared $CDCl_3$ solution of **IIIa′$_3$** displays the presence of both of them in a 1:1 ratio. On standing, one of the two isomers becomes the predominant species.

On the other hand, spectra of the complexes **IIa′$_2$** and **IIa″$_2$** show the presence of only one of the two possible isomers. Three distinct signals (doublets or a doublet of doublets) are observed for the olefin protons of acrylonitrile and methyl acrylate, when overlap by other signals does not prevent the assignment.

(v) Analogous considerations hold for type **II** complexes containing ligand **b**. The lack of symmetry in this ligand allows the formation of diastereomeric pairs in dimethyl fumarate and dimethyl maleate complexes, which have actually been observed in **IIb′$_5$** in an approximate ratio of 4:1.

Deplumbation of IIa′$_4$. Freshly prepared samples of **IIa′$_4$** are quite pure. After slow recrystallization,

(11) Schneider-Koglin, C.; Mathiasch, B.; Draeger, M. *J. Organomet. Chem.* **1993**, *448*, 39.

aiming to obtain crystals suitable for X-ray diffraction (see Experimental Section), microscopic examination of the crop has led us to ascertain that very few crystals of different nature accompany the main product. Repeated crystallizations from aged samples have shown some increase of the unknown species, suggesting a progressive decomposition process. An X-ray diffraction study has revealed the new species to be the deplumbation product [PtCl(Ph)(dmphen)(dimethyl maleate)] (**IVa′$_4$**).

This species has also been obtained in good yield through another procedure. When $AgBF_4$ is added to **IIa′$_4$** in a dichloromethane/acetonitrile solution, the formation of an orange oil is observed after removal of the solvents. On the grounds of previous results concerning cationic type **II** compounds,[12] we considered this material to be mainly [Pt($PbPh_2Cl$)(MeCN)(dmphen)-(dimethyl maleate)](BF_4). This material transforms in nitromethane solution as a deplumbation reaction takes place. Addition of LiCl to the reaction mixture leads to the attainment of **IVa′$_4$**, which actually exists in two isomeric forms differing in olefin orientation. However, after some days in chloroform solution only the most thermodynamically stable isomer is present, and its NMR spectrum is coincident with the spectrum of the crystals formed from **IIa′$_4$**.

Reaction of $PbMe_3Cl$ with Ia$_1$. The addition of an equimolar amount of $PbMe_3Cl$ to **Ia$_1$** in a toluene suspension affords the known five-coordinate species [PtClMe(dmphen)(C_2H_4)][13] in 60% yield. The reaction is complete in a few minutes, and the product is recovered by chloroform extraction of the crude precipitate.

The reaction was also monitored by ^1H NMR spectroscopy. The spectrum of a fresh deuteriochloroform sample, recorded ca. 3 min after the mixing the reagents, shows the presence of three products. One of them disappears progressively, while the concentration of the other two (in ca. 4:1 ratio) increases correspondingly. The two growing species are [PtClMe(dmphen)-(C_2H_4)] and, most probably, [$PtMe_4$(dmphen)]. The latter assignment is suggested by the observation of two methyl signals at δ 2.10 ($^2J_{Pt-H}$ = 74 Hz) and −1.01 ($^2J_{Pt-H}$ = 45 Hz) ppm, which can be attributed to the equatorial and axial methyls in an octahedral complex[14] and to the equivalence of the halves of the corresponding dmphen. Furthermore, another signal, which is attributed to $PbMe_4$, also grows.

More interesting for this study is the first fading species, precursor of the other compounds. The ^1H NMR signals that pertain to it show the halves of the chelate to be equivalent, as expected in a type **II** complex. The signals of the ethylene protons (two apparent doublets at δ 3.17 and 2.18 ppm) are also reasonably consistent with equatorial coordination in a bipyramidal trigonal geometry.[12] The axial positions could be occupied by −Cl and $-PbMe_3$ or alternatively by −Me and $-PbMe_2$-Cl. The first choice seems to be ruled out by the absence of the expected intense (9H) single resonance. Instead, two signals are observed, respectively at δ 0.36 ($^2J_{Pb-H}$ = 32 Hz) and −0.25 ($^2J_{Pt-H}$ = 68 Hz) ppm, in a 6:3 ratio. These results point to the presence of the ligand fragments $-PbMe_2Cl$ and −Me in the axial positions of the trigonal bipyramid and indicate that the reaction proceeds through the activation of the Pb−C bond, as depicted in Scheme 2.

Scheme 2

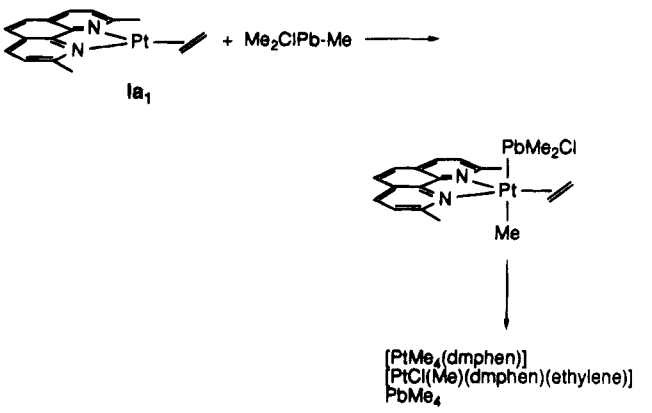

Addition of Cl_2 and HCl to IIa′$_4$. Gaseous hydrogen halides H−X and halogens X_2 are reported to react with square-planar platinum(II) complexes containing a Pt−Pb bond by cleaving the bimetallic linkage according to the following examples:[5,6]

$$[PtR(PbR_3)(PPh_3)_2] + HBr \rightarrow [PtR(Br)(PPh_3)_2] + \text{Pb-containing products}$$

$$[PtR(PbR_3)(PPh_3)_2] + Br_2 \rightarrow [PtR(Br)(PPh_3)_2] + \text{Pb-containing products}$$

The first step of the reaction is supposed to be the oxidative addition of the electrophile to the bimetallic square-planar complex. The corresponding octahedral product would subsequently undergo the reductive elimination of a plumbane.

A different reaction pathway is observed when gaseous HCl or Cl_2 are bubbled in a chloroform solution of **IIa′$_4$**. In these cases, the reaction affects the Pb−Ph linkage. Thus, the new five-coordinate complex **IIa‴$_4$**, characterized by the presence of the apical ligand fragment $-PbPhCl_2$, can be isolated (eq 2).

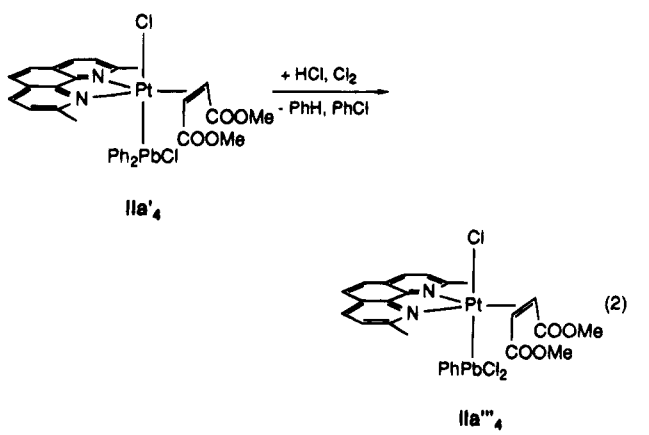

Complex **IIa‴$_4$** has been characterized through elemental analysis and NMR spectroscopy, even though only the proton spectrum has been run, owing to the very low solubility in the common solvents. The general

(12) Albano, V. G.; Natile, G.; Panunzi, A. *Coord. Chem. Rev.* **1994**, *133*, 67.
(13) Cucciolito, M. E.; De Felice, V.; Panunzi, A.; Vitagliano, A. *Organometallics* **1989**, *8*, 1180.
(14) Lashanizadehgan, M.; Rashidi, M.; Hux, J. E.; Puddephatt, R.; Ling, S. S. M. *J. Organomet. Chem.* **1984**, *269*, 317.

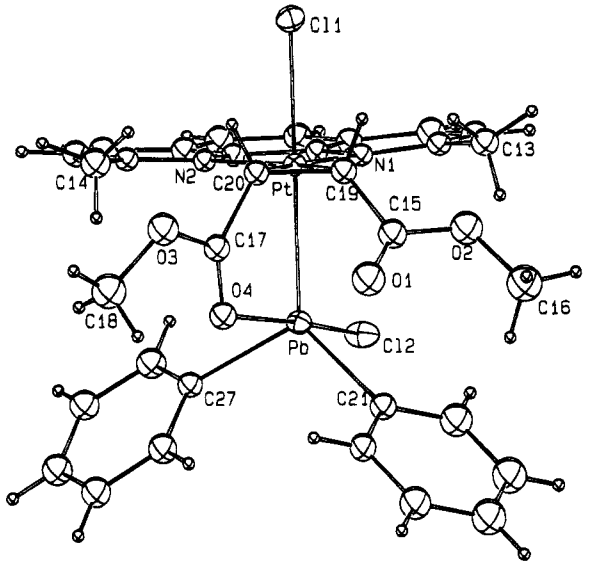

Figure 2. ORTEP drawing of [PtCl(PbPh$_2$Cl)(dmphen)(dimethyl maleate)] (**IIa'$_4$**).

Table 4. Relevant Bond Distances (Å) and Angles (deg) for IIa'$_4$

Pt–Cl(1)	2.447(6)	Pb–Cl(2)	2.618(6)
Pt–Pb	2.642(1)	Pb–C(21)	2.19(1)
Pt–C(19)	2.09(2)	Pb–C(27)	2.21(1)
Pt–C(20)	2.10(2)	Pb–O(4)	2.66(1)
Pt–N(1)	2.169(7)	C(19)–C(20)	1.48(3)
Pt–N(2)	2.180(7)	C(17)–C(20)	1.50(2)
C(19)–C(15)	1.49(2)	C(17)–O(4)	1.20(1)
C(15)–O(1)	1.16(2)	C(17)–O(3)	1.34(2)
C(15)–O(2)	1.31(2)	O(3)–C(18)	1.44(2)
O(2)–C(16)	1.44(2)		
Cl(1)–Pt–Pb	178.7(1)	N(2)–Pt–N(1)	75.7(2)
Cl(2)–Pb–C(21)	92.8(5)	O(4)–Pb–Cl(2)	174.7(3)
Cl(2)–Pb–C(27)	92.8(4)	O(4)–Pb–C(21)	89.6(6)
O(4)–Pb–C(27)	81.9(5)	C(27)–Pb–C(21)	110.0(6)
Pt–Pb–C(27)	119.6(4)	Pt–Pb–Cl(2)	101.2(1)
Pt–Pb–C(21)	127.3(4)	Pt–Pb–O(4)	81.0(3)

spectral features are consistent with the proposed bipyramidal trigonal geometry and indicate that only one of the two possible isomers exists in solution. In this case, the $^3J_{Pb-H}$ coupling constant between the olefin protons and the lead atom, which is not detectable in the spectra of the related type **II** species, could be measured (4 Hz).

Finally, we note that the possible alternative attempt to obtain complex **IIa'''$_4$** through the oxidative addition of $PbPhCl_3$ to the precursor [Pt(dmphen)(dimethyl maleate)] (**Ia$_4$**) is discouraged by the high instability of the organolead reagent.[15]

Structure of [PtCl(PbPh$_2$Cl)(dmphen)(dimethyl maleate)] (IIa'$_4$). The molecular structure of the title compound, determined by X-ray diffraction, is shown in Figure 2, and some relevant bond values are listed in Table 4. The molecule exhibits trigonal bipyramidal coordination around the platinum atom with the dmphen and dimethyl maleate ligands defining the equatorial plane. The chloride and $PbPh_2Cl$ ligands occupy the axial positions. The maleate ester is oriented with the C(O)OMe groups facing the $PbPh_2Cl$ ligand, and the interplanar angle between the two C(O)O groups is 56.4(9)°. The molecular conformation is asymmetric because neither the carboxylate groups nor the Ph and Cl substituents on the lead atom conform to a possible C_s symmetry. The actual orientation of the latter ligands is determined by the presence of a short Pb- - -O(4) contact (2.66(1) Å), which is well under the sum of the van der Waals radii (ca. 3.5 Å)[16] and is comparable to what found in compounds with similar coordination geometry, e.g., [$Ph_3PbO_2CCO_2Me$] (2.384(4) and 2.565(4) Å).[17] The attractive nature of this interaction is demonstrated by the torsion angle C(15)–C(19)–C(20)–C(17) (15.5(2)°) and by the Pt–C(20)–C(17) and Pt–C(19)–C(15) angles (117.79(2) and 131.30(2)°, respectively), which, in the absence of perturbing factors, were expected to be approximately zero (the former) and equal (the two latter). Another significant effect of the Pb–O interaction is that the ligand geometry around the lead atom turns toward the trigonal bipyramid (see Table 4). This additional linkage between the platinum and lead moieties adds stability to the compound, and its chemical effects are discussed in the next section.

The bond distances in the equatorial plane are normal[12] (Pt–N_{av}, 2.17(1)°; Pt–C_{av}, 2.09(2)°; C(19)–C(20), 1.48(3) Å) and are not worth discussing because of their high esd's. Of greater interest is the Pt–Pb distance (2.642(1) Å), the first determined for a trigonal bipyramidal Pt(II) complex. This value can be compared to that reported for the tin analogue [PtCl($SnPh_2Cl$)(dmphen)(ethylene)][8] (2.534(1) Å) and the mercury derivative [PtCl(HgMe)(dmphen)(dimethyl maleate)][9] (2.558(1) Å). Concerning the *trans* influence of these ligands on the chloride ion (Pt–Cl, 2.447(6), 2.478(3), and 2.590(6) Å, for the three species, respectively, and an average value of 2.30(2) Å for Cl^- *trans* to itself[12]), tin and lead seem to possess *trans*-influencing ability comparable to that of the alkyl carbon (2.457(2) Å in both [PtCl(Me){6-Me-py-2-CHN(CHMePh)}(ethylene)][18] and [PtCl{CH(CH$_2$)$_2$CH=CH(CH$_2$)$_2$CHOMe}(dmphen)][19]) while mercury appears to be a stronger destabilizer.

Structure of [PtCl(Ph)(dmphen)(dimethyl maleate)] (IVa'$_4$). The molecular structure of the title compound is illustrated in Figure 3, and bond distances and angles are listed in Table 5. The overall geometry is that expected, also in consideration of its formation from **IIa'$_4$**, just described. The coordination polyhedron is a trigonal bipyramid in which the chloride and phenyl ligands define the axial sites and the phenanthroline nitrogens and maleate double bond define the equatorial plane. The C(O)OMe groups in the maleate ester are oriented toward the site occupied by the phenyl ligand, in accord with the configuration found in the parent compound. Therefore the elimination of the organolead molecule and its substitution by the phenyl group do not disturb the bonding mode of this branched ligand. The molecule, as frozen in the crystal, lacks any symmetry because the conformations of the two C(O)OMe groups do not match the idealized C_s symmetry to which the remaining part of the molecule conforms. The angle between the planes of the carboxylate groups is

(15) Harrison, P. G. In *Comprehensive Organometallic Chemistry*; Pergamon Press: New York, 1982; Vol. 2, 650.

(16) Bondi, A. *J. Phys. Chem.* **1964**, *68*, 441.

(17) Glowacki, A.; Huber, F.; Preut, H. *J. Organomet. Chem.* **1986**, *306*, 9.

(18) Albano, V. G.; Braga, D.; De Felice, V.; Panunzi, A.; Vitagliano, A. *Organometallics* **1987**, *6*, 517.

(19) Albano, V. G.; Castellari, C.; Morelli, G.; Vitagliano, A. *Gazz. Chim. Ital.* **1989**, *119*, 235.

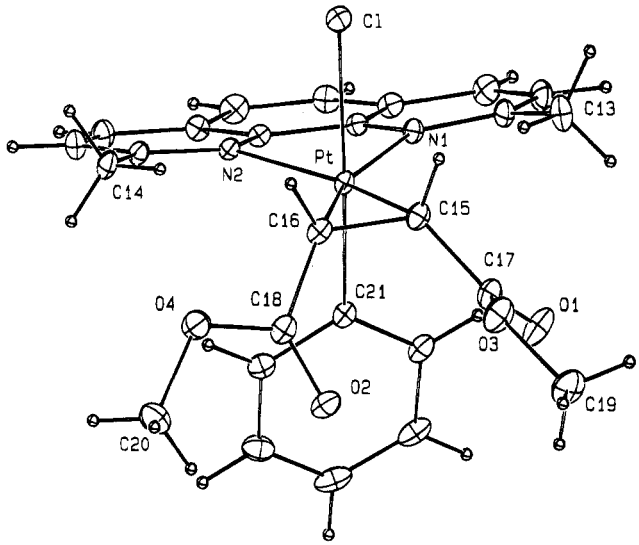

Figure 3. ORTEP drawing of [PtCl(Ph)(dmphen)(dimethyl maleate)] (**IVa′$_4$**).

Table 5. Relevant Bond Distances (Å) and Angles (deg) for IVa′$_4$

Pt–Cl	2.439(2)	C(16)–C(18)	1.48(1)
Pt–N(1)	2.165(5)	C(17)–O(1)	1.17(1)
Pt–N(2)	2.191(5)	C(17)–O(3)	1.32(1)
Pt–C(21)	2.033(7)	C(18)–O(2)	1.19(1)
Pt–C(15)	2.050(7)	C(18)–O(4)	1.34(1)
Pt–C(16)	2.078(6)	O(3)–C(19)	1.44(1)
C(15)–C(16)	1.45(1)	O(4)–C(20)	1.46(1)
C(15)–C(17)	1.51(1)		
O(2)···C(21)	3.09(1)	Cl···H(14B)	2.84(1)
O(2)···C(26)	3.11(1)	Pt···H(13B)	3.46(1)
O(1)···C(22)	3.08(1)	Pt···H(13C)	2.92(1)
C(18)···C(26)	3.16(1)	Pt···H(14A)	3.43(1)
O(1)···H(13B)	2.67(1)	Pt···H(14C)	3.07(1)
Cl···H(13C)	2.95(1)		
Cl–Pt–C(21)	175.1(2)	C(21)–Pt–C(15)	98.1(3)
Cl–Pt–N(1)	89.1(1)	C(21)–Pt–C(16)	95.1(3)
Cl–Pt–N(2)	89.8(1)	Pt–C(15)–C(17)	127.2(5)
Cl–Pt–C(15)	86.8(2)	Pt–C(16)–C(18)	120.3(5)
Cl–Pt–C(16)	89.0(2)	C(16)–C(15)–C(17)	122.5(7)
C(21)–Pt–N(1)	87.7(2)	C(15)–C(16)–C(18)	119.9(6)
C(21)–Pt–N(2)	85.8(2)	N(2)–Pt–N(1)	75.5(2)
C(17)–C(15)–C(16)–C(18)	8.8(2)		

67.6(3)°. Some geometrical peculiarities are apparent in Figure 3. The plane of the phenanthroline rings is tilted with respect to the equatorial coordination plane by 11.5°, and the methyl substituents are 0.14 and 0.12(1) Å above the ring plane. The Pt atom lies 0.459(5) Å under the ligand plane, with reference to Figure 3. This feature has been observed in other molecules of this kind[20] and has been attributed to the metal–H(methyl) contacts, but the optimization of the hydrogen–chloride and hydrogen–oxygen contacts can play a role. The phenyl ligand, as well, exhibits some tilting away from the maleate appendages in order to alleviate the contacts with that ligand.

The bond distances in the equatorial plane are normal but deserve some comment. The Pt–N interactions are slightly asymmetric (2.165 and 2.191(5) Å, average 2.18 Å) and range among the shortest found for the ligand in compounds of the same family, e.g., [PtCl$_2$(dmphen)(ethylene)][21] (2.236(5) Å), [PtCl(SnPh$_2$Cl)(dmphen)(ethylene)][8] (2.20$_{av}$ Å), [PtCl(H)(dmphen)(dimethyl maleate)][22] (2.19$_{av}$ Å), [PtCl(HgMe)(dmphen)(dimethyl maleate)][9] (2.175$_{av}$ Å), and [PtCl(py)(dmphen)(ethylene)]$^+$ [23] (2.233$_{av}$ Å). The Pt–C(maleate) distances are slightly asymmetric as well (2.050(7) and 2.078(6) Å, average 2.06 Å), and the C=C distance is 1.45(1) Å long. These values are equal, within experimental errors, to those found for the same ligand in [PtCl(HgMe)(dmphen)(dimethyl maleate)][9] (2.06(2)$_{av}$ and 1.46(3) Å) and [PtCl(H)(dmphen)(dimethyl maleate)][22] (2.05$_{av}$ and 1.45(1) Å). The high π-accepting ability of the dimethylmaleate ester can be appreciated if the C=C bond lengths just reported are compared to the shorter values found for the ethylene ligand in [PtCl$_2$(dmphen)(ethylene)][21] (1.41(1) Å), in [PtCl(SnPh$_2$Cl)(dmphen)(ethylene)][8] (1.41(2) Å), and in [PtCl(py)(dmphen)(ethylene)]$^+$ [23] (1.40(1) Å). The bond distances of the axial ligands, Pt–Cl (2.439(2) Å) and Pt–C(Ph) (2.033(7) Å), are of interest because this is the first report of a Pt–C(sp^2) distance in this family of compounds. It is slightly shorter than the Pt–C(sp^3) values found in [PtCl(Me){6-Me-py-2-CHN(CHMePh)}(ethylene)][18] (2.055(6) Å) and [PtCl(dmphen){CH(CH$_2$)$_2$CH=CH(CH$_2$)$_2$CH(OMe)}][19] (2.06(1) Å). Concerning the *trans* influence of this kind of carbon on the Pt–Cl bond (2.439(2) Å) it appears comparable but slightly smaller than that exerted by the alkyl carbon (2.457(2) Å) in both of the compounds just mentioned.

Discussion

It is reported that bimetallic complexes containing the Pt(II)–PbPh$_2$X fragment are not stable and that they collapse by elimination of an organoplumbane.[7,24] More precisely, a Pt(II)–PbPh$_2$Br-coordinated fragment was detected at low temperature by NMR spectroscopy,[7] while the –PbPh$_2$Cl fragment was stable in the coordination sphere of octahedral Pt(IV) species.[25] In addition, to our knowledge, no examples of Pt(II,IV)–PbMe$_2$Cl derivatives have yet appeared.

Our results show that Pt(II)–PbR$_2$Cl bonds can be stabilized by the coordinative saturation of the transition metal, prompted by the steric features of the N–N chelate.[12] More precisely, the oxidative addition of PbMe$_2$Cl$_2$ or PbPh$_2$Cl$_2$ to the type **I** Pt(0) species affords different products depending mostly on the features of the bidentate ligand (Scheme 1). In fact, only in the presence of dmphen and pimpy, with high sterical "in plane" requirements, the reaction leads to the isolation of five-coordinate type **II** complexes containing a Pt–PbR$_2$Cl bond. As a remarkable exception to the general observed trend, we note that, when the ethylene precursor **Ia$_1$** is reacted with PbMe$_2$Cl$_2$, the isolated product of the addition is the known mononuclear species [PtCl(Me)(dmphen)(ethylene)], which does not contain the organolead fragment despite the presence of dmphen. The reduced stability of the binuclear ethylene complexes might be a consequence of the inability of the

(20) Albano, V. G.; Castellari, C.; Cucciolito, M. E.; Panunzi, A.; Vitagliano, A. *Organometallics* **1990**, *9*, 1269.

(21) Fanizzi, F. P.; Intini, F. P.; Maresca, L.; Natile, G.; Lanfranchi, M.; Tiripicchio, A. *J. Chem. Soc., Dalton Trans.* **1991**, 1007.

(22) Albano, V. G.; Castellari, C.; Ferrara, M. L.; Panunzi, A.; Ruffo, F. *J. Organomet. Chem.* **1994**, *469*, 237.

(23) Albano, V. G.; Castellari, C.; Monari, M.; De Felice, V.; Panunzi, A.; Ruffo, F. *Organometallics* **1992**, *11*, 3665.

(24) Sokolov, V. I.; Bashilov, V. V.; Reutov, O. A. *J. Organomet. Chem.* **1975**, *97*, 299.

(25) Kuyper, J. *Inorg. Chem.* **1977**, *16*, 2171.

olefin to stabilize the Pt−Pb linkage through the mechanism illustrated in the structural section.

The phen or mphen derivatives are involved in a fast decomposition process according to Scheme 1. In particular, route i is followed if the N−N chelate lacks the suitable steric requirements and the organosubstituents on the lead atom are phenyl groups. It is conceivable that the first step of the decomposition process involves the loss of the olefin with the formation of the binuclear square-planar complex [PtCl(PbPh$_2$Cl)(N−N)] (**V**). This is involved in the deplumbation reaction, which might proceed *via* the mechanism already discussed by Baird in a previous paper.[26] However, neither the five-coordinate type **II** nor the four-coordinate type **V** species has been detected, as the deplumbation reaction leading to a type **III** product occurs very quickly.

The nonchemoselective decomposition ii is observed when the organo substituents on Pb are methyl groups. In this case, the collapse of the type **II** species, which are isolated only in the case N−N is dmphen or pimpy, is much more complicated than that of the analogous phenyl derivatives. This is not surprising since in organolead derivatives the Pb−alkyl bonds are less stable than the Pb−aryl bonds.[15]

Route iii has been observed only in a few cases. This is described in detail for **IIa′$_4$**, whose corresponding five-coordinate decomposition product **IVa′$_4$** has been characterized through X-ray diffraction. Similarly, attempts to recrystallize the ethylene derivative **IIa′$_1$** generally cause a partial deplumbation, leading to the five-coordinate product [PtCl(Ph)(dmphen)(ethylene)] (**IVa′$_1$**).

Concerning type iii demetalation, it is worth noting that complexes containing a Pt−Hg bond, analogous to type **II** species, demercuriate in solution only if they possess a net positive charge.[27] This suggests that the formation of **IVa′$_4$** from **IIa′$_4$** might involve a cationic intermediate. In fact, the attempt to obtain **IVa′$_4$** by fairly fast deplumbation of the acetonitrile/cationic complex derived from **IIa′$_4$**, followed by chloride recoordination, was successful. Conceivably, water in aged solutions during recrystallization of **IIa′$_4$** could play a role similar to that of acetonitrile in the attainment of a cationic labile intermediate.

In one case it has been used a triorganolead derivative, i.e., PbMe$_3$Cl. The result of the reaction suggests that the type of substituent groups on lead can dramatically influence the course of the reaction. In fact, the addition of PbMe$_3$Cl to **Ia$_1$** does not involve the cleavage of the Pb−Cl bond, the fission of the Pb−C bond being preferred. Regarding this point, we note that the congener tin[8] and germanium[28] derivatives actually react with the same Pt(0) precursor by Ge−Cl and Sn−Cl cleavage, while the rupture of the Pb−Cl bond has been observed when PbMe$_3$Cl is reacted with Pt(0) phosphine complexes.[7] However, the binuclear product of the reaction between PbMe$_3$Cl and **Ia$_1$** is poorly stable in solution and has not been isolated (see Scheme 2). This is possibly due to the presence of the two strong *trans*-labilizing groups, −Me and −PbMe$_2$Cl, in the apical positions of the trigonal bipyramid.

In the whole, type **II** complexes share many properties with the Pt(IV) complexes [PtCl(PbPh$_2$Cl)Me$_2$(N−N)] described earlier by Kuyper.[25] In fact, both classes of compounds are coordinatively saturated, and their stability appears to be strongly dependent on the steric features of the chelate ligand. In addition, analogously to the Pt(IV) species, type **II** complexes do not show any tendency to a reductive elimination/oxidative addition equilibrium (with the precursor **I** and the organolead chloride), in contrast with the homologous tin derivatives [PtCl(SnR$_2$Cl)(dmphen)(olefin)].[29]

The bimetallic linkage in complex **IIa′$_4$** proved to be resistant to HCl and Cl$_2$ attacks, in contrast to that reported for square-planar species in which the Pt−Pb bond was easily cleaved by the electrophile.[5,6] More precisely, HCl and Cl$_2$ cleave a Pb−Ph bond in **IIa′$_4$**, and the five-coordinate complex **IIa‴$_4$** is isolated in both cases. It is conceivable that the enhanced endurance of the Pt−Pb bond in **IIa′$_4$** is due to the already discussed Pb−O interaction and to the coordinative saturation of the Pt(II) atom, which plays a steric and electronic protective role. Particularly, the coordinative saturation of **IIa′$_4$** might prevent the oxidative addition of HCl and Cl$_2$, which is expected[5,6] to be the first step of the Pt−Pb rupture.

Conclusions

This work describes the synthesis of the first class of five-coordinate platinum(II) complexes containing a Pt−Pb bond.[4] The compounds of general formula [PtCl(PbR$_2$Cl)(N−N)(olefin)] (R = Me, Ph) also provide a substantial upgrowth of the chemistry of the Pt−Pb bond, as the linkage Pt(II)−PbR$_2$Cl has been stabilized for the first time. Our results confirm previous findings which indicated the coordinative saturation of the d^8 ion as the most important requisite for the stabilization of ligand fragments generally involved in decomposition processes. We recall that only N−N ligands with high aptitude for the stabilization of the trigonal bipyramidal geometry allowed, in fact, the isolation of type **II** complexes containing Pt−H[22] and Pt−Hg−alkyl[9] bonds.

The enhanced stability of the Pt(II)−PbR$_2$Cl fragment in the studied environment also protects the bimetallic bond from electrophilic attacks. Thus, HCl or Cl$_2$ do not cleave the Pt−Pb linkage, the Pb−R bond rupture instead being involved in the reaction.

The X-ray crystal structure of [PtCl(PbPh$_2$Cl)(dmphen)(dimethyl maleate)] reveals a large *trans* influence exerted by the organometal fragment, which agrees with previous findings concerning analogous type **II** complexes bearing organomercury[9] and -tin[8] ligands in axial positions.

Experimental Section

^{1}H NMR spectra were recorded at 270 or 200 MHz on a Bruker AC-270 or a Varian XL-200 spectrometer, respectively. PbPh$_2$Cl$_2$,[30] PbMe$_2$Cl$_2$,[31] PbMe$_3$Cl,[31] and the three-coordinate Pt(0) complexes[32] were obtained according to literature methods. Solvents and reagents were of RP analytical grade (Carlo Erba Co.), and unless otherwise stated, they were used without further purification.

(26) Baird, M. C. *J. Inorg. Nucl. Chem.* **1967**, *29*, 367.
(27) Cucciolito, M. E.; De Felice, V.; Giordano, F.; Ruffo, F. *J. Organomet. Chem.*, in press.
(28) Ruffo, F. Unpublished results, 1994.
(29) De Felice, V.; Panunzi, A.; Ruffo, F.; Åkermark, B. *Acta Chem. Scand.* **1992**, *46*, 499.
(30) Lieber, E.; Keane, F. M. *Inorg. Synth.* **1966**, *8*, 57.
(31) Gruettner, G.; Krause, E. *Chem. Ber.* **1916**, *49*, 1415.
(32) De Felice, V.; De Renzi, A.; Ruffo, F.; Tesauro, D. *Inorg. Chim. Acta* **1994**, *219*, 169.

Syntheses of IIa′$_1$. $PbPh_2Cl_2$ (0.100 g, 0.232 mmol) was added to a suspension of the three-coordinate species **Ia$_1$** (0.100 g, 0.232 mmol) in 4 mL of dry toluene in an ethylene atmosphere. After the solution had been stirred for 30 min, the brown solid was separated, washed with toluene and *n*-hexane, and dried under vacuum. The product was dissolved in the minimum amount of methylene chloride, and the solution was filtered through Florisil. The volume of the solution was then reduced under vacuum, and the product was crystallized by adding diethyl ether. The complex was washed with diethyl ether and dried under vacuum (yield: 0.080 g, 40%).

Synthesis of Other Type II Complexes. To 0.10 mmol of the appropriate three-coordinate species in 2 mL of chloroform was added a stoichiometric amount of PbR_2Cl_2 with stirring. After 30 min (12 h for **Ia$_5$** and **Ib$_5$**), the solution was filtered through a thin layer of Celite, and the volume of the solution was reduced under vacuum. The complex was crystallized by adding diethyl ether, washed with diethyl ether, and dried under vacuum (yield 60%−80%).

Addition of $PbPh_2Cl_2$ to Type Ic,d Complexes. To 0.10 mmol of the appropriate three-coordinate species in 2 mL of chloroform was added a stoichiometric amount of $PbPh_2Cl_2$ with stirring. After 24 h the mixture was filtered on a thin layer of Celite, and the solvent was removed under vacuum. The residue was washed with diethyl ether to obtain the pure type **III** complex. Selected ^{1}H NMR data (δ(ppm); 298 K; in $CDCl_3$, $CHCl_3$ (δ 7.26 ppm) as internal standard; abbreviations: d, doublet; no attribute, singlet) for **IIIc**: 8.73 ($^3J_{Pt-H}$ = 64 Hz, d, N=CH, 1 H); 7.46 ($^3J_{Pt-H}$ = 42 Hz, d, 2H); 3.52 (NCMe, 3 H). For **IIId**: 9.52 ($^3J_{Pt-H}$ = 15 Hz, N = CH, 1H); 8.67 ($^3J_{Pt-H}$ = 61 Hz, N = CH, 1H); 7.54 ($^3J_{Pt-H}$ = 53 Hz, d, 2H).

Addition of $PbMe_3Cl$ and $PbMe_2Cl_2$ to Ia$_1$. The procedure described for the syntheses of **IIa′$_1$** was repeated by using the appropriate electrophile. After workup of the reaction, the complex [PtCl(Me)(dmphen)(ethylene)][13] was isolated in 50%−60% yield. The addition of $PbMe_3Cl$ was also monitored through ^{1}H NMR spectroscopy. $PbMe_3Cl$ (0.010 g, 0.035 mmol) dissolved in 0.6 mL of deuteriochloroform was added to **Ia$_1$** (0.015 g, 0.035 mmol), and NMR spectra were recorded until no more changes in the reaction mixture were detected. Selected ^{1}H NMR data (δ(ppm); 298 K; in $CDCl_3$, $CHCl_3$ (δ 7.26 ppm) as internal standard; abbreviations: app, apparent; d, doublet; no attribute, singlet) for [PtMe($PbMe_2Cl$)(dmphen)(ethylene)]: 3.30 (NCMe, 6H); 3.17 (app d, CH=CH, 2H); 2.18 (app d, CH=CH, 2H); 0.36 ($^2J_{Pb-H}$ = 32 Hz, $PbMe_2$-Cl, 6H); −0.25 ($^2J_{Pt-H}$ = 68 Hz, Pt−Me, 3H). For [$PtMe_4$-(dmphen)]: 3.22 (NCMe, 6H); 2.10 ($^2J_{Pt-H}$ = 74 Hz, equatorial Pt−Me, 6H); −1.01 ($^2J_{Pt-H}$ = 74 Hz, axial Pt−Me, 6H).

Addition of HCl and Cl_2 to IIa′$_4$. HCl: Gaseous HCl (1.2 mL, ca. 0.050 mmol) was added to a solution of **IIa′$_4$** (0.050 g, 0.050 mmol) in the minimum amount of chloroform. After 1 h the yellow crystals of **IIa‴$_4$** were separated, which were washed with 1 mL of cold chloroform and dried under vacuum (yield: 0.030 g, 60%).

Cl_2: a solution of Cl_2 (0.0036 g, 0.050 mmol) in 0.200 mL of chloroform was added to a solution of **IIa′$_4$** (0.050 g, 0.050 mmol) in the minimum amount of chloroform. After 1 h the yellow crystals of **IIa‴$_4$** were separated, which were washed with 1 mL of cold chloroform and dried under vacuum (yield: 0.025 g, 53%).

Synthesis of IVa′$_4$. $AgBF_4$ (0.024 g, 0.12 mmol) in 1 mL of acetonitrile was added to a solution of **IIa′$_4$** (0.10 g, 0.10 mmol) in 2 mL of dichloromethane at 273 K under nitrogen. After 30 min of stirring, AgCl was removed by filtration and the solvents were removed under vacuum. The yellow-orange residue was dissolved in 2 mL of nitromethane, and after 48 h the formed precipitate was removed by filtration. The yellow solution was diluted with 2 mL of chloroform and vigorously shaken with 2 mL of LiCl-saturated water. The organic phase was dried over Na_2SO_4, and, after filtration, the volume of the solution was reduced under vacuum. Diethyl ether was added to afford a yellow precipitate, which was recovered by filtration, dried, and dissolved in 2 mL of chloroform. After the solution stood for 5 days, careful addition of *n*-hexane caused the crystallization of **IVa′$_4$** in the form of light yellow microcrystals (yield: 0.036 g, 54%). Selected ^{1}H NMR data for **IVa′$_4$** (δ(ppm): 298 K; in $CDCl_3$, $CHCl_3$ (δ 7.26 ppm) as internal standard; abbreviations: d, doublet; no attribute, singlet): 6.68 ($^3J_{Pt-H}$ = 36 Hz, d, 2H); 4.61 ($^2J_{Pt-H}$ = 86 Hz, CH=CH, 2H); 3.71 (NCMe, 6H); 3.43 (OMe, 6H). Anal. Calcd for $C_{26}H_{25}ClN_2O_4Pt$: C, 47.31; H, 3.82; N, 4.24. Found: C, 46.98; H, 3.88; N, 4.35.

Table 6. Crystal Data and Experimental Details for IIa′$_4$ and IVa′$_4$

chemical formula	$C_{32}H_{30}Cl_2N_2O_4PbPt\cdot 3CHCl_3$	$C_{26}H_{25}ClN_2O_4Pt\cdot 2H_2O$
fw	1337.86	696.07
syst	triclinic	monoclinic
space group	$P\bar{1}$ (No. 2)	$P2_1/n$ (No. 14)
a/Å	11.458(5)	10.550(2)
b/Å	11.678(2)	17.461(5)
c/Å	18.088(5)	15.710(5)
α, deg	74.90(1)	90
β, deg	75.83(2)	91.79(2)
γ, deg	79.66(2)	90
V, Å^3	2248.3(12)	2892.7(14)
Z	2	4
d_{calcd}/g cm^{-3}	1.98	1.95
μ(Mo Kα)/cm^{-1}	7.54	4.98
F(000)	1272	1360
2θ max, deg	50	60
scan type	ω	ω
ω scan width, deg	1.6 + 0.35 tan θ	1.1 + 0.35 tan θ
no. of reflns collcd	4902	8955
no. of unique obsd reflns [$F_o > 4\sigma(F_o)$]	3570	5476
$R(F_o)$, $wR(F_o^2)$	0.0774, 0.2045	0.0397, 0.1427
GOF	1.101	1.12

Crystallography. The diffraction experiments were carried out on an Enraf-Nonius CAD4 diffractometer at room temperature, using Mo Kα radiation. Crystal data for both compounds are given in Table 6. Slow diffusion of hexane in a chloroform solution of a powder sample of **IIa′$_4$** yielded bright yellow elongated prisms. The crystals lost their gemmy appearance within few minutes of their separation from the mother liquor, very probably because of evaporation of clathrated solvent. After several attempts we succeeded in sealing a crystal fragment in a glass capillary and undertook the diffraction experiment. The crystal suffered severe decay, and the data collection was stopped when the reflecting power was reduced to one-third of the starting value, leaving the reflection sphere of 25° not completely explored. The intensity data have been corrected for decay. A consequence of the experimental drawback is that the structure model was modest but sufficient to disclose the structural features of chemical interest. The structure was solved by Patterson and Fourier methods (SHELXS-86)[33] and was refined by full-matrix least-squares calculations (SHELXL-93)[33] using anisotropic thermal parameters for the heavy atoms only. In order to improve the reliability of the most significant bond parameters, all the available information was used in a constrained refinement. The dimethylphenanthroline molecule and Ph and Me fragments were treated as rigid groups, and the chemically equivalent distances in the dimethyl maleate ester were constrained to be equal within 0.02 Å. Three independent molecules of chloroform were found clathrated in the crystal and were refined as rigid groups. The coordinates of the structure model are reported in Table 7.

(33) Sheldrick, G. M. *SHELXS 86*; Göttingen, Germany, 1986; *SHELXL 93*; University of Göttingen: Göttingen, Germany, 1993.

Table 7. Fractional Atomic Coordinates ($\times 10^4$) and Equivalent Isotropic Displacement Parameters ($A^2 \times 10^3$) for [PtCl(PbPh$_2$Cl)(dmphen)(dimethyl maleate)]·3CHCl$_3$ [(IIa′$_4$)·3CHCl$_3$]

	x	y	z	U(eq)[a]
Pt	4070(1)	2199(1)	7696(1)	46(1)
Pb	3185(1)	887(1)	7025(1)	52(1)
Cl(1)	4876(5)	3384(5)	8345(4)	63(2)
Cl(2)	1313(5)	204(6)	8116(4)	79(2)
Cl(3)	−1506(7)	3039(8)	3015(5)	128(3)
Cl(4)	472(7)	2305(8)	1826(5)	128(3)
Cl(5)	218(10)	983(8)	3431(5)	156(4)
C(34)	−581(17)	1817(16)	2700(10)	102(10)
C(19)	4234(18)	3605(19)	6703(13)	63(6)
C(15)	3615(18)	3941(20)	6028(14)	76(7)
O(1)	4060(17)	3761(16)	5414(12)	100(6)
O(2)	2530(15)	4509(16)	6228(12)	96(6)
C(16)	1813(27)	4999(27)	5640(17)	115(11)
C(20)	5374(18)	2772(17)	6689(12)	57(5)
C(17)	5720(16)	2036(17)	6086(13)	61(6)
O(3)	6889(14)	2106(15)	5740(11)	90(5)
C(18)	7442(26)	1299(24)	5235(17)	106(10)
O(4)	5174(13)	1369(12)	5939(10)	68(4)
C(21)	2099(14)	1523(13)	6121(9)	66(6)
C(22)	855(14)	1855(15)	6310(9)	90(8)
C(23)	197(10)	2267(17)	5721(13)	109(10)
C(24)	783(16)	2347(17)	4942(11)	120(11)
C(25)	2028(16)	2015(16)	4753(8)	94(9)
C(26)	2686(10)	1603(13)	5343(11)	63(6)
N(1)	2489(6)	1995(5)	8645(4)	49(4)
N(2)	4581(5)	554(6)	8511(4)	49(4)
C(10)	1515(6)	2818(6)	8715(5)	57(5)
C(9)	571(6)	2608(7)	9376(6)	77(7)
C(8)	654(6)	1625(7)	9965(5)	81(7)
C(7)	1696(5)	782(6)	9906(4)	57(5)
C(6)	1888(7)	−267(7)	10501(5)	70(6)
C(5)	2928(8)	−998(7)	10435(5)	73(7)
C(4)	3870(6)	−770(5)	9758(5)	63(6)
C(3)	5003(7)	−1470(6)	9666(6)	73(7)
C(2)	5873(6)	−1113(7)	9025(6)	66(6)
C(1)	5654(5)	−115(7)	8449(5)	54(5)
C(11)	2596(5)	1021(5)	9237(4)	50(5)
C(12)	3703(5)	238(5)	9161(4)	52(5)
C(13)	1467(8)	3907(7)	8098(7)	76(7)
C(14)	6621(6)	255(9)	7750(6)	78(7)
C(27)	4025(13)	−975(10)	7025(11)	60(6)
C(28)	4420(14)	−1335(12)	6321(9)	77(7)
C(29)	4918(14)	−2511(14)	6318(9)	78(7)
C(30)	5020(14)	−3326(10)	7019(11)	87(8)
C(31)	4626(15)	−2966(13)	7723(9)	88(8)
C(32)	4128(14)	−1790(15)	7726(9)	88(8)
Cl(6)	7842(9)	4702(8)	6403(5)	138(4)
Cl(7)	8548(9)	3112(7)	7777(6)	150(4)
Cl(8)	8301(11)	5675(8)	7598(8)	180(5)
C(33)	7739(22)	4493(15)	7409(11)	127(14)
C(35)	2895(22)	5184(18)	−314(13)	123(13)
Cl(9)	2053(13)	4031(10)	236(8)	198(6)
Cl(10)	1978(17)	6337(13)	−826(10)	396(19)
Cl(11)	3567(18)	5725(19)	270(13)	358(16)

[a] U(eq) is defined as one-third of the trace of the orthogonalized U_{ij} tensor.

Microscopic examination of specimens of **IIa′$_4$** obtained by slow recrystallization revealed that some crystals were more fresh and brilliant than others. These are similar in color to the main constituents of the crop but are more equant in shape. In order to ascertain whether these crystals were air stable polymorphs of **IIa′$_4$** or new molecules, we undertook a complete structural determination. The crystal behaved well during the experiment, and the structure was solved and refined without difficulties. It contained the new molecule [PtCl(Ph)(dmphen)(dimethyl maleate)] (**IVa′$_4$**) and two molecules of water in the asymmetric unit. Some residual peaks (in the range 2−3 e Å^{-3}) in a region wide enough to allocate clathrated solvent remained unexplained in terms of a recognizable molecule. The structure model, optimized by full-matrix least-squares calculations, comprises anisotropic thermal motion for the non-hydrogen atoms and their calculated positions. Most of the hydrogen atoms appeared in the difference-Fourier map, and this has helped to define the conformation of the Me groups. The atomic coordinates are reported in Table 8. The SHELX programs have been used for all of the computations.[33]

Table 8. Fractional Atomic Coordinates ($\times 10^4$) and Equivalent Isotropic Displacement Parameters ($A^2 \times 10^3$) for [PtCl(Ph)(dmphen)(dimethyl maleate)]·2H$_2$O [(IVa′$_4$)·2H$_2$O]

	x	y	z	U(eq)[a]
Pt	2071(1)	1835(1)	724(1)	41(1)
Cl	1609(2)	1537(1)	−770(1)	55(1)
N(1)	4044(5)	1561(3)	535(3)	45(1)
N(2)	2218(4)	609(3)	1005(3)	40(1)
C(1)	4901(6)	2032(4)	204(5)	57(2)
C(2)	6186(7)	1825(4)	245(4)	69(2)
C(3)	6571(7)	1140(5)	566(5)	69(2)
C(4)	5665(6)	633(4)	884(4)	53(2)
C(5)	5964(7)	−110(4)	1216(5)	61(2)
C(6)	5055(7)	−587(4)	1460(5)	65(2)
C(7)	3760(6)	−363(3)	1417(4)	50(1)
C(8)	2757(7)	−846(4)	1628(5)	62(2)
C(9)	1548(6)	−596(4)	1494(5)	59(2)
C(10)	1286(6)	130(3)	1194(4)	47(1)
C(11)	4410(5)	868(3)	841(4)	44(1)
C(12)	3440(5)	363(3)	1107(4)	41(1)
C(13)	4468(9)	2748(5)	−187(7)	82(3)
C(14)	−47(6)	393(4)	1058(5)	58(2)
C(15)	1359(7)	2905(4)	466(5)	56(2)
C(16)	354(6)	2415(3)	761(4)	51(2)
C(17)	1721(8)	3644(4)	904(6)	69(2)
C(18)	−234(6)	2575(4)	1587(5)	57(2)
C(19)	1019(12)	4906(5)	1102(7)	107(4)
C(20)	−1988(10)	2292(7)	2421(7)	102(3)
O(1)	2708(7)	3792(3)	1229(5)	99(2)
O(2)	145(6)	3010(3)	2124(4)	74(2)
O(3)	800(6)	4147(3)	771(5)	87(2)
O(4)	−1292(5)	2159(4)	1647(4)	77(2)
C(21)	2535(6)	1996(3)	1977(4)	48(1)
C(22)	3646(7)	2368(4)	2220(5)	62(2)
C(23)	4080(9)	2352(5)	3073(6)	77(3)
C(24)	3414(9)	1971(5)	3664(6)	83(3)
C(25)	2323(9)	1619(5)	3433(5)	73(2)
C(26)	1867(7)	1618(4)	2594(5)	59(2)
O(5)	2428(10)	974(6)	5769(6)	122(3)
C(27)	9631(19)	−467(11)	3497(13)	175(7)
C(28)	8706(17)	−773(10)	2847(11)	154(6)
O(6)	7694(18)	467(11)	3496(12)	261(8)

[a] U(eq) is defined as one-third of the trace of the orthogonalized U_{ij} tensor.

Acknowledgment. We thank the Consiglio Nazionale delle Ricerche and Ministero della Ricerca Scientifica e Tecnologica for financial support and the Centro Interdipartimentale di Metodologie Chimico-Fisiche, Università di Napoli "Federico II", for the use of the Varian XL-200 and Bruker AC-270 NMR spectrometers.

Supporting Information Available: Tables of bond distances and angles and positional and thermal parameters for **IIa′$_4$** and **IVa′$_4$** (18 pages). Ordering information is given on any current masthead page.

OM950242L

Preparation of New Bis(arene)ruthenium(II) Complexes. X-ray Crystal Structures of $[(\eta^6\text{-biphenyl})_2Ru][BF_4]_2$ and the *syn* and *anti* Isomers of $[(\eta^6\text{-fluorene})_2Ru][BF_4]_2$

Leigh Christopher Porter,* Swamy Bodige, and Henry Edward Selnau, Jr.

Department of Chemistry, The University of Texas at El Paso, El Paso, Texas 79968

Henry Hall Murray III and Jonathan M. McConnachie

Corporate Research, Exxon Research and Engineering Company, Annandale, New Jersey 08801

Received December 14, 1994[⊗]

New sandwich complexes of the type $[bis(\eta^6\text{-arene})Ru][BF_4]_2$, where the arenes are biphenyl, bibenzyl, fluorene, and *trans*-stilbene, have been synthesized. These complexes were prepared by reacting the $[(acetone)_3(\eta^6\text{-arene})Ru]^{2+}$ dication with the appropriate arene in refluxing trifluoroacetic acid. A crystal structure determination of the $[(\eta^6\text{-biphenyl})_2Ru][BF_4]_2$ complex establishes that the metal ion lies coordinated between two biphenyl ligands and binds in an η^6 manner to one of the arene rings of each. The X-ray crystal structure of the $[(\eta^6\text{-fluorene})_2Ru][BF_4]_2$ complex was also determined and found to be similar with respect to the coordination of the transition metal. However, in the fluorene complex two isomeric forms (*syn* and *anti*) were found to be present in the same lattice in equal proportion, differing principally with respect to the relative orientation of the methylene bridges.

Introduction

Transition-metal sandwich complexes of polycyclic aromatic hydrocarbons (PAH's) constitute a potentially vast source of new systems exhibiting a number of interesting and potentially significant electronic properties.[1-4] Bis(arene) complexes of iron and ruthenium have recently found use as structural elements in the construction of new molecular solids exhibiting interesting features of structure and conductivity.[1,2] In instances where the ligands consist of large polycyclic aromatic hydrocarbons, band structure calculations have been carried out and predict a wealth of low-dimensional solid-state phenomena, including conductivity.[3]

Our interest in the structures and properties of transition-metal complexes containing PAH's as ligands prompted us to explore new synthetic procedures.[5] The synthetic procedures that were developed during the course of these investigations proved to be sufficiently general to enable a variety of new Ru^{II} sandwich complexes to be synthesized, the preparation of many of which until now has remained elusive. In this paper we describe the syntheses of ruthenium(II) sandwich complexes of biphenyl, bibenzyl, fluorene, and *trans*-stilbene. In addition we describe the X-ray crystal structures of $[(\eta^6\text{-biphenyl})_2Ru][BF_4]_2$ and two isomeric forms (*syn* and *anti*) of $[(\eta^6\text{-fluorene})_2Ru][BF_4]_2$, the last two found cocrystallized within the same lattice.

Experimental Section

All manipulations were carried out using standard Schlenk techniques under oxygen-free nitrogen or an inert-atmosphere glovebox. Methanol was dried and distilled over finely divided Mg metal, and all halogenated solvents were distilled over P_2O_5. Biphenyl, bibenzyl, fluorene, and *trans*-stilbene were all purchased from Aldrich Chemical Co., Inc., and used as received. Ruthenium(III) chloride hydrate was obtained from the Engelhard Corporation. Preparation of the $[(1,5\text{-COD})RuCl_2]_n$ polymer was carried out using the reported literature procedure.[6] The chloro-bridged Ru^{II} dimers of biphenyl, bibenzyl, fluorene, and *trans*-stilbene having the general formula $[(\eta^6\text{-arene})RuCl_2]_2$ were all prepared using a modification of the literature procedure.[7] NMR spectra were recorded on a Bruker AM-250 spectrometer using either DMSO-d_6 or CD_3NO_2 dried over 4 Å molecular sieves and referenced internally to TMS. Crystallographic data were collected at ambient temperature on either a Siemens R3m/V diffractometer or an Enraf-Nonius CAD-4 instrument.

Preparation of dimeric $[(\eta^6\text{-arene})RuCl_2]_2$ Complexes. In a typical reaction, a 100 mL flask was charged with 1.0 g

[⊗] Abstract published in *Advance ACS Abstracts,* August 1, 1995.

(1) (a) Ward, M. D. *Organometallics* **1987**, *6*, 754. (b) Ward, M. D.; Johnson, D. C. *Inorg. Chem.* **1987**, *26*, 4213. (c) Ward, M. D.; Fagan, P. J.; Calabrese, J. C.; Johnson, D. C. *J. Am. Chem. Soc.* **1989**, *111*, 1719. (d) Li, S.; White, H. S.; Ward, M. D. *Chem. Mater.* **1992**, *4*, 1082. (e) Fagan, P. J.; Ward, M. D. *Sci. Am.* **1992**, 48.

(2) (a) Lehn, J.-M. *Angew. Chem., Int. Ed. Engl.* **1988**, *27*, 89. (b) Carter, R. L., Ed. *Molecular Electronic Devices*; Marcel Dekker: New York, 1982. (c) Miller, J. S. *Extended Linear Chain Compounds*; Plenum: New York, 1982–1983; Vols. 1–3. (d) Desiraju, G. *Crystal Engineering*; Elsevier: New York, 1989. (e) Miller, J. S.; Epstien, A. J.; Reiff, W. M. *Science* **1988**, *240*, 40.

(3) (a) Burdett, J. K.; Canadell, E. *Organometallics* **1985**, *4*, 805. (b) Lauher, J. W.; Elian, M.; Summerville, R. H.; Hoffmann, R. *J. Am. Chem. Soc.* **1976**, *98*, 3219.

(4) Bush, B. F.; Lynch, V. M.; Lagowski, J. J. *Organometallics* **1987**, *6*, 1267. (b) Bush, B. F.; Lagowski, J. J. *J. Organomet. Chem.* **1990**, *386*, 37.

(5) (a) Suravajjala, S.; Polam, J. R.; Porter, L. C. *J. Organomet. Chem.* **1993**, *461*, 201. (b) Polam, J. R.; Suravajjala, S.; Porter, L. C. *Organometallics* **1994**, *13*, 37. (c) Porter, L. C.; Polam, J. R.; Mahmoud, J. *Organometallics* **1994**, *13*, 2092. (d) Porter, L. C.; Polam, J. R.; Bodige, S. *Inorg. Chem.* **1995**, *34*, 998. (e) Suravajjala, S.; Porter, L. C. *Acta Crystallogr.* **1994**, *C50*, 1678.

(6) Albers, M. O.; Ashworth, T. V.; Oosthuizen, H. E.; Singleton, E. *Inorg. Synth.* **1987**, *26*, 68.

(7) (a) Pertici, P.; Vitulli, G.; Bigelli, C.; Lazzaroni, R. *J. Organomet. Chem.* **1984**, *275*, 113. (b) Pertici, P.; Vitulli, G.; Lazzaroni, R.; Salvadori, P. *J. Chem. Soc., Dalton Trans.* **1982**, 1019.

0276-7333/95/2314-4222$09.00/0

Chart 1

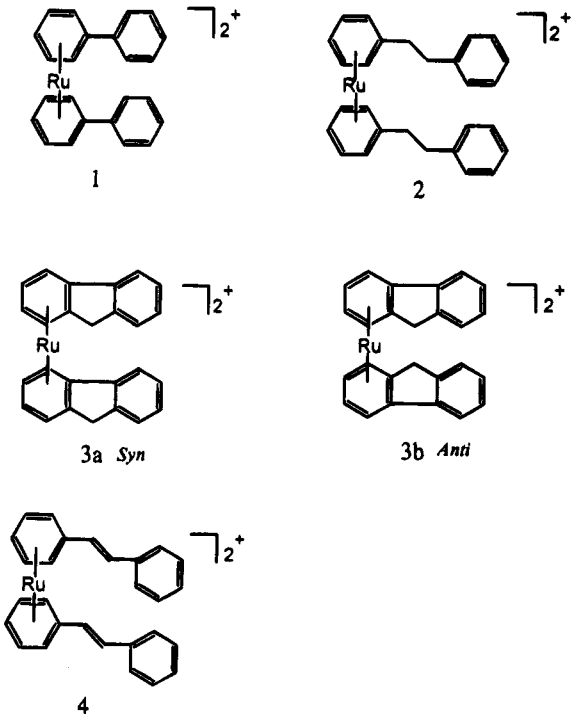

of the $[(1,5\text{-COD})RuCl_2]_n$ polymer, 2.0 g of the appropriate arene, 10.0 g (153 mmol) of zinc dust, and 20 mL of freshly distilled THF. The reaction mixture was refluxed for 24 h, after which the solvent was removed under reduced pressure. The residue was then treated with 40 mL of freshly distilled pentane and the pentane solution transferred via a cannula into a fresh 100 mL Schlenk flask. Removal of the solvent under reduced pressure resulted in the isolation of an oily residue which was immediately dissolved in 10 mL of acetonitrile. To this was then added 4 mL of a 1 M HCl–etherate solution and the solution stirred for 24 h. Addition of 20 mL of diethyl ether to the reaction mixture resulted in the precipitation of the chloro-bridged dimer, which was then filtered, washed twice with two 10 mL aliquots of diethyl ether, and dried *in vacuo*. Yields for the preparation of these dimeric complexes typically range from 10 to 20%, and full discussion of these complexes will be subject of a subsequent paper.

Preparation of $[(\eta^6\text{-biphenyl})_2Ru][BF_4]_2$ (1). Model Procedure for $[(\eta^6\text{-arene})_2Ru]^{2+}$ Complexes. A mixture of 0.15 mmol of the chloro-bridged dimer, $[(\eta^6\text{-biphenyl})RuCl_2]_2$ and 0.60 mmol (0.177 g) of $AgBF_4$ in 10 mL of acetone were stirred together for 15 min at room temperature. The solution fraction was then transferred to a second Schlenk flask using a cannula, one end of which was covered with fine filter paper to exclude the entrainment of any AgCl precipitate. Removal of the solvent under reduced pressure produced an oily orange-yellow residue. To this was added was added 5 mL of trifluoroacetic acid followed by the 0.100 g (0.65 mmol) of biphenyl. The reaction mixture was refluxed for 5 min and cooled to room temperature. Removal of the solvent under reduced pressure resulted in the formation of an oil which was triturated with 10 mL of methanol, producing an off-white powder. The product was isolated by filtration and washed with 5 mL each of methanol and diethyl ether. The compound was recrystallized from a nitromethane-diethyl ether solution yielding 0.086 g of a white powder in 49% yield. Mp: 258–260 °C dec. Anal. Calcd for $C_{24}H_{20}B_2F_8Ru$: C, 49.43; H, 3.46. Found: C, 48.71; H, 3.48.

Preparation of $[(\eta^6\text{-bibenzyl})_2Ru][BF_4]_2$ (2). This complex was prepared by following the procedure described for **1**. Using 0.106 g (0.15 mmol) of the $[(\eta^6\text{-bibenzyl})RuCl_2]_2$ dimer, 0.117 g (0.60 mmol) of $AgBF_4$, and 0.100 g (0.55 mmol) of bibenzyl, the off-white, air-stable compound **2** was isolated in 56% (0.107 g) yield. Mp: 230–232 °C dec. Anal. Calcd for $C_{28}H_{28}B_2F_8Ru$: C, 52.61; H, 4.42. Found: C, 51.82; H, 4.41.

Table 1. Summary of Crystal Data for $[(\eta^6\text{-biphenyl})_2Ru][BF_4]_2$ and $[(\eta^6\text{-fluorene})_2Ru][BF_4]_2$

empirical formula	$C_{24}H_{20}B_2F_8Ru$	$C_{26}H_{20}B_2F_8Ru$
fw	583.1	607.1
cryst syst	monoclinic	monoclinic
space group	$P2_1/n$	$P2_1/c$
a (Å)	12.206(6)	13.839(3)
b (Å)	14.836(7)	18.829(4)
c (Å)	13.479(6)	9.454(2)
β (deg)	111.50(4)	106.96(3)
V (Å^3)	2271(2)	2356.3(9)
Z	4	4
ϱ (Mg m^{-3})	1.705	1.711
μ (mm^{-1})	0.751	0.727
radiation	Mo Kα (0.710 73 Å)	Mo Kα (0.710 73 Å)
weighting scheme	$w^{-1} = \sigma^2(F) + 0.0029F^2$	$w^{-1} = \sigma^2(F) + 0.0037F^2$
final R	0.062	0.063
final R_w	0.0682	0.0959
goodness of fit	0.89	1.27

Preparation of $[(\eta^6\text{-fluorene})_2Ru][BF_4]_2$ (3). This complex was prepared by following the procedure described for **1**. Using 0.100 g (0.15 mmol) of the $[(\eta^6\text{-fluorene})RuCl_2]_2$ complex, 0.117 g (0.60 mmol) of $AgBF_4$, and 0.100 g (0.55 mmol) of fluorene, the yellow air-stable product **3** was isolated. The yield was 0.118 g (60%). Mp: 210–212 °C dec. Anal. Calcd for $C_{26}H_{20}B_2F_8Ru$: C, 51.43; H, 3.33. Found: C, 51.18; H, 3.30.

Preparation of $[(\eta^6\text{-}trans\text{-stilbene})_2Ru][BF_4]_2$ (4). This complex was prepared by following the procedure described for **1**. Using 0.105 g (0.15 mmol) of the $[(\eta^6\text{-}trans\text{-stilbene})RuCl_2]_2$ dimer, 0.117 g (0.60 mmol) of $AgBF_4$, and 0.100 g (0.55 mmol) of *trans*-stilbene, we isolated 0.118 g of a clean yellow powder in 62% yield. Mp: 300-302 °C dec. Anal. Calcd for $C_{28}H_{24}B_2F_8Ru$: C, 52.94; H, 3.81. Found: C, 52.69; H, 3.86.

Results

Crystallographic Determination of the Structures. Details concerning the crystallographic experimental procedures are summarized in Table 1. Intensity data collection for the $[(\eta^6\text{-fluorene})_2Ru][BF_4]_2$ complex was carried out at 298 K using an Enraf-Nonius CAD-4 diffractometer. For the $[(\eta^6\text{-biphenyl})_2Ru][BF_4]_2$ complex a Siemens R3m/V diffractometer also operating at room temperature was used. Both instruments were equipped with graphite-monochromated Mo Kα radiation. Structure solution and refinement was carried out using the SHELXTL-PC collection of crystallographic software[8] utilizing scattering factors that included terms for anomalous dispersion.[9] The data for both structures were corrected for Lorentz and polarization effects and for absorption.

Structure determination of $[(\eta^6\text{-biphenyl})_2Ru][BF_4]_2$. Crystals suitable for an X-ray crystal structure determination were obtained following crystallization from an acetone–nitromethane solution at room temperature. A single irregularly shaped pale yellow fragment was selected and mounted on the end of a glass fiber in a random orientation. Monoclinic symmetry was suggested on the basis of the interaxial angles and confirmed by axial rotation photographs.

(8) Sheldrick, G. M. SHELXTL-PLUS (PC version): An Integrated System for Solving, Refining and Displaying Crystal Structures from Diffraction Data; University of Gottingen: Gottingen, Germany, 1990.
(9) *International Tables for X-ray Crystallography*; Kynoch Press (present distributor D. Reidel, Dordrecht, The Netherlands): Birmingham, U.K., 1974; Vol. IV.

Refined cell parameters were determined from the setting angles of 35 reflections with $7° < 2\theta < 30°$. Three standards measured every 97 data showed only minor variations in intensity (<2.0%) over the period of data collection. A total of 3147 reflections ($+h,+k,\pm l$; $h_{max} = 13$, $k_{max} = 16$, $l_{max} = 14$) with $3.5° < 2\theta < 45°$ were collected using the ω-scanning technique in bisecting geometry, resulting in 2987 unique reflections with $R_{int} = 1.45\%$ following the merging of equivalent reflections. Absorption corrections were applied empirically on the basis of several strong reflections spanning a range of 2θ values (minimum and maximum transmission 0.712 and 0.748, respectively). The crystal was assigned to the $P2_1/n$ space group following an inspection of the systematically absent reflections. Refinement was based on F using weights of the form $w^{-1} = [\sigma^2(F) + 0.0029(F^2)]$. A careful inspection of the difference Fourier map revealed that one of the BF_4^- counterions was disordered and a satisfactory resolution was obtained by including three of the four F atoms in three alternate positions with 50% occupancy factors using isotropic thermal parameters. Refinement using this disorder model resulted in B–F bond lengths that were found to be somewhat longer than those found in other complexes containg BF_4^- counterions. For the final cycle the maximum shift/error was 0.007 (mean shift/error = 0.001) with minimum and maximum residual electron densities of 0.61 and −0.68 e Å^{-3}. Convergence to conventional R values of $R = 0.062$ and $R_w = 0.068$ with a goodness of fit of 0.89 was obtained for 329 variable parameters and 2987 reflections with $I > 3\sigma(I)$.

Structure Determination of [(η^6-fluorene)$_2$Ru][BF$_4$]$_2$. Amber, well-formed crystals suitable for an X-ray crystal structure determination were obtained following crystallization from a DMSO–water solution at room temperature. A total of 4835 reflections ($+h,+k,\pm l$; $h_{max} = 17$, $k_{max} = 23$, $l_{max} = 11$) with $4.0° < 2\theta < 52.0°$ were collected using the $2\theta-\theta$ scanning technique and corrected for Lorentz and polarization effects. This led to 4629 unique reflections with $R_{int} = 1.18\%$ and 2692 observed reflections with $I > 2\sigma(I)$. Absorption corrections were applied empirically on the basis of azimuthal scans of several strong reflections spanning a range of 2θ values. The structure was solved using direct methods; however, it quickly became apparent that the ligands of the structure (but not the transition metal) were disordered. This made it necessary to inspect very carefully the difference Fourier maps in order to correctly assign the regions of residual electron density to the appropriate fluorene ligand. One of the problems that was encountered centered on the degree of overlap exhibited by several of the fluorene carbon atoms. This necessitated refining these atoms using only isotropic thermal parameters so that correlations between their temperature factors and fractional atomic coordinates were minimized. Hydrogen atoms were included in idealized positions with fixed isotropic U values of 0.08 Å^2. After the refinement had converged to a satisfactory state, the occupancies of the disordered carbon atoms were refined. This led to an increase in correlations between occupancy factors and thermal parameters but provided occupancies that indicated a 50:50 mix of the two isomers. Refinement was based on F using weights of the form $w^{-1} = [\sigma^2(F) + 0.0037(F^2)]$. Convergence to conventional R values of $R = 0.0627$ and $R_w = 0.0959$ with a goodness of fit of 1.27 was obtained for 322 variable parameters and 2692 reflections with $I > 2\sigma(I)$.

Table 2. ^{1}H NMR Absorptions of the Complexes[a]

compd no.	solvent	chem shift
1	DMSO-d_6	6.96 (t, 2H, J = 5.41), 7.06 (t, 4H, J = 7.34 Hz), 7.29 (t, J = 6.66 Hz), 7.50 (m, 10H)
2	DMSO-d_6	2.92 (s, 8H), 6.90 (m, 10H), 7.2–7.4 (m,10H)
3[b]	CD_3NO_2	2.88 (d, 2H, J = 23.60 Hz), 3.21 (d, 2H, J = 23.81 Hz), 3.82 (d, 2H, J = 23.78 Hz),3.92 (d, 2H, J = 23.82 Hz) 6.96 (m, 10H),7.10 (d, 2H, J = 7.63 Hz), 7.40 (m, 12H),7.64 (m, 6H), 7.83 (d, 2H, J = 7.71 Hz)
4	DMSO-d_6	6.8 (d, 4H, J = 16.24 Hz), 6.85 (t, 2H, J = 5.82 Hz), 6.96 (t, 4H, J = 6.02 Hz),7.23 (m, 8H), 7.34 (d, 4H, J = 7.00 Hz), 7.55 (d, 2H, J = 16.32 Hz)

[a] Chemical shifts are given in ppm and J values in Hz. [b] Combined data for both the *syn* and *anti* isomers.

Discussion

Four [2(η^6-arene)$_2$Ru]$^{2+}$ sandwich complexes have been prepared using biphenyl, bibenzyl, fluorene, and *trans*-stilbene. Chloro-bridged (η^6-arene)Ru^{II} dimers having the general formula [(η^6-arene)RuCl$_2$]$_2$ were used as starting materials in each case. These dimers are readily cleaved by halide abstraction[10a] using 4 equiv of AgBF$_4$ in acetone to give a tris(acetone) complex of Ru^{II} containing an η^6-coordinated arene. The three molecules of acetone are only weakly coordinating and, hence, are easily displaced in the presence of the appropriate arene in refluxing trifluoroacetic acid.[10b]

Elemental analyses consistent with structures having the formula [(η^6-arene)$_2$Ru][BF$_4$]$_2$ were obtained for the complexes prepared in this investigation. All exhibited good solubility in nitromethane and DMSO and poor solubility in solvents such as methanol or halogenated solvents such as chloroform and dichloromethane. Overall yields typically were found to range from 40% to 60%, and in all instances the products were isolated as clean air-stable complexes. In these reactions the final step leading to the formation of the (η^6-arene)$_2$Ru^{II} complex was essentially complete after a few minutes, and refluxing the reaction mixture for extended periods of time proved to be unnecessary. In fact, product yields decreased noticeably following prolonged heating using trifluoroacetic acid as the solvent. We suspect the reason for this reflects one or more competing side reactions, and while the exact nature of the products being formed under these conditions remains uncertain, ^{13}C NMR data have in at least one instance revealed the presence of coordinated trifluoroacetate.

^{1}H and ^{13}C NMR data were obtained for all the complexes, since a considerable amount of information concerning how the arene binds to the transition metal can be quickly obtained by examining the proton and carbon chemical shifts of the arene ligands. In the ^{1}H NMR spectra of all these complexes we find that the resonances for the protons associated with the bound carbons are shifted downfield slightly (Table 2). In contrast, the ^{13}C NMR resonances (Table 3) for the

(10) (a) Bennett, M. A.; Matheson, T. W. *J. Organomet. Chem.* **1979**, *175*, 87. (b) Bennett, M. A.; Matheson, T. W.; Roberston, G. B.; Steffen, W. L.; Turney, T. W. *J. Chem. Soc., Chem. Commun.* **1979**, 32.

Table 3. ^{13}C NMR Absorptions of the Complexes[a]

compd no.	solvent	chem shift
1	DMSO-d_6	92.11, 93.14, 94.09, 112.17, 127.99, 128.51, 129.27, 132.05
2	DMSO-d_6	34.44, 35.62, 93.41, 94.17, 94.26, 94.53, 126.51, 128.43, 128.52, 139.30
3[b]	CD_3NO_2	35.66, 35.74, 87.40, 87.51, 92.07, 92.14, 92.62, 92.70, 92.76, 92.94, 115.74, 116.23, 116.49, 117.23, 125.47, 125.77, 127.50, 129.70, 130.29, 134.48, 134.63, 145.96
4	DMSO-d_6	90.6, 92.5, 93.7, 110.5, 117.9, 127.8, 128.7, 130.3, 134.4, 142.4

[a] Chemical shifts are given in ppm. [b] Combined data for both the *syn* and *anti* isomers.

Table 4. Atomic Coordinates ($\times 10^4$) and Equivalent Isotropic Displacement Coefficients ($Å^2 \times 10^3$) for the Biphenyl Complex

	x	*y*	*z*	*U*(eq)[a]
Ru(1)	1429(1)	8673(1)	7660(1)	38(1)
F(1)	4995(8)	10587(6)	8527(7)	181(5)
F(2)	4372(5)	9734(3)	7110(8)	165(5)
F(3)	5252(5)	11044(4)	7106(6)	130(4)
F(4)	3475(4)	11018(4)	7157(6)	125(4)
F(5)	715(7)	8648(4)	3070(10)	155(6)
F(6)	−558(9)	8446(5)	3885(7)	128(5)
F(6A)	−1029(28)	8548(19)	3212(34)	69(9)
F(7)	−1161(10)	8586(7)	2245(8)	174(6)
F(7A)	−632(28)	7732(29)	2253(24)	73(10)
F(8)	−267(11)	7322(5)	2868(17)	216(12)
F(8A)	292(22)	7542(19)	3896(19)	58(8)
B(1)	4511(8)	10578(6)	7474(12)	85(5)
B(2)	−203(9)	8191(6)	3059(12)	85(6)
C(11)	−2273(7)	9291(6)	5794(5)	69(3)
C(12)	−3412(7)	9263(7)	5795(6)	87(4)
C(13)	−3799(7)	8569(7)	6237(7)	86(4)
C(14)	−3067(8)	7863(7)	6643(6)	78(4)
C(15)	−1914(6)	7848(5)	6655(5)	59(3)
C(16)	−1519(6)	8582(5)	6229(5)	51(3)
C(21)	341(6)	7796(4)	6318(5)	49(3)
C(22)	1509(6)	7814(5)	6349(5)	57(3)
C(23)	2067(6)	8645(5)	6331(5)	59(3)
C(24)	1446(6)	9434(5)	6266(5)	56(3)
C(25)	283(6)	9425(5)	6237(5)	54(3)
C(26)	−300(6)	8593(4)	6245(4)	46(2)
C(31)	1344(6)	7945(5)	9068(5)	51(3)
C(32)	2500(7)	7890(6)	9063(5)	66(3)
C(33)	3135(6)	8662(6)	9015(6)	68(3)
C(34)	2602(6)	9513(5)	8977(5)	63(3)
C(35)	1444(6)	9588(5)	8980(5)	56(3)
C(36)	811(6)	8799(5)	9044(4)	49(3)
C(41)	−859(7)	8195(6)	9458(6)	74(4)
C(42)	−2008(8)	8245(7)	9430(7)	87(4)
C(43)	−2693(8)	8949(7)	8980(7)	80(4)
C(44)	−2246(7)	9652(6)	8561(6)	77(4)
C(45)	−1097(6)	9616(5)	8589(5)	58(3)
C(46)	−416(5)	8875(5)	9031(4)	49(3)

[a] Equivalent isotropic *U*, defined as one-third of the trace of the orthogonalized $\mathbf{U}_{ij}$ tensor.

carbon atoms attached to the transition metal are found to be shifted upfield *ca.* 10−20 ppm relative to the free arene. In the ^1H and ^{13}C NMR spectra of the fluorene complex, evidence for both the *syn* and *anti* isomers in solution was present. Careful peak integration of the methylene protons for the two isomers revealed that they were both present in solution in equal amounts.

Description of the Structure of [(η^6-biphenyl)$_2$Ru][BF$_4$]$_2$. A cursory description of the structure of this complex has appeared; however not until now has a thorough crystallographic investigation of this complex been reported.[11] Fractional atomic coordinates and selected bond angles and distances are given in Tables

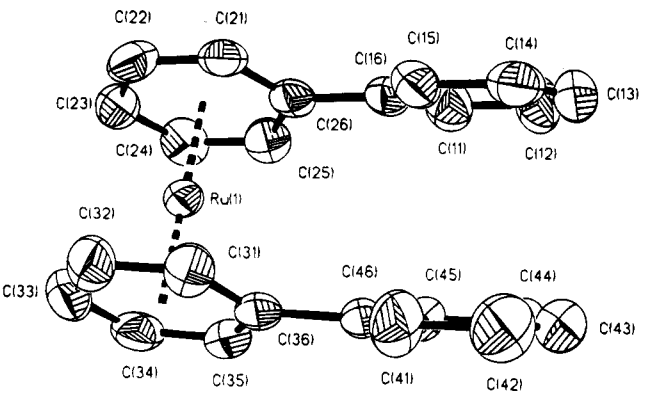

Figure 1. View of the [(η^6-biphenyl)$_2$Ru]$^{2+}$ ion illustrating the coordination of the ruthenium atom and the atomic labeling scheme. Thermal ellipsoids have been drawn at the 50% probability level. The hydrogen atoms have been omitted for clarity.

Table 5. Selected Bond lengths (Å) for the Biphenyl Complex

Ru(1)−C(21)	2.229(6)	Ru(1)−C(22)	2.210(8)
Ru(1)−C(23)	2.200(9)	Ru(1)−C(24)	2.198(8)
Ru(1)−C(25)	2.216(6)	Ru(1)−C(26)	2.271(5)
Ru(1)−C(31)	2.220(7)	Ru(1)−C(32)	2.196(7)
Ru(1)−C(33)	2.211(6)	Ru(1)−C(34)	2.211(7)
Ru(1)−C(35)	2.232(7)	Ru(1)−C(36)	2.262(7)

4 and 5, respectively, and in Figure 1 is shown a view of the complex. The structure of free biphenyl has been the subject of many investigations, both theoretical and experimental. From theoretical investigations of biphenyl in the gas phase there is found one energy minimum where the two arene rings display a torsion angle of 44.4° along with two energy maxima which occur at $x = 0$ and 90°.[12] In the solid state biphenyl appears to be planar,[13] and the gas-phase energy barrier to rotation has been estimated to range from 6.5 to 9.2 kJ/mol.[14] In the X-ray crystal structure of [(η^6-biphenyl)$_2$Ru][BF$_4$]$_2$ the two phenyl rings are twisted with torsion angles that measure 24.6 and 25.0° for the two independent biphenyl groups, probably as a consequence of crystal-packing forces.[15]

Description of the X-ray Crystal Structure of [(η^6-Fluorene)$_2$Ru][BF$_4$]$_2$. In the X-ray crystal structure of the [(η^6-fluorene)$_2$Ru][BF$_4$]$_2$ complex two isomers are present in equal proportion in the lattice. This complex therefore constitutes a rare example of conformational isomerization in which the two isomers cocrystallize. Views of the *syn* and *anti* isomers of [(η^6-fluorene)$_2$Ru][BF$_4$]$_2$ illustrating the atomic numbering scheme are presented in Figures 2 and 3. A listing of fractional atomic coordinates and a summary of pertinent bond angles and distances is given in Tables 6 and 7, respectively.

An inspection of the figures of the two isomers shows that they differ with respect to the relative orientations of the two methylene bridges and, to a lesser extent,

(11) Plitzko, K.-D.; Wherle, G.; Gollas, B.; Rapko, B.; Dannheim, J.; Boekelheide, V. *J. Am. Chem. Soc.* **1990**, *112*, 6556.
(12) Almenningen, A.; Bastiansen, O.; Fernholt, L.; Cyvin, B. N.; Cyvin, S. J.; Samdal, S. *J. Mol. Struct.* **1985**, *128*, 59.
(13) (a) Robertson, G. B. *Nature* **1961**, *191*, 593. (b) Charbonneau, G.-P.; Delugeard, Y. *Acta Crystallogr.* **1976**, *B33*, 1586. (c) Charbonneau, G.-P.; Delugeard, Y. *Acta Crystallogr.* **1976**, *B32*, 1420.
(14) Hafelinger, G.; Regelmann, C. *J. Comput. Chem.* **1987**, *8*, 1057.
(15) (a) Belsky, V. K.; Zavodnik, V. E.; Vozzhennikov, V. M. *Acta Crystallogr.* **1984**, *C40*, 1210. (b) Gerkin, R. E.; Lundstedt, A. P.; Reppart, W. J. *Acta Crystallogr.* **1984**, *C40*, 1892.

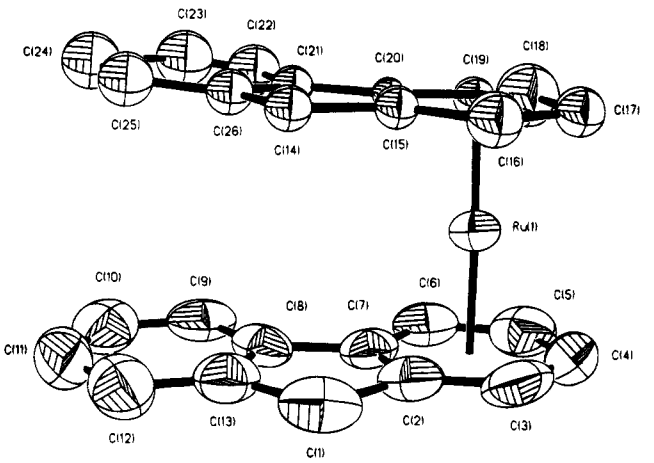

Figure 2. View of the *syn*-[(η^6-fluorene)$_2$rRu]$^{2+}$ ion illustrating the coordination of the ruthenium atom and the atomic labeling scheme. Thermal ellipsoids have been drawn at the 50% probability level. The hydrogen atoms have been omitted for clarity.

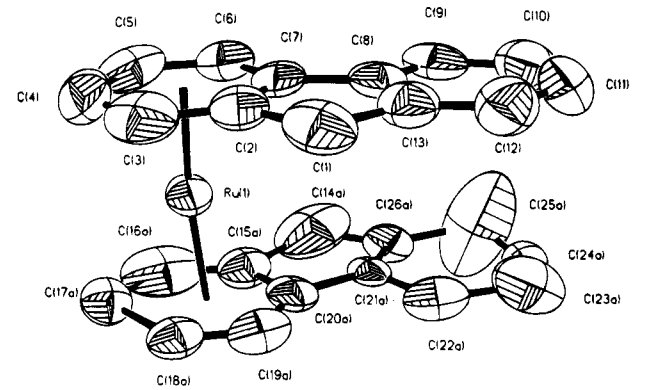

Figure 3. View of the *anti*-[(η^6-fluorene)$_2$Ru]$^{2+}$ ion with thermal ellipsoids drawn for all atoms, including those that are refined isotropically at the 50% probability level. The hydrogen atoms have been omitted for clarity.

the angle of rotation that the fluorene ligands make with respect to each other. In the *anti* form of the complex the methylene bridges are located on opposite sides and the two fluorene rings are slightly staggered. In the *syn* isomer the methylene bridges are located on the same side; however, the carbon atoms of the two coordinated arene rings are nearly perfectly eclipsed. The *syn* and *anti* isomers are unique; neither can be interconverted by a simple rotation of the one of the fluorene rings. In both isomers the Ru atom coordinates in an η^6 manner to one of the arene rings of each of the two fluorenes. In these two sandwich complexes we find the separation between the coordinated arene rings to measure 3.449−3.465 Å for the *syn* and *anti* isomers, respectively. A similar range of values has been observed in the crystal structures of two isomeric forms of [(η^6-4-(methylisopropyl)benzene)(η^6-fluorene)][BF_4]$_2$,[5a,e] as well as other unsymmetrical Ru^{2+} sandwich complexes that have recently been prepared using a large polycyclic benzenoid aromatic as one of the ligands.[5] There are no substantial out-of-plane deviations of any of the arene C atoms, and for both isomers the fluorene molecule is folded about the methylene bridge where the angles range from a minimum of 3.2° to a maximum of 4.3°. In the crystal structure of free fluorene this angle is only 1.3°; hence, the 4.3° angle seen in the

Table 6. Atomic Coordinates (×10^4) and Equivalent Isotropic Displacement Coefficients (Å^2 × 10^3) for the Fluorene Complex

	x	*y*	*z*	*U*(eq)[a]
Ru(1)	2742(1)	9115(1)	668(1)	52(1)
F(1)	4500(11)	11436(7)	4480(14)	196(8)
F(2)	5436(7)	11857(4)	3146(7)	122(4)
F(3)	5954(10)	11918(4)	5593(8)	153(6)
F(4)	5887(9)	10882(4)	4478(10)	143(5)
F(5)	742(8)	8235(6)	−5764(10)	152(5)
F(6)	1218(11)	9245(5)	−4621(17)	194(8)
F(7)	−71(13)	8633(8)	−4196(17)	239(10)
F(8)	1468(10)	8323(6)	−3414(12)	179(7)
B(1)	5518(14)	11552(9)	4410(15)	88(7)
B(2)	824(15)	8625(9)	−4569(17)	93(7)
C(1)	1900(8)	10269(6)	2825(12)	79(5)
C(2)	1744(7)	9601(5)	1932(10)	55(4)
C(3)	1978(9)	8922(8)	2383(13)	87(5)
C(4)	1791(9)	8350(6)	1345(16)	84(6)
C(5)	1348(9)	8503(7)	−129(15)	84(5)
C(6)	1138(7)	9216(6)	−624(12)	66(4)
C(7)	1337(6)	9758(5)	478(11)	55(4)
C(8)	1219(6)	10513(5)	261(11)	55(4)
C(9)	883(7)	10902(7)	−999(12)	71(4)
C(10)	837(8)	11635(8)	−825(17)	93(6)
C(11)	1111(9)	11956(7)	558(19)	93(6)
C(12)	1445(9)	11536(7)	1808(15)	84(5)
C(13)	1523(7)	10834(6)	1648(12)	65(4)
C(14)	4062(11)	10612(7)	1338(15)	35(3)
C(15)	4022(13)	9832(9)	985(29)	32(4)
C(16)	4372(23)	9350(18)	2054(37)	83(11)
C(17)	4288(15)	8629(13)	1452(26)	49(6)
C(18)	3842(16)	8475(12)	−132(30)	55(5)
C(19)	3420(11)	9033(9)	−1236(16)	33(3)
C(20)	3606(10)	9757(9)	−593(18)	22(3)
C(21)	3285(20)	10432(14)	−1525(42)	60(7)
C(22)	2917(22)	10570(18)	−2954(39)	89(10)
C(23)	2922(20)	11393(18)	−2937(36)	68(7)
C(24)	3232(22)	11918(16)	−1801(46)	83(9)
C(25)	3632(17)	11623(15)	−244(27)	63(5)
C(26)	3602(13)	10826(13)	−321(25)	41(4)
C(14A)	3100(24)	9840(15)	−2441(32)	114(9)
C(15A)	3593(16)	9451(17)	−929(25)	65(6)
C(16A)	3748(24)	8708(19)	−531(37)	94(10)
C(17A)	4132(17)	8520(12)	936(33)	55(6)
C(18A)	4334(14)	9133(13)	1869(22)	41(5)
C(19A)	4181(21)	9808(16)	1591(37)	84(10)
C(20A)	3834(17)	9969(12)	189(37)	66(6)
C(21A)	3445(17)	10482(15)	−957(35)	51(6)
C(22A)	3663(18)	11107(17)	29(27)	67(7)
C(23A)	3400(19)	11844(13)	−886(39)	69(6)
C(24A)	3116(20)	11789(19)	−2397(35)	72(7)
C(25A)	2911(22)	11157(18)	−3197(36)	79(10)
C(26A)	3082(20)	10642(13)	−2341(41)	62(6)

[a] Equivalent isotropic *U*, defined as one-third of the trace of the orthogonalized $\mathbf{U}_{ij}$ tensor.

Table 7. Selected Bond Lengths (Å) for the Fluorene Complex[a]

Ru(1)−C(2)	2.267(11)	Ru(1)−C(3)	2.210(4)
Ru(1)−C(4)	2.170(14)	Ru(1)−C(5)	2.184(12)
Ru(1)−C(6)	2.208(9)	Ru(1)−C(7)	2.253(9)
Ru(1)−C(15)	2.177(18)	Ru(1)−C(16)	2.296(28)
Ru(1)−C(17)	2.245(21)	Ru(1)−C(18)	2.239(27)
Ru(1)−C(19)	2.265(17)	Ru(1)−C(20)	2.267(17)
Ru(1)−C(15A)	2.258(27)	Ru(1)−C(16A)	2.175(39)
Ru(1)−C(17A)	2.176(24)	Ru(1)−C(18A)	2.164(17)
Ru(1)−C(19A)	2.327(28)	Ru(1)−C(20A)	2.340(27)

[a] A complex listing of bond lengths and angles is available as part of the supporting information.

structure of the *syn* isomer may reflect the effects of unfavorable steric interactions involving the bridging methylene groups.[15]

Attempts were made to extend this work to include fused-ring systems such as naphthalene, anthracene, and phenanthrene. In all instances we were unable to

isolate the needed chloro-bridged dimeric starting material, the reasons for which we are not completely certain. It may be possible to prepare dimeric complexes containing these ligands using the procedures described here; however, the yields are not likely to be high. We find that fused-ring PAH's tend to be inferior as ligands when compared to the types of ligand systems used in these investigations.[16] Alternately, it may be necessary to develop a different synthetic approach that does not require as a principal step the preparation of the chloro-bridged dimer. Investigations related to the preparation of new complexes containing other ligands such as fused polycyclic benzenoid aromatics are currently in progress.

(16) Bennett, M. A.; Neuman, H.; Thomas, M.; Qiwang, X.; Pertici, P.; Vitulli, G.; Salvadori, P. *Organometallics* **1991**, *10*, 3237.

Acknowledgment is made to the donors of the Petroleum Research Fund, administered by the American Chemical Society, and to the Robert A. Welch Foundation. We especially wish to thank Engelhard Corp. for their generous gift of ruthenium trichloride and F. Cervantes-Lee for assisting with the collection of the intensity data.

Supporting Information Available: Tables of crystal data, bond lengths and angles for the BF_4^- anions, atomic positional parameters for hydrogen atoms, and anisotropic thermal parameters for the biphenyl and fluorene complexes (9 pages). Ordering information is given on any current masthead page.

OM940954W

Synthesis, Structure, and Reactivities of Trifluoromethyl-Substituted (π-Vinylcarbene)iron Complexes

Take-aki Mitsudo,* Ken-ichi Fujita, Shingo Nagano, Toshi-aki Suzuki, and Yoshihisa Watanabe*

Division of Energy and Hydrocarbon Chemistry, Graduate School of Engineering, Kyoto University, Sakyo-ku, Kyoto, 606-01 Japan

Hideki Masuda

Department of Applied Chemistry, Nagoya Institute of Technology, Gokiso-cho, Showa-ku, Nagoya, 466 Japan

Received January 9, 1995[⊗]

Bis(triphenylphosphine)nitrogen(1+) tetracarbonylhydridoferrate reacts with hexafluoro-2-butyne to give bis(triphenylphosphine)nitrogen(1+) [1−3-η-2,3-bis(trifluoromethyl)acryloyl]-tricarbonylferrate (**1**) in 90% yield. Complex **1** crystallizes in the triclinic space group $P\bar{1}$ with a = 13.029(6) Å, b = 16.812(9) Å, c = 10.341(8) Å, α = 103.61(5)°, β = 96.64(5)°, γ = 68.29(4)°, and Z = 2. Complex **1** reacts with $(CH_3)_3OBF_4$ to give [1−3-η-1-methoxy-2,3-bis-(trifluoromethyl)prop-2-en-1-ylidene]tricarbonyliron (**4**). Complex **4** reacts with pyrrolidine to give [1−3-η-1-*N*-pyrrolidino-2,3-bis(trifluoromethyl)prop-2-en-1-ylidene]tricarbonyliron (**6**), which belongs to the monoclinic space group $P2_1$ with a = 8.058(2) Å, b = 10.847(4) Å, c = 17.766(4) Å, β = 99.00(2)°, and Z = 4. Complex **4** reacts with triphenylphosphine to afford [1−4-η-3,4-bis(trifluoromethyl)vinylketene]dicarbonyl(triphenylphosphine)iron (**8**). Complex **4** reacts with 2 mol equiv of carbon monoxide to give 1,1,1,1-tetracarbonyl-3-methoxy-4,5-bis(trifluoromethyl)ferracyclopent-3-en-2-one (**9**). Complex **4** reacts with ethoxyethyne to give [2 + 3] adducts [1−4-η-1-ethoxy-3-methoxy-4,5-bis(trifluoromethyl)-1,3-cyclopentadiene]-tricarbonyliron (**13**). Complex **13** crystallizes in the triclinic space group $P\bar{1}$ with a = 7.6177-(8) Å, b = 14.646(2) Å, c = 7.488(1) Å, α = 99.73(1)°, β = 98.08(1)°, γ = 98.97(1)°, and Z = 2.

Introduction

Since our discovery of a (π-vinylcarbene)iron (or (η^3-vinylcarbene)- or (η^3-allylidene)iron) complex in 1976,[1,2] the chemistry of π-vinylcarbene complexes has been developed.[3−9] These complexes are often postulated to be key intermediates in the reactions of carbene complexes with acetylenes involving the Dötz reaction[9,10] and polymerization of acetylenes.[11,12] Hofmann et al. theoretically examined the reaction of a carbene−metal (metal: Cr, Mo, W, etc.) double bond with acetylene and found that the direct route to a π-vinylcarbene complex is preferable to that to the metallacyclobutene complex (Scheme 1).[11]

Although fundamental reactivities of (π-vinylcarbene)iron complexes have been investigated and very interesting character was revealed,[3−9,13−22] their reactivity is not fully disclosed mainly because of the

[⊗] Abstract published in *Advance ACS Abstracts,* August 1, 1995.

(1) (a) Mitsudo, T.; Nakanishi, H.; Inubushi, T.; Morishima, I.; Watanabe, Y.; Takegami, Y. *J. Chem. Soc., Chem. Commun.* **1976**, 416. (b) Mitsudo, T.; Watanabe, Y.; Nakanishi, H.; Morishima, I.; Inubushi, T.; Takegami, Y. *J. Chem. Soc., Dalton Trans.* **1978**, 1298.

(2) Nakatsu, K.; Mitsudo, T.; Nakanishi, H.; Watanabe, Y.; Takegami, Y. *Chem. Lett.* **1977**, 1447.

(3) (a) Klimes, J.; Weiss, E. *Angew. Chem.* **1982**, *94*, 207; *Angew. Chem., Int. Ed. Engl.* **1982**, *21*, 205. (b) Jens, K. J.; Weiss, E. *Chem. Ber.* **1984**, *117*, 2469. (c) Valeri, T.; Meier, F.; Weiss, E. *Chem. Ber.* **1988**, *121*, 1093.

(4) (a) Hermann, W. A.; Fischer, R. A.; Herdtweck, E. *Angew. Chem.* **1987**, *99*, 1286; *Angew. Chem., Int. Ed. Engl.* **1987**, *26*, 1284. (b) Fischer, R. A.; Ficsher, R. W.; Herrmann W. A.; Herdweck, E. *Chem. Ber.* **1989**, *122*, 2035.

(5) (a) Mayr, A.; Asaro, M. F.; Glines, T. J. *J. Am. Chem. Soc.* **1987**, *109*, 2215. (b) Mayr, A.; Asaro, M. F.; Glines, T. J.; Engen, D. V.; Tripp, G. M. *J. Am. Chem. Soc.* **1993**, *115*, 8187.

(6) Garrett, K. E.; Sheridan, J. B.; Pourreau, D. B.; Feng, W. C.; Geoffroy, G. L.; Staley, D. L.; Rheingold, A. L. *J. Am. Chem. Soc.* **1989**, *111*, 8383.

(7) Feng, S. G.; Gamble, A. S.; Templeton, J. L. *Organometallics* **1989**, *8*, 2024.

(8) Park, J.; Kang, S.; Whang, D.; Kim, K. *Organometallics* **1992**, *11*, 1738.

(9) Barluenga, J.; Aznar, F.; Matin, A.; Granda, S. G.; Carreno, E. P. *J. Am. Chem. Soc.* **1994**, *116*, 11191.

(10) (a) Dötz, K. H. *Angew. Chem.* **1975**, *87*, 672; *Angew. Chem., Int. Ed. Engl.* **1975**, *14*, 644. (b) Dötz, K. H. *Pure Appl. Chem.* **1983**, *55*, 1689. (c) Dötz, K. H. *Angew. Chem.* **1984**, *96*, 573; *Angew Chem., Int. Ed. Engl.* **1984**, *23*, 587. (d) Wulff, W. D.; Tang, P. C.; Chan, K. S.; McCallum, J. S.; Yang, D. C.; Gilbertson, S. R. *Tetrahedron* **1985**, *41*, 5813. (e) Dötz, K. H.; Popall, M. *Tetrahedron* **1985**, *41*, 5797. (f) Yamashita, A.; Scahill, T. A.; Toy, A. *Tetrahedron Lett.* **1985**, *26*, 2969. (g) Wulff, W. D.; Gilbertson, S. R.; Springer, J. P. *J. Am. Chem. Soc.* **1986**, *108*, 520. (h) Semmelhack, M. F.; Tamura, R.; Springer, J. P. *J. Am. Chem. Soc.* **1984**, *106*, 5363. (i) Semmelhack, M. F.; Park, J. *Organometallics* **1986**, *5*, 2550. (j) Bos, M. E.; Wulff, W. D.; Miller, R. A.; Chamberlin, S.; Brandvold, T. A. *J. Am. Chem. Soc.* **1991**, *113*, 9293. (k) Wulff, W. D.; Bax, D. M.; Brandvold, T. A.; Chan, K. S.; Gilbert, A. M.; Hsung, R. P.; Mitchell, J.; Clardy, J. *Organometallics* **1994**, *13*, 102.

(11) Hofmann, P.; Hammerle, M.; Unfried, G. *New J. Chem.* **1991**, *15*, 769.

(12) (a) Masuda, T.; Sasaki, N.; Higashimura, T. *Macromolecules* **1975**, *8*, 717. (b) Katz, T. J.; Lee, S. J. *J. Am. Chem. Soc.* **1980**, *102*, 422. (c) Katz, T. J.; Haber, S. M.; Kendrick, R. D.; Yunoni, C. S. *J. Am. Chem. Soc.* **1985**, *107*, 2182. (d) Lerisalles, J.; Rose-Munch, F.; Rudler, H.; Daran, J. C.; Dromzee, Y.; Jeannim, Y.; Ades, D.; Fontanille, M. *J. Chem. Soc., Chem. Commun.* **1981**, 1055.

(13) Mitsudo, T.; Watanabe, H.; Sasaki, T.; Takegami, Y.; Watanabe, Y. *Organometallics* **1989**, *8*, 368.

0276-7333/95/2314-4228$09.00/0

Scheme 1

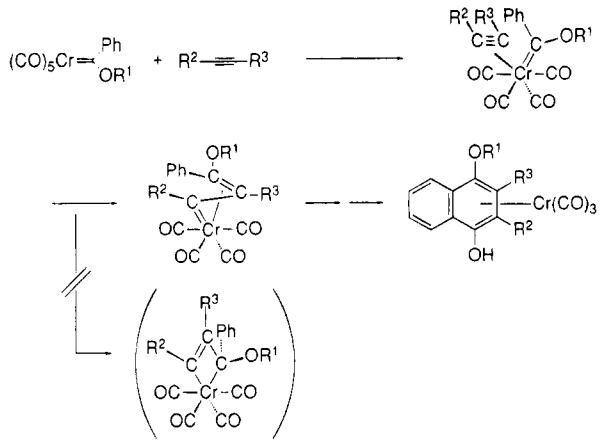

limitation of the substituents on the vinylcarbene skeleton. Since the (π-vinylcarbene)iron complexes prepared by us had methoxycarbonyl groups,[1] the reactivities toward nucleophiles could not be fully examined because of the high reactivity of these groups. In this study, we report the synthesis, structure and reactivities of trifluoromethyl-substituted (π-vinylcarbene)iron complexes.

Results and Discussion

A trifluoromethyl-substituted (π-vinylcarbene)tricarbonyliron complex was successfully prepared by the method developed by us.[1,2] The reactions performed in this work are summarized in Scheme 2.

Preparation of [PPN][(*trans*-2,3-bis(trifluoromethyl)-π-acryloyl)tricarbonyliron] (1). [PPN][HFe(CO)$_4$] was treated with hexafluoro-2-butyne (1 atm) in dichloromethane at room temperature for 6 h. Addition of diethyl ether to the reaction mixture gave a 1:1 adduct **1** as pale-yellow crystals in 90% yield. The adduct was not an alkenyliron complex **2** but a (η^3-acryloyl)tricarbonyliron anion complex; insertion of a carbon monoxide molecule between the alkenyl–iron bond occurred.[1,2] The IR spectrum of **1** showed ν(C≡O) absorptions at 2020 and 1927 cm^{-1} and ν(C=O) absorption of an acryloyl at 1722 cm^{-1}.[1] The ^{1}H NMR spectrum of **1** showed a signal of a coordinated olefinic proton at 3.08 ppm (q, $^3J_{HF}$ = 8.2 Hz). The ^{13}C NMR spectrum of **1** showed a signal assigned to carbonyl carbon of an acryloyl group at δ 233.3 ppm and signals of coordinated olefinic carbons at δ 35.9 (q, $^2J_{CF}$ = 36.8 Hz) and 22.0 (dq, $^2J_{CF}$ = 36.8 Hz, $^2J_{CH}$ = 153.0 Hz). These spectral data are compared with those of bis(triphenylphosphine)nitrogen(1+) (*trans*-2,3-bis(methoxycarbonyl)-π-acryloyl)tricarbonyliron (**3**): ν(C≡O) 2015, 1937, 1900 cm^{-1}, ν(C=O) 1742 cm^{-1}, ^{1}H NMR δ 3.67, ^{13}C NMR δ 235.7, 37.1 (d, J_{CH} = 159 Hz, olefin), 25.1 (s, olefin).[1] The difference of the spectra between **1** and **3** is the ^{13}C NMR signals of the coordinated olefinic carbons. In **1**, the signal of the center carbon was found at 35.9 ppm, which was in lower field than that of the terminal carbon by 13.9 ppm. In **3**, the signal of the center carbon is found at 25.1 ppm which is higher field than that of the terminal carbon by 12.0 ppm. The chemical shifts of the coordinated olefins are quite sensitive to the substituents.

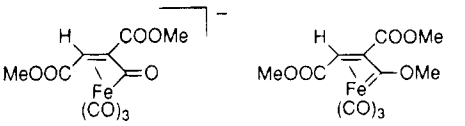

3 5

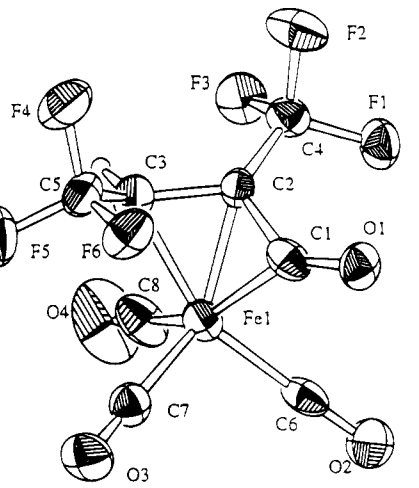

Figure 1. ORTEP[32] view of **1**. (The [PPN]$^+$ counterion is omitted for clarity.) Thermal ellipsoids are shown at the 30% probability level.

X-ray Crystal Structure of 1. The molecular geometry and atom-numbering system of **1** are shown in Figure 1, while Tables 1–3 summarize the results obtained. This complex has an η^3-acryloyl ligand with two trifluoromethyl groups in *trans* configuration with respect to the C(2)=C(3) bond, which shows that the addition of the [PPN][HFe(CO)$_4$] to hexafluoro-2-butyne is *trans*. The *trans*-addition of the hydride to acetylenes was also observed in the preparation of **3**.[1] The molecular geometry of **1** was revealed to be very close to that of **3**.[22] Nakamura et al. also reported that Cp_2MoH_2 reacts with acetylenes to give *trans*-adducts.[23]

Preparation of [1–3-η-(*trans*-1,2-bis(trifluoromethyl)vinyl)methoxycarbene]tricarbonyliron (4). The methylation of **1** with Me_3OBF_4 and recrystallization from *n*-pentane at −78 °C gave orange crystals of **4** in 38% yield. Complex **4** is an orange liquid which solidifies at ca. 3 °C. This complex is very volatile and can be easily distilled at 25 °C under a reduced pressure (1 Torr). The IR spectrum of **4** showed a characteristic absorption of a π-vinylcarbene skeleton at 1541 cm^{-1}

(14) Mitsudo, T.; Ishihara, A.; Kadokura, M.; Watanabe, Y. *Organometallics* **1986**, *5*, 238.
(15) Mitsudo, T.; Watanabe, H.; Watanabe, K.; Watanabe, Y.; Kafuku, K.; Nakatsu, K. *Organometallics* **1982**, *1*, 612.
(16) Mitsudo, T.; Ogino, Y.; Komiya, Y.; Watanabe, H.; Watanabe, Y. *Organometallics* **1983**, *2*, 1202.
(17) Mitsudo, T.; Sasaki, T.; Watanabe, Y.; Takegami, Y.; Nishigaki, S.; Nakatsu, K. *J. Chem. Soc., Chem. Commun.* **1978**, 252.
(18) Mitsudo, T.; Sasaki, T.; Watanabe, Y.; Takegami, Y.; Nakatsu, K.; Kinoshita, K.; Miyagawa, Y. *J. Chem. Soc., Chem. Commun.* **1978**, 579.
(19) Mitsudo, T.; Watanabe, H.; Sasaki, T.; Watanabe, Y.; Takegami, Y.; Kafuku, K.; Kinoshita, K.; Nakatsu, K. *J. Chem. Soc., Chem. Commun.* **1981**, 22.
(20) Mitsudo, T.; Watanabe, H.; Komiya, Y.; Watanabe, Y.; Takegami, Y.; Nakatsu, K.; Kinoshita, K.; Miyagawa, Y. *J. Organomet. Chem.* **1980**, *190*, C39.
(21) Mitsudo, T.; Watanabe, H.; Watanabe, K.; Watanabe, Y.; Takegami, Y. *J. Organomet. Chem.* **1981**, *214*, 87.
(22) Nakatsu, K.; Inai, Y.; Mitsudo, T.; Watanabe, Y.; Nakanishi, H.; Takegami, Y. *J. Organomet. Chem.* **1978**, *159*, 111.
(23) Otsuka, S.; Nakamura, A.; Minamida, H. *J. Chem. Soc., Dalton Trans.* **1969**, 1148.

Scheme 2

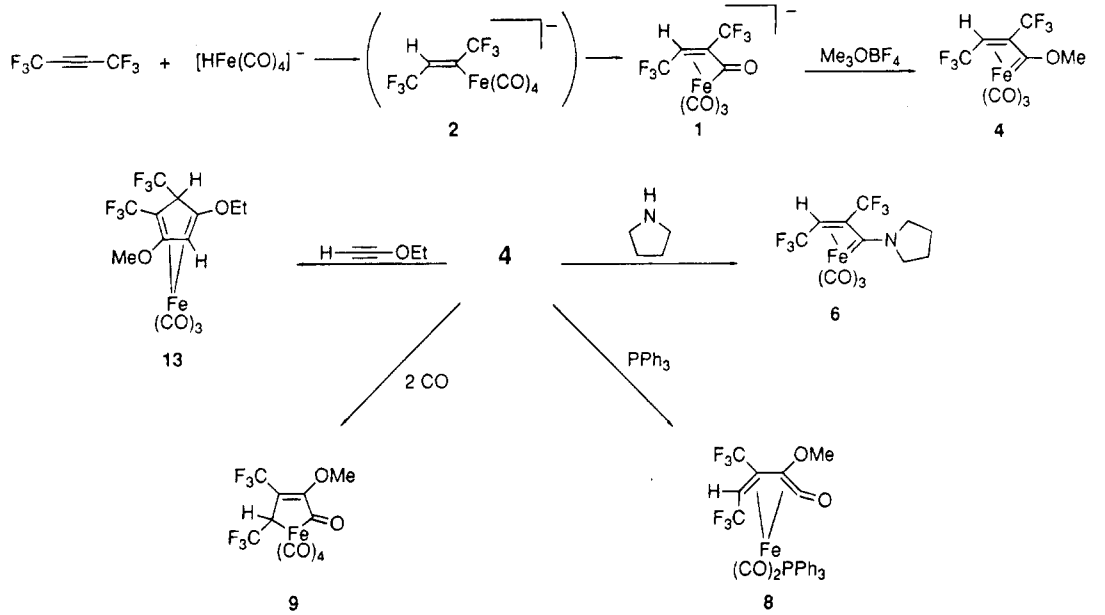

Table 1. Summary of Crystal Data, Collection Data, and Refinement Data for 1, 6, and 13

	1	6	13
	Description of Crystal		
color	pale-yellow	yellow	orange
habit	cubic	plate	prismatic
max cryst dimens (mm)	0.30 × 0.30 × 0.30	0.15 × 0.15 × 0.07	0.10 × 0.30 × 0.40
cryst syst	triclinic	monoclinic	triclinic
space group	$P\bar{1}$	$P2_1$	$P\bar{1}$
unit cell params			
a (Å)	13.029(6)	8.058(2)	7.6177(8)
b (Å)	16.812(9)	10.847(4)	14.646(2)
c (Å)	10.341(8)	17.766(4)	7.488(1)
α (deg)	103.61(5)		99.73(1)
β (deg)	96.64(5)	99.00(2)	98.08(1)
γ (deg)	68.29(4)		98.97(1)
V (Å^3)	2044(2)	1533.7(8)	801.3(2)
Z	2	4	2
formula	$C_{44}H_{31}F_6NO_4P_2Fe$	$C_{12}H_9F_6N_1O_3Fe$	$C_{13}H_{10}F_6O_5Fe$
fw	869.52	385.05	416.06
D_{calc} (g cm^{-3})	1.412	1.667	1.724
μ_{calc} (cm^{-1})	5.17	10.57	10.22
	Data Collection		
radiation (λ, Å)		Mo $K\alpha$ (0.710 69)	
scan technique		$\omega-2\theta$	
scan width (deg)	1.15 + 0.30 tan θ	1.20 + 0.30 tan θ	1.15 + 0.30 tan θ
$2\theta_{max}$ (deg)	60	60	60
no. of rflns measd	10848	7446	5009
	Structure Determination		
no. of rflns used ($I > 3\sigma(I)$)	2923	3247	1800
no. of params varied	523	487	267
data/param ratio	5.59	6.67	6.74
goodness of fit	2.01	1.90	1.45
R^a	0.057	0.066	0.045
$R_w{}^a$	0.060	0.079	0.022
highest peak of resid electron density (e Å^{-3})	0.36	0.38	0.33

[a] $R = \Sigma||F_o| - |F_c||/\Sigma|F_o|$; $R_w = [\Sigma w(|F_o| - |F_c|)^2/\Sigma wF_o^2]^{1/2}$.

as well as ν(C≡O) at 2081, 2024, and 2006 cm^{-1}. The characteristic ^{13}C NMR signal at δ 264.7 ppm was assigned to a carbene carbon. The spectrum also showed signals of coordinated olefinic carbons at δ 51.6 (q, $^2J_{CF}$ = 44.1 Hz) and at δ 39.8 (dq, $^2J_{CF}$ = 38.3 Hz, $^1J_{CH}$ = 150.1 Hz)]. The ^{1}H-NMR signal of the coordinated olefinic proton was found at 3.94 ppm as a quartet ($^3J_{HF}$ = 6.5 Hz). These spectral data were similar to those of the corresponding methoxycarbonyl-substituted (π-vinylcarbene)iron complex **5**: ν(C≡O) 2050, 2000, 1980, ν(C−C−C$_{asyn}$) 1523 cm^{-1}, ^{1}H NMR δ 4.30 ppm, ^{13}C NMR δ 270.9, 208.6, 51.4 (s, olefin), 41.8 (d, J_{CH} = 164 Hz, olefin).[1] On the basis of these spectral data, complex **4** was inferred as a trifluoromethyl-substituted (π-vinylcarbene)iron complex. This inference was confirmed by the X-ray analysis of its derivatives.

Reaction of 4 with Pyrrolidine. The First (π-Aminovinylcarbene)iron Complex. The complex **4** reacted with pyrrolidine at 25 °C to give yellow crystals of [(1-pyrrolidino)(π-vinyl)carbene]iron complex **6** in 41%

Table 2. Atomic Coordinates for 1

atom	x	y	z
Fe(1)	0.2850(1)	0.29278(9)	0.6396(1)
P(1)	0.6635(2)	0.2695(1)	0.1833(2)
P(2)	0.7358(2)	0.0888(1)	0.2310(2)
F(1)	0.0905(5)	0.3777(4)	0.8952(5)
F(2)	−0.0418(5)	0.4494(4)	0.7756(6)
F(3)	0.1011(5)	0.4858(3)	0.8274(5)
F(4)	0.0099(6)	0.4083(4)	0.3956(6)
F(5)	0.1775(6)	0.3588(4)	0.3322(6)
F(6)	0.1091(5)	0.2744(4)	0.3890(5)
O(1)	0.1273(5)	0.2056(4)	0.6689(6)
O(2)	0.4041(7)	0.1804(5)	0.8268(7)
O(3)	0.3934(6)	0.1859(5)	0.3913(7)
O(4)	0.4004(9)	0.4211(7)	0.726(1)
N(1)	0.6626(5)	0.1751(4)	0.1804(6)
C(1)	0.1608(8)	0.2607(8)	0.6504(9)
C(2)	0.1239(8)	0.3540(6)	0.6686(9)
C(3)	0.1533(8)	0.3804(6)	0.561(1)
C(4)	0.0696(9)	0.4162(7)	0.790(1)
C(5)	0.115(1)	0.3555(8)	0.423(1)
C(6)	0.3591(8)	0.2251(7)	0.755(1)
C(7)	0.3531(9)	0.2286(7)	0.488(1)
C(8)	0.3570(10)	0.3732(8)	0.694(1)
C(9)	0.7535(7)	0.2675(6)	0.0624(8)
C(10)	0.8061(8)	0.3266(6)	0.0798(9)
C(11)	0.8753(9)	0.3212(7)	−0.016(1)
C(12)	0.8899(9)	0.2577(9)	−0.130(1)
C(13)	0.836(1)	0.1980(8)	−0.150(1)
C(14)	0.7678(8)	0.2034(7)	−0.053(1)
C(15)	0.5286(7)	0.3347(6)	0.1399(8)
C(16)	0.4438(9)	0.3058(6)	0.1282(10)
C(17)	0.3376(9)	0.3555(8)	0.096(1)
C(18)	0.3163(8)	0.4397(7)	0.0763(9)
C(19)	0.4022(10)	0.4689(6)	0.0913(10)
C(20)	0.5056(8)	0.4197(6)	0.1213(9)
C(21)	0.6985(8)	0.3238(6)	0.3421(9)
C(22)	0.8065(9)	0.3040(6)	0.3851(10)
C(23)	0.8340(9)	0.3379(7)	0.517(1)
C(24)	0.750(1)	0.3913(8)	0.602(1)
C(25)	0.6426(9)	0.4115(7)	0.558(1)
C(26)	0.6174(8)	0.3777(6)	0.431(1)
C(27)	0.8765(7)	0.0779(5)	0.2661(9)
C(28)	0.9409(8)	0.0718(6)	0.1625(10)
C(29)	1.0475(9)	0.0717(7)	0.190(1)
C(30)	1.0908(9)	0.0799(7)	0.314(1)
C(31)	1.0307(10)	0.0838(7)	0.416(1)
C(32)	0.9237(8)	0.0835(6)	0.3934(10)
C(33)	0.7319(8)	−0.0028(6)	0.1024(8)
C(34)	0.8089(8)	−0.0859(6)	0.1051(9)
C(35)	0.8021(9)	−0.1560(6)	0.006(1)
C(36)	0.722(1)	−0.1435(7)	−0.093(1)
C(37)	0.6447(9)	−0.0606(7)	−0.0957(10)
C(38)	0.6518(8)	0.0086(6)	0.0034(10)
C(39)	0.6828(7)	0.0840(6)	0.3818(8)
C(40)	0.6730(8)	0.0073(6)	0.3970(10)
C(41)	0.6379(9)	0.0051(7)	0.518(1)
C(42)	0.6143(9)	0.0762(9)	0.620(1)
C(43)	0.6235(8)	0.1520(7)	0.6041(10)
C(44)	0.6577(8)	0.1560(6)	0.4850(9)

yield. IR absorptions of metal carbonyl groups in **6**, 2062, 1993, and 1975 cm^{-1}, shifted to the lower wavenumber comparing with those of the mother complex **4**, 2081, 2024, and 2006 cm^{-1}, which shows the enhanced back-donation of the d-electrons to the carbonyl π^* orbitals in **6**. ^1H NMR spectrum exhibited a signal of an olefinic proton at δ 3.36 ppm, which was found in higher field than that of the complex **4** by 0.55 ppm. The ^{13}C NMR spectrum of **6** showed a signal of a carbene carbon at δ 222.0 ppm, which was found at higher field than those in usual examples of amino-substituted carbene complexes.[24] The signals of methylene carbons of pyrrolidine were found at δ 57.5, 55.1, 25.9 and 25.1 ppm, which exhibited that free rotation of the pyrrolidine ring is suppressed. In conclusion, all spectral data for **6** were fully consistent with the structure of the [(1-pyrrolidino)(π-vinyl)carbene]iron complex. The complex **6** is, to our knowledge, the first example of a (π-aminovinylcarbene)iron complex.

(24) For example: Klabunde, U.; Fischer, E. O. *J. Am. Chem. Soc.* **1967**, *89*, 7141.

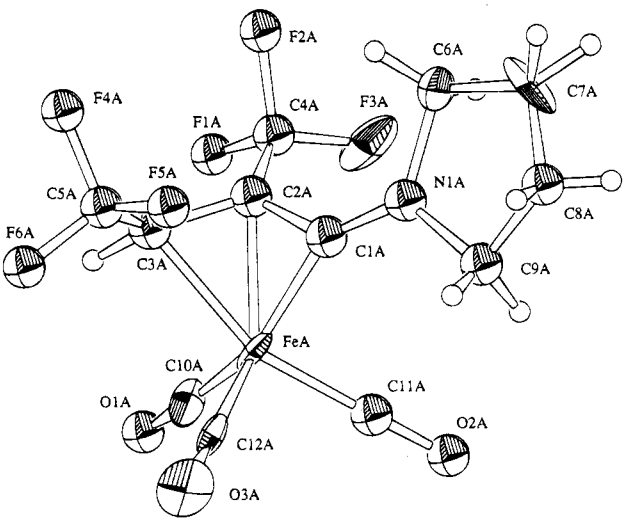

Figure 2. ORTEP view of **6**. Thermal ellipsoids are shown at the 30% probability level.

Table 3. Selected Bond Lengths and Angles in Complex 1

	Bond Lengths (Å)		
Fe(1)−C(1)	1.91(1)	C(1)−O(1)	1.22(1)
Fe(1)−C(2)	1.989(9)	C(6)−O(2)	1.14(1)
Fe(1)−C(3)	2.04(1)	C(7)−O(3)	1.14(1)
Fe(1)−C(6)	1.79(1)	C(8)−O(4)	1.12(1)
Fe(1)−C(7)	1.79(1)	C(4)−F(1)	1.35(1)
Fe(1)−C(8)	1.87(1)	C(4)−F(2)	1.35(1)
C(1)−C(2)	1.43(1)	C(4)−F(3)	1.34(1)
C(2)−C(3)	1.43(1)	C(5)−F(4)	1.37(1)
C(2)−C(4)	1.49(1)	C(5)−F(5)	1.34(1)
C(3)−C(5)	1.47(1)	C(5)−F(6)	1.36(1)
	Bond Angles (deg)		
C(1)−Fe(1)−C(2)	43.1(4)	Fe(1)−C(1)−O(1)	147.4(9)
C(1)−Fe(1)−C(3)	73.9(4)	Fe(1)−C(1)−C(2)	71.5(6)
C(1)−Fe(1)−C(6)	88.9(5)	O(1)−C(1)−C(2)	138.4(10)
C(1)−Fe(1)−C(7)	107.6(4)	Fe(1)−C(2)−C(1)	65.4(6)
C(1)−Fe(1)−C(8)	149.1(4)	Fe(1)−C(2)−C(3)	71.0(6)
C(2)−Fe(1)−C(3)	41.5(3)	Fe(1)−C(2)−C(4)	127.7(7)
C(2)−Fe(1)−C(6)	115.6(4)	C(1)−C(2)−C(3)	112.0(8)
C(2)−Fe(1)−C(7)	128.5(4)	C(1)−C(2)−C(4)	124.1(9)
C(2)−Fe(1)−C(8)	109.3(4)	C(3)−C(2)−C(4)	123.7(9)
C(3)−Fe(1)−C(6)	157.0(4)	Fe(1)−C(3)−C(2)	67.4(6)
C(3)−Fe(1)−C(7)	98.9(4)	Fe(1)−C(3)−C(5)	119.5(7)
C(3)−Fe(1)−C(8)	92.4(5)	C(2)−C(3)−C(5)	121.8(9)
C(6)−Fe(1)−C(7)	100.9(4)	Fe(1)−C(6)−O(2)	177(1)
C(6)−Fe(1)−C(8)	95.1(5)	Fe(1)−C(7)−O(3)	177.1(10)
C(7)−Fe(1)−C(8)	101.8(5)	Fe(1)−C(8)−O(4)	179(1)

X-ray Crystal Structure of 6. The crystal contains two independent enantiomers in a unit cell that happened to be oriented in a decidedly polar fashion with respect to the crystal *b*-axis. The molecular geometry and atom-numbering system of **6** are shown in Figure 2, while Tables 1, 4, and 5 summarize the results obtained. These results confirmed that **6** is a [(1-pyrrolidino)(π-vinyl)carbene]iron complex. The geometry of this complex was a very distorted trigonal bipyramid with C(1) and C(10) at the axial apices (C(1A)−Fe(A)−C(10A) 146.3(5)°) and other carbon atoms, C(11) and C(12), and the C(2)=C(3) groups on the equatorial plane.[2] The Fe(1)−C(1) bond lengths, 1.876(7) and 1.868(8) Å, are longer than that in **5** (1.819(3)

Table 4. Atomic Coordinates for 6

atom	x	y	z
Fe(A)	0.4761(2)	1.000	0.09745(8)
Fe(B)	0.4068(2)	0.6783(2)	0.39996(8)
F(1A)	0.262(1)	0.7371(7)	0.1498(5)
F(1B)	−0.0037(8)	0.4453(7)	0.4337(5)
F(2A)	0.0362(8)	0.7762(7)	0.0757(5)
F(2B)	0.177(1)	0.4075(6)	0.3610(4)
F(3A)	0.255(1)	0.7266(6)	0.0302(5)
F(3B)	0.2495(9)	0.4048(6)	0.4806(5)
F(4A)	0.0138(9)	1.091(1)	0.1664(5)
F(4B)	0.0845(9)	0.8513(7)	0.4229(5)
F(5A)	0.1441(8)	1.1760(7)	0.0884(4)
F(5B)	−0.1122(8)	0.7569(8)	0.3506(5)
F(6A)	0.233(1)	1.1921(9)	0.2058(5)
F(6B)	0.066(1)	0.8637(7)	0.3028(5)
O(1A)	0.667(1)	0.878(1)	0.2298(6)
O(1B)	0.720(1)	0.605(1)	0.4946(6)
O(2A)	0.700(1)	0.923(1)	−0.0072(6)
O(2B)	0.476(1)	0.9390(8)	0.3746(7)
O(3A)	0.586(1)	1.2575(8)	0.1191(6)
O(3B)	0.480(1)	0.560(1)	0.2594(5)
N(1A)	0.2292(8)	0.9946(8)	−0.0497(4)
N(1B)	0.2942(8)	0.6730(7)	0.5546(4)
C(1A)	0.2905(9)	0.9889(8)	0.0195(5)
C(1B)	0.2954(9)	0.6663(7)	0.4843(5)
C(2A)	0.249(1)	0.924(1)	0.0839(5)
C(2B)	0.198(1)	0.599(1)	0.4220(5)
C(3A)	0.264(1)	0.997(1)	0.1504(5)
C(3B)	0.157(1)	0.672(1)	0.3561(5)
C(4A)	0.205(1)	0.793(1)	0.0843(7)
C(4B)	0.158(1)	0.466(1)	0.4236(7)
C(5A)	0.170(1)	1.116(1)	0.1528(6)
C(5B)	0.052(1)	0.787(1)	0.3580(6)
C(6A)	0.062(1)	0.945(1)	−0.0856(6)
C(6B)	0.162(1)	0.626(1)	0.5969(6)
C(7A)	0.046(2)	0.975(1)	−0.1637(7)
C(7B)	0.201(2)	0.683(2)	0.6728(6)
C(8A)	0.174(2)	1.067(2)	−0.1736(7)
C(8B)	0.361(2)	0.748(2)	0.6780(8)
C(9A)	0.310(1)	1.062(1)	−0.1086(6)
C(9B)	0.419(1)	0.747(1)	0.6053(7)
C(10A)	0.597(2)	0.926(1)	0.1785(7)
C(10B)	0.600(1)	0.635(1)	0.4561(7)
C(11A)	0.612(1)	0.956(1)	0.0332(7)
C(11B)	0.453(1)	0.837(1)	0.3850(7)
C(12A)	0.546(1)	1.156(1)	0.1115(5)
C(12B)	0.457(1)	0.610(1)	0.3140(6)

Å).[2] The C(1)−N(1) bond lengths of 1.25(1) and 1.25(1) Å are somewhat shorter than an ordinary C=N bond (1.30 Å). These results and the low wavenumbers of ν(C≡O) of **6** mentioned above strongly suggest the large contribution of the structure **7** (eq 1).

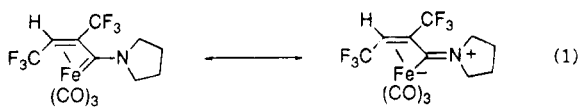

(1)

6 7

Reaction of 4 with Triphenylphosphine. The complex **4** reacted with triphenylphosphine at 25 °C to give yellow crystals of a η^4-vinylketene complex **8** in 79% yield. IR absorptions of metal carbonyl groups, 2041 and 1985 cm^{-1}, which shifted to the lower wavenumber comparing with those of **4**, showed coordination of triphenylphosphine to the iron atom. The IR absorption of 1719 cm^{-1} and the ^{13}C NMR signal at δ 233.6 ppm showed the existence of an organic carbonyl group. All spectral data showed that **8** was a η^4-vinylketene complex.[13] In this reaction the insertion of carbon monoxide between the carbene carbon and iron occurred, which had been observed in the reaction of π-vinylcarbene complexes with tertiary phosphines.[13]

Table 5. Selected Bond Lengths and Angles in Complex 6

Bond Lengths (Å)			
Fe(A)−C(1A)	1.876(7)	C(12A)−O(3A)	1.15(2)
Fe(A)−C(2A)	1.990(9)	C(4A)−F(1A)	1.33(1)
Fe(A)−C(3A)	2.073(9)	C(4A)−F(2A)	1.36(1)
Fe(A)−C(10A)	1.80(1)	C(4A)−F(3A)	1.32(1)
Fe(A)−C(11A)	1.77(1)	C(5A)−F(4A)	1.34(1)
Fe(A)−C(12A)	1.79(1)	C(5A)−F(5A)	1.31(1)
C(1A)−C(2A)	1.43(1)	C(5A)−F(6A)	1.30(2)
C(2A)−C(3A)	1.41(1)	N(1A)−C(6A)	1.50(1)
C(2A)−C(4A)	1.46(1)	N(1A)−C(9A)	1.51(1)
C(3A)−C(5A)	1.50(2)	C(6A)−C(7A)	1.41(2)
C(1A)−N(1A)	1.25(1)	C(7A)−C(8A)	1.46(2)
C(10A)−O(1A)	1.12(2)	C(8A)−C(9A)	1.47(2)
C(11A)−O(2A)	1.14(2)		
Bond Angles (deg)			
C(1A)−Fe(A)−C(2A)	43.3(4)	N(1A)−C(1A)−C(2A)	134.8(8)
C(1A)−Fe(A)−C(3A)	73.5(3)	Fe(A)−C(2A)−C(1A)	64.1(4)
C(1A)−Fe(A)−C(10A)	146.3(5)	Fe(A)−C(2A)−C(3A)	72.8(5)
C(1A)−Fe(A)−C(11A)	90.5(4)	Fe(A)−C(2A)−C(4A)	128.3(7)
C(1A)−Fe(A)−C(12A)	111.2(4)	C(1A)−C(2A)−C(3A)	113.0(9)
C(2A)−Fe(A)−C(3A)	40.6(4)	C(1A)−C(2A)−C(4A)	124.7(9)
C(2A)−Fe(A)−C(10A)	106.5(5)	C(3A)−C(2A)−C(4A)	122.2(9)
C(2A)−Fe(A)−C(11A)	117.5(5)	Fe(A)−C(3A)−C(2A)	66.5(5)
C(2A)−Fe(A)−C(12A)	132.3(5)	Fe(A)−C(3A)−C(5A)	117.4(8)
C(3A)−Fe(A)−C(10A)	90.6(5)	C(2A)−C(3A)−C(5A)	121.7(8)
C(3A)−Fe(A)−C(11A)	157.8(5)	C(1A)−N(1A)−C(6A)	126.2(8)
C(3A)−Fe(A)−C(12A)	102.4(5)	C(1A)−N(1A)−C(9A)	124.0(7)
C(10A)−Fe(A)−C(11A)	94.7(6)	C(6A)−N(1A)−C(9A)	109.7(7)
C(10A)−Fe(A)−C(12A)	101.1(5)	Fe(A)−C(10A)−O(1A)	178(1)
C(11A)−Fe(A)−C(12A)	97.7(5)	Fe(A)−C(11A)−O(2A)	177(1)
Fe(A)−C(1A)−N(1A)	150.2(7)	Fe(A)−C(12A)−O(3A)	178(1)
Fe(A)−C(1A)−C(2A)	72.6(5)		

Reaction of 4 with Carbon Monoxide. Complex **4** reacted with 50 atm of carbon monoxide at 50 °C to give yellow crystals of **9** in 63% yield. On the basis of the spectral data, **9** was revealed to be a ferracyclopentenone complex shown in Scheme 2. In the reactions of the methoxycarbonyl-substituted (π-vinylcarbene)iron complexes with carbon monoxide, the insertion of carbon monoxide between the carbene carbon and iron occurred to afford η^4-vinylketene complexes or a pyrone complex.[12] In the reaction of trifluoromethyl-substituted (π-vinylcarbene)iron complex **4**, two molecules of carbon monoxide were introduced into the complex to afford the ferracyclopentenone complex **9**. This result shows the substituent effect of the trifluoromethyl groups. In contrast, in the reaction of **5** with carbon monoxide, only 1 mol of carbon monoxide was introduced and the cyclization to a pyrone complex **10** occurred (eq 2). The carbonylation of a monomethoxycarbonyl-substituted vinylcarbeneiron complex **11** gave only a η^4-vinylketene complex **12** even under 80 atm of carbon monoxide (eq 3).

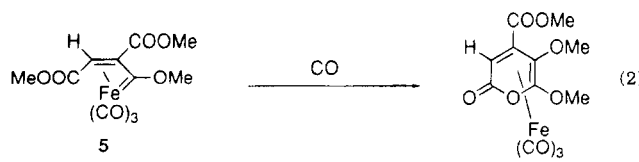

(2)

5 10

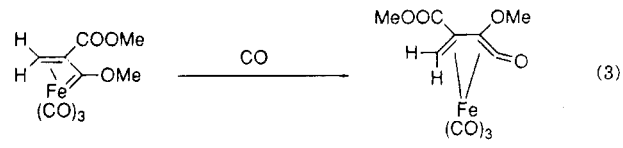

(3)

11 12

Reaction of 4 with Ethoxyethyne and X-ray Crystal Structure of the Product. Complex **4** re-

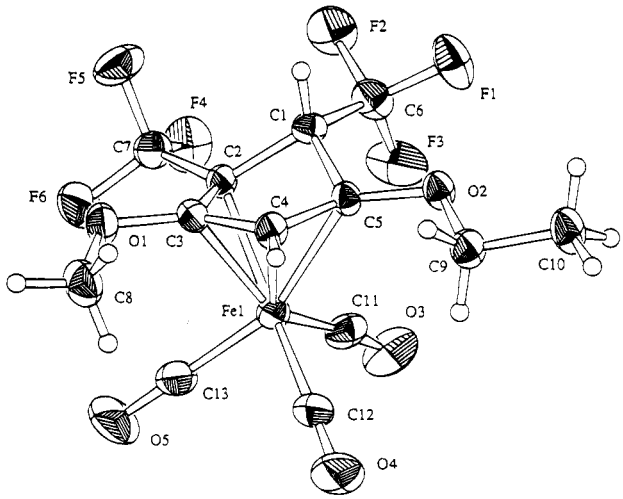

Figure 3. ORTEP view of **13**. Thermal ellipsoids are shown at the 30% probability level.

Table 6. Atomic Coordinates for 13

atom	x	y	z
Fe(1)	0.43303(9)	0.68362(5)	0.29506(10)
F(1)	0.5734(4)	0.9898(2)	0.2536(4)
F(2)	0.3075(4)	0.9519(2)	0.1049(4)
F(3)	0.4966(4)	0.8641(2)	0.0488(4)
F(4)	0.0937(4)	0.7754(2)	−0.0103(4)
F(5)	−0.0301(4)	0.8224(2)	0.2166(4)
F(6)	−0.0250(3)	0.6760(2)	0.1327(4)
O(1)	0.1108(4)	0.6880(2)	0.4999(4)
O(2)	0.6907(4)	0.8820(2)	0.5035(4)
O(3)	0.5894(5)	0.6899(3)	−0.0405(5)
O(4)	0.6922(5)	0.5812(2)	0.4575(6)
O(5)	0.1830(5)	0.5041(2)	0.1480(6)
C(1)	0.3838(6)	0.8668(3)	0.3327(6)
C(2)	0.2479(5)	0.7736(3)	0.2837(6)
C(3)	0.2559(6)	0.7369(3)	0.4500(6)
C(4)	0.4319(6)	0.7679(3)	0.5485(6)
C(5)	0.5236(5)	0.8282(3)	0.4507(6)
C(6)	0.4422(7)	0.9152(3)	0.1827(7)
C(7)	0.0733(6)	0.7617(3)	0.1577(8)
C(8)	0.1493(9)	0.6329(4)	0.6356(10)
C(9)	0.8114(7)	0.8506(4)	0.6386(8)
C(10)	0.9874(8)	0.9168(4)	0.6775(9)
C(11)	0.5293(6)	0.6934(3)	0.0929(7)
C(12)	0.5928(6)	0.6224(3)	0.3944(7)
C(13)	0.2793(6)	0.5741(3)	0.2054(7)

acted with ethoxyethyne at room temperature to give orange crystals of a 1:1 adduct **13** in 50% yield. Other acetylenes such as dimethyl acetylenedicarboxylate, phenylacetylene, diphenylacetylene, or hexafluoro-2-butyne did not react with **4** under the same conditions. Since the structure of the complex **13** could not be inferred on the basis of spectral data, X-ray analysis was performed.

The molecular geometry and atom-numbering system of **13** are shown in Figure 3, while Tables 1, 6, and 7 summarize the results obtained. These results indicate that **13** is a (cyclopentadiene)iron complex. The cyclopentadiene ligand is the usual envelope-shaped one, with an "endo" trifluoromethyl group at the methylene group. Apparent [2 + 3] cycloaddition of ethoxyethyne and the vinylcarbene ligand occurred to form the cyclopentadiene ligand. Ethoxyethyne is reasonably oriented to afford the product; electron-sufficient terminal acetylenic carbon is bound to the electron-deficient vinylcarbene carbon.

Possible Mechanism for the Formation of 13. The formation of **13** by the reaction of **4** with ethoxyethyne may be rationalized as follows (see Scheme 3). First, the insertion of ethoxyethyne between the carbene carbon and iron occurs to afford a ferracyclohexadiene intermediate **14**. Then reductive elimination occurs to form the cyclopentadieneiron complex **13**. The direction of the insertion of ethoxyethyne into the carbon−iron double bond may be controlled by the nucleophilic attack of the terminal acetylenic carbon to the carbene carbon. The trifluoromethyl group at the methylene group of the cyclopentadiene was endo to the iron atom. The reason is not clear at the present time, however, there is a possibility that the exo-isomer formed may be reactive to form complicated cyclopentadienyl complexes by abstraction of the active methylene proton resulting the isolation of the endo isomer as a sole product.

Table 7. Selected Bond Lengths and Angles in Complex 13

Bond Lengths (Å)			
Fe(1)−C(2)	2.078(4)	C(4)−C(5)	1.406(5)
Fe(1)−C(3)	2.059(4)	C(5)−O(2)	1.355(4)
Fe(1)−C(4)	2.083(5)	C(6)−F(1)	1.337(5)
Fe(1)−C(5)	2.191(4)	C(6)−F(2)	1.338(5)
Fe(1)−C(11)	1.789(5)	C(6)−F(3)	1.303(5)
Fe(1)−C(12)	1.774(5)	C(7)−F(4)	1.333(5)
Fe(1)−C(13)	1.796(5)	C(7)−F(5)	1.337(5)
C(1)−C(2)	1.534(5)	C(7)−F(6)	1.327(5)
C(1)−C(5)	1.525(5)	O(1)−C(8)	1.428(6)
C(1)−C(6)	1.508(6)	O(2)−C(9)	1.451(5)
C(2)−C(3)	1.434(5)	C(9)−C(10)	1.487(7)
C(2)−C(7)	1.487(5)	C(11)−O(3)	1.153(5)
C(3)−C(4)	1.402(5)	C(12)−O(4)	1.140(5)
C(3)−O(1)	1.354(4)	C(13)−O(5)	1.141(5)
Bond Angles (deg)			
C(2)−Fe(1)−C(3)	40.6(1)	Fe(1)−C(2)−C(7)	129.5(3)
C(2)−Fe(1)−C(4)	66.6(2)	C(1)−C(2)−C(3)	105.3(4)
C(2)−Fe(1)−C(5)	63.2(1)	C(1)−C(2)−C(7)	122.2(4)
C(2)−Fe(1)−C(11)	102.2(2)	C(3)−C(2)−C(7)	120.4(4)
C(2)−Fe(1)−C(12)	158.3(2)	Fe(1)−C(3)−O(1)	127.4(3)
C(2)−Fe(1)−C(13)	98.3(2)	Fe(1)−C(3)−C(2)	70.4(3)
C(3)−Fe(1)−C(4)	39.6(1)	Fe(1)−C(3)−C(4)	71.2(3)
C(3)−Fe(1)−C(5)	64.0(2)	O(1)−C(3)−C(2)	123.5(4)
C(3)−Fe(1)−C(11)	142.6(2)	O(1)−C(3)−C(4)	129.1(4)
C(3)−Fe(1)−C(12)	119.5(2)	C(2)−C(3)−C(4)	107.2(4)
C(3)−Fe(1)−C(13)	92.8(2)	Fe(1)−C(4)−C(3)	69.3(3)
C(4)−Fe(1)−C(5)	38.3(1)	Fe(1)−C(4)−C(5)	75.0(3)
C(4)−Fe(1)−C(11)	138.0(2)	C(3)−C(4)−C(5)	106.9(4)
C(4)−Fe(1)−C(12)	92.0(2)	Fe(1)−C(5)−O(2)	131.2(3)
C(4)−Fe(1)−C(13)	123.3(2)	Fe(1)−C(5)−C(1)	93.3(3)
C(5)−Fe(1)−C(11)	99.9(2)	Fe(1)−C(5)−C(4)	66.7(2)
C(5)−Fe(1)−C(12)	102.8(2)	O(2)−C(5)−C(1)	117.2(3)
C(5)−Fe(1)−C(13)	156.7(2)	O(2)−C(5)−C(4)	127.7(4)
C(11)−Fe(1)−C(12)	96.4(2)	C(1)−C(5)−C(4)	108.1(4)
C(11)−Fe(1)−C(13)	97.8(2)	C(3)−O(1)−C(8)	115.9(4)
C(12)−Fe(1)−C(13)	90.2(2)	C(5)−O(2)−C(9)	115.7(3)
C(2)−C(1)−C(5)	94.1(3)°	O(2)−C(9)−C(10)	108.0(4)
C(2)−C(1)−C(6)	120.2(4)	Fe(1)−C(11)−O(3)	173.0(5)
C(5)−C(1)−C(6)	118.5(4)	Fe(1)−C(12)−O(4)	178.3(5)
Fe(1)−C(2)−C(1)	97.6(3)	Fe(1)−C(13)−O(5)	179.3(5)
Fe(1)−C(2)−C(3)	69.0(2)		

Experimental Section

All manipulations were performed under a dry argon atmosphere with standard Schlenk techniques. Dichloromethane and 1,2-dichloroethane were distilled from $CaCl_2$; diethyl ether was distilled from benzophenone ketyl; *n*-pentane and benzene were distilled from sodium. Bis(triphenylphosphine)nitrogen(1+) hydridotetracarbonyliron[1b] and trimethyloxonium tetrafluoroborate[25] were prepared by literature methods. Other reagents were used as obtained from com-

(25) Meerwein, H. *Organic Syntheses*; Wiley: New York, 1973; **1973**, Collect. Vol. V, p 1096.

Scheme 3

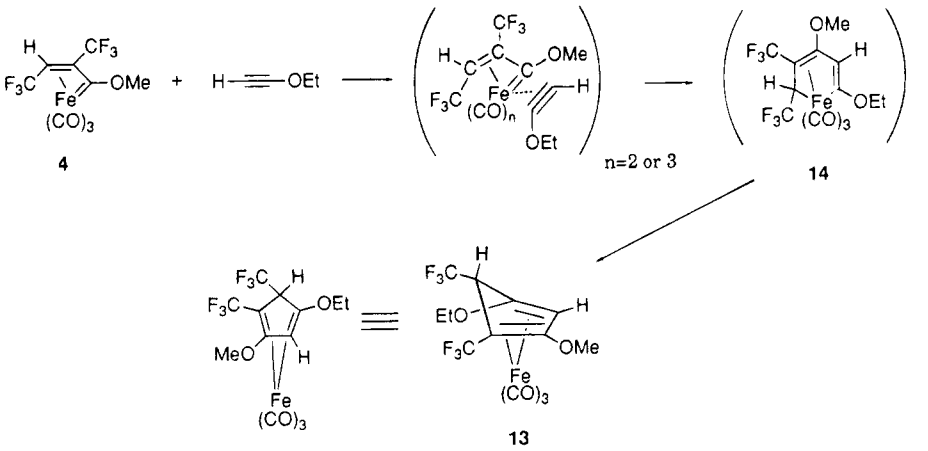

mercial sources. Melting points were determined under an argon atmosphere on a Yanagimoto micro melting point apparatus. Infrared spectra were recorded on a Shimadzu FTIR-8100 spectrometer and calibrated with a polystyrene standard. ^{1}H NMR spectra were obtained on a JEOL JNM FX-90 or a JEOL GSX-270 spectrometer. ^{13}C NMR spectra were recorded on a JEOL JNM FX-100 or a JEOL GSX-270 spectrometer.

Preparation of [PPN][(*trans*-2,3-bis(trifluoromethyl)-π-acryloyl)tricarbonyliron] (1). Into a 50 mL two-necked cylindrical flask, connected with a gas buret filled with hexafluoro-2-butyne and an argon line through a three way stopcock, were placed under an argon atmosphere a magnetic stirring bar, 7.29 g (10.3 mmol) of bis(triphenylphosphine)-nitrogen(1+) (PPN) hydridotetracarbonyliron, and dichloromethane (10 mL). To the solution was introduced hexafluoro-2-butyne, and then the solution was stirred at room temperature for 6 h. After concentration of the solution, the addition of diethyl ether (40 mL) gave pale-yellow crystals of [PPN][(*trans*-2,3-bis(trifluoromethyl)-π-acryloyl)tricarbonyliron] (**1**) (8.02 g, 9.2 mmol, 90%).

Data for 1. Mp: 128–130 °C. IR (KBr): ν(C≡O) 2020 (vs), 1927 (vs) cm^{-1}, ν(C=O) 1722 (vs) cm^{-1}. ^{1}H NMR (CD_2Cl_2): δ 7.5–7.3 (m, 30H, PPN), 3.08 (q, 1H, $^3J_{HF}$ = 8.2 Hz, CH). ^{13}C NMR (CD_2Cl_2): δ 233.3 (s, C=O), 213.2 (s, Fe-CO), 135.3–123.9 (m, CF_3, CF_3, PPN), 35.9 (q, $^2J_{CF}$ = 36.8 Hz, olefin), 22.0 (dq, $^2J_{CF}$ = 36.8 Hz, $^2J_{CH}$ = 153.0 Hz, olefin). Anal. Calcd for $C_{44}H_{31}F_6NO_4P_2Fe$: C, 60.77; H, 3.59; F, 1.61. Found: C, 60.67; H, 3.36; F, 1.57.

Preparation of [1–3-η-(*trans*-1,2-bis(trifluoromethyl)-vinyl)methoxycarbene]tricarbonyliron (4). To a solution of **1** (1.74 g, 2.0 mmol) in dichloromethane (5.0 mL) was added 0.31 g (2.1 mmol) of Me_3OBF_4 at 0 °C, and the mixture was stirred at 0 °C for 0.3 h and then at room temperature for 1.2 h. After evaporation of the solvent, the residue was extracted with 60 mL of *n*-pentane. The extract was concentrated under a reduced pressure, and then the solution was cooled at −78 °C to give orange crystals of **4** (0.27 g, 0.78 mmol, 38%).

Data for 4. Mp: ca. 3 °C. IR (neat): ν(C≡O) 2081 (vs), 2024 (vs), 2006 (vs) cm^{-1}, ν(C–C–C$_{asyn}$) 1541 (s) cm^{-1}. ^{1}H NMR ($CDCl_3$): δ 4.59 (s, 3H, OMe), 3.94 (q, 1H, $^3J_{HF}$ = 6.5 Hz, CH). ^{13}C NMR ($CDCl_3$): δ 264.7 (d, $^3J_{CH}$ = 5.5 Hz, carbene), 206.7 (s, Fe-CO), 127.1 (q, $^1J_{CF}$ = 270.8 Hz, CF_3), 121.2 (q, $^1J_{CF}$ = 275.8 Hz, CF_3), 68.3 (q, $^1J_{CF}$ = 150.1 Hz, OMe), 51.6 (q, $^2J_{CF}$ = 44.1 Hz, olefin), 39.8 (dq, $^2J_{CF}$ = 38.3 Hz, $^1J_{CH}$ = 150.1 Hz, olefin). MS (*m*/*z*): 346 (M$^+$) (calcd 345.97). Anal. Calcd for $C_9H_4F_6O_4Fe$: C, 31.25; H, 1.17; F, 32.95. Found: C, 31.36; H, 1.16; F, 32.99.

Reaction of 4 with Pyrrolidine. To a solution of **4** (0.14 g, 0.40 mmol) in 1,2-dichloroethane (1.0 mL) was added 35 μL (0.42 mmol) of pyrrolidine, and the solution was stirred at room temperature for 0.5 h. After evaporation of the solvent, the residue was extracted with *n*-pentane. The extract was recrystallized from *n*-pentane at −78 °C to give yellow crystals of [(1-pyrrolidino)(π-vinyl)carbene]iron complex **6** (0.063 g, 0.16 mmol, 41%).

Data for 6. Mp: 47–50 °C. IR (KBr): ν(C≡O) 2062 (vs), 1993 (vs), 1975 (vs) cm^{-1}. ^{1}H NMR ($CDCl_3$): δ 3.97–3.78 (m, 2H, NCH_2), 3.72–3.59 (m, 2H, NCH_2), 3.36 (q, 1H, $^3J_{HF}$ = 7.4 Hz, CH), 2.24–1.98 (m, 4H, β-CH_2CH_2). ^{13}C NMR ($CDCl_3$): δ 222.0 (d, $^3J_{CH}$ = 9.2 Hz, carbene), 209.2 (s, Fe–CO), 128.1 (q, $^1J_{CF}$ = 272.1 Hz, CF_3), 124.0 (q, $^1J_{CF}$ = 273.3 Hz, CF_3), 57.5 (t, $^1J_{CH}$ = 145.3 Hz, NCH_2), 55.1 (t, $^1J_{CH}$ = 144.3 Hz, NCH_2), 49.4 (q, $^2J_{CF}$ = 40.4 Hz, olefin), 37.6 (dq, $^2J_{CF}$ = 36.8 Hz, $^1J_{CH}$ = 156.3 Hz, olefin) 25.9 (t, $^1J_{CH}$ = 135.2 Hz, β-CH_2), 25.1 (t, $^1J_{CH}$ = 132.4 Hz, β-CH_2). Anal. Calcd for $C_{12}H_9F_6NO_3Fe$: C, 37.43; H, 2.36; N, 3.64. Found: C, 37.60; H, 2.28; N, 3.60.

Reaction of 4 with Triphenylphosphine. To a solution of **4** (0.20 g, 0.56 mmol) in 1,2-dichloroethane (0.5 mL) was added 0.15 g (0.57 mmol) of triphenylphosphine, and then the mixture was stirred at room temperature for 2.5 h. After evaporation of the solvent the residue was recrystallized from *n*-pentane–diethyl ether (10:3) to give yellow crystals of η^4-vinylketene complex **8** (0.27 g, 0.44 mmol, 79%).

Data for 8. Mp: 97–101 °C. IR (KBr): ν(C≡O) 2041 (vs), 1985 (vs) cm^{-1}. ^{1}H NMR ($CDCl_3$): δ 7.51–7.33 (m, 15H, PPh_3), 3.48 (q, 1H, CH), 2.97 (s, br, 3H, OMe). ^{13}C NMR ($CDCl_3$): δ 236.8 (d, $^2J_{CP}$ = 13 Hz, C=O), 213.8 (m, Fe–CO), 134.7–126.8 (m, Ph), 123.1 (q, $^1J_{CF}$ = 275.9 Hz, CF_3), 120.0 (q, $^1J_{CF}$ = 272.2 Hz, CF_3), 80.6 (s, *C*–OMe), 67.1 (q, $^2J_{CF}$ = 148.9 Hz, *C*CF_3), 56.8 (q, $^1J_{CH}$ = 147.7 Hz, OMe), 41 (dq, *C*(CF_3)H). Anal. Calcd for $C_{27}H_{19}F_6O_4PFe$: C, 53.32; H, 3.15; F, 18.74. Found: C, 53.13; H, 2.99; F, 18.52.

Reaction of 4 with Carbon Monoxide. A solution of **4** (0.20 g, 0.57 mmol) in 1,2-dichloroethane (1.5 mL) was placed into a 50 mL autoclave, which was charged with 50 atm of carbon monoxide. The mixture was stirred at 50 °C for 8.2 h. After evaporation of the solvent, the residue was recrystallized from *n*-pentane–dichloromethane (4:5) to give yellow crystals of ferracyclopentenone complex **9** (0.14 g, 0.36 mmol, 63%).

Data for 9. Mp: 68–70 °C. IR (KBr): ν(C≡O) 2135 (vs), 2087 (s, sh), 2051 (vs), 2022 (m, sh) cm^{-1}. ^{1}H NMR (CD_2Cl_2): δ 3.86 (s, 3H, OMe), 3.74 (q, 1H, $^3J_{HF}$ = 10.1 Hz, CH). ^{13}C NMR (CD_2Cl_2): δ 239.4 (s, acyl), 202.5–199.0 (m, Fe–CO), 167.3 (s, *C*–OMe), 138.0–136.4 (m, *C*CF_3), 130.2 (dq, $^1J_{CF}$ = 278.0 Hz, $^3J_{CH}$ = 8.3 Hz CF_3), 123.4 (q, $^1J_{CF}$ = 275.1 Hz, CF_3), 60.6 (q, $^1J_{CH}$ = 147.7 Hz, OMe), 30.6 (dq, $^1J_{CF}$ = 137.9 Hz, $^2J_{CF}$ = 31.9 Hz, *C*(CF_3)H). Anal. Calcd for $C_{11}H_4F_6O_6Fe$: C, 32.86; H, 1.00. Found: C, 32.75; H, 1.09.

Reaction of 4 with Ethoxyethyne. To a solution of **4** (0.20 g, 0.56 mmol) in dichloromethane (2.0 mL) was added 0.14 mL of ethoxyethyne (in hexane 50 wt %, 0.73 mmol) at −78 °C. The mixture was stirred at room temperature for 10 h and then chromatographed on silica gel. Elution with benzene gave an orange-yellow solution. After evaporation of the solvent, the residue was recrystallized from *n*-pentane–

dichloromethane (2:1) to give orange crystals of (η^4-cyclopentadiene)iron complex **13** (0.12 g, 0.29 mmol, 50%).

Data for 13. Mp: 62–66 °C. IR (KBr): ν(C≡O) 2054 (vs), 1997 (vs), 1972 (vs) cm^{-1}. ^{1}H NMR ($CDCl_3$): δ 5.23 (s, 1H, CH), 3.93 (q, $^3J_{HF}$ = 8.4 Hz, CF_3C–H), 3.89 (s, OMe), 3.54–3.37 (m, 2H, OCH_2CH_3), 1.23 (t, 3H, $^1J_{CH}$ = 7.0 Hz, OCH_2CH_3). ^{13}C NMR ($CDCl_3$): δ 208.8 (s, Fe–CO), 132.9 (s, C–OMe), 124.6 (q, $^1J_{CF}$ = 271.5 Hz, CF_3), 123.7 (q, $^1J_{CF}$ = 279.4 Hz, CF_3), 93.7 (s, C–OEt), 67.7 (t, $^1J_{CH}$ = 141.6 Hz, OCH_2CH_3), 59.8 (dq, $^1J_{CH}$ = 132.4 Hz, $^2J_{CF}$ = 29.4 Hz, $C(CF_3)H$), 57.4 (q, $^1J_{CH}$ = 146.5 Hz, OMe), 54.5 (d, $^1J_{CH}$ = 180.1 Hz, CH), 43.9 (q, $^2J_{CF}$ = 38.6 Hz, CCF_3), 14.6 (q, $^1J_{CH}$ = 127.5 Hz, OCH_2CH_3). Anal. Calcd for $C_{13}H_{10}F_6O_5Fe$: C, 37.53; H, 2.42; F, 27.40. Found: C, 38.41; H, 2.64; F, 27.11.

X-ray Structure Determinations of 1, 6, and 13. The crystal data and experimental details for **1**, **6**, and **13** are summarized in Table 1. Diffraction data for **1** and **13** were obtained with a Rigaku AFC-7R, and those for **6**, with an Enraf-Nonius CAD4 four-circle automated diffractometer. The reflection intensities were monitored by three standard reflections at every 150 mesurements for **1** and **13** and at every 2 h for **6**, respectively, and the decays of intensities for these crystals were within 2%. Reflection data were corrected for Lorentz and polarization effects. Absorption corrections were empirically applied for **6** and **13**, while azimuthal scans of several reflections indicated no need for an absorption correction for **1**.

The structures were solved by direct methods using MITHRIL90[26] for **1**, SIR88[27] for **6**, and SHELX86[28] for **13**, respectively, and refined anisotropically for non-hydrogen atoms by full-matrix least-squares calculations. All refinements were continued until all shifts were smaller than one-third of the standard deviations of the parameters involved. Atomic scattering factors and anomalous dispersion terms were taken from the literature.[29] All hydrogen atoms for the three complexes were included as isotropic in the structure factor calculations at the final stage of refinement; the positions for **1** and **6** were located on the idealized positions, and those for **13**, on difference Fourier maps. The absolute configuration of the complex **6** with space group $P2_1$ was determined by the anomalous dispersion method. The final R and R_w values were 0.057 and 0.060 for **1**, 0.066 and 0.079 for **6**, and 0.045 and 0.022 for **13**, respectively. The final difference Fourier maps did not show any significant features except the ghost peaks close to Fe atoms. The calculations were performed on an IRIS Indigo computer by using the program system teXsan[30] for **1** and **13** and on a micro VAX-3100 computer by the program system SDP-MolEN[31] for **6**.

The final atomic parameters for non-hydrogen atoms for **1**, **6**, and **13** are given in Tables 2, 4, and 6, respectively, and the selected bond lengths and angles are summarized in Tables 3, 5, and 7, respectively.

Supporting Information Available: Tables of X-ray parameters, positional and thermal parameters, and bond distances and angles (46 pages). Ordering information is given on any current masthead page.

OM950014R

(26) MITHRIL90: Gilmore, C. J. MITHRIL-an integrated direct methods computer program; Univ. of Glasgow, Scotland, 1990.

(27) Cascarano, G.; Giacovazzo, C.; Burla, M. C.; Polidori, G.; Camalli, M.; Spagna, R.; Viterbo, D. *SIR88*; University of Bari: Bari, Italy, 1988.

(28) SHELX86: Sheldrick, G. M. In *Crystallographic Computing 3*; Sheldrick, G. M., Kruger, C., Goddard, R., Eds.; Oxford University Press: Oxford, U.K., 1985; pp 175–189.

(29) (a) Ibers, J. A.; Hamilton, W. C. *International Tables for X-Ray Crystallography*; Kynoch: Birmingham, U.K., 1974; Vol. IV. (b) Cromer, D. T.; Waber, G. T. *International Tables for X-Ray Crystallography*; Kynoch, Birmingham, U.K., 1974; Vol. IV. (c) Ibers, J. A.; Hamilton, W. C. *Acta Crystallogr.* **1964**, *17*, 781. (d) Creagh, D. C.; McAuley, W. J. *International Tables for X-Ray Crystallography*; Wilson, A. J. C., Ed.; Kluwer Academic Publishers: Boston, MA, 1992; Vol. C. (e) Creagh, D. C.; Hubbell, J. H. *International Tables for X-Ray Crystallography*; Wilson, A. J. C., Ed.; Kluwer Academic Publishers: Boston, MA, 1992; Vol. C.

(30) teXsan: Crystal Structure Analysis Package, Molecular Structure Corp., 1985, 1992.

(31) SDP-MolEN: *An Interactive Structure Solution Procedure*; Enraf-Nonius: Delft, The Netherlands, 1990.

(32) Johnson, C. K. *ORTEP Report ORNL-3794*; Oak Ridge National Laboratory: Oak Ridge, TN, 1965.

Stoichiometric Homologation of 1,3-Butadiene by Reaction with the Iridium Methylene Complex $Ir{=}CH_2[N(SiMe_2CH_2PPh_2)_2]$

Michael D. Fryzuk,* Xiaoliang Gao, and Steven J. Rettig†

Department of Chemistry, University of British Columbia, 2036 Main Mall, Vancouver, BC, Canada V6T 1Z1

Received April 12, 1995®

The reaction of the iridium methylene complex $Ir{=}CH_2[N(SiMe_2CH_2PPh_2)_2]$ with 1,3-butadiene leads to the formation of a new complex with the formula $Ir(C_5H_8)[N(SiMe_2CH_2PPh_2)_2]$ in which 1 equiv of butadiene has been incorporated. By a series of NMR experiments, the structure was established as containing a σ-η^3-pentenyl unit. The X-ray crystal structure confirms the stereochemistry of the hydrocarbyl unit as being anti-exo, with the tridentate ancillary ligand adopting the facial orientation. Labeling studies indicate that the formation is diastereoselective as a result of the orientation of the incoming double bond in the early stages of the reaction mechanism.

Introduction

The reaction of metal–alkylidene complexes with 1,3-butadiene in an olefin metathesis type reaction has not been examined in detail[1–3] either because the reaction can be considered as nonproductive after one or two cycles or due to the possibility that a conjugated diene can act as a catalyst poison.[4] However, cyclopropanation of conjugated dienes by a metal-catalyzed diazoalkane addition is an important reaction leading to the formation of vinylcyclopropanes[5–7] that can be further elaborated[8] and are important in their own right in natural product chemistry. As shown below in Scheme 1 for the case of a transition-metal methylene complex reacting with 1,3-butadiene, both the olefin metathesis (path **a**) and the cyclopropanation (path **b**) reactions can be envisioned as proceeding through a common vinyl-substituted metallacyclobutane type intermediate.[9] Such an intermediate has the further option of rearranging via a β-elimination sequence (path **c**) to ultimately result in homologation.

All of these pathways in Scheme 1 have their origin in the reaction of olefins with a methylene unit attached to a metal to generate a metallacyclobutane. For group 8 metals, numerous studies have documented the synthesis and reactivity of metallacyclobutane derivatives.[10,11] However, the intermediate metallacyclobutane formed from 1,3-butadiene has yet another, so far unrecognized pathway for rearrangement; because there is a metal–carbon σ-bond with a proximate β-double bond, one could anticipate a ring expansion to form a six-membered ring (eq 1). In this paper we document a variant of such a transformation for the reaction of an iridium methylene complex with 1,3-butadiene.

Scheme 1

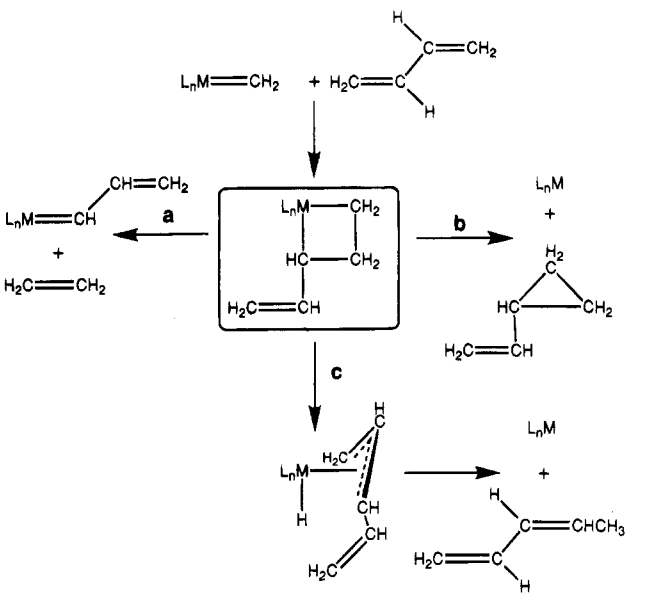

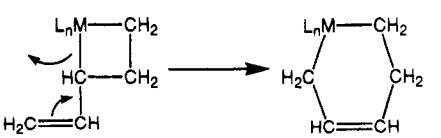

(1)

We have previously shown that the 16-electron iridium(I) methylene complex $Ir{=}CH_2[N(SiMe_2CH_2PPh_2)_2]$ (**1**) is reactive to a variety of small molecules and unsaturated substrates such as allene and certain olefins.[12–14] Undoubtedly, it is the coordinative unsaturation at the metal center in concert with the reactive

† Professional Officer: UBC Crystal Structure Service.

® Abstract published in *Advance ACS Abstracts,* July 15, 1995.

(1) Ivin, K. J. *Olefin Metathesis*; Academic Press: New York, 1983.
(2) Dragutan, V.; Balaban, A. T.; Dimonie, M. *Olefin Metathesis and Ring-Opening Polymerization of Cycloolefins*; Wiley: Bucharest, 1985.
(3) Streck, R. *J. Mol. Catal.* **1992,** *76,* 359.
(4) Zerpner, D.; Holtrup, W.; Streck, R. *J. Mol. Catal.* **1986,** *36,* 153.
(5) Aratani, T. *Pure Appl. Chem.* **1985,** *57,* 1838.
(6) Doyle, M. P. *Chem. Rev.* **1986,** *86,* 919.
(7) Green, J.; Sinn, E.; Woodward, S.; Butcher, R. *Polyhedron* **1993,** *12,* 991.
(8) March, J. *Advanced Organic Chemistry*; Wiley: Toronto, 1985; p 1019.
(9) Wulff, W. D.; Yang, D. C.; Murray, C. K. *Pure Appl. Chem.* **1988,** *60,* 137.
(10) Puddephatt, R. J. *Coord. Chem. Rev.* **1980,** *33,* 149.
(11) Jennings, P. W.; Johnson, L. L. *Chem. Rev.* **1994,** *94,* 2241.
(12) Fryzuk, M. D.; Joshi, K.; Rettig, S. J. *Organometallics* **1991,** *10,* 1642.
(13) Fryzuk, M. D.; Gao, X.; Joshi, K.; MacNeil, P. A.; Massey, R. L. *J. Am. Chem. Soc.* **1993,** *115,* 10581.

0276-7333/95/2314-4236$09.00/0

$Ir{=}CH_2$ fragment that renders this methylene derivative susceptible to further transformations. However, the tridentate ancillary ligand is apparently able to moderate the reactivity somewhat since the starting methylene **1** is remarkably thermally stable; by comparison, two related 18-electron methylene complexes of iridium, $Ir{=}CH_2(CO)I(PPh_3)_2$ and $(\eta^5\text{-}C_5Me_5)Ir{=}CH_2(PMe_3)$, are stable only to −50 and −40 °C, respectively.[15,16] An additional consequence of the presence of the ancillary tridentate ligand of **1** is that the stereochemistry of the resulting products reflects considerable inherent diastereoselectivity. The reaction of **1** with 1,3-butadiene also displays complete diastereoselectivity in the formation of the 1-σ,3-η^3-pentenyl unit attached to iridium.

Results and Discussion

1,3-Butadiene reacts with the methylene complex **1** over a period of 1 h at room temperature to give a single product by both ^1H and $^{31}P\{^1H\}$ NMR spectroscopies. Elemental analyses are consistent with the formula $Ir(C_5H_8)[N(SiMe_2CH_2PPh_2)_2]$, **2**; in other words, only 1 equiv of 1,3-butadiene is incorporated into the methylene complex **1** (eq 2).

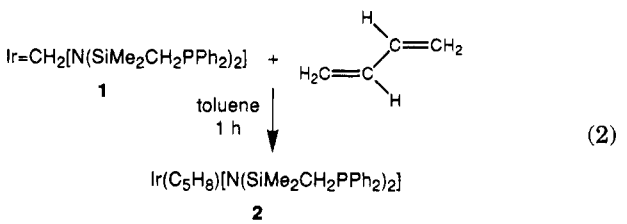

(2)

The $^{31}P\{^1H\}$ NMR spectrum of **2** shows that there are two doublets that are assigned to inequivalent phosphines coupled together with a coupling constant of 7.3 Hz, the latter typical of a cis-disposition of the phosphorus donors of the tridentate ligand. Unlike the reaction of olefins with **1** which generates allyl−hydride complexes, no hydride signal in the ^1H NMR spectrum of complex **2** could be located. Instead, the resonances of all eight inequivalent protons on the C_5H_8 unit were apparent and could be assigned on the basis of decoupling and NOE experiments. The lack of symmetry of the C_5H_8 unit was also mirrored in the ancillary tridentate ligand in that all four silyl methyl groups and all four backbone methylene protons were found to be inequivalent. In the $^{13}C\{^1H\}$ NMR spectrum of **2** there were observed five peaks consistent with the five inequivalent carbons of the C_5H_8 unit of which three resonances were typical of an allyllic unit: a singlet and two doublets at 108.35, 44.16, and 54.90 ppm, respectively, with the latter two resonances coupled to phosphorus (d, $^2J_{CP}$ = 35.1 Hz; d, $^2J_{CP}$ = 23.5 Hz); the remaining two resonances were observed at 28.01 (s) and −37.29 (s ppm).

A structure that is consistent with the spectroscopic parameters is shown below. The connectivity is based on NOE experiments; these NOE spectra are shown in Figure 1. The cis-disposition of the phosphorus donors

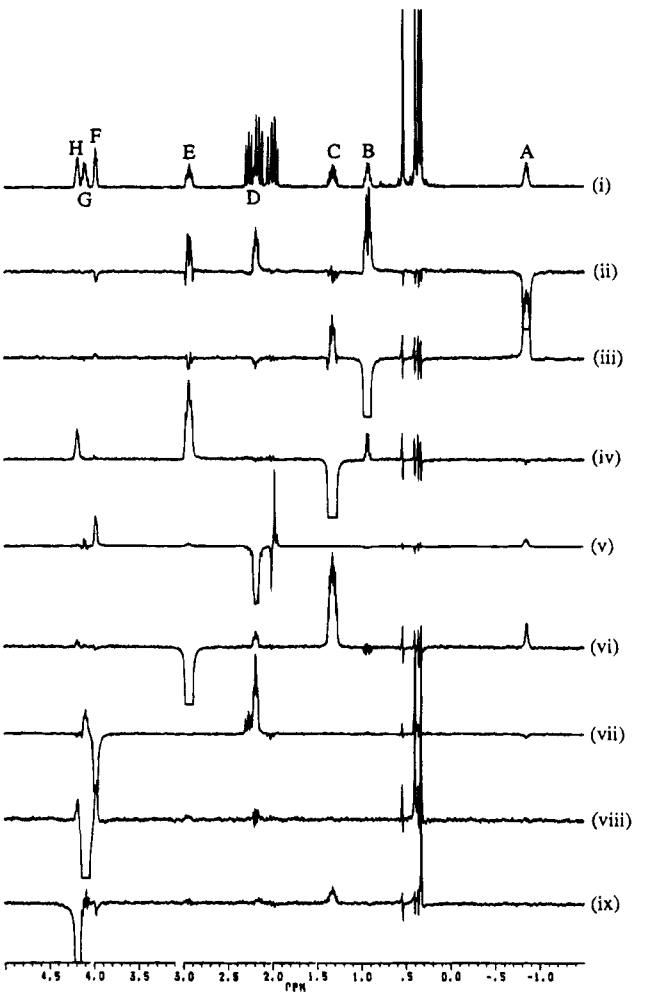

Figure 1. NOE difference spectra for $Ir(\sigma\text{-}\eta^3\text{-}C_5H_8)[N(SiMe_2CH_2PPh_2)_2]$ (**2**): (i) normal 400 MHz ^1H NMR spectrum from −1.5 to 5.0 ppm; (ii) irradiation of peak A; (iii) irradiation of peak B; (iv) irradiation of peak C; (v) irradiation of peak D; (vi) irradiation of peak E; (vii) irradiation of peak F; (viii) irradiation of peak G; and (ix) irradiation of peak H. See also Chart 1.

necessarily puts the tridentate ligand into a facial orientation leaving the remaining three sites of the presumed octahedral Ir center for the C_5H_8 unit. The two upfield multiplets at −0.93 and 0.84 ppm in the ^1H NMR spectrum are probably due to the protons of the carbon directly attached to the iridium via a σ-bond; in other words, these two resonances belong to H_1/H_2 attached to C_a. This was confirmed by repeating the reaction with the deuterium labeled methylene complex $Ir{=}CD_2[N(SiMe_2CH_2PPh_2)_2]$ (d_2-**1**) which gave rise to d_2-**2** but with these two upfield resonances absent in the ^1H NMR spectrum.

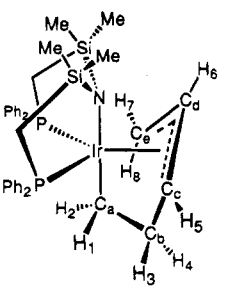

2

(14) Fryzuk, M. D.; Gao, X.; Rettig, S. J. *J. Am. Chem. Soc.* **1995**, *117*, 3106.
(15) Clark, G. R.; Roper, W. R.; Wright, A. H. *J. Organomet. Chem.* **1984**, *273*, C17.
(16) Klein, D. P.; Bergman, R. G. *J. Am. Chem. Soc.* **1989**, *111*, 3079.

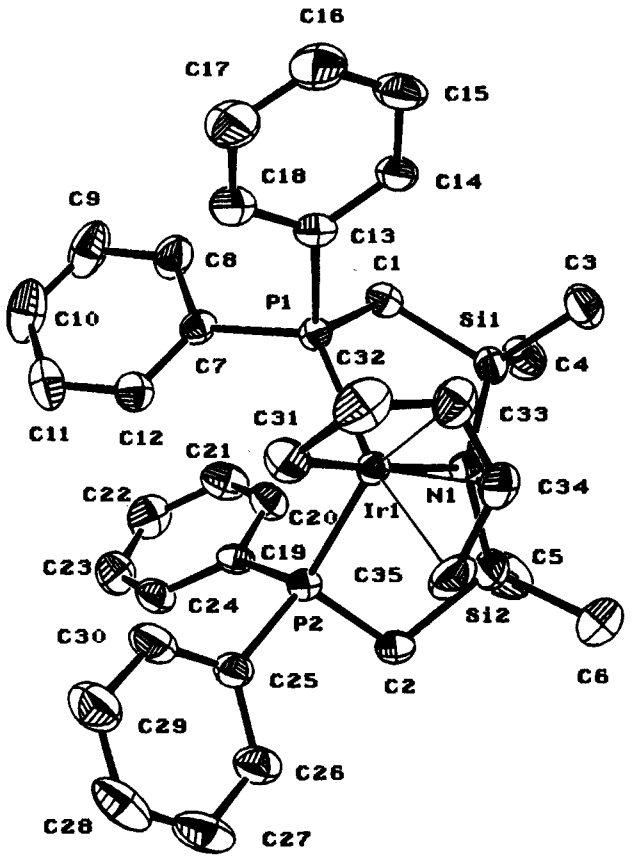

Figure 2. Molecular structure and numbering scheme for Ir(σ-η^3-C_5H_8)[N($SiMe_2CH_2PPh_2$)$_2$] (**2**).

Irradiation of the most upfield resonance, peak A, resulted in enhancement of peaks B (25%), D (11%), and E (7%), while irradiation of peak B produced enhancements at peaks A (23%) and C(8%). This allows a preliminary assignment of H_1 to peak B and H_2 to peak A since the latter would be expected, after irradiation, to transfer magnetization to both H_4 (peak E) and anti proton H_8 (peak D), attached to carbon C_e at the other end of the C_5H_8 moiety. This also suggests that peak C is due to H_3 since it is enhanced by the vicinal H_1. Irradiation of peak C (H_3) results in enhancements in peaks E (H_4, 29%), B (H_1, 5%), and H (7%); the enhancement of peak H at 4.11 ppm allows its assignment to H_5, the syn proton attached to carbon C_c. When peak D (H_8) is irradiated, enhancements at peaks F (16%), A (H_2, 6%), and E (H_4, 2%); assignment of peak F to the syn proton H_7 attached to the same carbon as H_8 is consistent with this particular experiment. At this point, the only peak not assigned is peak G at 4.02 ppm, which, by default, must be due to H_6, the central proton of the allyllic unit. Confirmation of this was complicated by the proximity of the resonances due to the syn protons H_5 and H_7 (peaks H and F, respectively), however, one can observe that irradiation of peak F (H_7) does result in enhancement of peak G, the central proton resonance. In addition, irradiation of peak G does show enhancements to both peaks F and H, as expected. More importantly however, irradiation of peak G (H_6) produced enhancements in two of the four silyl methyl resonances. This latter result allows the stereochemistry of the η^3-allyl unit to be assigned as exo since the central carbon of this moiety points toward the disilylamido portion of the tridentate ancillary ligand. In fact, in keeping with nomenclature previously established for

Scheme 2

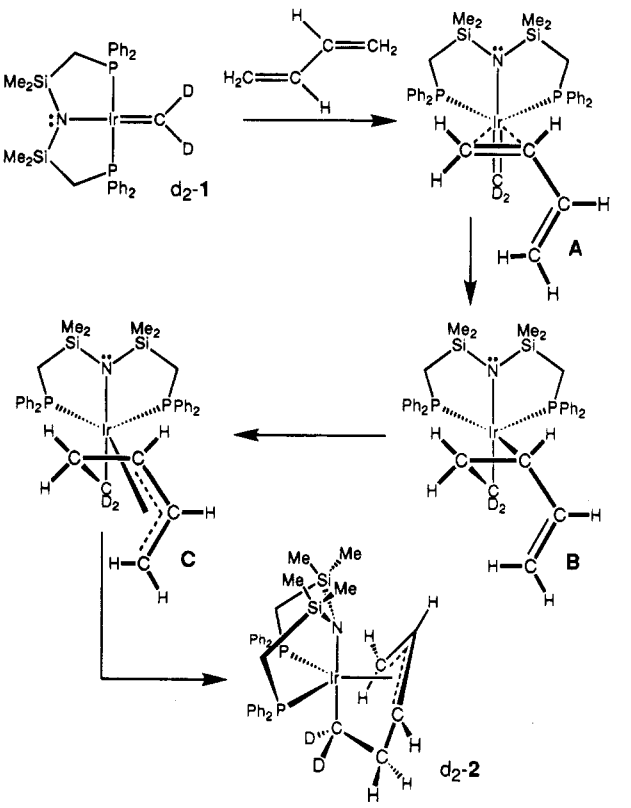

the reaction of the methylene complex **1** with olefins,[14] the stereochemistry of the C_5H_8 unit is described as anti-exo. Interestingly, irradiation of both syn protons H_5 and H_7 in turn produces enhancements of the appropriate proximate silyl methyl resonances, as expected on the basis of the proposed structure.

Crystal Structure Analysis of Ir(σ-η^3-C_5H_8)[N($SiMe_2CH_2PPh_2$)$_2$]. The stereochemistry determined by NMR spectroscopy was confirmed by single-crystal X-ray diffraction. The molecular structure and numbering scheme are shown in Figure 2; selected bond lengths and bond angles appear in Table 3. The facial orientation of the tridentate ligand is evident and is characterized by a P1–Ir–P2 bond angle of 107.74(8)°, with P1–Ir–N and P2–Ir–N being 87.1(1) and 83.3(2)°, respectively. The C_5H_8 unit is bound to the iridium in an anti-exo configuration; there is a direct iridium–carbon bond to C31 which is trans to the amide donor with N–Ir–C31 being 174.4(3)° and an Ir–C31 bond length of 2.108(8) Å. This carbon is attached to C32, which is the anti substituent to the allyl unit; this carbon lies 20° out of the plane defined by the three carbons of the allyl moiety, C33, C34, and C35. The angle subtended by these carbons, C33–C34–C35, is 122.8(9)°, close to the expected 120° for an allyl unit. The bond lengths within the allyl unit are typical of such systems: C33–C34, 1.36(1) Å; C34–C35, 1.40(1) Å. The distances between the allyl carbons and the iridium are as follows: Ir–C33, 2.241(8) Å; Ir–C34, 2.166(8) Å; and Ir–C35, 2.224(8) Å; these distances are essentially identical to those found for the related allyl–hydride complexes.[14]

Mechanism of Formation. As mentioned in the introduction, the reaction of certain electron deficient olefins with the methylene complex **1** results in the diastereoselective formation of allyl hydride derivatives.[14] As described here, 1,3-butadiene reacts with **1**

Chart 1

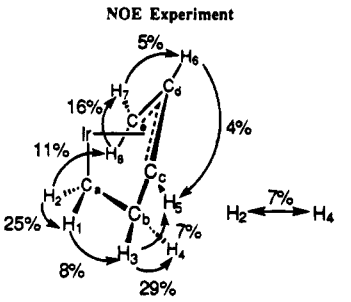

^{1}H NMR[a]	δ	^{1}H{^{31}P}[b]	coupling constants
P(C_6H_5)$_2$	6.6–7.8 (m)		
H_1	0.84 (m)	m	
H_2	−0.93 (m)	m	
H_3	1.26 (m)	m	
H_4	2.85 (m)	m	
H_5	4.11 (t)	m	
H_6	4.02 (m)	m	
H_7	3.90 (m)	d	$^3J_{HH}$ = 7.8 Hz
H_8	2.11 (m)	d	$^3J_{HH}$ = 10.2 Hz
$SiCH_2P$	2.20 (dd)	d	$^3J_{HH}$ = 13.3 Hz, $^3J_{PH}$ = 11.3 Hz
$SiCH_2P$	2.08 (t)	d	$^3J_{HH}$ = 14.2 Hz, $^3J_{PH}$ = 14.2 Hz
$SiCH_2P$	1.95 (t)	d	$^3J_{HH}$ = 13.5 Hz, $^3J_{PH}$ = 13.5 Hz
$SiCH_2P$	1.91 (t)	d	$^3J_{HH}$ = 14.4 Hz, $^3J_{PH}$ = 14.4 Hz
SiMe	0.44 (s)	s	
SiMe	0.32 (s)	s	
SiMe	0.27 (s)	s	
SiMe	0.25 (s)	s	

[a] C_6D_6, 400 MHz. [b] Simplification of the multiplet pattern upon broad-band decoupling.

to produce exclusively the anti-exo isomer of **2**. On the basis of the mechanism previously suggested for the olefin reactions, a similar mechanism can be envisioned as shown in Scheme 2; to take into account the labeling experiment, the dideuteriated methylene complex d_2-**1** is used in the scheme.

The first step involves coordination of the 1,3-butadiene to the methylene complex **1** via η^2 interaction to form intermediate **A** in which the coordinated end of the diene lies perpendicular to the Ir=C π-system. In agreement with semiempirical MO calculations,[14] such an approach allows overlap of the HOMO of a bent metal fragment with the appropriate π^* orbital of the coordinated double bond. Subsequent carbon–carbon bond formation occurs to generate **B**, which has a highly puckered iridacyclobutane unit and a vinyl substituent on an α-carbon. This presumably can undergo ring expansion by using the exocyclic double bond to form **C**; counterclockwise rotation of the allyllic unit in **C** will generate the observed product **2**. The carbon–carbon bond formation to generate **B** can be considered to go via another possible intermediate shown below as **D**; however, this puts the exocyclic vinyl group at the central carbon of the puckered iridacyclobutane and thus cannot ring expand.

Conclusions

The results of this study show that the iridium methylene compound Ir=CH_2[$N(SiMe_2CH_2PPh_2)_2$] can react with 1,3-butadiene to undergo a stoichiometric carbon–carbon bond formation. This reaction probably involves an initial formation of a vinyl-substituted iridacyclobutane unit which undergoes a diastereoselective expansion to generate a 1-σ,3-η^3-pentenyl unit bound to the Ir[$N(SiMe_2CH_2PPh_2)_2$] fragment in an anti-exo configuration. In a formal sense, this represents a one-carbon homologation of 1,3-butadiene, albeit bound to a metal complex. The stability of this hydrocarbyl unit attached to iridium is remarkable and might explain why certain alkylidene-containing catalysts are poisoned by the presence of conjugated dienes.[4]

Table 1. Crystallographic Data[a]

compd	Ir(C_5H_8)[$N(SiMe_2CH_2PPh_2)_2$]
formula	$C_{35}H_{44}IrNP_2Si_2$
fw	789.08
color, habit	colorless, plate
cryst syst	monoclinic
space group	$P2_1/c$
a, Å	10.710(3)
b, Å	18.261(4)
c, Å	17.976(4)
β°	96.81(2)
V, Å^3	3491(2)
Z	4
ϱ_{calc}, g/cm^3	1.501
F(000)	1584
μ, cm^{-1}	39.92
crystal size, mm^3	0.05 × 0.20 × 0.35
transmissn factors	0.68–1.00
scan type	ω–2θ
scan range, deg in ω	1.10 + 0.35 tan θ
scan speed, deg/min	16 (up to 8 rescans)
data collected	$+h,+k,\pm l$
$2\theta_{max}$, deg	60
crystal decay, %	negligible
tot. no. of reflns	10 777
tot. no. of unique reflns	10 479
R_{merge}	0.070
no. of reflns with $I \geq 3\sigma(I)$	3684
no. of variables	371
R	0.035
R_w	0.027
gof	1.28
max Δ/σ (final cycle)	0.01
residual density, e/Å^3	−0.71 to 0.57 (near Ir)

[a] Temperature, 294 K; Rigaku AFC6S diffractometer; Mo Kα radiation (λ = 0.710 69 Å); graphite monochromator; takeoff angle, 6.0°; aperature, 6.0 × 6.0 mm^2 at a distance of 285 mm from the crystal; stationary background counts at each end of the scan (scan/background time ratio 2:1, up to 8 rescans); $\sigma^2(F^2) = [S^2(C + 4B)]/Lp^2$ (S = scan rate, C = scan count, B = normalized background count); function minimized, $\sum w(|F_o| - |F_c|)^2$ where $w = 4F_o^2/\sigma^2(F_o^2)$, $R = \sum||F_o| - |F_c||/\sum|F_o|$, $R_w = (\sum w(|F_o| - |F_c|)^2/\sum w|F_o|^2)^{1/2}$, and gof = $[\sum w(|F_o| - |F_c|)^2/(m - n)]^{1/2}$. Values given for R, R_w, and gof are based on those reflections with $I \geq 3\sigma(I)$.

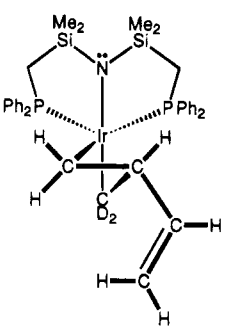

Experimental Section

General Procedures. All experimental procedures were identical to that previously described.[17] The preparation of Ir=CH_2[$N(SiMe_2CH_2PPh_2)_2$] follows that of the improved procedure described in the literature.[13]

Preparation of Ir(σ-η^3-C_5H_8)[$N(SiMe_2CH_2PPh_2)_2$]. To a toluene solution (15 mL) of the methylene complex **1** (90 mg,

(17) Fryzuk, M. D.; Huang, L.; McManus, N. T.; Paglia, P.; Rettig, S. J.; White, G. S. *Organometallics* **1992**, *11*, 2979.

Table 2. Final Atomic Coordinates (Fractional) and B_{eq} (Å^2)[a]

atom	x	y	z	B_{eq}
Ir(1)	0.36934(3)	0.27027(2)	0.50062(2)	2.91(1)
P(1)	0.2840(2)	0.30809(11)	0.38449(11)	3.0(1)
P(2)	0.3798(2)	0.14533(10)	0.49894(13)	3.34(9)
Si(1)	0.5668(2)	0.32357(12)	0.38467(13)	3.7(1)
Si(2)	0.6496(2)	0.19556(13)	0.4924(2)	4.8(1)
N(1)	0.5541(5)	0.2622(3)	0.4534(3)	3.2(3)
C(1)	0.4083(7)	0.3235(4)	0.3252(4)	3.5(4)
C(2)	0.5432(7)	0.1223(4)	0.5269(4)	4.3(4)
C(3)	0.6046(8)	0.4188(4)	0.4206(5)	5.2(5)
C(4)	0.6848(8)	0.3031(5)	0.3180(5)	5.8(5)
C(5)	0.7521(10)	0.1505(5)	0.4294(6)	8.5(7)
C(6)	0.7622(9)	0.2264(6)	0.5763(6)	8.6(6)
C(7)	0.1637(7)	0.2534(4)	0.3282(4)	3.3(4)
C(8)	0.1305(8)	0.2690(5)	0.2536(5)	5.4(4)
C(9)	0.0348(9)	0.2315(6)	0.2118(5)	6.8(5)
C(10)	−0.0276(9)	0.1774(6)	0.2450(6)	6.7(6)
C(11)	0.0058(8)	0.1592(5)	0.3188(6)	5.4(5)
C(12)	0.1011(8)	0.1983(4)	0.3609(4)	4.1(4)
C(13)	0.1998(8)	0.3961(4)	0.3846(4)	3.7(4)
C(14)	0.2627(8)	0.4628(4)	0.3849(4)	4.1(4)
C(15)	0.1989(10)	0.5289(4)	0.3891(5)	5.7(5)
C(16)	0.0731(10)	0.5286(5)	0.3943(6)	6.4(6)
C(17)	0.0077(9)	0.4641(6)	0.3940(6)	6.4(6)
C(18)	0.0705(9)	0.3974(5)	0.3883(5)	5.2(5)
C(19)	0.3438(7)	0.0935(4)	0.4119(4)	3.3(4)
C(20)	0.3994(8)	0.1161(4)	0.3499(5)	4.5(4)
C(21)	0.3759(9)	0.0810(5)	0.2822(5)	5.4(5)
C(22)	0.2988(10)	0.0204(5)	0.2751(5)	5.8(5)
C(23)	0.2459(9)	−0.0031(4)	0.3365(6)	5.4(5)
C(24)	0.2664(8)	0.0323(4)	0.4039(5)	4.2(4)
C(25)	0.2896(9)	0.0971(4)	0.5644(4)	3.9(4)
C(26)	0.3460(9)	0.0559(4)	0.6239(5)	5.0(5)
C(27)	0.2752(13)	0.0252(5)	0.6752(5)	6.9(6)
C(28)	0.1484(12)	0.0344(5)	0.6679(6)	6.8(6)
C(29)	0.0895(9)	0.0740(5)	0.6093(6)	6.7(6)
C(30)	0.1616(9)	0.1044(5)	0.5590(5)	5.8(5)
C(31)	0.2003(8)	0.2887(4)	0.5470(5)	4.7(4)
C(32)	0.2276(10)	0.3663(5)	0.5732(5)	6.3(6)
C(33)	0.3618(9)	0.3793(5)	0.5571(5)	5.0(5)
C(34)	0.4589(9)	0.3386(5)	0.5900(4)	4.7(5)
C(35)	0.4424(8)	0.2700(5)	0.6217(4)	5.8(4)

[a] $B_{eq} = (8/3)\pi^2\sum\sum U_{ij}a_ia_j(\mathbf{a}_i\cdot\mathbf{a}_j)$.

0.1124 mmol) was charged 1,3-butadiene (15 mL, 1 atm). The purple color gradually faded, and after 1 h a light yellow solution formed. The solution was stirred for 1 more h and was pumped to dryness. Recrystallization of the residue in hexanes gave colorless crystals. Slow evaporation of the mother liquor to almost dryness gave a second crop of crystals. The two crops of crystals were washed with cold hexanes (−30 °C, 2 × 2 mL) and were dried under vacuum. The yield of this compound was 76 mg, 86%. Anal. Calcd for $C_{35}H_{44}IrNP_2Si_2$: C, 53.28; H, 5.62; N, 1.77. Found: C, 53.64; H, 5.70; N, 1.85. $^{31}P\{^1H\}$ NMR (500 MHz, C_6D_6, δ): −5.54 (d, $^2J_{PP}$ = 7.3 Hz), −8.42 (d, $^2J_{PP}$ = 7.3 Hz). $^{13}C\{^1H\}$ NMR (C_6D_6, 400 MHz, δ): 5.32 (s, SiMe); 5.36 (s, SiMe); 5.92 (s, SiMe), 9.04 (s, SiMe); 24.26 (d, $^1J_{PC}$ = 16.4 Hz, $SiCH_2P$); 30.10 (d, $^1J_{PC}$ = 22.3 Hz, $SiCH_2P$); σ-η^3-C_5H_8 ligand, 44.16 (d, $^2J_{CP}$ = 35.1 Hz, C_e); 108.35 (s, C_d); 54.90 (d, $^2J_{CP}$ = 23.5 Hz, C_c); 28.01 (s, C_b); −37.29 (s, C_a); PPh_2, 127−133 (overlapping). See also Chart 1.

X-ray Crystallographic Analysis of Ir(C_5H_8)[N($SiMe_2CH_2PPh_2$)$_2$]. Crystallographic data appear in Table 1. The final unit-cell parameters were obtained by least-squares refinement on the setting angles for 25 reflections with 2θ = 8.7−15.5°. The intensities of three standard reflections, measured every 200 reflections throughout the data collection, showed only small random fluctuations. The data were processed[18] and corrected for Lorentz and polarization effects and absorption (empirical, based on azimuthal scans for three reflections).

(18) *TEXSAN/TEXRAY Structure Analysis Package*, Version 5.1; Molecular Structure Corporation: The Woodlands, TX, 1985.

Table 3. Bond Lengths (Å) and Bond Angles (deg) with Estimated Standard Deviations

Bond Lengths			
Ir(1)−P(1)	2.284(2)	C(10)−C(11)	1.37(1)
Ir(1)−P(2)	2.285(2)	C(11)−C(12)	1.39(1)
Ir(1)−N(1)	2.249(5)	C(13)−C(14)	1.392(9)
Ir(1)−C(31)	2.108(8)	C(13)−C(18)	1.40(1)
Ir(1)−C(33)	2.241(8)	C(14)−C(15)	1.39(1)
Ir(1)−C(34)	2.166(8)	C(15)−C(16)	1.36(1)
Ir(1)−C(35)	2.224(8)	C(16)−C(17)	1.37(1)
P(1)−C(1)	1.823(7)	C(17)−C(18)	1.40(1)
P(1)−C(7)	1.836(7)	C(19)−C(20)	1.39(1)
P(1)−C(13)	1.843(7)	C(19)−C(24)	1.39(1)
P(2)−C(2)	1.812(8)	C(20)−C(21)	1.37(1)
P(2)−C(19)	1.831(8)	C(21)−C(22)	1.38(1)
P(2)−C(25)	1.834(8)	C(22)−C(23)	1.37(1)
Si(1)−N(1)	1.686(6)	C(23)−C(24)	1.37(1)
Si(1)−C(1)	1.895(8)	C(25)−C(26)	1.39(1)
Si(1)−C(3)	1.885(8)	C(25)−C(30)	1.37(1)
Si(1)−C(4)	1.880(8)	C(26)−C(27)	1.38(1)
Si(2)−N(1)	1.688(6)	C(27)−C(28)	1.36(1)
Si(2)−C(2)	1.908(8)	C(28)−C(29)	1.37(1)
Si(2)−C(5)	1.860(9)	C(29)−C(30)	1.37(1)
Si(2)−C(6)	1.90(1)	C(31)−C(32)	1.51(1)
C(7)−C(8)	1.376(9)	C(32)−C(33)	1.52(1)
C(7)−C(12)	1.379(9)	C(33)−C(34)	1.36(1)
C(8)−C(9)	1.38(1)	C(34)−C(35)	1.40(1)
C(9)−C(10)	1.37(1)		
Bond Angles			
P(1)−Ir(1)−P(2)	107.74(8)	Ir(1)−N(1)−Si(2)	114.0(3)
P(1)−Ir(1)−N(1)	87.1(1)	Si(1)−N(1)−Si(2)	133.4(3)
P(1)−Ir(1)−C(31)	92.5(2)	P(1)−C(1)−Si(1)	109.8(4)
P(1)−Ir(1)−C(33)	96.5(2)	P(2)−C(2)−Si(2)	110.0(4)
P(1)−Ir(1)−C(34)	126.7(3)	P(1)−C(7)−C(8)	120.5(6)
P(1)−Ir(1)−C(35)	162.0(2)	P(1)−C(7)−C(12)	120.5(6)
P(2)−Ir(1)−N(1)	83.3(2)	C(8)−C(7)−C(12)	119.0(7)
P(2)−Ir(1)−C(31)	102.1(2)	C(7)−C(8)−C(9)	121.2(8)
P(2)−Ir(1)−C(33)	153.9(2)	C(8)−C(9)−C(10)	119.4(9)
P(2)−Ir(1)−C(34)	124.5(3)	C(9)−C(10)−C(11)	120.7(9)
P(2)−Ir(1)−C(35)	89.9(2)	C(10)−C(11)−C(12)	119.4(9)
N(1)−Ir(1)−C(31)	174.4(3)	C(7)−C(12)−C(11)	120.3(8)
N(1)−Ir(1)−C(33)	108.0(3)	P(1)−C(13)−C(14)	121.8(7)
N(1)−Ir(1)−C(34)	89.2(3)	P(1)−C(13)−C(18)	120.2(6)
N(1)−Ir(1)−C(35)	98.4(3)	C(14)−C(13)−C(18)	117.9(7)
C(31)−Ir(1)−C(33)	66.5(3)	C(13)−C(14)−C(15)	121.2(8)
C(31)−Ir(1)−C(34)	86.6(3)	C(14)−C(15)−C(16)	119.8(9)
C(31)−Ir(1)−C(35)	80.3(3)	C(15)−C(16)−C(17)	120.9(9)
C(33)−Ir(1)−C(34)	35.8(3)	C(16)−C(17)−C(18)	119.9(9)
C(33)−Ir(1)−C(35)	65.5(3)	C(13)−C(18)−C(17)	120.3(8)
C(34)−Ir(1)−C(35)	37.1(3)	P(2)−C(19)−C(20)	117.8(6)
Ir(1)−P(1)−C(1)	109.9(3)	P(2)−C(19)−C(24)	124.6(6)
Ir(1)−P(1)−C(7)	121.2(2)	C(20)−C(19)−C(24)	117.7(7)
Ir(1)−P(1)−C(13)	113.9(2)	C(19)−C(20)−C(21)	121.6(8)
C(1)−P(1)−C(7)	106.0(3)	C(20)−C(21)−C(22)	120.0(8)
C(1)−P(1)−C(13)	104.9(3)	C(21)−C(22)−C(23)	118.6(8)
C(7)−P(1)−C(13)	99.4(3)	C(22)−C(23)−C(24)	121.9(8)
Ir(1)−P(2)−C(2)	108.0(2)	C(19)−C(24)−C(23)	120.2(8)
Ir(1)−P(2)−C(19)	121.5(2)	P(2)−C(25)−C(26)	122.8(7)
Ir(1)−P(2)−C(25)	116.1(3)	P(2)−C(25)−C(30)	120.4(7)
C(2)−P(2)−C(19)	102.5(3)	C(26)−C(25)−C(30)	116.6(8)
C(2)−P(2)−C(25)	106.0(4)	C(25)−C(26)−C(27)	120.9(9)
C(19)−P(2)−C(25)	103.1(3)	C(26)−C(27)−C(28)	120(1)
N(1)−Si(1)−C(1)	105.6(3)	C(27)−C(28)−C(29)	120.2(9)
N(1)−Si(1)−C(3)	113.3(3)	C(28)−C(29)−C(30)	119(1)
N(1)−Si(1)−C(4)	117.0(3)	C(25)−C(30)−C(29)	123.3(9)
C(1)−Si(1)−C(3)	109.9(3)	Ir(1)−C(31)−C(32)	97.4(5)
C(1)−Si(1)−C(4)	105.4(4)	C(31)−C(32)−C(33)	103.9(7)
C(3)−Si(1)−C(4)	105.3(4)	Ir(1)−C(33)−C(32)	91.9(5)
N(1)−Si(2)−C(2)	106.6(3)	Ir(1)−C(33)−C(34)	69.1(5)
N(1)−Si(2)−C(5)	116.0(4)	C(32)−C(33)−C(34)	121.7(9)
N(1)−Si(2)−C(6)	114.3(4)	Ir(1)−C(34)−C(33)	75.1(5)
C(2)−Si(2)−C(5)	107.8(4)	Ir(1)−C(34)−C(35)	73.7(5)
C(2)−Si(2)−C(6)	107.3(4)	C(33)−C(34)−C(35)	122.8(9)
C(5)−Si(2)−C(6)	104.5(5)	Ir(1)−C(35)−C(34)	69.2(4)
Ir(1)−N(1)−Si(1)	112.6(3)		

The structure was solved by heavy atom methods, the coordinates of the Ir, P, and Si atoms being determined from the Patterson function and those of the remaining non-

hydrogen atoms from subsequent difference Fourier syntheses. All non-hydrogen atoms were refined with anisotropic thermal parameters. Hydrogen atoms were fixed in idealized positions (C–H = 0.98 Å, $B_H = 1.2B_{\text{bonded atom}}$). A secondary extinction correction (Zachariasen isotropic type I) was applied, the final value of the extinction coefficient being 1.37 (6) × 10^{-7}. Neutral atom scattering factors for all atoms and anomalous dispersion corrections for the non-hydrogen atoms were taken from the *International Tables for X-Ray Crystallography*.[19] Final atomic coordinates and equivalent isotropic thermal parameters are given in Table 2, and selected bond lengths and angles appear in Table 3. Hydrogen atom parameters, anisotropic thermal parameters, complete tables of bond lengths and bond angles, torsion angles, intermolecular contacts, and least-squares planes are included as supporting information.

(19) *International Tables for X-Ray Crystallography*; Kynoch Press: Birmingham, England, 1974; Vol. IV, pp 99–102, 149–150.

Acknowledgment. Financial support was provided by NSERC of Canada. We thank Johnson-Matthey for the generous loan of iridium salts.

Supporting Information Available: Tables of hydrogen atom parameters, anisotropic thermal parameters, all bond lengths and bond angles, torsion angles, intermolecular contacts, and least-squares planes (15 pages). Ordering information is given on any current masthead page.

OM950266S

Stereochemistry and Mechanism of Chloropalladation of Acetylenes

Jan-E. Bäckvall,* Ylva I. M. Nilsson, and Roberto G. P. Gatti

Department of Organic Chemistry, University of Uppsala, Box 531, S-751 21 Uppsala, Sweden

Received April 11, 1995[⊗]

The stereochemistry of chloropalladation of acetylenes has been studied. Chloropalladation adducts from terminal acetylenes were trapped *in situ* by reaction with either allyl chloride or 1,3-cyclohexadiene. It was found that the stereochemistry of the chloropalladation reaction was dependent on the chloride ion concentration. At a low chloride concentration cis chloropalladation predominates, whereas at a high chloride concentration there is a preference for trans chloropalladation.

Vinylpalladium complexes are versatile reactive intermediates in a number of catalytic reactions.[1-3] In these reactions, such as vinyl couplings,[1] carbonylations,[2] and Heck reactions,[3] the vinylpalladium species is generated by oxidative addition of a vinyl halide or triflate to palladium(0). Another way of generating a vinylpalladium complex is by the addition of a nucleophile (coordinated or free) to an (acetylene)palladium(II) complex. Although the latter approach has had limited applications in catalytic reactions,[4] recently the use of hydropalladation[5] and chloropalladation[6,7] of an acetylene has been used to generate vinylpalladium in palladium(II)-catalyzed reactions. In one of the latter reactions, developed in our laboratory,[7] dienyne **1** afforded product **2** in a palladium(II)-catalyzed oxidation reaction (eq 1). The reaction was suggested to proceed

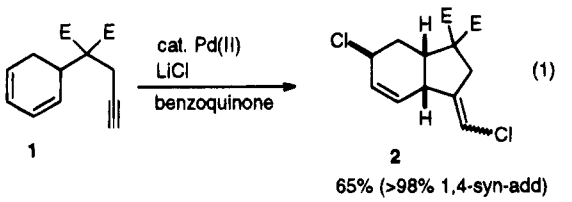

1 2

65% (>98% 1,4-syn-add)

via a chloropalladation of the acetylene followed by insertion of one of the double bonds of the conjugated diene in the vinyl–palladium bond (Scheme 1). The π-allyl complex formed is subsequently attacked by a chloride anion to give product **2**. In the reaction given in eq 1 the product is a mixture of double bond isomers indicating that the chloropalladation is nonstereospecific. Since chloropalladation of olefins,[8] dienes,[9] and vinylcyclopropanes[10] is known to take place by external

Scheme 1

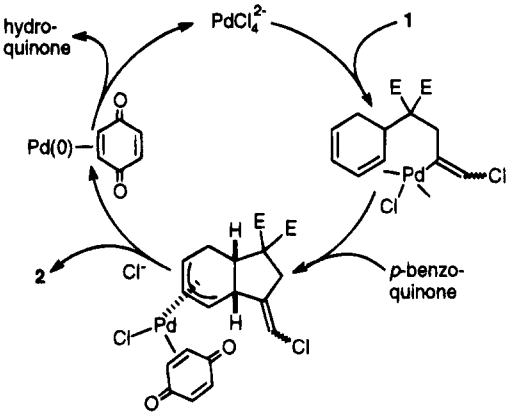

chloride attack, i.e., trans chlorpalladation, we were intrigued by the observation that acetylenes seem to undergo both cis and trans chloropalladation.[6,7,11,12] We therefore decided to study the stereochemistry and mechanism of chloropalladation of acetylenes.

Results and Discussion

Chloropalladation of Alkynes. In the work by Kaneda[4a] only cis chloropalladation was observed with substituted acetylenes. This is in contrast to the work by us[7] and others,[6] where the results indicate competing trans and cis chloropalladation with substituted acetylenes. In fact, in some cases trans chloropalladation predominated over the cis chloropalladation.

In the present study the chloropalladation of a few substituted acetylenes have been studied under different reaction conditions. Two different methods to trap the vinylpalladium species from chloropalladation was used. The first method, which has previously been used

[⊗] Abstract published in *Advance ACS Abstracts,* July 15, 1995.

(1) (a) Negishi, E. *Acc. Chem. Res.* **1982**, *15*, 340. (b) Stille, J. K. *Angew. Chem., Int. Ed. Engl.* **1986**, *25*, 508. (c) Miyaura, N.; Maeda, K.; Suginome, H.; Suzuki, A. *J. Org. Chem.* **1982**, *47*, 2117.

(2) Schoenberg, A.; Heck, R. F. *J. Org. Chem.* **1974**, *39*, 3327.

(3) (a) Cabri, W.; Candiani, I. *Acc. Chem. Res.* **1995**, *28*, 2. (b) Heck, R. F. *Org. React.* **1982**, *27*, 345.

(4) (a) Kaneda, K.; Uchiyama, T.; Fujiwara, Y.; Imanaka, T.; Teranishi, S. *J. Org. Chem.* **1979**, *44*, 55. (b) Lambert, C.; Utimoto K.; Nozaki, H. *Tetrahedron Lett.* **1984**, *25*, 5323. (c) Kosugi, M.; Sakaya, T.; Ogawa, S.; Migita, T. *Bull. Chem. Soc. Jpn.* **1993**, *66*, 3058. (d) Larock, R. C.; Riefling, B. *Tetrahedron Lett.* **1976**, 4661.

(5) Trost, B. M. *Acc. Chem. Res.* **1990**, *23*, 34.

(6) (a) Ma, S; Lu, X. *J. Org. Chem.* **1991**, *56*, 5120. (b) Ma, S.; Lu, X. *J. Org. Chem.* **1993**, *58*, 1245.

(7) Bäckvall, J. E.; Nilsson, Y. I. M; Andersson, P. G.; Gatti, R. G. P.; Wu, J. *Tetrahedron Lett.* **1994**, *35*, 5713.

(8) (a) Wipke, W. T.; Goeke, G. L. *J. Am. Chem. Soc.* **1974**, *96*, 4244. (b) Wiger, G.; Albelo, G.; Rettig, M. F. *J. Chem. Soc., Dalton Trans.* **1974**, 2242.

(9) Bäckvall, J. E. Unpublished results.

(10) (a) Bäckvall, J. E.; Björkman, E. E. *J. Chem. Soc., Chem. Commun.* **1982**, 693 (b) Bäckvall, J. E.; Wilhelm, D.; Nordberg, R. E.; Norin, T. *Organometallics* **1985**, *4*, 1296.

(11) (a) Mann, B. E.; Bailey, P. M.; Maitlis, P. M. *J. Am. Chem. Soc.* **1975**, *97*, 1275. (b) Yukawa, T. T.; Tsutsumi, S. *Inorg. Chem.* **1968**, *7*, 1458.

(12) Maitlis, P. M.; Espinet, P.; Rusell, M. J. H. In *Comprehensive Organometallic Chemistry*; Wilkinson, G., Stone, F. G. A., Abel, E. W., Eds.; Pergamon Press: London, 1982; Vol. 6, p 455.

0276-7333/95/2314-4242$09.00/0

Scheme 2

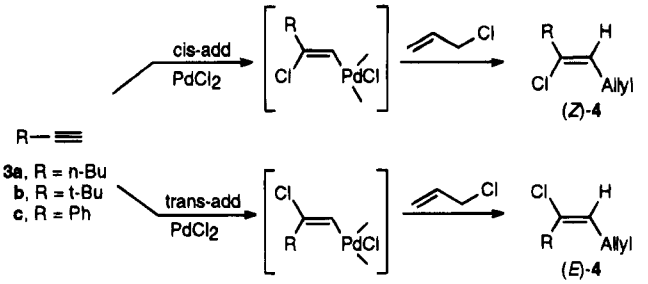

Table 1. Chloropalladation of 1-Hexyne: Trapping with 1-Chloro-2-propene[a]

entry	$[Cl^-]_{tot.}$[b] (M)	[1-hexyne] (M)	*Z*-4a:*E*-4a[c] (cis-add:trans add)[d]
1	0.08	0.03	98:2
2	0.2	0.2	93:7
3	0.53	0.2	80:20
4	1.0	0.2	64:36
5	1.0	0.03	58:42
6	2.0	0.2	49:51
7	2.0	0.03	31:69

[a] The reactions were performed in acetone–acetic acid (4:1) with $PdCl_2$ and added LiCl in the presence of excess 1-chloro-2-propene. The ratio of $[PdCl_2]$:[1-hexyne]:[1-chloro-2-propene] was 0.3:1:10. [b] The $[Cl^-]_{tot.}$ refers to the total amount of Cl^- including that on $PdCl_2$. [c] The yield of **4a** (based on 1-hexyne) was in the range of 70–80%. The stereochemistry was determined by ^1H NMR. [d] Refers to the chloropalladation across the triple bond.

in several instances,[4ac,13] involves trapping by allyl chloride (eq 2). The second method utilizes 1,3-cyclo-

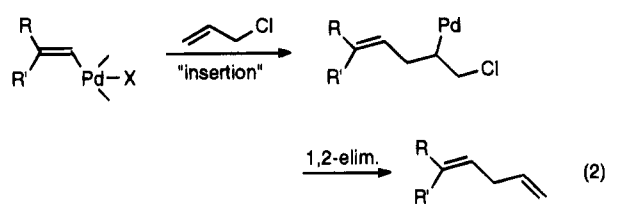

hexadiene as the trapping molecule. The latter method was employed because of the uncertainty that the first method, i.e. palladium-catalyzed reaction between an acetylene and allyl halide, may involve an alternative pathway via a (π-allyl)palladium intermediate.[14]

A. Trapping with Allyl Chloride. The acetylene (**3**) was allowed to react with palladium chloride at low temperature in acetone–acetic acid (4:1) in the presence of allyl chloride which led to the formation of (*E*)- and (*Z*)-**4** (Scheme 2). The concentrations of the Cl^- (as LiCl) and the substrate were varied. Reaction of 1-hexyne (**3a**) with $PdCl_2$–LiCl at a low chloride concentration afforded mainly isomer (*Z*)-**4a** ((*Z*)-**4a**:(*E*)-**4a** = 98:2) consistent with a pathway via 98% cis chloropalladation (Table 1, entry 1). An increased chloride concentration increased the relative amount of trans chloropalladation as indicated by the increase of (*E*)-**4a**. At a total chloride concentration, $[Cl^-]_{tot.}$,[15] of 2 M there was a slight preference for (*E*)-**4a**. The stereochemical outcome was slightly dependent on the substrate concentration. Thus, at 2 M $[Cl^-]_{tot.}$ the ratio (*Z*)-**4a**:(*E*)-**4a** at substrate concentration 0.2 and 0.03 M was 49:51 and 31:69, respectively (entries 6 and 7). A similar effect by the substrate concentration was observed at 1 M $[Cl^-]_{tot.}$ (entries 4 and 5).

Table 2. Chloropalladation of Substituted Alkynes: Trapping with 1-Chloro-2-propene[a]

entry	substrate[b]	$[Cl^-]_{tot.}$[c] (M)	product[d]	*Z*:*E*[e] (cis-add:trans add)
1	**3a**	0.08	**4a**	98:2
2		2.0		31:69
3	**3b**	0.08	**4b**	100:0
4		2.0		100:0
5	**3c**	0.08	**4c**	98:2
6		2.0		71:29
7	**5**	0.08	**6**	54:46
8		2.0		62:38

[a] The reactions were performed in acetone–acetic acid (4:1) with $PdCl_2$ and added LiCl in the presence of excess 1-chloro-2-propene. The ratio of $[PdCl_2]$:[substrate]:[1-chloro-2-propene] was 0.3:1:10. [b] The concentration of the substrate was 0.03 M in all cases. [c] The $[Cl^-]_{tot.}$ refers to the total amount of Cl^- including that on $PdCl_2$. [d] The yields were in the range of 60–80% except in entry 4 where the yield was ~20%. [e] The stereochemistry was determined by ^1H NMR.

Some other acetylenes were also studied in order to determine the effect of the substituent on the stereochemical outcome. The sterically hindered *tert*-butylacetylene (**3b**) (Table 2, entries 3 and 4) was dramatically different from 1-hexyne (entries 1 and 2) and gave only (*Z*)-**4b** from cis chloropalladation (100% cis addition) under all chloride concentrations studied. Phenylacetylene (**3c**) showed a chloride concentration dependence but weaker than that of 1-hexyne (**3a**), and at $[Cl^-]_{tot.}$ concentrations of 0.03 and 2 M **3c** gave (*Z*)-**4c** and (*E*)-**4c** in ratios of 98:2 and 71:29, respectively (entries 5 and 6).

A disubstituted acetylene **5** was also studied (eq 3). Acetylene **5** afforded a mixture of (*Z*)- and (*E*)-**6** in ratios of 54:46 and 62:38 at low and high chloride concentrations, respectively (Table 2, entries 7 and 8).

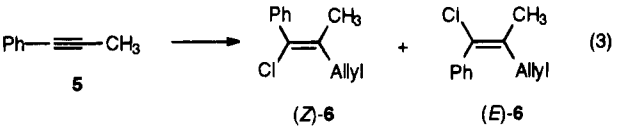

B. Trapping with 1,3-Cyclohexadiene. In an alternative trapping method 1,3-cyclohexadiene was used as trapping molecule. It is known that vinylpalladium species add to conjugated dienes to give (π-allyl)palladium intermediates in catalytic Heck type reactions.[16–18] Thus, 1,4-functionalizations of conjugated dienes via vinylpalladation followed by nucleophilic

(13) Liebeskind, L. S.; Bombrun, A. *J. Org. Chem.* **1994**, *59*, 1149.

(14) Formation of a π-allyl complex from the allyl chloride followed by insertion of the acetylene and subsequent reductive elimination was considered as an alternative pathway. In fact in one study[4c] this pathway is likely since Pd(0) intermediates were present. In another case[4a] the π-allyl pathway was ruled out on the basis of the regiochemical outcome of the reaction.

(15) The $[Cl^-]_{tot.}$ refers to the total amount of Cl^- including those on palladium(II), and therefore the concentration of chloride ions in solution will be lower than the $[Cl^-]_{tot.}$ given. At high chloride concentration and low palladium(II) salt concentrations, however, the chloride ion concentration in solution is approximately equal to $[Cl^-]_{tot.}$.

(16) Bäckvall, J. E. In *Advances in Metal-Organic Chemistry*; Liebeskind, L. S., Ed.; JAI Press: Greenwich, CT, 1989; Vol. 1, pp 135–175.

(17) (a) Heck, R. F. *Acc. Chem. Res.* **1979**, *12*, 146. (b) Patel, B. A.; Kao, L. C.; Cortese, N. A.; Minkievics, J. V.; Heck, R. F. *J. Org. Chem.* **1979**, *44*, 918. (c) Connor J. M.; Stallman, B. J.; Clark, W. G.; Shu, A. Y. L.; Spada R. E.; Stevenson, T. M.; Dieck, H. A. *J. Org. Chem.* **1983**, *48*, 807. (d) Shi, L.; Narula, C. K.; Mak, K. T.; Kao, L.; Xu, Y.; Heck, R. F. *J. Org. Chem.* **1983**, *48*, 3894.

(18) Larock, R. C.; Harrison, L. W.; Hsu, M. H. *J. Org. Chem.* **1984**, *49*, 3664.

Scheme 3

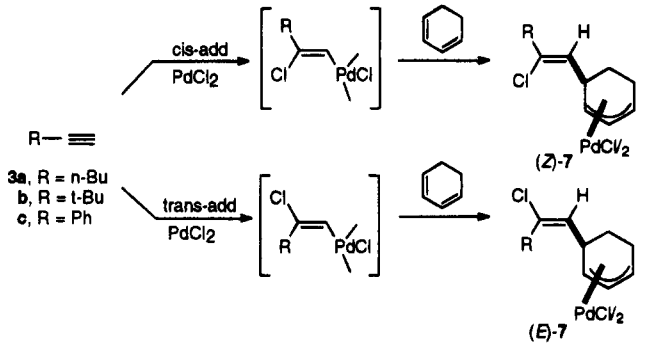

Table 3. Chloropalladation of 1-Hexyne: Trapping with 1,3-Cyclohexadiene[a]

entry	$[Cl^-]_{tot.}$[b] (M)	[1-hexyne] (M)	*Z*-7a:*E*-7a[c] (cis-add:trans add)[d]
1	0.06	0.03	98:2
2	0.12	0.03	86:14
3	0.81	0.2	72:28
4	3.0	0.2	50:50
5	1.5	0.03	41:59
6	2.0	0.03	33:67

[a] The reactions were performed in acetone–acetic acid (4:1) with $PdCl_2$ and added LiCl (no added LiCl in entry 1) in the presence of excess cyclohexadiene. The ratio of $[PdCl_2]$:[1-hexyne]:[cyclohexadiene] was 1:1:10. [b] The $[Cl^-]_{tot.}$ refers to the total amount of Cl^- including that on $PdCl_2$. [c] The yield of **7a** (based on 1-hexyne) was in the range of 70–80%. The stereochemistry was determined by ^1H NMR. [d] Refers to the chloropalladation across the triple bond.

attack on the π-allyl intermediate have been reported.[17,18] In our trapping of the vinylpalladium intermediate the (π-allyl)palladium complexes were isolated and characterized (Scheme 3). The double bond stereochemistry of (*Z*)- and (*E*)-**7** was established by ^1H NMR NOE measurements.

Reaction of **3a** with equimolar amounts of $PdCl_2$ in the presence of 10 equiv of 1,3-cyclohexadiene produced (π-allyl)palladium complexes (*Z*)-**7a** and (*E*)-**7a** in a ratio of 98:2 indicating that mainly cis chloropalladation takes place (Table 3, entry 1). An increase of the chloride concentration increased the relative amount of (*E*)-**7a**. At 0.12, 1.5, and 2 M $[Cl^-]_{tot.}$ and substrate concentrations of 0.03 M, the ratio (*Z*)-**7a**:(*E*)-**7a** was 86:14, 41:59, and 33:67, respectively, indicating a predominance of trans chloropalladation at higher chloride concentrations (entries 2, 5, and 6). The results are in accordance with those obtained from the trapping with allyl chloride. Also for the 1,3-cyclohexadiene trapping the stereochemical outcome was dependent on the concentration of the substrate (Table 3).

Acetylenes **3b,c** were also studied with 1,3-cyclohexadiene as the trapping molecule. The results obtained (Table 4) are in accordance with the results in Table 2, where allyl chloride was employed as a trapping molecule.

C. Attempts To Isolate the Intermediate Chloropalladation Adduct. The reaction between **3a** and Li_2PdCl_4 was followed by ^1H NMR at low temperature (−60 to 0 °C) in acetone-d_6–acetic acid-d_4 (4:1). The acetylene was slowly consumed, but it was not possible to observe any significant amount of the expected vinylpalladium complex from chloropalladation. It appears that the chloropalladation adducts *cis* and *trans*-**A** are in equilibrium with the π-acetylene complex (Scheme 4).

Table 4. Chloropalladation of Substituted Alkynes: Trapping with 1,3-Cyclohexadiene[a]

entry	substrate[b]	$[Cl^-]_{tot.}$[c] (M)	product[d]	*Z*:*E*[e] (cis-add:trans add)
1	**3a**	0.06	**7a**	98:2
2		2.0		33:67
3	**3b**	0.06	**7b**	100:0
4		2.0		100:0
5	**3c**	0.06	**7c**	100:0
6		2.0		45:55

[a] The reactions were performed in acetone–acetic acid (4:1) with $PdCl_2$ and added LiCl (no added LiCl in entries 1, 3, and 5) in the presence of excess cyclohexadiene. The ratio of $[PdCl_2]$:[substrate]:[cyclohexadiene] was 1:1:10. [b] The concentration of the substrate was 0.03 M in all cases. [c] The $[Cl^-]_{tot.}$ refers to the total amount of Cl^- including that on $PdCl_2$. [d] The yields were in the range of 50–70%. [e] The stereochemistry was determined by ^1H NMR.

Scheme 4

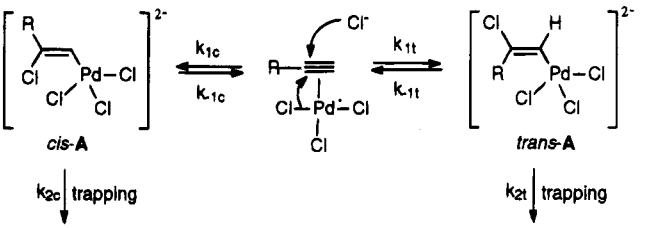

Since the trapping of *cis*- and *trans*-**A** may occur with slightly different rates (k_{2c} differs from k_{2t}), the results from the trapping experiments do not necessarily reflect the relative amounts between *cis*- and *trans*-**A** in an equilibrium situation. However, with a large excess and high concentration of the trapping molecule, the trapping reaction may become faster than the retro-chloropalladation, e.g. k_{2c}[*cis*-**A**][trapping molecule] > k_{-1c}[*cis*-**A**]. This would explain the difference between the experiments carried out at different concentrations (e.g. entry 4 versus entry 5 and entry 6 versus entry 7 in Table 1; cf. also entries 4 and 5, Table 3). Since a ratio of 1:10 between the acetylene and the trapping molecule was maintained in all cases, the concentration of trapping molecule was 0.3 and 2 M at the two different concentrations.

There is also an example in the literature where the chloropalladation adduct from an acetylene has been isolated (eq 4).[11b] In this reaction the *trans*-chloropal-

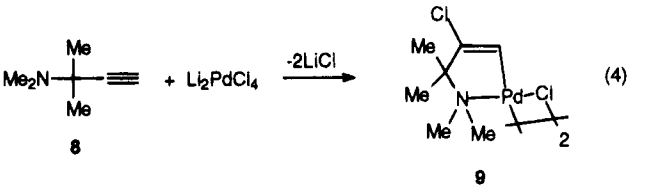

(4)

ladation adduct **9** obtained from **8** is stabilized by intramolecular coordination. Also in this case it is possible that a kinetic cis chloropalladation occurs, but due to the nitrogen coordination the thermodynamic product will be **9**, which also can be isolated. We have prepared **9** and confirmed its structure.[19] The dimer **9**, which occurs as a 1:1.5 mixture of its cisoid and transoid dimeric forms, was transformed to the monomer **10**. Irradiation of the vinylic proton gave an NOE

(19) In the original study the stereochemistry of **9** was not explicitly proven but proposed on the analogy of the corresponding oxy adducts previously reported by Cope: Cope, A. C.; Klieman, J. M.; Friedrich, E. C. J. *J. Am. Chem. Soc.* **1965**, *87*, 3272.

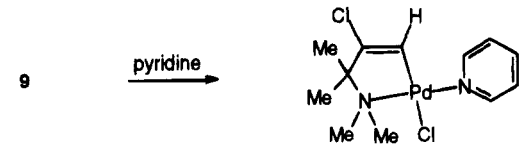

10

on the α protons of the pyridine ring of 8.3% but no detectable NOE on any of the methyl groups. Furthermore, there was no NOE between the pyridine protons and any of the methyl groups.

Further confirmation of the structure of complex **10** was given by the $^3J_{C,H}$ coupling constant of 6.7 Hz between the vinylic proton and the allylic carbon. The magnitude of the coupling constant requires that the proton and carbon are trans to one another.[20]

Experimental Section

General Methods. NMR spectra were recorded for $CDCl_3$ solutions with a Varian 400 spectrometer, ^1H at 400 MHz and ^{13}C at 100.5 MHz, using chloroform-d_1 (7.26 ppm, ^1H, 77.0 ppm, ^{13}C) as internal standard. Commercial acetone (99.5%), acetic acid, lithium chloride (99%), propiolic acid (98%), 1-hexyne (**3a**) (98%), phenylacetylene (**3c**) (98%), 3,3-dimethyl-1-butyne (**3b**) (98%), and 1,3-cyclohexadiene (97%) were purchased from Aldrich and used without further purification. Allyl chloride was purchased from BDH laboratory reagents and was used without further purification. $PdCl_2$ was obtained from Johnson Matthey. $Pd(PhCN)_2Cl_2$ was prepared according to a literature procedure.[21] Compound **8** was prepared according to ref 22. Merck silica gel 60 (240–400 mesh) was used for flash chromatography.

General Procedure for the Chloropalladation of Acetylenes: Trapping with Allyl Chloride. To $PdCl_2$ (0.032 g, 0.18 mmol) and the appropriate amount of LiCl (0–39.6 mmol) in acetone–acetic acid (4:1) (2.5 or 20 mL) at −78 °C was added the acetylene (0.61 mmol) followed by 1-chloro-2-propene (0.466 g, 6.09 mmol). The reaction was stirred at −78 °C for 30 min and then allowed to warm up over night. Water (10 mL) was added, and the mixture was extracted with ether (3 × 15 mL). The combined organic layers were washed with 2 M NaOH (until the water layer was neutralized) followed by brine (10 mL). All aqueous washings were back-extracted with ether. The combined organic layers were dried ($MgSO_4$), and the solvent was removed on a rotary evaporator. The crude product was purified by flash chromatography (pentane).

General Procedure for the Chloropalladation of Acetylenes: Trapping with 1,3-Cyclohexadiene. To $PdCl_2$ (0.108 g, 0.61 mmol) and the appropriate amount of LiCl (0–38.8 mmol) in acetone–acetic acid (4:1) (2.5 mL or 20 mL) at −78 °C was added the acetylene (0.61 mmol) followed by cyclohexadiene (0.488 g, 6.09 mmol). The reaction was stirred at −78 °C for 30 min and then allowed to warm up over night. Water (10 mL) was added, and the mixture was extracted with CH_2Cl_2 (3 × 15 mL). The combined organic layers were washed with water (until the water layer was neutralized) followed by brine (10 mL). All aqueous washings were back-extracted with CH_2Cl_2. The combined organic layers were dried ($MgSO_4$), and the solvent was removed on a rotary evaporator. The crude product was purified by flash chromatography (pentane:$CHCl_3$, 1:1).

(*Z*)-5-Chloro-1,4-nonadiene ((*Z*)-4a):[4a] ^1H NMR δ 5.85–5.70 (m, 1 H, *H*C=CH_2), 5.47 (dt, *J* = 6.7, 1.0 Hz, 1 H, ClC=CH), 5.08–4.98 (m, 2 H, HC=C*H*$_2$), 2.92 (tm, *J* = 6.7 Hz, 2 H, C=CHC*H*$_2$CH=C), 2.35–2.30 (m, 1 H, C=CC*H*$_2$CH$_2$), 1.57–1.49 (m, 2 H, $CH_2CH_2CH_2$), 1.37–1.27 (m, 2 H, CH_2CH_3), 0.906 (t, *J* = 7.2 Hz, 3 H, CH_3); ^{13}C NMR δ 135.9, 135.4, 122.3, 115.2, 39.2, 32.8, 29.5, 21.7, 13.8. NOE difference experiments gave a significant NOE between the vinyl proton on the trisubstituted olefin and the CH_2 in the butyl group.

(*E*)-5-Chloro-1,4-nonadiene ((*E*)-4a): ^1H NMR δ 5.85–5.70 (m, 1 H, *H*C=CH_2), 5.61 (t, *J* = 7.7 Hz, 1 H, ClC=CH), 5.08–4.98 (m, 2 H, HC=C*H*$_2$), 2.78 (m, 1 H, C=CHC*H*$_2$CH=C), 2.35–2.30 (m, 1 H, C=CC*H*$_2$CH$_2$), 1.57–1.49 (m, 2 H, $CH_2CH_2CH_2$), 1.37–1.27 (m, 2 H, CH_2CH_3), 0.914 (t, *J* = 7.2 Hz, 3 H, CH_3). NOE difference experiments gave a significant NOE between the bis-allylic CH_2 and the CH_2 in the butyl group.

(*Z*)-5-Chloro-6,6-dimethyl-1,4-heptadiene ((*Z*)-4b): ^1H NMR δ 5.86–5.75 (m, 1 H, *H*C=CH_2), 5.52 (t, *J* = 8.0 Hz, 1 H, ClC=CH), 5.05 (dm, *J* = 17 Hz, 1 H, HC=CH*H* (trans)), 4.99 (dm, *J* = 10 Hz, 1 H, HC=CH*H* (cis)), 2.92 (tm, *J* = 6.2 Hz, 2 H, C=CHCH_2CH=CH_2), 1.18 (s, 3 H, CH_3); ^{13}C NMR δ 145.9, 135.6, 119.2, 115.1, 38.6, 33.0, 28.9. NOE difference experiments gave a significant NOE between the vinyl proton on the trisubstituted olefin and the CH_3 protons in the *tert*-butyl group.

(*Z*)-1-Chloro-1-phenyl-1,4-pentadiene ((*Z*)-4c):[4a] ^1H NMR δ 7.65–7.55 (m, 2 H, –Ph), 7.45–7.3 (m, 3 H, –Ph), 6.17 (t, *J* = 7.6 Hz, 1 H, ClC=CH), 6.0–5.85 (m, 1 H, *H*C=CH_2), 5.18 (dq, *J* = 12, 1.7 Hz, 1 H, HC=CH*H* (trans)), 5.10 (dq, *J* = 10, 1.7 Hz, 1 H, HC=CH*H* (cis)), 3.18 (m, 2 H, CH_2); ^{13}C NMR δ 138.1, 134.8, 133.7, 128.4, 128.2, 126.4, 124.9, 115.8, 33.8. NOE difference experiments gave a significant NOE between the vinyl proton on the trisubstituted olefin and the *ortho*-protons in the phenyl group.

(*E*)-1-Chloro-1-phenyl-1,4-pentadiene ((*E*)-4c): ^1H NMR δ resolved peaks 6.03 (t, *J* = 7.8 Hz, 1 H, ClC=CH), 2.86 (ddt, *J* = 7.8, 6.0, 1.6 Hz, 2 H, CH_2).

(*Z*)-1-Chloro-2-methyl-1-phenyl-1,4-pentadiene ((*Z*)-6):[4a] ^1H NMR δ 7.36–7.20 (m, 5 H, Ph), 5.73 (ddt, *J* = 17.0, 10.0, 6.2 Hz, 1 H, *H*C=CH_2), 5.05 (dm, *J* = 17.0 Hz, 1 H, HC=CH*H* (trans)), 5.01 (dm, *J* = 10.0 Hz, 1 H, HC=CH*H* (cis)), 3.17 (dm, *J* = 6.2 Hz, 2 H, CH_2), 2.27 (t, *J* = 0.6 Hz, 3 H, CH_3); ^{13}C NMR δ 141.5, 134.3, 134.1, 128.5, 128.0, 127.2, 126.9, 116.0, 39.4, 22.9. NOE difference experiments gave a significant NOE between the methyl protons and the *ortho*-protons in the phenyl group. Anal. Calcd for $C_{12}H_{13}Cl$: C, 74.80, H, 6.80. Found: C, 74.54, H, 6.86.

(*E*)-1-Chloro-2-methyl-1-phenyl-1,4-pentadiene ((*E*)-6): ^1H NMR δ 7.38–7.28 (m, 5 H, Ph), 5.76 (ddt, *J* = 16.9, 10.0, 6.2 Hz, 1 H, *H*C=CH_2), 5.08 (dq, *J* = 10.0, 1.5 Hz, 1 H, HC=CH*H* (cis)), 5.03 (dq, *J* = 16.9, 1.6 Hz, 1 H, HC=CH*H* (trans)), 2.79 (dt, *J* = 6.2, 1.5 Hz, 2 H, CH_2), 1.98 (s, 3 H, CH_3); ^{13}C NMR δ 139.1, 135.3, 132.2, 128.9, 128.2, 128.0, 127.4, 116.5, 39.6, 19.7. NOE difference experiments gave a significant NOE between the bis-allylic CH_2 and the *ortho*-protons in the phenyl group.

[4-{(*Z*)-2-Chloro-1-hexen-1-yl}-η^3-cyclohexen-3-yl]palladium Chloro Dimer ((*Z*)-7a): ^1H NMR δ 5.81 (d, *J* = 8.5 Hz, 1 H, C=CH), 5.47 (dd, *J* = 7, 6.5 Hz, 1 H, CH-central η^3-allyl), 5.11–5.06 (m, 1 H, CH_2CH-η^3-allyl), 4.81 (dm, *J* = 6.5 Hz, 1 H, CHC*H*-η^3-allyl), 2.38 (m, 1 H, C*H*CH=), 2.34 (t, *J* = 7.5 Hz, 2 H, C=CClCH_2), 2.31–2.23 (m, 1 H, CH_2CH_2CHCH=), 2.05–1.97 (m, 1 H, CH_2CH_2CHCH=), 1.69–1.60 (m, 1 H, CH_2CH_2CHCH=), 1.54 (quint, *J* = 7.5 Hz, 2 H, $CH_2CH_2CH_2$), 1.32 (sext, *J* = 7.5 Hz, 2 H, CH_2CH_3), 1.26–1.16 (m, 1 H, CH_2CH_2CHCH=), 0.91 (t, *J* = 7.5 Hz, 3 H, CH_3); ^{13}C NMR δ 135.3, 127.4, 100.9, 81.6, 80.5, 39.0, 37.1, 29.7, 29.4, 26.4, 21.7, 13.8. NOE difference experiments gave a significant NOE between the vinyl proton and the CH_2 in the butyl group.

[4-{(*E*)-2-Chloro-1-hexen-1-yl}-η^3-cyclohexen-3-yl]palladium Chloro Dimer ((*E*)-7a): ^1H NMR δ resolved peaks 5.97 (dm, *J* = 10 Hz, 1 H, C=CH), 4.74 (dm, *J* = 6.2 Hz, 1 H, CHC*H*-η^3-allyl).

[4-{(*Z*)-2-Chloro-3,3-dimethyl-1-buten-1-yl}-η^3-cyclohexen-3-yl]palladium Chloro Dimer ((*Z*)-7b): ^1H NMR δ 5.92 (d, *J* = 8.4 Hz, 1 H, C=CH), 5.47 (t, *J* = 6.6 Hz, 1 H,

(20) Vogeli, U.; von Philipsborn, W. *Org. Magn. Reson.* **1975**, *7*, 617.
(21) Kharasch, M. S.; Seyler, R. C.; Mayo, F. R. *J. Am. Chem. Soc.* **1938**, *60*, 882.
(22) Hennon, G. F.; Nelson, K. W. *J. Am. Chem. Soc.* **1957**, *79*, 2142.

CH-central η^3-allyl), 5.13–5.08 (m, 1 H, CH_2CH-η^3-allyl), 4.83 (dm, J = 6.6 Hz, 1 H, $CHCH$-η^3-allyl), 2.44–2.36 (m, 1 H, $CHCH$=), 2.30–2.16 (m, 1 H, CH_2CH_2CHCH=), 2.06–1.96 (m, 1H, CH_2CH_2CHCH=), 1.71–1.58 (m, 1 H, CH_2CH_2CHCH=), 1.30–1.20 (m, 1 H, CH_2CH_2CHCH=), 1.20 (s, 9 H, 3 × CH_3); ^{13}C NMR δ 145.2, 124.6, 101.0, 81.7, 80.5, 38.7, 37.2, 29.3, 22.8, 26.4. NOE difference experiments gave a significant NOE between the vinyl proton and the CH_3 protons in the *tert*-butyl group. Anal. Calcd for $C_{24}H_{36}Cl_4Pd_2$: C, 42.44; H, 5.34. Found: C, 42.17; H, 5.16.

[4-{(*Z*)-2-Chloro-2-phenyl-ethen-1-yl}-η^3-cyclohexen-3-yl]palladium Chloro Dimer ((*Z*)-7c): ^{1}H NMR δ 7.70–7.64 (m, 2 H, Ph), 7.37–7.28 (m, 3 H, Ph), 6.59 (d, J = 8.9 Hz, 1 H, C=CH), 5.51 (app t, J = 6.8 Hz, 1 H, CH-central η^3-allyl), 5.18–5.11 (m, 1 H, CH_2CH-η^3-allyl), 4.97–4.90 (m, 1 H, $CHCH$-η^3-allyl), 2.71–2.58 (m, 1 H, $CHCH$=), 2.41–2.25 (m, 1 H, CH_2CH_2CHCH=), 2.11–1.98 (m, 1 H, CH_2CH_2CHCH=), 1.80–1.66 (m, 1 H, CH_2CH_2CHCH=), 1.38–1.23 (m, 1 H, CH_2CH_2-CHCH=); ^{13}C NMR δ 137.5, 132.9, 129.3, 128.5, 128.2, 126.5, 101.1, 80.6, 37.9, 29.0, 26.3. NOE difference experiments gave a significant NOE between the vinyl proton and the *ortho*-protons in the phenyl group. Anal. Calcd for $C_{28}H_{28}Cl_4Pd_2$: C, 46.76; H, 3.92. Found: C, 46.87; H, 3.94.

[4-{(*E*)-2-Chloro-2-phenyl-ethen-1-yl}-η^3-cyclohexen-3-yl]palladium Chloro Dimer ((*E*)-7c): ^{1}H NMR δ resolved peaks 6.34 (d, J = 9.2 Hz, 1 H, C=CH), 5.44 (app t, J = 6.7 Hz, CH-central η^3-allyl), 5.09–5.00 (m, 1 H, CH_2CH-η^3-allyl), 4.81–4.75 (m, 1 H, $CHCH$-η^3-allyl).

Complex 9. This complex was prepared from **8**[22] according to Yukawa and Tsutsumi.[11b] It was found to consist of two dimeric forms, one transoid dimer and one cisoid dimer. The ratio between the diasteromeric dimers was 1:1.4 (it is not possible to assign which is the major isomer). ^{1}H NMR: δ 5.87, 5.82 (two s, 1H, vinylic proton, 42% integral on 5.87), 2.74, 2.73 (two s, 6H, NMe_2), 1.42(s, 6H, CMe_2). ^{13}C NMR: δ (signals in each bracket correspond to one carbon) [132.4], [131.7, 130.3], [76.3, 76.2] [46.9, 46.6], [23.7].

Complex 10. To 18.2 mg of **4** (0.032 mmol) in $CDCl_3$ (0.5 mL) in an NMR tube was added 5.0 mg of pyridine (0.063 mmol). The tube was shaken, and NMR spectra were recorded. Only one isomer was observed: ^{1}H NMR δ 8.74–8.71 (m, 2H, α-pyridine protons), 7.78–7.73 (m, H, γ-pyridine proton), 7.33–7.29 (m, 2H, β-pyridine protons), 5.79 (s, 1H, vinyl), 2.87 (s, 6H, Me_2), 1.43 (s, 6H, Me_2); ^{13}C NMR δ 153.3, 137.7, 137.4, 133.9, 125.0, 76.3, 46.7, 23.9. Irradiation of the vinylic proton gave an NOE on the α protons of the pyridine ring of 8.3%. Furthermore, there was a $^3J_{C,H}$ coupling constant of 6.7 Hz between the vinylic proton and the allylic carbon.

Acknowledgment. We are grateful to the Swedish Natural Science Research Council for financial support and to Johnson Matthey for a loan of $PdCl_2$. We thank Dr. Adolf Gogoll for help concerning NMR problems.

OM950261V

Sterically Induced P–C Bond Cleavage: Routes to Substituent-Free Phosphorus Complexes of Zirconium

Maria C. Fermin, Jianwei Ho, and Douglas W. Stephan*

Department of Chemistry and Biochemistry, University of Windsor, Windsor, Ontario, Canada N9B 3P4

Received April 7, 1995[⊗]

The reaction of Cp_2ZrHCl with 1 equiv of K[PH(C_6H_2-2,4,6-*t*-Bu_3)] and excess KH in THF yields the dark red product [$Cp_2ZrH(P(C_6H_2$-2,4,6-*t*-$Bu_3))K(THF)_2]_2$, **4**. The complex Cp^*_2-Zr(PH(C_6H_2-2,4,6-*t*-Bu_3))Cl, **5**, is derived from the reaction of $Cp^*_2ZrCl_2$ with KPH(C_6H_2-2,4,6-*t*-Bu_3). Generation of **5** via the reaction of $Cp^*_2ZrCl_2$ with excess KH and phosphine results in P–C bond cleavage as evidenced by the formation of the diamagnetic species (Cp^*_2-Zr)$_2(\mu$-$P_2)$, **6**, and the paramagnetic compound ($Cp^*_2Zr)_2(\mu$-P), **7**. Compound **7** is the first dimetallaphosphallene to be structurally characterized. In an alternate synthetic route, reaction of 2 equiv of $PH_2(C_6H_2$-2,4,6-*t*-Bu_3) with ($Cp^*_2Zr(N_2))_2(\mu$-N_2) yields P–C bond cleavage, as the species $Cp^*_2Zr[(PH)_2]$, **8**, is formed. Reaction of **8** with KH leads to the generation of species [$Cp^*_2Zr(P_2)$][$K(THF)_x]_2$, **9**, which reacts with $Cp^*_2ZrCl_2$ to give **6** quantitatively. In a subsequent reaction, compound **6** undergoes reaction slowly with excess $PH_2(C_6H_2$-2,4,6-*t*-Bu_3) in the presence of KH to give compound **10**. X-ray crystallographic study of **10** revealed the asymmetric unit to contain $Cp^*_2ZrP_3K(THF)_{1.5}$. This species forms an infinite polymeric structure in the solid state. The nature of the bonding in species **7**, **8**, and **10** has been examined via EHMO calculations. The chemistry described herein demonstrates that high steric demands may induce P–C bond cleavage, thus offering a feasible metal-mediated route to substituent-free P complexes.

Introduction

Interest in the subdiscipline of inorganometallic chemistry has been prompted by academic interest in new reactivity patterns, the notion of metal-mediated syntheses of organic heterocycles, and the possibility of structural and mechanistic insight relating to MOCVD processes. Recently, much interest has focused on early metal inorganometallics. In early metal–imides (M=NR),[1] rich new chemistry has been uncovered principally by the research groups of Bergman and Wolczanski. Related oxide (M=O) and sulfide (M=S)[2] systems have also been studied with a view to the incorporation of heteroatoms into organic compounds. In a similar manner, recent studies of Zr–phosphinidenes (M=PR) have revealed a broad range of reactivity including C–H and P–H activation, as well as a variety of insertion or metathesis reactions which offer metal-mediated syntheses of both organophosphorus species[4] and main group–phosphorus compounds.[5] In general, early metal–heteroatom multiple bonds are stabilized by employing sterically demanding ancillary groups. This is particularly true in the case of phosphinidene derivatives as examplified by the complexes Cp_2Zr-(PC_6H_2-2,4,6-*t*-Bu_3)(PMe_3),[6] ($Me_3SiNCH_2CH_2)_3NTa$=PR,[7] and $(silox)_3Ta$=PPh.[8]

During the course of the development of synthetic routes to early metal–phosphinidenes, we have observed that the use of sterically demanding substituents may facilitate P–C bond cleavage. Two such examples of this phenomenon, the pseudopyramidal species ($CpZr(\mu^3$-$C_5H_4))_3P$, **1**,[9] and the planar, mixed-valent compound $(Cp_2Zr)_2(\mu^2$-Cl)(μ^3-P)(Cp_2ZrCl), **2**,[10] have been previously reported. In each case these compounds were derived from reactions of low-valent Zr reagents with $PH_2(C_6H_2$-2,4,6-*t*-Bu_3), clearly the result of P–C bond cleavage.

* E-mail: Stephan@UWindsor.ca.

⊗ Abstract published in *Advance ACS Abstracts,* August 1, 1995.

(1) (a) Walsh, P. J.; Hollander, F. J.; Bergman, R. G. *J. Am. Chem. Soc.* **1988**, *110*, 8729. (b) Walsh, P. J.; Carney, M. J.; Bergman, R. G. *J. Am. Chem. Soc.* **1991**, *113*, 6343. (c) Walsh, P. J.; Hollander, F. J.; Bergman, R. G. *J. Organomet. Chem.* **1992**, *428*, 13. (d) Bennett, J. L.; Wolczanski, P. T. *J. Am. Chem. Soc.* **1994**, *116*, 2179. (e) Schaller, C. P.; Bonanno, J. B.; Wolczanski, P. T. *J. Am. Chem. Soc.* **1994**, *116*, 4133. (f) Cummins, C. C.; Schaller, C. P.; Van Duyne, G. D.; Wolczanski, P. T.; Chan, A. W. E.; Hoffmann, R. *J. Am. Chem. Soc.* **1991**, *113*, 2985. (g) Banaszak Hall, M. M.; Wolczanski, P. T. *J. Am. Chem. Soc.* **1992**, *114*, 3854.

(2) (a) Parkin, G.; Bercaw, J. E. *J. Am. Chem. Soc.* **1989**, *111*, 391. (b) Carney, M. J.; Walsh, P. J.; Hollander, F. J.; Bergman, R. G. *J. Am. Chem. Soc.* **1989**, *111*, 8751. (c) Whinnery, L. L.; Hening, L. M.; Bercaw, J. E. *J. Am. Chem. Soc.* **1991**, *113*, 7575. (d) Carney, M. J.; Walsh, P. J.; Bergman, R. G. *J. Am. Chem. Soc.* **1990**, *112*, 6426. (e) (3) (a) Fagan, P. J.; Nugent, W. A. *J. Am. Chem. Soc.* **1988**, *110*, 2310. (b) Fagan, P. J.; Ward, M. D.; Caspar, J. V.; Calabrese, J. C.; Krusic, P. J. *J. Am. Chem. Soc.* **1988**, *110*, 2981. (c) Doxsee, K. M.; Dhen, G. S.; Knobler, C. B. *J. Am. Chem. Soc.* **1989**, *111*, 9129. (d) Buchwald, S. L.; Watson, B. T.; Wannamaker, W. M.; Dewan, J. C. *J. Am. Chem. Soc.* **1989**, *111*, 4486. (e) McGrane, P. L.; Jensen, M.; Livinghouse, T. *J. Am. Chem. Soc.* **1992**, *114*, 5459. (f) Buchwald, S. L.; Nielsen, R. B.; Dewan, J. C. *J. Am. Chem. Soc.* **1987**, *109*, 1590. (g) Buchwald, S. L.; Nielsen, R. B. *J. Am. Chem. Soc.* **1988**, *110*, 3171. (h) Buchwald, S. L.; Fisher, R. A.; Davis, W. M. *Organometallics* **1989**, *8*, 2082. (i) Fisher, R. A.; Nielsen, R. B.; Davis, W. M.; Buchwald, S. L. *J. Am. Chem. Soc.* **1991**, *113*, 165.

(4) Geissler, B.; Wettling, T.; Barth, S.; Binger, P.; Regitz, M. *Synthesis* **1994**, 1337.

(5) Hou, Z.; Stephan, D. W. *J. Am. Chem. Soc.* **1992**, *114*, 10088.

(6) Hou, Z.; Breen, T. L.; Stephan, D. W. *Organometallics* **1993**, *12*, 3158.

(7) Cummins, C. C.; Schrock, R. R.; Davis, W. M. *Angew. Chem., Int. Ed. Engl.* **1993**, *32*, 756.

(8) Bonanno, J. B.; Wolczanski, P. T.; Lobkovsky, E. B. *J. Am. Chem. Soc.* **1994**, *116*, 11159.

(9) Ho, J.; Stephan, D. W. *Organometallics* **1992**, *11*, 1014.

(10) Ho, J.; Rousseau, R.; Stephan, D. W. *Organometallics* **1994**, *13*, 1918.

0276-7333/95/2314-4247$09.00/0

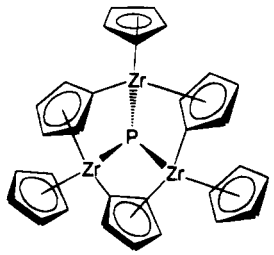

1

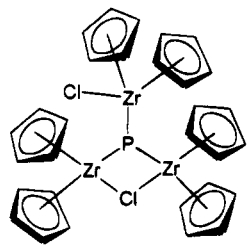

2

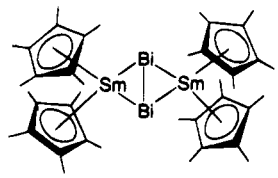

3

Such sterically induced pnictogen–carbon bond cleavages are not without precedent. Evans and co-workers have described the compound $(Cp^*_2Sm)_2(\mu\text{-}Bi_2)$, **3**, which is derived from Bi–C bond cleavage in the reaction of Cp^*_2Sm with $BiPh_3$.[11] Our observations in the zirconium–phosphorus systems suggested to us that control of such P–C bond cleavage reactions would provide a synthetic strategy to substituent-free phosphorus–early metal complexes, a class of compounds which has drawn little attention.[12] Furthermore, we reasoned that controlled steric congestion would provide insight regarding the nature of the reaction sequence as P–C cleavage would be shut down. Thus, in this paper we describe in detail a rational, systematic investigation of both the utility and limitations of sterically induced P–C bond cleavage reactions in the synthesis of substituent-free phosphorus–zirconium complexes. In addition, the nature of both the structure and bonding of such Zr–bare-P complexes is examined and discussed. A preliminary report of some of the chemistry described herein has been previously communicated.[13]

Experimental Section

General Data. All preparations were done under an atmosphere of dry, O_2-free N_2 employing either Schlenk line techniques or a Vacuum Atmospheres inert atmosphere glovebox. Solvents were reagent grade, distilled from the appropriate drying agents under N_2, and degassed by the freeze–thaw method at least three times prior to use. ^1H and $^{13}C\{^1H\}$ NMR spectra were recorded on a Bruker AC-300 operating at 300 and 75 MHz, respectively. ^{31}P and $^{31}P\{^1H\}$ NMR spectra were recorded on a Bruker AC-200 operating at 81 MHz. Trace amounts of protonated solvents were used as references, and chemical shifts are reported relative to $SiMe_4$ and 85% H_3PO_4, respectively. FAB mass spectra were recorded employing the Kratos MS-50 at Georgia Tech. Nitrobenzylglycerol was used as the matrix, and the high-resolution (HR) mass spectral results are reported using the most abundant isotopes. Combustion analyses were performed by Galbraith Laboratories Inc., Knoxville, TN, or Schwarzkopf Laboratories, Woodside, NY. $PH_2(C_6H_2\text{-}2,4,6\text{-}t\text{-}Bu_3)$ was purchased from Quantum Chemical Co. $[(Cp^*_2Zr(N_2))_2(N_2)]$ was prepared by published methods.[14]

Synthesis of $[Cp_2ZrH(P(C_6H_2\text{-}2,4,6\text{-}t\text{-}Bu_3))K(THF)_2]_2$, 4: $PH_2(C_6H_2\text{-}2,4,6\text{-}t\text{-}Bu_3)$ (140 mg, 0.5 mmol) in THF (10 mL) was treated with excess KH, generating $K[PH(C_6H_2\text{-}2,4,6\text{-}t\text{-}Bu_3)]$. A 1 equiv amount of Cp_2ZrHCl (130 mg, 0.5 mmol) was added. The mixture was stirred for 0.5 h and stood for 24 h. The solution was filtered, the volume was reduced to about half of the original amount, and pentane was added. Red orange crystals of **4** were deposited in a yield of 10%. ^1H NMR (C_6D_6, 25 °C) δ: 7.60 (m, 2H); 5.58 (s, 10H); 3.56 (m, 8H); 1.71 (s, 9H); 1.41 (m, 8H); 1.32 (s, 18H). ^{31}P NMR (C_6D_6, 25 °C) δ: 565.5. Anal. Calcd for $C_{38}H_{60}ClPZr$: C, 67.66; H, 8.97. Found: C, 67.60; H, 8.90.

Synthesis of $Cp^*_2Zr(PH(C_6H_2\text{-}2,4,6\text{-}t\text{-}Bu_3))Cl$, 5: $PH_2(C_6H_2\text{-}2,4,6\text{-}t\text{-}Bu_3)$ (280 mg, 1.0 mmol) in THF (10 mL) was treated with excess KH, generating $K[PH(C_6H_2\text{-}2,4,6\text{-}t\text{-}Bu_3)]$. The excess KH was removed by filtration, and $Cp^*_2ZrCl_2$ (453 mg, 1.0 mmol) was added. The mixture became red-brown, was stirred for 30 min, and stood overnight. The solution was filtered, the volume was reduced, and pentane was diffused slowly into the mixture. Orange-brown crystals of **5** were deposited in 95% yield. An alternative method involves the use of $Li[PH(C_6H_2\text{-}2,4,6\text{-}t\text{-}Bu_3)]$, generated by the reaction of $PH_2(C_6H_2\text{-}2,4,6\text{-}t\text{-}Bu_3)$ with BuLi. ^1H NMR (C_6D_6, 25 °C) δ: 7.59 (b s, 1H); 7.49 (b s, 1H); 6.17 (d, 1H); 1.79 (s, 30H); 1.56 (s, 9H); 1.35 (s, 18H). ^{31}P NMR (THF, 25 °C) δ: 117.0 ($|J_{P-H}|$ = 297 Hz). Anal. Calcd for $C_{38}H_{60}ClPZr$: C, 67.66; H, 8.97. Found: C, 67.60; H, 8.80.

Synthesis of $(Cp^*_2Zr)_2(\mu\text{-}P_2)$, 6: (i) Compound **5** was generated in THF solution as described above. Excess KH was added to the reaction mixture. The mixture stood for 24 h and was then filtered. The solvent was removed, and the residue was washed with pentane to give compound **6** in 60% yield. (ii) To a solution of **9** (25 mg, 0.05 mmol) in THF (5 mL) was added $Cp^*_2ZrCl_2$ (23 mg, 0.05 mmol). The solution was stirred overnight, and then the solvent was removed in vacuo. The residue was washed with a small amount of cold pentane and dried in vacuo. This afforded the brown product **6** in 80% yield. ^1H NMR (C_6D_6, 25 °C) δ: 2.09 (s). ^{31}P NMR (C_6D_6, 25 °C) δ: 959.5. Anal. Calcd for $C_{40}H_{60}P_2Zr_2$: C, 61.18; H, 7.70. Found: C, 61.02; H, 7.57. FAB-HRMS: *m/e* (calcd) 786.3159; found, 786.3150.

Synthesis of $(Cp^*_2Zr)_2(\mu\text{-}P)$, 7: From the reaction mixture described for preparation i of **6**, the pentane washing was concentrated and stood overnight, affording brown crystals of **7** in 10% yield. EPR (THF): g = 1.989, $\langle a_P \rangle$ = 26 G.

Synthesis of $Cp^*_2Zr((PH)_2)$, 8: To a solution of $(Cp^*_2Zr(N_2))_2(N_2)$ (150 mg, 0.185 mmol) in benzene (5 mL) was added $PH_2(C_6H_2\text{-}2,4,6\text{-}t\text{-}Bu_3)$ (206 mg, 0.743 mmol). The mixture was stirred for 30 min, and the solvent was removed in vacuo. The residue was washed with a minimum amount of cold pentane. This afforded **8** as a brown powder in 90%–95% yield. ^1H NMR (C_6D_6, 25 °C) δ: 1.70 (s, 30H), 4.68 (d of d, 2H). ^{31}P NMR (C_6D_6, 25 °C) δ: 134.3, $|J_{P-H}|$ = 310 Hz, $|J_{P-H}|$ = 21.3 Hz. ^{13}C NMR (C_6D_6, 25 °C) δ: 117.3, 11.55 ppm. Anal. Calcd for $C_{20}H_{32}P_2Zr$: C, 56.44; H, 7.58. Found: C, 56.36; H, 7.48.

Generation of $[Cp^*_2Zr(P_2)][K(THF)_x]_2$, 9: To a solution of **8** (50 mg, 0.117 mmol) in THF (5 mL) was added KH (10 mg, 0.264 mmol). The mixture was vigorously stirred overnight. Excess KH was removed by filtration, and the solvent was removed in vacuo. The residue was washed with pentane, dried, and isolated as a brown powder in 83% yield (based on NMR). ^1H NMR (C_6D_6, 25 °C) δ: 1.66 (s). ^{31}P NMR (C_6D_6, 25 °C) δ: 450.4 (s). ^{13}C NMR (C_6D_6, 25 °C) δ: 117.2, 11.68.

(11) Evans, W. J.; Gonzoales, S. L.; Ziller, J. W. *J. Am. Chem. Soc.* **1991**, *113*, 9880.

(12) (a) Rosenthal, G.; Corbett, J. D. *Inorg. Chem.* **1988**, *27*, 53. (b) Scherer, O. J.; Vondung, J.; Wolmershauser, G. *Angew. Chem., Int. Ed. Engl.* **1989**, *28*, 1355. (c) Scherer, O. J.; Schwalb, J.; Swarowsky, H.; Wolmershauser, G.; Kaim, W.; Gross, R. *Chem. Ber.* **1988**, *121*, 443. (d) Scherer, O. J.; Swarowsky, H.; Wolmershauser, G.; Kaim, W.; Kohlmann, S. *Angew. Chem., Int. Ed. Engl.* **1987**, *26*, 1153. (e) Hey, E.; Lappert, M. F.; Atwood, J. L.; Bott, S. G. *J. Chem. Soc., Chem. Commun.* **1987**, 597.

(13) Fermin, M. C.; Ho, J.; Stephan, D. W. *J. Am. Chem. Soc.* **1994**, *116*, 6033.

(14) Manriquez, J. M.; McAlister, D. R.; Rosenberg, E.; Shiller, A. M.; Williamson, K. L.; Chan, S. I.; Bercaw, J. E. *J. Am. Chem. Soc.* **1978**, *100*, 3078.

Table 1. Crystallographic Data

	4	5	7	10
formula	$C_{36}H_{54}KO_2PZr$	$C_{38}H_{60}ClPZr$	$C_{40}H_{60}PZr_2$	$C_{26}H_{42}KO_{1.5}P_3Zr$
fw	680.11	674.54	754.32	601.86
cryst color	red-orange	orange-brown	red-black	red
cryst size (mm^3)	0.42 × 0.20 × 0.28	0.35 × 0.35 × 0.30	0.32 × 0.30 × 0.28	0.30 × 0.32 × 0.22
a (Å)	14.891(7)	27.441(2)	14.720(9)	15.205(4)
b (Å)	14.107(6)	12.748(4)		13.302(4)
c (Å)	10.192(9)	10.026(2)	19.464(13)	15.481(5)
α (deg)	94.27(6)			
β (deg)	73.45(6)			104.39(2)
γ (deg)	115.53(3)			
cryst syst	triclinic	orthorhombic	tetragonal	monoclinic
space group	$P\bar{1}$ (No. 2)	$Pna2_1$ (No. 33)	$P\bar{4}2_1c$ (No. 114)	$P2/c$ (No. 13)
vol ($Å^3$)	1849(2)	3783(2)	4217(5)	3033(2)
D_{calcd} (g cm^{-3})	1.22	1.18	1.34	1.32
Z	2	4	4	4
abs coeff, μ (cm^{-1})	4.81	4.26	6.24	6.76
radiation, λ (Å)	Mo Kα (0.710 69)	Mo Kα (0.710 69)	Mo Kα (0.710 69)	Mo Kα (0.710 69)
temp (°C)	24	24	24	24
scan speed (deg/min)	8.0 ($\theta/2\theta$) (1–3 scans)	8.0 ($\theta/2\theta$) (1–3 scans)	8.0 ($\theta/2\theta$) (1–3 scans)	8.0 ($\theta/2\theta$) (1–3 scans)
scan range (deg)	1.0 below $K\alpha_1$, 1.0 above $K\alpha_2$	1.0 below $K\alpha_1$, 1.0 above $K\alpha_2$	1.0 below $K\alpha_1$, 1.0 above $K\alpha_2$	1.0 below $K\alpha_1$, 1.0 above $K\alpha_2$
bkgd/scan ratio	0.5	0.5	0.5	0.5
no. of data collcd	5667	3779	2193	5041
2θ range (deg)	4.5–50.0	4.5–50.0	4.5–50.0	4.5–50.0
index range	$\pm h \pm k l$	hkl	hkl	$\pm hkl$
no. of data with $F_o^2 > 3\sigma(F_o^2)$	1606	1155	857	1189
no. of variables	245	179	95	116
transmissn factors	0.558–1.000	0.965–1.000	0.934–1.000	0.947–1.000
R (%)[a]	9.62	5.92	6.56	8.23
R_w (%)[a]	9.72	5.25	7.32	9.48
largest Δ/σ	0.01	0.06	0.001	0.002
goodness of fit	2.13	1.75	2.28	2.28

[a] $R = \Sigma||F_o| - |F_c||/\Sigma|F_o|$, $R = [\Sigma(|F_o| - |F_c|)^2|/\Sigma|F_o|^2]^{0.5}$.

Synthesis of $Cp^*_2ZrP_3K(THF)_{1.5}$, 10: Compound **6** (30 mg, 0.038 mmol) was dissolved in THF (5 mL) and treated with a mixture of $PH_2(C_6H_2$-2,4,6-*t*-$Bu_3)$ (42 mg, 0.152 mmol) and excess KH (4 mg, 0.10 mmol). The mixture was vigorously stirred overnight and stood for 1 week, and the excess KH removed by filtration. The solvent was removed in vacuo, the residue was washed with a small amount of cold pentane, and the product was isolated as a brown solid in 72%–78% yield. This material could be recrystallized from THF/pentane. After the solution stood for several days at −35 °C, red crystals of **10** were deposited in 30% yield. ^1H NMR (C_6D_6, 25 °C) δ: 1.87 (s). ^{31}P NMR (C_6D_6, 25 °C) δ: 490.4 (d), 245.6 (t), $|J_{P-P}| = 598$ Hz. Anal. Calcd for $C_{26}H_{42}KP_3O_{1.5}Zr$: C, 51.99; H, 7.05. Found: C, 51.88; H, 6.99.

X-ray Data Collection and Reduction. X-ray quality crystals of **4**, **5**, **7**, and **10** were obtained directly from the preparation as described above. The crystals were manipulated and mounted in capillaries in a glovebox, thus maintaining a dry, O_2-free environment for each crystal. Diffraction experiments were performed on a Rigaku AFC6 diffractometer equipped with graphite-monochromatized Mo Kα radiation. The initial orientation matrix was obtained from 20 machine-centered reflections selected by an automated peak search routine. These data were used to determine the crystal systems. Automated Laue system check routines around each axis were consistent with the crystal system. Ultimately, 25 reflections ($20° < 2\theta < 25°$) were used to obtain the final lattice parameters and the orientation matrices. Crystal data are summarized in Table 1. The observed extinctions were consistent with the space groups. The data sets were collected in three shells ($4.5° < 2\theta < 50.0°$), and three standard reflections were recorded every 197 reflections. Fixed scan rates were employed. Up to four repetitive scans of each reflection at the respective scan rates were averaged to ensure meaningful statistics. The number of scans of each reflection was determined by the intensity. The intensities of the standards showed no statistically significant change over the duration of the data collections. The data were processed using the TEXSAN crystal solution package operating on an SGI Challenger mainframe with remote X-terminals. The reflections with $F_o^2 > 3\sigma F_o^2$ were used in the refinements.

Structure Solution and Refinement. Non-hydrogen atomic scattering factors were taken from the literature tabulations.[15,16] The Zr and P atom positions were determined using direct methods, employing either the SHELX-86 or Mithril routines. The remaining non-hydrogen atoms were located from successive difference Fourier map calculations. The refinements were carried out by using full-matrix least-squares techniques on F, minimizing the function $\omega(|F_o| - |F_c|)^2$, where the weight ω is defined as $4F_o^2/2\sigma(F_o^2)$ and F_o and F_c are the observed and calculated structure factor amplitudes. In the final cycles of each refinement, all the Zr, P, O, K, and Cl atoms were assigned anisotropic temperature factors. Carbon atoms were assigned anisotropic thermal parameters, and in some cases cyclopentadienyl and phenyl rings were constrained to be regular pentagons and hexagons, respectively, in order to maintain a reasonable data:variable ratio. Empirical absorption corrections were applied to the data sets on the basis of either ψ-scan data or a DIFABS calculation and employed the software resident in the TEXSAN package. Hydrogen atom positions were calculated and allowed to ride on the carbon to which they are bonded, assuming a C–H bond length of 0.95 Å. In the case of **4**, the hydride on Zr was located via difference map calculations, at a distance of 1.36 Å from Zr. Hydrogen atom temperature factors were fixed at 1.10 times the isotropic temperature factor of the carbon atom to which they are bonded. All hydrogen atom contributions were calculated but not refined. The final values of R, R_w, and the

(15) (a) Cromer, D. T.; Mann, J. B. *Acta Crystallogr., Sect. A: Cryst. Phys., Diffr., Theor. Gen. Crystallogr.* **1968**, *A24*, 324. (b) *Ibid.* **1968**, *A24*, 390.

(16) Cromer, D. T.; Waber, J. T. *International Tables for X-ray Crystallography*; Kynoch Press: Birmingham, England, 1974.

maximum Δ/σ on any of the parameters in the final cycles of the refinements are given in Table 1. The locations of the largest peaks in the final difference Fourier map calculation as well as the magnitude of the residual electron densities in each case were of no chemical significance. Positional parameters, hydrogen atom parameters, thermal parameters, and bond distances and angles have been deposited as supporting information.

Molecular Orbital Calculations.[17] Extended Hückel calculations were performed and visualized employing the Cache Software system operating on a Power Mac 7100 computer. Initial coordinates and geometric parameters were taken from X-ray data. The models for calculations were simplified by use of cyclopentadienyl ligands rather than pentamethylcyclopentadienyl groups.

Results and Discussion

Synthesis. We have previously reported that elimination of primary phosphine or H_2 provides access to the phosphinidene species $Cp_2Zr(PC_6H_2\text{-}2,4,6\text{-}t\text{-}Bu_3)(PMe_3)$ (eqs 1 and 2).[5,9] We reasoned that subsequent

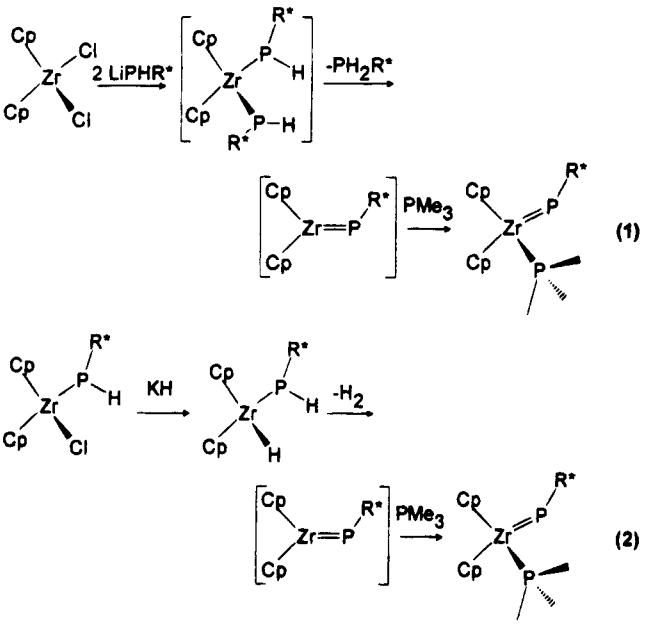

P–C bond cleavage might be induced if an additional hydride ligand could be incorporated in place of the stabilizing phosphine (i.e., PMe_3). In our initial efforts to this end, the reaction of Cp_2ZrHCl with 1 equiv of the $K[PH(C_6H_2\text{-}2,4,6\text{-}t\text{-}Bu_3)]$ and excess KH was performed in THF. The reaction becomes dark red, and the evolution of gas, presumably H, was observed. Monitoring of the reaction mixture by ^{31}P NMR revealed two low-field singlet resonances, a weak signal at 621.0, and a stronger one at 565.5 ppm. These chemical shifts are similar to those attributable to the previously reported species $Cp_2Zr(PC_6H_2\text{-}2,4,6\text{-}t\text{-}Bu_3)(\mu\text{-}Cl)Li(DME)$, suggesting that the present products are also phosphinidene-bridged derivatives.[6] Species **4**, which gives rise to the resonance at 565.5 ppm, was isolated in 10% yield, while the minor product, resulting in the ^{31}P resonance at 621.0 ppm, was not isolable and thus remains uncharacterized. ^1H NMR for species **4** confirmed the presence of both cyclopentadienyl and supermesityl fragments as well as coordinated THF. X-ray crystallography confirmed the formulation of **4** as the phosphinidene–hydride complex $[Cp_2ZrH(PC_6H_2\text{-}2,4,6\text{-}t\text{-}Bu_3)K(THF)_2]_2$, **4** (*vide infra*, Scheme 1). Although the hydride was not detected by ^1H NMR spectroscopy, recent studies of Zr–hydride anions suggest that the hydride resonance from **4** is probably obscured by the THF signals.[18] Attempts to observe the hydride via IR spectroscopy were also unsuccessful; nonetheless, the presence of the hydride was unequivocally confirmed by crystallography.

The orange-brown product $Cp^*_2Zr(PH(C_6H_2\text{-}2,4,6\text{-}t\text{-}Bu_3))Cl$, **5**, was prepared via reaction of $Cp^*_2ZrCl_2$ with 1 equiv of $K[PH(C_6H_2\text{-}2,4,6\text{-}t\text{-}Bu_3)]$ (eq 3). ^1H and ^{31}P

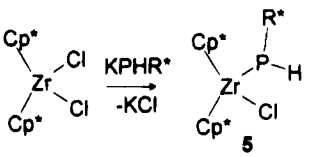

(3)

NMR data are consistent with the formulation of **5**, and this was also confirmed crystallographically (*vide infra*). Use of excess phosphide in the preparation of **5** did not lead to further substitution, and thus the diphosphide species $Cp^*_2Zr(PH(C_6H_2\text{-}2,4,6\text{-}t\text{-}Bu_3))_2$ was not readily accessible. In contrast, complexes $Cp^*_2Zr(PH(C_6H_2\text{-}2,4,6\text{-}Me_3))_2$ and $Cp_2Zr(PH(C_6H_2\text{-}2,4,6\text{-}t\text{-}Bu_3))_2$ have been prepared.[6] Thus it appears that the present combination of pentamethylcyclopentadienyl ligands and supermesityl phosphide presents a highly sterically demanding environment about the Zr center that precludes formation of the analogous diphosphide.

Generation of **5** via the reaction of $Cp^*_2ZrCl_2$ with phosphide in the presence of excess KH resulted in further reaction. Solvent removal and washing of the residue with pentane afforded the extraction of a new product, compound **6** in 15%–20% yield. This compound **6** exhibits a singlet $^{31}P\{^1H\}$ resonance at 959.0 ppm and a ^1H NMR resonance attributable to pentamethylcyclopentadienyl rings. The absence of resonances attributable to the supermesityl fragment is consistent with P–C bond cleavage. Although the spectroscopy is less than definitive, the ^{31}P NMR chemical shift does indicate a much more deshielded P environment in **6** compared to that seen in **1** (^{31}P NMR δ: 782.6 ppm).[9] Numerous attempts to obtain X-ray quality crystals of **6** were unsuccessful; however, elemental analysis, FAB-MS, and additional chemical data (*vide infra*) led to the formulation of **6** as $(Cp^*_2Zr)_2(\mu\text{-}P_2)$ (Scheme 2). Although unconfirmed by X-ray methods, **6** is thought to be a structural analog of the species $(Cp^*_2Sm)_2(\mu\text{-}Bi_2)$ **3**.[11]

In addition to **6**, a second product, **7**, was isolated from the reaction of **5** and KH. The pentane washings of the initial residue afford crystals of **7** in 10% yield. This paramagnetic product exhibits a doublet EPR resonance at $g = 1.989$, with a P hyperfine coupling constant of 26 G consistent with the coupling of a P atom to a lone unpaired electron on Zr. X-ray crystallographic study (*vide infra*) of **7** revealed the formulation as $(Cp^*_2Zr)_2(\mu\text{-}P)$ (Figure 1).

(17) CaChe Worksystem Software is an integrated modeling, molecular mechanics, and molecular orbital computational software package and is a product of CaChe Scientific Inc.

(18) Fermin, M. C.; Stephan, D. W. Unpublished results.

Table 2. Positional Parameters for 4, 5, 7, and 10

atom	x	y	z	atom	x	y	z
			$[Cp_2ZrH(PC_6H_2$-2,4,6-t-$Bu_3)K(THF)_2]_2$, **4**			
Zr(1)	0.0990(2)	0.3499(2)	0.0587(2)	C(17)	0.173(2)	0.157(2)	−0.344(2)
K(1)	−0.1060(4)	0.0761(4)	−0.0301(6)	C(18)	0.105(2)	0.049(2)	−0.264(2)
P(1)	0.1476(5)	0.1978(5)	−0.0023(6)	C(19)	0.106(2)	0.214(2)	−0.325(2)
O(1)	−0.169(2)	0.150(2)	−0.212(2)	C(20)	0.198(2)	0.134(2)	−0.493(2)
O(2)	−0.275(2)	0.073(2)	0.165(3)	C(21)	0.559(2)	0.357(2)	−0.464(3)
C(1)	0.229(1)	0.438(1)	−0.164(1)	C(22)	0.551(2)	0.345(2)	−0.613(3)
C(2)	0.151(1)	0.473(1)	−0.145(2)	C(23)	0.623(2)	0.470(2)	−0.442(3)
C(3)	0.152(1)	0.532(1)	−0.029(2)	C(24)	0.620(2)	0.298(3)	−0.463(3)
C(4)	0.229(1)	0.534(1)	0.024(1)	C(25)	0.380(2)	0.261(2)	0.027(2)
C(5)	0.277(1)	0.476(1)	−0.059(2)	C(26)	0.493(2)	0.277(2)	0.016(2)
C(6)	0.095(1)	0.376(1)	0.306(2)	C(27)	0.308(2)	0.148(2)	0.099(2)
C(7)	0.026(1)	0.412(1)	0.284(2)	C(28)	0.364(2)	0.338(2)	0.123(3)
C(8)	−0.059(1)	0.326(2)	0.259(2)	C(29)	−0.138(4)	0.257(3)	−0.238(5)
C(9)	−0.043(1)	0.236(1)	0.265(2)	C(30)	−0.165(3)	0.263(3)	−0.351(5)
C(10)	0.052(1)	0.267(1)	0.294(2)	C(31)	−0.225(3)	0.161(3)	−0.397(3)
C(11)	0.2684(8)	0.223(1)	−0.146(1)	C(32)	−0.219(3)	0.097(2)	−0.309(4)
C(12)	0.2675(8)	0.220(1)	−0.283(1)	C(33)	−0.323(5)	0.139(3)	0.144(4)
C(13)	0.361(1)	0.260(1)	−0.387(1)	C(34)	−0.435(4)	0.070(6)	0.185(7)
C(14)	0.4549(8)	0.303(1)	−0.354(1)	C(35)	−0.450(5)	−0.012(4)	0.273(5)
C(15)	0.4558(8)	0.306(1)	−0.218(1)	C(36)	−0.347(3)	0.006(3)	0.261(4)
C(16)	0.363(1)	0.266(1)	−0.114(1)				
			$Cp^*_2Zr(PH(C_6H_2$-2,4,6-t-$Bu_3))Cl$, **5**			
Zr(1)	0.32892(7)	0.4890(1)	0.3265(1)	C(19)	0.3158(9)	0.672(2)	0.057(3)
Cl(1)	0.2880(3)	0.4096(5)	0.5188(9)	C(20)	0.2956(8)	0.460(2)	−0.031(3)
P(1)	0.3544(2)	0.3331(4)	0.2058(8)	C(21)	0.4020(7)	0.235(1)	0.220(2)
C(1)	0.4206(6)	0.497(2)	0.383(2)	C(22)	0.4450(8)	0.234(1)	0.134(2)
C(2)	0.3944(7)	0.499(2)	0.509(2)	C(23)	0.4849(8)	0.197(2)	0.179(2)
C(3)	0.3677(8)	0.588(2)	0.506(3)	C(24)	0.4904(7)	0.154(1)	0.303(3)
C(4)	0.3785(7)	0.638(1)	0.391(2)	C(25)	0.4477(8)	0.135(2)	0.378(2)
C(5)	0.4093(7)	0.583(1)	0.305(3)	C(26)	0.4027(7)	0.174(1)	0.331(3)
C(6)	0.4600(7)	0.422(1)	0.355(3)	C(27)	0.4423(8)	0.275(1)	−0.007(2)
C(7)	0.400(1)	0.432(2)	0.620(3)	C(28)	0.4456(9)	0.385(2)	−0.021(3)
C(8)	0.3406(9)	0.626(2)	0.621(3)	C(29)	0.3998(8)	0.236(2)	−0.081(2)
C(9)	0.3717(8)	0.747(2)	0.370(3)	C(30)	0.488(1)	0.233(2)	−0.088(3)
C(10)	0.4344(8)	0.611(2)	0.181(3)	C(31)	0.5420(8)	0.120(2)	0.368(3)
C(11)	0.2502(8)	0.459(1)	0.185(3)	C(32)	0.560(1)	0.042(2)	0.267(3)
C(12)	0.2386(7)	0.533(1)	0.286(2)	C(33)	0.539(1)	0.077(2)	0.508(4)
C(13)	0.2623(8)	0.616(2)	0.252(2)	C(34)	0.575(1)	0.202(2)	0.359(4)
C(14)	0.291(1)	0.595(2)	0.144(3)	C(35)	0.3565(8)	0.130(2)	0.415(3)
C(15)	0.2836(7)	0.501(2)	0.099(2)	C(36)	0.3612(9)	0.021(2)	0.409(3)
C(16)	0.2243(9)	0.363(2)	0.186(3)	C(37)	0.357(1)	0.166(2)	0.550(3)
C(17)	0.1994(8)	0.524(2)	0.395(2)	C(38)	0.3091(8)	0.153(2)	0.340(3)
C(18)	0.2530(8)	0.712(2)	0.308(3)				
			$(Cp^*_2Zr)_2(\mu$-P), **7**				
Zr(1)	0.8306(1)	0.4717(1)	0.1610(1)	C(10)	0.799(2)	0.404(2)	−0.017(2)
P(1)	1.0000	0.5000	0.1458(5)	C(11)	0.807(2)	0.409(2)	0.283(1)
C(1)	0.829(2)	0.564(1)	0.048(1)	C(12)	0.733(2)	0.373(2)	0.239(1)
C(2)	0.778(2)	0.612(2)	0.098(1)	C(13)	0.767(2)	0.311(2)	0.190(1)
C(3)	0.701(1)	0.568(1)	0.117(1)	C(14)	0.864(2)	0.311(2)	0.203(1)
C(4)	0.699(2)	0.487(2)	0.077(1)	C(15)	0.889(2)	0.366(2)	0.256(1)
C(5)	0.775(2)	0.482(2)	0.038(1)	C(16)	0.797(2)	0.464(2)	0.344(2)
C(6)	0.909(2)	0.590(2)	0.003(1)	C(17)	0.633(2)	0.393(2)	0.259(2)
C(7)	0.804(2)	0.709(2)	0.117(1)	C(18)	0.715(2)	0.251(2)	0.147(1)
C(8)	0.626(2)	0.600(2)	0.163(2)	C(19)	0.919(2)	0.243(2)	0.168(2)
C(9)	0.615(2)	0.423(3)	0.067(2)	C(20)	0.977(2)	0.370(2)	0.293(1)
			$[Cp^*_2ZrP_3K(THF)_{1.5}]_n$, **10**				
Zr(1)	0.2204(2)	0.2807(3)	0.0064(2)	C(11)	0.063(1)	0.297(1)	0.050(1)
K(1)	0.5800(4)	0.4374(6)	0.1588(5)	C(12)	0.049(1)	0.338(1)	−0.035(1)
P(1)	0.3578(6)	0.3313(7)	0.1300(6)	C(13)	0.101(1)	0.427(1)	−0.029(1)
P(2)	0.2782(6)	0.3876(7)	−0.1047(6)	C(14)	0.147(1)	0.440(1)	0.060(1)
P(3)	0.3749(6)	0.4059(7)	0.0158(6)	C(15)	0.124(1)	0.360(1)	0.109(1)
O(1)	1/2	0.576(2)	1/4	C(16)	0.020(2)	0.200(1)	0.075(2)
O(2)	0.652(2)	0.275(2)	0.107(2)	C(18)	0.105(2)	0.497(2)	−0.107(1)
C(1)	0.2142(9)	0.0778(9)	0.0276(8)	C(17)	−0.013(2)	0.295(2)	−0.121(1)
C(2)	0.1725(8)	0.098(1)	−0.0619(9)	C(19)	0.212(1)	0.527(2)	0.098(2)
C(3)	0.239(1)	0.133(1)	−0.1027(8)	C(20)	0.159(2)	0.344(2)	0.211(1)
C(4)	0.3224(8)	0.1333(9)	−0.0384(9)	C(21)	0.557(3)	0.641(3)	0.308(3)
C(5)	0.3069(8)	0.0994(9)	0.0421(8)	C(22)	0.538(3)	0.746(3)	0.278(3)
C(6)	0.167(1)	0.038(1)	0.098(1)	C(23)	0.688(4)	0.269(4)	0.036(3)
C(8)	0.224(1)	0.164(2)	−0.2010(9)	C(24)	0.737(4)	0.181(5)	0.044(4)
C(7)	0.0709(8)	0.086(2)	−0.107(1)	C(25)	0.713(5)	0.126(5)	0.114(5)
C(9)	0.415(1)	0.166(2)	−0.054(1)	C(26)	0.649(3)	0.177(5)	0.146(3)
C(10)	0.379(1)	0.088(2)	0.131(1)				

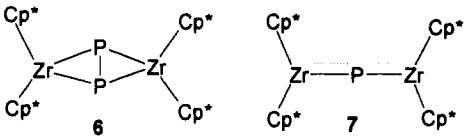

Complexes **6** and **7** are clearly derived from intriguing P–C bond cleavage reactions that occur in this "one-pot synthesis". However, because of the poor yields and the generation of both diamagnetic and paramagnetic products, an alternative synthetic route to such substituent-free phosphorus derivatives was sought. The reaction of 2 equiv of $PH_2(C_6H_2$-2,4,6-t-$Bu_3)$ with $(Cp^*_2Zr(N_2))_2(\mu$-$N_2)$[14] in benzene at 25 °C proceeds smoothly with the evolution of N_2, to give upon subsequent workup a brown product, **8**, in 75%–90% isolated yield. ^{1}H NMR showed resonances attributable to the pentamethylcyclopentadienyl ligands and two PH protons. No resonances due to the supermesityl substituents were observed, clearly indicating that P–C bond cleavage had occurred. These spectroscopic data together with the observation of two P–H coupling constants, 310.0 and 21.3 Hz, are consistent with the formulation of **8** as $Cp^*_2Zr[(PH)_2]$ (Scheme 2). Similar spectroscopic parameters have been described for the species $Cp_2Mo[(PH)_2]$, although this compound was prepared via the reaction of P_4 with Cp_2MoH_2.[19]

Reaction of **8** with KH proceeds rapidly with the generation of H_2 and species **9**, which exhibits a ^{31}P-{^{1}H} resonance at 449.5 ppm. The ^{1}H NMR spectrum of **9** shows only resonances attributable to pentamethylcyclopentadienyl and THF protons, consistent with the formulation of **9** as $[Cp^*_2Zr(P_2)][K(THF)_x]_2$ (Scheme 2). Subsequent addition of 1 equiv of $Cp^*_2ZrCl_2$ to a solution of **9** yields **6** quantitatively as evidenced by the appearance of the clean ^{31}P NMR resonance at 959.0 ppm.

Compound **9** reacts slowly with excess $PH_2(C_6H_2$-2,4,6-t-$Bu_3)$ in the presence of KH over the period of 1 week. The ^{31}P NMR resonance attributable to **9** is replaced by a doublet at 490.4 and a triplet at 245.6 ppm, with a $|J_{P-P}|$ value of 598 Hz. This magnitude of the coupling constant infers direct P–P bonding. Following workup and recrystallization, red-brown crystals of a new species **10** were isolated in 30% yield. X-ray

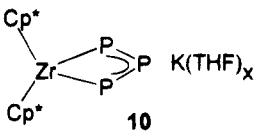

crystallographic study of **10** was employed to determine that the asymmetric unit contained $Cp^*_2ZrP_3K(THF)_{1.5}$ (*vide infra*).

Structural Studies. A crystallographic study of **4** confirmed its formulation as $[Cp_2ZrH(P(C_6H_2$-2,4,6-t-$Bu_3))]K(THF)_2$. The contents of the asymmetric unit are depicted in Figure 1. Two cyclopentadienyl ligands, a phosphinidene, and a hydride complete the pseudotetrahedral coordination sphere of Zr. The Zr–C bond distances are typical, while the Zr–P distance is 2.528(2) Å. This Zr–P distance is slightly longer than the Zr–P distance of 2.505(4) Å found in $Cp_2Zr(PC_6H_2$-2,4,6-t-$Bu_3)(PMe_3)$[13] and is consistent with the anionic nature of the Zr center in **4**. The charge of this complex anion is balanced by a potassium atom. Two molecules of THF are coordinated to the K with K–O distances of 2.75(3) and 2.71(3) Å. The K atom is also loosely associated with the P of the phosphinidene ligand of two symmetry-related Zr-complex anions (K–P distances are 3.497(9) Å). Thus, the Zr anions and K cations form a dimeric association in the solid state (Figure 2). The resulting P–K–P and K–P–K angles are 98.0(2) and 82.0(2)°, respectively.

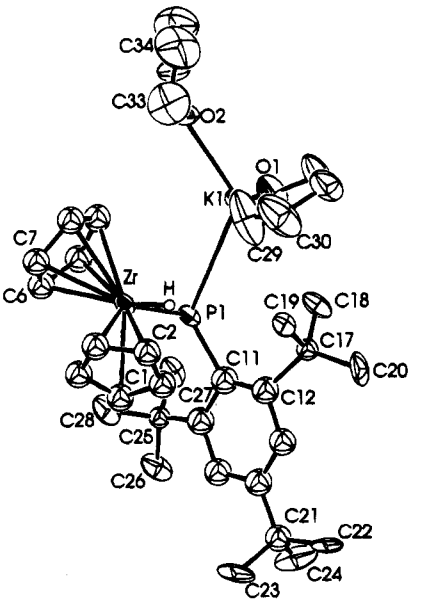

Figure 1. ORTEP drawing of the asymmetric unit of **4**; 30% thermal ellipsoids are shown; hydrogen atoms are omitted for clarity.

Scheme 1

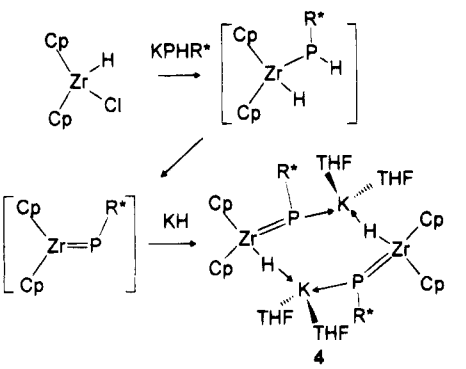

Scheme 2

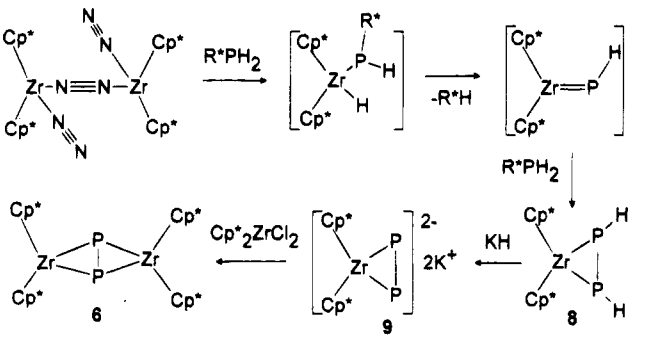

(19) Green, J. C.; Green, M. L. H.; Morris, G. E. *J. Chem. Soc., Chem. Commun.* **1974**, 212.

Table 3. Selected Bond Distances (Å) and Angles (deg) for 4, 5, 7, and 10

$[Cp_2ZrH(PC_6H_2\text{-}2,4,6\text{-}t\text{-}Bu_3)K(THF)_2]_2$, **4**

Distances

Zr(1)–K(1)	3.993(6)	Zr(1)–P(1)	2.528(8)	Zr(1)–C(1)	2.51(1)	Zr(1)–C(2)	2.52(2)
Zr(1)–C(3)	2.49(2)	Zr(1)–C(4)	2.46(1)	Zr(1)–C(5)	2.47(1)	Zr(1)–C(6)	2.51(2)
Zr(1)–C(7)	2.52(2)	Zr(1)–C(8)	2.55(1)	Zr(1)–C(9)	2.56(1)	Zr(1)–C(10)	2.53(2)
K(1)–P(1)	3.497(9)	K(1)–P(1)	3.67(1)	K(1)–O(1)	2.75(3)	K(1)–O(2)	2.71(3)
P(1)–C(11)	1.88(1)						

Angles

K(1)–Zr(1)–P(1)	60.0(2)	Zr(1)–P(1)–K(1)	153.8(2)	Zr(1)–P(1)–C(11)	117.0(5)
Zr(1)–K(1)–P(1)	133.7(2)	P(1)–K(1)–P(1)	98.0(2)	K(1)–P(1)–K(1)	82.0(2)

$Cp^*_2Zr(PH(C_6H_2\text{-}2,4,6\text{-}t\text{-}Bu_3))Cl$, **5**

Distances

Zr(1)–Cl(1)	2.484(8)	Zr(1)–P(1)	2.558(7)	Zr(1)–C(1)	2.58(2)	Zr(1)–C(2)	2.57(2)
Zr(1)–C(3)	2.49(2)	Zr(1)–C(4)	2.55(2)	Zr(1)–C(5)	2.57(2)	Zr(1)–C(11)	2.62(2)
Zr(1)–C(12)	2.58(2)	Zr(1)–C(13)	2.63(2)	Zr(1)–C(14)	2.56(3)	Zr(1)–C(15)	2.60(2)
P(1)–C(21)	1.88(2)						

Angles

Cl(1)–Zr(1)–P(1)	97.1(2)	Zr(1)–P(1)–C(21)	138.8(8)

$(Cp^*_2Zr)_2(\mu\text{-}P)$, **7**

Distances

Zr(1)–P(1)	2.545(3)	Zr(1)–C(1)	2.59(2)	Zr(1)–C(2)	2.53(2)	Zr(1)–C(3)	2.52(2)
Zr(1)–C(4)	2.55(2)	Zr(1)–C(5)	2.54(2)	Zr(1)–C(11)	2.57(2)	Zr(1)–C(12)	2.54(3)
Zr(1)–C(13)	2.61(2)	Zr(1)–C(14)	2.55(3)	Zr(1)–C(15)	2.57(3)		

Angles

Zr(1)–P(1)–Zr(1)	166.6(4)

$[Cp^*_2ZrP_3K(THF)_{1.5}]_n$, **10**

Distances

Zr(1)–P(1)	2.550(8)	Zr(1)–P(2)	2.55(1)	Zr(1)–P(3)	2.853(9)	Zr(1)–C(11)	2.62(2)
Zr(1)–C(12)	2.64(2)	Zr(1)–C(13)	2.65(2)	Zr(1)–C(14)	2.64(1)	Zr(1)–C(15)	2.62(2)
Zr(1)–C(1)	2.72(1)	Zr(1)–C(2)	2.68(1)	Zr(1)–C(3)	2.66(1)	Zr(1)–C(4)	2.69(1)
Zr(1)–C(5)	2.74(1)	K(1)–K(1)	4.16(2)	K(1)–P(1)	3.59(1)	K(1)–P(1)	3.47(1)
K(1)–P(2)	3.41(1)	K(1)–P(3)	3.37(1)	K(1)–P(3)	3.61(1)	K(1)–O(1)	2.77(2)
K(1)–O(2)	2.63(3)	P(1)–P(3)	2.10(1)	P(2)–P(3)	2.09(1)		

Angles

P(1)–Zr(1)–P(2)	90.2(3)	P(1)–Zr(1)–P(3)	45.3(3)	P(2)–Zr(1)–P(3)	44.9(3)
P(1)–K(1)–P(1)	89.1(3)	P(1)–K(1)–P(2)	150.5(3)	P(1)–K(1)–P(3)	34.9(2)
P(1)–K(1)–P(3)	118.9(3)	P(1)–K(1)–O(1)	78.8(4)	P(1)–K(1)–O(2)	95.2(6)
P(1)–K(1)–P(2)	117.9(3)	P(1)–K(1)–P(3)	124.0(3)	P(1)–K(1)–P(3)	151.9(3)
P(1)–K(1)–O(1)	80.9(4)	P(1)–K(1)–O(2)	85.2(7)	P(2)–K(1)–P(3)	117.5(3)
P(2)–K(1)–P(3)	34.4(2)	P(2)–K(1)–O(1)	93.2(5)	P(2)–K(1)–O(2)	98.6(7)
P(3)–K(1)–P(3)	84.1(3)	P(3)–K(1)–O(1)	88.0(3)	P(3)–K(1)–O(2)	94.9(6)
P(3)–K(1)–O(1)	100.8(5)	P(3)–K(1)–O(2)	94.3(8)	O(1)–K(1)–O(2)	164.8(9)
Zr(1)–P(1)–K(1)	140.2(4)	Zr(1)–P(1)–K(1)	142.7(4)	Zr(1)–P(1)–P(3)	75.0(3)
K(1)–P(1)–K(1)	72.3(3)	K(1)–P(1)–P(3)	67.0(3)	K(1)–P(1)–P(3)	122.7(5)
Zr(1)–P(2)–K(1)	152.8(3)	Zr(1)–P(2)–P(3)	75.3(4)	K(1)–P(2)–P(3)	78.0(4)
Zr(1)–P(3)–K(1)	136.2(4)	Zr(1)–P(3)–K(1)	127.3(3)	Zr(1)–P(3)–P(1)	59.7(3)
Zr(1)–P(3)–P(2)	59.8(4)	K(1)–P(3)–K(1)	95.9(3)	K(1)–P(3)–P(1)	78.1(3)
K(1)–P(3)–P(2)	159.1(5)	K(1)–P(3)–P(1)	171.7(5)	K(1)–P(3)–P(2)	67.7(4)
P(1)–P(3)–P(2)	119.5(6)	K(1)–O(1)–K(1)	97(1)		

with two pentamethylcyclopentadienyl ligands, a chloride atom, and a phosphide fragment comprising the coordination sphere. The Zr–P distance of 2.558(7) Å is slightly longer than the Zr–P distance of 2.543(3) Å seen in the analogous species, $Cp_2ZrCl(PC_6H_2\text{-}2,4,6\text{-}t\text{-}Bu_3)$.[10] While this is attributed to the relative increase in the steric demands about the Zr center in **5**, the electronic effects of the stronger π-donation from the pentamethylcyclopentadienyl ligands cannot be overlooked. A second feature that appears to reflect the steric congestion in **5** is the Zr–P–C angle (138.8(8)°). This is some 10° greater than the analogous parameter in $Cp_2ZrCl(PC_6H_2\text{-}2,4,6\text{-}t\text{-}Bu_3)$ (Zr–P–C angle 128.4(2)°).[10] The Zr–Cl distance and P–Zr–Cl angle in **5** of 2.484(8) Å and 97.1(2)° compare with the corresponding parameters of 2.494(3) Å and 98.61(9)° in $Cp_2ZrCl(PC_6H_2\text{-}2,4,6\text{-}t\text{-}Bu_3)$.

The results of the structural determination of **7** are depicted in Figure 4. The molecule is simply two bis(pentamethylcyclopentadienyl)zirconium units linked by a single P atom. The Zr–C distances are typical, while the Zr–P distance is 2.545(3) Å. This is slightly longer than the Zr–P distances in **4** and $Cp_2Zr(PC_6H_2\text{-}2,4,6\text{-}t\text{-}Bu_3)(PMe_3)$[6] and is consistent with Zr–P multiple-bond character. The crystallographic symmetry dictates strict 2/*m* symmetry. Thus, the two Zr–P distances are equivalent, and the geometry at P approaches linearity with a Zr′–P–Zr angle of 166.6(4)°. The imposed symmetry dictates that the Cp* centroid–centroid vectors on the two Zr atoms be perpendicular (Figure 4b). This dimetallaphosphaallene[20] represents the first such species to be structurally characterized, although the related arsina- and stibacumulenes $(Cp^*Mn(CO)_2)_2(\mu\text{-}E)$ (E = As, Sb) have been reported.[21] Furthermore, **7** is also a rare example of a mixed-valent Zr(IV)/Zr(III) compound.[22]

(20) A brief report of the synthesis of $[(Cp^*Mn(CO)_2)_2P]X$ has appeared, although no structural data were reported. Strube, A.; Heuser, J.; Huttner, G.; Lang, H. *J. Organomet. Chem.* **1988**, *365*, C9.

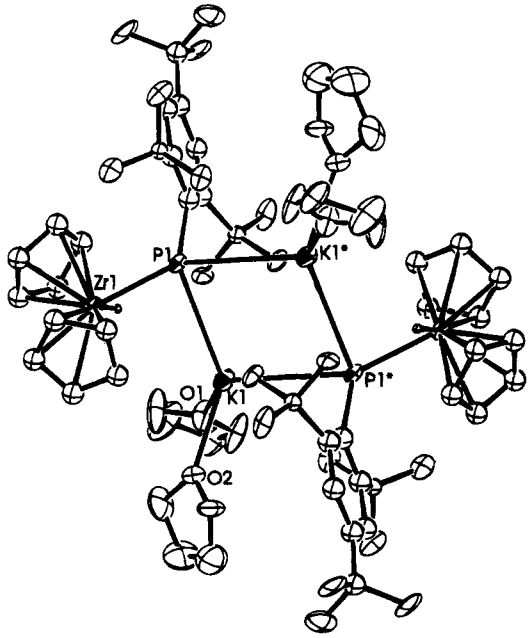

Figure 2. ORTEP drawing of **4** showing the dimeric nature in the solid state; 30% thermal ellipsoids are shown; hydrogen atoms are omitted for clarity.

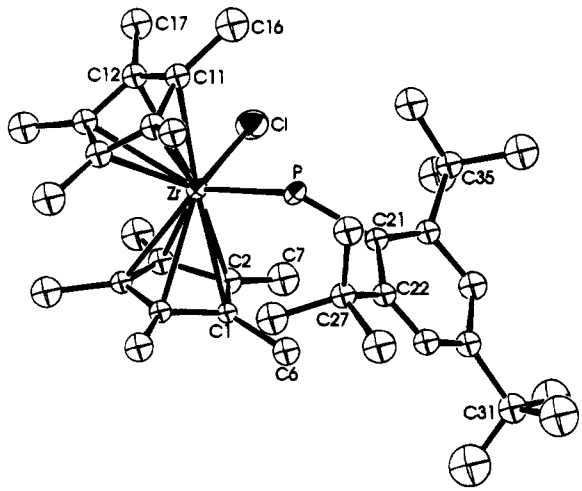

Figure 3. ORTEP drawing of **5**; 30% thermal ellipsoids are shown; hydrogen atoms are omitted for clarity.

The structure of compound **10** was determined and the contents of the asymmetric unit is depicted in Figure 5. Two pentamethylcyclopentadienyl ligands and three phopshorus atoms constitute the coordination sphere of Zr. The three phosphorus atoms in a plane are bonded to Zr such that the Zr–P distances are 2.550(8), 2.55-(1), and 2.853(9) Å. The P–P distances average 2.10-(1) Å. Ignoring the central P atom that exhibits the longer Zr–P distance, the geometry about Zr is pseudo-tetrahedral. The dissymmetric interaction of the P_3 fragment and Zr is in contrast to that typically seen for metal complexes of P_3 rings. In a number of such cases, a triangle of P atoms bonds symmetrically to the metal.[23] A structurally related species, $Cp_2ZrP_4(P(SiMe_3)_2)_2$, **11**,was prepared by Lappert et al. via the

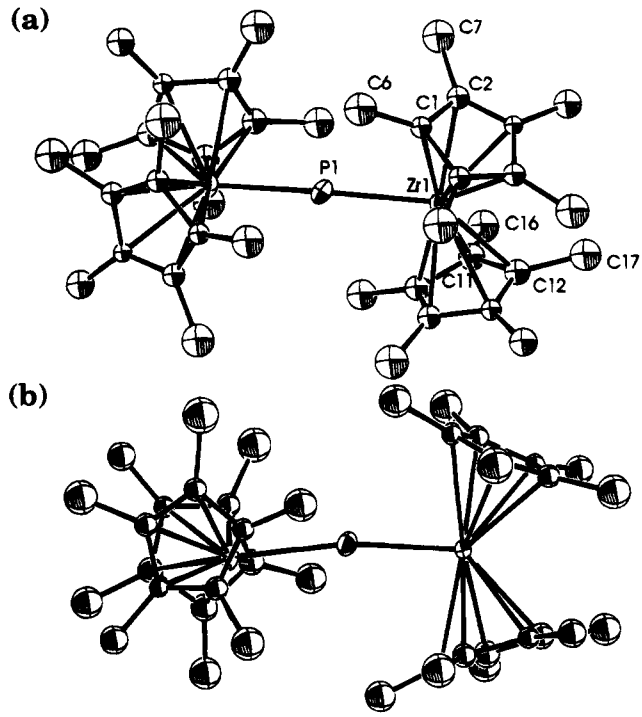

Figure 4. ORTEP drawing of the asymmetric unit of **7**; 30% thermal ellipsoids are shown; hydrogen atoms are omitted for clarity. The two views, a and b, are approximately orthogonal to each other.

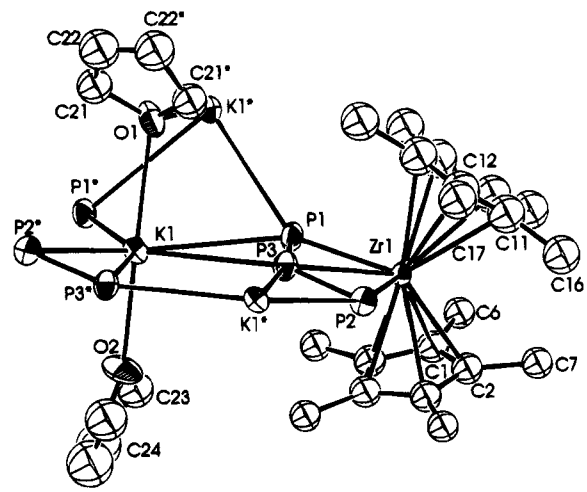

Figure 5. ORTEP drawing of the asymmetric unit of **10**; 30% thermal ellipsoids are shown; hydrogen atoms are omitted for clarity.

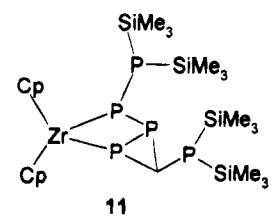

11

reaction of P_4 with $Cp_2Zr(P(SiMe_3)_2)_2$.[24] The Zr–P and P–P bond lengths in **10** are somewhat shorter than those observed in **11** (Zr–P distances, 2.632(3), 2.607-

(21) (a) Strube, A.; Huttner, G.; Zsolnai, L. *Angew. Chem., Int. Ed. Engl.* **1988**, *27*, 1529. (b) Strube, A.; Huttner, G.; Zsolnai, L. *Z. Anorg. Allg. Chem.* **1989**, *577*, 263. (c) Bringewski, F.; Huttner, G.; Imhof, W. *J. Organomet. Chem.* **1993**, *448*, C3.

(22) Ho, J.; Hou, Z.; Drake, R. J.; Stephan, D. W. *Organometallics* **1993**, *12*, 3145.

(23) Reviews on bare main group metal complexes include: (a) Scherer, O. J. *Angew. Chem., Int. Ed. Engl.* **1990**, *29*, 1104. (b) Herrmann, W. A. *Angew. Chem., Int. Ed. Engl.* **1986**, *25*, 56. (c) DiVaira, M.; Stoppioni, P.; Peruzzini, M. *Polyhedron* **1987**, *6*, 351.

(24) Hey, E.; Lappert, M. F.; Atwood, J. L.; Bott, S. G. *J. Chem. Soc., Chem. Commun.* **1987**, 597.

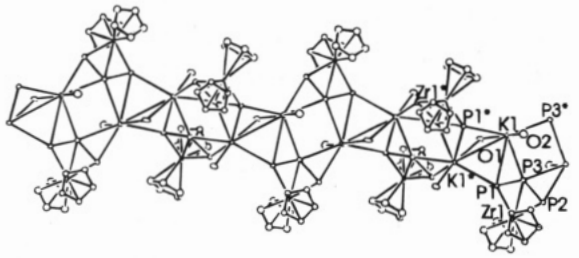

Figure 6. ORTEP drawing revealing the extended polymeric nature of **10** in the solid state; 30% thermal ellipsoids are shown; hydrogens, Cp*-methyl carbons, and the carbons of THF molecules are omitted for clarity.

(4); P–P distance, 2.241(4) Å.)[24] This is consistent with the net charge on anion $[Cp_2ZrP_3]^-$ of **10**.

Each of the P atoms exhibits an electrostatic interaction with K atoms at distances ranging from 3.37(1) to 3.61(1) Å. Each of the K atoms is situated in the plane of five P atoms. Two THF molecules complete the coordination spheres of K. One of these THF molecules bridges two K atoms, and thus the K–O distances of 2.63(1) and 2.77(2) Å reflect the terminal and bridging sites. The net result is an infinite lattice in the solid state in which $[Cp^*_2ZrP_3]$ units are bridged by K atoms, yielding the extended array (Figure 6).

Mechanistic Considerations

The reaction of potassium supermesityl phosphide with Cp_2ZrHCl is presumed to proceed through the intermediate $Cp_2ZrH(PH(C_6H_2\text{-}2,4,6\text{-}t\text{-}Bu_3))$ with loss of H_2 to generate a transient phosphinidene, in much the same way as that previously suggested for the trapping of the generated phosphinidene by PMe_3 to yield $Cp_2Zr(PC_6H_2\text{-}2,4,6\text{-}t\text{-}Bu_3)(PMe_3)$ (eq 2).[9] In the presence of KH, the transient phosphinidene is trapped as **4** (Scheme 1). When larger ancillary ligands, (i.e., pentamethylacyclopentadienyl ligands) are present, the analogous phosphinidene–hydride anion is not stable and P–C bond cleavage results affording **6** and **7**. These views are supported by observations made while monitoring the one-pot synthesis of **6** and **7** by $^{31}P\{^1H\}$ NMR spectroscopy. These experiments confirmed the initial formation of **5** in the reaction mixture, as evidenced by the appearance of the resonance at 117.0 ppm. Over the next $^1/_2$ h, this resonance gradually diminished and was replaced by a doublet of doublets at 134.3 ppm, attributed to species **8**. When the solution was left to stand, this signal was subsequently replaced by resonances attributable to two products, the minor component **9** and the major product **6**, as evidenced by the resonances at 449.5 and 959.0 ppm. These observations suggest that **8** and **9** are intermediates en route to the P_2 product, **6**. In addition, the isolation of **7** from the one-pot mixture, albeit in low yield, is viewed as the trapping of a short-lived P_1 intermediate. It is noteworthy, however, that the mixed-valent nature of **7** suggests a reaction sequence involving reduction. This aspect of the mechanism remains poorly understood.

The initial step in the reaction of $PH_2(C_6H_2\text{-}2,4,6\text{-}t\text{-}Bu_3)$ with $(Cp^*_2Zr(N_2))_2(\mu\text{-}N_2)$[14] is thought to be the oxidative addition of the PH bond to Zr (Scheme 2). The resulting hydride–phosphide intermediate is reactive. We propose that the steric demands about the metal center induce P–C bond cleavage from the intermediate species $Cp^*_2ZrH(PH(C_6H_2\text{-}2,4,6\text{-}t\text{-}Bu_3))$, yielding the transient intermediate $Cp^*_2Zr(PH)$. This is supported by the observation of RH in the reaction mixtures via ^1H NMR spectroscopy. Subsequent P–H addition and RH elimination reactions with a second equivalent of phosphine yields **8**. A similar mechanism involving a reactive phosphinidene intermediate has been implicated in the formation of $Cp^*_2Zr[(P(C_6H_2\text{-}2,4,6\text{-}Me_3))_2]$.[6,25] Thus, it appears that, in the case of the analogous phosphide–hydride intermediates $Cp_2ZrH(PH(C_6H_2\text{-}2,4,6\text{-}t\text{-}Bu_3))$ and $Cp^*_2ZrH(PH(C_6H_2\text{-}2,4,6\text{-}t\text{-}Bu_3))$, the lesser steric demands of ancillary ligands in the former favor H_2 elimination while the greater steric congestion in the latter induces P–C bond cleavage.

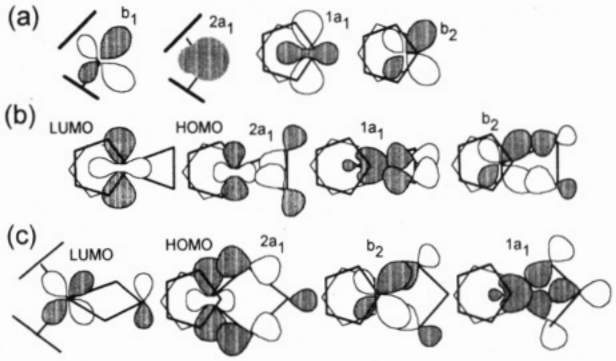

Figure 7. Schematic depiction of (a) the frontier orbitals of Cp_2Zr. (b) The LUMO, HOMO, and Zr–P bonding orbitals for $Cp_2Zr[(PH)_2]$. (c) The LUMO, HOMO, and Zr–P bonding orbitals for $[Cp_2ZrP_3]^-$. The depicted orbitals were derived from EHMO calculations.

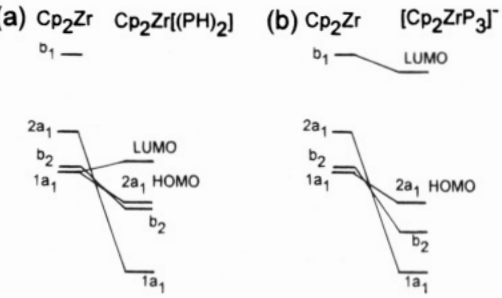

Figure 8. Truncated orbital energy diagrams of the bonding for the Cp_2Zr fragment and the species (a) $Cp_2Zr[(PH)_2]$ and (b) $[Cp_2ZrP_3]^-$.

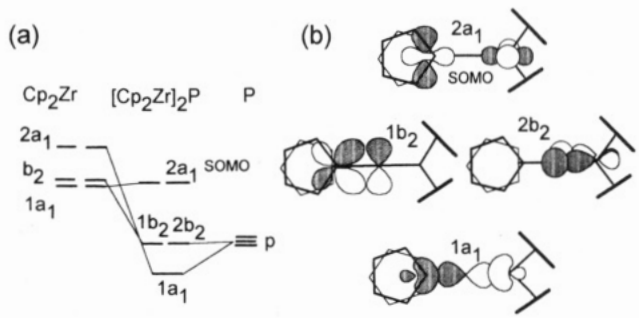

Figure 9. (a) Truncated orbital energy diagram for the Cp_2Zr and P fragments and the species $(Cp_2Zr)_2(\mu\text{-P})$. (b) Schematic depiction of the SOMO and the Zr–P bonding orbitals.

Extended Hückel Molecular Orbital Calculations. The bonding in **7**, **8**, and **10** was probed by

(25) Ho, J.; Breen, T. L.; Ozarowski, A. J.; Stephan, D. W. *Inorg. Chem.* **1994**, *33*, 865.

EHMO calculations using suitably simplified models. Overlap of the P−P π-bond with the $1a_1$ frontier orbital of the Cp_2Zr fragment (Figure 7(a))[26] yields the $2a_1$ molecular orbital in $Cp_2Zr[(PH)_2]$. A σ-bonding interaction (b_2 symmetry) arises from the mixing of P p-orbitals with the b_2 frontier orbital of the Cp_2Zr fragment. The HOMO ($2a_1$) for $Cp_2Zr[(PH)_2]$ is primarily P p-orbitals with a lesser contribution for the $1a_1$ of the Cp_2Zr fragment. The LUMO, like most metallocene(IV) derivatives, remains primarily the $1a_1$ frontier orbital of the Cp_2Zr. Similar bonding occurs in $[Cp_2ZrP_3]^-$ although the b_2 molecular orbital is more stable than that in $Cp_2Zr[(PH)_2]^-$ (Figure 8). This is attributed to the greater overlap of the P p-orbitals with the b_2 metallocene fragment frontier orbital as a result of the greater P−Zr−P angle. This P−Zr−P angle also alters the nature of the HOMO in $[Cp_2ZrP_3]^-$ as more significant overlap of P p-orbitals with the $1a_1$ metallocene fragment frontier orbital results. The LUMO is an admixture of the metal-based b_1 frontier orbital with a contribution from a p-orbital on the central P atom. The primary σ interaction in $(Cp_2Zr)_2(\mu\text{-P})$ arises from the mixing of the p_z-orbital on P with the $1a_1$ orbitals of the Cp_2Zr fragments (Figure 9). Each of the two remaining orthogonal p-orbitals on P are of the correct symmetry for interaction with the b_2 orbitals of the respective Cp_2Zr fragments. This orthogonal π-interactions are similar to those seen in allenes. The singly occupied orbital in this Zr(IV)/Zr(III) species is of $2a_1$ symmetry and is the admixture of the two $1a_1$ Cp_2Zr fragment orbitals.

(26) Lauher, J., Hoffmann, R. *J. Am. Chem. Soc.* **1976**, *98*, 1729.

Summary. The above chemistry demonstrates that a sterically demanding environment may induce P−C bond cleavage and thus provide access to substituent-free P derivatives. The generality of this approach and the utility of the derived products in the construction of main group polyatomic anion complexes is currently being explored.

Acknowledgment. Support from the Petroleum Research Fund administered by the American Chemical Society is gratefully acknowledged. Support from the NSERC of Canada is also acknowledged.

Supporting Information Available: Tables of crystallographic parameters, hydrogen atom parameters, and thermal parameters (29 pages). Ordering information is given on any current masthead page.

OM9502502

Lewis Acid Catalysis of the Rearrangement of a Dipalladium Acetylene Adduct to a Vinylidene-Bridged Complex

Constanze Kluwe and Julian A. Davies*

Departments of Chemistry and Medicinal and Biological Chemistry, University of Toledo, Toledo, Ohio 43606

Received February 21, 1995[⊗]

The crystallographically characterized vinylidene complex $[Pd_2Cl_2(\mu\text{-dppm})_2(\mu\text{-}\sigma\text{-C=C-}(SCH_3)_2)]$ (**3**); dppm = bis(diphenylphosphino)methane) was prepared by the reaction of $[Pd_2Cl_2(\mu\text{-dppm})_2]$ with $CH_3SC{\equiv}CSCH_3$ in the presence of $HBF_4{\cdot}Et_2O$ as well as through an isomerization of the acetylene adduct $[Pd_2Cl_2(\mu\text{-dppm})_2(\mu\text{-}CH_3SCCSCH_3)]$ (**1**) catalyzed by several Lewis acids. Treatment of the related acetylene adduct $[Pd_2Cl_2(\mu\text{-dmpm})_2(\mu\text{-}CH_3SCCSCH_3)]$ (**2**; dmpm = bis(dimethylphosphino)methane) with $HBF_4{\cdot}Et_2O$ yielded the tetranuclear palladium complex $[Pd_4(\mu\text{-Cl})_2(\mu\text{-dmpm})_2(\mu\text{-}SCH_3)_4][BF_4]_2$ (**4**), which was also characterized crystallographically.

Introduction

The products in the reactions of the metal–metal-bonded dipalladium(I) complexes $[Pd_2Cl_2(\mu\text{-dppm})_2]$ and $[Pd_2Cl_2(\mu\text{-dmpm})_2]$ with acetylenes are typically 1,2-dimetalated olefins (acetylene adducts) or 1,1-dimetalated olefins (vinylidene complexes).[1] The formation of the former is favored with acetylenes bearing electron-withdrawing groups, while formation of the latter involves an unusual 1,2-shift reaction. Such shift reactions may be observed in cases where heteroatomic groups (Cl, SR, NR_2, etc.) are involved.[1c,2] It has been shown that coordination of acetylenes, including examples without electron-withdrawing substituents, to form 1,2-dimetalated olefins may be facilitated by acid catalysis.[3] We recently reported that the $HBF_4{\cdot}Et_2O$-catalyzed reaction of $[Pd_2Cl_2(\mu\text{-dppm})_2]$ and the unsymmetrically substituted acetylene $CH_3SC{\equiv}CCH_3$ gave not an acetylene adduct but rather the vinylidene complex $[Pd_2Cl_2(\mu\text{-dppm})_2(\mu\text{-}\sigma\text{-C=C(CH}_3)(SCH_3))]$, while without acid catalysis no reaction was observed. In contrast, the uncatalyzed reactions of $[Pd_2Cl_2(\mu\text{-dppm})_2]$ and $[Pd_2Cl_2(\mu\text{-dmpm})_2]$ with the symmetrical sulfur-substituted acetylene $CH_3SC{\equiv}CSCH_3$ yielded the acetylene adducts $[Pd_2Cl_2(\mu\text{-dppm})_2(\mu\text{-}CH_3SCCSCH_3)]$ (**1**) and $[Pd_2Cl_2(\mu\text{-dmpm})_2(\mu\text{-}CH_3SCCSCH_3)]$ (**2**).[4] Our results were opposite to those reported by Miller and Angelici[2h] for the reactions of the mononuclear ruthenium(II) complex $[RuCl(P(CH_3)_3)_2Cp]$ with $CH_3SC{\equiv}CSCH_3$ and $CH_3SC{\equiv}CCH_3$, in which a facile 1,2-migration of SCH_3 and formation of a vinylidene complex was observed only in the reaction with the symmetrical acetylene $CH_3SC{\equiv}CSCH_3$.

We now report the synthesis of $[Pd_2Cl_2(\mu\text{-dppm})_2(\mu\text{-}\sigma\text{-C=C(SCH}_3)_2)]$ (**3**) by reaction of $[Pd_2Cl_2(\mu\text{-dppm})_2]$ and $CH_3SC{\equiv}CSCH_3$ in the presence of $HBF_4{\cdot}Et_2O$ and through isomerization of **1** catalyzed by various Lewis acids, as well as the formation of $[Pd_4(\mu\text{-Cl})_2(\mu\text{-dmpm})_2(\mu\text{-}SCH_3)_4][BF_4]_2$ (**4**) by treatment of **2** with $HBF_4{\cdot}Et_2O$. These results provide new insight into the role of Lewis acids in these types of reactions.

Experimental Section

General Procedures. All reactions were carried out under argon atmospheres using standard Schlenk techniques unless otherwise noted. The solvents were outgassed and freshly distilled under argon prior to use. Methylene chloride was distilled from calcium carbide. All other chemicals were used as received from commercial sources.

NMR spectra were recorded on Varian VXR-400 or Gemini-200 NMR spectrometers. The chemical shifts for the ^1H NMR spectra were referenced to internal $(CH_3)_4Si$ or to $(CH_3)_4Si$ *via* the signal resulting from the residual protons of the deuterated solvent; for $^{31}P\{^1H\}$ NMR spectra, the shifts were referenced to external 85% H_3PO_4. The C, H, N analyses were carried out on a PE 2400 elemental analyzer.

The compounds $[Pd_2Cl_2(\mu\text{-dppm})_2]$,[5] $[Pd_2Cl_2(\mu\text{-dmpm})_2]$,[6] and $CH_3SC{\equiv}CSCH_3$[7] were prepared by following the literature procedures. $[Pd_2Cl_2(\mu\text{-dppm})_2(\mu\text{-}CH_3SCCSCH_3)]$ (**1**) and $[Pd_2Cl_2(\mu\text{-dmpm})_2(\mu\text{-}CH_3SCCSCH_3)]$ (**2**) were prepared as described previously.[4]

$[Pd_2Cl_2(\mu\text{-dppm})_2(\mu\text{-}\sigma\text{-C=C(SCH}_3)_2)]$. (a) $[Pd_2Cl_2(\mu\text{-dppm})_2]$ (126 mg, 0.12 mmol) was dissolved in CH_2Cl_2 (15 mL). $CH_3SC{\equiv}CSCH_3$ (22 μL, 0.17 mmol) was first added slowly, dropwise, through a rubber septum with a syringe. Next, $HBF_4{\cdot}Et_2O$ (1 μL) was added. The solution was stirred for 48 h. Over this period of time the mixture had turned cloudy. After the

[⊗] Abstract published in *Advance ACS Abstracts,* August 15, 1995.

(1) (a) Lee, C.-L.; Hunt, C. T.; Balch, A. L. *Inorg. Chem.* **1981**, *20*, 2498. (b) Balch, A. L.; Lee, C.-L.; Lindsay, C. H.; Olmstead, M. M. *J. Organomet. Chem.* **1979**, *177*, C22. (c) Davies, J. A.; Pinkerton, A. A.; Syed, R.; Vilmer, M. *J. Chem. Soc., Chem. Comm.* **1988**, 47.

(2) (a) Horvath, I. T.; Palyi, G.; Marko, L. *J. Chem. Soc., Chem. Commun.* **1979**, 1054. (b) Horvath, I. T.; Palyi, G.; Marko, L.; Andretti, G. D. *Inorg. Chem.* **1983**, *22*, 1049. (c) Löwe, C.; Hund, H.-U.; Berke, H. *J. Organomet. Chem.* **1989**, *371*, 311. (d) Fogg, D. E.; MacLaughlin, S. A.; Kwek, K.; Cherkas, A. A.; Taylor, N. J.; Carty, A. J. *J. Organomet. Chem.* **1988**, *352*, C17. (e) Adams, R. D.; Chen, G.; Pompeo, M. P.; Yin, J. *Organometallics* **1991**, *10*, 2541. (f) Adams, R. D.; Chen, G.; Chen, L.; Yin, J. *Organometallics* **1993**, *12*, 2644. (g) Werner, H.; Baum, M.; Schneider, D.; Windmüller, B. *Organometallics* **1994**, *13*, 1089. (h) Miller, D. C.; Angelici, R. J. *Organometallics* **1991**, *10*, 79. (i) Bruce, M. I. *Chem. Rev.* **1991**, *91*, 197.

(3) Higgins, S. J.; Shaw, B. L. *J. Chem. Soc., Chem. Commun.* **1986**, 1629.

(4) Davies, J. A.; Kirschbaum, K.; Kluwe, C. *Organometallics* **1994**, *13*, 3664.

(5) Balch, A. L.; Benner, L. S. *Inorg. Synth.* **1982**, *21*, 47.

(6) Davies, J. A.; Dutremez, S.; Vilmer, M. *J. Prakt. Chem.* **1992**, *334*, 34.

(7) Brandsma, L. *Preparative Acetylene Chemistry*; Elsevier: New York, 1971; p 92.

0276-7333/95/2314-4257$09.00/0

Table 1. X-ray Data for $[Pd_2Cl_2(\mu\text{-dppm})_2(\mu\text{-}\sigma\text{-}C{=}C(SCH_3)_2)]$ (3) and $[Pd_4(\mu\text{-Cl})_2(\mu\text{-dmpm})_2(\mu\text{-}SCH_3)_4][BF_4]_2\cdot{}^1/_2CH_2Cl_2$ ($4\cdot{}^1/_2CH_2Cl_2$)

	3	$4\cdot{}^1/_2CH_2Cl_2$
formula	$Pd_2Cl_2P_4S_2C_{54}H_{50}$	$Pd_4Cl_2P_4S_4C_{14}B_2F_8H_{40}\cdot{}^1/_2CH_2Cl_2$
fw	1170.73	1173.19
$F(000)$	2368	1096
cryst dimens, mm	0.11 × 0.10 × 0.20	0.30 × 0.10 × 0.03
radiation (λ, Å)	Mo Kα (0.710 73)	Mo Kα (0.710 73)
temp, K	150 ± 1	294 ± 1
space group	tetragonal, $P4_1$	triclinic, $P\bar{1}$
a, Å	21.115(4)	11.799(2)
b, Å		12.256(3)
c, Å	14.368(2)	15.599(3)
α, deg		72.21(2)
β, deg		83.00(2)
γ, deg		67.29(2)
V, Å^3	6404(3)	1981(1)
Z	4	2
D_{calc}, g/cm^3	1.21	1.97
μ, cm^{-1}	8.3	23.1
no. of params	531	336
R	0.049	0.055
R_w	0.050	0.068
S	1.18	1.64
max resd density, e/Å^3	0.69	1.17

stirring was stopped, a light yellow solid settled immediately out of solution. It proved to be air stable and was isolated by filtration and washed with cold CH_2Cl_2 (5 mL). The yield was 92 mg (0.078 mmol, 65%). Anal. Calcd for $Pd_2P_4Cl_2S_2C_{54}H_{50}$: C, 55.42; H, 4.27. Found: C, 54.47; H, 4.15. NMR ($CDCl_3$): ^{1}H, δ 1.27 (6H, s, SCH_3), 6.9–8.1 (40H, m, C_6H_5), 2.8 (2H, m, PCH_2P), 3.0 (2H, m, PCH_2P); $^{31}P\{^1H\}$, δ 10.3 (s). (b) In an alternative synthesis, $[Pd_2Cl_2(\mu\text{-dppm})_2(\mu\text{-}CH_3SCCSCH_3)]$ (**1**; 115 mg, 0.098 mmol) was dissolved in CH_2Cl_2 (10 mL). $HBF_4\cdot Et_2O$ (1 μL) was added and the solution stirred for 48 h. A light yellow solid precipitated out of solution and was isolated by filtration. The yield was 85 mg (0.073 mmol, 74%). The signals in the recorded $^{31}P\{^1H\}$ and ^{1}H NMR spectra of the isolated complex were in agreement with those described above. $[Pd_2Cl_2(\mu\text{-dppm})_2(\mu\text{-}\sigma\text{-}C{=}C(SCH_3)_2)]$ (**3**) was also obtained in similar reactions where $[Pd_2Cl_2(\mu\text{-dppm})_2(\mu\text{-}CH_3SCCSCH_3)]$ (**1**) was treated with either catalytic amounts of $BF_3\cdot Et_2O$ or 1 equiv of $[PtCl_2(cod)]$.

$[Pd_4(\mu\text{-Cl})_2(\mu\text{-dmpm})_2(\mu\text{-}SCH_3)_4][BF_4]_2$. To a solution of $[Pd_2Cl_2(\mu\text{-dmpm})_2(\mu\text{-}CH_3SCCSCH_3)]$ (**2**) (30 mg, 0.044 mmol) in CH_2Cl_2 (15 mL) was added $HBF_4\cdot Et_2O$ (3 μL). The solution was stirred for 48 h. During this time the color of the solution changed from orange to yellow. Yellow crystals were grown by slow evaporation of CH_2Cl_2. The isolated solid proved to be air stable.

X-ray Structure Determination. General Methods. A single crystal selected for data collection was mounted on a glass fiber in a random orientation. X-ray diffraction data were collected with an Enraf-Nonius CAD4 diffractometer in the $\omega-2\theta$ mode. Data were collected to a maximum 2θ of 52°. Lorentz and polarization corrections and an empirical absorption correction were applied to the data. The structure was refined by full-matrix least-squares methods where the function minimized was $\sum w(|F_o| - |F_c|)^2$ and the weight w was defined as $4F_o^2/\sigma^2(F_o^2)$. Scattering factors were taken from the standard literature.[8] Anomalous dispersion effects were included in F_c. The unweighted and weighted agreement factors are defined as $R = \sum||F_o| - |F_c||/\sum|F_o|$ and $R_w = (\sum w(|F_o| - |F_c|)^2/\sum|F_o|^2)^{1/2}$. All calculations were performed on a VAX 3100 computer using MolEN.[9]

(8) Cromer, D. T.; Waber, J. T. *International Tables for X-ray Crystallography*; Kynoch Press: Birmingham, England, 1974; Vol. IV.
(9) Fair, C. K.; *MolEN: An Interactive Intelligent System for Crystal Structure Analysis*; User Manual; Enraf-Nonius: Delft, The Netherlands, 1990.

$[Pd_2Cl_2(\mu\text{-dppm})_2(\mu\text{-}\sigma\text{-}C{=}C(SCH_3)_2)]$. Yellow single crystals were grown by slow evaporation of the solvent, methylene chloride. The tetragonal unit cell constants and the orientation matrix for data collection were obtained from least-squares refinement, using the setting angles of 25 reflections in the range $7 < \theta < 13°$. As a check on crystal stability the intensities of three representative reflections were measured every 60 min, indicating a total loss in intensity of 4.0%. An anisotropic decay correction was applied with correction factors on I in the range from 0.954 to 1.187. A total of 6888 reflections were collected, of which 6523 were unique. Intensities of equivalent reflections were averaged; the agreement factors were 5.8% based on I and 4.4% based on F_o. A total of 3310 reflections with $F_o^2 > 3.0\sigma(F_o^2)$ were used in the calculations.

Structure Solution and Refinement. The positions of the two Pd atoms in the asymmetric unit were found by direct methods. The remaining atoms were located by repeated least-squares refinements followed by difference Fourier syntheses. The positions of the hydrogen atoms were calculated and included in the least-squares refinement as riding atoms; $U_{iso} = 1.3[U_{eq}(\text{bonding atom})]$. The carbon atoms C(5), C(10), C(15), C(24), C(47), C(50), C(52), C(53), and C(54) were refined with isotropic thermal parameters. All other non-hydrogen atoms were refined with anisotropic thermal parameters. The final cycle of refinement included 531 variable parameters and converged with $R = 0.049$ and $R_w = 0.050$. Further details relevant to the data collection and structure refinements are given in Table 1.

$[Pd_4(\mu\text{-Cl})_2(\mu\text{-dmpm})_2(\mu\text{-}SCH_3)_4][BF_4]_2\cdot{}^1/_2CH_2Cl_2$. Yellow single crystals were grown by slow evaporation of the solvent, methylene chloride. The triclinic unit cell constants and the orientation matrix for data collection were obtained from least-squares refinement, using the setting angles of 25 reflections in the range $7 < \theta < 15°$. As a check on crystal stability the intensities of three representative reflections were measured every 60 min, indicating a total loss in intensity of 3.8%. An anisotropic decay correction was applied with correction factors on I in the range from 0.960 to 1.093. A total of 8158 reflections were collected, of which 7752 were unique. Intensities of equivalent reflections were averaged; the agreement factors were 2.8% based on I and 2.3% based on F_o. A total of 3158 reflections with $F_o^2 > 3.0\sigma(F_o^2)$ were used in the calculations.

Structure Solution and Refinement. The positions of the four Pd atoms in the asymmetric unit were found by direct methods. The remaining atoms were located by repeated least-squares refinements followed by difference Fourier syntheses. The positions of the hydrogen atoms of the tetranuclear palladium complex were calculated and included in the least-squares refinement as riding atoms; $U_{iso} = 1.3[U_{eq}(\text{bonding atom})]$. All non-hydrogen atoms of the tetranuclear palladium complex were refined with anisotropic thermal parameters. For both BF_4^- anions each fluorine was found to be equally disordered over two positions. All atoms of the anions were refined with isotropic thermal parameters. Highly disordered solvent was also found in the asymmetric unit. The model refined contained $^1/_2$ equiv of CH_2Cl_2 per tetranuclear palladium complex disordered over four positions. The positions of the non-hydrogen atoms were found in the difference Fourier map and fixed during refinements (Cl(a) to Cl(h), C(21) to C(23)). The isotropic thermal parameters were refined; hydrogen positions were not calculated. The final cycle of refinement included 336 variable parameters and converged with $R = 0.055$ and $R_w = 0.068$. Further details relevant to the data collection and structure refinements are given in Table 1.

Results and Discussion

Syntheses of $[Pd_2Cl_2(\mu\text{-dppm})_2(\mu\text{-}\sigma\text{-}C{=}C(SCH_3)_2)]$ (3). Stirring a solution of $[Pd_2Cl_2(\mu\text{-dppm})_2]$ in CH_2Cl_2

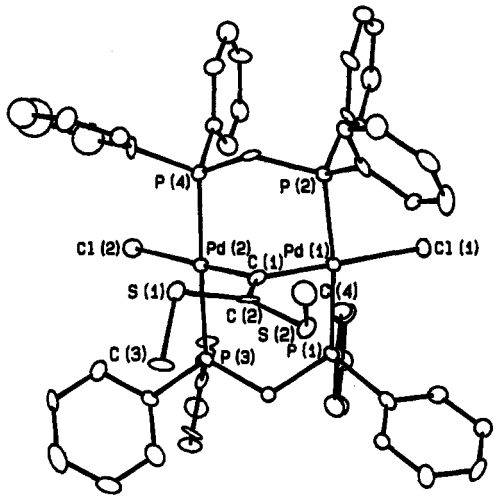

Figure 1. ORTEP diagram of $[Pd_2Cl_2(\mu\text{-dppm})_2(\mu\text{-}\sigma\text{-}C{=}C(SCH_3)_2)]$ (**3**), showing 50% probability thermal ellipsoids.

with excess $CH_3SC{\equiv}CSCH_3$ in the presence of a small amount of $HBF_4{\cdot}Et_2O$ under an inert atmosphere over a period of 48 h yielded a light yellow solid which settled from solution and proved to be air stable. The $^{31}P\{^1H\}$ NMR spectrum of the complex in $CDCl_3$ showed a singlet at 10.3 ppm. The ^1H NMR spectrum ($CDCl_3$) included a singlet for the methyl protons at 1.27 ppm. This chemical shift was very similar to that of 1.17 ppm found for the methyl protons in $[Pd_2Cl_2(\mu\text{-dppm})_2(\mu\text{-}CH_3SCCSCH_3)]$ (**1**) (cf. 2.37 ppm for the free acetylene).

The same complex, **3**, could also be obtained from the reaction of **1** with $HBF_4{\cdot}Et_2O$ in CH_2Cl_2. If very small (catalytic) amounts of acid were used, only one product, **3**, was formed and the reaction was slow. When the amount of acid was increased, the reaction proceeded faster, but the formation of side products, including the mononuclear complex $[PdCl_2(dppm)]$, was observed.

Single crystals suitable for X-ray analysis were grown by slow evaporation of the solvent CH_2Cl_2. The X-ray crystal structure determination revealed that a symmetrical vinylidene complex (**3**; Figure 1) had been formed by rearrangement of the acetylene adduct, **1**. The two palladium atoms in **3** were held together by two mutually *trans* dppm ligands. The vinylidene moiety lay in the equatorial plane. Palladium exhibited an approximate square-planar coordination geometry which was completed by two terminal chloride ligands. The α-carbon (C(1)) of the vinylidene moiety symmetrically bridged the two palladium atoms. The β-carbon (C(2)) was disubstituted with two SCH_3 groups (for significant bond lengths and bond angles refer to Table 2).

The rearrangement of **1** to **3** was also observed in the presence of other Lewis acids ($BF_3{\cdot}Et_2O$ and $[PtCl_2(cod)]$ (cod = 1,5-cyclooctadiene)) under similar conditions (Scheme 1). These results show that Lewis acids not only facilitate the insertion of acetylenes into palladium–palladium bonds as reported previously[3] but also catalyze the rearrangement of heteroatom-substituted acetylene adducts to the vinylidene isomers. This catalytic rearrangement has, to our knowledge, not been observed previously.

In terms of mechanism, it seemed possible that the Lewis acid (e.g. H^+) coordinates to sulfur in the initiating step. The possibility of a subsequent carbon–sulfur bond cleavage, elimination of CH_3SH, and formation of

Table 2. Selected Bond Angles and Distances for $[Pd_2Cl_2(\mu\text{-dppm})_2(\mu\text{-}\sigma\text{-}C{=}C(SCH_3)_2)]$ (3)

(a) Bond Angles (deg)

Cl(1)–Pd(1)–P(1)	92.5(1)	Cl(2)–Pd(2)–P(3)	95.0(1)
Cl(1)–Pd(1)–P(2)	95.3(1)	Cl(2)–Pd(2)–P(4)	92.4(1)
Cl(1)–Pd(1)–C(1)	178.4(4)	Cl(2)–Pd(2)–C(1)	177.7(4)
P(1)–Pd(1)–P(2)	172.1(1)	P(3)–Pd(2)–P(4)	171.8(2)
P(1)–Pd(1)–C(1)	88.8(4)	P(3)–Pd(2)–C(1)	86.2(4)
P(2)–Pd(1)–C(1)	83.5(4)	P(4)–Pd(2)–C(1)	86.3(4)
Pd(1)–C(1)–Pd(2)	110.2(7)	S(1)–C(2)–S(2)	119.9(8)
Pd(1)–C(1)–C(2)	122(1)	S(1)–C(2)–C(1)	118(1)
Pd(2)–C(1)–C(2)	127(1)	S(2)–C(2)–C(1)	122(1)

(b) Distances (Å)

Pd(1)–Cl(1)	2.412(3)	Pd(2)–Cl(2)	2.401(4)
Pd(1)–P(1)	2.308(4)	Pd(2)–P(3)	2.330(4)
Pd(1)–P(2)	2.333(4)	Pd(2)–P(4)	2.302(4)
Pd(1)–C(1)	2.00(1)	Pd(2)–C(1)	1.96(1)
S(1)–C(2)	1.79(2)	S(2)–C(2)	1.76(1)
C(1)–C(2)	1.35(2)	Pd(1)···Pd(2)	3.245(1)

a σ,π-acetylide intermediate was considered. To test this possibility, the rearrangement of **1** to **3** was performed in the presence of excess EtSH and, in other experiments, excess PhSH and CH_3OH in order to attempt trapping of a σ,π-acetylide intermediate by external nucleophiles. Such a process would generate an unsymmetrical vinylidene complex by addition to the β-carbon, while readdition of CH_3SH would generate the symmetrical vinylidene complex **3**. In all cases **3** was the only reaction product. In low-temperature $^{31}P\{^1H\}$ NMR studies (CD_2Cl_2), performed at −60 °C, no evidence of a σ,π-acetylide intermediate could be found and it was not possible to characterize any other intermediate. The experimental results thus did not support the possibility of a rearrangement *via* a σ,π-acetylide formed by elimination of CH_3SH. However, for the uncatalyzed reactions of the terminal alkynes acetylene and phenylacetylene with $[Ir_2I_2(CO)(\mu\text{-}CO)(\mu\text{-dppm})_2]$ Xiao and Cowie[10] suggested that the rearrangement of the acetylene adduct to the vinylidene complex proceeded *via* a hydrido–acetylide intermediate. Previous theoretical calculations by Hoffmann and Silvestre[11] had shown that a concerted mechanism for a 1,2-hydride shift was unlikely for a binuclear complex, while the isomerization *via* an acetylide–hydride intermediate was feasible. In the present case an analogous mechanism would involve initial transfer of the SCH_3 group, presumably following protonation, from carbon to palladium. Indeed, formation of free CH_3SH is unlikely on the basis of results of experiments in the presence of added nucleophiles and the fact that the boiling point of CH_3SH is so low that free CH_3SH would be lost from solution. We note, however, that no intermediate analogous to that proposed by Xiao and Cowie was observed in low-temperature NMR studies (see above).

A CH_2Cl_2 solution of **3** was treated with $HBF_4{\cdot}Et_2O$, and a bright orange solution was obtained. The $^{31}P\{^1H\}$ NMR spectrum of the reaction solution in $CDCl_3$ exhibited a signal at 8.3 ppm (cf. **3**: 10.3 ppm). The ^1H NMR spectrum included a resonance at 1.88 ppm which was assigned to the methyl protons (cf. **3**: 1.27 ppm). The magnitude of the downfield shift was in agreement with that observed after protonation of $(CH_3)_2S$ with $HBF_4{\cdot}Et_2O$ (from 2.04 to 2.69 ppm). These data suggested that protonation occurred on the sulfur atoms

(10) Xiao, J.; Cowie, M. *Organometallics* **1993**, *12*, 463.
(11) Hoffmann, R.; Silvestre, J. *Helv. Chim. Acta* **1985**, *68*, 1461.

Scheme 1

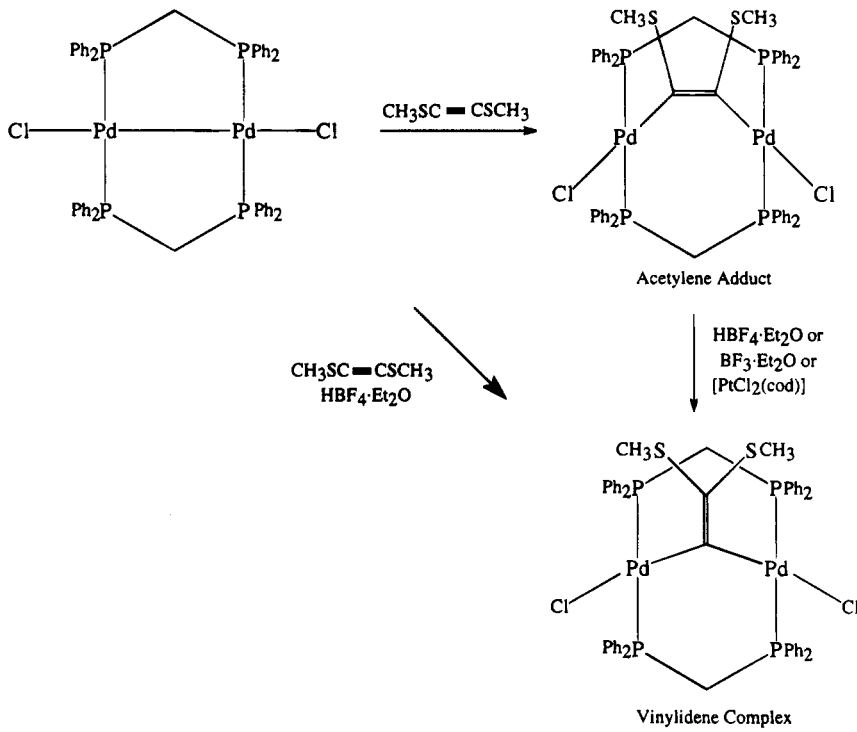

of the vinylidene moiety. Attempts to obtain crystals suitable for X-ray diffraction have thus far been unsuccessful.

Reaction of $[Pd_2Cl_2(\mu\text{-dmpm})_2(\mu\text{-}CH_3SCCSCH_3)]$ (2) with $HBF_4\cdot Et_2O$. Addition of catalytic amounts of acid led only to the recovery of **2**. However, addition of about $^1/_2$ equiv of $HBF_4\cdot Et_2O$ to **2** in CH_2Cl_2 followed by stirring for 48 h led to a change in the color of the solution from orange to yellow. The $^{31}P\{^1H\}$ NMR spectrum ($CDCl_3$) of the reaction solution showed a complex set of multiplets. Slow evaporation of the solvent CH_2Cl_2 from the reaction mixture yielded yellow crystals suitable for X-ray analysis. The isolated crystals proved to be a tetranuclear palladium complex (**4**; Figure 2). The four palladium atoms occupied a plane. Two long and two short palladium–palladium distances were found. These short metal–metal distances (Pd(1)···Pd(4) = 3.053(2) Å, Pd(2)···Pd(3) = 3.027(2) Å) were supported by two bridging chloride ligands, while the long distances (Pd(1)···Pd(3) = 3.161(1) Å, Pd(2)···Pd(4) = 3.192(2) Å) result from bridging by two dmpm ligands. The metal–metal distances for the chloro-/mercapto-bridged moieties $\{Pd_2X_4(\mu\text{-Cl})(\mu\text{-SMe})\}$ were unusually short compared with palladium–palladium separations in analogous dinuclear palladium(II) complexes (e.g. *cis*-$[Pd_2Cl_2(\mu\text{-Cl})(\mu\text{-SEt})(PMe_2Ph)_2]$,[12] 3.234(1) Å; *cis*-$[Pd_2Cl_2(\mu\text{-Cl})(\mu\text{-SMe})(PMe_3)_2]$,[13] 3.294(4)

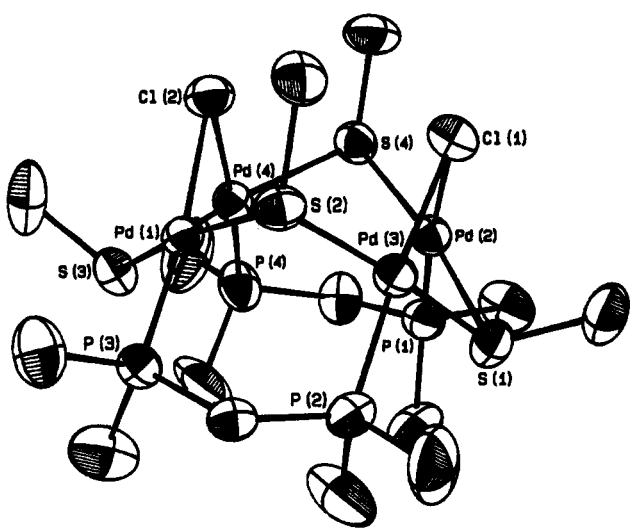

Figure 2. ORTEP diagram of $[Pd_4(\mu\text{-Cl})_2(\mu\text{-dmpm})_2(\mu\text{-}SCH_3)_4][BF_4]_2$ (**4**), showing 50% probability thermal ellipsoids.

Table 3. Selected Bond Angles and Distances for $[Pd_4(\mu\text{-Cl})_2(\mu\text{-dmpm})_2(\mu\text{-}SCH_3)_4][BF_4]_2\cdot{}^1/_2CH_2Cl_2$ ($4\cdot{}^1/_2CH_2Cl_2$)

(a) Bond Angles (deg)

Cl(2)–Pd(1)–S(2)	96.5(2)	Cl(1)–Pd(3)–S(1)	84.3(2)
Cl(2)–Pd(1)–S(3)	84.1(2)	Cl(1)–Pd(3)–S(2)	97.5(2)
Cl(2)–Pd(1)–P(3)	173.9(1)	Cl(1)–Pd(3)–P(2)	174.5(2)
S(2)–Pd(1)–S(3)	171.0(2)	S(1)–Pd(3)–S(2)	175.1(2)
S(2)–Pd(1)–P(3)	86.2(2)	S(1)–Pd(3)–P(2)	90.4(2)
S(3)–Pd(1)P(3)	94.2(2)	S(2)–Pd(3)–P(2)	87.9(2)
Cl(1)–Pd(2)–S(1)	84.2(2)	Cl(2)–Pd(4)–S(3)	84.2(2)
Cl(1)–Pd(2)–S(4)	96.6(2)	Cl(2)–Pd(4)–S(4)	96.5(2)
Cl(1)–Pd(2)–P(1)	175.3(1)	Cl(2)–Pd(4)–P(4)	174.4(1)
S(1)–Pd(2)–S(4)	171.2(1)	S(3)–Pd(4)–S(4)	173.4(2)
S(1)–Pd(2)–P(1)	92.5(2)	S(3)–Pd(4)–P(4)	92.3(2)
S(4)–Pd(2)–P(1)	87.2(2)	S(4)–Pd(4)–P(4)	87.5(2)
Pd(2)–Cl(1)–Pd(3)	77.5(1)	Pd(1)–S(2)–Pd(3)	85.4(2)
Pd(1)–Cl(2)–Pd(4)	78.7(1)	Pd(1)–S(3)–Pd(4)	81.9(1)
Pd(2)–S(1)–Pd(3)	80.6(1)	Pd(2)–S(4)–Pd(4)	86.2(2)

(b) Distances (Å)

Pd(1)···Pd(4)	3.053(2)	Pd(3)–Cl(1)	2.416(5)
Pd(1)–Cl(2)	2.407(5)	Pd(3)–S(1)	2.338(5)
Pd(1)–S(2)	2.326(5)	Pd(3)–S(2)	2.333(5)
Pd(1)–S(3)	2.333(5)	Pd(3)–P(2)	2.220(5)
Pd(1)–P(3)	2.230(5)	Pd(4)–Cl(2)	2.408(5)
Pd(2)···Pd(3)	3.027(2)	Pd(4)–S(3)	2.326(5)
Pd(2)–Cl(1)	2.418(5)	Pd(4)–S(4)	2.344(4)
Pd(2)–S(1)	2.340(6)	Pd(4)–P(4)	2.231(6)
Pd(2)–S(4)	2.326(5)	Pd(1)···Pd(3)	3.161(1)
Pd(2)–P(1)	2.244(5)	Pd(2)···Pd(4)	3.192(2)

(12) Jain, V. K.; Patel, R. P.; Muralidharan, K. V.; Bohra, R. *Polyhedron* **1989**, *8*, 2151.

Table 4. Positional Parameters and B_{eq} Values for $[Pd_2Cl_2(\mu\text{-dppm})_2(\mu\text{-}\sigma\text{-}C{=}C(SCH_3)_2)]$ (3)

atom	x	y	z	B (Å^2)[a]
Pd(1)	0.48591(5)	0.22249(5)	0.983	1.28(2)
Pd(2)	0.56674(5)	0.11507(5)	1.09281(9)	1.39(2)
Cl(1)	0.3898(2)	0.2841(2)	0.9781(3)	2.20(7)
Cl(2)	0.5710(2)	0.0439(2)	1.2229(3)	2.49(8)
S(1)	0.6889(2)	0.1496(2)	0.9447(3)	2.09(8)
S(2)	0.5960(2)	0.2168(2)	0.8136(3)	2.15(8)
P(1)	0.4404(2)	0.1395(2)	0.9032(3)	1.44(8)
P(2)	0.5453(2)	0.2994(2)	1.0607(3)	1.30(7)
P(3)	0.5281(2)	0.0399(2)	0.9885(3)	1.49(7)
P(4)	0.6108(2)	0.1965(2)	1.1774(3)	1.69(8)
C(1)	0.5669(6)	0.1737(6)	0.987(1)	1.7(3)
C(2)	0.6110(7)	0.1779(6)	0.919(1)	1.9(3)
C(3)	0.7086(7)	0.1043(7)	0.842(1)	3.2(4)
C(4)	0.6607(7)	0.2717(7)	0.794(1)	3.3(4)
C(5)	0.4930(6)	0.0718(6)	0.8822(9)	1.3(3)*
C(6)	0.6178(6)	0.2700(6)	1.1123(9)	1.5(3)
C(7)	0.3712(6)	0.1055(6)	0.962(1)	1.6(3)
C(8)	0.3506(6)	0.1282(7)	1.045(1)	2.1(3)
C(9)	0.2987(7)	0.1021(8)	1.088(1)	3.5(4)
C(10)	0.2685(7)	0.0508(7)	1.049(1)	3.1(3)*
C(11)	0.2906(7)	0.0258(7)	0.967(1)	3.3(4)
C(12)	0.3413(7)	0.0522(7)	0.920(1)	2.9(4)
C(13)	0.4105(6)	0.1583(6)	0.787(1)	1.7(3)
C(14)	0.3540(6)	0.1894(6)	0.779(1)	2.1(3)
C(15)	0.3276(7)	0.2049(7)	0.696(1)	2.2(3)*
C(16)	0.3614(7)	0.1907(7)	0.615(1)	3.3(4)
C(17)	0.4174(7)	0.1604(7)	0.625(1)	2.9(4)
C(18)	0.4426(7)	0.1452(6)	0.707(1)	1.8(3)
C(19)	0.5067(6)	0.3433(6)	1.154(1)	1.6(3)
C(20)	0.5376(7)	0.3937(6)	1.194(1)	2.1(3)
C(21)	0.5124(7)	0.4254(6)	1.271(1)	2.6(4)
C(22)	0.4553(7)	0.4035(7)	1.307(1)	2.6(3)
C(23)	0.4268(7)	0.3539(7)	1.268(1)	2.7(4)
C(24)	0.4494(6)	0.3218(6)	1.1907(9)	1.3(3)*
C(25)	0.5741(6)	0.3604(6)	0.981(1)	1.8(3)
C(26)	0.5395(6)	0.3744(6)	0.900(1)	2.0(3)
C(27)	0.5591(7)	0.4177(7)	0.837(1)	2.9(3)
C(28)	0.6160(7)	0.4486(6)	0.852(1)	2.8(4)
C(29)	0.6522(7)	0.4356(7)	0.926(1)	2.3(3)
C(30)	0.6315(6)	0.3925(6)	0.991(1)	1.7(3)
C(31)	0.5906(7)	−0.0111(6)	0.945(1)	1.9(3)
C(32)	0.6436(6)	−0.0206(7)	1.002(1)	2.4(3)
C(33)	0.5906(7)	−0.0374(6)	0.856(1)	2.9(4)
C(34)	0.6389(6)	−0.0757(6)	0.827(1)	2.4(3)
C(35)	0.6905(7)	−0.0861(8)	0.884(1)	3.7(4)
C(36)	0.6931(6)	−0.0584(7)	0.970(1)	2.7(3)
C(37)	0.4693(6)	−0.0176(6)	1.0287(9)	1.4(3)
C(38)	0.4378(7)	−0.0071(7)	1.114(1)	2.3(3)
C(39)	0.4552(6)	−0.0723(6)	0.979(1)	2.1(3)
C(40)	0.4109(7)	−0.1135(7)	1.011(1)	2.9(4)
C(41)	0.3805(7)	−0.1017(7)	1.092(1)	3.1(4)
C(42)	0.3934(7)	−0.0483(7)	1.144(1)	2.4(3)
C(43)	0.5671(7)	0.2180(7)	1.280(1)	2.0(3)
C(44)	0.5105(7)	0.1894(7)	1.300(1)	2.6(3)
C(45)	0.4744(7)	0.2062(7)	1.379(1)	3.1(4)
C(46)	0.4963(7)	0.2535(7)	1.436(1)	2.9(4)
C(47)	0.5529(7)	0.2838(8)	1.417(1)	3.1(4)*
C(48)	0.5881(7)	0.2660(6)	1.341(1)	2.3(3)
C(49)	0.6914(6)	0.1829(6)	1.217(1)	2.3(3)
C(50)	0.7438(7)	0.2092(7)	1.180(1)	2.3(3)*
C(51)	0.8026(7)	0.1963(7)	1.209(1)	3.3(4)
C(52)	0.814(1)	0.1563(9)	1.275(1)	5.6(5)*
C(53)	0.762(1)	0.131(1)	1.327(2)	10.2(8)*
C(54)	0.700(1)	0.142(1)	1.291(2)	7.2(6)*

[a] Starred values denote atoms refined isotropically. Anisotropically refined atoms are given in the form of the isotropic equivalent displacement parameter defined as $^4/_3[a^2B(1,1) + b^2B(2,2) + c^2B(3,3) + ab(\cos\gamma)B(1,2) + ac(\cos\beta)B(1,3) + bc(\cos\alpha)B(2,3)]$.

Å) but too long for palladium−palladium bonding interactions. The metal−metal distances for the dmpm-/mercapto-bridged moieties $\{Pd_2X_4(\mu\text{-dmpm})(\mu\text{-SMe})\}$ were in the range observed for related A-frame complexes containing dmpm ligands (e.g. $[Pd_2Cl_2(\mu\text{-CO})(\mu\text{-dmpm})_2]$,[14] 3.171(1) Å) and also excluded support by palladium−palladium bonding. The nearly square-planar coordination environment around each palladium center was completed by four bridging SCH_3 groups. The tetranuclear palladium complex was found to be a dication. Two BF_4^- counterions were found in

Table 5. Positional Parameters and B_{eq} Values for $[Pd_4(\mu\text{-Cl})_2(\mu\text{-dmpm})_2(\mu\text{-}SCH_3)_4][BF_4]_2 \cdot {}^1/_2CH_2Cl_2$ ($4\cdot{}^1/_2CH_2Cl_2$)

atom	x	y	z	B (Å^2)[a]
Pd(1)	0.0464(1)	0.2007(1)	0.74289(8)	3.04(3)
Pd(2)	0.4305(1)	0.0818(1)	0.83574(9)	3.32(3)
Pd(3)	0.2946(1)	−0.0295(1)	0.75654(9)	3.17(3)
Pd(4)	0.1818(1)	0.3170(1)	0.82026(9)	3.25(3)
Cl(a)	0.219	0.453	0.045	14(3)*
Cl(b)	0.002	0.589	−0.045	9(2)*
Cl(d)	0.142	0.549	−0.002	16(3)*
Cl(c)	−0.138	0.537	−0.021	7(1)*
Cl(e)	0.562	0.404	1.003	7(1)*
Cl(f)	0.314	0.639	1.038	8(1)*
Cl(g)	−0.051	0.488	−0.020	12(2)*
Cl(h)	0.187	0.469	0.020	10(2)*
Cl(1)	0.3404(4)	−0.0693(4)	0.9125(3)	4.1(1)
Cl(2)	0.0522(4)	0.2050(4)	0.8955(3)	4.1(1)
S(1)	0.4947(4)	−0.0313(4)	0.7304(3)	4.0(1)
S(2)	0.0891(4)	−0.0096(4)	0.7764(3)	3.6(1)
S(3)	0.0368(4)	0.4034(4)	0.7061(3)	3.9(1)
S(4)	0.3413(4)	0.2137(4)	0.9258(3)	3.8(1)
P(1)	0.5282(4)	0.2092(4)	0.7632(3)	3.7(1)
P(2)	0.2716(4)	0.0023(5)	0.6107(3)	4.2(1)
P(3)	0.0197(4)	0.2095(4)	0.6015(3)	3.2(1)
P(4)	0.2856(5)	0.4372(5)	0.7483(4)	5.0(1)
F(1)	0.017(2)	0.809(2)	0.649(2)	7.0(6)*
F(2)	−0.188(2)	0.830(2)	0.643(1)	6.0(5)*
F(3)	−0.071(2)	0.768(2)	0.770(2)	6.6(6)*
F(4)	−0.166(3)	0.957(3)	0.705(2)	12(1)*
F(5)	−0.115(2)	0.850(2)	0.774(2)	9.5(8)*
F(6)	−0.165(3)	0.965(3)	0.643(2)	10.4(9)*
F(7)	−0.005(2)	0.864(2)	0.633(2)	6.3(6)*
F(8)	−0.141(2)	0.769(2)	0.663(2)	7.0(6)*
F(9)	0.361(3)	0.333(3)	0.434(2)	10.8(9)*
F(10)	0.501(4)	0.399(4)	0.411(3)	16(1)*
F(11)	0.331(3)	0.548(3)	0.369(2)	9.6(8)*
F(12)	0.443(2)	0.394(2)	0.309(2)	7.0(6)*
F(13)	0.285(2)	0.424(2)	0.443(2)	8.7(7)*
F(14)	0.477(2)	0.429(2)	0.437(1)	6.0(5)*
F(15)	0.326(2)	0.549(2)	0.326(2)	8.6(7)*
F(16)	0.387(3)	0.346(3)	0.347(2)	9.8(8)*
C(1)	0.115(1)	0.071(1)	0.572(1)	3.1(4)
C(2)	0.057(1)	−0.069(2)	0.894(1)	4.9(5)
C(3)	0.552(2)	0.226(1)	0.645(1)	5.1(5)
C(4)	0.590(2)	−0.185(2)	0.786(1)	5.6(6)
C(5)	0.451(1)	0.365(1)	0.771(1)	4.6(5)
C(6)	0.674(1)	0.165(2)	0.811(1)	5.3(5)
C(7)	−0.134(1)	0.221(2)	0.584(1)	6.2(6)
C(8)	0.046(2)	0.333(2)	0.514(1)	5.9(6)
C(9)	0.289(2)	0.128(2)	1.030(1)	5.1(6)
C(10)	−0.104(2)	0.485(2)	0.756(1)	7.2(7)
C(11)	0.245(2)	0.574(2)	0.782(2)	9(1)
C(12)	0.276(2)	0.493(2)	0.631(1)	10.1(9)
C(13)	0.333(2)	−0.136(2)	0.579(2)	10.1(9)
C(14)	0.343(2)	0.104(2)	0.538(1)	8.8(8)
C(21)	0.441	0.496	1.083	0(2)*
C(22)	0.066	0.453	0.045	3(1)*
C(23)	0.018	0.487	0.019	7(5)*
B(1)	−0.102(2)	0.842(2)	0.685(2)	5.5(6)*
B(2)	0.390(2)	0.428(2)	0.388(2)	7.0(7)*

[a] Starred values denote atoms refined isotropically. Anisotropically refined atoms are given in the form of the isotropic equivalent displacement parameter defined as $^4/_3[a^2B(1,1) + b^2B(2,2) + c^2B(3,3) + ab(\cos\gamma)B(1,2) + ac(\cos\beta)B(1,3) + bc(\cos\alpha)B(2,3)]$.

(13) Padilla, E. M.; Golen, J. A.; Richmann, P. N.; Jensen, C. M. *Polyhedron* **1991**, *10*, 1343.
(14) Kullberg, M. L.; Kubiak, C. P. *Inorg. Chem.* **1986**, *25*, 26.

Scheme 2

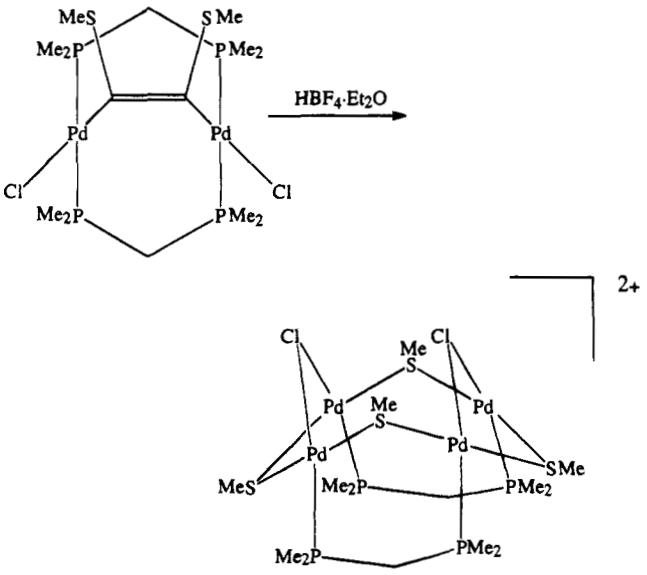

the asymmetric unit. A vinylidene complex could not be isolated from this reaction (refer to Scheme 2).

Conclusions. Our results indicated that Lewis acids not only facilitate the formation of acetylene adducts by protonation of the metal–metal bond, as described earlier,[3] but also catalyze certain 1,2-heteroatom shift reactions and the formation of vinylidene complexes. The mechanism of the isomerization is the subject of further investigation. Formation of the tetranuclear palladium complex upon treatment of **2** with $HBF_4 \cdot Et_2O$ supports the proposal that an early step in the reaction of dipalladium adducts of sulfur-substituted acetylenes with Lewis acids is C–S bond cleavage.

Acknowledgment. We are grateful to Dr. Bruce Cheesman for his assistance in the low-temperature NMR studies. The financial support of the donors of the Petroleum Research Fund, administered by the American Chemical Society, is acknowledged. X-ray facilities were provided by the College of Arts and Sciences Instrumentation Center.

Supporting Information Available: Tables of crystal data and intensity measurement and structure solution details, thermal parameters, and all bond distances and angles for **3** and **4** (16 pages). Ordering information is given on any current masthead page.

OM950135R

Structure and Bonding of the Transition Metal Methyl and Phenyl Compounds MCH_3 and MC_6H_5 (M = Cu, Ag, Au) and $M(CH_3)_2$ and $M(C_6H_5)_2$ (M = Zn, Cd, Hg)[1]

Iris Antes[†] and Gernot Frenking*

Fachbereich Chemie, Philipps-Universität Marburg, Hans-Meerwein-Strasse, D-35032 Marburg, Germany

Received February 22, 1995[⊗]

Quantum mechanical calculations of the geometries and metal–carbon bond dissociation energies using relativistic pseudopotentials with large valence basis sets for the metals are reported for MCH_3 and MC_6H_5 (M = Cu, Ag, Au) and for $M(CH_3)_2$ and $M(C_6H_5)_2$ (M = Zn, Cd, Hg). The Cu–CH_3 bond length calculated at the MP2 level is significantly shorter (1.866 Å) than predicted in most previous studies. This is due to relativistic effects, which are important for accurate calculations of the geometries of copper compounds. The calculated Ag–C(phenyl) bond length (2.091 Å) is much longer than the experimental value of the alleged silver aryl complex (1.902 Å) reported by Lingnau and Strähle (*Angew. Chem., Int. Ed. Engl.* **1988**, *27*, 436). The other theoretical bond lengths are in excellent agreement with experimental values. It seems unlikely that the measured compound is a silver aryl complex. The calculated metal–carbon dissociation energies at CCSD(T) are slightly lower than the experimental values. The calculations predict that the M–C bond strengths of the group 11 methyl and phenyl compounds have the order Au > Cu > Ag, while the group 12 elements have the order Zn > Cd > Hg. The NBO method and the topological analysis of the electron density distribution show that the metal–carbon bonds are strongly polarized toward the carbon ends. The M–C polarization decreases from the first to the second and third transition metal rows. The NBO analysis gives only one M–C bond for the $M(CH_3)_2$ and $M(C_6H_5)_2$ compounds. The M–C bonds of the latter compounds are clearly more ionic than the group 11 methyl and phenyl compounds.

1. Introduction

The ubiquitous utility of organometallic reagants for synthetic purposes stands in striking contrast to the poor knowledge about the structures and particularly the bond energies of transition metal compounds.[2] One example is the ongoing controversy about the "higher-order" and "lower-order" cuprates. Although cuprates are among the most versatile organometallic molecules in organic synthesis, the structure of the active species is still a topic of controversial discussions.[3] Another example concerns the structure of aryl–copper and aryl–silver compounds. In 1988 Lingnau and Strähle (LS) reported the first synthesis of monocoordinated Cu and Ag aryl compounds M(Ar) (M = Cu, Ag; Ar = 2,4,6-$Ph_3C_6H_2$).[4] A surprising feature of the X-ray structure analysis of the complexes was that the Cu–C and Ag–C bond lengths were nearly the same (Cu–C = 1.890 Å; Ag–C = 1.902 Å). The identification of the alleged metal complexes has recently been challenged by Haaland et al.[5] These authors reexamined the results of LS,[4] and they suggested that the observed molecules may be the bromine derivatives BrAr rather than M(Ar). They estimated that the Ag–C(aryl) bond length should be approximately 2.08 Å rather than 1.902 Å.[5] The estimate was based upon experimentally known metal–hydride and metal–chloride distances, which are 0.16–0.23 Å longer for silver than for copper.[6] Ab initio calculation of $CuCH_3$ and $AgCH_3$ predicted also that the Ag–CH_3 bond is 0.27 Å longer than the Cu–CH_3 bond.[5] This makes it highly unlikely that the Ag–C(aryl) distance is nearly as long as the Cu–C(aryl) bond.

The use of ab initio methods to obtain accurate data for the structures and properties of molecules has become a routine in the chemistry of light-atom molecules. However, there is still the belief that heavy-atom molecules, particularly transition metal complexes, cannot be calculated with the same accuracy by quantum chemical methods. This assumption is not true. Transition metal complexes can be calculated very reliably using nonlocal gradient corrected density func-

[†] Present address: Institut für Organische Chemie, Universität Zürich, Zürich, Switzerland.

(1) Theoretical Studies of Organometallic Compounds. XIV. Part XIII: Frenking, G.; Dapprich, S.; Ehlers, A. W.; Otto , M.; Vyboishchikov, S. F. Proceedings of the NATO Advanced Study Institute, Metal–Ligand Interactions: Structure and Reactivity, Cetraro, Italy, September 5–16, 1994; Russo, N., Ed.; Kluwer Academic Publishers: Amsterdam, in print.

[⊗] Abstract published in *Advance ACS Abstracts,* July 15, 1995.

(2) *Bonding Energetics in Organometallic Compounds*; Marks, T. J., Ed.; ACS Symposium Series 428; American Chemical Society: Washington, DC, 1990.

(3) (a) Lipshutz, B. H.; James, B. *J. Org. Chem.* **1994**, *59*, 7585. (b) Bertz, S. H. *J. Am. Chem. Soc.* **1990**, *112*, 4031; **1991**, *113*, 5470. (c) Stemmler, T.; Penner-Hahn, J. E.; Knochel, P. *J. Am. Chem. Soc.* **1993**, *115*, 348. (d) Stemmler, T. L.; Barnhart, T. M.; Penner-Hahn, J. E.; Tucker, C. E.; Knochel, P.; Böhme, M.; Frenking, G. Submitted for publication.

(4) Lingnau, R.; Strähle, J. *Angew. Chem.* **1988**, *100*, 409; *Angew. Chem., Int. Ed. Engl.* **1988**, *27*, 436.

(5) Haaland, A.; Rypdal, K.; Verne, H. P.; Scherer, W.; Thiel, W. R. *Angew. Chem.* **1994**, *106*, 2515; *Angew. Chem., Int. Ed. Engl.* **1994**, *33*, 2443.

(6) Huber, K. P.; Herzberg, G. *Molecular Spectra and Molecular Structure. Vol. IV: Constants of Diatomic Molecules*; Van Nostrand: New York, 1979.

0276-7333/95/2314-4263$09.00/0

tional theory (DFT)[7] or classical ab initio methods in combination with pseudopotentials.[8] It has been demonstrated in several studies of different transition metal complexes that standard ab initio methods using pseudopotentials give very accurate geometries and bond energies of heavy-atom molecules.[8,9]

We reported recently about theoretically predicted structures of cuprates.[10] In this paper we present calculated equilibrium geometries and metal–carbon bond dissociation energies of the methyl and phenyl compounds of the elements of group 11 MCH_3 and MC_6H_5 (M = Cu, Ag, Au). We also calculated the compounds $M(CH_3)_2$ and $M(C_6H_2)_2$ of group 12 elements (M = Zn, Cd, Hg). The theoretically predicted bond lengths are given at the MP2 level of theory. Bond dissociation energies are calculated at the MP2 level and using coupled-cluster theory[11] at the CCSD(T)[12] level. The bonding situation of the molecules has been examined using the natural bond orbital (NBO) partitioning scheme[13] and the topological analysis of the electron density distribution.[14]

The calculations reported here have been carried out with different pseudopotentials than in our previous studies.[8,10] The pseudopotentials developed by the group of Stoll and Preuss[15] have a much higher number of valence basis functions than the pseudopotential reported by Hay and Wadt.[16] Thus, the valence basis set for the metals in this study has TZ+P quality. Also, the pseudopotentials of group 12 elements Zn, Cd, and Hg suggested by Hay and Wadt[16b] have a large core, i.e., the $(n-1)s^2(n-1)p^6$ outermost core electrons are included in the core potentials. The Stoll/Preuss pseudopotentials for Zn, Cd, and Hg have a 20-electron valence space.[15] Another advantage of the latter pseudopotentials is that relativistic effects are included for Cu and Zn, while the Hay/Wadt pseudopotentials of the fourth row are nonrelativistic.[16] It has been shown that relativistic effects cannot be neglected for accurate calculations of the bond lengths and bond energies of Cu compounds.[17ab]

The methyl compounds $M(CH_3)_n$ of group 11 and 12 elements have been investigated previously by several groups.[17bc,18–23] There are no ab initio studies of the phenyl compounds $M(C_6H_5)_n$ known to us. The geometry of $Hg(C_6H_5)_2$ has been optimized using MNDO.[24]

2. Computational Methods

The geometries of the molecules have been optimized at the Hartree–Fock (HF) and MP2 (Møller–Plesset perturbation theory terminated at second order)[25] levels of theory. For the geometry optimizations an all-electron 6-31G(d) basis set was used for carbon and hydrogen.[26] Relativistic pseudopotentials were employed for the metals.[15] The $(n-1)s^2(n-1)p^6(n)s^2(n-1)d^x$ electrons of the metals are calculated explicitly. This means that the group 11 elements Cu, Ag, and Ag have 19 valence electrons and that the group 12 elements Zn, Cd, and Hg have 20 valence electrons. A large basis set [311111/22111/411] has been used for the valence electrons.[15] This basis set combination is denoted as basis set I.

Improved total energies were calculated for the methyl compounds using coupled-cluster theory[11] with single and double excitations and a noniterative estimate of the triple excitations CCSD(T).[12] For the latter calculations a 6-31+G(d) basis set is used for carbon and hydrogen.[27] The valence basis set I of the metals is augmented by a set of *f*-type polarization functions.[28] This basis set combination is denoted as basis set II. The total energies of the phenyl compounds of Cu, Ag, and Au were also calculated at the CCSD(T) level using basis sets augmented by a set of *f*-type functions at the metals, but only 6-31G(d) at the other atoms. The total energies of the diphenyl compounds of Zn, Cd, and Hg are given at MP2/I. The vibrational frequencies and zero-point energies (ZPE) were calculated at HF/I. The ZPE corrections are scaled by a factor of 0.89.[29] All structures reported here are minima on the potential energy surface, i.e., the eigenvalues of the Hessian matrix are all positive.

The calculations have been carried out using the program packages Gaussian 92,[30] Turbomole,[31] and ACES II.[32] For the

(7) Li, J.; Schreckenbach, G.; Ziegler, T. *J. Am. Chem. Soc.* **1995**, *117*, 486.
(8) Review: Frenking, G.; Antes, I.; Böhme, M.; Dapprich, S.; Ehlers, A. W.; Jonas, V.; Neuhaus, A.; Otto, M.; Stegmann, R.; Veldkamp, A.; Vyboishchikov, S. F. In *Reviews in Computational Chemistry*; Vol. 7, Lipkowitz, K. B., Boyd, D. B. Eds.; VCH: New York, in press.
(9) (a) Ehlers, A. W.; Frenking, G. *J. Am. Chem. Soc.* **1994**, *116*, 1514. (b) Veldkamp, A.; Frenking, G. J. *Am. Chem. Soc.* **116**, 4937 (1994). (c) Neuhaus, A.; Veldkamp, A.; Frenking, G. *Inorg. Chem.* **1994**, *33*, 5278. (d) Dapprich, S.; Frenking, G. *Angew. Chem.* **1995**, *107*, 383; *Angew. Chem., Int. Ed. Engl.* **1995**, *34*, 354.
(10) Böhme, M.; Frenking, G.; Reetz, M. T. *Organometallics* **1994**, *13*, 4237.
(11) Cizek, J. *J. Chem. Phys.* **1966**, *45*, 4256.
(12) (a) Pople, J. A.; Krishnan, R.; Schlegel, H. B.; Binkley, J. S. *Int. J. Quantum Chem.* **1978**, *14*, 545. (b) Bartlett, R. J.; Purvis, G. D. *Ibid.* **1978**, *14*, 561. (c) Purvis , G. D.; Bartlett, R. J. *J. Chem. Phys.* **1982**, *76*, 1910. (d) Raghavachari, K.; Trucks, G. W.; Pople, J. A.; Head-Gordon, M. *Chem. Phys. Lett.* **1989**, *157*, 479. (e) Bartlett, R. J. Watts, J. D.; Kucharski, S. A.; Noga, J. *Ibid.* **1990**, *165*, 513.
(13) Reed, A. E.; Curtiss, L. A.; Weinhold, F. *Chem. Rev.* **1988**, *88*, 899.
(14) Bader, R. F. W. *Atoms in Molecules: A Quantum Theory*; Oxford University Press: Oxford, 1990.
(15) (a) Dolg, M.; Wedig, U.; Stoll, H.; Preuss, H. *J. Chem. Phys.* **1987**, *86*, 866. (b) Andrae, D.; Häussermann, U.; Dolg, M.; Stoll, H.; Preuss, H. *Theor. Chim. Acta* **1990**, *77*, 123.
(16) (a) Hay, P. J.; Wadt, W. R. *J. Chem. Phys.* **1985**, *82*, 299. (b) Hay, P. J.; Wadt, W. R. *J. Chem. Phys.* **1985**, *82*, 270.
(17) (a) Barnes, L. A.; Rosi, M.; Bauschlicher, C. W. *J. Chem. Phys.* **1990**, *93*, 609. (b) Bauschlicher, C. W.; Langhoff, S. R.; Partridge, H.; Barnes, L. A. *J. Chem. Phys.* **1989**, *91*, 2399. (c) Sodupe, M.; Bauschlicher, C. W.; Lee, T. J. *Chem. Phys. Lett.* **1992**, *189*, 266.
(18) (a) Schwerdtfeger, P.; Boyd, P. D. W.; Burrell, A. K.; Robinson, W. T.; Taylor, M. T. *Inorg. Chem.* **1990**, *29*, 3593. (b) Schwerdtfeger, P. *J. Am. Chem. Soc.* **1990**, *112*, 2818. (c) Schwerdtfeger, P.; Boyd, P. D. W.; Brienne, S.; McFeathers, J. S.; Dolg, M.; Liao, M.-S.; Schwarz, W. H. E. *Inorg. Chim. Acta* **1993**, *213*, 233.
(19) Kippels, C.; Thiel, W.; McKean, D. C.; Coats, A. M. *Spectrochim. Acta* **1992**, *48A*, 1067.
(20) Reinhold, J.; Steinfeld, N.; Schüler, M.; Steinborn, D. *J. Organomet. Chem.* **1992**, *425*, 1.
(21) Ziegler, T.; Tschinke, V.; Becke, A. *J. Am. Chem. Soc.* **1987**, *109*, 1351.
(22) (a) Chen, H.; Krasowski, M.; Fitzgerald, G. *J. Chem. Soc.* **1993**, *98*, 8710. (b) Sosa, C.; Andzelm, J.; Elkin, B. C.; Wimmer, E.; Dobbs, K. D.; Dixon, D. A. *J. Phys. Chem.* **1992**, *96*, 6630. (c) Kaupp, M.; Stoll, H.; Preuss, H. *J. Comput. Chem.* **1990**, *11*, 1029. (d) Jayatilaka, D.; Amos, R. D.; Koga, N. *Chem. Phys. Lett.* **1989**, *163*, 151.
(23) Almenningen, A.; Helgaker, T. U.; Haaland, A.; Samdal, S. *Acta Chem. Scand.* **1982**, *A36*, 159.
(24) Rhodes, C. J.; Glidewell, C.; Agirbas, H. *J. Chem. Soc., Faraday Trans.* **1991**, *87*, 3171.
(25) (a) Møller, C.; Plesset, M. S. *Phys. Rev.* **1934**, *46*, 618. (b) Binkley, J. S.; Pople, J. A. *Int. J. Quantum Chem.* **1975**, *9*, 229.
(26) (a) Hehre, W. J.; Ditchfield, R.; Pople, J. A. *J. Chem. Phys.* **1971**, *56*, 2257. (b) Hariharan, P. C.; Pople, J. A. *Theor. Chim. Acta* **1973**, *28*, 213.
(27) Clark, T.; Chandrasekhar, J.; Spitznagel, G. W.; Schleyer, P. v. R. *J. Comput. Chem.* **1983**, *4*, 294.
(28) The exponents for the *f* functions are: $f_{Cu} = 1.3375$; $f_{Ag} = 1.3375$; $f_{Au} = 1.1447$; $f_{Zn} = 1.500$; $f_{Cd} = 1.500$; $f_{Hg} = 1.500$.
(29) Hout, R. F.; Levi, B. A.; Hehre, W. J. *J. Comput. Chem.* **1982**, *3*, 234.
(30) *Gaussian 92, Revision C*; Frisch, M. J.; Trucks, G. W.; Head-Gordon, M.; Gill, P. M. W.; Wong, M. W.; Foresman, J. B.; Johnson, B. G.; Schlegel, H. B.; Robb, M. A.; Replogle, E. S.; Gomperts, R.; Andres, J. L.; Raghavachari, K.; Binkley, J. S.; Gonzalez, C.; Martin, R. L.; Fox, D. J.; Defrees, D. J.; Baker, J.; Stewart, J. J. P.; Pople, J. A. Gaussian, Inc.: Pittsburgh, PA, 1992.

Table 1. Calculated and Experimental Metal–C Bond Lengths (Å) of Group 11 and 12 Methyl and Phenyl Compounds

molecule	sym	our HF/I	our MP2/I	other	exptl
$CuCH_3$	C_{3v}	1.970	1.866	1.936;[c] 1.921;[g] 1.923;[j] 1.86[h]	
$Cu(CH_3)_2^-$	D_{3h}	2.019	1.922	1.917;[i] 1.927;[i] 1.963[j]	1.935[a]
$AgCH_3$	C_{3v}	2.180	2.111	2.146;[c] 2.06[h]	
$AuCH_3$	C_{3v}	2.077	2.017	2.190[d]	
CuC_6H_5	C_{2v}	1.960	1.850		
AgC_6H_5	C_{2v}	2.165	2.091		
AuC_6H_5	C_{2v}	2.049	1.981		
$Zn(CH_3)_2$	D_{3h}	1.979	1.925	1.912;[i] 1.910;[e] 1.940[k]	1.928[b]
$Cd(CH_3)_2$	D_{3h}	2.162	2.123	2.119;[i] 2.123[e]	2.110[b]
$Hg(CH_3)_2$	D_{3h}	2.135	2.104	2.080[f]	2.093[b]
$Zn(C_6H_5)_2$	D_{2d}	1.963	1.914		
$Cd(C_6H_5)_2$	D_{2d}	2.143	2.110		
$Hg(C_6H_5)_2$	D_{2d}	2.112	2.085		2.092[l]

[a] Reference 34. [b] Reference 35. [c] MCPF level, ref 17b. [d] HF level, ref 18a. [e] DFT level, ref 22a. [f] MP2 level, ref 18c. [g] CCSD(T) level, ref 17c. [h] DFT level, ref 21. [i] DFT level, ref 22b. [j] MP2 level, ref 10. [k] CISD level, ref 22c. [l] Reference 41.

Table 2. Calculated and Experimental Metal–C Bond Dissociation Energies D_e and D_o[i] (kcal/mol) of Group 11 and 12 Methyl and Phenyl Compounds. Geometries are Optimized at MP2/I (see Table 1)

molecule	sym	HF/II[a] D_e	MP2/II[a] D_e	MP2/II[a] D_o	CCSD(T)/II[a] D_e	CCSD(T)/II[a] D_o	other D_e	exptl D_o
$CuCH_3$	C_{3v}	14.6	58.7	55.5	52.1	48.9	48.4;[e] 56.9[h]	53.3[b]
$AgCH_3$	C_{3v}	7.2	43.1	39.9	40.8	37.6	36.2;[e] 42.3[h]	
$AuCH_3$	C_{3v}	18.0	62.5	58.6	58.1	54.0	11.3[f]	
CuC_6H_5[a]	C_{2v}	24.9	74.0	72.2	65.1	63.3		
AgC_6H_5[a]	C_{2v}	17.0	58.3	56.7	53.8	52.2		
AuC_6H_5[a]	C_{2v}	26.3	80.2	78.2	72.4	70.4		
$Zn(CH_3)_2$[d]	D_{3h}	47.4	90.4	83.1	81.1	73.8		84.8[c]
$Cd(CH_3)_2$[d]	D_{3h}	33.6	73.8	66.7	67.8	60.7		67.2[c]
$Hg(CH_3)_2$[d]	D_{3h}	23.9	66.6	58.7	60.5	52.6	58.7[g]	57.9[c]
$Zn(C_6H_5)_2$[d]	D_{2d}	70.6	123.2	118.9				
$Cd(C_6H_5)_2$[d]	D_{2d}	55.3	109.2	105.2				
$Hg(C_6H_5)_2$[d]	D_{2d}	45.1	103.3	99.0				75.3[c]

[a] The 6-31G(d) basis set is used for the phenyl compounds of Cu, Ag, and Au. For the diphenyl compounds of Zn, Cd, and Hg basis set I is employed. [b] Reference 39. [c] Taking the differences of the heats of formation, reference 38. [d] Dissociation energy with respect to both methyl and phenyl groups, respectively. [e] MCPF level, ref 17b. [f] HF level, ref 18a. [g] MP2 level, ref 18c. [h] DFT level, ref 21. [i] The D_o values include the ZPE corrections.

topological analysis of the electron density distribution the programs GRID, CONTOUR, SADDLE, and GRDVEV were employed.[33]

3. Results and Discussion

Table 1 shows the theoretically predicted and experimentally observed metal–carbon bond lengths. The M–C bond dissociation energies are shown in Table 2.

The calculated $Cu-CH_3$ bond length at MP2/I (1.866 Å) is significantly shorter than the previously reported distances at the MCPF level (1.936 Å)[17b] and at CCSD(T) (1.921 Å).[17c] It is also shorter than the MP2 value (1.923 Å) given in our earlier study.[10] Because the basis sets in these studies[17b,c] were rather large, it can be ruled out that the differences are due to basis set effects. However, the latter three values have been obtained without the consideration of relativistic effects, while the present value was calculated with a relativistic pseudopotential.[15] Previous calculations gave Cu^+-CO bond lengths of $CuCO^+$ $r = 1.985$ Å (nonrelativistic) and 1.941 Å (relativistic).[17a] It has also been shown that relativistic effects increase the $Cu-CH_3$ bond energy by 3 kcal/mol.[17b] The present study suggests that the $Cu-CH_3$ interatomic distance is significantly influenced by relativistic contributions. It should be pointed out that a previous DFT calculation[21] gave a $Cu-CH_3$ bond length of 1.86 Å, which agrees with our value (1.866 Å). The short DFT value for the $Cu-CH_3$ distance is due to a fortuitous error cancellation. The DFT calculation was carried out using a local nonrelativistic functional.[21] Nonlocal corrections would make the bond longer, and relativity would contract it.

The conclusion about the importance of relativistic contributions is supported by the calculated Cu–C bond distance of dimethyl cuprate, $Cu(CH_3)_2^-$. The experimental value for the Cu–C bond length is 1.935 Å.[34] Our previously reported value given by a nonrelativistic MP2 calculation is 1.963 Å.[10] The relativistic MP2/I value given here is 1.922 Å, which is in good agreement with experiment. The DFT results for $Cu(CH_3)_2^-$ are very similar to our data (Table 1).

The calculated MP2/I values for the M–C bond lengths of $AgCH_3$ (2.111 Å) and $AuCH_3$ (2.017 Å) are shorter than calculated before at the MCPF level for $AgCH_3$ (2.146 Å)[17b] and at the HF level for $AuCH_3$ (2.190 Å).[18a] The DFT value for the $Au-CH_3$ bond distance is shorter (2.06 Å)[21] than given here. A local functional including relativistic effects was employed for the latter calculation.[21] Nonlocal corrections would yield a longer $Au-CH_3$ bond, which would be in agreement with the MP2 value reported here. Table 1 shows that the M–C bond lengths of the $M(CH_3)_2$ molecules (M = Zn, Cd, Hg) predicted at MP2/I are in excellent agreement with the experimental data. The experimental values have been taken from an IR spectroscopic study.[35] Other experimental values using IR or electron diffraction are nearly the same as those given in Table 1.[23,36] Because of the good agreement between the MP2/I values and the experimental data for the M–C distances of the $M(CH_3)_2$ compounds, we believe that the theoretical values for the $Cu-CH_3$, $Ag-CH_3$, and $Au-CH_3$ bond lengths calculated at MP2/I should be accurate within ±0.02 Å.

The calculated $Cu-C_6H_5$ and $Ag-C_6H_5$ bond lengths at MP2/I are very interesting because of the controversy[5] about the synthesis of the copper and silver aryl complexes reported by Lingnau and Strähle.[4] The calculations predict that the Cu–C(phenyl) bond length is 1.850 Å. The calculated Ag–C(phenyl) bond length is 2.091 Å. The former value is in reasonable agreement with the experimental Cu–C(phenyl) bond length re-

(31) (a) Häser, M.; Ahlrichs, R. *J. Comput. Chem.* **1989**, *10*, 104. (b) Ahlrichs, R.; Bär, M.; Häser, M.; Horn, H.; Kölmel, C. *Chem. Phys. Lett.* **1989**, *162*, 165. (c) Horn, H.; Weiss, H.; Häser, M.; Ehrig, M.; Ahlrichs, R. *J. Comput. Chem.* **1991**, *12*, 1058. (d) Häser, M.; Almlöf, J.; Feyereisen, M. W. *Theor. Chim. Acta* **1991**, *79*, 115.

(32) *ACES II, an ab initio program system*; Stanton, J. F.; Gauss, J.; Watts, J. D.; Lauderdale, W. J.; Bartlett, R. J. University of Florida: Gainesville, FL, 1991.

(33) Biegler-König, F. W.; Bader, R. F. W.; Ting-Hua, T. *J. Comput. Chem.* **1982**, *3*, 317.

(34) Hope, H.; Olmstaed, M. M.; Power, P. P.; Sandell, J.; Xu, X. *J. Am. Chem. Soc.* **1985**, *107*, 4337.

(35) McKean, D. C.; McQuillan, G. P.; Thompson, D. W. *Spectrochim. Acta* **1980**, *36A*, 1009.

(36) (a) Kasiwabara, K.; Konakan, S.; Iijima, T.; Kimura, M. *Bull. Chem. Soc. Jap.* **1973**, *46*, 407. (b) McKean, D. C.; Duncan, J. L.; Batt, L. *Spectrochim. Acta* **1973**, *29A*, 1037. (c) Rao, S.; Stroicheff, B. P.; Turner, R. *Can. J. Phys.* **1960**, *38*, 1516.

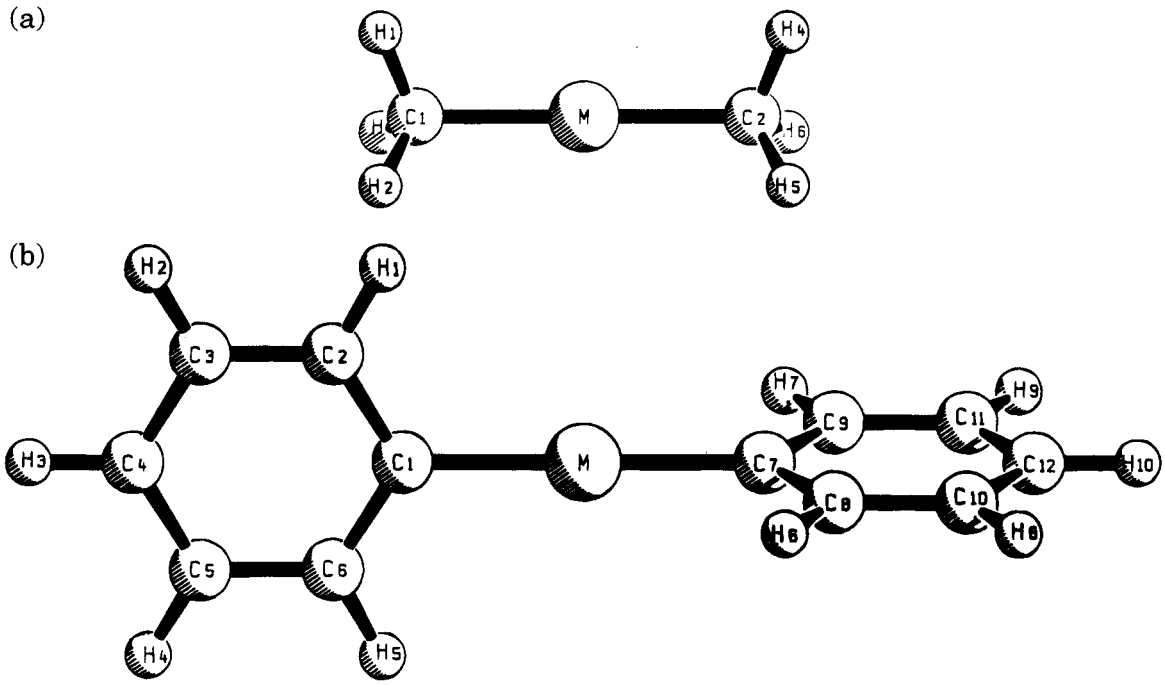

Figure 1. Calculated lowest energy conformations of (a) $M(CH_3)_2$ (M = Zn, Cd, Hg) and (b) $M(C_6H_5)_2$ (M = Zn, Cd, Hg).

ported by LS (1.890 Å). The calculated Ag–C(phenyl) distance at MP2/I is much longer, however, than the value reported by LS (1.902 Å). Because of the good agreement of the other calculated metal–carbon bond lengths at MP2/I with experimental values shown in Table 1, we think that the bond distance reported by LS refers to a different compound. The calculated results support the suggestion of Haaland et al.[5] that the complex observed by LS is not a silver–aryl complex. It should be noted that the calculated Ag–C_6H_5 bond length at MP2/I is in excellent agreement with the estimate made by Haaland et al. for a silver–aryl bond length (2.08 Å).[5] The calculations predict that the metal–C(phenyl) bond lengths of the group 11 and 12 metals are 0.01–0.03 Å shorter than the respective metal–C(methyl) bond lengths (Table 1). The MP2/I result for the Hg–C distance of $Hg(C_6H_5)_2$ (2.085 Å) is in excellent agreement with the experimental value (2.092 Å),[41] while a previously reported MNDO value is somewhat too short (2.002 Å).[24]

The dimethyl compounds have been calculated with staggered (D_{3d}) and eclipsed (D_{3h}) conformations. The D_{3h} form was in all cases more stable than the D_{3d} form. However, the energy differences were very low at all levels of theory (<0.05 kcal/mol). This indicates nearly free rotation around the M–methyl bonds. The instantaneous symmetry of $M(CH_3)_2$ (M = Zn, Cd, Hg) and $Cu(CH_3)_2^-$ is D_3. This is in agreement with several experimental studies of these molecules which made it clear that the barrier of internal rotation is negligible.[37] The calculations predict that in the diphenyl compounds the phenyl rings are orthogonal to each other (D_{2d} symmetry, Figure 1).

The M–C bond dissociation energies are shown in Table 2. The energies refer to the dissociation into the metal atoms in the electronic ground state (^2S for Cu, Ag, and Au; ^1S for Zn, Cd, and Hg) and the methyl and phenyl radicals, respectively. The experimental values for the dissociation energies of $M(CH_3)_2$ (M = Zn, Cd, Hg) and $Hg(C_6H_5)_2$ have been derived from the heats of formation of the fragments.[38] The theoretically predicted bond energies at CCSD(T)/II//MP2/I are higher than in previous theoretical studies except the DFT calculations,[21] but they are still lower than experimentally observed. The DFT results have been obtained using local DFT theory, which tends to overestimate the bond strength. On the other hand, relativistic effects are not included in the DFT calculations. Because relativistic effects increase the Cu–CH_3 bond strength,[17b] the DFT value for the dissociation energy is subject to a fortuitous error cancellation. For $M(C_6H_5)_2$ (M = Zn, Cd, Hg) the dissociation energies could only be calculated at MP2/I because of the size of the molecules.

The theoretical dissocation energies predicted at the MP2/II level are higher than at CCSD(T)/II (Table 2). The D_0 values for the methyl compounds at MP2/II are in very good agreement with experiment. We think that this is fortuitous. The dissociation energy for $Hg(C_6H_5)_2$ predicted at MP2/I is clearly too high (Table 2). We want to point out that the trend of the bond energies among the different series is the same for the MP2 and CCSD(T) results. Because the calculated differences of the bond energies appear to be quite reliable among a series, the MP2/I results for the $M(C_6H_5)_2$ compounds may be used to estimate the dissociation energies for M = Zn and Cd. Using the experimental D_0 value of $Hg(C_6H_5)_2$ as reference data, the MP2/I calculations predict that D_0 of $Cd(C_6H_5)_2$ should be ~81 kcal/mol and D_0 of $Zn(C_6H_5)_2$ should be ~95 kcal/mol.

It is interesting to note that the calculations predict for the bond strength of the methyl and phenyl com-

(37) (a) Boyd, D. R. J.; Thompson, H. W.; Williams, R. L. *Discuss. Faraday Soc.* **1950**, *9*, 154. (b) Butler, I. S.; Newbury, M. L. *Spectrochim. Acta* **1977**, *A33*, 699 and references therein.

(38) The heat of formation at 298 K was used. In order to calculate D_0 values at 0 K, the differences of DH_f were taken. In addition, the differences in the number of degrees of freedom of translational (3 pV = 1.8 kcal/mol) and rotational motion (1.5 pV = 0.9 kcal/mol) plus the work term (2 pV = 1.2 kcal/mol) were taken. The corrections refer to the loss of two groups. Lias, S. G.; Bartmess, J. E.; Liebman, J. F.; Holmes, J. L.; Levin, R. D.; Mallard, W. G. *J. Phys. Chem. Ref. Data* **1988**, *17* (Suppl. 1).

Table 3. Calculated and Experimental First and Second Metal–CH_3 Bond Dissociation Energies D_e and D_o (kcal/mol) of $M(CH_3)_2$ (M = Zn, Cd, Hg). Geometries are Optimized at MP2/I (see Table 1)

molecule	diss.	HF/II D_e	MP2/II D_e	CCSD(T)/II D_e	CCSD(T)/II D_o	exptl D_o
$Zn(CH_3)_2$	first	43.9	75.1	70.0	65.9	68.0[a]
$Zn(CH_3)_2$	second	3.5	15.3	11.2	8.2	16.6[b]
$Cd(CH_3)_2$	first	34.6	64.6	60.3	56.2	
$Cd(CH_3)_2$	second	−1.0	9.2	7.5	4.5	
$Hg(CH_3)_2$	first	35.2	66.1	60.9	56.0	51.6[c]
$Hg(CH_3)_2$	second	−11.3	0.5	−0.4	−3.4	7.0[c]

[a] Reference 40. [b] Reference 39. [c] Taking the differences of the heats of formation, ref 38.

Table 4. Results of the NBO Analysis for the Metal–C Bonds and Partial Charges q at MP2/I[a]

molecule	occ	%M	%s(M)	%p(M)	%d(M)	BO	q(M)	q(C)
$CuCH_3$	2.000	21.5	94.7	0.3	5.0	0.68	+0.58	−1.22
$AgCH_3$	2.000	25.9	94.1	0.9	5.0	0.78	+0.49	−1.13
$AuCH_3$	2.000	38.1	84.6	0.3	16.1	0.96	+0.26	−0.93
CuC_6H_5	1.963	19.3	95.1	0.3	4.6	0.62	+0.62	−0.50
AgC_6H_5	1.954	19.6	95.5	2.1	2.4	0.61	+0.60	−0.45
AuC_6H_5	1.974	34.7	83.5	0.2	16.3	0.91	+0.33	−0.29
$Zn(CH_3)_2$[b]	1.997	20.0	95.9	1.5	2.6	0.46	+1.33	−1.33
$Cd(CH_3)_2$[b]	1.996	22.7	93.9	1.5	4.6	0.49	+1.26	−1.29
$Hg(CH_3)_2$[b]	1.995	29.2	86.9	1.1	12.0	0.52	+1.10	−1.22
$Zn(C_6H_5)_2$[b]	1.967	17.8	96.8	0.7	2.5	0.43	+1.38	−0.65
$Cd(C_6H_5)_2$[b]	1.965	19.9	94.8	0.7	4.5	0.45	+1.33	−0.60
$Hg(C_6H_5)_2$[b]	1.970	26.8	87.6	0.4	12.0	0.50	+1.16	−0.54

[a] Occ gives the occupancy of the M–C natural bond orbital; %M gives the metal part of the M–C bond; %s(M), %p(M), and %d(M) give the hybridization of the M–C bond at the metal end; BO gives the Wiberg bond order; q(M) and q(C) give the atomic partial charges of the metal and the carbon atom of the M–C bond. [b] The NBO analysis gives only one M–C bond.

pounds of group 11 elements the order Au > Cu > Ag. A different order is calculated for the first, second, and third row transition metal (TM) elements of group 12. Here, the bond strength of the dimethyl and diphenyl compounds decreases with the order Zn > Cd > Hg. Thus, the third row TM element of group 11 has the strongest bond, while the third row TM element of group 12 has the weakest bonds (Table 2). This is in agreement with the experimental values for the dissociation energies of the dimethyl compounds of Zn, Cd, and Hg (Table 2).

We calculated also the first and second M–CH_3 dissociation energies of the dimethyl compounds $M(CH_3)_2$ (M = Zn, Cd, Hg). The results are shown in Table 3. The calculations predict that the first dissociation energy is much higher than the second. This is in agreement with experimental studies of $Zn(CH_3)_2$ and $Hg(CH_3)_2$.[38–40] The calculations suggest that $HgCH_3$ is hardly bound.

We analyzed the bonding situation of the metal–alkyl and metal–aryl compounds using the NBO method.[13] The results are shown in Table 4. The metal–carbon bonds of $CuCH_3$, $AgCH_3$, and $AuCH_3$ are polarized toward the carbon end. The polarization decreases with the order Cu > Ag ≫ Au. The NBO analysis suggests that in the methyl compounds the Au–C bond is clearly more covalent than the Ag–C and Cu–C bond. This becomes evident by the calculated polarization given by %M, the Wiberg bond order, BO, and the partial charges at the metal atoms (Table 4). The metal–C bonds have nearly pure s-character at the metals with very little d-contribution. This holds also for the phenyl compounds of Cu, Ag, and Au. The polarization of the M–C bonds toward the carbon end is higher, however, for the phenyl compounds than for the methyls. This is reasonable, because the latter molecules have sp^2 carbon atoms, while in the methyl compounds the carbon atoms are sp^3 hybridized.

The NBO analysis gives only one metal–carbon bond orbital for the dimethyl and diphenyl compounds of Zn, Cd, and Hg. This means that the best Lewis structure of these molecules should be written in mesomeric forms:

$$H_3C{-}M^+\ CH_3^- \leftrightarrow H_3C^-\ M^+{-}CH_3$$

The calculated atomic partial charges at the metal atoms of the dimethyl and diphenyl compounds of group 12 elements are significantly higher (>1.0) than those of the group 11 elements. The polarization of the M–C bond toward the carbon end of the group 12 elements (only one bond) is even higher than for the group 11 molecules. This indicates that the group 12 dimethyl and diphenyl compounds are more ionic and less covalent than the group 11 methyl and phenyl compounds. The polarization of the M–C bonds toward carbon has the order Zn > Cd ≫ Hg. The hybridization at the metal atoms has, in all cases, dominantly s-character of the M–C bonds and very little d-contribution, which is a little higher for the Au and Hg compounds than for the other molecules.

The polar character of the metal–carbon bond is also revealed by the Laplacian of the electron density distribution, $\nabla^2\rho(\mathbf{r})$. Figure 2 shows the contour line diagrams of $\nabla^2\rho(\mathbf{r})$ for $AuCH_3$, AuC_6H_5, $Hg(CH_3)_2$, and $Hg(C_6H_5)_2$. The difference of the shape of the Laplacian distribution of the M–C and C–H bonds reflects the different nature of the bonds. The C–H bonds exhibit a continuous area of charge concentration ($\nabla^2\rho(\mathbf{r}) < 0$, solid lines), while the charge concentration of the M–C bonds is localized at the carbon ends. The Laplacian distributions of the other molecules are very similar and, therefore, are not shown here.

4. Summary

The theoretically predicted geometries at the MP2/I level of theory for the methyl and phenyl compounds MCH_3 and MC_6H_5 (M = Cu, Ag, Au), $Cu(CH_3)_2^-$, and $M(CH_3)_2$ and $M(C_6H_5)_2$ (M = Zn, Cd, Hg) are in very good agreement with available experimental values. The relativistic effect upon the Cu–C bond length is remarkable. The calculated value using relativistic pseudopotentials at MP2/I is clearly shorter (1.866 Å) than in most previous studies. The calculated Ag–C_6H_5 bond length is significantly longer than the Ag–C distance of the silver–aryl complex reported by Lingnau and Strähle.[4] It is highly unlikely that the measured complex is really a silver compound. The theoretical metal–carbon bond dissociation energies calculated at the CCSD(T)/II level are slightly lower than experimental data. The calculated M–C bond strengths of the

(39) (a) Armentrout, P. B.; Kickel, B. L. *Organometallic Ion Chemistry*; Freiser, S. B., Ed.; Kluwer: Dordrecht, in press. (b) P. Armentrout, personal communication, 1994.
(40) McMillan, D. F.; Golden, D. M. *Ann. Rev. Phys. Chem.* **1982**, *33*, 493.
(41) Vilkov, L. V.; Anashkin, M. G.; Mamaeva, G. I. *J. Struct. Chem. USSR* **1968**, 372.

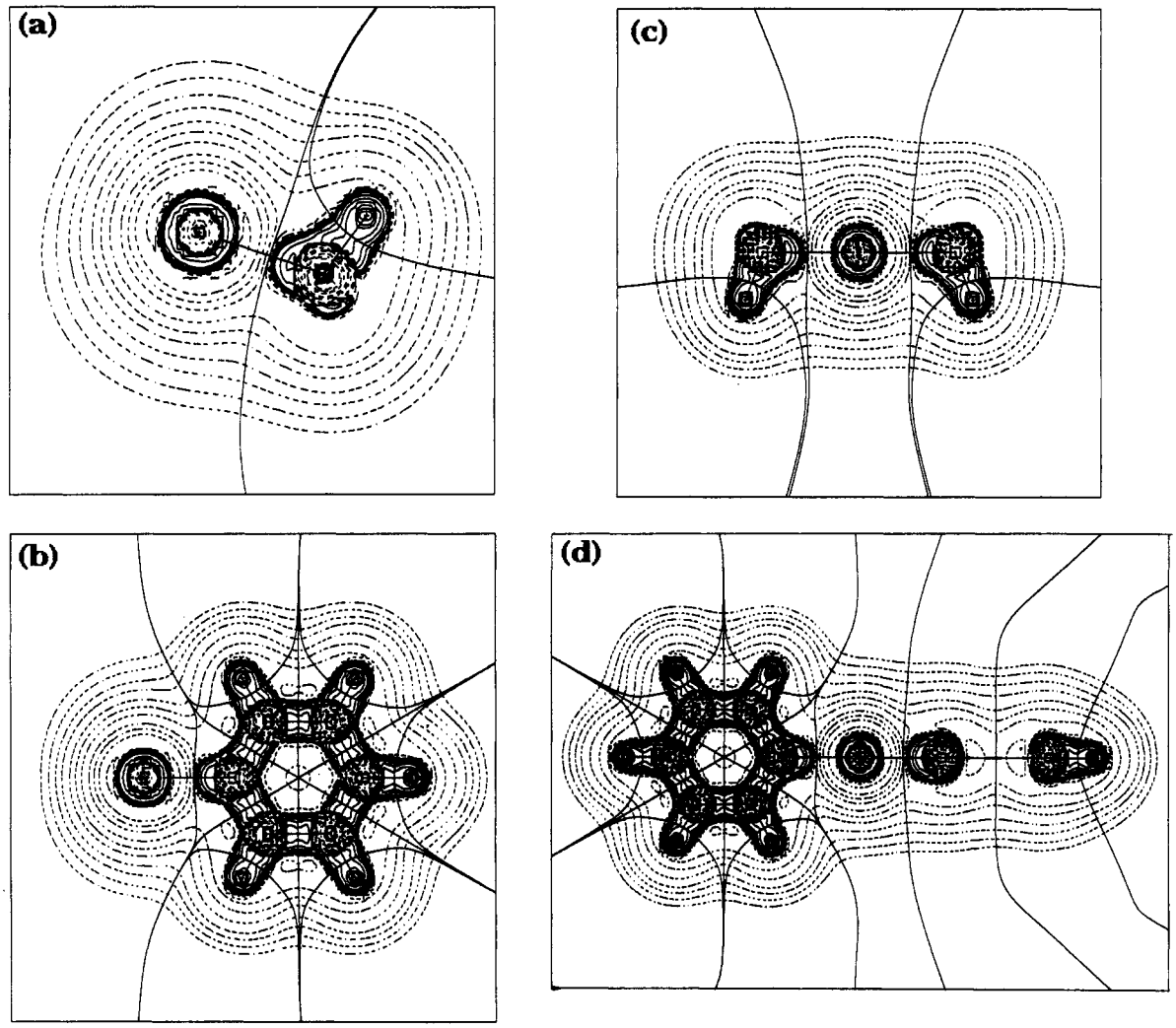

Figure 2. Contour line diagrams of the Laplacian distribution $\nabla^2\rho(\mathbf{r})$ at MP2/I for (a) $AuCH_3$, (b) AuC_6H_5, (c) $Hg(CH_3)_2$, and (d) $Hg(C_6H_5)_2$. Dashed lines indicate charge depletion ($\nabla^2\rho(\mathbf{r}) > 0$), and solid lines indicate charge concentration ($\nabla^2\rho(\mathbf{r}) < 0$). The solid lines connecting the atomic nuclei are the bond paths, the solid lines separating the atomic nuclei indicate the zero-flux surfaces in the plane. The crossing points of the bond paths and zero-flux surfaces are the bond critical points, $\mathbf{r}_b$.

methyl and phenyl compounds have the order Au > Cu > Ag for the group 11 elements. The order for the group 12 elements is Zn > Cd > Hg.

The analysis of the bonding situation indicates that the metal–carbon bonds are polarized toward the carbon end. The polarization shows the TM order first row > second row ≫ third row. The dimethyl and diphenyl compounds of Zn, Cd, and Hg have metal–C bonds which are more ionic than the methyl and phenyl compounds of Cu, Ag, and Au. The best Lewis structure of the former compounds has mesomeric forms with only one M–C bond. The atomic partial charges at Zn, Cd, and Hg are clearly larger than at Cu, Ag, and Au. The metal part of the M–C bonds has mainly s-character.

Acknowledgment. We thank Prof. Tom Ziegler for helpful information concerning the DFT calculations reported in ref 21. This work has been supported by the Deutsche Forschungsgemeinschaft (SFB 260 and Graduiertenkolleg) and the Fonds der Chemischen Industrie. We acknowledge generous support and excellent service by the computer centers HRZ Marburg, HHLRZ Darmstadt, and HLRZ Jülich.

OM950141N

Single and Double Base-Induced Migrations and Rearrangements of Group 14 Ligand Bimetallic Complexes, $(\eta^5\text{-}C_5H_5)(CO)_mM(ER_2)_nM(CO)_m(\eta^5\text{-}C_5H_5)$ (M = Fe (m = 2), W, Mo (m = 3); $(ER_2)_n$ = $(SiMe_2)_2$, $(SiMe_2)_5$, $GeMe_2$, $SnMe_2$)

Sneh Sharma,[†] Jorge Cervantes,[‡] Jose Luis Mata-Mata,[‡] Mari-Carmen Brun,[†] Francisco Cervantes-Lee,[†] and Keith H. Pannell*,[†]

Departments of Chemistry, University of Texas at El Paso, El Paso, Texas 79968, and Universidad de Guanajuato, Guanajuato, GTO 36050 Mexico

Received May 11, 1995[⊗]

Treatment of the bimetallic complexes $[(\eta^5\text{-}C_5H_5)Fe(CO)_2]_2(ER_2)_n$, $Fp(ER_2)_nFp$ (**1**), $(ER_2)_n$ = Si_2Me_4 (**1a**), Si_5Me_{10} (**1b**), $GeMe_2$ (**1c**), and $SnMe_2$ (**1d**), with 1 equiv of lithium diisopropylamide, LDA, followed by quenching with MeI produced single-migration products $Fp(EMe_2)_n(\eta^5\text{-}C_5H_4)Fe(CO)_2Me$, (**2a,c,d** from **1a,c,d**, respectively), and a mixture of single-, **2b**, and double-, $[Me(CO)_2Fe(\eta^5\text{-}C_5H_4)]_2(ER_2)_n$ (**3b**), migration products from **1b**. Treatment of **1d** with of LDA, added slowly, also produced a novel dimeric complex $[(\eta^5\text{-}C_5H_4)Fe(CO)_2\text{-}SnMe_2]_2$ (**4**) containing both Fe–Sn and $(\eta^5\text{-}C_5H_4)$–Sn bonds. A single-crystal structure of this latter complex was determined. Treatment of the starting materials (**1a–d**) with 2 equiv of LDA followed by quenching with MeI yielded double-migration products, **3a–d**, in moderate yields, 30%–60%. Quenching the reaction between **1a** and either 1 or 2 equiv of LDA with Me_3SnCl yielded the analogous tin single- and double-migrated derivatives, **5** and **6**. Treatment of the analogous Mo and W tin complexes $[(\eta^5\text{-}C_5H_5)M(CO)_3]_2SnMe_2$, M = Mo, W, with LDA resulted in double-migration products, **7a,b**. However, similar treatment of the related tungsten germanium derivative resulted in cleavage of the W–Ge bond. After the reaction was quenched with MeI, $(\eta^5\text{-}C_5H_5)W(CO)_3Me$ was obtained.

Introduction

Since the report by Dean and Graham illustrating base-induced migrations of Ph_3Ge from Mo and W to the cyclopentadienyl ring in the system $(\eta^5\text{-}C_5H_5)M(CO)_3\text{-}GePh_3$ (M = Mo, W),[1] many other examples of this type of migration reaction have been reported. Thus silyl,[2] oligosilyl,[3] germyl,[4] stannyl,[4] and plumbyl[4] groups have all been shown to undergo such reactions. Certain carbon ligands have also been reported to migrate under similar conditions.[5]

We have observed that the reaction between $(\eta^5\text{-}C_5H_5)Fe(CO)_2SiMe_2SiMe_2Fe(CO)_2(\eta^5\text{-}C_5H_5)$ and lithium diisopropylamide, LDA, followed by treatment with MeI, resulted in the double-migration product $[MeFe(CO)_2\text{-}(\eta^5\text{-}C_5H_4)]_2SiMe_2SiMe_2$.[6] We now report an extension of this study to a variety of group 14 bridged bimetallic complexes, $[(\eta^5\text{-}C_5H_5)M(CO)_m]_2(ER_2)_n$ (M = Fe, Mo, W; ER_2 = Si_2Me_4, Si_5Me_{10}, $GeMe_2$, $SnMe_2$), in which both single and double migrations are possible and were observed under appropriate conditions. Together with the migration chemistry, a complex rearrangement resulted from the treatment of $FpSnMe_2Fp$ with LDA.

Experimental Section

All reactions were performed under inert atmospheres, N_2 or Ar, using dry oxygen-free solvents and reagents. Starting complexes $[(\eta^5\text{-}C_5H_5)M(CO)_m]_2(ER_2)_n$ were synthesized using published procedures;[6–9] LDA was used freshly prepared from *n*-BuLi and diisopropylamine; alumina for column chromatography was Fisher 70–200 mesh. NMR spectra were recorded on a Bruker NR 200 MHz multinuclear spectrometer.

Representative synthetic procedures are described below, and the melting points, elemental analyses (performed by Galbraith Laboratories Inc.), and spectral data of the new complexes are recorded in Table 1.

Synthesis of $Si_2Me_4[(\eta^5\text{-}C_5H_4)Fe(CO)_2SnMe_3]_2$, 6. In a 100-mL round-bottomed Schlenk flask was placed 0.32 g (0.68 mmol) of $[(\eta^5\text{-}C_5H_5)Fe(CO)_2]_2SiMe_2SiMe_2$ in 30 mL of THF. To this solution at 0 °C was added 3 mL (1.68 mmol) of freshly

[†] University of Texas at El Paso.

[‡] Universidad de Guanajuato.

[⊗] Abstract published in *Advance ACS Abstracts,* August 1, 1995.

(1) Dean, W. K.; Graham, W. A. G. *Inorg. Chem.* **1977**, *16*, 1061.

(2) (a) Berryhill, S. R.; Sharenow, B. J. *J. Organomet. Chem.* **1981**, *221*, 143. (b) Thum, G.; Ries, W.; Malisch, W. *J. Organomet. Chem.* **1983**, *252*, C67. (c) Berryhill, S. R.; Clevenger, G. L.; Burdurli, Y. P. *Organometallics* **1985**, *4*, 1509. (d) Heah, P. C.; Gladysz, J. A. *J. Am. Chem. Soc.* **1984**, *106*, 7636. (e) Crocco, G. L.; Gladysz, J. A. *J. Chem. Soc. Chem. Commun.* **1985**, 283. (f) Pannell, K. H.; Rozell, J. M.; Lii, J.; Tien-Mayr, S.-Y. *Organometallics* **1988**, *7*, 2525.

(3) (a) Pannell, K. H.; Hernandez, C.; Cervantes, J.; Cassias, J.; Vincenti, S. P. *Organometallics* **1986**, *5*, 1056. (b) Crocco, J. L.; Young, C. S.; Lee, K. E.; Gladysz, J. A. *Organometallics* **1988**, *7*, 2158.

(4) Cervantes, J.; Vincenti, S. P.; Kapoor, R. N.; Pannell, K. H. *Organometallics* **1989**, *8*, 744.

(5) (a) Abbot, S.; Baird, G. J.; Davies, S. G.; Dordor-Hedgecock, I. M.; Maberly, T. D.; Walker, J. C.; Warner, P. *J. Organomet. Chem.* **1985**, *289*, C17. (b) Pannell, K. H.; Vincenti, S. P.; Scott, R. C. *Organometallics* **1987**, *6*, 1593.

(6) Pannell, K. H.; Cervantes, J.; Parkanyi, L.; Cervantes-Lee, F. *Organometallics* **1990**, *9*, 859.

(7) (a) Job, C. R.; Curtis, M. D. *Inorg. Chem.* **1973**, *12*, 2514. (b) Scibelli, J. V.; Curtis, M. D. *Synth. React. Inorg. Met.-Org. Chem.* **1978**, *8*, 399.

(8) Patil, H. R. H.; Graham, W. A. G. *Inorg. Chem.* **1966**, *5*, 1401.

(9) (a) O'Conner, J.; Corey, E. R. *Inorg. Chem.* **1967**, *6*, 968. (b) Biryukov, B. P.; Struchkov, Yu. T. *Zh. Strukt. Khim.* **1968**, *9*, 488.

0276-7333/95/2314-4269$09.00/0

Table 1. Spectral Properties for New Complexes[a]

$(\eta^5\text{-}C_5H_5)Fe(CO)_2SiMe_2SiMe_2(\eta^5\text{-}C_5H_4)Fe(CO)_2Me$, **2a**	
yield; mp; anal. C, H, calcd (found)	40%; 55 °C; C, 47.14 (46.98); H, 4.99 (5.07)
^1H	0.3 (SiMe), 0.1 (FeMe), 4.2 (C_5H_5), 4.8, 5.1 (C_5H_4)
^{13}C	−22.4 (FeMe), −2.3 (SiMe), 3.3 (SiFe), 83.1 (C_5H_5), 88, 93 (C_5H_4), 216, 218 (CO)
^{29}Si	15.9, −16.3
ν(CO)	2010, 1999, 1956, 1948
$(\eta^5\text{-}C_5H_5)Fe(CO)_2(SiMe_2)_5(\eta^5\text{-}C_5H_4)Fe(CO)_2Me$, **2b**	
^{29}Si	23.1 (Fe−Si), −18.4, −31.3, −38.8, −42.4
$(\eta^5\text{-}C_5H_5)Fe(CO)_2GeMe_2(\eta^5\text{-}C_5H_4)Fe(CO)_2Me$, **2c**	
yield; mp; anal. C, H, calcd (found)	66%; 65 °C; C, 43.38 (43.24); H, 3.85 (3.91)
^1H	0.45 (FeMe), 0.75 (GeMe), 3.91 (C_5H_5), 4.27, 4.44 (C_5H_4)
^{13}C	−22.4 (FeMe), 5.56 (GeMe), 71.9 (C_5H_5), 83.7, 91.1, 97.9 (C_5H_4), 215.5, 218.6 (CO)
ν(CO)	2002, 1954
$(\eta^5\text{-}C_5H_5)Fe(CO)_2SnMe_2(\eta^5\text{-}C_5H_4)Fe(CO)_2Me$, **2d**	
yield; mp; anal. C, H, calcd (found)	50%; 42 °C; C, 39.52 (38.97); H, 3.51 (3.44)
^1H	0.49 (FeMe), 0.70 (SnMe), 4.08 (C_5H_5), 4.35, 4.41 (C_5H_4)
^{13}C	−22.6 (FeMe), −4.2 (SnMe), 81.6 (C_5H_5), 82.2, 87.9, 93.6 (C_5H_4), 214.8, 216.6 (CO)
^{119}Sn	120.0
ν(CO)	2008, 1996, 1951 (bd)
$(SiMe_2)_5[(\eta^5\text{-}C_5H_4)Fe(CO)_2Me]_2$, **3b**	
yield; mp; anal. C, H calcd (found)	34%; C, 46.45 (46.12); H, 6.55 (7.01)
^1H	0.08, 0.10, 0.33, 0.41, (Me), 4.28(C_5H_4)
^{29}Si	−18.6, −40.3, −42.9
ν(CO)	1987, 1978, 1941, 1933
$GeMe_2[(\eta^5\text{-}C_5H_4)Fe(CO)_2Me]_2$, **3c**	
yield; mp; anal. C, H calcd (found)	29%; yellow-orange oil; C, 44.64 (44.55); H, 4.16 (4.24)
^1H	0.42 (GeMe), 0.6 (FeMe), 4.3, 4.4 (C_5H_4)
^{13}C	−1.82 (GeMe), −22.7 (FeMe), 87.5, 92.2 (C_5H_4), 217.8(CO)
ν(CO)	2010, 1957
$SnMe_2[(\eta^5\text{-}C_5H_4)Fe(CO)_2Me]_2$, **3d**	
yield; mp; anal. C, H calcd (found)	60%; brown-orange oil; C, 40.74 (40.23); H, 3.79 (4.08)
^1H	0.1 (SnMe), 0.25 (FeMe), 4.5, 4.7 ($\eta^5\text{-}C_5H_4$)
^{13}C	−22.7 (FeMe), −8.8(SnMe), 88.3, 94.3 (C_5H_4), 217.9 (CO)
^{119}Sn	−26.6
ν(CO)	2010, 1956
$[(\eta^5\text{-}C_5H_4)Fe(CO)_2SnMe_2]_2$, **4**	
yield; mp; anal. C, H calcd (found)	25%; 158−160 °C; C, 33.29 (33.70); H, 3.10 (3.04)
^1H	0.50 (Me), 4.28, 4.66 (C_5H_4)
^{13}C	−4.46 (Me), 83.6, 86.8, 91.5 (C_5H_4), 215.5 (CO)
^{119}Sn	124.2
ν(CO)	1987, 1942
$(\eta^5\text{-}C_5H_5)Fe(CO)_2SiMe_2SiMe_2(\eta^5\text{-}C_5H_4)Fe(CO)_2SnMe_3$, **5**	
yield; mp; anal. C, H calcd (found)	30%; 75 °C; C, 39.85 (39.47); H, 4.77 (5.08)
^1H	0.28 (SiMe), 0.48 (SnFe), 4.12 (C_5H_5), 4.15, 4.17 (C_5H_4)
^{13}C	−4.8 (SiFe), −3.4 (SiMe), −2.07 (SnMe), 82.7 (C_5H_5), 83.06, 86.8 (C_5H_4), 215.3, 215.6 (CO)
^{29}Si	16, −16.1
ν(CO)	2010, 1990, 1956, 1940
$Si_2Me_4[(\eta^5\text{-}C_5H_4)Fe(CO)_2SnMe_3]_2$, **6**	
yield; mp; anal. C, H calcd (found)	65%; 178 °C; C, 36.22 (36.32); H, 4.81 (4.65)
^1H	0.28 (SiMe), 0.48 (SnMe), 4.2, 4.22 (C_5H_4)
^{13}C	−2.94 (SnMe), −4.5 (SiMe), 87.4, 89.04 (C_5H_4), 215.8 (CO)
^{29}Si	−23.2
ν(CO)	1990, 1940
$SnMe_2[(\eta^5\text{-}C_5H_4)Mo(CO)_3Me]_2$, **7a**	
yield; mp; anal. C, H calcd (found)	29%; 84−86 °C; C, 36.02 (36.05); H, 3.02 (3.13)
^1H	0.47 (SnMe), 0.52 (MoMe), 4.6, 4.9 (C_5H_4)
^{13}C	−21.7 (MoMe), −8.2 (SnMe), 92.4, 97.7, 98.7 (C_5H_4), 227.3 (CO)
ν(CO)	2020, 1941, 1934
$SnMe_2[(\eta^5\text{-}C_5H_4)W(CO)_3Me]_2$, **7b**	
yield; mp; anal. C, H calcd (found)	41%; 98−100 °C; C, 28.50 (28.57); H, 2.39 (2.30)
^1H	0.58 (SnMe), 0.7 (WMe), 4.7, 5.0 (C_5H_4)
^{13}C	−34.4 (WMe), −7.9 (SnMe), 90.9, 96.9, 97 (C_5H_4), 216.7(CO)
ν(CO)	2016, 1933, 1922
$SiMeH[(\eta^5\text{-}C_5H_4)Fe(CO)_2Me]_2$, **8**	
yield; mp; anal. C, H calcd (found)	29%; unstable oil, no analysis
^1H	0.40 (FeMe), 1.44 (SiMe), 4.3, 4.4 (C_5H_4), 4.8 (Si−H)
^{13}C	−4.8 (SiMe), −22.4 (FeMe), 81.1, 87.4, 93.6 (C_5H_4), 217.8 (CO)
ν(CO)	2010, 1957, 2142 (SiH)

[a] NMR spectra were recorded in C_6D_6, and IR spectra were recorded in hexane. Chemical shifts are in δ, and ν(CO) are in cm^{-1}.

prepared LDA in the same solvent. The solution was stirred for 30 min, after which time infrared monitoring indicated the absence of the starting material and the concomitant formation of a species exhibiting ν(CO) stretching frequencies at 1882, 1867, 1812, and 1753 cm^{-1}. To this solution at 0 °C was added 0.35 g (1.75 mmol) of Me_3SnCl. The solution was stirred for 30 min and warmed to room temperature. Infrared analysis indicated new ν(CO) bands at 1978 and 1928 cm^{-1}. The solvent was removed *in vacuo*, and the residue was extracted with 50 mL of hexane, filtered, and concentrated to 3 mL, and placed upon a 1 × 15 cm alumina column. Development of the column with hexane produced a yellow band which was eluted with a 20:80 methylene chloride–hexane solvent mixture. Subsequent to removal of the solvent, recrystallization from hexane yielded complex **6a** as a yellow crystalline solid (0.35 g, 0.44 mmol, 65%).

Synthesis of $GeMe_2[(\eta^5\text{-}C_5H_4)Fe(CO)_2Me]_2$, 3c. To 30 mL of a THF solution of $[(\eta^5\text{-}C_5H_5)Fe(CO)_2]_2GeMe_2$ (0.3 g, 0.65 mmol) was added 3 mL (1.68 mmol) of a 0.56 M LDA solution at 0 °C. The solution turned deep orange, and after the solution had been stirred for 2 h IR spectroscopy indicated the presence of ν(CO) bands at 1882, 1867, 1812, and 1753 cm^{-1}. Addition of an excess of MeI resulted in the solution becoming green-brown and exhibiting ν(CO) bands at 2000 and 1946 cm^{-1}. The solvent was removed, and the residue was extracted into hexane, filtered, concentrated to 5 mL, and placed upon an alumina column, 1 × 15 cm. Elution with hexane developed a yellow band, which was collected and, after solvent removal, yielded **3c** as a yellow orange oil (0.092 g, 0.19 mmol, 29%).

A similar procedure was used to obtain $SiMeH[(\eta^5\text{-}C_5H_4)Fe(CO)_2Me]_2$, **8** (29%), and $SnMe_2[(\eta^5\text{-}C_5H_4)Fe(CO)_2Me]_2$, **3d** (0.24 g, 0.46 mmol, 60%).

Synthesis of $SnMe_2[(\eta^5\text{-}C_5H_4)W(CO)_3Me]_2$, 7b. To 30 mL of a THF solution of $[(\eta^5\text{-}C_5H_5)W(CO)_3]_2SnMe_2$ (0.3 g, 0.36 mmol) was added 3 mL (1.68 mmol) of a 0.56 M LDA solution at 0 °C. The solution turned deep orange, and after the solution had been stirred for 2 h an IR spectrum indicated the presence of ν(CO) bands at 1894, 1801, and 1712 cm^{-1}. An excess of MeI was added, and after 1 h infrared spectroscopic analysis showed the presence of ν(CO) bands at 2009, 1970, and 1913 cm^{-1}. The solvent was removed *in vacuo*, and the residue was extracted with 50 mL of hexane, filtered, and, after solvent removal, the residue was dissolved in 5 mL of CH_2Cl_2 and placed on a 1 × 15 cm alumina column. Elution with hexane developed a yellow band which was recovered and, subsequent to solvent removal and recrystallization from hexane, yielded **7b** as a yellow solid (0.13 g, 0.15 mmol, 42%).

The same synthetic procedure was applied to obtain $SnMe_2[(\eta^5\text{-}C_5H_4)Mo(CO)_3Me]_2$, **7a** (26%).

Treatment of $FpSnMe_2Fp$, 1d, with 1 Equiv of LDA. To a THF solution (60 mL) of **1d** (1.0 g, 1.99 mmol) was added 4.4 mL of a 0.56 M solution of freshly prepared LDA in THF at 0 °C. There was an immediate color change from yellow to red-orange. The solution was stirred for 1 h, at which time infrared monitoring indicated the formation of new bands at 1980, 1930, 1884, 1868, 1781, and 1750 cm^{-1} showing the formation of a substituted $[Fp]^-$ salt. This solution was then treated with an excess of MeI at 0 °C, and the resulting solution was warmed to room temperature. The solvent was removed under reduced pressure, and the residue was dissolved in hexane, 10 mL, and placed upon a 2.5 × 10 cm alumina chromatography column. The resulting yellow band was eluted with hexane and after collection a crude product mixture was obtained. Fractional crystallization from hexane yielded an initial crop of $[(\eta^5\text{-}C_5H_4)Fe(CO)_2SnMe_2]_2$, **4**, as a yellow crystalline material (0.32 g, 0.49 mmol, 25%). A second crop of crystalline material yielded $FpSnMe_2(\eta^5\text{-}C_5H_4)Fe(CO)_2Me$ (0.51 g, 0.99 mmol, 50%).

Synthesis of $(\eta^5\text{-}C_5H_5)Fe(CO)_2SiMe_2SiMe_2[(\eta^5\text{-}C_5H_4)Fe(CO)_2Me]$, 2a. To 30 mL of a THF solution of $[(\eta^5\text{-}C_5H_5)Fe(CO)_2]_2SiMe_2SiMe_2$ (0.25 g, 0.53 mmol) was added 1 mL (0.56 mmol) of a 0.56 M LDA solution at 0 °C. The solution turned deep orange, and after the solution had been stirred for 30 min an IR spectrum exhibited six ν(CO) bands (1991, 1933, 1882, 1867, 1812, and 1753 cm^{-1}). Addition of an excess of methyl iodide resulted in the formation of a brown-green color and new ν(CO) bands at 2000, 1991, 1942, and 1937 cm^{-1}. Removal of the solvent *in vacuo* was followed by extraction into a 70:30 hexane–methylene chloride solvent mixture. This solution was filtered, concentrated to 5 mL, and placed upon an alumina column, 1 × 15 cm. Elution with a hexane–methylene chloride solvent mixture (90:10) developed a yellow band which was collected. Recrystallization from the same solvent mixture yielded **2a** (0.15 g, 0.2 mmol, 38%).

The same procedure was applied to obtain the corresponding Me_3Sn derivative, $(\eta^5\text{-}C_5H_5)Fe(CO)_2SiMe_2SiMe_2(\eta^5\text{-}C_5H_4)Fe(CO)_2SnMe_3$, **5**.

Table 2. Structure Determination Summary for 4

Crystal Data	
empirical formula	$C_{18}H_{20}Fe_2O_4Sn_2$
color; habit	yellow fragment
cryst size (mm^3)	0.40 × 0.28 × 0.40
cryst syst	triclinic
space group	$P\bar{1}$
unit cell dimens	a = 7.749(2) Å
	b = 9.161(3) Å
	c = 15.649(5) Å
	α = 91.35(3)°
	β = 97.90(2)°
	γ = 103.67(3)°
volume	1067.4(6) $Å^3$
Z	2
fw	649.4
density (calcd)	2.021 Mg/m^3
abs coeff	3.676 mm^{-1}
F(000)	624
Data Collection	
diffractometer	Siemens R3m/V
radiation	Mo Kα (λ = 0.710 73 Å)
temp (K)	295
monochromator	highly oriented graphite crystal
2θ range	3.5–45.0°
scan type	ω
scan speed	variable; 3.00–15.00 deg/min. in ω
scan range (ω)	1.20°
bkgd measmt	stationary crystal and stationary counter at beginning and end of scan, each for 25.0% of total scan time
std reflns	3 measd every 97 reflns
index ranges	$0 \le h \le 8, -9 \le k \le 9, -16 \le l \le 16$
no. of reflns collcd	3056
no. of independent reflns	2811 (R_{int} = 1.06%)
no. of obsd reflns	2582 ($F > 3.0\sigma(F)$)
abs cor	semiempirical
min/max transmissn	0.0516/0.0858
Solution and Refinement	
syst used	Siemens SHELXTL PLUS (VMS)
soln	direct methods
refinement method	full-matrix least-squares
quantity minimized	$\sum w(F_o - F_c)^2$
abs structure	N/A
extinction cor	χ = 0.0102(3), where $F^* = F[1 + 0.002\chi F^2/\sin(2\theta)]^{-1/4}$
hydrogen atoms	riding model, fixed isotropic U
wting scheme	$w^{-1} = \sigma^2(F) + 0.0011F^2$
no. of params refined	236
final R indices (obsd data)	R = 2.35%, wR = 3.91%
R indices (all data)	R = 2.68%, wR = 4.74%
goodness-of-fit	1.04
largest and mean Δ/σ	1.598, 0.455
data-to-param ratio	10.9:1
largest difference peak	0.56 e $Å^{-3}$
largest difference hole	−0.47 e $Å^{-3}$

Structural Determination of 4. Crystallographic data were collected on a Siemens R3m/V single-crystal diffractometer, and the structure was solved using the SHELEXTL-PLUS software package. All the relevant data are provided in the accompanying Tables 2–5 and supporting information.

Table 3. Atomic Coordinates (×10⁴) and Equivalent Isotropic Displacement Coefficients (Å² × 10³)

	x	y	z	U(eq)[a]
Sn(1)	−6324(1)	−2170(1)	5485(1)	44(1)
Fe(1)	−5012(1)	119(1)	6523(1)	41(1)
O(1)	−5803(6)	−1865(4)	7894(3)	79(2)
O(2)	−1529(5)	−473(5)	6534(3)	86(2)
C(1)	−6692(6)	1201(5)	5759(3)	50(2)
C(2)	−5102(6)	−1905(5)	4316(3)	47(2)
C(3)	−4074(7)	2440(5)	6554(3)	53(2)
C(4)	−5360(8)	2095(6)	7117(3)	59(2)
C(5)	−6956(7)	1304(6)	6624(3)	61(2)
C(6)	−9165(7)	−2634(7)	5025(4)	78(2)
C(7)	−5806(9)	−4219(6)	5980(4)	77(3)
C(8)	−5513(7)	−1090(6)	7347(3)	53(2)
C(9)	−2919(6)	−254(5)	6519(3)	52(2)
Sn(2)	571(1)	5577(1)	8687(1)	44(1)
Fe(2)	1070(1)	7636(1)	9876(1)	40(1)
O(3)	1733(6)	9892(4)	8619(3)	75(2)
O(4)	−2758(5)	7354(4)	9542(3)	72(2)
C(10)	2787(7)	8899(5)	10925(3)	61(2)
C(11)	1349(7)	7940(5)	11214(3)	52(2)
C(12)	1331(6)	6413(5)	10994(3)	44(2)
C(13)	2839(6)	6498(5)	10552(3)	51(2)
C(14)	3723(6)	8030(6)	10493(3)	57(2)
C(15)	2804(8)	4675(7)	8444(4)	76(2)
C(16)	−652(9)	6164(7)	7456(3)	84(3)
C(17)	1465(6)	8972(5)	9106(3)	49(2)
C(18)	−1239(6)	7456(5)	9668(3)	49(2)

[a] Equivalent isotropic U defined as one-third of the trace of the orthogonalized U_{ij} tensor.

Table 4. Selected Bond Lengths (Å) for 4

Sn(1)−Fe(1)	2.539(1)	Sn(2)−Fe(2)	2.541(1)
Sn(1)−C(2)	2.166(5)	Sn(2)−C(12)	2.173(4)
Sn(1)−C(7)	2.151(5)	Sn(2)−C(16)	2.165(6)
Fe(1)−C(8)	1.743(5)	Fe(2)−C(17)	1.743(5)

Table 5. Selected Bond Angles (deg) for 4

C(2)−Sn(1)−Fe(1)	110.2(1)	C(12a)−Sn(2)−Fe(2)	109.5(1)
C(6)−Sn(1)−C(7)	106.7(1)	C(15)−Sn(2)−C(16)	107.2(3)
C(8)−Fe(1)−C(9)	92.7(2)	C(17)−Fe(2)−C(18)	92.0(2)

Results and Discussion

Treatment of the disilyl-, monogermyl-, and monostannyl-bridged bimetallic complexes **1a,c,d** with 1 equiv of LDA resulted in a single migration, such that quenching with MeI resulted in the formation of $Fp(ER_2)_n$-(η^5-C_5H_4)$Fe(CO)_2Me$, $(ER_2)_n$ = Si_2Me_4, $GeMe_2$, $SnMe_2$, **2a,c,d**, eq 1. Quenching the reaction between **1a** and

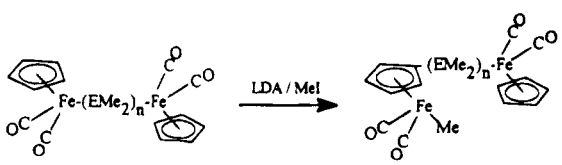

(1)

LDA with Me_3SnCl resulted in the corresponding trimethyltin complex. NMR analysis of the crude reaction product provided no evidence for significant double migrations in these experiments.

Treatment of the same complexes **1a,c,d** with 2 equiv of lithium diisopropylamide in THF followed by quenching of the resulting metal carbonylate ions with either MeI (and in some cases Me_3SnCl) resulted in the isolation of the corresponding methyl (or stannyl) double-migration products in moderate to good yields, 30%−65%, eq 2.

In the case of the pentasilyl-bridged bimetallic complex, **1b**, treatment with 1 equiv of LDA always resulted

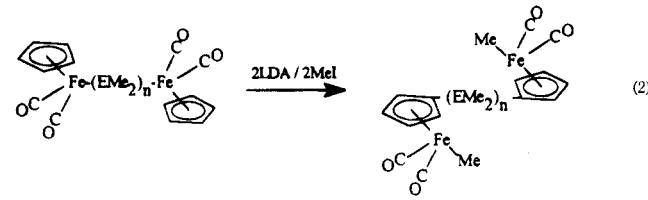

(2)

in a mixture of single **and** double migration. Changing LDA addition rates and temperatures did not change this outcome. We have been able to characterize the single-migration products only by ^{29}Si NMR spectroscopy in these mixtures. Addition of excess LDA, >2 equiv, permitted isolation of the pure double-migration product.

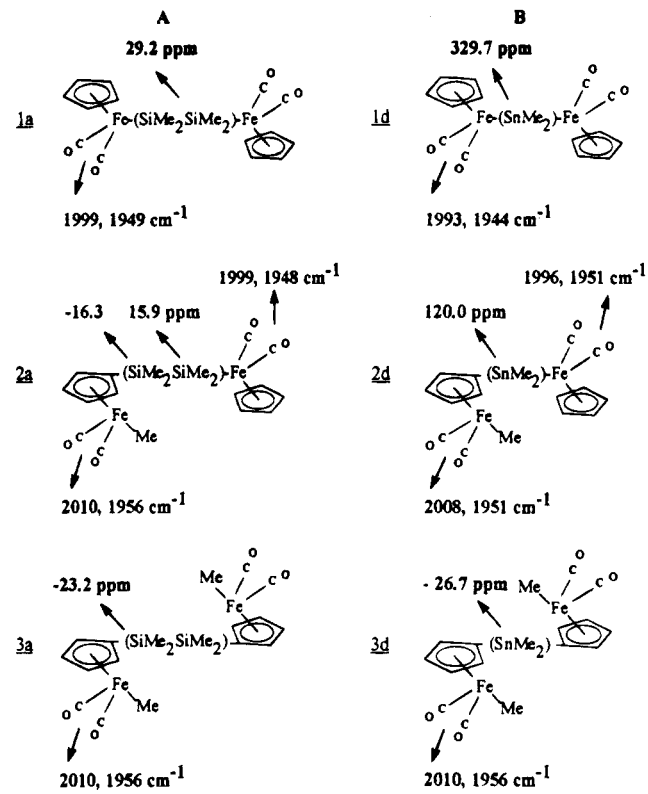

Figure 1. ν(CO), ^{119}Sn and ^{29}Si NMR data for starting materials and for single- and double-migrated products, **1a,d**, **2a,d**, and **3a,d**.

The above results suggest that when the two Fe centers are close, bridged by only 1 or 2 atoms, initial deprotonation of one cyclopentadienyl ring and migration of the group 14 element to the ring produces an anion that significantly reduces the ability of the second cyclopentadienyl group to deprotonate, i.e., step **A** (eq 3a) is significantly favored over step **B** (eq 3b). Only

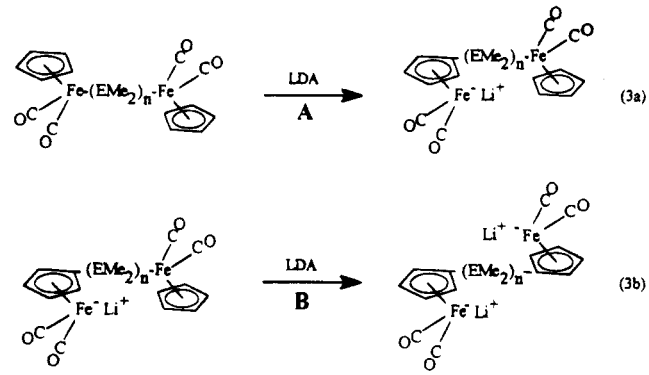

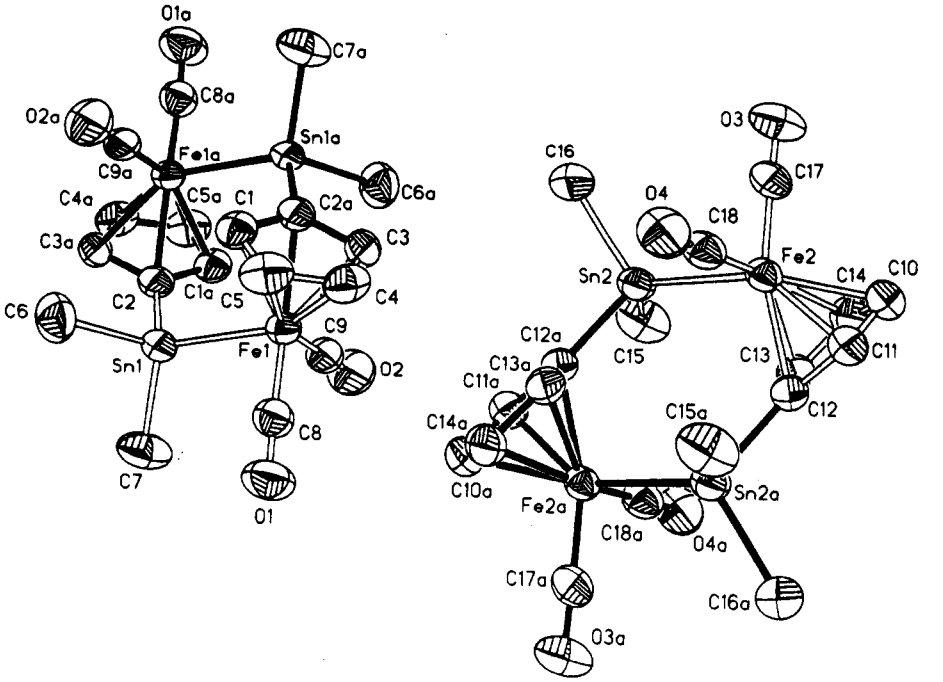

Figure 2. Structure of **4**.

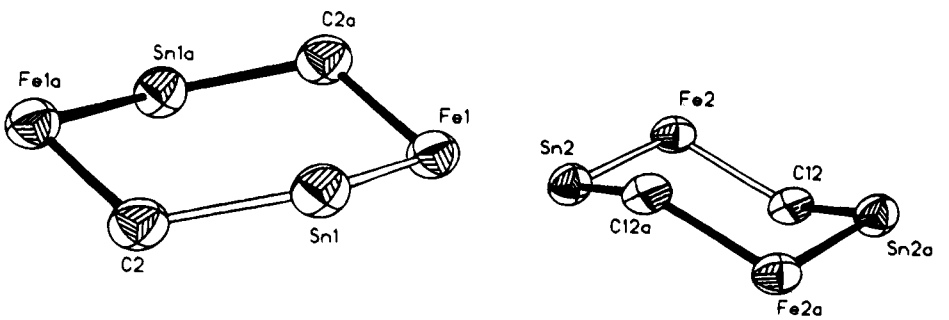

Figure 3. Conformations of the Sn–C–Fe–Sn–C–Fe ring in **4**.

upon completion of the first process does the second process, **B**, commence. The inductive effect of negative charge at one end of the bridge may be expected to retard the deprotonation at the other end. A one- or two-atom bridging unit can transmit this effect, but with longer chains the effect is attenuated and the two ends of the complex act as independent and equivalent units.

The spectroscopic data for the new complexes are most informative with respect to detailing the changes in coordination at the transition metal center. Figure 1a illustrates the trends observed for the tranformations **1a** → **2a** → **3a**, and Figure 1b does the same from the transformation **1d** → **2d** → **3d**. Thus the infrared stretching frequencies for the CO groups in $[(\eta^5\text{-}C_5H_5)Fe(CO)_2]_2SnMe_2$ at 1993 and 1944 cm^{-1} changed to 2010 and 1956 cm^{-1} upon transformation to the double-migration product $SnMe_2[(C_5H_4)Fe(CO)_2Me]_2$ that now contains Fe–C bonds. The ^{119}Sn NMR signal for the two complexes changed from 329.7 to −26.7 ppm. Both these observations are in accord with previously reported data, and the spectra of the intermediate single-migration products exhibited bands associated with each "end" of the group 14 bridging ligand.[4,6] Similarly the IR and ^{29}Si NMR data for the series **1a**, **2a**, and **3a** change in a systematic manner.

Analysis of the crude reaction mixtures using multinuclear NMR and GC/MS sometimes exhibited products from reactions involving the cleavage of the M–Sn and M–Ge bonds in the starting materials, especially when an excess of LDA was used. Such reactions have been observed previously,[4] and in the present study the double-migration product was sometimes contaminated with such cleavage products. For example, treatment of $[(\eta^5\text{-}C_5H_5)Fe(CO)_2]_2SnMe_2$ with an excess of LDA followed by quenching with Me_3SnCl resulted in small amounts of $FpSnMe_3$, as determined by ^{119}Sn NMR (+143.5 ppm) and GC/mass spectrometry *via* the intermediacy of Fp^-Li^+.

A greater amount of the cleavage reaction occurred when we studied the molybdenum complex $[(\eta^5\text{-}C_5H_5)Mo(CO)_3]_2SnMe_2$, and quenching with MeI produced $(\eta^5\text{-}C_5H_5)Mo(CO)_3Me$ together with the double-migration product, **7a**. Several purification steps were needed in order to obtain a pure analytical sample of **7a**, hence the relatively low recovered yield. Finally, the reaction of $[(\eta^5\text{-}C_5H_5)W(CO)_3]_2GeMe_2$ with LDA resulted in cleavage of the W–Ge bond to yield $[(\eta^5\text{-}C_5H_5)W(CO)_3Me]$ upon quenching with MeI.

Formation of $[(\eta^5\text{-}C_5H_4)Fe(CO)_2SnMe_2]_2$, 4. The reaction between $FpSnMe_2Fp$ and LDA was a complex reaction. Rapid addition of the 2 equiv of base resulted in double migration; however, addition of 1 equivalent resulted in both a single-migration product and the distinctive reaction product **4**. The mechanism for the formation of **4** is not clear. Clearly kinetic aspects of the chemistry are involved, including possible participation of intermediates from the Fe–Sn cleavage reactions

noted above; however, one of many speculative processes could be involved.

We obtained crystals of **4** suitable for a single-crystal X-ray analysis, and the structure of the complex is illustrated in Figure 2. It is similar to the analogous silicon complex recently reported by Sun and co-workers from the thermal rearrangement of $[(\eta^5\text{-}C_5H_4)Fe(CO)_2]_2(\mu\text{-}SiMe_2SiMe_2)$.[10] The asymmetric unit consists of two molecular fragments, A and B. Fragment A contains atoms Fe1, Sn1, O1, O2, and C1–C9, and fragment B contains Fe2, Sn2, O3, O4, and C10–C18. Each fragment, through crystallographic symmetry, generates a dimeric molecule having a molecular center of symmetry coinciding with a crystallographic one at $-1/2$, 0, $1/2$ for A and at 0, $1/2$, 1 for B. The dimers have similar conformations but different orientations in the unit cell. The Fe–Sn bond length of 2.539(1) Å is in the normal range for such bonds, and the six-membered ring Fe–C–Sn–Fe–C–Sn assumes a typical chair conformation when viewed in the absence of ancillary atoms for clarity, Figure 3.

(10) Sun, H.; Xu, S.; Zhou, X.; Wang, H.; Wang, R.; Yao, X. *J. Organomet. Chem.* **1993**, *444*, C41.

Acknowledgment. This research was supported by the R. A. Welch Foundation, Houston, TX; the NSF (Grant No. RII-88-02973); and a joint NSF/CONACyT Collaborative Research Award, No. Int-9002051.

Supporting Information Available: Tables listing anisotropic and isotropic displacement coordinates, H atom coordinates, torsion angles, and bond lengths and bond angles for **4** (7 pages). Ordering information is given on any current masthead page.

OM950341Z

Electron Transfer Reactions of the Organometallic Free Radical $CpMo(CO)_3^{\bullet}$ with Triphenylpyrylium Ion and Triphenylpyranyl Radical

Tae-Jin Won and James H. Espenson*

Ames Laboratory and Department of Chemistry, Iowa State University, Ames, Iowa 50011

Received June 9, 1995[⊗]

The title compound, a 17-electron organometallic free radical, undergoes reversible electron transfer in two steps in acetonitrile. It is oxidized by the triphenylpyrylium ion (TPP^+) to $[CpMo(CO)_3NCCH_3]^+$ and reduced by $TPP^{\bullet}$ to $[CpMo(CO)_3]^-$. Three of the four rate constants for the forward and reverse directions of these two steps were evaluated directly by flash photolysis and stopped-flow techniques. The results were considered in light of data for similar reactions of $[CpMo(CO)_3]^{\bullet}$ with $TMPD^{\bullet+}$ and TMPD (TMPD = *N,N,N′,N′*-tetramethyl-1,4-phenylenediamine). Notable differences were found, due entirely to the 0.55 V difference in E° for the two A^+/A couples. On the other hand, surprising agreement was found between the rate constants for a pair of reactions that differ by 10^8 in their equilibrium constants. Both of these rate constants are at the diffusion-controlled level. We thus conclude that the minor species $[CpMo(CO)_3{\cdot}NCCH_3]^{\bullet}$ (sometimes referred to as a 19e radical), the binding constant of which is only $\sim 10^{-4}$ L mol^{-1}, may carry the diffusion-controlled reactions with TPP^+ and $TMPD^{\bullet+}$. Reduction to the 18e molybdenum anion, however, does not proceed with the involvement of the coordinated solvent.

Introduction

Organometallic radicals[1] with 17 electrons can be produced by a number of techniques, depending on their lifetimes and stabilities.[2-5] Some of these 17e radicals are stable toward dimerization,[5-7] especially when bulky ligands are present to impede metal–metal bond formation; most have short lifetimes, including $CpMo(CO)_3^{\bullet}$, **1**. This radical is easily created in laser flash photolysis experiments by the photolysis of the stable Mo–Mo dimer, eq 1.

$$[CpMo(CO)_3]_2 \xrightarrow{h\nu} 2CpMo(CO)_3^{\bullet} \qquad (1)$$

When $CpMo(CO)_3^{\bullet}$ encounters an electron donor, the radical can be reduced to the stable 18e anion, $CpMo(CO)_3^-$; with an acceptor, the organometallic radical can be oxidized to the cation. Concurrent with oxidation, a ligand or solvent is added so as to give another 18e species, $CpMo(CO)_3L^+$. When the electron acceptor is $TMPD^{\bullet+}$ and the donor TMPD (TMPD = *N,N,N′,N′*-tetramethyl-1,4-phenylenediamine), these electron transfer processes (eqs 2 and 3) are so rapid, and so favorable thermodynamically, that net disproportionation of $CpMo(CO)_3^{\bullet}$ (eq 4) prevails over radical combination (eq 5). As a result, light energy is stored in the separated organometallic ions which lie in free energy above the dimer, since the reverse of reaction 4 is negligible.

$$CpMo(CO)_3^{\bullet} + TMPD \rightleftharpoons CpMo(CO)_3^- + TMPD^{\bullet+} \qquad (2)$$

$$CpMo(CO)_3^{\bullet} + TMPD^{\bullet+} \xrightarrow{CH_3CN} CpMo(CO)_3NCCH_3^+ + TMPD \qquad (3)$$

$$2CpMo(CO)_3^{\bullet} + CH_3CN \rightarrow CpMo(CO)_3^- + CpMo(CO)_3NCCH_3^+ \qquad (4)$$

$$2CpMo(CO)_3^{\bullet} \xrightarrow{k_c} [CpMo(CO)_3]_2 \qquad (5)$$

In place of TMPD we have chosen to investigate TPP^+, the triphenylpyrylium cation, **2**, and its pyranyl radical,

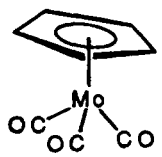

1

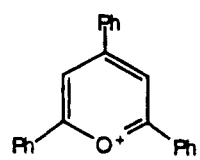

2

$TPP^{\bullet}$, because $E^\circ(TPP^+/TPP^{\bullet})$ lies −0.55 V negative of $E^\circ(TMPD^{\bullet+}/TMPD)$. The respective potentials are −0.39

⊗ Abstract published in *Advance ACS Abstracts,* August 1, 1995.

(1) (a) Muetterties, E. L.; Sosonsky, B. A.; Zamaraev, K. I. *J. Am. Chem. Soc.* **1975**, *97*, 5299–5300. (b) Sweany, R. L.; Halpern, J. *J. Am. Chem. Soc.* **1977**, *99*, 8335–8337. (c) Bullock, R. M.; Samsel, E. G. *J. Am. Chem. Soc.* **1990**, *112*, 6886–6898. (d) Trogler, W. C., Ed. *Organometallic Radical Processes*; Elsevier: New York, 1990; Vol. 22.

(2) (a) Pickett, C. J.; Pletcher, D. *J. Chem. Soc., Chem. Commun.* **1974**, 660–661. (b) Treichel, P. M.; Wagner, K. P.; Mueh, H. J. *J. Organomet. Chem.* **1975**, *86*, C13–C16. (c) Zang, Y.; Gosser, D. K.; Rieger, P. H.; Sweigart, D. A. *J. Am. Chem. Soc.* **1991**, *113*, 4062–4068. (d) Rourke, F.; Gash, R.; Crayston, J. A. *J. Organomet. Chem.* **1992**, *423*, 223–239.

(3) Krusic, P. J.; Stoklosa, H.; Manzer, L. E.; Meakin, P. *J. Am. Chem. Soc.* **1975**, *97*, 667–669.

(4) Meckstroth, W. K.; Walters, R. T.; Waltz, W. L.; Wojcicki, A.; Dorfman, L. M. *J. Am. Chem. Soc.* **1982**, *104*, 1842–1846.

(5) Kidd, D. R.; Cheng, C. P.; Brown, T. L. *J. Am. Chem. Soc.* **1978**, *100*, 4103–4107. (b) Hallock, S. A.; Wojcicki, A. *J. Organomet. Chem.* **1973**, *54*, C27–C29.

(6) Moelwyn-Hughes, T. J.; Garner, A. W. B.; Gordon, N. *J. Organomet. Chem.* **1970**, *26*, 373–387.

(7) Watkins, W. C.; Jaeger, T.; Kidd, C. E.; Fortier, S.; Baird, M. C.; Kiss, G.; Roper, G. C.; Hoff, C. D. *J. Am. Chem. Soc.* **1992**, *114*, 907–914.

0276-7333/95/2314-4275$09.00/0

and +0.16 V *versus* SSCE.[8-10] This means that different aspects of the reactivity would be manifest in its combination with $CpMo(CO)_3^{\bullet}$. That is to say, the potential differences give rise to the particular interplay of the kinetic and equilibrium constants that define the course of this reaction network, and the net outcomes will be markedly different in the two systems. As remarked previously, the net result with TMPD/$TMPD^{\bullet+}$ is that disproportionation of the molybdenum radical predominated; that is, eq 4 (the sum of eqs 2 and 3) was the net result of electron transfer, these events occurring simultaneously with an amount of the dimerization reaction, an irreversible reaction. The net balance between disproportionation and dimerization was governed by the TMPD concentration employed in a given experiment. With an electron donor that has an $E°$ quite different from that of TMPD, however, the result of the reaction sequence was anticipated to be very different. We sought to quantify all of the changes in one such case, since the results would bear very directly on the consequences of photochemical excitation in complex systems. For this purpose the $TPP^+/TPP^{\bullet}$ system seemed well-suited, not only because its potential was so greatly shifted, but because both cation and radical can be studied directly, allowing a particularly thorough and direct characterization of the reaction steps.

It did prove feasible to determine directly three of the four rate constants by the application of millisecond stopped-flow and microsecond flash photolysis techniques, allowing more complete characterization of the entire set of chemical reactions.

Experimental Section

The reagents $Cp_2Mo_2(CO)_6$ and 2,4,6-triphenylpyrylium tetrafluoroborate were obtained from Aldrich Chemical Co. Solutions were prepared daily in HPLC-grade acetonitrile, and $[Cp_2Mo_2(CO)_6]$ was determined spectrophotometrically ($\epsilon^{384} = 1.69 \times 10^4$ L mol^{-1} cm^{-1}).[11] The anion $CpMo(CO)_3^-$ was prepared by using potassium hydride to reduce the dimer. Solutions of $TPP^{\bullet}$ were prepared by stirring an acetonitrile solution of $[TPP^+]$ $[BF_4^-]$ with granular zinc as described in the literature.[12]

All operations that used or produced $TPP^{\bullet}$ or $CpMo(CO)_3^{\bullet}$ were carried out under argon with the strict exclusion of oxygen. For laser flash photolysis, a known amount of substrate (TPP^+ or $TPP^{\bullet}$) was added to a solution of $Cp_2Mo_2(CO)_6$ in acetonitrile. This solution was subjected to a 0.6 μs flash from a flashlamp-pumped dye laser containing Coumarin 522B in an apparatus described previously.[13] Stopped-flow measurements were carried out with a DX-17MV instrument from Applied Photophysics Ltd.

Results

Kinetics of Dimerization of the $TPP^{\bullet}$ Radical. We shall first treat the dimerization reaction which was encountered during the kinetic studies of electron transfer. The reaction has a relaxation time of the order of milliseconds, and it became necessary to conduct a precise evaluation of the kinetics to allow for this equilibrium step during the electron transfer reactions. The equilibrium constant has been reported: $K_6 = 800$ L^{-1} mol in acetonitrile at $T = 25$ °C[14] (eq 6).

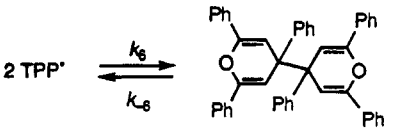

(6)

The reaction was studied by the concentration jump technique: an equilibrated solution of the triphenylpyranyl radical, prepared as described in the experimental section, was suddenly diluted to half its volume in the stopped-flow instrument. This caused the reaction to shift to a new equilibrium position. The relaxation was monitored at 550 nm, an absorption maximum for $TPP^{\bullet}$. The kinetic curves were fit to eq 7

$$\delta_t = \frac{\alpha\delta_0 e^{-\alpha k_{-6} t}}{\alpha + 48_0 K_6 (1 - e^{-\alpha k_{-6} t})} \tag{7}$$

where $\alpha = 1 + 4K_6[TPP^{\bullet}]_e$ and $\delta = ([P]_t - [P]_e)/2$.[15,16] This treatment gave $k_{-6} = (2.0 \pm 0.1) \times 10^2$ s^{-1}. From K_6, we obtained $k_6 = 1.6 \times 10^5$ L mol^{-1} s^{-1} at 25 °C; the dimerization of the triphenylpyranyl radical is roughly 10^2 times more rapid than the dimerization of the triphenylmethyl radical.[17]

For this and for other parts of the kinetic analysis the molar absorptivity of $TPP^{\bullet}$ was required. Various solutions of $TPP^{\bullet}$ and its dimer were prepared, and the absorbance of each was plotted against the concentration of $TPP^{\bullet}$ itself after allowance, from the value of K_6, for the extent of formation of the nonabsorbing dimer. Over the concentration range studied, 50–80 μM TPP, Beer's law was obeyed, giving $\epsilon(TPP^{\bullet}) = (4.67 \pm 0.07) \times 10^3$ L mol^{-1} cm^{-1} at its 550 nm peak.

General Scheme. Both $CpMo(CO)_3^{\bullet}$ and $TPP^{\bullet}$ react rapidly with oxygen. Consequently, all solutions were purged with high-purity argon. It is useful to define the electron transfer steps and their rate constants at an early stage, to allow clear reference to a kinetic model that is fairly complex. This is done in eqs 8 and 9.

$$CpMo(CO)_3^{\bullet} + TPP^+ \underset{k_{-8}}{\overset{k_8(CH_3CN)}{\rightleftharpoons}} CpMo(CO)_3NCCH_3^+ + TPP^{\bullet} \tag{8}$$

$$CpMo(CO)_3^{\bullet} + TPP^{\bullet} \underset{k_{-9}}{\overset{k_9}{\rightleftharpoons}} CpMo(CO)_3^- + TPP^+ \tag{9}$$

The first reaction provides for solvent addition to give the 18e product $CpMo(CO)_3NCCH_3^+$, cf. eq 8, but consideration of the timing of solvent (acetonitrile) incorporation, relative to electron transfer, will be deferred. Reactions 8 and 9 are shown as being reversible, but the value of k_{-8} was anticipated from the thermodynamics and established by the kinetic analysis

(8) Pragst, F.; Ziedig, R.; Seydenitz, U.; Driesel, D. *Electrochim. Acta* **1980**, *25*, 341–352.
(9) Bockman, T. M.; Kochi, J. K. *New J. Chem.* **1992**, *16*, 39–49.
(10) Grabner, E. W.; Hessberger, H. *J. Phys. Chem.* **1987**, *91*, 226.
(11) J. Balla, J. H. Espenson and A. Bakac *J. Phys. Chem.* **1995**, *99*, 3598.
(12) Hawata, H.; Niizuma, S. *Bull. Chem. Soc. Jpn.* **1989**, *62*, 2279.
(13) Connolly, P.; Espenson, J. H.; Bakac, A. *Inorg. Chem.* **1986**, *25*, 2169.
(14) Wintgens, V.; Pouliquen, J.; Kossanyi, J.; Heintz, M. *Nouv. J. Chim.* **1986**, *10*, 345–350.
(15) King, E. L. *Int. J. Chem. Kinet.* **1982**, *14*, 580.
(16) Espenson, J. H. *Chemical Kinetics and Reaction Mechanisms*, 2nd ed.; McGraw-Hill Book Co.: New York, 1995; pp 50–54.
(17) Kristjansdottir, S. S.; Moody, A. E.; Norton, J. R. *Int. J. Chem. Kinet.* **1992**, *24*, 895.

to be so small relative to the other rate constants that the reverse of reaction 8 did not contribute appreciably to the kinetics.

Three separate types of kinetic determinations were feasible. The first two are based on laser flash photolysis. They consisted in the generation of the molybdenum radical by photohomolysis of $[CpMo(CO)_3]_2$ in the presence of (a) TPP^+ and (b) $TPP^•$. To a good approximation, as explained shortly, these determinations allowed the direct evaluation of k_8 and k_9, with due provision for the competing dimerization of $CpMo(CO)_3^•$, eq 5. The third type of experiment employed the stopped-flow technique to evaluate directly the kinetics of the reaction between $CpMo(CO)_3^-$ and TPP^+, as represented by k_{-9}.

In preliminary experiments it was found that the laser excitation of $[CpMo(CO)_3]_2$ in the presence of TPP^+ at 490 or 500 nm also causes the excitation of TPP^+ and the generation of some $TPP^•$ by a photoprocess not thoroughly characterized. Fortunately, this phenomenon could be avoided by the use of a laser dye that provided a 526 nm excitation. This wavelength resulted in no formation of $TPP^•$, yet this longer wavelength sufficed quite well for the photodissociation of the molybdenum dimer. Consequently, only 526 nm radiation was used in all the experiments described in this work. In practical terms, about 25% of the $[CpMo(CO)_3]_2$ was dissociated when it was present at 10–50 μM concentration. A test was run to show that the accepted value[11,18] of $k_c = 2.16 \times 10^9$ L mol^{-1} s^{-1} in acetonitrile could be duplicated.

Reduction of TPP^+ by $CpMo(CO)_3^•$. No reaction occurred in the dark between the molybdenum dimer and TPP^+. When solutions of $[CpMo(CO)_3]_2$ containing suitable concentrations of TPP^+ were photolyzed at 526 nm, the molybdenum radical was formed. After the flash the ensuing buildup of $TPP^•$ could be monitored at 550 nm. Attempted measurements at 380 nm, the maximum wavelength for the molybdenum dimer, were not successful since TPP^+ also absorbs at that wavelength, greatly complicating the kinetic analysis. Experiments were carried out under the following concentration conditions: 20–30 μM $[CpMo(CO)_3]_2$ (which gives $[CpMo(CO)_3]_0 \sim 10$–15 μM) and 30–80 mM TPP^+. The relatively high TPP^+ concentrations were needed, lest the competing radical combination pathway of eq 5 predominate. The kinetic treatment requires the consideration of both reactions 5 and 8, since appreciable amounts of the molybdenum radical disappeared by each pathway under these conditions. The rate of disappearance of $CpMo(CO)_3^•$ is given by the combined rates of the two reactions (eq 10).

$$-\frac{d[CpMo(CO)_3^•]}{dt} = 2k_c[CpMo(CO)_3^•]^2 + k_8[TPP^+][CpMo(CO)_3^•] \quad (10)$$

The solution of this equation[19–21] for the case $[TPP^+]_0 \gg [CpMo(CO)_3^•]_0$ can be expressed in terms of the increase with time of the absorbance of $TPP^•$ at 550 nm (eq 11):

$$Abs_t = Abs_0 + \frac{\epsilon_{TPP^•}k_\psi}{2k_c} \ln\left\{1 + \frac{2k_c[CpMo(CO)_3^•]_0}{k_\psi}(1 - e^{-k_\psi t})\right\} \quad (11)$$

where $k_\psi = k_8[TPP^+]$. All of the quantities in this equation are known save for k_ψ, which was obtained by nonlinear least-squares fitting. Since the accuracy of $[CpMo(CO)_3]_0$ is limited, it, too, was floated in the fitting procedure for eq 10. One such experiment is depicted in Figure 1, which also displays the fitted curve. The rate constant was determined by fitting five experimental curves at each $[TPP^+]$, which gave values of k_ψ that agreed to within a standard error of 8%. The values of k_ψ were directly proportional of $[TPP^+]$, giving $k_8 = (2.52 \pm 0.11) \times 10^6$ L mol^{-1} s^{-1} at 23 °C in acetonitrile.

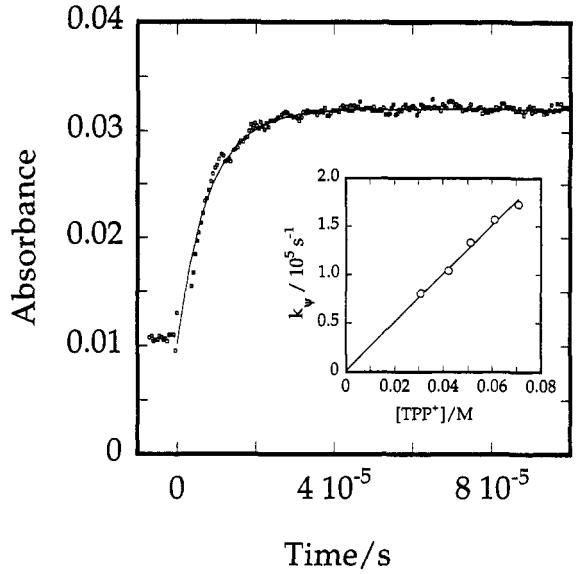

Figure 1. Absorbance–time trace for the reduction of TPP^+ ion by $CpMo(CO)_3^•$ in acetonitrile. The trace was monitored at 550 nm, where $TPP^•$ has an absorption maximum. Conditions: $[Cp_2Mo_2(CO)_6] = 20$ μM, $[TPP^+] = 0.07$ M, and $[CpMo(CO)_3^•] \sim 10$ μM. The smooth curve shows the fit of the data to eq 11. The inset shows that the values of k_ψ are directly proportional to $[TPP^+]$.

Oxidation of $TPP^•$ by $CpMo(CO)_3^•$. Estimates from the Marcus equation and from preliminary experiments on the reaction between $CpMo(CO)_3^•$ and $TPP^•$ indicated that k_9 would approach the diffusion-controlled limit. The magnitude of this rate constant, the necessity of using >10 μM $CpMo(CO)_3^•$ to attain a sufficient absorbance change, the need for ≥0.14 mM $TPP^•$ for the kinetic treatment to be applicable, and the need for ≤0.18 mM $TPP^•$ to stay within the time scale for the flash photolysis apparatus used governed the allowable concentration conditions. These conditions also drove the reaction to >95% completion, allowing k_{-9} to be ignored in these experiments. The absorbance–time curves were fit to first-order kinetics and yielded values of k_ψ that were directly proportional to $[TPP^•]$: $k_\psi = k_9[TPP^•]$ This treatment, presented in Figure 2, afforded $k_9 = (2.09 \pm 0.03) \times 10^9$ L mol^{-1} s^{-1} at 23 °C in acetonitrile.

(18) Balla, J.; Espenson, J. H.; Bakac, A. *Organometallics* **1994**, *13*, 1073.
(19) Scott, S. L.; Espenson, J. H.; Zhu, Z. *J. Am. Chem. Soc.* **1993**, *115*, 1789–1797.
(20) Scott, S. L.; Espenson, J. H.; Chen, W.-J. *Organometallics* **1993**, *12*, 4077–4084.
(21) Zhu, Z.; Espenson, J. H. *Organometallics* **1994**, *13*, 1893–1898.

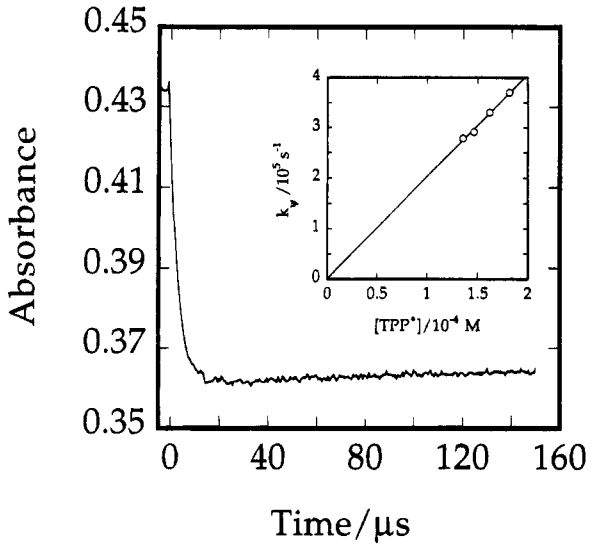

Figure 2. Typical kinetic trace for the oxidation of TPP• by $CpMo(CO)_3$• in acetonitrile. The reaction was monitored at 550 nm, where TPP• has an absorption maximum. Conditions: $[Cp_2Mo_2(CO)_6] = 30\ \mu M$, [TPP•] = 17 mM, and $[CpMo(CO)_3\bullet] \sim 10\ \mu M$. The small rising portion at long times corresponds to the re-equilibration of TPP• and $(TPP)_2$ as in eq 6. The inset shows the first-order rate constant is directly proportional to [TPP•] over the limited range of concentrations where measurements were possible.

On a longer time scale the absorbance started to drift upward, which is also apparent in Figure 2. This was traced simply to the re-equilibration of the TPP• dimerization equilibrium, eq 6. Both the timing of this event and the amplitude of the absorbance change are consistent with such an assignment. The dimerization of TPP• could be and was ignored for the data analysis in the main reaction, as it was a very minor component on the time scale used for the determination of k_9.

Oxidation of $CpMo(CO)_3^-$ by TPP^+. When solutions of these ions in acetontrile were mixed, the brilliant yellow color of the triphenylpyrylium ion faded immediately, and the solution took on the pink color of TPP•. The molybdenum dimer was also formed to a certain extent, and it is also pink, but the intensity of the color and, more specifically, the UV–vis absorption spectrum identified the formation of TPP•. The spectral changes occurred on the millisecond time scale and could be shown to occur according to the reverse of reaction 9.

The data could not be fit by considering k_{-9} alone, however, and they did not fit first-order kinetics when concentrations were adjusted such that $[TPP^+]_0 \gg [CpMo(CO)_3^-]_0$. The reason is that $CpMo(CO)_3$• formed in that step partitions between two reactions, namely, oxidation of TPP^+ (eq 8) and return to $CpMo(CO)_3^-$; irreversible radical recombination (eq 5) was unimportant under these conditions. This family of kinetic equations has no closed-form solution that expresses the monitored variable (Abs_{550} or [TPP•]) as a function of time. To deal with this situation we used a numerical integration routine for kinetic data that allowed for the refinement of kinetic parameter(s) within the model. This program is called FITSIM,[22] and it is a component of modeling program KINSIM.[23,24] The concentration conditions for these experiments were as follows: $[CpMo(CO)_3^-] = 3.6–8.5\ \mu M$ and $[TPP^+] = 4.9–12.2$ mM. Under these conditions <2% of the TPP• is transformed to $(TPP)_2$, and so reaction 6 was ignored. Values of k_c and k_8 were set at their known values, such that k_{-9} was the only fitted parameter. This refinement procedure gave $k_{-9} = (1.13 \pm 0.07) \times 10^4\ L\ mol^{-1}\ s^{-1}$ at 23 °C in acetonitrile.

Another approach to the analysis of the kinetic data for the reaction of $CpMo(CO)_3^-$ and TPP^+ is to integrate the rate law making the steady-state approximation for the reactive molybdenum radical. This treatment ignores the dimerization of $CoMo(CO)_3$•, but that is clearly valid under these conditions. Integration affords eq 12

$$\{2(k_9/k_8)x_0 + [TPP^+]\} \ln x - 2(k_9/k_8)x = -kt + I \quad (12)$$

where $x = [CpMo(CO)_3^-]$ and $k = k_{-9}[TPP^+]^2$. Analysis of the stopped-flow data by this method, with the values of k_8 and k_9 set at their determined values, gave $k_{-9} = (1.1 \pm 0.1) \times 10^4\ L\ mol^{-1}\ s^{-1}$, which agrees with the value obtained by numerical analysis.

A reaction was conducted between $CpMo(CO)_3^-$ (0.20 mM) and TPP^+ (10 mM) in argon-saturated acetonitrile in the dark. After 4 h the products were analyzed by HPLC, and no $[CpMo(CO)_3]_2$ was found. This confirmed experimentally the same conclusion that one could arrive at by considering the various competitive reactions under this set of conditions.

Discussion

We shall consider first the thermodynamics of each electron transfer reaction between the mononuclear organomolybdenum species and the pyrylium cation–pyranyl radical. Comparisons with the TMPD system are desirable. These are the applicable electrode potentials in acetonitrile, relative to SSCE.

$$CpMo(CO)_3NCCH_3^+ \xrightarrow{(-0.50)^{25}} CpMo(CO)_3\bullet \xrightarrow{(-0.080)^{25}} CpMo(CO)_3^-$$

$$TPP^+ \xrightarrow{(-0.39)^8} TPP\bullet$$

$$TMPD^{\bullet+} \xrightarrow{(+0.16)^{10}} TMPD$$

The value of K_9 calculated from ΔE° is 1.7×10^5, which agrees quite well with the quotient of the independently determined values of the forward and reverse rate constants, $k_9/k_{-9} = 1.8 \times 10^5$. This agreement lends confidence that the correct kinetic treatments have been applied to the composite set of reactions.

It was earlier found[11,17] that TMPD catalyzes the disproportionation of $CpMo(CO)_3$•, as written in eq 4. More precisely stated, the metal radical partitions

(22) Zimmerle, C. T.; Frieden, C. *Biochem. J.* **1989**, *258*, 381–387.

(23) Barshop, B. A.; Wrenn, R. F.; Frieden, C. *Anal. Biochem.* **1983**, *130*, 134.

(24) Frieden, C. *Methods Enzymol.* **1994**, *240*, 311–322.

(25) Pugh, J. R.; Meyer, T. J. *J. Am. Chem. Soc.* **1992**, *114*, 3784.

Table 1. Summary of Kinetic and Thermodynamic Data for the Reactions of $CpMo(CO)_3^•$ with Electron Acceptor–Donor Pairs[a,b]

	A = TPP		A = TMPD	
reaction	rate const[c]	equil. const	rate const[c]	equil. const
$Mo^• + A^+ = Mo^+ + A$	$k_f = 2.5 \times 10^6$ $k_r \sim 300$ (calcd)	3.5×10^3	$k_f = 1.8 \times 10^6$ $k_r \sim 10^{-3}$ (calcd)	10^{11}
$Mo^• + A = Mo^- + A^+$	$k_f = 2.1 \times 10^9$ $k_r = 1.13 \times 10^4$	1.7×10^5	$k_f = 1.5 \times 10^7$ $k_r = 7.9 \times 10^9$	1.9×10^{-3}

[a] In acetonitrile at 23 °C. [b] $A^+ = TPP^+$ and $TMPD^{•+}$; $A = TPP^•$ and TMPD. "Mo" = $CpMo(CO)_3$. [c] In L mol^{-1} s^{-1}.

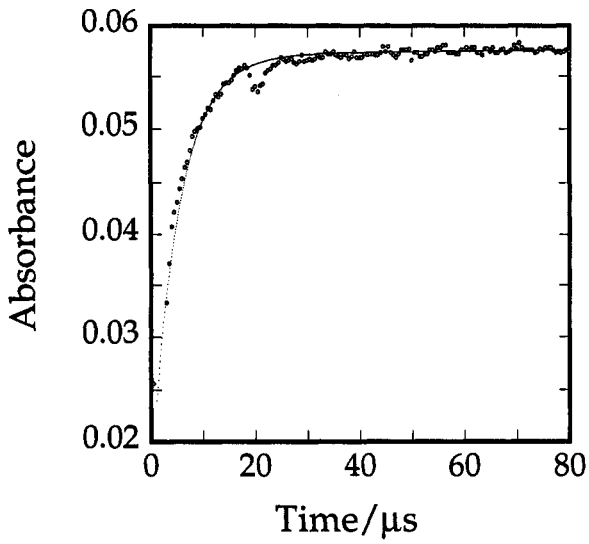

Figure 3. Simulated absorbance–time curve generated by the KINSIM program overlaid with the experimental trace for the reduction of TPP^+ ion by $CpMo(CO)_3^•$ in acetonitrile. Conditions: 32 μM $[CpMo(CO)_3]_2$, 61 mM TPP^+, and ~16 μM $CpMo(CO)_3^•$.

between the thermally irreversible radical combination reaction, eq 5, and the two single-electron steps, eqs 2 and 3. The proportion of recovered $[CpMo(CO)_3]_2$ and of the ionic molybdenum products depends on the concentration of TMPD taken. The implied stoichiometry is correct, however, only in the limited context of the equilibrium constants and rate constants that define the TMPD system. With $TPP^+/TPP^•$, however, the stoichiometric results are different, since the kinetic and thermodynamic balance has been altered.

Stoichiometry of Reactions Involving $TPP^+/TPP^•$. The values of the rate constants and equilibrium constants are quite different in the TPP system as compared to TMPD, as summarized in Table 1. These comparisons make it clear that, in phenomenological terms, TPP and TMPD are expected to and do behave differently. The equilibrium constants themselves do not define the "final" position in practical terms, because the irreversible dimerization of $CpMo(CO)_3^•$ enters the picture. In other words, it is the combination of rate constants and equilibrium constants and of the initial concentrations that determines where the reactions come to rest. A corollary is as follows: since the molybdenum ions, $CpMo(CO)_3NCCH_3^+$ and $CpMo(CO)_3^-$, are never in equilibrium with the dimer, the system as a whole does not attain a true thermodynamic equilibrium in any reasonable time.

To aid in an understanding of these differences and their origins, certain numerical simulations were carried out for each of the reactions examined, setting the concentrations at values typical, or near the midpoint,

Table 2. Final Concentrations Simulated[a] for the Various Combinations of Starting Materials Used in the Experimental Study

start				final				
conc/μM		conc/mM		conc/μM				
$[Mo^•]$	$[Mo^-]$	$[TPP^•]$	$[TPP^+]$	$2[Mo_2]$	$[Mo^-]$	$[Mo^+]$	$[TPP^•]$	$[TPP^+]$
15	0	0	60	2.4	~0.9	12	11	B
15	0	0.16	0	1.3	14	~0	B	14
0	15	0	10	~0	~0	15	29	B

[a] Results obtained with the use of the program KINSIM.[20–22] B = bulk concentration, substantially unchanged. "Mo" = $CpMo(CO)_3$.

of those used in this work. Three such simulations were made in the TPP system, corresponding to the three families of kinetics experiments reported herein. Each simulation consisted of entering into the modeling program KINSIM[21–23] the set of initial concentrations, having specified the value of k_c and the four rate constants from Table 1. The program displayed the evolution of each concentration over time and in its final state. Figure 3 shows the overlay of one of the simulations compared with the experimental absorbance–time trace. Note that no provision was needed for the extremely slow, albeit thermodynamically favorable, reaction between $CpMo(CO)_3^-$ and $CpMo(CO)_3NCCH_3^+$. The results of certain kinetic simulations are presented in Table 2. Among other things, they allow a description of the reaction stoichiometry. In terms of the percentage of molybdenum reagent that undergoes a given reaction, the findings are as follows:

(a) $CpMo(CO)_3^•$ + TPP^+: 78% reaction 8, 16% reaction 9, and 6% reaction 5. Roughly, this amounts to the formation of $CpMo(CO)_3^+$ and $TPP^•$, but reduction and dimerization of the molybdenum radical occur to minor extents.

(b) $CpMo(CO)_3^•$ + $TPP^•$: 91% reaction 9 and 9% reaction 5. The principal products are thus $CpMo(CO)_3^-$ and TPP^+, with some radical recombination.

(c) $CpMo(CO)_3^-$ + TPP^+: 100% each of reaction 8 and the reverse of reaction 9. To high accuracy the result is the combination of the two (eq 13).

$$CpMo(CO)_3^- + 2TPP^+ = CpMo(CO)_3^+ + 2TPP^• \quad (13)$$

Kinetic Considerations. The value of k_9, 2.1×10^9 L mol^{-1} s^{-1}, is so close to the diffusion-controlled limit in acetonitrile, 1.9×10^{10} L mol^{-1} s^{-1}, that an analysis in terms of Marcus–Hush theory is not realistic. On the other hand, it does reaffirm that the electron exchange rate constants of both partners, $CpMo(CO)_3^•/CoMo(CO)_3^-$ and $TPP^+/TPP^•$, are quite large. This is not unexpected since inner-shell reorganization should be minimal.

The values of the rate constants for the oxidation of $CpMo(CO)_3^•$ by TPP^+ ($k_8 = 2.5 \times 10^6$ L mol^{-1} s^{-1}) and

by $TMPD^{\bullet+}$ ($k_3 = 1.8 \times 10^6$ L mol^{-1} s^{-1}) are surprisingly similar, given that the equilibrium constants for reactions 8 and 3 differ by 8 orders of magnitude (refer to Table 1). Were one to consider this similarity in terms of the Marcus cross-relation, it would then be necessary to postulate what is clearly untenable: a remarkable difference in the electron exchange rate constants for the $TPP^+/TPP^{\bullet}$ and $TMPD^{\bullet+}/TMPD$ partners.

It seems instead that both reactions are proceeding at a diffusion-controlled rate, the reagents being $[CpMo(CO)_3{\cdot}NCCH_3]^{\bullet}$ and TPP^+ (or $TMPD^{\bullet+}$). This adopts the point of view advocated by Tilset,[26] who points out that (a) the equilibrium constant for the oxidation of the molybdenum radical with coordinated acetonitrile to the 18e organometallic cation is 10^{25} times that for the oxidation of the 17e radical to the immediate 16e product, (b) the standard reduction potential is 1.4 V more negative for the couple with coordinated acetonitrile than without, and (c) the solvated organometallic radical, sometimes called a 19e radical, binds acetonitrile very loosely, $10^{-6} < K_{14} < 10^{-3}$ L mol^{-1}, as shown in reaction 14.

If this viewpoint is adopted, the value of k_8 would then be $K_{14}k_{15}$. Analogously, k_3 would be the product of K_{14}

$$CpMo(CO)_3^{\bullet} + CH_3CN \overset{K_{14}}{\rightleftharpoons} [CpMo(CO)_3NCCH_3^{\bullet}] \quad (14)$$

$$[CpMo(CO)_3NCCH_3^{\bullet}] + TPP^+ \xrightarrow{k_{15}} CpMo(CO)_3NCCH_3^{+} + TPP^{\bullet} \quad (15)$$

and the bimolecular rate constant between the 19e radical and TPP^+. If this composite rate constant is taken to be the diffusion-controlled value in acetonitrile, 1.9×10^{10} L mol^{-1} s^{-1}, on the basis that both reactions 3 and 8 have nearly the same experimental rate constant, then $K_{14} = 1.3 \times 10^{-4}$ (from k_8) and 0.9×10^{-4} (from k_3). Because of this agreement, we are now inclined to this view; the values of K_{14} are in excellent agreement despite their being derived from reactions that present a large difference in driving force.

Acknowledgment. This work was supported by the U.S. Department of Energy, Office of Basic Energy Sciences, Division of Chemical Sciences, under Contract No. W-7405-Eng-82. We gratefully acknowledge discussions with J. Balla and A. Bakac.

OM950442X

(26) Tilset, M. *Inorg. Chem.* **1994**, *33*, 3121–3126.

Photoinduced Electron Transfer from Polygermane to C_{60} Studied by Laser Flash Photolysis

Akira Watanabe,[†] Osamu Ito,*[,†] and Kunio Mochida[‡]

Institute for Chemical Reaction Science, Tohoku University Katahira, Aoba-ku, Sendai 980-77, Japan, and Department of Chemistry, Faculty of Science, Gakushuin University, 1-5-1, Mejiro, Tokyo 171, Japan

Received March 6, 1995[⊗]

Electron transfer from poly(phenylmethylgermylene) (PMePhGe) to photoexcited C_{60} in benzene–acetonitrile solution has been investigated by 532 nm laser flash photolysis in the near-IR region. The transient absorption band of the C_{60} triplet state ($^3C_{60}$*) appeared immediately after nanosecond laser exposure. With the decay of $^3C_{60}$*, the absorption bands of the radical anion of C_{60} ($C_{60}^{\bullet-}$) and the radical cation of PMePhGe appeared in the region 900–1600 nm. The rate constant of the electron transfer from PMePhGe to $^3C_{60}$* was determined to be 2.33×10^8 M^{-1} s^{-1}, which was similar to that for poly(methylphenylsilylene). Electron transfer from the singlet state of C_{60} ($^1C_{60}$*) was investigated by fluorescence quenching experiments using a picosecond fluorescence lifetime measurement system, and the quenching rate constant was determined to be 4.00×10^{10} M^{-1} s^{-1}. The rate constant of intersystem crossing from $^1C_{60}$* to $^3C_{60}$* was determined to be 1.10×10^9 s^{-1} by picosecond time-resolved absorption spectroscopy using a streak camera. Electron transfer from $^1C_{60}$* to PMePhGe and intersystem crossing from $^1C_{60}$* to $^3C_{60}$* are competitive, and the intersystem crossing is dominant in a dilute solution system. When a 355 nm laser was used as the excitation light, photochemical intermediates were produced from the direct photolysis of PMePhGe in addition to the electron transfer.

Introduction

It has been reported that photoexcited fullerenes act as good electron acceptors;[1-8] as electron donors, aromatic amines with π-electron-rich donors have been frequently used. Photoinduced electron transfer reactions have investigated by photochemical techniques such as transient electronic absorption spectroscopy. By these methods, it has been revealed that the electron transfer takes place via the triplet state of C_{60} ($^3C_{60}$*).

Photoinduced electric conductivity has been reported for polymers doped with C_{60}. Some π-donors have been reported[9-11] as showing photoconductivity. In our previous report,[12] we investigated photoinduced electron transfer from poly(vinylcarbazole) to $^3C_{60}$* by the laser flash photolysis method, from which the electron transfer mechanism has been revealed by following the decay of $^3C_{60}$* and rise of the radical anion of C_{60} ($C_{60}^{\bullet-}$) and cation radical of poly(vinylcarbazole) in the near-IR region. Laser flash photolysis was also successfully applied to poly(methyl methacrylate) doped with C_{60} and an aromatic amine.[13] In the case of σ-conjugated polymers such as polysilanes, photoconductivities have been investigated,[14,15] and electron transfer between C_{60} and polysilanes occurs in the initial step of carrier formation. We also succeeded in the observation of $C_{60}^{\bullet-}$ and the cation radical of polysilane in the near-IR region, in addition to $^3C_{60}$*.[16] In this paper, we will apply this technique to the system of polygermane and C_{60}. The formation of $C_{60}^{\bullet-}$ and polygermane radical cation by electron transfer via $^3C_{60}$* was studied by nanosecond laser flash photolysis. The possibility of electron transfer via the singlet state of C_{60} ($^1C_{60}$*) was investigated by fluorescence quenching experiments using a picosecond fluorescence lifetime measurement system.

Experimental Section

C_{60} (99.9%) was obtained from Texas Fullerene Corp. Poly(phenylmethylgermylene), abbreviated as PMePhGe in this study, was prepared by the Kipping reaction in toluene at 110 °C using Na.[17] The molecular weight was determined to be 5020 by GPC using monodispersed polystyrene as the standard; thus, the degree of polymerization (n) is 32. C_{60} and

[†] Tohoku University Katahira.
[‡] Gakushuin University.
[⊗] Abstract published in *Advance ACS Abstracts,* August 1, 1995.

(1) Sension, R.; Szarka, A. Z.; Smith, G. R.; Hochstrasser, R. M. *Chem. Phys. Lett.* **1991**, *185*, 179.
(2) Arbogast, J. W.; Foote, C. S. *J. Am. Chem. Soc.* **1991**, *113*, 8886.
(3) Arbogast, J. W.; Foote, C. S.; Kao, M. *J. Am. Chem. Soc.* **1992**, *114*, 2277.
(4) Biczok, L.; Linschitz, H. *Chem. Phys. Lett.* **1992**, *195*, 339.
(5) Osaki, T.; Tai, Y.; Tazawa, M.; Tanemura, S.; Inukawa, K.; Ishiguro, K.; Sawaki, Y.; Saito, Y.; Shinohara, H.; Nagashima, H. *Chem. Lett.* **1993**, 789.
(6) Nonell, S.; Arbogast, J. W.; Foote, C. S. *J. Phys. Chem.* **1992**, *96*, 4169.
(7) Guldi, D. M.; Hungerbuhler, H.; Janata, E.; Asmus, K.-D. *J. Chem. Soc., Chem. Commun.* **1993**, 84.
(8) Ghosh, H.; Pal, H.; Sapre, A. V.; Mittal, J. P. *J. Am. Chem. Soc.* **1993**, *115*, 11722.
(9) Wang, Y. *Nature* **1992**, *356*, 585.
(10) Wang, Y.; Herron, N.; Caspar, J. *Mater. Sci. Eng. B* **1993**, *B19*, 61.
(11) Yoshino, K.; Xiao, H. Y.; Nuro, K.; Kiyomatsu, S.; Morita, S.; Zakihdov, A. A.; Noguchi, T.; Ohnishi, T. *Jpn. J. Appl. Phys.* **1933**, *32*, L357.
(12) Watanabe, A.; Ito. O. *J. Chem. Soc. Chem. Commun.* **1994**, 1285.
(13) Gevaert, M.; Kamat, P. V. *J. Phys. Chem.* **1992**, *96*, 9883.
(14) Wang, Y.; West, R.; Yuan. C.-H. *J. Am. Chem. Soc.* **1993**, *115*, 3844.
(15) Kepler, R. G.; Cahill, P. A. *Appl. Phys. Lett.* **1933**, *63*, 1552.
(16) Watanabe, A.; Ito, O. *J. Phys. Chem.* **1994**, *98*, 7736.
(17) Mochida, K.; Chiba, H. *J. Orgnomet. Chem.* **1944**, *473*, 45.

0276-7333/95/2314-4281$09.00/0

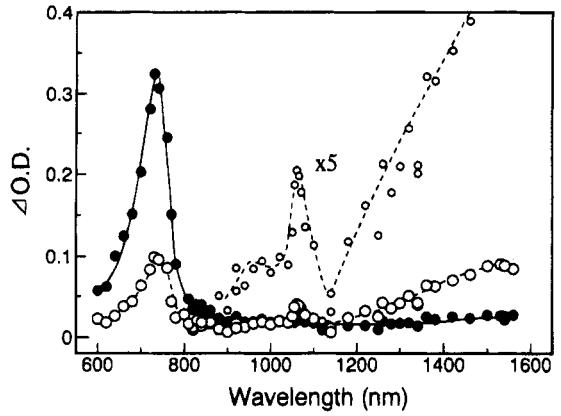

Figure 1. Transient absorption spectra obtained by 532 nm laser flash photolysis of 0.1 mM C_{60} in the presence of PMePhGe (5 mM in monomer unit) in a benzene–acetonitrile (2/1 (v/v)) solvent mixture: (●) 100 ns; (○) 1000 ns.

PMePhGe were dissolved in a benzene and acetonitrile solvent mixture (2/1 (v/v)) deaerated with nitrogen bubbling before the measurements.

The solution was excited by a Nd:YAG laser (Quanta-Ray, GCR-130, 6 ns fwhm) at 355 or 532 nm. A pulsed xenon flash lamp (Tokyo Instruments, XF80-60, 15 J, 60 μs fwhm) was used for the probe beam, which was detected with a Ge-APD module (Hamamatsu Photonics, C5331-SPL) after passing through the photochemical quartz vessel (10 mm × 10 mm) and a monochromator. The Ge-APD module consists of a germanium avalanche photodiode (B2834), a high-speed current-to-voltage amplifier, and a high-voltage bias circuit on a compact board and shows high sensitivity in the frequency range 0.004–100 MHz.[12,16,18] The output from Ge-APD was recorded with a digitizing oscilloscope (HP 54510B, 300 MHz) and analyzed by a personal computer (NEC, PC98). The transient absorption spectra in the UV–visible region were measured with an optical multichannel system (UNISOKU, USP-500) after the appropriate delay time. The solution UV–visible absorption spectra were recorded with a Hitachi U-3400 spectrometer.

The fluorescence lifetimes were measured using an argon ion laser (Spectra-Physics, BeamLok 2060-10-SA), a pumped Ti:sapphire laser (Spectra-Physics, Tsunami 3950-L2S, 1.5 ps fwhm) with a pulse selector (Spectra-Physics, Model 3980), a frequency doubler (GWU-23PS), and a streak scope (Hamamatsu Photonics, C4334-01). Intersystem crossing from $^1C_{60}$* to $^3C_{60}$* was observed using a picosecond time-resolved absorption spectrometer which consists of an active/passive mode-locked Nd:YAG laser (Continuum, PY61C-10, 30 ps fwhm), optical delay lines, and a streak scope (Hamamatsu Photonics, C2830). A continuum probe light with relatively long duration (50 ns) is generated by the breakdown of Xe gas focusing the 1064 nm laser beam onto the Xe tube.[19,20] All experiments were carried out at 20 °C.

Results and Discussion

Figure 1 shows the transient absorption spectra in the near-IR region obtained after the laser flash photolysis of C_{60} with 532 nm light in the presence of 5 mM (in monomer units) of PMePhGe in a mixed solvent (benzene–acetonitrile, 2/1 (v/v)). The absorption band at 730 nm which appears immediately after laser exposure is attributed to $^3C_{60}$*.[21–24] With the decay of the absorption intensity of $^3C_{60}$*, the intensities of the

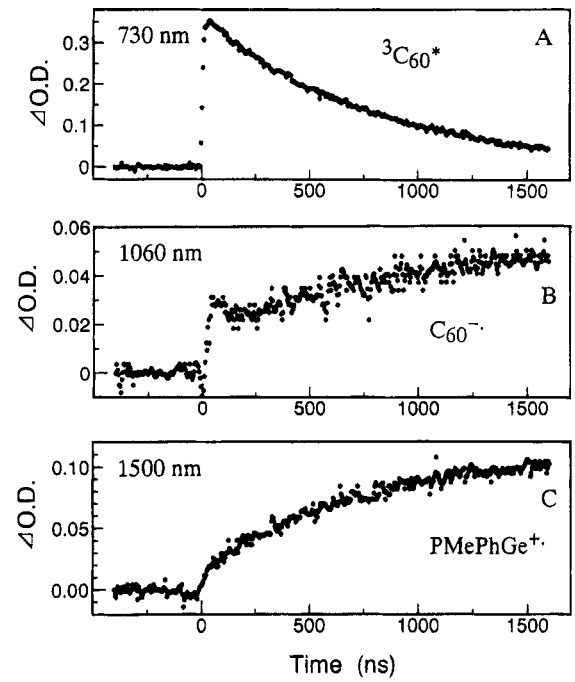

Figure 2. Absorption-time profiles obtained by 532 nm laser flash photolysis of 0.1 mM C_{60} in the presence of 5 mM PMePhGe in a benzene–acetonitrile mixed solvent (2/1 (v/v)): (A) 730 nm; (B) 1060 nm; (C) 1500 nm.

absorption bands increase in the region 900–1600 nm. The absorption band at 1030 nm is a characteristic band of the radical anion of C_{60} ($C_{60}^{\bullet-}$).[25,26] The broad absorption band extending from 1200 to 1600 nm may be attributed to the radical cation of PMePhGe (PhMeGe$^{\bullet+}$) in analogy to the broad absorption bands of the radical cations of polysilanes in a similar region.[27,28] Such radical ions generated by the electron transfer were not observed in neat benzene. $^3C_{60}$* is the only transient species observed by nanosecond laser flash photolysis in a nonpolar solvent, benzene. The same result was obtained in our previous study on electron transfer between C_{60} and poly(methylphenylsilylene) (PMePhSi).[16] The electron transfer from PMePhSi to $^3C_{60}$* shows a clear solvent polarity effect, where the electron transfer rate increases with the solvent polarity. A similar solvent polarity effect has been reported for the electron transfer from a low-molecular-weight donor to $^3C_{60}$* or $^3C_{70}$*.[5,29]

In Figure 2, the time profiles of the absorption bands observed under the conditions described in Figure 1 are shown. The absorption intensity of $^3C_{60}$* at 730 nm decays with a lifetime of ca. 500 ns in the presence of 5

(18) Watanabe, A.; Ito, O. *Jpn. J. Appl. Phys.* **1995**, *34*(1), 194.
(19) Sumitani, K.; Yoshihara, K. *Bull. Chem. Soc. Jpn* **1982**, *55*, 85.
(20) Ito, T.; Hiramatsu, M.; Hosoda, M.; Tsuchiya, Y. *Rev. Sci. Instrum.* **1991**, *62*, 1415.
(21) Arbogast, J. W.; Darmanyan, A. P.; Foote, C. S.; Rubin, Y.; Diederich, F. N.;Alvarez, M. M.; Anz, S. J.; Whetten, R. L. *J. Phys. Chem.* **1991**, *95*, 11.
(22) Kajii, Y.; Nakagawa, T.; Suzuki, S.; Achiba, Y.; Obi, K.; Shibuya, K. *Chem. Phys. Lett.* **1991**, *181*, 100.
(23) Sension, R. J.; Phillips, C. M.; Szarka, A. Z.; Romanow, W. J.; Macghie, A. R.; McCauley, J. P.; Smith, A. B., III; Hochstrasser, R. M. *J. Phys. Chem.* **1991**, *95*, 6075.
(24) Dimitrijevic, N. M.; Kamat, P. V. *J. Phys. Chem.* **1992**, *96*, 4811.
(25) Kato, T.; Kodama, T.; Shida, T.; Nakagawa, T.; Matsui, Y.; Suzuki, S.; Shiromaru, H.; Yamauchi, K.; Achiba, Y. *Chem. Phys. Lett.* **1991**, *180*, 446.
(26) Gasyna, Z.; Andrews, L.; Schatz, P. N. *J. Phys. Chem.* **1992**, *96*, 1525.
(27) Ushida, K.; Kira, A.; Tagawa, S.; Yoshida, Y.; Shibata, H. *Polym. Mater. Sci. Eng.* **1992**, *66*, 299.
(28) Irie, S.; Irie, M. *Macromolecules* **1992**, *25*, 1766.
(29) Biczok, L.; Linschitz, H. *Chem. Phys. Lett.* **1992**, *195*, 339.

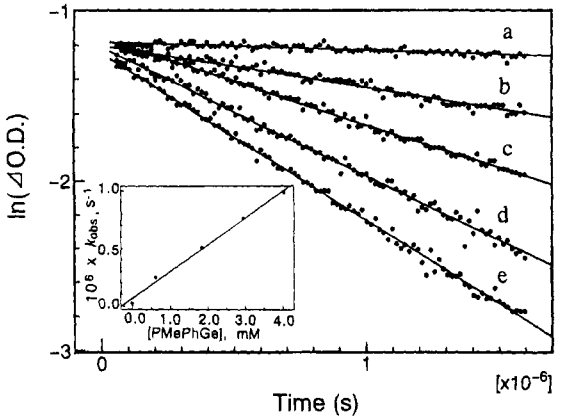

Figure 3. First-order plots for the decay of $^3C_{60}$* at 730 nm in the presence of PMePhGe in a benzene–acetonitrile mixed solvent (2/1 (v/v)). PMePhGe concentration: (a) 0 mM; (b) 0.6 mM; (c) 1.8 mM; (d) 2.9 mM; (e) 4.0 mM. Excitation was at 532 nm. Insert: dependence of the pseudo-first-order rate constant (k_{obsd}) for the decay of $^3C_{60}$* on the concentration of PMePhGe in the monomer unit.

Scheme 1

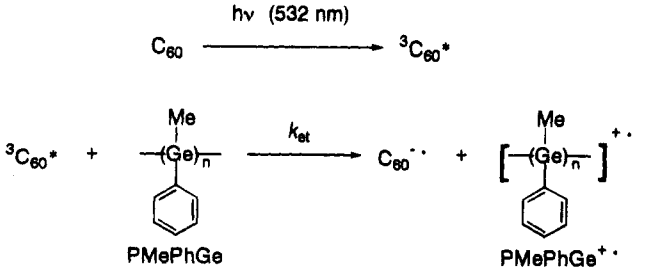

mM of PMePhGe, whereas $^3C_{60}$* decays slowly in the absence of PMePhGe with a lifetime of 2300 ns. The PMePhGe$^{\bullet+}$ band at 1500 nm increases rather smoothly with time as an exponential curve. The absorption intensity of $C_{60}^{\bullet-}$ at 1060 nm increases up to 1600 ns, accompanied by the decay of $^3C_{60}$*, although the initial fast rise is seen in Figure 2B immediately after 532 nm laser pulse excitation. This suggests the existence of a direct path for the electron transfer forming $C_{60}^{\bullet-}$ without passing through $^3C_{60}$*. This direct path is electron transfer via $^1C_{60}$*. The electron transfer process is discussed later using picosecond time-resolved spectroscopy.

From the transient absorption spectra and their profiles, it is revealed that the electron transfer takes place via $^3C_{60}$* with photoexcitation of C_{60} by 532 nm light, which is not absorbed by PMePhGe (Scheme 1).

The reaction rate constant of the electron transfer step (k_{et}) was determined by the decay rate of $^3C_{60}$* at 730 nm; in the presence of PMePhGe at a concentration greater than 0.6 mM, the decay of $^3C_{60}$* obeys the first-order kinetics as shown in Figure 3. The slopes of the first-order plots yield the first-order rate constants (k_{obs}), which increase with the concentration of PMePhGe. The pseudo-first-order plot of k_{obs} against [PMePhGe] (concentration based on monomer repeating unit) is shown in the insert in Figure 3, where a straight line can be obtained. From the slope of the line, the second-order rate constant for the quenching reaction of $^3C_{60}$* with PMePhGe was evaluated to be 2.33×10^8 M^{-1} s^{-1}. From the correspondence of the quenching rate of $^3C_{60}$* with the rise in rates for $C_{60}^{\bullet-}$ and PMePhGe$^{\bullet+}$ as seen in Figure 2, the quenching rate constant thus obtained is attributed to the k_{et} value in Scheme 1.

It is well-known that the k_{et} value depends on the electron donor ability of the counterpart of the electron transfer of C_{60} and on solvent polarity. The ionization energy (IP) of PMePhGe was estimated to be 5.4–5.5 eV,[30] which is in the same range as that for polysilanes (IP = 5.6 eV);[31] thus, the k_{et} value of 2.33×10^8 M^{-1} s^{-1} for PMePhGe is quite similar to that for polysilane with a degree of polymerization comparable to that reported in our previous report (2.11×10^8 M^{-1} s^{-1} in the same solvent).[18] On the other hand, aromatic amines such as *p*-phenylenediamine (IP = 6.8 eV)[32] have k_{et} values of ca. 5×10^9 M^{-1} s^{-1},[3] which is ca. 22 times greater than the observed k_{et} values for PMePhGe. The IP value for a solid polymer film measured by the AC (air counter) method is 1.0–1.5 eV lower than the usual IP value for low-molecular-weight compounds.[31] In a previous paper, we calculated the electron transfer rate constant for PMePhSi using the Rehm–Weller equation and the oxidation potential of PMePhSi (0.93 V vs Ag/Ag^+).[16] In the case of PMePhGe, the oxidation potential has not been reported, but the IP data suggest that the oxidation potential of PMePhGe is quite similar to that of PMePhSi. The calculated value 1.60×10^{10} M^{-1} s^{-1} in a benzene–acetonitrile (2/1) mixed solvent is 69 times greater than the observed value ($k_{et} = 2.33 \times 10^8$ M^{-1} s^{-1}). The inconsistency can be explained by considering the local concentration effect of the polymer chain in a dilute solution. In quenching experiments determining the k_{et} value of the polymer, the donor concentration was based on the monomer repeating units which are concentrated locally. If we imagine electron transfer between C_{60} and a polymer chain, both of which are macromolecules, the quencher concentration becomes lower and the rate constant becomes higher by a factor of the degree of polymerization (32 for PMePhGe). The corrected value considering the local concentration effect corresponded well with the calculated value.

The back-electron-transfer reaction from $C_{60}^{\bullet-}$ to PMePhGe$^{\bullet+}$ seems to be slow; at least, back electron transfer was not observed in 1500 ns, as shown in the time profiles of $C_{60}^{\bullet-}$ and PMePhGe$^{\bullet+}$ in Figure 2. This indicates that the positive charge (hole) of PMePhGe$^{\bullet+}$ migrates quickly along the Ge–Ge main chain apart from $C_{60}^{\bullet-}$, which decreases the chance of the hole encountering the electron.

As mentioned above, the initial fast rise in Figure 2B suggests the possibility of electron transfer via $^1C_{60}$*. A fluorescence quenching experiment is effective in investigating the electron transfer quenching via $^1C_{60}$*.[33] Figure 4 shows the fluorescence spectra of C_{60} in the absence and in the presence of PMePhGe, which were observed by photon counting measurements using a Ti: sapphire laser (375 nm) and a streak camera. The relative fluorescence intensity decreases in the presence of PMePhGe. The fluorescence lifetimes were measured by decay curves, and the fitting curves are shown in

(30) Mochida, K.; Shimoda, M.; Kurosu, H.; Kojima, A. *Polyhedron* **1994**, *13*, *3039*.
(31) Yokoyama, K.; Tokoyama, M. *Solid State Commun.* **1989**, *70*, 241.
(32) Lias, S. G.; Bartmess, J. E.; Holmes, J. L.; Levin, R. D.; Libman, J. F.; Mallard, W. G. *J. Phys. Chem. Ref. Data, Suppl.* **1988**, *17*, Suppl. 1.
(33) Williams, R. M.; Verhoeven, J. W. *Chem. Phys. Lett.* **1992**, *194*, 446.

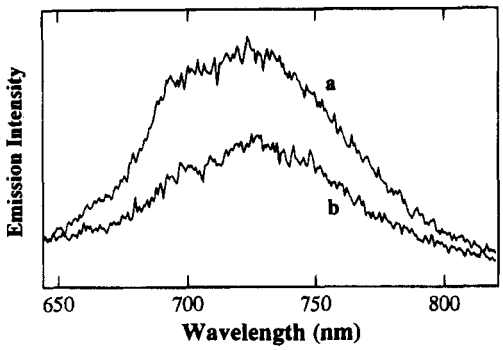

Figure 4. Fluorescence spectra of 0.1 mM C_{60} in the absence (a) and in the presence (b) of PMePhGe (5 mM in monomer unit) in a benzene–acetonitrile 2/1 mixed solvent (2/1) obtained by excitation from the 375 nm pulse of a Ti: sapphire laser.

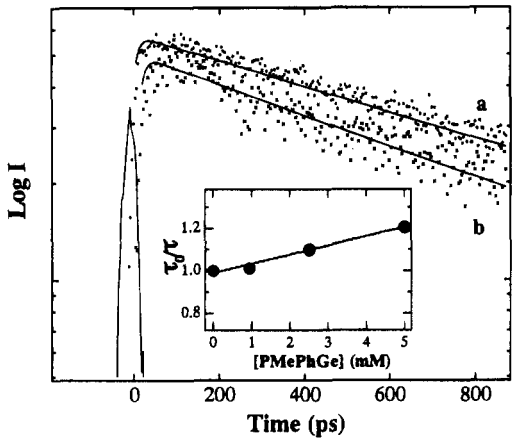

Figure 5. Decay curves of C_{60} fluorescence in the absence (a) and in the presence (b) of PMePhGe (5 mM in monomer unit) in a benzene–acetonitrile (2/1). The insert shows the Stern–Volmer plot of τ/τ_0 against PMePhGe concentration.

Figure 5. The fluorescence lifetime of C_{60} in a benzene–acetonitrile (2/1) mixed solvent was determined to be 1.09 ns. The Stern–Volmer plot, τ_0/τ vs PMePhGe concentration, where τ_0 and τ are fluorescence lifetimes in the absence and in the presence of PMePhGe, is shown as an insert in Figure 5. From the slope and τ_0, the rate constant for quenching of electron transfer from PMePhGe to $^1C_{60}$* was determined to be 4.00×10^{10} M^{-1} s^{-1}. The electron transfer via $^1C_{60}$* gives a rather large rate constant. The electron transfer process is competitive with intersystem crossing from $^1C_{60}$* to $^3C_{60}$*.

Figure 6 shows the absorption–time profile for $^3C_{60}$* at 740 nm obtained by picosecond time-resolved spectroscopy using a streak scope. The growth of the transient absorption corresponds to the formation of $^3C_{60}$* from $^1C_{60}$* by intersystem crossing. By curve fitting as shown in Figure 6, the rate constant for intersystem crossing, k_{isc}, was determined to be 1.10×10^9 s^{-1}. We can estimate the ratio of electron transfer via $^1C_{60}$* to that via $^3C_{60}$* using these rate constants and considering the concentration of PMePhGe (5 mM) in the solution: the electron transfer ratios via $^1C_{60}$* and via $^3C_{60}$* are 15 and 85%, respectively, for a 5 mM PMePhGe solution. The ratio of electron transfer via $^1C_{60}$* increases with increasing concentration of σ-conjugated polymer. In Figure 2, the fast rise of $C_{60}^{\bullet-}$ is attributable to electron transfer via $^1C_{60}$*. In a condensed system such as a C_{60}-doped polysilane film which

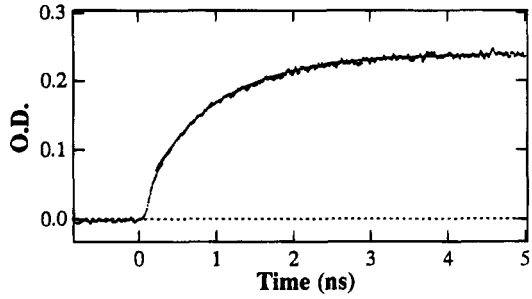

Figure 6. Absorption–time profile of $^3C_{60}$* (740 nm) obtained by picosecond laser flash photolysis using a streak camera for 0.1 mM C_{60} in the absence of PMePhGe.

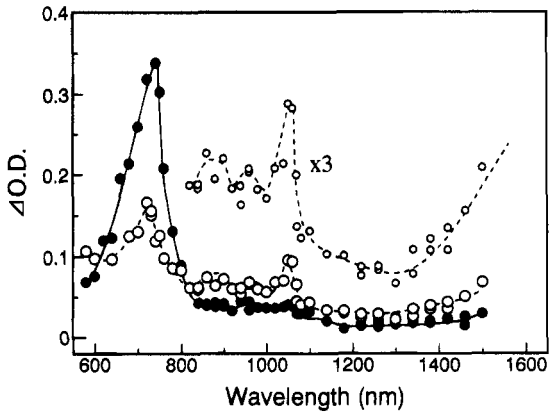

Figure 7. Transient absorption spectra obtained by 355 nm laser flash photolysis of 0.1 mM C_{60} and 5 mM PMePhGe in a benzene–acetonitrile mixed solvent (2/1): (●) 100 ns; (○) 1000 ns.

shows a high photoconductivity, electron transfer via $^1C_{60}$* may be dominant.

When both C_{60} and PMePhGe were photoexcited with 355 nm laser light, the transient absorption spectra were different from those of Figure 1, as shown in Figure 7. The most prominent difference is the decrease in the intensity of the broad absorption band longer than 1200 nm which is characteristic of $PMePhGe^{\bullet+}$. This suggests the formation of some photochemical intermediates of PMePhGe with direct 355 nm laser exposure; intermediates such as free radicals and carbene-type germylenes quickly trap $PMePhGe^{\bullet+}$ formed by electron transfer to $^3C_{60}$*.

In addition, some absorption bands appear in the region 800–1000 nm, which seems to increase in place of the decay of $^3C_{60}$*. The absorption bands between 800 and 1000 nm are similar to those reported for the free radicals, which are produced by the reaction between C_{60} and alkyl radical ($R^{\bullet}$); $R-C_{60}^{\bullet}$.[34] Thus, we can attribute the new absorption bands in the 800–1000 nm region to the free radicals which can be produced by the reaction between C_{60} (or $^3C_{60}$*) and polygermane radicals.

Figure 8A shows the transient spectrum obtained by the direct photolysis of PMePhGe; the absorption bands were observed at 380 and 475 nm. The transient absorption band at 380 nm can be attributed to the germyl radicals, as shown in Scheme 2.[35,36] The transient absorption at 475 nm can be considered as being due to either the Ge-centered radicals or germylenes

(34) Guldi, D. M.; Hungerbuhler, H.; Janata, E.; Asmus, K.-D. *J. Phys. Chem.* **1993**, *97*, 11258.

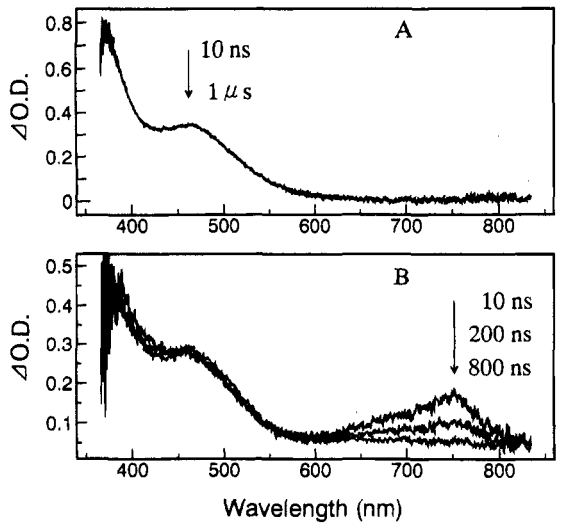

Figure 8. Absorption spectra obtained by 355 nm laser flash photolysis in the visible region of 5 mM PMePhGe (A) and 0.1 mM C_{60} and 5 mM PMePhGe (B) in a benzene–acetonitrile mixed solvent (2/1).

Scheme 2

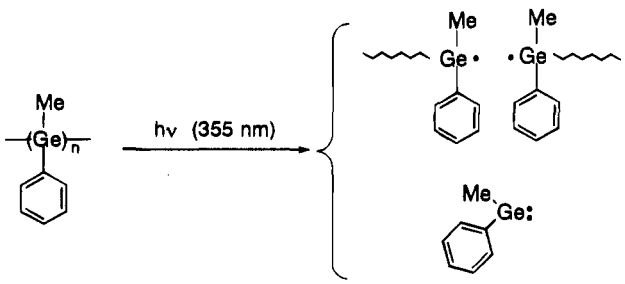

(Scheme 2).[35,36] The decay rates of the 380 and 475 nm bands were not prominent within 1000 ns, suggesting that these photolytic intermediates from PMePhGe are stable in benzene–acetonitrile solvent within the time scale of a few microseconds. This is in agreement with the observation for polysilanes that photolytic intermediates such as Si-centered radicals and silylenes in the polymer backbone are long-lived compared with the low-molecular-weight ones.

In Figure 8B, the transient spectra in the visible region obtained by the 355 nm laser photolysis of both C_{60} and PMePhGe are shown; the absorption band at 740 nm due to $^3C_{60}$* was observed in addition to the photolytic intermediates at 475 nm. The absorption intensity of $^3C_{60}$* decreases with time by accepting electrons from PMePhGe; the decay of $^3C_{60}$* with 355 nm laser excitation is faster than that of $^3C_{60}$* with 532 nm laser excitation in Figures 1 and 2. The absorption intensities at 380 and 475 nm show slow decay, suggesting that photolytic intermediates of PMePhGe at 380 and 475 nm do not play a role as electron donors to $^3C_{60}$*.

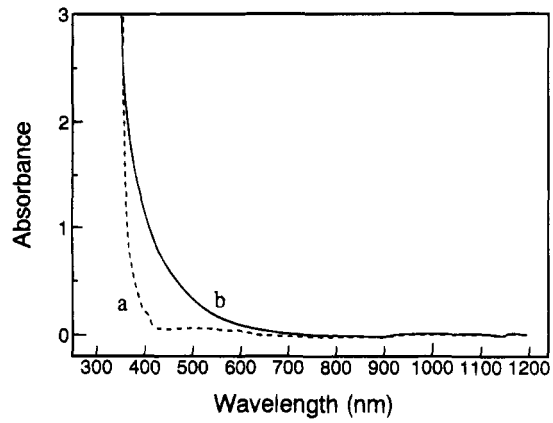

Figure 9. Absorption spectra before (a) and after (b) irradiation of 0.1 mM C_{60} and 5 mM PMePhGe in a benzene/acetonitrile mixed solvent (2/1) with 355 nm laser light of 20 mJ energy for 5 min.

On prolonged 355 nm laser irradiation of C_{60} and PMePhGe, the color of the solution changed from purple to dark brown; the absorption spectra of the solution are shown in Figure 9. Before irradiation, a weak absorption band of C_{60} is seen at 450–600 nm and intense one shorter than 375 nm includes both C_{60} and PMePhGe. After irradiation, a new absorption appears, extending from 375 to 700 nm. C_{60} itself was photostable, and no color change was observed by 355 nm light irradiation. PMePhGe itself is photounstable, but photolysis products do not show intense color. Thus, the observed absorption change may be attributed to the reaction between C_{60} and photochemical intermediates of PMePhGe such as that shown in Scheme 2.

In conclusion, rate constants for electron transfer from PMePhGe to $^3C_{60}$*, electron transfer from PMePhGe to $^1C_{60}$*, and intersystem crossing from $^1C_{60}$* to $^3C_{60}$* were determined to be 2.33×10^8 M^{-1} s^{-1}, 4.00×10^{10} M^{-1} s^{-1}, and 1.10×10^9 s^{-1}, respectively. Electron transfer via $^1C_{60}$* and intersystem crossing are competitive processes. In a dilute solution of C_{60} containing an electron donor in a low concentration, the electron transfer proceeds mainly via $^3C_{60}$* after the intersystem crossing from $^1C_{60}$* to $^3C_{60}$*.

Acknowledgment. We are grateful to Mr. Motoyuki Watanabe, Mr. Haruhisa Saito, and Mr. Musubu Koishi (Hamamatsu Photonics) for their technical support in setting up the picosecond time-resolved absorption and emission spectrometer (URAS system of the Institute for Chemical Reaction Science, Tohoku University).

OM950172I

(35) Mochida, K.; Kimijima, K.; Chiba, H.; Wakasa, M.; Hayashi, H. *Organometallics* **1994**, *13*, 404.
(36) Watanabe, A.; Matsuda, M. *Macromolecules* **1992**, *25*, 484.

Clusters Containing a Quadruply Bridging CO Ligand. Syntheses, Crystal Structures, and Solution Dynamics of $CpWRu_4(CO)_{14}H$ and $Cp^*MRu_4(CO)_{14}H$ (M = Mo, W)

Chi-Jung Su,[†] Yun Chi,*[,†] Shie-Ming Peng,*[,‡] and Gene-Hsiang Lee[‡]

Departments of Chemistry, National Tsing Hua University, Hsinchu 30043, Taiwan, Republic of China, and National Taiwan University, Taipei 10764, Taiwan, Republic of China

Received April 19, 1995[⊗]

The pentametal carbonyl cluster compounds $CpWRu_4(CO)_{14}(\mu_3\text{-H})$ (**4**), $Cp^*MoRu_4(CO)_{14}(\mu_3\text{-H})$ (**5**), and $Cp^*WRu_4(CO)_{14}(\mu_3\text{-H})$ (**6**) were obtained by condensation of $Ru_3(CO)_{12}$ with the corresponding anionic reagents $[CpW(CO)_3][PPN]$ and $[Cp^*M(CO)_3][PPN]$ (M = Mo, W) in the ratio 3:2 in refluxing THF solution, followed by treatment with excess CF_3CO_2H in CH_2Cl_2 at room temperature. The Cp derivative **4** possesses a trigonal-bipyramidal Ru_4W core in which the W atom is located at an equatorial position and the hydride lies on a WRu_2 triangular face. In contrast, the Cp* derivatives **5** and **6** adopt an edge-bridged tetrahedral geometry with a tentacle Cp*M fragment bridging a Ru–Ru edge, on which the novel μ_4-η^2-CO ligand is associated with the local butterfly Ru_3M array (M = Mo, W). The solution dynamics of these three cluster compounds are discussed.

Transition-metal clusters containing a quadruply bridging CO ligand form a very interesting class of organometallic compounds.[1] The unique μ_4-η^2-CO ligand of these clusters is bound to three metal atoms through the carbon atom and to one metal atom through its oxygen atom. Because of the multisite interaction with metal atoms, this bonding mode weakens the C–O bond substantially. As a result, it is implicated as a key intermediate for the reduction of CO on metal clusters[2] and the formation of carbido clusters through direct CO bond cleavage.[3]

The first structure of clusters containing a μ_4-CO ligand was for the tetrairon anionic cluster $[HFe_4(CO)_{13}]^-$.[4] From the variable-temperature ^{13}C NMR data Shriver further demonstrated that it exists as two isomers in equilibrium.[5] As indicated in Scheme 1, one isomer displays a butterfly framework with a μ_4-CO ligand, while the other has a more crowded tetrahedral geometry. As revealed by the X-ray structures of the related complexes $[Fe_4(CO)_{13}(CuPPh_3)][PPN]$ and $[Fe_4(CO)_{13}(HgCH_3)][PPN]$, the tetrahedral isomer contains 1 edge-bridging, 10 terminal, and 2 semibridging CO ligands on the coordination sphere with slightly elongated Fe–Fe bond distances.[6]

Scheme 1

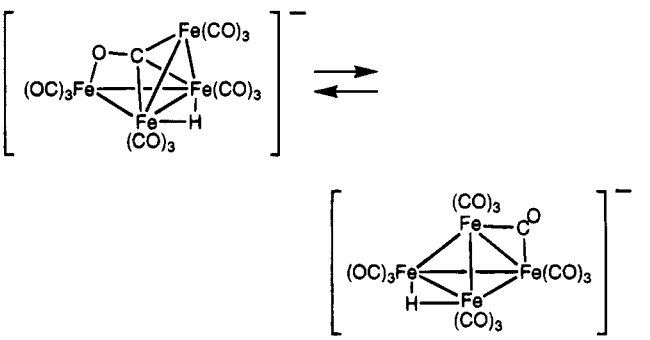

Recently, our research group has prepared a series of closely related tetranuclear carbonyl clusters, $CpWRu_3(CO)_{12}H$ (**1**), $Cp^*WRu_3(CO)_{12}H$ (**2**), and $Cp^*MoRu_3(CO)_{12}H$ (**3**), which also showed the related tautomerization of butterfly and tetrahedral isomers (Scheme 2).[7] In this cluster system, each individual isomer was fully identified according to its X-ray crystal structures, by the solution ^1H and ^{13}C NMR spectral properties, and by comparison with the related crystal structure of osmium derivatives $CpWOs_3(CO)_{12}H$ and $Cp^*WOs_3(CO)_{12}H$.[8] Our results not only allowed us to establish the exact core arrangement of each isomer and the location of its ancillary ligands but also enabled a profound understanding of the μ_4-CO exchange process.[7b] Thus, our system supplements what has not been found in the $[HFe_4(CO)_{13}]^-$ system[4–6] and serves as an alternative model to probe the various factors that control the generation of the μ_4-CO ligands in cluster compounds.

In this paper, we extend our studies of this subject to pentanuclear cluster compounds that possess the em-

[†] National Tsing Hua University.
[‡] National Taiwan University.
[⊗] Abstract published in *Advance ACS Abstracts,* August 1, 1995.

(1) (a) Horwitz, C. P.; Shriver, D. F. *Adv. Organomet. Chem.* **1984**, *23*, 219. (b) Adams, R. D.; Babin, J. E.; Tasi, M. *Angew. Chem., Int. Ed. Engl.* **1987**, *26*, 685. (c) Wang, J.-C.; Lin, R.-C.; Chi, Y.; Peng, S.-H.; Lee, G.-H. *Organometallics* **1993**, *12*, 4061.
(2) (a) Muetterties, E. L.; Stein, J. *Chem. Rev.* **1979**, *79*, 479. (b) Whitmire, K. H.; Shriver, D. F. *J. Am. Chem. Soc.* **1980**, *102*, 1456.
(3) (a) Anson, C. E.; Bailey, P. J.; Conole, G.; Johnson, B. F. G.; Lewis, J.; McPartlin, M.; Powell, H. R. *J. Chem. Soc., Chem. Commun.* **1989**, 442. (b) Bailey, P. J.; Duer, M. J.; Johnson, B. F. G.; Lewis, J.; Conole, C.; McPartlin, M.; Powell, H. R.; Anson, C. E. *J. Organomet. Chem.* **1990**, *383*, 441. (c) Bailey, P. J.; Johnson, B. F. G.; Lewis, J. *Inorg. Chim. Acta* **1994**, *227*, 197. (d) Horwitz, C. P.; Shriver, D. F. *J. Am. Chem. Soc.* **1985**, *107*, 8147.
(4) (a) Hieber, W.; Werner, R. *Chem. Ber.* **1957**, *90*, 286. (b) Manassero, M.; Sansoni, M.; Longoni, G. *J. Chem. Soc., Chem. Commun.* **1976**, 919.
(5) Horwitz, C. P.; Shriver, D. F. *Organometallics* **1984**, *3*, 756.
(6) Horwitz, C. P.; Holt, E. M.; Brock, C. P.; Shriver, D. F. *J. Am. Chem. Soc.* **1985**, *107*, 8136.
(7) (a) Chi, Y.; Wu, F.-J.; Liu, B.-J.; Wang, C.-C.; Wang, S.-L. *J. Chem. Soc., Chem. Commun.* **1989**, 873. (b) Chi, Y.; Su, C.-J.; Farrugia, L. J.; Peng, S.-M.; Lee, G.-H. *Organometallics* **1994**, *13*, 4167.
(8) (a) Churchill, M. R.; Hollander, F. J.; Shapley, J. R.; Foose, D. S. *J. Chem. Soc., Chem. Commun.* **1978**, 534. (b) Peng, S.-M.; Lee, G.-H.; Chi, Y.; Peng, C.-L.; Hwang, L.-S. *J. Organomet. Chem.* **1989**, *371*, 197.

0276-7333/95/2314-4286$09.00/0

Scheme 2

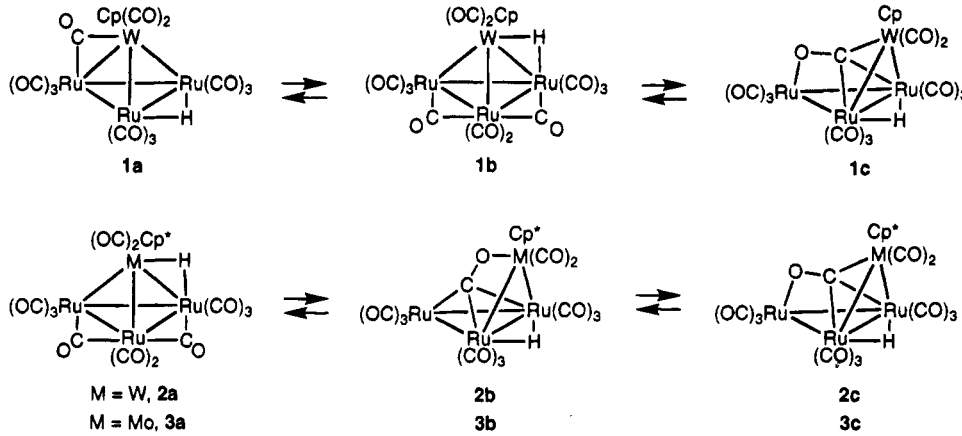

pirical formula $LMRu_4(CO)_{14}H$ (L = Cp, Cp*; M = Mo, W). The cluster compounds isolated, $CpWRu_4(CO)_{14}H$ (**4**), $Cp^*MoRu_4(CO)_{14}H$ (**5**), and $Cp^*WRu_4(CO)_{14}H$ (**6**), also exhibit two different skeletal arrangements, namely the trigonal bipyramid and edge-bridged tetrahedron. Thus, their interchange provides an additional example of the formation of the μ_4-CO ligand via reversible cluster equilibration. The chosen synthetic methodology was related to the redox–condensation procedures in the preparation of tetranuclear complexes **1**–**3**,[9] except that more vigorous conditions and a large excess of $Ru_3(CO)_{12}$ were required to improve the yields of pentametal complexes $LMRu_4(CO)_{14}H$.

Experimental Section

General Information and Materials. Infrared spectra were recorded on a Perkin-Elmer 2000 FT-IR spectrometer. ^1H and ^{13}C NMR spectra were recorded on Bruker AM-400 and AMX-300 instruments; chemical shifts are quoted with respect to the internal standard tetramethylsilane (^1H and ^{13}C NMR). Mass spectra were obtained on a JEOL-HX110 instrument operating in the fast atom bombardment (FAB) mode. All reactions were performed under a nitrogen atmosphere using deoxygenated solvents dried with an appropriate reagent. The progress of reactions was monitored by analytical thin-layer chromatography (5735 Kieselgel 60 F_{254}, Merck), and the products were separated on commercially available preparative thin-layer chromatographic plates (Kieselgel 60 F_{254}, Merck). The complexes $[Cp^*M(CO)_3][PPh_4]$ (M = Mo, W) were prepared from the reaction of Cp*Li slurry with $Mo(CO)_6$ or $W(CO)_6$ in refluxing THF solution, followed by addition of an aqueous solution of tetraphenylphosphonium chloride. The related Cp derivatives $[CpM(CO)_3][PPh_4]$ (M = Mo, W) were prepared under similar experimental conditions. Elemental analyses were performed at the NSC Regional Instrumentation Center at National Cheng Kung University, Tainan, Taiwan.

Reaction of $[CpW(CO)_3][PPh_4]$ with $Ru_3(CO)_{12}$. A THF solution (40 mL) of $Ru_3(CO)_{12}$ (400 mg, 0.63 mmol) and $[CpW(CO)_3][PPh_4]$ (280 mg, 0.42 mmol) was heated at reflux for 1 h under nitrogen, during which time the color turned from orange to dark red. The solvent was removed in vacuo to produce an oily residue. This residue was dissolved in 30 mL of dichloromethane, after which 2 mL of trifluoroacetic acid was added with vigorous stirring. The resulting solution was continuously stirred for 1 h at room temperature. Then the solvent was removed in vacuo and the residue was separated by thin-layer chromatography. Development with a mixture of dichloromethane and hexane in a 2:3 ratio produced two bands, which were removed from the silica gel plates to yield 25 mg of the black pentanuclear cluster $CpWRu_4(CO)_{14}H$ (**4**; 0.08 mmol, 5.6%) and 129 mg of the orange-red tetranuclear cluster $CpWRu_3(CO)_{12}H$ (**1**; 0.145 mmol, 34%) after recrystallization.

Spectral data for **4**: MS (FAB, ^{102}Ru, ^{184}W) *m/z* 1050 (M^+); IR (C_6H_{12}) ν(CO) 2088 (w), 2061 (vs), 2038 (s), 2030 (m), 2011 (w), 1997 (w), 1968 (vw) cm^{-1}; ^1H NMR (CD_2Cl_2, 230 K) δ 6.24 (s, 5H), −14.83 (s, J_{W-H} = 66 Hz); ^{13}C NMR (CD_2Cl_2, 200 K) δ 234.0 (2C, J_{W-C} = 155 Hz), 201.5 (3C), 192.4 (2C), 189.2 (2C), 188.7 (2C). Anal. Calcd for $C_{19}H_6O_{14}Ru_4W$: C, 21.81; H, 0.58. Found: C, 21.71; H, 0.61.

Reaction of $[Cp^*Mo(CO)_3][PPh_4]$ with $Ru_3(CO)_{12}$. A THF solution (40 mL) of $Ru_3(CO)_{12}$ (237 mg, 0.37 mmol) and $[Cp^*Mo(CO)_3][PPh_4]$ (163 mg, 0.25 mmol) was heated at reflux for 6 h under nitrogen, during which time the color turned from orange to dark brown. The solvent was evaporated under vacuum, and the oily residue was redissolved in 30 mL of dichloromethane. After addition of 1 mL of trifluoroacetic acid, the solution was stirred at room temperature for 1 h. After the volatile components were removed under vacuum, the residue was subjected to thin-layer chromatographic separation (dichloromethane–hexane, 2:3), producing 82 mg of the black pentanuclear cluster $Cp^*MoRu_4(CO)_{14}H$ (**5**; 0.08 mmol, 32%) and 32 mg of the black tetranuclear cluster $Cp^*MoRu_3(CO)_{12}H$ (**3**; 0.038 mmol, 15%). The ^{13}CO-enriched samples of **5** were prepared from the reactions of 50% enriched $Ru_3(CO)_{12}$ and regular $[Cp^*Mo(CO)_3][PPh_4]$ under similar conditions. Crystals of **5** suitable for an X-ray diffraction study were obtained from a layered solution of dichloromethane–methanol at room temperature.

Spectral data for **5**: MS (FAB, ^{102}Ru, ^{98}Mo) *m/z* 1033 (M^+); IR (C_6H_{12}) ν(CO) 2076 (m), 2062 (vw), 2043 (vs), 2034 (s), 2020 (s), 1996 (m, br), 1976 (w), 1856 (br, vw) cm^{-1}; ^1H NMR (CD_2Cl_2, 293 K) δ 2.01 (s, 15H, C_5Me_5), −15.08 (**5b**, 10%, 1H), −18.87 (**5a**, 90%, s, 1H); ^{13}C NMR (THF-d_8, 205 K) isomer **5a**, δ 292.1 (μ_4-CO), 240.6, 236.0 (br), 233.1 (Mo–CO), 228.6 (Mo–CO), 199.8 (3C), 199.5, 195.3, 194.9, 194.7, 193.5, 190.0. Anal. Calcd for $C_{24}H_{16}O_{14}Ru_4Mo$: C, 28.03; H, 1.57. Found: C, 27.88; H, 1.61.

Reaction of $[Cp^*W(CO)_3][PPh_4]$ with $Ru_3(CO)_{12}$. Condensation of $Ru_3(CO)_{12}$ with $[Cp^*W(CO)_3][PPh_4]$ in a 3:2 ratio under similar reaction conditions produced the analogous pentanuclear complex $Cp^*WRu_4(CO)_{14}H$ (**6**) and the tetranuclear cluster $Cp^*WRu_3(CO)_{12}H$ (**2**) in 17% and 23% yields, respectively.

Spectral data for **6**: MS (FAB, ^{102}Ru, ^{184}W) *m/z* 1120 (M^+); IR (CCl_4) ν(CO) 2075 (m), 2042 (vs), 2035 (s), 2018 (s), 1996 (br, m), 1974 (w), 1889 (br, vw), 1844 (br, w) cm^{-1}; ^1H NMR ($CDCl_3$, 294 K) δ 1.98 (s, 15H, C_5Me_5), −14.25 (**b**, 33%, s, J_{W-H} = 68 Hz), −19.01 (**a**, s, 67%); ^{13}C NMR (THF-d_8, 270 K) δ 302.0 (μ_4-CO), 228.9, 227.1 (J_{W-C} = 176 Hz), 219.1 (J_{W-C} = 148 Hz), 199.9 (3C), 196.0 (J_{C-H} = 12 Hz), 194.3 (J_{C-H} = 10 Hz), 193.8

(9) Cazanoue, M.; Lugan, N.; Bonnet, J.-J.; Mathieu, R. *Organometallics* **1988**, *7*, 2480.

and 192.7. Anal. Calcd for $C_{24}H_{16}O_{14}Ru_4W$: C, 25.82; H, 1.44. Found: C, 25.73; H, 1.49.

Hydrogenation of Cp*WRu$_4$(CO)$_{14}$H. A toluene solution (25 mL) of Cp*WRu$_4$(CO)$_{14}$H (42 mg, 0.038 mmol) was heated at reflux under 1 atm of dihydrogen for 20 min. The color turned slowly from dark brown to orange during the reaction. After the solution was cooled to room temperature, the solvent was removed and the residue separated by thin-layer chromatography (silica gel, dichloromethane–hexane, 1:4), giving 28 mg of Cp*WRu$_3$(CO)$_{11}$(μ-H)$_3$ (0.03 mmol, 79%) as red-orange needles after recrystallization from dichloromethane–methanol. Hydrogenation of the analogous pentanuclear clusters Cp*MoRu$_4$(CO)$_{14}$H and CpWRu$_4$(CO)$_{14}$H under similar conditions produced the trihydride complexes Cp*MoRu$_3$(CO)$_{11}$(μ-H)$_3$ and CpWRu$_3$(CO)$_{11}$(μ-H)$_3$ in 61% and 63% yields, respectively.

Reaction of Cp*WRu$_4$(CO)$_{14}$H with CO. A toluene solution (20 mL) of Cp*WRu$_4$(CO)$_{14}$H (21 mg, 0.019 mmol) was heated at reflux under 1 atm of CO for 1 h. After the solution was cooled to room temperature, the solvent was removed and the residue separated by thin-layer chromatography (silica gel; dichloromethane–hexane, 2:3), giving 5.7 mg of Ru$_3$(CO)$_{12}$ and 8.4 mg of Cp*WRu$_3$(CO)$_{12}$H (0.009 mmol, 47%).

X-ray Crystallography. Diffraction measurements of complexes **4** and **5** were carried out on a Nonius CAD-4 diffractometer. All reflections were corrected for Lorentz, polarization, and absorption effects. Data reduction and refinement were performed using the NRCC-SDP-VAX packages. Lattice parameters for **4** were determined from 25 randomly selected high-angle reflections with 2θ angles in the range 19.00–32.62°. The space group *Pbca* was identified on the basis of systematic absences and confirmed by successfully solving the crystal structure. Absorption corrections were made by the Ψ scan method; the minimum and maximum transmission factors were 0.75 and 1.00, respectively. Anisotropic thermal parameters were introduced for all nonhydrogen atoms. The bridging hydride ligand was located from a difference Fourier map and was included in the structure factor calculation. Full-matrix least-squares refinement with 44 atoms and 348 parameters gave $R_F = 0.028$ and $R_w = 0.022$, for 3160 reflections with $I > 2\sigma(I)$. The residual electron density on the difference Fourier map is about 0.70 e/Å^3.

Lattice parameters for **5** were determined from 25 selected reflections with 2θ angles in the range 16.12–34.64°. Empirical absorption corrections were performed, and the minimum and maximum transmission factors were 0.80 and 1.00, respectively. The structures were solved by using the NRCC-SDP-VAX packages and refined by least-squares cycles. The bridging hydride ligand was located from the difference Fourier map and was included in the structure factor calculation. The hydrogen atoms of the Cp* ligand were calculated at idealized positions with fixed temperature coefficients. Full-matrix least-squares refinement with 59 atoms and 393 parameters gave $R_F = 0.023$ and $R_w = 0.027$ for 4397 reflections with $I > 2\sigma(I)$. The combined data collection and refinement parameters are summarized in Table 1. Atomic positional parameters for **4** and **5** are presented in Tables 2 and 3, whereas selected bond angles and lengths are listed in Tables 4 and 5, respectively.

Table 1. Experimental Data for the X-ray Diffraction Studies[a]

compd	4	5
formula	$C_{19}H_6O_{14}WRu_4$	$C_{24}H_{16}O_{14}MoRu_4$
mol wt	982.38	1028.59
cryst syst	orthorhombic	monoclinic
space group	*Pbca*	$P2_1/c$
a (Å)	14.786(3)	10.468(1)
b (Å)	16.624(5)	16.804(2)
c (Å)	29.240(5)	17.251(3)
β (deg)		104.81(1)
V (Å^3)	4975(2)	2933(1)
Z	8	4
D_c (g/cm^3)	2.623	2.329
$F(000)$	3599	1960
2θ(max) (deg)	50	50
hkl ranges	0–17, 0–19, 0–24	−12 to +12, 0–19, 0–20
cryst size (mm)	0.10 × 0.13 × 0.17	0.08 × 0.25 × 0.35
μ(Mo Kα) (cm^{-1})	70.86	24.48
transmissn: max, min	1.00, 0.75	1.00, 0.80
no. of unique data	4362	5156
no. of data with $I > 2\sigma(I)$	3160	4397
no. of atoms and params	44, 348	72, 452
max Δ/σ ratio	0.040	0.003
R_F; R_w	0.028; 0.022	0.023; 0.027
GOF	1.58	2.41
D-map, max/min (e/Å^3)	+0.72/−0.66	+0.39/−0.53

[a] Features common to all determinations: Nonius CAD-4 diffractometer, λ(Mo Kα) = 0.709 30 Å, 25 °C; minimized function $\sum(w|F_o - F_c|^2)$, weighting scheme $(1/\sigma^2)(F_o)$, $w = 1/\sigma^2(F_o)$; GOF = $[\sum w|F_o - F_c|^2/(N_o - N_v)]^{1/2}$ (N_o = number of observations; N_v = number of variables.

Results and Discussion

The pentanuclear heterometallic cluster compound CpWRu$_4$(CO)$_{14}$H (**4**) was isolated in ca. 6% yield from the reaction of a 3:2 molar ratio of Ru$_3$(CO)$_{12}$ and [CpW(CO)$_3$][PPh$_4$] in refluxing THF solution for 2 h, followed by addition of excess CF_3CO_2H in dichloromethane at room temperature. The related Cp* derivatives Cp*MoRu$_4$(CO)$_{14}$H (**5**) and Cp*WRu$_4$(CO)$_{14}$H (**6**) were obtained in 15–17% yields under similar conditions from the related anionic complexes [Cp*M(CO)$_3$][PPh$_4$] (M = Mo, W). The conditions used to prepare complexes **4**–**6** are identical with those used previously to obtain the tetranuclear anionic clusters [LMRu$_3$(CO)$_{12}$]$^-$ and neutral clusters **1**–**3**,[7b,9] except that we added 1.5 equiv of Ru$_3$(CO)$_{12}$ to maximize the yield of pentanuclear derivatives and to suppress the tetranuclear derivatives. Attempts to synthesize the CpMo derivative CpMoRu$_4$(CO)$_{14}$H were unsuccessful, presumably due to the poor thermal stability that caused unwanted decomposition during the reaction and workup. This result is consistent with the poor yield of complex **4**.

The molecular formulas of these three pentanuclear clusters were obtained from FAB mass analyses. The solution IR spectrum of **4** shows the complex CO stretching bands in the region 2088–1968 cm^{-1} due to the terminal and bridging CO ligands. However, IR spectra of the Cp* derivatives **5** and **6** are distinct, exhibiting an additional broad CO stretching band at 1396 and 1357 cm^{-1} due to the quadruply bridging CO ligand. Encouraged by this finding, we carried out the single-crystal X-ray diffraction studies of both **4** and **5**.

Crystal Structure of 4. An ORTEP diagram of **4** is shown in Figure 1, and selected bond parameters are presented in Table 4. The metal core consists of a Ru$_4$W trigonal-bipyramidal arrangement, with atoms Ru(1) and Ru(2) defining the axial positions and atoms Ru(3), Ru(4), and W located at the equatorial positions. In addition to the Cp ligand, this molecule contains 14 CO ligands: 2 CO ligands on the W atom and 3 CO ligands on each Ru atom. Among these 14 CO ligands, 3 CO ligands adopt the semibridging mode. These CO ligands include the C(1)O(1) and the C(2)O(2) ligands on the W atom and the C(11)O(11) ligand on Ru(3), which possess nonlinear M–C–O angles in the range 158–162°.

Table 2. Atomic Coordinates and Equivalent Isotropic Displacement Coefficients for 4

	x	*y*	*z*	B_{eq} (Å^2)[a]
W	0.046387(22)	0.258646(23)	0.037099(17)	2.432(14)
Ru(1)	0.09697(5)	0.11133(4)	0.10349(4)	2.70(3)
Ru(2)	0.02908(5)	0.37807(4)	0.13881(4)	3.06(3)
Ru(3)	−0.01080(5)	0.21899(4)	0.17010(3)	2.49(3)
Ru(4)	0.17055(4)	0.26213(5)	0.15018(3)	2.39(3)
C(1)	−0.0278(6)	0.1597(6)	0.0321(5)	3.8(5)
C(2)	−0.0726(6)	0.3009(6)	0.0587(5)	3.9(5)
C(3)	0.1687(6)	0.0662(5)	0.0343(5)	3.3(4)
C(4)	0.0157(6)	0.0243(6)	0.0999(5)	4.0(5)
C(5)	0.1586(6)	0.0607(6)	0.1729(5)	3.9(5)
C(6)	0.0798(7)	0.4535(6)	0.0829(5)	5.3(6)
C(7)	−0.0779(7)	0.4394(6)	0.1387(5)	4.7(5)
C(8)	0.0706(7)	0.4336(6)	0.2136(5)	4.8(5)
C(9)	−0.1248(6)	0.1709(6)	0.1607(5)	4.1(5)
C(10)	0.0239(6)	0.1511(5)	0.2418(5)	4.0(5)
C(11)	−0.0563(6)	0.2997(6)	0.2291(5)	4.1(5)
C(12)	0.2730(6)	0.1948(6)	0.1591(5)	4.0(5)
C(13)	0.1740(6)	0.2874(6)	0.2423(5)	4.4(5)
C(14)	0.2420(6)	0.3488(6)	0.1201(4)	3.4(4)
C(15)	0.0113(9)	0.2691(14)	−0.0715(6)	14.5(13)
C(16)	0.0897(11)	0.2196(8)	−0.0676(5)	10.2(10)
C(17)	0.1534(7)	0.2674(9)	−0.0463(5)	7.3(7)
C(18)	0.1217(8)	0.3418(7)	−0.0381(5)	6.2(6)
C(19)	0.0362(8)	0.3436(9)	−0.0532(6)	9.3(8)
O(1)	−0.0858(4)	0.1161(4)	0.0136(3)	5.2(4)
O(2)	−0.1496(4)	0.3200(4)	0.0538(4)	5.4(4)
O(3)	0.2095(4)	0.0415(4)	−0.0083(3)	5.2(4)
O(4)	−0.0298(5)	−0.0284(4)	0.0999(4)	6.1(4)
O(5)	0.1975(5)	0.0264(5)	0.2133(4)	6.5(4)
O(6)	0.1107(6)	0.5049(5)	0.0524(4)	8.5(5)
O(7)	−0.1449(5)	0.4733(5)	0.1394(4)	6.9(4)
O(8)	0.0958(5)	0.4692(5)	0.2588(4)	7.3(5)
O(9)	−0.1947(4)	0.1400(5)	0.1561(4)	7.0(5)
O(10)	0.0395(5)	0.1133(4)	0.2880(3)	6.0(4)
O(11)	−0.0871(5)	0.3302(4)	0.2750(3)	6.4(4)
O(12)	0.3387(4)	0.1591(5)	0.1637(4)	6.5(5)
O(13)	0.1804(5)	0.2991(5)	0.2977(3)	7.0(5)
O(14)	0.2888(5)	0.3986(4)	0.1020(4)	5.9(4)
H	0.143(4)	0.219(4)	0.074(3)	3.5(19)

[a] B_{eq} is the mean of the principal axes of the thermal ellipsoid.

Table 3. Atomic Coordinates and Equivalent Isotropic Displacement Coefficients for 5

	x	*y*	*z*	B_{eq} (Å^2)[a]
Mo	0.32416(5)	0.12797(3)	0.19280(3)	1.805(19)
Ru(1)	0.04414(4)	0.16121(3)	0.11618(3)	1.902(18)
Ru(2)	−0.02036(4)	0.23953(3)	−0.03204(3)	2.056(18)
Ru(3)	0.24216(4)	0.22831(3)	0.04715(3)	1.847(19)
Ru(4)	0.07334(5)	0.32994(3)	0.10793(3)	2.165(19)
C(1)	0.2020(5)	0.2490(3)	0.1636(3)	2.09(24)
C(2)	0.2799(6)	0.0425(3)	0.1092(3)	2.5(3)
C(3)	0.1951(6)	0.0711(3)	0.2407(3)	2.8(3)
C(4)	−0.0353(6)	0.1701(4)	0.2006(3)	3.1(3)
C(5)	−0.0171(6)	0.0551(3)	0.0936(3)	2.46(25)
C(6)	−0.1462(6)	0.1979(3)	0.0303(3)	2.7(3)
C(7)	−0.0837(6)	0.1737(3)	−0.1239(3)	2.8(3)
C(8)	−0.1280(6)	0.3250(3)	−0.0797(3)	2.6(3)
C(9)	0.1449(6)	0.2832(3)	−0.0669(3)	2.7(3)
C(10)	0.3301(6)	0.1573(3)	−0.0073(3)	2.8(3)
C(11)	0.3811(6)	0.3016(3)	0.0613(3)	2.7(3)
C(12)	0.1303(6)	0.3888(4)	0.2068(4)	4.0(3)
C(13)	0.1129(7)	0.4146(4)	0.0441(4)	3.9(3)
C(14)	−0.1097(6)	0.3576(4)	0.1002(4)	3.8(3)
C(15)	0.5035(5)	0.1542(3)	0.3059(3)	2.35(23)
C(16)	0.4639(5)	0.0755(3)	0.3128(3)	2.58(25)
C(17)	0.4815(5)	0.0314(3)	0.2452(3)	2.36(23)
C(18)	0.5354(5)	0.0841(3)	0.1966(3)	2.27(24)
C(19)	0.5477(5)	0.1609(3)	0.2344(3)	2.32(24)
C(20)	0.5084(6)	0.2183(4)	0.3660(4)	3.7(3)
C(21)	0.4307(7)	0.0401(4)	0.3859(4)	4.2(4)
C(22)	0.4707(6)	−0.0571(3)	0.2365(4)	3.6(3)
C(23)	0.5924(6)	0.0600(4)	0.1286(4)	3.5(3)
C(24)	0.6090(6)	0.2340(4)	0.2099(4)	3.6(3)
O(1)	0.2835(3)	0.24344(21)	0.23167(20)	2.26(16)
O(2)	0.2639(4)	−0.00998(24)	0.06582(24)	3.92(22)
O(3)	0.1416(4)	0.02911(25)	0.27445(24)	3.73(21)
O(4)	−0.0869(5)	0.1750(3)	0.2516(3)	5.4(3)
O(5)	−0.0582(4)	−0.00785(24)	0.0828(3)	4.30(23)
O(6)	−0.2564(4)	0.1919(3)	0.0313(3)	4.01(22)
O(7)	−0.1228(5)	0.1371(3)	−0.1797(3)	5.1(3)
O(8)	−0.1930(4)	0.37718(25)	−0.1081(3)	4.21(22)
O(9)	0.1774(4)	0.3174(3)	−0.11677(25)	4.25(23)
O(10)	0.3829(5)	0.1186(3)	−0.0432(3)	5.0(3)
O(11)	0.4596(5)	0.3497(3)	0.0658(3)	4.72(24)
O(12)	0.1639(6)	0.4225(3)	0.2648(3)	7.4(3)
O(13)	0.1457(6)	0.4637(3)	0.0071(3)	6.5(3)
O(14)	−0.2163(5)	0.3732(3)	0.0988(3)	6.1(3)
H	0.083(6)	0.152(3)	0.020(3)	5.5(16)

[a] B_{eq} is the mean of the principal axes of the thermal ellipsoid.

The metal−metal distances span the narrow range 2.935(1)−2.750(1) Å, with Ru−Ru distances (average 2.817 Å) being slightly shorter than the W−Ru distances (average 2.899 Å). The W−Ru(4) vector in the equatorial plane is the longest metal−metal bond within the whole molecule. The lengthening of this metal−metal bond is apparently due to the presence of the face-bridging hydride, which was located by difference Fourier synthesis. This hydride ligand is strongly associated with the W−Ru(4) edge (W−H = 1.75(6) Å and Ru(4)−H = 1.74(7) Å) but is weakly bonded to the opposite metal atom (Ru(1)−H = 2.00(7) Å).

Crystal Structure of 5. As indicated in Figure 2, compound **5** possesses a metal core of 1 Mo and 4 Ru atoms coordinated by 14 CO ligands, 1 face-bridging hydride, and a Cp* ligand. Selected bond distances are listed in Table 5. The skeleton consists of an edge-bridged tetrahedral arrangement with a pendant Cp*Mo(CO)$_2$ unit attached to the Ru$_4$ tetrahedron. All metal−metal bonds are normal, with Ru−Ru distances in the range 2.7448(7)−2.8720(7) Å and with Mo−Ru distances of 2.9445(8) and 2.9648(7) Å. As revealed by the difference Fourier synthesis, the hydride lies on the Ru(1)−Ru(2)−Ru(3) metal triangle. In addition, we observed three terminal CO ligands on the Ru(4) atom and two terminal CO ligands on each of the other three Ru atoms. The observed Ru−CO arrangement is completed by two bridging CO ligands on the Ru(1)−Ru(2) and Ru(2)−Ru(3) edges. One CO ligand, C(9)O(9), is close to the symmetric bridging mode with Ru(2)−C(9) = 2.104(6) Å and Ru(3)−C(9) = 2.176(6) Å, while the second is more asymmetric with Ru(1)−C(6) = 2.243(6) Å and Ru(2)−C(6) = 2.027(6) Å.

The most important feature is the presence of the unique μ_4-CO ligand. The carbon atom C(1) occupies the MoRu$_3$ butterfly crater of the cluster, and the oxygen atom O(1) is bonded to the bridging Cp*Mo(CO)$_2$ fragment. Thus, the orientation of the μ_4-CO ligand differs from that revealed by the solid-state structure of clusters **1** and **2**, in which the oxygen atom is tilted toward the wingtip Ru(CO)$_3$ fragment but is pointed away from the CpW(CO)$_2$ and Cp*W(CO)$_2$ fragments. The CO distance, C(1)−O(1) = 1.266(6) Å, is much longer than that of other terminal CO ligands within the molecule, indicating a significant reduction in the C−O bond order. The small dihedral angle of 117.4(2)° between the planes Mo−Ru(1)−Ru(3) and Ru(1)−Ru(3)−Ru(4) is undoubtedly due to the restriction imposed by the multiple-bonding interaction of the μ_4-CO ligand. These features are observed in many other clusters containing the encapsulated μ_4-CO fragment.[10,11]

Table 4. Selected Bond Distances (Å) and Bond Angles (deg) for 4

	Intermetallic Distances		
W–Ru(1)	2.892(1)	W–Ru(2)	2.871(1)
W–Ru(3)	2.898(1)	W–Ru(4)	2.935(1)
Ru(1)–Ru(3)	2.750(1)	Ru(1)–Ru(4)	2.892(1)
Ru(2)–Ru(3)	2.783(1)	Ru(2)–Ru(4)	2.854(1)
Ru(3)–Ru(4)	2.805(1)		
	Parameters Associated with CO Ligands		
W–C(1)	1.98(1)	Ru(1)–C(1)	2.48(1)
∠W–C(1)–O(1)	157.9(8)	W–C(2)	1.94(1)
Ru(2)–C(2)	2.56(1)	∠W–C(2)–O(2)	161.2(8)
Ru(1)–C(3)	1.91(1)	Ru(1)–C(4)	1.88(1)
Ru(1)–C(5)	1.88(1)	Ru(2)–C(6)	1.85(1)
Ru(2)–C(7)	1.88(1)	Ru(2)–C(8)	1.88(1)
Ru(3)–C(9)	1.88(1)	Ru(3)–C(10)	1.91(1)
Ru(2)–C(11)	2.58(1)	Ru(3)–C(11)	1.92(1)
∠Ru(3)–C(11)–O(11)	161.5(8)	Ru(4)–C(12)	1.89(1)
Ru(4)–C(13)	1.91(1)	Ru(4)–C(14)	1.89(1)
	Bond Distances Associated with the Cp Ligands		
W–C(15)	2.27(1)	W–C(16)	2.31(1)
W–C(17)	2.32(1)	W–C(18)	2.34(1)
W–C(19)	2.32(1)		
	Metal–Hydride Distances		
W–H	1.75(6)	Ru(1)–H	2.00(7)
Ru(4)–H	1.74(7)		

Table 5. Selected Bond Distances (Å) and Bond Angles (deg) for 5

	Intermetallic Distances		
Mo–Ru(1)	2.9445(8)	Mo–Ru(3)	2.9648(7)
Ru(1)–Ru(2)	2.8005(7)	Ru(1)–Ru(3)	2.8720(7)
Ru(1)–Ru(4)	2.8592(7)	Ru(2)–Ru(3)	2.7448(7)
Ru(2)–Ru(4)	2.8088(7)	Ru(3)–Ru(4)	2.8437(7)
	Parameters Associated with the μ_4-CO Ligand		
Mo–C(1)	2.387(5)	Mo–O(1)	2.131(3)
Ru(1)–C(1)	2.210(5)	Ru(3)–C(1)	2.184(5)
Ru(4)–C(1)	1.981(5)	C(1)–O(1)	1.266(6)
∠Ru(4)–C(1)–O(1)	135.6(4)	∠Mo–C(1)–O(1)	62.9(3)
∠Ru(1)–C(1)–Ru(3)	81.6(2)		
	Bond Distances Associated with Other CO Ligands		
Mo–C(2)	2.004(5)	Mo–C(3)	1.998(6)
Ru(1)–C(4)	1.859(6)	Ru(1)–C(5)	1.901(6)
Ru(1)–C(6)	2.243(6)	Ru(2)–C(6)	2.027(6)
Ru(2)–C(7)	1.906(6)	Ru(2)–C(8)	1.881(6)
Ru(2)–C(9)	2.104(6)	Ru(3)–C(9)	2.176(6)
Ru(3)–C(10)	1.896(6)	Ru(3)–C(11)	1.873(6)
Ru(4)–C(12)	1.930(6)	Ru(4)–C(13)	1.909(6)
Ru(4)–C(14)	1.943(6)		
	Bond Distances Associated with the Cp* Ligands		
Mo–C(15)	2.377(5)	Mo–C(16)	2.377(5)
Mo–C(17)	2.324(5)	Mo–C(18)	2.316(5)
Mo–C(19)	2.332(5)		
	Metal–Hydride Distances		
Ru(1)–H	1.82(6)	Ru(2)–H	1.90(6)
Ru(3)–(H)	2.05(6)		

NMR Analyses and Solution Fluxionality of 4. To acquire more information on the nature of these cluster complexes in solution, variable-temperature ^{1}H NMR spectra were recorded. At room temperature, complex **4** in CD_2Cl_2 exhibits a Cp signal at δ 5.76 and a very broad hydride signal at δ −15.36. Below 270 K the hydride signal broadens and turns into a sharp singlet with clearly visible satellite peaks due to the coupling with the W atom (Figure 3). As the temperature increases, the hydride signal also sharpens and the tungsten satellites also become observable near 313 K. This behavior is consistent with a "hidden-partner" exchange process, and the failure to observe the hidden partner is apparently due to an equilibrium heavily favoring the major component, thus resulting in the signal of the minor isomer being lost in the base line of the NMR spectrum.[12]

Because we observe J_{W-H} coupling to the hydride signal at low temperature, we speculate that the major isomer in solution possesses a structure identical with that already determined by X-ray diffraction and that the exchange is due to hydride migration from a WRu_2 face to other triangular faces of the trigonal-bipyramidal

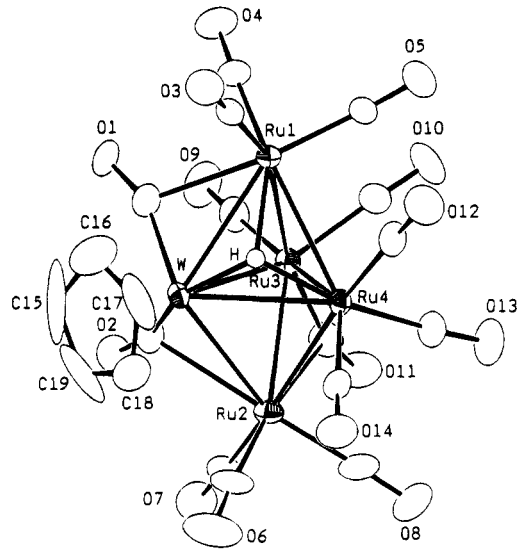

Figure 1. Molecular structure and atomic numbering scheme of **4**.

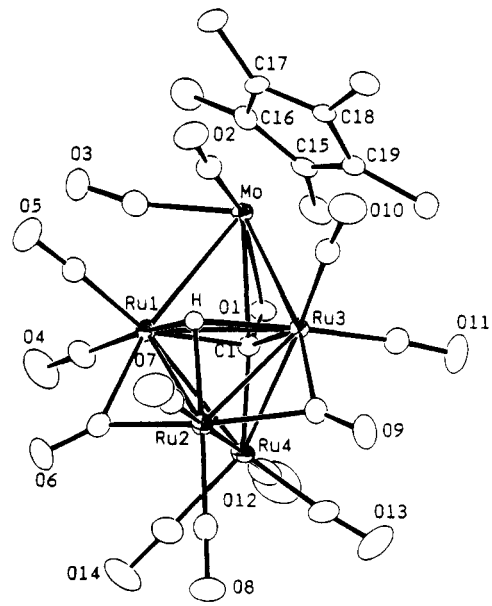

Figure 2. Molecular structure and atomic numbering scheme of **5**.

(10) (a) Kwek, K.; Taylor, N. J.; Carty, A. J. *J. Am. Chem. Soc.* **1984**, *106*, 4636. (b) Field, J. S.; Haines, R. J.; Mulla, F. *J. Organomet. Chem.* **1990**, *389*, 227. (c) Chi, Y.; Chuang, S.-H.; Liu, L.-K.; Wen, Y.-S. *Organometallics* **1991**, *10*, 2485.

(11) (a) Adams, R. D.; Babin, J. E.; Tasi, M. *Inorg. Chem.* **1988**, *27*, 2618. (b) Anson, C. E.; Bailey, P. J.; Conole, G.; Johnson, B. F. G.; Lewis, J.; McPartlin, M.; Powell, H. R. *J. Chem. Soc., Chem. Commun.* **1989**, 442. (c) Johnson, B. F. G.; Lewis, J.; McPartlin, M.; Pearsall, M.; Sironi, A. *J. Chem. Soc., Chem. Commun.* **1984**, 1089.

(12) (a) Okazawa, N.: Sorenson, T. S. *Can. J. Chem.* **1978**, *56*, 2737. (b) Anet, F. A. L.; Basus, V. J. *J. Magn. Reson.* **1978**, *32*, 339. (c) Nucciarone, D.; Taylor, N. J.; Carty, A. J. *Organometallics* **1988**, *7*, 127.

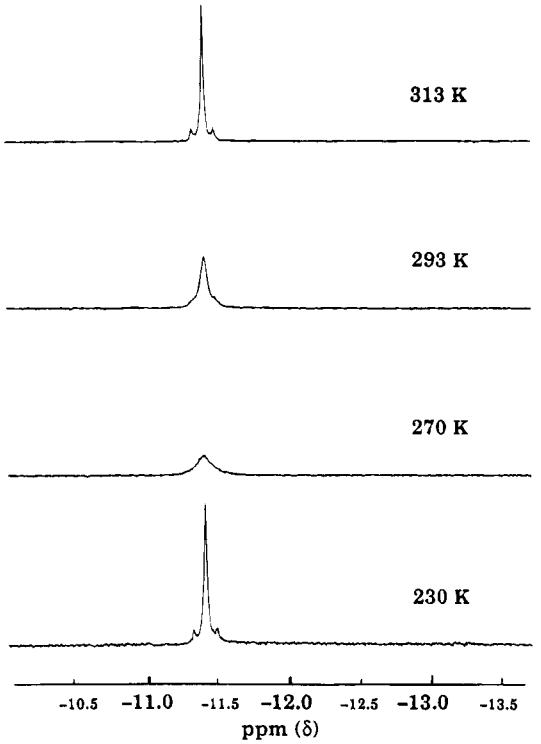

Figure 3. Variable-temperature ^{1}H NMR spectra of **4** in CD_2Cl_2 solution.

Scheme 3

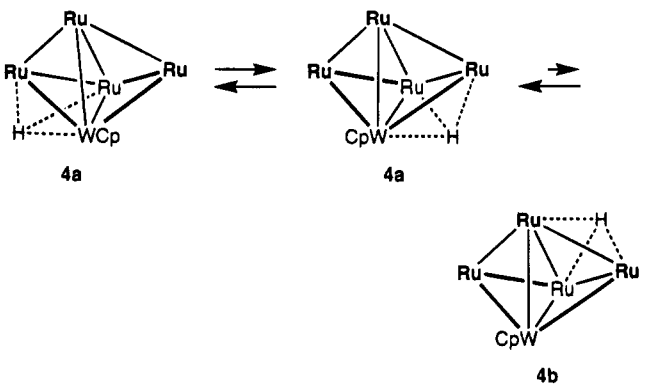

[a] Legend: Ru = $Ru(CO)_2$; **Ru** = $Ru(CO)_3$. Three bridging CO ligands, located on the boldface metal–metal bonds, are omitted for clarity.

cluster arrangement (Scheme 3). Evidence for the occurrence of such exchange motion comes from the observation of facile hydride migration in hydride cluster compounds.[13] The hydride exchange envisaged in Scheme 3 represents one such possibility, in which the hidden isomer **4b** is generated by hydride migration to a nearby Ru_3 triangular surface of the metal core.

In addition, the fluxionality of the major isomer is observed in the variable-temperature ^{13}C NMR studies. The spectrum recorded at 200 K shows only 11 of the 14 expected CO signals at δ 234.0 (J_{W-C} = 155 Hz), 201.5, 192.4, 189.2, and 188.7 in the intensity ratio 2:3:2:2:2. This pattern indicates the existence of a time-averaged plane of mirror symmetry which coincides with the equatorial WRu_2 triangle, generated by hydride

(13) (a) Chen, C.-C.; Chi, Y.; Peng, S.-M.; Lee, G.-H. *J. Chem. Soc., Dalton Trans.* **1993**, 1823. (b) Lin, R.-C.; Chi, Y.; Peng, S.-M.; Lee, G.-H. *Inorg. Chem.* **1992**, *31*, 3818. (c) Park, J. T.; Chi, Y.; Shapley, J. R.; Churchill, M. R.; Ziller, J. W. *Organometallics* **1994**, *13*, 813.

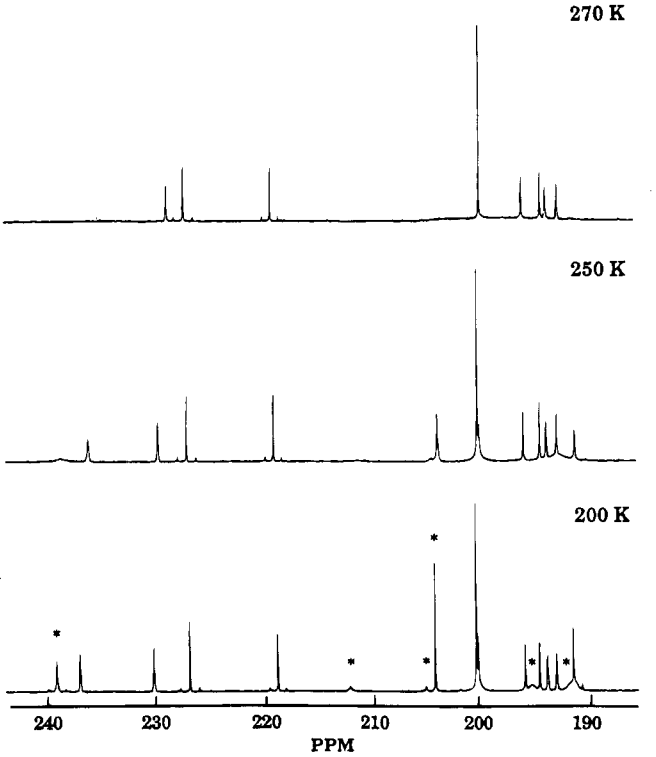

Figure 4. Variable-temperature ^{13}C NMR spectra of **6** in THF-d_8 solution. Signals marked with an asterisk are due to isomer **6b**.

migration between the adjacent WRu_2 faces. The existence of a mirror plane causes the bridging CO ligands on W–Ru edges to become equivalent and the terminal CO ligands on each axial Ru atom to possess an identical environment. Thus the signals occurring at δ 192.4, 189.2, and 188.7 are due to CO ligands on axial Ru atoms. Consistent with our hypothesis, these three signals broaden and coalesce into a very broad hump at δ 189.9 corresponding to six CO ligands when we raise the temperature to 253 K, due to the rapid threefold rotation. At 293 K, all CO resonances coalesce into the base line, indicating the coexistence of rapid isomerization with **4b** and CO scrambling between W and all Ru sites.

NMR Analyses and Solution Fluxionality of 5 and 6. The ^{1}H and ^{13}C NMR spectra of the Cp* derivatives **5** and **6** were recorded to illustrate its relationship with the Cp derivative. The ^{1}H NMR of **5** at 293 K shows, besides the Me signal due to the Cp* ligand, two hydride signals at δ −15.08 and −18.87 in the ratio 1:9, suggesting the presence of two isomers in solution. Similarly, the Cp^*WRu_4 derivative **6** also exhibits two hydride signals at δ −14.25 (J_{W-H} = 68 Hz) and −19.01 in a ratio of 1:3 in both CD_2Cl_2 and THF-d_8 solution. Because of the lack of J_{W-H} coupling to the more downfield hydride signal, the predominant species **5a** and **6a** are assigned to possess a structure already determined by X-ray studies.

In accordance with this assignment, the ^{13}C NMR spectrum of **6** at 270 K shows a series of nine CO signals at δ 302.0, 228.9, 227.1 (J_{W-C} = 176 Hz), 219.1 (J_{W-C} = 148 Hz), 199.9 (3C), 196.0, 194.3, 193.8, and 192.7 (Figure 4). The integrated intensity pattern is 1:1:1:1:3:1:1:1:1 starting from left to right. We speculate that all these resonances derive from the isomer **6a**, and they account for 11 of the 14 expected CO ligands. The first

Scheme 4

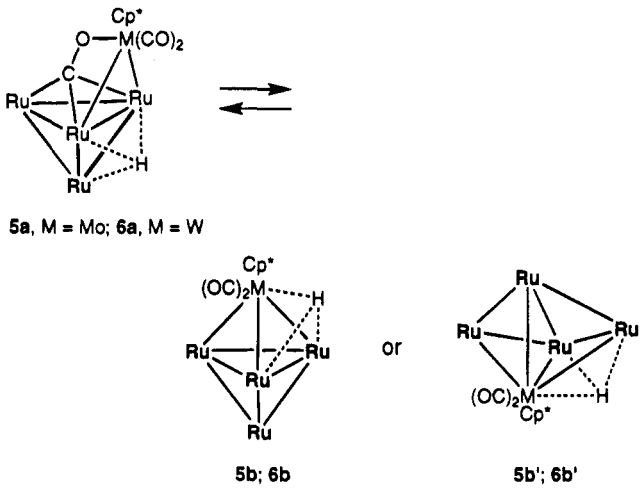

[a] Legend: Ru = $Ru(CO)_2$; **Ru** = $Ru(CO)_3$. Two bridging CO ligands, located on the boldface Ru–Ru bonds, are omitted for clarity.

five signals are produced by the μ_4-CO group, a bridging CO ligand, two CO ligands on the W atom, and the $Ru(CO)_3$ fragment located at the unique position opposite to the hydride ligand. The chemical shift of the μ_4-CO ligand is exceptional. Its value appears compatible with that of the triply bridging CO ligand (δ 308.0) in $Cp^*CpW_2Ru_2(CO)_6(CCPh)_2$[14] and is much lower field than that observed in the butterfly complexes $[Fe_4(\mu\text{-}X)(CO)_{13}]^-$ (X = H, $AuPPh_3$, HgR; R = Me, $CpFe(CO)_2$, $CpMo(CO)_3$; δ 284.9–279.8)[3d,15] and $LWRu_3(CO)_{12}(\mu\text{-}AuPPh_3)$ (L = Cp, Cp*; δ 272.8–255.1).[16] Partial assignment of the four high-field Ru–CO resonances has been achieved by turning off proton decoupling. This treatment allowed the CO signals at δ 196.0 and 194.3 to appear as doublets in the undecoupled spectrum, indicating that they are due to CO ligands *trans* to the hydride.

The other three Ru–CO signals of **6a** and some CO signals of **6b** came into view at lower temperature. First, three broad CO signals surface at δ 236.1, 199.5, and 191.3 at 250 K. We believe that they are due to a "$Ru(CO)_2(\mu\text{-}CO)Ru$" grouping of **6a**, for which the signal at δ 236.1 is due to the bridging CO ligand. By further cooling to 200 K, the CO signals of **6b** appear and the NMR spectrum becomes very complicated. Assignment of the CO resonance signals of **6b** is precluded because of their low intensity and high fluxionality. However, the slightly broad W–CO signal at δ 235.2, which exhibits a distinct coupling with the W atom (J_{W-C} = 157 Hz), the sharp $Ru(CO)_3$ resonance at δ 204.1, and several other broad peaks are definitely contributed by isomer **6b**.

On the basis of these limited ^{13}C NMR spectral data, the key structure of the minor component **6b** can be deduced. The existence of only one W–CO resonance at δ 239.0 and the lack of the respective μ_4-CO signal in the region below δ 239 strongly indicate that a trigonal-bipyramidal metal framework with nine M–M bonds is produced (Scheme 4), as formation of one additional M–M bond is required to compensate for the electronic unsaturation generated by removal of the μ_4-CO ligand from the edge-bridged tetrahedral arrangement of **6a** (eight M–M bonds). The great fluxionality of the CO ligands confirms the attachment of CO ligands to the close-packed trigonal-bipyramidal metal framework. This behavior is in full accord with the ^{13}C NMR fluxional behavior of the already discussed pentanuclear cluster **4** and the tetrahedral isomers **1**–**3**.

Although we are confident about the prediction of the skeletal arrangement, the exact disposition of the hydride and W atom in **6b** cannot be determined from available data. Although the large J_{W-H} coupling implied that the hydride ligand is directly coordinated to the W atom, this ligand may adopt either a triply bridging or a doubly bridging mode; we have no experimental evidence to differentiate them. Similarly, the W atom may be located at either an axial or an equatorial site. We favor the structure with the W atom at the axial site, as the direct generation of M–M bonding between the pendant $Cp^*W(CO)_2$ fragment and the $Ru(CO)_2$ fragment of **6a** is expected to lead readily to this trigonal-bipyramidal configuration. A subsequent cluster rearrangement following initial formation of the M–M bond might produce a more stable isomer with a W atom occupying an equatorial site, as shown in the alternative drawing **6b'** in Scheme 4. The crystal structure of **4** supports the latter assignment.

Finally, the ^{13}C NMR spectra of the Cp^*MoRu_4 complex **5** were also recorded. The variable-temperature spectra exhibit similar fluxional behavior, and the respective diagnostics are less clear due to the lack of J_{W-C} coupling. By using our previous discussion, the 12 CO signals at δ 292.1, 240.6, 236.0 (br), 233.1, 228.6, 199.8 (3C), 199.5, 195.3, 194.9, 194.7, 193.5, and 190.0, observed in the spectrum at 205 K, are assigned to the μ_4-CO group, two bridging CO ligands, two Mo–CO ligands, the CO ligands of a $Ru(CO)_3$ fragment, and seven inequivalent terminal Ru–CO ligands of the predominant, edge-bridged tetrahedral isomer **5a**, respectively. Three weak CO resonances at δ 219.2, 202.4, and 192.8 were also seen for the minor isomer **5b** at this temperature. No attempt was made to identify these signals due to their low abundance.

Reactivity Studies. Limited studies have been conducted to reveal basic reactivities. Complexes **5** and **6** react with CO in refluxing toluene to afford complexes **3** and **2** in moderate yields, respectively. Upon switching to H_2, we obtain the corresponding hydride complexes $Cp^*MoRu_3(CO)_{11}H_3$ and $Cp^*WRu_3(CO)_{11}H_3$ in high yields, which adopt a tetrahedral framework with hydride ligands located on one Ru–Ru and two M–Ru edges.[17] These results indicate that cluster degradation is the predominant pathway. The Cp derivative **4** follows the same reaction patterns presumably, but no attempt was made due to its scarcity.

Conclusion. In this work, we present the synthesis and structural characterization of neutral pentametal WRu_4 and $MoRu_4$ clusters with 1 hydride and 14 CO ligands. Their formation can be considered as a condensation between the tetranuclear anionic clusters $[LMRu_3(CO)_{12}]^-$ and $Ru_3(CO)_{12}$ to generate the penta-

(14) Hwang, D.-K.; Lin, P.-J.; Chi, Y.; Peng, S.-M.; Lee, G.-H. *J. Chem. Soc., Dalton Trans.* **1991**, 2161.
(15) Wang, J.; Sabat, M.; Horwitz, C. P.; Shriver, D. F. *Inorg. Chem.* **1988**, *27*, 552.
(16) Chen, C.-C.; Chi, Y.; Peng, S.-M.; Lee, G.-H. Unpublished results.
(17) (a) Chi, Y.; Cheng, C.-Y.; Wang, S.-L. *J. Organomet. Chem.* **1989**, *378*, 45. (b) Housecroft, C. E.; Matthews, D. M.; Rheingold, A. L.; Song, X. *J. Chem. Soc., Dalton Trans.* **1992**, 2855.

metal anionic clusters $[LMRu_4(CO)_{14}]^-$. These pentanuclear anions then react with a proton source to afford the isolated clusters $LMRu_4(CO)_{14}H$. The Cp derivative **4** shows a trigonal-bipyramidal core arrangement, in which the hydride ligand undergoes migration between the WRu_2 triangular faces and the Ru_3 faces. In contrast, the Cp* derivatives **5** and **6** show a different type of dynamic process, which involves a skeletal rearrangement between edge-bridged-tetrahedral and the trigonal-bipyramidal geometry and concurrent switching of one CO ligand between the novel μ_4-η^2 mode and the regular C-bound mode. The Cp* ligand favors the edge-bridged-tetrahedral arrangement because it provides greater steric repulsion than does the Cp ligand. This argument is consistent with the trend observed in complexes **1**–**3**, as the Cp* derivatives **2** and **3** contain more butterfly isomers (≥85%) than the corresponding Cp derivative **1** (~55%), and the Cp*-containing metal fragments invariably reside at the less congested wingtip positions. Finally, this enhanced steric interaction in the Cp* derivatives is confirmed by the observation that the C–Mo distances of the Cp* ligand in **6** (average 2.345 Å) are always longer than those of the C–W distances of the Cp ligand in **4** (average 2.31 Å).

Finally, these pentametal clusters are unstable relative to their tetrametal counterparts. Treatment of **5** and **6** with both CO and H_2 in refluxing toluene led to the formation of complexes **3** and **2** and the hydride complexes $Cp^*MoRu_3(CO)_{11}H_3$ and $Cp^*WRu_3(CO)_{11}H_3$. These degradation reactions formally proceed via expelling of the $Ru(CO)_2$ fragment and were confirmed by isolation of $Ru_3(CO)_{12}$ from the reaction mixture.

Acknowledgment. We thank the National Science Council of the Republic of China for financial support (Grant No. NSC 84-2113-M007-020).

Supporting Information Available: Tables of calculated positions of hydrogen atoms and anisotropic thermal parameters for **4** and **5** (6 pages). Ordering information is given on any current masthead page.

OM950286U

Synthesis and Structures of Vanadium(II) Alkynide Complexes: $[(LiTMEDA)_2V(\mu\text{-}C{\equiv}CPh)_4(TMEDA)]$ and $V(C{\equiv}CR)_2(TMEDA)_2$ (R = Ph, ^{t}Bu; TMEDA = *N,N,N′,N′*-Tetramethylethylenediamine)

Hiroyuki Kawaguchi and Kazuyuki Tatsumi*

Department of Chemistry, Faculty of Science, Nagoya University, Furo-cho Chikusa-ku, Nagoya 464-01, Japan

Received March 28, 1995[⊗]

The V(II) tetrakis- and bis(alkynide) complexes, $[(LiTMEDA)_2V(\mu\text{-}C{\equiv}CPh)_4(TMEDA)]$ (**1**) and $V(C{\equiv}CPh)_2(TMEDA)_2$ (**2**) have been synthesized from the reaction between $VCl_3(THF)_3$ and LiC≡CPh in THF in the presence of TMEDA (=*N,N,N′,N′*-tetramethylethylenediamine). In the case of the analogous $VCl_3(THF)_3$/LiC≡C^{t}Bu/TMEDA reaction system, only the bis(alkynide) complex $V(C{\equiv}C^tBu)_2(TMEDA)_2$ (**3**) was isolable. Reduction of vanadium occurred during these reactions, and use of a divalent vanadium chloride, $VCl_2(TMEDA)_2$, instead of $VCl_3(THF)_3$ was found to give **1**–**3** in higher yields. Complex **1** crystallizes in the monoclinic space group $P2_1/c$ with $Z = 4$ in a unit cell of dimensions $a = 15.761(4)$ Å, $b = 14.325(4)$ Å, $c = 22.614(9)$ Å, and $\beta = 98.38(4)°$. Crystals of **2** are orthorhombic, space group *Cmcm*, with $a = 10.045(5)$ Å, $b = 22.379(7)$ Å, $c = 12.306(4)$ Å, and $Z = 4$. Crystals of **3** are triclinic, space group $P\bar{1}$, with $a = 9.402(2)$ Å, $b = 9.833(2)$ Å, $c = 8.907(2)$ Å, and $Z = 1$. Reactions of these alkynide complexes with electrophiles such as Me_3SiCl, MeI, PhNCO, CO_2, and CO were examined.

While alkynide complexes are ubiquitous in organometallic chemistry,[1] those of group 4 and 5 transition metals are still scarce, and the only structurally characterized examples are limited to those consisting of bent-metallocene fragments.[2–4] This is probably due to a lack of steric bulk of alkynide ligands that may allow high reactivity at these electron-deficient metal centers.[5] We are interested in developing chemistry based on "alkynide rich" complexes of early transition metals and report herein the synthesis and structures of vanadium(II) complexes that carry two or four alkynides at a single metal center: $[(LiTMEDA)_2V(\mu\text{-}C{\equiv}CPh)_4(TMEDA)]$ (**1**), $V(C{\equiv}CPh)_2(TMEDA)_2$ (**2**), and $V(C{\equiv}C^tBu)_2(TMEDA)_2$ (**3**). The only previously reported tetrakis(alkynide) mononuclear complexes are $LiLn(C{\equiv}CR)_4(THF)$ (Ln = Sm, Er, Lu; R = ^{t}Bu, Ph).[6] These have been shown to form from the reaction of homoleptic alkyl lanthanide complexes with monosubstituted alkynes, but no structural information is yet available. A related lanthanide alkynide is $[(C_5Me_5)_2Yb][(\mu\text{-}C{\equiv}CPh)_4Yb]$, which has four *bridging* alkynides.[7]

Complexes **1**–**3** were synthesized from the reaction between $VCl_3(THF)_3$ and lithium salts of the corresponding alkynides, in which the vanadium atom was reduced from V^{III} to V^{II}. We also found that the prereduced V(II) chloride, $VCl_2(TMEDA)_2$,[8] reacted with these lithium alkynides to give **1**–**3** in higher yields. The organometallic chemistry of vanadium(II) is little explored, and is mostly based on half-sandwich-type cyclopentadienyl complexes.[9] We plan to utilize these alkynide V(II) compounds as an entry into such chemistry, and thus we also report some initial results of reactions of **2** and **3** with Me_3SiCl, MeI, PhNCO, CO_2, and CO.

Results and Discussion

Synthesis of Vanadium(II) Alkynides. Treatment of $VCl_3(THF)_3$ with 5 equiv of LiC≡CPh in THF/TMEDA at 0 °C formed a brown solution, and a gradual color change to purple was observed upon warming the solution to room temperature. Removal of the solvent followed by recrystallization of the resulting solid from hexane/TMEDA generated **1** as purple crystals (see eqs 1 and 2). When the amount of LiC≡CPh was decreased

$$VCl_3(THF)_3 + n\ LiC{\equiv}CPh \xrightarrow[/TMEDA]{THF} \begin{cases} n = 5 \rightarrow \mathbf{1} & (1) \\ n = 3 \rightarrow \mathbf{1} + \mathbf{2} & (2) \end{cases}$$

$[(LiTMEDA)_2V(\mu\text{-}C{\equiv}CPh)_4(TMEDA)]$	$V(C{\equiv}CPh)_2(TMEDA)_2$
1	**2**
eq (1) : 64% yield eq (2) : 4%	eq (2) : 71%

to 3 equiv, **2** was obtained as brown crystals, together with a small amount of **1**. In all cases, the vanadium

[⊗] Abstract published in *Advance ACS Abstracts,* July 15, 1995.

(1) Nast, R. *Coord. Chem. Rev.* **1982,** *47,* 89–124.

(2) (a) Erker, G.; Frömberg, W.; Benn, R.; Mynott, R.; Angermund, K.; Krüger, C. *Organometallics* **1989,** *8,* 991–920. (b) Lang, H.; Seyferth, D. *Z. Naturforsch.* **1990,** *212,* 45B.

(3) Teuben, J. H.; DeLiefde Meijer, H. J. *J. Organomet. Chem.* **1968,** *15,* 131–137.

(4) Evans, W. J.; Bloom, I.; Doedens, R. J. *J. Organomet. Chem.* **1984,** *265,* 249–255.

(5) (a) Heeres, H. J.; Teuben, J. H. *Organometallics* **1991,** *10,* 1980–1986. (b) Sekutowski, D. G.; Stucky, G. D. *J. Am. Chem. Soc.* **1976,** *98,* 1376–1382. (c) Evans, W. J.; Keyer, R. A.; Ziller, J. W. *Organometallics* **1993,** *12,* 2618–2633 and references therein.

(6) Evans, W. J.; Wayda, A. L. *J. Organomet. Chem.* **1980,** *202,* C6–C8.

(7) Boncella, J. M.; Tilley, T. D.; Andersen, R. A. *J. Chem. Soc., Chem. Commun.* **1984,** 710–712.

(8) Edema, J. J. H.; Gambarotta, S.; Stauthamer, W.; van Bolhuis, F.; Spek, A. L.; Smeets, W. J. *Inorg. Chem.* **1990,** *29,* 1302–1306.

0276-7333/95/2314-4294$09.00/0

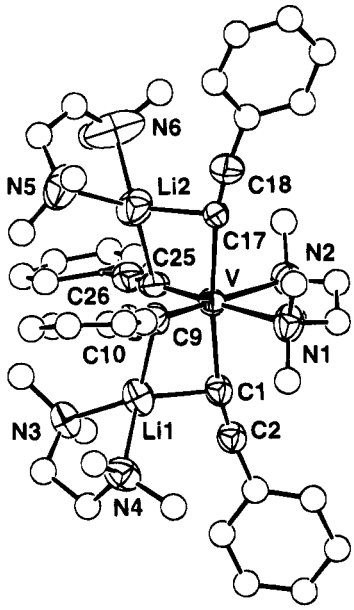

Figure 1. ORTEP drawing of the structure of $[(LiTMEDA)_2V(\mu\text{-}C{\equiv}CPh)_4(TMEDA)]$ (**1**).

center is reduced from V(III) to V(II), where the reducing agent is probably LiC≡CPh, thus consuming 1 equiv of LiC≡CPh during the reaction. Since **1** is soluble in hexane and other typical organic solvents, the lithium cations are probably tightly bound to the alkynides in solution. Interestingly the lithium-free neutral alkynide complex **2** is not very soluble in nonpolar organic solvents.

The tetrakisalkynide complex **1** was also synthesized in 84% yield from the reaction between the prereduced V(II) chloride $VCl_2(TMEDA)_2$ and 4 equiv of LiC≡CPh under similar reaction conditions. Likewise, the (1:2) $VCl_2(TMEDA)_2$/LiC≡CPh reaction system gave rise to **2** in 85% yield in addition to a small amount of **1**. Although this method starting from $VCl_2(TMEDA)_2$ gives the alkynide complexes of V(II) more cleanly and in higher yields, we have found it more convenient to use $VCl_3(THF)_3$ because of the additional steps required in the synthesis of $VCl_2(TMEDA)_2$.

Addition of 3 equiv of LiC≡C^{t}Bu to a THF/TMEDA solution of $VCl_3(THF)_3$ afforded **3** as brown-purple crystals (eq 3).[10] However, the reaction between 5 equiv

$$VCl_3(THF)_3 + 3\ LiC{\equiv}C^tBu \xrightarrow{THF/TMEDA} \underset{\textbf{3}}{V(C{\equiv}C^tBu)_2(TMEDA)_2} \quad (3)$$

56% yield

of LiC≡C^{t}Bu and $VCl_3(THF)_3$ resulted in an uncharacterized green product along with **3** (11%) as a side product, and our attempts to isolate the C≡C^{t}Bu analogue of **1** have not been successful.

The ^{1}H NMR spectra of **1**–**3** are not informative due to the paramagnetic nature of these V(II) compounds. The EI mass spectra of **2** and **3** consist of the parent molecular ion along with fragments resulting from loss of the alkynide group and/or TMEDA. On the other hand, the mass spectrum of the lithiated complex **1** did not provide us with useful information. The IR spectrum of **1** features a sharp band at 2000 cm^{-1} and a weaker band at 1964 cm^{-1}, both assignable to C≡C stretching vibrations. In the case of **2** and **3**, a single C≡C stretching band appears which is shifted to higher frequency relative to that of **1**: 2020 cm^{-1} for **2** and 2035 cm^{-1} for **3**. These $\nu_{C\equiv C}$ frequencies are lower than those of the V(III) alkynide complexes, $(C_5H_5)_2V(C{\equiv}CPh)$ (2060 cm^{-1})[3] and $(C_5H_5)_2V(C{\equiv}C^tBu)$ (2075 cm^{-1}).[4]

In the absence of TMEDA, neither the $VCl_3(THF)_3$/LiC≡CPh nor the $VCl_3(THF)_3$/LiC≡C^{t}Bu reaction system in THF gave characterizable products. Thus chelation by TMEDA of either V(II) or Li appears to be important to stabilize these alkynide complexes. However, in DME, the reaction between $VCl_3(THF)_3$ and LiC≡CPh allowed us to isolate a DME containing lithiated alkynide complex $Li_2(DME)_XV(C{\equiv}CPh)_4$ (**4**) as red-purple crystals (eq 4). The coordination geometry

$$VCl_3(THF)_3 + 5\ LiC{\equiv}CPh \xrightarrow{DME} \underset{\textbf{4}}{Li_2(DME)_XV(C{\equiv}CPh)_4} \quad (4)$$

at V(II) of **4** is thought to be similar to **1**. In fact the C≡C stretching bands for **4** appear at 2000 (s) and 1960 cm^{-1} (w), which are very close to those of **1**.

Structure of $[(LiTMEDA)_2V(\mu\text{-}C{\equiv}CPh)_4(TMEDA)]$ (1). The molecular structure of **1** is shown in Figure 1. A summary of crystal data, fractional coordinates, and selected bond distances and angles are given in Tables

Table 1. Crystal Data for $[(LiTMEDA)_2V(\mu\text{-}C{\equiv}CPh)_4(TMEDA)]$ (1), $V(C{\equiv}CPh)_2(TMEDA)_2$ (2), and $V(C{\equiv}C^tBu)_2(TMEDA)_2$ (3)

	1	2	3
formula	$C_{50}H_{68}N_6Li_2V$	$C_{28}H_{42}N_4V$	$C_{24}H_{50}N_4V$
fw	817.95	485.61	445.629
space group	$P2_1/c$ (No. 14)	$Cmcm$ (No. 63)	$P1$ (No. 2)
a, Å	15.761(4)	10.040(5)	9.402(2)
b, Å	14.325(4)	22.379(7)	9.833(2)
c, Å	22.614(9)	12.306(4)	8.907(2)
α, deg			108.61(2)
β, deg	98.38(4)		110.58(2)
γ, deg			73.18(1)
V, Å^3	5051(3)	2761(2)	715.9(3)
Z	4	4	1
D_{calcd}, g/cm^3	1.076	1.169	1.034
$2\theta_{max}$, deg	45.0	55.0	55.0
transmissn factors	0.92–1.00	0.90–1.00	0.96–1.00
no. of unique reflns	7032	1388	3130
no. of observns[a]	3137	865	2573
R	0.0688	0.0695	0.0661
R_w	0.0641	0.0705	0.0688
function minimized	$\Sigma w(\lvert F_o\rvert - \lvert F_c\rvert)^2$	$\Sigma w(\lvert F_o\rvert - \lvert F_c\rvert)^2$	$\Sigma w(\lvert F_o\rvert - \lvert F_c\rvert)^2$
least-squares wts	$1.5565/(\sigma^2(F)+0.0005F^2)$	$0.3181/(\sigma^2(F)+0.002F^2)$	$0.5929/(\sigma^2(F)+0.004F^2)$
no. of refined params	301	141	207

[a] $I > 3.0\sigma(I)$.

(9) (a) Hessen, B.; Teuben, J. H.; Lemmen, T. H.; Huffman, J. C.; Caulton, K. G. *Organometallics* **1985**, *4*, 946–948. (b) Hessen, B.; Lemmen, T. H.; Luttikhedde, H. J. G.; Teuben, J. H.; Petersen, J. L.; Huffman, J. C.; Jagner, S.; Caulton, K. G. *Organometallics* **1987**, *6*, 2354–2362.

(10) Use of $VCl_2(TMEDA)_2$, instead of $VCl_3(THF)_3$, again increased the yield of **3** to 73%.

(11) (a) Krausse, J.; Marx, G. *J. Organomet. Chem.* **1974**, *65*, 215–222. (b) Müller, E.; Krausse, J.; Schmiedeknecht, K. *J. Organomet. Chem.* **1972**, *44*, 127–140.

(12) Olmstead, M. M.; Power, P. P.; Shoner, S. C. *Organometallics* **1988**, *7*, 1380–1385.

Table 2. Positional Parameters and *U*(eq) Values (Å²) for [(LiTMEDA)₂V(μ-CrCPh)₄(TMEDA)] (1), V(C≡CPh)₂(TMEDA)₂ (2), and V(C≡C^{t}Bu)₂(TMEDA)₂ (3)

atom	*x*	*y*	*z*	*U*(eq)	atom	*x*	*y*	*z*	*U*(eq)
				[(LiTMEDA)₂V(μ-C≡CPh)₄(TMEDA)] (**1**)					
V	0.32221(7)	0.22753(8)	0.07117(5)	0.046	C22	−0.023(1)	0.190(2)	−0.1944(7)	0.250
N1	0.3956(4)	0.2470(5)	−0.111(2)	0.051	C23	−0.0360(8)	0.253(2)	−0.1542(5)	0.271
N2	0.3423(4)	0.0716(4)	0.0452(3)	0.070	C24	0.0165(6)	0.265(1)	−0.1021(4)	0.194
N3	0.3926(4)	0.3781(4)	0.2454(2)	0.065	C25	0.2653(4)	0.1827(5)	0.1461(3)	0.052
N4	0.4980(4)	0.4749(4)	0.1712(3)	0.069	C26	0.2412(4)	0.1437(5)	0.1896(3)	0.061
N5	0.0680(6)	0.3501(6)	0.1034(4)	0.105	C27	0.2208(5)	0.0939(6)	0.2403(4)	0.063
N6	0.0272(6)	0.1570(8)	0.0966(5)	0.127	C28	0.1990(5)	0.1372(6)	0.2901(4)	0.090
Li1	0.4051(8)	0.3647(7)	0.1539(5)	0.061	C29	0.1799(6)	0.0852(9)	0.3376(4)	0.109
Li2	0.1447(7)	0.2328(9)	0.0913(5)	0.079	C30	0.1830(6)	−0.009(1)	0.3380(5)	0.115
C1	0.4488(4)	0.2254(5)	0.1256(3)	0.051	C31	0.2021(6)	−0.0534(7)	0.2888(5)	0.106
C2	0.5227(5)	0.2130(5)	0.1489(3)	0.054	C32	0.2232(5)	−0.0033(7)	0.2408(4)	0.082
C3	0.6102(5)	0.1898(5)	0.1699(3)	0.054	C33	0.3431(5)	0.2875(6)	−0.0639(3)	0.087
C4	0.6511(5)	0.2118(5)	0.2275(3)	0.073	C34	0.4727(5)	0.3064(7)	0.0014(3)	0.119
C5	0.7353(6)	0.1870(6)	0.2458(4)	0.086	C35	0.4262(8)	0.1545(9)	−0.0223(4)	0.146
C6	0.7819(6)	0.1415(7)	0.2079(5)	0.101	C36	0.3748(7)	0.0798(7)	−0.0124(5)	0.141
C7	0.7432(6)	0.1184(6)	0.1520(5)	0.093	C37	0.4014(5)	0.0212(5)	0.0906(4)	0.110
C8	0.6586(5)	0.1430(5)	0.1330(3)	0.069	C38	0.2625(5)	0.0171(5)	0.0361(4)	0.109
C9	0.3056(4)	0.3743(5)	0.0750(3)	0.056	C39	0.4224(5)	0.2900(5)	0.2744(3)	0.083
C10	0.2933(4)	0.4568(6)	0.0653(3)	0.059	C40	0.3048(6)	0.3945(6)	0.2581(4)	0.124
C11	0.2776(5)	0.5518(5)	0.0462(4)	0.063	C41	0.4477(6)	0.4571(6)	0.2680(4)	0.105
C12	0.2942(5)	0.5793(6)	−0.0091(4)	0.091	C42	0.5216(6)	0.4683(7)	0.2360(4)	0.122
C13	0.2808(7)	0.6699(8)	−0.0293(4)	0.108	C43	0.4624(6)	0.5650(6)	0.1528(4)	0.123
C14	0.2477(7)	0.7324(8)	0.0055(6)	0.112	C44	0.5739(5)	0.4612(6)	0.1423(4)	0.117
C15	0.2313(7)	0.7112(7)	0.0594(5)	0.134	C45	0.0604(6)	0.4128(7)	0.0530(5)	0.149
C16	0.2442(6)	0.6184(7)	0.0792(4)	0.114	C46	0.1054(7)	0.3999(8)	0.1554(5)	0.174
C17	0.2035(4)	0.2219(5)	0.0087(3)	0.064	C47	−0.015(1)	0.314(1)	0.1102(9)	0.203
C18	0.1464(5)	0.2166(6)	−0.0331(3)	0.072	C48	−0.032(1)	0.226(2)	0.092(1)	0.268
C19	0.0869(6)	0.2075(8)	−0.0873(4)	0.091	C49	0.0251(7)	0.111(1)	0.1493(7)	0.279
C20	0.1011(7)	0.1423(8)	−0.1286(5)	0.132	C50	0.006(1)	0.093(1)	0.0509(8)	0.379
C21	0.043(1)	0.135(1)	−0.1818(6)	0.206					
				V(C≡CPh)₂(TMEDA)₂ (**2**)					
V	0.00	0.12755(5)	0.25	0.036	C9	0.00	−0.0873(1)	0.25	0.039
N	0.1743(5)	0.1264(2)	0.1274(4)	0.072	C10	−0.1186(8)	−0.1197(3)	0.25	0.053
C1	0.00	0.2249(4)	0.25	0.053	C11	−0.1164(9)	−0.1813(3)	0.25	0.063
C2	0.00	0.2788(1)	0.25	0.044	C12	0.166(3)	0.180(1)	0.040(2)	0.102
C3	0.00	0.3435(4)	0.25	0.047	C13	0.7819(6)	0.1415(7)	0.2079(5)	0.101
C4	0.00	0.3756(3)	0.1522(8)	0.066	C14	0.201(2)	0.0745(7)	0.075(1)	0.084
C5	0.00	0.4376(4)	0.157(1)	0.085	C15	0.296(2)	0.1440(6)	0.205(2)	0.102
C6	0.00	0.4676(5)	0.25	0.092	C13x[a]	0.202(2)	0.181(1)	0.075(2)	0.085
C7	0.00	0.0303(4)	0.25	0.049	C14x	0.160(2)	0.0722(9)	0.032(1)	0.110
C8	0.00	−0.0233(4)	0.25	0.048	C15x	0.287(2)	0.1079(6)	0.195(2)	0.095
				V(C≡C^{t}Bu)₂(TMEDA)₂ (**3**)					
V	0.00	0.50	0.50	0.048	C10	0.0117(7)	0.3075(7)	0.7119(7)	0.170
N1	0.1945(5)	0.4633(5)	0.7340(6)	0.079	C11	−0.1220(6)	0.2036(5)	0.4473(6)	0.094
N2	−0.0990(5)	0.3424(5)	0.5718(5)	0.070	C12	−0.2461(6)	0.4107(6)	0.6163(6)	0.102
C1	0.1221(3)	0.3104(3)	0.3541(3)	0.063	N1x[a]	0.2191(6)	0.4918(5)	0.7365(6)	0.097
C2	0.1938(3)	0.2049(3)	0.2780(3)	0.061	N2x	0.1429(5)	0.6426(5)	0.4748(5)	0.080
C3	0.2857(3)	0.0761(4)	0.25(0)	0.047	C7x	0.3015(7)	0.3282(6)	0.7308(6)	0.126
C4	0.2772(5)	−0.0624(4)	0.2317(6)	0.131	C8x	0.1797(6)	0.5401(6)	0.8888(6)	0.116
C5	0.2193(5)	0.0545(5)	0.0052(4)	0.131	C9x	0.3026(6)	0.05858(7)	0.7193(7)	0.160
C6	0.4536(4)	0.0880(5)	0.2492(6)	0.148	C10x	0.2796(6)	0.6275(7)	0.5959(2)	0.166
C7	0.3484(6)	0.3901(7)	0.7155(7)	0.138	C11x	0.0434(6)	0.8039(5)	0.4692(6)	0.104
C8	0.2129(6)	0.6007(6)	0.8745(6)	0.120	C12x	0.1647(6)	0.6017(6)	0.3017(5)	0.110
C9	0.1282(7)	0.3849(6)	0.8032(7)	0.172					

[a] Atoms designated with an x are disordered and were refined with half-occupancy.

1−3. Four phenyl acetylides and one TMEDA molecule are bound to the vanadium atom approximately in an octahedral array. There are two lithium cations, each bridging the α-carbons of a pair of *cis*-alkynide ligands. Each lithium is further coordinated by a TMEDA molecule, completing a tetrahedral coordination geometry. The distances between the lithiums and the β-carbons of the alkynides, ranging from 2.80(1) to 2.87(1) Å, are too long to invoke bonding interactions. Electron deficient early-transition metal complexes often accommodate lithium cations which are tightly bound to anionic ligands,[11,12] and in the yttrium alkynide complex, (C₅Me₅)₂Y(C≡C^{t}Bu)₂Li(THF), the lithium also coordinates to the α-carbons of the alkynides.[13] The Li−Cα distances of 2.20(1)−2.23(1) Å for **1** are comparable to those of (C₅Me₅)₂Y(C≡C^{t}Bu)₂Li(thf) (2.09(3) Å)[13] and (PhC≡CLiTMEDA)₄ (2.20(1) Å).[14] Despite the lithium coordination at the α-carbons, the V−C−C bond angles do not deviate much from linearity. The V−Li separations of 2.89(1) and 2.90(1) Å are longer than the sum of the ionic radius of Li^+ and V(II), 2.66 Å.[15] The average V−Li distance (2.615 Å) in a related homoleptic phenyl complex $[LiOEt_2]_4[VPh_6]$ is clearly shorter than that of **1**.[12] Thus direct bonding interactions, if any, between V(II) and Li^+ in **1** would be very small. The

(13) Evans, W. J.; Drummond, D. K.; Hanusa, T. P.; Olofson, J. M. *J. Organomet. Chem.* **1989**, *376*, 311−320.
(14) Schubert, B.; Weiss, E. *Angew. Chem. Int. Ed. Engl.* **1983**, *22*, 496−497.
(15) Shannon, R. D. *Acta Crystallogr.* **1976**, *A32*, 751−767.

Table 3. Selected Bond Distances (Å) and Angles (deg) for [(LiTMEDA)$_2$V(μ-C≡CPh)$_4$ (TMEDA)] (1), V(C≡CPh)$_2$(TMEDA)$_2$ (2), and V(C≡C^{t}Bu)$_2$(TMEDA)$_2$ (3)

	[(LiTMEDA)$_2$V(μ-C≡CPh)$_4$(TMEDA)] (**1**)		
V–C1	2.186(6)	Li2–N6	2.17(2)
V–C9	2.122(8)	Li1–C1	2.23(1)
V–C17	2.175(6)	Li1–C9	2.20(1)
V–C25	2.128(7)	Li2–C17	2.21(2)
V–N1	2.346(6)	Li2–C25	2.23(1)
V–N2	2.343(6)	Li2–C26	2.81(1)
V–Li1	2.89(1)	C1–C2	1.220(9)
V–Li2	2.90(1)	C9–C10	1.21(1)
Li1–N3	2.12(1)	C17–C18	1.210(9)
Li1–N4	2.15(1)	C25–C26	1.24(1)
Li2–N5	2.11(2)		
V–C1–C2	168.8(6)	C1–V–C9	95.7(2)
V–C9–C10	167.5(6)	C1–V–C17	173.2(3)
V–C17–C18	169.2(7)	C17–V–C25	94.8(3)
V–C25–C26	169.2(6)	C9–V–N1	89.6(3)
N3–Li1–N4	85.0(5)	C9–V–N2	167.6(2)
C1–Li1–C9	92.1(5)	C25–V–N1	168.7(2)
N5–Li2–N6	83.2(6)	C25–V–N2	90.0(2)
C17–Li2–C25	91.0(5)	N1–V–N2	79.3(2)
	V(C≡CPh)$_2$(TMEDA)$_2$ (**2**)		
V–C1	2.18(1)	C1–C2	1.21(1)
V–C7	2.18(1)	C7–C8	1.20(1)
V–N	2.311(5)		
C1–V–N	90.6(1)	C7–V–N	89.4(1)
N–V–N′	81.5(3)		
	V(C≡C^{t}Bu)$_2$(TMEDA)$_2$ (**3**)		
V–C1	2.179(2)	V–N1	2.288(4)
V–N2	2.358(5)	C1–C2	1.207(3)
V–C1–C2	177.8(2)	C1–V–N1	89.5(1)
N1–V–N2	81.0(2)	C1–V–N2	89.7(1)

V–C1–Li1–C9 quadrilateral is puckered, and so is the V–C17–Li2–C25 quadrilateral. The dihedral angle between the C1–V–C9 and C1–Li1–C9 planes is 28.9°, while the corresponding angle for the latter quadrilateral is 31.3°.

The V–C1 and V–C17 bonds, which are trans to each other, are 0.047–0.064 Å (6σ–8σ) longer than the other two V–C distances. The stronger trans influence of the alkynide donor relative to the N-donor of TMEDA must be one reason behind the different V–C bond lengths. Despite Li coordination at the α-carbons, the average V–C bond length of **1** (2.153 Å) is clearly shorter than the V(II)–alkyl (sp^3 carbon) and V(II)–aryl bonds (sp^2 carbon) in (C_5H_5)V(CH_3)(dmpe) (2.219(4) Å)[9a] and in *trans*-V(*o*-$C_6H_4NMe_2$)$_2$(py)$_2$ (2.233(4) Å).[8] The lithiated phenyl complex of V(II), [$LiOEt_2$]$_4$[VPh_6], has even longer V–C bonds (2.342(3)–2.383(3) Å).[12] On the other hand, the V(III)–alkynide distances in (C_5H_5)$_2$V(C≡C^{t}Bu) (2.075(5) Å)[4] and (C_5Me_4Et)$_2$V (C≡C$C_6H_2Me_3$) (2.03(1) Å)[16] are shorter than those of **1**. The C≡C distances of **1** fall in the normal range.[17] Thus neither Li coordination nor back-bonding from d^3 V(II) detectably lengthen the C≡C bond. The phenyl rings of the *trans*-alkynides are situated nearly parallel to each other, which are then approximately perpendicular to the phenyl rings of the other two alkynides.

Structures of V(C≡CPh)$_2$(TMEDA)$_2$ (2) and V(C≡C^{t}Bu)$_2$(TMEDA)$_2$ (3). The molecular structures

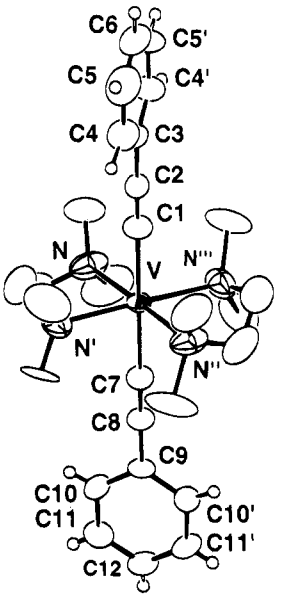

Figure 2. ORTEP drawing of the structure of V(C≡CPh)$_2$(TMEDA)$_2$ (**2**). Only one orientation of the disordered TMEDA ligands is shown.

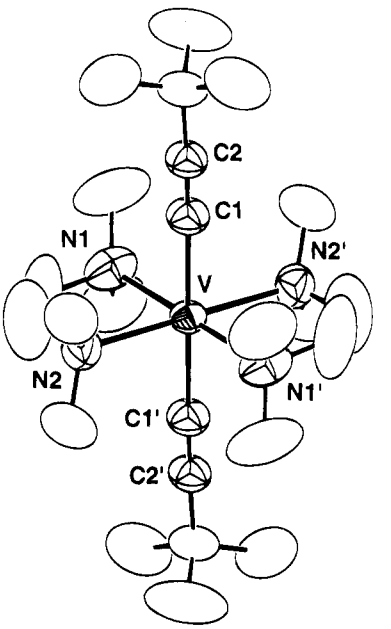

Figure 3. An ORTEP drawing of the structure of V(C≡C^{t}Bu)$_2$(TMEDA)$_2$ (**3**). The V atom is located on an inversion center, and only one of the positions of the disordered TMEDA ligand is shown.

of **2** and **3** are shown in Figures 2 and 3, respectively, and their crystal data are summarized in Tables 1–3. For both **2** and **3**, two alkynides coordinate V(II) in a trans configuration, while two TMEDA molecules form an equatorial girdle. In the case of **2**, there is crystallographic *mm* symmetry, in which one alkynide ligand, C1–C6, lies on one mirror plane, while the other ligand, C7–C12, lies on the perpendicular mirror plane. Thus, unlike **1**, the two trans phenyl groups are inherently perpendicular, and the C2–C1–V–C7–C8 spine is exactly linear. Due to this *mm* symmetry, the TMEDA ligands are disordered across the mirror planes. For **3** the vanadium atom sits at a crystallographic inversion center, so that the two alkynide groups are equivalent and so are the two TMEDA groups. These TMEDA ligands are again disordered.[18] The V–C bond lengths

(16) Köhler, F. H.; Prössdorf, W.; Schubert, U.; Neugebauer, D. *Angew. Chem., Int. Ed. Engl.* **1978**, *17*, 850–851.
(17) Evans, W. J.; Ulibarri, T. A.; Chamberlain, L. R.; Ziller, J. W.; Alvarez, D., Jr. *Organometallics* **1990**, *9*, 2124–2130 and references therein.

of **2** (2.18(1) Å) and **3** (2.179(4) Å) are practically identical, and differing the alkynide substituent does not affect the V–C bond length. Interestingly, the V–C bond lengths in these Li-free complexes, i.e., V–C1 and V–C19, are indistinguishable from those of **1**, in which the alkynides are trans to each other. The V–N distances, on the other hand, even in these sterically crowded bis-TMEDA complexes, are shorter than in **1**, in which they are trans to alkynides.

In the *Cmcm* space group, the two TMEDA chelates of **2** should assume either a $\lambda\lambda$ or a $\delta\delta$ configuration in order to avoid steric repulsion between the methyl groups of neighboring amine units. The N–V–N chelate angle of 81.5(3)° is slightly larger than that of **1** (79.3(2)°), and the V–N distance is shorter. The two phenyl groups, situated perpendicular to each other, are both staggered with respect to the nitrogen atoms of TMEDA. Complex **3** crystallizes in the space group $P\bar{1}$, and the TMEDA molecules are disordered in a different way from **2**. The inversion center at vanadium forces a pair of the symmetrically related TMEDA molecules to have the opposite configuration. The N1–V–N2 angle of 81.0(2)° is similar that of **2**.

With the exception of the V–N distances trans to an alkynide ligand in **1**, all other V–N distances appear normal. The V–N distance in **2**, 2.311(5) Å is very similar to that reported for $VCl_2(TMEDA)_2$, 2.319(2) Å (average).[8] The V–N distances in **3** vary widely. However, this variation is likely artificial, because of the disorder in this complex, and the average V–N distance in **3** is indistinguishable from that observed in the other compounds.

Reactions of 1–3. The neutral, bis(alkynide) complex **2** smoothly reacts with LiC≡CPh to afford **1** in good yield. The V(II) center accommodates four PhC≡C$^-$ ligands, resulting in the dianionic complex **1** (eq 5),

$$\underset{\mathbf{2}}{V(C{\equiv}CPh)_2(TMEDA)_2} + 2\,LiC{\equiv}CPh \xrightarrow{THF/TMEDA} \underset{\mathbf{1}}{[(LiTMEDA)_2V(\mu\text{-}C{\equiv}CPh)_4(TMEDA)]} \quad (5)$$

84% yield

while in the case of ^{t}BuC≡C$^-$, only two ligands are incorporated to form the neutral complex **2**. The choice may be delicately controlled by the size of the acetylide substituent and/or electronic factors.

The high-yield syntheses of the lithiated, anionic complex **1** and the neutral complexes **2** and **3**, which are the first alkynide complexes of V(II), provide us with a good opportunity to examine differences in the reactivity between neutral and anionic alkynide complexes and to compare this reactivity with that of electron rich metals. The reactivity of these complexes is an ongoing study, and we report here some initial results.

In the case of **1–3**, the alkynide ligands were found to react with organic electrophiles at the α-carbon. For instance, treatment of **1** with 2 equiv of Me_3SiCl and MeI resulted in formation of **2** along with $Me_3SiC{\equiv}CPh$ and MeC≡CPh, respectively (eq 6). Addition of phenyl isocyanate to a THF solution of **3**, and subsequent hydrolysis with aqueous HCl generated ^{t}BuC≡CC(O)-

$$\underset{\mathbf{1}}{[(LiTMEDA)_2V(\mu\text{-}C{\equiv}CPh)_4(TMEDA)]} + 2\,RX \longrightarrow \underset{\mathbf{2}}{V(C{\equiv}CPh)_2(TMEDA)_2} + RC{\equiv}CPh \quad (6)$$

RX = Me_3SiCl, 73% yield

MeI, 66%

NHPh. Thus, a facile insertion of isocyanate into the V–C σ-bond took place. Carbon dioxide inserted in a similar way for **1** and **2** and generated PhC≡CCO$_2$H after hydrolysis. Thus, in case of the vanadium(II) acetylide complexes **1–3**, electrophiles attack at C_α of the C≡C fragment. This is similar to the chemistry reported for $(C_5H_5)_2M(C{\equiv}CPh)_2$ (M = V, Ti), which was reported to react with HCl to produce HC≡CPh.[3] There is no evidence for enhanced nucleophilicity at the β carbon as has been observed for some electron rich acetylide compounds.[19–21]

Finally, **2** and **3** were found to react with carbon monoxide under mild conditions to yield a pyrophoric black precipitate with an IR band at 1850 cm^{-1}. This precipitate is tentatively identified as $[V(CO)_6]^-$ by reference to the ν_{CO} band of $[Na(diglyme)_2][V(CO)_6]$ (1859 cm^{-1}).[22] Compounds **2** and **3** may be reduced from V(II) to V(−I) upon reaction with CO. The vanadium(III) compound, $[V(Mes)_3(THF)]$, has also been shown to undergo reaction with CO to form $[V(CO)_6]^-$ (ν_{CO} = 1862 cm^{-1}) and MesC(O)Mes.[23]

Experimental Section

General Procedure. All reactions were carried out using standard Schlenk techniques under an argon atmosphere. Solvents were dried and distilled before use according to known methods. $VCl_3(THF)_3$[24] and $VCl_2(TMEDA)_2$[8] were prepared as reported. Infrared spectra were recorded on a Hitachi model 295, while EI mass spectra were obtained on a JEOL JMS-DX-303 spectrometer. Elemental analyses were performed on a LECO CHN-900 microanalyzer.

Preparation of [(LiTMEDA)$_2$V(μ-C≡CPh)$_4$(TMEDA)] (1). Method 1. A THF (30 mL) solution of LiC≡CPh (16.4 mmol) was added to $VCl_3(THF)_3$ (1.09 g, 2.92 mmol) in THF (30 mL) containing TMEDA (10 mL) at 0 °C. The solution was stirred at room temperature for 2 h, during which time the color gradually turned from brown to purple. After removal of solvent *in vacuo*, the purple residue was treated with hexane (100 mL)/TMEDA (1 mL). The hexane solution was centrifuged to remove insoluble LiCl and was concentrated to yield **1** as purple crystals (1.52 g, 64%): IR (Nujol) 2000 (s), 1964 (w) cm^{-1}; UV–visible (λ_{max}, nm, THF) 490. Anal. Calcd for $C_{50}H_{68}N_6Li_2V$: C, 73.42; H, 8.38; N, 10.27. Found: C, 72.02; H, 7.36; N, 9.32. All of the vanadium(II) alkynide complexes reported in this paper are sensitive to air and moisture, hindering attempts to obtain satisfactory elemental analyses.

Method 2. A THF (30 mL) solution of LiC≡CPh (16.4 mmol) was added at 0 °C to $VCl_2(TMEDA)_2$ (1.40 g, 4.05 mmol) in THF (30 mL)/TMEDA (2 mL). Workup similar to that in method 1 above yielded **1** (2.77 g, 84%).

(18) See supporting information, in which the disordered structures of **2** and **3** are described in detail.

(19) Kelly, C.; Lugan, N.; Terry, M. R.; Geffroy, G. L.; Haggerty, B. S.; Rheingold, A. L. *J. Am. Chem. Soc.* **1992**, *114*, 6735–6749.
(20) Birdwhistell, K. R.; Templeton, J. L. *Organometallics* **1985**, *4*, 2062–2064.
(21) Bruce, M. I. *Chem. Rev.* **1991**, *91*, 197–257.
(22) Connelly, N. G. Vanadium. In *Comprehensive Organometallic Chemistry*; Wilkinson, G., Stone, F. G. A., Abel, E. W., Eds.; Pergamon: Oxford, U.K., 1981; Vol. 3, Chapter 24, pp 648–649.
(23) Vivanco, M.; Ruiz, J.; Floriani, C.; Chiesi-Villa, A.; Rizzoli, C. *Organometallics* **1993**, *12*, 1794–1801.
(24) Manzer, L. E. *Inorg. Synth.* **1982**, *21*, 135.

Preparation of V(C≡CPh)$_2$(TMEDA)$_2$ (2). Method 1. A mixture of LiC≡CPh (8.95 mmol) and $VCl_3(THF)_3$ (1.10 g, 2.94 mmol) in THF (70 mL)/TMEDA (10 mL) was treated as described above to give **1** in 4% yield (based on vanadium, 0.26 g) and the brown solid insoluble in hexane. Compound **2** (1.02 g, 71%) was extracted from the brown residue by THF (100 mL)/TMEDA (5 mL). Data for **2**: IR (Nujol) 2020 (s) cm^{-1}; EI MS *m/e* 485 (M^+), 369 (M^+ − TMEDA). Anal. Calcd for $C_{28}H_{42}N_4V$: C, 69.25; H, 8.72; N, 11.54. Found: C, 69.96; H, 8.63; N, 11.38.

Method 2. Addition of LiC≡CPh (7.01 mmol) in THF (30 mL) to $VCl_2(TMEDA)_2$ (1.23 g, 3.47 mmol) in THF (40 mL)/TMEDA (2 mL) at 0 °C, followed by workup similar to the above yielded **1** (0.05 g, 2% based on vanadium) and **2** (1.34 g, 85%).

Preparation of V(C≡C^{t}Bu)$_2$(TMEDA)$_2$ (3). Method 1. The same procedure as used for **1** was followed. Reaction of LiC≡C^{t}Bu (12.7 mmol) in THF (30 mL) with $VCl_3(THF)_3$ (1.69 g, 4.52 mmol) in THF (40 mL)/TMEDA (5 mL) afforded **3** as brown purple crystals (1.13 g, 56%): IR (Nujol) 2035 (s) cm^{-1}; EI MS *m/e* 445 (M^+), 363 (M^+ − HC≡C^{t}Bu), 329 (M^+ − TMEDA), 247 (M^+ − TMEDA − HC≡C^{t}Bu); UV−visible (λ_{max}, nm, THF) 530. Anal. Calcd for $C_{24}H_{50}N_4V$: C, 64.69; H, 11.31; N, 12.57. Found: C, 63.76; H, 10.88; N, 12.36.

Method 2. Analogous to method 2 for the preparation of **2**, LiC≡C^{t}Bu (9.79 mmol) in THF (30 mL) and $VCl_2(TMEDA)_2$ (1.70 g, 4.80 mmol) in THF (50 mL)/TMEDA (4 mL) produced **3** (1.56 g, 73%).

Attempt to Isolate the C≡C^{t}Bu Analogue of 1. Method 1. A THF (30 mL) solution of LiC≡C^{t}Bu (19.6 mmol) was added to $VCl_3(THF)_3$ (1.45 g, 3.88 mmol) in THF (40 mL)/TMEDA (6 mL) at 0 °C. The solution was warmed to room temperature with stirring. Within a few minutes, the color of the solution changed from brown to greenish brown. After that, workup similar to **1** afforded **3** (0.19 g, 11%).

Method 2. Addition of LiC≡C^{t}Bu (12.7 mmol) in THF (30 mL) to $VCl_2(TMEDA)_2$ (1.02 g, 2.88 mmol) in THF (50 mL)/TMEDA (5 mL) followed by workup similar to method 1 above provided **3** (0.21 g, 16%).

Reaction of $VCl_3(THF)_3$ with LiC≡CPh in DME. LiC≡CPh (15.5 mmol) in DME (40 mL) was added to a DME (30 mL) solution of $VCl_3(THF)_3$ at 0 °C. As this solution was stirred at room temperature for 2 h, the color changed from brown to purple. The resulting solution was centrifuged to remove insoluble products. The purple solution was concentrated to afford $Li_2(DME)_xV(C{\equiv}CPh)_4$ (**4**) as red purple crystals (1.10 g): IR (Nujol) 2000 (s), 1960 (w) cm^{-1}.

Reaction of 2 with LiC≡CPh. A THF (20 mL)/TMEDA (1 mL) solution of **2** (0.46 g, 0.95 mmol) was treated as described for **1** with LiC≡CPh (1.90 mmol) in THF (10 mL). Compound **1** (0.64 g, 83%) was obtained as purple crystals.

Reaction of 1 with Me$_3$SiCl and MeI. Me_3SiCl (0.11ml, 0.87 mmol) in THF (5 mL) was added to a THF (20 mL) solution of **1** (0.33 g, 0.40 mmol) and TMEDA (1 mL) at room temperature. The initially purple solution immediately became brown and was stirred at room temperature for 1 h. The solvent and PhC≡CSiMe$_3$ were removed under vacuum to leave a brown crystalline solid, which was recrystallized from THF/TMEDA, giving **2** as brown crystals (0.14 g, 73%). Similar reaction with MeI afforded **2** in 66% yield. The GS−MS spectra of the solutions showed PhC≡CSiMe$_3$ and PhC≡CMe, respectively.

Reaction of 1 and 2 with CO$_2$. A THF (20 mL) solution of **1** (0.23 g, 0.28 mmol) was stirred under CO_2 (1 atm) for 1 h. Addition of aqueous HCl to the THF solution followed by extraction with ether gave PhC≡CCO$_2$H (0.11 g, 66%) as colorless crystals: IR (Nujol) 2660 (s), 2575 (s), 2220 (sh), 2198 (s), 1670 (s) cm^{-1}. The reaction of **2** (0.10 g, 0.21 mmol) and CO_2 followed by a similar workup also gave PhC≡CCO$_2$H (33 mg, 54%).

Reaction of 3 with PhNCO. Compound **3** (0.34 g, 0.76 mmol) was treated as described above with 2 equiv of PhNCO (0.17ml, 1.56 mmol) in THF (20 mL). ^{t}BuC≡CC(O)NHPh (0.19 g, 61%) was obtained as colorless crystals: IR (Nujol) 3240 (s), 3125 (s), 3060 (sh), 2280 (w), 2220 (s) cm^{-1}. Anal. Calcd for $C_{13}H_{15}NO$: C, 77.58; H, 7.51; N, 6.96. Found: C, 77.20; H, 7.53; N, 7.20.

Reaction of 2 and 3 with CO. A THF (20 mL) solution of **2** (0.13 g, 0.27 mmol) was stirred under CO (1 atm) at room temperature for 3 days. A black pyrophoric precipitate was obtained (40 mg), which has an IR band at 1850 cm^{-1} (Nujol) (cf. 1859 cm^{-1} for $[V(CO)_6]^-$ in THF).[21] Compound **3** (0.67 g, 1.51 mmol) also underwent a similar reaction with CO to give a black precipitate (61 mg).

Crystal Structure Determination of Complexes 1−3. Crystals of **1−3** suitable for X-ray analysis were mounted in glass capillaries and sealed under argon. Diffraction data were collected at room temperature on a Rigaku AFC5R diffractometer employing graphite-monochromated Mo Kα radiation (λ = 0.710 690 Å) and using the $\omega-2\theta$ scan technique. Refined cell dimensions and their standard deviations were obtained from least-squares refinements of 25 randomly selected centered reflections. Three standard reflections, monitored periodically for crystal decomposition or movement, showed only slight intensity variation (~1%) over the course of the data collections. The raw intensities were corrected for Lorentz and polarization effects. Empirical absorption corrections based on ψ scans were applied.

All calculations were performed with SHELX76. The structures of **1** and **2** were solved by the Patterson method, and the structure of **3** was solved by direct methods, locating in all three cases the vanadium position. The other atoms were found in subsequent Fourier maps, and the structures were refined by full-matrix least squares. Anisotropic refinement was applied to all non-hydrogen atoms, including the disordered carbon and/or nitrogen atoms in **2** and **3**. The hydrogen atoms on the two phenyl groups of **2** were located and refined isotropically, while the other hydrogens were put at calculated positions. Additional information is available as supporting information.

Acknowledgment. We are very grateful to Prof. T. Yoshida at the University of Osaka Prefecture for open access to the diffractometer for the crystal structure analysis of **3**. We also thank Prof. Roger E. Cramer for stimulating discussions and careful reading of the manuscript, who is at Nagoya University on sabbatical leave from University of Hawaii, U.S.A.

Supporting Information Available: Tables giving atomic coordinates and isotropic thermal parameters, bond distances and angles, hydrogen coordinates, and anisotropic thermal parameters of **1−3** and text and figures giving details on the disordered structures of **2** and **3** (23 pages). Ordering information is given on any current masthead page.

OM950226O

Synthesis, Structure, Fluxional Behavior, and Substitution Reaction of the Metal–Metal-Bonded Heterobimetallic Phosphido-Bridged Complex $CpW(CO)_2(\mu\text{-}CO)(\mu\text{-}PPh_2)Fe(CO)_3$

Shin-Guang Shyu,*,† Shu-Min Hsiao,†,‡ Kuan-Jiuh Lin,† and H.-M Gau‡

Institute of Chemistry, Academia Sinica, Taipei, Taiwan 11529, Republic of China, and Department of Chemistry, National Chung Hsing University, Taichung, Taiwan, Republic of China

Received April 25, 1995®

The heterobimetallic phosphido-bridged complexes $CpW(CO)_2(\mu\text{-}CO)(\mu\text{-}PPh_2)Fe(CO)_3$ (**4**) and $CpW(CO)_3(\mu\text{-}PPh_2)Fe(CO)_4$ (**5**) were prepared by the reaction of $CpW(CO)_3PPh_2$ with $Fe_2(CO)_9$. Photolysis of **5** produced **4**. The structures of **4** and **5** were determined by single-crystal X-ray diffraction. The W–Fe distance was 2.8308(22) Å in **4**, indicative of a W–Fe bond. The long distance between W and Fe (4.2434(20) Å) in **5** indicates no metal–metal bond in the complex. Fluxional behavior involving the exchange of all CO ligands in **4** was studied by variable-temperature ^{13}C NMR spectroscopy. Reaction between **4** and Lewis bases L (L = $P(OMe)_3$, PMe_3, PPh_2H, PPh_3, PEt_3) at ambient temperatures produced $CpW(CO)_2(\mu\text{-}PPh_2)Fe(CO)_3(L)$ (**6**) with L regiospecifically coordinated to Fe. However, **5** did not react with L under similar conditions. The structure of $CpW(CO)_2(\mu\text{-}PPh_2)Fe(CO)_3(PPh_2H)$ (**6c**) was determined by single-crystal X-ray diffraction.

Introduction

An interesting cooperativity effect between metals in bimetallic phosphido-bridged complexes is that a metal can activate the substitution reaction of the adjacent metal carbonyl through the formation of a metal–metal bond.[1] Thus, metal–metal bonds in the heterobimetallic phosphido-bridged complexes $CpW(CO)_2(\mu\text{-}PPh_2)Mo(CO)_5$ (**1**) and $CpFe(CO)(\mu\text{-}CO)(\mu\text{-}PPh_2)W(CO)_4$[2] (**2**) activate the Mo carbonyl ligand and the W carbonyl ligands correspondingly toward substitution by Lewis bases L (L = PMe_3, PPh_2H, $P(OMe)_3$) at ambient temperatures via the opening of the metal–metal bond to produce $CpW(CO)_3(\mu\text{-}PPh_2)Mo(CO)_4L$ and $CpFe(CO)_2(\mu\text{-}PPh_2)W(CO)_4L$ with the intramolecular transfer of one Mo carbonyl or one W carbonyl, respectively, to the adjacent metal.[1a,2] For the complex $CpW(CO)_2(\mu\text{-}PPh_2)W(CO)_5$ (**3**), similar activation of the carbonyl ligands on the $W(CO)_5$ moiety toward substitution by Lewis bases L by the adjacent W through the metal–metal bond was also observed at a higher reaction temperature to produce $CpW(CO)_2(\mu\text{-}PPh_2)W(CO)_4L$.[1b]

Systematic investigations on the influence of a metal on the chemistry of its adjacent metal in bimetallic complexes could be of importance for an understanding of the cooperativity effect in binuclear complexes and clusters. One way is by using different kinds of metal fragments and comparing their influences on a similar metal moiety as in the cases of complexes **2** and **3**. The other way is by using similar metal fragments and studing their influences on different kinds of metal moieties. Since the $CpW(CO)_2$ fragment can activate the substitution of its adjacent group VI element (Mo or W) carbonyl ligands in complexes **1** and **2**, it would be of interest to see whether the activation can be extended to group VIII elements.

The complex $CpW(CO)_2(\mu\text{-}CO)(\mu\text{-}PPh_2)Fe(CO)_3$[3] (**4**) was chosen as our target of study on the basis of the following three reasons. First, substitution of the second carbonyl ligand by phosphine in $Fe(CO)_4PR_3$ requires high temperature or a long period of UV irradiation.[4] If we consider that the metallophosphine $CpW(CO)_2PPh_2$ is a ligand similar to PR_3, it would be of interest to see whether $CpW(CO)_2$ can activate the substitution of the carbonyl ligands on Fe in this complex. Second, a single-crystal X-ray study of this complex revealed the presence of a bridging carbonyl ligand. This indicates $CpW(CO)_2$ has a strong interaction with the adjacent Fe carbonyl. This interaction may facilitate the substitution of the Fe carbonyl ligand such that the substitution can proceed under a relatively mild conditions.[2] Third, its non-metal–metal-bonded

† Academia Sinica.
‡ National Chung Hsing University.
® Abstract published in *Advance ACS Abstracts,* August 1, 1995.

(1) (a) Shyu, S.-G.; Hsu, J.-Y.; Lin, P.-J.; Wu, W.-J.; Peng, S. M.; Lee, G. H.; Wen, Y.-S. *Organometallics* **1994,** *13,* 1699. (b) Shyu, S.-G.; Wu, W.-J.; Peng, S. M.; Lee, G. H.; Wen, Y.-S. *J. Organomet. Chem.* **1995,** *489,* 113. (c) Regragui, R.; Dixneuf, P. H.; Taylor, N. J.; Carty, A. J. *Organometalllics* **1986,** *5,* 1. (d) Mercer, W. C.; Whittle, R. R.; Burkhardt, E. W.; Geoffroy, G. L. *Organometallics* **1985,** *4,* 68. (e) Powell, J.; Sawyer, J. F.; Stainer, M. V. R. *Inorg. Chem.* **1989,** *28,* 4461. (f) Powell, J.; Coutoure, C.; Gregg, M. R. *J. Chem. Soc., Chem. Commun.* **1988,** 1208.

(2) Shyu, S.-G.; Lin, P.-J.; Lin, K.-J.; Wen, Y.-S.; Chang, M.-C. *Organometallics* **1995,** *14,* 2253.

(3) Linder, E.; Heckmann, M.; Fawzi, R.; Hiller, W. *Chem. Ber.* **1991,** *124,* 2171.

(4) (a) Clifford, A. F.; Mukherjee, A. K. *Inorg. Chem.* **1963,** *2,* 151. (b) Lewis, J.; Nyholm, R. S.; Sandhu, S. S.; Stiddard, M. H. B. *J. Chem. Soc.* **1964,** 2825.

0276-7333/95/2314-4300$09.00/0

Table 1. Spectroscopic Data for 4–6[a]

complex	$^{31}P\{^1H\}$ NMR,[b,c] δ	^1H NMR,[b,d] δ	IR, ν(CO),[e] cm^{-1}
4	93.27 (s, J_{P-W} 257.6)	5.16 (s, 5H)	2072 m, 2041 s, 1977 s, 1925 s, 1851 m, 1736 m
5	−10.41 (s, J_{P-W} 130.79)	5.41 (s, 5H)	2040 s, 2023 s, 1943 s, 1911 s
6a	127.19 (d, $^2J_{P-P}$ 19.93, J_{P-W} 317.77, μ-PPh_2), 170.46 (d, $P(OMe)_3$)	5.14 (s, 5H), 3.62 (d, $^3J_{P-H}$ 12.0, 9H)	2034 w, 1962 s, 1913 s, 1837 s
6b	127.53 (d, $^2J_{P-P}$ 20.25, J_{P-W} 322.03, μ-PPh_2), 16.91 (d, PMe_3)	5.02 (s, 5H), 1.64 (d, $^2J_{P-H}$ 10.0, 9H)	2011 m, 1947 s, 1901 s, 1827 s
6c	132.43 (d, $^2J_{P-P}$ 21.80, J_{P-W} 324.76, μ-PPh_2), 41.22 (d, J_{P-H} 382.71, PPh_2H)	4.82 (s, 5H)	2025 w, 1958 m, 1905 s, 1832 s
6d	129.13 (d, $^2J_{P-P}$ 10.57; J_{P-W} 309.53, μ-PPh_2), 62.19 (d, PPh_3)	5.28 (s, 5H)	2004 m, 1946 s, 1912 s, 1838s
6e[h]	125.93 (d, $^2J_{P-P}$ 15.67, J_{P-W} 317.71, μ-PPh_2), 46.83 (d, PEt_3)	5.03 (s, 5H), 1.94 (m, 6H), 1.14 (m, 9H)	2003 w, 1941 s, 1904 s, 1834 m

[a] At room temperature. [b] J values in Hz. [c] In THF solution unless otherwise indicated. [d] In $CDCl_3$ solution unless otherwise indicated. Cp, Me, and H groups only. Abbreviations: s, singlet; d, doublet. [e] In THF solution unless otherwise indicated. Abbreviations: vs, very strong; s, strong; m, medium; w, weak; br, broad; sh, shoulder.

analogue $CpW(CO)_3(\mu\text{-}PPh_2)Fe(CO)_4$ (**5**) can be prepared and serves as a standard for comparison of their reactivities to reveal the influence of the metal–metal bond in **4**.

The heterobimetallic phosphido-bridged complexes **4** (with a metal–metal bond) and **5** (without a metal–metal bond) were synthesized. Reactions between **4** and Lewis bases L (L = $P(OMe)_3$, PMe_3, PPh_2H, PPh_3, PEt_3) produced $CpW(CO)_2(\mu\text{-}PPh_2)Fe(CO)_3L$ (**6**) with L regiospecifically coordinated to Fe under mild conditions. However, **5** did not react with L under similar conditions. This indicates that $CpW(CO)_2$ in **4** could enhance substitution of the adjacent Fe carbonyl through the formation of the metal–metal bond. Reported herein are the synthesis, structures, fluxional behavior, and reactivity studies of **4** and **5**. Scheme 1 shows reactions that comprise the main focus of our work. The products of the substitution reaction have been characterized spectroscopically, and the structure of $CpW(CO)_2(\mu\text{-}PPh_2)Fe(CO)_3(PPh_2H)$ (**6c**) was also determined by a single-crystal X-ray diffraction study.

Scheme 1

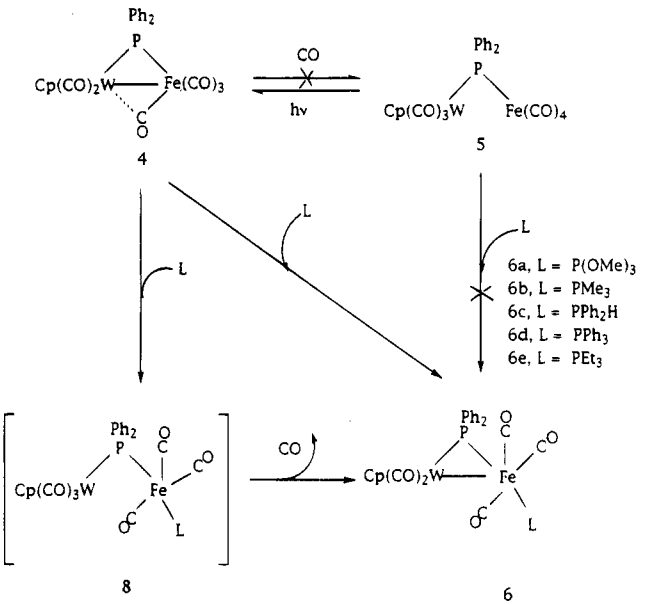

Experimental Section

Unless otherwise stated, all reactions and manipulations of air-sensitive compounds were carried out at ambient temperatures under an atmosphere of purified N_2 with standard procedures. A 450-W Hanovia medium-pressure quartz mercury-vapor lamp (Ace Glass) and a Pyrex Schlenk tube as a reaction vessel were used in the photoreactions. Infrared (IR) spectra were recorded on a Perkin-Elmer 882 infrared spectrophotometer. ^1H, ^{13}C, and ^{31}P NMR spectra were measured by using Bruker AMX-500, MSL-200, AC-200, and AC-300 spectrometers. ^{31}P NMR shifts are referenced to 85% H_3PO_4. Except as noted, NMR spectra were collected at room temperature. Electron impact (EI) and fast-atom bombardment (FAB) mass spectra were recorded on a VG 70-250S or a JEOL JMS-HX 110 mass spectrometer. Microanalyses were performed at the Microanalytic Laboratory at National Cheng Kung University, Tainan, Taiwan, and at Academia Sinica. Spectroscopic data (^{31}P and ^1H NMR and IR) of all new complexes are listed in Table 1.

Materials. THF was distilled from potassium and benzophenone under an atmosphere of N_2 immediately before use. Other solvents were purified according to established procedures.[5] Metal carbonyls ($W(CO)_6$, $Fe(CO)_5$), PPh_2Cl, PMe_3, PPh_2H, PEt_3, and PPh_3 were obtained from Strem, $P(OMe)_3$ was obtained from Merck, and ^{13}CO (99 atom % ^{13}C) was obtained from Isotec. Other reagents and solvents were obtained from various commercial sources and used as received. $Na[CpW(CO)_3]$,[6] $WCp(CO)_3PPh_2$,[7] and $Fe_2(CO)_9$[8] were prepared by literature procedures.

Synthesis of $CpW(CO)_2(\mu\text{-}CO)(\mu\text{-}PPh_2)Fe(CO)_3$ (4) and $CpW(CO)_3(\mu\text{-}PPh_2)Fe(CO)_4$ (5). A yellow solution of $Na[CpW(CO)_3]$ (9.30 g, 26.20 mmol) in 250 mL of THF was cooled to 0 °C. PPh_2Cl (4.7 mL, 26.20 mmol) was then added slowly to the above solution. After 1 h, the solution turned orange-red. $Fe_2(CO)_9$ (9.56 g, 26.20 mmol) was then added to the above solution. After the solution was stirred overnight, the solvent was removed and the residue was chromatographed on grade II Al_2O_3. Elution with CH_2Cl_2/hexane (1:6) afforded three fractions. A trace amount of yellow solid was obtained from the first band and was not identified. The red solid **4** was obtained from the second band which is dark red. Yield: 0.98 g (6%). Anal. Calcd for $C_{23}H_{15}FeO_6PW$: C, 41.95; H, 2.30. Found: C, 41.80; H, 2.04. MS (FAB): M^+ m/z 658.

The orange solid **5** was obtained from the third band after the solvent was removed. Yield: 9.17 g (53%). Anal. Calcd

(5) Perrin, D. D.; Armarego, W. L. F.; Perrin, D. R. *Purification of Laboratory Chemicals*; Pergamon: Oxford, U.K., 1966.

(6) Bender, R.; Braunstein, P.; Jud, J.-M.; Dusausoy, Y. *Inorg. Chem.* **1983**, *22*, 3394.

(7) (a) Adams, H.; Bailey, N. A.; Day, A. N.; Morris, M. J.; Harrison, M. M. *J. Organomet. Chem.* **1991**, *407*, 247. (b) Malisch, W.; Maisch, R.; Colquhoun, I. J.; Mcfarlane, W. *J. Organomet. Chem.* **1981**, *220*, C1.

(8) Eisch, J. J.; King, R. B. *Organometallic Synthesis*; Academic Press: New York, 1965.

for $C_{24}H_{15}FeO_7PW$: C, 42.02; H, 2.20. Found: C, 42.29; H, 2.56. MS (FAB): M^+ *m/z* 686.

Photolysis of 5. A solution of **5** (1.80 g, 2.62 mmol) in 40 mL of THF was irradiated with UV under N_2 for 3 h. The color of the solution changed from orange to dark red. The solvent was then removed, and the residue was chromatographed on grade II Al_2O_3. Elution with CH_2Cl_2/hexane (1:6) afforded four fractions. Only trace amounts of products were obtained from the first and second bands which were yellow and pink, respectively. They were not identified. The fourth fraction is unreacted **5** (0.16 g, 9%). After the solvent was removed from the third band, **4** was obtained as a red solid. Yield: 1.00 g (58%).

Synthesis of $CpW(CO)_2(\mu\text{-}PPh_2)Fe(CO)_3(P(OMe)_3)$ (6a). To a red solution of **4** (0.20 g, 0.30 mmol) in 30 mL of THF was added 280 μL of $P(OMe)_3$ (2.40 mmol) under N_2 at ambient temperature. After the mixture was stirred overnight, the solvent was removed. The residue was chromatographed on grade II Al_2O_3 and eluted with CH_2Cl_2/hexane (1:3) to afford two fractions. A trace amount of pink solid was obtained from the first band and was not identified. The second band was red. After the solvent was removed, **6a** was obtained as a red solid. Yield: 0.11 g (49%). Anal. Calcd for $C_{25}H_{24}FeO_8P_2W$: C, 39.84; H, 3.08. Found: C, 39.84; H, 3.30. MS (FAB): M^+ *m/z* 752.

Synthesis of $CpW(CO)_2(\mu\text{-}PPh_2)Fe(CO)_3(PMe_3)$ (6b). To a red solution of **4** (0.20 g, 0.30 mmol) in 30 mL of THF was added 0.30 mL (1.19 M in THF, 0.36 mmol) of PMe_3 under N_2 at ambient temperature. After the mixture was stirred ovenight, the solvent was removed. The residue was chromatographed on grade II Al_2O_3 and eluted with CH_2Cl_2/hexane (1:4) to afford two fractions. The first band was unreacted **4**. The second band was red. After the solvent was removed, **6b** was obtained as a red solid. Yield: 0.125 g (58%). Anal. Calcd for $C_{25}H_{24}FeO_5P_2W$: C, 42.53; H, 3.43. Found: C, 42.27; H, 3.38. MS (FAB): $M - CO^+$ *m/z* 705.

Synthesis of $CpW(CO)_2(\mu\text{-}PPh_2)Fe(CO)_3(PPh_2H)$ (6c). To a red solution of **4** (0.20 g, 0.30 mmol) in 25 mL of THF was added 100 μL of PPh_2H (0.57 mmol) under N_2 at ambient temperature. After the mixture was stirred overnight, the solvent was removed. The residue was chromatographed on grade II Al_2O_3 and eluted with CH_2Cl_2/hexane (1:3) to afford two fractions. The first band was unreacted **4**. The second band was red. After the solvent was removed, **6c** was obtained as a red solid. Yield: 0.16 g (63%). Anal. Calcd for $C_{34}H_{20}FeO_5P_2W$: C, 50.03; H, 3.21. Found: C, 49.61; H, 3.24. MS (FAB): M^+ *m/z* 816.

Synthesis of $CpW(CO)_2(\mu\text{-}PPh_2)Fe(CO)_3(PPh_3)$ (6d). To a red solution of **4** (0.18 g, 0.27 mmol) in 30 mL of THF was added 72 mg (0.27 mmol) of PPh_3 under N_2 at ambient temperature. The mixture was stirred for 41 h. After the solvent was removed, a red solid which is a mixture of **4** and **6d** was obtained. Complex **4** was removed by washing the mixture with 30 mL of CH_2Cl_2/hexane (2:3) solution. Complex **6d** was obtained as a red solid. Yield: 0.18 g (74%). Anal. Calcd for $C_{40}H_{30}FeO_5P_2W$: C, 53.90; H, 3.28. Found: C, 53.51; H, 3.01. MS (FAB): M^+ *m/z* 891.

Synthesis of $CpW(CO)_2(\mu\text{-}PPh_2)Fe(CO)_3(PEt_3)$ (6e). To a red solution of **4** (0.21 g, 0.32 mmol) in 30 mL of THF was added 0.35 mL (1.37 M, 0.48 mmol) of PEt_3 under N_2 at ambient temperature. The mixture was stirred overnight. The solvent was removed. The residue was chromatographed on grade II Al_2O_3 and eluted with CH_2Cl_2/hexane (1:6) to afford three fractions. Trace amounts of products were obtained from the first band and the second band. They were not identified. After the solvent was removed, the red solid **6e** was obtained from the third band. Yield: 0.167 g (69%). Anal. Calcd for $C_{28}H_{30}FeO_5P_2W$: C, 44.95; H, 4.04. Found: C, 44.75; H, 4.04. MS (FAB): M^+ *m/z* 748.

Reaction of 5 with PR_3 (R = Ph, OMe, Me) and PPh_2H. To a yellow solution containing 250 mg (0.36 mmol) of **5** in 20 mL of THF was added 100 μL (0.84 mmol) of $P(OMe)_3$. The solution was stirred in the dark at reflux temperature overnight. No color change was observed. Results of the ^{31}P NMR study of the reaction mixture indicated the existence of the unreacted **5** and $P(OMe)_3$ and small amounts of unidentified impurities.

Similar reaction conditions were applied to the reaction between **5** and PPh_3 (reflux for 18 h), PMe_3 (ambient temperature overnight), and PPh_2H (reflux for 33 h). No complex **6** was observed in the reaction product according to ^{31}P NMR spectra of the reaction mixtures.

Reaction between 4 and CO. A solution of **4** (0.20 g, 0.30 mmol) in 25 mL of THF in a 100 mL Schlenk flask was stirred under 1 atm of CO overnight at room temperature. A ^{31}P NMR study of the solution indicated that no reaction took place between **4** and CO.

Preparation of ^{13}CO-Enriched 4. A solution of **4** (0.60 g, 0.91 mmol) in 12 mL of THF in a 50 mL Pyrex Schlenk flask was irradiated with UV light under 1 atm of ^{13}CO for 2 h. Only **4** was observed in the ^{31}P NMR spectrum of the solution.

Structure Determination of 4, 5, and 6c. Crystals of complexes **4**, **5**, and **6c** were grown by slow diffusion of hexanes into the saturated solutions of the relevant complexes in CH_2Cl_2 at −15 °C. Suitable single crystals were chosen for indexing on an Enraf-Nonius CAD4 diffractometer with graphite-monochromated Mo Kα radiation (λ = 0.710 69 Å). The unit cell parameters and orientation matrix were established from a least-squares fit of 25 reflections. Intensity data were collected in the $\omega-2\theta$ scanning mode with three standard reflections monitored for intensity variation throughout the experiment. No significant variation in standards was observed, and crystal absorption was empirically corrected for using φ-scan through 360° for selected reflections with χ near 90°. For complexes **4** and **6c**, their structures were solved by direct methods, and E-maps from the starting set with the highest combined figure of merit revealed coordinates for W and Fe atoms. For **5**, the coordinates of W and Fe were obtained from Patterson syntheses. The remaining non-H atoms were located from the successive difference Fourier map. The hydrogen atoms in **6c** (P−H) were located from its difference Fourier maps as well. The chirality parameter η was refined with a value of 1.05 for **5**, indicating that the crystal was of a single polarity. The final full-matrix least-squares refinement on F converged to give the agreement values R = 0.034, 0.023, and 0.022 for **4**, **5**, and **6c**, respectively. The details of the crystal data and refinements are summarized in Table 2. The final positional parameters are listed in Tables 3 (**4**), 4 (**5**), and 5 (**6c**). Selected interatomic distances and bond angles are given in Tables 6 (**4** and **5**) and 7 (**6c**). All data reduction and refinements were carried out on a MicroVax3600 computer using NRCVAX[9] programs.

Results and Discussion

Synthesis, Spectroscopic Characterization, and Molecular Structures of 4 and 5. Complex **4** was first prepared by the reaction between $Li_2[CpW(CO)_2PPh_2]$ and $Fe(CO)_4Br_2$.[3] We synthesized the W−Fe complexes **4** and **5** by the reaction of $CpW(CO)_3PPh_2$ with $Fe_2(CO)_9$.

Photolysis of **5** with UV produced **4**. Unlike $CpFe(CO)(\mu\text{-}CO)(\mu\text{-}PPh_2)W(CO)_4$ (**2**),[10] **4** did not react with CO to open the metal−metal bond to reproduce **5**. The

(9) Gabe, E. J.; Lepage, Y.; Charland, J.-P.; Lee, F. L.; White, P. S. *J. Appl. Crystallogr.* **1989**, *22*, 384.
(10) Shyu, S.-G.; Lin, P.-J.; Wen, Y.-S. *J. Organomet. Chem.* **1993**, *443*, 115.

Table 2. Crystal and Intensity Collection Data for 4, 5, and 6c

	4	5	6c
mol formula	$C_{23}H_{15}FeO_6PW$	$C_{24}H_{15}FeO_7PW$	$C_{34}H_{26}FeO_5P_2$
mol wt	658.03	686.04	816.22
space group	$P2_1/c$	$Pca2_1$	$P2_1/n$
a (Å)	10.5270(11)	16.613(4)	13.909(2)
b (Å)	12.3458(12)	9.0392(10)	10.888(2)
c (Å)	17.544(3)	15.910(4)	19.973(3)
β (deg)	99.080(10)	90	92.598(11)
V (Å^3)	2251.6(5)	2389.2(9)	3021.6(9)
ϱ(calcd) (Mg m^{-3})	1.941	1.907	1.794
Z	4	4	4
cryst dimens (mm)	0.06 × 0.05 × 0.15	0.15 × 0.25 × 0.15	0.12 × 0.31 × 0.26
abs coeff μ(Mo Kα) (mm^{-1})	5.89	5.70	4.51
temp	room temp	room temp	room temp
radiation λ(Mo Kα) (Å)	0.710 69	0.710 69	0.710 69
2θ range (deg)	45	45	45
scan type	ω–2θ	ω–2θ	ω–2θ
no. of unique rflns	2940	1634	3938
no. of obsd rflns	1774 (>2.0$\sigma(I)$)	1368 (>2.0$\sigma(I)$)	3173 (>2.5$\sigma(I)$)
variables	290	308	308
R	0.034	0.023	0.022
R_w	0.031	0.022	0.023
S	1.13	1.21	1.27
ΔF (e/Å^3)	<0.586	<0.750	<0.380
$(\Delta/\sigma)_{max}$	0.000	0.007	0.003

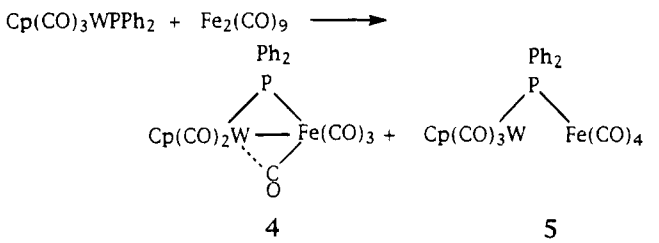

4 5

metallophosphine $CpW(CO)_3PPh_2$ reacting with $Fe(CO)_4$ from $Fe_2(CO)_9$ should produce **5**. The small amount of **4** obtained from the reaction might be due to the photolysis of **5** by laboratory fluorescence light during the reaction and the chromatography.

The absorption at 1736 cm^{-1} in the IR of **4** indicates the presence of a bridging or semibridging carbonyl ligand. The $^{31}P\{^1H\}$ NMR spectrum of **4** in THF at room temperature shows a resonance at 93.27 ppm with J_{P-W} = 257.6 Hz. This relatively downfield resonance reveals the existence of a metal–metal bond in the complex.[11] In contrast, the relatively upfield resonance at −10.41 ppm with J_{P-W} = 130.8 Hz in the $^{31}P\{^1H\}$ NMR of **5** indicates the opening of the W–P–Fe triangle in the complex.[11]

Complexes **4** and **5** were further characterized by single-crystal X-ray diffraction studies. Structures of them are shown in Figures 1 and 2.

In **5**, a W–Fe distance of 4.2434(20) Å indicates that there is no metal–metal bond between the metals. One can consider that the metallophosphine $CpW(CO)_3PPh_2$ is a ligand similar to PR_3. Thus, four CO groups and one $CpW(CO)_3PPh_2$ coordinate to the Fe^0 atom to form a distorted trigonal bipyramid.

In **4**, the Fe–C(6)–O(6) angle 141.1(12)° indicates a semibridging carbonyl.[12] We define δ_{A-B} as being $d_{AB} - (r_A + r_B)$, in which r is the covalent radius of the element and d_{AB} is the distance between the two elements (A and B).[13] δ_{Fe-C} (0.00 Å) is smaller than δ_{W-C} (0.16 Å), indicating primary coordination of the semibridging carbonyl ligand to Fe. Note that for Cp_2-

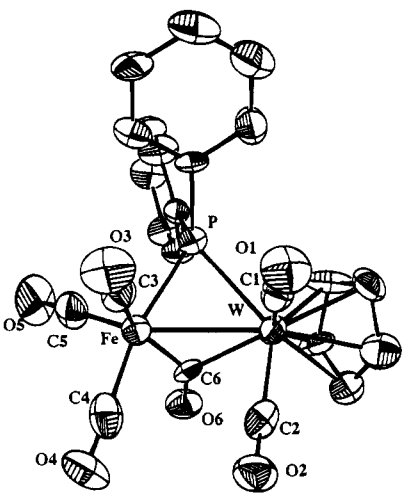

Figure 1. ORTEP drawing of **4**. Hydrogen atoms are omitted.

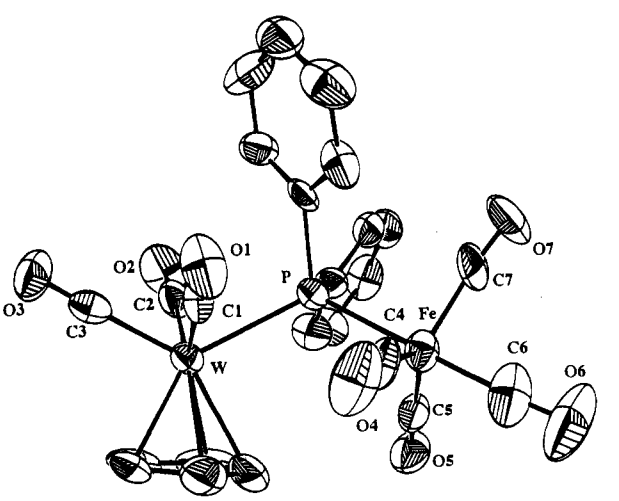

Figure 2. ORTEP drawing of **5**. Hydrogen atoms are omitted.

(11) (a) Carty, A. J.; Maclaughlin, S. A.; Nucciarone, D. In *Phosphorus-31 NMR Spectroscopy in Stereochemical Analysis. Organic Compounds and Metal Complexes*; Verkade, J. G., Quin, L. P., Eds.; VCH: New York, 1987; Chapter 16, and references cited therein. (b) Carty, A. J. *Adv. Chem. Ser.* **1982**, *No. 196*, 163. (c) Garrou, P. E. *Chem. Rev.* **1981**, *81*, 229.

(12) (a) Cotton, F. A. *Prog. Inorg. Chem.* **1976**, 21. (b) Lavin, M.; Crabtree, R. H. *Inorg. Chem.* **1986**, *25*, 805.

Table 3. Atomic Coordinates and Isotropic Thermal Parameters (Å²) for 4

atom	x	y	z	B_{iso}[a]
W	0.78860(6)	0.86609(5)	0.14682(4)	2.82(3)
Fe	0.77621(20)	0.72902(17)	0.1650(12)	3.00(10)
P	0.6630(4)	0.7023(3)	0.11310(22)	2.77(18)
O(1)	0.9915(12)	0.7013(10)	0.2281(7)	6.0(7)
O(2)	1.0311(11)	0.9389(11)	0.0749(7)	5.6(7)
O(3)	0.9557(11)	0.5504(10)	0.0703(7)	5.9(7)
O(4)	0.9423(13)	0.8044(12)	−0.0917(7)	6.4(8)
O(5)	0.5659(12)	0.6621(12)	−0.1005(7)	7.4(8)
O(6)	0.6598(10)	0.9428(8)	−0.0185(6)	4.2(5)
C(1)	0.9160(15)	0.7584(14)	0.1959(9)	3.8(8)
C(2)	0.9433(15)	0.9123(13)	0.1003(9)	3.6(8)
C(3)	0.8847(15)	0.6183(13)	0.0491(9)	3.6(8)
C(4)	0.8795(17)	0.7768(14)	−0.0501(9)	4.5(9)
C(5)	0.6485(16)	0.6851(14)	−0.0547(9)	4.3(8)
C(6)	0.7097(15)	0.8737(14)	0.0215(8)	3.5(8)
C(11)	0.8306(20)	0.9931(15)	0.2412(10)	5.4(10)
C(12)	0.7704(21)	1.0461(14)	0.1746(11)	5.1(11)
C(13)	0.6423(21)	1.0063(16)	0.1582(10)	5.4(11)
C(14)	0.6319(19)	0.9263(16)	0.2140(13)	5.7(11)
C(15)	0.7459(22)	0.9196(14)	0.2651(9)	4.8(10)
C(21)	0.4882(12)	0.7067(12)	0.0902(7)	2.5(6)
C(22)	0.4137(15)	0.6211(14)	0.1056(9)	4.2(8)
C(23)	0.2805(15)	0.6228(15)	0.0847(10)	5.0(9)
C(24)	0.2200(14)	0.7089(14)	0.0473(9)	4.2(8)
C(25)	0.2913(15)	0.7955(13)	0.0306(9)	4.1(8)
C(26)	0.4228(15)	0.7953(12)	0.0512(9)	3.6(8)
C(31)	0.6920(12)	0.5794(11)	0.1712(8)	2.2(6)
C(32)	0.7011(16)	0.5845(13)	0.2507(9)	4.1(9)
C(33)	0.7211(17)	0.4923(18)	0.2946(10)	5.0(10)
C(34)	0.7340(17)	0.3939(16)	0.2628(11)	5.1(10)
C(35)	0.7260(16)	0.3875(12)	0.1832(10)	4.3(8)
C(36)	0.7068(15)	0.4783(13)	0.1382(8)	3.7(8)

[a] $B_{iso} = {}^8/_3\pi^2\sum_{i,j}U_{ij}a_ia_ja^*_ia^*_j$.

Table 4. Atomic Coordinates and Isotropic Thermal Parameters(Å²) for 5

atom	x	y	z	B_{iso}[a]
W	0.01824(3)	0.14324(5)	0.00000	2.86(3)
Fe	−0.11530(12)	0.52355(20)	0.07072(19)	3.68(10)
P	−0.03993(21)	0.3206(4)	0.1148(3)	2.88(15)
O(1)	0.1445(5)	0.4009(9)	0.0026(13)	6.0(6)
O(2)	0.0123(7)	−0.0679(11)	0.1549(7)	6.6(6)
O(3)	0.1836(6)	−0.0223(10)	0.0104(12)	5.8(6)
O(4)	0.0050(7)	0.5991(12)	−0.0559(8)	7.6(7)
O(5)	−0.2531(6)	0.3310(10)	0.0359(7)	5.7(6)
O(6)	−0.2046(7)	0.7817(12)	0.0186(16)	10.6(12)
O(7)	−0.1166(10)	0.6462(14)	0.2409(9)	7.2(8)
C(1)	0.0984(7)	0.3070(13)	0.0045(16)	4.0(8)
C(2)	0.0129(11)	0.0136(21)	0.1010(11)	4.2(9)
C(3)	0.1223(8)	0.0406(13)	0.0057(13)	3.7(7)
C(4)	−0.0420(7)	0.5648(13)	−0.0007(19)	4.7(9)
C(5)	−0.1981(8)	0.4042(14)	0.0521(9)	4.1(7)
C(6)	−0.1711(9)	0.6779(17)	0.0386(12)	6.5(11)
C(7)	−0.1130(11)	0.5955(15)	0.1774(12)	5.1(9)
C(11)	0.0137(10)	0.0905(21)	−0.1406(9)	4.8(9)
C(12)	−0.0305(16)	−0.0169(21)	−0.1001(13)	6.2(12)
C(13)	−0.0972(10)	0.058(3)	−0.0641(10)	6.2(10)
C(14)	−0.0917(11)	0.2018(22)	−0.0877(10)	5.8(10)
C(15)	−0.0249(12)	0.2209(18)	−0.1338(10)	5.4(9)
C(21)	0.0466(7)	0.3784(14)	0.1816(8)	3.1(6)
C(22)	0.0722(8)	0.5203(15)	0.1781(9)	4.4(7)
C(23)	0.1449(11)	0.5591(21)	0.2227(12)	5.9(9)
C(24)	0.1816(9)	0.4577(23)	0.2742(12)	6.2(10)
C(25)	0.1487(11)	0.316(3)	0.2830(14)	6.1(10)
C(26)	0.0838(9)	0.2768(17)	0.2343(9)	4.1(7)
C(31)	−0.1059(7)	0.2252(15)	0.1912(8)	3.3(6)
C(32)	−0.1561(8)	0.1125(16)	0.1657(9)	4.7(7)
C(33)	−0.2103(9)	0.0504(16)	0.2183(10)	4.7(8)
C(34)	−0.2173(10)	0.1005(17)	0.2988(11)	5.1(8)
C(35)	−0.1675(10)	0.2116(18)	0.3269(9)	5.0(8)
C(36)	−0.1117(9)	0.2736(15)	0.2719(9)	3.9(7)

[a] $B_{iso} = {}^8/_3\pi^2\sum_{i,j}U_{ij}a_ia_ja^*_ia^*_j$.

$Nb(\mu\text{-}CO)(\mu\text{-}PPh_2)Fe(CO)_3$ (**7**)[13] the semibridging carbonyl ligand is coordinated in a primary fashion to Nb instead of Fe. The W−Fe distance (2.8308(22) Å) in **4** indicates the presence of a metal−metal bond. It is similar to the Fe−W distance (2.851(4) Å) in **2**, which also has a semibridging carbonyl ligand.[15]

Unlike the case for **2** and **7**, the bridging CO, the phosphido ligand, and the two metals in **4** are not coplanar.[14,15] Instead, **4** has a butterfly structure with a dihedral angle of 71.2(6)° between the two planes of the butterfly core (P−W−Fe−C(6)). Another interesting feature is that, for its Mo analogue $CpMo(CO)_2(\mu\text{-}PPh_2)Fe(CO)_4$, there is no bridging or semibridging carbonyl ligand in spite of the fact that the radii of Mo and W are similar.[16]

Variable-Temperature ^{13}C NMR and Fluxional Behavior of $CpW(CO)_2(\mu\text{-}CO)(\mu\text{-}PPh_2)Fe(CO)_3$. An unsymmetrical broad hump at 219 ppm was observed in the $^{13}C\{^1H\}$ NMR of **4** at room temperature, indicating a possible exchange of metal carbonyl ligands. In order to understand this fluxional behavior, variable-temperature ^{13}C NMR spectra of ^{13}CO-enriched **4** was taken (Figure 3).

At 190 K, the two CO signals C1,2 (δ 227.50, $^2J_{C-P}$ = 12.8 Hz, J_{C-W} = 154.71 Hz) and C2,1 (δ 218.12, J_{C-W} = 149.70 Hz) are assigned to CO ligands coordinated to W on the basis of the observation of their tungsten satellites (Figure 3A). The signal C6 (243.50 ppm, $^2J_{C-P}$ = 27.7 Hz) belongs to the semibridging carbonyl because the bridging carbonyl has a relatively downfield resonance position in ^{13}C NMR in comparison with that of the corresponding terminal carbonyls. The signal of the semibridging carbonyl ligand which is coordinated in a primary fashion to W in **2** has observable J_{W-P} satellites.[15] The absence of J_{W-P} satellites for the signal of C6 further indicates primary coordination of the semibridging carbonyl to Fe. The remaining signals (C3, C4, C5) are assigned to the other CO ligands on Fe.

We interpret the ^{13}C NMR observations as follows. Below 190 K, all carbonyls are rigid and no intramolecular exchange among carbonyl ligands occurs. At 210 K, exchange among the three iron carbonyl ligands and the semibridging CO takes place, as indicated by the broadening of their NMR signals (C3, C4, C5, C6). At 230 K, a coalescence point of the C3, C4, and C5 signals and broadening of the C6 and C1,2 signals are observed. These observations indicate two interesting phenomena. First, the exchange of the three Fe carbonyl ligands (C3, C4, and C5) is more rapid than the exchange of these ligands with the C6 carbonyl. Second, in addition to the exchange process between C6 and C3,4,5, the tungsten carbonyl C1,2 is involved in the exchange process. At 250 and 270 K, signals of C6, C1,2, and C3,4,5 were all broadened. At 298 and 320 K, broadening of the C2,1 signal indicates that the second tungsten carbonyl exchanges with the other carbonyl ligands in

(13) r_C = 0.77 Å, r_{Fe} = 1.16 Å, r_W = 1.30 Å: Emsley, J. *The Elements*; Oxford University Press: New York, 1989.

(14) Oudet, P.; Kubicki, M. M.; Moise, C. *Organometallics* **1994**, *13*, 4278.

(15) Shyu, S.-G.; Lin, P.-J.; Dong, T.-Y.; Wen, Y.-S. *J. Organomet. Chem.* **1993**, *460*, 229.

(16) Linder, E.; Stangle, M.; Hiller, W.; Fawzi, R. *Chem. Ber.* **1988**, *121*, 1421.

Table 5. Atomic Coordinates and Isotropic Thermal Parameters (Å²) for 6c

atom	x	y	z	B_{iso}[a]
W	0.04850(1)	0.93176(2)	0.21149(1)	2.08(1)
Fe	0.06008(5)	1.20016(7)	0.19011(3)	2.16(3)
P(1)	−0.05089(9)	1.09762(12)	0.24647(7)	2.15(5)
P(2)	0.19106(10)	1.23512(13)	0.13134(7)	2.47(6)
O(1)	−0.0531(3)	1.1453(4)	0.0668(2)	4.0(2)
O(2)	−0.0060(3)	1.4520(4)	0.1991(3)	5.9(3)
O(3)	0.1883(3)	1.2204(4)	0.3111(2)	4.4(2)
O(4)	0.0399(3)	0.8357(4)	0.3569(2)	4.1(2)
O(5)	0.2633(3)	0.9783(4)	0.2545(2)	4.0(2)
C(1)	−0.0072(4)	1.1624(5)	0.1151(3)	2.8(2)
C(2)	0.0201(4)	1.3537(5)	0.1952(3)	3.3(3)
C(3)	0.1383(4)	1.2088(5)	0.2649(3)	3.0(3)
C(4)	0.0431(4)	0.8763(5)	0.3027(3)	2.7(2)
C(5)	0.1825(4)	0.9653(5)	0.2391(3)	2.6(2)
C(6)	0.0987(4)	0.8087(6)	0.1234(3)	4.0(3)
C(7)	0.0262(4)	0.8820(5)	0.0957(3)	3.5(3)
C(8)	−0.0598(4)	0.8569(6)	0.1279(3)	3.4(3)
C(9)	−0.0398(5)	0.7636(6)	0.1753(3)	4.1(3)
C(10)	0.0597(5)	0.7336(5)	0.1715(3)	4.1(3)
C(11)	−0.0686(4)	1.1397(5)	0.3344(2)	2.5(2)
C(12)	−0.1549(4)	1.1912(6)	0.3537(3)	4.0(3)
C(13)	−0.1663(5)	1.2226(7)	0.4204(3)	5.5(4)
C(14)	−0.0947(5)	1.2013(7)	0.4674(3)	4.8(3)
C(15)	−0.0102(4)	1.1486(6)	0.4495(3)	3.8(3)
C(16)	0.0030(4)	1.1182(5)	0.3836(3)	3.0(3)
C(21)	−0.1747(3)	1.1118(5)	0.2104(2)	2.3(2)
C(22)	−0.2364(4)	1.0121(6)	0.2126(3)	3.5(3)
C(23)	−0.3303(4)	1.0206(6)	0.1873(3)	4.2(3)
C(24)	−0.3641(4)	1.1297(7)	0.1599(3)	4.3(3)
C(25)	−0.3043(4)	1.2286(6)	0.1578(3)	3.9(3)
C(26)	−0.2097(4)	1.2203(5)	0.1833(3)	3.2(3)
C(31)	0.1810(4)	1.3588(5)	0.0702(3)	2.8(2)
C(32)	0.2383(4)	1.4612(5)	0.0780(3)	4.0(3)
C(33)	0.2297(5)	1.5579(6)	0.0330(4)	5.0(3)
C(34)	0.1658(5)	1.5525(7)	−0.0212(4)	5.3(4)
C(35)	0.1080(5)	1.4501(7)	−0.0296(3)	5.0(4)
C(36)	0.1150(4)	1.3558(6)	0.0156(3)	3.9(3)
C(41)	0.2516(4)	1.1116(5)	0.0886(3)	2.4(2)
C(42)	0.3394(4)	1.0673(6)	0.1156(3)	3.7(3)
C(43)	0.3879(4)	0.9724(6)	0.0843(4)	4.7(3)
C(44)	0.3484(5)	0.9236(6)	0.0256(3)	4.8(3)
C(45)	0.2617(4)	0.9650(6)	−0.0012(3)	4.1(3)
C(46)	0.21134(4)	1.0580(6)	0.0304(3)	3.5(3)
H	0.270	1.267	0.166	4.2(13)

[a] $B_{iso} = {}^8/_3\pi^2\sum_{ij}U_{ij}a_ia_ja^*_ia^*_j$.

the complex. The coalescence point is obtained at 350 K when d_8-toluene is used as the solvent (Figure 3B).

In **2** and other monophosphido-bridged heterobimetallic complexes $CpW(CO)_2(\mu\text{-}PPh_2)M(CO)_5$ (M = Cr, Mo, W)[1a,10,15,17] with metal–metal bonds and semibridging carbonyl ligands, exchange of CO ligands was only observed among the semibridging carbonyl and the other three M (M = Mo, W) carbonyl ligands which are cis to the phosphido bridge. No exchange of carbonyl ligands between the two metals was observed. The exchange of carbonyl ligands between the two metals in **4** may be due to the more bridging-like carbonyl ligand which serves as an exchange path.[18] In **2** and other complexes with semibridging carbonyls, the interactions between the semibridging carbonyl ligands and the metal in the CpM (M = Fe, W) moiety are not so strong, as indicated by their structures, such that semibridging carbonyl ligands in these complexes cannot serve as an exchange path at ambient temperatures.

(17) Shyu, S.-G.; Hsu, J.-Y; Wen, Y.-S. *J. Organomet. Chem.* **1993**, *453*, 97.

(18) (a) Gansow, O. A.; Burke, A. R.; Vernon, W. D. *J. Am. Chem. Soc.* **1972**, *94*, 2550. (b) Gansow, O. A.; Burke, A. R.; Vernon, W. D. *J. Am. Chem. Soc.* **1976**, *98*, 5817.

Table 6. Selected Bond Lengths (Å) and Bond Angles (deg) in Complexes 4 and 5

complex **4**		complex **5**	
	Bond Lengths		
W–Fe	2.8308(22)	W···Fe	4.2434(20)
Fe–P	2.245(4)	Fe–P	2.329(4)
Fe–C(3)	1.815(17)	Fe–C(4)	1.707(22)
Fe–C(4)	1.815(20)	Fe–C(5)	1.773(14)
Fe–C(5)	1.770(17)	Fe–C(6)	1.752(17)
Fe–C(6)	1.925(18)	Fe–C(7)	1.818(18)
W–P	2.437(4)	W–P	2.615(4)
W–C(1)	1.986(17)	W–C(1)	1.993(13)
W–C(2)	2.016(18)	W–C(2)	1.991(18)
W–C(6)	2.226(14)	W–C(3)	1.964(14)
C(1)–O(1)	1.142(21)	C(1)–O(1)	1.143(15)
C(2)–O(2)	1.136(21)	C(2)–O(2)	1.130(21)
C(3)–O(3)	1.146(21)	C(3)–O(3)	1.168(16)
C(4)–O(4)	1.113(23)	C(4)–O(4)	1.22(3)
C(5)–O(5)	1.123(21)	C(5)–O(5)	1.157(18)
C(6)–O(6)	1.175(20)	C(7)–O(7)	1.136(20)
	Bond Angles		
W–P–Fe	74.27(13)	W–P–Fe	118.13(20)
P–Fe–C(3)	92.0(5)	P–Fe–C(4)	89.4(4)
P–Fe–C(4)	167.7(5)	P–Fe–C(5)	89.3(4)
P–Fe–C(5)	93.1(5)	P–Fe–C(6)	179.2(6)
P–Fe–C(6)	82.1(4)	P–Fe–C(7)	89.4(5)
P–W–C(1)	81.5(5)	P–W–C(1)	76.5(6)
P–W–C(2)	125.3(5)	P–W–C(2)	77.3(5)
P–W–C(6)	72.0(4)	P–W–C(3)	125.6(6)
Fe–C(3)–O(3)	178.2(14)	Fe–C(4)–O(4)	174.4(16)
Fe–C(4)–O(4)	178.7(16)	Fe–C(5)–O(5)	176.1(13)
Fe–C(5)–O(5)	176.8(17)	Fe–C(6)–O(6)	177.0(14)
Fe–C(6)–O(6)	141.1(12)	Fe–C(7)–O(7)	174.4(16)
W–C(1)–O(1)	175.3(14)	W–C(1)–O(1)	176.5(23)
W–C(2)–O(2)	179.2(13)	W–C(2)–O(2)	175.0(15)
W–C(6)–O(6)	133.0(12)	W–C(3)–O(3)	178.6(15)

Table 7. Selected Bond Lengths (Å) and Bond Angles (deg) in Complex 6c

	Bond Lengths		
W–Fe	2.9588(10)	W–C(4)	1.923(6)
Fe–P(1)	2.2479(15)	W–C(5)	1.953(6)
Fe–P(2)	2.2440(15)	C(1)–O(1)	1.148(7)
Fe–C(1)	1.779(6)	C(2)–O(2)	1.133(7)
Fe–C(2)	1.767(6)	C(3)–O(3)	1.137(7)
Fe–C(3)	1.810(6)	C(4)–O(4)	1.172(7)
W–P(1)	2.3975(14)	C(5)–O(5)	1.161(7)
	Bond Angles		
W–P(1)–Fe	79.06(5)	P(1)–W–C(5)	109.41(15)
P(1)–Fe–P(2)	159.77(6)	Fe–C(1)–O(1)	175.7(5)
P(1)–Fe–C(1)	87.72(17)	Fe–C(2)–O(2)	179.4(5)
P(1)–Fe–C(2)	102.45(18)	Fe–C(3)–O(3)	176.5(5)
P(1)–Fe–C(3)	90.75(17)	W–C(4)–O(4)	176.1(5)
P(1)–W–C(4)	84.98(16)	W–C(5)–O(5)	176.1(4)

Substitution Reaction between 4 and Lewis Bases L (L = $P(OMe)_3$, PMe_3, PPh_2H, PPh_3, PEt_3) and the Structure of 6c. Reaction of **4** with Lewis bases L (L = PMe_3, $P(OMe)_3$, PPh_2H, PPh_3, PEt_3) in THF at ambient temperatures yielded **6** with L regiospecifically coordinating to Fe. A downfield position of the phosphido-bridge phosphorus signal and the absence of J_{P-W} for the M–PR_3 signal in the ^{31}P NMR of **6** indicate the presence of a metal–metal bond and the coordination of L to Fe. The structure of **6c** was determined by a single-crystal X-ray diffraction study. Its structure is shown in Figure 4.

The W–Fe distance is 2.9588(10) Å, indicative of an Fe–W bond. It is 0.13 Å longer than the W–Fe bond (2.8308(22) Å) in **4**.[15] The long W–Fe bond in **6** may be due to the large steric repulsion between the Fe–PR_3 fragment and the CpW moiety. Interestingly, no bridging or semibridging carbonyl is observed in the

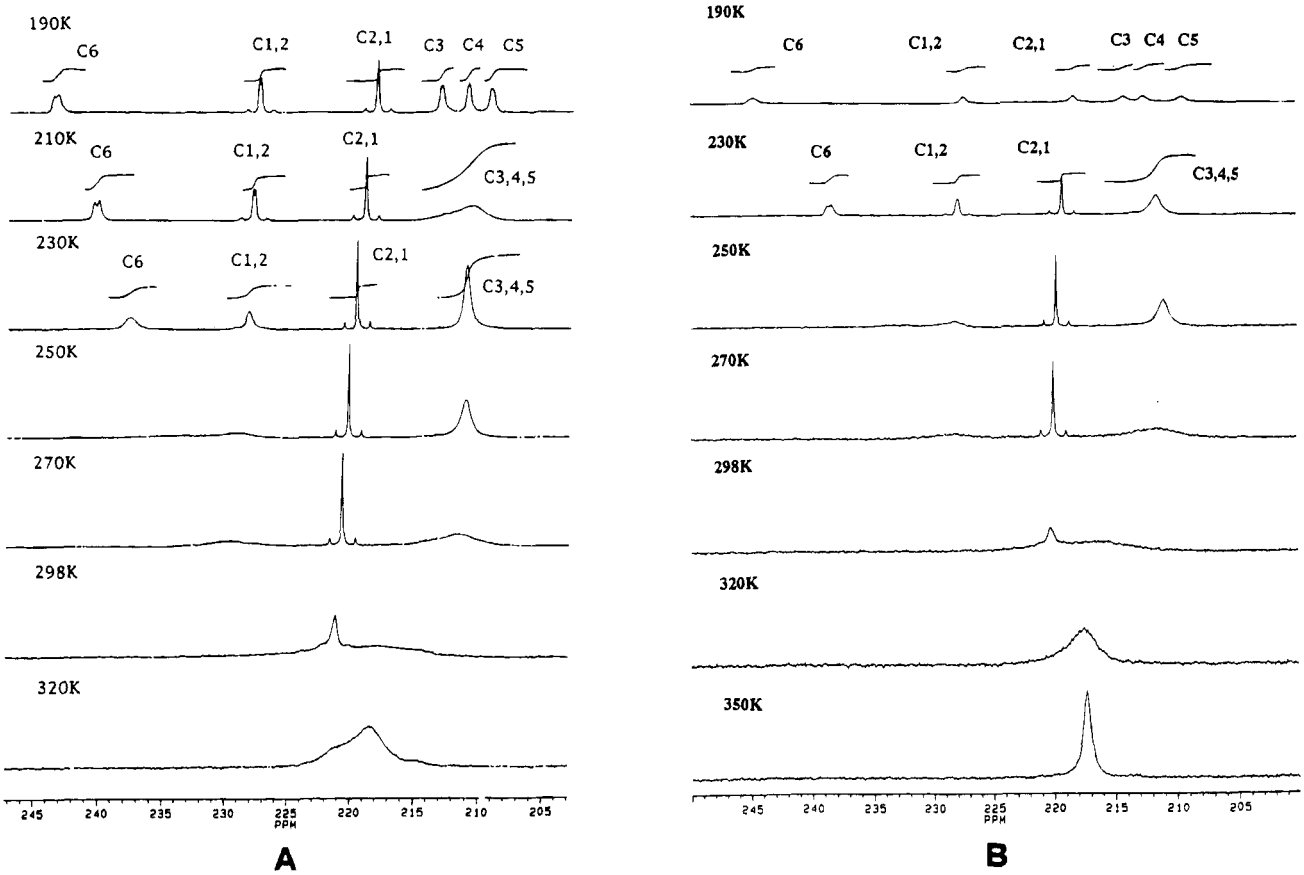

Figure 3. Variable-temperature $^{13}C\{^1H\}$ NMR spectra of **4** in CD_2Cl_2 (A) and in d_8-toluene (B). Only the carbonyl region is shown.

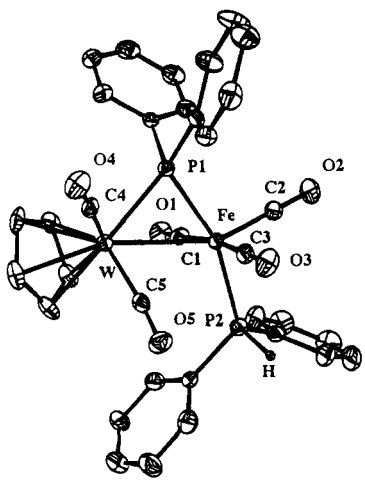

Figure 4. ORTEP drawing of **6c**. Except for the H on the PPh_2H ligand, hydrogen atoms are omitted.

complex. This is understandable since the interaction between W and the Fe carbonyl ligand is reduced because of the long distance between W and Fe in the complex.

Formation of **6** from the reaction between **4** and L may proceed through two possible paths. One is the direct substitution of one CO on Fe. The other possibility is that the addition product **8** is formed as an intermediate and loses a CO to produce **6** under the reaction conditions.[1a,2,19] However, when the reaction was followed by ^{31}P NMR spectroscopy, no intermediate was observed; the lifetime of the intermediate could be very short, resulting in the isolation of **6** as the only product.

Role of the Adjacent Metal. The labilization of CO on Ru by the adjacent metal through the metal–metal bond has been proposed in the $(CO)_4Ru(\mu\text{-}PPh_2)Co(CO)_3$ system,[1c] and the enhancement of substitution of group VI transition metal carbonyls in heterobimetallic phosphido complexes has been observed.[1a,b,2] For **5**, carbonyl ligands on Fe were inert toward L when a THF solution of **5** and L (L = $P(OMe)_3$, PPh_2H, PPh_3) was heated under reflux overnight. Complexes **4** and **5** have similar frameworks, except that **4** has a metal–metal bond and **5** does not. These observations clearly indicate that CO ligands on Fe in **4** were labilized by the metal–metal bond.

The Fe CO's in **4** are probably activated by the electron donation from Fe to its adjacent W through the metal–metal bond. This may result in a decrease in d–π^* transfer of the Fe CO's, which induces weakening of the Fe–CO bond in **4**. A similar electron density transfer from one metal to its adjacent metal through the metal–metal bond was proposed for $CpW(CO)_2(\mu\text{-}PPh_2)M(CO)_5$ (M = Mo, W),[1a,b] **2**,[2] and **7**.[14]

The electron-rich W may also labilize the Fe–CO group through the donation of an electron to the π^* orbital of the adjacent Fe–CO to form the semibridging carbonyl ligand. Theoretically, the higher the interaction between the adjacent metal and the semibridging carbonyl, the easier the carbonyl ligand can be substituted, since intramolecular migration of CO from one

(19) Haines, R. J.; Nolte, C. R. *J. Organomet. Chem.* **1972**, *36*, 163.

metal to the other was observed in reactions of **1** and **2** with phosphines.[1a,2] This is demonstrated by the fact that the tungsten CO is more easily substituted by phosphine in **2** than in **3**.[2] However, even though both complexes **4** and **7** have bridging carbonyl ligands, the carbonyl ligand on Fe in **7** is substituted by phosphine at a much higher temperature (refluxing toluene) than for **4** (room temperature).[14] This indicates that the property of the metal–metal bond should also be considered.

Addition reactions between **2** and Lewis bases L (L = $P(OMe)_3$, PMe_3, PPh_2H, PPh_3) open the metal–metal bond to form $CpFe(CO)_2(\mu\text{-}PPh_2)W(CO)_4L$. However, in similar reactions between **3** and $LCpW(CO)_2(\mu\text{-}PPh_2)W(CO)_4L$, the metal–metal bond remains intact.[2b] Similarly, **7** reacts with PMe_2Ph to produce $Cp_2(CO)Nb(\mu\text{-}PPh_2)Fe(CO)_3(PMe_2Ph)$ which has no metal–metal bond,[14] and **4** reacts with phosphine to produce **6**, which has a metal–metal bond.[1b] Whether a metal–metal bond remains intact after substitution may also depend on the adjacent metal and the metal–metal bond involved.

Conclusions

Heterobimetallic phosphido-bridged complexes without a metal–metal bond (**5**) and with a metal–metal bond (**4**) were synthesized in order to study the influence of the metal–metal bond in the substitution reaction. Structures of both complexes were determined by single-crystal X-ray diffraction methods. Fluxional behavior involving the exchange of CO's between metals was also studied.

Substitution of CO in **4** with Lewis bases L (L = $P(OMe)_3$, PMe_3, PPh_2H, PPh_3, PEt_3) was regiospecific on Fe. The reaction was enhanced by the adjacent W moiety through the metal–metal bond, which is suggested to reduce the electron density on Fe.

Acknowledgment. We are grateful to the National Science Council, Republic of China, and Academia Sinica for financial support of this work.

Supporting Information Available: Figures giving additional views and listings of calculated atomic coordinates, anisotropic thermal parameters, and bond distances and angles for compounds **4**, **5**, and **6c** (31 pages). Ordering information is given on any current masthead page.

OM950298F

Solution-State Interactions of Bis(pentamethylcyclopentadienyl)ytterbium, Cp^*_2Yb, with Trialkylphosphines and R_3PX Complexes (X = O, NR′, CHR″)

David J. Schwartz and Richard A. Andersen*

Chemistry Department and Chemical Sciences Division of Lawrence Berkeley Laboratory, University of California, Berkeley, California 94720

Received April 21, 1995[⊗]

The interactions formed between Cp^*_2Yb (**1**) and phosphines and R_3PX derivatives (X = O, NR′, CHR″) in solution have been investigated using multinuclear (^1H, ^{13}C, ^{31}P, ^{171}Yb) and variable-temperature NMR spectroscopy. Intermolecular exchange can be slowed at low temperature for 1:1 and 1:2 phosphine adducts, with a $^1J_{YbP}$ value of *ca.* 950 Hz for $Cp^*_2Yb(PEt_3)$ (**3**) and $Cp^*_2Yb(PMe_3)$ (**4**) and *ca.* 600 Hz for $Cp^*_2Yb(PMe_3)_2$ (**2**), $Cp^*_2Yb(dmpm)$ (dmpm = $Me_2PCH_2PMe_2$) (**5**), and $Cp^*_2Yb(1,2\text{-}(PMe_2)_2C_6H_4)$ (**6**). Adducts of **1** with Me_3PO and Et_3PNH undergo slow intermolecular exchange in solution at 25 °C (NMR time scale); both 1:1 adducts ($Cp^*_2Yb(OPMe_3)$, **7**; $Cp^*_2Yb(HNPEt_3)$, **9**) and 1:2 adducts ($Cp^*_2Yb(OPMe_3)_2$, **8**; $Cp^*_2Yb(HNPEt_3)_2$, **10**) have been isolated. The spectroscopic properties of two ylide adducts, $Cp^*_2Yb(Me_2PhPCHSiMe_3)$ (**12**) and $Cp^*_2Yb(Me_2PhPCH_2)$ (**13**), have also been investigated. Intermolecular exchange can be slowed at low temperature in both cases; in the former complex a second process, resulting in inequivalent Cp* rings and inequivalent P-bound methyl groups, can also be slowed at lower temperatures. The nature of this process is discussed in detail. The solid-state structure of **12** has been determined. The NMR values for all of the complexes are discussed in detail. In addition, the ^{171}Yb chemical shifts for **6**, **7**, and **12** have been measured, *via* $^1H/^{171}Yb$ indirect detection utilizing long-range J_{YbH} coupling, and are discussed.

Introduction

Weak interactions in solution between organometallic complexes and organic substrates have been implicated in a variety of important reactions, including C–H bond activation[1] and the Ziegler–Natta polymerization of olefins.[2] Consequently, a thorough understanding of the electronic and geometric consequences of such interactions is desirable.

The lanthanide metallocene Cp^*_2Yb (**1**) possesses several properties that make it amenable to the investigation of weak metal–ligand interactions in solution: it is bent,[3] thus requiring little reorganization energy upon binding of a third ligand; it is diamagnetic ($4f^{14}$ electronic configuration) and possesses an NMR-active metal isotope (^{171}Yb: $I = {}^1/_2$, 14.3%), allowing the use of NMR spectroscopy as an investigative tool; and the Yb center is Lewis-acidic. Several adducts of **1** (or related derivatives) with nonclassical Lewis bases have been isolated and characterized in the solid state; several of these adducts are shown in Figure 1.[4,5] All of the previously-reported $Cp^*_2YbL_n$ adducts were found to undergo fast intermolecular exchange in solution at all temperatures, on the NMR time scale, precluding a detailed study of the solution-state perturbations that result from the weak interactions present.

Given the favorable properties of **1** for such investigations, and the relative paucity of such studies (especially for the lanthanides and actinides, a result of the paramagnetism of almost all Ln/An complexes[6]), we felt such a study would be worthwhile and have recently undertaken an investigation of slow-exchange $Cp^*_2YbL_n$ systems. We have recently reported the details of the solution-state interactions formed between **1** and *cis*-P_2PtX_2 complexes (X = H, Me);[7] these adducts undergo slow intermolecular exchange in solution, and spin–spin coupling between the ^{171}Yb isotope and the ^1H, ^{13}C, ^{31}P, and ^{195}Pt nuclei of the P_2PtX_2 ligands is resolved.

Phosphine complexes of the lanthanides and actinides are relatively rare,[8] as a result of the hard nature of these metal centers and the soft nature of phosphines. Almost no solution-state investigations have been re-

* Address correspondence to this author at the Chemistry Department, University of California, Berkeley, CA 94720.

⊗ Abstract published in *Advance ACS Abstracts,* July 15, 1995.

(1) (a) Brookhart, M.; Green, M. L. H.; Wong, L. L. *Prog. Inorg. Chem.* **1988**, *36*, 1. (b) Arndsten, B. A.; Bergman, R. G.; Mobley, T. A.; Peterson, T. H. *Acc. Chem. Res.* **1995**, *28*, 154.

(2) (a) Jordan, R. F. *Adv. Organomet. Chem.* **1991**, *32*, 325. (b) Cossee, P. *J. Catal.* **1964**, *3*, 80. (c) Arlman, E. J.; Cossee, P. *J. Catal.* **1964**, *3*, 99. (d) Leclerc, M. K.; Brintzinger, H. H. *J. Am. Chem. Soc.* **1995**, *117*, 1651.

(3) (a) Andersen, R. A.; Boncella, J. M.; Burns, C. J.; Green, J. C.; Hohl, D.; Rosch, N. *J. Chem. Soc., Chem. Commun.* **1986**, 405. (b) Andersen, R. A.; Boncella, J. M.; Burns, C. J.; Blom, R.; Haaland, A.; Volden, H. V. *J. Organomet. Chem.* **1986**, *312*, C49. (c) Andersen, R. A.; Blom, R.; Boncella, J. M.; Burns, C. J.; Volden, H. V. *Acta Chem. Scand.* **1987**, *A41*, 24. (d) Green, J. C.; Hohl, D.; Rosch, N. *Organometallics* **1987**, *6*, 712.

(4) (a) Burns, C. J.; Andersen, R. A. *J. Am. Chem. Soc.* **1987**, *109*, 941. (b) Burns, C. J.; Andersen, R. A. *J. Am. Chem. Soc.* **1987**, *109*, 5853. (c) Burns, C. J.; Andersen, R. A. *J. Am. Chem. Soc.* **1987**, *109*, 915.

(5) Schumann, H.; Glanz, M.; Winterfeld, J.; Hemling, H.; Kuhn, N.; Kratz, T. *Angew. Chem., Int. Ed. Engl.* **1994**, *33*, 1733.

(6) The paramagnetic shift induced by Cp^*_2Eu has been used to study weak metal–ligand bonding in an indirect way: Nolan, S. P.; Marks, T. J. *J. Am. Chem. Soc.* **1989**, *111*, 8538.

(7) Schwartz, D. J.; Ball, G. E.; Andersen, R. A. *J. Am. Chem. Soc.* **1995**, *117*, 6027.

0276-7333/95/2314-4308$09.00/0

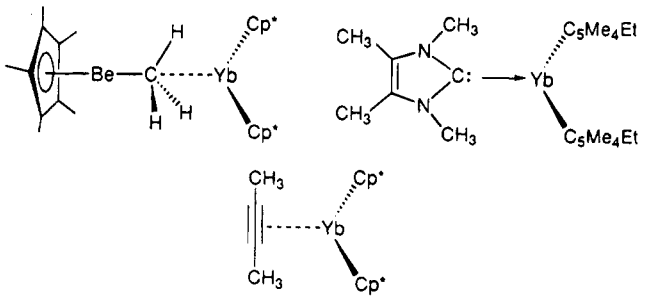

Figure 1. Examples of $Cp^{\ddagger}_2YbL_n$ complexes ($Cp^{\ddagger}$ = a Cp derivative) that have been crystallographically characterized.[4a,b,5]

ported for lanthanide and actinide complexes, in general, and for phosphine derivative complexes, more specifically. Herein, we report the results of an investigation of the solution-state interactions formed between **1** and phosphines, phosphine oxides (R_3PO), phosphine imines (R_3PNR'), and phosphine ylides (R_3PCHR''). The strength and nature of the interactions formed between **1** and phosphines, phosphine oxides and imines, and the isoelectronic (to phosphine oxides and imines) ylides have been found to vary significantly. In addition, a novel intramolecular dynamic process of an ylide adduct of **1** has been elucidated.

Results

Interactions with Phosphines. Addition of 2 equiv of PMe_3 to a dark brown toluene solution of **1** gives a bright green solution, from which green crystals of $Cp^*_2Yb(PMe_3)_2$ (**2**) may be isolated in 88% yield upon cooling to −80 °C. A similar synthetic procedure with 2 equiv of PEt_3 yields dark blue crystals of the 1:1 adduct $Cp^*_2Yb(PEt_3)$ (**3**), presumably a result of the larger size of PEt_3 relative to PMe_3. The ^1H and $^{31}P\{^1H\}$ NMR spectral values of **2** and **3** at 25 °C are very similar to the spectral values for the free compounds, showing that the solution-state interaction between **1** and these phosphines is relatively weak. The phosphine alkyl group protons and the phosphorus nucleus are not coupled to the ^{171}Yb nucleus, indicating fast intermolecular exchange occurs on the NMR time scale for both **2** and **3**.

Cooling a toluene-d_8 sample of the 1:2 PMe_3 adduct **2** to −101 °C results in broadened resonances in both the ^1H and $^{31}P\{^1H\}$ spectra (the values are given in Table 1), suggesting that the intermediate exchange region has been reached. Even though the width at half-height of the $^{31}P\{^1H\}$ resonance (at −49.2 ppm) is 135 Hz, a $^1J_{YbP}$ value of *ca.* 600 Hz is resolved. The $^{31}P\{^1H\}$ spectrum of a sample of **1** with *ca.* 0.8 equiv of PMe_3, at −83 °C, contains a sharp singlet at −45.4 ppm with ^{171}Yb satellites (Figure 2, the area of each satellite is approximately 7% of the area of the major resonance, as expected), presumably arising from the 1:1 adduct

Table 1. Low-Temperature ^1H, ^{31}P NMR Data for Phosphine Adducts of 1 (Toluene-d_8)[a]

sample	temp (°C)	δ(P)	$^1J_{YbP}$	δ(Cp*)[b]	δ(H)
PMe_3	−93	−62.0			0.78
1:2 adduct, **2**	−101	−49.2	600(20)[c]	2.28	0.64
1:1 adduct, **4**[d]	−93	−45.4	956	2.20	0.54
PEt_3	−93	−23.0			1.02 (Me) 1.18 (CH_2)
1:1 adduct, **3**	−103	−3.7	950	2.24	0.51 (Me) 1.15 (CH_2)
1 + xs PEt_3	−103	−16.3[e]	not resolved	2.24	0.80 (Me) 1.16 (CH_2)
dmpm	−65	−57.1			not measd
5	−65	−35.6	580	2.27	not measd
1,2-$(PMe_2)_2C_6H_4$	−20	−52.9			1.18
6[f]	−20	−38.4	656	2.06	1.02

[a] For this and all other tables, chemical shift values are given in ppm and coupling constants are given in Hz. [b] As mentioned in the text, many of the samples were made with a slight excess of **1**, to minimize intermolecular exchange; consequently, a free Cp* resonance at *ca.* 2.00 ppm was also present for these low-temperature samples. [c] For this and all other tables containing NMR data, estimated experimental uncertainties are given in parentheses, for values where the uncertainty is relatively large. [d] Values given were measured from a sample containing 0.8 equiv of PMe_3/1 equiv of **1**; see text. [e] The half-height width of this resonance is *ca.* 900 Hz; see text. [f] In addition, a $^3J_{YbPCH_3}$ of 2.7 Hz was resolved; see text.

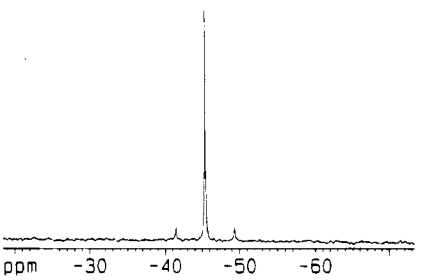

Figure 2. $^{31}P\{^1H\}$ spectrum of **2** at −83 °C, showing $^{171}Yb-^{31}P$ coupling of 956 Hz (121.5 MHz, toluene-d_8).

$Cp^*_2Yb(PMe_3)$ (**4**). The $^{171}Yb-^{31}P$ coupling is 956 Hz, roughly $^2/_3$ larger than the analogous value for the 1:2 PMe_3 adduct **2**. The ^1H spectrum of this sample at −83 °C contains resonances for both free and bound **1** (the spectral values are given in Table 1); coupling of ^{171}Yb to the alkyl protons of the bound phosphine ($^3J_{YbH}$) is not resolved. The slow exchange behavior of this sample at −83 °C, compared to the intermediate exchange observed for **2** at −101 °C, indicates that the barrier for intermolecular exchange is higher for **4** than for **2**; this will be discussed below.

Cooling a toluene-d_8 sample of the 1:1 PEt_3 adduct, **3**, to −103 °C results in slow intermolecular exchange on the NMR time scale; the observed $^1J_{YbP}$ value of 950 Hz is similar to the analogous value observed for the 1:1 PMe_3 derivative, **4**. Again, $^{3,4}J_{YbH}$ is not resolved (the NMR values for this sample are also given in Table 1). The coalescence temperature of the free and bound Cp* resonances is −89 °C.[9] The ^1H and $^{31}P\{^1H\}$ spectra of a sample of **1** and 2 equiv of PEt_3 contain broad resonances at −103 °C (^{31}P resonance, $w_{1/2}$ *ca.* 900 Hz), indicating that the exchange barrier is lower for the 2:1 PEt_3 derivative, relative to the 1:1 adduct, similar to the situation observed for the PMe_3 derivatives, above.

At this point, it was of interest to investigate the behavior of chelating phosphines with **1**. While Cp^*_2-

(8) (a) Hitchcock, P. B.; Holmes, S. A.; Lappert, M. F.; Tian, S. *J. Chem. Soc., Chem. Commun.* **1994**, 2691. (b) Tilley, T. D.; Andersen, R. A.; Zalkin, A. *Inorg. Chem.* **1983**, *22*, 856. (c) Tilley, T. D.; Andersen, R. A.; Zalkin, A. *J. Am. Chem. Soc.* **1982**, *104*, 3725. (d) Brennan, J. G.; Stults, S. D.; Andersen, R. A.; Zalkin, A. *Organometallics* **1988**, *7*, 1329 and references therein. (e) Schlesener, C. J.; Ellis, A. B. *Organometallics* **1983**, *2*, 529. (f) Brennan, J. G.; Andersen, R. A.; Robbins, J. L. *J. Am. Chem. Soc.* **1986**, *108*, 335. (g) Hitchcock, P. B.; Lappert, M. F.; MacKinnon, I. A. *J. Chem. Soc., Chem. Commun.* **1988**, 1557. (h) Fryzuk, M. D.; Haddad, T. S. *J. Chem. Soc., Chem. Commun.* **1990**, 1088.

Yb(dmpm) (**5**) has been reported,[8b] only the exchange-averaged room-temperature NMR data were measured. Cooling a sample of **5** to −65 °C results in slow exchange, with a $^1J_{YbP}$ coupling of 580 Hz (values given in Table 1); this value is unchanged at −90 °C. As found for the monodentate phosphine analogues above, coupling of ^{171}Yb to the phosphine alkyl protons is not resolved. A sample of **5** containing a slight excess of dmpm exhibits intermediate exchange behavior at −65 °C; although two resonances are visible in the $^{31}P\{^1H\}$ spectrum, arising from free dmpm and **5**, both are broad, with widths at half-height of *ca.* 450 Hz. This contrasts with the slow-exchange behavior at this temperature for **5**, in the absence of added dmpm. A similar phenomenon, with a faster exchange rate in the presence of excess phosphine, was found for many of the phosphine adducts and is likely a result of associative exchange in the presence of excess phosphine.[7,10]

The dmpe complex, $Cp^*_2Yb(dmpe)$, is insoluble in toluene and diethyl ether but dissolves in thf to give $Cp^*_2Yb(thf)_2$ and the free phosphine.[8b] This behavior indicates that $Cp^*_2Yb(dmpe)$ likely has a polymeric structure, with dmpe acting as a bridging rather than a chelating ligand. Addition of $Me_2PCH_2P(Me)CH_2PMe_2$ to a toluene solution of **1** results in the instantaneous precipitation of a bright green solid, presumably also with a polymeric structure; the ^{1}H NMR spectrum of this solid dissolved in thf-d_8 indicates the presence of $Cp^*_2Yb(thf)_2$ and the free phosphine, in a 1:1 ratio. A toluene solution of **1** and 1,2-$(PMe_2)_2C_6H_4$, in a *ca.* 2:1 molar ratio, is dark green-brown. The ^{1}H spectrum of this sample at 25 °C contains a broad Cp* resonance ($w_{1/2}$ = 35 Hz at 400 MHz), indicating intermediate intermolecular exchange; however, $^1J_{YbP}$ of 656 Hz is resolved in the $^{31}P\{^1H\}$ spectrum at this temperature (a result of the larger $^1J_{YbP}$ value, relative to the frequency difference between the free and bound Cp* resonances[11]). Cooling this sample results in decoalescence of the Cp* resonance into free and bound resonances, the latter arising from the 1:1 adduct $Cp^*_2Yb(1,2\text{-}(PMe_2)_2C_6H_4)$ (**6**); the $^1J_{YbP}$ value is unchanged upon cooling. We believe that the *cis* disposition of the Me_2P groups in 1,2-$(PMe_2)_2C_6H_4$, in contrast to dmpe and $Me_2PCH_2P(Me)CH_2PMe_2$, enforces bidentate rather than bridging interactions.[12] The ^{1}H and $^{31}P\{^1H\}$ NMR values measured on **6** at −20 °C are given in Table 1. Coupling of the ^{171}Yb nucleus to the methyl protons of the phosphine ligand, $^3J_{YbPCH_3}$, is resolved and is 2.7 Hz (measured at −30 °C).[13] Using this coupling constant, the HMQC pulse sequence[14] was utilized to acquire a

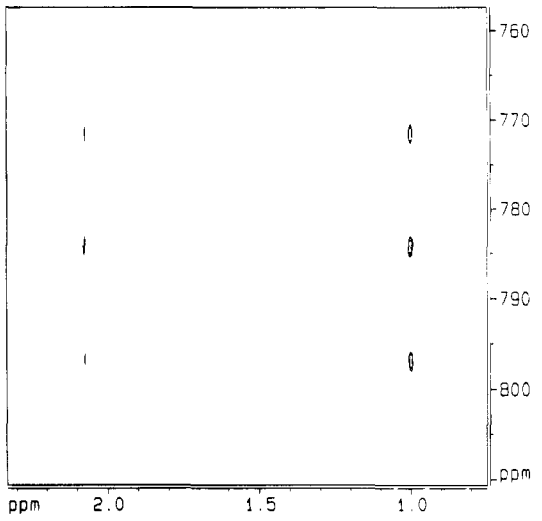

Figure 3. $^1H/^{171}Yb$ HMQC spectrum of **6** (300 MHz, toluene-d_8, −30 °C).

$^1H/^{171}Yb$ spectrum, at −30 °C (Figure 3). The ^{171}Yb (vertical) dimension of this spectrum shows that the ^{171}Yb chemical shift of **6** is +782 ppm (this value will be discussed below); $^{171}Yb-^{31}P$ coupling is resolved and is identical to the value measured from the 1-D $^{31}P\{^1H\}$ spectrum.

From Table 1 it can be seen that a low-field shift of the Cp* resonance of **1**, of *ca.* 0.20 ppm, occurs upon binding of a phosphine ligand. Such low-field shifts of the Cp* resonance are common upon coordination of a ligand to **1**.[7] The ^{1}H chemical shifts of the phosphine alkyl groups move slightly upfield upon coordination to **1**; the shift for the 1:1 adduct **4** ($\Delta(\delta)$ = −0.24 ppm) is roughly twice the shift for the 1:2 adduct, **2** ($\Delta(\delta)$ = −0.14 ppm). While the $-CH_2$ resonance of PEt_3 is shifted upfield by only 0.03 ppm upon coordination to **1**, the methyl resonance is shifted upfield by a surprisingly large 0.51 ppm. This shift may be indicative of a γ-agostic interaction; agostic interactions have been observed in the solid state for adducts of **1**.[4b,7,15] However, the $^1J_{CH_3}$ value of **3** at −103 °C is 127(1) Hz, unchanged from the analogous value for free PEt_3 at this temperature.[16]

The ^{31}P resonances for all of the phosphine complexes discussed above are shifted downfield *ca.* 13−21 ppm, consistent with the phosphines acting as Lewis bases toward the Yb center of **1**. The $^1J_{YbP}$ values for the 1:1 adducts **3** and **4** (956 Hz and 950 Hz, respectively) are roughly 60% larger than the analogous values for the 1:2 PMe_3 adduct **2** and the dmpm and 1,2-$(PMe_2)C_6H_4$ adducts, **5** and **6**, respectively. This indicates that each Yb−P interaction in the 1:2 adducts (considering **5** and **6** as 1:2 adducts, as they each have two P donors/Yb center) is weaker than the single Yb−P interaction in the 1:1 adducts.[17] The similar spectral values for the 1:2 PMe_3 and dmpm adducts, **2** and **5** ($\delta(^{31}P)$ perturba-

(9) All coalescence temperatures given in the text were measured at 300 MHz ^{1}H frequency and were measured on samples containing 1 equiv excess of **1**. These values may be used as a qualitative measure of the kinetic barrier to intermolecular exchange.

(10) The exchange rate is faster for samples containing excess phosphine, relative to samples containing a slight excess of **1**. Consequently, all stopped-exchange NMR values reported in the text were measured on samples containing *ca.* 1 equiv excess of **1**. It has been found that the number of excess equivalents of **1** present has no effect on the exchange rate; i.e., the exchange mechanism in the presence of excess **1** is dissociative.[7]

(11) Bryant, R. G. *J. Chem. Educ.* **1983**, *60*, 933.

(12) The recently-reported $[Yb(CH(SiMe_3)_2)_2(dmpe)]$ complex[8a] is soluble in toluene; only the exchange-averaged room temperature NMR data were reported.

(13) This coupling is likely unresolved for complexes **2**−**4** as a result of the broader resonances present at the low temperatures required to slow intermolecular exchange in these systems.

(14) (a) Bax, A.; Griffey, R. H.; Hawkins, B. L. *J. Magn. Reson.* **1983**, *55*, 301. (b) Bax, A.; Subramanian, S. *J. Magn. Reson.* **1986**, *67*, 565.

(15) The solid-state structure of $Cp^*_2Yb(OEt_2)$ has a γ-CH_3 interaction involving the methyl group of the diethyl ether ligand: Watson, P. L., Personal communication.

(16) Agostic complexes with unchanged $^1J_{CH}$ values are known. See ref 7 and: (a) Neve, F.; Ghedini, M.; Crispini, A. *Organometallics* **1992**, *11*, 3324. (b) Albinati, A.; Pregosin, P. S.; Wombacher, F. *Inorg. Chem.* **1990**, *29*, 1812. (c) Albinati, A.; Anklin, C. G.; Ganazoli, F.; Ruegg, H.; Pregosin, P. S. *Inorg. Chem.* **1987**, *26*, 503.

(17) This assumes that the hybridization of the ^{31}P and ^{171}Yb nuclei are the same in both the 1:1 and the 1:2 adducts; see ref 22, Chapter 4.

Table 2. ^1H, ^{31}P NMR Values for Phosphine Oxide and Imine Complexes of 1

sample	temp (°C)	δ(P)	$^2J_{YbP}$	δ(Cp*)	δ(H)
Me_3PO	25	29.4			0.83[a]
7	25	45.6	94.6	2.14	0.65
Et_3PNH	25	44.6			1.15 (CH_2)
					0.86 (Me)
9[b]	25	60.1	91.6	2.12	1.20 (CH_2)
					0.61 (Me)
$Et_3PNSiMe_3$[b]	−83	18.2			1.00 (CH_2)
					0.79 (Me)
					0.42 ($SiMe_3$)
11[b]	−83	33.6	7(1)	2.34	1.22 (CH_2)
					0.47 (Me)
					0.18 ($SiMe_3$)

[a] The $^2J_{PH}$ values for Me_3PO and **7** are identical, 12.8 Hz. [b] These samples in toluene-d_8; the others are in C_6D_6.

tions, $^1J_{YbP}$ values), indicate that chelation does not have a significant effect on the interactions formed between **1** and phosphines.[18]

Interactions with R_3PX Complexes (X = O, NR'). The $Cp^*_2Yb(OPMe_3)$ adduct (**7**), isolated in 83% yield as a yellow-orange crystalline solid, undergoes slow intermolecular exchange in C_6D_6 at 25 °C. This contrasts with the fast-exchange behavior at 25 °C that was observed for the phosphine adducts discussed above. While $^{171}Yb-^{31}P$ coupling is observed for **7** ($^2J_{YbP}$ = 94.6 Hz), long-range $^{171}Yb-^1H$ coupling ($^4J_{YbH}$) is not resolved. The ^1H and ^{31}P spectral values for **7** and Me_3PO are given in Table 2. When a toluene-d_8 sample of **7** (with 1 equiv of excess **1**[10]) is heated in the NMR probe, coalescence of the free and bound Cp* resonances occurs at 110 °C.[9] The $^{31}P\{^1H\}$ spectrum of a sample of $Cp^*_2Yb(SPPh_3)$ in C_6D_6 shows $^2J_{YbP}$ of 87 Hz,[19] similar to the analogous value found for **7**.

Addition of 2 equiv of Me_3PO to a toluene solution of **1** results in the precipitation of an orange solid, $Cp^*_2Yb(OPMe_3)_2$ (**8**), which is insoluble in toluene and aliphatic hydrocarbon solvents. The 1:2 adduct **8** dissolves in thf-d_8 with a slight darkening in color; the ^1H and $^{31}P\{^1H\}$ spectral features (broadened resonances, and slightly shifted Me_3PO chemical shift values, relative to those of free Me_3PO in thf-d_8) indicate competitive exchange with the solvent. While thf is competitive with Me_3PO as a ligand toward the Yb center of **1**, when thf is removed under reduced pressure, the pure complex **8** is re-isolated. When Et_2O is added to a sample of the 1:1 adduct **7**, a green solution with an orange precipitate results. Apparently, Et_2O can coordinate to an empty coordination site on the Yb center, lowering the barrier to intermolecular exchange (similar to the phenomenon discussed above for samples of **1** containing excess phosphine). The result is precipitation of the orange 1:2 adduct **8** and a solution containing the green $Cp^*_2Yb(Et_2O)$ adduct, the identity of which was confirmed by ^1H NMR spectroscopy.[21]

Figure 4. The two resonance structures for phosphine ylides.

The interaction formed between **1** and the phosphine imine Et_3PNH is similar to that found for Me_3PO. The ^1H NMR spectrum at 25 °C of a toluene-d_8 sample of the light orange $Cp^*_2Yb(HNPEt_3)$ adduct (**9**) indicates slow intermolecular exchange; a $^2J_{YbP}$ value of 91.6 Hz can be measured from the $^{31}P\{^1H\}$ spectrum. The values for this sample, and for uncomplexed Et_3PNH, are given in Table 2. Unfortunately, the ^1H resonance for the N−H proton is not resolved in either of these samples, at 25 °C or at −90 °C, presumably a result of ^{14}N quadrupolar or exchange broadening.[22] When 2 equiv of Et_3PNH are added to a toluene solution of **1**, the orange 1:2 adduct $Cp^*_2Yb(HNPEt_3)_2$ (**10**) precipitates from solution. Similar to **8**, this solid dissolves in thf-d_8, giving ^1H and $^{31}P\{^1H\}$ spectra that indicate competitive exchange with the solvent. A sample of **1** (2 equiv) and $Et_3PN(SiMe_3)$[23] undergoes fast exchange at 25 °C, on the NMR time scale. However the ^1H spectrum of this sample at −83 °C contains resonances for both free and bound Cp* rings (T_c = −50 °C[9]), and $^{171}Yb-^{31}P$ coupling is resolved in the $^{31}P\{^1H\}$ spectrum ($^2J_{YbP}$ = 7(1) Hz; values given in Table 2). The fast intermolecular exchange at 25 °C for $Cp^*_2Yb(Et_3PNSiMe_3)$ (**11**), as well as the much smaller $^2J_{YbP}$ value as compared to **9** ($^2J_{YbP}$ = 91.6 Hz), likely results from the sterically bulky $SiMe_3$ group preventing the Yb center from approaching the nitrogen nucleus as closely as in the Et_3PNH derivative, **9**.

Interactions with R_3PCHR' Complexes. Considering the relatively strong interactions formed between **1** and phosphine oxides and imines, it was of interest to examine the interaction of **1** with isoelectronic phosphine ylides. Two resonance forms can be drawn for phosphine ylides (Figure 4), and the chemical properties of ylides show that both forms are important. It is known that ylides generally have a slightly pyramidal geometry about the ylide carbon atom in the solid state,[24,25] $^1J_{CH}$ coupling constants suggesting sp^2 hybridization,[26,27] P−C distances consistent with a P=C double bond,[25,26] and a low barrier to rotation about the P−C bond,[24,28] and bind strongly to alkali metals *via* the carbon center.[26] Ylides typically also interact with transition metals *via* the carbon center.[24,29] Recent *ab initio* molecular orbital calculations have found that the dominant resonance structure for phosphine ylides is the dipolar one.[24]

(18) While chelation does not appear to affect the *enthalpic* strength of the Yb−P interactions, based on the NMR data, it does have an affect on the *entropic* contribution to the ΔG(interaction) value, as mentioned in the Discussion.

(19) Reaction of $Cp^*_2Yb(OEt_2)$ with Ph_3PS gives $[Cp^*_2Yb(\mu\text{-}S)]_2$.[20] Apparently, the base-free derivative **1** also reacts similarly, as a resonance for free Ph_3P becomes visible in the $^{31}P\{^1H\}$ spectrum of this sample over the course of several hours.

(20) Berg, D. J.; Burns, C. J.; Andersen, R. A.; Zalkin, A. *Organometallics* **1989**, *8*, 1865.

(21) Tilley, T. D.; Andersen, R. A.; Spencer, B.; Ruben, H.; Zalkin, A.; Templeton, D. H. *Inorg. Chem.* **1980**, *19*, 2999.

(22) Jameson, C. J.; Mason, J. In *Multinuclear NMR*; Mason, J., Ed.; Plenum Press: New York, 1987; Chapter 3.

(23) Birkofer, L.; Kim, S. M. *Chem. Ber.* **1964**, *97*, 2100.

(24) Dixon, D. A. In *Ylides and Imines of Phosphorus*; Johnson, A. W., Ed.; John Wiley & Sons, Inc.: New York, 1993; Chapter 2.

(25) Gilheany, D. G. *Chem. Rev.* **1994**, *94*, 1339.

(26) Kaska, W. C. *Coord. Chem. Rev.* **1983**, *48*, 1.

(27) Starzewski, K. A. O.; Feigel, M. *J. Organomet. Chem.* **1975**, *93*, C20.

(28) Liu, Z.-p.; Schlosser, M. *Tetrahedron Lett.* **1990**, *31*, 5753.

(29) Grim, S. O. In *Phosphorus-31 NMR Spectroscopy in Stereochemical Analysis: Organic Compounds and Metal Complexes*; Verkade, J. G., Quin, L. D., Eds.; VCH Publishers: Deerfield Beach, FL, 1987; Chapter 18.

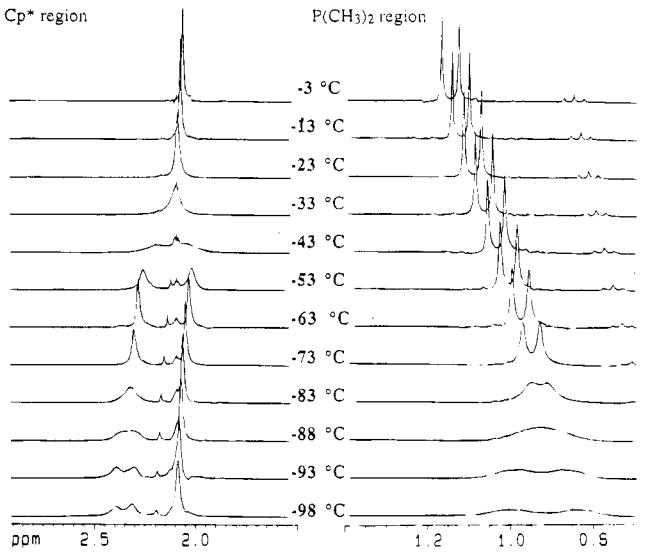

Figure 5. Variable-temperature ^1H spectra of **12**, with 1 equiv excess of **1** (300 MHz, toluene-d_8, −3 to −98 °C).

Addition of 1 equiv of $Me_2PhPCHSiMe_3$[30] to a toluene solution of **1** results in a dark green solution from which dark green crystals of $Cp^*_2Yb(Me_2PhPCHSiMe_3)$ (**12**) can be isolated in 55% yield. The ^1H and $^{31}P\{^1H\}$ spectra of a toluene-d_8 sample of **12**, containing an additional 1 equiv of **1**,[10] indicate that fast intermolecular exchange occurs at 25 °C. On cooling, two different fluxional processes can be distinguished, as indicated by the variable-temperature ^1H spectra, from −3 to −98 °C (Figure 5). The slower process is intermolecular exchange of free and bound **1**; the averaged Cp* resonance decoalesces into free and bound resonances upon cooling, with a $T_c = -40$ °C.[9] Further cooling results in inequivalent Cp* rings, as well as inequivalent phosphorus-bound methyl groups. The coalescence temperatures (two slightly different temperatures for this one process, as a result of the frequency differences between the inequivalent Cp* rings and the inequivalent methyl groups[11]) give an approximate $\Delta G^‡$ value of 9.2(2) kcal mol^{-1} for this fluxional process. The nature of these fluxional processes will be discussed in detail below.

A toluene-d_8 sample of the Me_2PhPCH_2[30] adduct, $Cp^*_2Yb(Me_2PhPCH_2)$ (**13**), with an additional 1 equiv of **1**, also undergoes fast intermolecular exchange at 25 °C; this exchange is slowed upon cooling ($T_c(Cp^*) = -68$ °C[9]). The two identical groups on the ylide carbon necessarily result in equivalent Cp* and PMe_2 groups at all temperatures. To investigate the details of the interactions between **1** and the ylides in solution, the ^1H, $^{13}C\{^1H\}$, and $^{31}P\{^1H\}$ NMR spectra were measured on samples of **12** and **13** (both samples containing 1 equiv excess of **1**), at −78 and −93 °C, respectively.[31] The spectral values of the two samples, as well as those of the two ylides at the same temperatures, are given in Table 3.

Examination of the values in Table 3 shows the usual downfield shift of the Cp* rings of **1**, and of the ^{31}P chemical shifts (the $\Delta(\delta P)$ values are slightly less than were observed for the phosphine, oxide, and imine derivatives, above), upon adduct formation.[32] Interestingly, the ylide proton resonance of **12** is shifted 0.69 ppm downfield from the value for the free ylide, while the analogous resonance for **13** is shifted in the opposite direction, by 0.65 ppm. The methyl and $SiMe_3$ spectral values are perturbed only slightly, consistent with a direct Yb−C interaction. The $^2J_{YbP}$ value for **12** is significantly smaller than the analogous value for **13**. This may be either a steric or an electronic effect; the sterically bulky $SiMe_3$ group is known to stabilize (i.e., delocalize) the ylidic negative charge.[26] The ^{13}C chemical shifts of the ylide carbons of both **12** and **13** are shifted downfield slightly upon adduct formation, consistent with C→Yb electron donation. The $^1J_{PC}$ values involving this carbon are roughly halved upon formation of the adducts; the values for **12** and **13** are similar to the analogous values for phosphonium salts, $(R_3PCHR'R'')^+$,[24] and for previously-reported M−ylide complexes.[33] Unfortunately, coupling between ^{171}Yb and the ylide ^1H and ^{13}C nuclei was not resolved, most likely a result of line broadening from the low temperature required to slow intermolecular exchange.[34]

To investigate the details of the Yb−ylide interaction in the solid state, **12** was characterized by X-ray crystallography, and an ORTEP diagram is shown in Figure 6. There are relatively few structurally characterized lanthanide−ylide complexes.[36] The crystallographic data, positional parameters, and selected intramolecular distances and angles are given in Tables 4−6. The quality of the X-ray data was not sufficient to locate the ylide H; it is assumed to be oriented roughly downward in Figure 6, based on the positions of the Yb, Si, and P atoms. The quality of the data was also not sufficient to allow anisotropic refinement on the carbon atoms; see the Experimental Section for details of the structure solution.

The Cp*−Yb−Cp* angle, the Yb−Cp* distances, and the Cp*−Yb−Cp*/Si−C24−P torsional angle (84°) of **12** are within the expected ranges.[4,7] The Yb−C21 distance, 2.69(2) Å, is indicative of a direct Yb−C interaction.[4,5,35] The P−C21 distance of 1.69(2) Å is within the range observed for M−ylide complexes.[26,38] The Yb−C21−Si angle (105°) is more acute than the Yb−C21−P angle (128°), resulting in a short Yb−methyl contact involving one of the methyl carbons on the Si atom (Yb−C22 = 3.15(2) Å). This likely results from a secondary Yb−methyl interaction, as the sum of the van der Waals radii[39] for a methyl group (2.00 Å) and Yb(II) is 3.70

(30) Schmidbaur, H.; Heimann, M. *Z. Naturforsch.* **1978**, *29b*, 485.
(31) These temperatures were chosen as they are well below the T_c(intermolecular exchange) temperatures.
(32) The ^{31}P chemical shift of ylides nearly always shifts downfield upon coordination to a metal; see ref 29.
(33) (a) Schumann, H.; Reier, F. W.; Dettlaff, M. *J. Organomet. Chem.* **1983**, *255*, 305. (b) Werner, H.; Schippel, O.; Wolf, J.; Schulz, M. *J. Organomet. Chem.* **1991**, *417*, 149.
(34) Several $^1H/^{13}C$ HMQC spectra were obtained on a sample of **12** at −78 °C; however Yb−C or Yb−H coupling was not resolved in any of them. A $^1J_{YbC}$ value of 0.32 Hz has recently been reported for $\{Yb[N(SiMe_3)C(tBu)CH(SiMe_3)]_2\}$.[8a] This value is unexpectedly small, considering the $^1J_{YbC}$ value of 48 Hz that we have found for (dippe)Pt(μ-CH_3)(μ-H)YbCp^*_2.[7] The $^1J_{YbC}$ value for $Yb[C(SiMe_3)_3]_2$ was not reported.[35]
(35) Eaborn, C.; Hitchcock, P. B.; Izod, K.; Smith, J. D. *J. Am. Chem. Soc.* **1994**, *116*, 12071.
(36) (a) Schumann, H.; Albrecht, I.; Reier, F.-W.; Hahn, E. *Angew. Chem., Int. Ed. Engl.* **1984**, *23*, 522. (b) Wong, W.-K.; Guan, J.; Ren, J.; Shen, Q.; Wong, W.-T. *Polyhedron* **1993**, *12*, 2749. (c) Wong, W.-K.; Guan, J. W.; Shen, Q.; Zhang, L. L.; Lin, Y.; Wong, W.-T. *Polyhedron* **1995**, *14*, 277.
(37) Walker, N.; Stuart, D. *Acta Crystallogr.* **1983**, *A39*, 158.
(38) A P=C double bond distance is 1.665 Å,[25] and a P−C single bond distance is 1.872 Å.[24]
(39) Pauling, L. In *The Nature of the Chemical Bond*, 3rd ed.; Cornell University Press: Ithaca, NY, 1960; pp 260−261.

Table 3. Low-Temperature ^{1}H, ^{13}C, and ^{31}P NMR Values for the Phosphine Ylide Complexes 12 and 13[a]

value[b]	$Me_2PhPCHSiMe_3$	**12**[c]	Me_2PhPCH_2	**13**[c]
δ(Cp*)		2.31		2.27
$\delta(CH)/^2J_{PH}$	−0.30/8.7	0.39/20.3	0.37/5.3	−0.28/12.6
$\delta(CH_3)/^2J_{PH}$	1.05/12.6	0.94/11.9	1.16/12.8	0.65/12.6
$\delta(Si(CH_3)_3)$	0.50	0.20		
$^1J_{CH}$(C−H)	136(1)	111(2)	150(1)	119(2)
$^1J_{CH}$(Me)	128(1)	129(1)	128(1)	129(1)
$^1J_{CH}(SiMe_3)$	116(1)	116(1)		
δ(P)	4.6	14.4	5.1	20.0
$^2J_{YbP}$		8(1)		37(1)
$\delta(CH)/^1J_{PC}$	−4.2/94	−2.5/53(2)	−6.1/92	−1.0/42(2)
$\delta(CH_3)/^1J_{PC}$	16.9/63	18.0/65(2)	15.7/67	15.1/62(2)
$\delta(Si(CH_3)_3)/^3J_{PC}$	4.9/4.2	3.5/unresolved		

[a] The values for $Me_2PhPCHSiMe_3$ and **12** were acquired at −78 °C. The values for Me_2PhPCH_2 and **13** were acquired at −93 °C. [b] All of these values were obtained from typical 1-D direct-detected spectra, with the exceptions of the $^1J_{CH}$ values (obtained from ^{13}C-filtered ^{1}H spectra) and the δ(C) and J_{PC} values for **12** and **13** (obtained from ^{1}H/^{13}C HMQC 2-D spectra). See the Experimental Section for details. [c] These samples contained 1 equiv excess of **1**.

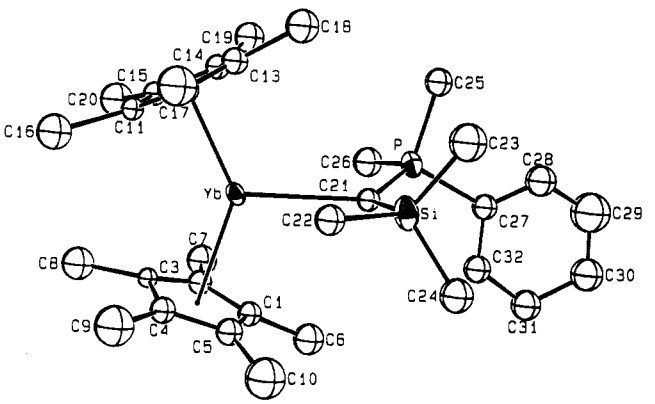

Figure 6. ORTEP diagram of $Cp^*_2Yb(Me_2PhPCHSiMe_3)$ (**13**), 50% probability thermal ellipsoids. The carbon atoms were refined isotropically; see the Experimental Section for details.

Å.[40] Consistent with this, the C(ylide)−Si−C(methyl) angle involving this methyl carbon center is slightly smaller than the other two C−Si−C angles (C21−Si−C22, 106°; C21−Si−C23, 116°; C21−Si−C24, 112°). As the hydrogen atoms were not located in the structure of **12**, further discussion on this point is not warranted. The Yb−C21−P angle, 128°, is within the expected range for M−ylide structures.[33b,41] Thus, interaction of **1** with $Me_2PhPCHSiMe_3$ involves a direct Yb−C interaction, supplemented by a secondary γ-CH_3 interaction, and adduct formation does not result in any unexpected perturbations of the ylide structure. The solid-state structure of **12**, with C_1 symmetry, is consistent with the low-temperature NMR data for this complex.

Discussion

Assuming that the kinetic barrier to intermolecular exchange serves as a qualitative indication of the thermodynamic strength of the Yb−L interaction,[42] the ligands studied above can be roughly ordered in decreasing strength of interaction toward **1**. For the 1:1 adducts, Me_3PO, Et_3PNH > ylides, PMe_3, PEt_3. This is easily rationalized by noting that the best ligands have hard heteroatom donors with lone pairs. Ylides and monodentate phosphines are roughly similar with respect to binding strength to **1**. For the 1:2 adducts (including the bidentate phosphine derivatives in this class), dmpm and 1,2-$(PMe_2)_2C_6H_4$ form stronger interactions with **1** than $(PMe_3)_2$ and $(PEt_3)_2$, the chelate effect resulting in a slightly better interaction relative to the monodentate analogues.[18] The 1:2 monodentate phosphine adducts have a lower kinetic barrier to intermolecular exchange than the analogous 1:1 adducts, indicating a weaker interaction in the former adducts; this result is consistent with the smaller ^{171}Yb−^{31}P coupling constants for the 1:2 adducts (Table 1).[17]

Comparison of the J_{YbP} values found for the complexes studied in this work to J_{MP} values that have been

Table 4. Crystallographic Data for $Cp^*_2Yb(Me_2PhPCHSiMe_3)$ (12)

chem formula	$C_{32}H_{51}PSiYb$
mol wt	667.86
cryst size (mm)	0.54 × 0.43 × 0.22
T (°C)	−100
space group	*Cc* (No. 9)
a (Å)	14.776(8)
b (Å)	14.852(8)
c (Å)	15.186(9)
β (deg)	104.80(4)
V (Å^3)	3222(3)
Z	4
d(calcd) (g cm^{-3})	1.377
μ(calcd) (cm^{-1})	30.0
rflns measd	$\pm h,\pm k,+l$
2θ range	3−45°
no. of rflns collcd	4428
abs corr[a]	T_{max} = 1.4, T_{min} = 0.58
no. of atoms in least squares	35
no. of unique rflns	2305
no. of rflns with $(F_o)^2 > 3\sigma(F_o)^2$	1874
p factor	0.05
no. of params	154
R[b]	0.0500
R_w	0.0616
R_{all}	0.0561
GOF	1.392
diff Fourier (e Å^{-3})	+1.01, −0.205

[a] The program DIFABS[37] was used for the absorption correction. [b] The definitions for R and R_w are as follows:

$$R = \frac{\sum||F_o| - |F_c||}{\sum|F_o|} \qquad R_w = \sqrt{\frac{\sum w(|F_o| - |F_c|)^2}{\sum w(F_o)^2}}$$

(40) Such a γ-CH_3 interaction involving the methyl of an $SiMe_3$ group and Yb has been reported for $Yb[(N(SiMe_3)_2]_2(dmpe)$.[8c]

(41) (a) Marder, T. B.; Fultz, W. C.; Calabrese, J. C.; Harlow, R.; Milstein, D. *J. Chem. Soc., Chem. Commun.* **1987**, 1543. (b) Kermode, N. J.; Lappert, M. F.; Skelton, B. W.; White, A. H.; Holton, J. *J. Organomet. Chem.* **1982**, *228*, C71 and references therein. (c) Buchanan, R. M.; Pierpont, C. G. *Inorg. Chem.* **1979**, *18*, 3608.

(42) The bent geometry of **1** and the overall lack of structural changes upon forming Lewis acid−base adducts with **1** results in the expectation that the kinetic barrier to exchange will serve as a qualitative indicator of the thermodynamic strength of the interaction.

Table 5. Atomic Coordinates and *B* Values (Å²) for the Atoms of 12[a-c]

atom	*x*	*y*	*z*	*B* (Å²)
Yb	0.000	0.25898(1)	0.000	1.46(1)
P	0.0389(3)	0.3176(3)	0.2616(3)	2.14(9)
Si	−0.1565(3)	0.2627(3)	0.1488(3)	2.4(1)
C1	0.053(1)	0.090(1)	0.060(1)	1.9(3)*
C2	0.116(1)	0.121(1)	0.016(1)	2.0(3)*
C3	0.082(1)	0.127(1)	−0.073(1)	1.3(3)*
C4	−0.018(1)	0.097(1)	−0.091(1)	2.1(3)*
C5	−0.030(1)	0.076(1)	−0.005(1)	2.2(3)*
C6	0.079(1)	0.055(1)	0.161(1)	3.2(4)*
C7	0.224(1)	0.140(1)	0.065(1)	3.3(4)*
C8	0.132(1)	0.134(1)	−0.150(1)	3.5(4)*
C9	−0.092(2)	0.084(2)	−0.184(2)	4.6(5)*
C10	−0.118(2)	0.032(2)	0.006(2)	4.8(5)*
C11	−0.003(1)	0.361(1)	−0.149(1)	1.5(3)*
C12	−0.077(1)	0.395(1)	−0.114(1)	2.3(3)*
C13	−0.038(1)	0.437(1)	−0.036(1)	2.1(3)*
C14	0.063(1)	0.427(1)	−0.011(1)	1.9(3)*
C15	0.083(1)	0.382(1)	−0.085(1)	1.7(3)*
C16	−0.021(1)	0.323(1)	−0.254(2)	3.6(4)*
C17	−0.178(2)	0.399(2)	−0.169(2)	4.2(5)*
C18	−0.087(1)	0.490(1)	0.025(1)	3.2(4)*
C19	0.132(1)	0.473(1)	0.061(1)	3.0(4)*
C20	0.180(1)	0.367(1)	−0.098(2)	3.8(4)*
C21	−0.028(1)	0.267(1)	0.168(1)	1.7(3)*
C22	−0.206(1)	0.251(1)	0.024(1)	2.5(4)*
C23	−0.213(2)	0.363(1)	0.187(2)	4.0(4)*
C24	−0.193(1)	0.165(1)	0.205(1)	3.3(4)*
C25	0.015(1)	0.436(1)	0.274(1)	2.5(3)*
C26	0.163(1)	0.310(1)	0.266(1)	3.0(4)*
C27	0.035(1)	0.266(1)	0.372(1)	2.2(3)*
C28	0.012(1)	0.311(1)	0.436(1)	3.2(4)*
C29	0.017(2)	0.272(2)	0.519(2)	5.5(6)*
C30	0.033(1)	0.180(1)	0.535(2)	3.7(4)*
C31	0.054(1)	0.128(1)	0.462(1)	3.1(4)*
C32	0.051(1)	0.175(1)	0.381(1)	2.6(3)*

[a] Numbers in parentheses give estimated standard deviations. [b] Equivalent isotropic thermal parameters are calculated as $(4/3)[a^2\beta_{11} + b^2\beta_{22} + c^2\beta_{33} + ab(\cos\gamma)\beta_{12} + ac(\cos\beta)\beta_{13} + bc(\cos\alpha)\beta_{23}]$. [c] Starred *B* values are for atoms that were included with isotropic thermal parameters.

Table 6. Selected Intramolecular Distances (Å) and Angles (deg) in 12a

	Bond Distances		
Yb−C21	2.69(2)	Yb−Cp1	2.44
Si−C21	1.85(2)	Yb−Cp2	2.43
P−C21	1.69(2)	Yb−P	3.963(5)
Yb−C22	3.15(2)	Yb−Si	3.624(6)
	Bond Angles		
Yb−C21−Si	104.6(6)	Yb−C21−P	128.4(9)
Cp1−Yb−Cp2	134.9(6)	Si−C21−P	120(1)
C21−Si−C22	106.2(9)	C21−Si−C23	116.5(9)
C21−Si−C24	111.7(8)		

[a] All distances and angles involving Cp* rings were calculated using the ring centroid positions.

reported in the literature is informative. There have been four $^1J_{YbP}$ values reported,[43] the most applicable being the values for $(Me_2\overline{PC(SiMe_3)PMe_2)_2}Yb(LiI)_2(thf)_3$ (497 Hz)[43b] and $Yb[\overline{N(SiMe_2CH_2PR_2)_2}]_2$ (R = Me, 665 Hz; R = Ph, 522 Hz);[43c] the ligands in these complexes all bear a negative charge, in contrast to the neutral phosphine ligands used in the present study. The reported values are similar to the $^1J_{YbP}$ values found for the 1:2 phosphine adducts in this study. There have been several $^2J_{MP}$ values reported for transition metal−ylide complexes. The values reported (reduced coupling constants, *K*, in parentheses),[44] *cis*-$(Me_3PCH_2)_2PtMe_2$, 92 Hz (8.77);[45] $[(Me_3PCH_2)Rh(PMe_3)_2(Cp)]I_2$, 4.5 Hz

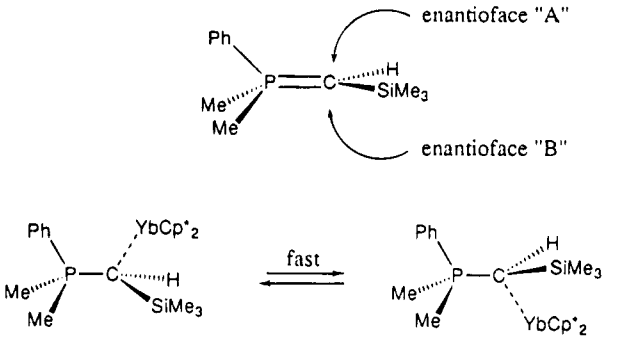

Figure 7. Fast inversion of the bound ylide enantioface resulting in inversion of the chirality at the ylide carbon, as required for P-bound methyl and Cp* group equivalency.

(−2.92);[46] *trans*-$[Pt(CH_2PR_3)(PR_3)_2X][Y]$ (X, Y = halides), *ca.* 100 Hz (9.53);[41b] and *cis*-$[Pt(CH_2PR_3)(PR_3)_2X][Y]$ (X, Y = halides), *ca.* 50 Hz (4.76),[41b] are similar to the values found for **12** ($^2J_{YbP}$ = 8 Hz, *K* = 0.933) and **13** ($^2J_{YbP}$ = 37 Hz, *K* = 4.32). In addition, the slight increase in the ylide $^2J_{PCH}$ value upon formation of the interaction with **1**, as observed in **12** and **13**, is a common result of coordination of ylides to metal centers.[33]

Two different fluxional processes can be slowed upon cooling a sample of **12** from 25 to −98 °C. The first process involves intermolecular exchange of free and bound **1**, and slowing of the second process results in inequivalent PMe_2 groups and inequivalent Cp* rings. As the Yb center is bound *via* the ylide carbon center, this carbon becomes chiral once intermolecular exchange is stopped, resulting in diastereotopic methyl groups. However, the methyl groups do not become inequivalent until a much lower temperature, at which point the Cp* rings also become inequivalent (Figure 5). Fast inversion of the chirality at the ylide carbon would make the PMe_2 groups equivalent. This fluxional process has an identical barrier as the process that results in equivalency of the bound Cp* rings of **12** between −40 and −84 °C and is most likely the same physical process.

Certain metal−ylide complexes are known to undergo phosphine exchange *via* metal carbene intermediates.[24,26] Addition of PMe_3 to a C_6D_6 solution of **12** results in no phosphine exchange after several hours at 25 °C, ruling out such a process. Consequently, the only way for fast inversion to occur at the ylide carbon is *via* fast interchange of **1** between the two ylide enantiofaces (Figure 7; the term enantioface is used with the P=C planar resonance form in mind). Since intermolecular exchange is slow below −40 °C, this process must occur without exchange of free and bound molecules of **1**. It is reasonable to assume that inversion at the ylide carbon involves the Yb center, as this is the only "labile" ligand.

(43) (a) Nief, F.; Ricard, L.; Mathey, F. *Polyhedron* **1993**, *12*, 19. (b) Karsch, H. H.; Ferazin, G.; Steigelmann, O.; Kooijman, H.; Hiller, W. *Angew. Chem., Int. Ed. Engl.* **1993**, *32*, 1739. (c) Fryzuk, M. D.; Haddad, T. S.; Berg, D. J. *Coord. Chem. Rev.* **1990**, *90*, 137.

(44) The reduced coupling constant is given by $K = (4\pi^2 J_{AB})/(h\gamma_A\gamma_B)$; all values given in the text are to the 10^{20} power and are in N A^{-2} m^{-3} units.

(45) Blaschke, G.; Schmidbaur, H.; Kaska, W. C. *J. Organomet. Chem.* **1979**, *182*, 251.

(46) Feser, R.; Werner, H. *Angew. Chem., Int. Ed. Engl.* **1980**, *19*, 940.

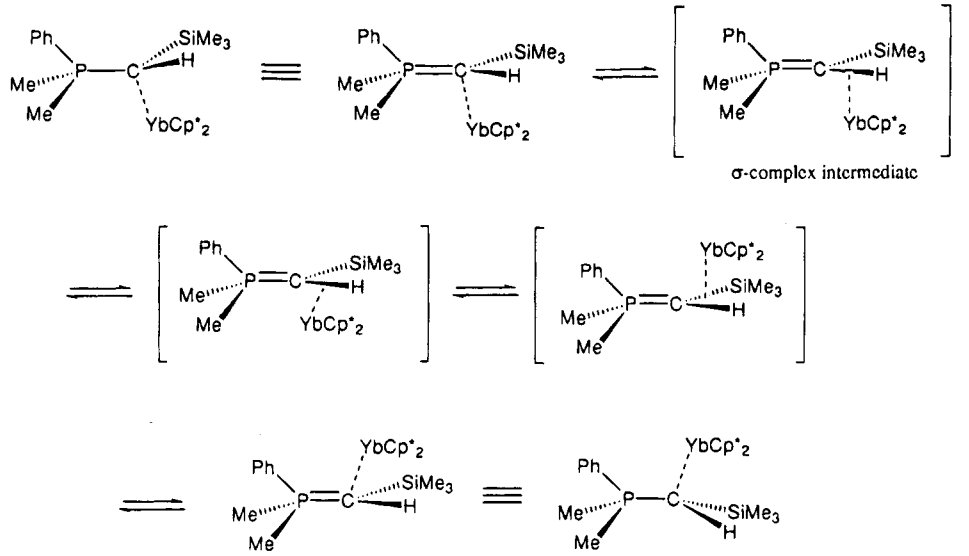

Figure 8. One possible mechanism for the fluxional process that results in equivalent PMe_2 groups and equivalent Cp* rings, without intermolecular exchange.

One possible mechanism for this inversion involves movement of **1** to the opposite ylide enantioface (the planar ylide resonance form is used for this discussion, for purposes of clarity) *via* a σ-complex involving the ylide C−H bond in the transition state (Figure 8).[47] This process, if fast on the NMR time scale, results in identical averaged environments for the two PMe_2 groups and for the two Cp* rings. A similar process with enantioface migration *via* a σ-complex, involving an olefinic C−H bond, has recently been invoked by Peng and Gladysz to explain the observation of intramolecular equilibration of the diastereomeric chiral Re complex $[CpRe(NO)PPh_3)(H_2C{=}CHR)][BF_4]$.[48,49] As Peng and Gladysz have noted, σ-complex interactions have been estimated at *ca.* 10 kcal mol^{-1} and consequently, can stabilize the transition state with respect to dissociation (i.e., intermolecular exchange).[48] Interaction of the electron-rich C−H bond of the ylide with the electrophilic Yb center is likely a favorable interaction.

Another possible mechanism for this fluxional process involves complete cleavage of the Yb−ylide interaction, with retention of Yb−P spin−spin coupling; this possibility assumes the presence of a solvent-caged species, for explaining the lack of intermolecular exchange.[50] Considering the Yb−methyl interaction that is present in the (ground-state) solid-state structure of **12** (Figure 6 and accompanying discussion), it is also possible that the inversion at the ylide carbon center occurs *via* a Yb−methyl interaction; this possibility is very similar to the σ-complex mechanism discussed above. Given the experimental evidence, none of these three possible mechanisms can be rigorously ruled out.

The $^1J_{CH}$ value of the ylide C−H bond of **12** decreases by 25 Hz upon formation of the interaction with **1**, consistent with a direct Yb−C interaction. Protonation of Me_3PCH_2 results in a decrease in $^1J_{CH}$ from 149 to 133 Hz,[51] while $^1J_{CH}$ for $Me_3PCH_2(Ni(CO)_3)$ (in which the Ni interacts with the ylide carbon, based on the solid-state structure of a related complex)[27] is 123 Hz. If there were a C−H−Yb interaction present in the ground state structure of **12**, the $^1J_{CH}$ value would probably be significantly smaller than the observed value of 111 Hz. Analogous $^1J_{CH}$ values for transition metal agostic complexes are reduced by as much as 50%, relative to the "free" values.[52] While it is clear that the ground-state Yb−ylide interaction involves a direct Yb−C interaction (supplemented by a Yb−methyl interaction), this does not rule out the presence of a σ-complex in the transition state of the fluxional process, as discussed above.

Examination of Figure 3 shows that, in addition to the ^{171}Yb correlations from the PMe_2 protons, correlations to the bound Cp* methyl protons are also present. This shows that spin−spin coupling between ^{171}Yb and these protons is present in **6**. We have measured the analogous value for **1**, and it is 2.5 Hz; this coupling will not vary much with the ligand, L, in $Cp^*_2YbL_n$ complexes. A $^1H/^{171}Yb$ HMQC spectrum of **7** at −7 °C,[53] optimized for this J_{YbH} value, gives a ^{171}Yb resonance (at +139 ppm) that is correlated to the Cp* protons. A similar experiment gives a ^{171}Yb resonance at +140 ppm for **12** (at −73 °C); this resonance is correlated with the $SiMe_3$ protons, indicating that long-range (4-bond) Yb−H communication is present. It appears that this method of indirectly detecting ^{171}Yb resonances, *via* long-range J_{YbH} coupling (involving either the Cp* protons or protons on the ligand, L), will be useful for any slow-exchange $Cp^*_2YbL_n$ complex.[54] The technique of using long range M−H coupling to indirectly detect

(47) Movement of the ylide molecule relative to **1** is identical to movement of **1** relative to the ylide molecule. For clarity, the latter frame of reference will be used for the discussion. Also, while rotation of the C(H)($SiMe_3$) moiety about the P−C bond may be occurring (the barrier to rotation about P−C ylide bonds is small),[28] this would not have a significant effect on the process under discussion.

(48) Peng, T.-S.; Gladysz, J. A. *J. Am. Chem. Soc.* **1992**, *114*, 4174.

(49) Similar interactions involving an olefinic C−H bond have been proposed to explain kinetic and isotopic effects in the $Cp^*Ir(PMe_3)(C_2H_4)$ system: (a) Stoutland, P. O.; Bergman, R. G. *J. Am. Chem. Soc.* **1985**, *107*, 4581. (b) Stoutland, P. O.; Bergman, R. G. *J. Am. Chem. Soc.* **1988**, *110*, 5732.

(50) See ref 48 for a more thorough discussion on this topic.

(51) Elser, V. H.; Dreeskamp, H. *Ber. Bunsen-Ges. Phys. Chem.* **1969**, *73*, 619.

(52) Crabtree, R. H. *Angew. Chem., Int. Ed. Engl.* **1993**, *32*, 789. While certain agostic complexes have $^1J_{CH}$ values that are relatively unchanged from the "free" $^1J_{CH}$ values, this is usually[16] a result of averaging of a smaller agostic $^1J_{CH}$ value with larger, unperturbed $^1J_{CH}$ values; this is not possible for **12**.

(53) Slight exchange broadening of the Cp* resonances is present in the 25 °C ^1H spectrum.

Table 7. Reported ^{171}Yb Chemical Shifts of $Cp^{\ddagger}_2YbL_n$ Complexes ($Cp^{\ddagger}$ = a Cp Derivative)

complex	$\delta(^{171}Yb)$, ppm	solvent/temp (°C)[a]	ref
Cp^*_2Yb, **1**[b]	−30	C_6D_6/25	this work
$(Cp^+)_2Yb$[b,c]	−16	toluene-d_8/24	56a
$(Cp^+)_2Yb(OEt_2)$[b-d]	−70	toluene-d_8/24	56a
$Cp^*_2Yb(OEt_2)$[d]	36	Et_2O/35	56b
$Cp^*_2Yb(thf)_2$[d]	0	thf/23	56b
$Cp^*_2Yb(NC_5H_5)_2$[d]	949	NC_5H_5/65	56b
$Cp^*_2Yb(\mu\text{-}H)_2Pt$(dcype)	572	toluene-d_8/25	7
$Cp^*_2Yb(\mu\text{-}H)_2Pt$(dcypp)	472	toluene-d_8/25	7
$Cp^*_2Yb(\mu\text{-}H)(\mu\text{-}Me)Pt$(dippe)	340	toluene-d_8/25	7
$Cp^*_2Yb(1,2\text{-}(PMe_2)C_6H_4)$, **6**	782	toluene-d_8/−30	this work
$Cp^*_2Yb(OPMe_3)$, **7**	139	toluene-d_8/−7	this work
$Cp^*_2Yb(Me_2PhPCHSiMe_3)$, **12**	140	toluene-d_8/−73	this work
$(Cp')_2Yb(thf)_2$[d,e]	242	thf/−30	56c
$(Cp'')_2Yb(thf)_2$[d,e]	316	thf/−30	56c
$(Cp^{py})_2Yb$[f]	457	C_6D_6, thf/31	56d
$(Cp'^{py})_2Yb$[f]	544	thf/31	56d
$(Cp^{py(s)})_2Yb$[f]	595	C_5D_5N/31	56d
$(Cp'^{py(s)})_2Yb$[f]	851	C_6D_6/31	56d

[a] It has been reported that ^{171}Yb chemical shifts have a significant temperature dependence.[56b] [b] We have found some evidence for a weak interaction of **1** with aromatic solvents such as C_6D_6; consequently, these may be averaged values. [c] $Cp^+ = 1,3\text{-}(SiMe_3)_2C_5H_3$. [d] The ^{171}Yb chemical shifts of these complexes are likely averaged values, as fast intermolecular exchange (with solvent) is likely present for these cases. [e] $Cp' = C_5Me_4P$; $Cp'' = C_5Me_4As$. [f] These Cp derivatives contain a pendant pyridyl arm: $Cp^{py} = C_5H_4[C(Me)_2CH_2C_5H_4N\text{-}2]$; $Cp'^{py} = C_5H_3(SiMe_3)[\{C(Me)_2CH_2C_5H_4N\text{-}2\}\text{-}3]$; $Cp^{py(s)} = C_5H_4[C(Me)_2C_5H_4N\text{-}2]$; $Cp'^{py(s)} = C_5H_3[(SiMe_3)\{C(Me)_2C_5H_4N\text{-}2\}\text{-}3]$; see ref 56d for details.

M spectra with increased sensitivity has been reported previously.[55]

Table 7 lists the ^{171}Yb chemical shifts of $Cp^{\ddagger}_2YbL_n$ complexes ($Cp^{\ddagger}$ = any Cp derivative) that have been reported to-date.[56] A rough correlation of the ^{171}Yb chemical shift with coordination number can be made. Specifically, the base-free compounds Cp^*_2Yb (**1**) and $(1,3\text{-}(SiMe_3)_2C_5H_3)_2Yb$ have chemical shifts of −30 and −16 ppm, respectively. The 1:1 adducts resonate slightly downfield, from 0 to +140 ppm (with the value for $(1,3\text{-}(SiMe_3)_2C_5H_3)_2Yb(OEt_2)$ being an exception), and the 1:2 adducts have chemical shifts from +340 to +950 ppm (with the value for $Cp^*_2Yb(thf)_2$ being an exception). Several of the values were measured under fast-exchange conditions (including the values for $(1,3\text{-}(SiMe_3)_2C_5H_3)_2Yb(OEt_2)$ and $Cp^*_2Yb(thf)_2$), as noted in Table 7, and so these chemical shift values are averaged values. While a dependence on coordination number is a common feature for metal chemical shifts, correlation of metal chemical shifts with specific chemical properties (as is frequently done for ^{1}H and ^{13}C chemical shifts) is often ambiguous.[22] The paramagnetic shielding contribution to the chemical shift, the dominant factor for metal chemical shifts, includes terms that are dependent on low-lying magnetic dipole-allowed transitions to excited states of the complex, the inverse cube of the distance of the valence p and d electrons from the metal nucleus, and the imbalance of electron distribution on the metal center.[22] In addition, relativistic effects on ^{171}Yb chemical shifts will be significant.[57] These factors are not well-understood for many metals[55a,58] and certainly not for $Cp^*_2YbL_n$ complexes; consequently, information contained within ^{171}Yb chemical shifts remains a mystery.

Conclusions

The interactions of **1** with phosphines have been found to have relatively high kinetic barriers, allowing investigation of the solution-state perturbations that result from such interactions. Both 1:1 and 1:2 adducts can be isolated; $^1J_{YbP}$ is significantly reduced for the 1:2 adducts, relative to the 1:1 adducts. The presence of >2 equiv of phosphine results in faster (associative) intermolecular exchange, a common feature of $Cp^*_2YbL_n$ systems.[7] The barrier to intermolecular exchange for phosphine oxide and imine adducts is much higher, and these adducts undergo slow exchange at 25 °C. Both 1:1 and 1:2 adducts can be isolated for these derivatives also; however, the latter are insoluble in hydrocarbon and aromatic solvents. The $^2J_{YbP}$ values for the 1:1 adducts are 1 order of magnitude less than the analogous one-bond values for the phosphine derivatives. While an adduct with the unsymmetrical ylide $Me_2PhPCHSiMe_3$ undergoes fast intermolecular exchange at 25 °C, this exchange can be slowed at low temperature. An intramolecular process, resulting in equivalent PMe_2 groups and equivalent Cp* rings, can also be slowed at a lower temperature; possible mechanisms for this process have been discussed.

We are continuing our investigations of the solution- and solid-state perturbations that result from the interactions of **1** with various nonclassical Lewis bases. As above, the NMR-active ^{171}Yb isotope will be utilized in these studies. Our focus remains on slow-exchange adducts, for which J_{YbX} values can be measured to give information concerning the nature of the Lewis acid–base interactions in the solution state. The results of these investigations will be reported at a later date.

(54) The potential of this technique for other $Cp^{\ddagger}ML_n$ complexes ($Cp^{\ddagger}$ = a Cp derivative; M = an NMR-active metal nucleus) is currently being explored: Ball, G. E. Work in progress.

(55) (a) Macchioni, A.; Pregosin, P. S.; Ruegger, H.; van Koten, G.; van der Schaaf, P. A.; Abbenhuis, R. A. T. M. *Magn. Res. Chem.* **1994**, *32*, 235. (b) Bonny, A.; McMaster, A. D.; Stobart, S. R. *Inorg. Chem.* **1978**, *4*, 935. (c) Benn, R.; Brevard, C. *J. Am. Chem. Soc.* **1986**, *108*, 5622. (d) Benn, R.; Brenneke, H.; Joussen, E.; Lehmkuhl, H.; Lopez Ortiz, F. *Organometallics* **1990**, *9*, 756.

(56) (a) Hitchcock, P. B.; Howard, J. A. K.; Lappert, M. F.; Prashar, S. *J. Organomet. Chem.* **1992**, *437*, 177. (b) Avent, A. G.; Edelman, M. A.; Lappert, M. F.; Lawless, G. A. *J. Am. Chem. Soc.* **1989**, *111*, 3423. (c) Nief, F.; Ricard, L.; Mathey, F. *Polyhedron* **1993**, *12*, 19. (d) van den Hende, J. R.; Hitchcock, P. B.; Lappert, M. F. *J. Organomet. Chem.* **1994**, *472*, 79.

(57) Mason, J. *Chem. Rev.* **1987**, *87*, 1299.

(58) Pregosin, P. S. In *Annual Reports on NMR Spectroscopy, Vol. 17*; Webb, G. A., Ed.; Academic Press Inc.: London, 1986.

Experimental Details

General Comments. All reactions and product manipulations were carried out under dry nitrogen using standard Schlenk and drybox techniques. Solvents and reagents were dried and purified as described previously.[59] Infrared spectra, melting points, elemental analyses, and the NMR spectra were obtained as previously described.[59]

^1H NMR shifts are relative to tetramethylsilane; the residual solvent peak was used as an internal reference. $^{31}P\{^1H\}$ NMR shifts are relative to 85% H_3PO_4 at δ 0.0, with shifts downfield of the reference considered positive. ^{171}Yb shifts are referenced to an absolute frequency scale relative to the reported frequency of $Cp^*_2Yb(thf)_2$[56b] and scaled according to the ^1H frequency of the particular machine used. In all cases where ^{171}Yb chemical shifts were being investigated, the HMQC pulse sequence was used,[14] and first a large sweep width in the ^{171}Yb dimension was used, followed by a smaller sweep width, to ensure that the resonance was not folded. The HMQC pulse sequence was also used to acquire $^1H/^{13}C$ spectra (to obtain the ^{13}C NMR data for **12** and **13**). The $^1J_{CH}$ values for **12**, **13**, and the free ylides were obtained from ^{13}C-filtered ^1H spectra, using the standard Bruker pulse sequence, with optimized 90° pulses and delays.

$Cp^*_2Yb(PMe_3)_2$ (2). Trimethylphosphine (0.086 mL, 0.84 mmol) was added dropwise to a solution of **1** (0.18 g, 0.41 mmol) in toluene (15 mL). The solution turned bright green, and a dark green crystalline solid precipitated from solution within minutes. The mixture was slowly cooled to −80 °C, yielding the product as dark green crystals (0.22 g, 88%), mp 110 °C (decomposition to a black solid). ^1H NMR (C_6D_6): δ 2.05 (s, 30H), 0.76 (s, 18H). $^{31}P\{^1H\}$ NMR (C_6D_6): δ −55.8 (s) ppm. IR: 2718 m, 1377 s, 1367 m, 1326 w, 1304 s, 1281 m, 1017 m, 960 s, 939 s, 839 w, 801 w, 722 m, 710 m, 668 w, 663 w, 624 w, 591 m cm^{-1}. Anal. Calcd for $C_{26}H_{48}P_2Yb$: C, 52.4; H, 8.12. Found: C, 52.3; H, 8.30.

$Cp^*_2Yb(PEt_3)$ (3). Triethylphosphine (0.060 mL, 0.40 mmol) was added dropwise to a toluene solution (15 mL) of **1** (0.12 g, 0.27 mmol). The resulting dark blue solution was concentrated to *ca.* 10 mL. Slow cooling to −80 °C yielded the product as dark blue crystals (0.10 g, 66%), mp 128 °C (decomposition to a dark brown oil). ^1H NMR (C_6D_6): δ 2.04 (s, 30H), 1.27 (6H, qd, $^3J_{HH}$ = 7.6 Hz, $^2J_{PH}$ = 1.6 Hz), 0.77 (9H, dt, $^3J_{PH}$ = 14.4 Hz, $^3J_{HH}$ = 7.6 Hz). $^{31}P\{^1H\}$ NMR (C_6D_6): δ −12.6 (s) ppm. IR: 2721 m, 1417 m, 1377 s, 1262 s, 1098 s, 1036 s, 1023 s, 865 w, 803 s, 766 m, 756 m, 702 m, 672 w, 622 w, 590 w cm^{-1}. Anal. Calcd for $C_{26}H_{48}P_2Yb$: C, 55.6; H, 8.08. Found: C, 55.5; H, 8.13.

$Cp^*_2Yb(1,2\text{-}(Me_2P)_2C_6H_4)$ (6). To a toluene solution (15 mL) of **1** (0.15 g, 0.34 mmol), 1,2-$(Me_2P)_2C_6H_4$ (0.056 mL) was added dropwise. The resulting dark green-brown solution was concentrated to *ca.* 10 mL and then filtered. Slow cooling to −40 °C yielded the product as maroon crystals (0.10 g, 46%); the compound did not melt sharply but darkened to a brown oil over the temperature range 260−290 °C. ^1H NMR (C_6D_6): δ 7.11 (m, 2H), 7.04 (m, 2H), 2.06 (s, 30H), 1.03 (s, 12H). $^{31}P\{^1H\}$ NMR (C_6D_6): δ −42.5 (s, $w_{1/2}$ = 40 Hz (see text), $^1J_{YbP}$ = 650 Hz) ppm. IR: 2720 m, 1426 s, 1376 s, 1299 s, 1283 w, 1277 w, 1134 w, 1119 m, 1018 w, 942 s, 907 s, 874 m, 827 w, 799 w, 753 s, 730 m, 718 m, 686 w, 677 w, 589 w, 463 m, 452 w cm^{-1}. Anal. Calcd for $C_{30}H_{46}P_2Yb$: C, 56.2; H, 7.23. Found: C, 56.3; H, 7.39.

$Cp^*_2Yb(OPMe_3)$ (7). A toluene solution (10 mL) of Me_3PO (0.040 g, 0.44 mmol) was added dropwise to a stirred solution of **1** (0.19 g, 0.43 mmol) in toluene (10 mL). The solution turned orange near the end of the addition. The solvent was removed under reduced pressure, giving the crude product as a yellow-orange solid. This solid was washed with pentane (2 × 20 mL) and dried under reduced pressure, giving the product as a fine yellow powder (0.19 g, 83%), mp 303−307 °C (dec). ^1H NMR (C_6D_6): δ 2.14 (s, 30H), 0.65 (d, 9H, $^2J_{PH}$ = 12.8 Hz) ppm. $^{31}P\{^1H\}$ NMR (C_6D_6): δ 45.6 (s, $^2J_{YbP}$ = 95 Hz) ppm. IR: 2720 m, 1417 m, 1377 m, 1344 w, 1309 s, 1296 s, 1154 s, 1108 w, 1022 w, 945 s, 857 s, 799 w, 747 m cm^{-1}. Anal. Calcd for $C_{23}H_{39}OPYb$: C, 51.6; H, 7.34. Found: C, 51.7; H, 7.08.

$Cp^*_2Yb(OPMe_3)_2$ (8). A toluene solution (10 mL) of Me_3PO (0.070 g, 0.76 mmol) was added dropwise to a toluene solution (10 mL) of **1** (0.15 g, 0.34 mmol). An orange solid precipitated from the solution during the addition. The solid was allowed to settle, the solvent was removed by cannula, and the solid was washed with toluene (2 × 10 mL). Drying under reduced pressure yielded the product as a pumpkin-colored solid (0.080 g, 38%), mp 290 °C (decomposition to a red-brown oil). ^1H NMR (thf-d_8): δ 1.85 (s, 15H, $w_{1/2}$ = 1 Hz), 1.53 (broad s, 9H, $w_{1/2}$ = 38 Hz; see text). $^{31}P\{^1H\}$ NMR (thf-d_8): δ 39.3 (broad s, $w_{1/2}$ = 480 Hz; see text) ppm. Free Me_3PO in thf-d_8 has the following values: ^1H NMR 1.34 (d, $^2J_{PH}$ = 12.8 Hz) ppm; $^{31}P\{^1H\}$ NMR 30.5 (s) ppm; IR 2717 w, 1377 m, 1344 w, 1308 s, 1295 s, 1182 s, 1166 s, 1021 w, 944 s, 861 m, 798 w, 750 m, 721 w cm^{-1}. A satisfactory elemental analysis was not obtained on this sample, since it was difficult to find a suitable crystallization solvent; see text. (The procedure used above gave a product that was consistently *ca.* 1% low in carbon).

$Cp^*_2Yb(HNPEt_3)$ (9). A toluene solution (10 mL) of Et_3PNH[60] (0.045 g, 0.34 mmol) was added dropwise to a toluene solution (10 mL) of **1** (0.15 g, 0.34 mmol). The resulting orange solution was stirred for 30 min and filtered. Slow cooling of the solution to −80 °C gave the product as a fine light orange powder (0.10 g, 51%), mp 240 °C (decomposition to a dark brown oil). ^1H NMR (toluene-d_8): δ 2.12 (s, 30H), 1.20 (dq, 6H, $^2J_{PH}$ = 12.1 Hz, $^3J_{HH}$ = 7.8 Hz), 0.61 (dt, 9H, $^3J_{PH}$ = 16.8 Hz, $^3J_{HH}$ = 7.8 Hz) ppm (the N−*H* resonance is not observed; see text). $^{31}P\{^1H\}$ NMR (toluene-d_8): δ 60.1 (s, $^2J_{YbP}$ = 92 Hz) ppm. IR: 2721 m, 1412 m, 1379 s, 1283 m, 1264 m, 1139 s, 1046 m, 1027 m, 1012 m, 983 w, 783 s, 769 s, 741 w, 724 m cm^{-1}. Anal. Calcd for $C_{26}H_{46}NPYb$: C, 54.2; H, 8.04. Found: C, 54.4; H, 7.76.

$Cp^*_2Yb(Me_2PhPCHSiMe_3)$ (12). To a stirred solution of **1** (0.12 g, 0.34 mmol) in toluene (10 mL), $Me_2PhPCHSiMe_3$[30] (0.061 mL) was added dropwise. The resulting dark green solution was filtered and slowly cooled to −40 °C, yielding the product as dark green crystals (0.10 g, 55%), mp 103 °C (dec). ^1H NMR (toluene-d_8): δ 7.4−7.0 (m, 5H), 2.14 (s, 30H), 1.22 (d, 6H, $^2J_{PH}$ = 12.5 Hz), 0.24 (d, 1H, $^2J_{PH}$ = 20.5 Hz), 0.16 (s, 9H) ppm. $^{31}P\{^1H\}$ NMR (toluene-d_8): δ 10.8 (s) ppm. IR: 1420 m, 1378 m, 1329 w, 1310 w, 1301 m, 1288 m, 1254 m, 1244 m, 1163 w, 1123 s, 1105 m, 1076 w, 1016 w, 958 s, 922 s, 917 s, 856 s, 832 s, 767 m, 747 s, 723 w, 697 m, 681 m, 639 m, 590 m, 491 m, 421 m cm^{-1}. Anal. Calcd for $C_{32}H_{51}PSiYb$: C, 57.6; H, 7.70. Found: C, 57.6; H, 8.0.

$Cp^*_2Yb(Me_2PhPCH_2)$ (13). To a stirred solution of **1** (0.15 g, 0.34 mmol) in toluene (10 mL), Me_2PhPCH_2[30] (0.047 mL) was added dropwise. The resulting dark maroon solution was slowly cooled to −80 °C, yielding the product as reddish-brown crystals (0.16 g, 79%), mp 166−178 °C. ^1H NMR (toluene-d_8): δ 7.2−6.95 (m, 5H), 2.06 (s, 30H), 1.05 (d, 6H, $^2J_{PH}$ = 12.8 Hz), −0.20 (d, 2H, $^2J_{PH}$ = 13.4 Hz) ppm. $^{31}P\{^1H\}$ NMR (toluene-d_8): δ 18.7 (s) ppm. IR: 2721 m, 1437 s, 1420 m, 1378 m, 1367 m, 1304 m, 1289 w, 1262 w, 1182 w, 1159 m, 1113 m, 1018 m, 1000 w, 977 m, 953 s, 925 s, 844 m, 819 w, 799 w, 760 m, 744 s, 725 s, 692 s, 667 m, 494 m, 419 m cm^{-1}. Anal. Calcd for $C_{29}H_{73}PYb$: C, 58.5; H, 7.29. Found: C, 58.2; H, 7.36.

X-ray Structure Determination of 12. X-ray-quality crystals of **12** were grown as described above. The crystals

(59) Schwartz, D. J.; Andersen, R. A. *J. Am. Chem. Soc.* **1995**, *117*, 4014.

(60) Birkofer, L.; Kim, S. M. *Chem. Ber.* **1964**, *97*, 2100. This compound was obtained as a crystalline white solid, crystallized from diethyl ether, in contrast to a colorless oil as reported.

were placed in Paratone N oil, mounted on the end of a cut quartz capillary tube, and placed under a flow of cold nitrogen on an Enraf-Nonius CAD4 diffractometer. Crystal data and numerical details of the structure determination are given in Tables 4–6. Intensities were collected with graphite-monochromatized Mo Kα (λ = 0.710 73 Å) radiation using the θ–2θ scan technique. Lattice parameters were determined using automatic peak search and indexing procedures. Intensity standards were measured every 1 h of data collection.

The raw intensity data were converted to structure factor amplitudes and their esd's by correction for scan speed, background, and Lorentz and polarization effects. Correction for crystal decomposition was not necessary. Analysis of the data, collected based on a triclinic unit cell, suggested a *C*-centered monoclinic lattice. A θ-independent differential absorption (DIFABS) correction[37] was applied to the raw data, using an isotropic model in the space group *P*1 as a basis for the correction (the Yb atoms were found using Patterson techniques; the non-hydrogen atoms were located using standard least-squares and Fourier techniques;[61,62] and hydrogens were included in this model, in positions assuming idealized bonding geometry about the carbon atoms).

The absorption-corrected data were transformed to a *C*-centered monoclinic unit cell, and the atomic positions were transformed to the space group *Cc*. The systematic absences were rejected, and the redundant data were averaged (R_{int} = 0.077). The carbon atoms were refined isotropically, the heavy atoms were refined anisotropically, and no hydrogen atoms were included in the final model. The enantiomorph that gave the best agreement with the data was used. Attempts to refine the carbon atoms anisotropically resulted in irrational thermal parameter values (nonpositive definite tensors), for many of these atoms.

The least-squares program minimized the expression, $\sum w(|F_o| - |F_c|)^2$, where w is the weight of a given observation. A value of 0.05 for the *p*-factor was used to reduce the weight of intense reflections in the refinements. The analytical forms of the scattering factor tables for the neutral atoms were used,[63a] and all non-hydrogen scattering factors were corrected for both real and imaginary components of anomalous dispersion.[63b]

Acknowledgment. This work was supported by the Director, Office of Energy Research, Office of Basic Energy Sciences, Chemical Sciences Division of the U.S. Department of Energy, under Contract No. DE-AC03-76F00098. We thank the National Science Foundation for a predoctoral fellowship to D.J.S.; Dr. Graham E. Ball for helpful discussions, including the idea of using long-range J_{YbH} coupling from the Cp* methyl groups of $Cp^*_2YbL_n$ complexes to indirectly detect ^{171}Yb spectra; Mr. Christopher D. Tagge for helpful discussions; and Dr. F. J. Hollander for helpful advice concerning X-ray crystallography.

Supporting Information Available: Complete tables of bond lengths and angles, anisotropic thermal parameters, and root mean square amplitudes of thermal vibration for **12** (12 pages). This material is contained in many libraries on microfiche, immediately follows this article in the microfilm version of the journal, and can be ordered from the ACS; see any current masthead page for ordering information.

OM9502906

(61) All calculations were performed on a DEC Microvax II or a DEC Microvax 4000 using locally modified Nonius-SDP software operating under Micro-VMS operating system.

(62) (a) Frenz, B. A. In *Structure Determination Package Users Guide*; Texas A & M University and Enraf-Nonius: College Station, TX, and Delft, The Netherlands, 1985. (b) Fair, C. K. In *MolEN Molecular Structure Solution Procedures*; Enraf-Nonius, Delft Instruments, X-ray Diffraction B.V.: Delft, The Netherlands, 1990.

(63) (a) Cromer, D. T.; Waber, J. T. In *International Tables for X-ray Crystallography, Vol. IV*; The Kynoch Press: Birmingham, England, 1974; Table 2.2B. (b) Cromer, D. T. *Ibid.*, Table 2.3.1.

Stereoselective Ring Expansion of 3-Vinyl-1-cyclopropenes To Give (η^5-Cyclopentadienyl)ruthenium and (η^4-Cyclohexadienone)iron Complexes. Exclusion of Planar Metallacyclohexadiene Intermediates and Relevance to the Dötz Reaction

Russell P. Hughes,*,† Hernando A. Trujillo,[1] and André J. Gauri

Burke Chemistry Laboratory, Dartmouth College, Hanover, New Hampshire 03755-3564

Received May 1, 1995[⊗]

trans-3-(β-Deuteriovinyl)-1,2,3-triphenyl-1-cyclopropene, **15**, reacts with $Fe_2(CO)_9$ to give the 2,4-cyclohexadieneone complex **16**, as a single isotopomer. The location of deuterium in the *endo*-position was confirmed by comparison of ^1H NMR spectra of **16** with its isotopomer **10** and by conversion of both isotopomers to their bis(trimethylphosphine) derivatives **17a,b**. NOE experiments on **17a** show a positive interaction between the *endo*-H and PMe_3; this resonance is missing in **17b**. Similarly, **15** reacts with $[Ru(C_5Me_5)Cl]_4$ or $[Ru(C_5Me_5)(MeCN)_3]^+BF_4^-$ to give only a single isotopomeric ruthenocene **9b**, containing no deuterium. Formation of single isotopomers in each reaction excludes any access to a planar metallacyclohexadiene, or any species with a symmetry plane bisecting the CHD group, as an intermediate or transition state along the reaction pathway. Internally consistent mechanisms for formation of the six- and five-membered rings are proposed to account for the stereochemical features of these and related reactions. Analogies are drawn between these reactions and those pathways proposed for the synthetically useful Dötz reaction for the synthesis of five- and six-membered organic rings.

Introduction

Numerous examples of the ring expansion of 3-vinyl-1-cyclopropenes to give five- and six-membered rings exist in the literature. Initial observations of thermal and photochemical formation of cyclopentadienes and indenes from vinylcyclopropenes[2] were followed by transition metal mediated preparation of cyclopentadienes and cyclopentadienyl complexes[3-8] and, with incorporation of a molecule of CO, phenols and cyclohexadienones.[9,10] The reaction manifold leading to these organic rings is similar to the synthetically useful Dötz reaction, in which five- and six-membered rings are formed from alkynes and group 6 Fischer carbene complexes.[11] A mechanism for the generic Dötz reaction is shown in Scheme 1.[11b] The unsaturated group bound to the carbene center can be a vinyl group, as shown, in which case monocyclic products are obtained, or part of a phenyl ring, leading eventually to benzannulated products. The first carbon–carbon bond-forming step is thought to involve formation of metallacyclobutene **1a** or the valence isomeric vinylcarbene **1b**; calculations favor the latter.[12] At this stage the choice of ring size is made. Incorporation of CO can occur, in a reaction which is known for vinylcarbene complexes, to afford a vinylketene intermediate **2** which can then cyclize to give a cyclohexadienone complex. Tautomerization and decomplexation from the metal center eventually affords a phenolic ring system.[13] However, a number of potentially significant equilibria involving intermediates **1a** and **1b** are possible. These may precede CO incorporation or may divert the reaction along another pathway to give a cyclopentadiene-based ring system. Coordination of the vinyl group of **1a** or **1b** affords intermediates

† E-mail address: RPH@DARTMOUTH.EDU.

⊗ Abstract published in *Advance ACS Abstracts,* August 15, 1995.

(1) American Chemical Society, Division of Organic Chemistry Fellow, 1990–1991; sponsored by the American Cyanamid Co.

(2) Padwa, A. *Org. Photochem.* **1979**, *4*, 261–326 and references therein. Breslow, R. In *Molecular Rearrangements*; (de Mayo, P., Ed.; Wiley: New York, 1963; Part 1, p 236. Zimmerman, H. E.; Hovey, M.C. *J. Org. Chem.* **1979**, *44*, 2331–2345. Zimmerman, H. E.; Kreil, K. J. *J. Org. Chem.* **1982**, *47*, 2060–2075. Zimmerman, H. E.; Fleming, S. A. *J. Org. Chem.* **1985**, *50*, 2539–2551.

(3) Grabowski, N. A.; Hughes, R. P.; Jaynes, B. S.; Rheingold, A. L. *J. Chem. Soc., Chem. Commun.* **1986**, 1694–1695.

(4) Egan, J. W., Jr.; Hughes, R. P.; Rheingold, A. L. *Organometallics* **1987**, *6*, 1578.

(5) Donovan, B. T.; Egan, J. W., Jr.; Hughes, R. P.; Spara, P. P.; Trujillo, H. A.; Rheingold, A. L. *Isr. J. Chem.* **1990**, *30*, 351.

(6) Hughes, R. P.; Robinson, D. J. *Organometallics* **1989**, *8*, 1015.

(7) Donovan, B. T.; Hughes, R. P.; Trujillo, H. A. *J. Am. Chem. Soc.* **1990**, *112*, 7076.

(8) Donovan, B. T.; Hughes, R. P.; Kowalski, A. S.; Trujillo, H. A.; Rheingold, A. L. *Organometallics* **1993**, *12*, 1038.

(9) Semmelhack, M. F.; Ho, S.; Steigerwald, M.; Lee, M. C. *J. Am. Chem. Soc.* **1987**, *109*, 4397. Semmelhack, M. F.; Ho, S.; Cohen, D.; Steigerwald, M.; Lee, M. C.; Lee, G.; Gilbert, A. M.; Wulff, W. D.; Ball, R. G. *J. Am. Chem. Soc.* **1994**, *116*, 7108.

(10) Cho, S. H.; Liebeskind L. S. *J. Org. Chem.* **1987**, *52*, 2631.

(11) (a) Dötz, K. H. *Angew. Chem., Int. Ed. Engl.* **1984**, *23*, 587. For a detailed discussion, and leading references, see: Bos, M. E.; Wulff, W. D.; Miller, R. A.; Chamberlin, S.; Brandvold, T. A. *J. Am. Chem. Soc.* **1991**, *113*, 9293. Other recent references include: Harvey, D. F.; Grenzer, E. M.; Gantzel, P. K. *J. Am. Chem. Soc.* **1994**, *116*, 6719. Barluenga, J.; Aznar, F.; Martín, A.; García-Granda, S.; Pérez-Carreno, E. *J. Am. Chem. Soc.* **1994**, *116*, 11191. Gross, M. F.; Finn, M. G. *J. Am. Chem. Soc.* **1994**, *116*, 10921. (b) For recent detailed mechanistic discussion see: Wulff, W. D.; Bax, B. M.; Brandvold, T. A.; Chan, K. S.; Gilbert, A. M.; Hsung, R. P.; Mitchell, J.; Clardy, J. *Organometallics* **1994**, *13*, 102.

(12) For calculations on metallacyclobutene and vinylcarbene isomers, see: Hofmann, P.; Hämmerle, M.; Unfied, G. *New J. Chem.* **1991**, *15*, 769.

(13) A nontautomerized cyclohexadienone complex has recently been isolated.[11b]

0276-7333/95/2314-4319$09.00/0

Scheme 1

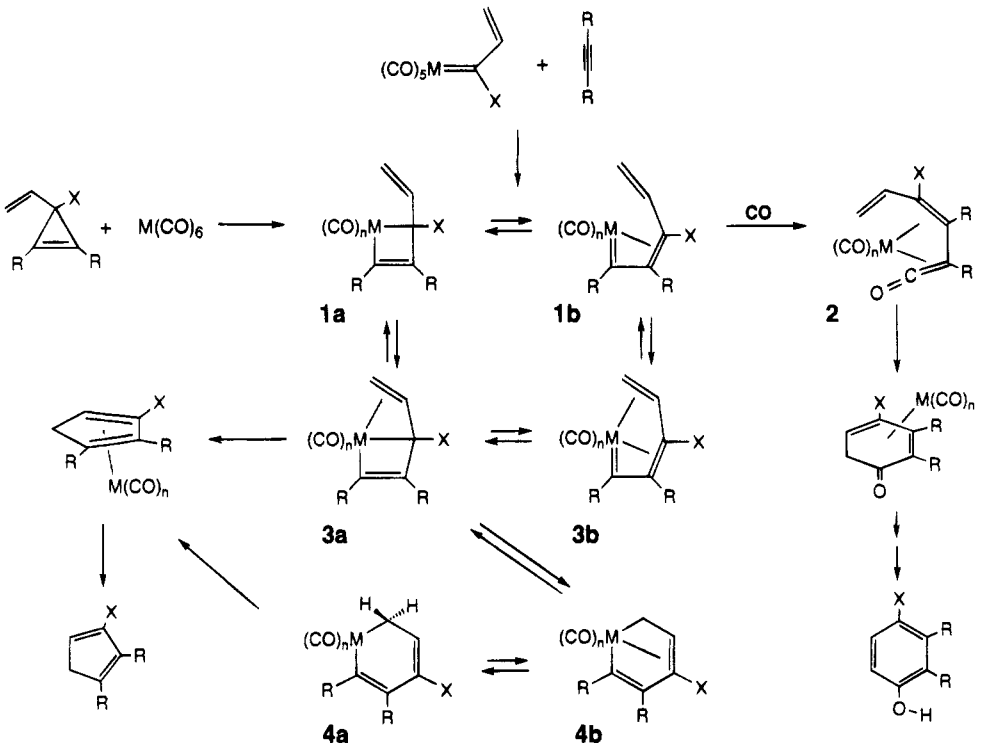

Scheme 2

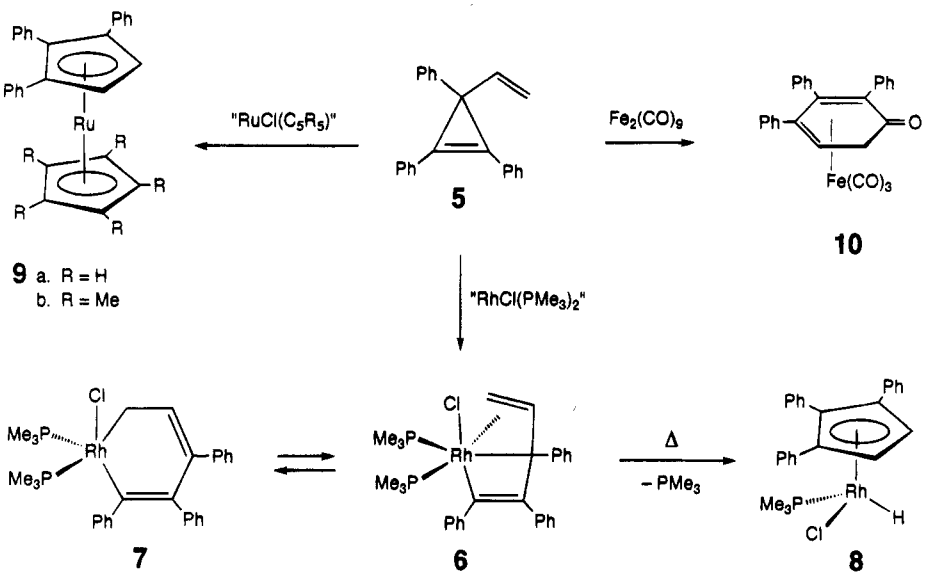

3a and **3b**. From **3a**, the metallacyclohexadiene intermediate **4a** can be accessed as shown, and formation of five-membered rings from such an intermediate is often shown as a direct coupling of the sp^3 and sp^2 carbon centers.

While the usual route into the Dötz reaction involves initial carbon–carbon bond formation from the metal–carbene complex and the alkyne, an alternative entry into the same reaction manifold can be afforded by direct reaction of a 3-vinyl-1-cyclopropene as shown in Scheme 1.[9,14] In our studies of the reactions of vinylcyclopropenes with transition metal centers, we have been have been able to isolate species with structures analogous to suggested intermediates in the Dötz reaction and to study their chemistry.[3–8] Some representative reactions of triphenylvinylcyclopropene **5** with transition metal centers are shown in Scheme 2. Reaction of **5** with the [$RhCl(PMe_3)_2$] fragment affords the pentadienediyl complex **6**, structurally analogous to intermediate **3a**; variable-temperature NMR studies show unambiguously that, while **6** is the ground state structure, it is in rapid equilibrium with the metallacyclohexadiene species **7** on the NMR time scale and can be converted to an acetylacetonato analogue containing a stable metallacyclohexadiene ring.[4] On heating, **6** loses PMe_3 and presumably undergoes cyclization to a cyclopentadiene ligand followed by *endo*-H migration to the metal to give **8**. A similar reaction is observed on reaction of **5** with the [$RuCl(C_5R_5)$] frag-

(14) The Dötz reaction manifold can be entered at a variety of other points. See: Huffman, M. A.; Liebeskind, L. S.; Pennington, W. T. *Organometallics*, **1992**, *11*, 255.

Scheme 3

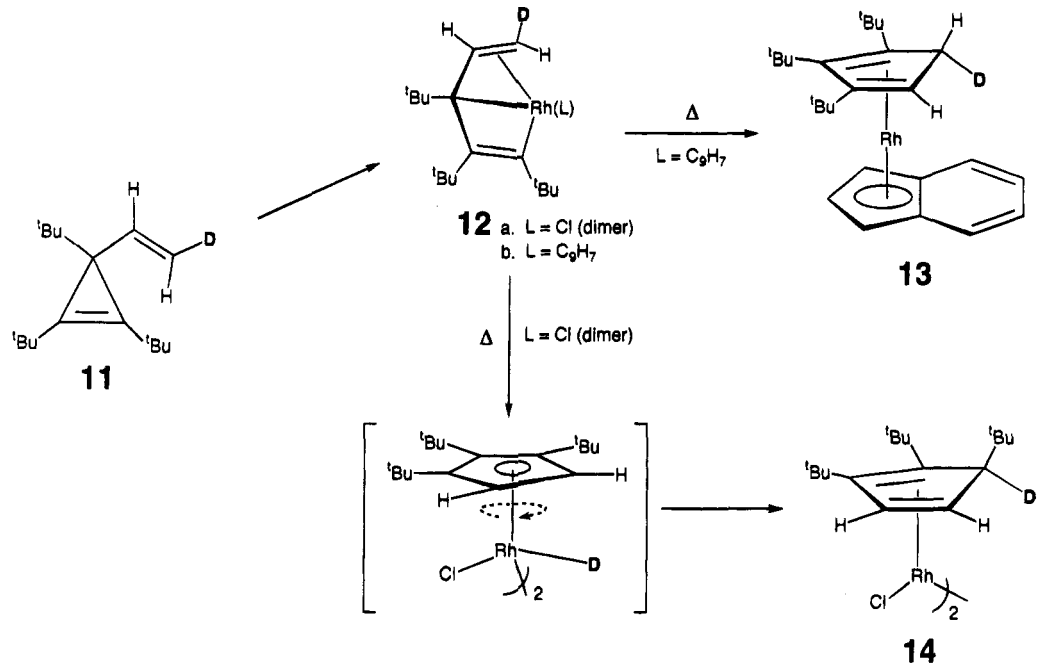

ments (R = H, Me), although fewer intermediates are observed.[6] These reactions afford complexes **9** presumably via a sequence of events analogous to those in the formation of **8** except that eventual elimination of HCl from the metal occurs to give the very stable ruthenocene structure. The reaction of **5** with $[Fe_2(CO)_9]$ affords only an η^4-cyclohexadienone complex **10**, the product of CO incorporation;[3] Semmelhack has shown that the same vinylcyclopropene reacts with $[Mo(CO)_6]$ to afford triphenylphenol via analogous chemistry.[9,14] Therefore, these transition metal promoted reactions of vinylcyclopropenes provide reasonable model systems for the formation of five- and six-membered rings in the Dötz reaction and afford opportunities to evaluate possible mechanisms for ring formation in the latter. Notably because the organic ring remains ligated to the metal, these reactions afford an opportunity to probe the stereochemistry of the ring formation reaction, unlike the Dötz reaction itself, in which any stereochemical information may be lost by decomplexation and tautomerization of the organic product.[11,13]

In order to probe whether a metallacyclohexadiene intermediate was necessarily required for cyclopentadiene ring formation, we previously investigated the reactions of the selectively deuterium-labeled tri-*tert*-butylvinylcyclopropene **11** with Rh(I) species, as shown in Scheme 3. The reaction of **11** with $[RhCl(C_2H_4)_2]_2$ afforded the dimeric pentadienediyl complex **12a**, in which the deuterium is exclusively in the *syn*-position shown. Isomerization to the *anti*-D isotopomer is extremely slow, providing an unambiguous demonstration that a planar metallacyclohexadiene analogous to **7** (or **4a**) is a very high energy intermediate in this system.[5] The major contribution to the instability of this particular metallacyclohexadiene arises from the steric problems associated with locating three *tert*-butyl groups on contiguous carbon atoms in a planar six-membered ring. Complex **12a** was converted to its mononuclear indenyl analogue **12b** without scrambling of deuterium. On heating of **12b**, the cyclopentadiene complex **13** was formed, with D exclusively in the *endo*-position, showing that the ring closure to give the cyclopentadiene neither requires nor even samples a planar metallacyclohexadiene intermediate.[7] Corresponding heating of the dimeric complex **12a** affords the rearranged cyclopentadiene complex **14**, by analogous closure of the ring to give *endo*-D followed by migration of D to the 16-electron Rh center and back to the ring, as shown;[8] this latter pathway is blocked in the corresponding 18-electron complex **13**.[7] These stereochemical results indicate that ring closure is probably best considered to occur by intramolecular addition of the Rh–C σ-bond to the Rh–olefin bond[7] and that simple reductive coupling from a metallacyclohexadiene is rigorously excluded in this sterically biased system.

Clearly the reactions involving **11** are sterically biased enough to completely exclude access to a metallacyclohexadiene intermediate and demonstrate that such a species is not necessary for formation of a five-membered ring. These results do not exclude metallacyclohexadienes as accessible intermediates in less biased systems, as demonstrated by the facility with which the rhodium complex **6** accesses metallacyclohexadiene **7** on the NMR time scale.[4] We now report the results of a similar mechanistic interrogation of the other reactions represented in Scheme 2 to see whether metallacyclohexadienes were sampled along reaction pathways that afford cyclopentadienyl or cyclohexadienone ligands.

Results and Discussion

In order to test for the presence of planar metallacyclohexadiene intermediates in these reactions, the selectively deuterated 1,2,3-triphenyl-3-vinyl-1-vinylcyclopropene (**15**) was required. Attempts to prepare this compound in a manner analogous to that used for the preparation of **11**,[5] by coupling of the triphenylcyclopropenyl cation with *trans*-(CHD=CHLi), failed. However, *in situ* conversion of the vinyllithium reagent to its magnesium analogue using $MgBr_2$, followed by coupling of the resultant *trans*-(CHD=CHMgBr) with

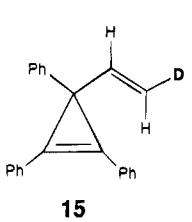

15

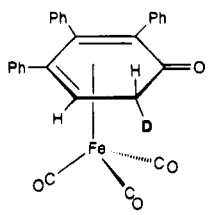

16

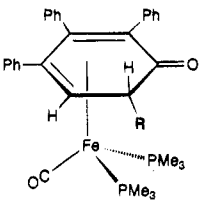

17 a. R = H
b. R = D

the triphenylcyclopropenyl cation, afforded the required **15** in 50% yield.[15] The ^1H and $^2H\{^1H\}$ NMR spectra of this compound confirm that the deuterium is located exclusively in the position shown.

Treatment of *trans*-deuterated vinylcyclopropene **15** with $[Fe_2(CO)_9]$ afforded the single *endo*-deuterated isotopomer **16**. The location of the deuterium on the *endo* face of the cyclohexadienone ring in **16** is indicated by the following observations. Faller has noted that vicinal ^1H NMR coupling constants are a reliable means to assign the resonances of the *exo*- and *endo*-hydrogens of a CH_2 group in coordinated cyclohexadienes and cyclopentadienes: the pucker of the coordinated ring reduces the vicinal coupling to the *exo* hydrogen in a Karplus fashion, while the coupling to the *endo* hydrogen is increased.[16] Examination of the vicinal coupling constants to the two geminal protons of **10** and **16** (Table 1) indicates that the resonance which disappears on deuteration is *endo*. To confirm this assignment, both isotopomers **10** and **16** were converted to the corresponding bis(trimethylphosphine) derivatives **17a,b**. Although the vicinal proton coupling constants for the *exo*- and *endo*-hydrogens of **17a** did not differ significantly from those in **10**, the observation of phosphorus–hydrogen coupling to only one geminal proton identified that proton as H_{exo};[17] comparison with the corresponding spectrum of **17b** illustrates that, in this complex, deuteration is observed in the position lacking an observable J_{HP}, i.e. the *endo* position. Finally, the NOE difference spectrum of **17a** showed an interaction between the methyl groups of a phosphine and only one of the geminal hydrogens, identifying its resonance as that for H_{endo}; this is the resonance missing in the spectrum of **17b**. The combined evidence of these NMR studies unambiguously locates the deuterium in the *endo* position of **16** as shown.

Since any reaction pathway involving a metallacyclohexadiene, or indeed any other species in which a plane of symmetry bisects the CHD group, must result in scrambling of the deuterium label between *exo* and *endo* positions in the final cyclohexadienone ring, observation of only one product isotopomer clearly demonstrates that none of the pathways to CO incorporation and subsequent ring closure can sample such a symmetric intermediate or transition state. With this constraint in mind, a reasonable mechanism is shown in Scheme 4. Insertion of the metal into the cyclopropene ring affords metallacyclobutene intermediate **18a**, which may be in equilibrium with its vinylcarbene valence tautomer **18b**. Incorporation of CO via an insertion reaction of **18a** affords the corresponding species **19a**. It is straightforward to envisage ring closure from **19a** by migratory insertion reaction of the iron–acyl bond to the coordinated deuteriovinyl group as shown. In order to maintain orbital overlap, such an insertion must result in the CHD terminus rotating as shown, with the inevitable result that deuterium is located in the *endo*-position of the resultant ring. This provides a pathway for formation of the six-membered ring consistent with that proposed for five-membered cyclopentadiene ring formation in the rhodium-based system shown in Scheme 3.[7,8] An alternative picture

Table 1. Coupling Constants and NOEs to the CH_2 Protons of 10 and 17a

		17a		
	10 $^3J_{HH}$[a]	$^3J_{HH}$[a]	J_{HP}[a]	NOE to PMe_3
endo	4.3[b]	3.7[c]	n.o.[d]	+
exo	1.9	1.8	6.0	n.o.[d]

[a] in Hz. [b] This resonance is absent in the deuterated compound **16**. [c] This resonance is absent in the deuterated compound **17b**. [d] n.o.: not observed.

Scheme 4

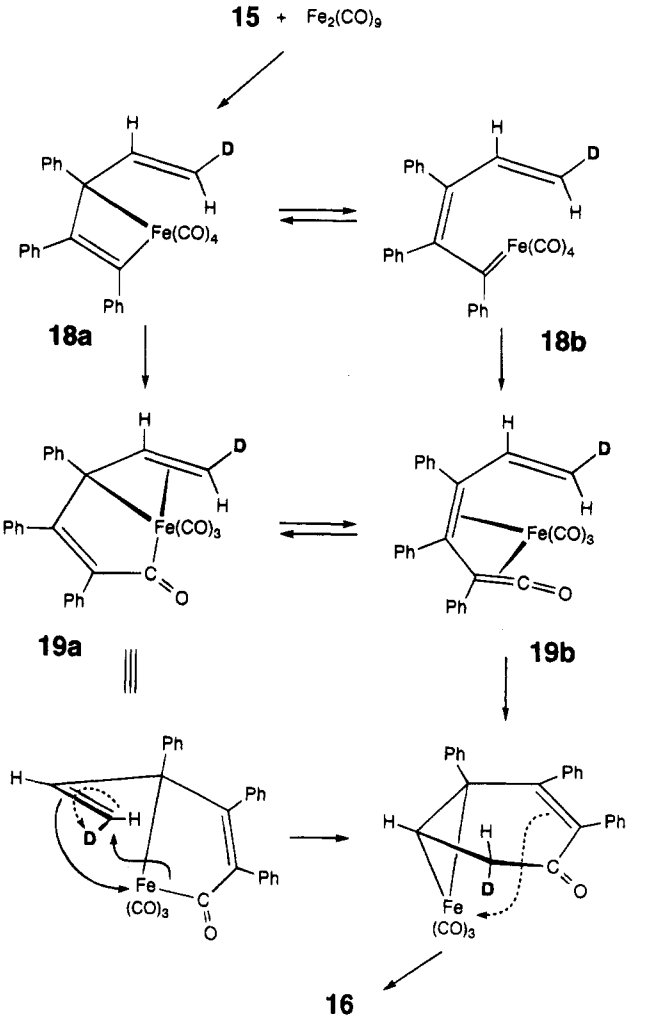

(15) A similar procedure has been used to afford other isotopically labeled vinylcyclopropenes: Hughes, R. P.; Trujillo, H. A.; Rheingold, A. L. *J. Am. Chem. Soc.* **1993**, *115*, 1583.

(16) Faller, J. W. *Inorg. Chem.* **1980**, *19*, 2857. See also: Szajek, L. P.; Shapley, J. R. *Organometallics* **1991**, *10*, 2512. Bailey, N. A.; Blunt, E. H.; Fairhurst, G.; White, C. *J. Chem. Soc., Dalton Trans.* **1980**, 829. Schrock, R. R.; Osborn, J. A. *Inorg. Chem.* **1970**, *9*, 2339. Birch, A. J.; Cross, P. E.; White, D. A. *J. Chem. Soc. A* **1968**, 332. Birch, A. J.; Chamberlain, K. B.; Hass, M. A.; Thompson, D. J. *J. Chem Soc., Perkins Trans.* **1973**, 1882. Birch, A. J.; Chamberlain, K. B.; Thompson, D. J. *J. Chem. Soc., Perkins Trans.* **1973**, 1900.

(17) Indirect J_{HP} couplings appear to have a strong dependence on bond angles. See, for example, ref 15 and: Mavel, G. *Annu. Rep. NMR Spectrosc.* **1973**, *5B*, 30.

Scheme 5

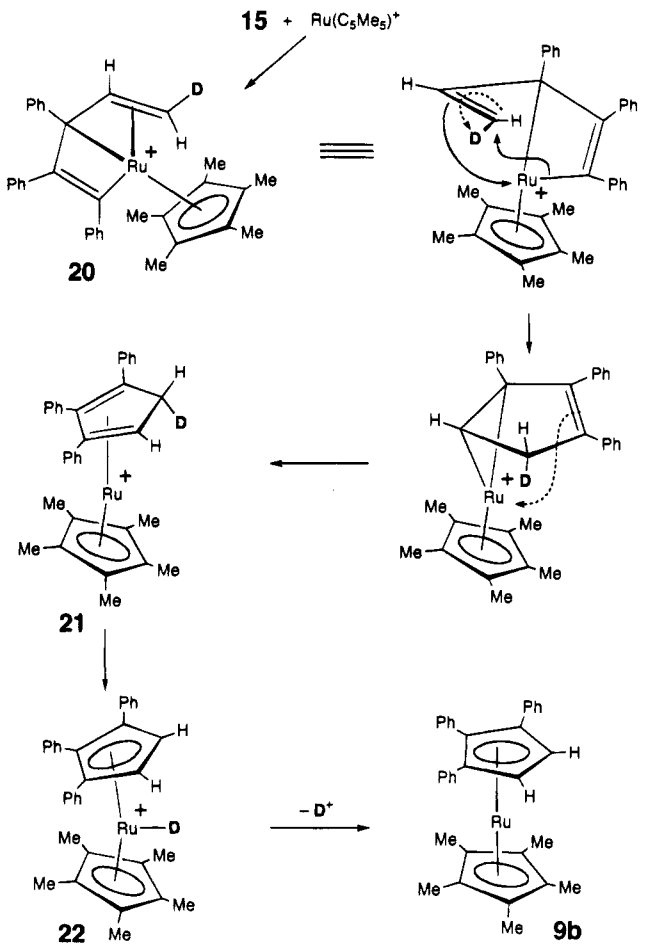

of the ring closing step derives from consideration of a butadienylcarbene intermediate **18b**;[11] CO insertion would afford **19b**, electrocyclic closure of which would also have to be stereospecific with rotation of the CHD group of the uncoordinated olefin in the same sense required to give *endo*-deuterium. Such a pathway is not available for the five-membered ring formation discussed above or that encountered in the system discussed below.

We next treated **15** with two different sources of the $[Ru(C_5Me_5)]^+$ fragment, the tetrameric $[RuCl(C_5Me_5)]_4$ and the monomeric $[Ru(C_5Me_5)(MeCN)_3]^+$. In each case the product obtained was the previously characterized ruthenocene **9b**[6] in which no trace of deuterium above natural abundance was observed by $^2H\{^1H\}$ NMR spectroscopy. The proposed mechanism is shown in Scheme 5. Ring closure from intermediate **20** to give **21** places deuterium selectively in the *endo*-position, from which it can transfer to ruthenium to give **22**, and thence be eliminated as D^+. This pathway is stereochemically consistent with all the previous examples in rhodium[7,8] and iron (*vide supra*) based chemistry. We specifically discount the possibility that a different stereochemistry for ring closure occurs to give the *exo*-D isotopomer of **21** followed by loss of *exo*-D^+. Such a pathway would violate the principle of microscopic reversibility; reversible protonation of ruthenocene has been shown unambiguously to occur, not via *exo*-attack at a cyclopentadienyl ring but exclusively at the ruthenium center with no subsequent transfer from protonated ruthenium to a cyclopentadienyl ring.[18]

These results delineate a consistent picture of the stereochemistry of this kind of ring closure reaction by excluding planar metallacyclohexadiene intermediates *en route* to formation of either five- or six-membered organic rings. By analogy, they demonstrate unambiguously that such intermediates are not required in the Dötz reaction. Taken in conjunction with previous results,[7,8] they also suggest that reductive elimination or coupling reactions involving allylic ligands occur from the η^3-allylic form rather than from the η^1-allylic isomer.

Experimental Section

General Procedures. All reactions were performed in oven-dried glassware, using standard Schlenk techniques, under an atmosphere of nitrogen which had been deoxygenated over BASF catalyst and dried over Aquasorb. Hydrocarbon reaction solvents and ether were distilled under nitrogen from benzophenone ketyl; halogenated solvents were distilled from 4 Å molecular sieves. Aromatic and unsaturated components of 35–65 °C petroleum ether were removed before distillation by prolonged standing over H_2SO_4 (concentrated) followed by washing with Na_2CO_3 (10% aqueous). ^1H (300 MHz), $^2H\{^1H\}$ (46.1 MHz), $^{13}C\{^1H\}$ (75.4 MHz), and $^{31}P\{^1H\}$ (121 MHz) NMR spectra were recorded on a Varian XL-300 Spectrometer at 25 °C. Chemical shifts are reported as ppm downfield of either TMS (^1H, ^2H, and ^{13}C NMR, referenced to the solvent) or external 85% H_3PO_4 (^{31}P NMR). Coupling constants are reported in Hz. IR spectra were recorded on a Bio-Rad Digilab FTS-40 Fourier transform infrared spectrophotometer. Melting points of samples in capillaries sealed under vacuum were obtained using an Electrothermal or a Thomas Hoover device and are uncorrected. Elemental analyses were performed by Spang (Eagle Harbor, MI).

Trimethylphosphine was purchased from Strem. Deuterioacetic acid was obtained from Aldrich. $[Fe_2(CO)_9]$,[19] triphenylvinylcyclopropene **5**,[20] *trans*-bis(tributylstannyl)ethylene,[21] $[Ru(C_5Me_5)(\mu^3\text{-}Cl)]_4$,[22] $[Ru(C_5Me_5)(NCMe)_3]BF_4$,[23] triphenylcyclopropenyl tetrafluoroborate,[24] and $MgBr_2$/ether complex[25] were prepared by literature routes.

***trans*-3-(β-Deuteriovinyl)-1,2,3-triphenyl-1-cyclopropene, 15.** *n*-Butyl lithium (4.6 mL of 2.81 M hexanes solution, 13 mmol, 1 equiv) was added to a −78 °C solution of *trans*-bis(tributylstannyl)ethylene (7.0 mL, 13 mmol, 1.0 equiv) in THF (90 mL). The resulting pale yellow solution was stirred 1 h at −78 °C and then quenched with DOAc (0.75 mL, 13 mmol, 1 equiv) and warmed to room temperature. The colorless mixture was cooled back to −78 °C and treated with a second equivalent of n-BuLi (4.6 mL, 13 mmol). After being stirred for 1 h at −78 °C, the yellow mixture was treated with $MgBr_2$/ether complex (6.0 mL, 16 mmol, 1.2 equiv) and allowed to warm to room temperature, giving a clear yellow solution. The solution was added to a −78 °C slurry of 1,2,3-triphenylcyclopropenyl bromide (2.26 g, 6.56 mmol, 0.5 equiv) in THF (90 mL), warmed to room temperature, and stirred 8 h to give a pale yellow solution. The reaction was quenched with aqueous ammonium chloride (100 mL, 20%), and the layers were separated. The aqueous layer was extracted with ether

(18) Mueller-Westerhoff, U. T.; Haas, T. J.; Swiegers, G. F.; Leipert, T. K. *J. Organomet. Chem.* **1994**, *472*, 229.
(19) Braye, E. H.; Hübel, W. *Inorg. Synth.* **1966**, *8*, 178.
(20) (a) Padwa, A.; Blacklock, T. J.; Getman, D.; Hatanaka, N.; Loza, R. *J. Org. Chem.* **1978**, *43*, 1481. (b) Zimmerman, H. E.; Aasen, S. M. *J. Org. Chem.* **1978**, *43*, 1493.
(21) (a) Corey, E. J.; Wollenberg, R. H. *J. Org. Chem.* **1975**, *40*, 3788. (b) Bottaro, J. C.; Hanson, R. N.; Seitz, D. E. *J. Org. Chem.* **1981**, *46*, 5221.
(22) Fagan, P. J.; Ward, M. D.; Calabrese, J. C. *J. Am. Chem. Soc.* **1989**, *111*, 1698.
(23) The BF_4 salt was prepared by substituting $AgBF_4$ for AgOTf in Fagan's preparation of the triflate.[22]
(24) Breslow, R.; Chang, H. W. *J. Am. Chem. Soc.* **1961**, *83*, 2367.
(25) Maercker, A.; Roberts, J. D. *J. Am. Chem. Soc.* **1966**, *88*, 1742.

(3 × 50 mL); the combined organic layers were washed with water (3 × 50 mL) and brine (2 × 10 mL). Drying over $MgSO_4$ and evaporation left a yellow oil, which was purified by flash chromatography (SiO_2, 5 × 16 cm). Elution with hexanes (2.5 L) gave Bu_4Sn followed by the desired vinylcyclopropene (1.00 g, 50%) as soapy white crystals after evaporation. ^1H NMR (C_6D_6): δ 6.98–7.68 (m, 15 H, Ph), 6.70 (d, 1H, J = 17.2, H_a), 5.32 (d, 1H, J = 17.3, H_{cis}). $^2H\{^1H\}$ NMR (C_6H_6): δ 5.14 (br, D_{trans}).

[2–5-η-(2,3,4-Triphenyl-2,4-cyclohexadienone)]tricarbonyliron, 10. A suspension of $Fe_2(CO)_9$ (0.70 g, 1.9 mmol, 1.1 equiv) and triphenylvinylcyclopropene **5** (0.50 g, 1.7 mmol) in ether (30 mL) was stirred for 7 h and then filtered through Celite and concentrated. The mixture was applied to a chromatography column (SiO_2, 1.7 × 9 cm, 20 °C) under nitrogen. A yellow band eluted with ether (30 mL) and was evaporated to dryness. Recrystallization of the residue from ether gave **10** (371 mg, 47%) as yellow needles. Mp: 146–149 °C, dec. Calcd for $C_{27}H_{18}FeO_4$: 70.15, C; 3.92, H. Found: 69.98, C; 4.01, H. ^1H NMR ($CDCl_3$): δ 7.0–6.1 (m, 15H, Ph), 3.05 (dd, 1H, J_{HH} = 4.0, 1.8, =C*H*), 2.70 (dd, 1H, J_{HH} = 18.9, 4.0, H_{endo}), 2.30 (dd, 1H, J_{HH} = 18.9, 1.8, H_{exo}). $^{13}C\{^1H\}$ NMR ($CDCl_3$): δ 209.6 (Fe–*C*O), 194.9 (*C*=O), 137.2–126.0 (Ph), 111.2 (CPh), 104.5 (CPh), 84.2 (CPh), 51.4 (*C*H), 36.2 (CH_2). IR (KBr, cm^{-1}): ν_{CO} = 2060 vs, 2005 vs, 1993 vs, 1690 m.

The *endo*-deuterated isotopomer **16** was prepared as described for the protic compound above, using deuterated triphenylvinylcyclopropene **15**. ^1H NMR (C_6D_6): δ 7.02–6.08 (m, 15H, Ph), 3.07 (d, 1H, J_{HH} = 1.9, H_4), 2.29 (br, 1H, H_{exo}). $^2H\{^1H\}$ NMR (C_6D_6): δ 2.66 (br, D_{endo}). IR (CCl_4, cm^{-1}): ν_{CO} = 2060 vs, 2000 vs, 1992 vs, 1683 m.

[2–5-η-(2,3,4-Triphenyl-2,4-cyclohexadienone)]carbonylbis(trimethylphosphine)iron, 17a. A solution of **10** (26 mg, 56 μmol) and trimethylphosphine (23 μL, 0.27 mmol, 5 equiv) in benzene (10 mL) was irradiated for 30 min (Canrad-Hanovia 450 W medium-pressure Hg-arc lamp, Pyrex filter, 10 °C), over which time the yellow solution darkened. The mixture was freeze-dried, dissolved in a minimum of ether, and purified by chromatography (1 × 12 cm SiO_2, under nitrogen, 20 °C). The bis(phosphine) complex eluted with ether (20 mL) as an orange band, which was evaporated to give **17a** (12 mg, 39%). An analytical sample was recrystallized by slow evaporation of ether. Mp: 120 °C, dec 130 °C. Calcd for $C_{31}H_{36}FeO_2P_2$: 66.68, C; 6.50, H. Found: 66.68, C; 6.51, H. ^1H NMR (C_6D_6): δ 6.72–7.71 (m, 15H, Ph), 2.71 (ddd, 1H, J_{HH} = 18.5, 1.8, J_{HP} = 6.0, H_{exo}), 2.52 (dd, 1H, J_{HH} = 18.5, 3.7, H_{endo}), 2.38 (dddd, 1H, J_{HH} = 3.6, 1.8, J_{HP} = 9.6, 0.5, CH), 1.34 (d, 9H, J_{HP} = 7.5, PMe_3), 0.52 (d, 9H, J_{HP} = 8.1, PMe_3). $^{31}P\{^1H\}$ NMR (C_6D_6): δ 25.68 (d, J_{PP} = 22.3, PMe_3), 14.35 (d, J_{PP} = 22.1, PMe_3). IR (CCl_4, cm^{-1}): ν_{CO} = 1890 vs, 1653 m.

The deuterated isotopomer **17b** was prepared similarly from **16** and trimethylphosphine. ^1H NMR: identical to that of the protic material above except for the absence of the δ 2.52 peak and the associated 18.5 and 3.6 Hz couplings. $^2H\{^1H\}$ NMR (C_6D_6): δ 2.52 (br, D_{endo}). $^{31}P\{^1H\}$ NMR (C_6D_6) and IR (ν_{CO}; CCl_4) were identical to those of the protic material above.

(η^5-Pentamethylcyclopentadienyl)(η^5-1,2,3-triphenylcyclopentadienyl)ruthenium, 9b. (a) From [Ru(C_5Me_5)(NCMe)$_3$]BF_4. Triphenylvinylcyclopropene **5** (53 mg, 0.18 mmol, 1.1 equiv) was added to a greenish-yellow solution of [Ru(C_5Me_5)(NCMe)$_3$]BF_4 (73 mg, 0.16 mmol) in CH_2Cl_2 (10 mL) at ambient temperature. The resulting rust-colored solution was stirred overnight, during which time its color faded to amber. The residue left on evaporation was extracted with petroleum ether (3 × 15 mL); evaporation of the yellow extracts left **9b** as a white solid (71 mg, 82%). The ^1H NMR ($CDCl_3$) of the product was identical to that reported in the literature:[6] δ 7.00–7.29 (m, 15H, Ph), 4.62 (s, 2H, H_{Cp}), 1.67 (s, 15 H, Me).

The analogous reaction of deuterated vinylcyclopropene **15** produced an identical product for which no residual deuterium was detectable by ^1H or ^2H NMR.

(b) From [Ru(C_5Me_5)Cl]$_4$. Deuterated **15** (92 mg, 0.31 mmol, 1.0 equiv) was added to a solution of [Ru(C_5Me_5)Cl]$_4$ (84 mg, 0.31 mmol Ru) in CH_2Cl_2 (15 mL). The mixture was stirred overnight and evaporated, and the residue was extracted with petroleum ether. Removal of solvent from the yellow extracts left **9b** as a yellow oil which solidified on the addition of ether and subsequent evaporation (147 mg, 89%). The ^1H NMR spectrum of the product was identical to that prepared from [Ru(C_5Me_5)(NCMe)$_3$]BF_4; no residual deuterium was detected by ^1H or $^2H\{^1H\}$ NMR.

Acknowledgment. We are grateful to the National Science Foundation for generous financial support of this work and to Johnson Matthey Aesar/Alfa for a loan of ruthenium chloride.

OM9503149

Substitution Reactions of a μ-Thioether Ligand in Dinuclear Cyclopentadienylmolybdenum Complexes

D. S. Tucker, S. Dietz, K. G. Parker, V. Carperos, J. Gabay, B. Noll, and M. Rakowski DuBois*

Department of Chemistry and Biochemistry, University of Colorado, Boulder, Colorado 80309

Charles F. Campana

Siemens Industrial Automation, 6300 Enterprise Lane, Madison, Wisconsin 53719

Received February 27, 1995[⊗]

The thermal reaction of the thioether-bridged complex $[(CpMo)_2(S_2CH_2)(\mu\text{-}SMe)(\mu\text{-}SMe_2)]$-OTf (**1**) with electron donors leads to the elimination of dimethyl sulfide and the formation of structures which incorporate new ligands into the dimer. For example, reaction of **1** with excess LiCl results in the formation of $(CpMo)_2(S_2CH_2)(\mu\text{-}SMe)(\mu\text{-}Cl)$ (**2**), which has been isolated and characterized by an X-ray diffraction study. Dimers with μ-bromide and with μ-η^2-alkyne ligands have also been prepared by thioether substitution reactions and characterized spectroscopically. The reaction of **1** with two-electron donors led to the formation of dimers with new terminal ligands of the formula $[(CpMoL)_2(S_2CH_2)(\mu\text{-}SMe)]OTf$ with L = ^{t}BuNC (**6a**), $C_6H_5CH_2NC$ (**6b**), and CO (**7**). The X-ray diffraction study of one isomer of **7** established that the cation contained cis carbonyl ligands and an equatorial configuration for the methanethiolate substituent. The complexes with terminal isocyanide ligands are thermally stable, but the complex with carbon monoxide ligands undergoes ligand exchange reactions at high temperatures. The potential reactivity of the carbon monoxide ligands in **7** with nucleophiles and with oxidants has been explored. For example, the reaction of **7** with Me_3NO in acetonitrile solution results in the loss of one carbonyl ligand and the formation of $[CpMo(CO)(S_2CH_2)(\mu\text{-}SMe)(MeCN)MoCp]OTf$ (**9**), a potential precursor to coordinatively unsaturated complexes.

Introduction

We have recently reported the synthesis of dinuclear cyclopentadienylmolybdenum complexes with a μ-thioether ligand, e.g., $[(CpMo)_2(S_2CH_2)(\mu\text{-}SMe)(\mu\text{-}SMe_2)]OTf$ (**1**).[1] The thioether ligand in **1** is thermally labile, and when the thermolysis in a sealed tube was followed by NMR spectroscopy, evidence for a reversible process was observed (eq 1).

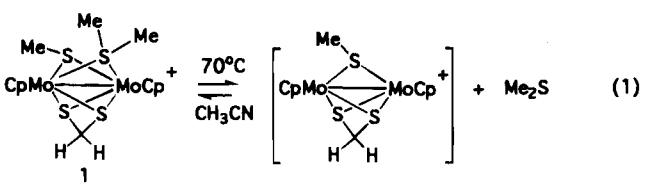

(1)

The three-sulfur product may involve some stabilization by solvent coordination, but this intermediate has not been successfully isolated or characterized. Nevertheless, reaction 1 has been used in the synthesis of new thioether complexes via substitution of the labile bridge with a free dialkyl sulfide. In addition, thermal reactions of **1** with cyclic thioethers have led to a number of desulfurization reactions, as shown in eq 2.[1]

More recently we have extended the ligand substitution chemistry of **1** to synthesize molybdenum complexes which contain new types of ligands in the dinuclear structure. Thermal reactions of **1** with atoms or groups

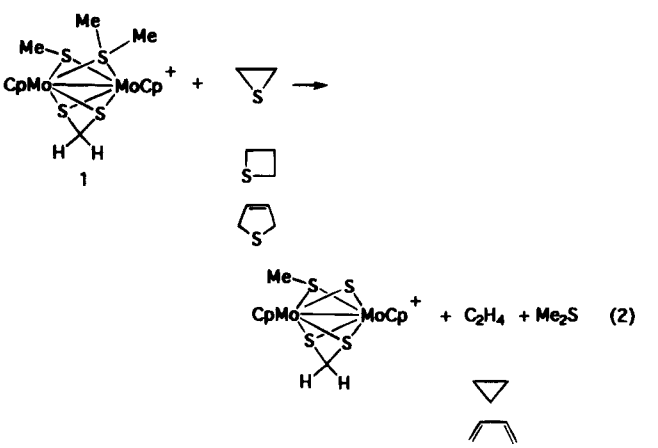

(2)

which can act as four-electron donors lead to products with new bridging ligands, while conventional two-electron donors serve as terminal ligands at each metal center. This paper reports the syntheses and characterizations of several examples of these new derivatives.

Results and Discussion

Synthesis of μ-Halide Derivatives. A chloride anion is similar in size and electronegativity to a thiolate sulfur, and substitution of this halide into the dinuclear molybdenum structure was expected to be facile. The reaction of **1** with excess lithium chloride was carried out in refluxing acetonitrile. Two products were formed in the reaction as shown in eq 3. An analogous reaction was also characterized for the MeCp derivatives.

[⊗] Abstract published in *Advance ACS Abstracts,* August 15, 1995.

(1) Gabay, J.; Dietz, S.; Bernatis, P.; Rakowski DuBois, M. *Organometallics* **1993,** *12,* 3630.

0276-7333/95/2314-4325$09.00/0

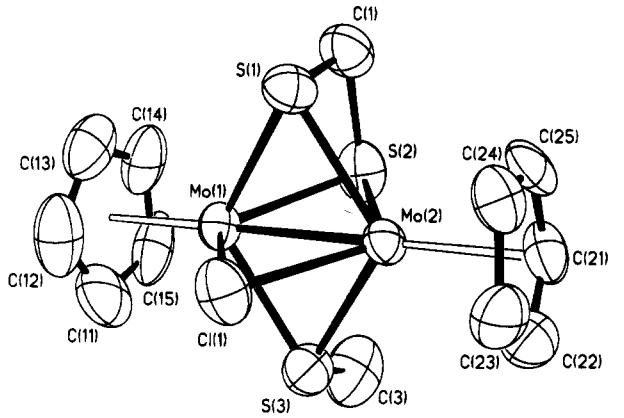

Figure 1. Perspective drawing and numbering scheme for $(CpMo)_2(S_2CH_2)(\mu\text{-}SMe)(\mu\text{-}Cl)$ (**2**). Thermal ellipsoids are shown at the 50% probability level.

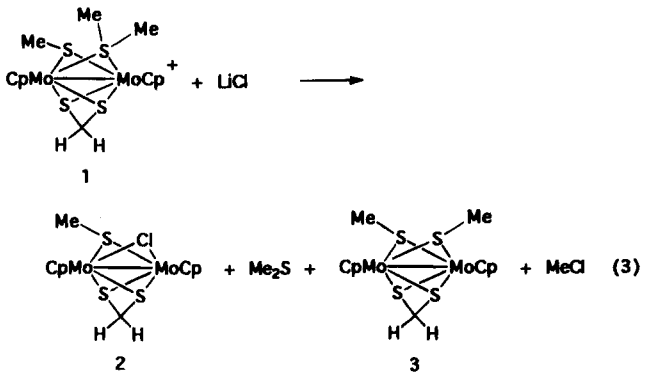

The chloride-bridged derivative **2** was the major product, but approximately 20% of the material was converted to the neutral bis(thiolate) derivative, which has been prepared previously.[2] Methyl chloride is presumably a byproduct in the formation of the bis(thiolate) product, but efforts to detect this volatile species were not made. The demethylation of **1** by nucleophiles has been characterized previously, however. For example, reaction of **1** with cyanide ion in DMSO was found to produce **3** and acetonitrile.[1]

The neutral complexes **2** and **3** were difficult to separate, but **2** could be isolated in pure form as dark green crystals by recrystallization at low temperatures. The mass spectrum of **2** was consistent with the proposed formulation, and the ^1H NMR spectrum suggested that the single chloride ligand occupied a symmetrical bridging position. Two isomers of the product were apparent in the spectrum, and these are attributed to slow inversion at the thiolate sulfur. A single crystal was isolated from a hexane/CH_2Cl_2 solution and characterized by an X-ray diffraction study. Two molecules were observed per asymmetric unit. The structural features were very similar, and an Ortep plot of one of the molecules is shown in Figure 1. Selected bond distances and angles are given in Table 1 and positional parameters in Table 2. The product contains a molecular (but not a crystallographic) plane of symmetry perpendicular to the metal-metal vector with the chloride and three thiolate sulfur bridges lying in this plane. The average Mo–S thiolate bond distance, 2.439(4) Å, is very similar to those observed for the neutral bis(thiolate) analogue **3**.[2] The average Mo–Cl distance of 2.495(4) Å is slightly longer than the Mo–S bonds, but the value is similar to the Mo–Cl distance of 2.484(1) Å reported for the related Mo(III) dimer $[R\text{–}CpMo(\mu\text{-}Cl)_2]_2$.[3] The longer M–Cl distance results in an average Mo–Cl–Mo angle of 63.08(10)° in **2**, compared to the average Mo–S–Mo angle of 64.70(11)°.

The redox properties of **2** were studied by cyclic voltammetry. Complex **2** was found to undergo a reversible oxidation at −0.29 V vs Fc (ΔE_p = 80 mV) and a second well defined quasi-reversible oxidation at +0.32 V vs Cp_2Fe (ΔE = 140 mV). The facile two-

Table 1. Selected Bond Distances and Angles for $(CpMo)_2(S_2CH_2)(\mu\text{-}SCH_3)(\mu\text{-}Cl)$ (2)

Distances (Å)			
Mo(1)–Mo(2)	2.610(2)	Mo(2)–S(1)	2.450(4)
Mo(1)–S(2)	2.435(4)	Mo(2)–S(2)	2.415(4)
Mo(1)–Cl(1)	2.508(4)	Mo(2)–S(3)	2.447(4)
Mo(1)–S(1)	2.462(4)	Mo(2)–Cl(1)	2.504(4)
Mo(1)–S(3)	2.411(4)	S(2)–C(1)	1.91(2)
S(1)–C(1)	1.77(2)	S(3)–C(3)	1.79(2)
Angles (deg)			
Mo(1)–S(1)–Mo(2)	64.18(11)	Mo(1)–S(1)–C(1)	93.9(6)
Mo(1)–S(2)–Mo(2)	65.11(12)	Mo(2)–S(1)–C(1)	93.7(6)
Mo(1)–S(3)–Mo(2)	64.99(11)	Mo(1)–S(2)–C(1)	91.5(5)
Mo(1)–Cl(1)–Mo(2)	62.77(10)	Mo(2)–S(2)–C(1)	91.5(5)
Mo(1)–S(3)–C(3)	108.0(7)	Mo(2)–S(3)–C(3)	111.2(7)

Table 2. Atomic Coordinates ($\times 10^4$) and Equivalent Isotropic Displacement Parameters ($Å^2 \times 10^3$) for $C_{12}H_{15}S_3ClMo_2$ (2)

	x	y	z	U_{eq}[a]
Mo(1)	1149(1)	1750(1)	4714(1)	42(1)
Mo(2)	200(1)	3158(1)	3879(1)	40(1)
Mo(3)	6297(1)	1550(1)	1535(1)	38(1)
Mo(4)	5107(1)	1066(1)	2577(1)	44(1)
S(1)	−26(3)	1529(3)	3345(3)	52(1)
S(2)	1618(3)	2495(3)	3431(3)	64(1)
S(3)	1362(3)	3351(3)	5248(3)	58(1)
S(5)	5065(3)	329(3)	1153(3)	52(1)
S(6)	6749(3)	450(3)	2737(3)	61(1)
S(7)	6368(3)	2271(3)	2993(2)	49(1)
Cl(1)	−429(3)	2296(3)	5078(3)	61(1)
Cl(2)	4702(3)	2333(3)	1462(3)	62(1)
C(1)	854(13)	1627(12)	2656(11)	68(5)
C(2)	7242(11)	1412(11)	3525(10)	61(5)
C(3)	2500(13)	3769(15)	5034(14)	97(7)
C(4)	5538(12)	−821(11)	1276(11)	66(5)
C(11)	2057(20)	1184(17)	5981(14)	97(7)
C(12)	1297(16)	523(16)	5735(16)	90(7)
C(13)	1384(14)	158(13)	4915(15)	78(6)
C(14)	2172(15)	551(13)	4697(15)	82(6)
C(15)	2588(13)	1206(14)	5354(16)	82(6)
C(21)	291(12)	4444(12)	3031(11)	61(5)
C(22)	−72(12)	4785(13)	3755(12)	65(5)
C(23)	−931(14)	4363(12)	3792(12)	70(5)
C(24)	−1172(12)	3709(12)	3056(11)	62(5)
C(25)	−427(12)	3794(12)	2586(10)	57(4)
C(31)	7795(13)	1967(13)	1416(11)	66(5)
C(32)	7608(11)	1143(12)	916(10)	51(4)
C(33)	6867(12)	1327(13)	202(11)	60(4)
C(34)	6628(14)	2270(15)	273(11)	76(6)
C(35)	7176(15)	2675(13)	1026(12)	73(5)
C(41)	4191(18)	1426(16)	3583(18)	97(7)
C(42)	4872(16)	746(17)	3960(12)	82(6)
C(43)	4631(17)	−52(14)	3461(17)	91(7)
C(44)	3859(19)	108(20)	2837(16)	100(7)
C(45)	3582(18)	990(24)	2906(19)	118(8)

[a] U_{eq} is defined as one-third of the trace of the orthogonalized U_{ij} tensor.

(2) McKenna, M.; Wright, L. L.; Miller, D. J.; Tanner, L.; Haltiwanger, R. C.; Rakowski DuBois, M. *J. Am. Chem. Soc.* **1983**, *105*, 5329.

(3) Green, M. L. H.; Izquierdo, A.; Martin-Polo, J. J.; Mtetwa, V. S. B.; Prout, K. *J. Chem. Soc., Chem. Commun.* **1983**, 538.

electron-oxidation behavior is similar to that of the series of neutral Mo(III) dimers which contain four-bridging thiolate ligands.[4] For example, under similar conditions oxidation waves were observed for **3** at −0.36 V (ΔE_p = 90 mV) and at +0.35 V (ΔE_p = 100 mV) vs Cp_2Fe. The one-electron-oxidation product of **2**, $[(CpMo)_2(S_2CH_2)(\mu\text{-SMe})(\mu\text{-Cl})]OTf$, could be isolated as a purple solid from the reaction of **2** with 1 equiv of silver triflate. The FAB^+ mass spectrum showed envelopes at *m/e* values identical with those observed in the EI spectrum of **2**. We were curious whether the mixed-valence derivative might show enhanced lability in ligand substitution reactions, but a reaction with $LiNEt_2$, for example, resulted in rapid electron transfer and regeneration of **2**.

Ligand substitution reactions have been observed for **2** under thermal conditions. For example, **2** reacted with excess LiBr in refluxing acetonitrile to form $(CpMo)_2(S_2CH_2)(\mu\text{-SMe})(\mu\text{-Br})$ (**4**) (eq 4). ^1H NMR reso-

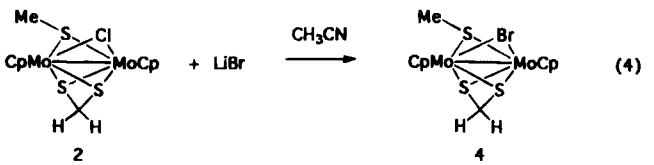

2 4 (4)

nances for two isomers of **4** are slightly shifted relative to those of **2**, and the reaction could therefore be monitored spectroscopically. The substitution reaction proceeded slowly, and 86% conversion was observed after 6 days. The mechanism of this rather unusual μ-halide substitution reaction has not been established, but preliminary studies with other solvents suggest that acetonitrile greatly facilitates the reaction. More detailed mechanistic studies are planned. Product **4** could also be prepared by the reaction of **1** with LiBr.

Reactions of 1 with Alkynes. New organometallic derivatives of the molybdenum dimers have been prepared by the thermal reaction of **1** with unsaturated carbon ligands. For example, the reactions of **1** with alkynes (1-butyne, phenylacetylene) were carried out in acetonitrile at elevated temperatures to form new derivatives of the formula $[(CpMo)_2(S_2CH_2)(\mu\text{-SMe})(\mu\text{-}\eta^2\text{-HCCR})]OTf$ (**5a,b**) (eq 5).

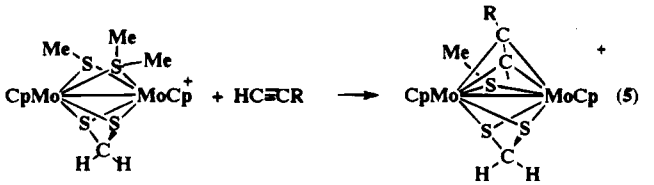

(5)

5a: R = Et
5b: R = Phenyl

The alkyne ligand in **5** is proposed to act as a η^2 bridging unit that donates two electrons to each molybdenum ion. The proposed structure is consistent with the ^1H NMR data, which indicate that the products contain equivalent cyclopentadienyl ligands and equivalent hydrogens in the methanedithiolate ligand. The resulting structure can be formulated as a dimer of molybdenum(III) ions with an 18e count at each metal center. Evidence is observed in the spectra for two noninterconverting isomers of each product. At least two isomers are expected, since the two possible orientations of the alkyne substituent will not be equivalent with respect to the methanethiolate ligand. Formation of additional isomers resulting from inversion at the methanethiolate sulfur may be sterically hindered in this product.

The proposed bonding mode of the alkyne ligand in **5** is similar to the dimetallotetrahedrane structure characterized for the lower valent molybdenum carbonyl derivatives $[CpMo(\mu\text{-RCCR})(CO)_2]_2$.[5] These derivatives have been found to undergo alkyne exchange at temperatures >120 °C and slow alkyne hydrogenation at similar temperatures. CO dissociation was proposed to be an initial step in these reactions.[6] Alkyne coupling reactions have also been characterized for the carbonyl derivatives under more rigorous thermal (130−160 °C) or photochemical conditions.[7] The alkyne-bridged products **5**, described here, do not have the CO dissociation pathway available for generation of a vacant coordination site. Complex **5b** has been found to be stable in acetonitrile solution under hydrogen pressure up to temperatures of 150 °C.

Reactions of 1 with Two Electron Donors. The reactions of **1** with two-electron-donor ligands have also been investigated. For example, thermolysis of **1** in the presence of excess isocyanide leads to the formation of a new type of structure which contains two terminal 2e donors and three bridging thiolates, **6a,b** (eq 6).

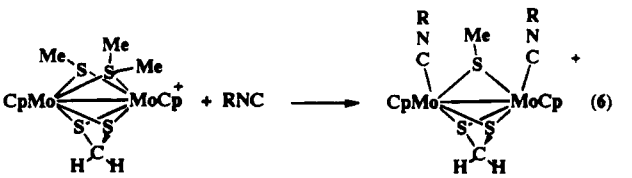

(6)

6a: R = t-Bu
6b: R = Benzyl

Compounds **6** have been isolated in analytically pure form and characterized spectroscopically. In the infrared spectrum of **6a,** the strong C=N stretch observed at 2108 cm^{-1} is consistent with a terminal bonding mode for the RNC ligands. For this derivative only a single isomer with equivalent Cp and isocyanide ligands is observed in the NMR spectrum. A cis arrangement of the isocyanide and Cp ligands is consistent with the observed NMR symmetry. In contrast, two isomers are observed in the NMR spectrum of the benzyl isocyanide derivative **6b**. These may correspond to cis and trans isomers, but two isomers that differ only in the orientations of the thiolate methyl group are also possible. The Mo(III) isocyanide complexes are stable in air and show no evidence of terminal ligand dissociation at temperatures up to 115 °C.

A similar structure with terminal carbonyl ligands was produced when **1** was reacted with CO (150 psi) at

(4) Casewit, C. J.; Haltiwanger, R. C.; Noordik, J.; Rakowski DuBois, M. *Organometallics* **1985**, *4*, 119.

(5) (a) Barley, W. I., Jr.; Chisholm, M. H.; Cotton, F. A.; Rankel, L. A. *J. Am. Chem. Soc.* **1978**, *100*, 5764. (b) Klingler, R. J.; Butler, W.; Curtis, M. D. *J. Am. Chem. Soc.* **1975**, *97*, 3535.

(6) Slater, S.; Muetterties, E. L. *Inorg. Chem.* **1980**, *19*, 3337.

(7) (a) Knox, S. A. R.; Stansfield, R. F. D.; Stone, F. G. A.; Winter, M. J.; Woodward, P. *J. Chem. Soc., Dalton Trans.* **1982**, 173. (b) Curtis, M. D. *Polyhedron* **1987**, *6*, 759 and references therein. (c) Winter, M. J. *Adv. Organomet. Chem.* **1989**, *29*, 101 and references therein.

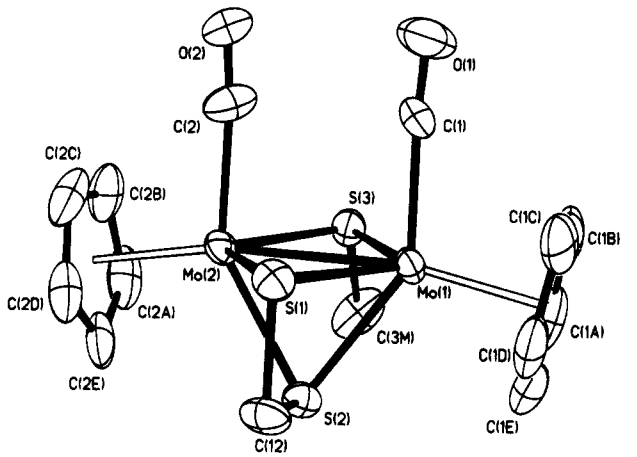

Figure 2. Perspective drawing and numbering scheme for $[(CpMoCO)_2(S_2CH_2)(\mu\text{-SMe})]^+$, the cation of **7**. Thermal ellipsoids are shown at the 50% probability level.

100 °C in acetonitrile (eq 7).[8] Attempts to carry out this

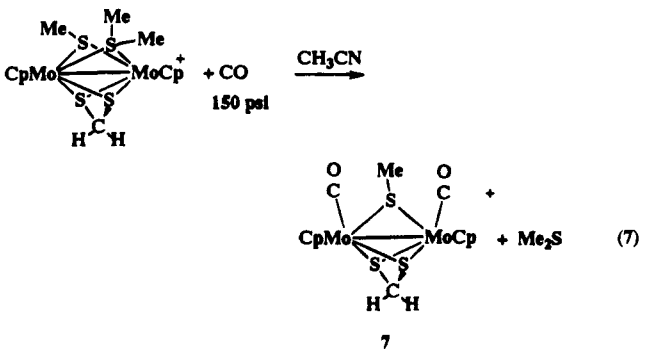

reaction at lower CO pressures and temperatures resulted in significantly lower yields of **7**. Complex **7** showed a single IR stretch in the carbonyl region at 2010 cm^{-1}. The NMR spectrum again showed evidence for two isomers in varying ratios, depending on isolation and crystallization techniques. The isomer possibilities described above for **6b** are also applicable here. Isomers with cis carbonyl ligands would be consistent with the single IR stretch in the CO region, provided that the vibrational modes of the two CO ligands on adjacent metals are not coupled. The large difference in NMR chemical shifts for the SMe resonances in the two isomers (1.63 and 2.60 ppm) may reflect different methyl orientations in the two derivatives.

Although repeated attempts to obtain crystals of **7** have resulted in twinned crystals, the structure has been successfully solved. The large unit cell contains 4 asymmetric units and 16 molecules. The dinuclear cations within the cell are similar in their structural parameters, and one of these is shown in Figure 2. Positional parameters are listed in Table 3, and selected bond distances and angles are given in Table 4. The structure of the discrete cation confirms the cis orientation of the carbon monoxide ligands and the presence of both bridging methanethiolate and methanedithiolate ligands. The two eclipsed carbonyl ligands appear to fill the vacant coordination sites created by the displacement of the dimethyl sulfide ligand, with little rearrangement of the remaining core of the molecule. The Mo–Mo distance in the triply bridged structure has lengthened to 2.784(2) Å, which is significantly longer than the metal–metal distances of about 2.60 Å in related quadruply bridged structures. The Mo–C distances for the carbonyl ligands average 2.068 Å, while the Mo–S distances for the symmetrically bridged thiolate ligands are about 2.46 Å. The angles between the molybdenum ions and the centroid of the Cp ligands, Mo–Mo–Cp(centroid), are 169.6 and 169.2°. These bond lengths and angles are similar to those reported for other cationic Mo(III) dimers with three bridging sulfur ligands and two terminal carbonyls, such as $[(CpMoCO)_2(\mu\text{-SMe})_3]Br$[9a] and $[(Cp^*MoCO)_2(\mu\text{-SMe})_2(\mu\text{-SH})]BF_4$.[9b] In each of the previously reported structures, two methanethiolate ligands are nearly parallel with the carbonyls (in an axial conformation), while in **7** the substituents on the thiolate ligands are oriented away from the carbon monoxide ligands. The smaller degree of steric hindrance for the carbonyls in **7** may lead to differences in reactivity for these ligands compared to those in previous structures.

Reaction 7 can be reversed when **7** is heated to ~110 °C in the presence of excess dimethyl sulfide. The lability of the CO ligands was also studied by monitoring the exchange of ^{13}CO into the complex by IR spectroscopy. New IR bands for the labeled complex were observed at 1997 and 1963 cm^{-1}. Significant CO exchange was only observed at relatively high temperatures of 105–110 °C.

Reactivity of $[(CpMo(CO))_2(S_2CH_2)(\mu\text{-SMe})]OTf$. A study of the reactions of **7** with nucleophiles has been initiated. Although the molybdenum ions are coordinatively saturated, nucleophilic addition to break a M–M bond or addition at an unsaturated ligand site are possibilities in this system. Addition of $LiEt_3BH$ to an isomeric mixture of **7** resulted in a rapid color change from orange to yellow. The product was purified by column chromatography and characterized by spectroscopic data. On the basis of ^1H and ^{13}C NMR data the product is identified as a cyclopentadiene complex, which results from hydride addition to one cyclopentadienyl ligand (eq 8). Two isomers are apparent in the spectrum arising from nucleophilic addition to the two isomers of **7**.

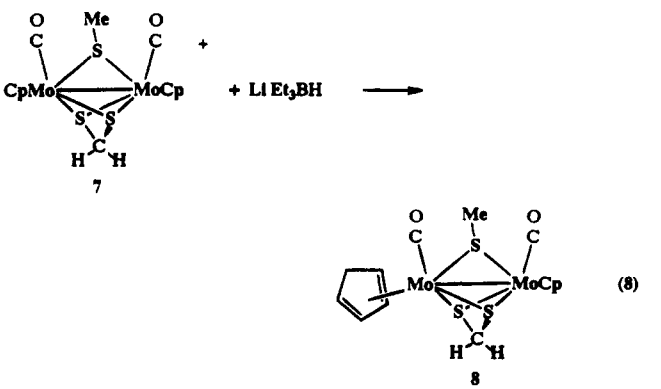

The NMR spectrum of the major isomer shows a singlet for the unchanged cyclopentadienyl ligand (5.85

(8) In previous work, carbonylation of Cp'Ru dimers with bridging disulfide ligands has led to dinuclear sulfur-bridged structures with terminal carbonyl ligands: Ogilvy, A. E.; Rauchfuss, T. B. *Organometallics* **1988**, *7*, 1884.

(9) (a) Gomes de Lima, M. B.; Guerchais, J. E.; Mercier, R.; Petillon, F. Y. *Organometallics* **1986**, *5*, 1952. (b) Schollhammer, P.; Petillon, F. Y.; Pichon, R.; Poder-Guillou, S.; Talarmin, J.; Muir, K. W.; Manojlovic-Muir, L. *Organometallics* **1995**, *14*, 2277.

Table 3. Atomic Coordinates (×10⁴) and Equivalent Isotropic Displacement Parameters (Å² × 10³) for 7

	x	y	z	U(eq)		x	y	z	U(eq)
Mo(1)	7304(1)	2496(1)	1827(1)	39(1)	C(6A)	5727(11)	8247(11)	849(3)	92(5)
Mo(2)	10007(1)	2485(1)	1790(1)	43(1)	C(6B)	5522(10)	7290(12)	872(2)	78(4)
S(1)	8795(4)	2015(3)	2141(1)	47(1)	C(6C)	5443(9)	6903(10)	651(2)	65(4)
S(2)	8743(4)	3775(3)	1961(1)	49(1)	C(6D)	5596(9)	7645(12)	494(2)	76(4)
C(12)	8862(17)	3202(10)	2243(2)	60(4)	C(6E)	5769(12)	8475(11)	617(3)	97(5)
S(3)	8517(3)	2865(4)	1472(1)	52(1)	Mo(7)	6323(1)	7566(1)	1969(1)	35(1)
C(3M)	8478(20)	4105(12)	1398(3)	94(8)	Mo(8)	8979(1)	7441(1)	1895(1)	42(1)
C(1)	7285(11)	1146(8)	1698(2)	62(3)	S(10)	7377(3)	7919(4)	1595(1)	50(1)
O(1)	7200(16)	422(9)	1633(3)	98(5)	S(11)	7413(4)	6192(3)	1794(1)	50(1)
C(2)	9934(13)	1126(9)	1660(3)	72(4)	C(78)	7241(18)	6731(11)	1503(2)	72(5)
O(2)	10019(14)	438(9)	1581(3)	96(5)	S(12)	7923(3)	7164(4)	2272(1)	50(1)
C(1A)	5427(11)	3262(12)	1719(3)	96(5)	C(12M)	7881(15)	5917(10)	2344(3)	61(4)
C(1B)	5205(9)	2312(13)	1711(2)	94(5)	C(7)	6545(11)	8919(7)	2080(2)	47(3)
C(1C)	5297(10)	1947(11)	1930(3)	89(5)	O(7)	6564(14)	9661(8)	2145(3)	88(5)
C(1d)	5579(10)	2693(12)	2081(2)	81(4)	C(8)	9139(12)	8815(9)	2005(2)	67(4)
C(1E)	5620(11)	3493(10)	1948(3)	91(5)	O(8)	9229(18)	9560(9)	2051(3)	115(6)
C(2A)	11790(11)	3242(11)	1642(3)	90(5)	C(7A)	4571(11)	6929(10)	2172(2)	64(4)
C(2B)	11987(10)	2276(12)	1619(2)	90(5)	C(7B)	4438(10)	7891(10)	2166(2)	61(3)
C(2C)	12073(11)	1890(11)	1842(3)	90(5)	C(7C)	4270(10)	8177(9)	1936(2)	59(3)
C(2D)	11938(10)	2615(12)	1995(2)	81(4)	C(7D)	4283(9)	7386(10)	1798(2)	56(3)
C(2E)	11775(10)	3453(10)	1877(3)	82(4)	C(7E)	4466(10)	6605(9)	1946(2)	56(3)
Mo(3)	1193(1)	2565(1)	523(1)	34(1)	C(8A)	10835(11)	6620(13)	1984(3)	105(5)
Mo(4)	−1467(1)	2456(1)	599(1)	47(1)	C(8B)	11124(10)	7576(14)	1987(2)	113(6)
S(4)	143(4)	2934(3)	895(1)	44(1)	C(8C)	10977(11)	7908(12)	1761(3)	107(5)
S(5)	100(4)	1195(3)	701(1)	47(1)	C(8D)	10573(11)	7148(13)	1627(2)	89(5)
C(34)	327(14)	1736(8)	983(2)	43(3)	C(8E)	10498(12)	6360(11)	1764(3)	95(5)
S(6)	−435(3)	2171(3)	227(1)	49(1)	S(13)	4162(6)	462(4)	1148(1)	76(2)
C(6M)	−359(19)	888(10)	159(3)	74(5)	O(131)	3795(19)	1388(9)	1215(2)	115(6)
C(3)	967(11)	3935(8)	419(2)	53(3)	O(132)	5584(12)	309(15)	1168(4)	160(9)
O(3)	1026(14)	4678(9)	356(2)	84(4)	O(133)	3596(24)	124(13)	938(3)	194(11)
C(4)	−1634(11)	3839(8)	500(3)	65(4)	C(13)	3554(17)	−302(10)	1360(3)	104(6)
O(4)	−1781(14)	4584(10)	448(4)	118(7)	F(131)	3886(19)	−1162(8)	1326(3)	141(7)
C(3A)	2926(10)	1941(10)	320(2)	61(3)	F(132)	2295(16)	−281(15)	1380(5)	244(11)
C(3B)	3055(9)	2911(10)	327(2)	50(3)	F(133)	3978(28)	−55(12)	1568(2)	226(11)
C(3C)	3240(10)	3190(9)	559(2)	50(3)	S(14)	3358(6)	5469(4)	1347(1)	75(2)
C(3D)	3224(9)	2370(10)	695(2)	54(3)	O(141)	3814(22)	5052(13)	1555(2)	127(9)
C(3E)	3068(11)	1623(9)	543(2)	66(4)	O(142)	3752(18)	6357(9)	1281(3)	113(6)
C(4A)	−3338(11)	1631(12)	516(2)	86(5)	O(143)	1955(13)	5274(16)	1309(5)	213(12)
C(4B)	−3624(10)	2589(13)	515(3)	103(5)	C(14)	3994(17)	4678(11)	1133(2)	85(5)
C(4C)	−3447(11)	2920(12)	745(3)	108(6)	F(141)	3723(23)	4956(12)	926(2)	191(9)
C(4D)	−3044(11)	2161(13)	875(2)	96(5)	F(142)	3663(19)	3806(8)	1166(3)	140(6)
C(4E)	−2992(12)	1373(11)	739(3)	87(4)	F(143)	5267(14)	4714(16)	1153(4)	242(11)
Mo(5)	10201(1)	7491(1)	667(1)	45(1)	S(15)	3032(6)	260(4)	2413(1)	77(2)
Mo(6)	7510(1)	7476(1)	702(1)	37(1)	O(151)	2797(19)	1231(9)	2464(2)	113(6)
S(7)	8701(4)	7010(3)	353(1)	52(1)	O(152)	4085(13)	−203(13)	2536(3)	122(7)
S(8)	8791(4)	8779(3)	533(1)	47(1)	O(153)	2882(20)	−8(13)	2173(2)	137(7)
C(56)	8651(16)	8209(10)	250(2)	65(4)	C(15)	1651(15)	−311(12)	2539(3)	96(5)
S(9)	8995(4)	7864(3)	1020(1)	49(1)	F(151)	1689(19)	−1209(10)	2499(3)	171(7)
C(9M)	8962(17)	9128(10)	1084(3)	67(5)	F(152)	562(12)	35(14)	2461(3)	177(8)
C(5)	10207(12)	6130(8)	790(3)	64(3)	F(153)	1612(13)	−176(10)	2764(2)	112(4)
O(5)	10311(13)	5393(9)	858(3)	99(5)	S(16)	4467(6)	5249(4)	85(1)	73(1)
C(6)	7583(10)	6130(8)	892(2)	47(3)	O(161)	4559(19)	4975(12)	325(2)	115(6)
O(6)	7573(16)	5420(10)	910(3)	113(6)	O(162)	4727(18)	6221(9)	36(3)	119(6)
C(5A)	12104(11)	8227(11)	773(2)	86(4)	O(163)	3422(13)	4809(11)	−46(2)	96(5)
C(5B)	12300(10)	7279(12)	786(2)	86(4)	C(16)	5838(15)	4676(11)	−44(3)	87(4)
C(5C)	12198(10)	6910(11)	562(3)	86(5)	F(161)	5853(14)	4809(9)	−268(2)	105(4)
C(5D)	11938(11)	7655(12)	415(2)	89(5)	F(162)	5805(17)	3764(9)	−3(3)	132(6)
C(5E)	11893(11)	8467(10)	546(3)	85(4)	F(163)	6939(12)	5000(14)	36(3)	161(7)

[a] U(eq) is defined as one-third of the trace of the orthogonalized U_{ij} tensor.

ppm) and four multiplets for the four inequivalent vinyl hydrogens on the cyclopentadiene ring (5.82, 5.69, 3.82, and 3.40 ppm). An AB pattern centered at 3.62 ppm is assigned to the geminal hydrogens. When Et_3BD^- was used as the nucleophile, this AB pattern collapsed to a broadened singlet at 3.51 ppm (Figure 3). A second set of similar but less intense resonances are observed for the minor isomer (see Experimental Section). A ^{13}C NMR DEPT experiment on the product also supported the proposed formulation. Two CH_2 resonances were observed for each isomer, and these are assigned to the S_2CH_2 ligand (65.06 and 67.63 ppm) and to the methylene group of the cyclopentadiene ligand (40.41 and 47.42 ppm).

The cyclopentadiene complex **8** can be formally described as a mixed-valence Mo(I)−Mo(III) dimer with the η^4-cyclopentadiene ligand coordinated to Mo(I). A single metal−metal bond would complete the 18-electron count at each metal center. The infrared spectrum of **8** reflects the unsymmetrical electron distribution of the dimer. A strong C−O stretch is observed at 1966 cm^{-1}, as well as weaker lower energy stretches at 1904 and 1898 cm^{-1}. The latter absorbances are expected to result from the CO interaction with the more electron-rich molybdenum ion. The addition of triflic acid to **8** reversed the hydride addition to re-form the starting complex **7** and presumably H_2.

The relatively high CO stretching frequency in **7**

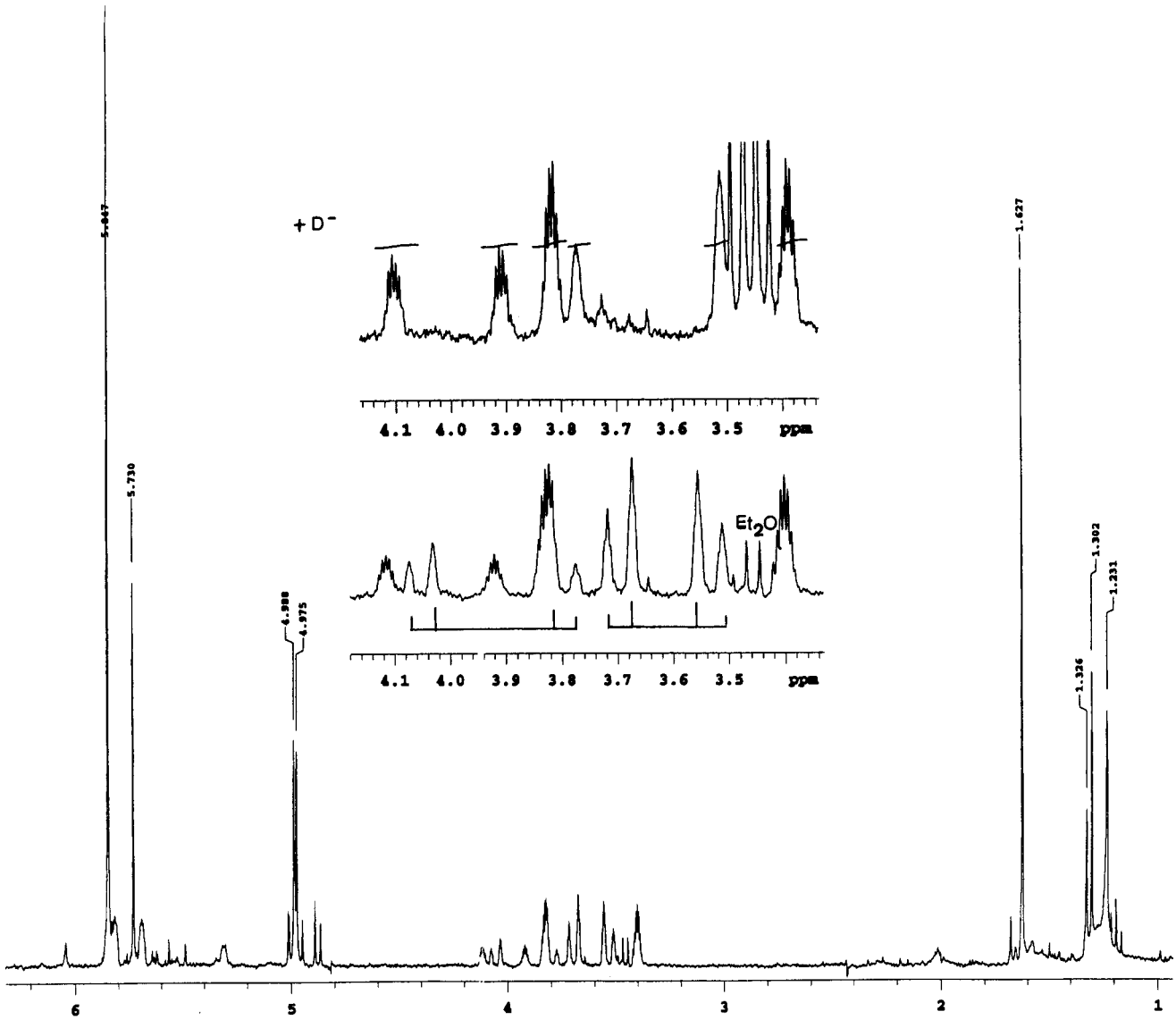

Figure 3. 300 MHz ^{1}H NMR spectrum of (CpMoCO)(S_2CH_2)(μ-SMe)(CO)MoC_5H_6 (**8**) in $CDCl_3$. Insets show expanded regions of the spectra from 3.0 to 4.2 ppm for this product and for the analogous product resulting from deuteride attack.

Table 4. Selected Bond Distances and Angles for [(CpMoCO)$_2$(S_2CH_2)(μ-SMe)]OTf (7)

	Distances (Å)		
Mo(1)–C(1)	2.060(11)	Mo(2)–C(2)	2.077(12)
Mo(1)–S(3)	2.458(4)	Mo(2)–S(3)	2.449(4)
Mo(1)–S(2)	2.470(4)	Mo(2)–S(2)	2.458(4)
Mo(1)–S(1)	2.469(4)	Mo(2)–S(1)	2.474(4)
C(1)–O(1)	1.101(14)	C(2)–O(2)	1.084(14)
S(1)–C(12)	1.790(13)	S(2)–C(12)	1.822(12)
S(3)–C(3M)	1.82(2)	Mo(1)–Mo(2)	2.784(2)
	Angles (deg)		
Mo(1)–S(1)–Mo(2)	68.54(10)	Mo(1)–C(1)–O(1)	175.9(13)
Mo(1)–S(2)–Mo(2)	68.79(12)	Mo(2)–C(2)–O(2)	172.4(14)
Mo(1)–S(3)–Mo(2)	69.11(10)	Mo(2)–Mo(1)–C(1)	88.6(3)
S(1)–Mo(1)–C(1)	90.7(4)	Mo(1)–Mo(2)–C(2)	89.9(4)
S(1)–Mo(2)–C(2)	91.6(4)	S(1)–Mo(1)–S(3)	111.01(12)
S(3)–Mo(1)–C(1)	84.4(4)	S(1)–Mo(1)–S(2)	66.63(14)
S(3)–Mo(2)–C(2)	84.9(4)	S(1)–C(12)–S(2)	97.3(5)

suggested that the carbonyl ligand would be susceptible to nucleophilic attack,[10] but we have not identified spectroscopic evidence for this pathway. Other examples of nucleophilic addition of hydrides and of alkyllithium reagents to Cp rather than to carbonyl ligands in cationic metal complexes have been reported previously.[11]

Several techniques for promoting CO dissociation from a metal complex have been developed, and we have begun to explore this type of reaction with **7**. The removal of a single carbonyl ligand from **7** would result in a coordinatively unsaturated dinuclear complex which may show interesting further reactivity. For example, loss of carbon monoxide could lead to a bridging interaction of the remaining carbonyl ligand which might promote further reactions of this ligand. Complex **7** reacted with 1 equiv of Me_3NO in acetonitrile at room temperature to form a single new air-sensitive product in high yield (eq 9). The same complex could

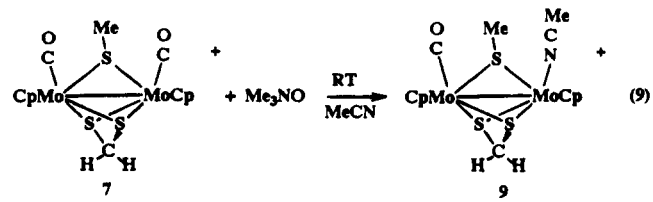

(9)

also be prepared by heating **7** in acetonitrile under

(10) Darensbourg, D. J.; Darensbourg, M. Y. *Inorg. Chem.* **1970**, *9*, 1691. Angelici, R. J. *Acc. Chem. Res.* **1972**, *5*, 335.

nitrogen pressure at 110 °C, but the purity of the product diminished under these conditions. Spectroscopic data for the product support its formulation as an acetonitrile adduct, **9**.

The ^{1}H NMR spectrum shows resonances for inequivalent Cp ligands and methanedithiolate protons, and in CD_2Cl_2 a singlet at 2.42 ppm is assigned to the nitrile methyl. The latter resonance is not observed in CD_3CN, suggesting that the coordinated nitrile undergoes exchange in this solvent. A strong infrared absorption at 1979 cm^{-1} is assigned to ν_{CO} of the terminal carbonyl, but the nitrile stretch has not been identified. A strong band at 1260 cm^{-1} is associated with the ionic triflate anion.[12] Attempts to carry out the reaction of **7** with trimethylamine *N*-oxide in a noncoordinating solvent, such as dichloromethane, did not give a characterizable product. We were also unsuccessful in removing the remaining carbonyl ligand in **9** by reaction with additional Me_3NO. The nitrile ligand in **9** appears to be significantly more labile than the carbonyl ligands in **7**, and further work to explore the reactivity of **9** and related derivatives with weakly coordinated ligands is in progress.

Conclusions and Summary. Synthetic procedures have been developed for the preparation of dinuclear cyclopentadienylmolybdenum complexes which contain three bridging sulfur atoms and a variable fourth bridge. For example, new complexes which contain bridging halides or hydrocarbons have been isolated and characterized. The extensive ligand-based reactivity of the dimers containing four sulfur bridges has been well established. The extension of the synthetic procedures described here should permit us to study the scope of this reactivity as new ligands are substituted into the bridge position.

New cyclopentadienylmolybdenum dimers which contain three bridging sulfurs and a two-electron-donor terminal ligand on each metal have also been synthesized. The series of terminal ligands in these structures, RNC, CO, and MeCN, show an increasing ease of dissociation, and the consequences of a more readily accessible vacant coordination site are being explored in ongoing work.

Experimental Section

Reactions were carried out under a nitrogen atmosphere using standard Schlenk techniques. Solvents were dried and degassed before use. The molybdenum complexes $[CpMo)_2(S_2CH_2)(SMe)(\mu\text{-}SMe_2)]OTf$ and $[(MeCpMo)_2(S_2CH_2)(\mu\text{-}SMe)(\mu\text{-}SMe_2)]OTf$ were synthesized according to published procedures.[1]

$(CpMo)_2(S_2CH_2)(\mu\text{-}SCH_3)(\mu\text{-}Cl)$, 2. $[(CpMo)_2(S_2CH_2)(\mu\text{-}SCH_3)(\mu\text{-}S\{CH_3\}_2)]OTf$ (**1**; 0.078 g, 0.12 mmol), LiCl (0.18 g, 4.1 mmol), and CH_3CN (20 mL) were combined in a Schlenk flask. The solution was heated to reflux for 11 h, while the color changed from orange to green. Solvent was removed *in vacuo*, affording a 4:1 mixture of **2** and $(CpMo)_2(S_2CH_2)(\mu\text{-}SCH_3)_2$ (**3**). Yield: 0.093 g, 62%. The green solid product was dissolved in Et_2O (2 × 5 mL) and chromatographed on neutral alumina with hexanes (80 mL), removing a clear band, which was discarded. Elution with Et_2O (200 mL) afforded a green band containing both products. Slow cooling of a 5:1 hexanes/Et_2O solution of the product mixture to −70 °C afforded green crystalline **2**. ^{1}H NMR ($CDCl_3$): δ 5.77, 5.76 (2s, 10 H, Cp, two isomers), 5.41, 5.34 (2s, 2 H, S_2CH_2), 1.49, 1.47 (3s, 2 H, SCH_3). $^{13}C\{^1H\}$NMR ($CDCl_3$): δ 93.79 (s, Cp), 74.60 (s, S_2CH_2), 22.77 (s, SCH_3). MS (EI$^+$; *m/e*) 482 (P), 467 (P − CH_3), 436 (P − CH_3 − S), 421 (P − CH_3, S − CH_2). Oxidations in acetonitrile with 0.1 M $(n\text{-}Bu)_4NBF_4$ (V vs Cp_2Fe): $E^\circ = -0.29$, $\Delta E = 80$ mV; $E^\circ = 0.37$, $\Delta E = 240$ mV.

A similar procedure was followed to prepare $(MeCpMo)_2(S_2CH_2)(\mu\text{-}SCH_3)(\mu\text{-}Cl)$. ^{1}H NMR data ($CDCl_3$; δ): 5.79−5.57 (10 H, m, Cp, CH_2); 2.02 (6 H, s, MeCp); 1.49, 1.35 (3 H, s, SCH_3). MS (EI; *m/e*): 510 (P), 495(P − Me), 463 (P − SMe), 449 ($Cp'MoS)_2Cl$). Anal. Calcd for $C_{14}H_{19}ClMo_2S_3$: C, 32.92; H, 3.75; Cl, 6.94; S, 18.83. Found: C, 32.98; H, 3.62; Cl, 6.88; S, 18.49.

Table 5. Crystal Data, Data Collection Conditions, and Solution and Refinement Details for $(CpMo)_2(S_2CH_2)(\mu\text{-}SCH_3)(\mu\text{-}Cl)$ (2) and $[(CpMo(CO))_2(S_2CH_2)(\mu\text{-}SMe)]OTf$ (7)

compd	**2**	**7**
formula	$C_{24}H_{30}Cl_2Mo_4S_6$	$C_{15}H_{15}F_3Mo_2O_5S_4$
color and habit	black cube	red needle
cryst dimens, mm	0.15 × 0.15 × 0.10	0.7 × 0.07 × 0.07
space group	$P2_1/c$	B2(1)
cryst syst	monoclinic	monoclinic
unit cell dimens		
a, Å	14.084(2)	10.265(2)
b, Å	14.151(2)	14.233(3)
c, Å	15.419(3)	57.735(12)
β, deg	100.17(3)	90.14(3)
V, Å^3	3024.8(8)	8436(3)
formula units/cell, *Z*	4	16
fw	965.50	652.39
density (calcd), g/cm^3	2.120	2.055
abs coeff, mm^{-1}	2.227	1.636
F(000), e	1888	5120
radiation	Mo Kα (λ = 0.710 73 Å)	
temp, K	293(2)	173(2)
θ range, deg	1.97−22.71	0.71−26.38
scan type	2θ−θ	ω oscillation, 0.3°
no. of rflns collected	4351	21 316
no. of unique rflns	4014 (R_{int} = 5.04%)	12 720 (R_{int} = 0.0300)
no. of obsd rflns	2667 ($F > 4.0\sigma(F)$)	10 195 ($F > 4.0\sigma(F)$)
final residuals (obsd data)[a]		
R1	0.0715	0.0669
wR2	0.1670	0.1345
goodness of fit	0.990	1.140
largest diff peak, e/Å^3	1.579	1.455
largest diff hole, e/Å^3	−1.060	−0.651

[a] $R_1 = \{\Sigma||F_o| - |F_c||\}/\Sigma|F_o|$; $wR_2 = \{\Sigma[w(F_o^2 - F_c^2)^2]^{1/2}\}/\{\Sigma w(F_o^2)^2]\}$.

X-ray Diffraction Study of $(CpMo)_2(S_2CH_2)(\mu\text{-}SMe)(\mu\text{-}Cl)$ (2). The complex was crystallized by cooling a saturated hexane/methylene chloride solution (5:1). The product crystallized in space group $P2_1/c$ with two molecules per asymmetric unit. Data were collected on a Siemens P3/F diffractometer. The molybdenum positions were determined by direct methods, and the other atoms were located using difference Fourier calculations in SHELX. All hydrogens were refined in fixed ideal positions. All non-hydrogen atoms were refined anisotropically during the final cycles of full-matrix least-squares refinement. The chloride atoms were assigned on the basis of chemical evidence. The largest difference peak was 1.58 e/Å^3 and is 1.15 Å from

(11) (a) Brunner, J.; Langer, M. *J. Organomet. Chem.* **1973**, *54*, 221. (b) Whitesides, T. H.; Shelly, J. *J. Organomet. Chem.* **1975**, *92*, 215. (c) For other references to nucleophilic attack on Cp ligands, see: Kirchner, K.; Taube, H. *J. Am. Chem. Soc.* **1991**, *113*, 7039 and references therein.

(12) Lawrence, G. A. *Chem. Rev.* **1986**, *86*, 17.

S6. Details of the crystal data and experimental conditions and a summary of the solution refinement information are given in Table 5 and in the supporting information.

$(CpMo)_2(S_2CH_2)(\mu\text{-}SCH_3)(\mu\text{-}Br)$ (4). Method a. Complex **1** (0.021 g, 0.032 mmol) LiBr (0.30 g, 3.4 mmol) and CH_3CN (15 mL) were combined in a Schlenk flask. The solution was heated to reflux for 16 h while the color changed from orange to green. Solvent was removed *in vacuo*. Extraction of a green solution with hexanes (2 × 50 mL) afforded a 3:2 mixture of **4** and $(CpMo)_2(S_2CH_2)(\mu\text{-}SCH_3)_2$ (**3**). Yield of **4:** 0.014 g, 50% yield.

Method b. $[(CpMo)_2(S_2CH_2)(\mu\text{-}SCH_3)Cl]$ (**2**; 0.010 g, 0.021 mmol), LiBr (0.10 g, 1.1 mmol), and CH_3CN (15 mL) were combined in a Schlenk flask. The solution was heated to reflux for 16 h. Solvent was removed *in vacuo*. A ^1H NMR spectrum of the product showed 31% conversion of **2** to **4**. CH_3CN (15 mL) was added to the product, and the mixture was heated to reflux for 6 days. A ^1H NMR spectrum of the product mixture showed 86% conversion of **2** to **4**. ^1H NMR ($CDCl_3$; δ) 5.74, 5.71 (2s, 10 H, Cp, two isomers); 5.46, 5.34 (2s, 2 H, S_2CH_2); 1.51, 1.50 (2s, 3 H, SCH_3).

$[(CpMo)_2(\mu_2\text{-}1\text{-}Butyne)(S_2CH_2)(\mu\text{-}SCH_3)]OTf$ (5a). Complex **1** (0.044 g, 0.067 mmol) and CH_3CN (15 mL) were added to a 100 mL high-pressure vessel equipped with a pressure gauge, an inlet for 1-butyne, and an inlet for N_2/evacuation. The vessel was evacuated and backfilled with 1-butyne (cp grade) and finally filled with 1-butyne to 30 psi. The solution was heated to 98 °C for 11 h. The final color was orange-yellow. Solvent was removed *in vacuo*, affording orange-yellow solid **5a** (0.044 g, 0.067 mmol). Recrystallization from slow addition of Et_2O to a CH_2Cl_2 solution of **5a** gave yellow needles. ^1H NMR ($CDCl_3$; δ) 6.08, 6.07 (2s, 10 H, Cp, two isomers); 6.00, 5.63 (2s, 1 H, HC=); 4.97, 4.77 (2s, 2 H, S_2CH_2); 2.89, 2.80 (2q, J = 8 Hz, 2 H, CH_2CH_3); 1.72, 1.70 (2s, 3 H, SCH_3); 1.12, 1.11 (2t, J = 8 Hz, 3H, CH_2CH_3). MS: *m/e* 501 (P − OTf), 447 (P − C_4H_6 − OTf), 401 (P − C_4H_6 − SCH_3 − OTf). Anal. Calcd for $C_{17}H_{21}S_4O_3F_3Mo_2$: C, 31.39; H, 3.25. Found: C, 31.35; H, 3.36.

$[(CpMo)_2(\mu_2\text{-}Phenylacetylene)(S_2CH_2)(\mu\text{-}SCH_3)]OTf$ (5b). Complex **1** (0.120 g, 0.182 mmol), CH_3CN (20 mL) and phenylacetylene (1.5 mL, 14 mmol) were combined in a Schlenk flask. The solution was heated to reflux for 16 h, while the color changed from orange to orange-yellow. Solvent was removed *in vacuo*, affording orange-yellow solid **5b**. Attempts to recrystallize this product by slow cooling in a variety of solvents (CH_2Cl_2, CH_2Cl_2/THF, and CH_2Cl_2/Et_2O) as well as by slow diffusion of pentane into a CH_2Cl_2 solution of **5b** were unsuccessful. Yield: 64%. ^1H NMR (CD_3CN; δ) 7.34, 7.22 (2m, 5 H, Ph, two isomers); 6.24, 6.06 (2s, 1 H, HCCPh); 6.15, 6.14 (2s, 10 H, Cp); 4.90, 4.74 (2s, 2 H, S_2CH_2); 1.76, 1.75 (2s, 3 H, SCH_3).

$[\{CpMo_2(CN^tBu)\}_2(S_2CH_2)(\mu\text{-}SCH_3)]OTf$, (6a). Complex **1** (0.040 g, 0.061 mmol), CH_3CN (20 mL), and CN^tBu (0.10 mL, 0.89 mmol) were combined in a Schlenk flask. The solution was heated to reflux for 14 h, while the color changed from orange to red. Solvent was removed *in vacuo*, affording red solid **6a**. Recrystallization by slow addition of Et_2O to a CH_2Cl_2 solution of **6a** gave red plates. Yield: 64%. IR (CH_2Cl_2): ν_{CN} 2108 (s), 2068 (sh), 2034 (sh) cm^{-1}. ^1H NMR (CD_3CN; δ) 5.69 (s, 10 H, Cp), 5.43 (s, 2 H, S_2CH_2); 1.57 (s, 3 H, SCH_3); 1.36 (s, 18 H, ^tBu). $^{13}C\{^1H\}$ NMR (CD_3CN; δ) 93.03 (C_5H_5); 75.90 (S_2CH_2); 30.81 (CMe_3); 26.40 (SCH_3). MS *m/e* 613 (P − OTf), 532 (P − CN^tBu − OTf) , 447 (P − $2CN^tBu$ − OTf), 432 (P − $2CN^tBu$ − CH_3 − OTf). Anal. calcd for $C_{18}H_{14}S_4O_3F_3Mo_2$: C 36.22; H, 4.36. Found: C, 36.02; H, 4.40.

$[\{CpMo(CNBz)\}_2(S_2CH_2)(\mu\text{-}SCH_3)]OTf$ (6b). Complex **1** (0.015 g, 0.023 mmol), CH_3CN (10 mL), and CNBz (0.24 mL, 1.0 mmol) were combined in a Schlenk flask. The solution was heated to reflux for 11 h, while the color changed from orange to red. Solvent was removed *in vacuo*, affording red solid **6b**. ^1H NMR ($CDCl_3$; δ) 7.32 (m, 6 H, Ph); 7.15 (m, 4 H, Ph); 5.53, 5.51 (2s, 10 H, Cp, two isomers); 5.41, 5.40 (2s, 2 H, S_2CH_2, two isomers); 1.58, 1.59 (2s, 4 H, $CNCH_2Ph$); 2.50, 1.57 (2s, 3 H, SCH_3, two isomers).

$[\{CpMo(CO)\}_2(S_2CH_2)(\mu\text{-}SCH_3)]OTf$ (7). Complex **1** (0.044 g, 0.067 mmol) and CH_3CN (20 mL) were added to a 100 mL high-pressure vessel equipped with a pressure gauge, an inlet for CO, and an inlet for N_2/evacuation. The vessel was evacuated and backfilled with CO (cp grade) three times and finally filled with CO to 150 psi. The solution was heated to 100 °C for 14 h. The final color was orange. Solvent was removed *in vacuo*, affording **7.** Yield: 0.043 g, 0.066 mmol, 98%. Recrystallization via slow cooling of a CH_2Cl_2 solution of **7** to −70 °C gave orange cubes. IR (CH_2Cl_2): ν_{CO} 2010 (s) cm^{-1}. ^1H NMR ($CDCl_3$; δ): isomer identified by X-ray diffraction study, 6.08 (s, 10 H, Cp), 5.43 (s, 2 H, S_2CH_2), 1.63 (s, 3 H, SCH_3); second isomer 6.10 (s, 10 H, Cp), 5.47 (s, 2 H, S_2CH_2), 2.60 (s, 3 H, SCH_3). $^{13}C\{^1H\}$NMR (CD_3CN; from crystals of one isomer, ^{13}C-enriched CO; δ): 231.72 (s, CO), 95.11 (s, C_5H_5), 71.69 (s, CH_2), 23.79 (s, CH_3). MS *m/e* 503 (P − OTf), 447 (P − 2CO − OTf), 431 (P − 2CO − CH_3 − OTf), 399 (P − 2CO − SCH_3 − OTf). Reduction potential in acetonitrile with 0.1 M $(n\text{-}Bu)_4NBF_4$: $E°$ = −1.47 V vs $FeCp_2$, ΔE = 80 mV. Anal. Calcd for $C_{15}H_{15}S_3O_5F_3Mo_2$: C, 27.62; H, 2.32. Found: C, 27.58; H, 2.30.

X-ray Diffraction Study of $[(CpMoCO)_2(S_2CH_2)(\mu\text{-}SMe)]OTf$, (7). The complex was crystallized from a CH_2Cl_2/pentane solution and isolated as red-orange needles. Data were collected on a Siemens SMART CCD-based diffractometer with an LT-2 low-temperature apparatus operating at 173 K. The needle direction of the crystal coincided with the a axis of the unit cell. A total of 1320 frames were collected as 0.3° ω oscillations, each exposed for 10.0 s. The maximum resolution was 0.90 Å.

This specimen was originally indexed as monoclinic $P2_1$ with cell dimensions, a = 10.265 Å, b = 14.233 Å, c = 29.308 Å, and β = 99.95°. Although the structure was successfully solved using these parameters, refinement was unsatisfactory. The crystal may also be indexed as orthorhombic C, but this did not resolve problems with refinement. Oscillation images viewed during data collection indicated that twinning may be present. Conversion of the primitive monoclinic cell to the unconventional, but equivalent, B-centered cell reported herein facilitates refinement of the crystal structure as a pseudo-orthorhombic twin by bringing β nearer to 90°. The twin lattice is related to the indexed lattice by the matrix [1,0,0,0,−1,0,0,0,1]. The ratio between the two components in this specimen is 0.109 91. Careful

examination of the data did not reveal the presence of higher symmetry. Solution and refinement were performed with the SHELXTL suite of programs.[13] Details of the crystal data and experimental conditions and a summary of the solution refinement information are given in Table 5 and in the supporting information.

Synthesis of $CpMo(CO)(\mu\text{-}S_2CH_2)(\mu\text{-}SMe)(CO)MoC_5H_6$ (8). $LiBEt_3H$ (70 μL, 0.070 mmol) was added dropwise to a solution of **7** (50 mg, 0.077 mmol) in 10 mL of dry, degassed tetrahydrofuran with stirring. The original brown-orange solution immediately turned pale orange; the reaction mixture was stirred for an additional 15 min. The solvent was removed in vacuo, and the oily, orange residue was extracted with hexanes. The hexane solvent was removed in vacuo to give the solid orange product. In some cases the product was further purified by chromatography on neutral alumina, first with pentane and then with ether as eluent to obtain a yellow band. Yield: 25 mg, 60%. Two isomers were observed in the NMR spectrum in a 2:1 ratio. ^1H NMR ($CDCl_3$; δ): major isomer, 5.85 (s, 5 H, Cp), 5.84, 5.69, 3.82, 3.40 (4 m, C_4H_4), 4.98 (AB, S_2CH_2), 3.62 (AB, Cp CH_2), 1.63 (s, SCH_3); minor isomer, 5.73 (s, 5 H, Cp), 5.60, 5.30, 4.12, 3.91 (4m, C_4H_4), 4.9 (S_2CH_2), 3.93 (AB, Cp CH_2), 1.30 (SMe). ^{13}C NMR (δ): major isomer, 91.33 (C_5H_5), 82.2, 82.0, 65.0, 64.2 (C_4H_4), 65.06 (S_2CH_2), 40.41 (Cp CH_2), 24.95 (SMe); minor isomer, 91.88 (C_5H_5), 83.15, 81.90, 72.03, 71.68 (C_4H_4), 67.63 (S_2CH_2), 47.42 (Cp CH_2), 23.78 (SMe). The FAB^+ mass spectrum for the product was similar to that observed for the starting reagent **7**.

$[(CpMo)_2(CO)(CH_3CN)(S_2CH_2)(\mu\text{-}SCH_3)]OTf$ (9). A THF (20 mL) solution of Me_3NO (0.04 g, 0.06 mmol) was added to an orange THF (20 mL) solution of $[(CpMoCO)_2(S_2CH_2)(\mu\text{-}SCH_3)]OTf$ (**7**; 0.042 g, 0.062 mmol) over 15 min. The resulting solution was yellow. Solvent removal gave a yellow solid. Recrystallization via slow addition of toluene to a CH_3CN solution of **4** afforded dark orange needles. IR (CH_2Cl_2): ν_{CO} 1979 cm^{-1}. ^1H NMR (CD_2Cl_2); δ) 6.03 (s, 5 H, Cp); 5.68 (s, 5 H, Cp); 5.88 (d, ^2J = 7.9 Hz, 1 H, S_2CH_2), 5.07 (d, ^2J = 7.9 Hz, 1 H, S_2CH_2); 2.42 (s, 3 H, CH_3CN); 1.67 (s, 3 H, SCH_3). MS (FAB): *m/e* 518 (P − OTf), 476 (P − NCMe − OTf), 448 (P − NCMe − CO − OTf), 403 (P − NCMe − CO − SMe − OTf). The complex decomposed slowly in the solid state under nitrogen, and elemental analyses were not attempted.

Acknowledgment. This work was supported by a grant from the National Science Foundation.

Supporting Information Available: Complete tables of crystal data and refinement details, bond lengths and angles, anisotropic displacement parameters, and hydrogen atom coordinates for **2** and **7** (21 pages). Ordering information is given on any current masthead page.

OM950156L

(13) Sheldrick, G. M. SHELXTL; Siemens: Madison, WI, 1995.

Tetraferrocenylethylene, a Chiral, Organometallic Propeller: Synthesis, Structure, and Electrochemistry

Benno Bildstein,*,† Peter Denifl,† Klaus Wurst,† Max André,‡ Martin Baumgarten,§ Jan Friedrich,§ and Ernst Ellmerer-Müller||

Institut für Allgemeine, Anorganische, und Theoretische Chemie, Universität Innsbruck, Innrain 52a, A-6020 Innsbruck, Austria, Biochemie GmbH, A-6250 Kundl, Austria, Max-Planck-Institut für Polymerforschung, D-55021 Mainz, Germany, and Institut für Organische Chemie, Universität Innsbruck, Innrain 52a, A-6020 Innsbruck, Austria

Received April 24, 1995®

Tetraferrocenylethylene is synthesized from diferrocenyl ketone by three different reductive carbon–carbon bond-forming methodologies: (a) an ultrasound-promoted McMurry reaction with low-valent titanium, (b) a modified Clemmensen reduction with zinc and trimethylchlorosilane, and (c) an aluminum-assisted oxygen–tellurium exchange in diferrocenyl ketone and subsequent thermolysis. Mechanistically, the first two methods involve carbenoid intermediates, whereas the third method consists of a twofold extrusion process from a preformed cyclic dimer of diferrocenyl telluroketone. Tetraferrocenylethylene shows spectral properties which are in accord with a sterically highly congested conformation. Noteworthy features include the very low C=C stretching vibration of 1474 cm^{-1} in the Raman spectrum, indicative of an elongated and weak C=C double bond, and the magnetic inequivalence of the ^1H and ^{13}C NMR signals of the hydrogens and carbons of the substituted cyclopentadienyl rings, indicative of a frozen molecular propeller conformation. An X-ray single-crystal structure analysis shows tetraferrocenylethylene to be a chiral, strongly twisted, and sterically congested olefin. The bond length of 138.1 pm of the central double bond and the angles of twisting and torsion are close in value to those of the most distorted olefins known. The helical chirality stems from the uniform twisting of the four alternatingly arranged ferrocenyl substituents. Electrochemically, tetraferrocenylethylene can be oxidized to the tetracation in accord with the number of ferrocenyl units. The donor ability of tetraferrocenylethylene compared to ferrocene itself is strongly enhanced with $\Delta E^1_{1/2} = -220$ mV.

Introduction

The normal properties of the olefinic double bond in ethylene can be substantially altered by fourfold attachment of sterically demanding, electron-donating or electron-accepting groups. Perturbation of the preferred molecular geometry by bulky substituents can lead to twisting of the double bond or to pyramidalization of the olefinic carbon atoms and to elongation of the C=C double bond. Electron-donating substituents reduce the oxidation potential, whereas electron-accepting substituents increase the electron affinity of the olefinic double bond. In comparison to ethylene these effects result in molecular distortion[1] of these tetrasubstituted olefins and in unusual redox behavior and reactivity.[2]

In this context, tetraferrocenylethylene is an interesting target compound because of the electron-donating properties and steric requirements of the ferrocenyl moiety. Structurally, the fourfold substitution of the carbon–carbon double bond should result in a highly strained molecule with an exceptionally elongated olefinic bond. Stereochemically, the twisting of the cyclopentadienyl rings in relation to the C=C plane should cause atropisomerism. Electronically, the powerful electron-donating capacity of the ferrocenyl moieties[3] will substantially ease oxidation.

Here we report the synthesis, characterization (NMR, IR, UV–vis, Raman, MS), structure (X-ray), attempted separation of enantiomers by HPLC, and electrochemistry (CV, PES) of tetraferrocenylethylene.[4]

Results and Discussion

Preparation of Tetraferrocenylethylene (1). Compound **1** can be prepared by three different synthetic routes, as outlined in Scheme 1.

Method a. The ultrasound-promoted McMurry reac-

† Institut für Allgemeine, Anorganische, und Theoretische Chemie, Universität Innsbruck.
‡ Biochemie GmbH.
§ Max-Planck Institut für Polymerforschung.
|| Institut für Organische Chemie, Universität Inssbruck.
® Abstract published in *Advance ACS Abstracts,* July 15, 1995.

(1) (a) Luef, W., Keese, R. Strained Olefins: Structure and Reactivity of Nonplanar Carbon-Carbon Double Bonds. *Top. Stereochem.* **1991**,*20*, 231. (b) Bock, H.; Ruppert, K.; Näther, C.; Havlas, Z.; Herrmann, H.-F.; Arad, C.; Göbel, I.; John, A.; Meuret, J.; Nick, S.; Rauschenbach, A.; Seitz, W.; Vaupel, T.; Solouki, B. *Angew. Chem.* **1992**, *104*, 564; *Angew. Chem., Int. Ed. Engl.* **1992**, *31*, 550. (c) Borden, W. T. *Chem. Rev.* **1989**, *89*, 1095.

(2) (a) Wiberg, N. *Angew. Chem.* **1968**, *80*, 809; *Angew. Chem., Int. Ed. Engl.* **1968**, *7*, 766. (b) Hoffmann, R. W. *Angew. Chem.* **1968**, *80*, 823; *Angew. Chem., Int. Ed. Engl.* **1968**, *7*, 754. (c) Hocker, J.; Merten, R. *Angew. Chem.* **1972**, *84*, 1022; *Angew. Chem., Int. Ed. Engl.* **1972**, *11*, 964. (d) Lappert, M. F. *J. Organomet. Chem.* **1988**, *358*, 185. (e) Fatiadi, A. J. *Synthesis* **1986**, 249. (f) Fatiadi, A. J. *Synthesis* **1987**, 85. (g) Fatiadi, A. J. *Synthesis* **1987**, 959.

(3) (a) Watts, W. E. *J. Organomet. Chem. Libr.* **1979**, *7*, 399. (b) Watts, W. E. In *Comprehensive Organometallic Chemistry*; Wilkinson, G., Stone, F. G. A., Abel, E. W., Eds.; Pergamon: Oxford, U.K., 1982; Vol. 8, Chapter 59, p 1051.

(4) Part of this work has been presented as a poster at the XVth International Conference on Organometallic Chemistry, Warsaw, Poland, Aug 9–14, 1992 and at the Xth FECHEM Conference on Organometallic Chemistry, Agia Pelagia, Crete, Greece, Sept 5–10, 1993.

0276-7333/95/2314-4334$09.00/0

Scheme 1[a]

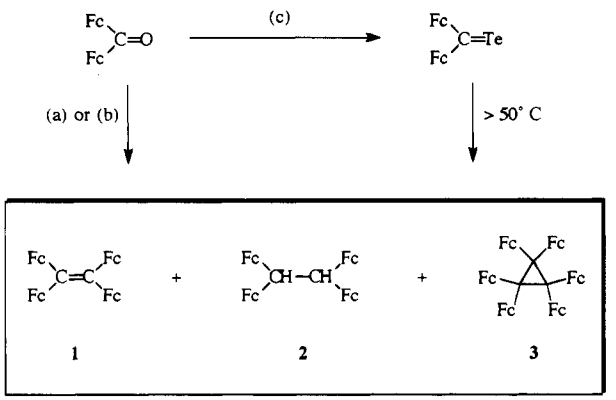

[a] Legend: (a) $TiCl_3$·3THF/Li/DME/ultrasound; (b) Zn/Me_3SiCl/THF; (c) Me_2Al–Te–$AlMe_2$/dioxane; Fc = ferrocenyl.

tion[5] of diferrocenyl ketone gives a high yield of **1** (80%) in a mixture with tetraferrocenylethane[6] (**2**) and traces of hexaferrocenylcyclopropane (**3**). Unsuccessful attempts to synthesize compound **1** from diferrocenyl ketone or from diferrocenyl thioketone by a McMurry reaction have been reported.[7] The failure to obtain olefinic products has been attributed to steric hindrance, but the combination of the proper choice of reducing agent ($TiCl_3$·3THF/Li versus the more common hydride-containing $TiCl_3$/$LiAlH_4$ or versus $TiCl_4$/Zn) and improved reaction conditions (ultrasonic enhancement[8] of the heterogeneous McMurry reaction) results in complete consumption of the starting material diferrocenyl ketone with a good yield of a product mixture of **1**, **2**, and **3**. Although the exact nature of the low-valent Ti reagent and the mechanism of the McMurry reaction is still under discussion,[9] the small traces of hexaferrocenylcyclopropane (**3**), a formal trimer of diferrocenylmethylidene, indicates the involvement of carbenoid intermediates, which either couple to olefin **1** or oligomerize to cyclopropane **3**. Ethane **2** is formed most likely by hydrogen abstraction from the solvent.

Method b. Reduction of diferrocenyl ketone by Zn/Me_3SiCl similarly affords a mixture of mainly **1** with **2** as byproduct. Mechanistically, this reaction can be viewed as a modification[10] of the more familiar Clemmensen reduction, in which the proton has been replaced by a silicon electrophile, whose high oxophilicity removes the carbonyl oxygen as hexamethyldisiloxane and generates an organozinc carbenoid, which forms products **1** and **2** in a manner analogous to that in method a. In this case, no trimerization product **3** can be detected.

Method c. Thermolysis of diferrocenyl telluroketone, prepared from diferrocenyl ketone by reaction with bis(dimethylaluminum) telluride,[11] yields almost quantitatively elemental tellurium and olefin **1** and traces of **2**. Probably this redox disproportionation is analogous to other reductive carbon–carbon bond-forming reactions of selenoketones by a twofold extrusion process.[12] First the telluroketone reacts in a [2 + 2] cycloaddition to give the dimer 2,2,4,4-tetraferrocenyl-1,3-ditelluretane. This proposed reaction is based on the recent mass spectroscopic evidence and X-ray structure[13] of the first 1,3-ditelluretanes and on the analogous reactions of sterically protected germanethione, germaneselone, stannanethione, and stannaneselone compounds.[14] Tetraferrocenylethylene (**1**) is formed from this cyclic dimer of diferrocenyl telluroketone by stepwise extrusion of elemental tellurium; the first extrusion yields tetraferrocenyltellurirane, which fragments further to afford **1** in a second extrusion step (Scheme 2).

Scheme 2. Twofold Te-Extrusion Mechanism for Method c[a]

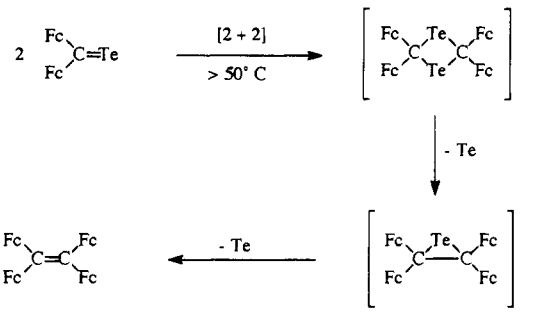

[a] Fc = ferrocenyl.

In terms of availability of starting materials, yield of ethylene **1**, and convenience of reaction conditions, method b is the preferred preparation of compound **1**. Both methods (a) and (c) involve a multiple-step procedure: either the preparation of the McMurry reagent from $TiCl_3$·3THF and Li powder or the cumbersome and stench-affected synthesis of bis(dimethylaluminum) telluride from bis(triorganostannyl) telluride and trimethylaluminum,[11,13a] respectively.

For all three synthetic routes the purification of **1** necessitates its separation from the byproduct **2**. Unfortunately, these two compounds have very similar physical properties and are therefore difficult to separate by conventional means. After prepurification of **1** by fractional crystallization and column chromatography on silica the remaining traces of byproduct **2** are removed either chemically or physically. Chemically, extended treatment with palladium on activated carbon in refluxing decalin selectively reduces **2** to diferrocenylmethane, which can be separated from **1** by conventional column chromatography. Physically, HPLC purification of **1** is achieved on a 150 mg scale on Nucleosil C_{18} (10 μm) as stationary phase with THF/H_2O as mobile phase, taking into consideration the low solubility of **1**, **2**, and **3** in conventional HPLC solvent mixtures and the oxidative decomposition of **1** in polar

(5) (a) McMurry, J. E. *Chem. Rev.* **1989**, *89*, 1513. (b) Lenoir, D. *Synthesis* **1989**, 883. (c) Betschart, D.; Seebach, D. *Chimia* **1989**, *43*, 39. (d) McMurry, J. E. *Acc. Chem. Res.* **1983**, *16*, 405.

(6) Paulus, H.; Schlögl, K.; Weissensteiner, W. *Monatsh. Chem.* **1982**, *113*, 767.

(7) (a) Lenoir, D., Burghard, H. *J. Chem. Res. Synop.* **1980**, 396. (b) Sato, M.; Asai, M. *J. Organomet. Chem.* **1992**, *430*, 105.

(8) Nayak, S. K.; Banerji, A. *J. Org. Chem.* **1991**, *56*, 1940.

(9) Fürstner, A. *Angew. Chem.* **1993**, *105*, 171; *Angew. Chem., Int. Ed. Engl.* **1993**, *32*, 164.

(10) (a) Motherwell, W. B.; Nutley, C. J. *Contemp. Org. Synth.* **1994**, *1*, 219. (b) Motherwell, W. B. *Aldrichim. Acta* **1992**, *25*, 71. (c) Banerjee, A. K.; de Carrasco, M. C. S.; Frydych-Houge, C. S. V.; Motherwell, W. B. *J. Chem. Soc., Chem. Commun.* **1986**, 1803.

(11) Denifl, P.; Bildstein, B. *J. Organomet. Chem.* **1993**, *453*, 53.

(12) (a) Guziez, F. S., Jr.; SanFilippo, L. J.; Murphy, C. J.; Moustakis, C. A.; Cullen, E. R. *Tetrahedron* **1985**, *41*, 4843. (b) Back, T. G.; Barton, D. H. R.; Britten-Kelly, M. R.; Guziec, F. S., Jr. *J. Chem. Soc., Perkin Trans. 1* **1976**, 2079.

(13) (a) Segi, M.; Koyama, T.; Takata, Y.; Nakajima, T.; Suga, S. *J. Am. Chem. Soc.* **1989**, *111*, 8749. (b) Boese, R.; Haas, A.; Limberg, C. *J. Chem. Soc., Dalton Trans.* **1993**, 2547.

(14) Okazaki, R.; Tokitoh, N.; Ishii, A.; Ishii, N.; Matsuashi, Y.; Matsumoto, T.; Suzuki, H. *Phosphorus; Sulfur Silicon Relat. Elem.* **1992**, *67*, 49.

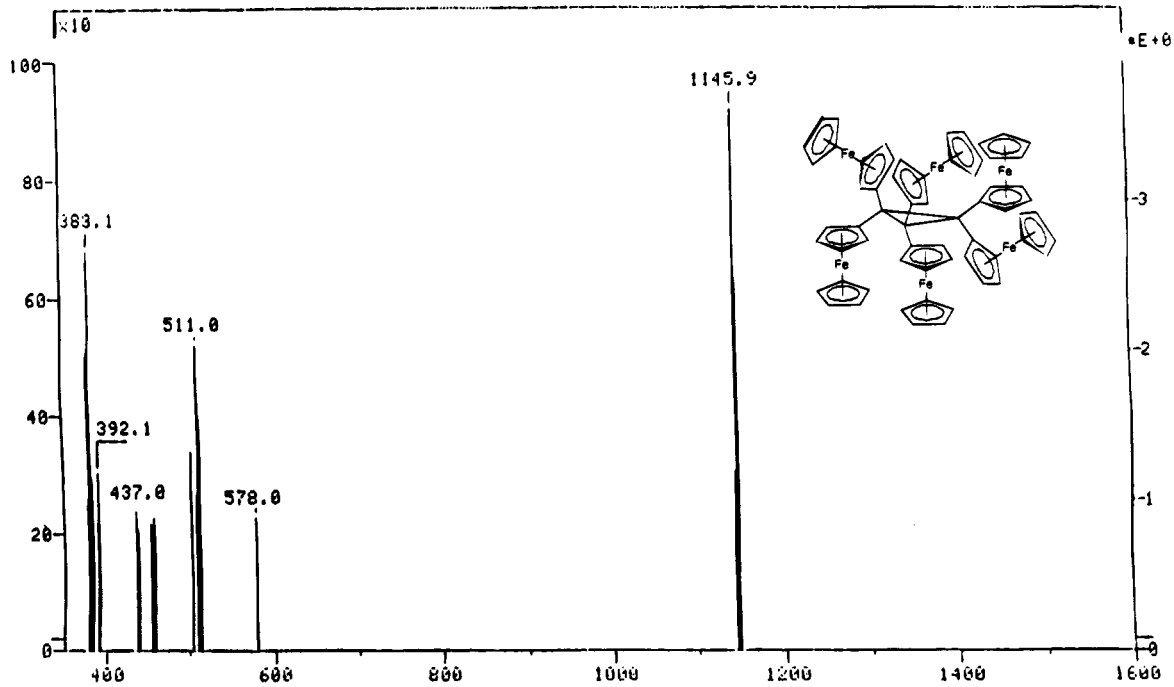

Figure 1. FAB-MS of hexaferrocenylcyclopropane (**3**).

solvents. In the case of method a cyclopropane **3** can be obtained in a total yield of 7 mg from collecting the corresponding fractions of three chromatographic separations. Due to this limited amount of **3** only characterization by FAB-MS (Figure 1) was possible.

Properties of Tetraferrocenylethylene. Compound **1** remains unchanged in the solid state (mp > 350 °C) under an inert atmosphere (Ar) at ambient temperature but decomposes in oxygen-containing solution over time to insoluble unidentified oxidized products. A preliminary screening of the chemical properties of **1** include the following reactions. The typical reactivity of ferrocene is partially retained in **1**; fourfold Friedel–Crafts acylation with acetyl chloride affords tetrakis(1-acetylferrocenyl)ethylene together with some less acetylated products in 75% overall isolated yield. Unexpectedly, a Mannich reaction with bis(dimethylamino)methane/H_3PO_4/CH_3CO_2H or with a preformed iminium salt[15] $(Me_2N{=}CH_2)^+$ gives no aminomethylated product. The central double bond in olefin **1** is unreactive, probably for steric reasons. Attempted complex formation with transition-metal carbonyls[2d] under thermal or photochemical activation and attempted dioxetane formation with singlet oxygen[16] give no reaction.

In the ^1H NMR spectrum of **1** (Figure 2) the 16 hydrogens of the substituted cyclopentadienyl rings are magnetically equivalent for all four ferrocenyl substituents and magnetically inequivalent for the four hydrogens of each cyclopentadienyl unit, resulting in one set of four slightly broadened singlets. No resolved coupling for this ABCD spin system could be obtained, although the usually observed $^1H-^1H$ coupling constants for ferrocene derivatives are in the range of 1–3 Hz.[17] Cooling does not change the appearance of these signals, indicating no exchange equilibrium. The halfwidth of the residual proton of the solvent $CDCl_3$ indicates paramagnetic impurities (partially oxidized **1**)

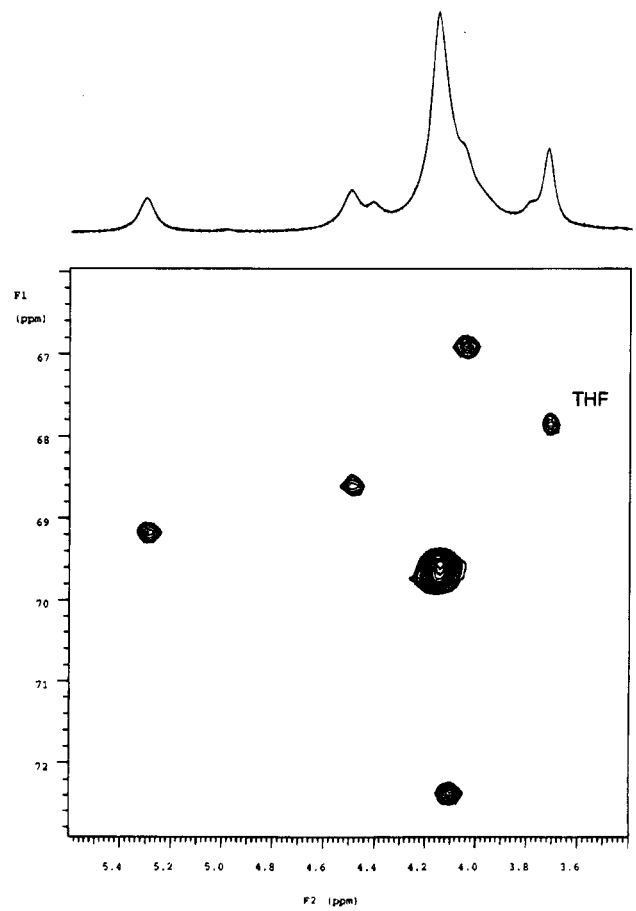

Figure 2. Pulsed field gradient enhanced HSQC of tetraferrocenylethylene (**1**).

(15) Kinast, G.; Tietze, L.-F. *Angew. Chem.* **1976**, *88*, 261; *Angew. Chem., Int. Ed. Engl.* **1976**, *15*, 239.

(16) (a) Adam, W. In *Small Ring Heterocycles. Part III. Oxirenes, Arene Oxides, Oxaziridines, Dioxetanes, Thietanes, Thietes, Thiazetes, and Others;* Hassner, A., Ed.; Wiley-Interscience: New York, 1985; Chapter IV, p 351. (b) Adam, W.; Cilento, G. *Angew. Chem.* **1983**, *95*, 525; *Angew. Chem., Int. Ed. Engl.* **1983**, *22*, 529. (c) Adam, W.; Encarnación, L. A. A. *Chem. Ber.* **1982**, *115*, 2592.

(17) Levenberg, M. I.; Richards, J. H. *J. Am. Chem. Soc.* **1964**, *86*, 2634.

as being responsible for the unresolved coupling in the ^{1}H NMR spectrum. We tried to remove these detrimental traces by treating a THF solution of **1** with excess Li powder as a reducing agent and filtering the resulting suspension under an atmosphere of argon, but no improvement in the signal width was observed. The ^{13}C NMR spectrum (Figure 2) shows five signals for the substituted cyclopentadienyl ring in addition to one signal for the unsubstituted cyclopentadienyl ring. We interpret this as evidence for a "frozen propeller" conformation in solution, where each ferrocenyl group is locked in a position with little or no rotational freedom due to steric interactions. Similar arguments have been reported for other tetrasubstituted olefinic molecular propellers.[18] The ^{13}C NMR shift of the olefinic carbon is observed at 133.7 ppm, which is rather unexceptional for a C=C bond, in accord with the location of the corresponding ^{13}C NMR signals in other highly strained olefins.[1a] In contrast, the Raman-active C=C stretching vibration of 1474 cm^{-1} is very low in comparison to those for other distorted olefins,[1a] indicating reduced π-bond order and considerable twist caused by steric repulsions of the four ferrocenyl groups.

A detailed interpretation of the UV–vis and PE spectral data is hampered by the ferrocenyl substituents. Comparison of the visible absorptions of **1** with UV–vis data for sterically congested alkenes[1a,19] and for metallocenes[20] hints at an assignment of the absorption at 503 nm (log ϵ = 3.50) as indicative of a strongly twisted and partially conjugated C=C bond. The PE spectrum of **1** shows the expected ionizations for the ferrocenyl moiety (6.74 and 9.00 eV):[21] one shoulder at 6.14 eV and one band at 10.06 eV. Vertical ionization potentials of sterically strained olefins show decreased values (8.8–7.9 eV)[1a] in comparison to that of ethylene (10.51 eV). A further shifting of the first ionization to lower energy (6.1 eV for tetrakis(dimethylamino)ethylene, for example) has been observed in electron-rich olefins,[22] which makes these compounds strong reducing agents comparable to alkaline-earth metals (Ca, 6.1 eV). In our case, an assignment of the 6.14 eV band in **1** to the ionization of the C=C bond is not corroborated by cyclic voltammetric measurements (see Electrochemistry) and by the unobserved chemical reactivity of **1** as a reducing agent (with the exception of the partial oxidative decomposition of **1** in solution). The 10.06 eV band in **1**, on the other hand, seems to be too high in energy for a sterically congested and electron-rich olefinic compound such as tetraferrocenylethylene.

Electrochemistry. Oligoferrocenes, such as ferrocene itself, usually undergo reversible one-electron oxidations of each ferrocene unit, where the separation of the consecutive half-wave potentials may vary over a wide range, depending on the interaction and substitution pattern of the ferrocenyl subunits.[23] Electrochemical measurements of **1** yield four distinct oxidation steps with formation of the tetracation (see Table 1), demonstrating the highly efficient donor capacity of tetraferrocenylethylene. The good donor ability is also established by a drastically diminished first half-wave oxidation potential of 0.09 V compared to ferrocene itself (0.31–0.32 V). Under standard conditions used for cyclic voltammetric detection of the oxidation potentials in solution, the last step occurs somewhat irreversibly, probably due to decreased solubility leading to adsorption phenomena of the compound on the electrode surface. The rectangular voltammogram (Figure 3), on the other hand, enables the clear determination of the fourth half-wave potential at 0.62 V. The separation of the half-wave potentials do not allow us to identify a clear assignment of the interactions between the cis/trans forms of the 1,2-substituted ethylene or with the 1,1′-substituted units. Therefore, the following model compounds were included in the studies to serve as references for specific ferrocene–ferrocene interactions: tetraferrocenylethane (**2**), 1,1-diferrocenylethylene (**4**), diferrocenylmethane (**5**), *trans*-1,2-diferrocenylethylene (**6**), and 1,2-diferrocenylethane (**7**) (Table 1). The saturatively bridged tetraferrocenylethane (**2**) is characterized by four oxidation steps, as found for **1**, but the complete oxidation process occurs in a much smaller potential range ($\Delta[E^1-E^4]$ = 370 mV, versus 530 mV for **1**). Thus, the ethane moiety diminishes the interaction between the ferrocene substituents as expected and shows the smaller oxidation power indicated by a positively shifted first oxidation potential. The relatively large difference of the first two oxidation potentials of **2** stem from a considerable Coulomb

Table 1. Half-Wave Potentials (V)[a] of 1 in Comparison to Model Compounds 2, 4, 5, 6, and 7[b]

	1	2	4	5	6	7
$E^1_{1/2}$	0.09	0.20	0.35	0.26	0.25	0.28
$E^2_{1/2}$	0.26	0.37	0.48	0.37	0.41	0.28
E^3	0.41[c]	0.52[c]				
E^4	0.62[c]	0.57[c]				

[a] Versus SCE at 100 mV/s in 0.1 M [TBA]PF_6/CH_2Cl_2 at −30 °C. [b] Legend: **2**, tetraferrocenylethane; **4**, 1,1-diferrocenylethylene; **5**, diferrocenylmethane; **6**, trans-1,2-diferrocenylethylene; **7**, 1,2-diferrocenylethane. [c] Determined by rectangular voltammetry because of partial adsorption on electrode surface.

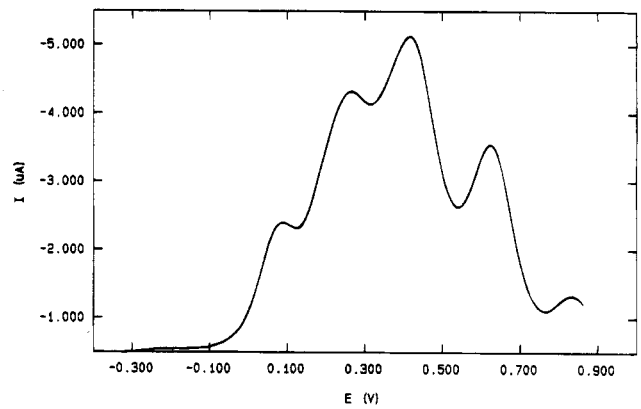

Figure 3. Rectangular voltammogram of tetraferrocenylethylene (**1**).

(18) (a) Gur, E.; Kaida, Y.; Okamoto, Y.; Biali, S. E.; Rappoport, Z. *J. Org. Chem.* **1992**, *57*, 3689. (b) Maeda, K.; Okamoto, Y.; Toledano, O.; Becker, D.; Biali, S. E.; Rappoport, Z. *J. Org. Chem.* **1994**, *59*, 5473. (c) Columbus, I.; Biali, S. E. *J. Org. Chem.* **1994**, *59*, 3402.

(19) Beck, A.; Gompper, R.; Polborn, K.; Wagner, H.-U. *Angew. Chem.* **1993**, *105*, 1424; *Angew. Chem., Int. Ed. Engl.* **1993**, *32*, 1352.

(20) Sohn, Y. S.; Hendrickson, D. N.; Gray, H. B. *J. Am. Chem. Soc.* **1971**, *93*, 3603.

(21) Zerner, M. C.; Loew, G. H.; Kirchner, R. F.; Mueller-Westerhoff, U. T. *J. Am. Chem. Soc.* **1980**, *102*, 589.

(22) (a) Cetinkaya, B.; King, G. H.; Krishnamurthy, S. S.; Lappert, M. F.; Pedley, J. B. *J. Chem. Soc., Chem. Commun.* **1971**, 1370. (b) Bock, H.; Borrmann, H.; Havlas, Z.; Oberhammer, H.; Ruppert, K.; Simon, A. *Angew. Chem.* **1991**, *103*, 1733; *Angew. Chem., Int. Ed. Engl.* **1991**, *30*, 1678.

(23) (a) Levanda, C.; Beechgard, K.; Cowan, D. O. *J. Org. Chem.* **1976**, *41*, 2700. (b) Jaitner, P.; Schottenberger, H.; Gamper, S.; Obendorf, D. *J. Organomet. Chem.* **1994**, *475*, 113.

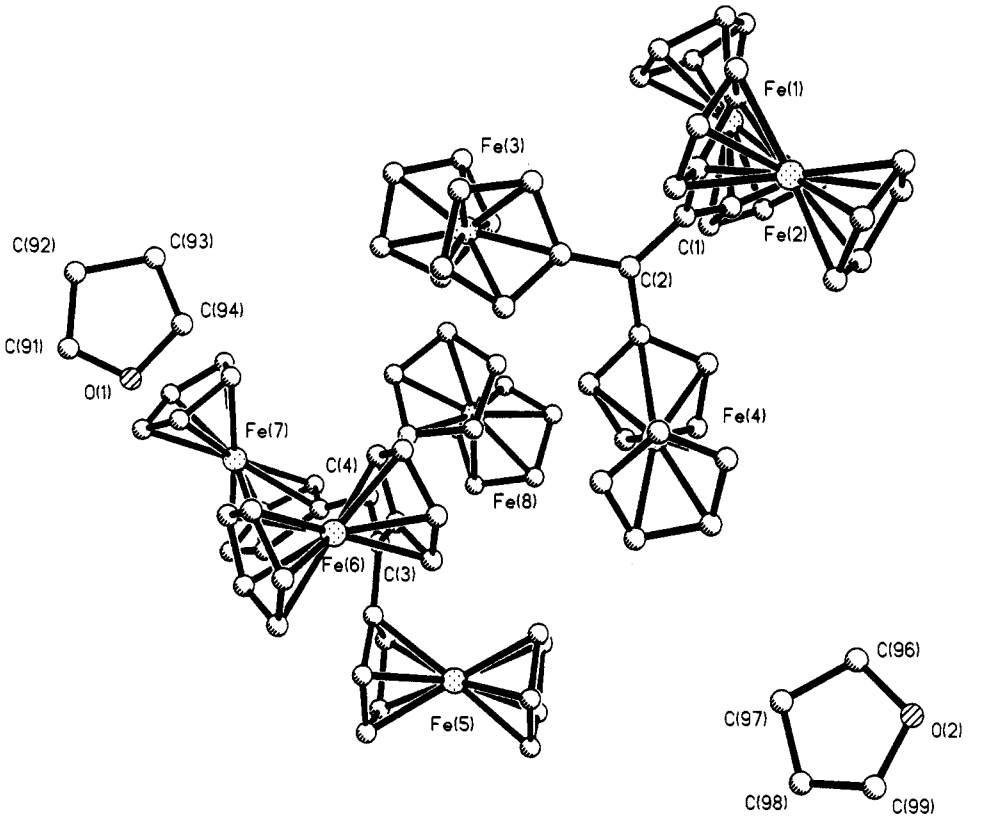

Figure 4. Molecular structure of tetraferrocenylethylene (**1**), showing the two independent molecules A and B and the two THF molecules in the asymmetric unit.

interaction (in contrast to **7**), which seems somewhat unusual for ethane-bridged ferrocenes but may be explained by the large steric demands of two ferrocenyl moieties on each carbon center, such that no anti conformation can be chosen as in 1,2-diferrocenylethane (**7**), where no such interaction can be envisaged.

X-ray Diffraction Structure of Tetraferrocenylethylene. The above results are in accord with a conformationally distorted olefin. For an exact description of the molecular structure of **1**, a single-crystal X-ray diffraction study proved necessary. The growth of suitable crystals of **1** is difficult, because this compound tends to form very thin platelets and decomposes partially in solution. After many attempts, suitable crystals were finally obtained from a concentrated solution of **1** in a mixture of THF and H_2O, kept overnight under argon at 4 °C. Figure 4 shows the contents of the asymmetric unit; the crystallographic data are listed in Table 2, and the final positional parameters are given in Table 3. Compound **1** is chiral, displays D_2 molecular symmetry in the crystal, and crystallizes as the racemate with two crystallographically independent molecules A and B and with two molecules of THF. The THF molecules and the two structurally slightly different molecules A and B seem to be necessary to obtain a sufficient crystal packing. Figures 5 and 6 show the two independent molecules of the asymmetric unit in the same orientation, illustrating their similarity. Molecules A and B differ only slightly in their torsion angles and in the bond length of the C=C double bond (Table 4). The central double bond is elongated to 138.4(7) pm in molecule A and 137.8(8) pm in molecule B (mean value 138.1 pm). Comparably high values are 140.2 pm for bis[1,3-bis-(dicyanomethylene)indan-2-ylidene][19] and 136.9[24] and 137.0 pm[25] for tetrasilylethylenes. The molecular struc-

Table 2. Crystal Data and Structure Refinement for 1

mol formula	$[C_{42}H_{36}Fe_4]\cdot[C_4H_8O]$
fw	[764.14]·[72.11]
cryst system	triclinic
space group	$P\bar{1}$ (No. 2)
unit cell dimens	a = 1162.4(8) pm
	b = 1581.3(9) pm
	c = 2067.0(10) pm
	α = 107.02(5)°
	β = 94.8(7)°
	γ = 99.21(4)°
vol	3.551(4) nm^3
Z	4
temp	183(2) K
radiation	Mo Kα (λ = 71.073 pm)
density (calcd)	1.564 Mg/m^3
abs coeff	1.639 mm^{-1}
F(000)	1728
color, habit	red platelet
cryst size	0.8 × 0.4 × 0.1 mm
θ range for data collection	5.02–23.03°
index ranges	$-12 \le h \le 12$, $-16 \le k \le 16$, $-22 \le l \le 22$
no. of rflns collected	10 546
no. of indep rflns	8924 (R_{int} = 0.0289)
no. of rflns with $I > 2\sigma(I)$	6788
abs cor	DIFABS
refinement method	full-matrix least-squares on F^2
data/restraints/parameters	8260/0/919
goodness of fit on F^2	1.039
final R indices ($I > 2\sigma(I)$)	R1 = 0.0413, wR2 = 0.0890
R indices (all data)	R1 = 0.0687, wR2 = 0.1215
largest diff peak and hole	393 and −422 e nm^{-3}

(24) Sakurai, H.; Ebata, K.; Kabuto, C.; Nakadaira, Y. *Chem. Lett.* **1987**, 301.
(25) Sakurai, H.; Tobita, H.; Nakadaira, Y.; Kabuto, C. *J. Am. Chem. Soc.* **1982**, *104*, 4288.

Table 3. Atomic Coordinates ($\times 10^{-4}$) and Equivalent Isotropic Displacement Parameters ($pm^2 \times 10^{-1}$) for 1[a]

	x	y	z	U(eq)		x	y	z	U(eq)
				Molecule A					
Fe(1)	4668(1)	5916(1)	1778(1)	22(1).	C(27)	6351(6)	3110(3)	527(3)	35(2)
Fe(2)	7008(1)	3328(1)	1521(1)	26(1)	C(28)	6022(5)	3900(3)	950(3)	28(1)
Fe(3	9111(1)	7060(1)	877(1)	22(1)	C(29)	7092(5)	4523(3)	1291(3)	22(1)
Fe(4)	10114(1)	6590(1)	3230(1)	25(1)	C(30)	9231(5)	8403(3)	1399(3)	33(2)
C(1)	7224(4)	5438(3)	1797(2)	19(1)	C(31)	9623(6)	8295(4)	756(3)	40(2)
C(2)	8276(4)	6043(3)	1903(2)	19(1)	C(32)	8677(7)	7780(4)	255(3)	48(2)
C(10)	4633(5)	6600(4)	1081(3)	35(2)	C(33)	7719(6)	7558(4)	583(3)	42(2)
C(11)	3569(5)	6588(4)	1380(3)	32(1)	C(34)	8062(5)	7943(4)	1289(3)	36(2)
C(12)	3013(5)	5684(4)	1240(3)	34(1)	C(35)	10182(5)	6452(3)	1373(3)	22(1)
C(13)	3726(5)	5130(4)	861(3)	36(2)	C(36)	10439(5)	6354(4)	702(3)	29(1)
C(14)	4722(5)	5694(4)	761(3)	33(1)	C(37)	9415(5)	5895(4)	242(3)	29(1)
C(15)	6082(5)	6597(3)	2472(3)	23(1)	C(38)	8510(5)	5718(3)	625(3)	23(1)
C(16)	5053(5)	6582(4)	2797(3)	26(1)	C(39)	8970(4)	6055(3)	1340(2)	19(1)
C(17)	4538(5)	5677(4)	2695(3)	28(1)	C(40)	11653(6)	6238(4)	2919(3)	41(2)
C(18)	5261(4)	5134(3)	2316(3)	22(1)	C(41)	11808(6)	6644(5)	3630(3)	49(2)
C(19)	6238(4)	5684(3)	2181(2)	19(1)	C(42)	10996(6)	6135(5)	3906(3)	53(2)
C(20)	6075(6)	2973(4)	2233(3)	43(2)	C(43)	10343(6)	5408(5)	3370(4)	48(2)
C(21)	6377(5)	2210(4)	1783(3)	41(2)	C(44)	10743(5)	5474(4)	2766(3)	40(2)
C(22)	7610(6)	2342(4)	1824(3)	39(2)	C(45)	9551(4)	7508(3)	2804(3)	23(1)
C(23)	8079(5)	3195(4)	2299(3)	39(2)	C(46)	9712(5)	7844(3)	3524(3)	26(1)
C(24)	7137(6)	3584(4)	2554(3)	43(2)	C(47)	8977(5)	7244(4)	3773(3)	27(1)
C(25)	8034(5)	4086(3)	1077(3)	29(1)	C(48)	8365(5)	6529(3)	3207(3)	25(1)
C(26)	7580(6)	3231(4)	605(3)	35(2)	C(49)	8700(4)	6687(3)	2596(2)	19(1)
				Molecule B					
Fe(5)	13682(1)	11325(1)	4953(1)	24(1)	C(67)	12166(5)	8689(3)	2235(3)	30(1)
Fe(6)	13790(1)	9486(1)	2481(1)	22(1)	C(68)	12066(5)	9609(3)	2396(3)	25(1)
Fe(7)	12323(1)	12877(1)	2382(1)	22(1)	C(69)	12600(4)	10061(3)	3088(3)	18(1)
Fe(8)	9181(1)	11359(1)	3501(1)	22(1)	C(70)	11031(5)	12618(5)	1584(3)	40(2)
C(3)	12651(4)	11035(3)	3429(2)	19(1)	C(71)	11894(7)	13346(4)	1592(3)	45(2)
C(4)	11839(4)	11476(3)	3214(2)	16(1)	C(72)	12962(6)	13032(4)	1527(3)	45(2)
C(50)	12146(5)	10997(4)	5330(3)	34(1)	C(73)	12761(6)	12113(4)	1479(3)	41(2)
C(51)	13090(5)	11415(4)	5868(3)	36(2)	C(74)	11559(6)	11862(4)	1514(3)	40(2)
C(52)	13958(5)	10883(4)	5774(3)	36(2)	C(75)	11564(5)	13118(3)	3262(3)	23(1)
C(53)	13570(5)	10138(4)	5178(3)	34(1)	C(76)	12354(5)	13898(3)	3256(3)	27(1)
C(54)	12446(5)	10217(4)	4910(3)	31(1)	C(77)	13495(5)	13699(3)	3203(3)	27(1)
C(55)	13479(5)	12313(3)	4536(3)	31(1)	C(78)	13419(5)	12788(3)	3173(3)	25(1)
C(56)	14510(6)	12586(4)	5017(3)	38(2)	C(79)	12227(4)	12421(3)	3228(2)	19(1)
C(57)	15264(5)	11969(4)	4807(3)	30(1)	C(80)	9189(5)	11685(4)	4530(3)	37(2)
C(58)	14714(4)	11320(3)	4187(3)	24(1)	C(81)	9728(5)	12442(4)	4358(3)	37(2)
C(59)	13599(5)	11528(3)	4000(3)	22(1)	C(82)	8907(5)	12642(4)	3914(3)	37(2)
C(60)	15593(5)	9826(4)	2713(3)	30(1)	C(83)	7849(5)	12021(4)	3813(3)	37(2)
C(61)	15246(5)	8965(4)	2195(3)	36(2)	C(84)	8014(5)	11428(4)	4188(3)	34(2)
C(62)	14603(5)	9097(4)	1636(3)	37(2)	C(85)	9694(5)	11216(3)	2561(3)	25(1)
C(63)	14535(6)	10023(4)	1794(3)	41(2)	C(86)	8635(5)	10610(4)	2508(3)	29(1)
C(64)	15161(5)	10462(4)	2461(3)	36(2)	C(87)	8838(5)	10051(4)	2910(3)	33(1)
C(65)	13056(5)	9404(3)	3332(3)	25(1)	C(88)	10036(5)	10305(3)	3210(3)	29(1)
C(66)	12779(5)	8572(3)	2813(3)	28(1)	C(89)	10595(4)	11028(3)	2988(3)	20(1)
				THF A					
O(1)	13592(7)	10244(5)	370(3)	105(2)	C(93)	11763(10)	9791(9)	-334(8)	131(5)
C(91)	13685(10)	10663(7)	-130(5)	99(3)	C(94)	12516(11)	9590(8)	212(6)	118(4)
C(92)	12742(13)	10155(6)	-682(5)	105(4)					
				THF B					
O(2)	12311(8)	4523(5)	5548(5)	139(3)	C(98)	13795(8)	5717(7)	5640(5)	98(3)
C(96)	11879(8)	5007(6)	5129(5)	83(3)	C(99)	13519(10)	4849(8)	5754(6)	101(3)
C(97)	12926(7)	5667(6)	5085(4)	73(2)					

[a] U(eq) is defined as one third of the trace of the orthogonalized $\mathbf{U}_{ij}$ tensor.

ture of **1** can be described as a twisted olefin (molecule A, 33.5°; molecule B, 36.7°; mean value 35.1°; Figure 7), which is substituted by four ferrocenyl groups; each of these ferrocenyl substituents shows no out-of-plane bending with the twisted central double bond. In other words, no pyramidalization of the olefinic sp^2 carbons occurs, but each ferrocenyl group is uniformly twisted in reference to the C=C plane (molecule A, 21.8°; molecule B, 24.4°; mean value 23.1°; Figure 8) due to steric hindrance of the inner ortho hydrogens of the substituted cyclopentadienyl rings. The four ferrocenyl substituents are alternatingly transoid attached to the central double bond, resulting in a helical vinyl propeller system, which exists in two enantiomeric forms, differing only in the sign of the twist angle of the four ferrocenyl substituents. Comparable vinyl propellers are fourfold aryl-substituted sterically congested olefins, which have been recently reported.[18]

Attempts at Chromatographic Separation of the Enantiomers of Tetraferrocenylethylene. Since attempts to separate tetraferrocenylethane (**2**) by column liquid chromatography on triacetylcellulose as chiral stationary phase (CSP) failed,[6] several chiral stationary phases were tested for the separation of the enantiomers of tetraferrocenylethylene (**1**) by HPLC. No chiral separation was obtained on (+)-poly(triphenylmethyl methacrylate) (CHIRALPAK OT(+)), which

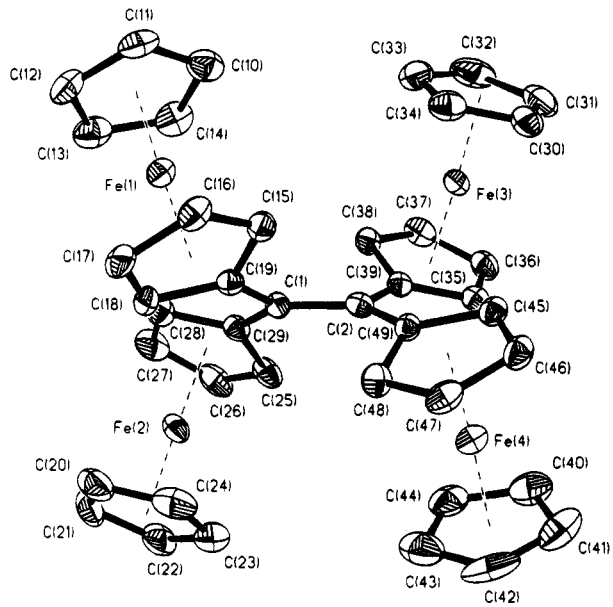

Figure 5. Molecular structure of molecule A of tetraferrocenylethylene (**1**), showing the atom-numbering scheme.

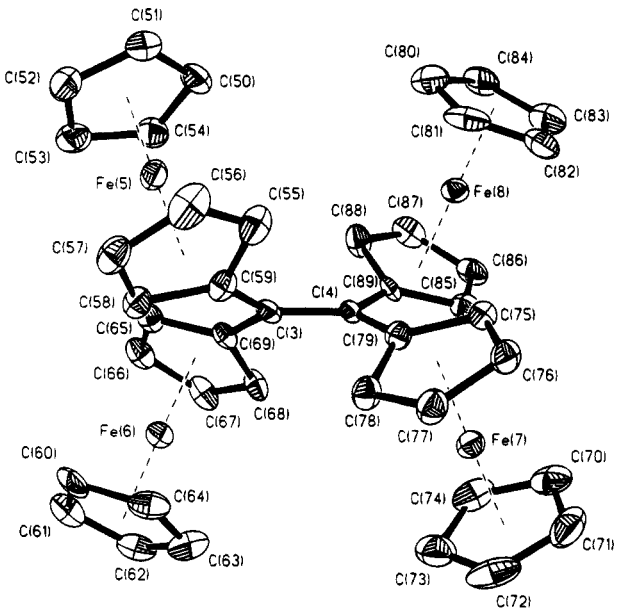

Figure 6. Molecular structure of molecule B of tetraferrocenylethylene (**1**), showing the atom-numbering scheme.

proved an appropriate CSP for the analogous dissymmetric tetramesitylethylene[18] as well as for planar chiral ferrocene compounds.[26] Also, cellulose carbamate (CHIRALCEL OD-R) in the reversed-phase mode exhibited no enantiomeric selectivity. In addition, cyclodextrins as CSP have been examined, assuming a possible separation via inclusion complexes in the reversed-phase mode. No chiral separation was obtained with a γ-cyclodextrin bonded phase, recommended for the chiral separation of dissymmetric molecules,[27] or with permethylated β-cyclodextrin. Usually permethylated β-cyclodextrin should exhibit enhanced chiral selectivity and shorter retention times for very apolar molecules compared to unmodified β-cyclodextrin used for separation of assymmetric metallocene compounds.[28] In all cases unambiguous assignment of enantiomeric peaks by online polarometric detection was not possible due to enhanced pseudorotation effects.[29] The so far unsuccessful resolution of **1** is understandable by inspection of a van der Waals plot of **1**. The highly symmetrical ball-like shape of tetraferrocenylethylene leaves little opportunity to form a diastereomeric complex with a chiral stationary phase. In further experiments capillary electrophoresis will be examined as an alternative separation system.

Experimental Section

General Comments. All the reactions were carried out in the absence of air using standard Schlenk techniques and vacuum-line manipulations. Solvents were deoxygenated, purified, and dried prior to use. Instrumentation: Bruker AC 200, Bruker AM 300, Varian UNITYplus 500 (^{1}H and ^{13}C NMR); Nicolet 510 FT-IR (IR); Nicolet 910 FT-Raman (Raman); Bruins Instruments Omega 20 (UV–vis); Varian CH-7, Finnigan MAT 95 (MS); Siemens P4 (X-ray); Waters 510/486/746 (HPLC); EG&G Princeton Applied Research Potentiostat (CV). Microanalyses were obtained from the Department for Microanalysis, University of Vienna, Vienna, Austria. Diferrocenyl ketone,[30] diferrocenyltelluroketone,[11] $TiCl_3$·3THF,[31] 1,1-diferrocenylethylene,[32] diferrocenylmethane,[33] *trans*-1,2-diferrocenylethylene,[34] and 1,2-diferrocenylethane[34] were prepared according to literature methods or were obtained as side products and had properties in accord with literature values.

Tetraferrocenylethylene (1). Method a. A suspension of 1.13 g (5 mmol) of $TiCl_3$·3THF in 100 mL of DME (dimethoxyethane) was reduced with 0.11 g (15 mmol) of lithium powder by immersing the reaction vessel in an ultrasonic cleaning bath (Bandelin SONOREX SUPER RK 255H) at room temperature for 30 min. To the resulting black suspension was added 0.5 g (1.25 mmol) of diferrocenyl ketone, and sonication was continued for an additional $^1/_2$ h. The mixture was poured into water, the organic materials were extracted with three portions of ether, and the combined organic layers were washed with water and dried with $CaCl_2$. After removal of all volatile materials *in vacuo*, the product mixture was prepurified by flash chromatography on silica with ether/*n*-hexane (3/5) as eluent, affording 0.45 g of red, microcrystalline material, consisting of mainly (>80%) tetraferrocenylethene (**1**), tetraferrocenylethane (**2**), and traces (<1%) of hexaferrocenylcyclopropane (**3**). For a relative amount of 80% in this product mixture this corresponds to a 360 mg, 0.47 mmol, 75% yield of **1**, based on starting diferrocenyl ketone.

Method b. A Schlenk vessel was charged with 100 mg of Zn powder, 0.10 mL of freshly distilled HCl-free trimethylchlorosilane, and 30 mL of THF. To this stirred suspension was added dropwise a solution of 100 mg (0.25 mmol) of diferrocenyl ketone, dissolved in 15 mL of THF. After the mixture was stirred at 0 °C for 2 h, workup similar to that in method a yielded 83 mg of a red amorphous product mixture,

(26) Yamazaki, Y.; Morohashi, N.; Hosono, K. *J. Chromatogr.* **1991**, *542*, 129.
(27) Stulcup, A. M.; Jin, H. L.; Armstrong, D. W. *J. Liq. Chromatogr.* **1990**, *13*(1), 473.
(28) Armstrong, D. W.; DeMond, W.; Czech, B. P. *Anal. Chem.* **1985**, *57*, 481.
(29) Däppen, R.; Voigt, P.; Maystre, F.; Bruno, A. *Anal. Chim. Acta* **1993**, *282*, 47.
(30) O'Connor Salazar, D. C.; Cowan, D. O. *J. Organomet. Chem.* **1991**, *408*, 219 and references cited therein.
(31) Manzer, L. E. *Inorg. Synth.* **1982**, *21*, 137.
(32) 1,1-Diferrocenylethylene was prepared by Wittig olefination of diferrocenyl ketone and had properties in accord with values reported by: Rinehart, K. L.; Kittle, P. A.; Ellis, A. F. *J. Am. Chem. Soc.* **1960**, *82*, 2082.
(33) Diferrocenylmethane was obtained by reduction of **2** with palladium on activated carbon (see Experimental Section) and had properties in accord with values reported by: Pauson, P. L.; Watts, W. E. *J. Chem. Soc.* **1962**, 3880.
(34) *trans*-1,2-Diferrocenylethylene, with 1,2-diferrocenylethane as byproduct, was obtained by reductive coupling of ferrocenecarboxaldehyde with Zn/trimethylchlorosilane (analogous to method b for the preparation of 1) and had properties in accord with values reported by: Pauson, P. L.; Watts, W. E. *J. Chem. Soc.* **1963**, 2990.

Table 4. Selected Bond Lengths (pm) and Angles (deg) for 1

	molecule A	molecule B
Bond Lengths		
C(1)–C(2)/C(3)–C(4)	138.4(7)	137.8(8)
C(1)–C(19)/C(3)–C59)	148.6(10)	147.8(12)
C(1)–C(29)/C(3)–C(69)	149.3(7)	148.4(7)
C(2)–C(39)/C(4)–C(89)	147.3(10)	147.5(9)
C(2)–C(49)/C(4)–C(79)	148.3(9)	148.1(7)
Fe(1)/Fe(5)–cent(subst Cp)[a]	164.9(19)	165.6(20)
Fe(1)/Fe(5)–cent(unsubst Cp)[a]	165.3(19)	165.9(20)
Fe(2)/Fe(6)–cent(subst Cp)[a]	165.0(19)	165.0(19)
Fe(2)/Fe(6)–cent(unsubst Cp)[a]	165.3(19)	165.5(20)
Fe(3)/Fe(8)–cent(subst Cp)[a]	165.1(19)	164.8(19)
Fe(3)/Fe(8)–cent(unsubst Cp)[a]	165.6(20)	165.3(20)
Fe(4)/Fe(7)–cent(subst Cp)[a]	164.8(19)	165.4(19)
Fe(4)/Fe(7)–cent(unsubst Cp)[a]	165.0(19)	165.5(20)
mean C_{ring}–C_{ring} in subst Cp of Fe(1)/Fe(5)	141.8(8)	142.2(9)
mean C_{ring}–C_{ring} in unsubst Cp of Fe(1)/Fe(5)	141.6(9)	142.2(9)
mean C_{ring}–C_{ring} in subst Cp of Fe(2)/Fe(6)	141.8(9)	142.0(8)
mean C_{ring}–C_{ring} in unsubst Cp of Fe(2)/Fe(6)	140.7(9)	141.9(9)
mean C_{ring}–C_{ring} in subst Cp of Fe(3)/Fe(8)	142.0(9)	142.2(9)
mean C_{ring}–C_{ring} in unsubst Cp of Fe(3)/Fe(8)	140.4(11)	141.0(9)
mean C_{ring}–C_{ring} in subst Cp of Fe(4)/Fe(7)	141.8(8)	142.3(7)
mean C_{ring}–C_{ring} in unsubst Cp of Fe(4)/Fe(7)	140.3(10)	140.4(9)
Angles		
twist angle C(1)–C(2)/C(3)–C(4)[b]	33.51(0.69)	36.75(0.74)
pyramidalization of C(1)/C(3)[c]	0.43(1.12)	0.85(1.11)
pyramidalization of C(2)/C(4)[c]	0.19(0.97)	1.50(0.89)
torsion angle C(1)/C(3)–Cp of Fe(1)/Fe(5)	22.95(0.80)	24.83(0.94)
torsion angle C(1)/C(3)–Cp of Fe(2)/Fe(6)	21.97(0.81)	23.79(0.87)
torsion angle C(2)/C(4)–Cp of Fe(3)/Fe(8)	20.31(0.77)	23.72(0.85)
torsion angle C(2)/C(4)–Cp of Fe(4)/Fe(7)	21.78(0.85)	25.38(0.85)

[a] cent = centroid of Cp. [b] Twist angle = mean value of dihedral angles C(29)–C(1)–C(2)–C(39) and C(19)–C(1)–C(2)–C(49) for molecule A and mean value of dihedral angles C(69)–C(3)–C(4)–C(89) and C(59)–C(3)–C(4)–C(79) for molecule B. [c] Pyramidalization is defined as in ref 1a.

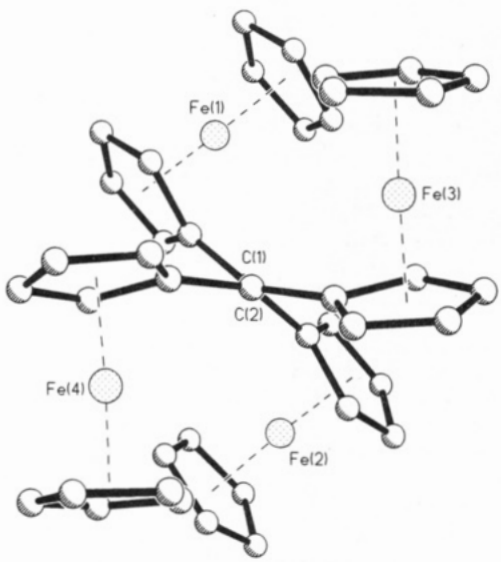

Figure 7. Molecular structure of molecule A of tetraferrocenylethylene (**1**), viewed down the olefinic C(1)-C(2) bond, showing the twist angle.

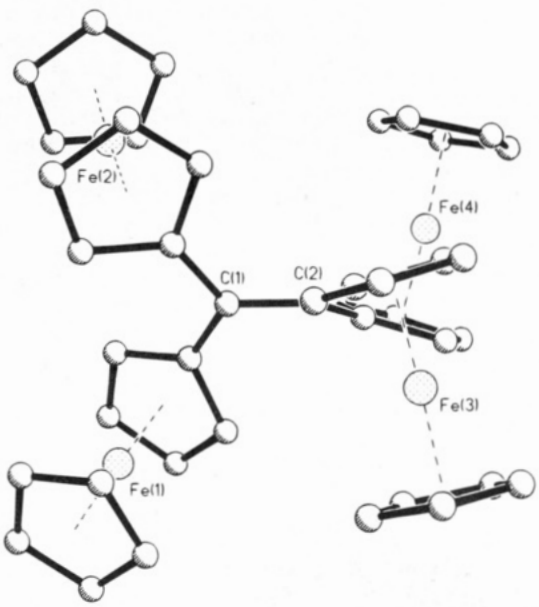

Figure 8. Molecular structure of molecule A of tetraferrocenylethylene (**1**), showing the torsion angle (twisting in reference to the C=C plane) of the ferrocenyl substituents.

consisting of mainly (>80%) tetraferrocenylethene (**1**) and tetraferrocenylethane (**2**). For a relative amount of 80% in this product mixture this corresponds to a 66 mg, 0.087 mmol, 70% yield of **1**, based on starting diferrocenyl ketone.

Method c. A Schlenk vessel with an attached reflux condenser was charged with 30 mL of toluene, 1.57 g (3.27 mmol) of bis(tri-*n*-butylstannyl) telluride, and 1.63 mL (3.27 mmol) of a 2.0 M trimethylaluminum–toluene solution. After the mixture was stirred at 110 °C for 16 h, the solvent and all volatile materials were removed on a vacuum line, leaving a white solid residue, which was dissolved in 30 mL of dioxane. To the resulting colorless solution was added 0.65 g (1.63 mmol) of diferrocenyl ketone, and within a few minutes the blue color of diferrocenyl telluroketone indicated initation of the reaction. Stirring was continued for 15 min at room temperature and for 3 h at 95 °C, during which time the color of the reaction mixture changed from dark blue to dark red with precipitation of elemental tellurium in the form of a metallic mirror on the wall of the reaction vessel. After the mixture was cooled to cool to room temperature, the following workup was performed without exclusion of air. The reaction mixture was poured into ice/water and extracted with four portions of ether; the combined organic layers were washed with three portions of water, dried with Na_2SO_4, and evaporated to dryness, leaving an oily crude product, which contains

1 and **2** in addition to organotin compounds and diferrocenyl ketone, formed by hydrolysis of diferrocenyl telluroketone. The organotin compounds were separated by flash chromatography on silica.[35] First the organic stannanes were eluted with *n*-hexane, and second the mixture of **1**, **2**, and diferrocenyl ketone was eluted with dichloromethane. This mixture was separated into a diferrocenyl ketone fraction and a product fraction by a second flash chromatography on silica with dichloromethane/*n*-hexane (2/1) as eluent, yielding 0.41 g of a red amorphous product mixture, consisting of mainly (>80%) tetraferrocenylethene **1** and tetraferrocenylethane (**2**). For a relative amount of 80% in this product mixture this corresponds to a 328 mg, 0.43 mmol, 53% yield of **1**, based on starting diferrocenyl ketone.

Separation of Tetraferrocenylethylene (1) from Tetraferrocenylethane (2) by Selective Reduction of 2. A Schlenk vessel with an attached reflux condenser was charged with a solution of 380 mg of a mixture of **1** and **2** dissolved in 20 mL of dry, deoxygenated decalin and with 300 mg of palladium (10%) on activated carbon. After 70 h at reflux temperature (bp 191 °C) the solvent decalin was removed on a vacuum line at 90 °C bath temperature; the residue was dissolved in a small volume of dichloromethane and purified by chromatography on silica with dichloromethane/*n*-hexane (1/2) as eluent. The first fraction consists of diferrocenylmethane,[33] directly followed by the second fraction of tetraferrocenylethylene (**1**). Recrystallization from THF/water (10/1) yields 174 mg (46% yield based on 380 mg starting material) in the form of thin, red platelets.

Separation of Tetraferrocenylethylene (1) from Tetraferrocenylethane (2) by Preparative HPLC. The low solubility of **1**, **2**, and **3** in conventional HPLC solvent mixtures, the oxidative decomposition of **1** in polar solvents, and the similarity in molecular shape of **1** and **2** makes the separation by HPLC difficult. The optimization of HPLC parameters results in a compromise in high loadability, efficiency of separation, and tolerance of **1** toward oxidative decomposition: column dimensions, 250 × 16 mm; stationary phase, Nucleosil C_{18} (10 μm); mobile phase, 60% THF/40% H_2O; flow rate, 16 mL/min; detection, UV (300 nm); column temperature, ambient; injection volume, 2 mL, 150 mg in 2 mL of THF. Product mixtures from McMurry reactions (method a for the synthesis of tetraferrocenylethylene) contain small traces of hexaferrocenylcyclopropane (**3**), which are easily separated from **1** and **2** by HPLC. A total yield of 7 mg of **3** could be obtained from collecting the corresponding fractions of three chromatographic separations.

Characterization of 1. Mp: >350 °C. Anal. Calcd for $C_{42}H_{36}Fe_4$: C, 66.02; H, 4.75. Found: C, 65.43; H, 4.61. UV–vis (hexane, λ_{max}) [nm/log ϵ]: 203/4.56, 314/3.70, 351/3.61, 399/3.65, 503/3.50. MS (EI, 70 eV) [*m*/*z*]: 764 (M^+), 643 (M^+ − CpFe), 578 (M^+ − $(Cp)_2Fe$), 382 ($M^+/2$), 317 (($M^+/2$) − CpH). MS (FAB) [*m*/*z*]: 764 (M^+). IR (KBr) [cm^{-1}]: 3097 m, 1560 vw, 1510 vw, 1460 w, 1412 w, 1396 w, 1295 w, 1108 s, 1052 m, 1000 m, 920 w, 814 s. Raman (KBr) [cm^{-1}]: 1474 s, 1386 m, 1269 m, 1210 m, 1168 s, 1058 m, 326 m. ^1H NMR ($CDCl_3$; 500 MHz) [ppm] (Figure 2): 4.13 (s, 20 H, unsubst Cp); 4.03, 4.1, 4.43, 5.27 (each signal: unresolved m, 4 H, C(2)–C(5) of subst Cp). ^{13}C NMR ($CDCl_3$; 50 MHz, 75 MHz) [ppm] (Figure 2): 69.6 (unsubst Cp); 66.9, 68.3, 69.1, 72.4, (C(2)–C(5) of subst Cp); 90.3 (C(1) of subst Cp); 133.7 (olefinic C). CV (CH_2Cl_2; 250 K) [V] (Table 1, Figure 3): +0.09, +0.26, +0.41, +0.62. PE (HeI; 320–340 °C) [eV]: 6.14, 6.74, 9.00, 10.06.

Characterization of 2. Spectral parameters and a single-crystal structure analysis concur with published data.[6]

Characterization of 3. MS (FAB) [m/z] (Figure 1): 1146 (M^+).

X-ray Structure Analysis of 1. A Siemens P4 diffractometer with graphite-monochromatized Mo Kα radiation (λ = 71.073 pm) was used for data collection (Table 2). The unit cell parameters were determined and refined from 25 randomly selected reflections, obtained by P4 automatic routines. Data were measured via ω-scan and corrected for Lorentz and polarization effects. Scattering factors for neutral atoms and anomalous dispersion corrections were taken from ref 36, and an empirical absorption correction[37] was made. The structure was solved by direct methods, SHELXS-86,[38] and refined by a full-matrix least-squares procedure using SHELXL-93.[39] All non-hydrogen atoms were refined with anisotropic displacement parameters (Tables 2–4). Hydrogen atoms were placed in calculated positions.

Cyclic Voltammetry. The cyclic (CV) and rectangular voltammetric experiments were carried out with an EG&G Potentiostat (Princeton Applied Research). All the measurements of the ferrocenes were taken under strictly inert conditions (N_2, Ar) in dichloromethane (CH_2Cl_2) at −30 °C with 0.1 M tetrabutylammonium hexafluorophosphate ([TBA]PF_6) as the conducting salt. As a reference for the absolute calibration of the redox potentials we used cobaltocenium/cobaltocene versus a standard calomel electrode (SCE; $E^1_{1/2}$ = −1.040 V). The measurements were performed with a scan rate of typically 100 mV/s. A gold disk (1 mm) was used as the working electrode and a platinum wire as the counter electrode. A silver wire was employed as a quasi reference electrode for the calibration of cobaltocenium/cobaltocene.

Acknowledgment. We thank the FWF, Vienna, Austria (Grant No. P10182) for financial support. We are grateful to Prof. Laszlo Szepes, University of Budapest, for PE measurements, Dr. Bill Willis, University of Connecticut, IMS, Storrs, CT, for preliminary valence band XPS measurements, Prof. F. R. Kreissl, Anorganisch-Chemisches Institut der Technischen Universität München, München, Germany, for FAB mass spectra, and Dr. Fleischer, Nicolet Instrument GmbH, Offenbach, Germany, for FT-Raman spectra.

Supporting Information Available: Tables of crystal data and structure refinement details, anisotropic thermal parameters, fractional atomic coordinates and isotropic thermal parameters for the non-hydrogen atoms, all bond lengths and angles, and fractional atomic coordinates for the hydrogen atoms (15 pages). Ordering information is given on any current masthead page.

OM950296V

(35) Farina, V. *J. Org. Chem.* **1991**, *56*, 4985.

(36) *International Tables for X-ray Crystallography*; Kynoch Press: Birmingham, U.K., 1974; Vol. IV, pp 72–98.

(37) North, A. C. T.; Phillips, D.; Mathews, F. S. *Acta Crystallogr.* **1968**, *A24*, 351.

(38) Sheldrick, G. M. SHELXS-86: Program for Crystal Structure Solutions; University of Göttingen, Göttingen, Germany, 1986.

(39) Sheldrick, G. M. SHELXL-93: Program for the Refinement of Crystal Structures; University of Göttingen, Göttingen, Germany, 1993.

Homogeneous Catalysis. Mechanism of Diastereoselective Hydroacylation of 3-Substituted-4-pentenals Using Chiral Rhodium Catalysts

Richard W. Barnhart and B. Bosnich*

Department of Chemistry, The University of Chicago, 5735 South Ellis Avenue, Chicago, Illinois 60637

Received May 31, 1995[⊗]

Catalytic hydroacylation of 4-pentenals using [Rh(diphosphine)]$^+$ catalysts leads to the formation of cyclopentanones. Catalytic kinetic resolution of racemic 3-phenyl-4-pentenal using the chiral catalyst, [Rh((*S*)-binap)]$^+$, leads not only to the diastereoselective formation of β-phenylcyclopentanone but also to the diastereoselective production of 4-phenyl-4-pentenal. The kinetics of the formation of these two products, together with deuterium distribution studies, indicates that hydroacylation proceeds by a variety of reversible steps. The 4-phenyl-4-pentenal is formed by carbonyl deinsertion–insertion steps. Although the steps appear to be reversible, equilibrium is not established. It is concluded that asymmetric hydroacylation is not governed by a single enantioselective step, but rather that the enantioselection is controlled by a number of reversible steps involving reaction intermediates.

Catalytic intramolecular hydroacylation of 4-pentenals (eq 1) is promoted by complexes of the type [Rh-

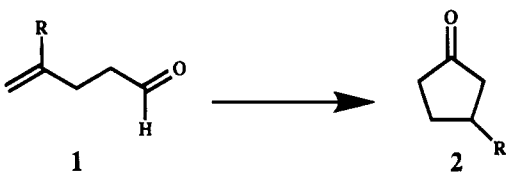

1 2 (1)

(diphosphine)(*S*)$_2$]$^+$ where S is a weakly coordinating solvent molecule.[1,2] The turnover number depends on the nature of the diphosphine and to some extent on the solvent and is controlled by a secondary reaction, namely, the formation of the catalytically inactive species [Rh(diphosphine)(CO)$_2$]$^+$ formed by decarbonylation of **1**. Despite the presence of the secondary decarbonylation path, turnover numbers of the order of 500 can be achieved with high turnover frequency, making the process practical for the production of β-substituted cyclopentanones **2**. Incorporation of the chiral diphosphine (*S*)-binap **3** generates a catalyst

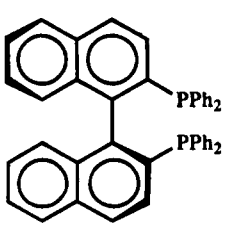

(S)-binap

3

which converts 4-substituted-4-pentenals **1** bearing tertiary or ester or ketone groups into essentially optically pure products **2**.[3]

This high enantioselectivity has prompted us to consider the possibility that efficient kinetic resolutions of 3-substituted pentenals (eq 2) might be achieved

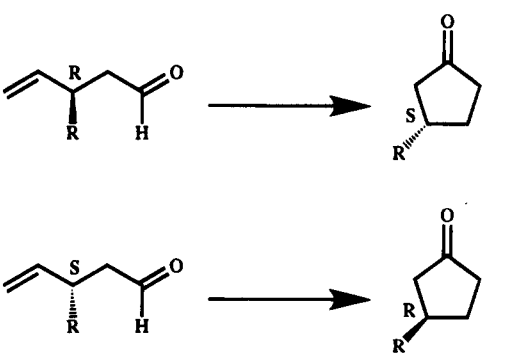

(2)

using the (*S*)-binap catalyst. The efficiency of the kinetic resolution relies on achieving a favorable differentiation for the rates of conversion of the two enantiomers of the substrate.[4,5] Two 3-substituted pentenals were investigated, namely when R = Ph and t-Bu. Although only modest kinetic resolution was observed, the origins of this resolution is surprising. We

[⊗] Abstract published in *Advance ACS Abstracts,* August 15, 1995.

(1) Fairlie, D. P.; Bosnich, B. *Organometallics* **1988**, *7*, 936.

(2) Fairlie, D. P.; Bosnich, B. *Organometallics* **1988**, *7*, 946.

(3) (a) Barnhart, R. W.; Wang, X.; Noheda, P.; Bergens, S. H.; Whelan, J.; Bosnich, B. *J. Am. Chem. Soc.* **1994**, *116*, 1821. (b) Wu, X. M.; Funakoshi, K.; Sakai, K. *Tetrahedron Lett.* **1992**, *33*, 6331.

(4) (a) Kuhn, W.; Knopf. E. *Z. Phys. Chem. B* **1930**, *7*, 292. (b) Newman, P.; Rutkin, P.; Mislow, K. *J. Am. Chem. Soc.* **1958**, *80*, 465. (c) Horeau, A. *Tetrahedron* **1975**, *31*, 1307. (d) Horeau, A. *Tetrahedron Lett.* **1962**, 965. (e) Balavoine, G.; Moradpour, A.; Kagan, H. B. *J. Am. Chem. Soc.* **1974**, *96*, 5152. (f) Martin, V. S.; Woodard, S. S.; Katsuki, T.; Yamada, Y.; Ikeda, M.; Sharpless, K. B. *J. Am. Chem. Soc.* **1981**, *103*, 6237.

(5) James and Young have reported kinetic resolutions of 2,2′-disubstituted-4-pentenals and a 3,3′-disubstituted-4–-pentenal using [Rh(chiraphos)$_2$]Cl at ~150 °C. See: (a) James, B. R.; Young, C. G. *J. Chem. Soc., Chem. Commun.* **1983**, 1215. (b) James, B. R.; Young, C. G. *J. Organomet. Chem.* **1985**, *285*, 321.

0276-7333/95/2314-4343$09.00/0

Table 1. Product Ratios for the Hydroacylation of the 3-Substituted Pentenals Using the [Rh(chiral diphosphine)]$^+$ Catalysts at 25 °C

Substrate	Diphosphine	Solvent	Products (%)		
			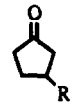	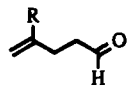	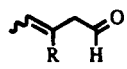
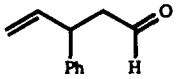	(S) - binap	CH_2Cl_2	51	42	7
	(S) - binap	acetone	91	5	5
	(S,S) - chiraphos	CH_2Cl_2	21	79	0
	(S,S) - chiraphos	acetone	38	62	0
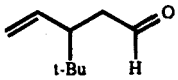	(S) - binap	CH_2Cl_2	97	3	0
	(S,S) - chiraphos	CH_2Cl_2	90	10	0

report the results here together with the possible mechanism and its implications for enantioselection.

1. Results

Table 1 lists the results using ~4 mol % of the catalysts incorporating the (*S*)-binap and (*S,S*)-chiraphos ($Ph_2PCH(CH_3)CH(CH_3)PPh_2$) ligands and the two 3-substituted-4-pentenal substrates. The ratios of products are those observed when all of the 3-substituted pentenal has been consumed. Since the rates of catalysis of the 4-substituted pentenals are at least 15 times slower than that of the 3-substituted pentenal substrates, it is possible to determine the ratio of the cyclopentanone product to that of the 4-substituted pentenal derived directly from the 3-substituted pentenal with good accuracy. The double-bond migration products, when observed, do not react further with the catalysts; thus, in all cases examined 3-substituted pentenals give both the cyclopentanone product and the 4-substituted pentenal. These ratios vary with the nature of the catalyst, the solvent, and the substrate. Eventually the 4-substituted pentenal is converted to the final cyclopentanone product.

Because the absolute configuration of the β-phenylcyclopentanone has been established[6] and because the cyclopentanone and the 4-phenylpentenal are formed in nearly equal proportions in CH_2Cl_2 solution using the (*S*)-binap catalyst, we chose this system for closer study. The small amount of double-bond migration that is observed with this system is not expected to affect the overall conclusion even if the process is diastereoselective in the sense that the (*R*)- and (*S*)-3-phenylpentenals have different rates of double-bond migration.

The time dependent evolution of the various isomers of the substrate and products is given in Table 2. The percent distribution of isomers was determined after quenching the catalysis by rapid addition of oxygen and removal of the inactivated catalyst by passing the solution through Florisil. The ratios of the various species were established by ^1H NMR spectroscopy. The enantiomer ratios of the substrate and the β-phenylcyclopentanone enantiomers were determined by ^{13}C NMR spectroscopy of the SAMP,[7] **4**, hydrazones of the aldehydes and ketones. The absolute configuration of the prevailing enantiomer of β-phenylcyclopentanone was established by optical rotation.[6] The absolute configu-

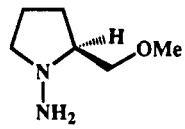

4

ration of the prevailing enantiomer of the remaining 3-phenyl-4-pentenal was determined indirectly by converting these pentenals to the β-phenylcyclopentanone by means of the achiral catalyst derived from the dcpe ($(C_6H_{11})_2PCH_2CH_2P(C_6H_{11})_2$) ligand.[1] It should be noted that (*R*)-3-phenyl-4-pentenal correlates with the (*S*)-β-phenylcyclopentanone absolute configuration because of the priority conventions. Inspection of the substrate and product enantiomer ratios (Table 2) reveals that the faster-disappearing substrate enantiomer does not produce the faster-appearing product enantiomer. This surprising result suggests that the substrate enantiomers have different rates for the production of the 4-phenyl-4-pentenal. An analysis of the data (Table 2) indicates that the relative rate constants for the pseudo-first-order catalytic production of the products is as illustrated in Scheme 1. The (*S*)-3-phenylpentenal is converted to the 4-phenylpentenal nearly 7 times faster than the corresponding conversion of the (*R*) enantiomer, but the (*R*)-3-phenylpentenal is transformed to the β-phenylcyclopentanone about twice as fast as the (*S*) enantiomer. Consequently, an unusual kinetic resolution operates where the (*S*)-β-phenylcyclopentanone is kinetically amplified not only by the faster catalytic rate of the (*R*)-3-phenylpentenal to the cyclopentanone product but also by the more rapid conversion of the (*S*)-3-phenylpentenal to the 4-phenylpentenal.

2. Mechanism

Mechanistic pathways that provide an explanation for the formation of the products are shown in Scheme 2.[2] The steps in Scheme 2 are the following, starting from the (*R*)-3-phenylpentenal **5**. Oxidative addition of the formyl C–H bond leads to **6**, which, upon hydride–olefin insertion, gives the metallocyclohexane **7**, which can reductively eliminate to give the (*S*) product. Alternatively, **7** may decarbonylate to give the metallocyclo-

(6) Taber, D. F.; Raman, K. *J. Am. Chem. Soc.* **1983**, *105*, 5935. Posner, G. H.; Hulce, M. *Tetrahedron Lett.* **1984**, *25*, 379.
(7) Enders, D.; Eichenauer, H. *Tetrahedron Lett.* **1977**, 191.

Scheme 1

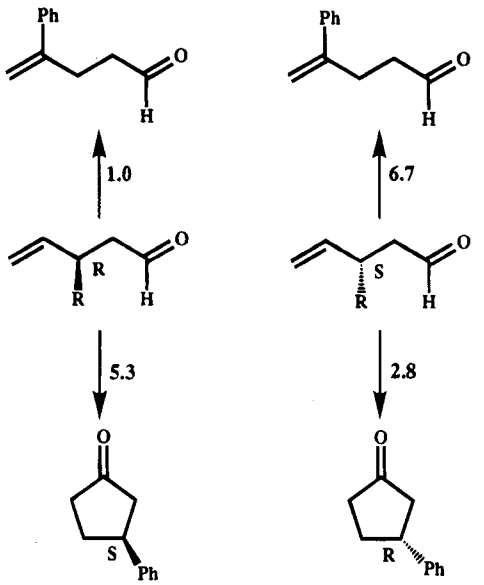

pentane **8**, which, upon carbonyl reinsertion at the other metal–carbon bond, gives **9**, which also can give the (*S*) product; but the metallocyclohexane **9** can β-hydride eliminate to **10**, and **10** can reductively eliminate to the 4-phenylpentenal **12**. In principle, the intermediate **10** can invert its enantiomeric olefin coordination to give the diastereomer **11**, which now can enter the (*S*)-3-phenylpentenal **17** domain via the intermediates **13** → **14** → **15** → **16**. It will be noted that the conformations of the metallocycles are shown and are those in which the phenyl group is in the preferred equatorial disposition. Scheme 2 illustrates how the 3-phenylpentenal substrates **5** and **17** can be converted to the 4-phenylpentenal **12**, an unusual form of metal-catalyzed isomerization. Further, the mechanism embodied in Scheme 2 implies that, if the system is under complete equilibrium via all of the equilibrating species, the ee would be the same from either the 4-phenylpentenal or from either of the two enantiomers of the 3-phenylpentenal, implying that the irreversible reductive elimination of the metallocyclohexanes (**7**, **9**, **13**, **15**) to give the products is the enantioselective step. This is not the case for any of the present systems. Thus, although the 4-*tert*-butylpentenal is converted to the β-*tert*-butylcyclopentanone in >99% ee by the (*S*)-binap catalyst in CH_2Cl_2 solution,[3a] the (*R*,*S*)-3-*tert*-butylpentenal gives only 20% ee after 70% reaction using the same catalyst under the same conditions. Were the equilibrium established and the product-forming reductive elimination the enantioselective step, we would expect the same ee starting from either substrate. Similarly, the 3-phenylpentenal analogues undergo kinetic resolution (Table 2) rather than producing a constant ee of 35%, which is observed for the 4-phenylpentenal. The lack of complete equilibration among the intermediates indicates that the enantioselection of 4-substituted pentenals using these chiral catalysts is not governed by a single enantioselective step. Rather, the ee is controlled by the relative rates of a number of reversible steps involving a variety of intermediates and probably including the rate of a final irreversible reductive elimination step. If this is generally the case for hydroacylation with these catalysts, identifying the origins of the enantioselection is made exceedingly difficult.[8]

That each step in Scheme 2, aside from the product-forming step, is likely to be reversible was demonstrated by the use of formyl-deuterated 3-phenylpentenal with the (*S*)-binap catalyst. When the deuterated substrate was mixed with the catalyst in CH_2Cl_2 solution, ^2H NMR showed that there was rapid deuterium scrambling between the formyl position and the terminus of the double bond where both the cis and trans positions were occupied by deuterium. The probable mechanism for this deuterium scrambling is illustrated in Scheme 3, which invokes the formation of the catalytically unproductive five-membered metallocycle **19** followed by β-elimination to give **20**, which in turn eliminates to the substrate. As a consequence, deuterium is found in both the α- and β-positions of the cyclopentanone product as well as in the α- and β-positions of the 4-phenylpentenal (see Scheme 2). No deuterium is found at the 4-position of the 3-phenylpentenal **23**. This suggests that the rate of elimination of the six-membered metallocycle **21** to give **23** via **22**, if elimination occurs at all, is a much slower process than that of the 4-phenyl analogue, **10** → **12** or **11** → **12** (Scheme 2). Consistently, when the 4-phenylpentenal is the substrate, no 3-phenylpentenal is observed during catalysis. This is the case for both the binap and chiraphos catalysts in either acetone or CH_2Cl_2 solution and for the 4-*tert*-butylpentenal using either catalyst in CH_2Cl_2 solution. Since the structural relationship between the transformed substrate and the phosphine of the intermediates is not known, it seems imprudent to speculate on the origins of these rate differences. Speculation is further restrained by the solvent effects observed (Table 1) which may imply that solvent coordination is present in the intermediates.

3. Conclusions

These results demonstrate that the mechanism of hydroacylation with these catalysts must involve numerous intermediate steps, most of which appear to be reversible. The steps preceding the product-forming step do not appear to be at equilibrium, for, if they were, the corresponding 3-substituted and 4-substituted pentenals would give the same ee. The enantioselection appears to be controlled at least to some extent by these intermediates, an assertion which is supported by the diastereoselective production of the 4-phenylpentenal. Finally, the existence of the carbonyl deinsertion–insertion steps suggests that 4-substituted pentenals may form products from any of the intermediates **7**, **9**, **13**, and **15** rather than from only **9** and **13**.

Experimental Section

The following compounds were prepared according to literature methods: [Rh((*S*)-binap)(NBD)]ClO_4,[9] [Rh((*S*,*S*)-chiraphos)]$_2(ClO_4)_2$,[1] and [Rh(dcpe)(NBD)]ClO_4.[1] Reagents were purified by standard methods.

3-Phenyl-4-pentenal. This substrate was prepared by the Hg^{2+}-catalyzed vinylation of cinnamyl alcohol followed by Claisen rearrangement.[10] A mixture of cinnamyl alcohol (9.00 mL, 70 mmol), butyl vinyl ether (200 mL), and $Hg(OAc)_2$ (0.80

(8) Wang, X; Bosnich, B. *Organometallics* **1994**, *13*, 4131.
(9) Miyashita, A.; Yasuda, A.; Takya, H.; Toriumi, K.; Ito, T.; Sauchi, T.; Noyori, R. *J. Am. Chem. Soc.* **1980**, *102*, 7932.
(10) Watanabe, W. H.; Conlon, L. E. *J. Am. Chem. Soc.* **1957**, *79*, 2828.

Scheme 2

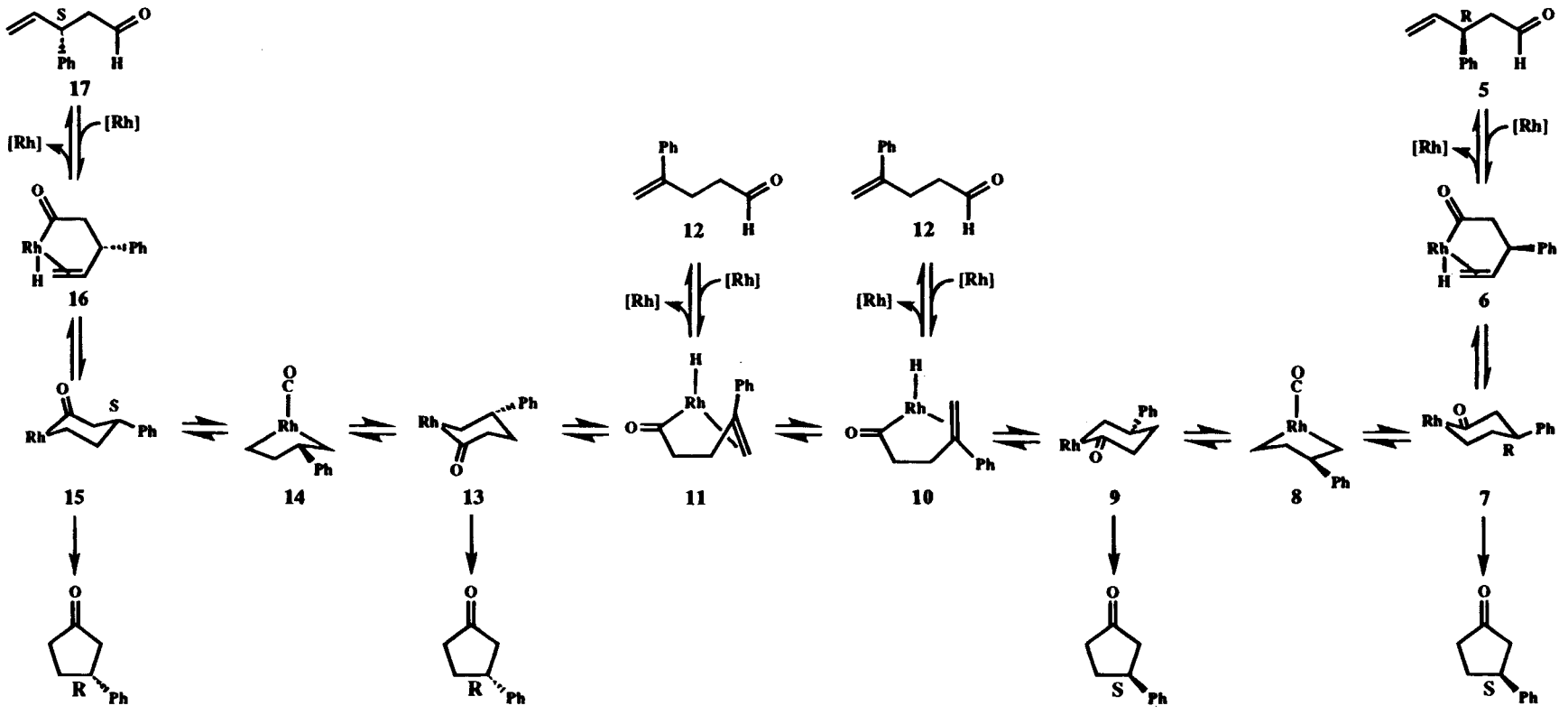

Table 2. Product and Substrate Distributions and Enantiomer Ratios during the Conversion of 3-Phenyl-4-pentenal (4.6×10^{-3} M) Catalyzed by [Rh((*S*)-binap)]ClO_4 (1 mol %) in CH_2Cl_2 Solutions at 25 °C

	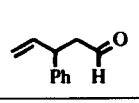		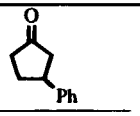		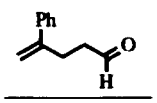	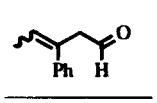
Time (min)	% remaining	R : S	% product	S : R	% product	% product
6	68	56 : 44	16	65 : 35	14	2
11	42	64 : 36	25	68 : 32	28	5
20	10	72 : 28	44	72 : 28	41	5
45	0	——	51	74 : 26	42	7

Scheme 3

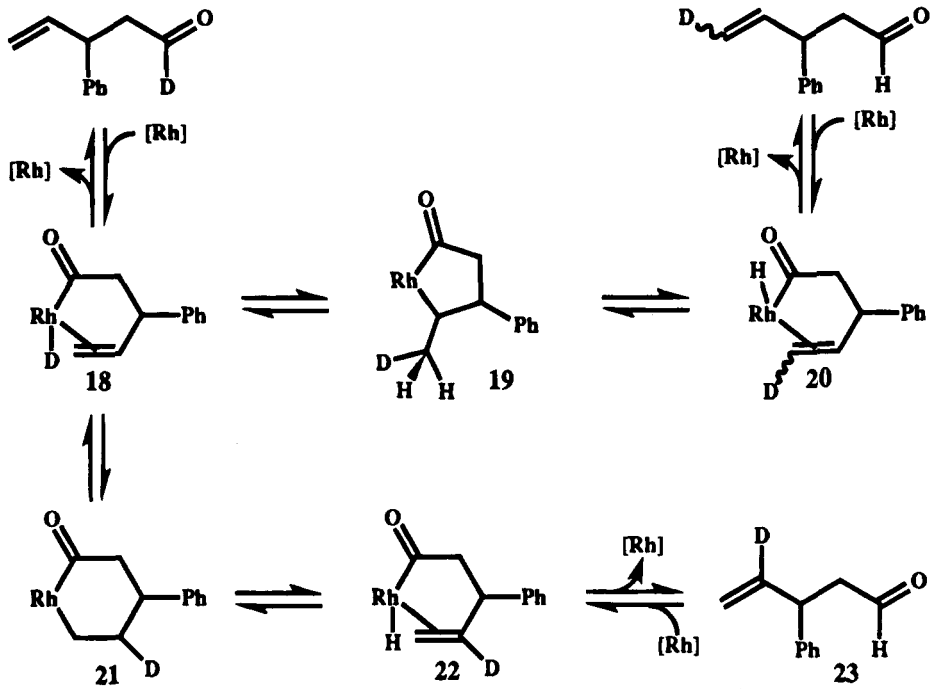

g, 2.5 mmol) was refluxed under N_2 for 24 h. The mixture was cooled to room temperature, and K_2CO_3 (2.0 g, 14 mmol) was added. After the mixture had been stirred for 30 min, it was filtered using pentane as a rinse. The solvents were distilled off under vacuum. The product was distilled under vacuum to yield a colorless liquid, which was purified twice by flash chromatography (silica gel, 12% EtOAc in hexane): 4.34 g, 39% yield; bp 53–56 °C (0.4 mmHg); ^{1}H NMR (500 MHz, $CDCl_3$) δ 9.66 (t, J = 1.6 Hz, 1 H), 7.30–7.15 (m, 5H), 5.95 (m, 1H), 5.08 (d, J = 9.9 Hz, 1 H), 5.04 (d, J = 17.3 Hz, 1 H), 3.93 (q, J = 7.1 Hz, 1 H), 2.82 (m, 2 H).

3-*tert*-Butyl-4-pentenal. This compound was also prepared by Hg^{2+}-catalyzed vinylation of the 3-substituted allyl alcohol followed by Claisen rearrangement. The allyl alcohol (4,4-dimethyl-2-pentenol) was prepared by the method of Kulkarni[11] in 50% yield. The volatility of the product aldehyde and high boiling point of butyl vinyl ether (bp 96 °C) makes it necessary to do the vinylation at a lower temperature in ethyl vinyl ether (bp 33 °C), isolate the allyl vinyl ether, and carry out the Claisen rearrangement in a separate step.

A mixture of 4,4-dimethyl-2-pentenol (2.47 g, 22 mmol), ethyl vinyl ether (60 mL), and $Hg(OAc)_2$ (0.50 g, 1.6 mmol) was refluxed for 9 h under N_2. After the reaction was cooled to room temperature and K_2CO_3 (0.65 g, 4.7 mmol) was added with stirring for 15 min, the mixture was filtered and the solids were washed with Et_2O. After the solvents were removed by rotary evaporator, the product was dissolved in Et_2O and run through a plug of silica gel (15 g), giving the impure allyl vinyl ether as a colorless oil.

The thermal Claisen rearrangement results in substantial polymerization and very low yields of product. The rearrangement proceeds rapidly and cleanly at room temperature with the addition of Et_2AlCl and PPh_3.[12]

Et_2AlCl (40 mL of a 1.0 M solution in hexane, 40 mmol) was rapidly added dropwise to a solution of PPh_3 (14.14 g, 54.0 mmol) in dry degassed CH_2Cl_2 (50 mL) under Ar. The solution was stirred at room temperature for 25 min before the addition of the impure allyl vinyl ether (2.78 g, 20.0 mmol). The reaction was stirred for 15 min, dry Et_2O (100 mL) was added, and the reaction was immediately poured into a 1.0 M solution of tartaric acid (50 mL), causing the rapid evolution of gas. The mixture was separated, and the organic phase was washed with brine (3 × 50 mL) and dried over Na_2SO_4. The resulting white solid (product in 2.7 equiv of PPh_3) was dissolved in CH_2Cl_2 (100 mL) under N_2, and MeI (7.7 mL, 54 mmol) was added dropwise over 20 min, causing the solvent to reflux. The reaction was stirred overnight at room temperature and then concentrated to about 50 mL on a rotary evaporator. Addition of Et_2O caused immediate precipitation of off-white crystalline $[Ph_3PMe]I$. Additional Et_2O was added before filtration, and the solids were washed with CH_2Cl_2/Et_2O. The filtrate was evaporated to give a deep yellow oil. The product was purified twice by flash chromatography (silica gel, 7% EtOAc in hexane) to give pure product as a colorless oil: 0.62 g, 22% yield (assuming pure starting allyl vinyl ether); ^{1}H NMR (400 MHz, CD_2Cl_2) δ 9.61 (m, 1 H), 5.74–5.65 (m, 1 H), 5.09–4.99 (m, 2 H), 2.53–2.48 (m, 1 H), 2.42–2.36 (m, 1 H), 2.32–2.25 (m, 1 H), 0.89 (s, 9 H).

1-Deuterio-3-phenyl-4-pentenal. A solution of $NaBD_4$ (0.26 g, 6.2 mmol, in 25 mL EtOH) was added dropwise over 5 min to a stirring solution of 3-phenyl-4-pentenal (1.00 g, 6.2 mmol, in 35 mL EtOH). After the reaction mixture had been stirred for 15 min, it was concentrated to about 5 mL on a rotary evaporator. After the addition of 0.5 M HCl (55 mL, 27.5 mmol), the reaction was extracted with Et_2O (4 × 25 mL). The organic layer was washed with H_2O (3 × 30 mL) until neutral and was then washed with brine (1 × 30 mL) and dried over Na_2SO_4, yielding 1.02 g (100%) as a colorless oil. The crude alcohol was oxidized by the method of Swern[13] using oxalyl chloride as the activator and triethylamine as the base. The deuterated aldehyde was purified by flash chromatography (silica gel, 10% EtOAc in hexane) to give a colorless oil in 84% yield from the starting aldehyde. The substitution at the formyl position was 67% atom D. The reduction and oxidation was repeated once more to give aldehyde with >90% atom D at the formyl position.

Catalytic Reactions. The NMR scale and small preparative scale catalytic reactions have been previously described.[3a]

To measure the reaction composition (i.e., the percentages of 3-phenyl-4-pentenal, 4-phenyl-4-pentenal, 3-phenyl-3-pentenal, and 3-phenylcyclopentanone) and to simultaneously measure the ee's of 3-phenyl-4-pentenal and 3-phenylcyclo-

(11) Kelkar, S. V.; Reddy, G. B.; Kulkarni, G. H. *Indian J. Chem.* **1991**, *30B*, 504.
(12) Takai, K.; Mori, I.; Oshima, K.; Nozaki, H. *Tetrahedron Lett.* **1981**, *22*, 3985.
(13) Omura, K.; Swern, D. *Tetrahedron* **1978**, *34*, 1651.

pentanone during catalysis, it was necessary to run large catalytic reactions and remove aliquots that could be quenched and later analyzed.

Under Ar in flame-dried glassware was dissolved [Rh((*S*)-binap)(NBD)]ClO_4 (34.0 mg, 0.0371 mmol) in dry, degassed CH_2Cl_2 (800 mL). Oxygen-free H_2 was bubbled through the solution for 10 min, and then the catalyst solution was stirred under H_2 (1 atm) for 40 min. Argon was bubbled through the solution for 35 min to purge all excess H_2. The solution was placed in a water bath to restore it to room temperature before injecting the 3-phenyl-4-pentenal (593 mg, 3.70 mmol). The reaction was stirred at room temperature. Aliquots (~110 mL) were transferred under Ar to flame-dried 250 mL flasks where they were quenched by pulling air through the mixture for 30 s. Pentane (50 mL) was added to each aliquot before passing it through Florisil (2 g) followed by CH_2Cl_2 (50 mL). The colorless solutions were placed under Ar and kept at −20 °C until they could be further analyzed. ^1H NMR was used to measure percent composition of the reaction mixture. Since all species have the same formula weight and since all species have one carbonyl group, it is possible to calculate the required amount of (*S*)-(−)-1-amino-2-(methoxymethyl)pyrrolidine (SAMP) from the total mass of the aliquot. The diastereomeric SAMP derivatives were made by the method of Enders[7] using 1.1 equiv of SAMP to ensure complete reaction of all carbonyl groups.

^{13}C NMR of the diastereomeric mixture was used to measure the ee's of the 3-phenylcyclopentanone product and 3-phenyl-4-pentenal starting material. The hydrazone may be syn or anti with respect to the 3-substituent of the cyclopentanone and syn or anti with respect to the carbon chain of the aldehyde. For the 3-substituted cyclopentanones, the syn and anti isomers form in approximately equal amounts to give four possible diastereomers, one pair for each enantiomer of the cyclopentanone product. For the aldehyde only the less hindered anti hydrazone is formed, giving one diastereomer for each enantiomer of 3-phenyl-4-pentenal.

The imine carbon of the hydrazone of the cyclopentanone has a ^{13}C NMR resonance at 168 to 171 ppm in $CDCl_3$. The two downfield resonances are assigned as the syn and anti isomers of the (*R*)-(+)-3-phenylcyclopentanone. The upfield peaks correspond to (*S*)-(−) product. Absolute configuration assignments were made using pure 3-phenylcyclopentanone prepared from 4-phenyl-4-pentenal and the literature assignment of a negative optical rotation as the (*S*) enantiomer.[3a,6]

The benzylic carbon of the hydrazone of the 3-phenyl-4-pentenal shows a ^{13}C NMR resonance at 48.1−48.2 ppm in $CDCl_3$. In 4-phenyl-4-pentenal and 3-phenyl-3-pentenal the phenyl group is conjugated to the olefin, shifting the benzylic carbon resonance and leaving the region at 48 ppm clear.

The following procedure was used to assign the absolute configuration of the 3-phenyl-4-pentenal. A small preparative scale catalytic reaction was carried out. The reaction was quenched as above after 15 min. The composition of the reaction mixture was as follows: 33% 3-phenyl-4-pentenal, 35% 4-phenyl-4-pentenal, 25% 3-phenylcyclopentanone, and 6% 3-phenyl-3-pentenal. The mixed aldehydes were separated from the cyclopentanone by flash chromatography (silica gel, 7%, EtOAc in hexane). The achiral catalyst [Rh(dcpe)(NBD)]-ClO_4 (where dcpe = 1,2-bis(dicyclohexylphosphino)ethane) cyclizes 3-phenyl-4-pentenal to 3-phenylcyclopentanone and 4-phenyl-4-pentenal more than 10× faster than it cyclizes 4-phenyl-4-pentenal. Since this catalyst is achiral, any ee in the cyclopentanone must have its origins in the nonracemic 3-phenyl-4-pentenal which was kinetically resolved by the [Rh((*S*)-binap)]ClO_4 catalyst. Any 4-phenyl-4-pentenal that cyclizes will simply decrease the ee by diluting the product with racemic product. This product is 3-phenylcyclopentanone. The relationship between absolute configuration, optical rotation, and ^{13}C NMR imine peak position of the SAMP derivative has already been made above.

Calculation of the Rate Constants. The percent composition of the aliquots was found by ^1H NMR of the crude mixtures after quenching by air and removal of catalyst by Florisil. The ee's of enantiomeric compounds (3-phenyl-4-pentenal and 3-phenylcyclopentanone) were found by ^{13}C NMR of the SAMP derivatives. The assumption was made that there was no exchange between the (*R*) and (*S*) regimes except through 4-phenyl-4-pentenal, which was slow to react under these conditions. A second assumption was made that the double-bond migration from chiral 3-phenyl-4-pentenal to achiral unreactive 3-phenyl-3-pentenal was approximately equal for the (*R*) and (*S*) enantiomers. If this assumption is not true, its effect on the outcome will be small and its effect on the conclusions will be inconsequential because the total amount of double-bond migration product formed is small compared to the amounts of cyclized product and 4-phenyl-4-pentenal formed.

The amounts of (*R*)-3-phenyl-4-pentenal at time *t* can easily be calculated using eq 3

$$n_{R\text{-SM}} = (n_{\text{total}}) \times (\%\ \text{composition}_{\text{SM}}) \times (\%\ \text{R}) \quad (3)$$

where $n_{R\text{-SM}}$ is the number of moles of (*R*) starting material at time *t*, n_{total} is the total number of moles of racemic starting material, % $\text{composition}_{\text{SM}}$ is the percent of starting material in the mixture at time *t*, and % $R = [R_{\text{SM}}/(R_{\text{SM}} + S_{\text{SM}})] \times 100\%$.

The amount of (*S*)-3-phenylcyclopentanone at time *t* ($n_{S\text{-cycl}}$) can be found similarly (eq 4)

$$n_{S\text{-cycl}} = (n_{\text{total}}) \times (\%\ \text{composition}_{\text{cycl}}) \times (\%\ S) \quad (4)$$

where $n_{S\text{-cycl}}$ is the number of moles of (*S*)-3-phenylcyclopentanone at time *t*, n_{total} is the number of total moles of racemic starting material, % $\text{composition}_{\text{cycl}}$ is the percent of 3-phenylcyclopentanone in the mixture at time *t*, and % $S = [S_{\text{cycl}}/(S_{\text{cycl}} + R_{\text{cycl}})] \times 100\%$.

The above assumptions lead to eqs 5 and 6

$$n_{R\text{-total}} = n_{S\text{-total}} = {}^1/_2 n_{\text{total}} = 36.8\ \text{mmol} \quad (5)$$

$$n_{R\text{-total}} = n_{R\text{-SM}} + n_{S\text{-cycl}} + n_{R\text{-4-Ph}} + {}^1/_2 n_{\text{dbm}} \quad (6)$$

where $n_{R\text{-total}}$ is the number of moles of compounds in or from the (*R*) domain, $n_{R\text{-4-Ph}}$ is the number of moles of 4-phenyl-4-pentenal formed from (*R*) starting material at time *t*, and n_{dbm} is the total number of moles of double-bond migration product formed at time *t*.

By eq 6 the amount of achiral 4-phenyl-4-pentenal formed can be mathematically separated as coming from the (*R*) or (*S*) starting material and can be found for each time *t* by solving for $n_{R\text{-4-Ph}}$. So the concentrations of all species are now known at each time t and can be used to calculate observed first-order rate constants.

Acknowledgment. This work was supported by grants from the National Institutes of Health.

OM9504056

Titanium–Ethylene Complexes Proposed To Be Intermediates in Ziegler–Natta Catalysis. Can They Be Detected through Vibrational Spectroscopy?

Vidar R. Jensen* and Knut J. Børve

Department of Chemistry, University of Bergen, Allégaten 41, N-5007 Bergen, Norway

Nina Westberg and Martin Ystenes

Department of Inorganic Chemistry, The Norwegian Institute of Technology, N-7034 Trondheim, Norway

Received November 18, 1994[⊗]

Quantum chemical prediction of geometry and vibrational frequencies has been performed at the SCF level of theory for the two lowest states, $^2A_1$ (**1**) and $^4B_1$ (**2**), of $Ti(C_2H_4)^+$, for $Cl_2Ti(CH_3)(C_2H_4)^+$, for the neutral, bimetallic, $AlH_2(\mu\text{-}Cl)_2TiCl_2(CH_3)(C_2H_4)$, and finally, for unperturbed C_2H_4 as a reference. For the latter three species, MP2 theory and gradient-corrected density functional theory have also been applied. The titanium–ethylene bond in **1** has a distinct covalent character, with large changes in ethylene geometry upon coordination. For the rest of the complexes only minor changes in the geometry of the ethylene unit appear upon coordination. Constrained space orbital variation (CSOV) calculations on **2** reveal that the titanium–ethylene bond consists of contributions from both intraunit polarization of Ti^+ and C_2H_4 and charge transfer from C_2H_4 to the metal. This type of bond also seems to be present in the two larger complexes, and, in spite of the small effects on ethylene geometry, the coordination nevertheless influences the frequencies, and also the IR intensities, substantially. In two regions of the spectra, dominated by the C–C stretching vibration and the out-of-plane deformation modes of ethylene, respectively, the predicted changes are particularly distinct and should be useful for spectral identification of titanium–ethylene complexes.

1. Introduction

The many advantageous properties of Ziegler–Natta catalysts have inspired numerous scientific studies during the last decades, and researchers have suggested several mechanistic schemes for the olefin polymerization using these catalysts, see, e.g., refs 1–6. Most of the proposed mechanisms involve a metal–monomer π complex intermediate. No direct proof for the existence of this complex has, however, been presented yet, but there are several observations that indicate its existence. Establishing whether such a complex is part of the propagation mechanism should therefore be given priority.

In a study concerning the polymerization of 4-methylpentene with a VCl_3 catalyst, Burfield[7] reported several indications (e.g., from IR spectra) of the presence of an olefin complex at −78 °C. The compound was catalytically active at room temperature. Grubbs and Miyashita[8] reported a stereospecific isomerization of the d_4-labeled dicyclopentadienyl titanacyclopentane that suggests an intermediate with two ethylene molecules attached to the titanium atom. This intermediate has a structure similar to modern homogeneous Ziegler–Natta catalysts. There is also indirect evidence of complex formation as the surface available for CO adsorption is reduced[9] when ethylene is introduced to an active $TiCl_3$ catalyst. Likewise, the retardation of the polymerization by internal olefins[10–12] or even more by nonconjugated diolefins[13] indicate that these olefins are able to complex and block the active center. The claims of the existence of a metal–monomer π complex during chain propagation is supported by reports of weak charge-transfer complexes of ethylene with $VOCl_3$ and $TiCl_4$.[14]

In addition to these experimental observations, quantum chemical calculations also indicate the existence of a metal–monomer intermediate in Ziegler–Natta catalysis. The metal–monomer interaction is generally found to be weak in octahedral metal complexes. Novaro *et al.*,[15,16] performing *ab initio* restricted Hartree–

* To whom correspondence should be addressed.

[⊗] Abstract published in *Advance ACS Abstracts,* August 1, 1995.

(1) Cossee, P. *Tetrahedron Lett.* **1960**, *17*, 12.
(2) Cossee, P. *J. Catal.* **1964**, *3*, 80.
(3) Ivin, K. J.; Rooney, J. J.; Stewart, C. D.; Green, M. L. H.; Mahtab, R. J. *J. Chem. Soc., Chem. Commun.* **1978**, 604.
(4) Brookhart, M.; Green, M. L. H. *J. Organomet. Chem.* **1983**, *250*, 395.
(5) Brookhart, M.; Green, M. L. H.; Pardy, R. B. A. *J. Chem. Soc., Chem. Commun.* **1983**, 691.
(6) Ystenes, M. *J. Catal.* **1991**, *129*, 383.
(7) Burfield, D. R. *J. Organomet. Chem.* **1978**, *150*, 321.
(8) Grubbs, R. H.; Miyashita, A. *J. Am. Chem. Soc.* **1978**, *100*, 1300.
(9) Fries, R. W.; Mirabella, F. M. In *Transition Metal Catalyzed Polymerizations*; Quirk, R. P., Ed.; Cambridge Univ. Press: Cambridge, 1988; p 314.
(10) Henrici-Olivé, G.; Olivé, S. *J. Organomet. Chem.* **1969**, *16*, 359.
(11) Burfield, D. R. In *Transition Metal Catalyzed Polymerizations*; Quirk, R., Ed.; MMI Symposium Series 4; Harwood: New York, 1983; p 171.
(12) Karol, F. J.; Wagner, B. E.; Cann, K. J. Lecture at the 199th ACS meeting, Boston, April 26, 1990.
(13) Solli, K.-A.; Vindstad, B. K.; Wester, T.; Ystenes, M. In *Catalyst design for tailor-made polyolefins*; Soga, K., Terano, M., Eds.; Kodansha: Tokyo, Japan, 1994; p 35.
(14) Krauss, H.-L.; Nickl, J. *Z. Naturforsch.* **1965**, *20b*, 630.

0276-7333/95/2314-4349$09.00/0

Fock (RHF) calculations on $Al(CH_3)_2(\mu\text{-}Cl)_2TiCl_2(CH_3)(C_2H_4)$, found a titanium–ethylene bond of only 3–4 kcal/mol. An even weaker metal–olefin attraction, as calculated with the modified coupled pair functional (MCPF) method and reasonably large basis sets, was recently reported for a similar model complex.[17] Somewhat higher ethylene-binding energies (7–11 kcal/mol) have been calculated for Ti(III) and Ti(IV) complexes in which the starting metal–halide fragments are frozen in a square-pyramidal configuration during ethylene coordination.[18]

In cationic complexes the ability to bind ethylene is expected to be much stronger as a result of the attractive charge-induced dipole force. Sodupe *et al.*[19] found two close-lying states for the $Ti(C_2H_4)^+$ complex, the high-spin state $^4B_1$ being only about 5 kcal/mol less stable than the covalently bound $^2A_1$. The latter has a calculated ethylene-binding energy of 24.2 kcal/mol at the MCPF level of theory. Eisch *et al.*[20] identified the cationic titanocene monoalkyl complex, $Cp_2Ti(CH_2SiMe_3)^+$, as the active species in a homogeneous ethylene polymerization, and others have obtained similar results.[21,22] These catalysts are charged entities and should therefore be expected to form relatively strong bonds with the olefin; in fact, large ethylene-binding energies (33–49 kcal/mol) have been calculated for cationic ethylene complexes of the type $[L_2M(CH_3)(C_2H_4)]^+$ (M = Ti, Zr; L = Cl or Cp type ligands).[23–28] However, the ethylene-binding energies in these models are probably overestimated due to lack of counterions and solvent effects in the models. These and other problems, e.g., insufficient treatment of electron correlation, have been noted,[29] for many of the calculations on cationic Ziegler–Natta systems. Furthermore, recent calculations which include effects of electron correlation[17,30,31] indicate that the π complex is not a stationary point on the potential energy surface due to spontaneous insertion, while others have noted a very shallow minimum for the π complex.[32]

Nevertheless, the significant affinity for the monomer which should be present in the cationic catalysts makes them promising candidates in the search for metal–monomer complexes in Ziegler–Natta catalysts. Thus, if the mechanism of Ziegler–Natta polymerization involves π-complexation of the monomer, it should be possible to detect these complexes, e.g., through vibrational spectroscopy of systems containing active cationic species. One of the aims of the present study is to provide a theoretical vibrational analysis of metal–ethylene complexes whose structures are close to what is postulated to be the case in Ziegler–Natta catalysts. The method of correlating theoretical and experimental vibrational spectra is a powerful and well-established method to detect, or to verify the structure of, molecular compounds, although so far to a lesser extent for inorganic species.[33–36] Other purposes of the present calculations are to assist the characterization of the titanium–ethylene bond in complexes and, if possible, to correlate vibrational shifts to bond characteristics. Finally, the present quantum chemical force fields of titanium–ethylene complexes are interesting as such and may be used when constructing force fields for molecular mechanics calculations.

The complexes chosen for the present study were the two lowest states, $^2A_1$ and $^4B_1$, of the simple metal cation model, $Ti(C_2H_4)^+$, the more realistic cationic model, $Cl_2Ti(CH_3)(C_2H_4)^+$, where ethylene has been found to insert into the titanium–methyl bond,[37] and finally, the neutral, bimetallic model, $AlH_2(\mu\text{-}Cl)_2TiCl_2(CH_3)(C_2H_4)$. The latter may be described as a contact ion pair consisting of $Cl_2Ti(CH_3)(C_2H_4)^+$ and $H_2AlCl_2^-$, which mimics the experimentally detected cocatalyst counterion, $AlCl_4^-$.[20] The inclusion of a counterion in one of the models is interesting, as the degree of charge separation in the homogeneous catalysts is still unclear. We have thus covered a broad range of different aspects of the postulated models of the active center, such as several different coordination numbers, different oxidation states, and both mono- and bimetallic centers.

No quantum chemical vibrational analyses of any related olefin complexes have so far been presented in the literature. Quantum chemical vibrational analyses of $TiCl_4$ and methylated derivatives[38] show that such calculations may lead to good predictions, although the accuracy may be slightly less than one could hope for. As neither experimental nor theoretical frequencies have been reported for titanium–ethylene complexes, we have no direct measure of the accuracy that can be expected for the present calculations. Therefore, we have tried to locate changes in the spectra upon ethylene coordination which show little dependence on the choice of model system and which are robust with respect to the method of calculation.

2. Computational Details

Restricted determinants were used as wave functions in all the present calculations.

(15) Giunchi, G.; Clementi, E.; Ruiz-Vizcaya, M. E.; Novaro, O. *Chem. Phys. Lett.* **1977**, *49*, 8.
(16) Novaro, O.; Blaisten-Barojas, E.; Clementi, E.; Giunchi, G.; Ruiz-Vizcaya, M. E. *J. Chem. Phys.* **1978**, *68*, 2337.
(17) Jensen, V. R.; Børve, K. J.; Ystenes, M. *J. Am. Chem. Soc.* **1995**, *117*, 4109.
(18) Jensen, V. R.; Ystenes, M.; Wärnmark, K.; Åkermark, B.; Svensson, M.; Siegbahn, P. E. M.; Blomberg, M. R. A. *Organometallics* **1994**, *13*, 282.
(19) Sodupe, M.; Bauschlicher, C. W., Jr.; Langhoff, S. R.; Partridge, H. *J. Phys. Chem.* **1992**, *96*, 2118. The state referred to as $^4B_1$ in the present work is denoted $^4B_2$ by Sodupe *et al.*
(20) Eisch, J. J.; Caldwell, K. R.; Werner, S.; Krüger, C. *Organometallics* **1991**, *10*, 3417.
(21) Alelyunas, Y. W.; Jordan, R. F.; Echols, S. F.; Borkowsky, S. L.; Bradley, P. K. *Organometallics* **1991**, *10*, 1406.
(22) Yang, X.; Stern, C. L.; Marks, T. J. *J. Am. Chem. Soc.* **1991**, *113*, 3623.
(23) Kawamura-Kuribayashi, H.; Koga, N.; Morokuma, K. *J. Am. Chem. Soc.* **1992**, *114*, 2359.
(24) Fujimoto, H.; Yamasaki, T.; Mizutani, H.; Koga, N. *J. Am. Chem. Soc.* **1985**, *107*, 6157.
(25) Jolly, C.; Marynick, D. S. *J. Am. Chem. Soc.* **1989**, *111*, 7968.
(26) Castonguay, L. A.; Rappé, A. K. *J. Am. Chem. Soc.* **1992**, *114*, 5832.
(27) Kawamura-Kuribayashi, H.; Koga, N.; Morokuma, K. *J. Am. Chem. Soc.* **1992**, *114*, 8687.
(28) Axe, F. U.; Coffin, J. M. *J. Phys. Chem.* **1994**, *98*, 2567.
(29) Jensen, V. R.; Siegbahn, P. E. M. *Chem. Phys. Lett.* **1993**, *212*, 353.
(30) Meier, R. J.; van Doremaele, G. H. J.; Iarlori, S.; Buda, F. *J. Am. Chem. Soc.* **1994**, *116*, 7274.
(31) Weiss, H.; Ehrig, M.; Ahlrichs, R. *J. Am. Chem. Soc.* **1994**, *116*, 4919.
(32) Woo, T. K.; Fan, L.; Ziegler, T. *Organometallics* **1994**, *13*, 2252.
(33) Pyykkö, P. *J. Chem. Soc., Chem. Commun.* **1990**, 933.
(34) Dymek, C.; Einarsrud, M.-A.; Wilkes, J.; Øye, H. *Polyhedron* **1988**, *7*, 1139.
(35) Einarsrud, M.-A.; Rytter, E.; Ystenes, M. *Vib. Spectrosc.* **1990**, *1*, 61.
(36) Ystenes, M. *Spectrochim. Acta* **1994**, *50A*, 219.
(37) Uppal, J. S.; Johnson, D. E.; Staley, R. H. *J. Am. Chem. Soc.* **1981**, *103*, 508.
(38) Bauschlicher, C. W., Jr.; Taylor, P. R.; Komornicki, A. *J. Chem. Phys.* **1990**, *92*, 3982.

2.1. Basis Sets. For titanium, Wachters' primitive (14s, 9p,5d) basis[39] was contracted to (10s,8p,3d) with the standard modifications as implemented in GAMESS:[40] The most diffuse s function was removed and replaced by one s function spanning the 3s–4s region ($\alpha_s = 0.209$), two p functions to describe the 4p region were added ($\alpha_p = 0.156, 0.0611$), and one diffuse d-primitive was added ($\alpha_d = 0.0743$). Chlorine and aluminum were described by ECPs according to Hay and Wadt.[41] The valence basis sets were double-ζ in the 3s and 3p regions. For chlorine, a d function with exponent 0.75 was also included in the valence basis set. Hydrogen and carbon were described by 6-31G(d) basis sets.[42,43] For carbon, the d exponent was 0.8.

In the second-order Møller–Plesset perturbation theory (MP2) and the gradient-corrected density functional theory (DFTG) calculations, the basis set of hydrogens in ethylene and the methyl group was augmented by one p function ($\alpha_p = 1.1$), yielding a 6-31G(d,p) basis. The two hydrogens attached to Al were described by 6-31G basis sets as in the SCF calculations. The correlated calculations were performed using a spherical harmonic basis, while a Cartesian basis including the s component of the d-shells was used in all reported SCF calculations.

2.2. Geometry Optimizations and Hessian Calculations. All ethylene Hessians were calculated analytically. The Hessians for the metal–ethylene complexes were calculated by numerical differentiation of the analytically determined gradients.

All geometry optimizations and Hessian calculations at the self-consistent field (SCF) Hartree–Fock (HF) level of theory were performed using the GAMESS set of programs.[40] Geometries were converged to a maximum gradient below 10^{-5} hartree/bohr. The HF numerical force field calculations were carried out with a Cartesian displacement of 0.01 bohr for each atom in the positive directions.

All MP2 and DFTG calculations were performed using the Gaussian set of programs,[44] and all valence electrons were correlated in the MP2 calculations. Geometries were converged to maximum gradient and displacement of 4.5×10^{-4} hartree/bohr and 1.8×10^{-3} bohr, respectively. The numerical force field calculations were carried out with a Cartesian displacement of 0.001 Å for each atom in all six directions. The DFTG method chosen was the Gaussian 92/DFT variation of Becke's three-parameter functional,[45] which includes Becke's 1988 exchange functional correction[46] and the correlation functional of Lee, Yang, and Parr,[47] the latter consisting of both local and nonlocal terms. The exchange and correlation functionals were evaluated using the default grid of Gaussian 92/DFT.

The reported SCF, MP2, and DFTG calculations were performed on local workstations at the University of Bergen and at the Norwegian Institute of Technology, Trondheim. Some of the larger calculations were performed on the CRAY Y-MP4D/464 and the Intel Paragon A/4 at SINTEF, Trondheim.

2.3. Constrained Space Orbital Variations (CSOV). The CSOV approach facilitates the decomposition of the energy of interaction between two molecules and is thoroughly described by Bagus *et al.*[48,49] A detailed study of ligand and metal charge rearrangements is thus enabled, and in particular, it is possible to distinguish between energetic contributions from intraunit polarization and interunit charge transfer and covalent bonding. This is achieved through the partitioning of the occupied and virtual orbital space in subsets belonging to each molecule and then optimizing the combined system by allowing orbitals in different subsets to interact according to a careful and systematic procedure.

An orbital set for the combined system was prepared from frozen, SCF-optimized orbitals for the isolated reactant molecules. The open shell orbitals on Ti^+ were chosen in accordance with their orientation in the complex. The two sets of frozen orbitals were orthogonalized in a Schmidt procedure, according to the following order of the orbitals: occ(ethylene), occ(Ti), virt(Ti), virt(ethylene), where occ(x) (virt(x)) are the occupied (virtual) orbitals of x. The CSOV calculations were thus carried out as described in ref 48 for the study of metal–ligand bonding in Al_4CO and Al_4NH_3. The CSOV calculations were performed with the STOCKHOLM[50] set of programs.

2.4. Vibrational Analysis. All frequencies were calculated within the harmonic approximation. The MOLVIB and GAMFORCE programs were applied[51,52] in assignment of the vibrations.

To aid the interpretation of the force field, the Cartesian Hessian matrix was transformed to an M-dimensional valence force field matrix. Such a transformation is only unique when $M = 3N - 6$ (N is the number of atoms). This requires a set of coordinates which often does not describe the physical situation well. For example, angles may obtain no intrinsic resistance toward deformation. This often leads to valence force matrices with very large interaction constants, and render an interpretation of the force constants close to impossible. A more appropriate set of valence coordinates can normally be obtained with $M > 3N - 6$. However, this leads to a force field matrix which is not uniquely defined. Tests with several different coordinate sets gave stretching force constants that were almost invariant to the choice of the other coordinates. The only significant variations were found when the sets were unphysical, which was easily detected as some off-diagonal constants became larger than the corresponding diagonal force constants. The force field used in this work included all stretching and bending coordinates between bonding atoms plus a torsion of the Al–Cl–Ti–Cl ring. No large off-diagonal force constants were found in the force field matrix.

For assignment of the ethylene modes the valence force constants were transformed to a set of symmetry force constants within the D_{2h} symmetry. When the potential energy distribution (PED) is calculated in terms of these symmetry constants, the D_{2h} symmetry of the vibration is found. In this way it is also possible to assign the ethylene modes to a dominating D_{2h} symmetry species even when the D_{2h} symmetry is lost. It is then possible to follow the changes in the individual modes upon complexation, although some precautions must be taken as this approach is an approximation. Nevertheless, for all ethylene modes in this work significantly more than 50% of the PED could be attributed to symmetry force constants of the given symmetry, and hence the assignments were obvious.

(39) Wachters, A. J. H. *J. Chem. Phys.* **1970**, *52*, 1033.
(40) Schmidt, M. W.; Baldridge, K. K.; Jensen, J. H.; Koseki, S.; Gordon, M. S.; Nguyen, K. A.; Windus, T. L.; Elbert, S. T. *Q. C. P. E. Bull.* **1990**, *10*, 52.
(41) Hay, P. J.; Wadt, W. R. *J. Chem. Phys.* **1985**, *82*, 284.
(42) Ditchfield, R.; Hehre, W. J.; Pople, J. A. *J. Chem. Phys.* **1971**, *54*, 724.
(43) Hehre, W. J.; Ditchfield, R.; Pople, J. A. *J. Chem. Phys.* **1972**, *56*, 2257.
(44) Frisch, M. J.; Trucks, G. W.; Schlegel, H. B.; Gill, P. M. W.; Johnson, B. G.; Wong, M. W.; Foresman, J. B.; Robb, M. A.; Head-Gordon, M.; Replogle, E. S.; Gomperts, R.; Andres, J. L.; Raghavachari, K.; Binkley, J. S.; Gonzalez, C.; Martin, R. L.; Fox, D. J.; Defrees, D. J.; Baker, J.; Stewart, J. J. P.; Pople, J. A. *Gaussian 92/DFT, Revision F.4*; Gaussian Inc.: Pittsburgh, PA, 1993.
(45) Becke, A. D. *J. Chem. Phys.* **1993**, *98*, 5648.
(46) Becke, A. D. *Phys. Rev. A* **1988**, *38*, 3098.
(47) Lee, C.; Yang, W.; Parr, R. G. *Phys. Rev. B* **1988**, *37*, 785.
(48) Bagus, P. S.; Hermann, K.; Bauschlicher, C. W., Jr. *J. Chem. Phys.* **1984**, *80*, 4378.
(49) Pettersson, L. G. M.; Bagus, P. S. *Phys. Rev. Lett.* **1986**, *56*, 500.
(50) STOCKHOLM is a general purpose quantum chemical set of programs written by P. E. M. Siegbahn, M. R. A. Blomberg, L. G. M. Pettersson, B. O. Roos, and J. Almlöf. Contact Prof. Per E. M. Siegbahn at the Department of Physics, University of Stockholm, Stockholm, Sweden, for further information.
(51) Sundius, T. *J. Mol. Struct.* **1990**, *218*, 321.
(52) Bache, Ø. *GAMFORCE*; Department of Inorganic Chemistry, Norwegian Institute of Technology, Trondheim, Norway, 1991.

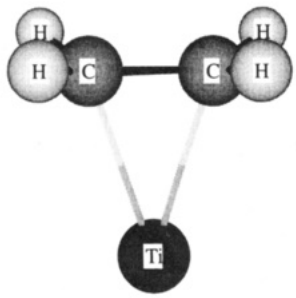

1

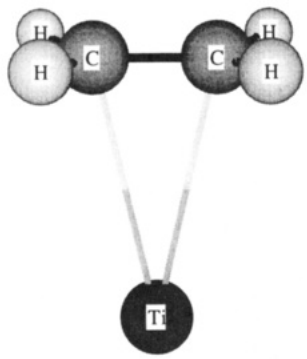

2

Figure 1. Two states, $^2A_1$ (**1**) and $^4B_1$ (**2**), of the complex $Ti(C_2H_4)^+$ as optimized at the RHF level.

Table 1. Structural Parameters for Ethylene[a]

params	RHF	MP2	DFTG	expt[b]
C−C	1.317	1.336	1.331	1.339
C−H	1.076	1.081	1.087	1.085
∠HCH	116.4	116.9	116.3	117.8

[a] Units: distances, Å; angles, deg. [b] From ref 72.

3. Results and Discussion

The first part of this section presents the calculated structures in terms of geometrical parameters. Attempts are also made, through the use of geometrical parameters, bond energies, CSOV energies of interaction, and population analyses, to characterize the titanium−ethylene bond in the various complexes. In the last part of this section, the vibrational spectra analyses are presented, with focus on the monomer modes and the modes due to the metal−monomer interactions.

3.1. Structures. The structures of the two states, $^2A_1$ (**1**) and $^4B_1$ (**2**), of $Ti(C_2H_4)^+$ are shown in Figure 1. In both of these complexes, the midpoint of the C−C bond is kept at the origin, the C−C bond is directed along the x axis, and the titanium atom is located on the negative z axis. The structures (**3** and **4**) of the two larger complexes $Cl_2Ti(CH_3)(C_2H_4)^+$ and $AlH_2(\mu\text{-}Cl)_2TiCl_2(CH_3)(C_2H_4)$ are shown in Figures 2 and 3. The wave functions of **3** and **4** transform according to the fully symmetric irreducible representation of the corresponding point groups. The structures were found to possess C_s symmetry, except for the MP2- and DFTG-optimized geometries of $Cl_2Ti(CH_3)(C_2H_4)^+$ (**3′** and **3″**, C_1 symmetry). In all cases, the presented structures are the ones which were found to have the lowest energy

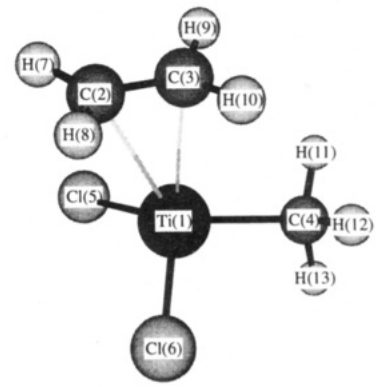

3

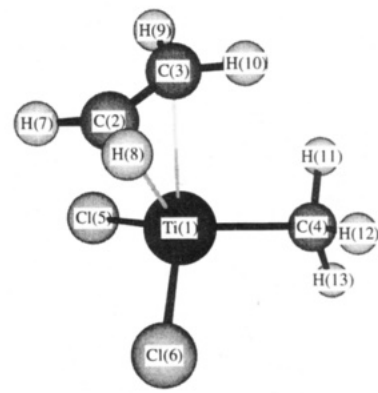

3′

Figure 2. Complex $Cl_2TiCH_3(C_2H_4)^+$ as optimized at the RHF (**3**) and MP2 (**3′**) levels. As is evident from Table 3, the DFTG-optimized structure (**3″**) is close to **3′**.

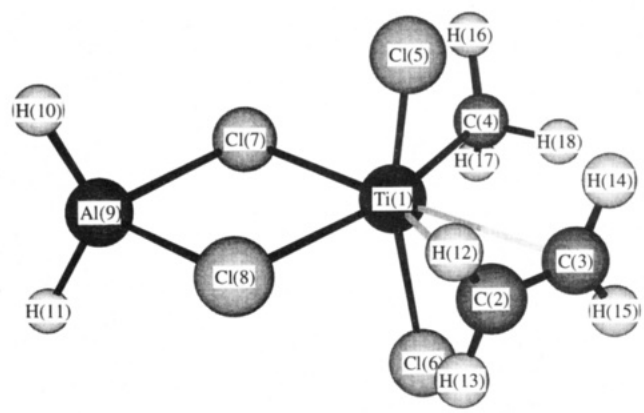

4′

Figure 3. Complex $AlH_2(\mu\text{-}Cl)_2TiCl_2(CH_3)(C_2H_4)$ as optimized at the MP2 (**4′**) level. As is evident from Table 4, the RHF-optimized structure (**4**) is similar to **4′**.

in the region of the potential energy surface where ethylene is parallel, or close to parallel, to the metal−methyl bond.

From the ethylene C−C and the Ti−ethylene distances in Tables 1−4, it is evident that a regular covalent bond to ethylene is found only in the $^2A_1$ state of $Ti(C_2H_4)^+$. The $^2A_1$ state of $Ti(C_2H_4)^+$ has, by far, the shortest metal−monomer bond of the complexes studied, the Ti−C distance being 2.192 Å at the RHF level. The

Table 2. Selected Structural Parameters from ROHF Geometry Optimization of the Two Lowest-Lying States of $Ti(C_2H_4)^+$ [a]

distances	$^2A_1$	$^4B_1$	angles	$^2A_1$	$^4B_1$
Ti–C	2.192	2.872	∠TiCH	110.2	99.6
C–C	1.394	1.333	∠HC H	114.6	116.6
C–H	1.080	1.078	∠H-bend[a]	13.0	3.0

[a] Units: distances, Å; angles, deg. [b] ∠H-bend denotes the out-of-plane bending of the hydrogen atoms.

Table 3. Selected Structural Parameters from RHF (3), MP2 (3′), and DFTG (3″) Geometry Optimization of $Cl_2Ti(CH_3)(C_2H_4)^+$ [a]

distances	3	3′	3″	angles	3	3′	3″
Ti(1)–C(2)	2.776	2.607	2.712	∠Ti(1)C(2)H(7)	104.2	98.9	101.8
Ti(1)–C(3)	2.472	2.489	2.421	∠Ti(1)C(2)H(8)	104.2	105.0	106.9
Ti(1)–C(4)	2.000	2.022	2.005	∠Ti(1)–C(3)H(9)	97.6	96.0	94.7
Ti(1)–H(11)	2.555	2.509	2.553	∠Ti(1)C(3)H(10)	97.6	101.6	99.3
Ti(1)–H(12)	2.555	2.546	2.552	∠Ti(1)C(4)H(11)	108.0	103.0	106.9
Ti(1)–H(13)	2.563	2.688	2.616	∠Ti(1)C(4)H(12)	108.0	105.6	106.9
C(2)–C(3)	1.345	1.358	1.355	∠Ti(1)C(4)H(13)	108.7	116.2	111.6
C(3)–C(4)	3.403	3.478	3.495	∠Cl(5)Ti(1)C(4)	106.4	106.6	106.9
C(2)–H(7)	1.077	1.085	1.089	∠Cl(6)Ti(1)C(4)	106.4	106.6	106.8
C(2)–H(8)	1.077	1.084	1.088	∠Cl(5)Ti(1)Cl(6)	120.8	113.3	115.0
C(3)–H(9)	1.081	1.087	1.093	∠Ti(1)C(2)C(3)	62.9	79.4	87.0
C(3)–H(10)	1.081	1.086	1.092	∠C(2)C(3)C(4)	123.7	110.3	117.2
C(4)–H(11)	1.088	1.100	1.100	∠H(7)C(2)H(8)	117.0	117.3	116.7
C(4)–H(12)	1.088	1.097	1.100	∠H(9)C(3)H(10)	117.3	117.6	117.2
C(4)–H(13)	1.087	1.091	1.097	∠H(11)C(4)H(12)	111.5	111.4	111.5
Ti(1)–Cl(5)	2.179	2.135	2.160	∠H(12)C(4)H(13)	110.0	110.4	109.9
Ti(1)–Cl(6)	2.179	2.134	2.160	∠C(4)Ti(1)C(2)C(3)	0.0	34.9	33.9

[a] Units: distances, Å; angles, deg.

Table 4. Selected Structural Parameters from RHF (4) and MP2 (4′) Geometry Optimization of $AlH_2(\mu\text{-}Cl)_2TiCl_2(CH_3)(C_2H_4)$ [a]

distances	4	4′	angles	4	4′
Ti(1)–C(2)	3.046	2.771	∠Ti(1)C(2)H(12,13)	97.4	98.0
Ti(1)–C(3)	3.048	2.798	∠Ti(1)C(3)H(14,15)	98.0	99.3
Ti(1)–C(4)	2.037	2.079	∠Ti(1)C(4)H(16,17)	109.0	114.2
Ti(1)–H(16,17)	2.600	2.712	∠Ti(1)C(4)H(18)	105.3	93.3
Ti(1)–H(18)	2.549	2.410	∠Cl(7)Ti(1)C(2)	153.3	156.6
C(2)–C(3)	1.330	1.351	∠Cl(8)Ti(1)C(2)	74.4	75.9
C(3)–C(4)	3.693	3.585	∠Cl(8)Ti(1)C(4)	169.5	162.6
C(2)–H(12,13)	1.074	1.081	∠Ti(1)C(2)C(3)	77.3	74.9
C(3)–H(14,15)	1.075	1.082	∠C(2)C(3)C(4)	110.8	110.2
C(4)–H(16,17)	1.081	1.086	∠C(3)C(4)H(16,17)	124.0	123.2
C(4)–H(18)	1.087	1.104	∠C(3)C(4)H(18)	49.6	42.0
Ti(1)–Cl(5,6)	2.278	2.239	∠H(12)C(2)H(13)	117.0	117.7
Ti(7)–Cl(7)	2.390	2.412	∠H(14)C(3)H(15)	117.3	117.9
Ti(1)–Cl(8)	2.860	2.600	∠H(16)C(4)H(17)	111.8	112.7
Cl(7)–Al(9)	2.527	2.409	∠Cl(5)Ti(1)Cl(6)	157.5	160.7
Cl(8)–Al(9)	2.289	2.333	∠Cl(7)Ti(1)Cl(8)	78.9	80.7
Al(9)–H(10,11)	1.578	1.594	∠Cl(7)Al(9)Cl(8)	88.2	86.6
			∠H(10)Al(9)H(11)	128.5	127.8
			∠Cl(5)Ti(1)Cl(6)Cl(7)	164.0	179.5

[a] Units: distances, Å, angles, deg.

C–C bond of the ethylene moiety is also very long (1.394 Å at the RHF level) compared to free ethylene. Hence the ethylene π bond is significantly weakened. Ethylene C–C bonds of this length are normally found in the transition state of olefin insertion, see, e.g., refs 23 and 24. In the other complexes, ethylene C–C bond distances of 1.330–1.345 Å are found at the RHF level, indicating only a minor weakening of the ethylene π bond.

Theoretically predicted geometries of the cationic π complex $Cl_2Ti(CH_3)(C_2H_4)^+$ have been presented by several authors.[23–25,28,31] The most relevant studies for comparison are perhaps the recent papers by Axe and Coffin[28] and Weiss *et al.*[31] since optimized geometries at the MP2 level are presented in both of these papers and, in ref 28, also at the DFTG level. The structures optimized at the HF, MP2, and DFTG levels of theory in refs 28 and 31 are close to ours, although some differences may be noticed. The present HF and MP2 metal–ligand distances, and in particular the titanium–methyl distances (2.000–2.022 Å) are somewhat longer than their reported distances (1.95–1.99 Å), probably due to the use of a larger metal basis set in the present calculations. The difference between the two Ti–C(ethylene) distances (0.12 Å) is also smaller than reported at the MP2 level (~0.4 Å) in refs 28 and 31.

The present bond distances calculated at the DFTG level are close to the distances reported by Axe *et al.* for their DFTG calculations using combined nonlocal corrections by Becke[46] and Perdew[53] (Becke–Perdew) as well as a combination of the nonlocal corrections by Perdew and Wang[54] and Perdew[53] (Perdew–Perdew). The present MP2- and DFTG-optimized structures are of C_1 symmetry while C_s symmetry was imposed by Axe and Coffin.[28] Nevertheless, the Ti–ethylene distances in ref 28 are close to the present distances, and in particular this is true for the calculations with the Becke–Perdew corrections. The calculations involving the Perdew–Perdew nonlocal corrections are seen to predict somewhat longer bond distances (~0.01–0.03 Å) than the present DFTG results.

The longest Ti–ethylene distance (Ti–C above 3 Å at the SCF level) is found for the neutral model complex **4**, shown in Figure 3. The bonding interaction probably involves dipole-induced dipole forces and σ-donation from ethylene (~0.2e, from Mulliken population analysis at the MP2 level). The binding forces are weak, as illustrated by the fact that no stationary point due to π coordination of ethylene was located for this complex at the DFTG level. As expected when including treatment of dynamical correlation, MP2 predicts shorter bond distances for the weak bonds in **4** than does SCF. In particular this is the case for the Ti(1)–C(2,3) distances, which are shortened by almost 0.3 Å. The asymmetry of the double Ti–Cl–Al bridge is also reduced, through shortening of the longest Ti–Cl distances. Finally, Ti(1)–H(18) is reduced to 2.410 Å (compared to the SCF result of 2.549 Å) when including effects of electron correlation at the MP2 level, and this may be due to a very weak agostic interaction from methyl.

Transition metal compounds generally offer many close-lying states, a fact which constitutes a challenge for theorists in the field. Rigorous treatment of correlation effects is often deemed necessary. However, the HF approximation may be able to provide reasonable geometries in cases where near degeneracies are absent, as has been seen in a series of studies involving transition metals.[19,55–64] The HF configuration is a good zeroth-order wave function for the two states of Ti-

(53) Perdew, J. P. *Phys. Rev. B* **1986**, *33*, 8822.
(54) Perdew, J. P.; Wang, Y. *Phys. Rev. B* **1986**, *33*, 8800.
(55) Dobbs, K. D.; Hehre, W. J. *J. Comput. Chem.* **1987**, *8*, 861.
(56) Dobbs, K. D.; Hehre, W. J. *J. Comput. Chem.* **1987**, *8*, 880.
(57) Blomberg, M. R. A.; Siegbahn, P. E. M.; Svensson, M. *J. Am. Chem. Soc.* **1992**, *114*, 6095.
(58) Siegbahn, P. E. M. *Chem. Phys. Lett.* **1993**, *205*, 290.
(59) Siegbahn, P. E. M. *J. Am. Chem. Soc.* **1993**, *115*, 5803.
(60) Siegbahn, P. E. M. *Theor. Cheim. Acta* **1993**, *86*, 219.
(61) Siegbahn, P. E. M.; Blomberg, M. R. A.; Svensson, M. *J. Am. Chem. Soc.* **1993**, *115*, 4191.
(62) Blomberg, M. R. A.; Siegbahn, P. E. M.; Svensson, M. *J. Phys. Chem.* **1993**, *97*, 2564.

$(C_2H_4)^+$,[19] and certainly is expected to be so also in **3** and **4**, which formally are d^0 complexes. The weight of the reference configuration (square of the coefficient) was found to be as low as 0.67 in a MCPF calculation on $H_2Al(\mu\text{-}Cl)_2TiCl_2CH_3(C_2H_4)$.[17] However, this rather low value is caused by the large number of correlated electrons in the calculation[48] rather than by important competing configurations, as illustrated by the fact that no excited configuration has a coefficient larger than 0.06.

With the HF configuration being a good zeroth-order representation of the wave function in all the present complexes, multireference treatment of correlation effects should not be required in order to obtain reasonable descriptions of geometries and relative energies in these complexes.

For further evaluation of the SCF-optimized geometries it is useful to compare some parts of the neutral structures **4** and **4'** with experimentally determined structural parameters of related compounds. The RHF- and MP2-optimized Ti(1)−Cl(5) distances of 2.278 and 2.239 Å, respectively, are in excellent agreement with X-ray diffraction data for terminal Ti−Cl bonds, 2.22−2.31 Å,[65] in titanium tetrachloride ester complexes. Likewise, the calculated Ti−methyl distances, 2.037 and 2.079 Å, agree well with the Ti−C distance of 2.042 Å found in electron diffraction studies of $TiCl_3CH_3$.[66] The calculated Al−H distances of 1.578 and 1.594 Å fit well in between the Al−H bond lengths in $[Cp_2Ti(\mu\text{-}H)_2AlH_2](CH_3)_2NC_2H_4N(CH_3)_2C_6H_6$, which were determined by X-ray crystallography to be 1.459 and 1.659 Å.[67]

3.2. Characterization of the Titanium−Ethylene Bond. Information about the calculated metal−ethylene-binding energies may add to the understanding of the mechanism involved in the coordination. Ethylene-binding energies, relative to ground state reactants, of 24.2 and 19.0 kcal/mol have been reported for the complexes **1** and **2**,[9] respectively (calculated using the modified coupled pair functional method (MCPF)). Formation of the $^2A_1$ state complex (**1**), with an electron pair present in the π back-donation orbital ($5b_1$), requires pre-excitation of Ti^+. The $^4B_1$ state (**2**), however, needs no rearrangements of the metal electrons upon ethylene coordination and thus turns out to have almost as large an ethylene-binding energy as **1**. As expected, the HF approximation fails to compensate for the loss of exchange energy when forming the low-spin state (**1**), which is thus 23.6 kcal/mol less stable than the ground state reactants at this level (ROHF). The corresponding value (15.7 kcal/mol) for **2** is more in line with the MCPF result.

Reducing the amount of repulsive valence electrons compared to **2** will tend to increase the strength of the metal−alkene bond.[29] This is the case in **3**, for which the present value of the MP2 binding energy is 42.6 kcal/mol. And finally, removing the positive charge on the metal fragment by including a counterion, as in **4**, reduces the bond strength considerably. The present MP2 result for the ethylene-binding energy in **4** is 1.5 kcal/mol, and no stationary point due to π coordination of ethylene was located for this complex with a DFTG method.

Table 5. Interaction Energies Given Relative to Separated Ti^+ and Ethylene, E_{int} [kcal/mol], and Dipole Moments (Calculated with Ti at the Origin), μ [D], for the CSOV SCF Wave Functions for the $^4B_1$ State of $Ti(C_2H_4)^+$ at the SCF Equilibrium Geometry[a]

	step	E_{int}	ΔE_{int}	μ	$\Delta\mu$
0.	frozen orbital interaction	−6.4		+0.64	
1.	Ti^+ polarization, Ti basis only	−1.2	+5.2	+1.78	+1.14
2.	Ti^+ donation, Ti + virtual C_2H_4 basis	−0.7	+0.5	+1.70	−0.08
3.	C_2H_4 polarization, C_2H_4 basis only	+3.5	+4.2	+2.29	+0.59
4.	C_2H_4 donation, C_2H_4 + virtual Ti basis	+13.3	+9.8	+3.50	+1.21
5.	C_2H_4 donation, C_2H_4 + virtual and active Ti bases	+15.4	+2.1	+4.22	+0.72
full	SCF	+15.7	+0.3	+4.29	+0.07

[a] Energies are given relative to separated Ti^+ and ethylene.

To obtain more insight into the nature of the apparently noncovalent metal−monomer bonds, it was decided to perform CSOV calculations[48,49] (cf. Computational Details) on the smallest of these complexes, the $^4B_1$ state of $Ti(C_2H_4)^+$. The titanium−ethylene-binding energy for the $^4B_1$ state, as calculated using the ROHF method, is seen to be fairly well in agreement with the MCPF value. ROHF is the level of theory used in the CSOV calculations. By means of the CSOV approach, it is possible to decompose the interaction energy between ethylene and titanium into a sum of chemically significant terms. It is of particular interest to distinguish between contributions from intraunit polarization, leading to a charge-induced dipole bond, and charge transfer, leading to a donation/back-donation bond. The interaction energy, E_{int}, relative to separated Ti^+ and ethylene is given along with the dipole moments, μ, in Table 5 for each CSOV step. The interaction energy is defined as $E_{int} = E(Ti^+) + E(C_2H_4) - E(Ti(C_2H_4)^+)$, and thus $E_{int} > 0$ indicates attraction.

The CSOV calculations were initiated, CSOV step 0, by using the frozen orbitals for the two noninteracting units Ti^+ and C_2H_4 at the equilibrium geometry. The orbitals were, however, properly orthogonalized. The negative value of E_{int} indicates that the interaction between the two frozen subsystems is repulsive. Then, in CSOV step 1, the Ti^+ orbitals were allowed to vary while the ethylene part of the orbital space was kept fixed, thus accounting for polarization of Ti^+ in the field of a frozen ethylene molecule. In step 2, the Ti orbitals were also allowed to mix with the virtual orbitals of ethylene, permitting charge transfer from Ti^+ to ethylene. Then, in step 3, the relaxed orbitals of Ti^+ were fixed and the ethylene orbitals were optimized within the ethylene orbital space. Since no virtual titanium orbitals were included in the variation, this should give a measure of the polarization of ethylene. In step 4, the virtual orbitals of Ti^+ were also included in the variation, and thus charge transfer from ethylene to Ti^+

(63) Bauschlicher, C. W., Jr.; Langhoff, S. R. *J. Phys. Chem.* **1991**, *95*, 2278.
(64) Rosi, M.; Bauschlicher, C. W., Jr. *Chem. Phys. Lett.* **1990**, *166*, 189.
(65) Rytter, E.; Kvisle, S.; Nirisen, Ø.; Ystenes, M.; Øye, H. A. In *Transition Metal Catalyzed Polymerizations: Ziegler−Natta and Metathesis Polymerizations*; Quirk, R., Ed.; Cambridge University Press, U.K., 1988; p 292.
(66) Berry, A.; Dawoodi, Z.; Derome, A. E.; Dickinson, J. M.; Downs, A. J.; Green, J. C.; Green, M. L. H.; Hare, P. M.; Payne, M. P.; Rankin, D. W. H.; Robertson, H. E. J. *J. Chem. Soc., Chem. Commun.* **1986**, 520.
(67) Lobkovskii, E. B.; Soloveichik, G. L.; Sisov, A. I.; Bulychev, B. M.; Gusev, A. I.; Kirillova, N. I. *J. Organomet. Chem.* **1984**, *265*, 167.

Table 6. Ethylene Frequencies/IR Intensities as Calculated at Various Levels of Theory[a]

mode[b]		description	SCF	MP2	DFTG	expt[c]	expt[d]
ν_{11}	B_{3u}	r (C–H stretch)	3079/1.0	3166/0.6	3247/0.7	3106 s	3234
ν_5	B_{1g}	r	3056/0	3145/0	3221/0	3103	3232
ν_1	A_g	r	3010/0	3072/0	3161/0	3026	3153
ν_9	B_{2u}	r	2989/0.6	3056/0.3	3146/0.4	2989 s	3147
ν_2	A_g	R (C=C stretch), α (C–C–H bend)	1670/0	1627/0	1714/0	1623	1655
ν_{10}	B_{2u}	α	1449/0.14	1434/0.09	1484/0.13	1444 s	1473
ν_3	A_g	α, R	1347/0	1331/0	1388/0	1342	1370
ν_6	B_{1g}	α	1218/0	1192/0	1241/0	1236	1245
ν_4	A_u	τ (ethylene torsion)	1040/0	1027/0	1067/0	1023	1044
ν_7	B_{1u}	τ, μ (C–C–H_2 out-of-plane bend)	986/2.4	934/1.9	974/1.9	949 vs	969
ν_8	B_{2g}	μ	989/0	884/0	959/0	943	959
ν_{12}	B_{3u}	α	807/0.0	796/0.0	831/0.02	826 vw	843

[a] The calculated frequencies are for harmonic modes. The SCF frequencies are scaled by a factor 0.9 and the MP2 frequencies by 0.9434.[73] Frequencies in cm^{-1}; IR intensities in $D^2\ u^{-1}\ A^{-2}$. Intensities below 0.01 are given as 0.0. [b] The ethylene molecule is oriented with the C–C bond along the z-axis and with the x-axis normal to the plane containing the molecule. [c] Observed anharmonic frequencies taken from ref 74. Intensities are visual estimates, v = very, w = weak, s = strong. [d] The harmonic frequencies are those recommended by Duncan *et al.*[75]

was accounted for. Finally, in step 5, the singly occupied orbitals of Ti^+ were included in the variational procedure, accounting for covalency between these orbitals and the ethylene orbitals.

According to the values of E_{int}, and the corresponding changes between successive CSOV steps, ΔE_{int}, the dominating contributions to the interaction energy are intraunit polarization of Ti^+ and C_2H_4 (9.4 kcal/mol), and charge transfer (donation) from C_2H_4 to Ti^+ (11.9 kcal/mol). It is evident that donation from the metal to ethylene (step 2) is unimportant. The corresponding values of μ and $\Delta\mu$ show that, for all the significant contributions, the dipole moment, as calculated with Ti at the origin, increases. The change in μ is either a result of the polarization of metal electrons away from ethylene, as in CSOV step 1, or of the polarization of ethylene charge toward the metal, as in steps 3–5. In step 1, most of the polarization can be attributed to the two unpaired electrons located in a_1 orbitals on titanium. The 4s orbital is seen to cause most of the increase in μ occurring in this step, while both orbitals experience a marked contraction in the z-direction which reduces the repulsive interaction with ethylene. The reason for nonzero dipole moment of the superimposed frozen orbital systems (step 0) is that the orbital orthogonalization procedure removes some electron density from the intermolecular region.

To conclude, the metal–alkene bonding in **2** seems to consist of intraunit polarization and ethylene donation, both being equally important. A Ti–C distance of 2.872 Å may seem unexpectedly long when compared to 2.192 Å in **1** and is a consequence of the rather repulsive high-spin coupled valence electrons of the metal, essentially the $3d^24s^1$ configuration.

Addition of covalent ligands to titanium results in a shorter bond toward ethylene, as seen in **3** (Figure 2, Table 3), where the Ti(1)–C(3) distance is below 2.5 Å for all the three methods used for optimization. Only a slight prolongation of the ethylene C–C bond (~0.02 Å) takes place upon coordination. The formal electron configuration of the metal (d^0), in **3** and **4**, hinders the formation of a covalent type donation/back-donation bond. The relatively strong metal–ethylene bond probably involves both ethylene donation and charge-induced dipole forces, as found in **2**. The relaxation due to polarization of the metal electron is expected to be less than in **2** as there are no unpaired electrons present. The Mulliken population analysis indicates that the ethylene donation should be significant for this system, with an estimated reduction in ethylene charge of ~0.3e at the MP2 level. Significant asymmetric coordination of ethylene is seen to be preferred at all three levels of theory (**3**, **3′**, and **3″**), the Ti(1)–C(3) distance being 0.1–0.3 Å longer than Ti(1)–C(2).

3.3. Vibrational Frequencies. The main results from the vibrational analysis are summarized in Tables 6–9. Table 6 gives the ethylene frequencies as calculated at the various levels of theory, as well as the observed ethylene frequencies. Tables 7 and 8 compare the vibrational frequencies, which can be attributed to the ethylene unit, and also frequencies which can be assigned to translation (liberation) and rotation (torsion) of the ethylene unit relative to the titanium fragment. In addition, for **3**, **3′**, and **3″** the section of the spectrum most suitable for detection (800–1800 cm^{-1}) is given in Figure 4 and is compared with the ethylene spectrum calculated at the corresponding level of theory. These spectra, based on the calculated frequencies and intensities, are simulated as Lorentzian functions with a common fwhm of 20 cm^{-1}. In Table 9, the most important force constants (as calculated at the SCF level) are compared. The SCF frequencies are scaled by a factor of 0.9, and the force constants are accordingly scaled by $0.81 = 0.9^2$.

Figure 5 gives the stretching force constants (scaled) for **4**.

The scaled SCF and MP2 frequencies in ethylene (Table 6) show expected and tolerable deviations from the experimental fundamentals, while the rather new DFTG functionals employed lead to frequencies that are generally close to the experimental harmonic ones. Except for ν_2 (calculated 1714, experimental harmonic 1655 cm^{-1}), DFTG performs very well in all regions of the spectrum. The overestimation of ν_2 at both the SCF and DFTG levels is caused by the incompleteness of the one-particle basis sets.[68] Tables 7 and 8 list the frequencies of the various complexes, as calculated at the SCF and the two correlated levels, respectively. In both tables the calculated frequencies of ethylene are given as reference. The modes that can be attributed to the ethylene molecule, have been labeled according to the symmetry of the corresponding mode in isolated

(68) Børve, K. J.; Jensen, V. R. Manuscript in preparation.

Table 7. Ethylene Frequencies in the Various Complexes, as Calculated at the SCF Level[a,b]

mode[c]		description	frequency/IR intensity[e] ethylene ^1A_g	**1** $^2A_1$	**2** $^4B_1$	**3** $^1A'$	**4** $^1A'$
ν_{11}	B_{3u}	r	3079/1.0	3024/0.02	3065/0.04	3083/0.2	3094/0.03
ν_5	B_{1g}	r	3056/0	3003/0	3046/0	3021/0.07	3072/0.01
ν_1	A_g	r	3010/0	2947/0.2	2982/0.01	2995/0.05	3009/0.02
ν_9	B_{2u}	r	2989/0.6	2934/0.01	2968/0.1	2935/0.2	2993/0.02
ν_2	A_g	R, α	1670/0	1505/0.05	1617/0.8	1594/1.0	1632/0.6
ν_{10}	B_{2u}	α	1449/0.14	1427/0.3	1451/0.2	1439/0.4	1450/0.2
ν_3	A_g	α, R	1347/0	1167/1.4	1330/0.6	1315/1.2	1338/0.3
ν_6	B_{1g}	α	1218/0	1206/0	1222/0	1222/0.01	1224/0.4
ν_4	A_u	τ	1040/0	841/0	1052/0	1033/0.0	1044/0.0
ν_7	B_{1u}	τ, μ	986/2.4	903/0.7	1057/5.0	994/4.4	1044/3.3
ν_8	B_{2g}	μ	989/0	982/2.0	1024/0.03	1119/1.3	1020/1.2
ν_{12}	B_{3u}	α	807/0.0	801/0.0	822/0.01	820/0.03	819/0.01
	B_{3g}	rot., β		538/0.4	297/0.08	335/0.1	314/0.2
	B_{2g}	rot., T (asym)		292/0.5	143/0.4	139/0.4	171/0.1
	B_{1u}	trans., T (sym)		272/0.8	123/0.1	249/0.6	43/0.2
	B_{3u}	trans., γ (wag)[f]				104/0.1	137/0.2
	B_{2u}	trans. (rock)[f]				150/0.0	133/0.01
	B_{1g}	rot. (twist)[f]				62/0.03	114/0.01

[a] The calculated frequencies are for harmonic modes, scaled 0.9 relative to the SCF/6-31G(d) frequencies. [b] Compounds **1**–**4** are ethylene–titanium complexes, see Figures 1–3. [c] The symmetries refer to the framework of an unperturbed ethylene molecule. For the titanium–ethylene complexes, where the symmetry is lower and mixing may occur, the modes are assigned according to the main contribution to the vibration. [d] The valence coordinates given are the ones responsible for the main contributions to the potential energy distribution. The ethylene valence coordinates are defined in Table 6. "Rot." and "trans" refer to rotation (torsion) or translation (liberation) of the whole ethylene molecule. T. Ti–C (ethylene) stretch; T_m, Ti–C (methyl) stretch; β, Ti–C–H (ethylene) bend; γ, C(ethylene)–Ti–C(methyl) bend; (twist), (rock) and (wag) refer to the whole ethylene unit vs the rest of the complex. [e] Frequencies in cm^{-1}; IR intensities in $D^2\ u^{-1}\ Å^{-2}$. Intensities below 0.01 are given as 0.0. [f] The assignment of these modes is tentative due to extensive coupling with other vibrations.

Table 8. Ethylene Frequencies in the Two Largest Complexes, at the MP2 and DFTG Levels[a]

mode[c]		description[d]	frequency/IR intensity[e] ethylene MP2 ^1A_g	**3′** MP2 ^1A	**3″** DFTG ^1A	**4′** MP2 $^1A'$
ν_{11}	B_{3u}	r	3166/0.6	3146/0.2	3255/0.2	3179/0.01
ν_5	B_{1g}	r	3145/0	3117/0.06	3199/0.09	3161/0.0
ν_1	A_g	r	3072/0	3040/0.2	3156/0.13	3072/0.01
ν_9	B_{2u}	r	3056/0.3	3017/0.3	3105/0.3	3063/0.0
ν_2	A_g	R, α	1627/0	1573/0.3	1640/0.5	1585/0.3
ν_{10}	B_{2u}	α	1434/0.09	1424/0.3	1475/0.4	1426/0.2
ν_3	A_g	α, R	1331/0	1313/0.3	1363/0.3	1319/0.2
ν_6	B_{1g}	α	1192/0	1197/0.0	1241/0.0	1197/0.0
ν_4	A_u	τ	1027/0	1035/0.01	1054/0.01	1024/0.0
ν_7	B_{1u}	τ, μ	934/1.9	979/0.6	1005/2.1	996/3.1
ν_8	B_{2g}	μ	884/0	1046/2.1	1102/1.0	953/0.09
ν_{12}	B_{3u}	α	796/0.0	804/0.02	840/0.03	805/0.0
	B_{3g}	rot., β		293/0.12	310/0.05	320/0.4
	B_{2g}	rot., T (asym)		162/0.11	148/0.2	208/0.4
	B_{1u}	trans., T (sym)		262/0.10	269/0.2	64/0.04
	B_{3u}	trans., γ (wag)		129/0.13	136/0.08	162/0.03
	B_{2u}	trans. (rock)[f]		155/0.02	160/0.02	157/0.0
	B_{1g}	rot. (twist)[f]		23/0.0	12/0.0	127/0.0

[a] The calculated frequencies are for harmonic modes. The MP2 frequencies have been scaled by a factor 0.9434.[73] [b] Compounds **3′**, **3″**, and **4′** are ethylene–titanium complexes, see Figure 2 and 3. [c] The symmetries refer to the framework of an unperturbed ethylene molecule. For the bound ethylene, where the symmetry is lower and mixing may occur, the modes are assigned according to the main contribution to the vibration. [d] The valence coordinates given are the ones responsible for the main contribution of the potential energy distribution, and are based on the SCF calculations. See Table 6 for the definition of the valence coordinates. [e] Frequencies in cm^{-1}, IR intensities in $D^2\ u^{-1}\ Å^{-2}$. Intensities below 0.01 are given as 0.0. [f] The assignment of these modes is tentative due to extensive coupling with other vibrations. See Table 7.

Table 9. Selected Force Constants (SCF/6-31G(*d*)/Scaled 0.81) for the Ethylene Group and the Titanium–Carbon Bonds[a]

	ethylene	**1**	**2**	**3**	**4**
F_R	9.29	5.45	8.47	7.97	8.65
F_r	5.00	4.88	5.00	5.06/4.88	5.08/5.09
H_α	0.94	0.69	0.87	0.88/0.78	0.88/0.90
H_τ	0.17	0.12	0.11	0.13	0.11
H_μ	0.15	0.13	0.10	0.14/0.09	0.09/0.09
F_T		0.72	0.13	0.31/0.24	0.15/0.17
H_β		0.16	0.07	0.09/0.10	0.07/0.07
F_{T_m}				1.89	1.85
H_γ				0.35	0.31
f_{Rr}	0.08	0.06	0.07	0.10/0.06	0.09/0.08
$h_{R\alpha}$	0.23	0.11	0.17	0.17/0.15	0.19
f_{RT}		0.29	0.01	−0.12/0.07	0.06/0.00
f_{TT}		−0.07	−0.02	0.06	−0.08

[a] F and f in mdyn $Å^{-1}$, H in mdyn Å rad^{-2}, and h in mdyn rad^{-1}. When the two ethylene carbons are not equivalent, two values are given for each parameter. The first value is then associated with the ethylene carbon closest to the methyl group. See Table 6 for the a definition of the valence coordinates in ethylene. The other valence coordinates are as follows: T, Ti–C (ethylene) stretch; T_m, Ti–C (methyl) stretch; β, Ti–C–H (ethylene) bend; γ, C(ethylene)–Ti–C(methyl) bend.

ethylene (cf. Computational Details). As the D_{2h} symmetry is destroyed upon complexation, modes that are IR inactive in ethylene may show up with considerable IR intensity in the complexes. The mode descriptions given in the tables are in all cases mainly based on the SCF calculations. The comparison between SCF results and the correlated calculations is difficult for the lowest frequencies reported, as it was not always possible to correlate unambiguously these modes from the various complexes. In particular, this is a problem for **3′** and **3″**, as the complex lost the mirror plane in the correlated calculations. These difficulties, however, hardly influence the internal ethylene vibrations.

The modes suitable for detection of ethylene coordination are mainly related to the out-of-plane deformation or to the C–C stretch in ethylene. In all the present complexes there is found a lowering of ν_2, an A_g mode dominated by the C–C stretch, which for **1** is reduced by 165 cm^{-1}. This reduction is predicted to be in the range 53–76 cm^{-1} for the charged complexes and close to 40 cm^{-1} for the neutral complex, **4**. The predicted change in ν_2 is thus in accordance with the correspond-

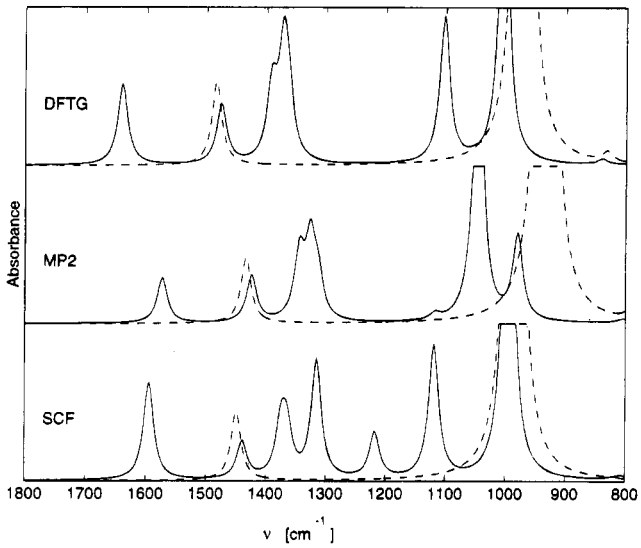

Figure 4. Simulated IR absorption (arbitrary units) spectra of $Cl_2TiCH_3(C_2H_4)^+$ based on the harmonic frequencies and intensities as calculated at SCF, MP2 and DFTG levels. SCF frequencies have been scaled by 0.90 and MP2 frequencies by 0.9434. The corresponding simulated ethylene spectra (dashed lines) are given for comparison. The highest peaks have been cut in order to reduce their dominance in the spectra. The spectra are simulated as Lorentzian functions with a common fwhm of 20 cm^{-1}.

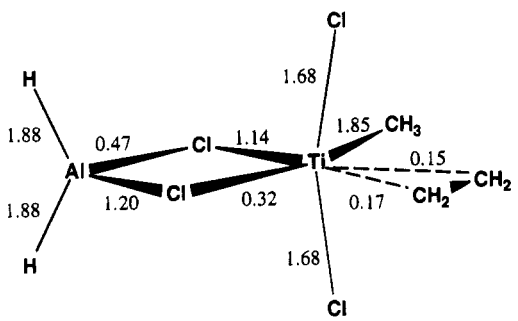

Figure 5. Stretching force constants in **4** calculated at the SCF level, scaled by a factor 0.81. The asymmetry of the Al–Cl–Ti–Cl ring is evident. For **3** the Ti–Cl stretching force constant is 2.38 mdyn $Å^{-1}$.

ing reduction (~50 cm^{-1}) reported by Burfield[7] for a VCl_3–4-methylpentene complex. Except for complex **1**, the IR intensity for this mode seems to be large enough for detection, especially as there are no other modes in this region of the spectrum. For the strongest complexation (**1**), the calculations also predict a significant effect on ν_3, due to a strong coupling between the ν_2 and ν_3 modes in ethylene. In **3**, ν_3 also gives rise to one of the strongest bands in the IR spectrum, and should thus be easily identified.

The modes related to the out-of-plane deformation in ethylene are especially useful as they seem to give information about the strength and type of the metal–ethylene bond in question. For these modes, there seem to be two opposing effects; a weakening of the π bond of ethylene gives softer force constants for these modes, and a direct interaction with titanium gives higher frequencies. As a consequence, a weak or noncovalent metal–ethylene bond leads to increased frequencies for two of these modes, ν_7 and ν_8. The total shift may be evenly distributed among the two modes, as in **4**, or unevenly, as in **3**. The large shifts to shorter wavelengths calculated for ν_8 in **3** are particularly evident in Figure 4, where it is also seen that this mode obtains significant IR intensity upon coordination. The changes in ν_7 and ν_8 are distinct even for the weakest metal–ethylene bond studied, with upward shifts of 62 and 69 cm^{-1} calculated at the MP2 level for **4**. In contrast, a strong bond with a covalent character leads to a substantial reduction in the frequencies of ν_4 and ν_7, 83 and 199 cm^{-1}, for **1**. The significant shifts predicted for the out-of-plane deformation modes, together with the strong IR intensity seen for ν_7 in particular, make these modes good candidates for detection of titanium–ethylene π complexes.

The C–H stretching region may reflect the existence of strong titanium–ethylene complexes. For **1**, a significant reduction in frequency is seen for all of these four modes. For the weaker complexes, only small or no changes are seen. A specific problem is that the modes appear to get a lower IR intensity after coordination, and hence detection may be difficult.

The low-frequency modes, especially those connected to rotation or translation of the ethylene entity, are probably less useful for the detection of the complexation. Their frequencies are uncertain and cannot be checked against known modes, and they would probably produce much weaker bands in the far IR spectrum than modes related to the rest of the complex. The Ti–Cl stretching modes may dominate this part of the spectrum, with strong and broad bands.[69,70]

Significant differences may be noticed when comparing the various methods mode by mode. For example, the SCF calculation predicts (Figure 4) that the CH_3 umbrella vibration should be observable as a significant band at 1217 cm^{-1} in the IR spectrum. The correlated calculations predict that this mode should have a lower frequency (1117 and 1179 cm^{-1}) and also a much lower IR activity. In hydrocarbons, this mode normally has a frequency at about 1375 cm^{-1}, while it is close to 1200 cm^{-1} in trimethylaluminum and trimethylgallium.[71] Some differences in the region 1300–1400 cm^{-1} are also evident from Figure 4. This region contains three overlapping peaks; two CH_3 deformation modes in addition to ν_3. All the calculations predict that the two CH_3 deformation modes are close to degenerate and have higher frequencies than ν_3. The latter difference is seen to be larger at the SCF level than for the two correlated methods.

In spite of some differences between the results from the various methods, the directions of the shifts which have been found suitable for detection of π complex

(69) Ystenes, M.; Rytter, E. *Spectrosc. Lett.* **1987**, *20*, 519.
(70) Ystenes, M.; Rytter, E. *Spectrochim. Acta* **1992**, *48A*, 543.
(71) Kvisle, S. Aluminum Alkyls in Low Temperature Matrices. Ph.D. Thesis, Department of Inorganic Chemistry, The Norwegian Institute of Technology, Trondheim, Norway, 1983.
(72) Duncan, J. L.; Wright, I. J.; Van Lerberghe, D. *J. Mol. Spectrosc.* **1972**, *42*, 463.
(73) Pople, J. A.; Scott, A. P.; Wong, M. W.; Radom, L. *Isr. J. Chem.* **1993**, *33*, 345. A scale factor of 0.9427 is reported for full MP2/6-31G(d) fundamental frequencies. Anthony P. Scott reports in an electronic mail posting to the Computational Chemistry List (**gopher://info-meister.osc.edu:73/1m/archived-messages/94/08/10**) that the scale factor for frozen core MP2/6-31G(d) has been estimated at 0.9434.
(74) Shimanouchi, T., Ed. *Tables of Molecular Vibrational Frequencies.* National Bureau of Standards: Washington, DC, 1972; Consolidated Volume 1, NSRDS-NBS-39.
(75) Duncan, J. L.; McKean, D. C.; Mallison, P. D. *J. Mol. Spectrosc.* **1973**, *45*, 221.

formation are seen to be independent of the methods applied in the present study. The applied computational methods are also seen to predict roughly the same magnitude for the shifts. An exception is the two out-of-plane ethylene deformation modes in **3**, ν_7 and ν_8, where the SCF calculation predicts that most of the shift occurs in the ν_8 mode, probably because the complex has C_s symmetry at this level of theory. However, the good agreement between the shifts calculated for **3** at the two correlated levels is encouraging. None of the shifts calculated for ν_2, ν_7, and ν_8 differs by more than 20 cm^{-1} between the MP2 and DFTG methods. The fact that no titanium–ethylene π complex was found for **4** with the DFTG method is taken as a reminder that it is still not clear whether these complexes, proposed to be intermediates in Ziegler–Natta catalysis, represent local minima on the potential energy surface of ethylene insertion reaction. Even if such local minima exist, it is an open question whether the lifetimes of the complexes are sufficient for experimental detection.

3.4. Important Features of the Force Field. The calculated force constants in Table 9 reflect the changes that appear in ethylene upon coordination. The changes are particularly clear for **1**: the C–C bond becomes weaker, and the C–C–H angle is less rigid. The Ti–C stretching constants increase with shorter Ti–ethylene bond lengths, and this is accompanied by an increasing force constant for the Ti–C–H bend. The large and positive f_{RT} (C–C/C–Ti interaction) is also expected, as a shortening of the Ti–ethylene bond leads to a longer C–C bond. A negative f_{TT} (C–Ti/C–Ti interaction) shows that the Ti–ethylene bond is best described as a nonclassic bond to the center of the π bond and not as independent Ti–C bonds.

The nonclassic bond character is not that evident for **3**, where the asymmetric complexation leads to different effects for the two carbon atoms. The two F_T constants differ with more than 25%, which is also reflected in a difference of 0.3 Å between the lengths of these two bonds at both the SCF and DFTG levels. Furthermore, the two f_{RT} constants have different signs, and f_{TT} is positive. This means that shortening the Ti–ethylene bond should cause the ethylene entity to rotate (B_{2g}), and a rotation should cause shortening or lengthening of the C–C bond, depending on the direction of rotation. The explanation is probably that the complex is approaching a classic bond situation for the Ti–C bond closest to the methyl group. A further strengthening of this bond causes a weakening of the metal–ethylene π bond and thus a shortening of the ethylene C–C bond. A feature that reflects the positive value of f_{TT} is that the frequency of the asymmetric Ti–ethylene stretch is significantly lower than for the symmetric counterpart.

The force field for **4** behaves more as expected, with a negative f_{TT} and positive f_{RT} for both Ti–C bonds. However, one of the latter interactions is reduced to nil, probably because of the very weak metal–ethylene interaction, with Ti–C distances above 3 Å. The weak titanium–ethylene interaction is reflected in the low calculated frequencies (43 and 64 cm^{-1}) for the symmetric Ti–ethylene stretch.

4. Conclusions

Ethylene was found to be covalently bound in the $^2A_1$ state of $Ti(C_2H_4)^+$. For the other complexes studied, the olefin geometry is much closer to that of free ethylene, with only a small weakening of the ethylene π bond during coordination. In the $^4B_1$ state of $Ti(C_2H_4)^+$, detailed CSOV calculations show that the bond to ethylene is composed of intramolecular polarization and ethylene-to-metal donation. The rather weak metal–monomer interaction in this complex is caused by the repulsive high-spin coupled valence electrons of the metal. Adding covalent ligands to titanium results in a stronger donation/polarization bond toward ethylene as calculated for $Cl_2Ti(CH_3)(C_2H_4)^+$. The weakest titanium–ethylene bond, apparently also of the donation/polarization type, was found for the neutral, bimetallic $AlH_2(\mu\text{-}Cl)_2TiCl_2(CH_3)(C_2H_4)$. At the DFTG level, no stationary point due to π coordination of ethylene was found for this system.

The calculations show that detection of metal–monomer complexes by means of vibrational spectroscopy should be feasible mainly in two frequency domains. (i) The changes in the fundamental dominated by the ethylene C–C stretching vibration (ν_2) may be substantial. For a strong, covalent type titanium–ethylene bond, the shift may be so large that the mode becomes difficult to identify in the vibrational spectrum of the complex. This mode is not IR-active in free ethylene, but it should be easily detected in Raman, and it is significantly activated for IR even for the weakest coordination studied in this work. (ii) Modes related to out-of-plane deformations of ethylene, in particular ν_7 and ν_8, are especially useful as they seem to contain information about the strength and type of metal–ethylene bond in question. A donation/polarization type metal–ethylene bond leads to increased frequencies for one or both of these modes, whereas a strong, covalent type bond gives a substantial reduction of ν_7. The latter mode is among the strongest in the IR spectrum of ethylene and maintains its intensity in the complexes. In case of a strong, covalent type titanium–ethylene bond, the C–H stretching region is also significantly affected. If the metal–ethylene bond is dominated by donation and polarization, the shifts are small, and the intensities of these bands in the complexes are also reduced.

Acknowledgment. A scholarship from the Norwegian Institute of Technology is gratefully acknowledged (V.R.J.), as is financial support from The Norwegian Academy of Science and Letters and Den norske stats oljeselskap a.s. (VISTA, Grant No. V6415) and a grant of computing time from the Norwegian Supercomputing Committee (TRU). The authors want to thank Intel Corporation for support through the SINTEF/Intel Paragon Supercomputer Partnership Agreement. V.R.J. also appreciates additional funding from Anders Jahres Fond. Finally, we would like to thank Dr. Bjørn K. Alsberg for help with visualization of the IR spectra.

OM940879P

Reactions of Silenes: A New Silene to Silene Thermal Rearrangement

Paul Lassacher, Adrian G. Brook,* and Alan J. Lough

Lash Miller Chemical Laboratories, University of Toronto, Toronto M5S 1A1, Canada

Received May 9, 1995[⊗]

Photolysis of the acylsilane $(Me_3Si)TipSiCOAd$ at room temperature gave rise to two geometric isomers of $(Me_3Si)TipSi{=}C(OSiMe_3)Ad$ which are less reactive than previously reported silenes. The formation of the phenylacetylene adducts of these silenes required heating to 90 °C, and no reaction was observed with (trimethylsilyl)acetylene, styrene, or 2,4-hexadiene. The formation of their methanol adducts required heating to 100 °C and proved to be a stereospecific process. If the original silene was heated at 120 °C for 5 days, in hopes of eliminating hexamethyldisiloxane and forming a silyne, a new rearranged silene $(Tip)MeSi{=}C(SiMe_2OSiMe_3)Ad$ was formed, which proved to be more reactive, giving adducts with phenylacetylene and methanol. A crystal structure of the silacyclobutene formed from this rearranged silene with phenylacetylene unequivocally confirmed its proposed structure. Heating of the rearranged silene to 150 °C resulted in its complete decomposition to unidentified products, and extended photolysis gave no change. The silenes $(Me_3Si)RSi{=}C(OSiMe_3)Ad$ (R = Mes, Tip) reacted with benzophenone to give 1,2-siloxetanes but did not react with acetone. If *E*-$Me_3Si(Mes)Si{=}C(OSiMe_3)Ad$ was heated together with styrene, a [2 + 2] cycloaddition product was formed. The cophotolysis of $(Me_3C)(Me_3Si)_2SiCOAd$ with phenylacetylene or (trimethylsilyl)acetylene gave rise to silene cycloadducts, each a mixture of stereoisomers, suggesting that the intermediate silene also existed as a mixture of geometric isomers.

It is well established that the 1,3-shift of a trimethylsilyl group from silicon to oxygen in acylpolysilanes under photochemical or thermal conditions gives rise to silenes.[1-3] Many of these silenes are in equilibrium with their head to head dimers and/or readily revert to their parent acylsilanes.[1,4] Silenes of the family $(Me_3Si)RSi{=}(OSiMe_3)Ad$ have been made, and with R = *t*-Bu only a single geometric isomer of a relatively stable silene was initially reported to have been formed.[5] When R = Mes, a mixture of relatively stable geometric isomers was obtained and characterized for the first time.[6] Unlike previously described silenes these species did not revert to their parent acylsilanes on heating but instead slowly decomposed. We speculated that this decomposition might involve the elimination of hexamethyldisiloxane from the silenes, which would lead to the formation of compounds containing the hitherto unknown silicon–carbon triple bond, as shown in Scheme 1.

Also, by introduction of increasingly sterically hindered R and R′ groups into the silenes, it was hoped that the elimination process would be facilitated and the stability of the triple bonded species would be increased.

Scheme 1

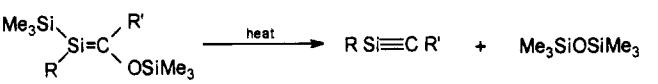

Scheme 2

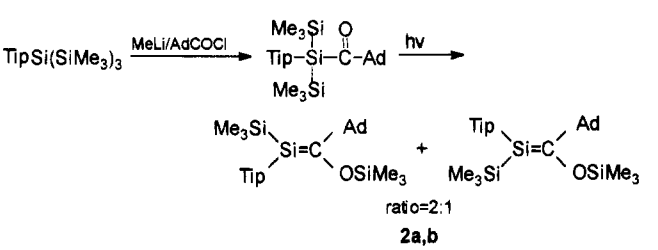

To test this rationale, the 2,4,6-triisopropylphenyl (Tip) group was introduced into the adamantoylsilane **1,** as shown in Scheme 2. Upon photolysis under mild conditions at room temperature in deuteriobenzene, the new silene geometric isomers **2a,b** were formed.

Numerous attempts to separate and crystallize these silenes from various solvents have not been successful to date, but the silenes have been fully characterized by ^1H, ^{13}C, and ^{29}Si NMR and MS spectroscopy, as well as by their phenylacetylene adducts **3a,b** and their methanol adducts **4a,b** (Scheme 3).

Thus, when phenylacetylene was added to a 2:1 mixture of silenes **2a,b** (as established by ^1H NMR spectroscopy), a 2:1 mixture of the related 1-silacyclobut-2-enes **3a,b** was formed after the solution was heated at 90 °C for 12 h. These findings agree with the results of previous experiments,[6] in which it has been shown

⊗ Abstract published in *Advance ACS Abstracts,* July 15, 1995.

(1) Brook, A. G.; Harris, J. W.; Lennon, J.; El Sheik, M. *J. Am. Chem. Soc.* **1979**, *101*, 83.
(2) Brook, A. G.; Nyburg, S. C.; Abdesaken, F.; Gutekunst, B.; Gutekunst, G.; Kallury, R., K. M. R.; Poon, Y. C.; Chang, Y. M.; Wong-Ng, W. *J. Am. Chem. Soc.* **1982**, *104*, 5667.
(3) Brook, A. G.; Vorspohl, K.; Ford, R. R.; Hesse, M.; Chatterton, W. J. *Organometallics* **1987**, *6*, 2128.
(4) Brook, A. G.; Nyburg, S. C.; Reynolds, W. F.; Poon, Y. C.; Chang, Y. M.; Lee, J. S.; Picard, J. P. *J. Am. Chem. Soc.* **1979**, *101*, 6750.
(5) Baines, K. M.; Brook, A. G.; Ford, R. R.; Lickiss, P. D.; Saxena, A. K.; Chatterton, W. J.; Sawyer, J. F; Behnam, B. A. *Organometallics* **1998**, *8*, 693.
(6) Brook, A. G.; Baumegger, A.; Lough, A. J. *Organometallics* **1992**, *11*, 3088.

0276-7333/95/2314-4359$09.00/0

Scheme 3

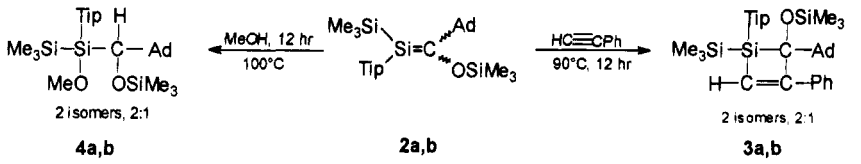

that the reaction of phenylacetylene with silenes is highly regio- and stereospecific. However, if (trimethylsilyl)acetylene was used as the reagent, no reaction occurred, even after heating of the solution for a prolonged time.

Reaction of methanol with a 2:1 mixture of silenes **2a,b** did not immediately occur at room temperature and proved to be a stereospecific process. If the reaction mixture was kept at room temperature for 16 h, the major silene isomer reacted exclusively to give a single methanol adduct **4a** whereas the minor silene isomer remained unreacted, as shown by ^{1}H and ^{29}Si NMR spectroscopy. The preparation of pure **4a** was achieved by quenching the reaction mixture with silica gel at this time, followed by chromatography and recrystallization. To obtain a 2:1 mixture of the methanol adducts **4a,b** the reaction mixture had to be kept at 100 °C for 12 h, at which time NMR spectroscopy showed the silenes had completely reacted. Attempted separation of this mixture of isomers has not been successful and so **4b** could not be obtained free of **4a**. Even if the acylsilane **1** was cophotolyzed with methanol, most of the silenes remained unreacted after photolysis and the reaction mixture had to be treated as above to obtain the adducts **4a,b**. The reaction of silenes with methanol has generally been observed to be a nonstereospecific process,[7] and the bulkiness of the Tip group is probably the reason that the reaction is stereospecific in this case. In the case of the mesityl-substituted silenes the reaction with methanol has been shown to be nonstereospecific.[6]

CID (collision-induced dissociation) MS experiments with silenes **2a,b** showed a small peak at m/z = 378, which could be attributed to the hoped-for silyne, as well as a peak at m/z = 162, attributable to hexamethyldisiloxane. These products could arise from the elimination reaction according to Scheme 1. The relative intensity of the signal attributed to the triple-bonded species is higher in the case of the Tip-substituted silenes than with the mesityl-substituted silene analogs. However, the intensity of their peaks compared to the molecular ion indicates that this reaction pathway is not very important under mass spectrometric conditions.

If the silenes **2a,b** were heated, either in deuterioxylene or neat, at 120 °C for 5 days, no evidence was found for formation of a silyne, but a remarkable rearrangement to a new silene **6** occurred. This reaction could be followed easily by ^{1}H NMR spectroscopy and gave a 95% yield of a single geometric isomer of **6** together with a small amount of unidentified byproducts. A possible mechanism for the formation of **6** is shown in Scheme 4.

The initially formed silenes **2a,b** either sequentially or concertedly must exchange the location of their Me_3-

Scheme 4

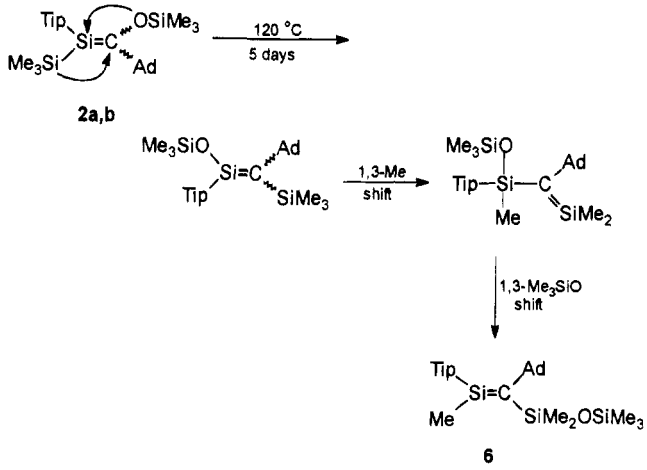

Si and Me_3SiO groups. Then a 1,3-methyl shift from sp^3-hybridized to sp^2-hybridized silicon occurs, followed by a 1,3-shift of a trimethylsiloxy group from sp^3-hybridized to sp^2-hybridized silicon yielding **6**. Other Me_3SiO-substituted silenes have been shown to undergo similar rearrangements involving Me_3Si and Me_3SiO interchange, as well as 1,3-Me and 1,3-Me_3SiO migrations under photochemical conditions,[5] but this was the first time that shifts of Me_3Si and Me_3SiO groups which are attached to the silicon–carbon double bond of silenes of this type have been observed to occur thermally. However, thermal 1,3-shifts of methyl groups in silenes with quite different structures have been observed by both Eaborn[8] and Wiberg,[9] and Auner[10] has observed 1,3-shifts of siloxy groups even at low temperatures. If silene **6** was photolyzed for an extended period, no further reaction occurred, but if it was heated to temperatures above 150 °C, complete decomposition took place. The position of the ^{29}Si NMR signal of the sp^2-hybridized silicon atom of **6** at 108.0 ppm lies in between the positions of signals of silenes of the family Me_2Si=, which usually give resonance signals at 126–144 ppm,[5,11] and those of the families $(Me_3Si)_2Si$= and $(Me_3Si)RSi$=, which give signals at 51–73 ppm.[5,12] The ^{13}C chemical shift of the sp^2-hybridized carbon at 127.3 ppm follows the same trend with the comparable ranges 77–118 ppm and 190–214 ppm, respectively, for the sp^2-hybridized carbon atom in the families of silenes discussed above.

When phenylacetylene was added to silene **6** at room temperature, a single adduct **8** was formed (Scheme 5), whose geometry is shown by the structure diagram in

(7) Kiro, M.; Maroyama, T.; Sakurai, H. *J. Am. Chem. Soc.* **1991**, *113*, 3986.

(8) Eaborn, C.; Happer, D. A.; Hitchcock, P. B.; Hopper, S. P.; Safa, K. D.; Washburne, S. S.; Walton, D. A. R. *J. Organomet. Chem.* **1980**, *186*, 309.

(9) Wiberg, N.; Köpf, H. *Chem. Ber.* **1987**, *120*, 653.

(10) Ziche, W.; Auner, N.; Behm, J. *Organometallics* **1992**, *11*, 3805.

(11) Wiberg, N.; Wagner, G.; Mueller, G. *Angew. Chem., Int. Ed. Eng.* **1985**, *24*, 229.

(12) Brook, A. G.; Abdesaken, F.; Gutekunst, G.; Plavac, N. *Organometallics* **1982**, *1*, 994.

Scheme 5

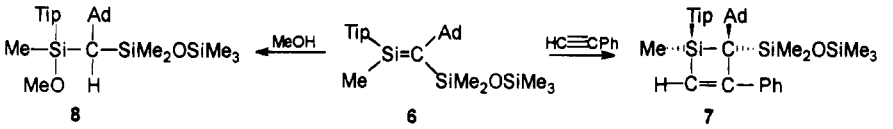

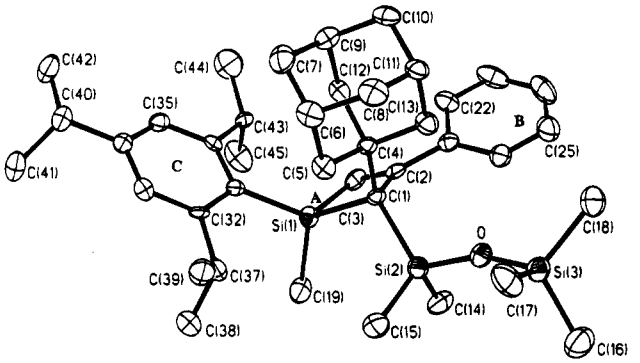

Figure 1.

Table 1. Summary of Crystal Data, Details of Intensity Collection, and Refinement Parameters

empirical formula	$C_{40}H_{62}OSi_3$
M_r	643.17
cryst size, mm	0.35 × 0.25 × 0.32
cryst class, space group	orthorhombic, *Pbca*
a, Å	19.268(3)
b, Å	18.712(3)
c, Å	20.726(3)
V, Å^3	7473(2)
Z	8
D_{calc}, Mg m^{-3}	1.143
μ(Mo Kα), mm^{-1}	0.156
F(000)	528
ω scan width, deg	0.53
range θ collcd, deg	3.0–22.5
index ranges	*h*, −10 to 12; *k*, −20 to 20; *l*, −22 to 2
tot. no. refls	3869
no. obsd data [$I > 2s(I)$]	2536
R [$I > 2\sigma(I)$]	0.038
w*R*2 (all data)	0.084
goodness of fit	0.866
largest/mean Δ/σ	0.001/0.000
params refined	411
max/min density in ΔF map, e/Å^3	0.177/−0.205

Figure 1. Tables 1 and 2 show the details of the X-ray structure determination and the atomic coordinates and thermal parameters in **7**.

On the assumption that silene **6** reacted with phenylacetylene suprafacially the geometry of the adduct **7** indicates that the geometry of silene **6** must be *E*. This is most surprising because it had been anticipated that the preferred geometry would be that where there was minimal steric interaction between the bulky Tip and Ad groups, as would exist in the *Z* isomer.

If silene **6** was treated with methanol, the reaction proved to be stereospecific, as in the case of **2** above, and a single adduct **8** was formed (geometry unknown). The steric bulk of the Tip group, and the fact that it is not freely rotating, as shown by the ^{1}H and ^{13}C NMR data, suggest that the silene **6** is locked in a conformation which allows addition of methanol from only one direction.

When the silenes **2a,b** were treated with benzophenone, only a single isomeric adduct of the siloxetane **5** was formed. The fact that no second isomer could be detected in this reaction again seems to be due to the bulkiness of the Tip group, because when the mesityl-substituted silenes reacted with benzophenone, two isomers of **9** were formed (Scheme 6).

Table 2. Atomic Coordinates (×10^4) and Equivalent Isotropic Displacement Parameters (Å^2 × 10^3) for 1[a]

	x	*y*	*z*	*U*(eq)
Si(1)	2071(1)	8606(1)	3334(1)	22(1)
Si(2)	3166(1)	9006(1)	4432(1)	25(1)
Si(3)	3769(1)	9183(1)	5854(1)	29(1)
O	3320(1)	9183(1)	5191(1)	32(1)
C(1)	2224(2)	8756(2)	4280(1)	18(1)
C(2)	1757(2)	9420(2)	4147(2)	20(1)
C(3)	1577(2)	9413(2)	3524(2)	24(1)
C(4)	1857(2)	8200(2)	4746(1)	18(1)
C(5)	2174(2)	7454(2)	4669(1)	26(1)
C(6)	1818(2)	6903(2)	5097(2)	29(1)
C(7)	1055(2)	6860(2)	4916(2)	36(1)
C(8)	1893(2)	7124(2)	5801(2)	33(1)
C(9)	716(2)	7588(2)	5019(2)	31(1)
C(10)	789(2)	7804(2)	5724(2)	30(1)
C(11)	1550(2)	7851(2)	5896(2)	26(1)
C(12)	1081(2)	8138(2)	4591(1)	26(1)
C(13)	1909(2)	8399(2)	5466(1)	26(1)
C(14)	3389(2)	9848(2)	4005(2)	38(1)
C(15)	3807(2)	8311(2)	4193(2)	38(1)
C(16)	4555(2)	9721(2)	5766(2)	51(1)
C(17)	4025(2)	8255(2)	6041(2)	43(1)
C(18)	3209(2)	9593(2)	6479(2)	36(1)
C(19)	2771(2)	8843(2)	2745(1)	34(1)
C(21)	1528(2)	9970(2)	4618(2)	23(1)
C(22)	881(2)	10277(2)	4538(2)	35(1)
C(23)	654(2)	10813(2)	4943(2)	47(1)
C(24)	1066(3)	11055(2)	5438(2)	45(1)
C(25)	1701(2)	10739(2)	5534(2)	38(1)
C(26)	1932(2)	10205(2)	5130(2)	30(1)
C(31)	1625(2)	7766(2)	3019(1)	18(1)
C(32)	1994(2)	7112(2)	2986(1)	18(1)
C(33)	1669(2)	6494(2)	2787(1)	24(1)
C(34)	982(2)	6473(2)	2597(1)	21(1)
C(35)	626(2)	7116(2)	2606(1)	23(1)
C(36)	930(2)	7755(2)	2813(1)	19(1)
C(37)	2766(2)	7076(2)	3122(2)	27(1)
C(38)	3175(2)	7090(2)	2494(2)	40(1)
C(39)	3003(2)	6427(2)	3518(2)	35(1)
C(40)	655(2)	5774(2)	2396(2)	28(1)
C(41)	1041(2)	5429(2)	1835(2)	40(1)
C(42)	−110(2)	5831(2)	2232(2)	42(1)
C(43)	501(2)	8437(2)	2780(2)	22(1)
C(44)	−274(2)	8324(2)	2816(2)	55(1)
C(45)	669(2)	8853(2)	2178(2)	50(1)

[a] *U*(eq) is defined as one-third of the trace of the orthogonalized U_{ij} tensor.

Scheme 6

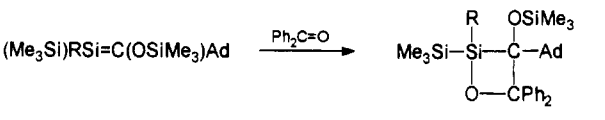

5 R = Tip
9 R = Mes

The ring silicon atoms of these cycloaddition products showed resonances at 35–39 ppm in their ^{29}Si NMR spectra. This is the region where the ring silicon atoms of known siloxetanes and disiloxetanes (both of which have silicon and oxygen atoms in a four-membered ring)

Scheme 7

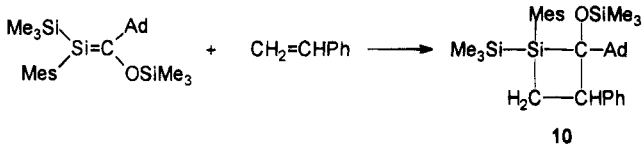

10

are known to resonate.[13] The proposed structure is also confirmed by the resonance frequencies of the ring carbon atoms and by all other spectroscopic methods.

It was remarkable to find that neither the silenes **2a,b** nor the related mesityl-substituted silenes reacted with acetone at room temperature. Even after 2 weeks at 40 °C a mixture of **2a,b** and acetone in deuteriobenzene showed only the original silene signals in their NMR spectra. Heating of a solution of the Mes silenes for 16 h resulted in the formation of at least 5 products (as shown by ^{1}H NMR spectroscopy) which could not be separated.

The stereospecific cycloaddition reactions which have been described above led us to examine the stereoselectivity of the reactions of some other unsaturated molecules with *E*-$Me_3Si(Mes)Si{=}C(OSiMe_3)Ad$. This silene could be easily obtained by heating a mixture of *Z* and *E* isomers of the silene to 120 °C for 5 h, at which time NMR spectroscopy showed all the *Z* isomer had decomposed, but more than 95% of the *E* isomer remained. It has already been shown[6] that only one isomeric silacyclobutene is formed if the *E*-silene is treated with (trimethylsilyl)acetylene.[6] The reaction of the *E*-silene with benzophenone also gave rise to only one isomer (geometry unknown) of the siloxetane **9**, isolated in 85% yield, showing that this reaction is also highly stereospecific.

Heating *E*-$(Me_3Si)MesSi{=}C(OSiMe_3)Ad$ with styrene cleanly gave rise to only one isomer (geometry unknown) of the [2 + 2] cycloaddition product, the silacyclobutane **10** (Scheme 7).

2,4-Hexadiene did not react at all with this silene, suggesting that the electronic properties of phenyl groups activate double bonds toward reactions with silenes.

The fact that acetylenes have been shown to react in a highly regio- and stereospecific manner with silenes led us to examine their reactions with the silene $(Me_3Si)(Me_3C)Si{=}C(OSiMe_3)Ad$ which was previously reported to have been formed as a single geometric isomer based on NMR evidence.[5] When the parent acylsilane of this silene was cophotolysed with either phenyl- or (trimethylsilyl)acetylenes, the formation of two isomeric adducts, **11a,b** and **12a,b** respectively, was observed by NMR spectroscopy, suggesting strongly that the intermediate silene must also have existed as a pair of geometric isomers, in contrast to the previous observations[5] (Scheme 8).

In summary, it has been found that when very bulky groups such as Tip are attached to the sp^2-hybridized silicon atom of a silene, the additions of methanol, benzophenone, styrene, and phenylacetylene are stereospecific reactions, only one isomeric product being formed from one of the silene geometric isomers. The related mesityl silene also reacted stereospecifically with

Scheme 8

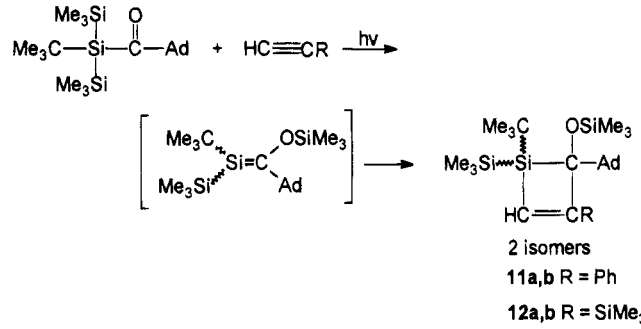

2 isomers
11a,b R = Ph
12a,b R = $SiMe_3$

benzophenone, styrene, and phenylacetylene. The bulky groups greatly reduce the reactivity of the silenes toward the above reagents, and in some cases no reaction occurs at all. Attempts to thermally induce the loss of hexamethyldisiloxane from these silenes to form a silyne failed, and a clean thermal silene-to-silene rearrangement was observed under the conditions employed.

Experimental Section

All experiments were performed with oven-dried glassware under nitrogen using standard inert-atmosphere and vacuum-line techniques. All reaction solvents were dried and distilled prior to use: diethyl ether and tetrahydrofuran were dried over sodium benzophenone ketyl, hexanes were dried over sodium–potassium alloy, and benzene was dried over lithium aluminum hydride. Photolyses were carried out using three 100-W PAR 38 mercury spot lamps, whose output is mainly at 360 nm and longer wavelengths.

All ^{1}H NMR spectra were obtained on a Gemini 200 spectrometer, and a Varian XL400 machine was used to record ^{13}C and ^{29}Si spectra. The spectra were run in C_6D_6 unless otherwise specified. Where necessary, APT and DEPT pulse sequences were used in obtaining ^{13}C spectra to allow unambiguous assignment of signals. Most ^{29}Si spectra were obtained using the DEPT pulse sequence.

All mass spectra were run on a VG 70-250S mass spectrometer operating in the electron impact (EI) mode for both low- and high-resolution mass spectra.

Elemental analyses were performed by Galbraith Laboratories Inc., Knoxville, TN.

Melting points are uncorrected.

Synthesis of (2,4,6-Triisopropylphenyl)bis(trimethylsilyl)adamantoylsilane (1). Compound **1** was prepared by the cleavage of $(Tip)Si(SiMe_3)_3$ in THF with 1 equiv of MeLi, the resulting red solution being added at −78 °C to 1 equiv of AdCOCl in THF. After the mixture was stirred at −78 °C for 1 h and then at room temperature for 5 h; workup gave 43% of **1** after recrystallization from methanol. Mp: 128–130 °C. Anal. Calcd for $C_{32}H_{47}OSi_3$: C, 71.04; H, 10.43. Found: C, 70.72; H, 10.06. ^{1}H NMR: δ 0.42 (18 H, s, Me_3Si), 1.16 (6 H, d, p-Me), 1.31 (12 H, d, o-Me) 1.50–1.95 (15 H, m, Ad), 2.73 (1 H, m, p-CH), 3.25(2 H, m, o-CH), 7.12 (2 H, s, CH Tip). ^{13}C NMR (δ): 2.32 ($SiMe_3$); 23.96 (p-CH_3); 26.80 (o-CH_3); 28.77 (Ad CH); 34.29 (p-CH); 36.08 (o-CH); 36.95, 38.96 (Ad CH_2); 52.41 (q-Ad); 122.16 (Tip CH); 130.23, 149.91, 155.68 (q-Tip); 249.99 (C=O). ^{29}Si NMR: δ −13.67 (Me_3Si), −45.53 (central Si). IR: 1610 cm^{-1} (C=O). MS [*m/z* (%)] (EI): 540 (5.3, M^+); 525 (12.1, M^+ − Me); 499 (M^+ − *i*-Pr); 467 (53, M^+ − $SiMe_3$); 377 (69, M^+ − COAd); 303 (100).

Photolysis of Acylsilane 1. Formation of Silenes 2a,b. A solution of 0.4 g (0.74 mmol) of acylsilane **1** in 0.6 mL of deuteriobenzene was photolyzed for 1 h at about 10 °C in a sealed NMR tube under nitrogen. At this time the ^{1}H, ^{13}C, and ^{29}Si NMR spectra showed no evidence of the starting material and revealed the presence of 2 sets of signals,

(13) (a) Brook, A. G.; Chatterton, W. J.; Sawyer, J. F.; Hughes, D. W.; Vorspohl, K. *Organometallics* **1987**, *6*, 1246. (b) Michalczyk, M. J.; West, R.; Michl, J. *J. Chem. Soc., Chem. Commun.* **1984**, 1525.

attributed to silenes **2a,b** present in the ratio 2:1. The spectra showed no change when stored at room temperature for months or even when heated to 60 °C for 1 week. Numerous attempts to crystallize the silenes from various solvents have failed to date. Data for **2a** (major isomer) are as follows. ^{1}H NMR: δ −0.11, 0.30 (each 9 H, s, $SiMe_3$); 1.21, 1.30, 1.43 (each 6 H, d, Me); 1.52−2.10 (15 H, m, Ad); 2.79 (1 H, m, p-CH); 3.75 (2 H, m, o-CH); 7.07 (2 H, s, Tip CH). The coupling constants J of all the doublets in this and all the following compounds always lay in the range 6.2 and 6.95 Hz, and their magnitude was not specific to o- or p-CH_3 groups. ^{13}C NMR: δ 1.22 (Me_3Si); 2.59 ($OSiMe_3$); 24.41, 25.10, 25.80 (Me); 29.39 (Ad CH); 35.06 (p-CH); 38.13 (o-CH); 37.72, 42.73 (Ad CH_2); 43.66 (q-Ad); 121.08 (Tip CH); 131.90, 150.85, 155.51 (q-Tip); 195.86 (C sp^2). ^{29}Si NMR: δ 40.33 (Si sp^2); 12.51 ($OSiMe_3$); −13.09 ($SiMe_3$). Data for **2b** (minor isomer) are as follows. ^{1}H NMR: δ 0.28, 0.39 (each 9 H, s, $SiMe_3$); 1.14, 1.31, 1.44 (each 6 H, d, Me); 1.52−2.10 (15 H, m, Ad with 2a); 2.75 (1 H, m, p-CH overlapping with **2a**); 4.07 (2 H, m, o-CH); 7.05 (2 H, s, Tip CH). ^{13}C NMR: δ 1.52 (Me_3Si); 2.38 ($OSiMe_3$); 24.26, 24.43, 25.30 (Me); 29.25 (Ad CH); 34.80 (p-CH); 38.80 (o-CH); 37.55, 42.15 (Ad CH_2); 45.16 (q-Ad); 121.22 (Tip CH); 133.64, 154.92, 155.59 (q-Tip); 191.04 (sp^2 C). ^{29}Si NMR: δ 43.31 (Si sp^2); 12.95 ($OSiMe_3$); −16.17 ($SiMe_3$). CID-MS [*m/z* (%)] of isomers (linked scan (B/E) done in first field free region (FFR) using CO_2 as collision gas, 80% transmission): 525 (27, M^+ − Me); 498 (62, $M^+ - C_3H_6$); 467 (97, M^+ − $SiMe_3$), 391 (33), 339 (51), 135 (100, Ad).

Synthesis of the Silacyclobutenes 3a,b. A slight excess of dry phenylacetylene was added to a mixture of silenes **2a,b** prepared as above. After heating of the sample to 60 °C, ^{13}C NMR spectroscopy showed the presence of 2 adducts in the ratio 2:1. Several recrystallizations from various solvents did not change the ratio of the products, but chromatography on silica gel (using hexanes as eluent) gave rise to pure **3a** together with **3b**, slightly contaminated with **3a**. Data for **3a** (major isomer, recrystallized from acetone) are as follows. Mp: 152−155 °C. ^{1}H NMR: δ −0.01, 0.34 (each 9 H, s, $SiMe_3$); 1.24 (6 H, d, p-Me); 1.26, 1.32, 1.34, 1.55 (each 3 H, d, o-Me); 1.55−2.15 (15 H, m, Ad); 2.81, 3.42, 3.66 (each 1 H, m, CH); 7.02 (1 H, s, ring CH); 7.12−7.20 and 7.66−7.69 (7 H, m, arom H). ^{13}C NMR: δ 1.43, 3.16 ($SiMe_3$); 24.16 (p-Me); 22.84, 26.26, 26.74, 27.39 (o-Me) 29.41 (Ad CH); 32.88, 34.84, 36.48 (CH); 37.58, 39.70 (Ad CH_2); 41.30 (q-Ad); 98.90 (ring C-Ad); 121.14, 121.40 (Tip-CH); 127.27, 127.81, 129.11 (Ph CH); 131.30 (Ph ipso); 142.18, 150.39, 154.98, 155.71 (q-Tip); 144.06 (ring =CH); 166.90 (ring =CPh). ^{29}Si NMR: δ 7.57 ($OSiMe_3$); −9.68 (ring Si); −16.21 ($SiMe_3$). Anal. Calcd for $C_{40}H_{62}OSi_3$: C, 74.72; H, 9.73. Found: C, 74.58; H, 9.54. HRMS: Calcd, 642.4109; found, 642.4098. MS [*m/z* (%)] (EI): 642 (5, M^+); 569 (52, M^+ − $SiMe_3$); 319 (42); 277 (90); 245 (75); 135 (100, Ad); 73 (97, $SiMe_3$). Data for **3b** (minor isomer, together with **3a**) are as follows. ^{1}H NMR: δ 0.34, 0.49 (each 9 H, s, $SiMe_3$); 1.21 (6 H, d, p-Me); 1.32, 1.34, 1.41, 1.50 (each 3 H, d, o-Me); 1.40−1.90 (15 H, m, Ad); 2.78, 3.39, 3.84 (each 1 H, m, CH); 6.89 (1 H, s, ring CH); 7.10−7.30 and 7.80−7.84 (7 H, m, arom H). ^{13}C NMR: δ 1.57, 4.23 ($SiMe_3$); 23.08, 23.73, 24.05, 26.31, 26.85, 28.32 (Me); 29.26 (Ad CH); 31.42, 31.99, 34.68 (CH); 37.15, 39.64 (Ad CH_2); 41.59 (q-Ad); 97.83 (ring C-Ad); 120.99, 122.03 (Tip-CH); 127.20, 127.81, 128.33 (Ph CH); 132.42 (Ph ipso); 141.74, 151.10, 154.32, 155.78 (q-Tip); 139.63 (ring =CH); 159.98 (ring =C-Ph). ^{29}Si NMR: δ 3.27 ($OSiMe_3$); −12.63 (ring Si); −20.10 ($SiMe_3$).

Formation of the Methanol Adducts 4a,b. A solution of 0.4 mg of acylsilane **1** in 0.6 mL of deuterotoluene was photolyzed in a capped NMR tube for 1 h, at which point no further starting material was present. To this was added 0.05 mL of dry methanol, and the reaction mixture had to be maintained at 100 °C for 24 h before a quantitative formation of the methanol adducts was obtained. Chromatography and recrystallization from acetone yielded a 2.5:1 **4a,b** mixture of isomers which could not be separated by these methods. To get the pure major isomer, the reaction mixture was not heated but was kept at room temperature for 16 h, at which point NMR spectroscopy showed that only silene **2a** had reacted. The mixture was quenched with silica gel, chromatographed (using hexanes:ethyl acetate = 100:1 as eluent) and recrystallized from acetone to give pure **4a**. Data for **4a** are as follows. Mp: 85−87 °C. ^{1}H NMR: δ 0.29, 0.35 (each 9 H, s, $SiMe_3$); 1.18 (6 H, d, p-Me); 1.42 (12 H, d, o-Me); 1.50−1.95 (15 H, m, Ad); 2.65 (1 H, m, p-CH); 3.32 (3 H, s, OMe); 3.73 (3 H, m, HCAd and o-CH); 7.20 (2 H, s, Tip H). ^{13}C NMR: δ 1.33, 1.76 ($SiMe_3$); 23.99, 26.12, 26.61 (Me); 28.96 (Ad CH); 33.09 (o-CH); 34.44 (p-CH); 37.41, 41.17 (Ad CH_2); 38.45 (q-Ad); 52.24 (O-Me); 79.99 (HCAd); 122.27 (Tip CH); 130.23, 150.55, 156.85 (Tip C). ^{29}Si NMR: δ 15.39 ($OSiMe_3$); 1.42 (Si−OMe); −16.01 ($SiMe_3$). HRMS: M^+ − H calcd for $C_{33}H_{59}O_2Si_3$ 571.3823, found 571.3831; M^+ − Me, calcd for $C_{32}H_{57}O_2Si_3$ 557.3666; found 557.3649. MS [*m/z* (%)] (EI): 571 (0.5, M^+ − H); 557 (14, M^+ − Me); 499 (27, M^+− $SiMe_3$); 467; 335 (100, Me_3SiSi-(OMe)Tip$^+$). Anal. Calcd for $C_{33}H_{60}O_2Si_3$: C, 69.16; H, 10.55. Found: C, 68.99; H, 10.94. Data for **4b** (together with **4a**) are as follows. ^{1}H NMR: δ 0.18, 0.46 (each 9 H, s, $SiMe_3$); 1.21 (6 H, d, p-Me); 1.40 (12 H, d, o-Me); 1.50−1.90 (15 H, m, Ad); 2.65 (1 H, m, p-CH); 3.46 (3 H, s, OMe); 3.73 (3 H, m, p-CH); 3.73 (1 H, s, HCAd); 7.22 (2 H, s, Tip H). ^{13}C NMR: δ 1.33, 1.76 ($SiMe_3$); 23.99, 26.12, (Me); 29.01 (Ad CH); 33.09 (o-CH); 34.50 (p-CH); 37.41, 41.37 (Ad CH_2); 38.38 (q-Ad); 52.35 (O-Me); 83.47 (HCAd); 122.08 (Tip CH); 131.84, 150.31, 156.85 (Tip C). ^{29}Si NMR: δ 15.18 ($OSiMe_3$); −1.78 (Si−OMe); −16.40 ($SiMe_3$).

Synthesis of the Siloxetane 5. After 400 mg of the acylsilane **1** (0.74 mmol) in 0.6 mL of C_6D_6 was photolyzed for 1 h, 135 mg of benzophenone (0.75 mmol) dissolved in 0.4 mL of C_6D_6 was added and the reaction mixture was kept at 50 °C for 1 h, at which time NMR spectroscopy showed no remaining starting material. The solvent was removed, and the resulting white foam was recrystallized twice from Et_2O to give 0.42 g of **5** (yield = 80%). The spectroscopic data showed no evidence of the formation of a second isomer. Data for **5** are as follows. Mp: 125−128 °C. ^{1}H NMR: δ −0.12, 0.47 (each 9 H, s, $SiMe_3$); 1.07, 1.24, 1.36, 1.54 (each 3 H, d, Me); 1.26 (6 H, d, p-Me); 1.55- 2.20 (15 H, m, Ad); 2.81, 3.14, 4.02 (each 1 H, m, CH); 6.95−8.05 (12 H, m, arom H). ^{13}C NMR: δ 2.17, 4.45 ($SiMe_3$); 24.11 (2 C, Me), 22.95, 24.42, 27.90, 28.46, (Me); 29.22 (Ad CH); 31.83, 34.73, 35.27 (CH); 37.04, 38.66 (Ad CH_2); 42.30 (q-Ad); 99.68, 111.13 (q-ring C) 120.48, 122,12 (Tip CH); 126.73, 127.02, 126.84, 127.65, 129.90, 130.54 (Ph CH); 145.18, 146.63, 150.72, 153.84, 157.91 (arom q-C). ^{29}Si NMR: δ 39.03 (ring Si); 4.01 ($OSiMe_3$); −16.69 ($SiMe_3$). HRMS: Calcd for $C_{45}H_{66}O_2Si_3$, 722.4371; found, 722.4377. MS [*m/z* (%)] (EI): 722 (6.6, M^+); 707 (2, M^+ − Me); 649 (83, M^+ − $SiMe_3$); 402 (100, $(Me_3SiO)AdC{=}CPh_2^+$).

Synthesis of the Silene 6. The silenes **2a,b**, prepared as above, were heated to 120−125 °C for 5 days, either in deuterioxylenes or neat. The reaction was monitored via ^{1}H NMR spectroscopy, and after 5 days 95% of **6** was formed, together with some unidentified byproducts. Numerous attempts to crystallize this new silene from various solvents failed, but the spectroscopic data for **6** and its reaction products **7** and **8** confirm the proposed structure. Data for **6** are as follows. ^{1}H NMR: δ 0.25 (9 H, s, $SiMe_3$); 0.57 (6 H, s, $SiMe_2$); 0.94 (3 H, s, SiMe); 1.14, 1.26, 1.42 (each 6 H, d, Me); 1.52−2.10 (15 H, m, Ad); 2.72 (1H, m, p-CH); 3.69 (2 H, m, o-CH); 7.04 (2 H, s, Tip CH). ^{13}C NMR: δ 2.62 (3 C, Me_3Si); 4.92 (1 C, SiMe); 8.86 (2 C, $SiMe_2$); 23.85, 24.09, 25.84 (each 2 C, Me); 30.11 (Ad CH); 34.73 (p-CH); 39.53 (o-CH); 37.29, 47.80 (Ad CH_2); 40.98 (q-Ad); 121.49 (Tip CH); 127.29 (sp^2 C); 138.76 (Tip C-ipso); 151.38, 151.88 (q-Tip). ^{29}Si NMR (also using ^{29}Si{^{1}H} coupled spectra) (δ): 108.08 (quartet, SiMe); 1.90 (septet, $SiMe_2$); 5.53 (m, $SiMe_3$). MS [*m/z* (%)] (EI): 540 (11, M^+); 525 (13, M^+ − Me); 467 (100, M^+ − $SiMe_3$); 337 (26, M^+ − Tip). HRMS: M^+, calcd for $C_{32}H_{56}OSi_3$ 540.3639, found 540.3612; M^+ − Me, calcd for $C_{31}H_{53}OSi_3$ 525.3404, found 525.3612

Synthesis of the Silacyclobutene 7. To a solution of silene **6** in deuteriotoluene (prepared as above) was added a slight excess of phenylacetylene. The reaction mixture was kept at 90 °C for 16 h. At this time NMR spectroscopy showed the reaction to be complete. The product was purified by chromatography using hexanes as eluent and subsequent recrystallization from acetone. Figure 1 shows a view of **7**. Mp: 112–114 °C. ^{1}H NMR: δ 0.30 (9 H, s, $SiMe_3$); 0.51 (3 H, s, SiMe); 0.69, 0.76 (each 3 H, s, $SiMe_2$); 1.19 (6 H, d, p-Me); 1.32–1.46 (4 d, o-Me, overlapping with Ad); 1.40–2.20 (Ad); 2.78, 3.28, 4.14 (each 1 H, m, CH); 6.80 (1 H, s, ring CH); 7.10–7.30 and 7.90-8.00 (7 H, m, Tip and Ph–CH). ^{13}C NMR (in $CDCl_3$): δ 2.21 (Me_3Si); 4.80, 5.15, 8.12 (SiMe); 22.73, 23.83, 23.88, 24.11, 26.74, 27.10 (Me); 29.25 (Ad CH); 32.74, 34.12, 35.84 (CH); 36.71, 42.26 (Ad CH_2); 40.20 (q-Ad); 57.94 (ring C-Ad); 136.48 (ring =CH) 163.89 (ring =CPh); 121.11, 121.58 (Tip CH); 127.28, 127.43, 127.53 (Ph CH); 135.31 (Ph ipso); 142.15, 149.91, 153.66, 154.55 (q-Tip). ^{29}Si NMR δ 6.86 ($OSiMe_3$); 5.28 ($SiMe_2$); −9.70 (ring Si). HRMS: M^+, calcd for $C_{40}H_{62}OSi_3$ 642.4108; found 642.4132. MS [*m/z* (%)] (EI): 642 (5, M^+); 627 (4, M^+ − Me); 335 (100, $TipSiMe(OSiMe_3)^+$); 147 (75, $Me_3SiOSiMe_2^+$); 73 (43, Me_3Si^+).

Synthesis of the Methanol Adduct 8. To a solution of silene **6** (prepared as above) was added a slight excess of dry methanol, resulting in an exothermic reaction and the disappearance of the yellow color. After 1 h at room temperature the solvent and excess methanol were removed under vacuo, and the resulting white foam was purified by chromatography on silica gel (using hexanes:ethyl acetate = 100:1 as eluent) and subsequent recrystallization from acetone. Data for **8** are as follows. Mp: 94–97 °C. ^{1}H NMR: δ.0.22 (9 H, s, $SiMe_3$); 0.51, 0.53 (each 3 H, s, $SiMe_2$); 0.91 (3 H, s, SiMe); 1.18, 1.37, 1.39 (each 6 H, d, Me); 1.59–2.15 (15 H, m, Ad); 2.75 (1 H, m, p-CH); 3.09 (3 H, s, OMe); 1.53 (1H, s, Ad-C-H 3.70 (2 H, m, o-CH); 7.19 (2 H, s, Tip CH). ^{13}C NMR: δ 2.42 (Me_3Si); 5.33 (SiMe); 6.05, 6.17 ($SiMe_2$); 23.99, 24.02, 26.36 (Me); 29.39 (Ad CH); 32.00, 34.48, 35.92 (CH); 36.59 (q-Ad); 37.07, 45.47 (Ad CH_2); 49.59 (OMe) 122.16 (Tip CH); 132.57, 150.04, 155.58 (q-Tip). ^{29}Si NMR (also using ^{29}Si{^{1}H} coupled spectra) (δ): 9.49 ($OSiMe_3$); 7.15 ($SiMe_2$); 6.30 (SiOMe). HRMS: M^+, calcd for $C_{33}H_{60}O_2Si_3$ 572.3901; found 572.3883; M^+ − Me, calcd for $C_{32}H_{57}O_2Si_3$ 557.3666; found 557.3653. MS [*m/z* (%)] (EI): 572 (2, M^+); 557 (30, M^+ − Me); 541 (7, M^+ − OMe); 369 (34, M^+ − Tip); 277 (100, $TipSi(OMe)Me^+$); 147 (34, $Me_3SiOSiMe_2^+$); 73 (17, $SiMe_3^+$). Anal. Calcd for $C_{33}H_{60}O_2Si_3$: C, 69.16; H, 10.55. Found: C, 68.86; H, 10.78.

Synthesis of the Siloxetane 9. A solution of 415 mg of mesitylbis(trimethylsilyl)adamantoylsilane in 0.7 mL of deuterioxylenes was photolyzed for 50 min. At this time ^{1}H NMR spectroscopy showed complete conversion to silene geometric isomers in the ratio 1.4:1. This solution was heated to 120 °C for 5 h, at which time the minor isomer was completely decomposed but more than 90% of the major isomer remained undestroyed. A solution of 165 mg of benzophenone in 0.3 mL of C_6D_6 was added at room temperature, and NMR spectroscopy showed all the silene to be reacted after 30 min. Recrystallization from hexanes yielded pure **9** (85%). The ^{29}Si and some of the ^{13}C NMR data of a second isomer could be obtained when the reaction was carried out without destroying the minor silene isomer, but this product could not be separated from the major isomer, and most ^{1}H and ^{13}C NMR signals overlapped. Data for **9** are as follows. Mp: 145–147 °C. ^{1}H NMR: δ −0.22, 0.39 (each 9 H, s, $SiMe_3$); 1.60–2.2 (15 H, m, Ad); 2.06, 2.43, 2.90 (each 3 H, s, CH_3); 6.63, 6.77 (each 1 H, s, Mes-H); 6.90–7.30 and 7.71–8.02 (10 H, m, Ph-H).^{13}C NMR: δ 1.09, 2.99 ($SiMe_3$); 21.07, 24.42, 28.09 (CH_3); 29.29 (Ad CH); 37.21, 39.74 (Ad CH_2); 41.56 (q-Ad); 100.13, 109.73 (ring C); 126.44, 126.95 (Mes CH); 142.34, 145.96, 136.01, 146.70 (q-Mes); 127.2–132.5 (Ph C, partial overlapping). ^{29}Si NMR: δ 36.25 (ring Si); 3.27 ($OSiMe_3$); −15.85 ($SiMe_3$). HRMS: calcd for $C_{39}H_{54}O_2Si_3$, 638.3422; found, 638.3450. MS [*m/z* (%)] (EI): 638 (3, M^+); 565 (74, M^+ − $SiMe_3$); 402 (100, $Ad(Me_3SiO)C{=}CPh_2^+$). Anal. Calcd for $C_{39}H_{54}O_2Si_3$: C, 73.29; H, 8.52. Found: C, 72.43; H, 8.54. Assignable data for the second isomers are as follows. ^{13}C NMR: δ −0.45, 4.99 ($SiMe_3$) 94.04, 106.09 (ring C). ^{29}Si NMR: δ 34.53 (ring Si); 5.77 ($OSiMe_3$); −14.88 ($SiMe_3$).

Synthesis of the Styrene Adduct 10. A solution of 420 mg of mesityl-bis(trimethylsilyl)adamantoylsilane in 0.7 mL of deuterioxylenes was photolyzed for 1 h. The sealed NMR tube was then heated to 120 °C for 5 h at which time NMR spectroscopy showed that just the major isomer remained and the minor isomer had decomposed completely. After the addition of 0.10 mL of styrene the solution was heated to 100 °C for 1 h. Chromatography (using hexanes as eluent) and subsequent recrystallization from ethanol gave 150 mg of pure **10**. Mp: 105–108 °C. ^{1}H NMR (all NMR data in $CDCl_3$) (δ): −0.27, 0.13 (each 9 H, s, $SiMe_3$); 1.4–2.0 (17 H, m, Ad and CH_2 ring); 2.24, 2.32, 2.46 (each 3 H, s, Mes CH_3); 3.58 (1 H, m, CH ring); 6.79 (2 H, s, Mes CH); 7.11–7.39 (5 H, m, Ph H). ^{13}C NMR: δ 0.19, 2.94 ($SiMe_3$); 21.17, 24.72, 26.17 (Mes CH_3); 21.99 (CH_2 ring); 28.81 (Ad CH); 37.22, 39.35 (Ad CH_2); 40.54 (q Ad); 48.52 (CH ring); 100.37 (q ring C); 125.53, 127.92, 129.08 (each 1 C, arom CH); 127.62, 129.67 (each 2 C, Ph CH); 131.29 (Ph ipso); 138.49, 143.35, 144.74, 146.01 (q-C Mes). ^{29}Si NMR: δ 4.44 ($OSiMe_3$); −10.70 (ring Si); −15.43 ($SiMe_3$). MS [*m/z* (%)] (EI): 560 (2, M^+); 545 (4, M^+ − Me); 487 (33, M^+ − $SiMe_3$); 456 ($Mes(SiMe_3)Si{=}C(OSiMe_3)Ad^+$ − H). HRMS: Calcd for $C_{33}H_{49}OSi_3$ (M^+ − Me), 545.3091; found, 545.3066.

Synthesis of the Silacyclobutenes 11a,b. A solution of 0.2 g of bis(trimethylsilyl)*tert*-butyladamantoylsilane (0.5 mmol) and a slight excess of phenylacetylene in 0.6 mL of deuteriobenzene was photolyzed for 1 h. ^{1}H NMR spectroscopy showed no remaining starting material but the formation of two isomeric adducts in the ratio 2.75:1, which could not be separated by chromatography or crystallization from various solvents. Data for **11a** (major isomer) are as follows. ^{1}H NMR: δ 0.38, 0.39 each 9 H, s, $SiMe_3$); 1.24 (9 H, s, CH_3); 1.55–2.10 (15 H, m, Ad); 6.57 (1 H, s, HC=); 7.08–7.23 and 7.69–7.76 (5 H, m, Ph H). ^{13}C NMR: δ 3.06, 4.82 ($SiMe_3$); 22.95 (q-C); 30.09 (CH_3); 29.36 (Ad CH); 37.27, 40.39 (Ad CH_2); 39.99 (q-Ad); 98.69 (ring C-Ad); 127.60, 127.65, 128.49 (Ph H); 138.03 (ring HC=); 141.98 (Ph ipso); 168.01 (ring PhC=). ^{29}Si NMR: δ 4.61 ($OSiMe_3$); 1.84 (ring Si); −18.57 ($SiMe_3$). Data for **11b** (minor isomer) are as follows. ^{1}H NMR: δ −0.18, 0.01 (each 9 H, s, $SiMe_3$); 1.16 (9 H, s, CH_3); 1.55–2.10 (Ad, overlapping with **11a**); 6.61 (1 H, s, HC=); 6.90–7.30 and 7.79–7.82 (Ph H, overlapping with **11a**). ^{13}C NMR: δ 0.88, 1.07 ($SiMe_3$); 21.39 (q-C); 29.52 (CH_3); 28.15 (Ad CH); 37.28, 41.01 (Ad CH_2); 40.00 (q-Ad, overlapping with **11a**); 139.7 (Ph ipso); 162.95 (PhC=); the other signals overlapped with **11a.** ^{29}Si NMR: δ 13.52 ($OSiMe_3$); −13.67 (ring Si); −19.21 ($SiMe_3$). MS (both isomers together) [*m/z* (%)] (EI): 497 (2, M^+); 482 (4, M^+ − Me); 424 (10, M^+ − $SiMe_3$); 339 (75, M^+ − $SiCMe_3$-$SiMe_3$); 135 (95, Ad); 73 (100, $SiMe_3$).

Synthesis of the Silacyclobutenes 12a,b. The same procedure as above was used, except that (trimethylsilyl)-acetylene was the reagent employed. The isomers, formed in the ratio 2:1, were not separable. Data for **12a** are as follows. ^{1}H NMR: δ 0.30, 0.33, 0.36 (each 9 H, s, $SiMe_3$); 1.21 (CH_3); 1.67–2.08 (15 H, m, Ad); 7.20 (ring HC=). ^{13}C NMR: δ 1.50, 2.89, 4.77 ($SiMe_3$); 22.35 (q-C); 29.38 (Ad CH); 30.19 (CH_3); 37.32, 40.10 (Ad CH_2); 39.39 (q-Ad); 100.34 (ring C-Ad); 157.29 (ring HC=); 179.92 (TMS-C=). ^{29}Si NMR: δ 11.03 ($OSiMe_3$); 3.46 (ring Si); −12.73, −19.42 ($SiMe_3$). HRMS (together with **12b**): Calcd for $C_{26}H_{52}OSi_4$, 492.3095; found 492.3087. Data for **12b** are as follows. ^{1}H NMR: δ 0.35, 0.31, 0.30 (each 9 H, s, $SiMe_3$); 1.95 (9 H, s, CH_3); 1.67–2.08 (Ad overlapping with 12a); 7.11 (ring HC=). ^{13}C NMR: δ 1.02, 2.33, 3.89 ($SiMe_3$); 25.72 (q-C); 29.82 (Ad CH); 30.66 (CH_3); 37.21, 40.38 (Ad CH_2); 40.25 (q-Ad); 101.68 (ring C-Ad); 153.10 (ring HC=); 172.41 (ring Me_3SiC=). ^{29}Si NMR: δ 5.75 ($OSiMe_3$); 5.43 (ring Si); −12.17, −15.80 ($SiMe_3$). MS (together with **12a** [*m/z* (%)] (EI): 492 (3, M^+); 477 (7, M^+ − Me); 435 (100, M^+ − CMe_3);

419 (15, $M^+ - SiMe_3$); 147 (70, $Me_3SiOSiMe_2^+$); 135 (82, Ad); 73 (86, $SiMe_3$).

X-ray Structural Determination. The cyclobutene ring **A** in **7** (see Figure 1) forms a least-squares plane with maximum deviation of 0.011(2) Å from the plane for atom C(2). The atom C(21) in ring **B** is almost in the plane formed by ring **A** (with a deviation of only 0.021(5) Å for C(21) from the fitted plane of ring **A**), and the aromatic ring **B** is twisted by 33.4(2)° from the plane of ring **A**.

The geometry of the molecule is affected by both bond and angle strain. Angles which are noticably large for tetrahedral geometry are C(3)–Si(1)–C(31), C(1)–Si(1)–C(31), and C(4)–C(1)–Si(2), which are 121.3(2), 121.12(12), and 119.2(2)°, respectively, and the angle C(21)–C(2)–C(1) of 127.4(3)° is larger than expected for sp^2 orbital hybridization. The distances Si(1)–C(1) = 2.002(3) Å, Si(1)–C(31) = 1.907(3) Å, and Si(2)–C(1) = 1.900(3) Å are significantly lengthened for C–Si bonds, and C(1)–C(4) = 1.585(4) Å is also noticably long. These bond length and angle distortions appear to be caused by a combination of the effects of cyclobutene ring strain and the steric bulk of the substituent groups present.

Intensity data for the crystal structure were collected on a Siemens P4 diffractometer at 173 K, using graphite-monochromated Mo Kα radiation (λ = 0.710 73 Å). The ω scan technique was applied with variable scan speeds ranging from 3 to 30°/min. The intensities of 3 standard reflections measured every 97 reflections showed no intensity decay. No correction was made for absorption.

The structure was solved by direct methods. Non-hydrogen atoms were refined anisotropically by full-matrix least-squares, using all data, to minimize $\sum w(F_o^2 - F_c^2)^2$, where $w^{-1} = \sigma^2(F^2) + (0.0367P)^2$ and $P = (F_o^2 + 2F_c^2)/3$. Hydrogen atoms were positioned on geometric grounds (C–H = 0.96 Å), and an overall hydrogen atom thermal parameter was refined to a value of 0.042(1) $Å^2$. Crystal data, data collection, and least-squares parameters are listed in Table 1. The atomic coordinates are listed in Table 2, and some important bond lengths and bond angles are listed in Table 3. All calculations were performed using SHELXTL-PC[14] and SHELXL-93[15] on a 486-66 personal computer. Figure 1 is a view of the molecule showing the crystallographic labeling scheme.

Table 3. Bond Lengths (Å) and Bond Angles (deg) for Compound 7

	Ring Lengths		
Si(1)–C(1)	2.002(3)	C(1)–C(2)	1.559(4)
Si(1)–C(3)	1.827(3)	C(2)–C(3)	1.338(4)
	Other Lengths		
Si(1)–C(31)	1.907(3)	C(1)–C(4)	1.585(4)
Si(2)–C(1)	1.900(3)		
	Ring Angles		
C(1)–Si(1)–C(3)	75.58(13)	C(1)–C(2)–C(3)	108.2(3)
Si(1)–C(1)–C(2)	81.5(2)	C(2)–C(3)–Si(1)	94.6(2)
	Other Angles		
C(3)–Si(1)–C(31)	121.3(2)	C(21)–C(2)–C(1)	127.4(3)
C(1)–Si(1)–C(31)	121.12(12)	Si(2)–O–Si(3)	155.7(2)
C(4)–C(1)–Si(2)	119.2(2)		

Acknowledgment. P.L. is grateful to the Austrian Science Foundation for an "Erwin Schroedinger" scholarship. This research was supported by the Natural Sciences and Engineering Research Council of Canada.

Supporting Information Available: Tables of bond lengths and bond angles, anisotropic displacement parameters, and hydrogen atom coordinates and thermal parameters (5 pages). Ordering information is given on any current masthead page.

OM950336V

(14) Sheldrick, G. M. SHELXTL/PC, Siemens Analytical X-ray Instruments Inc., Madison, WI.

(15) Sheldrick, G. M. SHELXL-93, Program for Crystal Structure Refinement, University of Gottingen, Germany.

Group and Site Selective σ-Bond Metathesis Reactions of $CH_3ScCH_2CH_3^+$ with [2,2-D_2]Propane, [1,1,1,4,4,4-D_6]-*n*-Butane, [2-D]Isobutane, and *n*-Pentane†

Kevin C. Crellin, Serge Geribaldi,‡ M. Widmer,§ and J. L. Beauchamp*

Arthur Amos Noyes Laboratory of Chemical Physics, California Institute of Technology, Pasadena, California 91125

Received February 15, 1995⊗

Fourier transform ion cyclotron resonance mass spectrometry has been used to examine the reactions of $CH_3ScCH_2CH_3^+$ with [D_4]methane, ethane, [2,2-D_2]propane, [1,1,1,4,4,4-D_6]-*n*-butane, [2-D]isobutane, *n*-pentane, and [D_{12}]-*n*-pentane. $CH_3ScCH_2CH_3^+$ is not observed to react with methane or ethane, but for propane, *n*-butane, isobutane, and *n*-pentane σ-bond metathesis with ethane elimination is the initial and dominant reaction observed, with further dehydrogenation of the resulting products occurring as additional reaction channels. For propane, *n*-butane, and isobutane, no methane elimination is observed. For *n*-pentane, methane elimination is a minor reaction channel. For propane, *n*-butane, and isobutane, the initial σ-bond metathesis involves predominantly the primary C–H bonds of the hydrocarbon. These processes are facile at room temperature and occur with little or no activation energy. Measured total bimolecular rate constants with [2,2-D_2]propane, [1,1,1,4,4,4-D_6]-*n*-butane, [2-D]isobutane, and *n*-pentane are 0.87×10^{-10}, 0.98×10^{-10}, 1.7×10^{-10} and 6.4×10^{-10} cm^3 s^{-1} molecule^{-1}, respectively. With the butanes and pentane a second intramolecular metathesis reaction follows the initial addition to yield a metallacycle product. In accordance with earlier theoretical predictions these metathesis reactions appear to proceed via an allowed four-center mechanism similar to that of a $2_\sigma + 2_\sigma$ cycloaddition. The higher reactivity of the metal-ethyl bond compared to the metal–methyl bond and the observed C–H bond specificity are also in agreement with theoretical predictions.

Introduction

Previous studies in our laboratory have revealed the exceptional reactivity of $Sc(CD_3)_2^+$ with small alkanes.[1] A four-center cycloaddition mechanism was invoked for σ-bond metathesis occurring at the metal center (Scheme 1), in accord with the prediction of Steigerwald and Goddard that certain organometallic systems containing an extremely acidic (in the Lewis sense) metal center should exhibit this kind of reactivity.[2] These reactions of $Sc(CD_3)_2^+$ with small alkanes do not involve oxidative addition mechanisms since Sc^+ has only two valence electrons, which precludes the formation of more than two strong σ bonds.[3] The reactions also exhibit a high degree of site specificity, with attack at the primary position of a small alkane favored over attack at secondary or tertiary positions.[1] This result agrees well with theoretical predictions of the enthalpies of these reactions as calculated by Perry and Goddard.[4] Similar site specificity has also been observed for reactions of

Scheme 1

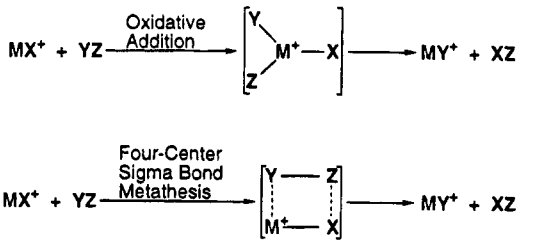

Co^+ with propane in the gas phase[5] and for reactions of iridium complexes in solution.[6]

Though the reactivity of $Sc(CD_3)_2^+$ has been investigated, no studies have yet been done on the reactivity of mixed ligand systems such as $CH_3ScCH_2CH_3^+$. By examining the reactions of $CH_3ScCH_2CH_3^+$, we can investigate how the reactivity changes as larger ligands are introduced to the metal center. We can also attempt to elucidate the factors that favor the reactivity of one ligand over that of another ligand and observe the effect that a second and larger ligand might have on the selectivity previously seen in smaller systems.[1] The focus of the present work is to examine the relative reactivities of the metal–methyl and metal–ethyl bonds. Theoretical results of Perry and Goddard indicate that the Sc^+–C bond in Sc^+–CH_3 is approximately 5 kcal

† Contribution No. 9052.
‡ Present Address: Universite de Nice-Sophia Antipolis, Laboratoire de Chemie Physique Organique, 06108 Nice Cedex 2, France.
§ Present Address: Zyma SA, DT-QC, CH-1260 Nyon, Switzerland.
⊗ Abstract published in *Advance ACS Abstracts,* July 15, 1995.

(1) Crellin, K. C.; Geribaldi, S.; Beauchamp, J. L. *Organometallics* **1994**, *13*, 3733.
(2) Steigerwald, M. L.; Goddard, W. A., III. *J. Am. Chem. Soc.* **1984**, *106*, 308.
(3) (a) Tolbert, M. A.; Beauchamp, J. L. *J. Am. Chem. Soc.* **1984**, *106*, 8117. (b) Beauchamp, J. L.; van Koppen, P. A. M. *Energetics of Organometallic Species*; Simoes, J. A. M., Ed.; Kluwer Academic Publishers: Dordrecht, The Netherlands, 1992.
(4) Perry, J. K.; Goddard, W. A., III. *J. Am. Chem. Soc.* **1994**, *116*, 5013.
(5) van Koppen, P. A. M.; Brodbelt-Lustig, J.; Bowers, M. T.; Dearden, D. V.; Beauchamp, J. L.; Fisher, E. R.; Armentrout, P. B. *J. Am. Chem. Soc.* **1991**, *113*, 2359.
(6) (a) Wax, M. J.; Stryker, J. M.; Buchanan, J. M.; Kovac, C. A.; Bergman, R. G. *J. Am. Chem. Soc.* **1984**, *106*, 1121. (b) Buchanan, J. M.; Stryker, J. M.; Bergman, R. G. *J. Am. Chem. Soc.* **1986**, *108*, 1537.

0276-7333/95/2314-4366$09.00/0

mol^{-1} stronger than the Sc^+-C bond in $Sc^+-CH_2CH_3$.[4] From this we can estimate that the process shown in reaction 1 should be about 5 kcal mol^{-1} more endothermic than the process shown in reaction 2. This suggests

$$CH_3\text{-}Sc^+\text{-}CH_2CH_3 \rightarrow CH_3 + Sc^+\text{-}CH_2CH_3 \quad (1)$$

$$CH_3\text{-}Sc^+\text{-}CH_2CH_3 \rightarrow CH_3CH_2 + Sc^+\text{-}CH_3 \quad (2)$$

that the methyl and ethyl groups should behave differently for reactions of $CH_3ScCH_2CH_3^+$ with small alkanes. It might also be suspected that replacement of one of the methyl groups by an ethyl group could affect the reactivity of the remaining methyl group compared to the reactivity observed for methyl groups in $Sc(CD_3)_2^+$. Synergistic effects of one ligand upon another metal–ligand bond strength within the same complex have been observed in the gas phase even for linear, two-ligand metal complexes.[7] Thus it is possible that $CH_3ScCH_2CH_3^+$ may exhibit a trans influence,[8] with the ethyl group affecting the bond energy or other properties of the remaining Sc^+-CH_3 bond. Since $Sc(CD_3)_2^+$ shows a preference for attack at the primary positions of small alkanes,[1] we have used labeled compounds to see if any site selectivity is observed in the reactions of $CH_3ScCH_2CH_3^+$ with hydrocarbons. In this study we report the results of the reaction of $CH_3ScCH_2CH_3^+$ with [D_4]-methane, ethane, [2,2-d_2]propane, [1,1,1,4,4,4-D_6]-*n*-butane, [2-D]isobutane, and *n*-pentane.

Experimental Section

Reactions were investigated with Fourier transform ion cyclotron resonance spectrometry (FT-ICR), of which a number of reviews are available.[9] Only details relevant to these experiments are outlined here. A 1-in.^{3} trapping cell is located between the poles of a Varian 15-in. electromagnet maintained at 1.0 T. Data collection is accomplished with an IonSpec Omega 386 FT-ICR data system and associated electronics. Neutral gases are introduced into the cell by separate leak valves, and their pressures are measured with a Schultz-Phelps ion gauge calibrated against an MKS 390 HA-00001SP05 capacitance manometer. Uncertainties in absolute pressures are estimated to be ±20%. Labeled [2,2-D_2]propane (98% D), [1,1,1,4,4,4-D_6]-*n*-butane (98% D), and [2-D]isobutane (98% D) were obtained commercially from Merck Sharp and Dohme. Labeled [D_4]-methane (99% D) and labeled [D_{12}]-*n*-pentane (98% D) were obtained commercially from Cambridge Isotope Laboratories. All reactant gases utilized were purified by freeze–pump–thaw cycling.

Sc^+ ions were produced by laser ablation of a scandium metal target with an N_2 laser at 337.1 nm.[1,10] The reactant ion was generated by reaction of Sc^+ with *n*-pentane, and unwanted ions were ejected from the cell using double resonance techniques[11] and/or frequency sweep excitation.[12] Reactionsof isolated $CH_3ScCH_2CH_3^+$ with *n*-pentane were examined first. Some experiments were performed with mixed samples of *n*-pentane and [D_{12}]-*n*-pentane in order to confirm the presence of certain structures. These mixed reagent experiments will be discussed in more detail in the Results and Discussion sections. The pentane pressures used in these experiments were in the range (2–3) × 10^{-7} Torr. Labeled methane, ethane, labeled propane, labeled *n*-butane, or labeled isobutane were then added along with the *n*-pentane, and reactions due to the additional alkane were observed. The pressure of the additional methane or ethane used was about 1 × 10^{-6} Torr, while the pressure of the additional alkanes larger than ethane were typically in the range (3–7) × 10^{-7} Torr. Rate constants were determined in a straightforward manner, from slopes of semilog plots of the decay of reactant ion abundance versus time and the pressure of the neutral reactant. The reported rate constants are averages of several different sets of experimental data taken at different pressures of the neutral gases. Errors are estimated to be ±20% due to uncertainties in absolute pressure determination. All experiments were performed at ambient temperature. To insure accurate product distributions, all distributions given in the next section were determined at short reaction times, before any subsequent secondary reactivity could affect the observed product distribution.

Results

Reaction of Sc^+ with *n*-Pentane: Generation of $CH_3ScCH_2CH_3^+$. A typical mass spectrum showing the products of the reaction of Sc^+ with *n*-pentane is presented in Figure 1a. Figure 1b shows a typical semilogarithmic plot of the decay of the Sc^+ abundance with time and the temporal variation of product ion abundances following the isolation of Sc^+. The initial processes observed are reactions 3–7. The metallacycle

$$Sc^+ + CH_3(CH_2)_3CH_3 \xrightarrow{35\%} CH_3\text{-}Sc^+\text{-}CH_2CH_3 + CH_2CH_2 \quad (3)$$

$$\xrightarrow{20\%} \text{[Sc}^+\text{-cyclopentane]} + H_2 \quad (4)$$

$$\xrightarrow{15\%} ScC_5H_8^+ + 2H_2 \quad (5)$$

$$\xrightarrow{10\%} \text{[Sc}^+\text{-cyclobutane]} + CH_4 \quad (6)$$

$$\xrightarrow{20\%} ScC_4H_6^+ + CH_4 + H_2 \quad (7)$$

product of reaction 6, ion II, has been previously observed.[1,3a] Studies of the reaction of Sc^+ with labeled *n*-butane show that 1,3 dehydrogenation of the *n*-butane to form $ScC_4H_8^+$ is observed, which is consistent with the formation of II.[3a] In addition, the previously observed reaction of labeled isobutane with $Sc(CD_3)_2^+$ leads to the formation of ion III, which is the only structure consistent with the observed mass peak.[1] The postulated metallacycle product of reaction 4, ion I, is

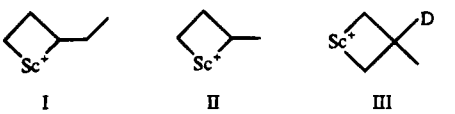

I II III

analogous to the metallacycle formed in reaction 6 and to ion III. Reactions 5 and 7 are observed when the nascent products of reactions 4 and 6 dehydrogenate. For the reaction of Sc^+ with *n*-pentane, the total

(7) Kappes, M. M.; Jones, R. W.; Staley, R. H. *J. Am. Chem. Soc.* **1982**, *104*, 888.
(8) (a) Huheey, J. E. *Inorganic Chemistry*, 3rd ed.; Harper and Row: New York, 1983; Chapter 11. (b) Hartley, F. R. *Chem. Soc. Rev.* **1973**, *2*, 163. (c) Appleton, T. G.; Clark, H. C.; Manzer, L. E. *Coord. Chem. Rev.* **1973**, *10*, 335.
(9) (a) Marshall, A. G. *Acc. Chem. Res.* **1985**, *18*, 316. (b) Comisarow, M. B. *Anal. Chim. Acta.* **1985**, *178*, 1.
(10) (a) Azzaro, M.; Breton, S.; Decouzon, M.; Geribaldi, S. *Int. J. Mass Spectrom. Ion Proc.* **1993**, *128*, 1. (b) Cody, R. B.; Burnier, R. C.; Reents, W. D., Jr.; Carlin, T. J.; McCrery, D. A.; Lengel, R. K.; Freiser, B. S. *Int. J. Mass Spectrom. Ion Phys.* **1980**, *33*, 37.
(11) Anders, L. R; Beauchamp, J. L.; Dunbar, R. C.; Baldeschwieler, J. D. *J. Chem. Phys.* **1966**, *45*, 1062.
(12) Comisarow, M. B.; Marshall, A. G. *Chem. Phys. Lett.* **1974**, *26*, 489.

bimolecular rate constant k is 1.2×10^{-9} cm^3 s^{-1} molecule^{-1} and the reaction efficiency k/k_{ADO} is 0.85.[13]

$CH_3ScCH_2CH_3^+$ can react further with n-pentane as shown in reactions 8–18. A typical semilogarithmic plot

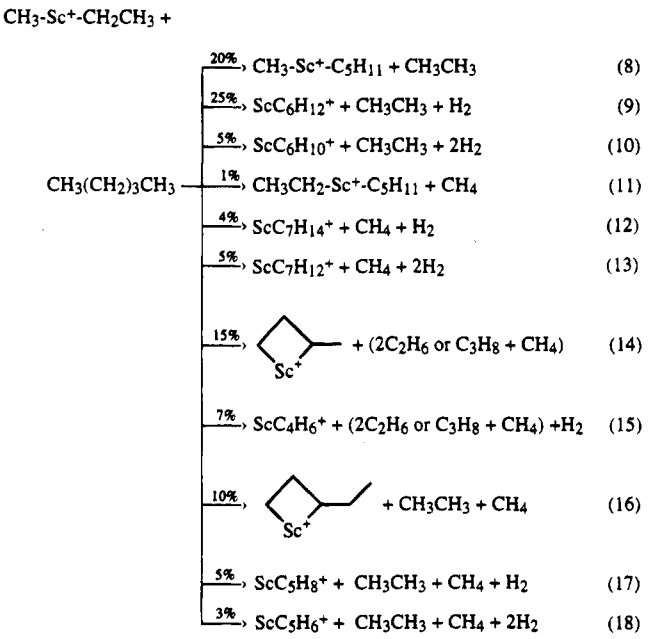

of the decay of the $CH_3ScCH_2CH_3^+$ abundance with time and the temporal variation of product ion abundances following the isolation of $CH_3ScCH_2CH_3^+$ is shown in Figure 2. It is postulated that reaction 16 occurs when the vibrationally excited products of reactions 8 or 11 have enough energy for a second intramolecular metathesis reaction, resulting in the observed metallacycle product. The neutral products of reactions 14 and 15 are uncertain. Reactions 9, 10, 12, 13, 15, 17, and 18 are observed when the nascent products of reactions 8, 11, 14, and 16 dehydrogenate. The reaction of $CH_3ScCH_2CH_3^+$ with n-pentane will be discussed in more detail in the next section.

Since $CH_3ScC_5H_{11}^+$ is the predominant product of the reaction of $CH_3ScCH_2CH_3^+$ with n-pentane, it was also isolated so that its reactivity with n-pentane could be examined. A semilogarithmic plot of the temporal variation of ion abundances following the isolation of $CH_3ScC_5H_{11}^+$ is shown in Figure 3. Reactions 19–23

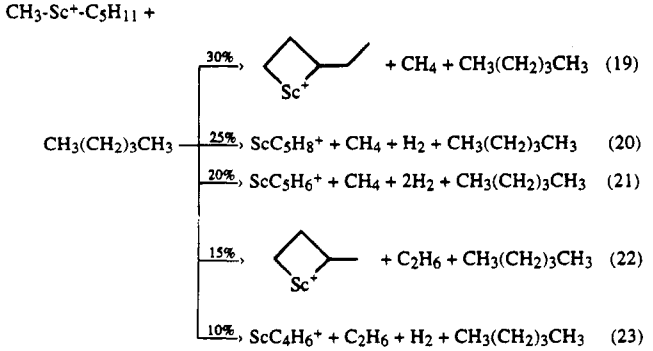

are the initial processes observed, and it appears that adduct formation with the neutral n-pentane generates enough energy to either collisionally or chemically activate the $CH_3ScC_5H_{11}^+$ ion. This strongly suggests that $CH_3ScC_5H_{11}^+$ is, in fact, a precursor to the metallacycle species and supports our postulate that the metallacycle of reaction 16 results from vibrationally excited $CH_3ScC_5H_{11}^+$ ions. At longer reaction times, the abundance of both metallacycle products decrease and the formation of $ScC_nH_m^+$ products with $n \geq 7$ and $m \geq 12$ is observed. Reactions 20, 21, and 23 are observed when the nascent products of reactions 19 and 22 dehydrogenate. For the reaction of $CH_3ScC_5H_{11}^+$ with n-pentane, the total bimolecular rate constant k is 1.6×10^{-10} cm^3 s^{-1} molecule^{-1} and the reaction efficiency k/k_{ADO} is 0.15.[13] Reaction 3 was utilized to generate the $CH_3ScCH_2CH_3^+$ ion, which was then isolated as shown in Figure 4a for further study of its reactivity.

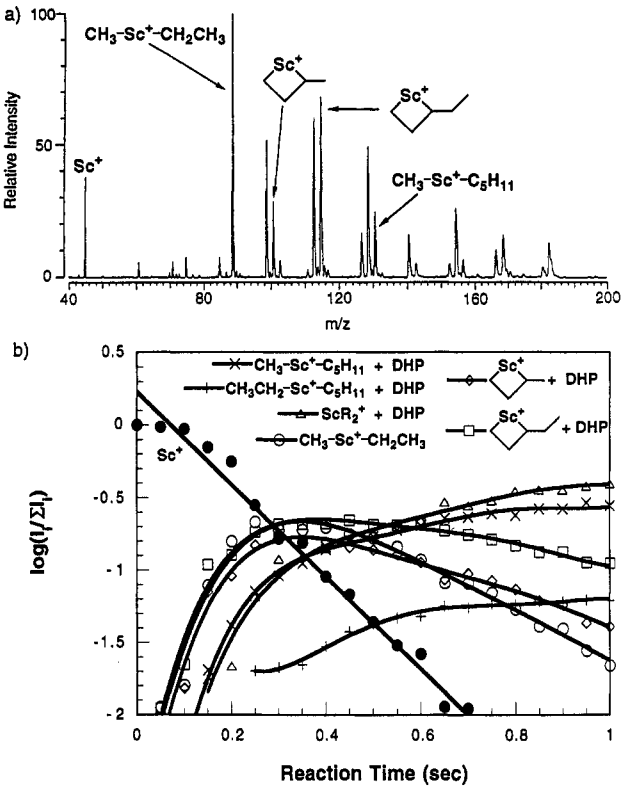

Figure 1. (a) Products of the reaction of Sc^+ with n-pentane. Spectrum taken 450 ms after isolation of Sc^+. Peaks at m/z 141 and 143 correspond to dehydrogenated $CH_3CH_2ScC_5H_{11}^+$. The main peaks above m/z 145 correspond to ScR_2^+, R = alkyl. The peaks at m/z 61 and 103 correspond to ScO^+ and $ScOC_3H_6^+$, respectively. The peaks at m/z 71, 75, and 85 correspond to $ScC_2H_2^+$, $Sc(CH_3)_2^+$, and CH_3ScCCH^+, respectively. (b) Semilogarithmic plot of the decay of the Sc^+ abundance with time for a single experimental run. The line is a fit to the data. The constant Sc^+ abundance observed in the first 100-ms "induction period" is most likely due to translationally excited Sc^+ ions that must cool down before they can react. The temporal variation of the product ion distribution for the reaction of Sc^+ with n-pentane is also shown. The relative intensities of the Sc^+–alkyl products involving n-pentane include the contribution from secondary dehydrogenated products which are associated with the main Sc^+–alkyl peaks and formed by subsequent unimolecular reactions of the primary Sc^+–alkyl products. Note the lack of deviation from linearity of the data, which suggests that little or no excited Sc^+ is present.

Reaction of $CH_3ScCH_2CH_3^+$ with n-Pentane. Elucidation of Structures. Reactions 8–18 are observed with n-pentane (see Figures 2 and 4b). Both single loss

(13) Collision rates are calculated using ADO theory: Su, T.; Bowers, M. T. *Int. J. Mass Spec. Ion Phys.* **1973**, *12*, 347.

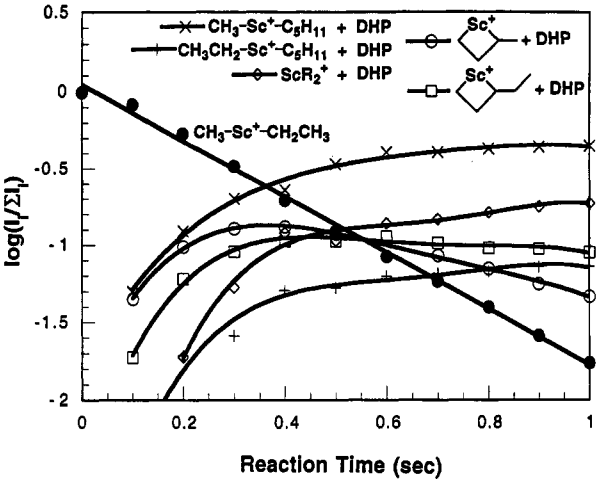

Figure 2. Semilogarithmic plot of the decay of the $CH_3ScCH_2CH_3^+$ abundance with time for a single experimental run. The line is a fit to the data. The temporal variation of the product ion distribution for the reaction of $CH_3ScCH_2CH_3^+$ with *n*-pentane is also shown. The relative intensities of the Sc^+−alkyl products involving *n*-pentane include the contribution from secondary dehydrogenated products which are associated with the main Sc^+−alkyl peaks and formed by subsequent unimolecular reactions of the primary Sc^+−alkyl products. Note the lack of deviation from linearity of the data, which suggests that little or no excited $CH_3ScCH_2CH_3^+$ is present.

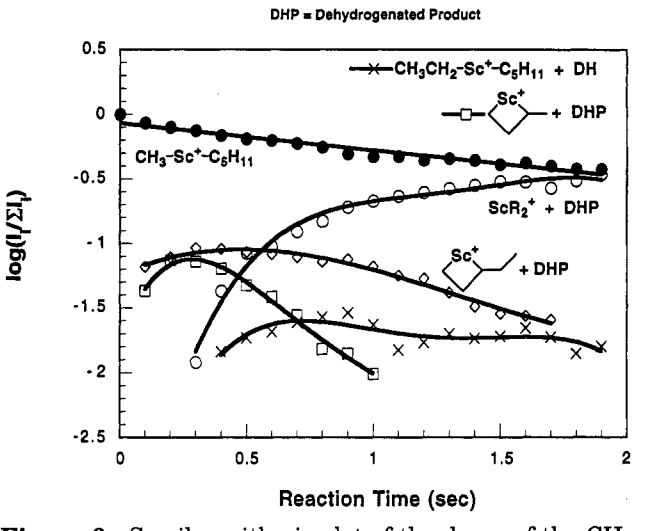

Figure 3. Semilogarithmic plot of the decay of the $CH_3ScC_5H_{11}^+$ abundance with time for a single experimental run. The line is fit to the data. The temporal variation of product ion distribution for the reaction of $CH_3ScC_5H_{11}^+$ with *n*-pentane is also shown. The relative intensities of the Sc^+−alkyl products involving *n*-pentane include the contribution from secondary dehydrogenated products which are associated with the main Sc^+−alkyl peaks and formed by subsequent unimolecular reactions of the primary Sc^+−alkyl products.

and multiple loss of hydrogen are observed from all the nascent products of reactions 8, 11, 14, and 16. For the reaction of $CH_3ScCH_2CH_3^+$ with *n*-pentane the total bimolecular rate constant k is 6.4×10^{-10} cm^3 s^{-1} molecule^{-1} and the reaction efficiency k/k_{ADO} is 0.55.[13] In order to determine if an isotope effect is present we also observed the reaction of $CD_3ScCD_2CD_3^+$ with [D_{12}]-*n*-pentane. The reaction with labeled *n*-pentane shows the same product distribution as in the unlabeled case,

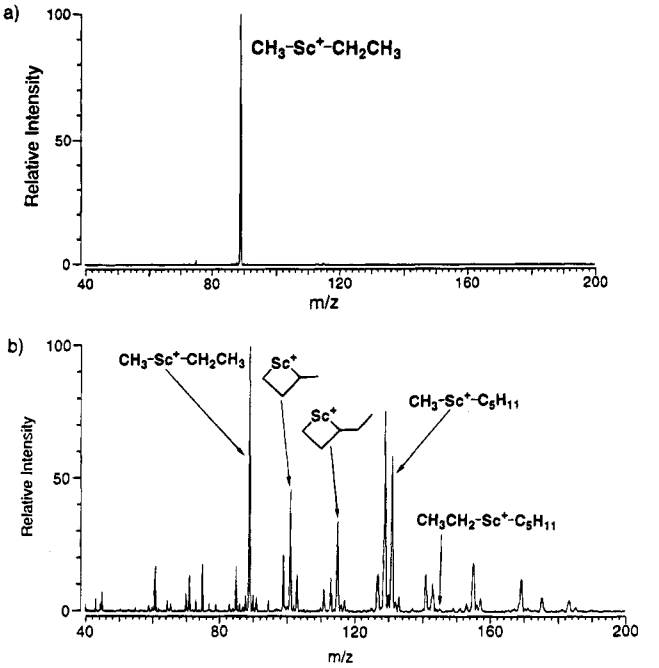

Figure 4. (a) Demonstration of our ability to isolate the $CH_3ScCH_2CH_3^+$ ion from unwanted products of the reaction of Sc^+ with *n*-pentane. Spectra taken 400 ms after generation of Sc^+. (b) Products of the reaction of $CH_3ScCH_2CH_3^+$ with *n*-pentane. Spectrum taken 400 ms after the isolation of $CH_3ScCH_2CH_3^+$. Peaks at m/z 141 and 143 correspond to dehydrogenated $CH_3CH_2ScC_5H_{11}^+$. The main peaks above m/z 145 correspond to ScR_2^+, R = alkyl. The peaks at m/z 61 and 103 correspond to ScO^+ and $ScOC_3H_6^+$, respectively. The peaks at m/z 71, 75, and 85 correspond to $ScC_2H_2^+$, $Sc(CH_3)_2^+$, and CH_3ScCCH^+, respectively.

and the total bimolecular rate constant k is 6.5×10^{-10} cm^3 s^{-1} molecule^{-1} and the reaction efficiency k/k_{ADO} is 0.56.[13]

Reactions of $CH_3ScCH_2CH_3^+$ and $CD_3ScCD_2CD_3^+$ with *n*-pentane/[D_{12}]-*n*-pentane mixtures were also observed to provide corroborating evidence that the major product is in fact $CH_3ScC_5H_{11}^+$ and not $CH_3CH_2ScC_4H_9^+$, both of which have the same mass. When $CH_3ScCH_2CH_3^+$ was isolated and reacted with labeled *n*-pentane, only reaction 24 was observed. Reaction 25

$$CH_3\text{-}Sc^+\text{-}CH_2CH_3 + CD_3(CD_2)_3CD_3 \rightarrow CH_3\text{-}Sc^+\text{-}C_5D_{11} + CH_3CDH_2 \quad (24)$$

$$CH_3\text{-}Sc^+\text{-}CH_2CH_3 + CD_3(CD_2)_3CD_3 \not\rightarrow CH_3CH_2\text{-}Sc^+\text{-}C_4D_9 + C_2D_3H_3 \quad (25)$$

was not seen (Figure 5a). Analogously, when $CD_3ScCD_2CD_3^+$ was isolated and reacted with unlabeled *n*-pentane, only reaction 26 was observed. Reaction 27

$$CD_3\text{-}Sc^+\text{-}CD_2CD_3 + CH_3(CH_2)_3CH_3 \rightarrow CD_3\text{-}Sc^+\text{-}C_5H_{11} + CD_3CD_2H \quad (26)$$

$$CD_3\text{-}Sc^+\text{-}CD_2CD_3 + CH_3(CH_2)_3CH_3 \not\rightarrow CD_3CD_2\text{-}Sc^+\text{-}C_4H_9 + C_2D_3H_3 \quad (27)$$

did not occur (Figure 5b). These observations support our assertion that the major product of the reaction between $CH_3ScCH_2CH_3^+$ and *n*-pentane is $CH_3ScC_5H_{11}^+$.

Reaction of $CH_3ScCH_2CH_3^+$ with Methane and Ethane. The possible exchange reactions of $CH_3ScCH_2CH_3^+$ with CD_4 were not observed. We estimate that

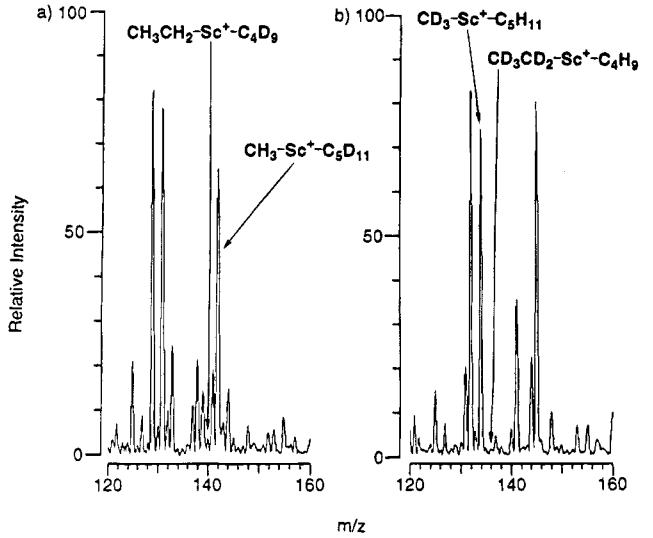

Figure 5. (a) Products of the reaction of $CH_3ScCH_2CH_3^+$ with a mixture of *n*-pentane and [D_{12}]-*n*-pentane between *m/z* 120 and 160. Spectrum taken 600 ms after the isolation of $CH_3ScCH_2CH_3^+$. Note the absence of any $CH_3CH_2ScC_4D_9^+$ product. (b) Products of the reaction of $CD_3ScCD_2CD_3^+$ with a mixture of *n*-pentane and [D_{12}]-*n*-pentane between *m/z* 120 and 160. Spectrum taken 700 ms after the isolation of $CD_3ScCD_2CD_3^+$. Note the absence of any $CD_3CD_2ScC_4H_9^+$ product.

for the reaction of $CH_3ScCH_2CH_3^+$ with methane the total bimolecular rate constant k is $\leq 1 \times 10^{-12}$ cm^3 s^{-1} molecule^{-1}. The possible exchange reactions of $CD_3ScCD_2CD_3^+$ with CH_3CH_3 were also not observed. Labeled *n*-pentane was used since we did not possess labeled ethane. We estimate that for the reaction of $CH_3ScCH_2CH_3^+$ with ethane the total bimolecular rate constant is less than 1×10^{-12} cm^3 s^{-1} molecule^{-1}.

Reaction of $CH_3ScCH_2CH_3^+$ with Propane. Reactions 28 and 29 were observed with labeled propane

$$CH_3\text{-}Sc^+\text{-}CH_2CH_3 + CH_3CD_2CH_3 \xrightarrow{90\%} CH_3\text{-}Sc^+\text{-}CH_2CD_2CH_3 + CH_3CH_3 \quad (28)$$

$$CH_3CD_2CH_3 \xrightarrow{10\%} CH_3\text{-}Sc^+\text{-}CD(CH_3)_2 + CH_3CDH_2 \quad (29)$$

(see Figure 6a), but reactions in which the methyl group instead of the ethyl group was exchanged were not observed. For the reaction of $CH_3ScCH_2CH_3^+$ with labeled propane, the total bimolecular rate constant k is 0.87×10^{-10} cm^3 s^{-1} molecule^{-1} and the reaction efficiency k/k_{ADO} is 0.08.[13]

Reaction of $CH_3ScCH_2CH_3^+$ with *n*-Butane. Reactions 30–32 were observed with labeled *n*-butane (see Figure 6b). Methyl exchange reactions were not seen. It is postulated that reaction 32 occurs when the

$$CH_3\text{-}Sc^+\text{-}CH_2CH_3 + CD_3(CH_2)_2CD_3 \xrightarrow{30\%} CH_3\text{-}Sc^+\text{-}CD_2(CH_2)_2CD_3 + CH_3CDH_2 \quad (30)$$

$$\xrightarrow{5\%} CH_3\text{-}Sc^+\text{-}CH(CD_3)CH_2CD_3 + CH_3CH_3 \quad (31)$$

$$\xrightarrow{65\%} \text{[D-Sc-D metallacycle]} + CH_3CDH_2 + CH_4 \quad (32)$$

vibrationally excited product of reaction 30 or 31 has enough energy for a second intramolecular metathesis

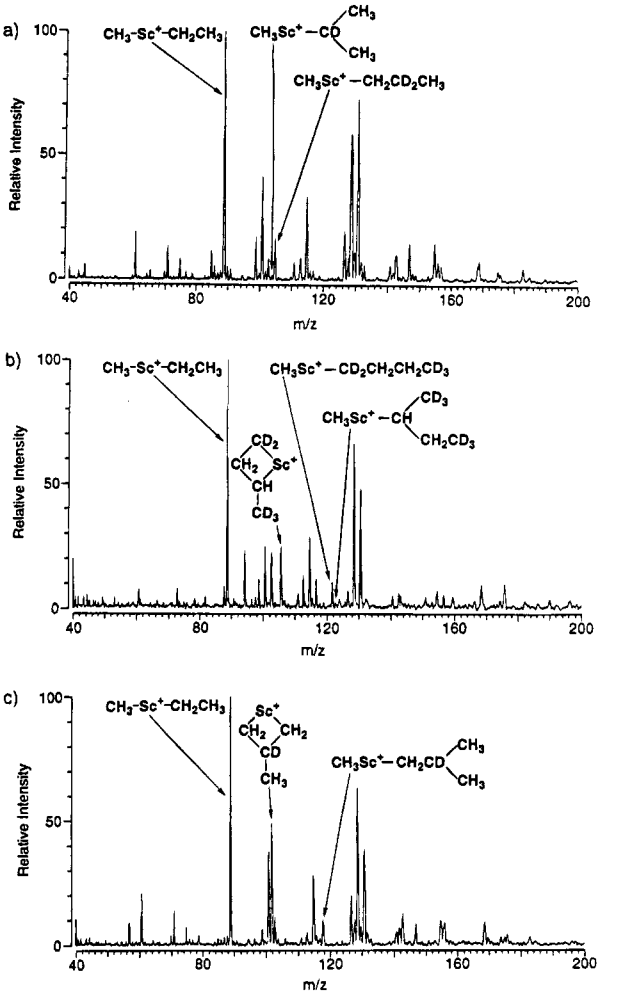

Figure 6. (a) Products of the reaction of $CH_3ScCH_2CH_3^+$ with [2,2-D_2]propane. Spectrum taken 250 ms after the isolation of $CH_3ScCH_2CH_3^+$. The main peaks above *m/z* 125 correspond to ScR_2^+, R = alkyl. The peak at *m/z* 61 corresponds to ScO^+. The peaks at *m/z* 71, 75, and 85 correspond to $ScC_2H_2^+$, $Sc(CH_3)_2^+$, and CH_3ScCCH^+, respectively. (b) Products of the reaction of $CH_3ScCH_2CH_3^+$ with [1,1,1,4,4,4-D_6]-*n*-butane. Spectrum taken 250 ms after the isolation of $CH_3ScCH_2CH_3^+$. The main peaks above *m/z* 125 correspond to ScR_2^+, R = alkyl. The peaks at *m/z* 61 and 73 correspond to ScO^+ and $ScC_2H_4^+$, respectively. (c) Products of the reaction of $CH_3ScCH_2CH_3^+$ with [2-D]isobutane. Spectrum taken 250 ms after the isolation of $CH_3ScCH_2CH_3^+$. The main peaks above *m/z* 125 correspond to ScR_2^+, R = alkyl. The peak at *m/z* 61 corresponds to ScO^+. The peaks at *m/z* 71 and 75 correspond to $ScC_2H_2^+$ and $Sc(CH_3)_2^+$, respectively.

reaction, resulting in the metallacycle product. It should be noted that the labeling of the hydrocarbon products shown in reaction 32 assumes that the initial metathesis occurs as shown in reaction 30. However, since reaction 31 is also observed as a minor reaction pathway, hydrocarbon products with the opposite labeling are also present but in significantly smaller quantities. For the reaction of $CH_3ScCH_2CH_3^+$ with labeled *n*-butane, the total bimolecular rate constant k is 0.98 $\times 10^{-10}$ cm^3 s^{-1} molecule^{-1} and the reaction efficiency k/k_{ADO} is 0.09.[13]

Reaction of $CH_3ScCH_2CH_3^+$ with Isobutane. Reactions 33 and 34 were observed with labeled isobutane (see Figure 6c). No reactivity is observed at the tertiary site of isobutane. Reaction 34 occurs when the vibra-

Table 1. Summary of the Observed Reactivity of $CH_3ScCH_2CH_3^+$ with the Small Alkanes Examined in This Study[a]

process			tot. rates (cm^3 $molecule^{-1}$ s^{-1})	reacn efficiency (k/k_{coll})
$CH_3-Sc^+-CH_2CH_3$ +	methane	→ no reaction	$<10^{-12}$	<0.001
	ethane	→ no reaction	$<10^{-12}$	<0.001
	propane	→ $CH_3-Sc^+-(CH_2)_2CH_3 + C_2H_6$	9×10^{-11}	0.09
	n-butane	→ $CH_3-Sc^+-(CH_2)_3CH_3 + C_2H_6$	1×10^{-10}	0.10
	isobutane	→ $CH_3-Sc^+-CH_2CH(CH_3)_2 + C_2H_6$	2×10^{-10}	0.20
	n-pentane	90% → $CH_3-Sc^+-(CH_2)_4CH_3 + C_2H_6$	6×10^{-10}	0.60
		10% → $CH_3CH_2-Sc^+-(CH_2)_4CH_3 + CH_4$		

[a] Only the initial reaction observed with each alkane is noted in the table.

tionally excited product of reaction 33 has enough

CH_3-Sc^+-CH_2CH_3 +

$(CH_3)_3CD$ — 80%, CH_3-Sc^+-$CH_2CD(CH_3)_2 + CH_3CH_3$ (33)

$(CH_3)_3CD$ — 20%,  $+ CH_3CH_3 + CH_4$ (34)

energy for a second intramolecular metathesis reaction to yield the metallacycle product. For the reaction of $CH_3ScCH_2CH_3^+$ with labeled isobutane, the total bimolecular rate constant k is 1.7×10^{-10} cm^3 s^{-1} $molecule^{-1}$ and the reaction efficiency k/k_{ADO} is 0.15.[13]

Discussion

Reaction of $CH_3ScCH_2CH_3^+$ with Small Alkanes. Overview. Table 1 summarizes the observed reactivity of $CH_3ScCH_2CH_3^+$ with the small alkanes examined in this study. Only the initial reaction observed with each alkane is noted in this summary of our results. With propane, *n*-butane, isobutane, and *n*-pentane σ-bond metathesis reactions occur where an ethyl group of $CH_3ScCH_2CH_3^+$ is replaced by either an *n*-propyl, an *n*-butyl, an isobutyl, or an *n*-pentyl group. Reaction efficiencies range from approximately 0.1 for propane to 0.55 for *n*-pentane. Methyl group replacement was observed only for the reaction of $CH_3ScCH_2CH_3^+$ with *n*-pentane, and even in this case methyl group replacement was only responsible for 10% of the reactivity (Table 1). In the reaction with *n*-butane, isobutane, and *n*-pentane, the *n*-butyl, isobutyl, and *n*-pentyl groups undergo a second intramolecular σ-bond metathesis reaction (reactions 14, 16, 32, and 34) to form a four-membered metallacycle. Similar reactivity was seen for the reaction of $Sc(CD_3)_2^+$ with *n*-butane and isobutane.[1] These metathesis reactions could proceed via an oxidative addition/reductive elimination pathway or via a four-center intermediate (see Scheme 1). Again, since Sc^+ only has two valence electrons with which to form strong σ-bonds,[3] we favor a four-center mechanism for these metathesis reactions.

Since the labeled hydrocarbons contained deuterium, it was possible that kinetic isotope effects would be present. Thus we examined the reaction of $CD_3ScCD_2CD_3^+$ with [D_{12}]-*n*-pentane so that we could observe any possible kinetic isotope effects. The total bimolecular rate constants measured with *n*-pentane and [D_{12}]-*n*-pentane were practically identical ($k_H/k_D = 0.98$). The product distributions observed with *n*-pentane and [D_{12}]-*n*-pentane were also indistinguishable. Thus we conclude that isotope effects are unimportant in this system, even though the reaction is not occurring at the collision limit. This result is not surprising, since $Sc(CD_3)_2^+$ also exhibited no isotope effects in its reactions with small alkanes.[1]

When $CH_3ScCH_2CH_3^+$ was reacted with *n*-pentane we expected the major product to be $CH_3ScC_5H_{11}^+$. However, it was possible that this product could actually be $CH_3CH_2ScC_4H_9^+$, which has the same mass as $CH_3ScC_5H_{11}^+$. To discount this possibility, we performed experiments in which $CH_3ScCH_2CH_3^+$ or $CD_3ScCD_2CD_3^+$ were reacted with *n*-pentane/[D_{12}]-*n*-pentane mixtures. Regardless of whether $CH_3ScCH_2CH_3^+$ or $CD_3ScCD_2CD_3^+$ was the reactant ion, only mass peaks corresponding to $CH_3ScC_5D_{11}^+$ or $CD_3ScC_5H_{11}^+$ were seen. No peaks corresponding to $CH_3CH_2ScC_4D_9^+$ or $CD_3CD_2ScC_4H_9^+$ were observed (Figure 5). In addition to showing that $CH_3ScC_5H_{11}^+$ is the major product of the reaction of $CH_3ScCH_2CH_3^+$ with *n*-pentane, these results also provide evidence that the ion product of reaction 3 is $CH_3ScCH_2CH_3^+$ and not an isomer such as the $Sc(C_3H_8)^+$ adduct.

Group Specificity. Group specificity was observed in the reactions of $CH_3ScCH_2CH_3^+$ with propane, *n*-butane, isobutane, and *n*-pentane. For propane, *n*-butane and isobutane the initial metathesis reactions (reactions 28–31 and 33) exhibit *only* ethyl exchange. No methyl exchange is seen in the initial metathesis reactions. For *n*-pentane the initial metathesis process (reactions 8 and 11) exhibits mostly ethyl exchange: 10% or less of the initial metathesis process is due to methyl exchange for *n*-pentane. From these observations it is apparent that ethyl exchange is *much* more favorable than methyl exchange with every alkane we examined.

To explain these observations, we first note that Perry and Goddard[4] have performed theoretical calculations which predict that the Sc^+-CH_3 bond is about 5 kcal mol^{-1} stronger than the $Sc^+-CH_2CH_3$ bond. Thus, even though the $H-CH_3$ bond is about 4 kcal mol^{-1} stronger than the $H-CH_2CH_3$ bond,[14] overall it is still energetically more favorable (by 1 kcal mol^{-1}) to exchange an ethyl group than to exchange a methyl group (see Table 2). A larger difference probably characterizes the activation energies for the competitive processes, however, since, in the transition state, the weaker metal–

(14) McMillan, D. F.; Golden, D. M. *Ann. Rev. Phys. Chem.* **1982**, *33*, 493.

Table 2. Predicted Reaction Enthalpy[a,b] for the σ-Bond Metathesis Reaction $ScR^+ + R'H \rightarrow ScR'^+ + RH$

R	R′ = CH_3	C_2H_5	n-C_3H_7	i-C_3H_7	t-C_4H_9
CH_3	0.0	1.0	−4.2	1.9	2.2
C_2H_5	−1.0	0.0	−5.2	0.9	1.2
n-C_3H_7	4.2	5.2	0.0	6.1	6.4
i-C_3H_7	−1.9	−0.9	−6.1	0.0	0.3
t-C_4H_9	−2.2	−1.2	−6.4	−0.3	0.0

[a] In kcal mol^{-1}. [b] Data from ref 4.

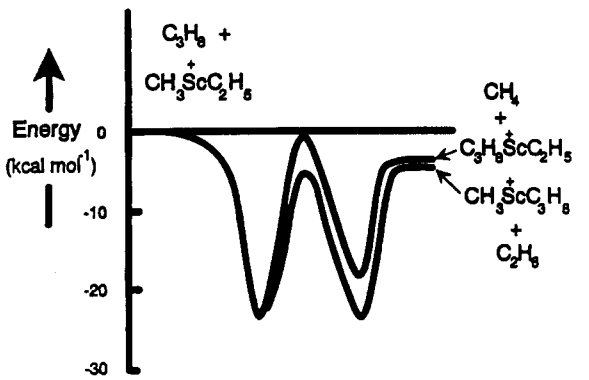

Figure 7. Schematic of a general potential energy surface showing how the nature of the ligand being lost can affect the electrostatic potential wells present. Note that the stronger electrostatic interaction of ethane with Sc^+ and the fact that the $Sc^+-CH_2CH_3$ bond energy is about 5 kcal mol^{-1} less than the Sc^+-CH_3 bond energy lowers the potential energy curve for the formation of ethane below the curve for the formation of methane. Both effects conspire to make loss of the ethyl group much more favorable than loss of the methyl group.

carbon bond is probably being ruptured prior to formation of the stronger C−H bond in the products. This is illustrated in Figure 7 for propane. In addition, ethane has a stronger electrostatic interaction than methane with Sc^+ due to its larger polarizability. Thus losing ethane rather than methane should give rise to a deeper potential energy well in the exit channel. This may also lower the energy of the transition state for this process, as shown in Figure 7. These effects conspire to make the loss of ethane more favorable than the loss of methane.

In the case of propane, n-butane, and isobutane it appears that the electrostatic potential wells are deep enough to lower the energy of the transition state for loss of ethane below the energy of the reactants but not deep enough to lower the energy of the transition state for methane loss below the energy of the reactants. Thus there is a net barrier to the loss of methane, but no barrier to the loss of ethane. This is why no methyl exchange is observed for the reaction of $CH_3ScCH_2CH_3^+$ with propane and the isomeric butanes. On the other hand, n-pentane has a higher polarizability[15] than either propane[16] or the isomeric butanes.[17] Thus the initial electrostatic potential energy well formed with n-pentane is deeper than with propane or the isomeric butanes. This lowers the energy of the transition state for methane loss enough that it is below the energy of the reactants when n-pentane is the neutral reactant. However, the energy of the transition state for ethane loss is still lower than that for methane loss, so that ethane loss is still the major process observed. These observations support the prediction of Perry and Goddard[4] that the $Sc^+-CH_2CH_3$ bond is weaker than the Sc^+-CH_3 bond.

Site Specificity. In addition to group specificity, site specificity was also observed for the reactions of $CH_3ScCH_2CH_3^+$ with propane, n-butane, and isobutane (see Figure 6). For propane and n-butane the initial metathesis reactions (reactions 28−31) show a marked preference for attack at primary rather than secondary C−H bonds. For isobutane the initial metathesis reaction (reaction 33) occurs only at primary C−H bonds. No attack is seen at the tertiary site.

These results are identical to those observed with $Sc(CD_3)_2^+$,[1] and these results are again counterintuitive, considering that secondary and tertiary C−H bonds are weaker than primary C−H bonds.[14] However, Perry and Goddard,[4] in their recent theoretical study of Sc^+-C bond strengths in Sc−alkyl$^+$ species, found that the differences in bond strengths of Sc^+-R for the series R = CH_3, C_2H_5, i-C_3H_7, and t-C_4H_9 match closely the differences in bond strengths for H−R. This would suggest that the exchange reaction $Sc^+-R + R'-H \rightarrow Sc^+-R' + R-H$ should be thermoneutral for this series, but alkyl groups larger than ethyl are able to bend around and interact with the Sc^+ center. This additional interaction or "solvation" with an alkyl group can further stabilize the Sc^+ center. For example, the n-propyl substituent further stabilizes the Sc^+ center by about 3 kcal mol^{-1} with this additional "solvation".[4] This stabilization, which should be present in the transition state for the reactions as well, explains the observed preference exhibited by $CH_3ScCH_2CH_3^+$ for reaction at primary sites with the larger alkanes in this study.

Reaction at primary C−H bonds may also be favored by the structure of the most stable Sc^+−alkyl adduct. Perry *et al.* have found that the Co^+−propane adduct is more stable when it exhibits η^4 coordination to the two primary carbons than when it exhibits η^2 coordination to the secondary carbon.[18] $CH_3ScCH_2CH_3^+$ may show similar behavior when it forms an adduct with propane.

Our results in this system contrast with results obtained by Weinberg and Sun,[19] who found that, in the case of propane reacting with a Pt surface, attack at secondary C−H bonds is preferred over attack at primary C−H bonds. However, reactions on iridium complexes in solution,[6] Co^+ with propane in the gas phase,[5] and $Sc(CD_3)_2^+$ with small alkanes in the gas phase[1] have shown a preference for attack at primary C−H bonds.

(15) For n-pentane, α = 9.99 Å^3: Maryott, A. A.; Buckley, F. *U.S. Natl. Bur. Stand.* **1953**, Circular No. 537.
(16) For propane, α = 6.29 Å^3: Maryott, A. A.; Buckley, F. *U.S. Natl. Bur. Stand.* **1953**, Circular No. 537.
(17) For n-butane α = 8.20 Å^3: Maryott, A. A.; Buckley, F. *U.S. Natl. Bur. Stand.* **1953**, Circular No. 537.

(18) Perry, J. K.; Ohanessian, G.; Goddard, W. A., III. *J. Phys. Chem.* **1993**, *97*, 5238.
(19) Weinberg, W. H.; Sun, Y. *Science* **1991**, *253*, 542.

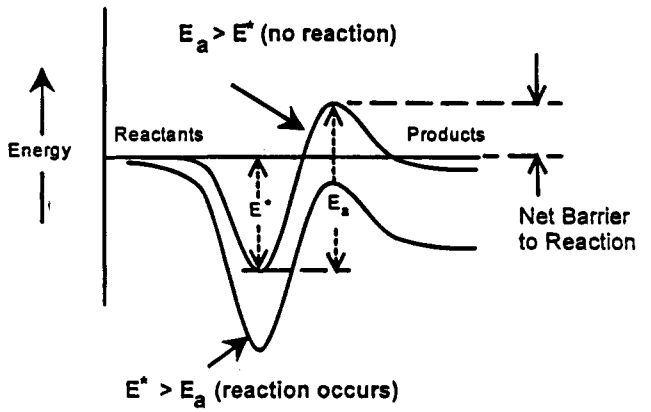

Figure 8. Schematic of a general potential energy surface showing how the initial electrostatic potential well can affect the height of a barrier relative to the energy of the reactants. Deepening the initial electrostatic well can lower the barrier to reaction below the energy of the reactants. The upper curve would be appropriate for the reaction of $CH_3ScCH_2CH_3^+$ with methane or ethane. The lower curve would be appropriate for the reaction of $CH_3ScCH_2CH_3^+$ with propane, the isomeric butanes or *n*-pentane.

Overall Reaction Efficiencies. The largest rate constant we observed was for the reaction of $CH_3ScCH_2CH_3^+$ with *n*-pentane. The rate constant for reaction with pentane was about 3.8 times larger than that for reaction with isobutane, while the rate constant for reaction with isobutane was about 1.7 times larger than that for reaction with *n*-butane and about 2.0 times larger than that for reaction with propane. Ethane and methane are not observed to react at all with $CH_3ScCH_2CH_3^+$. This trend is analogous to the trend seen with $Sc(CD_3)_2^+$.[1] The increase in reaction efficiency seen as the alkane reacting with $CH_3ScCH_2CH_3^+$ increases in size can be accounted for by the deeper potential wells which result from the increased polarizabilities of the larger alkanes. This makes it easier to overcome intrinsic barriers to σ-bond metathesis (Figure 8). These results are reminiscent of the reactions of Co^+ with hydrocarbons, where larger hydrocarbons deepen the electrostatic potential well for the Co^+–alkane adduct, more strongly binding the alkane to Co^+ and providing more energy for chemical activation.[5,18]

Furthermore, the kinetic efficiencies observed for $CH_3ScCH_2CH_3^+$ reacting with propane, *n*-butane, and isobutane are lower than for $Sc(CD_3)_2^+$ reacting with the same alkanes.[1] This observation suggests that, compared to the energy of the reactants, the energy of the transition state for the reaction of $CH_3ScCH_2CH_3^+$ with propane, *n*-butane or isobutane is higher than the energy of the transition state for the reaction of $Sc(CD_3)_2^+$ with the same alkane. This effect could be due to extra steric interactions introduced by the larger ethyl group or a possible trans effect[8] of the methyl and ethyl groups upon each other's bond strength with Sc^+. Similar synergistic effects in two-ligand gas phase metal-ion complexes have been previously observed.[7] The group specificity observed in the reactions of $CH_3ScCH_2CH_3^+$ with propane, *n*-butane, isobutane, and *n*-pentane is another example of how the replacement of one methyl group with an ethyl group synergistically affects the reactivity of the remaining methyl group compared to the reactivity observed for methyl groups in $Sc(CD_3)_2^+$.

The observation that ethane and methane do not react with $CH_3ScCH_2CH_3^+$ appears to be in accordance with the theoretical prediction of Perry and Goddard[4] that the degenerate metathesis reaction of methane with $Sc(CH_3)_2^+$ has a net barrier of about 12 kcal mol^{-1}. Table 2 shows the theoretical values calculated by Perry and Goddard for several metathesis reactions involving small alkanes. Even though methyl and ethyl exchange reactions with both $CH_3ScCH_2CH_3^+$ and $Sc(CD_3)_2^+$ are calculated to be approximately thermoneutral, $CH_3ScCH_2CH_3^+$ reacts with neither methane nor ethane, and $Sc(CD_3)_2^+$ does not react with methane,[1] providing experimental support for the presence of an overall barrier to these reactions. In these cases, the energy of the transition state is apparently higher than the energy of the reactants (upper curve of Figure 8). However, both $CH_3ScCH_2CH_3^+$ and $Sc(CD_3)_2^+$ react with alkanes larger than ethane. In these cases the energy of the transition state is below the energy of the reactants so that no net barrier to reaction exists, as shown by the lower curve in Figure 8. Our observation that both $CH_3ScCH_2CH_3^+$ and $Sc(CD_3)_2^+$ react with alkanes larger than ethane is in accordance with the prediction of Steigerwald and Goddard.[2]

Reaction of Sc^+ and *n*-Pentane and Reaction of Subsequent Product Ions with *n*-Pentane. The reaction of Sc^+ with *n*-pentane produced a complex mixture of products. At long times many high-mass $R'ScR^+$ products, where R and R′ are alkyl groups, were observed. In order to determine which ions were the precursors of these species, various product ions of the reaction of Sc^+ with *n*-pentane were isolated and allowed to react in turn with *n*-pentane. $CH_3ScCH_2CH_3^+$ reacted with *n*-pentane to produce mostly $CH_3ScC_5H_{11}^+$, $CH_3CH_2ScC_5H_{11}^+$, I, II, and small amounts of $R'ScR^+$ products of higher mass which result from subsequent reactions of the main product ions. $CH_3ScC_5H_{11}^+$ also reacted with *n*-pentane to produce mostly $R'ScR^+$ where R and R′ are larger than ethyl. What is of interest here is that $CH_3ScCH_2CH_3^+$ reacted with *n*-pentane via a σ-bond metathesis involving only C–H bond activation, as was seen previously for the reaction of $Sc(CD_3)_2^+$ with small alkanes.[1] The reaction of $CH_3ScCH_2CH_3^+$ with alkanes smaller than *n*-pentane, as observed in this study, also involved only C–H bond activation. But the facts that $CH_3ScC_5H_{11}^+$ can produce $R'ScR^+$ where either R or R′ is not a pentyl group and that II can be formed from $CH_3ScC_5H_{11}^+$ seem to suggest that some intermolecular and intramolecular C–C bond activation is occurring.

Observation of the reaction of $CH_3ScC_5H_{11}^+$ with *n*-pentane also provided us with direct evidence that intramolecular σ-bond metathesis does occur. Metallacycles I and II were both observed to form from isolated $CH_3ScC_5H_{11}^+$. These products could only be observed if intramolecular σ-bond metathesis were occurring. This supports our postulate that excited CH_3ScR^+ ions, where R = *n*-butyl, isobutyl, or pentyl, can perform a second intramolecular σ-bond metathesis reaction to form metallacyclic products.

Acknowledgment. We wish to thank J. K. Perry and Professor W. A. Goddard III for their theoretical work on this system.[4] This work was supported by the National Science Foundation under Grant CHE-9108318, by a grant from AMOCO, and by the Office of Naval Research.

OM950126I

Heterocyclic Systems Containing Lead(IV). 5.[1] Redistributions between Diaryllead Sulfides $[R_2PbS]_3$ and $[R'_2PbS]_3$ (R, R' = Ph, o-, m-, and p-Tol, 2,4-, 2,5-, and 3,4-Xyl, and p-Anis). $\pi-\pi'$ Charge Flow in Mixed Species via σ^*-LUMO's[†]

Heike Stenger, Barbara M. Schmidt, and Martin Dräger*

Institut für Anorganische Chemie und Analytische Chemie der Johannes Gutenberg-Universität, D-55099 Mainz, Germany

Received May 1, 1995[⊗]

Eight lead–sulfur heterocycles of the type $[R_2PbS]_3$ have been synthesized. Vibrational data for all compounds and crystal structures for $[o\text{-}Tol_2PbS]_3$ and $[p\text{-}Tol_2PbS]_3$ have been determined. The core of each molecule consists of a six-membered ring in a flexible twisted-boat conformation. Equimolar mixtures of the heterocycles dissolved in $CDCl_3$ immediately reached the steady state of the dynamic equilibrium between the starting materials and the redistribution species $[(R_2PbS)_2(R'_2PbS)]$ and $[(R_2PbS)(R'_2PbS)_2]$. Thirteen combinations have been followed by ^{207}Pb-NMR spectroscopy (six chemical shifts in an intensity ratio of (1):(1):(1:2):(1:2) and two spin–spin AB systems) and by FD mass spectrometry (mixed units with a Pb_4S_4 core). From these results and the crystal structure data, a possible course of the redistribution is proposed. Two differently substituted pure heterocycles slowly form a dimer containing two five-coordinated lead atoms. This dimer rearranges by a fast intramolecular nucleophilic attack at these atoms into a ladder structure with a Pb_4S_4 core and two extraladder groups –SPb which are shown to cleave off in the mass spectrum. The slow reversal of the rearrangement leads back to the pure heterocycles or results in the mixed species. The AB systems of the mixed heterocycles result in two-bond couplings $^2J(^{207}Pb–S–^{207}Pb)$. The ^{207}Pb-NMR chemical shifts are discussed in an order of $\pi-\pi'$ charge flow between units R_4Pb_2/R'_2Pb via σ^*-LUMO's which extend over the entire ring core. ^2J decreases along with an increasing charge flow.

Introduction

The investigation of redistribution experiments[2–4] between organolead and -tin heterocycles of the type $[R_2MS]_3$ (M = Sn, Pb; R = organyl) resulted in four- and six-membered mixed lead–tin rings.[1] NMR and mass spectrometric studies, just as the crystallographic study of a reaction intermediate, allowed the postulation of a mechanism for the synthesis and redistribution course.[1] In this paper we examine a number of exchange experiments between various aryl-substituted lead compounds $[R_2PbS]_3$ and $[R'_2PbS]_3$. Mixed six-membered redistribution species which contain differently substituted lead atoms are formed (Scheme 1).

Results obtained from NMR, mass spectrometric, and structure determination studies will be discussed in relation to the mechanism stated in the above mentioned work. ^{207}Pb-NMR chemical shifts and two-bond spin–spin couplings ^2J(Pb–S–Pb) of the exchanged systems are reported. The values of the ^{207}Pb-NMR chemical shifts for the redistribution species can be included in a consistent system of $\pi-\sigma^*-\pi'$ charge flow between the aromatic substituents R/R' in the 1,3-position. In a previous paper, dealing with asymmetrically substituted dilead species, we related values of the one-bond spin–spin coupling ^1J(Pb–Pb) with a $\pi-\sigma^*-\pi'$ charge migration between groups in a 1,2-position.[5] In asymmetrically substituted mononuclear lead compounds, e.g. $Ph_nPb(p\text{-}Tol)_{4-n}$ (n = 0–4), a $\pi-\sigma^*-\pi'$ charge flow is responsible for the nonlinear course of group 14 chemical shifts.[6] Previously, this effect had been simplistically termed as "sagging".[7]

Results

Starting Materials. The trimeric diorganolead sulfides used for the redistribution experiments were synthesized by reaction of the corresponding dihalogenides with hydrogen sulfide. The lead–sulfur het-

[†] This paper includes parts of the intended Ph.D. thesis of H.S.

[⊗] Abstract published in *Advance ACS Abstracts,* August 1, 1995.

(1) Part 4: Flöck, O. R.; Dräger, M. *Organometallics* **1993**, *12*, 4623.

(2) For general information with regard to redistribution equilibria see: Moedritzer, K. *Adv. Organomet. Chem.* **1968**, *6*, 171. Lockhart, J. C. *Redistribution Reactions*; Academic Press: New York, London, 1970.

(3) For detailed discussions of group 14 redistribution reactions see: Moedritzer, K. *Organomet. Chem. Rev.* **1966**, *1*, 179. *Comprehensive Organometallic Chemistry*; Wilkinson, G., Stone, F. G. A., Abel, E. W., Eds.; Pergamon: Oxford, U.K. 1982; Vol. 2; pp 27 and 169 (Si), pp 417 and 446 (Ge), p 606 (Sn). Haiduc, I.; Zuckerman, J. J. *Basic Organometallic Chemistry*; de Gruyter: Berlin, New York, 1985; pp 132 and 139 (Si), pp 146 and 152 (Ge), pp 154 and 156 (Sn). Wrackmeyer, B. *Annu. Rep. NMR Spectrosc.* **1985**, *16*, 73 (Sn). *The Chemistry of Organic Silicon Compounds*; Patai, S., Rappoport, Z., Eds.; Wiley: Chichester, U.K., 1989; Part 2, p 1402. *Chemistry of Tin*; Harrison, P. G., Ed.; Blackie: Glasgow, London, 1989; p 188.

(4) Redistribution reactions in which lead atoms are involved are detailed in: Shapiro, H.; Frey, F. W. *The Organic Compounds of Lead*; Wiley: New York, 1968; p 92. Calingaert, G.; Beatty, H. A. *J. Am. Chem. Soc.* **1939**, *61*, 2749 (creation of the term "redistribution reaction" and first systematic study). Calingaert, G.; Beatty, H. A.; Soroos, H. *J. Am. Chem. Soc.* **1940**, *62*, 1099 (redistribution of R_4Pb compounds).

(5) Koglin, H.-J.; Behrends, K.; Dräger, M. *Organometallics* **1994**, *13*, 2733.

0276-7333/95/2314-4374$09.00/0

Scheme 1[a]

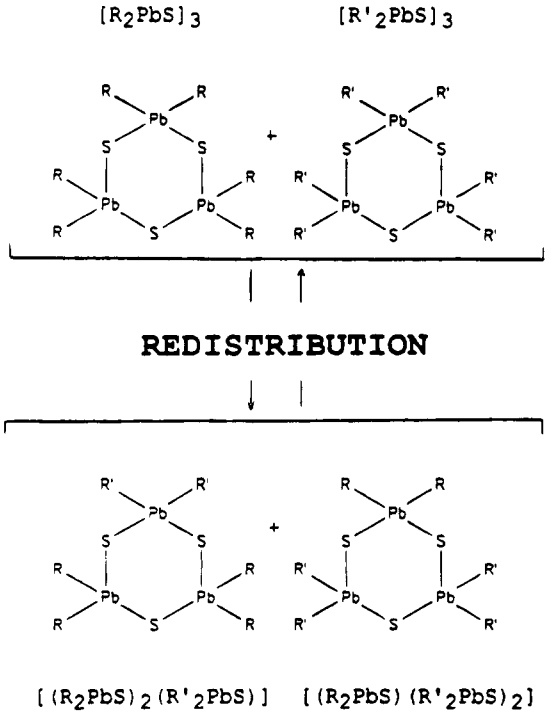

[a] R, R′: Ph, o-Tol, m-Tol, p-Tol, 2,4-Xyl, 2,5-Xyl, 3,4-Xyl, p-Anis.

erocycles slowly decompose in solution and must be protected from light. The results are summarized in Table 1.

Crystal Structures. The structure determinations of $[o\text{-}Tol_2PbS]_3$ (Figure 1) and of $[p\text{-}Tol_2PbS]_3$ reveal approximately C_2-symmetric six-membered rings in a chiral twisted-boat conformation. The centrosymmetric crystal structures contain both enantiomers. Table 2 gives the relevant bond lengths and angles for the above two compounds and also the relevant values for $[Ph_2PbS]_3$, used as a comparison.[8] Both bond lengths, Pb–S (averages 2.498, 2.500, 2.491 Å) and Pb–C (averages 2.22, 2.20, 2.19 Å), scatter only slightly and are distinctly shorter than the standard single-bond values of O'Keefe and Brese.[9]

All three molecular structures contain tetrahedrally coordinated lead atoms with distinctly enlarged C–Pb–C angles. Only in the case of the compound $[p\text{-}Tol_2PbS]_3$, one of the three $S_2Pb(p\text{-}Tol)_2$ tetrahedra receives a fifth intermolecular contact by a sulfur atom of a neighboring molecule (Pb···S 3.477(4) Å). A center of symmetry of the unit cell doubles this contact, and a dimeric unit arises (Figure 2). With respect to a single-bond value of 2.50 Å, the Pauling type bond order of the intermolecular contact amounts to BO 0.14.[10]

Vibrational Data. The stetching modes ν(Pb–S) for the central core of the compounds $[R_2PbS]_3$ reflect the approximate 2-fold axis found in the crystal structures

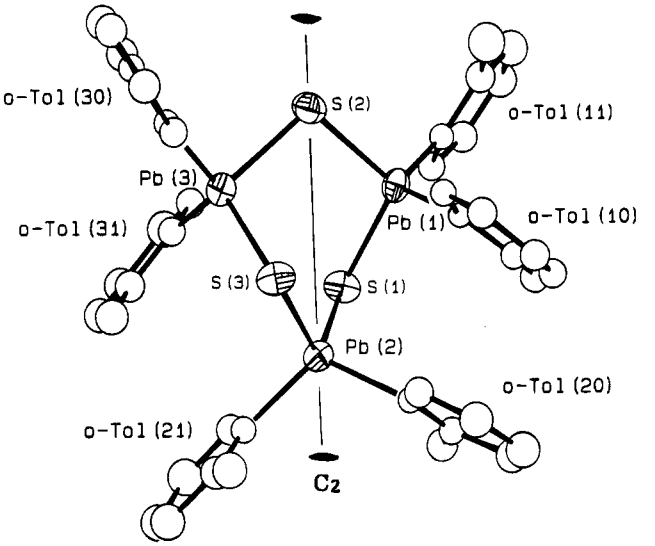

Figure 1. ORTEP drawing of $[o\text{-}Tol_2PbS]_3$. The approximate 2-fold axis (S(2)–Pb(2)) is outlined. Group identifications are as given in Table 6. Thermal ellipsoids are at the 50% probability level for Pb and S and at the 30% probability level for C.

of $[o\text{-}Tol_2/p\text{-}Tol_2/Ph_2PbS]_3$ and suggest that the other rings occupy a similar twisted-boat conformation. In addition to the asymmetric and symmetric modes ν_{as}(Pb–S) (strong IR absorptions, weak Raman emissions) and ν_s(Pb–S) (very strong Raman emissions, medium to strong IR absorptions), a third frequency appears nearly midway between the two other frequencies in most of the spectra (Table 1). The intensities of this "central" stretching vibration ν_c(Pb–S) are nonuniform.

Redistributions Followed by ^{207}Pb-NMR Spectroscopy. According to Scheme 1, ring-segment exchange reactions between differently substituted pure lead heterocyclic systems, $[R_2PbS]_3$ and $[R'_2PbS]_3$, result in an equilibrium between four kinds of six-membered ring species. Two of these are the starting materials, each showing one ^{207}Pb-NMR signal. The two redistribution species each contain two differently substituted lead nuclei, giving rise to two ^{207}Pb signals with an intensity ratio of 1:2, respectively. Starting with equimolar amounts of substances, in all experiments an overall intensity ratio of (1):(1):(1:2)(1:2) has been found in good approximation, indicating a statistical redistribution. All investigated mixtures immediately reached the steady state of the dynamic redistribution equilibrium. This is in contrast with the delayed setting up of the equilibrium if tin atoms are involved (see Figure 2 and Table 4 of ref 1). Low-temperature studies and temperature-dependent NMR experiments shall be the subject of a future paper.

Figure 3 shows as an example the six ^{207}Pb signals found in the exchange experiment $[Ph_2PbS]_3/[2,4\text{-}Xyl_2PbS]_3$. These six signals result from the four different rings containing only one chemical kind of ^{207}Pb nuclei in each ring. If one of the two redistribution species contained two chemically different ^{207}Pb nuclei, an AB spin pattern of four satellites would appear. These satellites would surround the two resonances of the respective ring species asymmetrically, amounting to a joint intensity of at most $^1/_5$ of the total intensity. An

(6) Charissé, M.; Mathiasch, B.; Dräger, M.; Russo, U. *Polyhedron*, in press.
(7) Harris, R. K.; Kennedy, J. D.; McFarlane, W. In *NMR and the Periodic Table*; Harris, R. K., Mann, B. E., Eds.; Academic Press: London, New York, San Francisco, 1978; p 309.
(8) Schmidt, B. M.; Dräger, M. *J. Organomet. Chem.* **1990**, *399*, 63.
(9) O'Keefe, M.; Brese, N. E. *J. Am. Chem. Soc.* **1991**, *113*, 3226 (sum of radii Pb–S = 2.56 Å and Pb–C = 2.31 Å; proposed corrections for electronegativity −0.03 and −0.01 Å).
(10) Kolb, U.; Beuter, M.; Gerner, M.; Dräger, M. *Organometallics* **1994**, *13*, 4413.

Table 1. Preparative and Physical Data of the Compounds $[R_2PbS]_3$

$$3R_2PbX_2 + 3H_2S + 6NEt_3 \xrightarrow[\text{darkness}]{20-25\ ^\circ C/\text{toluene}} [R_2PbS]_3 + 6NEt_3{\cdot}HX$$

R	X	yield[a] (%)	color	mp (°C)	formula (M_r)	elemental anal. (%)		stretching vibrations ν(Pb−S)[b]		
						C_{obs} (C_{calc})	H_{obs} (H_{calc})	ν_{as}(Pb−S)[c]	ν_c(Pb−S)[c]	ν_s(Pb−S)[c]
Ph	OAc	66	yellow	115	$C_{36}H_{30}Pb_3S_3$ (1179.60)	36.74 (36.63)	2.74 (2.54)	335 s (333 w)	324 s (314 w)	289 s (286 vs)
o-Tol	Br	78	yellow	128	$C_{42}H_{42}Pb_3S_3$ (1263.60)	39.50 (39.89)	3.43 (3.32)	326 sh, s (326 w)	320 vs (319 w)	291 s (291 s)
m-Tol	I	69	yellow/orange	81	$C_{42}H_{42}Pb_3S_3$ (1263.60)	40.32 (39.89)	3.50 (3.32)	326 s[d]	*e*, *d*	289 s (288 m)
p-Tol	I	61	yellow	110	$C_{42}H_{42}Pb_3S_3$ (1263.60)	39.80 (39.89)	3.61 (3.32)	330 s (336 m)	*e* (315 w)	294 w (293 s)
2,4-Xyl	Br	56	pale yellow	180	$C_{48}H_{54}Pb_3S_3$ (1347.60)	43.58 (42.74)	4.23 (4.01)	324 s (324 w)	302 m (297 sh, s)	282 m (287 vs)
2,5-Xyl	I	97	pale yellow	169	$C_{48}H_{54}Pb_3S_3$ (1347.60)	42.96 (42.74)	4.37 (4.01)	328 m (326 w)	314 m (313 w)	288 m (291 vs)
3,4-Xyl	Br	7	colorless	114	$C_{48}H_{54}Pb_3S_3$ (1347.60)	42.83 (42.74)	4.09 (4.01)	324 s[e]	303 m (300 vs)	282 s (284 sh, w)
p-Anis	I	48	pale yellow	134	$C_{42}H_{42}O_6Pb_3S_3$ (1359.60)	38.73 (37.07)	3.55 (3.09)	338 sh, s[e]	320 s (318 w)	301 s (290 s)

[a] Precipitated from toluene by petroleum ether (60−70 °C). R = p-Anis: recrystallized from $CHCl_3$/EtOH (1:1). [b] IR absorptions (Raman emissions in parentheses). [c] Asymmetric (as) and symmetric (s) stretching modes assigned preferentially to Pb and S off the 2-fold axis. Central (c) stretching mode influenced preferentially by Pb and S on the 2-fold axis. [d] Decomposition in the laser beam. [e] No appearance in the experimental spectrum.

Table 2. Bond Lengths and Bond Angles of the Heterocycles $[o\text{-}Tol_2PbS]_3$ and $[p\text{-}Tol_2PbS]_3$ Compared to $[Ph_2PbS]_3$[8] with Esd's in Parentheses

atom[a]	$[o\text{-}Tol_2PbS]_3$	$[p\text{-}Tol_2PbS]_3$	$[Ph_2PbS]_3$
	Bond Lengths (Å)		
Pb(1)−S(1)	2.493(3)	2.490(5)	2.499(6)
Pb(1)−S(2)	2.481(4)	2.523(4)	2.491(6)
Pb(2)−S(1)	2.492(3)	2.509(3)	2.492(7)
Pb(2)−S(3)	2.517(4)	2.496(4)	2.488(6)
Pb(3)−S(2)	2.507(4)	2.478(4)	2.489(7)
Pb(3)−S(3)	2.495(4)	2.504(5)	2.488(6)
Pb−C	2.20−2.24(1)	2.18−2.23(2)	2.16−2.21(2)
	Bond Angles (deg)		
S(1)−Pb(1)−S(2)	107.1(1)	105.5(1)	109.9(2)
C(10)−Pb(1)−C(11)	117.8(5)	118.4(5)	118.7(7)
S(3)−Pb(2)−S(1)	109.5(1)	110.9(1)	108.9(2)
C(20)−Pb(2)−C(21)	116.8(5)	131.0(5)	118.1(9)
S(2)−Pb(3)−S(3)	105.2(1)	107.2(1)	109.4(2)
C(30)−Pb(3)−C(31)	119.1(5)	116.1(6)	113.7(9)
Pb(2)−S(1)−Pb(1)	100.8(1)	108.4(2)	103.7(2)
Pb(1)−S(2)−Pb(3)	102.9(1)	101.3(2)	104.6(2)
Pb(3)−S(3)−Pb(2)	100.4(1)	101.4(1)	105.0(2)

[a] Atom identifications as given in Figures 1 and 2 and in Tables 6 and 7.

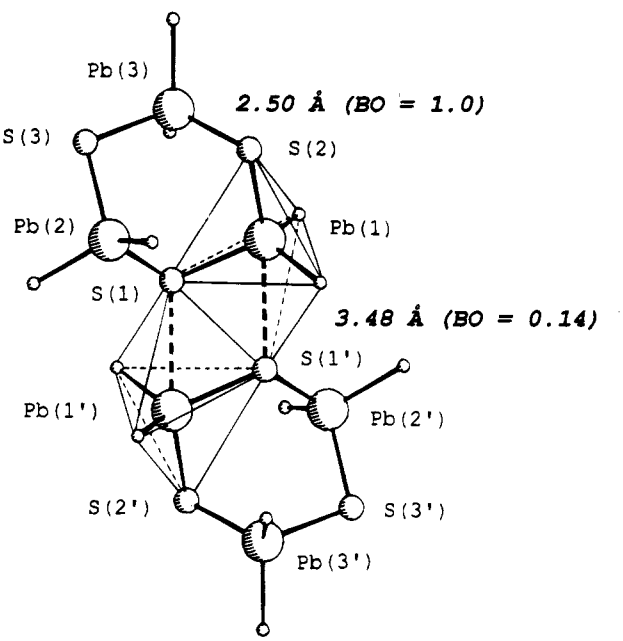

Figure 2. Dimeric molecular unit of $[p\text{-}Tol_2PbS]_3$, connected by intermolecular Pb···S interactions. The two edge-shared monocapped tetrahedra are outlined. PLUTO drawing with C(ipso) provided only for better clarity. Group identifications are as given in Table 7.

equivalent AB pattern of four satellites holds for the second redistribution species. Figure 3 shows both AB systems.

The eight expected AB satellites were only clearly discernible in some spectra. In some cases the satellites were obscured by the main signals being close together. Therefore a mathematical analysis of the visible signals was required (see Experimental Section). Thirteen exchange experiments were performed (Table 3). In seven cases both spin−spin couplings $^2J(^{207}Pb-S-^{207}Pb)$ were determined; in two additional cases, only one of the two independent couplings was determined.

Redistributions Followed by FD Mass Spectrometry. Solutions of the 8 starting compounds as well as 11 redistribution mixtures in $CDCl_3$ were examined by FD mass spectrometry in the range *m/e* 1000−1800. Table 4 summarizes the results and gives the most likely assignments. In most of the spectra the units Pb_4S_4 and Pb_4S_3 with varying amounts of organic substituents occur. In nearly all cases the redistribution mixtures show fragments with two kinds of aromatic groups. Overall, the cleavage of the lead−carbon bond seems to be easy. If in addition redistribution of these bonds takes place (see ref 4), it could not be concluded definitely.

Discussion

Course of the Redistribution. Scheme 2 summarizes the outcome of the redistribution experiments. The two flexible starting rings **1** (Figure 1, twisted-boat conformation; Figure 3, two ^{207}Pb-NMR signals) combine

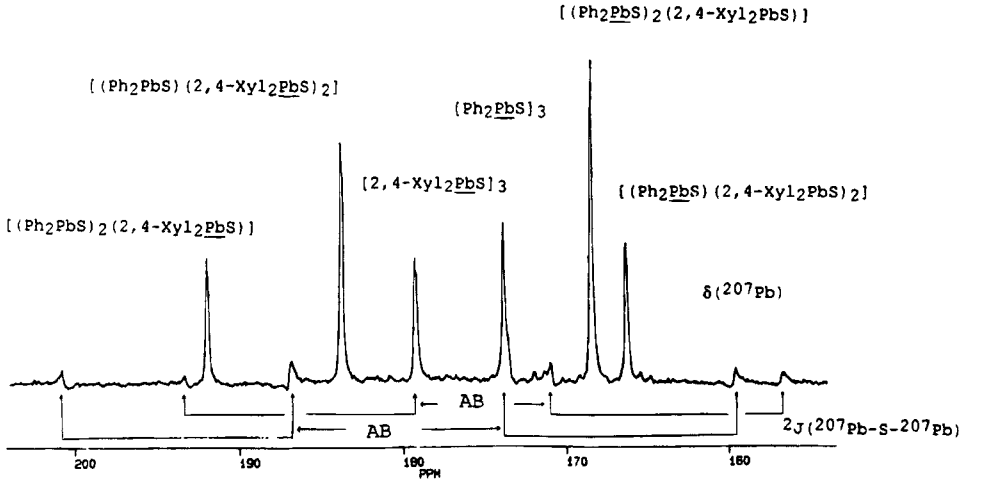

Figure 3. ^{207}Pb NMR spectrum of the redistribution system $[Ph_2PbS]_3/[2,4\text{-}Xyl_2PbS]_3$. Signals are assigned to the underlined lead atoms. The two AB systems are indicated by arrows.

Table 3. ^{207}Pb NMR Chemical Shifts (ppm[a]) and Coupling Constants $^2J(^{207}Pb-S-^{207}Pb)$ (Hz) for the Redistribution Species

		$\delta(^{207}Pb)$ ($^2J(^{207}Pb-S-^{207}Pb)$					
			$[(R_2PbS)_2(R'_2PbS)]$		$[(R_2PbS)(R'_2PbS)_2]$		
R	R'	$[R_2PbS]_3$					$[R'_2PbS]_3$
Ph	p-Tol	173.3	171.4 (244.9)	184.7 (244.2)	169.4 (244.6)	182.7 (247.5)	180.8
Ph	m-Tol	172.7	171.7 (*b*)	180.3 (*b*)	170.6 (*b*)	179.3 (*b*)	178.3
Ph	o-Tol	173.5	175.0 (266.7)	169.1 (266.7)	180.5 (237.3)	169.7 (237.0)	173.0
Ph	2,4-Xyl	173.7	168.3 (233.0)	191.9 (234.2)	166.2 (239.8)	183.7 (238.0)	179.2
Ph	2,5-Xyl	173.1	168.7 (233.8)	183.1 (233.8)	165.7 (231.8)	177.6 (231.8)	173.8
Ph	p-Anis	173.2	171.0 (264.8)	190.3 (264.8)	168.4 (258.6)	188.2 (258.6)	185.7
p-Tol	m-Tol	180.9	181.7 (*b*)	177.2 (*b*)	182.4 (*b*)	178.2 (*b*)	179.0
p-Tol	o-Tol	181.3	179.4 (*b*)	175.3 (*b*)	180.3 (243.8)	172.9 (244.0)	173.3
p-Tol	2,4-Xyl	181.3	181.3 (271.6)	177.0 (271.5)	186.4 (279.8)	177.6 (270.2)	179.1
p-Tol	2,5-Xyl	181.3	178.6 (*b*)	177.0 (*b*)	178.3 (*b*)	176.0 (*b*)	174.8
o-Tol	m-Tol	172.6	173.8 (*b*)	176.1 (*b*)	175.7 (*b*)	178.7 (*b*)	178.9
o-Tol	3,4-Xyl	173.3	171.8 (*b*)	184.2 (*b*)	174.1 (295.8)	181.4 (294.3)	182.5
2,4-Xyl	2,5-Xyl	178.9	179.7 (290.1)	172.1 (296.8)	178.9 (275.6)	173.9 (279.8)	174.4

[a] Solvent $CDCl_3$. [b] Not determinable.

in a slow nucleophilic attack of sulfur at four-coordinated lead atoms to form the weakly bonded dimer **2** (Figure 2: BO 0.14). The reverse of the equilibrium (1) is fast. A second nucleophilic attack (eq 2) of the encircled sulfur atoms at five-coordinated lead atoms in a different part of the dimer is also fast and is favored conformationally by the flexibility of the six-membered rings and mechanistically by the fact that a nucleophilic attack at a five-coordinated center is faster than at a four-coordinated center (concept of frontier orbital controlled nucleophilic attack[10,11]).

Overall, the dimer **2** rearranges to the intermediate **3**. This has been identified by FD mass spectrometry as a fragment with four lead atoms: the weakly connected extracyclic groups −SPb at the six-coordinated lead atoms have been cleaved off. The lifetime of **3** is short in terms of the NMR time scale. However with respect to mass spectrometry, the decompositions, (2) or (3), of the intermediates are slow. The ladderlike structure of **3** (12 atoms) is equivalent to the reaction intermediate $[Sn_4O_2(SH)_2)Cl_2]$ (10 atoms), which could be intercepted during the synthesis of the ring $[cHex_2SnS]_3$.[1] In both cases the extracyclic groups, −Cl or −SPb, stabilize the central core by an additional bond (pointed line). Previous examples of ladder structures contain similar modes of stabilization.[12]

The following step (eq 3) is the "central" step of the redistribution. The left and right parts of **3** rearrange and form a dimer **4** which contains different kinds of lead atoms in its six-membered rings. **4** cleaves quickly (reaction 4) into the two rings **5** which are detectable by their ^{207}Pb-NMR signals (Figure 3: 1:2 pattern twice and AB-satellite system). Known facts about redistribution equilibria including the other group 14 elements (R_4M compounds and group 16 bridged units M−X−M) point in the same direction of an initiation by a nucleophilic attack at M nuclei (see ref 3). This initiating nucleophilic attack gets faster in the order Si < Ge < Sn < Pb: control of the $GeR_4/GeCl_4$ redistribution is by means of a catalyst,[13] and that of the $SnR_4/SnCl_4$ redistribution (Kocheshkov reaction) is by temperature only.[14] In the case of cyclosilathianes a ring contraction on heating has been observed,[15] and a monomeric silathione is discussed as a possible intermediate.[16]

Charge Flow and Spin−Spin Coupling. The second outcome of Figure 3 is that of the positions of the ^{207}Pb-NMR chemical shifts of the rings **1** and **5** and of the values of the spin−spin couplings $^2J(^{207}Pb-S-$

(11) Chuit, C.; Corriu, R. J. P.; Reye, C.; Young, J. C. *Chem. Rev.* **1993**, *93*, 1371.

(12) Harrison, P. G.; Begley, M. J.; Molloy, K. C. *J. Organomet. Chem.* **1980**, *186*, 213. Vollano, J. F.; Day, R. O.; Holmes, R. R. *Organometallics* **1984**, *3*, 745. Dakternieks, D.; Gable, R. W.; Hoskins, B. F. *Inorg. Chim. Acta* **1984**, *85*, L43.

(13) Van der Kerk, G. J. M.; Rijkens, F.; Janssen, M. J. *Recl. Trav. Chim. Pays-Bas* **1962**, *81*, 764.

(14) Kocheshkov, K. A. *Chem. Ber.* **1926**, *62*, 996.

Table 4. Mass Spectrometrical Data for 8 Pure Species $[R_2PbS]_3$ and for 11 Redistribution Systems $[R_2PbS]_3/[R'_2PbS]_3$

R	R′	*m/e* (rel abundance (%))	attribution R	R′	Pb	S	R	R′	*m/e* (rel abundance (%))	attribution R	R′	Pb	S
Ph		1346 (100)	5		4	4	Ph	p-Tol	1431 (85)	4	2	4	4 (−CH_3)
		1376 (30)	5		4	5			1446 (65)	4	2	4	4
		1616 (53)	9		4	3			1461 (25)	2	4	4	4 (−CH_3)
o-Tol		1082 (26)	4		3	3	Ph	o-Tol	1391 (22)	6		4	3
		1322 (20)	4		4	4			1404 (100)	5	1	4	3
		1472 (100)	6		4	3			1419 (26)	6		4	4
m-Tol		1087 (23)	4		3	4 (−$2CH_3$)			1433 (42)	5	1	4	4
		1476 (100)	6		4	3			1460 (21)	3	3	4	4
		1567 (39)	7		4	4 (−$2CH_3$)	Ph	2,4-Xyl	1102 (72)	5		3	3
p-Tol		1322 (60)	4		4	4			1130 (98)	4	1	3	3
		1471 (100)	6		4	3			1156 (100)	3	2	3	3
		1504 (22)	6		4	4			1546 (18)	4	3	4	3
2,4-Xyl		1077 (94)	6		2	1	Ph	2,5-Xyl	1517 (52)	5	2	4	3
		1107 (50)	6		2	2			1544 (100)	4	3	4	3
		1181 (84)	5		3	2 (−$2CH_3$)			1571 (20)	3	4	4	3
		1597 (100)	7		4	2 (−$2CH_3$)	p-Tol	m-Tol	1474 (100)		6	4	3
2,5-Xyl		1077 (22)	6		2	1	p-Tol	o-Tol	1089 (100)		6	2	4
		1181 (22)	5		3	2 (−$2CH_3$)	p-Tol	2,4-Xyl	1520 (100)	5	1	4	4
		1421 (28)	7		3	2			1533 (18)	4	2	4	4
		1599 (100)	7		4	2 (−$2CH_3$)			1560 (21)	2	4	4	4
3,4-Xyl		1181 (37)	5		3	2 (−$2CH_3$)	p-Tol	2,5-Xyl	1144 (20)	5		3	2
		1418 (38)	5		4	2			1158 (100)	4	1	3	2
		1596 (100)	7		4	2 (−$2CH_3$)			1172 (48)	3	2	3	2
p-Anis		1198 (100)	3		4	3 (−$3CH_3$)	o-Tol	m-Tol	1474 (100)		6	4	3
		1569 (32)	6		4	4 (−OCH_3)	o-Tol	2,4-Xyl	1156 (100)	4	1	3	2
Ph	p-Tol	1388 (22)	6		4	3			1278 (30)	5	1	3	3
		1404 (84)	4	2	4	3 (−CH_3)			1534 (15)	4	2	4	4
		1417 (100)	6		4	4	2,4-Xyl	2,5-Xyl	1186 (100)		5	3	2 (−$2CH_3$)

Scheme 2[a]

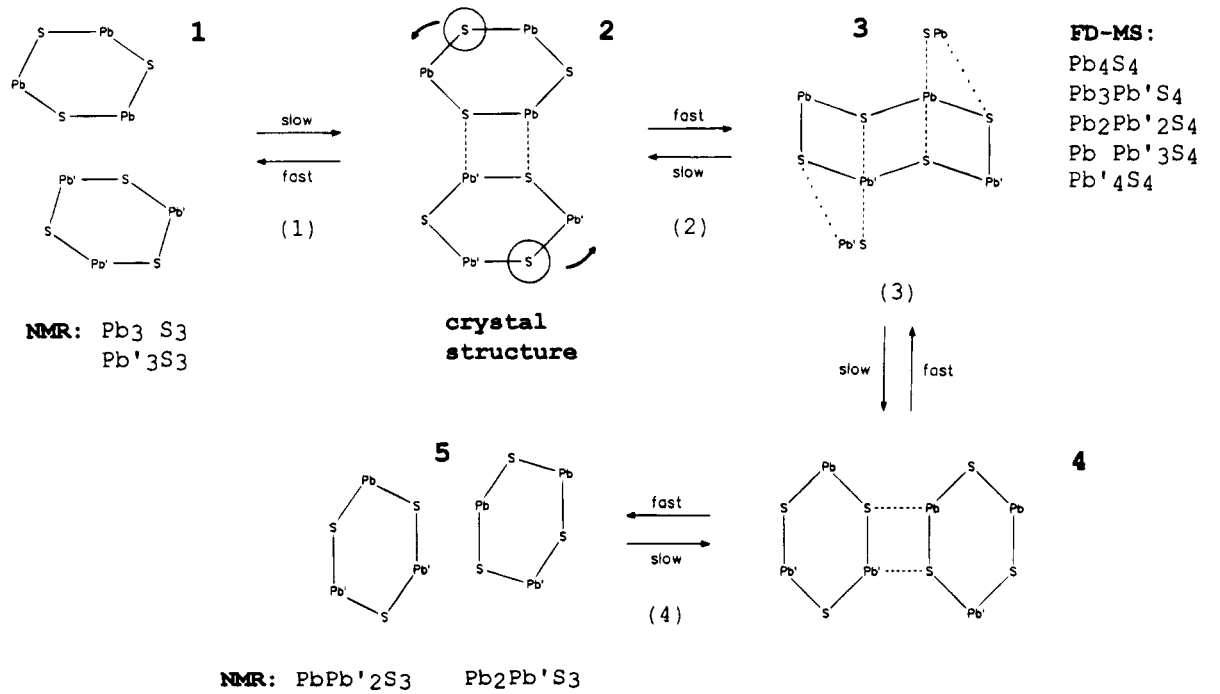

[a] Pb: PbR_2. Pb′: PbR_2'. Two bonds: lead 4-coordinated. Three bonds: lead 5-coordinated. Four bonds: lead 6-coordinated.

^{207}Pb) in **5**. $\delta(^{207}Pb)$ of the eight starting materials $[R_2PbS]_3$ (Table 3) increases by changing the substituent R in the order shown in (5) from 173 to 186 ppm ($\Delta\delta$ =

$$\text{Ph} \leq \text{o-Tol} < \text{2,5-Xyl} < \text{m-Tol} \leq \text{2,4-Xyl} < \text{p-Tol} < \text{3,4-Xyl} < \text{p-Anis} \quad (5)$$

+13 ppm). A similar downfield shift for $\delta(^{207}Pb)$ from −180 to −152 ppm ($\Delta\delta$ = +28 ppm) exists along the series R_4Pb in which the individual compounds contain two more aryl groups.[17]

The given order of $\delta(^{207}Pb)$ in the pure compounds $[R_2PbS]_3$ with six equal substituents R_6 accounts for a balanced charge distribution at the three equivalent lead nuclei. A distinction between two members of the series can be described by the difference shown in (6).

(15) Millard, M. M.; Pazdernik, L. J. *J. Organomet. Chem.* **1973**, *51*, 135. Millard, M. M.; Pazdernik, L. J.; Haddon, W. F.; Lundin, R. E. *J. Organomet. Chem.* **1973**, *52*, 283.
(16) Weidenbruch, M.; Schäfer, A.; Rankers, R. *J. Organomet. Chem.* **1980**, *195*, 171.
(17) Schneider-Koglin, C.; Mathiasch, B.; Dräger, M. *J. Organomet. Chem.* **1994**, *469*, 25.

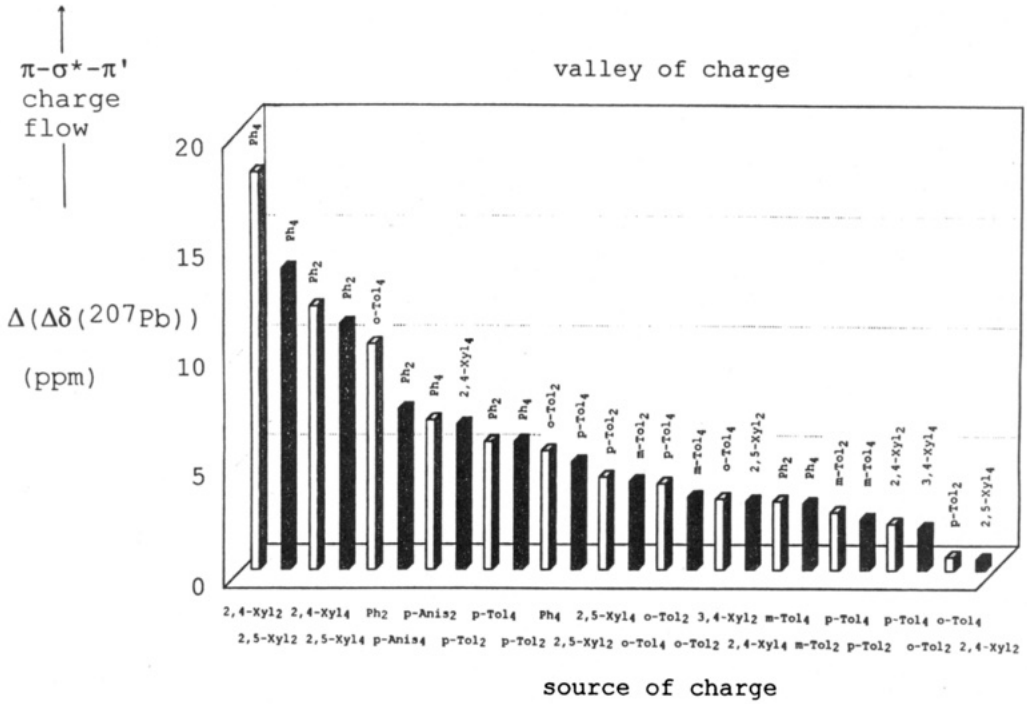

Figure 4. Charge migration via σ^*-LUMO's between $[R_2PbS]_2$ and $[R'_2PbS]$ units of the investigated 13 redistribution systems. Definition of $\Delta(\Delta\delta(^{207}Pb))$ provided by eqs 6–8.

$$\Delta\delta(R_6) = \delta(R_6) - \delta(R'_6) \quad (6)$$

With respect to the redistribution species **5**, the 2-fold three equivalent lead nuclei of **1** are no longer equivalent and split into two sets of two (Table 3). This splitting can also be described by a difference of chemical shifts (eq 7)in each individual ring. If (7) is corrected

$$\Delta\delta(R_2/R'_4) = \delta(R_2) - \delta(R'_4) \quad (7)$$

by (6), the total difference $\Delta(\Delta\delta)$ (eq 8)accounts for a

$$\Delta\,(\Delta\delta(^{207}Pb)) = \Delta\delta(R_2/R'_4) - \Delta\delta(R_6) \quad (8)$$

net charge flow from $[R_2Pb]$ to $[R'_2Pb]_4$ or vice versa. The differences $\Delta(\Delta\delta)$ for the 26 redistributed species **5** are given in the graph of Figure 4. For all mixed rings, this graph shows a source of charge (π-system) and a valley of charge (π'-system). The charge is transferred via delocalized σ^*-LUMO's which extend over the whole lead–sulfur ring core.[18]

With respect to the two-bond spin–spin couplings $^2J(^{207}Pb–S–^{207}Pb)$ of the redistribution species **5**, a range from 230 to 300 Hz has been found (Table 3). The individual values are generally consistent with the amount of π–σ^*–π' charge transfer shown in Figure 4. Increasing the exchange of charge indicates a definite lower value of ^2J (Figure 5). A similar relationship has been found between the charge flow and the one-bond coupling $^1J(^{207}Pb–^{207}Pb)$ in asymmetric systems $R_3Pb–PbR'_3$.[5] Also in the latter system, an extending σ^*-LUMO is responsible for the transfer of charge. Obviously, both spin–spin interactions ^1J and ^2J can be weakened by populated LUMO's.[19]

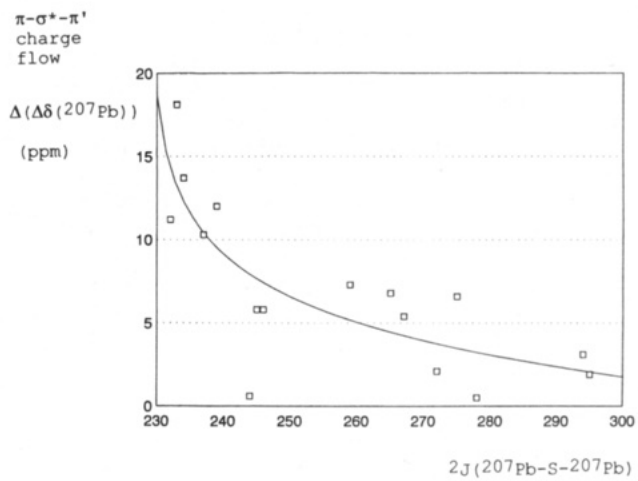

Figure 5. Plot of charge migration $\Delta(\Delta\delta)$ (ppm) versus the spin–spin coupling constants $^2J(^{207}Pb–S–^{207}Pb)$ (Hz) for the redistribution systems.

Experimental Section

General Considerations. Solvents were dried by standard techniques and were generally distilled prior to use. Organometallic lead compounds were obtained by known methods: Hexaorganyldiplumbanes Ar_6Pb_2 by Grignard reaction of ArMgBr with $PbCl_2$ and 1,2-dibromoethane in dry THF,[20] Ar_4Pb by pyrolysis of the corresponding Ar_6Pb_2 substances,[21] Ar_2PbBr_2 by cleavage of Ar_6Pb_2 with Br_2 in $CHCl_3$,[22] and Ar_2PbI_2 according to Ar_2PbBr_2 by treatment of Ar_4Pb with iodine in $CHCl_3$.[23] Melting points were determined in glass capillaries in a Kofler melting block. C and H analyses were obtained from the Institut für Organische Chemie, Universität Mainz, with a Perkin-Elmer 240 CHN Analyzer. Solution-state ^{207}Pb NMR spectra were recorded on a Bruker WP 80/

(18) Pacchioni, G.; Bagus, P. S. *Inorg. Chem.* **1992**, *31*, 4391.

(19) In view of the several counteracting contributions to spin–spin coupling, chemically strongly related systems must be chosen for any comparison of coupling constants: Harris, R. K. *Nuclear Magnetic Resonance Spectroscopy, A Physicochemical View*; Pitman Books Ltd.: London, 1983; p 211. Previous discussions of ^1J and ^2J at Sn centers refer preferentially to the geometrical alignment of the occupied orbitals ("bond angles"): Lockhart, T. P.; Manders, W. F. *J. Am. Chem. Soc.* **1987**, *109*, 7015. Lockhart, T. P.; Puff, H.; Schuh, W.; Reuter, H.; Mitchell, T. N. *J. Organomet. Chem.* **1989**, *366*, 61.

(20) Willemsens, L. C.; van der Kerk, G. J. M. *J. Organomet. Chem.* **1970**, *21*, 123.

Table 5. Crystallographic Data and Structure Determination Details for [o-Tol$_2$PbS]$_3$ and [p-Tol$_2$PbS]$_3$

	[o-Tol$_2$PbS]$_3$	[p-Tol$_2$PbS]$_3$
	Crystal Data[a]	
formula; M_r	$C_{42}H_{42}Pb_3S_3$; 1264.60	$C_{42}H_{42}Pb_3S_3$; 1264.60
cryst habit; color	oblique platelets; yellow	rhombic plate; yellow
face indices (dist from a common origin inside the cryst (mm))	100, $\bar{1}00$ (0.165); 1$\bar{1}$0, $\bar{1}$10 (0.200); 110, $\bar{1}\bar{1}$0 (0.105); 001, 00$\bar{1}$ (0.048)	100, $\bar{1}00$ (0.125); 010, 0$\bar{1}$0 (0.145); 001, 00$\bar{1}$ (0.080)
cryst syst; space group	monoclinic; $P2_1/n$ (No. 14)	triclinic; $P\bar{1}$ (No. 2)
unit cell dimens		
a(Å), α(deg)	13.193(2)	13.315(3), 85.64(4)
b(Å), β(deg)	17.358(5), 94.73(2)	13.501(3), 65.01(3)
c(Å), γ(deg)	17.872(7)	13.594(4), 67.32(1)
least-squares fit	23 rflns, θ = 18–22°	48 rflns, θ = 23–28°
packing: V (Å^3); Z; F(000)	4079(2); 4; 2352	2033(1); 2; 1176
D_{calcd}; D_{exptl} (g cm^{-3})	2.06; 1.95 (20°)	2.07; 1.96
	Intensity Data Collection[b]	
temp (°C); θ-range (deg); (sin θ)$_{max}$/λ (Å^{-1})	−65; 1.5–25.0; 0.590	−80; 1.5–25.0; 0.595
range of hkl	+17,+22,±23	+17,±17,±17
ref rflns	3, every 4000 s	3, every 4000 s
loss of intensity (%) (time (days)); corrcn	40 (10); linear	20 (12); linear
no. of rflns: measd; indep (int R)	10 525; 9774 (0.037)	10 127; 9713 (0.078)
no. of rflns: used, limit	5385, with $I > 2\sigma(I)$	6956, with $I > 2\sigma(I)$
μ; abs corrcn	120.6; numerical by face indices	120.9; numerical by face indices
range of transm	0.1100–0.3220	0.0729–0.2219
	Refinement	
choice of thermal params	Pb, S anisotropic, C isotropic	Pb, S anisotropic, C isotropic
var; ratio reflns/var; last shifts	225; 19; <0.005σ	225; 31; <0.004σ
final R; R_w	0.0479; 0.0575	0.0519; 0.0781
weight scheme w^{-1}	$\sigma^2(F) + 0.0017F^2$	$\sigma^2(F) + 0.0025F^2$
final diff Fourier max (e Å^{-3})	1.0, near Pb	2.0, near Pb

[a] Mo Kα_1; λ = 0.709 26 Å. [b] Mo Kα; λ = 0.710 69 Å; graphite monochromator.

DS instrument (digital resolution 0.5 Hz) at 16.74 MHz. Chemical shifts are given with reference to external $PbMe_4$. Solutions of 100–200 mg of compounds/3 mL of $CDCl_3$ were used. FD mass spectra were obtained using a Finigan MAT 8230 instrument (field desorption potential: 6 kV). Raman spectra were recorded on a SPEX 1403 spectrometer (excitation with a He/Ne laser at 633 nm and with a Kr laser at 647 nm; microcrystalline samples in capillaries). Infrared spectra in the region 4000–200 cm^{-1} were recorded on a Galaxy 2030 FTIR spectrometer as cesium iodide pellets.

Syntheses. Under exclusion of light, trimeric diorganyllead sulfides were synthesized by treating (aryl)$_2$PbX$_2$ (X = Br, I) with NEt_3 and hydrogen sulfide gas in dry toluene ([Ph_2PbS]$_3$: reaction of $Ph_2Pb(OAc)_2$ with H_2S in dilute acetic acid[24]). A representative detailed procedure follows for the compound [m-Tol$_2$PbS]$_3$. To a solution of 5 g m-Tol$_2$PbI$_2$ (7.8 mmol) in dry toluene, 1.65 g (16.3 mmol) of triethylamine was added dropwise with stirring at 0 °C. After complete addition, the mixture was allowed to warm to room temperature. A hydrogen sulfide filled balloon was placed over the reaction flask while the mixture was stirred at ambient temperature rapidly. A white solid of NEt_3·HX started to precipitate within a few seconds, and after a period of 60 min the reaction had been completed (indicated by the occurrence of a black precipitate of PbS) and the rubber balloon was removed. The resulting solution was filtered; solvent from the mother liquor was then removed under reduced pressure, being careful not to exceed 30 °C. The resulting yellow liquid was subjected to an atmosphere of petroleum ether (60–70 °C) at room temperature. Protected from light, a yellow-orange solid was obtained after several weeks in 69% yield. Table 1 summarizes the results obtained.

Crystal Structure Determinations. Yellow single crystals of [o-Tol$_2$PbS]$_3$ and [p-Tol$_2$PbS]$_3$ were obtained by slow diffusion of petroleum ether into a toluene solution under exclusion of light. Crystal data, as well as details of intensity data collections and refinements, are given in Table 5. The crystals were fixed with glue and sealed in thin-walled glass capillaries. The densities were obtained by flotation in Thoulet's solution. Integrated intensities were collected on an Enraf-Nonius CAD4 diffractometer. The structures were solved by Patterson syntheses in the case of [p-Tol$_2$PbS]$_3$, using direct methods for [o-Tol$_2$PbS]$_3$. The refinements resulted in good convergences and in even distributions of the variances. Fractional atomic coordinates and equivalent isotropic thermal displacements are given in Tables 6 and 7. Besides several locally written routines, local versions of SHELX-76 and SHELX-86 were used for the calculations and those of ORTEP and PLUTO-78 for the drawings.

NMR Redistribution Conditions. To investigate exchange reactions equimolar mixtures of about 0.13 M (100–300 mg/3 mL) of each starting substance were applied. Measurements for all redistribution experiments were carried out in $CDCl_3$ at room temperature. Considering the slow decomposition of lead heterocycles in solution, the starting materials were dissolved shortly before they were submitted for the NMR experiments. The decomposition occurred slowly compared to exchange velocity, with no influence on NMR studies.

Evaluation of the NMR Spectra. Two satellite peaks appeared with a joint intensity of 20% of the respective main signal according to an AB system (Figure 3) for each main signal of the redistribution species. In some NMR spectra the outer satellite peaks were not visible; these could be calculated by applying eqs 9 and 10,where d is the distance between the

$$d = \sqrt{(E_1 - E_4)(E_2 - E_3)} \quad (9)$$

$$^2J = E_1 - E_2 = E_3 - E_4 \quad (10)$$

main signals (Hz), J is the coupling constant (Hz), and E_n values (n = 1–4) are the positions of the satellite peaks (Hz). The determination of the difference term ($E_1 - E_4$) was possible by using the values of the inner signals E_2 and E_3 and of the

(21) *Gmelin Handbook of Inorganic Chemistry*; Springer-Verlag: Berlin, 1981; Organolead Compounds Part 3.
(22) Bähr, G.; Langer, E. *Houben-Weyl, Methoden der Organischen Chemie*, 4th ed.; Thieme-Verlag: Stuttgart, Germany, 1975; Vol. XIII/7, p 20.
(23) Gilman, H.; Bailie, J. C. *J. Am. Chem. Soc.* **1939**, *61*, 731.
(24) Polis, A. *Ber. Dtsch. Chem. Ges.* **1887**, *20*, 3331.

Table 6. Fractional Atomic Coordinates and Equivalent Isotropic Thermal Parameters for [o-Tol$_2$PbS]$_3$ (Monoclinic $P2_1/n$; Esd's in Parentheses)

group[a]	atom	x	y	z	U(eq),[b] Å^2
core	Pb(1)	0.78384(4)	0.95841(3)	0.15306(3)	0.0384(2)
	Pb(2)	0.68360(3)	0.79691(3)	0.27391(3)	0.0353(2)
	Pb(3)	0.71623(4)	1.00086(3)	0.35736(3)	0.0395(2)
	S(1)	0.3756(2)	0.3856(2)	0.3302(1)	0.043(1)
	S(2)	0.2024(2)	0.5612(2)	0.2501(2)	0.050(2)
	S(3)	0.2065(2)	0.3699(2)	0.1284(2)	0.047(1)
o-Tol (10)	C(10)	0.0796(9)	0.3815(7)	0.3334(6)	0.039(2)[c]
	C(101)	0.0088(10)	0.3949(8)	0.2734(7)	0.048(3)[c]
	C(102)	−0.0748(11)	0.3455(10)	0.2638(9)	0.065(4)[c]
	C(103)	−0.0863(12)	0.2840(9)	0.3115(9)	0.064(4)[c]
	C(104)	−0.0168(11)	0.2751(8)	0.3745(8)	0.056(3)[c]
	C(105)	0.0690(10)	0.3225(8)	0.3848(8)	0.051(3)[c]
	C(106)	0.1453(12)	0.3108(9)	0.4553(9)	0.064(4)[c]
o-Tol (11)	C(11)	0.2509(9)	0.5149(7)	0.4569(7)	0.043(3)[c]
	C(111)	0.3474(10)	0.5032(8)	0.4929(8)	0.053(3)[c]
	C(112)	0.3676(11)	0.5366(9)	0.5639(9)	0.063(4)[c]
	C(113)	0.2977(13)	0.5797(11)	0.5968(10)	0.078(5)[c]
	C(114)	0.2004(13)	0.5920(11)	0.5618(10)	0.079(5)[c]
	C(115)	0.1772(11)	0.5598(9)	0.4900(9)	0.064(4)[c]
	C(116)	0.0743(15)	0.5751(13)	0.4461(12)	0.098(6)[c]
o-Tol (20)	C(20)	0.2165(9)	0.2069(7)	0.2695(7)	0.042(3)[c]
	C(201)	0.1265(11)	0.1940(9)	0.2262(9)	0.062(4)[c]
	C(202)	0.0586(13)	0.1366(11)	0.2498(11)	0.083(5)[c]
	C(203)	0.0845(14)	0.0987(11)	0.3196(11)	0.086(5)[c]
	C(204)	0.1741(13)	0.1137(10)	0.3606(10)	0.075(4)[c]
	C(205)	0.2459(10)	0.1701(8)	0.3344(7)	0.050(3)[c]
	C(206)	0.3455(12)	0.1776(10)	0.3802(9)	0.070(4)[c]
o-Tol (21)	C(21)	0.4580(9)	0.2568(8)	0.1804(7)	0.046(3)[c]
	C(211)	0.5519(11)	0.2801(9)	0.2246(9)	0.062(4)[c]
	C(212)	0.6421(14)	0.2535(12)	0.1979(11)	0.089(5)[c]
	C(213)	0.6370(15)	0.2045(11)	0.1350(11)	0.087(5)[c]
	C(214)	0.5515(14)	0.1846(11)	0.0925(11)	0.087(5)[c]
	C(215)	0.4538(13)	0.2110(10)	0.1189(10)	0.072(4)[c]
	C(216)	0.3571(14)	0.1897(11)	0.0754(11)	0.087(5)[c]
o-Tol (30)	C(30)	0.2142(9)	0.5730(8)	0.0496(7)	0.046(3)[c]
	C(301)	0.1342(11)	0.5431(9)	0.0024(8)	0.057(3)[c]
	C(302)	0.0806(12)	0.5896(10)	−0.0531(10)	0.073(4)[c]
	C(303)	0.1097(12)	0.6662(11)	−0.0561(9)	0.073(4)[c]
	C(304)	0.1912(13)	0.6947(10)	−0.0112(10)	0.075(4)[c]
	C(305)	0.2442(10)	0.6491(8)	0.0448(7)	0.049(3)[c]
	C(306)	0.3298(12)	0.6858(10)	0.0944(9)	0.071(4)[c]
o-Tol (31)	C(31)	0.4501(10)	0.4981(8)	0.1638(8)	0.054(3)[c]
	C(311)	0.4920(11)	0.5374(9)	0.2310(8)	0.058(3)[c]
	C(312)	0.5963(14)	0.5350(11)	0.2511(11)	0.084(5)[c]
	C(313)	0.6563(13)	0.4913(10)	0.2032(10)	0.076(5)[c]
	C(314)	0.6208(13)	0.4521(10)	0.1376(10)	0.075(4)[c]
	C(315)	0.5103(12)	0.4558(9)	0.1196(9)	0.065(4)[c]
	C(316)	0.4705(13)	0.4145(11)	0.0536(10)	0.080(5)[c]

[a] Labeling as given in Figure 1 and used in Table 2. [b] U(eq) = one-third of the trace of the orthogonalized $\mathbf{U}(ij)$ tensor. [c] Isotropic thermal parameter.

distance d. The positions E_1 and E_4 were calculated including the value of the center point between the signals of the redistribution species.[25]

FD Mass Spectrometric Conditions. For FD mass spectrometric experiments, mixtures of the lead heterocycles in the molar ratio 1:1 in $CDCl_3$ were used. Analogous to the NMR studies, the starting substances were dissolved shortly before being examined by mass spectrometry.

(25) Abraham, R. J. *Analysis of High Resolution NMR Spectra*; Elsevier Publishing Co.: Amsterdam, London, New York, 1971.

Table 7. Fractional Atomic Coordinates and Equivalent Isotropic Thermal Parameters for [p-Tol$_2$PbS]$_3$ (Triclinic $P\bar{1}$; Esd's in Parentheses)

group[a]	atom	x	y	z	U(eq),[b] Å^2
core	Pb(1)	0.12120(4)	0.46597(4)	1.10874(4)	0.0255(2)
	Pb(2)	0.26786(4)	0.19822(4)	0.89923(4)	0.0279(2)
	Pb(3)	0.20395(5)	0.17995(4)	1.20404(4)	0.0310(2)
	S(1)	0.0845(2)	0.3681(2)	0.9877(2)	0.029(1)
	S(2)	0.2826(3)	0.3244(2)	1.1525(3)	0.034(1)
	S(3)	0.2830(3)	0.0620(2)	1.0329(3)	0.041(2)
p-Tol (10)	C(10)	−0.0353(11)	0.5215(10)	1.2673(10)	0.030(2)[c]
	C(101)	−0.0144(12)	0.5538(11)	1.3525(10)	0.032(2)[c]
	C(102)	−0.1135(14)	0.5930(13)	1.4558(13)	0.045(3)[c]
	C(103)	−0.2263(12)	0.5944(11)	1.4752(10)	0.032(2)[c]
	C(104)	−0.2424(12)	0.5675(11)	1.3932(11)	0.035(2)[c]
	C(105)	−0.1476(11)	0.5294(10)	1.2864(10)	0.029(2)[c]
	C(106)	−0.3294(15)	0.6354(14)	1.5874(14)	0.050(3)[c]
p-Tol (11)	C(11)	0.2109(11)	0.5779(10)	1.0298(10)	0.028(2)[c]
	C(111)	0.1459(12)	0.6830(11)	1.0380(10)	0.032(2)[c]
	C(112)	0.2048(12)	0.7541(11)	0.9889(11)	0.035(2)[c]
	C(113)	0.3291(12)	0.7138(11)	0.9328(11)	0.034(2)[c]
	C(114)	0.3920(13)	0.6066(12)	0.9252(12)	0.042(3)[c]
	C(115)	0.3368(13)	0.5333(12)	0.9736(12)	0.040(3)[c]
	C(116)	0.3931(16)	0.7909(15)	0.8731(15)	0.055(4)[c]
p-Tol (20)	C(20)	0.1914(11)	0.1377(10)	0.8104(10)	0.028(2)[c]
	C(201)	0.1850(12)	0.1786(11)	0.7181(10)	0.033(2)[c]
	C(202)	0.1223(14)	0.1480(12)	0.6720(12)	0.042(3)[c]
	C(203)	0.0740(13)	0.0701(12)	0.7224(11)	0.038(3)[c]
	C(204)	0.0833(14)	0.0316(12)	0.8099(12)	0.043(3)[c]
	C(205)	0.1467(13)	0.0648(12)	0.8545(12)	0.039(3)[c]
	C(206)	0.0020(19)	0.0410(17)	0.6701(17)	0.068(5)[c]
p-Tol (21)	C(21)	0.4262(11)	0.2384(10)	0.8389(10)	0.029(2)[c]
	C(211)	0.4308(12)	0.3208(11)	0.7744(11)	0.036(2)[c]
	C(212)	0.5333(15)	0.3592(14)	0.7405(13)	0.050(3)[c]
	C(213)	0.6251(13)	0.2959(11)	0.7788(11)	0.037(2)[c]
	C(214)	0.6152(14)	0.2166(13)	0.8384(12)	0.043(3)[c]
	C(215)	0.5173(12)	0.1832(11)	0.8706(11)	0.036(2)[c]
	C(216)	0.7257(18)	0.3312(16)	0.7485(16)	0.060(4)[c]
p-Tol (30)	C(30)	0.2962(12)	0.0752(11)	1.2981(11)	0.036(2)[c]
	C(301)	0.2496(13)	0.0121(12)	1.3697(11)	0.038(3)[c]
	C(302)	0.3118(14)	−0.0543(13)	1.4270(13)	0.045(3)[c]
	C(303)	0.4225(12)	−0.0563(11)	1.4091(11)	0.036(2)[c]
	C(304)	0.4686(13)	0.0068(12)	1.3348(12)	0.040(3)[c]
	C(305)	0.4117(14)	0.0719(13)	1.2781(12)	0.044(3)[c]
	C(306)	0.4972(16)	−0.1375(15)	1.4683(14)	0.055(4)[c]
p-Tol (31)	C(31)	0.0069(13)	0.2322(11)	1.2769(11)	0.038(3)[c]
	C(311)	−0.0567(13)	0.2631(12)	1.3935(11)	0.039(3)[c]
	C(312)	−0.1858(18)	0.2987(16)	1.4412(16)	0.062(4)[c]
	C(313)	−0.2471(14)	0.3100(13)	1.3762(13)	0.046(3)[c]
	C(314)	−0.1778(14)	0.2753(12)	1.2646(12)	0.042(3)[c]
	C(315)	−0.0498(13)	0.2400(12)	1.2147(12)	0.038(3)[c]
	C(316)	−0.3833(19)	0.3604(17)	1.4229(17)	0.065(5)[c]

[a] Labeling as given in Figure 2 and used in Table 2. [b] U(eq) = one-third of the trace of the orthogonalized $\mathbf{U}(ij)$ tensor. [c] Isotropic thermal parameter.

Acknowledgment. We gratefully acknowledge financial support from the Deutsche Forschungsgemeinschaft, Bonn-Bad Godesberg, Germany, and the Fonds der Chemischen Industrie, Frankfurt/Main, Germany.

Supporting Information Available: Tables listing anisotropic displacement parameters, all bond lengths and bond angles, and torsion angles for [o-Tol$_2$PbS]$_3$ and [p-Tol$_2$PbS]$_3$ (6 pages). Ordering information is given on any current masthead page.

OM950318D

Syntheses and Structures of Diruthenium Triple-Decker Complexes with Bridging 1,2,4-Triphospholyl and 1-Arsa-3,4-Diphospholyl Anions

Peter B. Hitchcock, Julian A. Johnson,[1] and John F. Nixon*

School of Chemistry and Molecular Sciences, University of Sussex, Brighton, East Sussex BN1 9QJ, U.K.

Received March 22, 1995[⊗]

Yellow-brown oils, characterized spectroscopically as [Cp*Ru(η^5-C_2-*t*-Bu_2P_3)], **11**, and [Cp*Ru(η^5-C_2-*t*-Bu_2AsP_2)], **12**, were isolated from the reaction of [Cp*Ru(CH_3CN)$_3$][PF_6], **6**, with [Li(C_2-*t*-Bu_2P_3)], **2**, or [Li(C_2-*t*-Bu_2AsP_2)], **4**, respectively. Both **11** and **12** reacted further with **6** to give the triple-decker complexes [Cp*Ru(μ-η^5:η^5-C_2-*t*-Bu_2P_3)RuCp*][PF_6], **7**, and [Cp*Ru(μ-η^5:η^5-C_2-*t*-Bu_2AsP_3)RuCp*][PF_6], **8**, in which the triphospholyl or arsadiphospholyl anions bridge two ruthenium centers. Both **7** and **8** have been characterized by single-crystal X-ray crystal structure determinations. Crystal data for $C_{30}H_{48}F_6P_4Ru_2$, **7**: M = 848.7, $P2_12_12_1$, a = 12.642(9) Å, b = 15.151(10 Å, c = 18.176(10) Å, V = 3481.4 Å^3, D_{calcd} = 1.62 g cm^{-3} (Z = 4) μ = 10.8 cm^{-1} for Mo Kα radiation (λ = 0.7107 Å), final R = 0.055, R_w = 0.057, from 2716 observed reflections (3437 measured). Data for $C_{30}H_{48}AsF_6P_3Ru_2$, **8**: M = 892.7, $P2_12_12_1$, a = 12.650(9) Å, b = 15.147(8) Å, c = 18.111(10) Å, V = 3470.1 Å^3, D_{calcd} = 1.71 g cm^{-3} (Z = 4) μ = 19.9 cm^{-1} for Mo Kα radiation (λ = 0.7107 Å), final R = 0.049, R_w = 0.053, from 2760 observed reflections (3430 measured). Attempts to prepare mixed-metal triple-decker complexes by reacting [Fe(η^5-C_5R_5)(η^5-C_2-*t*-Bu_2P_3)] (R = H, **14a**; R = Me, **14b**] or [Fe(η^5-C_5R_5)($\eta^4$5-C_2-*t*-Bu_2AsP_2)] (R = H, **15a**; R = Me, **15b**) with **6** were unsuccessful. Likewise, when either **14a** or **15a** is treated with **6** the intermediate complexes [Fe(η^5-C_5H_5)(η^5-C_2-*t*-Bu_2P_3)RuCp*(CH_3CN)$_2$][PF_6], **17**, or [Fe(η^5-C_5H_5)(η^5-C_2-*t*-Bu_2AsP_2)RuCp*(CH_3CN)$_2$][PF_6], **18**, were isolated and spectroscopically characterized. When these were heated in nitromethane, a ring transfer occurred and the triple-decker species **7** or **8** was observed. Similar reactions involving **14b** or **15b** led directly to **7** or **8** without detection of any intermediate complexes.

Introduction

The synthesis of phospholyl anions of the type $C_nR_nP_{5-n}$ (n = 0–5) and their complexation to transition metals is a contemporary theme in the rapidly expanding area of phosphorus–carbon multiple-bond chemistry.[2,3] Many mono- and polymetallic systems, containing a variety of coordination modes of phospholyl anions, have now been structurally characterized,[2] and the particular focus on this work is the study of complexes containing the di- and triphospholyl anions [(C_3-*t*-Bu_3P_2)$^-$], **1**, and [(C_2-*t*-Bu_2P_3)$^-$], **2**.[3] Several polymetallic complexes in which **2** behaves as a bridging ligand are known,[4–7] but so far no triple-decker complexes in which **2**, or any other phospholyl anion, bridges two metals in a μ-η^5:η^5 fashion have been isolated. There is one report by Grimes and co-workers[8] of a triple-decker complex containing a terminal phospholyl ligand. In contrast, the triple-decker complexes [Cp*Fe(μ-η^5:η^5-E_5)FeCp*][PF_6] (E = P, As), in which the pentaphospholyl **3a** or pentaarsolyl **3b**[9] anions bridge two Fe atoms, are known, as are homo- and heterobimetallic triple-decker complexes containing group 8 metals in which either Cp[10] of Cp*[11] ligand bridge the metals. The stability of 30-valence electron complexes of this type was predicted by Hoffman in 1976,[12] and calculations by Malar[13] have

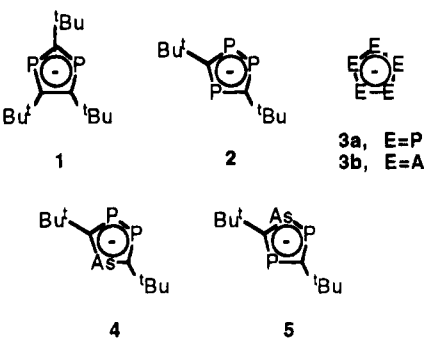

⊗ Abstract published in *Advance ACS Abstracts,* August 1, 1995.

(1) Present address: CSIRO Division of Minerals, P.O. Box 124, Port Melbourne 3207, Australia.

(2) Mathey, F. *Coord. Chem. Rev.* **1994**, *137*, 1.

(3) Nixon, J. F. *Chem. Rev.* **1988**, *88*, 1327; *Chem. Ind.* **1993**, 404; *Coord. Chem. Rev.*, in press.

(4) Bartsch, R.; Hitchcock, P. B.; Nixon, J. F. *J. Organomet. Chem.* **1988**, *340*, C37.

(5) Bartsch, R.; Gelessus, A.; Hitchcock, P. B.; Nixon, J. F. *J. Organomet. Chem.* **1992**, *430*, C10.

(6) Müller, C.; Bartsch, R.; Fischer, A.; Jones, P. G. *J. Organomet. Chem.* **1993**, *453*, C16.

(7) Müller, C.; Bartsch, R.; Fischer, A.; Jones, P. G. *Polyhedron* **1993**, *12*, 1383.

(8) Chase, K. J.; Bryan, R. F.; Woode, M. K.; Grimes, R. N. *Organometallics* **1991**, *10*, 2631.

(9) Scherer, O. J.; Brück, T.; Wolmerhäuser, G. *Chem. Ber.* **1989**, *122*, 2049. Scherer, O. J.; Blath, C.; Wolmerhäuser, G. *J. Organomet. Chem.* **1990**, *387*, C21. Rink, B.; Scherer, O. J.; Wolmerhäuser, G. *Chem. Ber.* **1995**, *128*, 71.

(10) Herberich, G. E.; Englert, E.; Marken, F.; Hoffmann, P. *Organometallics* **1993**, *12*, 4039.

(11) (a) Kudinov, A. R.; Rybinskya, M. I.; Struchkov, Yu. T.; Yanovskii, A. I.; Petrovskii, P. V. *J. Organomet. Chem.* **1987**, *336*, 187. (b) Lumme, P. O.; Turpeinen, U.; Kudinov, A. R.; Rybinskya, M. I. *Acta Crystallogr.* **1990**, *C46*, 1410.

0276-7333/95/2314-4382$09.00/0

shown the aromaticities of phosphorus-containing analogues of cyclopentadienyl anions are no less than 86% relative to $[C_5H_5^-]$; thus there seemed a strong likelihood for the possible synthesis of triple-decker complexes containing phospholyl anions by similar methods to those previously reported.

In this paper we describe the synthesis, characterization, and X-ray crystallographic studies of the diruthenium triple-decker complexes $[Cp^*Ru(\mu\text{-}\eta^5\text{:}\eta^5\text{-}C_2\text{-}t\text{-}Bu_2P_3)RuCp^*][PF_6]$, **7**, $[Cp^*Ru(\mu\text{-}\eta^5\text{:}\eta^5\text{-}C_2\text{-}t\text{-}Bu_2AsP_2)RuCp^*][PF_6]$, **8**, and $[Cp^*Ru(\mu\text{-}\eta^5\text{:}\eta^5\text{-}C_2\text{-}t\text{-}Bu_2PAsP)RuCp^*][PF_6]$, **9**, in which **2** and the recently reported[14,15] 1-arsa-3,4-diphospholyl and 3-arsa-1,4-diphospholyl anions, **4** and **5**, ligate in a $\mu\text{-}\eta^5\text{:}\eta^5$ mode. The attempted preparation of mixed-metal triple-decker complexes is also reported.

Results and Discussion

The synthesis of several iron complexes containing the anions **1** and **2** have been described,[4-7,16] and we have very recently reported the syntheses of several metal complexes containing the anions **4** and **5**.[14,15] Despite this, apart from a very recent paper by Mathey and coworkers,[17] there has been little attention paid to phospholyl complexes of ruthenium. The CpRu derivatives of the anions **1** and **2** have been synthesized and characterized,[18] and we now report the Cp*Ru derivatives of **1**, **2**, **4**, and **5**. Treatment of a 1,2-dimethoxyethane (DME) solution of $[Cp^*Ru(CH_3CN)_3][PF_6]$, **6**, with an equimolar amount of the lithium salt of either **2** or **4** gave the complexes $[Cp^*Ru(\eta^5\text{-}C_2\text{-}t\text{-}Bu_2P_3)]$, **11**, and $[Cp^*Ru(\eta^5\text{-}C_2\text{-}t\text{-}Bu_2AsP_2)]$, **12**, respectively (Scheme 1). Both compounds were characterized by NMR (^1H, $^{31}P\{^1H\}$) and mass spectroscopy. The ^1H NMR spectrum of **11** showed the expected two singlets due to Me and *t*-Bu protons. In addition to these signals, a weak singlet was observed, which was attributed to small amounts of $[Cp^*Ru(\eta^5\text{-}C_3\text{-}t\text{-}Bu_3P_2)]$, **10**, which is formed due the unavoidable cosynthesis of **1** with **2**.[16]

The $^{31}P\{^1H\}$ spectrum of **11** showed a triplet and doublet (J = 44 Hz), which is typical of $^2J_{P,P}$ coupling in metal complexes of **2**.[4-6,16] A weak singlet also observed in this spectrum is attributed to **10**. The ^1H NMR spectrum of **12** showed two singlets due to Cp* and *t*-Bu protons and several other signals in the Cp* and *t*-Bu regions. The $^{31}P\{^1H\}$) spectrum of **12** exhibited a singlet at δ 36.8 ppm, and several other resonances were also observed. Previous work[14] has shown that the synthesis of pure **4** cannot be achieved and that small amounts of **1**, **2**, and **5** are always present. Thus the extra signals occurring in both the ^1H and $^{31}P\{^1H\}$ spectra are attributed to $[Cp^*Ru(\eta^5\text{-}C_2\text{-}t\text{-}Bu_2AsP)]$, **13**, an isomer of **12**, and to **10** and **11**. The NMR spectroscopic data of complexes **10**–**13** are summarized in Table 1.

Scheme 1

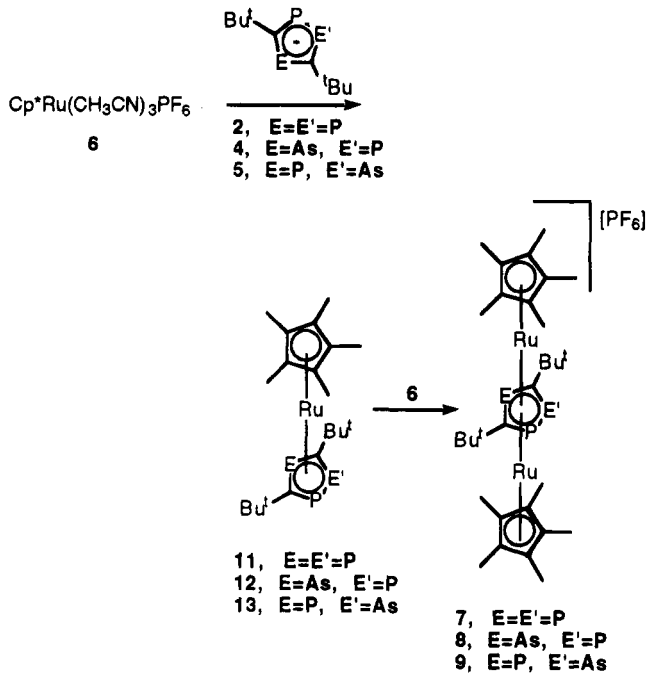

Table 1. Selected ^1H and ^{31}P NMR Spectroscopic Data[a] for New Mononuclear Phospholyl and Arsadiphospholyl Compounds 10–13 and 15b–16b

compd	^1H NMR δ (ppm)	$^{31}P\{^1H\}$ NMR δ (ppm)
10	1.60 (s, 18H); 1.87 (s, 15H)	21.8
11	1.39 (s, 18H); 1.80 (s, 15H)	18.0 (t); 36.2 (d) [$^2J_{P_A,P_X}$ = 43.0 Hz]
12	1.39 (s, 18H); 1.80 (s, 15H)	36.8
13	1.38 (s, 18H); 1.79 (s, 15H)	16.3 (t); 66.7 (d) [$^2J_{P_A,P_X}$ = 43.0 Hz
15b	1.49 (s, 18H); 1.70 (s, 15H)	49.9
16b	1.50 (s, 18H); 1.69 (s, 15H)	37.0 (t); 81.7 (d) [$^2J_{P_A,P_X}$) = 45.2 Hz]

[a] ^1H NMR: C_6D_6, 250 MHz. $^{31}P\{^1H\}$ NMR: C_6D_6, 101.3 MHz.

When $[Cp^*Ru(CH_3CN)_3][PF_6]$, **6**, was treated with a 2-fold excess of either **2** or **4** or when complexes **10** or **11** were treated with **6**, the novel triple-decker complexes $[Cp^*Ru(\mu\text{-}\eta^5\text{:}\eta^5\text{-}C_2\text{-}t\text{-}Bu_2P_3)RuCp^*][PF_6]$, **7**, and $[Cp^*Ru(\mu\text{-}\eta^5\text{:}\eta^5\text{-}C_2\text{-}t\text{-}Bu_2AsP_2)RuCp^*][PF_6]$, **8**, were formed from the respective rections (Scheme 1). Prolonged heating of the reaction mixtures led to decomposition of the compexes. Both **7** and **8** were isolated as orange air-stable powders, soluble in THF, acetone, and chloroform but insoluble in ether and petroleum ether. The ^1H NMR spectra of both **7** and **8** showed, as expected, one resonance due to the Me protons and one resonance due to the *t*-Bu protons. In addition, the spectrum of **8** showed two resonances (δ 1.33 and 1.81) due the Me and *t*-Bu protons, respectively, of $[Cp^*Ru(\mu\text{-}\eta^5\text{:}\eta^5\text{-}C_2\text{-}t\text{-}Bu_2PAsP)RuCp^*][PF_6]$, **9**, which was formed in addition to **8**. A small amount of **7** was also detected in the ^1H NMR spectrum of **8**, but this could be easily separated by fractional crystallization.

The $^{31}P\{^1H\}$ NMR spectrum of **7** showed an AX_2 pattern, ($^2J_{P,P}$ = 36 Hz), shifted *ca.* 40 ppm upfield from the value observed for **11**, as well as a septet due to the $[PF_6]^-$ anion. A similar upfield shift is observed when the complex $[Cp^*Fe(\eta^5\text{-}P_5)]$ reacts with $[CpFe(C_6H_6)][PF_6]$ to form $[Cp^*Fe(\mu\text{-}\eta^5\text{:}\eta^5\text{-}P_5)FeCp][PF_6]$.[8] Interestingly, no additional signals were observed in either the

(12) Lauher, J. W.; Elian, M.; Summerville, R. H.; Hoffman, R. *J. Am. Chem. Soc.* **1976**, *98*, 3219.
(13) Malar, E. J. P. *J. Org. Chem.* **1992**, *57*, 3694.
(14) Al-Juaid, S.; Hitchcock, P. B.; Johnson, J. A.; Nixon, J. F. *J. Organomet. Chem.* **1994**, *480*, 45.
(15) Bartsch, R.; Hitchcock, P. B.; Johnson, J. A.; Matos, R.; Nixon, J. F. *Phosphorus, Sulfur Silicon Relat. Elem.* **1993**, *77*, 45.
(16) Bartsch, R.; Hitchcock, P. B.; Nixon, J. F. *J. Chem. Soc., Chem. Commun.* **1987**, 1146.
(17) Carmichael, D.; Ricard, L.; Mathey, F. *J. Chem. Soc., Chem. Commun.* **1994**, 1167.
(18) Hitchcock, P. B.; Nixon, J. F.; Matos, R. *J. Organomet. Chem.* **1995**, *490*, 155.

Table 2. Selected ^1H and ^{31}P NMR Spectroscopic Data[a] for New Dinuclear Phospholyl and Arsadiphospholyl Compounds 7–9 and 17–19

compd	^1H NMR δ (ppm)	$^{31}P\{^1H\}$ NMR δ (ppm)
7	1.35 (s, 18H); 1.82 (s, 15H)	−2.37 (t); −34.2 (d) [$^2J_{P_A,P_X}$ = 37.0 Hz]
8	1.35 (s, 18H); 1.81 (s, 15H)	−28.2
9	1.33 (s, 18H); 1.82 (s, 15H)	13.5 (d); −40.9 (d) [$^2J_{P_A,P_X}$ = 36.9 Hz]
17	1.32 (s, 9H); 1.38 (s, 9H); 1.62 (s, 15H); 2.45 (s, 6H); 4.65 (s, 5H)	−6.46 (P_A); 95.0 (P_B); 27.6 (P_C) [$^1J_{P_A,P_B}$ = 437 Hz, $^2J_{P_A,P_C}$ = 47.0 Hz, $^2J_{P_B,P_C}$ = 48.3 Hz]
18	1.37 (s, 9H); 1.43 (s, 9H); 1.62 (s, 15H); 2.47 (s, 6H); 4.65 (s, 5H)	−5.20; 93.4 [$^1J_{P_A,P_X}$ = 447.0 Hz]
19	1.38 (s, 9H); 1.51 (s, 9H); 1.63 (s, 15H); 2.56 (s, 6H); 4.66 (s, 5H)	23.2; 114.5 [$^2J_{P_A,P_X}$ = 50.1 Hz]

[a] ^1H NMR: $CDCl_3$, 250 MHz. $^{31}P\{^1H\}$ NMR: $CDCl_3$, 101.3 MHz.

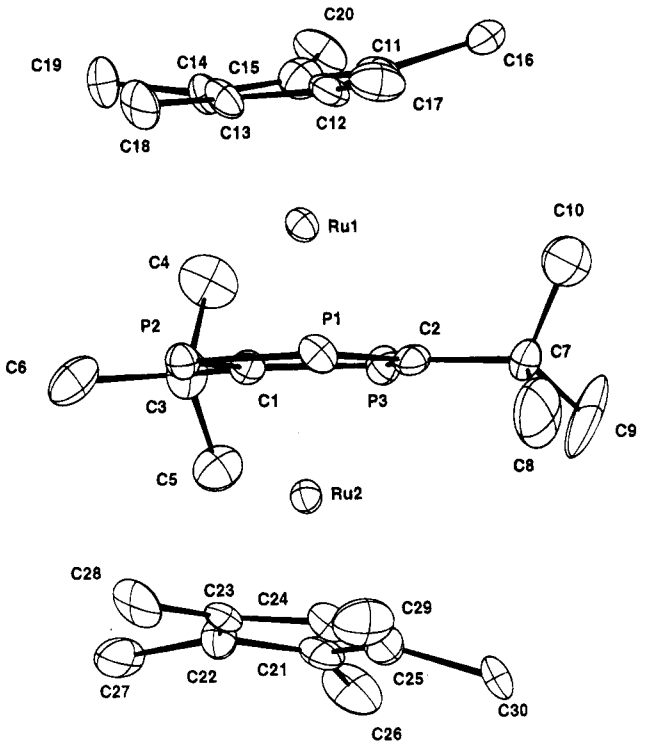

Figure 1. Molecular structure of compound **7**.

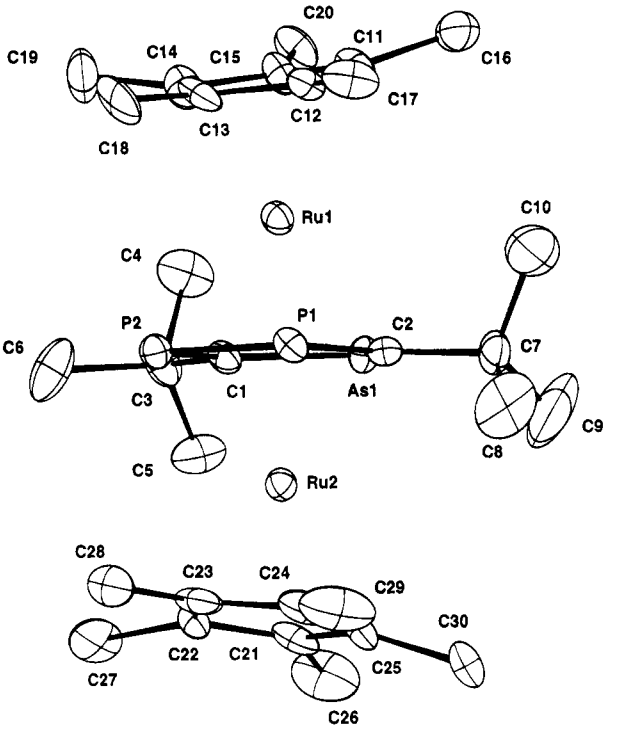

Figure 2. Molecular structure of compound **8**.

^1H or $^{31}P\{^1H\}$ NMR spectra of **7**, indicating that complex **10** had not reacted any further with **6** to give the triple-decker species in which **1** is ligated in a μ-η^5:η^5 fashion. This is probably due to the steric bulk of **1** since the presence of three *t*-Bu groups on the middle ring would inhibit coordination of two Cp*Ru fragments on either side of the ring. The $^{31}P\{^1H\}$ NMR spectrum of **8** showed a singlet together with AX pattern ($^2J_{P,P}$ = 36 Hz) assigned to **9**. In agreement with previous observations, both sets of signals are shifted *ca.* 60 ppm upfield relative to their parent complexes. Selected NMR spectroscopic data of complexes **7**–**9** are shown in Table 2.

The molecular structures of both **7** (Figure 1) and **8** (Figure 2) have been determined by single-crystal X-ray crystallographic studies and confirm the conclusions from the spectroscopic data. Interesting structural features of these complexes are the large dihedral angles between the Cp* rings and the middle ring (10.0° average for **7**) and (10.4° average for **8**), which are considerably bigger than those observed in the triple-decker complexes containing Cp or Cp* rings (typically about 2°)[10,11] (see Tables 3–6). These larger values could be attributed to the presence of bulky *t*-Bu substituents in the middle ring which would push out the Cp* rings on either side. A similarly high value (8.1°) is observed in the structurally related complex [Ru(η^5-C_2-*t*-Bu_2P_3)$_2$] which has recently been synthesized.[18] The two capping Cp* ligands in both complexes **7** and **8** are mutually eclipsed, and this orientation is consistent with other triple-decker species containing group 8 metals whose middle deck is either a Cp or Cp* ligand.[10,11b] The bond lengths within the middle ring of **7** are slightly longer than the bond lengths observed in [Ru(η^5-C_2-*t*-Bu_2P_3)$_2$],[18] and interestingly Scherer et al. report a similar small increase in the bond lengths of both the P_5^- and As_5^- ligands when their ligation mode changes from η^5 to μ-η^5:η^5.[8,9] An additional structural feature of **7** concerns the bond lengths between the each Ru atom and the center of the middle ring, (1.794 and 1.787 Å), which are marginally shorter than the bond length of 1.814 Å observed [Ru(η^5-C_2-*t*-Bu_2P_3)$_2$].[18] No comparison of the bond distances in complex **8** can be made due to the lack of structurally characterized complexes containing arsadiphospholyl anions. The average bond distances from each Ru atom to the C atoms in the Cp* ligands is 2.20 Å in **7** and 2.21 Å in **8**. These are slightly longer than those bond lengths observed in both decamethylruthenocene (2.17 Å)[19] and ruthenocene (2.186 Å).[20] A high disorder of

(19) Albers, M. O.; Liles, D. C.; Robinson, D. J.; Shaver, A.; Singleton, E.; Wiege, M.; Boeyens, J. C. A.; Levendis, D. C. *Organometallics* **1986**, *5*, 2321.

(20) Seiler, P.; Dunitz, J. D. *Acta Crystallogr., Sect. B.* **1980**, *B36*, 2946.

Table 3. Fractional Atomic Coordinates and Equivalent Thermal Parameters for Compound 7

	x	*y*	*z*	U_{eq}[a]
Ru(1)	0.87452(8)	0.80285(7)	0.26508(6)	0.032(1)
Ru(2)	0.67531(8)	0.96270(7)	0.30711(5)	0.031(1)
P(3)	0.6939(3)	0.7990(2)	0.3220(2)	0.039(2)
P(1)	0.8674(3)	0.9503(2)	0.3174(2)	0.038(2)
P(2)	0.7963(3)	0.9308(2)	0.2068(2)	0.036(2)
P(4)	0.7985(4)	0.5045(4)	0.9744(2)	0.072(3)
F(1)	0.8643(11)	0.4210(8)	0.9546(7)	0.147(10)
F(2)	0.8935(12)	0.5584(10)	0.9588(9)	0.188(12)
F(3)	0.8258(14)	0.4986(11)	1.0531(6)	0.197(13)
F(4)	0.7747(12)	0.5090(15)	0.8933(7)	0.240(15)
F(5)	0.7361(12)	0.5865(9)	0.9970(10)	0.185(13)
F(6)	0.7021(11)	0.4511(12)	0.9840(10)	0.292(14)
C(1)	0.7045(9)	0.8435(7)	0.2306(7)	0.033(6)
C(2)	0.7902(9)	0.8682(9)	0.3652(7)	0.036(7)
C(3)	0.6309(11)	0.8033(9)	0.1713(7)	0.046(7)
C(4)	0.6550(12)	0.7059(10)	0.1619(9)	0.069(10)
C(5)	0.5145(11)	0.8108(11)	0.1944(9)	0.061(9)
C(6)	0.6429(12)	0.8494(11)	0.0968(8)	0.065(10)
C(7)	0.8076(11)	0.8554(10)	0.4496(7)	0.046(8)
C(8)	0.8347(23)	0.9404(14)	0.4829(9)	0.126(17)
C(9)	0.7076(16)	0.8240(18)	0.4859(9)	0.124(16)
C(10)	0.8852(22)	0.7923(16)	0.4662(9)	0.187(18)
C(11)	0.9851(9)	0.6917(9)	0.2958(8)	0.044(7)
C(12)	1.0423(10)	0.7752(8)	0.2824(7)	0.043(8)
C(13)	1.0250(10)	0.7956(8)	0.2076(7)	0.044(7)
C(14)	0.9547(10)	0.7343(8)	0.1744(7)	0.038(7)
C(15)	0.9300(11)	0.6707(9)	0.2293(8)	0.051(8)
C(16)	0.9966(12)	0.6329(10)	0.3628(8)	0.060(9)
C(17)	1.1214(11)	0.8215(9)	0.3337(9)	0.061(9)
C(18)	1.0809(12)	0.8715(10)	0.1647(8)	0.063(9)
C(19)	0.9318(13)	0.7248(11)	0.0926(8)	0.064(10)
C(20)	0.8714(12)	0.5829(8)	0.2187(9)	0.058(9)
C(21)	0.5106(9)	1.0085(9)	0.3276(8)	0.046(8)
C(22)	0.5505(11)	1.0493(9)	0.2614(7)	0.048(8)
C(23)	0.6403(11)	1.0997(8)	0.2808(7)	0.045(8)
C(24)	0.6530(11)	1.0911(9)	0.3592(8)	0.052(9)
C(25)	0.5727(12)	1.0360(10)	0.3844(8)	0.059(9)
C(26)	0.4079(10)	0.9571(11)	0.3344(10)	0.076(11)
C(27)	0.5002(13)	1.0542(12)	0.1844(8)	0.092(11)
C(28)	0.7042(12)	1.1586(10)	0.2319(10)	0.083(10)
C(29)	0.7300(13)	1.1493(12)	0.4031(10)	0.079(11)
C(30)	0.5431(14)	1.0241(12)	0.4673(8)	0.080(10)

[a] U_{eq} is defined as one-third of the trace of the orthogonalized U_{ij} tensor.

Table 4. Fractional Atomic Coordinates and Equivalent Thermal Parameters for Compound 8

	x	*y*	*z*	U_{eq}[a]
Ru(1)	0.87450(8)	0.79930(6)	0.26492(5)	0.032(1)
Ru(2)	0.67581(8)	0.95852(6)	0.30782(5)	0.031(1)
As	0.69172(13)	0.78976(11)	0.32575(8)	0.032(1)
P(1)	0.87005(21)	0.94954(17)	0.31694(15)	0.034(1)
P(2)	0.79574(21)	0.92827(17)	0.20397(15)	0.034(1)
P(3)	0.79730(33)	0.50138(34)	0.97332(24)	0.075(3)
F(1)	0.8626(10)	0.4194(7)	0.9513(6)	0.136(9)
F(2)	0.8936(11)	0.5572(8)	0.9597(7)	0.158(10)
F(3)	0.8304(15)	0.4973(9)	1.0521(6)	0.203(13)
F(4)	0.7720(12)	0.5060(15)	0.8914(7)	0.244(14)
F(5)	0.7353(11)	0.5838(9)	0.9971(9)	0.176(11)
F(6)	0.6983(11)	0.4476(11)	0.9850(10)	0.298(13)
C(1)	0.7035(9)	0.8386(7)	0.2311(6)	0.034(6)
C(2)	0.7944(6)	0.8685(8)	0.3665(6)	0.036(6)
C(3)	0.6291(10)	0.7998(8)	0.1705(6)	0.043(6)
C(4)	0.6520(12)	0.7007(10)	0.1609(9)	0.072(10)
C(5)	0.5151(10)	0.8037(10)	0.1972(8)	0.063(8)
C(6)	0.6412(13)	0.854(11)	0.0953(7)	0.078(10)
C(7)	0.8128(10)	0.8573(9)	0.4508(7)	0.051(7)
C(8)	0.8425(20)	0.9448(13)	0.4847(9)	0.133(15)
C(9)	0.7152(17)	0.8304(20)	0.4871(9)	0.162(20)
C(10)	0.9038(21)	0.7994(15)	0.4666(10)	0.178(18)
C(11)	0.9875(9)	0.6888(8)	0.2969(7)	0.045(7)
C(12)	1.0446(10)	0.7723(8)	0.2828(7)	0.044(7)
C(13)	1.0237(9)	0.7937(8)	0.2060(7)	0.048(7)
C(14)	0.9538(10)	0.7295(8)	0.1733(7)	0.049(8)
C(15)	0.9305(9)	0.6673(8)	0.2311(7)	0.042(7)
C(16)	0.9991(12)	0.6286(9)	0.3621(8)	0.063(9)
C(17)	1.1199(10)	0.8190(8)	0.3324(8)	0.056(8)
C(18)	1.0785(11)	0.8687(9)	0.1641(8)	0.070(9)
C(19)	0.9294(13)	0.7198(10)	0.0907(7)	0.067(10)
C(20)	0.8712(11)	0.5807(7)	0.2186(7)	0.051(7)
C(21)	0.5097(9)	1.0030(8)	0.3281(8)	0.049(8)
C(22)	0.5510(10)	1.0438(8)	0.2612(7)	0.045(7)
C(23)	0.6409(10)	1.0941(8)	0.2805(8)	0.050(8)
C(24)	0.6543(10)	1.0866(9)	0.3604(8)	0.055(8)
C(25)	0.5734(10)	1.0323(9)	0.3886(7)	0.049(7)
C(26)	0.4076(11)	0.9546(11)	0.3358(11)	0.088(11)
C(27)	0.5012(14)	1.0499(10)	0.1842(8)	0.095(10)
C(28)	0.7048(11)	1.1530(9)	0.2293(9)	0.077(9)
C(29)	0.7308(13)	1.1454(11)	0.4046(10)	0.095(11)
C(30)	0.5463(14)	1.0227(12)	0.4694(8)	0.097(11)

[a] U_{eq} is defined as one-third of the trace of the orthogonalized U_{ij} tensor.

occupancy between the P and As atoms in the middle ring of **8** results from the cocrystallization of **8** and **9** from solution. This is not unexpected, as a similar disorder of occupany in both arsaphospholyl and arsadiphospholyl rings is observed in the structurally characterized complexes $[Fe(\eta^5\text{-}C_3Et_2HPAs)_2]$[21] and $[CpFe(\eta^5\text{-}C_2\text{-}t\text{-}Bu_2AsP_2)W(CO)_5]$.[14]

Surprisingly, the analogous diiron triple-decker complexes $[Cp^*Fe(\mu\text{-}\eta^5\text{:}\eta^5\text{-}C_2\text{-}t\text{-}Bu_2P_3)FeCp^*][PF_6]$ and $[Cp^*Fe(\mu\text{-}\eta^5\text{:}\eta^5\text{-}C_2\text{-}t\text{-}Bu_2AsP_2)FeCp^*][PF_6]$ could not be prepared from the reaction of either $[Cp^*Fe(\eta^5\text{-}C_2\text{-}t\text{-}Bu_2P_3)]$, **14b**, or $[Cp^*Fe(\eta^5\text{-}C_2\text{-}t\text{-}Bu_2AsP_2)]$, **15b**, with $[(C_5R_5)Fe(C_6H_6)][PF_6]$, (R = H, Me), even after prolonged reflux of the rection mixtures. In such reactions the starting materials were recovered quantitatively, and UV irradiation of the reaction mixtures only resulted in decomposition. In contrast, triple-decker complexes containing As_5 or P_5 rings as the bridging ligands are readily synthesized by visible-light irradiation of $[\eta^5\text{-}CpFe(C_6H_6)][PF_6]$ and either $(\eta^5\text{-}C_5Me_4R)Fe(\eta_5\text{-}As_5)]$ or $[(\eta^5\text{-}C_5Me_4R)Fe(\eta^5\text{-}P_5)]$ (R = Me, Et).[8,9] It is unclear why these types of diiron triple-decker complexes containing $\eta^5\text{-}(C_2\text{-}t\text{-}Bu_2P_3)$ and $\eta^5\text{-}(C_2\text{-}t\text{-}Bu_2AsP_2)$ rings do not also form in this way, although diiron triple-decker species with bridging Cp* ligands have previously been found to be less stable than their Ru analogues.[11a] It is possible that the triple-decker species $[Cp^*Fe(\mu\text{-}\eta^5\text{:}\eta^5\text{-}C_2\text{-}t\text{-}Bu_2P_3)FeCp^*][PF_6]$ and $[Cp^*Fe(\mu\text{-}\eta^5\text{:}\eta^5\text{-}C_2\text{-}t\text{-}Bu_2AsP_2)FeCp^*][PF_6]$ were formed in the above reactions, but the presence of displaced benzene induced degradation of the triple-decker species. A similar reaction in which benzene degrades diruthenium triple-decker complexes is known.[10]

The reaction of either $[CpFe(\eta^5\text{-}C_2\text{-}t\text{-}Bu_2P_3)]$, **14a**, or $[CpFe(\eta^5\text{-}C_2\text{-}Bu_2AsP_2)]$, **15a**, with $[Cp^*Ru(CH_3CN)_3][PF_6]$, **6**, did not lead to the expected mixed-metal triple-decker species. Instead, displacement of one acetonitrile ligand from **5** resulted in the formation of the new mixed-metallic complexes $[CpFe(\eta^5\text{-}C_2\text{-}t\text{-}Bu_2P_3)Ru(Cp^*)(CH_3CN)_2][PF_6]$, **17**, and $[CpFe(\eta^5\text{-}C_2\text{-}t\text{-}Bu_2P_3)Ru(Cp^*)(CH_3CN)_2][PF_6]$, **18**, respectively (Scheme 2). The compounds were identified on the basis of NMR spectroscopy (Table 2). The ^1H NMR spectrum of **17** showed two signals that can be assigned to *t*-Bu protons, one signal from the CH_3CN protons and one signal due to Cp protons. Similar resonances were observed in the ^1H NMR spectrum of **18**, together with extra signals due

(21) Sierra, M. L.; Charrier, C.; Mathey, F. *Bull. Chim. Soc. Fr.* **1993**, *130*, 521.

Table 5. Intramolecular Distances (Å) and Angles (deg) for Compound 7 with ESD's in Parentheses

(a) Bond Distances

Ru(1)–P(3)	2.508(4)	Ru(1)–P(1)	2.429(3)
Ru(1)–P(2)	2.421(3)	Ru(1)–C(1)	2.322(12)
Ru(1)–C(2)	2.330(12)	Ru(1)–C(11)	2.258(13)
Ru(1)–C(12)	2.185(13)	Ru(1)–C(13)	2.173(13)
Ru(1)–C(14)	2.196(12)	Ru(1)–C(15)	2.219(14)
Ru(1)–M1[a]	1.794	Ru(1)–M2[b]	1.840
Ru(2)–P(3)	2.506(4)	Ru(2)–P(1)	2.443(4)
Ru(2)–P(2)	2.429(4)	Ru(2)–C(1)	2.309(12)
Ru(2)–C(2)	2.297(12)	Ru(2)–C(21)	2.226(12)
Ru(2)–C(22)	2.2141(14)	Ru(2)–C(23)	2.176(12)
Ru(2)–C(24)	2.181(14)	Ru(2)–C(25)	2.211(15)
Ru(2)–M1	1.787	Ru(2)–M3[c]	1.846
P(3)–C(1)	1.798(13)	P(3)–C(2)	1.789(13)
P(1)–P(2)	2.223(5)	P(1)–C(2)	1.804(13)
P(2)–C(1)	1.813(12)	P(4)–F(1)	1.556(14)
P(4)–F(2)	1.48(2)	P(4)–F(3)	1.473(12)
P(4)–F(4)	1.507(14)	P(4)–F(5)	1.53(2)
P(4)–F(6)	1.47(2)	C(1)–C(3)	1.55(2)
C(2)–C(7)	1.56(2)	C(3)–C(4)	1.52(2)
C(3)–C(5)	1.53(2)	C(3)–C(6)	1.53(2)
C(7)–C(8)	1.46(3)	C(7)–C(9)	1.50(2)
C(7)–C(10)	1.40(3)	C(11)–C(12)	1.48(2)
C(11)–C(15)	1.43(2)	C(11)–C(16)	1.52(2)
C(12)–C(13)	1.41(2)	C(12)–C(17)	1.54(2)
C(13)–C(14)	1.42(2)	C(13)–C(18)	1.56(2)
C(14)–C(15)	1.42(2)	C(14)–C(19)	1.52(2)
C(15)–C(20)	1.53(2)	C(21)–C(22)	1.44(2)
C(21)–C(25)	1.36(2)	C(21)–C(26)	1.52(2)
C(22)–C(23)	1.41(2)	C(22)–C(27)	1.54(2)
C(23)–C(24)	1.44(2)	C(23)–C(28)	1.50(2)
C(24)–C(25)	1.39(2)	C(24)–C(29)	1.54(2)
C(25)–C(30)	1.56(2)		

(b) Bond Angles

M1–Ru(1)–M2	175.1	M1–Ru(2)–M3	174.9
C(1)–P(3)–C(2)	97.8(6)	P(2)–P(1)–C(2)	97.2(4)
P(1)–P(2)–C(1)	98.0(4)	F(1)–P(4)–F(2)	88.3(8)
F(1)–P(4)–F(3)	92.9(8)	F(1)–P(4)–F(4)	85.3(9)
F(1)–P(4)–F(5)	177.6(9)	F(1)–P(4)–F(6)	91.3(9)
F(2)–P(4)–F(3)	91.7(9)	F(2)–P(4)–F(4)	87.0(9)
F(2)–P(4)–F(5)	91.2(8)	F(2)–P(4)–F(6)	176(1)
F(3)–P(4)–F(4)	178(1)	F(3)–P(4)–F(5)	84.8(9)
F(3)–P(4)–F(4)	178(1)	F(3)–P(4)–F(5)	84.8(9)
F(3)–P(4)–F(6)	93(1)	F(4)–P(4)–F(5)	97(1)
F(4)–P(4)–F(6)	89(1)	F(5)–P(4)–F(6)	89.3(9)
P(3)–C(1)–P(2)	122.9(7)	P(3)–C(1)–C(3)	116.8(8)
P(2)–C(1)–C(3)	120.3(9)	P(3)–C(2)–P(1)	124.1(7)
P(3)–C(2)–C(7)	117.0(9)	P(1)–C(2)–C(7)	118.9(9)
C(1)–C(3)–C(4)	110(1)	C(1)–C(3)–C(5)	111(1)
C(1)–C(3)–C(6)	112(1)	C(4)–C(3)–C(5)	107(1)
C(4)–C(3)–C(6)	109(1)	C(5)–C(3)–C(6)	108(1)
C(2)–C(7)–C(8)	109(1)	C(2)–C(7)–C(9)	111(1)
C(2)–C(7)–C(10)	113(1)	C(8)–C(7)–C(9)	107(2)
C(8)–C(7)–C(10)	110(2)	C(9)–C(7)–C(10)	106(2)
C(12)–C(11)–C(15)	107(1)	C(12)–C(11)–C(16)	126(1)
C(15)–C(11)–C(16)	126(1)	C(11)–C(12)–C(13)	106(1)
C(11)–C(12)–C(17)	128(1)	C(13)–C(12)–C(17)	126(1)
C(12)–C(13)–C(14)	111(1)	C(12)–C(13)–C(18)	125(1)
C(14)–C(13)–C(18)	124(1)	C(13)–C(14)–C(15)	106(1)
C(13)–C(14)–C(19)	127(1)	C(15)–C(14)–C(19)	125(1)
C(11)–C(15)–C(14)	110(1)	C(11)–C(15)–C(20)	122(1)
C(14)–C(15)–C(20)	127(1)	C(22)–C(21)–C(25)	107(1)
C(22)–C(21)–C(26)	126(1)	C(25)–C(21)–C(26)	126(1)
C(21)–C(22)–C(23)	108(1)	C(21)–C(22)–C(27)	129(1)
C(23)–C(22)=C(27)	122(1)	C(22)–C(23)–C(24)	107(1)
C(22)–C(23)–C(28)	127(1)	C(24)–C(23)–C(28)	126(1)
C(23)–C(24)–C(25)	107(1)	C(23)–C(24)–C(29)	122(1)
C(25)–C(24)–C(29)	129(1)	C(21)–C(25)–C(24)	111(1)
C(21)–C(25)–C(30)	124(1)	C(24)–C(25)–C(30)	124(1)

[a] M1 is the centroid of the P(1)–P(2)–P(3)–C(1)–C(2) ring. [b] M2 is the centroid of the C(11)–C(15) ring. [c] M3 is the centroid of the C(21)–C(25) ring.

to the isomer of **18**, [CpFe(η^5-C_2-*t*-Bu_2PAsP)Ru(Cp*)-($CH_3CN)_2$][PF_6], **19**. The $^{31}P\{^1H\}$ NMR spectrum of **17** showed, as expected, an ABC pattern ($^1J_{PA,PB}$ = 437 Hz, $^2J_{PA,PC}$ = 44.7 Hz, $^2J_{PB,PC}$ = 50.1 Hz), the magnitude of the coupling constants being similar to those previously reported for $\eta^{5:1}$-ligated (C_2-*t*-Bu_2P_3) rings.[4-7] Two resonances were observed in the $^{31}P\{^1H\}$ NMR spectrum of **18** ($^1J_{PA,PB}$ = 447 Hz), the large coupling constant

Table 6. Intramolecular Distances (Å) and Angles (deg) for Compound 8 with ESD's in Parentheses

(a) Bond Distances

Ru(1)–As	2.565(2)	Ru(1)–P(1)	2.464(3)
Ru(1)–P(2)	2.455(3)	Ru(1)–C(1)	2.325(11)
Ru(1)–C(2)	2.347(11)	Ru(1)–C(11)	2.276(12)
Ru(1)–C(12)	2.215(12)	Ru(1)–C(13)	2.170(12)
Ru(1)–C(14)	2.209(13)	Ru(1)–C(15)	2.208(12)
Ru(2)–As	2.584(2)	Ru(2)–P(1)	2.466(3)
Ru(2)–P(2)	2.460(3)	Ru(2)–C(1)	2.313(11)
Ru(2)–C(2)	2.288(11)	Ru(2)–C(21)	2.236(12)
Ru(2)–C(22)	2.207(12)	Ru(2)–C(23)	2.158(12)
Ru(2)–C(24)	2.179(14)	Ru(2)–C(25)	2.250(13)
Ru(1)–M1[a]	1.841	Ru(1)–M3[c]	1.792
Ru(2)–M2[b]	1.839	Ru(2)–M3	1.782
As–C(1)	1.873(11)	As–C(2)	1.911(11)
P(1)–P(2)	2.275(4)	P(1)–C(2)	1.796(12)
P(2)–C(1)	1.856(11)	P(3)–F(1)	1.543(12)
P(3)–F(2)	1.503(14)	P(3)–F(3)	1.489(12)
P(3)–F(4)	1.520(14)	P(3)–F(5)	1.536(14)
P(3)–F(6)	1.51(2)	C(1)–C(3)	1.56(2)
C(2)–C(7)	1.55(2)	C(3)–C(4)	1.54(2)
C(7)–C(8)	1.51(2)	C(7)–C(9)	1.46(2)
C(7)–C(10)	1.47(3)	C(11)–C(12)	1.48(2)
C(11)–C(15)	1.43(2)	C(11)–C(16)	1.50(2)
C(12)–C(13)	1.45(2)	C(12)–C(17)	1.49(2)
C(13)–C(14)	1.44(2)	C(13)–C(18)	1.53(2)
C(14)–C(15)	1.44(2)	C(14)–C(19)	1.53(2)
C(15)–C(20)	1.53(2)	C(21)–C(22)	1.46(2)
C(21)–C(25)	1.43(2)	C(21)–C(26)	1.49(2)
C(22)–C(23)	1.41(2)	C(22)–C(27)	1.53(2)
C(23)–C(24)	1.46(2)	C(23)–C(28)	1.52(2)
C(24)–C(25)	1.41(2)	C(24)–C(29)	1.54(2)
C(25)–C(30)	1.51(2)		

(b) Bond Angles

M1–Ru(1)–M3	174.9	M2–Ru(2)–M3	174.9
C(1)–As–C(2)	93.0(5)	P(2)–P(1)–C(2)	97.6(4)
P(1)–P(2)–C(1)	97.2(4)	F(1)–P(3)–F(2)	88.6(7)
F(1)–P(3)–F(3)	93.7(8)	F(1)–P(3)–F(4)	84.1(9)
F(1)–P(3)–F(5)	178.0(8)	F(1)–P(3)–F(6)	92.7(8)
F(2)–P(3)–F(3)	87.3(9)	F(2)–P(3)–F(4)	89.1(8)
F(2)–P(3)–F(5)	90.2(7)	F(2)–P(3)–F(6)	177.8(9)
F(3)–P(3)–F(4)	176(1)	F(3)–P(3)–F(5)	84.7(9)
F(3)–P(3)–F(6)	94(1)	F(4)–P(3)–F(5)	97(1)
F(4)–P(3)–F(6)	89(1)	F(5)–P(3)–F(6)	88.6(8)
As–C(1)–P(2)	125.6(6)	As–C(1)–C(3)	116.5(8)
P(2)–C(1)–C(3)	117.9(8)	As–C(2)–P(1)	126.6(6)
As–C(2)–C(7)	114.4(8)	P(1)–C(2)–C(7)	119.0(8)
C(1)–C(3)–C(4)	109(1)	C(1)–C(3)–C(5)	109(1)
C(1)–C(3)–C(6)	113(1)	C(4)–C(3)–C(5)	105(1)
C(4)–C(3)–C(6)	109(1)	C(5)–C(3)–C(6)	111(1)
C(2)–C(7)–C(8)	110(1)	C(2)–C(7)–C(9)	110(1)
C(2)–C(7)–C(10)	112(1)	C(8)–C(7)–C(9)	106(2)
C(8)–C(7)–C(10)	104(1)	C(9)–C(7)–C(10)	114(2)
C(12)–C(11)–C(15)	107(1)	C(12)–C(11)–C(16)	127(1)
C(15)–C(11)–C(16)	125(1)	C(11)–C(12)–C(13)	105(1)
C(11)–C(12)–C(17)	128(1)	C(13)–C(12)–C(17)	126(1)
C(12)–C(13)–C(14)	111(1)	C(12)–C(13)–C(18)	124(1)
C(14)–C(13)–C(18)	125(1)	C(13)–C(14)–C(15)	106(1)
C(13)–C(14)–C(19)	126(1)	C(15)–C(14)–C(19)	127(1)
C(11)–C(15)–C(14)	111(1)	C(11)–C(15)–C(20)	124(1)
C(14)–C(15)–C(20)	124(1)	C(22)–C(21)–C(25)	108(1)
C(22)–C(21)–C(26)	127(1)	C(25)–C(21)–C(26)	125(1)
C(21)–C(22)–C(23)	108(1)	C(21)–C(22)–C(27)	129(1)
C(23)–C(22)–C(27)	122(1)	C(22)–C(23)–C(24)	107(1)
C(22)–C(23)–C(28)	126(1)	C(24)–C(23)–C(28)	126(1)
C(23)–C(24)–C(25)	109(1)	C(23)–C(24)–C(29)	123(1)
C(25)–C(24)–C(29)	127(1)	C(21)–C(25)–C(24)	108(1)
C(21)–C(25)–C(30)	126(1)	C(24)–C(25)–C(30)	125(1)

[a] M1 is the centroid of the C(11)–C(15) ring. [b] M2 is the centroid of the C(21)–C(25) ring. [c] M3 is the centroid of the As–P(1)–P(2)–C(1)–C(2) ring.

Scheme 2

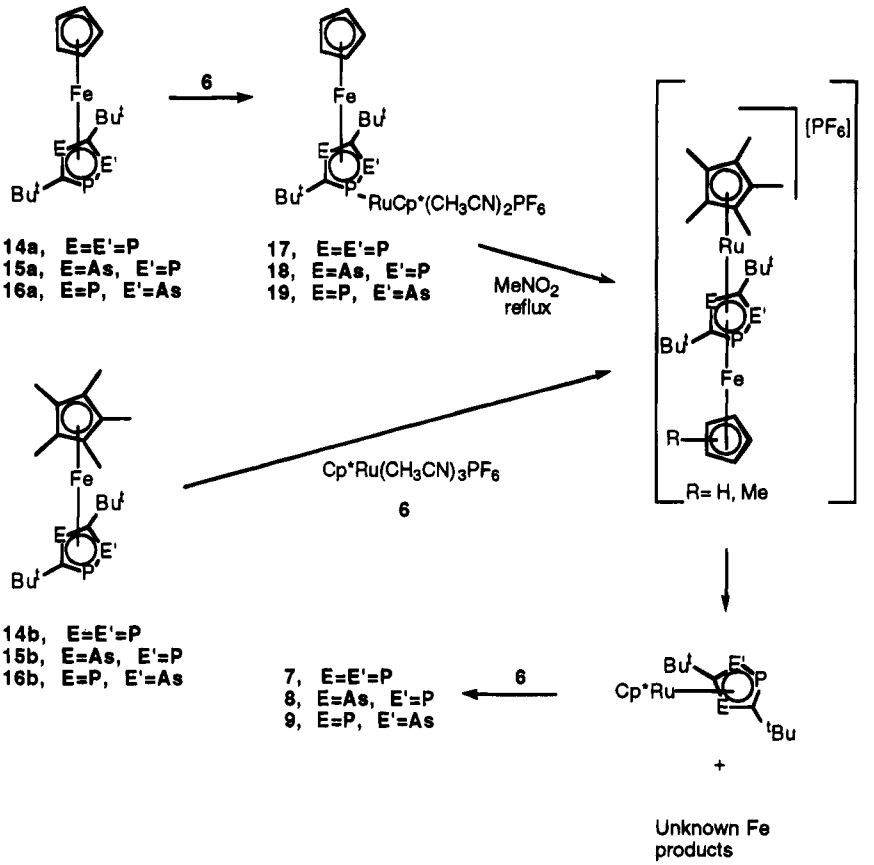

clearly showing that the two adjacent P atoms of C_2-*t*-Bu_2P_3 ring are *both* coordinated. Also observed in this spectrum was a set of signals showing an AX pattern ($^2J_{PA,PX}$ = 50.1 Hz) which arise from complex **19**. A similar attempt to prepare mixed-metal triple-decker complexes from the reaction of [Cp*Fe(η^5-C_2-*t*-Bu_2P_3)], **14b**, or [Cp*Fe(η^5-C_2-*t*-Bu_2AsP_2)], **15b**, with **6** led to the direct formation of the triple-decker species **7** and **8**, respectively (Scheme 2), as evidenced by their typical $^{31}P\{^1H\}$ NMR spectra. Also present in the reaction mixtures was the ruthenium species [Cp*Ru(η^5-C_2-*t*-Bu_2P_3)], **11**, or [Cp*Ru(η^5-C_2-*t*-Bu_2AsP_2)], **12**, respectively, both of which were easily separated from the triple-decker complexes. Both **7** and **8** were also formed by heating nitromethane solutions of either **17** or **18**. Monitoring these reactions by $^{31}P\{^1H\}$ NMR spectroscopy showed complexes **7** or **8** and **11** or **12** to be present. Thus from these detailed studies it is apparent that a ring-transfer reaction of the phospholyl or arsadiphospholyl ligands from the Fe atom to the Ru atom is taking place in each case.

These types of ring-transfer reactions were first identified by Maitlis *et al.*[22] and are particularly useful for the preparation of a variety of new metal cyclobutadiene complexes.[23,24] The mechanism of these reactions was first thought to proceed *via* monofacially bridged bimetallic species,[23] and the structural characterization of the monofacially-bridged Pd_2 complex, [$Pd_2(Al_2Cl_7)_2$-(μ-η^6-$C_6H_6)_2$],[25] strengthened this theory. However, similar cyclobutadiene species remained uncharacterized, and thus the mechanism is unproven. A second proposed mechanism, particularly for the ring transfer of η^5-borole ligands, has been suggested by Herberich *et al.*[26,27] This involves the formation of bifacially bridged (triple-decker) species by electrophilic stacking and subsequent decomposition by nucleophilic degradation with the ring being transferred from one metal to the other.

In a very recent paper, Herberich and Jansen[28] have established the intermediacy of this type of triple-decker complex in cyclopentadienyl ring-transfer reactions, in particular in the stereospecific transfer of isodicyclopentadienyl ligands from ruthenium to rhodium. In the case of the present study involving the transfer of phospholyl or arsadiphospholyl ligands, the Herberich mechanism also appears to be applicable. Thus the dinuclear complexes **17** or **18** might lose acetonitrile in refluxing nitromethane to give either [Cp*Fe(μ-η^5:η^5-C_2-*t*-Bu_2P_3)RuCp*][PF_6] or [Cp*Fe(μ-η^5:η^5-C_2-*t*-Bu_2AsP_2)-RuCp*][PF_6]. Alternatively the direct reaction of either [Cp*Fe(η^5-C_2-*t*-Bu_2P_3)], **14b**, or [Cp*Fe(η^5C_2-*t*-Bu_2AsP_2)], **15b**, with [Cp*Ru($CH_3CN)_3$][PF_6], **6**, would lead to the same products. These unstable species can then readily undergo nucleophilic degradation induced by displaced acetonitrile to give either [Cp*Ru(η^5-C_2-*t*-Bu_2P_3)], **11**, or [Cp*Ru(η^5-C_2-*t*-Bu_2AsP_2)], **12**, and [Cp*Fe($CH_3CN)_3$]$^+$. The presence of the triple-decker species **7** and **8** in these reactions is explained by an excess of **6** reacting

(22) Maitlis, P. M.; Games, M. L. *J. Am. Chem. Soc.* **1963**, *85*, 1887.
(23) Maitlis, P. M. *Adv. Organomet. Chem.* **1966**, *4*, 95.
(24) Garrou, P. *Adv. Organomet. Chem.* **1984**, *23*, 95.
(25) Allegra, G.; Immirzi, A.; Porri, L. *J. Am. Chem. Soc.* **1965**, *87*, 1394.
(26) Herberich, G. E.; Dunne, B. J.; Hessner B. *Angew. Chem., Int. Ed. Engl.* **1989**, *28*, 737.
(27) Herberich, G. E.; Büschges, U.; Dunne, B. J.; Hessner B.; Klaff, N.; Köffer, D. P. J.; Peters, K. *J. Organomet. Chem.* **1989**, *372*, 53.
(28) Herberich, G. E.; Jansen, U. J. *Organometallics* **1995**, *14*, 834.

with either **10** or **11** (Scheme 2). No iron-containing products were detected in the reaction mixture even though the unstable $[CpFe(CH_3CN)_3]^+$ cation is known to readily decompose to ferrocene at room temperature.[29] Likewise, neither pentamethyl- nor decamethylferrocenes were detected in similar solvent-induced nucleophilic degradation reactions previously reported for iron/ruthenium mixed-metal triple-decker complexes containing bridging cyclopentadienyl ligands,[10] and in this case a similar decomposition is believed to have occurred.

Conclusions

The formation of the diruthenium triple-decker complexes $[Cp^*Ru(\mu\text{-}\eta^5\text{:}\eta^5\text{-}C_2\text{-}t\text{-}Bu_2P_3)RuCp^*][PF_6]$, **7**, and $[Cp^*Ru(\mu\text{-}\eta^5\text{:}\eta^5\text{-}C_2\text{-}t\text{-}Bu_2AsP_2)RuCp^*][PF_6]$, **8**, by an electrophilic stacking mechanism is similar to the syntheses of other triple-decker systems of group 8 metals containing a variety of non-phosphorus containing bridging ligands. The occurrence of a ring-transfer reaction in the attempted formation of mixed-metal triple-decker complexes containing bridging phospholyl and arsadiphospholyl ligands suggests that these complexes probably have also been formed; however, their instability has prevented any characterization. The lack of stability of such intermediates is probably due to the presence of donor solvents in the reaction mixture which enhance the rate of nucleophilic degradation. Alternative synthetic routes to mixed-metal species are currently under investigation, as is the ligating potential of the phosphorus atoms in the middle decks of the novel cationic diruthenium complexes **7** and **8** described in this paper.

Experimental Section

All reactions were performed under an atmosphere of dry nitrogen gas using standard Schlenk techniques. The solvents 1,2-dimethoxyethane (DME), tetrahydrofuran (THF), petroleum ether 60−80° fraction (hereafter referred to as petroleum ether), and diethyl ether (ether) were distilled from Na/K alloy before use. Acetone and dichloromethane were distilled from $CaSO_4$ and CaH_2, respectively, before use. All NMR spectra were recorded on a Bruker AC-P250 spectrometer at the following frequencies: ^1H, 250.1 MHz, C_6D_6 or $CDCl_3$ internal reference; $^{31}P\{^1H\}$, 101.3 MHz, 85% H_3PO_4 external reference, recorded in $CDCl_3$ unless otherwise stated. Mass spectra (EI) were recorded on a Kratos MS80RF instrument, and melting points were measured on an Electrothermal melting point apparatus and are uncorrected. All microanalyses were carried out by Miss Mita Patel at the University of Sussex. The starting materials $[Li(C_2\text{-}t\text{-}Bu_2P_3)]$, **2**,[16] $[Li(C_2\text{-}t\text{-}Bu_2AsP_2)]$, **4**,[14] $[Cp^*Ru(CH_3CN)_3][PF_6]$, **6**,[30] $[Cp^*Fe(C_6H_6)][PF_6]$,[31] $[Cp^*Fe(\eta^5\text{-}C_2\text{-}t\text{-}Bu_2P_3)]$, **14b**,[6] $[CpFe(\eta^5\text{-}C_2\text{-}t\text{-}Bu_2P_3)]$, **14a**,[3] and $[CpFe(\eta^5\text{-}C_2\text{-}t\text{-}Bu_2AsP_2)]$, **15a**,[14] were prepared by published procedures. The complex $[Cp^*Fe(\eta^5\text{-}C_2\text{-}t\text{-}Bu_2AsP_2)]$, **15b**, was prepared in a similar manner to $[Cp^*Fe(\eta^5\text{-}C_2\text{-}t\text{-}Bu_2P_3)]$, **14b**,[6] as described below. All other reagents were used as received.

(Pentamethylcyclopentadienyl)(1-arsa-3,4-diphospha-2,5-di-*tert*-butylcyclopentadienyl)iron (15b). To a 10 cm^3 DME solution of $[FeCl_2]$ (0.26 g, 2.0 mmol) were added a solution of $[Li(C_5Me_5)]$ (2 mmol in 10 cm^3 of THF) and a 5 cm^3 DME solution of $[Li(C_2\text{-}t\text{-}Bu_2AsP_2)]$, **4** (2 mmol). The reaction mixture was stirred for 5 h, during which time a deep-red solution formed. Removal of solvent *in vacuo* gave a brown oil, which was extracted twice with petroleum ether. The combined extracts were eluted down a kieselgel column with petroleum ether, and two bands were collected. The orange first band was identified by ^1H NMR spectroscopy as $[Fe(C_5Me_5)_2]$.[32] The major red band was identified spectroscopically as a mixture of four complexes, namely, $[Cp^*Fe(\eta^5\text{-}C_2\text{-}t\text{-}Bu_2AsP_2)]$, **15b** {$^1H$ NMR (C_6D_6), δ 1.49 (s, *t*-Bu) 1.70 (s, C_5Me_5); $^{31}P\{^1H\}$ NMR ($CDCl_3$), δ 49.9; MS (70 eV, EI) *m/z* 466 [M^+, 40%], 328 [$M^+ - (t\text{-}BuC)_2$, 40%]}, as the predominant product, its isomer $[Cp^*Fe(\eta^5\text{-}C_2\text{-}t\text{-}Bu_2PAsP)]$, **16b** {$^1H$ NMR (C_6D_6), δ 1.50 (s, *t*-Bu), 1.69 (s, C_5Me_5); $^{31}P\{^1H\}$ NMR (C_6D_6), (AX) δ 37.0 P_A, 81.7 P_X, $^2J_{PA,PX}$ = 45.2 Hz}, and the previously reported[5] complexes $[Cp^*Fe(\eta^5\text{-}C_2\text{-}t\text{-}Bu_2P_3)]$, **14b**, and $[Cp^*Fe(\eta^5\text{-}C_3\text{-}t\text{-}Bu_3P_2)]$. Attempts to separate the individual components by fractional crystallization or sublimation were unsuccessful.

(Pentamethylcyclopentadienyl)(1,3,4-triphospha-2,5-di-*tert*-butylcyclopentadienyl)ruthenium (11). A 10 cm^3 DME solution of $[Li(C_2\text{-}t\text{-}Bu_2P_3)]$, **2** (1.0 mmol), was added slowly to **6** (0.45 g, 0.90 mmol) in DME (10 cm^3), and the resulting brown solution was stirred for 3 h. All volatile components were removed *in vacuo*, and the residual oil was extracted twice with petroleum ether. The yellow oil obtained after removal of solvent could not be purified by column chromatography because of decomposition but was identified spectroscopically as $[Cp^*Ru(\eta^5\text{-}C_2\text{-}t\text{-}Bu_2P_3)]$, **11** {$^1H$ NMR (C_6D_6) δ 1.39 (s, *t*-Bu), 1.80 (s, C_5Me_5); $^{31}P\{^1H\}$ NMR ($CDCl_3$) (AX_2) δ 18.0 P_A, 36.2 P_X, $^2J_{PA,PX}$ = 43.0 Hz; MS (70 eV, EI) *m/z* 468 [M^+, 25%], 411 [$M^+ - t$-Bu, 10%], 330 [$M^+ - (t\text{-}BuC)_2$, 35%]}, together with a small amount of $[Cp^*Ru(\eta^5\text{-}C_3\text{-}t\text{-}Bu_3P_2)]$, **10** {$^1H$ NMR (C_6D_6) δ 1.60 (s, *t*-Bu), 1.87 (s, C_5Me_5); $^{31}P\{^1H\}$ NMR ($CDCl_3$) δ 21.8}. The two products could not be separated by either fractional crystallization or sublimation.

(Pentamethylcyclopentadienyl)(1-arsa-3,4-diphospha-2,5-di-*tert*-butylcyclopentadienyl)ruthenium (12) was prepared in a similar manner from **6** (0.24 g, 0.48 mmol) and a 0.6 mmol solution of $[Li(C_2\text{-}t\text{-}Bu_2AsP_2)]$, **4** {$^1H$ NMR (C_6H_6) δ 1.39 (s, *t*-Bu), 1.80 (s, C_5Me_5); $^{31}P\{^1H\}$ NMR (C_6D_6) δ 36.8; MS (70 eV, EI) *m/z* 511 [M^+, 40%], 373 [$M^+ - (t\text{-}BuC)_2$, 40%]}.

(Pentamethylcyclopentadienyl)(3-arsa-1,4-diphospha-2,5-di-*tert*-butylcyclopentadienyl)ruthenium (13), an isomer of **12**, was also identified in the reaction products {^1H NMR (C_6D_6) δ 1.38 (s, *t*-Bu), 1.79 (s, C_5Me_5); $^{31}P\{^1H\}$ NMR (C_6D_6) (AX) δ 16.3 P_A, 66.7 P_X, $^2J_{PA,PX}$ = 43.0 Hz, as were **10** and **11**, but these complexes could not be separated by sublimation or fractional crystallization.

(μ-1,3,4-Triphospha-2,5-di-*tert*-butylcyclopentadienyl)-bis[(pentamethylcyclopentadienyl)ruthenium] Hexafluorophosphate (7). Both **6** (0.82 g, 1.60 mmol) and $[Li(C_2\text{-}t\text{-}Bu_2P_3)]$, **2** (0.80 mmol), were stirred for 6 h in DME (20 cm^3). All volatile components were then removed *in vacuo*, and the residual oil was washed with ether. The oil was taken up in THF and filtered through a 5 cm^3 pad of alumina (neutral, activity I), and the resulting orange solution was evaporated to dryness. Treatment of the oil obtained with ether afforded **7** (0.15 g, 22%) as an orange powder, mp = 234 °C (decomp). Anal. Calcd for $C_{30}H_{48}F_6P_4Ru_2$: C, 42.4; H, 5.60. Found: C, 42.1; H, 4.90. ^1H NMR ($CDCl_3$) δ 1.35 (s, *t*-Bu), 1.81 (s, C_5Me_5); $^{31}P\{^1H\}$ NMR ($CDCl_3$) (AX_2) δ −2.37 P_A, −34.2 P_X, $^2J_{PA,PX}$ = 37.0 Hz, PF_6 −142.6 (sept, $^1J_{P,F}$ = 708 Hz).

(μ-1-Arsa-3,4-diphospha-2,5-di-*tert*-butylcyclopentadienyl)bis[(pentamethylcyclopentadienyl)ruthenium] hexafluorophosphate (8) was prepared in a similar manner from **6** (0.82 g, 1.60 mmol) and $[Li(C_2\text{-}t\text{-}Bu_2AsP_2)]$, **4** (0.80 mmol), and isolated (0.08 g, 12%) as an orange powder, mp = 239 °C (decomp). Anal. Calcd for $C_{30}H_{48}AsF_6P_3Ru_2$: C. 40.5; H, 5.30. Found: C, 41.1; H, 4.90. ^1H NMR ($CDCl_3$) δ 1.35 (s, *t*-Bu), 1.81 (s, C_5Me_5); $^{31}P\{^1H\}$ NMR ($CDCl_3$) δ −28.2, PF_6 −142.6 (sept, $^1J_{P,F}$ = 708 Hz).

(μ-3-Arsa-1,4-diphospha-2,5-di-*tert*-butylcyclopentadienyl)bis[(pentamethylcyclopentadienyl)ruthenium]

(29) Gill, T. P.; Mann, K. R. *Inorg. Chem.* **1983**, *22*, 1986.
(30) Gill, T. P.; Mann, K. R. *Organometallics* **1982**, *1*, 485.
(31) Hamon, J.-R.; Astruc, D.; Michaud, P. *J. Am. Chem. Soc.* **1981**, *103*, 758.
(32) King, R. B.; Bisnette, M. B. *J. Organomet. Chem.* **1967**, *8*, 287.

hexafluorophosphate (9), an isomer of **7**, was also identified as a product from the above reaction {^{1}H NMR ($CDCl_3$) δ 1.33 (s, *t*-Bu), 1.81 (s, C_5Me_5); $^{31}P\{^1H\}$ NMR ($CDCl_3$) (AX) δ 13.5 P_A, −40.9 P_X, $^2J_{PA,PX}$ = 36.9 Hz, PF_6 −142.6 (sept, $^1J_{P,F}$ = 708 Hz)}, together with **7** which was separated by fractional crystallization.

Complexes **7**−**9** could also be prepared from the reactions of appropriate Cp*Fe precursors with [Cp*Ru(CH_3CN)$_3$][PF_6], **6**, in either DME or CH_2Cl_2, followed by workup as described above. In this way **7** was formed from [Cp*Fe(η^5-C_2-*t*-Bu_2P_3)], **14b**, in 30% yield, and **8** and its isomer **9** were formed in 27% yield from [Cp*Fe(η^5-C_2-*t*-Bu_2AsP_2)], **15b**, [Cp*Ru(η^5-C_3-*t*-Bu_3P_2)], and [Cp*Fe(η^5-C_2-*t*-Bu_2PAsP)], **16b**.

(Cyclopentadienyliron)(1,3,4-triphospha-2,5-di-*tert*-butylcyclopentadienyl)(pentamethylcyclopentadienyl)bis(acetonitrile)ruthenium Hexafluorophosphate (17). A 30 cm^3 CH_2Cl_2 solution of [CpFe(η^5-C_2-*t*-Bu_2P_3)], **14a** (0.11 g, 0.30 mmol), and [Cp*Ru(CH_3CN)$_3$][PF_6], **6**, was stirred for 5 h while being irradiated with a 100 W light. Removal of solvent *in vacuo* left an orange oily residue, which was redissolved in acetone and filtered through alumina (neutral, activity I). The solvent was again removed to leave an oily solid, which was identified spectroscopically as [CpFe(η^5-C_2-*t*-Bu_2P_3)RuCp*(CH_3CN)$_2$][PF_6], **17** {^{1}H NMR ($CDCl_3$) δ 1.32 (s, *t*-Bu), 1.38 (s, *t*-Bu), 1.62 (s, C_5Me_5), 2.45 (CH_3CN), 4.65 (s, C_5H_5); $^{31}P\{^1H\}$ NMR ($CDCl_3$) (ABC) δ_{PA} 95.0, δ_{PB} 27.6, δ_{PC} −6.46, $J_{PA,PB}$ = 437 Hz, $J_{PA,PC}$ = 47.0 Hz, $J_{PB,PC}$ = 48.3 Hz, PF_6 −142.9 (sept, $^1J_{P,F}$ = 712 Hz)}. The solid also contained a small, but inseparable, amount of **6**, as identified by ^{1}H NMR spectroscopy; thus satisfactory microanalytical data could not be obtained.

(Cyclopentadienyliron)(1-arsa-3,4-diphospha-2,5-di-*tert*-butylcyclopentadienyl)(pentamethylcyclopentadienyl)bis(acetonitrile)ruthenium hexafluorophosphate (18) was synthesized, as an oily solid, in a similar manner from **6** and [CpFe(η^5-C_2-*t*-Bu_2P_3)], **14a**. ^{1}H NMR ($CDCl_3$) δ 1.37 (s, *t*-Bu), 1.43 (s, *t*-Bu), 1.62 (s, C_5Me_5), 2.47 (CH_3CN), 4.65 (s, C_5H_5); $^{31}P\{^1H\}$ NMR ($CDCl_3$) (AB) δ_{PA} −5.20, δ_{PB} 93.4, $J_{PA,PB}$ 447 Hz, PF_6 −145.4 (sept, $^1J_{P,F}$ = 712 Hz).

(Cyclopentadienyliron)(3-arsa-1,4-diphospha-2,5-di-*tert*-butylcyclopentadienyl)(pentamethylcyclopentadienyl)bis(acetonitrile)ruthenium hexafluorophosphate (19), an isomer of **18**, was also found to be present in the resulting solid. ^{1}H NMR ($CDCl_3$) δ 1.38 (s, *t*-Bu), 1.51 (s, *t*-Bu), 1.63 (s, C_5Me_5), 2.56 (CH_3CN), 4.66 (s, C_5H_5); $^{31}P\{^1H\}$ NMR ($CDCl_3$) (AX) δ_{PA} 23.2, δ_{PX} 114.5, $J_{PA,PB}$ = 50.1 Hz, PF_6 −145.4 (sept, $^1J_{P,F}$ = 712 Hz). Again **6** was found to be present, and thus a satisfactory microanalysis could not be obtained.

Crystallography for Complex 7. Crystal data for $C_{30}H_{48}F_6P_4Ru_2$; M = 848.7; space group $P2_12_12_1$ (No. 19); cell parameters a = 12.642(9) Å, b = 15.151(10) Å, c = 18.176(10) Å, V = 3481.4 Å^3; Z = 4; D_{calcd} = 1.62 g cm^{-3}; $F(000)$ = 1720; μ = 10.8 cm^{-1} for Mo Kα radiation (λ = 0.7107 Å), T = 293 K.

Structure Determination for 7. Single crystals of [Cp*Ru(μ-η^5:η^5-C_2-*t*-Bu_2P_3)RuCp*][PF_6], **7**, were grown from chloroform/pentane. The 3437 unique reflections were collected from an air-stable red crystal of dimensions *ca.* 0.2 × 0.2 × 0.1 mm^3 on an Enraf-Nonius CAD4 in θ−2θ mode for 2° < 2σ < 25°, of which 2716 reflections had $|F^2| > 2\sigma(F^2)$. Structure solution was by heavy atom methods (SHELXS-86). A DIFABS absorption correction (max 1.15, min 0.88) was made; refinement by full-matrix least-squares with all heavy atoms anisotropic converged at R = 0.055, R' = 0.057.

Crystallography for Complex 8. Crystal data: $C_{30}H_{48}AsF_6P_3Ru_2$; M = 892.7; space group $P2_12_12_1$ (No. 19); a = 12.650(9) Å, b = 15.147(8) Å, c = 18.111(10) Å, V = 3470.1 Å^3; Z = 4; D_{calcd} = 1.71 g cm^{-3}; $F(000)$ = 1792; μ = 19.9 cm^{-1} for Mo Kα radiation (λ = 0.7107 Å), T = 293 K.

Structure Determination for 8. Single crystals of [Cp*Ru(μ-η^5:η^5-C_2-*t*-Bu_2AsP_2)RuCp*][PF_6], **8**, were grown from chloroform/pentane. The 3430 unique reflections were collected from an air-stable red crystal of dimensions *ca.* 0.25 × 0.25 × 0.05 mm^3 on an Enraf-Nonius CAD4 in θ−2θ mode for 2° < 2σ < 25°, of which 2760 had $|F^2| > 2\sigma(F^2)$. Structure solution was by heavy atom methods (SHELXS-86). A DIFABS absorption correction (max 1.15, min 0.91) was made; refinement by full-matrix least-squares with all heavy atoms anisotropic converged at R = 0.049, R' = 0.053. There is disorder between the P and As atoms such that the site labeled "As" has occupancy 0.5As + 0.5P and both P1 and P2 have occupancy 0.75P + 0.25As; appropriate averaged scattering factors were used.

Acknowledgment. We are grateful for financial support from the Science and Engineering Research Council (SERC).

Supporting Information Available: Tables of anisotropic temperature factors for **7** and **8** (4 pages). Ordering information is given on any current masthead page.

OM9502143

Redox-Induced Conversion Pathways in Rhodium and Iridium Complexes Containing C–S Bond Cleaved Benzo[*b*]thiophene

Claudio Bianchini,*[1a] Verónica Herrera,[1b] M. Victoria Jiménez,[1a] Franco Laschi,[1c] Andrea Meli,[1a] Roberto Sánchez-Delgado,[1b] Francesco Vizza,[1a] and Piero Zanello[1c]

Istituto per lo Studio della Stereochimica ed Energetica dei Composti di Coordinazione, ISSECC-CNR, Via J. Nardi 39, 50132 Firenze, Italy, Instituto Venezolano de Investigaciones Cientificas, IVIC, Caracas 1020-A, Venezuela, and Dipartimento di Chimica, Università di Siena, Pian dei Mantellini 44, 53100 Siena, Italy

Received June 12, 1995[⊗]

The thermally generated 16-electron fragments [(triphos)MH] (M = Rh, Ir) react with benzo[*b*]thiophene by C–S bond scission to yield the 2-vinylthiophenolate derivatives (triphos)M[η^3-S(C_6H_4)CH=CH_2] (M = Rh, **1**; Ir, **2**) which display a rich redox-induced reactivity [triphos = MeC(CH_2PPh_2)$_3$]. Removal of one electron from **1** or **2** leads to the corresponding paramagnetic cations $\mathbf{1}^+$ and $\mathbf{2}^+$, respectively; these compounds undergo a radical reaction with H• in solution to form the diamagnetic 2-ethylidenecyclohexadienethione complexes *anti*-[(triphos)M{η^4-S(C_6H_4)CH(CH_3)}]$^+$ (M = Rh, ***anti*-3**$^+$; Ir, ***anti*-6**$^+$) which isomerize to ***syn*-3**$^+$ and ***syn*-6**$^+$, respectively. Addition of one electron to ***syn*-3**$^+$ and ***syn*-6**$^+$ gives the neutral paramagnetic derivatives *syn*-[(triphos)M{η^4-S(C_6H_4)CH(CH_3)}] (M = Rh, ***syn*-3**; Ir, ***syn*-6**) which convert back to the starting complexes **1** and **2** by homolytic C–H bond cleavage liberating H•, and thus completing a full electrochemical cycle by addition/elimination of one electron and one H atom. The related 2-(3,3,3-triphenylpropylidene)-cyclohexadienethione complex [(triphos)Rh{η^4-S(C_6H_4)CH(CH_2CPh_3)}]PF_6 (**4PF$_6$**) undergoes similar reactions including loss of a trityl radical by a C–C bond cleavage reaction in the neutral derivative (triphos)Rh{η^4-S(C_6H_4)CH(CH_2CPh_3)} (**4**). Removal of a second electron from $\mathbf{1}^+$ or $\mathbf{2}^+$ leads to the dicationic species $\mathbf{1}^{2+}$ and $\mathbf{2}^{2+}$, which spontaneously lose a proton and produce the cationic metallabenzothiabenzene complexes [(triphos)M(η^2-*C*,*S*-C_8H_6S)]$^+$ (M = Rh, $\mathbf{5}^+$; Ir, $\mathbf{7}^+$). Finally, addition of one elecytron to $\mathbf{5}^+$ or $\mathbf{7}^+$ produces the corresponding neutral paramagnetic metallabenzothiabenzene complexes [(triphos)M(η^2-*C*,*S*-C_8H_6S)] (M = Rh, **5**; Ir, **7**). All the long-lived paramagnetic compounds have been characterized by X-band ESR spectroscopy.

Introduction

Given the complexity of the processes occurring in the hydrodesulfurization (HDS) process of fossil fuels as well as the relative scarcity of analytical and spectroscopic tools to investigate *in situ* heterogeneous reactions, the study of the coordination and reactivity of various sulfur-contaminants in crude oil with soluble metal complexes has emerged as a valid modeling approach for the elucidation of the HDS mechanism.[2]

Various bonding modes of model substrates such as thiophene (**T**), benzo[*b*]thiophene (**BT**), or dibenzothiophene (**DBT**),[3] and reactions leading to C–S bond cleavage,[4–11] hydrogenation,[4b,d,8a,12–15] and desulfurization[4d,8a,10,16–19] have been described in detail. In contrast, few studies have been reported on the electron-transfer chemistry of metal complexes containing intact or cleaved thiophenic molecules[8a,20] although electron-transfer processes on the catalyst surface have been suggested to play an important role in the HDS with molybdenum studies supported on alumina.[21–24]

In MoS_2/Al_2O_3 catalysts promoted by cobalt or nickel, there are metal sites in different oxidation states and environment. A number of model surface studies agree

⊗ Abstract published in *Advance ACS Abstracts,* August 1, 1995.

(1) (a) ISSECC-CNR, Firenze. (b) IVIC, Caracas. (c) Università di Siena.

(2) (a) Angelici, R. J. *Acc. Chem. Res.* **1988**, *21*, 387. (b) Wiegand, B. C.; Friend, C. M. *Chem. Rev.* **1992**, *92*, 491. (c) Angelici, R. J. In *Encyclopedia of Inorganic Chemistry*; King, R. B., Ed.; John Wiley & Sons: New York, 1994; Vol. 3, p 1433.

(3) (a) Angelici, R. J. *Coord. Chem. Rev.* **1990**, *105*, 61. (b) Rauchfuss, T. B. *Prog. Inorg. Chem.* **1991**, *39*, 259. (c) Sánchez-Delgado, R. A. *J. Mol. Catal.* **1994**, *86*, 287.

(4) (a) Bianchini, C.; Meli, A.; Peruzzini, M.; Vizza, F.; Frediani, P.; Herrera, V.; Sánchez-Delgado, R. A. *J. Am. Chem. Soc.* **1993**, *115*, 2731. (b) Bianchini, C.; Meli, A.; Peruzzini, M.; Vizza, F.; Moneti, S.; Herrera, V.; Sánchez-Delgado, R. A. *J. Am. Chem. Soc.* **1994**, *116*, 4370. (c) Bianchini, C.; Frediani, P.; Herrera, V.; Jiménez, M. V.; Meli, A.; Rincón, L.; Sánchez-Delgado, R. A.; Vizza, F. *J. Am. Chem. Soc.* **1995**, *117*, 4333. (d) Bianchini, C.; Jiménez, M. V.; Meli, A.; Moneti, S.; Vizza, F.; Herrera, V.; Sánchez-Delgado, R. A. *Organometallics* **1995**, *14*, 2342. (e) Bianchini, C.; Jiménez, M. V.; Meli, A.; Moneti, S.; Vizza, F. *J. Organomet. Chem.* **1995**, in press.

(5) (a) Spies, G. H.; Angelici, R. J. *Organometallics* **1987**, *6*, 1897. (b) Hachgenei, J. W.; Angelici, R. J. *J. Organomet. Chem.* **1988**, *355*, 359. (c) Chen, J.; Daniels, L. M.; Angelici, R. J. *J. Am. Chem. Soc.* **1990**, *112*, 199.

(6) (a) Jones, W. D.; Dong, L. *J. Am. Chem. Soc.* **1991**, *113*, 559. (b) Jones, W. D.; Chin, R. M. *Organometallics* **1991**, *11*, 2698. (c) Dong, L.; Duckett, S. B.; Ohman, K. F.; Jones, W. D. *J. Am. Chem. Soc.* **1992**, *114*, 151. (d) Chin, R. M.; Jones, W. D. *Angew. Chem., Int. Ed. Engl.* **1992**, *31*, 357. (d) Jones, W. D.; Chin, R. M. *J. Am. Chem. Soc.* **1992**, *114*, 9851. (f) Rosini, G. P.; Jones, W. D. *J. Am. Chem. Soc.* **1992**, *114*, 10767. (g) Jones, W. D.; Chin, R. M. *J. Organomet. Chem.* **1994**, *472*, 311. (h) Jones, W. D.; Chin, R. M.; Crane, T. W.; Baruch, D. M. *Organometallics* **1994**, *13*, 4448.

(7) Selnau, H. E.; Merola, J. S. *Organometallics* **1993**, *12*, 1583.

0276-7333/95/2314-4390$09.00/0

to consider edge Mo(II) as the active sites for the chemisorption of **T**.[21,23] The reduction Mo(IV) → Mo(II) has been proposed to be brought about by either bulk Mo valence band electrons or electron-transfer from neighboring molybdenum or promoter (Co, Ni) atoms connected by sulfur bridges.[21,24a]

Based on the observation that a pretreatment of the catalyst surface with H_2 is mandatory to make the catalyst susceptible for **T** chemisorption, it has also been suggested that H_2 participates in the reduction of Mo(IV).[23] Actually, electrons may be provided by H_2 when this reagent, adsorbed molecularly, dissociates heterolytically on the catalyst surface. As a matter of fact, the occurrence of heterolytic splitting reactions in hydrotreating catalysis has widely been demonstrated.[24] Thus, in addition to various bases (O^{2-}, OH^-, S^{2-}), a catalyst surface may host electrons, H^+ and H^- species, the latter two probably in the form of sulfhydryl (SH) and hydryl (MH) moieties.[24a]

To the best of our knowledge, the only works in which electrochemistry has been used as a method to study how electron transfers may influence the chemistry of thiophene ligands are those reported by Angelici and Rauchfuss (Chart 1).[5c,20d-f] In all cases, the addition of electrons to the starting complex results in a change of the bonding mode of the thiophene ligand from η^5 to η^4 and thus in increased chemical reactivity.[5c,8b,c] Elec-

Chart 1

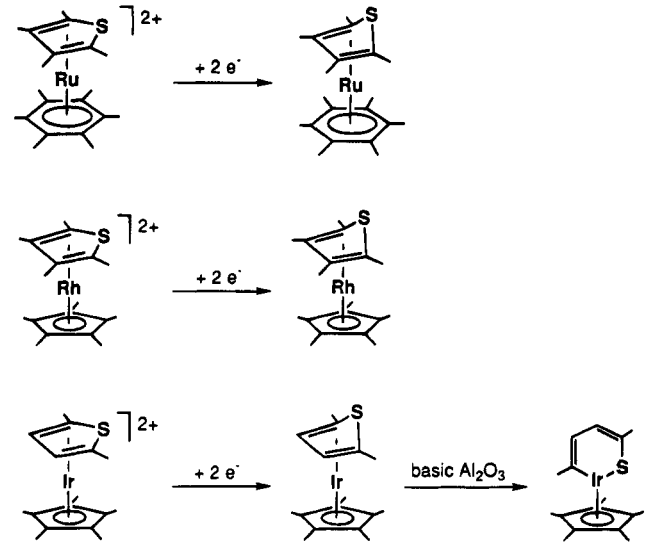

trochemical studies of complexes in which the metal center has inserted into a C–S bond of a thiophenic molecule are much rarer and of limited scope. In particular, Dessy and Pohl[20a] and later Rauchfuss[8a] have reported the electrochemical behavior of the benzothiaferroles $Fe_2(C_8H_6S)(CO)_6$ and $Fe_2(2,2'\text{-}C_4H_3SC_4H_3S)(CO)_6$ which undergo two one-electron reversible reductions.

In this paper, we report a study of the electron-transfer chemistry of various rhodium and iridium complexes obtained by metal-insertion into a C–S bond of **BT**, which is one of the most representative compounds of the least reactive sulfur-containing constituents of crude oil.[25]

Experimental Section

General Information. All reactions and manipulations were routinely performed under a nitrogen atmosphere by using standard Schlenk techniques. Tetrahydrofuran (THF) was distilled from $LiAlH_4$, stored over molecular sieves, and purged with nitrogen prior to use. Cobaltocene, $LiHBEt_3$ (1 M solution in THF), and $AgPF_6$ were purchased from Aldrich. All other chemicals were commercial products and were used as received without further purification. Literature methods were employed for the synthesis of (triphos)Rh[η^3-S(C_6H_4)-CH=CH_2] (**1**),[4c] [(triphos)Rh{η^4-S(C_6H_4)CH(CH_3)}]PF_6 (**3PF$_6$**),[4c] [(triphos)Rh{η^4-S(C_6H_4)CH(CH_2CPh_3)}]PF_6 (**4PF$_6$**),[4c] *syn*-[(triphos)Rh{η^4-SCHCHCH(CH_3)}]BPh_4,[4c] *anti*-[(triphos)Rh{η^4-SCHCHCH(CH_3)}]BPh_4,[4c] (triphos)Ir[η^3-S(C_6H_4)CH=CH_2] (**2**),[4b] [(triphos)Ir{η^4-S(C_6H_4)CH(CH_3)}]PF_6 (**6PF$_6$**),[4b] and [(triphos)-Ir(η^2-*C*,*S*-C_8H_6S)]PF_6 (**7PF$_6$**).[4b]

Deuterated solvents for NMR measurements were dried over molecular sieves. ^1H NMR and ^1H, ^1H 2D-COSY NMR spectra were obtained on either a Bruker ACP 200 (200.13 MHz) or a Bruker AVANCE DRX 500 (500.13 MHz) spectrometer. ^1H NMR shifts are recorded relative to tetramethylsilane (TMS) with the residual ^1H resonance in the deuterated solvent as secondary reference. $^{13}C\{^1H\}$ NMR spectra were recorded on the Bruker ACP 200 instrument operating at 50.32 MHz. The $^{13}C\{^1H\}$ NMR shifts are given relative to TMS with solvent as secondary reference. $^{31}P\{^1H\}$ NMR spectra were recorded on a Bruker ACP 200 spectrometer operating at 81.01

(8) (a) Ogilvy, A. E.; Draganjac, M.; Rauchfuss, T. B.; Bilson, S. R. *Organometallics* **1988**, *7*, 1171. (b) Luo, S.; Skaugset, A. E.; Rauchfuss, T. B.; Wilson, S. R. *J. Am. Chem. Soc.* **1992**, *114*, 1732. (c) Luo, S.; Rauchfuss, T. B.; Gan, Z. *J. Am. Chem. Soc.* **1993**, *115*, 4943. (d) Krautscheid, H.; Feng, Q.; Rauchfuss, T. B. *Organometallics* **1993**, *12*, 3273.

(9) Buys, I. E.; Field, L. D.; Hambley, T. W.; McQueen, A. E. D. *J. Chem. Soc., Chem. Commun.* **1995**, 557.

(10) Arce, A.; De Sanctis, Y.; Karam, A.; Deeming, A. J. *Angew. Chem., Int. Ed. Engl.* **1994**, *33*, 1381.

(11) (a) Garcia, J. J.; Maitlis, P. M. *J. Am. Chem. Soc.* **1993**, *115*, 12200. (b) Garcia, J. J.; Mann, B. E.; Adams, H.; Bailey, N. A.; Maitlis, P. M. *J. Am. Chem. Soc.* **1995**, *117*, 2179.

(12) Bianchini, C.; Herrera, V.; Jiménez, M. V.; Meli, A.; Sánchez-Delgado, R. A.; Vizza, F. *J. Am. Chem. Soc.*, in press.

(13) Jones, W. D.; Chin, R. M. *J. Am. Chem. Soc.* **1994**, *116*, 198.

(14) (a) Sánchez-Delgado, R. A.; González, E. *Polyhedron* **1989**, *8*, 1431. (b) Sánchez-Delgado, R. A. In *Advances in Catalyst Design*; Graziani, M.; Rao, C. N. R., Eds.; World Scientific Publishing Co.: Singapore, 1991; p 214. (c) Sánchez-Delgado, R. A.; Herrera, V.; Rincón, L.; Andriollo, A.; Martín, G. *Organometallics* **1994**, *13*, 553.

(15) (a) Fish, R. H.; Tan, J. L.; Thormodsen, A. D. *J. Org. Chem.* **1984**, *49*, 4500. (b) Fish, R. H.; Tan, J. L.; Thormodsen, A. D. *Organometallics* **1985**, *4*, 1743. (c) Fish, R. H.; Baralt, E.; Smith, S. J. *Organometallics* **1991**, *10*, 54. (d) Baralt, E.; Smith, S. J.; Hurwitz, I.; Horváth, I. T.; Fish, R. H. *J. Am. Chem. Soc.* **1992**, *114*, 5187.

(16) Arce, A. J.; Arrojo, P.; Deeming, A. J.; De Sanctis, Y. *J. Chem. Soc., Dalton Trans.* **1992**, 2423.

(17) (a) Riaz, U.; Curnow, O. J.; Curtis, M. D. *J. Am. Chem. Soc.* **1991**, *113*, 1416. (b) Riaz, U.; Curnow, O. J.; Curtis, M. D. *J. Am. Chem. Soc.* **1994**, *116*, 4357.

(18) Luo, S.; Ogilvy, A. E.; Rauchfuss, T. B.; Rheingold, A. L.; Wilson, S. R. *Organometallics* **1991**, *10*, 1002.

(19) Chen, J.; Daniels, L. M.; Angelici, R. J. *J. Am. Chem. Soc.* **1991**, *113*, 2544.

(20) (a) Dessy, R. E.; Pohl, R. L. *J. Am. Chem. Soc.* **1968** *90*, 1995. (b) Braitsch, D. M.; Kumarappan, R. *J. Organomet. Chem.* **1975**, *84*, C37. (c) Guerchais, V.; Astruc, D. *J. Organomet. Chem.* **1986**, *316*, 335. (d) Huckett, S. C.; Angelici, R. J. *Organometallics* **1988**, *7*, 1491. (d) Ogilvy, A. E.; Skaugset, A. E.; Rauchfuss, T. B. *Organometallics* **1989**, *8*, 2739. (f) Luo, S.; Rauchfuss, T. B.; Wilson, S. R. *J. Am. Chem. Soc.* **1992**, *114*, 8515. (g) Lockemeyer, J. R.; Rauchfuss, T. B.; Rheingold, A. L.; Wilson, S. R. *J. Am. Chem. Soc.* **1989**, *111*, 8828. (h) Skaugset, A. E.; Rauchfuss, T. B.; Stern, C. L. *J. Am. Chem. Soc.* **1990**, *112*, 2432.

(21) Anderson, A. B.; Al-Saigh, Z. Y.; Hall, W. K. *J. Phys. Chem.* **1988**, *92*, 803.

(22) Zonnevylle, M. C.; Hoffmann, R.; Harris, S. *Surf. Sci.* **1988**, *199*, 320.

(23) Diemann, E.; Weber, T.; Muller, A. *J. Catal.* **1994**, *148*, 288.

(24) (a) Neurock, M.; van Santen, R. A. *J. Am. Chem. Soc.* **1994**, *116*, 4427. (b) Topsoe, N.; Topsoe, H. *J. Catal.* **1993**, *139*, 641.

(25) (a) Thompson, C. J. In *Organic Sulfur Chemistry*; Freidlina, R. Kh., Skorova, A. E., Eds.; Pergamon: New York, 1981; p 201. (b) Porkorny, D.; Zdrazil, M. *Collect. Czech. Chem. Commun.* **1981**, *46*, 2185. (c) Kilanowski, D. R.; Gates, B. C. *J. Catal.* **1980**, *62*, 70.

Scheme 1

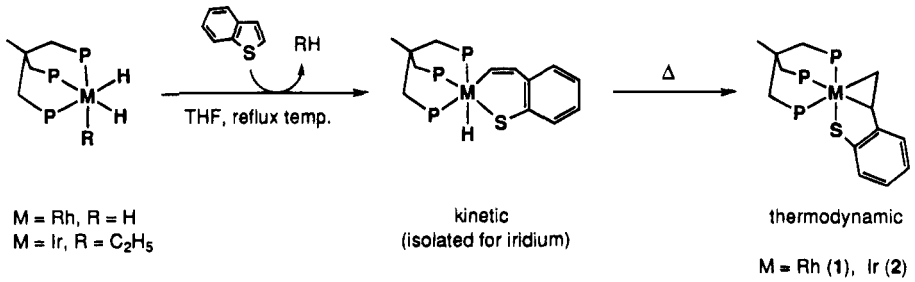

MHz. Chemical shifts are relative to external 85% H_3PO_4 with downfield values reported as positive. Broad band and selective $^1H\{^{31}P\}$ NMR experiments were carried out on the Bruker ACP 200 instrument equipped with a 5-mm inverse probe and a BFX-5 amplifier device. ^{13}C-DEPT and ^1H, ^{13}C 2D-HETCOR experiments were conducted on the Bruker ACP 200 spectrometer. Conductivities were measured with an Orion Model 990101 conductance cell connected to a Model 101 conductivity meter. The conductivity data were obtained at sample concentrations of ca. 10^{-3} M in nitroethane solutions at room temperature. The materials and the apparatus used for the electrochemical experiments have been described elsewhere.[26] Direct current voltammograms at a platinum electrode with periodical renewal of the diffusion layer (DCV) have been obtained as previously described.[26] Deaeration of solutions was performed by bubbling nitrogen for 15 min. Unless otherwise stated, the potential values are referred to an aqueous calomel electrode (SCE). Low-temperature macroelectrolysis tests were performed by using the Ag/AgCl reference electrode, the potential of which was −0.04 V *vs* SCE. Under the present experimental conditions, the ferrocenium/ferrocene couple was located at +0.44 V in dichloromethane solutions. X-Band ESR spectra were recorded with an ER 200 D-SRC Bruker spectrometer operating at $\omega_o = 9.78$ GHz. The operational microwave frequency (Bruker Microwave Bridge ER 041 MR) was tested with an XL 3120 microwave frequency counter. The control of the external magnetic field was obtained with a microwave bridge ER 041 MR Bruker wavemeter. The temperature was varied and controlled with an ER 4111 VT Bruker device with an accuracy of ±1 °C. In order to estimate accurate g_{iso} and g_{aniso} values over the temperature range of interest, the diphenylpicrylhydrazyl free radical (DPPH) was used as the H_0 external magnetic field marker (g_{iso}(DPPH) = 2.0036). In order to ensure quantitative reproducibility, the samples were placed into calibrated quartz capillary tubes permanently positioned in the resonance cavity.

Reactions of [(triphos)Rh{η^4-S(C_6H_4)CH(CH_3)}]PF_6 (3PF_6) and [(triphos)Rh{η^4-S(C_6H_4)CH(CH_2CPh_3)}]PF_6 (4PF_6) with $CoCp_2$. To a CH_2Cl_2 (20 mL) solution of either 3PF_6 or 4PF_6 (0.30 mmol) at room temperature was added 1 equiv of $CoCp_2$ (0.06 g, 0.30 mmol) in CH_2Cl_2 (20 mL). The resulting solution was stirred for ca. 3 h and then concentrated to dryness under vacuum. The ^1H and $^{31}P\{^1H\}$ NMR spectra of the residue, dissolved in CH_2Cl_2, showed the complete transformation of 3PF_6 or 4PF_6 to **1**. The reduction of 4PF_6 to **1** gave CPh_3H (^1H NMR singlet at 5.51 ppm).

Preparation of [(triphos)Rh(η^2-*C*,*S*-C_8H_6S)]PF_6 (5PF_6). To a stirred solution of (triphos)Rh[η^3-S(C_6H_4)CH=CH_2] (**1**) (0.20 g, 0.23 mmol) in THF (30 mL) at room temperature was added to a 2-fold excess of $AgPF_6$ (0.12 g, 0.46 mmol). There was an immediate color change from yellow to red. After 15 min, the reaction mixture was concentrated to ca. 10 mL under vacuum. The portionwise addition of *n*-heptane (20 mL) led to the precipitation of 5PF_6 as red microcrystals. They were collected by filtration on sintered-glass frits, washed with *n*-pentane, and dried in a stream of nitrogen; yield 86%. Anal. Calcd (found) for $C_{49}H_{45}F_6P_4RhS$: C, 58.46 (58.11); H, 4.50 (4.41); Rh, 10.22 (10.00); S, 3.18 (3.01). $^{31}P\{^1H\}$ NMR (CD_2Cl_2): 20 °C, A_3X spin systems, δ 27 (br); −70 °C, AM_2X spin system, δ −4.9 (dt, $J(P_AP_M)$ 23.3Hz, $J(P_ARh)$ 69.8 Hz, P_A), 42.5 (dd, $J(P_MRh)$ 104.6 Hz, P_M). ^1H NMR (THF-d_8, 20 °C): δ 8.39 (d, $J(H_4H_5)$ 7.8 Hz, H_4), 8.13 (m, $J(H_3H_2)$ 10.1 Hz, H_3), 8.04 (m, $J(H_2Rh)$ 2.4 Hz, H_2), 7.91 (d, $J(H_7H_6)$ 7.7 Hz, H_7), 7.68 (t, H_6), 7.62 (t, $J(H_5H_6)$ 7.6 Hz, H_5). $^{13}C\{^1H\}$ NMR (THF-d_8, 20 °C): δ 173.4 (quintet, $J(C_2P) \cong J(C_2Rh) \cong 24.6$ Hz, C_2); the resonances of the other **BT** carbons are masked by those of the phenyl carbons of the triphos ligand. Λ_M: 78 Ω^{-1} cm^2 mol^{-1}. When NEt_3 was added to the red solution, $[NHEt_3]PF_6$ precipitated by addition of *n*-heptane.

Reaction of [(triphos)Rh(η^2-*C*,*S*-C_8H_6S)]PF_6 (5PF_6) with LiHBEt$_3$. A solution of the rhodabenzothiabenzene complex 5PF_6 (0.03 g, 0.03 mmol) in THF-d_8 (1 mL) was placed into a Teflon capped resealable NMR tube under nitrogen. The solution was cooled to −70 °C and a 2-fold excess of $LiHBEt_3$ (1 M solution in THF, 60 μL, 0.06 mmol) was syringed into the tube. The ^1H and $^{31}P\{^1H\}$ NMR spectra, recorded at −70 °C, showed the immediate conversion of 5PF_6 to **1** with no detection of intermediate species.

Results and Discussion

The 16-electron fragments [(triphos)RhH] and [(triphos)IrH], generated *in situ* by thermolysis in THF of (triphos)RhH_3 and (triphos)Ir(H)$_2$(C_2H_5), respectively, have previously been shown to be active toward the oxidation addition of a C−S bond from **BT** [triphos = $MeC(CH_2PPh_2)_3$].[4c,e] The C−S insertion products are actually 2-vinylthiophenolate complexes of the formula (triphos)M{η^3-S(C_6H_4)CH=CH_2} (M = Rh, **1**; Ir, **2**) formed by reductive coupling of a terminal hydride with the vinyl moiety of a metallabenzothiabenzene intermediate (Scheme 1).[4b,c,e]

Formally, complexes **1** and **2** may be seen as the first reduction product of **BT** once the latter reagent has been cleaved by a metal center. In fact, the addition of H^+ to **1** or **2** results in the hydrogenation of the olefinic end of the 2-vinylthiophenolate ligand,[4b,c] while further reaction of the resulting 2-ethylidenecyclohexadienethione iridium complex with H_2 gives complete hydrogenation to 2-ethylthiophenolate (Scheme 2).[4b] On the other hand, the rhodium derivative **1** has recently been found to be an efficient catalyst precursor for the opening and hydrogenation of **BT** to 2-ethylthiophenol in homogeneous phase.[12] In light of these results as well as the importance of electron-transfer processes in the heterogeneous HDS, it seemed interesting to us to study the redox chemistry of **1** and **2**.

Electrochemistry of the 2-Vinylthiophenolate Rhodium Complex [(triphos)Rh(η^3-S(C_6H_4)CH=CH_2)] (1) and Characterization of its Redox Products. Figure 1a shows an overall picture of the redox

(26) Barbaro, P.; Bianchini, C.; Laschi, F.; Midollini, S.; Moneti, S.; Scapacci, G.; Zanello, P. *Inorg. Chem.* **1994**, *33*, 1622.

Scheme 2

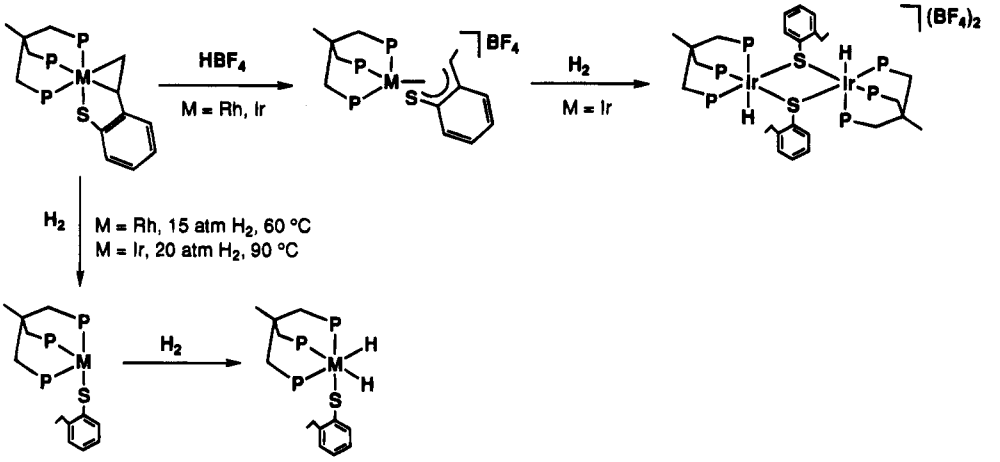

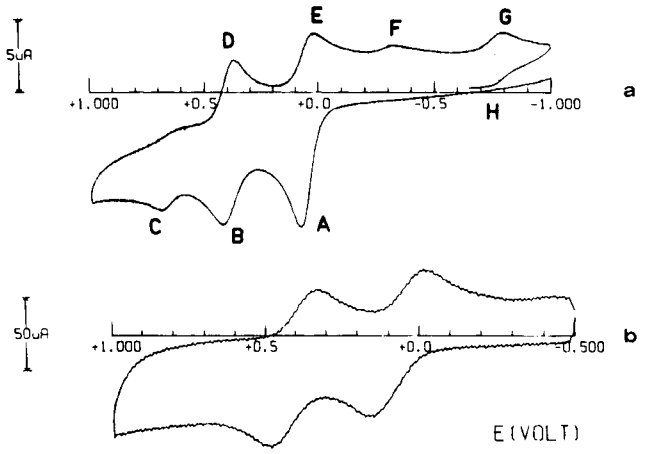

Figure 1. Cyclic voltammetric responses recorded at a platinum electrode on a CH_2Cl_2 solution containing **1** (0.7×10^{-3} mol dm^{-3}) and $[NBu_4]ClO_4$ (0.2 mol dm^{-3}). Scan rate: (a) 0.2 V s^{-1}; (b) 10.24 V s^{-1}.

behavior of the neutral complex **1** in dichloromethane solution at 20 °C.

Complex **1** displays two main sequential oxidation processes with some features of chemical reversibility at the peak-systems A/E and B/D, respectively, together with a few minor redox steps (namely, peaks C, F, and G), which, based on the response at high scan rates illustrated in Figure 1b, are clearly attributable to chemical complications following the two primary electron removals.

Controlled potential coulometric experiments directly performed in correspondence to the second anodic step (E_w = +0.5 V) consume about 1.1 electrons/molecule. Cyclic voltammetry (CV) and direct current voltammetry with periodical renewal of the diffusion layer on the solutions resulting from step-by-step macroelectrolysis, rationalize the underlying electrode mechanism.

After consumption of about 0.8 electrons/molecule at the first anodic step (E_w = +0.15 V), the electrolysis current almost drops out, and the original yellow solution turns green. The voltammetric profiles show the two peak-systems A/E and B/D (in a complementary fashion according to the formation of the monocation $\mathbf{1}^+$, see below) in a peak-height ratio reduced of about one-half as compared to the starting CV. Furthermore, in addition to the products responsible for the processes C and F, a new catho-anodic peak system is now visible at potentials slightly more negative than the peak system G/H (for comparative purposes with the electrochemistry of the iridium complex **2**, this new catho-anodic system will be hereafter as I/L). The further consumption of about 0.3 electron/molecule at the second anodic process puts an end to the electrolysis current, the solution becomes red and the voltammetric tests show only the presence of the almost overlapping catho-anodic peak-systems G/H and I/L.

On standing, the green solution obtained after exhaustive macroelectrolysis of **1** at the first anodic step slowly turns red-violet. CV measurements carried out in the course of this color change show that the intensity of the peak-system I/L increases with time at the expense of peak F which completely disappears after 1 h at room temperature, while peak C remains unaltered.

These experimental observables indicate that the neutral complex **1** undergoes two subsequent one-electron oxidations to the congeners $\mathbf{1}^+$ and $\mathbf{1}^{2+}$, respectively, both processes being complicated by chemical reactions.

Analysis[27] of the cyclic voltammograms relevant to the first anodic step with scan rates (varying from 0.02 V s^{-1} to 10.24 V s^{-1}) show the following: the i_{pc}/i_{pa} current ratio progressively increases from 0.65 to 1; the peak-to-peak separation progressively increases from 71 mV to 260 mV; the current function $i_{pc}/v^{-1/2}$ remains substantially constant. Taking into account that, under the same experimental conditions, the one-electron oxidation of ferrocene ($E^{0\prime}$ = +0.44 V) exhibits a rather similar trend in the peak-to-peak separation, these data suggest that the one-electron redox change $\mathbf{1}/\mathbf{1}^+$ involves an electrochemically reversible oxidation complicated by subsequent chemical reactions. Similar diagnostic parameters are observed for the second anodic process which converts $\mathbf{1}^+$ to $\mathbf{1}^{2+}$. Accordingly, both the transient monocation $\mathbf{1}^+$ and the dication $\mathbf{1}^{2+}$ are expected to substantially maintain the geometry of the neutral precursor and thus can be formulated as [(triphos)Rh(η^3-S(C$_6$H$_4$)CH=CH$_2$)]$^+$ and [(triphos)Rh(η^3-S(C$_6$H$_4$)-CH=CH$_2$)]$^{2+}$, respectively.[28]

On the basis of an X-ray structure analysis and

(27) Brown, E. R.; Sandifer, J. in *Physical Methods of Chemistry. Electrochemical Methods*, Rossiter, B. W. and Hamilton, J. F., Eds.; John Wiley & Sons: New York, 1986; Vol. 2, Chapter 4.

(28) Zanello, P. In *Stereochemistry of Organometallic and Inorganic Compounds*; Zanello, P., Ed.; Elsevier: Amsterdam, 1994; Vol. 5, Chapter 2.

Scheme 3

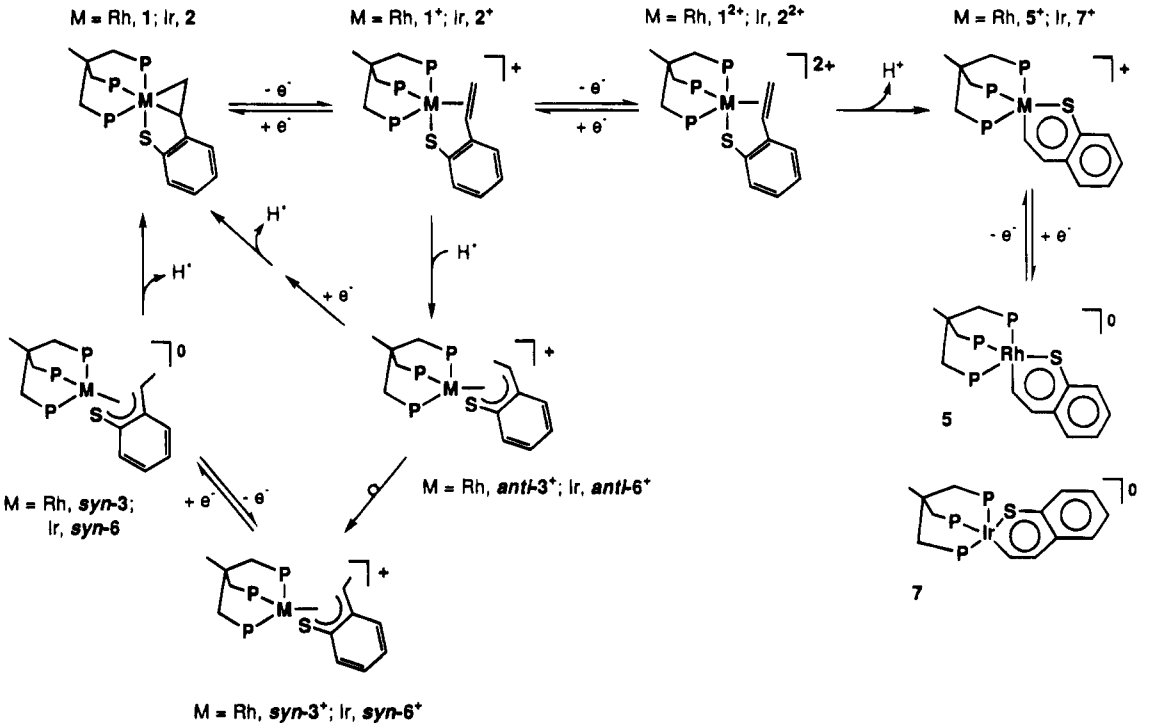

solution NMR data, the bonding interaction between rhodium and the double bond of the 2-vinylthiophenolate ligand in **1** was assigned a metallacyclopropane structure.[4c] Since removal of electrons from **1** is expected to reduce considerably the extent of $d\pi$ (metal) $\rightarrow \pi^*$ (olefin) back-bonding, $\mathbf{1}^+$ and $\mathbf{1}^{2+}$ are represented as π-olefin complexes in Scheme 3 which summarizes all the redox-induced transformations described in this work.

As shown above, the monocation $\mathbf{1}^+$ is fairly unstable in solution at room temperature ($t_{1/2} \cong 0.5$ s), which is confirmed by the fact that the value of the ratio $i_p(\mathbf{1}/\mathbf{1}^+)/i_p(\mathbf{1}^+/\mathbf{1}^{2+})$ is about 2 at low scan rates (below 0.5 V s^{-1}) and is 1 only at high scan rates (10.24 V s^{-1}). However, the complex is sufficiently stable in solution even at room temperature to allow its characterization by ESR spectroscopy. A detailed discussion of the ESR spectrum of $\mathbf{1}^+$ as well as all the other ESR-active compounds described in this work will be made in a forthcoming section to let the reader concentrate here on the type and nature of the chemical reactions which follow up the electron-transfer processes.

After macroelectrolysis of **1** in CH_2Cl_2 at −18 °C (E_w = +0.15 V), a sample of the solution was withdrawn and transferred under nitrogen into an ESR tube immersed in liquid nitrogen. The tube was positioned into an ESR spectrometer precooled at 100 K and variable-temperature spectra in X-band were acquired.

After the first ESR spectrum of $\mathbf{1}^+$ at 20 °C was acquired, subsequent spectra showed a significant decay of the paramagnetism with time. The green solution, however, became ESR-silent much before assuming a stable red-violet color. This evidence coupled with the electrochemical results indicate that the green paramagnetic cation $\mathbf{1}^+$ transforms into three diamagnetic compounds. Two of these are evidently related to each other: the complex responsible for peak F appears kinetically unstable as it spontaneously converts to a more stable species (responsible for the peak system I/L), which definitely imparts the red-violet color to the solution. The third minor species (responsible for peak C) apparently remains unaltered with time.

The stable red-violet complex has successfully been identified by means of the following procedure. A 100-mg sample of **1** was exhaustively electrolyzed at the potential of the first anodic step (E_w = +0.15 V) at room temperature. After *ca.* 1 h, the resulting solution was transferred under nitrogen into a Schlenk-type flask and the solvent was removed in vacuo. The dry residue was dissolved in CD_2Cl_2 and analyzed by $^{31}P\{^1H\}$ NMR spectroscopy which showed the formation of the known 2-ethylidenecyclohexadienethione complex [(triphos)Rh{η^4-S(C_6H_4)CH(CH_3)}]$^+$ ($\mathbf{3}^+$) in 90% yield.

Unequivocal experimental evidence in favor of the transformation of electrogenerated $\mathbf{1}^+$ into the thermodynamically stable product $\mathbf{3}^+$ was provided by a study of the electron-transfer properties of pure **3PF$_6$** independently prepared by protonation of **1** (Scheme 2).[4c] In fact, the redox fingerprint of **3PF$_6$** shown in Figure 2a, is identical with that of the red-violet product of degradation of $\mathbf{1}^+$ in CH_2Cl_2 solution (peak system I/L).

The reduction process of **3PF$_6$** consumes one electron/molecule in controlled potential coulometry (E_w = −1.1 V) and the CV parameters show that this redox step consists of an electrochemically reversible reduction complicated by slow chemical rearrangement of the electrogenerated product (the i_{pa}/i_{pc} ratio is 0.8 at 0.2 V s^{-1} and reaches the value of 1 at 2.0 V s^{-1}). Indeed, in accord with the backward profile shown in Figure 2a, exhaustive reduction of red-violet solutions of $\mathbf{3}^+$ obtained from either isolated **3PF$_6$** or exhaustive one-electron oxidation of **1**, ultimately restore the precursor **1** *via* the intermediacy of the neutral 2-ethylidenecyclohexadienethione complex (triphos)Rh{η^4-S(C_6H_4)CH(CH_3)} (**3**) (see below) (Scheme 3).

On the basis of these results, one may conclude that

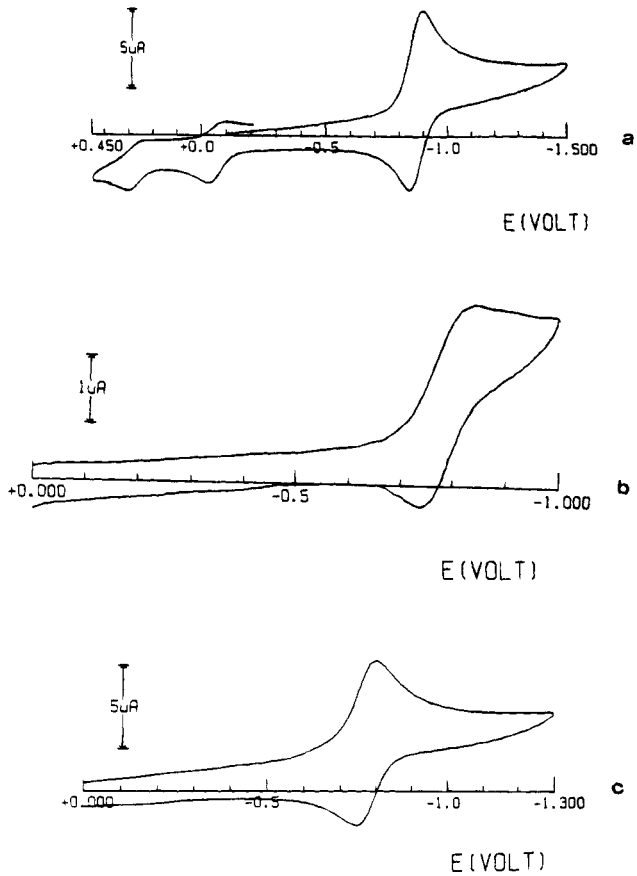

Figure 2. Cyclic voltammetric responses recorded at a platinum electrode on a CH_2Cl_2 solution containing $[NBu_4]ClO_4$ (0.2 mol dm^{-3}) and (a) **3PF$_6$** (0.5×10^{-3} mol dm^{-3}), scan rate 0.2 V s^{-1}; (b) **4PF$_6$** (0.7×10^{-3} mol dm^{-3}), scan rate 0.02 V s^{-1}; (c) **5PF$_6$** (0.5×10^{-3} mol dm^{-3}), scan rate 0.2 V s^{-1}.

the radical complex $\mathbf{1}^+$ converts in solution to the diamagnetic 2-ethylidenecyclohexadienethione complex $\mathbf{3}^+$. This transformation formally requires that a hydrogen atom is added to $\mathbf{1}^+$. The uptake of H$^\bullet$ species by paramagnetic complexes is not unusual; in most instances, hydrogen atoms are provided by the solvent or adventitious water.[29] In other cases, intermolecular hydrogen transfer between two radicals may occur.[30] In the second mechanistic hypothesis, two diamagnetic species would form which, however, is not observed in the case at hand. Accordingly, we are inclined to think that the formation of $\mathbf{3}^+$ proceeds by a radical mechanism in which a hydrogen atom is abstracted from the solvent by the paramagnetic complex $\mathbf{1}^+$ (although disfavored by bond energies, it is also possible that adventitious water can provide a hydrogen atom through an alternative pathway).

All our efforts to isolate or characterize in solution the product responsible for the cathodic peak F in Figure 1a were unsuccessful due to its spontaneous conversion to $\mathbf{3}^+$. This evidence coupled with the fact that the thermodynamically unstable species responsible for peak F regenerates the starting 2-vinylthiophenolate complex **1** by exhaustive reduction at $E_w = -0.45$ V suggest that the two products responsible for peaks F and I may be stereoisomers differing from each other

(29) Gotzig, J.; Otto, H.; Werner, H. *J. Organomet. Chem.* **1985**, *287*, 247.
(30) Mandon, D.; Astruc, D. *Organometallics* **1989**, *8*, 2372.

Scheme 4

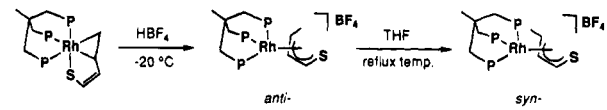

in the orientation of the methyl group with respect to the ethylidene double bond. Indeed, it has recently been reported that treatment of the butadienethiolate complex (triphos)Rh(η^3-SCH=CH-CH=CH_2) (similarly prepared by reaction of the trihydride (triphos)RhH_3 with **T**) with a protic acid gives the thiocrotonaldehyde complex *anti*-[(triphos)Rh{η^4-SCHCHCH(CH_3)}]$^+$ as kinetic product which isomerizes in solution to *syn*-[(triphos)Rh{η^4-SCHCHCH(CH_3)}]$^+$ (Scheme 4).[4c] Most importantly, the two thiocrotonaldehyde isomeric complexes exhibit irreversible reduction processes at quite different potentials (−1.3 and −1.0 V, respectively) as is observed for the 2-ethylidenecyclohexadienethione complexes presently discussed (−0.88 and −0.40 V, respectively).

In view of the overall experimental results and considerations, we suggest that the compound which spontaneously converts to $\mathbf{3}^+$ is actually *anti*-[(triphos)Rh{η^4-S(C_6H_4)CH(CH_3)}]$^+$ (***anti*-3**$^+$). Thus the stable, red-violet isomer can be quoted as ***syn*-3**$^+$ (Scheme 3).

In light of these results, a reaction between **1** and HBF_4·OEt_2 was carried out at −80 °C in an NMR tube (THF-d_8 as solvent) with the aim of intercepting the kinetic isomer ***anti*-3**$^+$. Even at this low temperature, ***syn*-3**$^+$ immediately formed, which suggests that, in contrast to the protonation of **1**,[4c] the radical reaction between $\mathbf{1}^+$ and H$^\bullet$ is still regioselective but not stereoselective.

All our attempts to identify the third product of degradation of $\mathbf{1}^+$ (the one responsible for peak C) were unsuccessful due to its low concentration.

The transformation of ***syn*-3**$^+$ into **1** upon exhaustive one-electron reduction at $E_w = -1.1$ V has been studied at low temperature. As anticipated by the CV studies, one-electron reduction of ***syn*-3**$^+$ gives the neutral derivative *syn*-(triphos)Rh{η^4-S(C_6H_4)CH(CH_3)} (***syn*-3**). Compound ***syn*-3**, which is sufficiently stable to allow its characterization by ESR spectroscopy, slowly converts ($t_{1/2} \cong 20$ s) at room temperature to **1** (Scheme 5a). The overall transformation of ***syn*-3**$^+$ into **1** has also been performed by chemical reduction of isolated **3PF$_6$** in CH_2Cl_2 with 1 equiv of cobaltocene (Scheme 5a).

From a chemical viewpoint, the spontaneous conversion of the paramagnetic complex **syn-3**, to the diamagnetic product **1** necessarily requires that a C−H bond in the former complex is homolytically cleaved. Examples of redox-promoted homolytic C−H bond cleavages in organometallic compounds have already been reported,[30,31] but certainly the occurrence of such a reaction path in a **BT** C−S insertion product assumes a particular relevance.

In an attempt to confirm the radical nature of the C−H bond cleavage undergone by the neutral 2-ethylidenecyclohexadienethione complex ***syn*-3**, the redox chemistry of the known 2-(3,3,3-triphenylpropylidene)-cyclohexadienethione congener [(triphos)Rh{η^4-S(C_6H_4)CH(CH_2CPh_3)}]PF_6 (**4PF$_6$**) has been studied (Scheme 5b).[4c]

(31) (a) Connelly, N. G. *Chem. Soc. Rev.* **1989**, *18*, 153. (b) Hayes, J. C.; Cooper, N. J. *J. Am. Chem. Soc.* **1982**, *104*, 5570.

Scheme 5

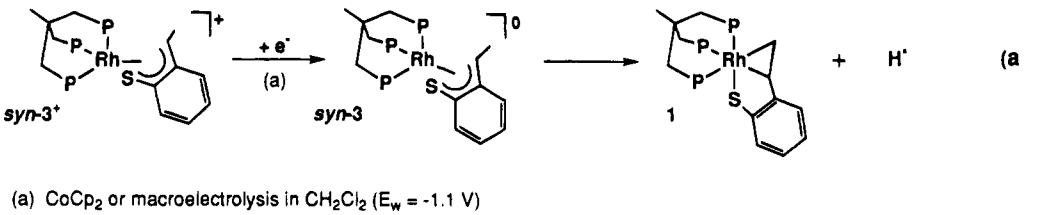

Figure 2b shows the cyclic voltammetric response exhibited by **4PF$_6$** in CH_2Cl_2. Controlled-potential coulometry (E_w = −1.0 V) shows that the reduction process involves one electron/molecule. The CV diagnostic criteria indicate that the redox change is complicated by slow degradation of the reduced species, while the large peak-to-peak separation (at 0.02 V s^{-1} ΔE_p is equal to 109 mV) suggests that a significative structural reorganization accompanies the one-electron addition. Consistently, the electrogenerated blue complex (triphos)Rh{η^4-S(C_6H_4)CH(CH_2CPh_3)} (**4**) is sufficiently stable ($t_{1/2} \cong 10$ s) to be characterized by ESR spectroscopy, but quantitatively converts in solution to the yellow starting complex **1** by homolytic C−C bond cleavage.

The driving force which makes C−C bond cleavage in **4** prevail over C−H bond cleavage is most likely due to the greater stability of the trityl radical as compared to H•. Although rarer than redox-promoted C−H bond cleavage reactions, examples of homolytic C−C bond scissions have also been reported.[32]

In conclusion, with the exception of the product responsible for peak C in Figure 1a (so far unidentified), all the redox-induced chemical transformations which follow the first oxidation step of **1** have been rationalized. It remains now to discuss the fate of the two-electron oxidized product **1**$^{2+}$.

As previously shown, the dication **1**$^{2+}$ is fairly stable in solution even at room temperature. However, on long standing ($t_{1/2} \cong 15$ s), it decomposes to give a red solution containing the product responsible for the peak system G/H of Figure 1a. Since this product is fully stable in solution, its preparation by chemical oxidation of **1** in THF with 2 equiv of $AgPF_6$ has been successful (Scheme 6). From this reaction, in fact, a diamagnetic red crystalline compound is obtained in quantitative yield which displays a reduction process in CH_2Cl_2 exactly in correspondence to the peak system G/H of Figure 1a with identical CV features (Figure 2c).

The diamagnetism of the compound obtained by two-electron oxidation of **1** has allowed its unambiguous

Scheme 6

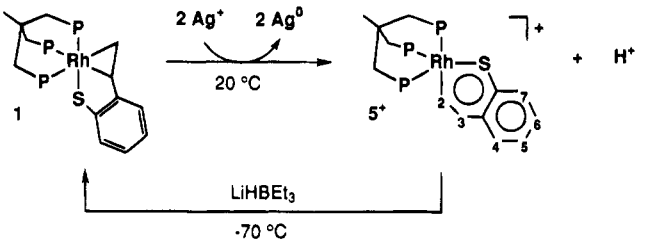

characterization by multinuclear NMR spectroscopy as the rhodabenzothiabenzene complex [(triphos)Rh(η^2-*C*,*S*-C_8H_6S)]PF_6 (**5PF$_6$**).

Compound **5PF$_6$** exhibits NMR parameters which are fully comparable with those of the iridium derivative [(triphos)Ir(η^2-*C*,*S*-C_8H_6S)]BPh_4 recently authenticated by an X-ray diffraction analysis.[4b] In particular, like the Ir analog, the rhodium complex is stereochemically nonrigid on the NMR timescale. At room temperature, the $^{31}P\{^1H\}$ NMR spectrum consists of a broad resonance centered at 27 ppm (A_3X spin system), while the slow exchange AM_2X regime is attained already at −50 °C [J(PP) = 23.3, $J(P_ARh)$ = 69.8, and $J(P_MRh)$ = 104.6 Hz]. As previously suggested on the basis of a computer simulation of the dynamic spectra of the iridium congener, the magnetic equivalence of the three phosphorus atoms of **5**$^+$ can be interpreted in terms of a non-bond-breaking interconversion between trigonal-bipyramidal and square-pyramidal structures. The spectrum in the slow exchange regime is consistent with a trigonal-bipyramidal geometry which, in fact, is the preferred one by the iridium analog in the solid state.[4b] The positions of C_2 (δ 173.4) in the $^{13}C\{^1H\}$ NMR spectrum and of the methyne hydrogens H_2 and H_3 (δ 8.04 and 8.13, respectively) in the ^1H NMR spectrum are in the proper range for delocalized six-membered metallathia rings[4a,5c] and match very close those found for the related iridium complex [δ 162.1 (C_2), 8.33 (H_2), 8.26 (H_3)].[4b] Conclusive experimental evidence in favor of the proposed structure of **5**$^+$ is provided by the reaction of isolated [**5**]PF_6 in THF with $LiHBEt_3$ which quantitatively gives the 2-vinylthiophenolate precursor **1**. By analogy with the same reaction of the iridabenzothiabenzene derivative,[4b,e] the formation of **1** most likely proceeds *via* a rhodium hydride intermediate, (triphos)-

(32) Connelly, N. G. in *Paramagnetic Organometallic Species in Activation Selectivity, Catalysis*; Chanon, M., Julliard, M., Poite, J. C., Eds.; Kluwer Academic Publishers: Holland, 1989.

Table 1. Formal Electrode Potentials (V, *vs* SCE) and Peak-to-Peak Separations (mV) for the Redox Changes Exhibited by the Present Complexes in CH_2Cl_2 Solution

rhodium			iridium		
redox change	$E^{\circ\prime}$	ΔEp^a	redox change	$E^{\circ\prime}$	ΔEp^a
$\mathbf{1/1^+}$	+0.04	84	$\mathbf{2/2^+}$	+0.09	66
$\mathbf{1^+/1^{2+}}$	+0.39	70	$\mathbf{2/2^{2+}}$	+0.32	87
***anti*-3$^+$/*anti*-3**	−0.40[b]	–	***anti*-6$^+$/*anti*-6**	−0.50[b]	–
***syn*-3$^+$/*syn*-3**	−0.88	72	***syn*-6$^+$/*syn*-6**	−0.89	72
$\mathbf{4^+/4}$	−0.79	111			
$\mathbf{5^+/5}$	−0.78	66	$\mathbf{7^+/7}$	−1.04	74

[a] Measured at 0.2 V s^{-1}. [b] Peak potential value for irreversible process.

$RhH(\eta^2\text{-}C,S\text{-}C_8H_6S)$, characterized by a localized electronic structure in the metallathiacycle (a double bond between C_2 and C_3).[4b] Like the Ir analog, the Rh hydrido complex rearranges to the 2-vinylthiophenolate complex by reductive coupling between the terminal hydride and the vinyl C_2 carbon atom. The energy barrier to this process is apparently much lower for rhodium than for iridium as no intermediate species was seen on the NMR timescale even when the reaction between $\mathbf{5PF_6}$ and $LiHBEt_3$ was carried out at −70 °C, whereas the hydride complex (triphos)$IrH(\eta^2\text{-}C,S\text{-}C_8H_6S)$ can be isolated at low temperature.[4b,e]

The transformation of $\mathbf{1^{2+}}$ into the rhodabenzothiabenzene complex $\mathbf{5^+}$ necessarily involves the loss of a proton from the dication, which, in fact, has experimentally been observed when the reaction between **1** and 2 equiv of Ag^+ was carried out in the presence of a proton scavenger such triethylamine.

Redox-induced heterolytic C−H bond cleavages resulting in H^+ elimination are well known in the literature. As an example, treatment of $Ru_2(\mu\text{-}CO)(\mu\text{-}CH_2)(\mu\text{-}dppm)Cp_2$ with 2 equiv of $[FeCp_2]^+$ as oxidant gives $Ru_2(\mu\text{-}CO)(\mu\text{-}CH)(\mu\text{-}dppm)Cp_2$ and H^+.[33]

As is evident from the electrochemical studies, $\mathbf{5^+}$ (either isolated or electrogenerated) displays a reduction process in correspondence to the peak-system G/H. The cyclic voltammetric features and the results of a controlled potential coulometry experiment are all consistent with a chemically and electrochemically reversible one-electron addition. As a matter of fact, the complex (triphos)$Rh(\eta^2\text{-}C,S\text{-}C_8H_6S)$ (**5**) can be electrogenerated in CH_2Cl_2 at $E_w = -1.0$ V, and this neutral species is rather long-lived under inert atmosphere ($t_{1/2} \cong 15$ s) to be characterized by ESR spectroscopy.

The formal electrode potentials for the redox changes exhibited by the rhodium complexes isolated or electrogenerated are summarized in Table 1.

Electrochemistry of the 2-Vinylthiophenolate Iridium complex [(triphos)Ir(η^3-S(C_6H_4)CH=CH_2)] (2) and Characterization of Its Redox Products. Figure 3a shows that the neutral complex **2**[4b] gives rise to a cyclic voltammetric picture rather similar to that shown by the rhodium analog **1**, the only significant difference being the presence of the peak-system (I/L) already in the reverse scan (Figure 1a). Peak F, which, as above discussed, is due to the chemical rearrangement of the one-electron oxidized product, is significantly more intense than in Figure 1a (correspondingly, the height of peak B is much lower than that of peak A, while an $i_p(A)/i_p(B)$ ratio of *ca.* 2.5 is observed at a scan rate of 0.2 V s^{-1}). Also, unlike the rhodium congener, comparable peak heights for the two one-electron steps $\mathbf{2/2^+}$ and $\mathbf{2^+/2^{2+}}$ are not observed even at high scan rates (the $i_p(A)/i_p(B)$ ratio is 1.5 at 10.24 V s^{-1}). These data are thus consistent with a faster chemical rearrangement of the electrogenerated monocation $[(triphos)Ir(\eta^3\text{-}S(C_6H_4)CH{=}CH_2)]^+$ ($\mathbf{2^+}$) as compared to the rhodium analog $\mathbf{1^+}$.

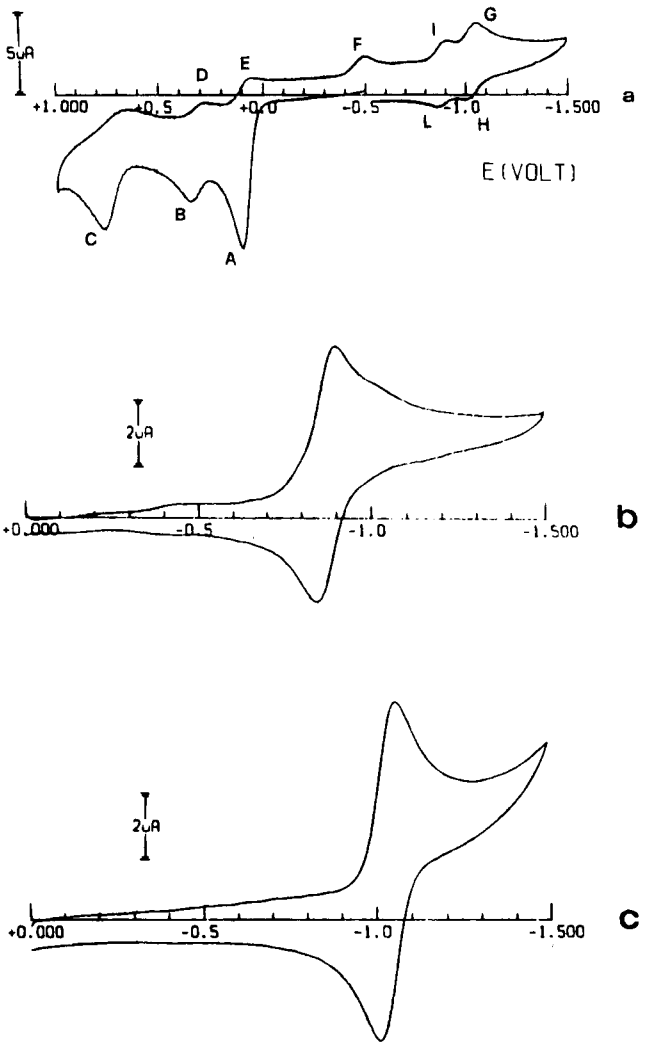

Figure 3. Cyclic voltammetric responses recorded at a platinum electrode on a CH_2Cl_2 solution containing $[NBu_4]ClO_4$ (0.2 mol dm^{-3}) and (a) **2** (0.8×10^{-3} mol dm^{-3}); (b) $\mathbf{6PF_6}$ (0.4×10^{-3} mol dm^{-3}); (c) $\mathbf{7PF_6}$ (0.6×10^{-3} mol dm^{-3}). Scan rate 0.1 V s^{-1}.

Apart from the different stabilities of some electrogenerated products (see below), the overall scheme of the redox-induced transformations of **2** is analogous to that of the rhodium congener **1** (Scheme 3). The monocation $\mathbf{2^+}$ converts to the 2-ethylidenecyclohexadienethione complex *anti*-[(triphos)Ir{η^4-S(C_6H_4)CH(CH_3)}]$^+$ (***anti*-6$^+$**) (peak F) by abstraction of a hydrogen atom from the environment. The *anti*-complex rearranges in solution to the thermodynamically stable isomer *syn*-[(triphos)Ir{η^4-S(C_6H_4)CH(CH_3)}]$^+$ (***syn*-6$^+$**), which can reversibly be reduced to the neutral paramagnetic derivative *syn*-(triphos)Ir{η^4-S(C_6H_4)CH(CH_3)} (***syn*-6**). In turn, the dication $\mathbf{2^{2+}}$ loses a proton convert-

(33) (a) Connelly, N. G.; Forrow, N. J.; Gracey, B. P.; Knox, S. A. R.; Orpen, A. G. *J. Chem. Soc., Chem. Commun.* **1985**, 14. (b) Connelly, N. G.; Forrow, N. J.; Knox, S. A. R.; Macpherson, K. A.; Orpen, A. G. *J. Chem. Soc., Chem. Commun.* **1985**, 16.

Table 2. X-Band ESR Parameters for the Present Complexes in CH_2Cl_2

	100 K					100 K				
complex	$g_l^{a,b}$	$g_m^{a,b}$	$g_h^{a,b}$	$\langle g\rangle^{a,c}$	300 K g_{iso}^{a}	$a_l^{b,d}$	$a_m^{b,d}$	$a_h^{b,d}$	$\langle a\rangle^{c,d}$	300 K a_{iso}^{d}
***syn*-3**	2.091	2.008	1.997	2.032	2.033	<30	<30	<30	<30	<30
5	2.088	2.009	1.998	2.032	2.033	<25	<20	<20	<22	<25
$\mathbf{1}^+$	2.080		2.018[e]	2.056	2.058	145		175[f]	155	155
										15
4	2.094	2.008	2.003	2.035	2.032	<30		<30	<30	<25
***syn*-6**	2.151	2.003		2.052	2.047	<30		<25	<30	<35
7A	2.116		1.928	2.053	2.050	197		231	208	228
						31		22	<28	<25
						26		18	<23	<25
7B	2.121		1.908	2.050	2.043	199		229	209	232
						31		22	<28	<25
						26		18	<23	<25

[a] ±0.005. [b] $g_l = g_m = g_\perp$, $g_h = g_\parallel$, $a_l = a_m = a_\perp$ and $a_h = a_\parallel$ for $\mathbf{1}^+$, **4**, **7A**, and **7B**. [c] $\langle g\rangle = 1/3(g_l + g_m + g_h)$, $= 1/3(g_\parallel + 2g_\perp)$; $\langle a\rangle = 1/3(a_l + a_m + a_h)$, $= 1/3(a_\parallel + 2a_\perp)$; l = low, m = medium, h = high. [d] ±3 G. [e] Evaluated from g_{iso} and $g_\perp$ calculations. [f] Evaluated from a_{iso} and $a_\perp$ calculations.

ing to the iridabenzothiabenzene [(triphos)Ir(η^2-*C*,*S*-C_8H_6S)]$^+$ ($\mathbf{7}^+$), which is reversibly reduced to the neutral derivative (triphos)Ir(η^2-*C*,*S*-C_8H_6S) (**7**).

When possible, all the redox products of **2** have been identified with the use of isolated compounds in independent electrochemical and/or chemical reactions. In particular, the complexes *syn*-[(triphos)Ir{η^4-S(C_6H_4)-$CH(CH_3)$}]PF_6 (**6PF$_6$**) and [(triphos)Ir(η^2-*C*,*S*-C_8H_6S)]-PF_6 (**7PF$_6$**) have been prepared according to published procedures[4b] and their redox properties compared with those of analogous products obtained by one- or two-electron oxidation of **2** (Figure 3). The paramagnetic complexes ***syn*-6** and **7** were characterized by ESR spectroscopy, whereas the inherent instability of $\mathbf{2}^+$ precluded its characterization.

The formal electrode potentials for the redox changes exhibited by the iridium complexes isolated or electrogenerated are summarized in Table 1. An inspection of the redox data shows that both oxidation steps of the starting Ir complex **2** occur at about the same potential values of the rhodium analog **1**, whereas a significant difference (*ca.* 0.3 V) is found only for the reduction of the metallabenzothiabenzene complexes $\mathbf{5}^+$ and $\mathbf{7}^+$.

Electron Spin Resonance of the Paramagnetic Rhodium and Iridium Complexes. Upon one- or two-electron oxidation of the 2-vinylthiophenolate complexes **1** or **2** in CH_2Cl_2, as many as three paramagnetic products each are directly or indirectly generated (Scheme 3). Five of these are sufficiently long-lived in solution to be characterized by X-band ESR spectroscopy: the Rh complexes $\mathbf{1}^+$, **syn-3** and **5**, and the Ir complexes **syn-6** and **7** (Table 2).

Rhodium Complexes. The room-temperature spectrum of $\mathbf{1}^+$ in CH_2Cl_2 solution is shown in Figure 4 (a, first derivative; b, second derivative).

The spectrum can confidently be interpreted in terms of a $S = {}^1/_2$ spin Hamiltonian. The ESR parameters are consistent with the presence of one unpaired electron localized on the metal center ($g_{iso} > g_e$) and strongly interacting with one phosphorus nucleus of triphos. The second derivative spectrum clearly shows two very different superhyperfine (shpf) ^{31}P couplings (155 and 15 G), which indicates that, like the diamagnetic precursor, $\mathbf{1}^+$ is not fluxional in solution even on the ESR timescale[34,35] (hyperfine (hpf) couplings to the ^{103}-Rh nucleus ($I = {}^1/_2$) are generally small or not visible in Rh(II) complexes with triphos).[34]

The spectrum at liquid nitrogen temperature yields

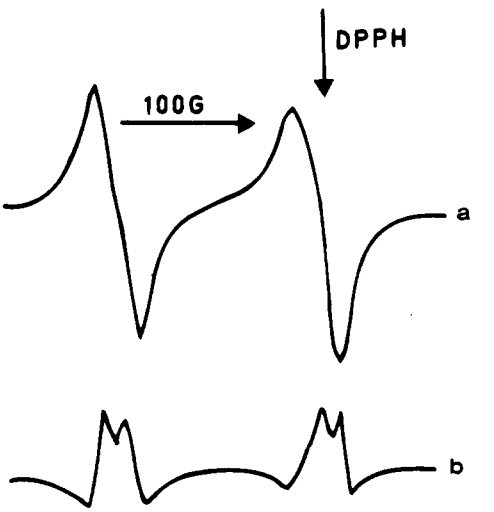

Figure 4. X-band ESR spectrum of $\mathbf{1}^+$ at 300 K (a), second derivative (b).

little additional information as it consists of a broad and partially resolved axial lineshape ($g_\parallel < g_\perp$). The large ^{31}P shpf coupling, still observed in the spectrum at 100 K, indicates that no major structural changes occur in going from fluid to glassy solution.

The neutral precursor **1** has previously been assigned an octahedral structure in which the Rh center is coordinated by a *fac* triphos ligand, a strongly bound double bond and a thiolate sulfur atom.[4c] Since the electrochemical properties relative to the $\mathbf{1}/\mathbf{1}^+$ redox step indicate an electrochemically reversible process, the monocation $\mathbf{1}^+$ is expected to maintain the primary geometry of the neutral precursor. Indeed, the large coupling constants observed in both the fluid and frozen solution spectra are consistent with a strong interaction of the unpaired electron with a phosphorus donor which faces the SOMO, as occurs for a low-spin d^7 metal ion in octahedral geometry (d_z2 SOMO).[36] A significant distortion from the idealized geometry, imposed by the Jahn–Teller effect, is confirmed by the coupling of the unpaired electron to one basal phosphorus only (15 G).

Mononuclear Rh(II) complexes are quite rare because

(34) Bianchini, C.; Peruzzini, M.; Laschi, F.; Zanello, P. In *Topics in Physical Organometallic Chemistry*; Gielen, M. F., Ed.; Freund Publishing House LTD.: London, 1992; Vol. 4, p 139.
(35) Bianchini, C.; Frediani, P.; Laschi, F.; Meli, A.; Vizza, F.; Zanello, P. *Inorg. Chem.* **1990**, *29*, 3402.
(36) Dunbar, K. R.; Haefner, S. C.; Pence, L. E. *J. Am. Chem. Soc.* **1989**, *111*, 5504 and references therein.

of their propensity for dimerization.[37] For this reason, most of the known mononuclear Rh(II) complexes are stabilized by bulky ligands among which tripodal polyphosphines with phenyl substituents play a predominant role.[34,36] A few Rh(II) compounds have been authenticated by X-ray analyses: the square-planar complexes $[Rh(MNT)_2]^{2-}$ [MNT = maleonitriledithiolate][38] and $[Rh(C_6Cl_5)_2\{P(OPh)_3\}_2]$,[39] and the distorted octahedral cation $[Rh(TMPP)_2]^{2+}$ [TMPP = tris(2,4,6-trimethoxyphenyl)phosphine].[36] Interestingly, the ESR spectrum of the latter complex exhibits axial symmetry with a d_z2 ground state.

The ESR spectra of the rhodium complexes ***syn*-3** and **5** are similar to each other and, like that of $\mathbf{1}^+$, can be interpreted in terms of a $S = {}^1/_2$ spin Hamiltonian with the unpaired electron localized on the metal center. In actuality, the method of formation of the two compounds is consistent with a different formal oxidation state of the metal: +2 in **5** and 0 in ***syn*-3**.

The spectral lineshapes of both compounds as a glass display three groups of anisotropic signals with $g_l > g_m > g_h$. Analogous rhombic structure and spectral parameters characterize the ESR spectrum of the Rh(0) complex **4**, which differs from ***syn*-3** only for the trityl substituent on the ylidene moiety. All glassy spectra are characterized by the absence of detectable couplings to either P or Rh nuclei (only upper limits for the magnetic couplings may be calculated from the linewidth of the signals).

As the temperature of the paramagnetic samples is increased, the intensities of the signals significantly decrease for ***syn*-3**, **4**, and **5**. The process is reversible with the temperature. At the glassy-fluid transition, the spectra consist of weak and relatively broard isotropic signals ($g_{av} = 2.033$) which reflect a large geometrical distortion of the coordination polyhedra.

As already mentioned, tripodal polyphosphine ligands such as triphos or $P(CH_2CH_2PPh_2)_3$ (PP_3) are capable of stabilizing a large number of mononuclear and dinuclear Rh(II) compounds,[34,40,41] while only one Rh(0) complex, namely the dimer (triphos)Rh(μ-CO)$_2$Rh(triphos), has been described.[42] All known mononuclear Rh(II) complexes with triphos or PP_3 are five-coordinate and generally exhibit distorted square-pyramidal structure,[34] although some examples of trigonal-bipyramidal compounds have also been reported.[40] The frozen-solution ESR spectra of the square-pyramidal complexes invariably show axial structure with a d_z2 ground state and are characterized by a strong magnetic interaction of the unpaired electron with one phosphorus nucleus of the polyphosphine ligand ($a_\perp \cong 210-213$ G; $a_{||} \cong 249-262$ G).[34] The rhombic structure and the absence of such a large coupling constant in the frozen solution spectra of **5** is thus suggestive of a trigonal-bipyramidal structure[40] which, in fact, is the structure adopted by the diamagnetic precursor $\mathbf{5}^+$ in solution at low temperature.

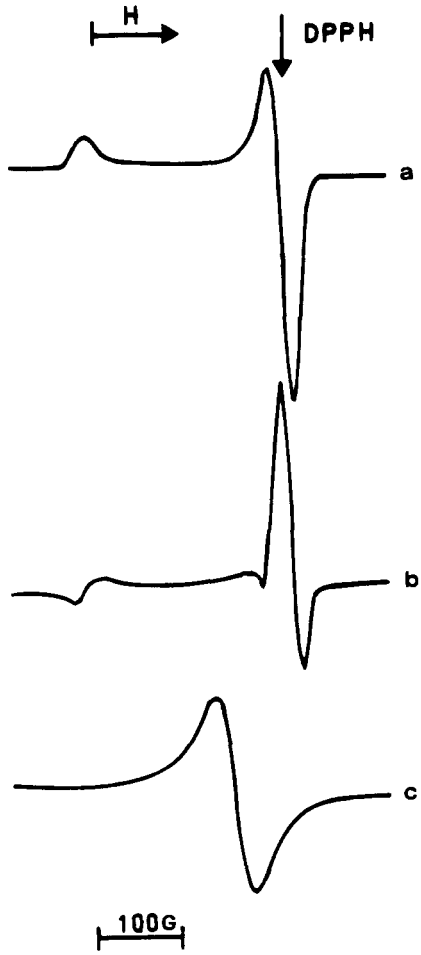

Figure 5. X-band ESR spectra of ***syn*-6** at 100 K (a), second derivative (b), and at 300 K (c).

By analogy with the ESR parameters (Table 2), a trigonal-bipyramidal structure may be assigned also to the Rh(0) complexes ***syn*-3** and **4** at low temperature. In actuality, based on low-temperature ^{31}P NMR studies, the diamagnetic precursors ***syn*-3**$^+$ and $\mathbf{4}^+$ have been assigned distorted square-pyramidal structures.[4c] Both compounds, however, are fluxional in solution where a low energy process allows a fast exchange between square-pyramidal and trigonal-bipyramidal structures.[43] The addition of one electron apparently stabilizes the trigonal-bipyramidal geometry.

Iridium Complexes. Figure 5 shows the X-band ESR spectra of the electrogenerated Ir(0) complex ***syn*-6** recorded at 100 K (a, first derivative; b, second derivative) and at room temperature (c) in CH_2Cl_2 solution.

Like the Rh analog ***syn*-3**, the remarkable orbital contribution of the Ir unpaired spin system causes extensive broadening of the anisotropic signals and the corresponding g_{aniso} values significantly differ from that of the free electron ($g_{iso} = 2.0023$).

(37) (a) Serpone, N.; Jamieson, M. A. In *Comprehensive Coordination Chamistry*; Wilkinson, G., Gillard, R. D., Mc Cleverty, J. A., Eds.; Pergamon Press: Oxford, U. K. 1987; Vol. 4, p. 1120. (b) Felthouse, T. R. *Prog. Inorg. Chem.* **1982**, *29*, 73 and references therein. (c) Boyar, E. B.; Robinson, S. D. *Coord. Chem. Rev.* **1983**, *50*, 109 and references therein.

(38) Billig, E.; Shupack, S. I.; Waters, J. H.; Williams, R.; Gray, H. B. *J. Am. Chem. Soc.* **1964**, *86*, 926.

(39) Garcia, M. P.; Jiménez, M. V.; Oro, L. A.; Lahoz, F. J.; Casas, J. M.; Alonso, P. *Organometallics* **1993**, *12*, 3257.

(40) Bianchini, C.; Laschi, F.; Masi, D.; Ottaviani, F. M.; Pastor, A.; Peruzzini, M.; Zanello, P.; Zanobini, F. *J. Am. Chem. Soc.* **1993**, *115*, 2723.

(41) Barbaro, P.; Bianchini, C.; Linn, K.; Mealli, C.; Meli, A.; Vizza, F. *Inorg. Chim. Acta* **1992**, *198–200*, 31.

(42) Cecconi, F.; Ghilardi, C. A.; Midollini, S.; Orlandini, A.; Zanello, P.; Heaton, B. T.; Huang, L.; Iggo, J. A.; Bordoni, S. *J Organomet. Chem.* **1987**, *353*, C5.

(43) (a) Bianchini, C.; Masi, D.; Mealli, C.; Meli, A.; Martini, G.; Laschi, F.; Zanello, P. *Inorg. Chem.* **1987**, *26*, 3683. (b) Rossi, A. R.; Hoffmann, R. *Inorg. Chem.* **1975**, *14*, 365.

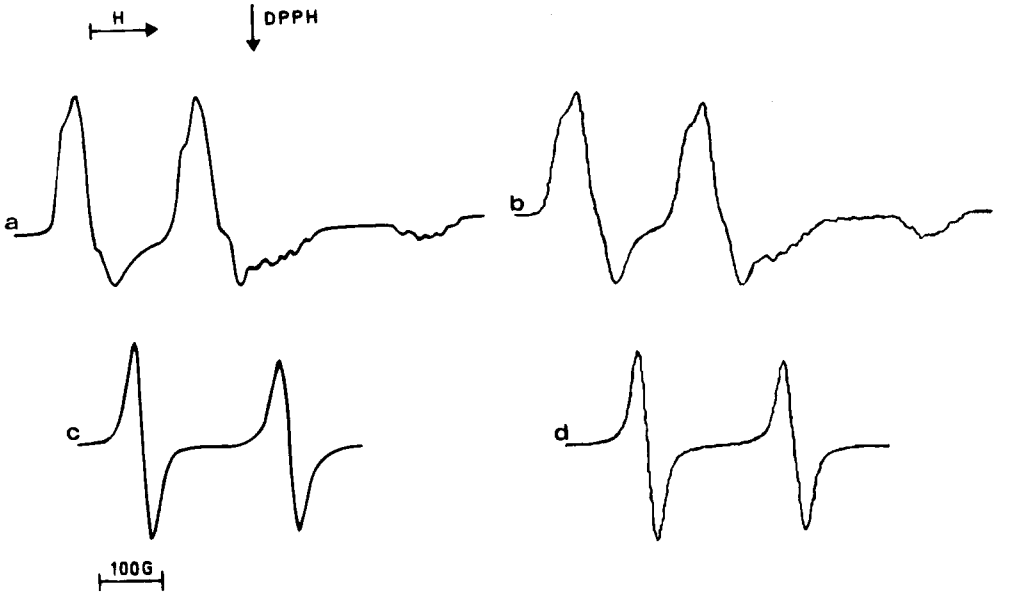

Figure 6. X-band ESR spectra of **7** at 100 K [experimental (a), computed (b)] and at 300 K [experimental (c), computed (d)].

The lineshape analysis of the glassy absorption pattern can be carried out in terms of a $S = {}^1/_2$ spin Hamiltonian, consistent with a low-spin d^7 metal ion. The second derivative spectrum and a computer simulation procedure[44] allow one to interpret the liquid nitrogen spectrum in terms of a well resolved axial symmetry ($g_{\parallel} > g_{\perp}$) with one unpaired electron localized on the metal center. A significant line-broadening effect largely biases the spectral anisotropic features and reflects the asymmetry of the overall coordination polyhedron. Neither hpf coupling of the electron to the ^{191}Ir and ^{193}Ir nuclei ($I = {}^3/_2$) nor shpf coupling to the ^{31}P nuclei is observed. Accordingly, only an upper limit for such magnetic interactions, if any, can be estimated from the corresponding anisotropic linewidths.

At the glassy-fluid transition phase, the axial spectrum evolves to the relevant unresolved isotropic one, with g_{iso} (190 K) = 2.038 ± 0.008 and ΔH_{iso} (190 K) = 55 ± 5 G. Raising the temperature, the signal sharpens (c) [ΔH_{iso} (300 K) = 35 ± 5 G], likely due to fast molecular dynamics which mediate the original anisotropies. Correspondingly, the g_{iso} value raises to 2.047 ± 0.005 at 300 K. This value well matches the calculated ⟨g⟩ value at 100 K [$^1/_3(g_{\parallel} + 2g_{\perp})$] and confirms that the complex maintains the same structure in the temperature range investigated.

From these data we can conclude that ***syn*-6** has a structure similar to that of the Rh analog ***syn*-3**, namely distorted trigonal-bipyramidal.

Figure 6 shows the X-band ESR spectra of the iridabenzothiabenzene complex **7** in CH_2Cl_2 at different temperatures. The glassy spectrum (Figure 6a) displays a complex lineshape, particularly broadened in the high-field regions. On the basis of computer simulation procedures,[42] the glassy spectrum can be interpreted in terms of a $S = {}^1/_2$ spin Hamiltonian with a well resolved metal-in-character axial structure ($g_{\parallel} < g_{\perp}$). Both the $g_{\perp}$ and $g_{\parallel}$ regions show shpf resolution with one large anisotropic splitting attributable to the strong magnetic coupling of the electron with one P nucleus and a less intense coupling to two slightly different P nuclei. Interestingly, the high-field parallel region exhibits a broad pseudo-quintuplet, resulting from the partial overlapping of two nearly equivalent 1:2:1 triplets. This spectral behavior can be interpreted assuming the presence of two geometric isomers, **7A** and **7B** (see below), with a slight prevalence of species A, characterized by similar g_{aniso} values (Table 2).

At the glassy-fluid transition, the axial structure collapses in a broad isotropic doublet with g_{iso} (190 K) = 2.056 ± 0.005 and a_{iso} (P) = 220 ± 5 G. The isotropic spectrum remains unaltered in the temperature range from 180 to 330 K where the magnetic parameters are in good agreement with the averaged anisotropic ones (Figure 6c). At higher temperature, the fluid solution doublet broadens [ΔH (330 K) = 30 ± 5 G] losing both spectral intensity and shpf resolution, while the g_{iso} value slightly decreases. Like ***syn*-6**, compound **7** displays ESR reversibility in the overall temperature range investigated. The observation of a broad doublet in fluid solution, which can properly be simulated only by assuming the presence of two isomers (Figure 6d), suggests that species **7A** and **7B** still exist at room temperature.

As previously mentioned, the diamagnetic precursor of **7** adopts a trigonal-bipyramidal structure in the solid state.[4b] In solution $\mathbf{7}^+$ is fluxional on the NMR timescale. The magnetic equivalence of the three phosphorus atoms of triphos in the fast exchange regime (^{31}P NMR A_3 spin system) is due to a fast interconversion between trigonal-bipyramidal and square-pyramidal structures which are separated by a very low energy barrier.[43] The glassy ESR spectra of **7A** and **7B** are unequivocally consistent with a distorted square-pyramidal structure such as that of the related Ir(II) complex (triphos)Ir(DBTC) (DBTC = 3,5-di-*tert*-butylcatecholate), which shows fully comparable ESR parameters.[41] It is therefore reasonable to conclude that, unlike the Rh analog **5**, the addition of one electron to $\mathbf{7}^+$ tips the balance in favor of the square-pyramidal structure.

ESR evidence for the existence of geometric isomers is not surprising for five-coordinate low-spin d^7 metal

(44) Lozos, G. P.; Hoffman, B. M.; Franz, C. G. *QCPE* **1974**, *11*, 265.

complexes with tripodal polyphosphine ligands, particularly when they adopt a distorted square-pyramidal structure and contain two different donor atoms in the basal plane.[34,40,45] Consistently, although it is only speculation, the difference between **7A** and **7B** may be caused by slightly different Jahn–Teller distortions related to the asymmetry of the cleaved **BT** ligand, which has a sulfur and a carbon atom bound to the metal.

Mononuclear Ir(II) complexes are a rarity,[46] although in the last few years some work has been done on the subject.[41,47,48] Single crystal X-ray structure determinations have been reported for the square-planar complexes $[Ir(mes)_2(SEt_2)_2]$[47] (mes = mesityl) and $[Ir(C_6Cl_5)_4]^{2-}$.[48]

Conclusions

We have previously shown that the thermally generated 16-electron fragments [(triphos)MH] (M = Rh, Ir) readily react with **BT** by a ring-opening C–S bond scission reaction to ultimately yield 2-vinylthiophenolate derivatives (triphos)M{η^3-S(C_6H_4) CH=CH_2} (M = Rh,[4c] **1**; Ir,[4b,e] **2**). These complexes display a rich redox-induced reactivity; by using a combination of chemical reactions, electrochemical studies, and EPR and NMR spectroscopic methods it has been possible to understand in depth a series of transformations that take place once the redox processes are initiated. The redox-induced transformations of the cleaved and partially reduced **BT** molecule include both homolytic and heterolytic C–H bond cleavage and formation.

In particular, removal of one electron from **1** or **2** leads to the corresponding paramagnetic cations $\mathbf{1}^+$ and $\mathbf{2}^+$; these complexes are rather unstable and undergo a radical reaction with H• in solution to form, as the kinetic products, the diamagnetic 2-ethylidenecyclohexadienethione compounds *anti*-[(triphos)M{η^4-S(C_6H_4)-CH(CH_3)}]$^+$ (M = Rh, ***anti*-3**$^+$; Ir, ***anti*-6**$^+$) which isomerize to the thermodynamically stable ***syn*-3**$^+$ (Rh) and ***syn*-6**$^+$ (Ir). Addition of one electron to ***syn*-3**$^+$ and ***syn*-6**$^+$ gives the neutral paramagnetic derivatives *syn*-[(triphos)M{η^4-S(C_6H_4)CH(CH_3)}] (M = Rh, ***syn*-3**; Ir, ***syn*-6**) which spontaneously convert back to the starting complexes **1** and **2** by a homolytic C–H bond cleavage liberating H•. In this way a full electrochemical cycle is completed by addition/elimination of one electron and one H atom. The radical nature of the C–H bond cleavage undergone by ***syn*-3** was confirmed by the redox chemistry of the related complex [(triphos)Rh{η^4-S(C_6H_4)CH(CH_2CPh_3)}]PF_6 (**4PF$_6$**), which induces loss of a trityl radical by a C–C bond cleavage reaction in the paramagnetic neutral derivative **4**.

On the other hand, removal of a second electron from $\mathbf{1}^+$ or $\mathbf{2}^+$ leads to the corresponding dicationic species $\mathbf{1}^{2+}$ and $\mathbf{2}^{2+}$, which undergo a heterolytic C–H bond splitting to lose a proton and produce the cationic metallabenzothiabenzene complexes [(triphos)M(η^2-*C*,*S*-C_8H_6S)]$^+$ (M = Rh, $\mathbf{5}^+$; Ir, $\mathbf{7}^+$). Although the Ir derivative $\mathbf{7}^+$ has previously been prepared by chemical methods,[4b] the Rh analogue seems to be available only by the electrochemical route herein described. Finally, additon of one electron to the monocationic complexes $\mathbf{5}^+$ and $\mathbf{7}^+$ produces the corresponding paramagnetic metallabenzothiabenzene complexes [(triphos)M(η^2-*C*,*S*-C_8H_6S)] (M = Rh, **5**; Ir, **7**).

In conclusion, the homogeneous modeling study reported in this paper provides new information which may contribute a better understanding of the mechanisms of HDS reactions on the surfaces of solid catalysts. One- and two-electron transfer processes have often been invoked to account for the activity of some Mo sites of HDS catalysts, as well as for the promoting effects of Co or Ni sites. Furthermore, the presence or possible formation of surface H•, H^+, and H^- species, associated with either the metal or the sulfur sites of the catalysts has long been recognized in the HDS literature. Thus the redox-induced reactions of ring-opened **BT** ligands identified in this paper are of particular interest since analogous transformations and species are to be expected also on HDS-active surfaces.

Acknowledgment. A grant to M.V.J. from Ministerio de Educatión y Ciencia (Spain) is gratefully acknowledged. C.B. thanks Progetto Strategico "Tecnologie Chimiche Innovative", CNR, Rome (Italy) for financial support.

OM950448M

(45) Bianchini, C.; Meli, A.; Peruzzini, Vacca, A.; Laschi, F.; Zanello, P.; Ottaviani, M. F. *Organometallics* **1990**, *9*, 360.

(46) Jardine, F. H.; Sheridan, P. S. In *Comprehensive Coordination Chamistry*; Wilkinson, G., Gillard, R. D., Mc Cleverty, J. A., Eds.; Pergamon Press: Oxford, U. K. 1987; Vol. 4, p 930.

(47) Danopoulos, A. A.; Wilkinson, G.; Hussain-Bates, B.; Hursthouse, M. B. *J. Chem. Soc., Dalton Trans.* **1992**, 3165.

(48) Garcia, M. P.; Jiménez, M. V.; Oro, L. A.; Lahoz, F. J.; Camellini Tiripicchio, M.; Tiripicchio, A. *Organometallics* **1993**, *12*, 4660.

Syntheses, Characterization, Crystal and Molecular Structures, and Solution Properties of $Et_2Ga(C_5H_5)$ and $EtGa(C_5H_5)_2$

O. T. Beachley, Jr.,* Daniel B. Rosenblum, Melvyn Rowen Churchill,* Charles H. Lake, and Lynn M. Krajkowski

Department of Chemistry, State University of New York at Buffalo, Buffalo, New York 14260

Received April 21, 1995[⊗]

The compounds $Et_2Ga(C_5H_5)$ and $EtGa(C_5H_5)_2$ have been prepared by ligand redistribution reactions in pentane solution between appropriate quantities of $GaEt_3$ and $Ga(C_5H_5)_3$. Both compounds have been fully characterized by elemental analyses, X-ray structural studies, cryoscopic molecular weight studies in benzene solution, mass spectroscopic studies, ^1H NMR studies of solutions, and ^1H NMR studies of melts. Both compounds exist as pure single compounds in the solid state. The compound $[Et_2Ga(C_5H_5)]_\infty$ crystallizes in the centrosymmetric triclinic space group $P\bar{1}$ (No. 2) with $a = 7.803(2)$ Å, $b = 15.839(4)$ Å, $c = 16.318(4)$ Å, $\alpha = 101.98(2)°$, $\beta = 95.23(2)°$, $\gamma = 102.72(2)°$, $V = 1904.5(8)$ Å^3, and $Z = 8$ (monomeric units). The structure consists of polymeric chains of $[Ga-C_5H_5]_\infty$ in which each gallium(III) center is linked to two ethyl ligands and is in contact with one carbon atom from each of two bridging C_5H_5 ligands. The other compound $[EtGa(C_5H_5)_2]_\infty$ crystallizes in the noncentrosymmetric orthorhombic space group $P2_12_12_1$ (No. 19) with $a = 8.213(5)$ Å, $b = 9.131(4)$ Å, $c = 14.277(10)$ Å, $V = 1070.7(11)$, and $Z = 4$ (monomeric units). The structure was refined to $R = 7.01\%$ for those 846 reflections above 6σ. This structure is also polymeric with $[Ga-C_5H_5]_\infty$ chains. Each gallium(III) center is also bonded to an ethyl ligand and a terminal η^1-C_5H_5 ligand. When the compounds are dissolved in benzene, toluene, cyclohexane, $CHCl_3$, or THF, ligand redistribution reactions occur to form equilibrium mixtures of species. However, when $[Et_2Ga(C_5H_5)]_\infty$ is melted, ^1H NMR spectral studies suggest the existence of only $Et_2Ga(C_5H_5)$, whereas when $[EtGa(C_5H_5)_2]_\infty$ is melted, a single compound does not exist and a mixture of $EtGa(C_5H_5)_2$, $Et_2Ga(C_5H_5)$, and $Ga(C_5H_5)_3$ is formed instead. Mass spectral studies of $Et_2Ga(C_5H_5)$ are consistent with the presence of $Et_2Ga(C_5H_5)$ in the gas phase, but when $[Et_2Ga(C_5H_5)]_\infty$ is heated and vaporized, uncertainty regarding the identities of the species in the gas phase arises due to the occurrence of the ligand redistribution reactions in the melt.

Heteroleptic organometallic compounds of the heavier group 13 elements have the potential to be novel precursors for the formation of semiconducting materials if different types of organic ligands in a given molecule have different propensities for selective elimination. However, these types of compounds tend to undergo ligand redistribution reactions to form symmetrized products[1,2] if and when an appropriate reaction pathway is available. Since a typical reaction pathway for ligand exchange utilizes a vacant coordination site on the group 13 element,[3] the isolable mixed ligand compounds are associated and have four-coordinate group 13 atoms. However, since the degree of association can change as the phase of the compound changes, it is necessary to characterize a compound as fully and completely as possible in order to prove the existence of a single compound in the solid, liquid, and gas phases and in solution. However, no compound with different organic ligands to our knowledge has been sufficiently characterized to demonstrate its existence in all phases. Only two gallium compounds, $[(t\text{-Bu})(Me_3SiC{\equiv}C)GaPEt_2]_2$[4] and $[Me_2Ga(C{\equiv}CPh)]_2$,[5-7] and six indium compounds, including $\{In[CH(SiMe_3)_2](i\text{-Pr})Cl\}_2$,[8] $[In(CH_2SiMe_3)(CH_2CMe_3)Cl]_2$,[2] $[(Me)(Me_3SiCH_2)InAs(SiMe_3)_2]_2$,[9] $[(Me)(Me_3SiCH_2)InP(SiMe_3)_2]_2$,[9] $[(Me)(Me_3CCH_2)InP(SiMe_3)_2]_2$,[10] and $[(Me_2In(C{\equiv}CMe)]_2$,[11] have been proven to exist in the solid phase and in benzene solution. However, of these compounds, only $[Me_2Ga(C{\equiv}CPh)]_2$ exists as the identical species in the solid and in solution. The other compounds isomerize or change the degree of association upon dissolution. The *trans* isomer in the solid state is converted to a *cis/trans* isomer mixture in solution. Even though only two gallium compounds with two organic substituents have been sufficiently characterized to prove their existence in both the solid and solution phases, other heteroleptic orga-

[⊗] Abstract published in *Advance ACS Abstracts,* August 1, 1995.

(1) Beachley, O. T., Jr.; Royster, T. L., Jr.; Arhar, J. R. *J. Organomet. Chem.* **1992**, *434*, 11.
(2) Beachley, O. T., Jr.; Maloney, J. D.; Churchill, M. R.; Lake, C. H. *Organometallics* **1991**, *10*, 3568.
(3) Wilkinson, G., Stone, F. G. A., Abel, E. W., Eds. *Comprehensive Organometallic Chemistry*; Pergamon Press: Oxford, 1982; Vol. 1, p 588 and references therein.
(4) Lee, K. E.; Higa, K. T.; Nissan, R. A. *Organometallics* **1992**, *11*, 2816.
(5) Jeffery, E. A.; Mole, T. *J. Organomet. Chem.* **1968**, *11*, 393.
(6) Lee, K. E.; Higa, K. T. *J. Organomet. Chem.* **1993**, *449*, 53.
(7) Tecle, B.; Ilsley, W. H.; Oliver, J. P. *Inorg. Chem.* **1981**, *20*, 2335.
(8) Neumüller, B. *Z. Naturforsch.* **1991**, *46b*, 1539.
(9) Wells, R. L.; McPhail, A. T.; Jones, L. J.; Self, M. F. *J. Organomet. Chem.* **1993**, *449*, 85.
(10) Wells, R. L.; McPhail, A. T.; Self, M. F. *Organometallics* **1993**, *12*, 3363.
(11) Fries, W.; Schwarz, W.; Hausen, H.-D.; Weidlein, J. *J. Organomet. Chem.* **1978**, *159*, 373.

0276-7333/95/2314-4402$09.00/0

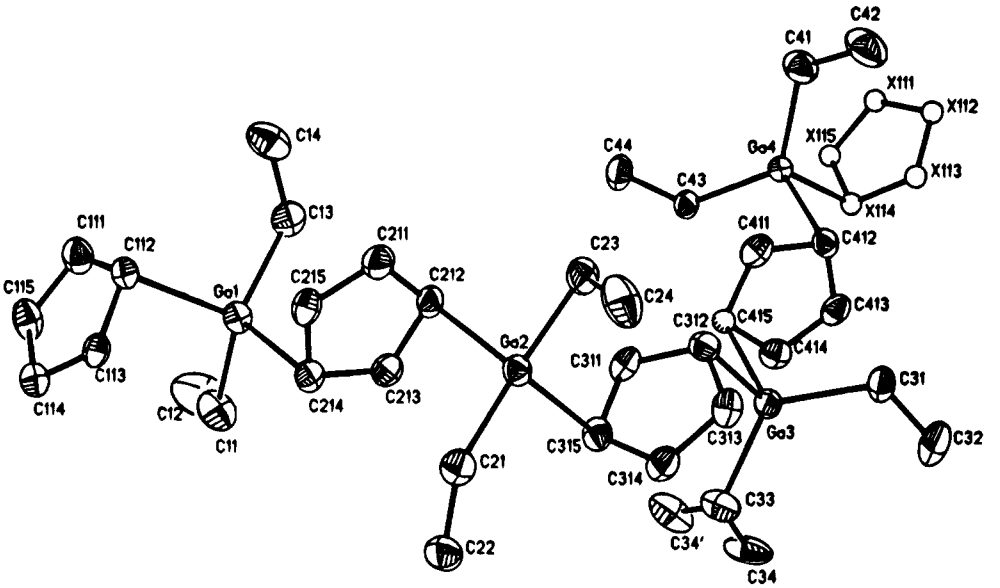

Figure 1. Structure of $[Et_2Ga(C_5H_5)]_\infty$. The figure shows the crystallographic asymmetric unit plus one additional C_5H_5 ligand, labeled X111 → X115 and symmetry-related to the ring C(111) → C(115) by the translation $(\vec{a} + \vec{b})$.

nogallium compounds, including $Me_2Ga(C_5H_5)$,[1,12-14] $Et_2Ga(C_5H_5)$,[12,13] $Me_2Ga(C{\equiv}CMe)$,[11] $Me_2Ga(C{\equiv}CSiMe_3)$,[6] $(t\text{-Bu})_2Ga(C{\equiv}CPh)$,[4] $Me_2Ga(CH{=}CH_2)$,[15] $Me_2Ga(t\text{-Bu})$,[16] and $MeGa(t\text{-Bu})_2$,[16] have been reported in the literature.

The two compounds $Me_2Ga(C_5H_5)$[1,12-14] and $MeGa(C_5H_5)_2$,[1] which are closely related to the ethyl derivatives described in this paper, have been extensively investigated. The compound $Me_2Ga(C_5H_5)$ exists in the solid state as a polymer.[14] The gallium atom is four-coordinate with two terminal methyl groups and cyclopentadienide groups which bridge the gallium atoms through the 1- and 3-positions. The liquid and gaseous phases were not fully characterized. When $[Me_2Ga(C_5H_5)]_\infty$ was dissolved in benzene, CCl_4, and THF, ligand redistribution reactions[1] occurred to form $MeGa(C_5H_5)_2$ and $GaMe_3$, which, in turn, underwent methyl and cyclopentadienide group exchange reactions. Thus, the occurrence of these reactions prevented the direct observation of the ^1H NMR lines of all three individual species. When an attempt was made to prepare $MeGa(C_5H_5)_2$,[1] $Me_2Ga(C_5H_5)$ and $Ga(C_5H_5)_3$ were isolated due to the occurrence of ligand redistribution reactions. Thus, $MeGa(C_5H_5)_2$ could neither be isolated as a single compound nor be characterized.

The level of understanding of organogallium compounds which contain only organic substituents but of two different types has increased significantly with the syntheses and complete characterizations of $Et_2Ga(C_5H_5)$ and of $EtGa(C_5H_5)_2$, a new compound. Both compounds have been prepared by ligand redistribution reactions between appropriate quantities of $GaEt_3$ and $Ga(C_5H_5)_3$ and have been found to exist as single compounds in the solid state as demonstrated by X-ray structural studies. In the liquid and gaseous states, $Et_2Ga(C_5H_5)$ exists as a single compound according to NMR and mass spectral studies, whereas $EtGa(C_5H_5)_2$ is in equilibrium with $Et_2Ga(C_5H_5)$ and $Ga(C_5H_5)_3$ in the melt. However, the situation is very different in solution as both compounds undergo ligand redistribution reactions (eqs 1 and 2) in benzene, toluene, THF,

$$2Et_2Ga(C_5H_5) \rightleftharpoons GaEt_3 + EtGa(C_5H_5)_2 \quad (1)$$

$$2EtGa(C_5H_5)_2 \rightleftharpoons Et_2Ga(C_5H_5) + Ga(C_5H_5)_3 \quad (2)$$

cyclohexane, and $CHCl_3$ (all solvents that were studied) to form symmetrized products. In addition, ligand exchange reactions involving ethyl groups and cyclopentadienide groups also occur but the rates are all typically slower than for the corresponding methyl derivatives. The equilibrium constants for the ligand redistribution reactions and the rates of the exchange reactions are dependent on solvent.

The synthesis of $Et_2Ga(C_5H_5)$ by a ligand redistribution reaction between $GaEt_3$ and $Ga(C_5H_5)_3$ in a 2:1 molar ratio, respectively, in pentane according to eq 3

$$2GaEt_3 + Ga(C_5H_5)_3 \xrightarrow[25\ ^\circ C]{C_5H_{12}} 3Et_2Ga(C_5H_5) \quad (3)$$

was straightforward and provided a near quantitative yield of the desired compound. The product had excellent elemental analyses for C and H and a sharp melting point. In contrast, the original metathesis reaction[12,13] between Et_2GaCl and NaC_5H_5 gave a relatively low yield (45%) of a product with poor elemental analyses. However, when $GaEt_3$ and $Ga(C_5H_5)_3$ were combined in pentane in a 1:2.00 molar ratio, respectively, in an attempt to prepare $EtGa(C_5H_5)_2$ according to eq 4, the

$$GaEt_3 + 2Ga(C_5H_5)_3 \xrightarrow[25\ ^\circ C]{C_5H_{12}} 3EtGa(C_5H_5)_2 \quad (4)$$

isolated product had unacceptable elemental analyses. The percent carbon was low, for example, at −4.56%, −2.0%, and −1.59% by difference for three independent samples from three different preparations. These data suggested to us that an equilibrium mixture of species

(12) Stadelhofer, J.; Weidlein, J.; Haaland, A. *J. Organomet.* **1975**, *84*, C1.
(13) Stadelhofer, J.; Weidlein, J.; Fischer, P.; Haaland, A. *J. Organomet. Chem.* **1976**, *116*, 55.
(14) Mertz, K.; Zettler, F.; Hausen, H.-D.; Weidlein, J. *J. Organomet. Chem.* **1976**, *122*, 159.
(15) Fries, W.; Sille, K.; Weidlein, J.; Haaland, A. *Spectrochim. Acta* **1980**, *36A*, 611.
(16) Cleaver, W. M.; Barron, A. R. *Chemtronics* **1989**, *4*, 146.

Table 1. Interatomic Distances (Å) for $Et_2Ga(C_5H_5)$

	(A) Ga–C(Cp) Distances		
Ga(1)···C(111)	2.817(6)	Ga(1)···C(211)	3.504(7)
Ga(1)–C(112)	2.245(6)	Ga(1)···C(212)	3.512(7)
Ga(1)···C(113)	2.791(6)	Ga(1)···C(213)	2.805(6)
Ga(1)···C(114)	3.501(7)	Ga(1)–C(214)	2.286(6)
Ga(1)···C(115)	3.467(7)	Ga(1)···C(215)	2.887(6)
Ga(2)···C(211)	2.792(6)	Ga(2)···C(311)	2.843(6)
Ga(2)–C(212)	2.272(6)	Ga(2)···C(312)	3.524(7)
Ga(2)···C(213)	2.844(6)	Ga(2)···C(313)	3.464(7)
Ga(2)···C(214)	3.514(7)	Ga(2)···C(314)	2.810(6)
Ga(2)···C(215)	3.444(7)	Ga(2)–C(315)	2.268(6)
Ga(3)···C(311)	2.813(6)	Ga(3)···C(411)	2.904(7)
Ga(3)–C(312)	2.277(6)	Ga(3)···C(412)	3.521(7)
Ga(3)···C(313)	2.849(6)	Ga(3)···C(413)	3.384(7)
Ga(3)···C(314)	3.493(7)	Ga(3)···C(414)	2.728(7)
Ga(3)···C(315)	3.510(7)	Ga(3)–C(415)	2.294(7)
Ga(4)···X(111)[a]	3.498(7)	Ga(4)···C(411)	2.804(7)
Ga(4)···X(112)[a]	3.504(7)	Ga(4)–C(412)	2.294(7)
Ga(4)···X(113)[a]	2.775(6)	Ga(4)···C(413)	2.888(7)
Ga(4)–X(114)[a]	2.262(6)	Ga(4)···C(414)	3.496(7)
Ga(4)···X(115)[a]	2.868(6)	Ga(4)···C(415)	3.510(7)
	(B) Ga–C_2H_5 Distances		
Ga(1)–C(11)	1.979(9)	Ga(3)–C(31)	1.975(5)
Ga(1)–C(13)	1.963(8)	Ga(3)–C(33)	1.958(9)
Ga(2)–C(21)	1.959(7)	Ga(4)–C(41)	1.945(9)
Ga(2)–C(23)	1.969(7)	Ga(4)–C(43)	1.955(5)
	(C) C–C(ethyl) Distances		
C(11)–C(12)	1.437(12)	C(33)–C(34)	1.350(29)
C(13)–C(14)	1.475(12)	C(33)–C(34′)	1.391(21)
C(21)–C(22)	1.508(10)	C(34)···C(34′)	1.486(33)
C(23)–C(24)	1.509(10)	C(41)–C(42)	1.502(12)
C(31)–C(32)	1.528(9)	C(43)–C(44)	1.529(9)
	(D) C–C(Cp) Distances		
C(111)–C(112)	1.432(9)	C(311)–C(312)	1.393(8)
C(112)–C(113)	1.392(9)	C(312)–C(313)	1.429(10)
C(113)–C(114)	1.399(7)	C(313)–C(314)	1.345(10)
C(114)–C(115)	1.421(10)	C(314)–C(315)	1.419(8)
C(115)–C(111)	1.363(10)	C(315)–C(311)	1.390(10)
C(211)–C(212)	1.410(9)	C(411)–C(412)	1.401(9)
C(212)–C(213)	1.398(9)	C(412)–C(413)	1.431(10)
C(213)–C(214)	1.420(9)	C(413)–C(414)	1.352(10)
C(214)–C(215)	1.436(9)	C(414)–C(415)	1.428(10)
C(215)–C(211)	1.337(10)	C(415)–C(411)	1.410(10)

[a] X(111) → X(115) are symmetry related to C(111) → C(115) by the translation $(\vec{a} + \vec{b})$.

had been formed by a ligand redistribution reaction of $EtGa(C_5H_5)_2$ (eq 2). Sublimation of the product at 25 °C would lead to the isolation of $EtGa(C_5H_5)_2$ contaminated with $Et_2Ga(C_5H_5)$, if these two compounds had similar volatilities and if $Ga(C_5H_5)_3$ was nonvolatile. In order to test this hypothesis, $GaEt_3$ and $Ga(C_5H_5)_3$ were mixed in a 1:2.24 molar ratio, respectively, in pentane in order to shift the equilibrium (eq 2) and minimize the formation of $Et_2Ga(C_5H_5)$. The crystalline product isolated by sublimation at 25 °C had excellent carbon, hydrogen, and gallium analytical data. Thus, the successful synthesis of $EtGa(C_5H_5)_2$ provides the first example of an isolable heteroleptic organogallium compound that contains two cyclopentadienide groups and one simple alkyl substituent. The closely related compound $MeGa(C_5H_5)_2$ could not be isolated[1] and was observed to decompose to $Me_2Ga(C_5H_5)$ and $Ga(C_5H_5)_3$ at room temperature. The only other example of a similar group 13 compound is $MeAl(C_5H_5)_2$.[17] The aluminum was found to be η^2-bound to each of the two cyclopentadienide rings.

(17) Fisher, J. D.; Wei, M.-Y.; Willett, R.; Shapiro, P. J. *Organometallics* **1994**, *13*, 3324.

Table 2. Selected Angles (deg) within $Et_2Ga(C_5H_5)$

	(A) Et–Ga–Et Angles		
C(11)–Ga(1)–C(13)	125.0(3)	C(31)–Ga(3)–C(33)	126.3(3)
C(21)–Ga(2)–C(23)	123.9(3)	C(41)–Ga(4)–C(43)	124.7(3)
	(B) Cp–Ga–Cp Angles		
C(112)–Ga(1)–C(214)	98.7(2)	C(312)–Ga(3)–C(415)	99.2(2)
C(212)–Ga(2)–C(315)	99.0(2)	C(412)–Ga(4)–X(115)[a]	100.0(2)

[a] See footnote *a* to Table 1.

The structure of $Et_2Ga(C_5H_5)$ in the solid state is a linear polymer as depicted in Figure 1, which also shows the atomic labelling scheme. The crystallographic asymmetric unit consists of a chain of four $Et_2Ga(C_5H_5)$ moieties which extends by the translation $\pm(\vec{a} + \vec{b})$ to form an infinite linear polymer of $[Et_2Ga(C_5H_5)]_\infty$. Interatomic distances are collected in Table 1. It should be noted that one ethyl group (that whose α-carbon is C(33)) is disordered, with the two sites for the β-carbon being defined by C(34) and C(34′).

The eight independent gallium(III)–ethyl bond lengths range from Ga(4)–C(41) = 1.945(9) Å to Ga(1)–C(11) = 1.979(9) Å, the mean value being 1.963 Å. Each gallium(III) center is also in contact with one carbon atom from each of two cyclopentadienide ligands. Thus Ga(1)–C(112) = 2.245(6) Å and Ga(1)–C(214) = 2.286(6) Å; Ga(2)–C(212) = 2.272(6) Å and Ga(2)–C(315) = 2.268(6) Å; Ga(3)–C(312) = 2.277(6) Å and Ga(3)–C(415) = 2.294(7) Å; and Ga(4)–C(412) = 2.294 (7) and Ga(4)–X(114) = 2.262(6) Å. [Here, X(114) = C(114) translated by $(\vec{a} + \vec{b})$.] All other Ga–C(Cp) distances are greater than 2.72 Å. The average Ga–C(Cp) contact distance is 2.275 Å, *i.e.*, 0.312 Å greater than the σ-bonding Ga–Et distances. Clearly these Ga–C(Cp) interactions are weak. The molecular structure bears a close resemblance and the crystal structure bears a superficial resemblance to $Me_2Ga(C_5H_5)$.[14] However, polymerization of this methyl analogue occurs by association along the 2_1-axis (in space group $P2_1/c$); Ga–Me bond lengths are 1.962(1)–1.972(1) Å, while the two independent Ga–C(Cp) bonding interactions are 2.215(2) and 2.314(2) Å.

The Et–Ga–Et angles (Table 2) are all slightly larger than the ideal *trigonal* value of 120° (*i.e.*, values of 123.9(3)–126.3(3)°, with an average value of 125.0°). The Cp–Ga–Cp contacts lie in a plane normal to the appropriate Et–Ga–Et plane with C–Ga–C angles of 98.7(2)–100.0(2)°, averaging 99.2°. Although each Ga(III) center appears to be in a typical distorted tetrahedral environment (*i.e.*, sp^3 hybridized around gallium), the distances and angles above suggest another possibility. Each Ga(III) atom has two normal σ-bonds to the ethyl groups and a two-electron three-centered bond across the C(Cp)–Ga–C(Cp) system as shown in the following canonical structure. Distances within each C_5H_5 system show the appropriate systematic pattern. The shortest C–C distance in each ring (*i.e.*, C(115)–C(111) = 1.363(10) Å, C(215)–C(211) = 1.337(10) Å, C(313)–C(314) = 1.345(10) Å, and C(413)–C(414) = 1.352(10) Å) is for that carbon–carbon bond in which neither of the carbon atoms interacts closely with a gallium(III) center. Other C–C(Cp) distances for the four distinct rings lie in the ranges 1.392(9)–1.432(9), 1.398(9)–1.436(9), 1.390(10)–1.429(10), and 1.401(9)–1.431(10) Å, respectively.

The polymeric nature of $EtGa(C_5H_5)_2$ is shown in Figure 2, which also shows the atomic labeling scheme.

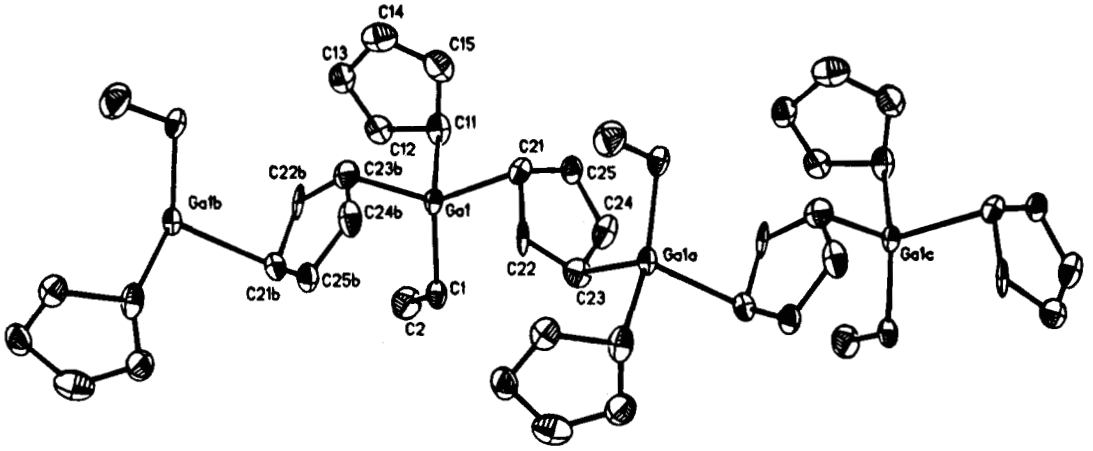

Figure 2. Structure of $[EtGa(C_5H_5)_2]_\infty$. The figure shows a portion of the strand of polymeric $[Ga(C_5H_5)_2(C_2H_5)]_\infty$ formed by translation of the basic asymmetric unit by the 2_1-axis along **b**.

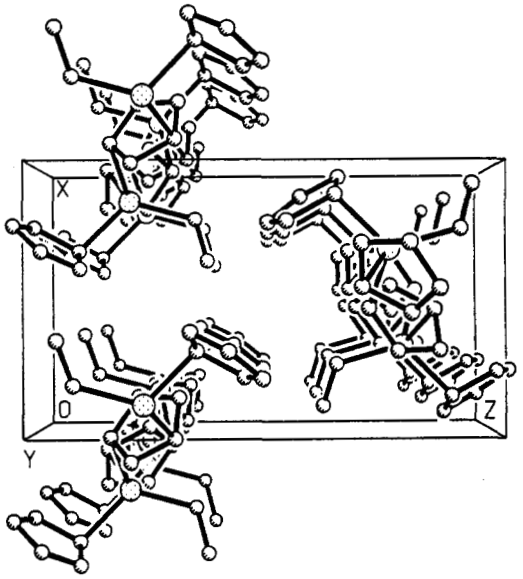

Figure 3. Packing of $[EtGa(C_5H_5)_2]_\infty$ molecules in the crystal. Note that polymerization occurs by way of the 2_1-axis down **b** and that there is no interchain cross-linking.

Association occurs by interaction of units along that 2_1-axis which runs along **b**. [A similar feature is found in $Me_2Ga(C_5H_5)$ but in a different space group ($P2_1/c$, rather than the present $P2_12_12_1$).] Figure 3 illustrates the crystallographic packing viewed down "**b**" and shows clearly that the structure consists of linear chains of $[EtGa(C_5H_5)_2]_\infty$ that are *not* cross-connected. Interatomic distances and angles are collected in Tables 3 and 4. This structural study is of lower accuracy than that for $Et_2Ga(C_5H_5)$, but, nevertheless, some valuable information may be gleaned from it.

The gallium(III) center forms simple σ-bonds to an ethyl group (Ga(1)–C(1) = 1.960(13) Å) and to a η^1-cyclopentadienide ligand (Ga(1)–C(11) = 2.032(15) Å). The second C_5H_5 ligand is bridged by two gallium atoms as in $[Et_2Ga(C_5H_5)]_\infty$. Each gallium atom, in turn, is in contact with two cyclopentadienide ligands, therefore forming the $[Ga{-}C_5H_5]_\infty$ backbone of the polymer. The important contacts are Ga(1)–C(21) = 2.232(12) Å and Ga(1)–C(23b) = 2.187(15) Å. The average Ga–C(Cp) distance of 2.210 Å is slightly shorter than the 2.275 Å in $Et_2Ga(C_5H_5)$ but is still substantially longer than the Ga–C_5H_5 σ-bonded distance of 2.032(15) Å. The C(1)–Ga(1)–C(11) angle is 119.7(6)° as compared to the C(21)–Ga(1)–C(23b) angle of 98.5(5)°.

Distances within the terminal η^1-C_5H_5 ligand are as expected, with two short bonds (C(12)–C(13) = 1.349(21) Å and C(14)–C(15) = 1.330(26) Å) and three longer bonds (1.419(23)–1.447(23) Å). The pattern in the bridging C_5H_5 ligand is not clear cut, with all five C–C bonds lying in the range 1.370(18)–1.423(19) Å. Even though $Et_2Ga(C_5H_5)$ and $EtGa(C_5H_5)_2$ exist as polymers in the solid state, cryoscopic molecular weight studies in benzene solution indicate the presence of only mon-

Table 3. Interatomic Distances (Å) for $EtGa(C_5H_5)_2$

(A) Distance of Ga(1) to Carbon Atoms of the "Bridging" C_5H_5 Ligands			
Ga(1)–C(21)	2.232(12)	Ga(1)···C(21b)[b]	3.475(17)
Ga(1)···C(22)	2.686(13)	Ga(1)···C(22b)[a]	2.688(16)
Ga(1)···C(23)	3.462(15)	Ga(1)–C(23b)[a]	2.187(15)
Ga(1)···C(24)	3.493(15)	Ga(1)···C(24b)[a]	2.921(16)
Ga(1)···C(25)	2.859(13)	Ga(1)···C(25b)[a]	3.575(17)
(B) Distance of Ga(1) to Carbon Atoms of the Terminal C_5H_5 Ligand			
Ga(1)–C(11)	2.032(15)	Ga(1)···C(14)	3.573(17)
Ga(1)···C(12)	2.819(16)	Ga(1)···C(15)	2.802(16)
Ga(1)···C(13)	3.593(17)		
(C) Ga–Et Bond Lengths			
Ga(1)–C(1)	1.960(13)	C(1)–C(2)	1.498(23)
(D) Distances within C_5H_5 Rings			
C(11)–C(12)	1.432(19)	C(21)–C(22)	1.423(19)
C(12)–C(13)	1.349(21)	C(22)–C(23)	1.370(18)
C(13)–C(14)	1.419(23)	C(23)–C(24)	1.411(20)
C(14)–C(15)	1.330(26)	C(24)–C(25)	1.388(19)
C(15)–C(11)	1.447(23)	C(25)–C(21)	1.411(18)

[a] The atoms C(21b) → C(25b) are as shown in Figure 2 and are related to the atoms C(21) → C(25) by the ORTEP symmetry code 3646 (*i.e.*, $1-x$, $-1/2+y$, $3/2+z$).

Table 4. Selected Angles (deg) for $EtGa(C_5H_5)_2$

C(1)–Ga(1)–C(11)	119.7(6)	C(21)–Ga(1)–C(23b)[a]	98.5(5)
C(1)–Ga(1)–C(21)	114.3(5)	C(11)–Ga(1)–C(21)	100.1(5)
C(1)–Ga(1)–C(23b)[a]	115.2(5)	C(11)–Ga(1)–C(23b)[a]	106.1(5)
Ga(1)–C(11)–C(12)	107.7(10)	Ga(1)–C(21)–C(22)	91.9(7)
Ga(1)–C(11)–C(15)	106.1(11)	Ga(1)–C(21)–C(25)	101.0(9)
		Ga(1)–C(23b)–C(22b)[a]	95.4(9)
Ga(1)–C(1)–C(2)	114.6(9)	Ga(1)–C(23b)–C(24b)[a]	106.6(10)
C(15)–C(11)–C(12)	105.2(13)	C(25)–C(21)–C(22)	106.5(10)
C(11)–C(12)–C(13)	109.1(13)	C(21)–C(22)–C(23)	109.0(11)
C(12)–C(13)–C(14)	107.1(14)	C(22)–C(23)–C(24)	107.7(12)
C(13)–C(14)–C(15)	110.7(15)	C(23)–C(24)–C(25)	108.4(12)
C(14)–C(15)–C(11)	107.4(15)	C(24)–C(25)–C(21)	108.1(12)

[a] See footnote *a* to Table 3.

Table 5. ^{1}H NMR Spectra of $Et_2Ga(C_5H_5)$

	assign[a]								
	Et_3Ga		$Et_2Ga(C_5H_5)$			$EtGa(C_5H_5)_2$			
solvent	CH_2	CH_3	CH_2	CH_3	C_5H_5	CH_2	CH_3	C_5H_5	K_{eq}
benzene	0.46	1.15	0.17	0.97	6.28	−0.30	0.75	6.28	4.1×10^{-3}
	0.44	*1.14*				*−0.29*	*0.75*	*6.13*	
toluene		1.13	0.19	1.01	6.23	−0.29	0.75	6.23	1.0×10^{-3}
	0.43	*1.14*				*−0.29*	*0.76*	*6.13*	
THF	0.27	1.07	0.09	0.99	6.02	−0.18	0.85	5.97	1.3×10^{-2}
	0.29	*1.07*				*−0.16*	*0.86*	*5.93*	
C_6H_{12}	0.63		0.27	1.03	6.28	−0.20	0.80	6.28	*b*
	0.69	*1.17*				*−0.25*	*0.78*	*6.17*	
$CHCl_3$	0.62	1.20	0.35	1.05	6.38	−0.25	0.80	6.38	*b*
	0.65	*1.15*				*−0.23*	*0.80*	*6.30*	

[a] Values in italics are for lines from pure compound dissolved in the appropriate solvent. [b] Integrations had large error due to weak, broad lines for the products.

Table 6. ^{1}H NMR Spectra of $EtGa(C_5H_5)_2$

	assign[a]							
	$EtGa(C_5H_5)_2$				$Et_2Ga(C_5H_5)$			
solvent	C_5H_5	CH_2	CH_3	C_5H_5	CH_2	CH_3	C_5H_5	K_{eq}
benzene	6.13	−0.29	0.75	6.13	0.17	0.97	6.13	3.3×10^{-2}
	5.93				*0.17*	*0.97*	*6.28*	
toluene	6.13	−0.29	0.76	6.13	0.19	0.99	6.13	4.6×10^{-2}
					0.19	*1.01*	*6.23*	
THF	5.85	−0.16	0.86	5.93	0.11	1.02	6.00	2.4×10^{-2}
	5.82				*0.09*	*0.99*	*6.02*	
C_6H_{12}	6.17	−0.25	0.78	6.17	0.30	1.03	6.17	2.7×10^{-2}
	5.92				*0.27*	*1.03*	*6.28*	
$CHCl_3$	6.30	−0.23	0.80	6.30	0.37	1.07	6.30	3.3×10^{-2}
					0.35	*1.05*	*6.38*	

[a] Values in italics are for lines from pure compound dissolved in the appropriate solvent.

omeric species. Thus, the polymers are broken during solvation by benzene.

Proton NMR spectral data (Table 5 and 6) demonstrate clearly that both $Et_2Ga(C_5H_5)$ and $EtGa(C_5H_5)_2$ undergo ligand redistribution reactions to form the equilibrium mixtures of species as indicated by eqs 1 and 2 in all solvents studied (benzene, toluene, cyclohexane, chloroform, and THF). Comparison of the chemical shifts (Tables 1 and 2) and the relative intensities of the lines for all species formed after a given compound was dissolved in a specific solvent confirms the identities of all species. The data also indicate that $Et_2Ga(C_5H_5)$ is more stable to a ligand redistribution reaction in a given solvent than is $EtGa(C_5H_5)_2$. When different solvents are compared for the same compound, the extent of reaction is different. Thus, the equilibrium constant K for redistribution of $Et_2Ga(C_5H_5)$ decreases in the order $C_4D_8O > C_6D_6 > C_7D_8 > C_6D_{12} \sim CDCl_3$ whereas for $EtGa(C_5H_5)_2$ K decreases in the order $C_7H_8 > C_6D_{12} \sim CDCl_3 \sim C_4D_8O \sim C_6D_6$. Thus, solvation effects appear to be very important. The data in Tables 5 and 6 also show that the relative rates of ligand exchange depend on the compound dissolved and the solvent. The rate of exchange of C_5H_5 groups between the different species in all solvents except THF is rapid on the NMR time scale as only one line for the C_5H_5 protons is observed in any given spectrum. In contrast, the rate of exchange of ethyl groups is more dependent on solvent. Coupling between the ethyl group protons of all species was observed for only THF solutions of $Et_2Ga(C_5H_5)$ but for all solutions of $EtGa(C_5H_5)_2$. For benzene solutions of $Et_2Ga(C_5H_5)$, ethyl group coupling was not observed for $GaEt_3$ only, whereas for toluene, cyclohexane, and $CDCl_3$ solutions, ethyl coupling was observed for lines for only $Et_2Ga(C_5H_5)$.

The last remaining question concerns the nature of $Et_2Ga(C_5H_5)$ and of $EtGa(C_5H_5)_2$ in the melt. Does a single compound or does an equilibrium mixture of species exist in the liquid phase? In order to answer this question, the ^{1}H NMR spectra of the melts were recorded. The reference for both spectra was C_6D_6, which had been sealed in a capillary tube and inserted into the NMR tube. The spectrum of the melt of $Et_2Ga(C_5H_5)$ at 45 °C was composed of one triplet, one quartet, and one singlet for methylene, methyl, and cyclopentadienide protons, respectively. In contrast, the spectrum of $EtGa(C_5H_5)_2$ exhibited five broad, poorly defined resonances. There were two resonances for methylene protons, two resonances for methyl protons, and one resonance for cyclopentadienide protons. The chemical shifts of the less intense set of methylene and methyl resonances were the same as those observed for the melt of $Et_2Ga(C_5H_5)$, whereas the others must be due to the ethyl protons of $EtGa(C_5H_5)_2$. The C_5H_5 protons were averaged to give a single line. Thus, $Et_2Ga(C_5H_5)$ melts at 35–36 °C whereas $EtGa(C_5H_5)_2$ decomposes at 39.0–39.4 °C. All data are consistent with the conclusions that $EtGa(C_5H_5)_2$ has a greater tendency to undergo ligand redistribution reactions to form mixtures of species and that cyclopentadienide groups exchange faster than do ethyl groups between gallium compounds.

In conclusion, the compounds $Et_2Ga(C_5H_5)$ and $EtGa(C_5H_5)_2$ exist as pure, single compounds in the solid state. When the compounds are melted, the integrity of $Et_2Ga(C_5H_5)$ is maintained whereas $EtGa(C_5H_5)_2$ undergoes ligand redistribution reactions to form $Ga(C_5H_5)_3$ and $Et_2Ga(C_5H_5)$. Dissolution causes all compounds to undergo ligand redistribution reactions and form new compounds. The hypothesis that the ligand redistribution reactions are prevented when the gallium is four-coordinate is supported by the X-ray structural studies. Both $Et_2Ga(C_5H_5)$ and $EtGa(C_5H_5)_2$ are polymers with four-coordinate gallium atoms in the solid state. The compounds undergo redistribution upon dissolution when monomers are formed. The cryoscopic molecular weight studies of both $Et_2Ga(C_5H_5)$ and $EtGa(C_5H_5)_2$ in benzene solution are consistent with the presence of monomeric species. Thus, if these hypotheses are used, $Et_2Ga(C_5H_5)$ exists as a single compound in the melt if the polymeric structure is maintained. In contrast, the decomposition of $EtGa(C_5H_5)_2$ in the melt to form $Ga(C_5H_5)_3$ and $Et_2Ga(C_5H_5)$ suggests the presence of monomeric $EtGa(C_5H_5)_2$ in the liquid phase. The compound $Ga(C_5H_5)_3$ is monomeric in the solid state.[18]

Experimental Section

All compounds described in this investigation were extremely sensitive to oxygen and moisture and were manipulated in a standard vacuum line or in a purified argon atmosphere. The starting material $Ga(C_5H_5)_3$ was prepared and purified by the literature method,[18] whereas $GaEt_3$ was purchased from Strem Chemicals and purified by vacuum distillation. Solvents were dried by conventional procedures. Infrared spectra of Nujol mulls between CsI plates were recorded by means of a Perkin-Elmer Model 683 spectrometer.

(18) Beachley, O. T., Jr.; Getman, T. D.; Kirss, R.; Hallock, R. B.; Hunter, W. C.; Atwood, J. L. *Organometallics* **1985**, *4*, 751.

Table 7. Data for X-ray Structural Studies of $Et_2Ga(C_5H_5)$ and $EtGa(C_5H_5)_2$

	$Et_2Ga(C_5H_5)$	$EtGa(C_5H_5)_2$
formula	$C_9H_{15}Ga$	$C_{12}H_{15}Ga$
cryst syst	triclinic	orthorhombic
space group	$P\bar{1}$ (No. 2)	$P2_12_12_1$ (No. 19)
a, Å	7.803(2)	8.213(5)
b, Å	15.839(4)	9.131(4)
c, Å	16.318(4)	14.277(10)
α, deg	101.98(2)	90.00
β, deg	95.23(2)	90.00
γ, deg	102.72(2)	90.00
V, Å^3	1904.5(8)	1070.7(11)
Z	8	4
fw	192.9	229.0
ϱ(calcd), g cm^{-3}	1.346	1.420
μ(Mo Kα), mm^{-1}	2.811	2.512
transmissn min/max	0.377/0.558	0.088/0.183
2θ range, deg	5.0−45.0	5.0−45.0
index ranges	h 0−8	h, 0−8
	k, −17 to 16	k, 0−9
	l, −17 to 17	l, 0−15
no. of reflns collcd	5551	846
no. of unique reflns	5024 (R_{int} = 0.97%)	846
no. of reflns >6σ	3226	694
R indices (all data)	R = 6.41%, R_w = 6.23%	R = 7.76%, R_w = 9.01%
R indices (6σ data)	R = 3.53%, R_w = 3.97%	R = 7.01%, R_w = 6.34%
largest diff peak, e/Å^3	0.54	1.65
deepest diff hole, e/Å^3	−0.41	−1.24

Absorption intensities are reported with the abbreviations w (weak), m (medium), s (strong), vs (very strong), and sh (shoulder). Mass spectra were obtained by electron impact by using a VG model 70-SE high-resolution mass spectrometer. Elemental analyses were performed by E+R Microanalytical Laboratories, Inc., Corona, NY. The ^{1}H NMR spectra were recorded at 400 MHz by using a Varian VXR-400 spectrometer. Proton chemical shifts are reported in δ units (ppm) and are referenced to $SiMe_4$ at 0.00 ppm. The following abbreviations were used to report the multiplicities of the lines: s (singlet), d (doublet), t (triplet), and br (broad). All samples for NMR spectra were contained in sealed NMR tubes. Melting points were observed in sealed capillaries filled with purified argon and are uncorrected. Molecular weights were measured cryoscopically in benzene by using an instrument similar to that described by Shriver and Drezdon.[19]

Synthesis of $Et_2Ga(C_5H_5)$. A 1.20 g (4.53 mmol) sample of $Ga(C_5H_5)_3$ was added to a flask that was connected to a 100 mL Schlenk flask by means of a glass elbow. Approximately 50 mL of pentane was condensed onto the $Ga(C_5H_5)_3$ at −196 °C. Then, 1.42 g (9.07 mmol) of $GaEt_3$ was vacuum distilled onto the pentane. Upon warming, a colorless solution formed. After 12 h at room temperature, the solvent was removed by vacuum distillation. The crude product was sublimed at 25 °C into the 100 mL Schlenk flask at −196 °C to yield 2.44 g (12.6 mmol, 92.9%) of $Et_2Ga(C_5H_5)$ as a colorless solid. Data for $Et_2Ga(C_5H_5)$. Mp 35−36 °C. IR (Nujol mull, cm^{-1}): 3077 (m), 2897 (vs), 2803 (w), 2720 (w), 1410 (m), 1228 (w), 1185 (w), 1106 (w), 1070 (w), 997 (m), 980 (s), 956 (w), 932 (w), 831 (m), 813 (s), 792 (vs), 747 (vs), 645 (m), 612 (s), 594 (m), 555 (m), 500 (m), 320 (m). MS (*m/e*, relative intensity): 163 ($EtGa(C_5H_5)^+$), 39%; 127 (Et_2Ga^+), 63%; 69 (Ga^+), 100%. Anal. Calcd for $C_9H_{15}Ga$: C, 56.03; H, 7.84. Found: C, 55.97; H, 7.74. Cryoscopic molecular weight, benzene solution, fw 192.9 (observed molality, observed mol wt, association): 0.0781, 224, 1.16; 0.0606, 262, 1.36; 0.0494, 237, 1.23; 0.0406, 251, 1.30; 0.0248, 248, 1.28.

Synthesis of $EtGa(C_5H_5)_2$. The compound $EtGa(C_5H_5)_2$ was synthesized by a ligand redistribution reaction between $Ga(C_5H_5)_3$ and $GaEt_3$ by using the above procedure. After 0.62 g (2.33 mmol) of $Ga(C_5H_5)_3$ and 0.16 g (1.04 mmol) of $GaEt_3$ were reacted in pentane solution, the pentane was removed by vacuum distillation to leave a colorless solid. Sublimation at 25 °C provided 0.603 g (2.63 mmol, 84.7% based on $GaEt_3$) of pure $EtGa(C_5H_5)_2$. Data for $EtGa(C_5H_5)_2$. Mp 39.0−39.4 °C (decomp). IR (Nujol mull, cm^{-1}): 3085 (w), 2713 (w), 1928 (vw), 1790 (vw), 1412 (w), 1300 (w), 1234 (vw), 1165 (vw), 1150 (vw), 1103 (w), 1072 (w), 1000 (w), 975 (m), 890 (w), 875 (w), 845 (m), 819 (m), 790 (m), 746 (vs), 657 (w), 635 (m), 540 (w), 389 (w), 361 (w), 330 (w). MS (*m/e*, relative intensity): 199 ($Ga(C_5H_5)_2^+$), 13%; 163 ($EtGa(C_5H_5)^+$), 33%; 69 (Ga^+), 100%. Anal. Calcd for $C_{12}H_{15}Ga$: C, 62.95; H, 6.60; Ga, 30.45. Found: C, 62.70; H, 6.71; Ga, 30.14. Cryoscopic molecular weight, benzene solution, fw 229.0 (observed molality, observed mol wt, association): 0.0860, 221, 0.97; 0.0646, 221, 0.96; 0.0429, 225, 0.98.

Table 8. Final Atomic Parameters (×10^4) and Equivalent Isotropic Displacement Coefficients (Å^2 × 10^3) for $Et_2Ga(C_5H_5)$

	x	y	z	U(eq)[a]
Ga(1)	−2539(1)	−5894(1)	1242(1)	57(1)
Ga(2)	1722(1)	−3722(1)	4079(1)	53(1)
Ga(3)	6549(1)	−1035(1)	3302(1)	56(1)
Ga(4)	3467(1)	927(1)	1485(1)	55(1)
C(11)	−1150(11)	−6512(5)	472(4)	94(4)
C(12)	−1454(16)	−6539(8)	−415(6)	179(8)
C(13)	−3430(9)	−4866(5)	1076(4)	80(3)
C(14)	−5062(11)	−4727(5)	1414(5)	109(4)
C(21)	2229(8)	−4787(4)	4376(4)	66(3)
C(22)	3501(9)	−5248(4)	3933(5)	82(3)
C(23)	962(9)	−2798(4)	4864(4)	74(3)
C(24)	1581(12)	−2748(5)	5779(4)	104(4)
C(31)	7687(8)	96(4)	4130(4)	70(3)
C(32)	9637(9)	438(5)	4046(5)	101(4)
C(33)	7733(11)	−1942(5)	2794(5)	91(4)
C(34)	9200(33)	−1760(15)	2419(18)	111(13)
C(34′)	7487(40)	−2327(14)	1931(12)	125(13)
C(41)	1779(10)	1539(5)	1991(5)	97(4)
C(42)	2248(13)	2110(6)	2876(7)	136(6)
C(43)	2833(8)	−137(4)	556(4)	63(3)
C(44)	1088(9)	−790(4)	584(5)	87(3)
C(111)	−5820(9)	−7155(4)	691(4)	76(3)
C(112)	−4908(8)	−6813(4)	1538(4)	57(2)
C(113)	−4064(7)	−7458(4)	1711(4)	53(2)
C(114)	−4391(8)	−8170(4)	1000(4)	62(3)
C(115)	−5450(10)	−7948(4)	361(4)	79(3)
C(211)	−1750(8)	−4454(5)	3256(4)	71(3)
C(212)	−294(8)	−4070(4)	2890(4)	60(2)
C(213)	306(8)	−4761(4)	2417(4)	63(3)
C(214)	−766(8)	−5572(4)	2517(3)	60(2)
C(215)	−2011(8)	−5339(4)	3067(4)	63(3)
C(311)	3574(7)	−2408(4)	3310(4)	62(3)
C(312)	4258(8)	−1633(4)	3941(4)	61(3)
C(313)	5278(8)	−1867(4)	4593(4)	70(3)
C(314)	5271(8)	−2733(4)	4351(4)	68(3)
C(315)	4164(8)	−3095(4)	3560(4)	62(3)
C(411)	4089(9)	−162(5)	2575(4)	69(3)
C(412)	5117(8)	694(4)	2617(4)	61(3)
C(413)	6673(9)	597(5)	2243(4)	72(3)
C(414)	6530(9)	−282(5)	1943(4)	69(3)
C(415)	4956(9)	−785(4)	2162(4)	68(3)

[a] Equivalent isotropic U, defined as one-third of the trace of the orthogonalized U_{ij} tensor.

Collection of X-ray Diffraction Data. In each case crystals were sealed (under very strict air- and moisture-free conditions) into thin-walled glass capillaries. The crystals were inspected under a binocular polarizing microscope to ensure that they were single; they were then accurately centered in a eucentric goniometer on an upgraded Syntex $P2_1$/Siemens P3 automated four-circle diffractometer. Determination of the Laue symmetry and unit cell parameters was carried out as described in detail previously.[20] Intensity data (Mo Kα, λ = 0.710 730 Å) were collected at room temperature

(19) Shriver, D. F.; Drezdzon, M. A. *The Manipulation of Air Sensitive Compounds*; Wiley: New York, 1986; p 38.

(20) Churchill, M. R.; Lashewycz, R. A.; Rotella, F. J. *Inorg. Chem.* **1977**, *16*, 265.

(24 ± 2 °C) using graphite-monochromatized radiation. Data were corrected for absorption and for Lorentz and polarization effects. Details are given in Table 7.

$Et_2Ga(C_5H_5)$. The crystal was of dimensions 0.2 × 0.2 × 0.3 mm³ and was mounted along its extended direction. The cell dimensions and diffraction symmetry ($\bar{1}$ only) indicated the triclinic crystal group. Possible space groups are the noncentrosymmetric space group $P1$ (No. 1) and the centrosymmetric space group $P\bar{1}$ (No. 2). The far more common, centrosymmetric $P\bar{1}$ was assumed; this was confirmed by the successful solution of the structure in this higher space group.

$EtGa(C_5H_5)_2$. The crystal was rather larger than would normally be preferred (approximatley 0.27 × 0.33 × 0.8 mm³) and not of high quality. However, no better crystal could be obtained. The cell parameters and diffraction symmetry (D_{2h}) indicated the orthorhombic crystal system. The systematic absences $h00$ for $h = 2n + 1$, $0k0$ for $k = 2n + 1$, and $00l$ for $l = 2n + 1$ uniquely define the noncentrosymmetric space group $P2_12_12_1$ (No. 19).

Determination of the Crystal Structures. All crystallographic calculations were carried out on a VAXstation 3100 computer system with use of the Siemens SHELXTL PLUS program package.[21] The analytical form of the scattering factors for neutral atoms was used with both of the real ($\Delta f'$) and imaginary ($i\Delta f''$) components of anomalous dispersion included in the calculations.[22] Structures were solved by direct methods and difference-Fourier syntheses. All non-hydrogen atoms were located, and the positional and anisotropic thermal parameters were refined. Hydrogen atoms were not located directly, but were included in calculated positions with d(C–H) = 0.95 Å.[23] Refinement was continued until convergence was reached. Each structure was checked by means of a final difference-Fourier synthesis. Specific details are listed in Table 7 or are outlined below.

$Et_2Ga(C_5H_5)$. Atomic coordinates are collected in Table 8. The crystallographic asymmetric unit contains four formula units; these are linked together and extended to form an infinite polymer. Final discrepancy indices are $R = 3.53\%$ for those 3226 data with $F_o > 6\sigma(F_o)$ and $R = 6.41\%$ for all 5024 unique reflections.

$EtGa(C_5H_5)_2$. Atomic coordinates are collected in Table 9. The crystallographic asymmetric unit is the monomeric formula unit. An infinite polymer is created by linkages involving the 2_1-axis along "**b**". Transmission factors were rather low (0.0883–0.1829) due to the larger than usual crystal that was used. Final discrepancy indices are, as expected, higher than for the previous structure, with $R = 7.01\%$ for those 694 reflections with $F_o > 6\sigma(F_o)$ and $R = 7.76\%$ for all 846 reflections. The absolute configuration of the crystal was determined by η-refinement, yielding the value $\eta = +0.4(2)$; although this value is not ideal, it confirms that we have chosen the correct enantiomeric crystal form.

(21) SHELXTL PLUS; Siemens Analytical Instrument Corp.: Madison, WI, 1988.
(22) *International Tables for X-Ray Crystallography*; Kynoch Press: Birmingham, England, 1974; Vol. 4, pp 99–101 and 149–150.
(23) Churchill, M. R. *Inorg. Chem.* **1973**, *12*, 1213.

Table 9. Final Atomic Parameters (×10⁴) and Equivalent Isotropic Displacement Coefficiets (Å² × 10³) for $EtGa(C_5H_5)_2$

	x	*y*	*z*	*U*(eq)[a]
Ga(1)	8407(2)	1876(1)	2276(1)	42(1)
C(1)	7780(15)	1759(12)	3598(9)	52(4)
C(2)	6315(26)	2650(17)	3854(12)	86(7)
C(11)	6665(18)	2148(13)	1280(11)	64(5)
C(12)	6042(16)	3606(16)	1368(11)	63(5)
C(13)	6626(20)	4432(16)	660(10)	75(5)
C(14)	7501(19)	3483(21)	54(12)	92(7)
C(15)	7506(23)	2123(20)	389(12)	87(7)
C(21)	9639(17)	−128(12)	1729(9)	54(4)
C(22)	10428(15)	−380(10)	2601(9)	54(4)
C(23)	9685(18)	−1531(16)	3045(10)	68(5)
C(24)	8314(17)	−1932(13)	2508(11)	71(5)
C(25)	8320(17)	−1116(12)	1687(9)	55(4)

[a] Equivalent isotropic U, defined as one-third of the trace of the orghogonalized $\mathbf{U}_{ij}$ tensor.

^1H NMR Spectral Studies of $Et_2Ga(C_5H_5)$ and $EtGa(C_5H_5)_2$ in Different Solvents. In a typical experiment, a small quantity (~10 mg) of the desired compound was placed in an NMR tube. Next, approximately 0.6 mL of the appropriate solvent was vacuum distilled into the NMR tube at −196 °C. The ^1H NMR spectrum (400 MHz) of the resulting solution was recorded upon warming of the solution to room temperature. The coupling constant for all triplets and quartets from ethyl groups was 8 Hz in all spectra. The NMR spectral data are provided in Tables 5 and 6.

^1H NMR Spectra of Molten $Et_2Ga(C_5H_5)$ and $EtGa(C_5H_5)_2$. A 3 mm diameter glass capillary was filled with approximately 0.5 mL of C_6D_6 and sealed under vacuum. This tube was then placed in an NMR tube which contained approximately 0.5 g of the appropriate compound. The NMR tube was then sealed by fusion. The NMR spectrum (400 MHz) of each compound was recorded at 45 °C. Data for $Et_2Ga(C_5H_5)$. ^1H NMR: −0.11 (q, $(CH_3\mathit{CH_2})_2Ga(C_5H_5)$, relative intensity 1.0); 0.84 (t, $(\mathit{CH_3}CH_2)_2Ga(C_5H_5)$, relative intensity 1.6); 6.06 (s, $(CH_3CH_2)_2Ga(\mathit{C_5H_5})$, relative intensity 1.4). Data for $EtGa(C_5H_5)_2$. ^1H NMR: −0.40 (broad, $(CH_3\mathit{CH_2})Ga(C_5H_5)_2$, relative intensity 2.1); 0.03 (broad, $(CH_3\mathit{CH_2})_2Ga(C_5H_5)$, relative intensity 1.0); 0.60 (broad, $(\mathit{CH_3}CH_2)Ga(C_5H_5)_2$, relative intensity 2.8); 0.83 (broad, $\mathit{CH_3}CH_2)_2Ga(C_5H_5)$, relative intensity 1.1); 6.00 (broad singlet, (C_5H_5), relative intensity 9.9).

Acknowledgment. This work was supported in part by the Office of Naval Research (O.T.B.). The upgrading of the X-ray diffractometer was made possible by Grant 89-13733 from the Chemical Instrumentation Program of the National Science Foundation.

Supporting Information Available: Complete tables of interatomic distances and angles, anisotropic thermal parameters, and calculated positions for hydrogen atoms (9 pages). Ordering information is given on any current masthead page.

OM950293I

Experimental and Theoretical Studies of the Gas-Phase Reactions of "Bare" Iron(I) with Tetralin

Katrin Seemeyer, Roland H. Hertwig, Jan Hrušák, Wolfram Koch,* and Helmut Schwarz*

Institut für Organische Chemie der Technischen Universität Berlin, Strasse des 17.Juni 135, D-10623 Berlin, Germany

Received March 29, 1995[⊗]

Extensive labeling studies have been employed to unravel the reaction mechanism of the Fe^+ mediated single and double dehydrogenation of tetralin (**1**). The reaction is both regio- and stereospecific, leading first to the 1,2-dihydronaphthalene–Fe^+ complex (**2**) and finally to the naphthalene–Fe^+ complex (**3**). In the course of the reaction the metal ion sticks to the same face of the hydrocarbon surface. The steric and electronic effects exerted by a CH_3- or a CH_3O-group attached at C(5) demonstrate that the metal ion migrates toward the initially saturated ring and is finally η^6-coordinated to this ring. The proposed reaction mechanism is supported by density functional calculations on the tetralin–Fe^+ complex **1**–Fe^+ as well as on the reaction products, i.e., 1,2-dihydronaphthalene–Fe^+ (**2**) and naphthalene–Fe^+ (**3**).

Introduction

Although metal ion-mediated dehydrogenations in the gas phase have been studied frequently,[1] the elucidation of the reaction mechanisms is often difficult due to (i) H/D equilibrations,[2] (ii) the operation of competing mechanisms, and/or (iii) "metabolic switching".[3] A fortunate case has been encountered for the metal complexes of tetralin (**1**), for which labeling experiments indicate that the M^+-mediated (M = Fe,[4] Co,[4,5] Ag[5]) consecutive losses of H_2 and $2H_2$ (see Scheme 1) in the gas phase to generate the naphthalene–M^+ complexes **3** are highly specific.

However, some questions regarding the bonding situation of **1**–M^+, **2**, and **3** as well as the details of the reaction mechanism are still unresolved. For example: Does the saturated ring in **1**–M^+ affect the coordination of the metal ion to the benzene submoiety as compared to benzene ifself? Is there a bonding interaction with the additional double bond in **2**? What is the hapticity of M^+ in **3**? If the mode of bonding in **1**–Fe^+, **2**, and **3** deviates from that of $M^+(C_6H_6)$, is this reflected in the bond dissociation energies (BDEs)? Does the metal ion influence the conformation of the nonaromatic ring? Which C–H position of the tetralin ring is first activated? Does the metal remain bonded to the aromatic ring throughout the whole reaction sequence or is it translocated to the initially saturated ring?

Here, we report the experimental results of the Fe^+-mediated single and double dehydrogenation of tetralin (**1**) in the gas phase. Preliminary results were reported previously.[4] The reaction mechanism has been elucidated by employing deuterium-labeled isotopomers and studying 5-substituted derivatives of tetralin. BDEs were determined by Cooks' kinetic method[6] and are augmented by quantum chemical calculations employing density functional theory (DFT).[7] This level of theory incorporates in an approximate fashion exchange interactions and electron correlation, which are both crucial for a proper description of open shell transition metal compounds. Density functional theory in the form of the local spin density approximation (LSDA) with additional nonlocal corrections has already successfully been applied to open shell transition metal systems.[8,9] While the geometries resulting from DFT calculations are generally in remarkable accord with experimental data or accurate calculations,[10] bond dissociation energies are often significantly too large.[7b,11] Fortunately, it has been shown that this behavior is systematic; hence, meaningful corrections can be made, and relative stabilities are reproduced correctly.[12] Another appeal-

Scheme 1

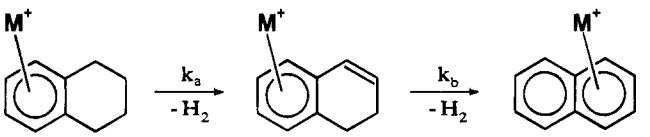

1-M^+ 2 3

[⊗] Abstract published in *Advance ACS Abstracts,* August 1, 1995.

(1) (a) Eller, K.; Schwarz, H. *Chem. Rev.* **1991**, *91*, 1121. (b) Eller, K. *Coord. Chem. Rev.* **1993**, *126*, 93.

(2) For an extreme example of extensive H/D exchange, see: Schwarz, J.; Schwarz, H. *Chem. Ber.* **1993**, *126*, 1257.

(3) (a) Prüsse, T.; Fiedler, A.; Schwarz, H. *Helv. Chim. Acta* **1991**, *74*, 1127. (b) Seemeyer, K.; Prüsse, T.; Schwartz, H. *Helv. Chim. Acta* **1993**, *76*, 1632. (c) Raabe, N.; Karrass, S.; Schwarz, H. *Chem. Ber.* **1994**, *127*, 261.

(4) Seemeyer, K.; Prüsse, T.; Schwarz, H. *Helv. Chim. Acta* **1993**, *76*, 113.

(5) Huang, Y.; Profilet, R. D.; Ng, J. H.; Ranasinghe, Y. A.; Rothwell, I. P.; Freiser, B. S. *Anal. Chem.* **1994**, *66*, 1050.

(6) (a) Cooks, R. G.; Kruger, T. L. *J. Am. Chem. Soc.* **1977**, *99*, 1279. (b) McLuckey, S. A.; Cameron, D.; Cooks, R. G. *J. Am. Chem. Soc.* **1981**, *103*, 1313. (c) Wright, L. G.; McLuckey, S. A.; Cooks, R. G. *Int. J. Mass Spectrom. Ion Phys.* **1982**, *42*, 115. (d) Chen, L.-Z.; Miller, J. M. *Org. Mass Spectrom.* **1992**, *27*, 883.

(7) (a) Parr, R. G.; Yang, W. *Density Functional Theory of Atoms and Molecules*; Oxford University Press: New Yory, 1989. (b) Ziegler, T. *Chem. Rev.* **1991**, *91*, 651.

(8) Ziegler, T.; Lee, J. *Can. J. Chem.* **1994**, *72*, 783.

(9) Russo, T. V.; Martin, R. L.; Hay, P. J. *J. Chem. Phys.* **1994**, *101*, 7729.

(10) See, e.g.: *Density Functional Methods in Chemistry*; Labanowski, J. K., Andzelm, J. W., Eds.; Springer-Verlag: Berlin, 1991.

(11) (a) Hertwig, R. H.; Koch, W. *J. Comput. Chem.* **1995**, in press. (b) Becke, A. D. *J. Chem. Phys.* **1992**, *96*, 2155. (c) *Ibid. J. Chem. Phys.* **1992**, *97*, 9173. (d) *Ibid. J. Chem. Phys.* **1993**, *98*, 5648.

0276-7333/95/2314-4409$09.00/0

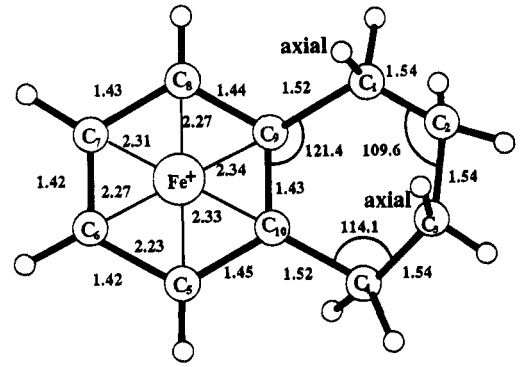

1-Fe$^+$

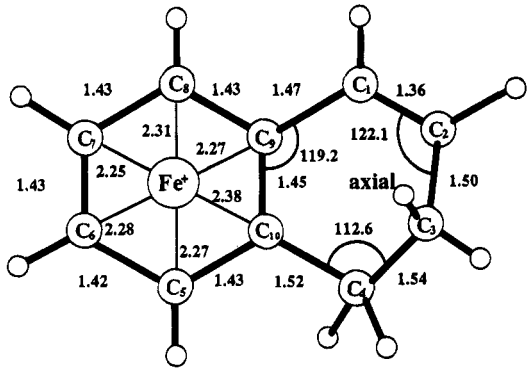

2'

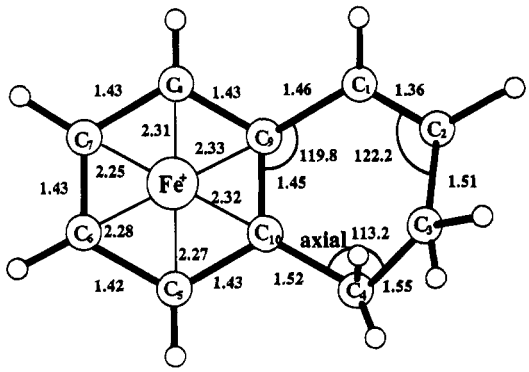

2''

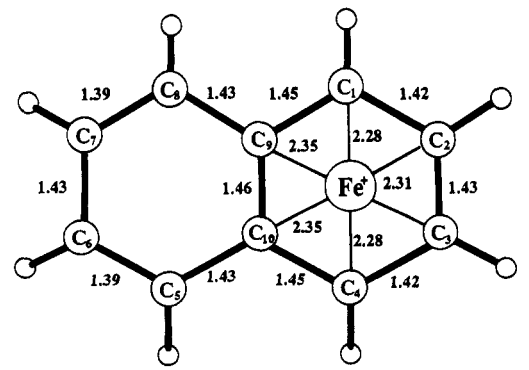

3

Figure 1. Calculated structures of **1**−Fe$^+$, **2**, and **3**. Bond lengths in Å, bond angles in degrees.

ing aspect of DFT is its rather modest demand with respect to computing resources, which makes the method an ideal tool to computationally approach this problem.

Experimental Section

As the experimental setup has been described repeatedly,[13,14] a brief description may suffice: A 1:1 mixture of Fe(CO)$_5$ and tetralin or its derivatives is bombarded with 100-eV electrons in the chemical ionization source (repeller voltage close to 0 V) of a modified four-sector tandem mass spectrometer of BEBE configuration (B stands for magnetic sector and E for electric sector), in which MS-I is the original VG ZAB-HF-2F part and MS-II is an AMD 604 mass spectrometer.[14] Although the actual mechanism by which the complexes are formed is yet unknown, the pressure in the ion source is high enough to permit collisional cooling, thus increasing the lifetime such that time-delayed decompositions after ca. 1 μs take place (metastable ion (MI) dissociation). To this end, the organometallic complexes of Fe$^+$ and tetralin (and its derivatives) having 8-keV translational energy are mass-selected by means of B(1)E(1). Unimolecular reactions occurring in the field-free region between E(1) and B(2) were monitored by scanning B(2). Spectra were recorded on-line and averaged by using signal-averaging techniques employing the AMD Intectra data system. In typical experiments, 15−20 spectra were recorded. All compounds were synthesized by standard laboratory procedures, purified by chromatographic means, and fully characterized by spectroscopic methods.

Computational Details

We applied the local spin density functional approximation[15] augmented by nonlocal corrections for exchange and correlation due to Becke[16] and Perdew[17] (BP). The calculations were carried out utilizing the program DGAUSS[18] employing a DZVP all electron basis set for carbon and hydrogen, and a DZVP basis combined with a norm conserving pseudopotential (NCPP)[19] describing the [Ar] core for iron. The geometries presented in Figure 1 were fully optimized in Cartesian coordinates without imposing any symmetry constraints. In a recent MCPF investigation, Bauschlicher et al.[20] identified the ground state of the Fe$^+$(C$_6$H$_6$) complex as $^4A_2$. We, therefore, also expect **1**−Fe$^+$, **2**, and **3** to be quartet states.[21]

Results and Discussion

The interpretation of the labeling results for tetralin (Table 1) is both unambiguous and straightforward and only compatible with a sequence of regiospecific 1,2-eliminations involving hydrogen atoms from C(1)/C(2) and/or C(3)/C(4). For example, the data of **1a,c**, and in particular the absence of HD loss for the first dehydrogenation, rule out a 2,3-elimination to generate the 1,4-

(12) (a) Hertwig, R. H.; Hrušák, J.; Schröder, D.; Koch, W.; Schwarz, H. *Chem. Phys. Lett.* **1995**, *236*, 194. (b) Holthausen, M. C.; Heinemann, C.; Cornehl, H. H.; Koch, W.; Schwarz, H., *J. Chem. Phys.* **1994**, *102*, 4931.

(13) (a) Prüsse, T. Ph.D. Thesis, Technische Universität Berlin, Berlin, Germany, 1991; D83. (b) Prüsse, T.; Schwarz, H. *Organometallics* **1989**, *8*, 2856.

(14) (a) Srinivas, R.; Sülzle, D.; Koch, W.; DePuy, C. H.; Schwarz, H. *J. Am. Chem. Soc.* **1991**, *113*, 5970. (b) Srinivas, R.; Sülzle, D.; Weiske, T.; Schwarz, H. *Int. J. Mass Spectrom. Ion Proc.* **1991**, *107*, 369.

(15) (a) Slater, J. C. *Phys. Rev.*, **1951**, *81*, 285. (b) Vosko, S. J.; Wilk, L.; Nusair, M. *Can. J. Phys.* **1980**, *58*, 1200. For a more recent and simpler formulation, see also: Perdew, J. P.; Wang, Y. *Phys. Rev. B* **1992**, *45*, 13244. (c) Gunnarson, O.; Lundqvist, I. *Phys. Rev. B* **1977**, 4274.

(16) Becke, A. D. *Int. J. Quantum Chem.* **1983**, *23*, 1915. *J. Chem. Phys.* **1986**, *84*, 4524; *Phys. Rev. A* **1988**, *38*, 3098.

(17) Perdew, J. P. *Phys. Rev. B* **1986**, *33*, 8822.

(18) DGAUSS 2.3, Cray Research, Inc., 1994.

(19) For a review on norm-conserving pseudopotentials, see: (a) Pickett, W. E. *Comput. Phys. Rep.* **1989**, *9*. (b) Chelikowski, J. R.; Cohen, M. L. University of Minnesota Institute Research Report UMSI 91/339; University of Minnesota: Minneapolis, MN, 1991.

(20) Bauschlicher, C. W., Jr.; Partridge, H.; Langhoff, S. R. *J. Am. Chem. Soc.* **1992**, *96*, 3273.

Scheme 2

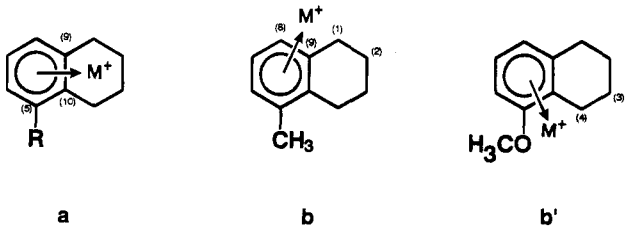

dihydronaphthalene–Fe^+ complex. Therefore, the product of the first reaction must correspond to the 1,2-dihydronaphthalene–Fe^+ complex **2** as shown in Scheme 1, and the mechanism is that of a combination of oxidative addition, β-hydrogen transfer, and reductive elimination of molecular hydrogen.

The data of the racemic pairs of **1c,d** convincingly demonstrate that the H(D) transfer to the metal ion center follows a *syn*-process. The complex of *cis*-labeled tetralin **1c** does not undergo HD loss; in contrast, the MI mass spectrum of the *trans*-complex **1d** contains signals for both H_2 and HD elimination, while D_2 is not eliminated.

Furthermore, as demonstrated earlier,[22] in the overall reaction the metal ion does not switch from one surface of the π-system to the other. This is evidenced by the MI spectrum of **1e**–Fe^+. If the Fe^+ cation would change the surface, one must observe the combined losses of H_2 + HD, irrespective from which side of the complex the first molecule of H_2 originates. This is *not* the case. Rather, the isotope distribution demands that throughout the whole reaction sequence the metal ion sticks to the same plane of the hydrocarbon surface to which it was bound initially.

In addition, earlier work[22] suggests that during these reactions the π-coordinated metal ion migrates toward the initially nonaromatic ring. For bicyclic [ML_n(polyene)] complexes, where ML_n = $Cr(CO)_3$ and CrCp, a theoretical analysis[23] of haptotropic rearrangements[24] has been conducted in great detail. Although this analysis does not pertain—in a strict sense—to the present study, there are some relations worth considering. In fact, three pathways deserve to be distinguished (Scheme 2).

The metal ion migrates in a symmetrical fashion toward the unsaturated ring across the central C(9)/C(10) bond (Scheme 2, path a). This path is not expected to be significantly affected by substituents attached to C(5); consequently, in the elimination of the first molecule of H_2, the positions C(1)/C(2) and C(3)/C(4) should participate equally. In contrast, if the metal ion follows the unsymmetrical paths b or b' (Scheme 2), one expects a preference for C(1)/C(2) or C(3)/C(4) depending on the nature of the substituent. For non or weakly complexing substituents, e.g., R = CH_3, M^+ is likely to be deflected *away from* R to the region of C(8)/C(9) (Scheme 2, path b). Consequently, the loss of the first H_2 molecule is predicted to preferentially involve C(1)/C(2). In contrast, substituents which are capable to compensate for the loss of π-electron complexation, e.g., R = OCH_3, are expected to direct the metal ion toward the region C(5)/C(10), thus favoring the activation of C(3)/C(4) C–H-bonds (Scheme 2, path b'). The data for the Fe^+ complexes of **4** and **5** (see Table 1) show that there is indeed a preferred directionality operative for the elimination of the first molecule of molecular hydrogen. For the 5-CH_3-substituted tetralin **4**, comparison of the isotopomers **4a,b** clearly demonstrates that the CH_3-group directs the metal ion *away* from its neighbors C(3)/C(4). This is evidenced by the increased ratio for the loss of H_2/HD = 5.6 from **4a**; in contrast, from the isotopomer **4b** this ratio drops to 1.3. If one assumes that the kinetic isotope effects associated with metal ion-mediated dehydrogenation of 5-substituted tetralins are approximately the same as for the tetralin isotopomer of **1b**, which amounts to 1.9 ± 0.2,[25] from a simple algebraic analysis it follows from the data of **4a,b** that the steric hindrance imposed by the CH_3-group amounts to a factor of ca. 2. Thus, the oxidative insertion of the metal ion in the sterically more easily accessible C(1)/C(2) region (path b) is preferred. We consider the effect of the methyl group to be steric rather than electronic in nature since the σ-constants of the linear free energy relationship,[26] which describe the electronic effect of a substituent at an aromatic ring, do not differ very much for an H-atom or a methyl group. Furthermore, if the methyl group would exert an electronic effect, this would be expected to have the same direction as that of the methoxy substituent (see below); this, however, is not the case. In contrast, the CH_3O substituent at C(5), i.e., **5**, clearly directs the metal ion toward the sterically more congested C(3)/C(4) region. This follows immediately from the large H_2/HD ratio of 14.5 for the complex **5a**–Fe^+. Obviously the loss of complexation energy associated with the migration of the Fe^+ is partially compensated for by coordination of the metal ion to the lone pair electrons of the methoxy group. The experiments with the 5-substituted derivatives of tetralin show that the metal ion, as expected, has to migrate toward the initially nonaromatic ring in order to induce the dehydrogenation. However, the experiments do not reveal the details of this migration: for example, does the oxidative addition commence with an insertion in the C(1) or the C(2) C–H bond? Therefore, DFT calculations were conducted in the hope to provide this missing link. The optimized structures of the quartet states of **1**–Fe^+, **2**, and **3** are shown in Figure 1. Comparsion between the complexed hydrocarbons and those of the free ligands is made in Table 2.

(21) In order to confirm this assumption we have investigated the sextet state of the complexes **1**–Fe^+, **2**, and **3**. The total energies for **1**–Fe^+, **2**, and **3** are nearly degenerate for both the quartet and sextet states. We rationalize this as follows: The calculated energy needed to excite the sextet ground state of the Fe^+ atom to its quartet state is overestimated by about 12 kcal/mol, which is not unexpected for DFT methods. On the other hand the order in the total energies between quartet and sextet is presumably reversed if we look at the complexes since we expect the quartet to be the ground state here in analogy to Fe^+–benzene. Consequently, the quartet should be significantly lower in energy. But, because this error in the atomic splitting is being propagated into the molecular total energies, the splitting between quartet and sextet structures in the case of **1**–Fe^+, **2**, and **3** is reduced by about the same amount (12 kcal/mol) in our calculations. Hence, we believe that all three complexes are in fact quartet states.

(22) Seemeyer, K.; Schwarz, H. *Helv. Chim. Acta* **1993**, *76*, 2384.

(23) Albright, T. A.; Hofmann, P.; Hoffmann, R.; Lillya, C. P.; Dobosh, P. A. *J. Am. Chem. Soc.* **1983**, *105*, 3396.

(24) Ark, N. T.; Elian, M.; Hoffmann, R. *J. Am. Chem. Soc.* **1978**, *100*, 110.

(25) For a comprehensive, detailed analysis of the isotope effects associated with the metal ion-mediated dehydrogenation of tetralin, see ref 4.

(26) (a) Taft, R. W. *Steric Effects in Organic Chemistry*; Newman, M. S., Ed.; Wiley: New York, 1956. (b) Taft, R. W.; Prize, E.; Fox, I. L.; Lewis, I. C.; Andersen, K. K.; Davis, G. T. *J. Am. Chem.* **1963**, *85*, 709, 3146. (c) Exner, O. *Correlation Analysis in Chemistry*; Chapman, N. B., Shorter, J., Eds.: Plenum Press: New York, 1978.

Table 1. Unimolecular Single and Double Dehydrogenation of Fe^+ Complexes of Tetralin and Its Derivatives[a]

		neutral eliminated				
no.	ligand	H_2	HD	$2H_2$ or D_2	H_2 + HD	H_2 + D_2 or 2HD
1	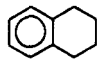	35		65		
1a	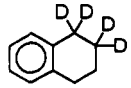	37		8		55
1b	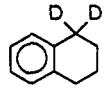	29	12		59	
1c	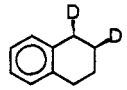	41		43		16
1d	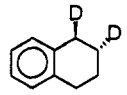	31	12			57
1e	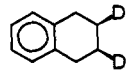	29	8	44		19
4	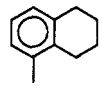	26		74		
4a	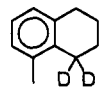	28	5		67	
4b	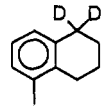	18	14		68	
5	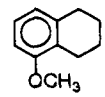	22		78		
5a	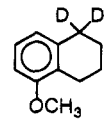	29	2	1[b]	68	
5b	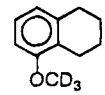	20		79	1	

[a] Data are normalized to Σ fragment intensities = 100%. [b] The quite minor loss of two H_2 (1%) from **5a**−Fe^+, which is not expected to take place if only the positions C(1)/C(2) and/or (C3)/C(4) serve as H_2 sources, originates from a new channel in which the CH_3O-substituent participates. This follows from the combined loss of H_2 + HD from the CD_3O-labeled isotopomer **5b**. It has been conjectured by a reviewer that this minor channel may result from Fe^+ in an excited state.

The salient feature of the three calculated structures **1**−Fe^+, **2**, and **3** is the η^6-coordination of the metal ion. The corresponding iron−carbon bond distances are within the range of 2.23−2.34 Å. Due to the absence of any symmetry constraints in **1**−Fe^+ and **2** and a low C_2-symmetry in **3**, the Fe−C bond lengths are not equal. From a comparison of the data collected in Table 2, it becomes evident that the structure of the ligand is only marginally altered by the presence of the iron. We note, however, that in each case the C−C bond lengths of the aromatic moiety are elongated by 0.01−0.02 Å as a result of the complexation with the iron.

The preference for the central position of the iron in all three complexes can be explained in terms of a MO picture by an overlap of the HOMO of the ligand with an empty sd-hybridized orbital of Fe^+, similar to the bonding of Fe^+ to benzene, which has recently been studied by Bauschlicher et al.[20] The total atomic charge on iron in **1**−Fe^+ is reduced to 0.72e, according to the Mulliken population analysis. This charge transfer

Table 2. Selected Bond Lengths, Bond Angles, and Torsion Angles of 1−Fe$^+$, 2′, and 3 and the Respective Free Ligands Tetralin, Dihydronaphthalene, and Naphthalene[a]

	1−Fe$^+$	tetralin	2′	dihydronaphthalene	3	naphthalene
C_1-C_2	1.54	1.54	1.36	1.36	1.42	1.39
C_2-C_3	1.54	1.54	1.50	1.52	1.43	1.43
C_3-C_4	1.54	1.54	1.54	1.56	1.42	1.39
C_4-C_{10}	1.52	1.53	1.52	1.52	1.45	1.43
C_9-C_{10}	1.43	1.42	1.45	1.42	1.46	1.44
$C_{10}-C_5$	1.45	1.41	1.43	1.40	1.43	1.43
C_5-C_6	1.42	1.40	1.42	1.41	1.39	1.39
C_6-C_7	1.42	1.41	1.43	1.41	1.43	1.43
C_7-C_8	1.43	1.40	1.43	1.41	1.39	1.39
C_8-C_9	1.44	1.41	1.43	1.41	1.43	1.43
C_9-C_1	1.52	1.52	1.47	1.47	1.45	1.43
$C_1-C_2-C_3$	109.6	110.7	122.1	122.0	120.7	120.3
$C_3-C_4-C_{10}$	114.1	113.2	112.6	114.5	120.2	120.8
$C_{10}-C_9-C_1$	121.4	113.3	119.2	119.4	120.2	118.9
$C_{10}-C_4-C_3-C_2$	51.9	46.7	47.2	36.0	−1.0	0.0
$C_9-C_1-C_2-C_3$	39.0	46.7	1.3	0.3	0.8	0.0

[a] All angles in degrees and bond lengths in Å.

leads to a small elongation of the aromatic C−C bonds (0.02 Å) and an out-of-plane distortion of the C−H bonds by 4°.

The conformation of the saturated ring in 1−Fe$^+$ is not significantly altered as compared to uncomplexed tetralin in that, in both systems, the nonaromatic ring adopts a half-chair conformation. With respect to possible sites for the first C−H bond activation in the course of the dehydrogenation reaction, the distances of the two relevant axial hydrogen atoms in 1−Fe$^+$ (as shown in Figure 1) are of importance. According to the stereoelectronic principle[27] these H atoms should be preferred, as their C−H bond orbitals are parallel to the π-orbitals of the aromatic ring so that stabilization of the newly formed π-orbital is achieved at an early stage. The distance of the iron to the axial hydrogen in position C(1) amounts to 3.56 Å, whereas the hydrogen in position C(2) is further away (3.79 Å). If the saturated ring of 1−Fe$^+$ would adopt a boat-like conformation, the axial hydrogen atom bound to C(2) would be the nearest. These simple geometrical arguments in conjunction with the experimental results of the tetralin isotopologues point to the conclusion that the first C−H bond activation commences at C(1). This is also in accord with investigations for the deprotonation/protonation of the $Cr(CO)_3$−2−methyltetralin complex in the condensed phase.[28]

The theoretical investigation of intermediate **2** requires some care. Whereas for 1−Fe$^+$ the conformation of the nonaromatic ring is by and large unaffected by the metal−ion complexation, there exists a difference for **2**. In fact, two different structures were located. In one case (**2′**) the C(3)-methylene group is slightly bent toward the iron center with a hydrogen atom in an axial position at a distance of 3.9 Å to the iron. In a second conformation **2″** the C(3)-methylene group is turned away from the iron. In the latter case the only axial hydrogen is located at C(4) at a distance of only 3.4 Å to the iron. Hence, the second H_2 elimination is likely to occur at C(4) starting from structure **2′**. Once the second dehydrogenation step is completed both rings have achieved aromaticity. Yet, the theoretical analysis

Table 3. Comparison of Bond Dissociation Energies of Fe$^+$L (in kcal/mol) as Determined by Cooks' Kinetic Method and Calculated by Density Functional (BP) for the Quartet States of Fe$^+$L[a]

	exptl	Δ	computed	Δ
benzene−Fe$^+$	48.6[30] (55)[31]	0	57.1	0
tetralin−Fe$^+$ (1−Fe$^+$)	53.1 (59.5)	4.5	63.2	6.1
dihydronaphthalene-Fe$^+$ (**2′**)	52.2 (58.6)	3.6	63.7	6.6
dihydronaphthalene−Fe$^+$ (**2″**)			62.5	5.4
naphthalene-Fe$^+$ (**3**)	51.2 (57.6)	2.6	60.3	3.2

[a] The data in brackets refer to the anchor point of BDE(Fe$^+$−C_6H_6) = 55 kcal/mol; Δ denotes the bond dissociation energy relative to BDE(Fe$^+$−C_6H_6).

clearly points to a η^6-coordination of the metal to one ring only. As the mechanism of dehydrogenation implies an oxidative insertion of the metal ion in a C−H bond of the saturated ring, it is very likely that in the course of the reaction the metal undergoes a translocation from the aromatic part to the originally saturated region of tetralin.

The structure of the final product of the double dehydrogenation reaction, i.e., the naphthalene−Fe$^+$ complex **3** is quite similar to those of 1−Fe$^+$ and **2**. As already mentioned, the metal ion is η^6-coordinated and the geometric features of the coordinated aromatic ring are only marginally affected by the presence of the uncomplexed ring. We note that the hydrogens are bent away from the plane by ca. 2°. The charge transfer component reduces the Mulliken charge on iron to 0.77e.

Next, we turn to the thermochemistry of the single and double dehydrogenation of tetralin. Based on the ΔH_f values[29] for tetralin (6.0 kcal/mol), dihydronaphthalene (28.0 kcal/mol), and naphthalene (35.9 kcal/mol), in the absence of Fe$^+$ these reactions are endothermic. In order to probe the effect of Fe$^+$ on the reaction enthalpy, we have both measured and calculated bond dissociation energies of "bare" Fe$^+$ to tetralin, dihydronaphthalene, and naphthalene. Considering a simple thermodynamic cycle it becomes clear that this endothermicity does not change dramatically as the BDEs differ by only a few kcal/mol (Table 3). In addition, the heats of dehydrogenation can be assessed theoretically by subtraction of the calculated total

(27) (a) Deslongchamps, P. *Stereoelectronic Effects in Organic Chemistry*; Pergamon Press: Oxford, 1983. (b) Winterfeldt, E. *Prinzipien und Methoden der stereoselektiven synthese*; Vieweg & Sohn: Braunschweig, Germany, 1987.

(28) Schmalz, H.-G.; Volk, T.; Batz, J. W. In preparation.

(29) (a) Lias, S. G.; Liebman, J. F.; Levin, R. D. *J. Phys. Chem. Ref. Data* **1984**, *13*, 695. (b) Lias, S. G.; Liebman, J. F.; Levin, R. D.; Kafafi, S. A. *NIST Standard Reference Database, Positive Ion Energetics*, Version 2.01; Gaithersburg, MD, January 1994.

energies of the dehydrogenated species and H_2 from the one of the hydrogenated parent compounds. By doing so we obtain the following results: Comparing the complexed and the free hydrocarbon system, we find that the heats of dehydrogenation differ by less than 1 kcal/mol. This difference lies within the error of the method, especially as zero-point vibrational energies have not been considered. Hence, complexation with iron does not change the reaction enthalpy of the dehydrogenation reaction of these hydrocarbons. A complete investigation of the reaction pathway, including transition states, which would also allow for an estimate on the thermodynamic barriers of these reactions would be highly demanding for this system and has therefore not been performed.

The experimental *relative* bond dissociation energies have been estimated by using Cooks' kinetic method[6] of determining the intensities of unimolecular losses of ligands L and L′ from mixed bis-ligated complexes $Fe^+(L)(L')$. Using the known BDE(Fe^+−benzene)[30,31] as a reference (Table 3) these relative values can be converted to *absolute* BDEs. The experimental and calculated BDEs for $Fe^+(C_6H_6)$ and **1**−Fe^+, **2**, and **3** are collected in Table 3.

The previously calculated[20] BDE (47.6 kcal/mol) for the C_{6v} symmetrical structure of $Fe^+(C_6H_6)$ is in good agreement with the experimental value of 48.6 kcal/mol[30] obtained recently in our laboratory; the agreement with a value reported by Freiser and co-workers (55 kcal/mol)[31] is less pleasing. For the purpose of calibration of our computational method we recalculated the BDE for $Fe^+(C_6H_6)$ using the same method and basis set as employed for **1**−Fe^+, **2**, and **3**. Apparently, our result of 57.1 kcal/mol for BDE(Fe^+−C_6H_6) agrees well with Freiser's[31] value. We note, however, that the density functional approach used in the present calculations tends to significantly overestimate binding energies. Although we are not able to unambiguously decide which of the two experimental values is more accurate, we suppose the value of >55 kcal/mol as too high. In fact, a more recent experimental determination of the BDE of $Fe^+(C_6H_6)$ that uses an entirely different approach leads to a BDE of 51 kcal/mol.[32] As to the relative BDEs, the disagreement is much less pronounced; in fact, we find satisfying agreement between theory and experiment. In any case, the data in Table 3, from both theory and experiment, strongly suggest that the driving force in the single and double dehydrogenation of tetralin—which, in the metal-free system and when complexed with iron, is *endothermic*—is provided by the energy gained in the initial attachment of "bare" Fe^+ to the π-system of tetralin **1**.

Conclusions

We have shown that the bonding of Fe^+ to tetralin **1** is similar to that of Fe^+−benzene; this η^6-coordination is retained also in the dihydronaphthalene−Fe^+ complex **2** and the naphthalene−Fe^+ complex **3**. Both our labeling experiments and the geometrical analysis of the structures resulting from our calculations strongly suggest that the first C−H bond activation occurs at C(1). Furthermore, the results obtained for 5-substituted derivatives of tetralin indicate that iron migrates across the hydrocarbon system with a directionality determined by the nature of the substituent. The BDEs of tetralin, dihydronaphthalene and naphthalene are slightly higher than the one of Fe^+−benzene and remain almost unchanged for all three complexes involved in the dehydrogenation reaction of tetralin. Therefore the endothermicity of the single and double dehydrogenation of tetralin is retained, if complexed with iron.

Acknowledgment. We are grateful to the Deutsche Forschungsgemeinschaft and the Fonds der Chemischen Industrie for the financial support of our work, to Dr. D. Schröder for stimulating comments. R.H.H. thanks Cray Research, Inc. for generously providing CPU time, and especially to Dr. G. Fitzgerald.

OM950232K

(30) Schröder, D.; Schwarz, H. *J. Organomet. Chem.*, in press.
(31) (a) Hettich, R. L.; Jackson, T. C.; Stanko, E. M.; Freiser, B. S. *J. Am. Chem. Soc.* **1986**, *108*, 5086. (b) Bruckner, S. W.; Freiser, B. S. *Polyhedron* **1988**, *16/17*, 1583 and references cited therein.
(32) Armentrout, P. B. Private communication, January 1995.

Notes

Synthesis of the (σ-1,3-Butadiyn-1-yl)titanocenes $(\eta^5\text{-}C_5H_4SiMe_3)_2Ti(C{\equiv}CC{\equiv}CC_2H_5)(Cl)$ and $(\eta^5\text{-}C_5H_4SiMe_3)_2Ti(C{\equiv}CC{\equiv}CC_2H_5)_2$ and Their Reactions with Copper(I) Halides

Heinrich Lang* and Christian Weber

Anorganisch-Chemisches Institut, Ruprecht-Karls-Universität Heidelberg, Im Neuenheimer Feld 270, D-69120 Heidelberg, Germany

Received May 1, 1995[⊗]

*Summary: The reaction of L_2TiCl_2 (**1**) ($L = \eta^5\text{-}C_5H_4SiMe_3$) with 1 equiv of $LiC{\equiv}CC{\equiv}CC_2H_5$ (**2**) yields $L_2Ti(C{\equiv}CC{\equiv}CC_2H_5)(Cl)$ (**3**). **3** reacts with **2** to afford $L_2Ti(C{\equiv}CC{\equiv}CC_2H_5)_2$ (**4a**); **4a** also can be prepared by treatment of **1** with 2 equiv of **2**. The compounds $L_2Ti(C{\equiv}CC{\equiv}CC_2H_5)(Cl)$ (**3**) and $L_2Ti(C{\equiv}CC{\equiv}CR)_2$ (**4a**, R = C_2H_5; **4b**, R = $SiMe_3$) can be used as organometallic chelating ligands for the stabilization of monomeric CuBr, yielding $[L_2Ti(C{\equiv}CC{\equiv}CC_2H_5)(Cl)]CuBr$ (**6**) or $[L_2Ti(C{\equiv}CC{\equiv}CR)_2]CuBr$ (**7a**, R = C_2H_5; **7b**, R = $SiMe_3$). The CuBr moiety in **6** is complexed by the chloro group and the inner C≡C triple bond of the 1,3-butadiyn-1-yl ligand, whereas in compounds **7a** and **7b** CuBr is coordinated by the inner C≡C triple bonds of the 1,3-butadiyn-1-yl ligands.*

Introduction

Recently, we reported the synthesis of the first stable mono(σ-alkynyl)titanocene species, $L_2Ti(C{\equiv}CR)(Cl)$ ($L_2 = (\eta^5\text{-}C_5H_2SiMe_3)_2(SiMe_2)_2$, $(\eta^5\text{-}C_5H_4SiMe_3)_2$; R = $SiMe_3$, $^tC_4H_9$, C_6H_5).[1-4] These compounds are stable in solution at ambient temperature as well as in the solid state and do not redistribute their ligands, RC≡C and Cl, so that the formation of the respective L_2TiCl_2 and $L_2Ti(C{\equiv}CR)_2$ compounds is not observed.[1,2] The $L_2Ti(C{\equiv}CR)(Cl)$ complexes react with polymeric copper(I) aggregates $[CuX]_n$ (X = singly bonded organic or inorganic ligand), to give complexed monomeric copper(I) moieties, $[L_2Ti(C{\equiv}CR)(Cl)]CuX$, in which the alkynyl ligand and the chloro group both are coordinated to the monomeric CuX fragment.[1,2]

In this study, we describe the synthesis of the first stable mono(σ-1,3-butadiyn-1-yl)titanocene chloride, $(\eta^5\text{-}C_5H_4SiMe_3)_2Ti(C{\equiv}CC{\equiv}CC_2H_5)(Cl)$, and the bis($\sigma$-1,3-butadiyn-1-yl)titanocene $(\eta^5\text{-}C_5H_4SiMe_3)_2Ti(C{\equiv}CC{\equiv}CC_2H_5)_2$. The reactions of these compounds with $[CuBr]_n$ are described.

Results and Discussion

The titanocene dichloride L_2TiCl_2 (**1**; $L = \eta^5\text{-}C_5H_4SiMe_3$)[5] reacted at −50 °C in diethyl ether with 1 molar equiv of $LiC{\equiv}CC{\equiv}CC_2H_5$ (**2**)[6] to form orange $L_2Ti(C{\equiv}CC{\equiv}CC_2H_5)(Cl)$ (**3**) in 59% yield. The bis(1,3-butadiyn-1-yl)titanocene $L_2Ti(C{\equiv}CC{\equiv}CC_2H_5)_2$ (**4a**) also was formed as a byproduct in 10% yield (eq 1).

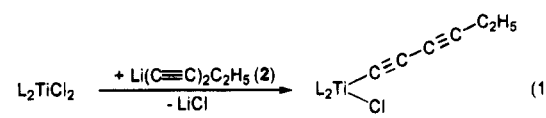

1 3 (1)

Product **3** after appropriate purification gave orange crystals of **3**, which are stable for months in the solid state. In solution compound **3** slowly redistributes its ligands, forming $L_2Ti(C{\equiv}CC{\equiv}CC_2H_5)_2$ (**4a**) and L_2TiCl_2 (**1**; $L = \eta^5\text{-}C_5H_4SiMe_3$).

Reaction of **3** with 1 molar equiv of **2** in diethyl ether, after appropriate workup, gave the air-stable deep red bis(σ-4-ethyl-1,3-butadiyn-1-yl)titanocene $L_2Ti(C{\equiv}CC{\equiv}CC_2H_5)_2$ (**4a**) in 86% yield. The preparation of compound **4a** also can be effected in 67% yield by treatment of L_2TiCl_2 (**1**)[5] with 2 molar equiv of $LiC{\equiv}CC{\equiv}CC_2H_5$ (**2**)[6] in diethyl ether at 25 °C (eq 2).

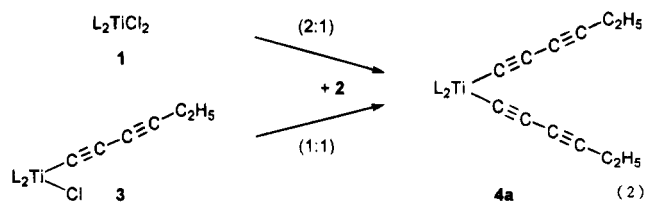

(2)

Addition of $L_2Ti(C{\equiv}CC{\equiv}CC_2H_5)(Cl)$ (**3**) or L_2Ti-

[⊗] Abstract published in *Advance ACS Abstracts,* August 1, 1995.

(1) Lang, H.; Blau, S.; Pritzkow, H.; Zsolnai, L. *Organometallics* **1995**, *14*, 1850.

(2) Lang, H.; Wu, I. Y.; Frosch, W.; Jacobi, A.; Pritzkow, H.; Nuber, B. Unpublished report.

(3) Lang, H.; Seyferth, D.; *Z. Naturforsch., B* **1990**, *45B*, 212. For the related $[(\eta^5\text{-}C_5H_5)_2Ti(C{\equiv}CSiMe_3)_2]$ compound, see: Woord, G. L.; Knobler, C. B.; Hawthorne, M. F. *Inorg. Chem.* **1989**, *28*, 382.

(4) For related zirconium compounds, see: Erker, G.; Frömberg, W.; Benn, R.; Mynott, R.; Angermund, K.; Krüger, C. *Organometallics* **1989**, *8*, 911.

(5) (a) Druce, P. M.; Kingston, B. M.; Lappert, M. F.; Spaiding, T. R.; Srivastava, *J. Chem. Soc. A* **1969**, 2106. (b) Lappert, M. F.; Pickett, C. J.; Riley, P. I.; Yarrow, P. I. W. *J. Chem. Soc., Dalton Trans.* **1980**, 805.

(6) Brandsma, L. *Preparative Acetylenic Chemistry*; 2nd ed.; Elsevier: Amsterdam, 1988; Chapter 5.9, p 51.

0276-7333/95/2314-4415$09.00/0

$(C{\equiv}CC{\equiv}CR)_2$ (**4a**, R = C_2H_5; **4b**, R = $SiMe_3$[7]) to a suspension of $[CuBr]_n$ (**5**) in an equimolar ratio in THF at 25 °C resulted in the formation of the bimetallic complex $[L_2Ti(C{\equiv}CC{\equiv}CC_2H_5)(Cl)]CuBr$ (**6**) or $[L_2Ti(C{\equiv}CC{\equiv}CR)_2]CuBr$ (**7a,b**) (eqs 3 and 4).

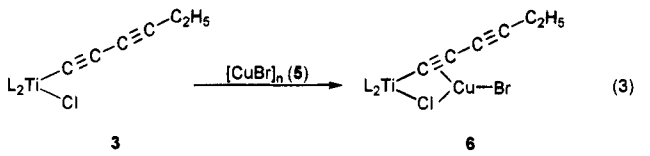

3 **6** (3)

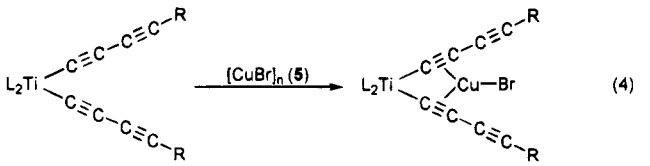

(4)

4a: R = C_2H_5
4b: R = $SiMe_3$

7a: R = C_2H_5 (96%)
7b: R = $SiMe_3$ (88%)

Compounds **6** and **7** are soluble in toluene, THF and acetone and can be precipitated as orange (compound **6**) or red (compounds **7a,b**) solids by cooling their THF/*n*-pentane solutions to −30 °C. In the solid state **6** can be handled in air only for short periods, while **7a,b** are stable in air for months.

Compounds **6** and **7** feature a monomeric copper(I) bromide entity, with the copper atom in an trigonal-planar environment.[1,8,9] The 4-ethyl-1,3-butadiyn-1-yl ligand and the chloro group of $L_2Ti(C{\equiv}CC{\equiv}CC_2H_5)(Cl)$ both are bonded to the monomeric CuBr moiety in compound **6**. In the dinuclear compounds **7a,b** the CuBr unit is complexed by the inner C≡C units of both $C{\equiv}CC{\equiv}CC_2H_5$ substituents. The outer C≡C bonds are noncoordinating. Even when a 5-fold excess of $[CuBr]_n$ is used, no reaction with the outer C≡C bonds can be observed.

Compounds **6** and **7** are monomeric in solution (cryoscopy in benzene). The mass spectra of compounds **6** and **7** are in agreement with this monomeric character.

The most characteristic features in the IR spectra of compounds **6** and **7** are two distinct C≡C stretching vibrations at 2197 and 1935 cm^{-1} for **6**, 2198 and 1952 cm^{-1} for **7a**, and 1997 as well as 1929 cm^{-1} for **7b**. The η^2-coordinated C≡C units of the 1,3-butadiyn-1-yl ligands thus are observed at lower wavenumber in each case. The η^2 coordination shift from the ν(C≡C) vibrations of the respective parent compounds (2032, 2023, and 2001 cm^{-1} in **3** and **4a,b**[2]) to lower wavenumbers indicates a bond weakening of the inner C≡C bonds in compounds **6** and **7**. The same observation has been made for compounds of the general type $[(\eta^5\text{-}C_5H_4SiMe_3)_2Ti(C{\equiv}CR)_2]CuX$ (X = singly bonded organic or inorganic ligand),[1,8,9] a phenomenon typical for π-bonding of alkynes to copper(I) fragments in which the alkyne unit acts as a donor ligand.[1,8,10]

The ^1H and $^{13}C\{^1H\}$ NMR spectra of compounds **3**, **4**, **6**, and **7** in $CDCl_3$ or C_6D_6 consist of sharp and well-resolved signals for each of the organic groupings present. The most remarkable feature about the ^1H NMR spectra is the appearance of multiplets (ratio 1:2:1 or 1:1:1:1, respectively) for the cyclopentadienyl protons of compounds **3** and **6**, while in the ^1H NMR spectra of **4** and **7** an AA'XX' resonance pattern is observed in the δ 6.0−6.7 region (J_{HH} = 2.3−2.6 Hz). This can be attributed to the unsymmetric (compounds **3** and **6**) or symmetric (compounds **4** and **7**) structures of compounds **3**, **4**, **6**, and **7**, respectively.

In the $^{13}C\{^1H\}$ NMR spectra of all new compounds reported, the expected four resonances due to the 1,3-butadiyn-1-yl ligands are found in the δ 65−140 region. The resonances of the carbon atoms of the C≡C moieties bonded to the titanium center are shifted to lower field (δ 120−140) as compared to the carbon signals of the RC≡C units (R = C_2H_5, $SiMe_3$) (δ 65−105) of the C≡C-C≡CR ligands.[8,11]

The potential use of compounds **3** and **4** for the synthesis of multimetallic complexes is the subject of further research.

Experimental Section

General Comments. All reactions were carried out under an atmosphere of nitrogen using standard Schlenk techniques. Diethyl ether was purified by distillation from sodium/benzophenone ketyl; *n*-pentane was purified by distillation from calcium hydride. Infrared spectra were obtained with a Perkin-Elmer 983G spectrometer. ^1H NMR spectra were recorded on a Bruker AC 200 spectrometer operating at 200.132 MHz in the Fourier transform mode; ^{13}C NMR spectra were recorded at 50.323 MHz. Chemical shifts are reported in δ units (parts per million) downfield from tetramethylsilane with the solvent as the reference signal. FD and EI mass spectra were recorded on a Finnigan 8230 mass spectrometer operating in the positive-ion mode. Melting points were determined using the analytically pure samples, sealed off in nitrogen-purged capillaries on a Gallenkamp MFB 595 010 M melting point apparatus. Microanalyses were performed by the Organisch-Chemisches Institut der Universität Heidelberg.

(A) Synthesis of $(\eta^5\text{-}C_5H_4SiMe_3)_2Ti(C{\equiv}CC{\equiv}CC_2H_5)(Cl)$ (3). To 1.0 g (2.54 mmol) of $(\eta^5\text{-}C_5H_4SiMe_3)_2TiCl_2$ (**1**)[5] in 150 mL of diethyl ether at −50 °C was added slowly 1 equiv of $LiC{\equiv}CC{\equiv}CC_2H_5$ (**2**) in diethyl ether.[6] After the reaction mixture had been stirred for 2 h at 25 °C, all volatiles were evaporated and the resulting dark red residue was extracted with 50 mL of *n*-pentane/diethyl ether (1:1). After filtration through Celite, the filtrate was cooled to −30 °C. An orange solid (650 mg; 1.49 mmol, 59%), **3**, crystallized.

Mp: 93 °C dec. IR (KBr): 2193 (m), 2032 (vs) [$\nu_{C\equiv C}$] cm^{-1}. ^1H NMR ($CDCl_3$): δ 0.29 (s, $SiMe_3$, 18H), 1.15 (t, J_{HH} = 7.5 Hz, CH_3, 3 H), 2.37 (q, J_{HH} = 7.5 Hz, CH_2, 2 H), 6.2 (m, C_5H_4, 2 H), 6.6 (m, C_5H_4, 4 H), 6.8 (m, C_5H_4, 2 H). $^{13}C\{^1H\}$ NMR ($CDCl_3$): δ 0.1 ($SiMe_3$), 13.7 (CH_3) 13.9 (CH_2), 65.8 ($C{\equiv}\mathit{C}CH_2$), 90.2 ($\mathit{C}{\equiv}CCH_2$), 114.9 (C_5H_4), 117.8 (C_5H_4), 119.6 ($^iC/C_5H_4$), 121.7 (Ti$\mathit{C}{\equiv}C$), 124.6 (C_5H_4), 126.2 (C_5H_4), 129.0 ($^iC/C_5H_4$), 136.0 (Ti$\mathit{C}{\equiv}C$). MS-FD [*m/z* (relative intensity)]: 436 (10), M^+; 399 (20), $M^+ - Cl$; 322 (100), $M^+ - Cl - C_4C_2H_5$. Anal. Calcd for $C_{22}H_{31}ClSi_2Ti$ (435.01): C, 60.75; H, 7.18. Found: C, 60.49; H, 6.98.

(7) Lang, H.; Weinmann, S.; Weber, C.; Wu, I. Y.; Nuber, B. *J. Organomet. Chem.*, submitted for publication.
(8) Lang, H.; Köhler, K.; Blau, S. *Coord. Chem. Rev.*, in press, and literature cited therein.
(9) Lang, H.; Weinmann, M. *Synlett*, in press, and literature cited therein.
(10) *E.g.*: (a) Villacorta, G. M.; Gibson, D.; Williams, I. D.; Whang, E.; Lippard, S. J. *Organometallics* **1987**, *6*, 2426. (b) Aalten, H. L.; van Koten, G.; Stam, C. H. *Inorg. Chem.* **1989**, *28*, 4140.
(11) Wrackmeyer, B.; Horchler, K. *Prog. NMR Spectrosc.* **1990**, *22*, 209.

(B) Synthesis of $(\eta^5\text{-}C_5H_4SiMe_3)_2Ti(C{\equiv}CC{\equiv}CC_2H_5)_2$ (4a). **(1) Reaction of 3 with 2.** One equivalent of **2**[6] was added to 0.5 g (1.15 mmol) of **3** in 200 mL of diethyl ether at −50 °C. After it was stirred for 2 h at 25 °C, the reaction mixture was worked up as described in (A). Crystallization at −30 °C yielded **4a** (470 mg, 0.99 mmol; 86%) as a dark red solid.

(2) Reaction of 1 with 2. The addition of 1.0 g (12.0 mmol) of **2**[6] to 2.4 g (6.0 mmol) of $(\eta^5\text{-}C_5H_4SiMe_3)_2TiCl_2$ (**1**)[5] in 100 mL of diethyl ether resulted in a color change from orange-red to deep red. After the mixture was stirred for 4 h at 25 °C, all volatiles were removed under high vacuum and the resulting residue was extracted with *n*-pentane and filtered through a pad of Celite. Crystallization of the residue from *n*-pentane at −30 °C yielded 1.9 g (4.0 mmol; 67%) of **4a**.

Mp: 108 °C dec. IR (KBr): 2189 (m), 2023 (vs) [$\nu_{C\equiv C}$] cm^{-1}. ^1H NMR ($CDCl_3$): δ 0.28 (s, $SiMe_3$, 18H), 1.16 (t, J_{HH} = 7.5 Hz, CH_3, 6 H), 2.37 (q, J_{HH} = 7.5 Hz, CH_2, 4 H), 6.37 (t, J_{HH} = 2.6 Hz, C_5H_4, 4 H), 6.65 (t, J_{HH} = 2.6 Hz, C_5H_4, 4 H). $^{13}C\{^1H\}$ NMR ($CDCl_3$): δ −0.07 ($SiMe_3$), 13.7 (CH_3), 14.0 (CH_2), 65.8 (C≡*C*CH_2), 92.5 (*C*≡CCH_2), 114.7 (C_5H_4), 118.4 (TiC≡*C*), 121.7 (C_5H_4), 126.4 ($^iC/C_5H_4$), 141.3 (Ti*C*≡C). MS-EI [*m/z* (relative intensity)]: 477 (8), M^+; 398 (16), $M^+ - C_4C_2H_5$; 322 (100), $M^+ - 2\,C_4C_2H_5$. Anal. Calcd for $C_{28}H_{36}Si_2Ti$ (476.7): C, 70.55; H, 7.61. Found: C, 70.22; H, 7.53.

(C) Synthesis of $[(\eta^5\text{-}C_5H_4SiMe_3)_2Ti(C{\equiv}CC{\equiv}CC_2H_5)(Cl)]\text{-}CuBr$ (6). To a solution of $(\eta^5\text{-}C_5H_4SiMe_3)_2Ti(C{\equiv}CC{\equiv}CC_2H_5)(Cl)$ (**3**; 290 mg, 0.67 mmol) in diethyl ether (20 mL) was added in one portion at 25 °C 100 mg (0.67 mmol) of $[CuBr]_n$. The suspension was stirred in the dark for 3 h and afterwards filtered through a pad of Celite (diethyl ether). When the filtrate was concentrated and cooled to −30 °C, compound **6** (370 mg, 0.64 mmol; 96%) was obtained as a red crystalline solid.

Mp: 67 °C dec. IR (KBr): 2197 (vs), 1935 (s) (η^2-coordinated) [$\nu_{C\equiv C}$] cm^{-1}. ^1H NMR ($CDCl_3$): δ 0.29 (s, $SiMe_3$, 18H), 1.24 (t, J_{HH} = 7.5 Hz, CH_3, 3 H), 2.44 (q, J_{HH} = 7.5 Hz, CH_2, 2 H), 6.1 (m, C_5H_4, 2 H), 6.2 (m, C_5H_4, 4 H), 6.4 (m, C_5H_4, 2 H), 6.6 (m, C_5H_4, 2 H). $^{13}C\{^1H\}$ NMR ($CDCl_3$): δ −0.7 ($SiMe_3$), 13.2 (CH_3), 14.3 (CH_2), 65.3 (C≡*C*CH_2), 108.8 (*C*≡CCH_2), 117.1 (C_5H_4), 117.5 (C_5H_4), 119.6 ($^iC/C_5H_4$), 120.9 (C_5H_4), 121.7 (C_5H_4), 122.9 (TiC≡*C*), 128.3 ($^iC/C_5H_4$), 129.8 (Ti*C*≡C). MS-FAB [*m/z* (relative intensity)]: 497 (40), M^+ − Br; 399 (20), $M^+ - Cu - Cl$; 322 (100), $M^+ - Cu - Cl - Br - C_4C_2H_5$. Anal. Calcd for $C_{22}H_{31}BrClCuSi_2Ti$ (578.46): C, 45.68; H, 5.40. Found: C, 43.37; H, 5.67 (compound **6** slowly decomposes on addditional attempted purification by crystallization).

(D) Synthesis of $[(\eta^5\text{-}C_5H_4SiMe_3)_2Ti(C{\equiv}CC{\equiv}CR)_2]Cu^IBr$ (7a, R = C_2H_5; 7b, R = $SiMe_3$). To a solution of $(\eta^5\text{-}C_5H_4\text{-}SiMe_3)_2Ti(C{\equiv}CC{\equiv}CR)_2$ (**4a**, R = C_2H_5, 400 mg, 0.84 mmol; **4b**, R = $SiMe_3$,[7] 475 mg, 0.84 mmol) in diethyl ether (20 mL) was added in one portion at 25 °C 120 mg (0.84 mmol) of $[CuBr]_n$. The suspension was stirred in the dark for 3 h and afterwards filtered through a pad of Celite. On concentration of the filtrate with subsequent cooling to −30 °C, compound **7a** (500 mg, 0.8 mmol; 96%) or **7b** (524 mg, 0.74 mmol; 88%) was obtained as a red crystalline solid.

7a: mp 170 °C dec. IR (KBr): 2198 (vs), 1952 (s) (η^2-coordinated) [$\nu_{C\equiv C}$] cm^{-1}. ^1H NMR ($CDCl_3$): δ 0.25 (s, $SiMe_3$, 18H), 1.26 (t, J_{HH} = 7.6 Hz, CH_3, 6 H), 2.53 (q, J_{HH} = 7.6 Hz, CH_2, 4 H), 6.06 (t, J_{HH} = 2.3 Hz, C_5H_4, 4 H), 6.21 (t, J_{HH} = 2.3 Hz, C_5H_4, 4 H). $^{13}C\{^1H\}$ NMR ($CDCl_3$): δ −0.1 ($SiMe_3$), 13.4 (CH_3), 14.6 (CH_2), 65.4 (C≡*C*CH_2), 101.3 (*C*≡CCH_2), 113.9 (C_5H_4), 117.1 (C_5H_4), 124.5 ($^iC/C_5H_4$), 126.4 (TiC≡*C*), 134.9 (Ti*C*≡C). MS-FD [*m/z* (relative intensity)]: 619 (55), M^+; 539 (100), M^+ − Br; 322 (90), $M^+ - CuBr - 2C_4C_2H_5$. Anal. Calcd for $C_{28}H_{36}BrCuSi_2Ti$ (620.11): C, 54.23; H, 5.85. Found: C, 54.46; H, 5.68.

7b: mp 210 °C dec. IR (KBr): 1997 (m), 1929 (vs) (η^2-coordinated) [$\nu_{C\equiv C}$] cm^{-1}. ^1H NMR ($CDCl_3$): δ 0.21 (s, $SiMe_3$, 18H), 0.27 (s, $SiMe_3$, 18H), 6.09 (t, J_{HH} = 2.4 Hz, C_5H_4, 4 H), 6.21 (t, J_{HH} = 2.4 Hz, C_5H_4, 4 H). $^{13}C\{^1H\}$ NMR ($CDCl_3$): δ −0.2 ($SiMe_3$), −0.1 ($SiMe_3$), 88.2 (C≡*C*Si), 105.7 (*C*≡CSi), 114.2 (C_5H_4), 117.3 (C_5H_4), 125.0 ($^iC/C_5H_4$), 125.2 (TiC≡*C*), 138.3 (Ti*C*≡C). MS-FD [*m/z*]: 708. Anal. Calcd for $C_{30}H_{44}BrCuSi_4Ti$ (708.37): C, 50.87; H, 6.26. Found: C, 50.11; H, 5.73.

Acknowledgment. We are grateful to the Deutsche Forschungsgemeinschaft, the Fonds der Chemischen Industrie, and Prof. Dr. G. Huttner for financial support. We thank Th. Jannack for carrying out the MS measurements.

OM9503196

Iridium-Catalyzed Reaction of Acetylene Hydrazones with a Hydrosilane and Carbon Monoxide. Synthesis of Nitrogen Heterocycles

Naoto Chatani, Shinshi Yamaguchi, Yoshiya Fukumoto, and Shinji Murai

Organometallics, **1995**, 14 (9), 4418-4420• DOI: 10.1021/om00009a053 • Publication Date (Web): 01 May 2002

Iridium-Catalyzed Reaction of Acetylene Hydrazones with a Hydrosilane and Carbon Monoxide. Synthesis of Nitrogen Heterocycles

Naoto Chatani, Shinshi Yamaguchi, Yoshiya Fukumoto, and Shinji Murai*

Department of Applied Chemistry, Faculty of Engineering, Osaka University, Suita, Osaka 565, Japan

Received May 15, 1995[⊗]

Summary: The reaction of acetylene hydrazones with a hydrosilane and carbon monoxide (CO) in the presence of $Ir_4(CO)_{12}$ as the catalyst gave six- or seven-membered nitrogen heterocycles having a (tert-butyldimethylsilyl)-methylene group at the 3-position.

Transition-metal-catalyzed reactions of hydrosilanes and CO[1] have been extensively studied by us[2-4] and other groups.[5-9] We reported that iridium complexes such as $Ir_4(CO)_{12}$ and $[IrCl(CO)_2]_n$ catalyzed the reaction of olefins with hydrosilanes and CO to give acylsilane derivatives.[3] We also reported that the reaction of 1,6-diynes with hydrosilanes and CO in the presence of $Ru_3(CO)_{12}/PCy_3$ resulted in the incorporation of two molecules of CO into the diynes to give catechol derivatives.[4] This reaction is a rare example of the catalytic incorporation of CO into diynes. Mechanistically, the reaction involves a new way of incorporating CO via an oxycarbyne complex.

The reactions of acetylenes with hydrosilanes and CO in the presence of rhodium complexes such as $Rh_4(CO)_{12}$, $Co_2Rh_2(CO)_{12}$, and $Rh_2(pfb)_4$ (pfb = perfluorobutyrate) have been found to result in silylformylation of acetylenes leading to α-silylacrylaldehydes by Matsuda,[5a] Ojima,[6a] and Doyle.[7] Recently, Alper reported the rhodium-catalyzed reaction of acetylenes with hydrosilanes and synthesis gas (H_2/CO = 1/1) leading to α-silylacrylaldehydes or α-(silylmethyl)acrylaldehydes depending on the structure of the acetylenes.[8] Acetylenes having a functional group at an appropriate, remote position are expected to undergo intramolecular cyclization, which is one of the most useful methods for the construction of a cyclic framework in organic synthesis. Indeed, the Rh-catalyzed reaction of propargyl alcohols and amines with hydrosilanes and CO afforded β-lactones and β-lactams, respectively.[5b,c] Ojima found a rather unusual cyclization of allyldipropargylamine.[6b] The formation of bicyclo[3.3.0]octenones from 1,6-diynes was reported by Ojima[6f] and Matsuda.[5e] A cyano group was found to remain intact in the rhodium-catalyzed reaction of a 1-acetylene-6-nitrile.[6d] Chemoselective silylformylation of the acetylene functionality was demonstrated in the reaction of 1-acetylene-ω-aldehydes (ω = 5–7), the aldehyde functionality being intact.[6e] However, an aldehyde functionality took part in the reaction to give a cyclized product without incorporation of CO under particular reaction conditions only in the case of 5-hexyn-1-al.[6e] While the reaction of acetylenes having some functional groups with hydrosilanes and CO has been studied as shown above, much remains to be explored. No examples of the Rh-catalyzed reaction of acetylenes having a carbon–nitrogen double bond with hydrosilanes and CO have appeared. In addition, there have been no reports on iridium-catalyzed reactions of acetylenes with a hydrosilane and CO. We now report that the reactions of acetylene hydrazones[10] with a hydrosilane and CO can be effected by iridium catalysts and give nitrogen heterocycles.

The reactions of acetylene hydrazone **1** with $HSiMe_2Bu^t$ (6 equiv) and CO (50 atm at room temperature) in CH_3CN at 140 °C gave the seven-membered nitrogen heterocycle **2** in 36% GC yield (eq 1). The reaction

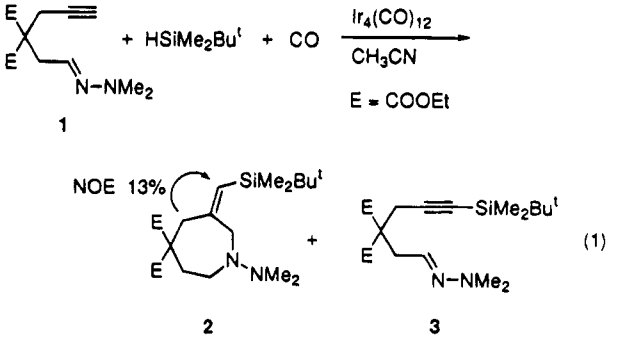

1 2 3 (1)

involves cyclization with incorporation of one molecule of CO and reduction of the incorporated CO carbon to a methylene group (2-position in **2**). A major side reaction

[⊗] Abstract published in *Advance ACS Abstracts,* August 1, 1995.

(1) For a recent review paper on transition-metal-catalyzed reactions of $HSiR_3$ and CO, see: Chatani, N.; Murai, S. *Synlett,* in press.

(2) For our recent papers on rhodium/$HSiR_3$/CO, see: Ikeda, S.; Chatani, N.; Kajikawa, Y.; Ohe, K.; Murai, S. *J. Org. Chem.* **1992,** *57,* 2. Ikeda, S.; Chatani, N.; Murai, S. *Organometallics* **1992,** *11,* 3494. Fukumoto, Y.; Chatani, N.; Murai, S. *J. Org. Chem.* **1993,** *58,* 4187. Fukumoto, Y.; Yamaguchi, S.; Chatani, N.; Murai, S. *J. Organomet. Chem.* **1995,** *489,* 215.

(3) For a recent paper on iridium/$HSiR_3$/CO, see: Chatani, N.; Ikeda, S.; Ohe, K.; Murai, S. *J. Am. Chem. Soc.* **1992,** *114,* 9710.

(4) For a recent paper on ruthenium/$HSiR_3$/CO, see: Chatani, N.; Fukumoto, Y.; Ida, T.; Murai, S. *J. Am. Chem. Soc.* **1993,** *115,* 11614.

(5) (a) Matsuda, I.; Ogiso, A.; Sato, S.; Izumi, Y. *J. Am. Chem. Soc.* **1989,** *111,* 2332. (b) Matsuda, I.; Ogiso, A.; Sato, S. *J. Am. Chem. Soc.* **1990,** *112,* 6120. (c) Matsuda, I.; Sakakibara, J.; Nagashima, H. *Tetrahedron Lett.* **1991,** *32,* 7431. (d) Matsuda, I.; Sakakibara, J.; Inoue, H.; Nagashima, H. *Tetrahedron Lett.* **1992,** *33,* 5799. (e) Matsuda, I.; Ishibashi, H.; Ii, N. *Tetrahedron Lett.* **1995,** *36,* 241.

(6) (a) Ojima, I.; Ingallina, P.; Donovan, R. J.; Clos, N. *Organometallics* **1991,** *10,* 38. (b) Ojima, I.; Donovan, R. J.; Shay, W. R. *J. Am. Chem. Soc.* **1992,** *114,* 6580. (c) Eguchi, M.; Zeng, Q.; Korda, A.; Ojima, I. *Tetrahedron Lett.* **1993,** *34,* 915. (d) Ojima, I.; Donovan, R. J.; Eguchi, M.; Shay, W. R.; Ingallina, P.; Korda, A.; Zeng, Q. *Tetrahedron* **1993,** *49,* 5431. (e) Ojima, I.; Tzamarioudaki, M.; Tsai, C.-Y. *J. Am. Chem. Soc.* **1994,** *116,* 3643. (f) Ojima, I.; Fracchiolla, D. A.; Donovan, R. J.; Banerji, P. *J. Org. Chem.* **1994,** *59,* 7594.

(7) Doyle, M. P.; Shanklin, M. S. *Organometallics* **1993,** *12,* 11. Doyle, M. P.; Shanklin, M. S. *Organometallics* **1994,** *13,* 1081.

(8) Zhou, J.-Q.; Alper, H. *Organometallics* **1994,** *13,* 1586.

(9) Wright, M. E.; Cochran, B. B. *J. Am. Chem. Soc.* **1993,** *115,* 2059.

(10) For a paper on cyclization of acetylene hydrazones, see: Jensen, M.; Livinghouse, T. *J. Am. Chem. Soc.* **1989,** *111,* 4495.

0276-7333/95/2314-4418$09.00/0

Table 1. Reaction of 1 with $HSiMe_2Bu^t$ and CO in the Presence of $Ir_4(CO)_{12}$[a]

run no.	temp, °C	pressure of CO, atm	2	3
1[b]	160	50	26	15
2	140	50	36	12
3[b]	120	50	28	10
4	140	15	40	14
5	140	10	53	18
6	140	5	41	25

[a] Reaction conditions: **1** (1 mmol), $HSiMe_2Bu^t$ (6 mmol), $Ir_4(CO)_{12}$ (0.02 mmol), CH_3CN (10 mL), 20 h. [b] The reaction was run on a 0.5 mmol scale.

was dehydrogenative silylation of acetylene leading to **3**.[11] The other byproduct was a siloxane, $(^tBuMe_2Si)_2O$. The *Z* stereochemistry of **2** was determined by NOE experiments. Specifically, irradiation of the methylene proton at the 4-position led to a 13% enhancement of the vinyl proton; however, no enhancement of the vinyl proton was observed on the irradiation of the methylene proton at the 2-position.

The selected results of the reaction of **1** under variable reaction conditions are shown in Table 1. In all cases, the byproduct **3** was formed. The reaction temperature of 140 °C gave a good result (runs 1–3). Although the reaction proceeded under CO pressure ranging from 5 to 50 atm, the reaction under 10 atm gave the highest yield of **2** (run 5). A lowered CO pressure increased the yield of byproduct **3**. The choice of solvent was crucial. The use of DMSO, DMF, THF, Et_2O, dioxane, CH_2Cl_2, toluene, and hexane did not give product **2**, but a complex mixture containing **3** was obtained in most cases (not shown in Table 1). The product **2** was formed only using CH_3CN as the solvent. Further manipulation of the reaction parameters to improve the yield of **2** was unsuccessful. Several other iridium complexes were examined for their catalytic activity. While $IrH(CO)(PPh_3)_3$, $IrCl(CO)(PPh_3)_2$, and $Na_2IrCl_6{\cdot}6H_2O$ were not effective, $Ir(COD)_2BF_4$ and $[IrCl(COD)]_2$ exhibited catalytic activity, affording **2**.

The reactions of substituted acetylene hydrazones were examined. However, no reaction occurred for the methyl-substituted derivative **4** even under more forcing reaction conditions. Thus, the present reaction seems applicable to only terminal acetylenes.

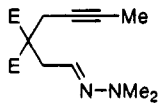

4

We have examined the reaction of a starting acetylene hydrazone that does not contain geminal substituents on the tether. The reaction of 5-hexynal dimethylhydrazone (**5**) with $HSiMe_2Bu^t$ and CO gave the expected product **6**, but in a low yield (eq 2), indicating the necessity of geminal substituents in the tether for effective cyclization as is often the case in cyclization reactions.[12] Shortening the length of the tether by one methylene unit gave the corresponding six-membered nitrogen heterocycle **9** (eq 3).

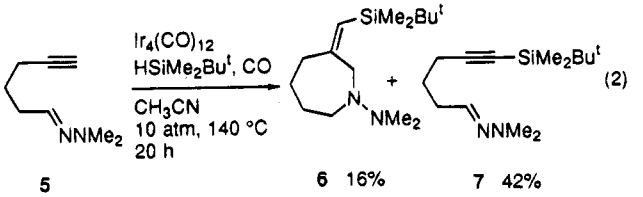

5 **6** 16% **7** 42%

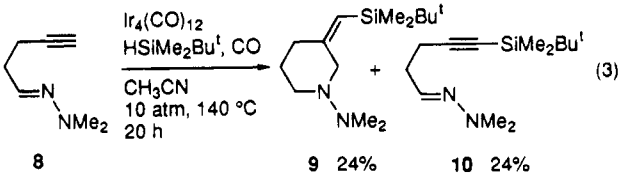

8 **9** 24% **10** 24%

In contrast to the extensive studies on Rh-catalyzed reactions,[5–8] there have been no reports, to the best of our knowledge, on Ir-catalyzed reactions of acetylenes with hydrosilanes and CO. The reaction of a simple acetylene under the same reaction conditions as those in eqs 1–3 was examined. Many products, including 1-(*tert*-butyldimethylsilyl)-1-octyne (51% yield), 1-(*tert*-butyldimethylsilyl)-1-octene (23%), **11** (7%), and **12** (20%) were obtained in the reaction of octyne (eq 4). No silylformylation product was observed under the reaction conditions, in contrast to Rh-catalyzed reactions of acetylenes.[5a, 6a, 7]

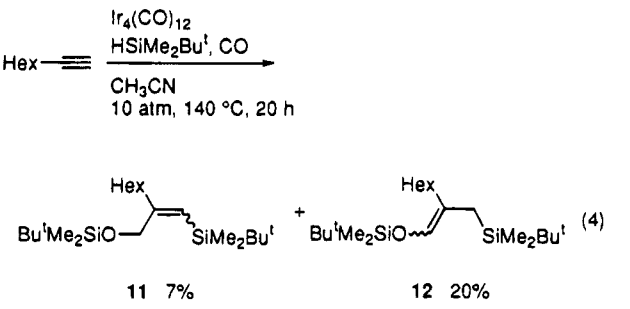

11 7% **12** 20%

In summary, the first examples of transition-metal-catalyzed reactions of acetylene species having a C–N double bond with a hydrosilane and CO are reported herein. The reaction provides a new method for the construction of nitrogen heterocycles. A reaction mechanism of formation of nitrogen heterocycles is not fully understood at present.[13]

Experimental Section

General Information. Boiling points (bp) refer to the air bath temperature for bulb-to-bulb distillation and are uncorrected. ^1H NMR and ^{13}C NMR spectra were recorded on a JEOL JMN-270 spectrometer in $CDCl_3$ with tetramethylsilane as an internal standard. Data are reported as follows: chemical shift in ppm (δ), multiplicity (s = singlet, d = doublet, t = triplet, quint = quintet, m = multiplet, and c = complex),

(11) Dehydrogenative silylation of terminal acetylenes is often encounterd in the hydrosilylation of acetylenes. For a recent paper, see: Esteruelas, M. A.; Olivan, M.; Oro, L. A.; Tolosa, J. I. *J. Organomet. Chem.* **1995**, *487*, 143.

(12) Forbes, M. D. E.; Patton, J. T.; Myers, T. L.; Maynard, H. D.; Smith, D. W., Jr.; Schulz, G. R.; Wagener, K. B. *J. Am. Chem. Soc.* **1992**, *114*, 10978.

(13) The reaction might proceed via the intermediacy of compounds shown below, although neither of these were not observed:

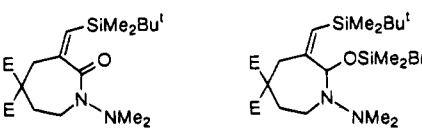

coupling constant (Hz), integration, and interpretation. Infrared spectra (IR) were obtained on a Hitachi IR-400 spectrometer; absorptions are reported in reciprocal centimeters. Mass spectra were obtained on a Shimadzu GCMS-QP 1000 with an ionization voltage of 70 eV. Elemental analyses and HRMS were performed by the Elemental Analyses Section of Osaka University. Analytical GC was carried out on a Shimadzu GC-14A gas chromatograph equipped with a Shimadzu Hicap CBP-10-M25−025 capillary column. Column chromatography was performed with SiO_2 (Wakogel).

Preparation of 3,3-Bis(ethoxycarbonyl)-5-hexynal Dimethylhydrazone (1). In a 300-mL three-necked round-bottomed flask, fitted with a dropping funnel and a reflux condenser, was placed 125 mL of absolute ethanol. To this was added 5.75 g (250 mmol) of freshly cut sodium. When most of the sodium had dissolved, a solution of redistilled diethyl malonate (250 mmol, 40 g) in ethanol (10 mL) was added from the dropping funnel over 30 min. Then a solution of 2-bromo-1,1-diethoxyethane (324 mmol, 64 g) in ethanol (40 mL) was added over 3 h. When the addition was complete, the reaction mixture was refluxed and stirred for 40 h. After it was cooled, the reaction mixture was diluted with 50 mL of water to dissolve the salt, and most of the ethanol was removed in vacuo. The aqueous layer was extracted with 80 mL of ether four times. The ethereal solution was dried over anhydrous magnesium sulfate. The solution was evaporated, and the product, diethyl (1,1-diethoxyethyl)malonate, was distilled under reduced pressure. The fraction boiling at about 90−125 °C/1 mmHg was collected and redistilled. The yield was 28.8 g (42% yield).

In a 300-mL three-necked round-bottomed flask, fitted with a dropping funnel and a reflux condenser, sodium ethoxide was prepared from 3.1 g (135 mmol) of sodium and 82 mL of absolute ethanol. When most of the sodium had dissolved, a solution of diethyl (1,1-diethoxyethyl)malonate (104 mmol, 28.7 g) in ethanol (20 mL) was added from the dropping funnel over 30 min. After the mixture was stirred for 1 h, a solution of propargyl bromide (135 mmol, 16 g) in ethanol (20 mL) was added over 40 min. When the addition was complete, the reaction mixture was stirred for 30 min. The reaction mixture was diluted with 25 mL of water to dissolve the salt, most of the ethanol was removed in vacuo, and 200 mL of water was added. The aqueous layer was extracted with 160 mL of ether four times. The ethereal solution was dried over anhydrous magnesium sulfate. The crude 5-yne 1-al diethyl acetal was obtained by evaporation of the solvent. The crude yield was 27.5 g (84% yield). The crude product was used in the next step without purification because its ^1H NMR spectrum showed that the crude product was essentially pure.

In a 500-mL three-necked round-bottomed flask were placed the 5-yne 1-al diethyl acetal (83 mmol, 26 g), acetone (330 mL), H_2O (5 mL), and Amberist-15 (3.3 g), and the solution was stirred at room temperature. After 20 h Amberist-15 (0.5 g) was again added and the solution was stirred for another 1.5 h. Filtration of Amberist-15 and evaporation gave the crude 5-yne 1-al (21.7 g, purity 86%). In a 100-mL three-necked round-bottomed flask fitted with a dropping funnel were placed Me_2NNH_2 (120 mmol, 7.2 g), CH_3COOH (0.4 mL), and a solution of 5-yne 1-al (40 mmol, 9.35 g) in ethanol (10 mL). Then, the resulting solution was stirred at reflux for 60 h. Evaporation followed by column chromatography on silica gel with 500 mL of hexane/EtOAc (7:1), 600 mL of hexane/EtOAc (3:1), and 900 mL of hexane/EtOAc (1:1) as eluants gave 3.36 g (30% yield) of pure **1** and 4.73 g of the 5-yne 1-al diethyl acetal (50% yield). ^1H NMR ($CDCl_3$): δ 1.25 (t, J = 7.3 Hz, 6H, CH_3), 2.01 (t, J = 2.7 Hz, 1H, CH≡), 2.72 (s, 6H, CH_3N), 2.87 (d, J = 2.7 Hz, 2H, CH_2CH≡), 2.96 (d, J = 5.4 Hz, CH_2C=), 4.20 (q, J = 7.3 Hz, 4H, CH_2O), 6.50 (t, J = 5.4 Hz, 1H, CH=). IR (neat): 3278, 2988, 2906, 2856, 2786, 1734, 1603, 1450, 1394, 1367, 1285, 1206, 1091, 916, 856, 814, 758 cm^{-1}; MS, *m/z* (relative intensity) 282 (9, M^+), 209 (11), 197 (41), 166 (17), 163 (15), 138 (18), 137 (16), 93 (13), 86 (62), 85 (100), 65 (19), 59 (14). Anal. Calcd for $C_{14}H_{22}N_2O_4$: C, 59.56; H, 7.85; N, 9.92. Found: C, 59.36; H, 7.90; N, 9.60.

Acetylene hydrazones **5** and **8** were prepared by the treatment of the corresponding aldehydes with dimethylhydrazine.

Catalytic Reaction of 1 with $HSiMe_2Bu^t$ and CO Leading to 1-(Dimethylamino)-5,5-bis(ethoxycarbonyl)-(*Z*)-3-((*tert*-butyldimethylsilyl)methylene)hexahydro-1*H*-azepine (2). In a 50-mL stainless steel autoclave were placed in order, $Ir_4(CO)_{12}$ (0.02 mmol, 22 mg), $HSiMe_2Bu^t$ (6 mmol, 1.0 mL), and **1** (1 mmol, 282 mg) in CH_3CN (10 mL). The autoclave was charged with carbon monoxide to 10 atm at 25 °C and then heated at 140 °C for 20 h. After the autoclave was cooled, the solvent was evaporated. Column chromatography on silica gel (hexane/EtOAc, 3/1) gave the pure product **2**. For the GLC yield, an appropriate hydrocarbon ($C_{22}H_{46}$) calibrated against purified products in CH_3CN/benzene was added as the standard after the catalytic reaction. ^1H NMR ($CDCl_3$): δ 0.05 (s, 6H, CH_3Si), 0.86 (s, 9H, Bu^t), 1.22 (t, J = 7.0 Hz, 3H, CH_3), 1.98−2.02 (m, 2H, CH_2), 2.32 (s, 6H, CH_3N), 2.74−2.78 (m, 2H, CH_2N), 2.99 (s, 2H, CH_2C=), 3.47 (s, 2H, CH_2N), 4.05−4.20 (m, 4H, CH_2O), 5.38 (s, 1H, CH=). ^{13}C NMR ($CDCl_3$): δ −4.26 (CH_3Si), 13.98 (CH_3), 17.07 (CSi), 26.42 (Bu^t), 35.22 (CH_2), 40.04 (CH_3N), 42.03 (CH_2C=), 45.14 (CH_2N), 56.02 (CH_2N), 57.29 (C), 60.99 (CH_2O), 127.04 (CH=), 152.70 (C=), 171.52 (C=O). IR (neat) 3088, 2940, 2860, 2776, 1733, 1608, 1500, 1462, 1388, 1364, 1304, 1237, 1183, 1133, 1095, 1058, 1018, 829, 778, 756, 700 cm^{-1}; MS: *m/z* (relative intensity) 412 (M^+, 17), 103 (14), 102 (13), 93 (13), 86 (18), 85 (56), 75 (40), 74 (13), 73 (100), 72 (20), 71 (10), 60 (34), 59 (59). HRMS: calcd for $C_{21}H_{40}O_4N_2Si$ (M^+) 412.2758, found 412.2773.

1-(Dimethylamino)-(*Z*)-3-((*tert*-butyldimethylsilyl)methylene)hexahydro-1*H*-azepine (6). ^1H NMR ($CDCl_3$) δ 0.09 (s, 6H, CH_3Si), 0.89 (s, 9H, Bu^t), 1.56 (c, 4H, CH_2), 2.35 (s, 6H, CH_3N), 2.35−2.41 (m, 2H, CH_2C=), 2.59 (t, J = 5.4 Hz, 2H, CH_2N), 3.53 (s, 2H, CH_2N), 5.30 (s, 1H, CH=). ^{13}C NMR ($CDCl_3$): δ −4.06 (CH_3Si), 17.18 (CSi), 26.54 (Bu^t), 30.33 (CH_2), 39.41 (CH_2), 40.04 (CH_3N), 49.09 (CH_2N), 57.29 (CH_2N), 121.85 (CH=), 160.16 (C=). IR (neat) 3100, 3080, 2942, 2858, 1607, 1466, 1359, 1343, 1247, 1140, 1082, 1005, 971, 875, 837 cm^{-1}. MS: *m/z* (relative intensity) 268 (M^+, 7), 166 (15), 102 (17), 98 (22), 86 (15), 83 (11), 79 (10), 75 (24), 74 (16), 73 (65), 59 (55), 57 (13), 56 (19), 55 (14), 45 (29), 44 (100). HRMS: calcd for $C_{15}H_{32}N_2Si$ (M^+) 268.2335, found 268.2336.

1-(Dimethylamino)-(*Z*)-3-(*tert*-butyldimethylsilylmethylene)hexahydroazine (9). ^1H NMR ($CDCl_3$): δ −0.10 (s, 9H, CH_3Si), 0.88 (s, 9H, Bu^t), 1.66 (quint, J = 5.4 Hz, 2H, CH_2), 2.13 (t, J = 5.4 Hz, 2H, CH_2), 2.40 (s, 6H, CH_3N), 2.71 (t, J = 5.4 Hz, 2H, CH_2N), 3.17 (s, 2H, CH_2N), 5.24 (s, 1H, CH=). ^{13}C NMR ($CDCl_3$): δ −3.97 (CH_3Si), 16.95 (SiC), 26.06 (CH_2), 26.40 (Bu^t), 38.22 (CH_2), 39.46 (CH_3N), 49.06 (CH_2N), 52.54 (CH_2N), 120.67 (CH=), 154.63 (C=). IR (neat): 3082, 2944, 2888, 1627, 1465, 1362, 1343, 1246, 1241, 1112, 1014, 951, 913, 886, 835, 799, 777, 706 cm^{-1}. MS: *m/z* (relative intensity) 254 (M^+, 26), 152 (22), 139 (80), 102 (47), 96 (12), 86 (10), 85 (69), 74 (20), 73 (100), 60 (12), 59 (78). HRMS: calcd for $C_{14}H_{30}N_2Si$ (M^+) 254.2178, found 254.2183.

Acknowledgment. This work is partially supported by grants from the Ministry of Education, Science, and Culture of Japan.

OM9503508

Carbon–Nitrogen Bond Formation by Reductive Elimination from Nickel(II) Amido Alkyl Complexes

Kwangmo Koo and Gregory L. Hillhouse*

Searle Chemistry Laboratory, Department of Chemistry, The University of Chicago, Chicago, Illinois 60637

Received June 15, 1995[⊗]

*Summary: Reaction of the azametallacyclohexane complex [(bpy)Ni{N(Tol)(CH$_2$)$_4$}] (**1**) with diacetylferrocenium tetrafluoroborate, O$_2$, or I$_2$ induces N–C reductive elimination, giving high yields of N-p-tolylpyrrolidine (**2**) upon chromatographic workup. Reaction of [(bpy)Ni(CH$_2$CMe$_2$-o-C$_6$H$_4$)] (**3**) with N$_3$Ph gives the azametallacycle [(bpy)Ni(NPh-o-C$_6$H$_4$CMe$_2$CH$_2$)] (**4**), which reacts with CO to give the lactam PhNC(O)CH$_2$CMe$_2$-o-C$_6$H$_4$ (**5**) and with HCl to give 2-tert-butyl-N-phenylaniline. Oxidation of **4** with [(AcCp)$_2$Fe$^+$], I$_2$, or O$_2$ results in N–C reductive elimination and affords high yields of the indoline PhN(CH$_2$CMe$_2$-o-C$_6$H$_4$) (**6**). The azametallacycle **4** is also thermally unstable with respect to C,N-reductive elimination to give **6**. Significantly lower yields of products resulting from N–C reductive elimination are realized when acyclic alkylnickel amides are oxidized. Thus, N,N-dimethyl-p-toluidine (**8**) is produced by the reaction of [(AcCp)$_2$Fe$^+$], I$_2$, or O$_2$ with [(bpy)Ni{N(Tol)(Me)}(Me)] (**7**), [(bpy)Ni{N(Ph)(Et)}(Et)] (**9**) reacts with I$_2$ to afford both N,N-diethylaniline (**10**) and N-ethylaniline (**11**) competitively, and [(bpy)Ni{N(Tol)(i-Bu)}(i-Bu)] (**12**) reacts with I$_2$ to give, primarily, N-isobutyl-p-toluidine (**14**), with smaller amounts of N,N-diisobutyl-p-toluidine (**13**).*

Introduction

Reductive-elimination reactions are ubiquitous across the transition-metal block and are among the most synthetically useful reactions in the organometallic chemist's arsenal. While reductive eliminations that form H–H, C–H, and C–C bonds are common,[1] similar reactions that form C–X bonds (where X is a heteroatom) are rare.[2,3] Nonetheless, reductive eliminations that form C–N bonds are strongly *implicated* in reactions such as Pd-catalyzed hetero cross-coupling reactions that form aryl amines[4] and the synthesis of organic amides and lactams from [(bpy)Ni(R)(NR$_2$)] and CO,[5] and two examples of C,N-reductive eliminations from well-characterized molecules have been reported.[6,7]

Scheme 1

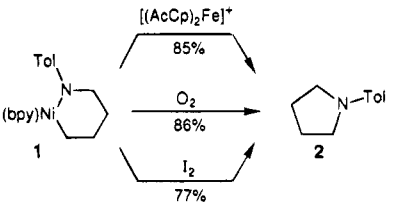

Herein we report on a general class of reductive-elimination reactions, from discrete nickel complexes possessing alkyl and amido ligands, that form new carbon–nitrogen bonds in product amines and indolines.

Results and Discussion

We recently reported that reaction of aryl azides with [(bpy)Ni(R)$_2$] (bpy ≡ 2,2′-bipyridine) derivatives provides a synthetic route to Ni(II) complexes containing aryl-amido ligands.[5] The azametallacycle [(bpy)Ni{N(Tol)-(CH$_2$)$_4$}] (**1**) is an isolable, thermally stable compound that undergoes thermal decomposition in benzene solution at ~130 °C. Remarkably, as shown in Scheme 1, reaction of solutions of **1** with either O$_2$ or I$_2$ at ambient temperature affords high yields of *N*-*p*-tolylpyrrolidine (**2**) upon chromatographic workup. Moreover, the one-electron oxidant 1,1′-diacetylferrocenium tetrafluoroborate also cleanly converts **1** to **2**, consistent with the notion that oxidation of Ni(II) to Ni(III) induces or facilitates C,N-reductive elimination. The ultimate fate of the Ni in these reactions has not been established, although free bipyridine is observed. Oxidatively induced reductive-elimination reactions that result in C–C bond formation are well established in organometallic chemistry, and several relevant nickel examples have been studied. For example, O$_2$ induces reductive elimination of cyclobutane from [(bpy)Ni(CH$_2$)$_4$][8] and chemical or electrochemical oxidation of Ni(II) to Ni(III) in [(bpy)Ni(R)$_2$] (R = alkyl, aryl) gives R–R-coupled products in high yields.[9]

In the course of examining the scope of this chemistry, we have studied the reaction of [(bpy)Ni(CH$_2$CMe$_2$-*o*-C$_6$H$_4$)] (**3**)[10] with N$_3$Ph at ambient temperature. As shown in Scheme 2, the reaction proceeds regiospecifically with insertion of the NPh fragment into the Ni–C(aryl) bond of **3** to give **4** and N$_2$. The regiochemistry of the insertion reaction was determined by quenching solutions of **4** with anhydrous HCl, giving 2-*tert*-butyl-*N*-phenylaniline (73% yield) on chromatographic workup. Similarly, reaction of solutions of **4** with carbon

[⊗] Abstract published in *Advance ACS Abstracts,* August 1, 1995.

(1) Collman, J. P.; Hegedus, L. S.; Norton, J. R.; Finke, R. G. *Principles and Applications of Organotransition Metal Chemistry*; University Science Books: Mill Valley, CA, 1987.

(2) For an example of C,S-reductive elimination, see: Barañano, D.; Hartwig, J. F. *J. Am. Chem. Soc.* **1995**, *117*, 2937.

(3) For examples of C,O-reductive eliminations, see: (a) Koo, K.; Hillhouse, G. L.; Rheingold, A. L. *Organometallics* **1995**, *14*, 456. (b) Matsunaga, P. T.; Mavropoulos, J. C.; Hillhouse, G. L. *Polyhedron* **1995**, *14*, 175. (c) Hoberg, H.; Schaefer, D.; Burkhart, G.; Krüger, C.; Romao, M. J. *J. Organomet. Chem.* **1984**, *266*, 203.

(4) (a) Guram, A. S.; Buchwald, S. L. *J. Am. Chem. Soc.* **1994**, *116*, 7901. (b) Paul, F.; Patt, J.; Hartwig, J. F. *J. Am. Chem. Soc.* **1994**, *116*, 7901.

(5) Matsunaga, P. T.; Hess, C. R.; Hillhouse, G. L. *J. Am. Chem. Soc.* **1994**, *116*, 3665.

(6) Berryhill, S. R.; Price, T.; Rosenblum, M. *J. Org. Chem.* **1983**, *48*, 158.

(7) Villanueva, L. A.; Abboud, K. A.; Boncella, J. M. *Organometallics* **1994**, *13*, 3921.

(8) Takahashi, S.; Suzuki, Y.; Sonogashira, K.; Hagihara, N. *J. Chem. Soc., Chem. Commun.* **1976**, *839*.

(9) Tsou, T. T.; Kochi, J. K. *J. Am. Chem. Soc.* **1978**, *100*, 1634.

(10) Cámpora, J.; Gutiérrez, E.; Monge, A.; Palma, P.; Poveda, M. L.; Ruíz, C.; Carmona, E. *Organometallics* **1994**, *13*, 1728.

0276-7333/95/2314-4421$09.00/0

Scheme 2

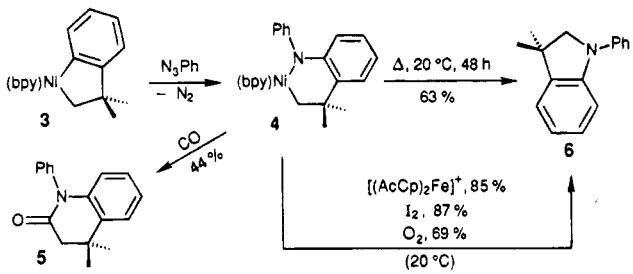

Scheme 3

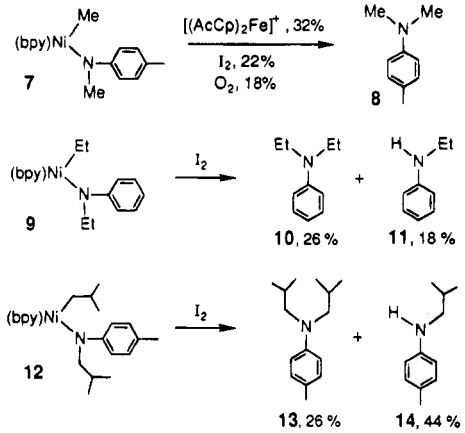

monoxide affords the lactam **5** as colorless crystals in 44% yield. An intriguing observation is that, unlike **1**, the azametallacycle **4** is thermally unstable with respect to C,N-reductive elimination to give the *N*-phenyl indoline **6**. Thus, stirring solutions of **4** for 2 days at ambient temperature affords **6** in 63% isolated yield. From a synthetic perspective, this Ni-based route to an indoline is interesting because it introduces the nitrogen functionality into the bicyclic ring system in the last step, in contrast to other protocols to indolines and indoles that incorporate nitrogen at earlier stages.[11] The most convenient route to the indoline **6**, however, is the treatment of **4** with an oxidizing agent (I_2, O_2, or $[(AcCp)_2Fe]^+$), which rapidly and cleanly effects the reductive elimination (Scheme 2).

Scheme 3 shows three acyclic alkylnickel(II) amido complexes, accessible by the reaction of aryl azides with dialkylnickel(II) derivatives,[5] that we have investigated with regard to C,N-reductive elimination to give trisubstituted arylamines. Oxidation of **7** by 1,1′-diacetylferrocenium gives **8** in 32% isolated yield. Somewhat lower yields of the C,N-coupled product are realized using I_2 or O_2 as the oxidant. In reactions of **7**, no secondary amine (i.e., MeNHTol) was detected, although in reactions of complexes having alkyl ligands with β-H atoms, the yields of secondary amines rival or exceed those of products derived from C,N-elimination. Thus, **9** reacts with I_2 to afford **10** (26%) and **11** (18%) competitively, while **12** reacts with I_2 to give **14** (44%) as the primary product, with smaller amounts of **13** (26%). The azametallacycle **1**, however, does not react to give a

(11) (a) Hegedus, L. S. *Angew. Chem., Int. Ed. Engl.* **1988**, *27*, 1113. (b) Tidwell, J. H.; Senn, D. R.; Buchwald, S. L. *J. Am. Chem. Soc.* **1991**, *113*, 4685. (c) Krolski, M. E.; Renaldo, A. F.; Rudisill, D. E.; Stille, J. K. *J. Org. Chem.* **1988**, *53*, 1170. (d) Kozikowski, A. P. *Heterocycles* **1981**, *16*, 267. (e) Robinson, B. *The Fischer Indole Synthesis*; Wiley-Interscience: New York, 1982. (f) Brown, R. K. *Indoles*: Wiley-Interscience: New York, 1972.

Scheme 4

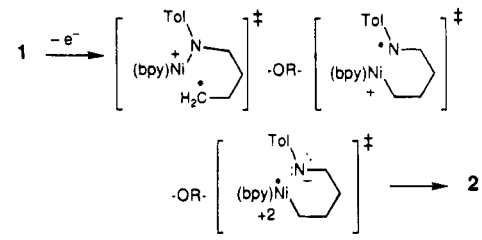

secondary amine product even though it possesses β-H atoms, perhaps because constraints imposed by the ligand's cyclic structure prevent the β-hydrogens from interacting with Ni. It is also noteworthy that the yields are considerably higher for C,N-reductive elimination from the cyclic derivatives **1** and **4** (75–87%) than for the acyclic examples **7**, **9**, and **12** (26–32%), suggesting that the mechanism of reductive elimination might be a stepwise sequence involving intermediates akin to those shown in Scheme 4. Such an *intramolecular* process for metallacycles such as **1** and **4** could be efficient and give rise to high yields of cyclic amines, but a similar process for acyclic molecules would be an *intermolecular* one in which cage escape results in diminished yields of C,N-coupled products.

Experimental Section

General Considerations. Reactions were carried out using standard high-vacuum and Schlenk techniques and dry, air-free solvents. ^1H and $^{13}C\{^1H\}$ NMR spectra were recorded in C_6D_6 solution using a General Electric Ω-500 spectrometer (^1H at 500 MHz; ^{13}C at 125.8 MHz). Infrared spectra were recorded on a Nicolet 20SXB spectrometer in Nujol mulls with KBr plates. Quantitative GC data were obtained on a Hewlett-Packard 5890 instrument with an integrator. Mass spectra were recorded on a VG Analytical LTD 70-70 EQ double-focusing (EB) mass spectrometer. Spectral data for new compounds are tabulated in Table 1. Elemental analyses were performed by Desert Analytics (Tucson, AZ). Authentic samples of *N*,*N*-dimethyl-*p*-toluidine (**8**), *N*,*N*-diethylaniline (**10**), and *N*-ethylaniline (**11**) were purchased from Aldrich Chemical Co. The following compounds were prepared according to literature procedures: [(bpy)Ni{N(Tol)(CH_2)$_4$}] (**1**),[5] [(bpy)Ni(CH_2CMe_2-*o*-C_6H_4)] (**3**),[10] [(bpy)Ni{N(Tol)(Me)}(Me)] (**7**),[5] [(bpy)Ni{N(Ph)(Et)}(Et)] (**9**),[5] and [(bpy)Ni(*i*-Bu)$_2$].[3b]

Preparation of 2. To a solution of **1** (0.07 g, 0.18 mmol) in C_6H_6 (10 mL) was added I_2 (0.047 g, 0.18 mmol). The solution was stirred at ambient temperature for 3 h, during which time the color changed from purple to dark yellow. The solution was filtered, the volatiles were removed under vacuum, and the residue was extracted with *n*-hexane (20 mL). The extracts were concentrated and chromatographed on silica gel (eluent *n*-hexane/ethyl acetate, 4:1) to give **2** (0.023 g, 77%) as a yellow oil. Using a procedure analogous to that described above, reaction of **1** with O_2 (1 atm) or $[(AcCp)_2Fe][BF_4]$ yielded **2** in 86% and 85% yields, respectively.

Preparation of 5. A sample of **3** (0.095 g, 0.27 mmol) in 15 mL of benzene was treated with N_3Ph (32 μL, 0.27 mmol) and stirred for 3 h at ambient temperature. The resulting purple solution of **4** was exposed to CO (1 atm) and stirred for an additional 10 min; then the solution was filtered and taken to dryness under vacuum and the residue extracted with hexane. The extracts were concentrated and chromatographed on silica gel using hexane/ethyl acetate (1:1) to give **5** (0.03 g, 44%) as colorless crystals (mp 118–119 °C).

Preparation of 6. (a) Oxidative Route. Using a procedure and workup analogous to that described for **5**, reaction of **3** (0.09 g, 0.25 mmol) with N_3Ph (30 μL, 0.25 mmol) for 3 h

Table 1. Spectroscopic Data for New Compounds

2: ^{1}H NMR δ 7.14 (d, 2 H, aryl), 6.52 (d, 2 H, aryl), 2.98 (t, 4 H, CH_2), 2.32 (s, 3 H, CH_3), 1.54 (t, 4 H, CH_2); $^{13}C\{^1H\}$ NMR δ 146.5, 129.9, 124.4, 122.2, 47.6, 25.4, 20.6; EIMS 160 ($M^+ - 1$)

5: ^{1}H NMR δ 7.2–7.1 (m, 4 H, aryl), 7.06 (d, 1 H, aryl), 7.04 (d, 1 H, aryl), 6.78 (quintet, 2 H, aryl), 6.42 (d, 1 H, aryl), 2.39 (s, 2 H, CH_2), 1.12 (s, 6 H, CH_3); $^{13}C\{^1H\}$ NMR δ 167.9, 141.2, 139.5, 134.6, 129.6, 129.4, 127.7, 127.1, 124.2, 123.1, 118.0, 46.5, 33.4, 27.2; EIMS 251 (M^+); IR ν(CO) 1677 cm^{-1}

6: ^{1}H NMR δ 7.22–7.11 (m, 5 H, aryl), 7.02 (t, 1H, aryl), 6.96 (d, 1H, aryl), 6.95 (t, 1H, aryl), 6.80 (t, 1 H, aryl), 3.30 (s, 2 H, CH_2), 1.14 (s, 6 H, CH_3); 1.14 (s, 6 H, CH_3); $^{13}C\{^1H\}$ NMR δ 145.9, 144.5, 140.4, 129.4, 127.6, 122.4, 121.0, 119.6, 117.9, 108.6, 66.2, 39.7, 27.7; EIMS 223 (M^+)

12: ^{1}H NMR δ 8.91–6.30 (m, 12 H, bpy/aryl), 3.58 (m, 1 H, CH), 3.26 (m, 1 H, NC*H*H), 2.98 (m, 1 H, NC*H*H), 2.38 (s, 3 H, CH_3), 1.90 (m, 1 H, CH), 1.36 (d, 6 H, CH_3), 1.30 (m, 2 H, $NiCH_2$), 1.25–1.20 (m, 6 H, CH_3); $^{13}C\{^1H\}$ NMR δ 158.4, 155.9, 152.2, 151.2, 149.7, 135.8, 134.9, 129.6, 125.3, 125.1, 120.2, 118.9, 118.0, 112.6, 61.2, 31.1, 30.9, 26.8, 24.9, 22.9, 22.7

13: ^{1}H NMR δ 7.06 (d, 2 H, aryl), 6.68 (d, 2 H, aryl), 2.98 (d, 4 H, CH_2), 2.26 (s, 3 H, CH_3), 2.03 (m, 2 H, CH), 0.82 (d, 12 H, CH_3); $^{13}C\{^1H\}$ NMR δ 154.0, 129.9, 120.4, 113.9, 60.9, 26.6, 20.4;[a] EIMS 219 (M^+)

14: ^{1}H NMR δ 7.13–6.30 (d, 2 H, aryl), 6.68 (d, 2 H, aryl), 3.09 (br, 1 H, NH), 2.67 (d, 2 H, CH_2), 2.24 (s, 3 H, CH_3), 1.60 (m, 1 H, CH), 0.80 (d, 6 H, CH_3); $^{13}C\{^1H\}$ NMR δ 146.9, 129.9, 125.9, 113.2, 52.2, 28.6, 20.6, 20.5; EIMS 163 (M^+)

[a] Two CH_3 resonances are accidentally degenerate (δ 20.4), confirmed by selective decoupling.

followed by addition of I_2 (0.06 g, 0.25 mmol) gave **6** (0.05 g, 87%) as a yellow oil after chromatography. Alternatively, reaction of solutions of **4** with O_2 (1 atm) or $[(AcCp)_2Fe][BF_4]$ yielded **6** in 69% and 85% yields, respectively.

(**b**) **Thermal Route.** Using a procedure and workup analogous to that described for **5**, reaction of **3** (0.10 g, 0.28 mmol) with N_3Ph (34 μL, 0.28 mmol) for 48 h gave **6** (0.04 g, 63%) as a yellow oil after chromatography.

Preparation of 8. To a solution of **7** (0.12 g, 0.33 mmol) in THF (15 mL) was added I_2 (0.083 g, 0.33 mmol). The solution was stirred at ambient temperature for 3 h, during which time the color changed from magenta to orange. Workup as for **5** (eluent *n*-hexane/Et_2O, 5:1) gave **8** (0.012 g, 22%) as a yellow oil. The product was identified by spectral comparison with an authentic sample. Using analogous procedures, reaction of **7** with O_2 (1 atm) or $[(AcCp)_2Fe][BF_4]$ yielded **2** in 18% and 32% yields, respectively.

Preparation of 10 and 11. A solution of **9** (0.16 g, 0.44 mmol) in toluene (20 mL) was treated with I_2 (0.11 g, 0.44 mmol) and stirred at ambient temperature for 2 h. The solution was filtered, the filtrate was reduced to dryness using a rotary evaporator, and the residue was extracted using Et_2O (20 mL), which was concentrated and then chromatographed on silica gel (eluent *n*-hexane/Et_2O, 10:1) to give **10** (0.017 g, 26%) and **11** (0.010 g, 18%), which were identified by spectral comparison with authentic samples.

Preparation of 12. To a solution of (bpy)Ni(*i*-Bu)$_2$ (0.48 g, 1.47 mmol) in THF (25 mL) was added N_3Tol (0.33 mL, 2.94 mmol) via syringe, the solution was stirred for 2 h at ambient temperature and filtered, the filtrate was reduced in volume to 5 mL under vacuum, and then *n*-pentane (20 mL) was added by vacuum transfer. The solution was cooled to −78 °C for 1 h, and the resulting crystalline magenta product was isolated by filtration, washed with cold *n*-pentane (3 × 5 mL), and dried to give **12** (0.51 g, 80%). Anal. Calcd for $C_{25}H_{33}N_3Ni$: C, 69.2; H, 7.66; N, 9.68. Found: C, 69.0; H, 7.68; N, 10.98.

Preparation of 13 and 14. Using a procedure analogous to that used for **10** and **11**, reaction of **12** (0.21 g, 0.48 mmol) with I_2 (0.12 g, 0.48 mmol) yielded **13** (0.027 g, 26%) and **14** (0.035 g, 44%) as yellow oils.

Acknowledgment. We are grateful to the National Science Foundation for financial support of this research through a grant to G.L.H. and to the government of South Korea for an Overseas Scholarship to K.K.

OM950458N

Expansion of the Nitrile Capped Cluster Fe3(CO)9(N.tplbond.CPh)

Harald Bantel, Pierre Suter, and Heinrich Vahrenkamp

Organometallics, **1995**, 14 (9), 4424-4426• DOI: 10.1021/om00009a055 • Publication Date (Web): 01 May 2002

Expansion of the Nitrile Capped Cluster $Fe_3(CO)_9(N{\equiv}CPh)$

Harald Bantel, Pierre Suter, and Heinrich Vahrenkamp*

Institut für Anorganische und Analytische Chemie der Universität Freiburg, Albertstrasse 21, D-79104 Freiburg, Germany

Received May 23, 1995[⊗]

*Summary: Treatment of the cluster $Fe_3(CO)_9(\mu_3\text{-}\eta^2\text{-}N{\equiv}CPh)$ (**1**) with the cluster expansion reagents $Fe_2(CO)_9$, $CpRh(CO)_2$, and $Ru_3(CO)_{12}$ results in the formation of the tetranuclear clusters $Fe_3(CO)_9ML_n(\mu_4\text{-}\eta^2\text{-}N{\equiv}CPh)$ (**2a**, $ML_n = Fe(CO)_3$; **2b**, $ML_n = RhCp$; **2c**, $ML_n = Ru(CO)_3$). The butterfly shape of these clusters and the unsymmetrical capping mode of the benzonitrile ligand were confirmed by structure determination of the Fe_3Ru cluster **2c**.*

Introduction

The reactivity and bonding of unsaturated organic molecules are not only modified by their attachment to transition metal centers, but they also vary considerably when the number of coordinated metal atoms is varied.[1-3] This has most often been demonstrated for alkynes,[1] and we have contributed studies on azoalkanes attached to two, three, or four metal atoms.[4-6] In order to enable such studies, clusters with varying size and composition must be available, to which the same organic substrate is attached. One way of obtaining these is the cluster expansion reaction by which organometallic fragments are condensed onto existing polynuclear metal–substrate combinations.[7] We have applied this technique to clusters containing alkynes,[8] vinylidenes,[9] or azoalkanes[10] as the organic substrates.

This note reports our findings for clusters containing a nitrile as the unsaturated substrate. The triiron benzonitrile cluster **1**,[11] whose preparation has recently been optimized,[12] was used as the starting compound. It was already observed in the first paper on **1**[11]that this cluster can be formed together with its tetranuclear homologue **2a**, and it was assumed[11] and later confirmed[13] that iron carbonyl units present in the reaction mixture effect the expansion from **1** to **2a**. Here we report the details of this expansion and of two related ones yielding the Fe_3Rh and Fe_3Ru clusters **2b** and **2c**.

$Fe_3(CO)_9(\mu_3\text{-}\eta^2\text{-}N{\equiv}CPh)$ **1**

$Fe_3(CO)_9ML_n(\mu_4\text{-}\eta^2\text{-}N{\equiv}CPh)$
2a, $ML_n = Fe(CO)_3$
2b, $ML_n = RhCp$
2c, $ML_n = Ru(CO)_3$

Experimental Section

The general experimental and spectroscopic techniques were as described before.[14] The starting compound **1** was prepared according to the improved procedure.[12] Reagents and solvents were obtained commercially.

2a. 150 mg (0.29 mmol) of **1** and 105 mg (0.29 mmol) of $Fe_2(CO)_9$ in 120 mL of hexane were stirred and irradiated by an immersed 150 W high-pressure Hg lamp in a Pyrex glass apparatus for 17 h. The mixture was evaporated to dryness by an oil pump. The residue was picked up in hexane and chromatographed with hexane over a 2 × 30 cm silica gel column. The first, brown, fraction contained 53 mg (35%) of unreacted **1**. The second, black, fraction yielded 81 mg (42%) of **2a** which was identified by its IR spectrum.[11] Extending the irradiation time reduced the yield of **2a**.

2b. 230 mg (0.42 mmol) of **1** and 95 mg (0.42 mmol) of $CpRh(CO)_2$ in 25 mL of toluene were stirred and heated to 100 °C for 20 h. All volatiles were removed in vacuo, and the residue was picked up in hexane and chromatographed over a 2 × 20 cm silica gel column. The first fraction (brown, eluted with hexane) contained 72 mg (31%) of unreacted **1**. The second fraction (black, eluted with hexane/benzene 10:1) yielded 80 mg (28%) of **2b** as black crystals, mp 135 °C (decomp). Anal. Calcd for $C_{21}H_{10}Fe_3NO_9Rh$: C, 36.51; H, 1.46; N, 2.03; mol wt, 690.8. Found: C, 36.70; H, 1.54; N, 1.97; mol wt, 691 (EI-MS).

2c: 155 mg (0.30 mmol) of **1** and 90 mg (0.14 mmol) of $Ru_3(CO)_{12}$ in 120 mL of hexane were irradiated as described above. The solution was filtered and evaporated to dryness. Crystallization from hexane yielded 180 mg (86%) of **2c** as a dark brown powder, mp 132 °C (decomp). Anal. Calcd for $C_{19}H_5Fe_3NO_{12}Ru$: C, 32.24; H, 0.71; N, 1.98; mol wt, 707.9. Found: C, 32.25; H, 0.89; N, 1.93.

Structure Determination. A brown-black crystal of **2c** (0.6 × 0.3 × 0.2 mm^3) was obtained by slow evaporation from a hexane solution. It belonged to the monoclinic space group $P2_1/n$ with a = 10.788(2) Å, b = 18.150(4) Å, c = 12.102(2) Å, β = 102.01(3)°, Z = 4, V = 2317.7(8) Å^3, d_{obsd} = 2.02, d_{calcd} = 2.03 g/cm^3. All crystallographic data were obtained with a Nonius CAD 4 diffractometer using Mo Kα radiation at room temperature. Using the $\omega/2\theta$ technique, 9091 reflections were measured in the 2θ range 5–53° for $-12 \le h \le 13$, $0 \le k \le 22$, and $-15 \le l \le 15$ which merged to 4698 unique reflections, of which 3957 had $I \ge 2\sigma(I)$. An empirical absorption correction[15] was applied (μ = 25.4 cm^{-1}). The structure was solved

⊗ Abstract published in *Advance ACS Abstracts,* August 1, 1995.

(1) Sappa, E.; Tiripicchio, A.; Braunstein, P. *Chem. Rev.* **1983**, *83*, 203.
(2) Adams, R. D.; Horvath, I. *Prog. Inorg. Chem.* **1985**, *33*, 127.
(3) Sappa, E.; Tiripicchio, A.; Braunstein, P. *Coord. Chem. Rev.* **1985**, *65*, 219.
(4) Wucherer, E. J.; Tasi, M.; Hansert, B.; Powell, A. K.; Garland, M. T.; Halet, J. F.; Saillard, J. Y.; Vahrenkamp, H. *Inorg. Chem.* **1989**, *28*, 3564.
(5) Tasi, M.; Powell, A. K.; Vahrenkamp, H. *Chem. Ber.* **1991**, *124*, 1549.
(6) Hansert, B.; Vahrenkamp H. *Chem. Ber.* **1993**, *126*, 2023.
(7) Vahrenkamp, H. *Adv. Organomet. Chem.* **1983**, *22*, 169.
(8) Bantel, H.; Powell, A. K.; Vahrenkamp, H. *Chem. Ber.* **1990**, *123*, 677.
(9) Albiez, T.; Powell, A. K.; Vahrenkamp, H. *Chem. Ber.* **1990**, *123*, 667.
(10) Hansert B.; Powell, A. K.; Vahrenkamp, H. *Chem. Ber.* **1991**, *124*, 2679.
(11) Keller, E.; Wolters, D. *Chem. Ber.* **1984**, *117*, 1572.
(12) Suter, P.; Vahrenkamp, H. *Chem. Ber.* **1995**, *128*, 793.
(13) Bantel, H.; Hansert, B.; Powell, A. K.; Tasi, M.; Vahrenkamp, H. *Angew. Chem.* **1989**, *101*, 1084; *Angew. Chem., Int. Ed. Engl.* **1989**, *28*, 1059.
(14) Deck, W.; Schwarz, M.; Vahrenkamp, H. *Chem. Ber.* **1987**, *120*, 1515.
(15) Walker, N.; Stuart, D. *Acta Crystallogr., Sect. A* **1983**, *39*, 158.

0276-7333/95/2314-4424$09.00/0

Table 1. Atomic Coordinates ($\times 10^4$) and Equivalent Isotropic Displacement Parameters ($Å^2 \times 10^3$) for 2c[a]

atom	x	y	z	U(eq)
Ru(1)	2259(1)	1660(1)	624(1)	21(1)
Fe(1)	1353(1)	590(1)	3560(1)	22(1)
Fe(2)	2464(1)	395(1)	1879(1)	21(1)
Fe(3)	2707(1)	1618(1)	2872(1)	20(1)
N(1)	1202(3)	1039(2)	2176(3)	20(1)
C(1)	−179(4)	2885(2)	1641(3)	26(1)
C(2)	−1243(4)	3288(3)	1763(4)	33(1)
C(3)	−2309(4)	2925(3)	1960(4)	32(1)
C(4)	−2319(4)	2167(3)	2034(4)	31(1)
C(5)	−1255(3)	1761(2)	1936(3)	24(1)
C(6)	−176(3)	2126(2)	1746(3)	20(1)
C(7)	953(3)	1676(2)	1650(3)	19(1)
C(8)	3758(4)	1441(3)	−41(4)	33(1)
O(8)	4617(4)	1315(3)	−407(3)	56(1)
C(9)	2147(4)	2650(3)	98(4)	29(1)
O(9)	2117(4)	3227(2)	−277(3)	43(1)
C(10)	1007(4)	1383(3)	−632(4)	33(1)
O(10)	193(3)	1228(2)	−1355(3)	47(1)
C(11)	605(4)	1261(3)	4301(3)	29(1)
O(11)	121(3)	1677(2)	4775(3)	40(1)
C(12)	37(4)	−41(3)	3364(4)	31(1)
O(12)	−811(4)	−428(2)	3241(4)	52(1)
C(13)	2271(4)	147(3)	4819(4)	29(1)
O(13)	2845(3)	−119(2)	5617(3)	45(1)
C(14)	4119(4)	301(3)	1832(4)	33(1)
O(14)	5160(3)	249(3)	1815(4)	53(1)
C(15)	2450(4)	−450(3)	2663(3)	27(1)
O(15)	2517(3)	−1040(2)	2997(3)	39(1)
C(16)	1760(4)	−29(2)	562(4)	30(1)
O(16)	1331(4)	−315(2)	−275(3)	45(1)
C(17)	3907(4)	1163(3)	3893(4)	31(1)
O(17)	4726(3)	913(2)	4542(3)	42(1)
C(18)	3867(4)	2103(3)	2262(4)	29(1)
O(18)	4759(3)	2421(2)	2167(3)	43(1)
C(19)	2389(3)	2424(3)	3673(3)	26(1)
O(19)	2222(3)	2937(2)	4156(3)	40(1)

[a] U(eq) is defined as one-third of the trace of the orthogonalized tensor U_{ij}.

with Patterson and Fourier methods and refined anisotropically, including the H atoms with fixed C−H distances (0.96 Å) and a common isotropic temperature factor. The final R value for 325 variables was 0.041 with residual electron density maxima of +1.1 and −2.2 e/Å^3. All calculations were done with the SHELX program system,[16] and the drawings were produced with SCHAKAL.[17] Table 1 lists the atomic parameters.

Results and Discussion

The three reagents $Fe_2(CO)_9$, $CpRh(CO)_2$, and $Ru_3(CO)_{12}$, which in our hands had proved to be the most productive ones for cluster expansion, were used successfully here to convert the Fe_3 cluster **1** into the Fe_3M clusters **2a−c**. When $Fe_2(CO)_9$ and $Ru_3(CO)_{12}$ were used, photochemical activation had to be applied to generate the respective $Fe(CO)_3$ and $Ru(CO)_3$ fragments necessary for cluster buildup. For $CpRh(CO)_2$ thermal treatment was sufficient to produce the required RhCp fragments. The yields of **2a−c** were reasonable to very good, indicating a high stability of the heteronuclear clusters under the reaction conditions.

The identification of the new clusters **2b,c** rests on their analogy with the known cluster **2a**[11] and on the structure determination of **2c** (see below). In their ^1H NMR spectra ($CDCl_3$) all three show the aromatic multiplets centered at ca. 7.6 ppm, and **2b** shows the presence of the RhCp unit by a singlet at 5.53 ppm. The IR data of the three products (Table 2) show only moderate similarity and thus are only of diagnostic value.

Table 2. CO Stretching Bands in the IR Spectra[a] of 2a−c

2a	2092 vw, 2059 s, 2025 vs, 2018 sh, 1990 w, 1938 w, 1930 sh
2b	2082 m, 2060 vw, 2022 vs, 2010 vs, 1980 vw, 1970 vw
2c	2098 m, 2085 vw, 2069 vs, 2060 m, 2036 s, 2005 w, 1994 w, 1982 m, 1927 w, 1944 m, 1922 m

[a] Hexane, cm^{-1}.

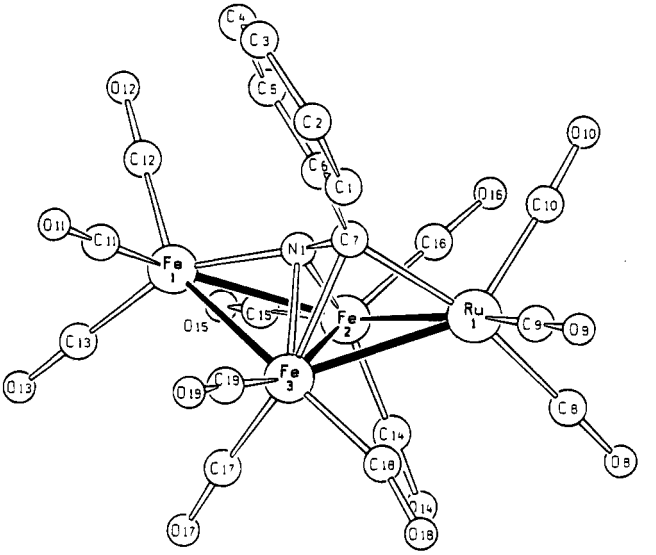

Figure 1. Molecular structure of **2c**. Selected bond lengths (Å): Ru1−Fe2, 2.736(1); Ru1−Fe3, 2.664(1); Fe2−Fe3, 2.511 (1); Fe1−Fe2, 2.592(1); Fe1−Fe3, 2.611(1); Fe1−N1, 1.839(3); Fe2−N1, 1.884(3); Fe3−N1, 1.970(3); Ru1−C7, 2.063(4); Fe3−C7, 2.149(4); N1−C7, 1.321(5).

The structure determination of **2c** (for details see Experimental Section) revealed the molecular shape shown in Figure 1. Compound **2c** corresponds closely in all molecular details to its Fe_4 homologue, **2a**.[11] Its metal atoms adopt the butterfly shape (dihedral angle 136.5°), which is common for η^2-capped tetranuclear species.[1,2,8−11] While the regular metal−metal distances deserve no further comment, the attachment of the capping nitrile ligand is somewhat unusual. Its nitrogen atom is located symmetrically in the center of the butterfly, interacting quite strongly with Fe1, Fe2, and Fe3 (average Fe−N distance, 1.90 Å) but not or only very weakly with Ru1 (distance 2.64 Å). The nitrile carbon atom, in contrast, is positioned quite unsymmetrically and interacts only with Fe3 and Ru1. A tentative bonding description of this atomic arrangement would assign a donor bond N1→Fe1, two normal σ bonds N1-Fe2 and C7-Ru1, and a π interaction between the N1−C7 multiple bond and Fe3. The nitrile would thus be a six-electron ligand, giving the butterfly cluster the correct total of 62 electrons. Its electron distribution, specifically its μ_3-η^2 parallel attachment to the Fe_2Ru triangle, is, however, reminiscent of the common mode of alkyne attachment to trinuclear clusters.[1] Looking at it this way, the cluster **2c** can be derived from a square-pyramidal Fe_2RuNC unit with Fe3 as the apex to which Fe1 is attached as a substituent.

(16) SHELXS and SHELXL; Sheldrick, G. M. Universität Göttingen: Göttingen, Germany, 1986 and 1993.
(17) SCHAKAL; Keller, E. Universität Freiburg: Freiburg, Germany, 1993.

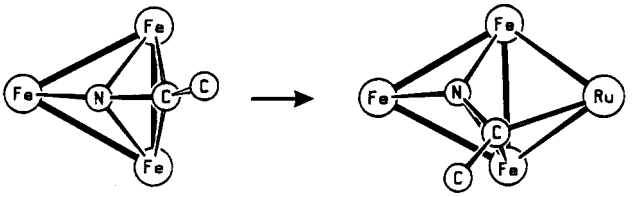

Figure 2. Evolution of the cluster cores in going from **1** to **2c**.

As usual, we hesitate to draw mechanistic conclusions from the structures of the starting cluster **1** and the respective products **2a**,**c**. Figure 2, which displays the molecular cores of **1**[11] and **2c** both projected onto the Fe_3 plane, would imply such a conclusion. It seems that the attachment of the $Ru(CO)_3$ unit to the intact cluster **1** mostly affects the orientation and bonding capacity of the nitrile carbon atom, which is the only nitrile constituent to which it becomes strongly associated. However, as discussed above, the whole cluster **2c** can be considered as generated from a Fe_2Ru(nitrile) entity to which a $Fe(CO)_3$ unit has been attached. We assume that the capping nitrile ligand can rotate above the trinuclear cluster allowing it to change its orientation when the incoming ML_n unit is attached. Accordingly the shape of the product cluster reflects the optimized bonding interactions among the four metal atoms and between the metal and nitrile C and N atoms, but it does not tell which organometallic unit was attached where. For this reason we would also avoid making a structural assignment of the Fe_3Rh cluster **2b**.

In conclusion we have provided another series of cluster expansions using fragment precursors. As in the previous examples the organic η^2 ligand capping the trinuclear starting cluster becomes attached to all four metal atoms of the resulting butterfly cluster. Its attachment and orientation with respect to the M_4 butterfly is specific for the η^2 ligand and varies considerably among the M_4 clusters capped by alkyne,[8] vinylidene,[9] azoalkane,[10] or nitrile ligands. It remains to be seen whether further variations may be provided by additional η^2 ligands (isonitrile, acyl, etc.) and whether the reactivity of μ_4-η^2-bound nitriles may be exploited.

Acknowledgment. This work was supported by the Volkswagen-Stiftung and the Fonds der Chemischen Industrie. We thank M. Ruf for help with the structure determination.

Supporting Information Available: Tables containing the details of data acquisition and refinement, all interatomic distances and angles, and anisotropic thermal parameters of non-hydrogen atoms (5 pages). Ordering information is given on any current masthead page.

OM950377R

Selectivity in the Aliphatic Palladation of Ketone Hydrazones. An Example of Palladium-Promoted Intramolecular Addition of a *N,N*-Dimethylhydrazone to an Alkene

Diego J. Cárdenas and Antonio M. Echavarren*

Departamento de Química Orgánica, Universidad Autónoma de Madrid, Cantoblanco, 28049 Madrid, Spain

Received March 28, 1995[⊗]

Summary: The efficacy of the aliphatic palladation reaction diminishes with the nucleophilicity of the hydrazone imino nitrogen; no benzylic or allylic C-H activation was observed. A γ,δ-unsaturated dimethylhydrazone reacts with $Pd(PPh_3)_2Cl_2$ to yield a palladacycle resulting from the addition of the imino group to a (η^2-alkene)palladium complex.

Introduction

We have recently reported the aliphatic palladation of *N,N*-dimethylhydrazones with $Pd(PPh_3)_2Cl_2$ or $Pd(AsPh_3)_2Cl_2$ (eq 1).[1] The palladation proceeds in the

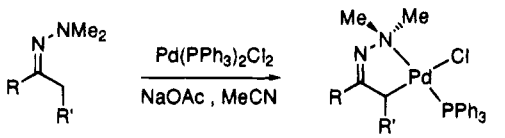

(1)

presence of sodium acetate in acetonitrile at 65–75 °C to give the desired five-membered palladacycles. This aliphatic palladation process[2] takes place regioselectively on the least-substituted α position of the hydrazone and leads to stable five-membered ring metallacycles which do not decompose by β-hydride elimination. Although the mechanism of this reaction was not determined in detail it was shown that the palladium(II) complex coordinates first with the imino nitrogen and that the addition of acetate promotes the formation of the palladacycle.

In this context, it is of interest to note a recent report on the activation of the benzylic positions of toluene and *p*-xylene with $Pd(PPh_3)_2Cl_2$ and related bromo and iodopalladium(II) complexes.[3] Even more remarkably, simple alkanes such as hexane and cyclohexane were activated with these palladium(II) complexes at 70–130 °C.[3] Although the aliphatic palladation reaction was shown to proceed satisfactorily with the examined *N,N*-dimethylhydrazones,[1] we wished to determine more precisely the scope and limitations of this process. In particular, it was of interest to examine the palladation of substrates possessing benzylic[4] and allylic[5] C-H that could be activated by the palladium(II) reagent. Additionally, we also studied the possible extension of the

Chart 1

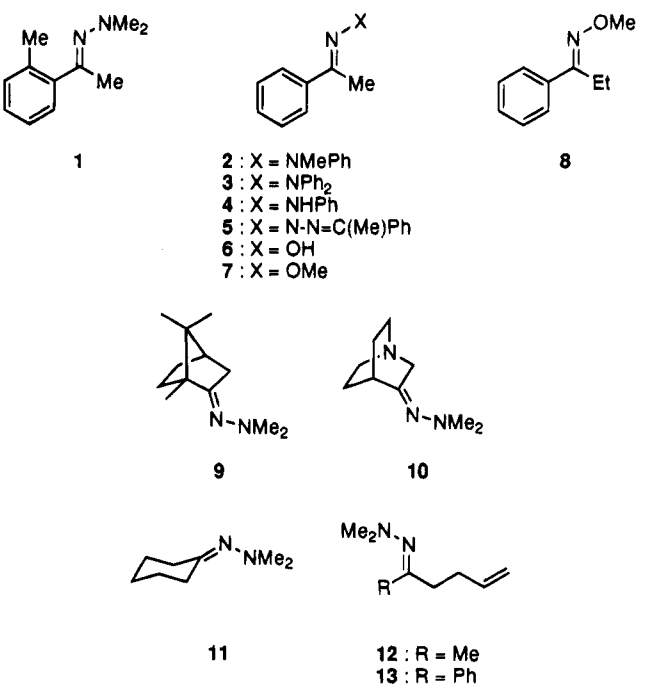

palladation reaction to other N-directing groups and the application to *N,N*-dimethylhydrazones of some cyclic ketones. In this paper we report the results of a study on the reactions of substrates **1**–**13** (Chart 1) with $Pd(PPh_3)_2Cl_2$ and the first example of an intramolecular attack of the imino nitrogen of a hydrazone to an alkene promoted by palladium.[6,7]

[⊗] Abstract published in *Advance ACS Abstracts,* July 1, 1995.

(1) Cárdenas, D. J.; Echavarren, A. M.; Vegas, A. *Organometallics* **1994**, *13*, 882.

(2) For recent references, see the following: Yoneda, A.; Hakushi, T.; Newkome, G. R.; Fronczek, F. R. *Organometallics* **1994**, *13*, 4912 and references therein.

(3) Vedernikov, A. N.; Kuramshin, A. I.; Solomonov, B. N. *J. Chem. Soc., Chem. Commun.* **1994**, 121.

(4) Benzylic palladation: (a) Hartwell, G. E.; Lawrence, R. V.; Smas, M. J. *J. Chem. Soc., Chem. Commun.* **1970**, 912. (b) Dehand, J.; Motet, C.; Pfeffer, M. *J. Organomet. Chem.* **1981**, *209*, 255. (c) Garber, A. R.; Garrou, P. E.; Hartwell, G. E.; Smas, M. J.; Wilkinson, J. R.; Todd, L. J. *J. Organomet. Chem.* **1975**, *86*, 219. (d) Steel, P. J.; Caygill, G. B. *J. Organomet. Chem.* **1987**, *327*, 101. (e) Deeming, A. J.; Rothwell, I. P. *J. Chem. Soc., Chem. Commun.* **1978**, 344. (f) Deeming, A. J.; Rothwell, I. P. *J. Chem. Soc., Dalton Trans.* **1978**, 1490. (g) Deeming, A. J.; Rothwell, I. P.; Hursthouse, M. B.; Malik, K. M. A. *J. Chem. Soc., Dalton Trans.* **1979**, 1899. (h) Ryabov, A. D. *J. Organomet. Chem.* **1984**, *268*, 91. (i) Pfeffer, M.; Wehman, E.; van Koten, G. *J. Organomet. Chem.* **1985**, *282*, 127. (j) Newkome, G. R.; Evans, D. W. *Organometallics* **1987**, *6*, 2592. (k) Ryabov, A. D.; Yatsimirsky, A. K. *Inorg. Chem.* **1984**, *23*, 789. (l) Albert, J.; Granell, J.; Sales, J.; Solans, X.; Font-Altaba, M. *Organometallics* **1986**, *5*, 2567. (m) Albert, J.; Ceder, R. M.; Gómez, M.; Granell, J.; Sales, J. *Organometallics* **1992**, *11*, 1536. (n) Barro, J.; Granell, J.; Sainz, D.; Sales, J.; Font-Bardia, M.; Solans, X. *J. Organomet. Chem.* **1993**, *456*, 147.

(5) (a) Chrisope, D. R.; Beak, P. *J. Am. Chem. Soc.* **1986**, *108*, 334. (b) Chrisope, D. R.; Beak, P.; Saunders, W. H. *J. Am. Chem. Soc.* **1988**, *110*, 230 and references therein.

(6) Hegedus, L. S. In *Comprehensive Organic Synthesis*; Trost, B. M., Fleming, I., Eds.; Pergamon: Oxford, 1991; Vol. 4, Chapter 3.1.

0276-7333/95/2314-4427$09.00/0

Chart 2

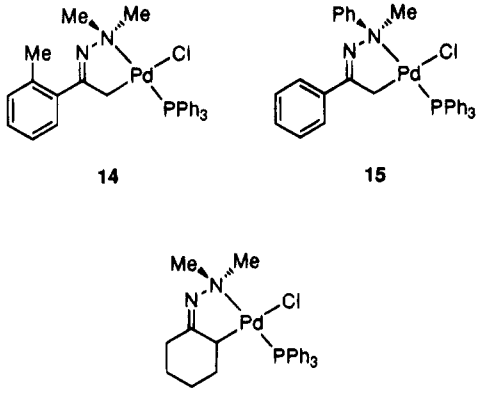

14 **15** **16**

Results and Discussion

Hydrazone **1**, obtained as a mixture of diastereomers, possesses three potentially reactive sites: aromatic, benzylic, and α-methyl. Reaction of **1** with $Pd(PPh_3)_2Cl_2$ and NaOAc in acetonitrile at 70 °C led exclusively to the formation of palladacycle **14** (Chart 2), isolated in 57% yield, as a result of the regioselective activation of the methyl α to the hydrazone function. None of the alternative palladation products was detected in the crude reaction mixture. On the other hand, *N*-methyl-*N*-phenylhydrazone **2** reacted with $Pd(PPh_3)_2Cl_2$ to give **15** as the only palladacycle. None of the alternative palladacycle derived from activation of the *N*-phenyl group could be observed. However, **15** was isolated in a lower yield (42% yield) than that obtained in the palladation of the corresponding *N*,*N*-dimethylhydrazone (97%).[1] This lower yield is consistent with the lower basicity, and increased steric hindrance, of the N-directing group of **2**. Accordingly, *N*,*N*-diphenylhydrazone **3** failed to yield a palladation product with $Pd(PPh_3)_2Cl_2$. A similar result was obtained with hydrazone **4**, azine **5**, oxime **6**, and methoximes **7** and **8**. In this last experiment, β-palladation, a known reaction with α,α-disubstituted oximes,[8] was not observed. It is of interest to note that in none of these experiments was aromatic palladation observed, in spite of the known activating effect of these functional groups.[9] These results provide further support that the coordination of triphenylphosphine considerably reduces the electrophilicity of palladium(II), leading to intermediate complexes which are unable to activate aromatic positions.

By reaction with $Pd(PPh_3)_2Cl_2$ under the usual reaction conditions, camphor and quinuclidinone hydrazones **9** and **10** gave rise to complex reaction mixtures, presumably containing coordination complexes. However, no aliphatic palladation products were obtained from **9** or **10**, even under forcing conditions. The failure with these rigid bicyclic substrates may be due to the unfavorable angle between the methylene C-H and the hydrazone, since cyclohexanone *N*,*N*-dimethylhydrazone (**11**) furnished palladacycle **16**. In this case, the isolated yield was low (36%) due to partial decomposition of the palladacycle under the reaction conditions.

Scheme 1

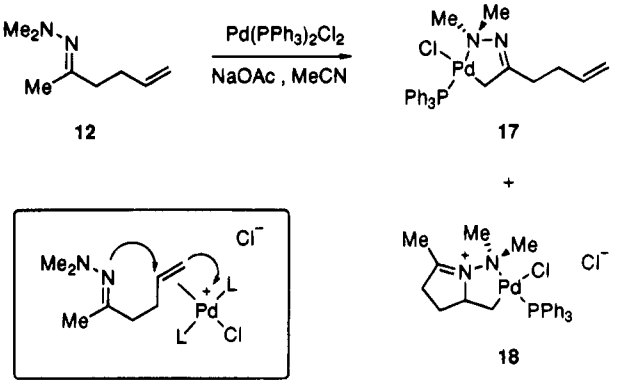

12 **17** + **18**

5-Hexen-2-one *N*,*N*-dimethylhydrazone (**12**), prepared as a mixture of *E* and *Z* diastereomers, was also examined to determine whether the allylic activation could compete with the usual pathway to form a (η^3-allyl)palladium(II) complex or, alternatively, to a six-membered (η^1-allyl)palladium complex with the metal coordinated to the amino nitrogen. However, **12** reacted with $Pd(PPh_3)_2Cl_2$ at 65 °C to give a mixture of two palladacycles which could be separated by column chromatography (Scheme 1). The minor product, isolated in 17% yield, was the expected palladacycle **17** resulting from the palladation on the least-substituted position.[1] Surprisingly, the polar derivative **18** was obtained as the major product. This derivative showed two doublets in the ^1H NMR spectrum at 3.07 ppm (J = 2.5 Hz) and 3.03 ppm (J = 2.0 Hz), corresponding to the diastereotopic *N*-methyls coupled to ^{31}P. In the ^{13}C NMR spectrum a low-field signal was observed at 208.33 ppm and was assigned to an iminium carbon. This resonance is shifted almost 29 ppm downfield as compared with the hydrazone carbon of **17**. The observation of a CH carbon at 61.13 ppm is also consistent with the cationic structure for **18**. Complex **18** is probably formed by a palladium-promoted attack of the imino nitrogen of **12** on the alkene, followed by coordination of the amino nitrogen of the hydrazone to palladium (Scheme 1). Nucleophilic additions of amines to alkene palladium complexes are precedented,[6,7] although this is to our knowledge the first example of a reaction of a hydrazone as the nucleophile.[10,11] Surprisingly, related hydrazone **13** was recovered unchanged under the conditions of Scheme 1, probably as a consequence of the diminished nucleophilicity of its imino nitrogen. The failure to obtain a palladation product on the methylene α to the hydrazone of **13** is also somewhat surprising,

(7) For the palladium-mediated intramolecular reaction of amines with alkenes leading to allylic functionalization, see the following: van der Schaaf, P.; Sutter, J.-P.; Grellier, M.; van Mier, G. P. M.; Spek, A. L.; van Koten, G.; Pfeffer, M. *J. Am. Chem. Soc.* **1994**, *116*, 5134 and references therein.

(8) (a) Constable, A. G.; McDonald, W. S.; Sawkins, L. C.; Shaw, B. L. *J. Chem. Soc., Chem. Commun.* **1978**, 1061. (b) Constable, A. G.; McDonald, W. S.; Sawkins, L. C.; Shaw, B. L. *J. Chem. Soc., Dalton Trans.* **1980**, 1992. (c) Carr, K.; Sutherland, J. K. *J. Chem. Soc., Chem. Commun.* **1984**, 1227. (d) Baldwin, J. E.; Nájera, C.; Yus, M. *J. Chem. Soc., Chem. Commun.* **1985**, 126. (e) Baldwin, J. E.; Jones, R. H.; Nájera, C.; Yus, M. *Tetrahedron* **1985**, *41*, 699. (f) Rocherolle, V.; López, J. C.; Olesker, A.; Lukacs, G. *J. Chem. Soc., Chem. Commun.* **1988**, 513. (g) Wells, A. P.; Kitching, W. *Organometallics* **1992**, *11*, 2750.

(9) Reviews: (a) Dehand, J.; Pfeffer, M. *Coord. Chem. Rev.* **1976**, *18*, 327. (b) Newkome, G. R.; Puckett, W. E.; Gupta, V. K.; Kiefer, G. E. *Chem. Rev.* **1986**, *86*, 451. (c) Omae, I. *Coord. Chem. Rev.* **1988**, *83*, 137. (d) Dunina, V. V.; Zalevskaya, O. A.; Potapov, V. M. *Russ. Chem. Rev.* **1988**, *57*, 250. (e) Ryabov, A. D. *Chem. Rev.* **1990**, *90*, 403.

(10) For an imine addition to an alkene iron(II) complex, see the following: Berryhill, S. R.; Price, T.; Rosenblum, M. *J. Org. Chem.* **1983**, *48*, 158.

(11) For the unrelated zirconium-promoted intramolecular addition of hydrazones to alkynes, see the following: Buchwald, S. L.; Wannamaker, M. W.; Watson, B. T. *J. Am. Chem. Soc.* **1989**, *111*, 4495.

since the related *N,N*-dimethylhydrazone of propiophenone furnished the corresponding palladacycle uneventfully.[1]

Conclusions

This study reveals that the efficacy of the aliphatic palladation reaction diminishes, as expected, with the nucleophilicity of the hydrazone imino nitrogen. The failure of rigid bicyclic hydrazones **9** and **10** suggests that a planar arrangement of the C-H and the hydrazone is required for the palladation reaction to proceed under normal conditions as has been demonstrated before in the benzylic C-H activation of methylquinolines.[9a] Under the conditions developed for this palladation reaction, no benzylic or allylic C-H activation was observed. However, the γ,δ-unsaturated dimethylhydrazone **12** leads to the formation of palladacycle **18**, a rare example of addition of an imino group to a (η^2-alkene)palladium complex.

Experimental Section

General Procedures. All reactions were carried out under an atmosphere of Ar. Solvents were dried before use by standard methods. $Pd(PPh_3)Cl_2$ was prepared by a known method.[12] The following hydrazones were prepared from the corresponding ketones according to known procedures: 1-(2-methylphenyl)-1-ethanone *N,N*-dimethylhydrazone (**1**),[13] acetophenone *N*-methyl-*N*-phenylhydrazone (**2**),[14] acetophenone *N,N*-diphenylhydrazone (**3**),[15] acetophenone *N*-phenylhydrazone (**4**),[16a] acetophenone azine (**5**),[16b] acetophenone oxime (**6**),[16c] acetophenone methoxime (**7**),[17] propiophenone methoxime (**8**),[17] (+)-camphor *N,N*-dimethylhydrazone (**9**),[18] and cyclohexanone *N,N*-dimethylhydrazone (**11**).[19]

Quinuclidinone *N,N*-Dimethylhydrazone (10). A mixture of quinuclidinone hydrochloride (860 mg, 5.94 mmol), NaOAc (487 mg, 5.94 mmol), and *N,N*-dimethylhydrazine (1.4 mL, 18.1 mmol) in EtOH (15 mL) was heated under refluxing conditions for 48 h. After the solution had been cooled to room temperature, the solvent was evaporated and the residue was suspended in EtOAc and filtered. The filtrate was evaporated, dissolved in Et_2O, dried ($MgSO_4$), and evaporated to give **11** as a greenish oil (592 mg, 51%) as a mixture of *E* and *Z* isomers. ^1H NMR (200 MHz, $CDCl_3$) δ 3.78 (s, 2H), 3.02 (m, 4H), 2.68 (m, 1H), 2.45 (s, 3H), 2.00 (s, 3H), 1.94 (m, 4H); $^{13}C\{^1H\}$ NMR (50 MHz, $CDCl_3$) δ 175.13, 169.77, 52.22*, 46.34, 45.36, 30.74*, 24.19*, 21.57* (the "*" denotes overlapping signals for both isomers).

5-Hexen-2-one *N,N*-Dimethylhydrazone (12). 5-Hexen-2-one (1.67 g, 17 mmol) and *N,N*-dimethylhydrazine (1.7 mL, 22.1 mmol) in toluene (25 mL) containing a catalytic amount of *p*-toluenesulfonic acid monohydrate (*ca.* 5 mg) was heated with azeotropic removal of water (Dean–Stark apparatus) for 24 h. After the mixture had been cooled to room temperature, it was diluted with Et_2O (50 mL), washed with water (3×), dried ($MgSO_4$), and evaporated to give **12** as an oil (88:12 mixture of *E* and *Z* isomers). The crude product (quantitative yield) was sufficiently pure and was not purified. *E* isomer: ^1H NMR (200 MHz, $CDCl_3$) δ 5.82 (ddt, J = 16.9, 10.4, 6.3 Hz, 1H), 5.04 (m, 2H), 2.43 (s, 6H), 2.30 (m, 4H), 1.95 (s, 3H); $^{13}C\{^1H\}$ NMR (50 MHz, $CDCl_3$) δ 166.08, 136.72, 114.33, 46.30 (2C), 37.44, 30.40, 15.98. *Z* isomer: ^1H NMR (200 MHz, $CDCl_3$) δ 5.82 (m, 1H), 5.05 (m, 2H), 2.41 (s, 6H), 2.28 (m, 4H), 1.93 (s, 3H); $^{13}C\{^1H\}$ NMR (50 MHz, $CDCl_3$) (only distinct signals) δ 168.04, 46.74 (2C), 29.74.

1-Phenyl-4-penten-1-one *N,N*-Dimethylhydrazone (13). To a solution of acetophenone *N,N*-dimethylhydrazone (675 mg, 4.16 mmol) in THF (5 mL) at −78 °C was added BuLi (2.6 mL, 1.6 M solution in hexane, 4.16 mmol). The mixture was slowly warmed up to −45 °C (*ca.* 1 h), and allyl iodide (0.38 mL, 4.16 mmol) was added. After 15 min at −45 °C the mixture was warmed up to 0 °C. After it had been stirred at this temperature for 1 h, the mixture was treated with aqueous NH_4Cl (saturated solution, pH 8, 5 mL). The aqueous phase was extracted with Et_2O, and the combined organic extracts were washed with water (3×) and dried ($MgSO_4$). The solvent was evaporated, and the residue was filtered through silica gel (10:1 hexane–EtOAc) to give **13** as a greenish oil (735 mg, 87%): ^1H NMR (200 MHz, $CDCl_3$) δ 7.62 (m, 2H), 7.37 (m, 3H), 5.81 (ddt, J = 17.0, 10.3, 6.5 Hz, 1H), 4.99 (m, 2H), 2.99 (m, 2H), 2.56 (s, 6H), 2.20 (m, 2H); $^{13}C\{^1H\}$ NMR (50 MHz, $CDCl_3$) δ 166.94, 137.05, 136.60, 128.55, 127.60, 126.33, 114.32, 47.12 (2C), 30.53, 26.87.

Aliphatic Palladation: General Procedure. A mixture of hydrazone (0.1–0.2 mmol), NaOAc (1 equiv), and $Pd(PPh_3)_2Cl_2$ (1 equiv) in acetonitrile (6–10 mL) was heated at 65–75 °C for 24–48 h. The originally yellow suspension usually remains unchanged, although in some instances an orange suspension or a solution was obtained. After it had been cooled to room temperature, the solvent was evaporated and the residue was chromatographed (flash grade silica gel) to yield the palladacycle as a pale yellow solid. Heating under reflux conditions or the use of impure hydrazone as the starting material led to lower yields and formation of metallic palladium.

Palladacycle 14. Reaction conditions: 70 °C, 15 h. Eluent: 3:1 hexane–EtOAc. Yield: 57%. ^1H NMR (300 MHz, $CDCl_3$) δ 7.72 (m, 6H), 7.41 (m, 9H), 7.09 (m, 4H), 3.18 [d, $^4J(^1H-^{31}P)$ = 2.4 Hz, 6H], 2.50 [d, $^3J(^1H-^{31}P)$ = 3.5 Hz, 2H], 2.23 (s, 3H); $^{13}C\{^1H\}$ NMR (50 MHz, $CDCl_3$; DEPT) δ 178.87 [d, $^3J(^{13}C-^{31}P)$ = 3.6 Hz; C], 135.14 (C), 134.46 [d, $^2J(^{13}C-^{31}P)$ = 11.7 Hz, PPh_3; CH], 130.96 [d, $^1J(^{13}C-^{31}P)$ = 49.2 Hz, PPh_3; C], 130.52 (CH), 130.45 [d, $^4J(^{13}C-^{31}P)$ = 2.3 Hz, PPh_3; CH], 128.57 (CH), 128.17 [d, $^3J(^{13}C-^{31}P)$ = 10.5 Hz, PPh_3; CH], 127.32 (CH), 125.49 (CH), 51.51 [d, $^3J(^{13}C-^{31}P)$ = 2.0 Hz, 2 CH_3], 42.49 [d, $^2J(^{13}C-^{3}1P)$ = 4.7 Hz, CH_2], 20.05 (CH_3) (one carbon signal was not observed); $^{31}P\{^1H\}$ (121.4 MHz, $CDCl_3$) δ 33.50; IR (KBr) 3040 (w), 2900 (w), 1605 (m), 1475 (s), 1440 (s), 1430 (s), 1380 (m), 1285 (m), 1175 (m), 1090 (s), 1000 (s), 935 (s), 745 (s), 720 (s), 690 (s), 525 (s), 425 (m); HRMS m/z calcd for $C_{29}H_{30}ClN_2PPd$, 578.0870; found 578.0865. Anal. Calcd for $C_{29}H_{30}ClN_2PPd$: C, 60.12; H, 5.22; N, 4.83. Found: C, 60.40; H, 5.50; N, 4.87.

Palladacycle 15. Reaction conditions: 65 °C, 44 h. Eluent: 3:1 hexane–EtOAc. Yield: 42%. ^1H NMR (300 MHz, $CDCl_3$) δ 7.72 (m, 6H), 7.60–7.30 (m, 16H), 7.25 (m, 3H), 3.74 [d, $^4J(^1H-^{31}P)$ = 2.1 Hz, 3H], 2.72 [dd, $J(^1H-^1H)$ = 16.9 Hz, $^3J(^1H-^{31}P)$ = 1.9 Hz, 1H], 2.44 [dd, $J(^1H-^1H)$ = 16.9 Hz, $^3J(^1H-^{31}P)$ = 4.8 Hz, 1H]; $^{13}C\{^1H\}$ NMR (50 MHz, $CDCl_3$; DEPT) δ 177.36 (C), 150.17 (C), 134.71 [d, $^2J(^{13}C-^{31}P)$ = 11.7 Hz, PPh_3; CH], 133.50 (C), 130.96 [d, $^1J(^{13}C-^{31}P)$ = 48.1 Hz, PPh_3; C], 130.57 [d, $^4J(^{13}C-^{31}P)$ = 2.5 Hz, PPh_3; CH], 130.45 (CH), 128.68 (CH), 128.26 [d, $^3J(^{13}C-^{31}P)$ = 10.7 Hz, PPh_3; CH], 128.25 (CH), 128.05 (CH), 125.87 (CH), 121.03 (CH), 49.23 (CH_3), 39.80 [d, $^2J(^{13}C-^{31}P)$ = 3.9 Hz, CH_2]; $^{31}P\{^1H\}$ (121.4 MHz, $CDCl_3$) δ 35.45; IR (KBr) 3035 (w), 2920 (w), 1620 (w), 1595 (w), 1575 (w), 1490 (s), 1440 (s), 1380 (w), 1270 (w), 1190 (w), 1105 (s), 1110 (m), 780 (s), 755 (s), 700 (vs), 535 (s), 510

(12) (a) *Gmelin Handbuch der Anorganischen Chemie*; Springer-Verlag: Weinheim, Germany; 1924; Palladium, Vol. 65. (b) Colquhoun, H. M.; Holton, J.; Thompson, D. J.; Twigg, M. V. *New Pathways for Organic Synthesis. Practical Applications of Transition Metals*; Plenum: New York, 1984.
(13) Newkome, G. R.; Bhacca, N. S. *J. Org. Chem.* **1971**, *36*, 1719.
(14) Karabatsos, G. J.; Krumel, K. L. *Tetrahedron* **1967**, *23*, 1097.
(15) Sharma, S. D.; Pandhi, S. B. *J. Org. Chem.* **1990**, *55*, 2196.
(16) (a) Vogel, A. *Vogel's Texbook of Practical Organic Chemistry*, 4th ed.; Longman: London, 1978; p 1112; (b) Ibid., p 1114; (c) Ibid., p 1113.
(17) Karabatsos, G. J.; Hsi, N. *Tetrahedron* **1967**, *23*, 1079.
(18) Chelucci, G.; Delogu, G.; Gladiali, S.; Soccolini, F. *J. Heterocycl. Chem.* **1986**, *23*, 1395.
(19) Newkome, G. R.; Fishel, D. L. *J. Org. Chem.* **1966**, *31*, 677.

(s), 365 (w); HRMS m/z calcd for $C_{33}H_{30}ClN_2PPd$, 626.0870; found, 626.0866. Anal. Calcd for $C_{33}H_{30}ClN_2PPd$: C, 63.17; H, 4.82; N, 4.46. Found: C, 63.40; H, 5.10; N, 4.27.

Palladacycle 16. Reaction conditions: 65 °C, 48 h. Eluent: 3:1 hexane–EtOAc. Yield: 31%. ^{1}H NMR (300 MHz, $CDCl_3$) δ 7.74 (m, 6H), 7.42 (m, 9H), 3.17 [d, $^4J(^1H-^{31}P)$ = 2.2 Hz, 3H], 3.04 [d, $^4J(^1H-^{31}P)$ = 2.4 Hz, 3H], 2.61 (m, 1H), 2.30 (m, 2H), 1.95–1.20 (m, 4H), 0.91 (m, 2H); $^{13}C\{^1H\}$ NMR (50 MHz, $CDCl_3$; DEPT) δ 183.46 (C), 134.79 [d, $^2J(^{13}C-^{31}P)$ = 11.7 Hz, PPh_3; CH], 131.12 [d, $^1J(^{13}C-^{31}P)$ = 46.9 Hz, PPh_3; C], 130.41 [d, $^4J(^{13}C-^{31}P)$ = 2.0 Hz, PPh_3; CH], 128.20 [d, $^3J(^{13}C-^{31}P)$ = 10.6 Hz, PPh_3; CH], 58.20 (CH), 51.74 [d, $^3J(^{13}C-^{31}P)$ = 2.0 Hz, CH_3], 51.57 [d, $^3J(^{13}C-^{31}P)$ = 1.7 Hz, CH_3], 37.51 (CH_2), 31.43 (CH_2), 28.86 (CH_2), 27.59 [d, $^4J(^{13}C-^{31}P)$ = 5.3 Hz, CH_2]; $^{31}P\{^1H\}$ (121.4 MHz, $CDCl_3$) δ 33.93; IR (KBr) 3050 (w), 2920 (m), 2860 (w), 1720 (w), 1640 (m), 1490 (m), 1340 (s), 1190 (m), 1130 (m), 1100 (s), 1000 (m), 970 (w), 940 (w), 920 (w), 755 (s), 720 (m), 705 (vs), 535 (vs), 510 (s), 360 (w); MS m/z 564 (0.2), 563 (0.1), 562 [0.3, 2 (M^+ – PPh_3) + 2], 561 (0.2), 560 (0.2), 559 (0.1), 544 (0.1), 542 (0.1), 508 (0.3), 506 (0.4), 505 (0.2), 278 (37), 277 (67), 262 (100), 183 (77), 108 (36); HRMS m/z calcd for $C_{26}H_{30}ClN_2PPd$, 542.0870; found, 542.0866.

Palladacycles 17 and 18. The palladation of **12** at 65 °C for 24 h gave a mixture of **17** and **18**. Chromatography (2:1 hexane–EtOAc) gave complex **17** (17%). Further elution with 1:1 hexane–EtOAc and EtOAc gave **18** (54%). Palladacycle **17**: ^{1}H NMR (300 MHz, $CDCl_3$) δ 7.72 (m, 6H), 7.43 (m, 9H), 5.68 (ddt, J = 17.9, 9.9, 6.7 Hz, 1H), 4.92 (m, 2H), 3.04 [d, $^4J(^1H-^{31}P)$ = 2.5 Hz, 6H], 2.28 (m, 4H), 2.10 [d, $^3J(^1H-^{31}P)$ = 3.5 Hz, 2H]; $^{13}C\{^1H\}$ NMR (50 MHz, $CDCl_3$; DEPT) δ 179.67 [d, $^3J(^{13}C-^{31}P)$ = 3.7 Hz; C], 137.14 (CH), 134.64 [d, $^2J(^{13}C-^{31}P)$ = 11.7 Hz, PPh_3; CH], 131.22 [d, $^1J(^{13}C-^{31}P)$ = 48.8 Hz, PPh_3; C], 130.51 [d, $^4J(^{13}C-^{31}P)$ = 2.2 Hz, PPh_3; CH], 128.25 [d, $^3J(^{13}C-^{31}P)$ = 10.5 Hz, PPh_3; CH], 115.20 (CH_2), 51.49 [d, $^3J(^{13}C-^{31}P)$ = 2.0 Hz, 2 CH_3], 40.38 [d, $^2J(^{13}C-^{31}P)$ = 4.6 Hz, CH_2], 32.06 (CH_2), 31.32 (CH_2); $^{31}P\{^1H\}$ (121.4 MHz, $CDCl_3$) δ 33.55; IR (KBr) 3040 (w), 2920 (w), 1485 (m), 1435 (s), 1105 (s), 1000 (m), 755 (s), 700 (s), 530 (s), 510 (s), 360 (w); MS m/z 546 (0.6), 544 (1.0), 542 (1.0, M^+), 508 (0.3), 506 (0.4), 505 (0.3), 262 (100), 183 (73); HRMS m/z calcd for $C_{26}H_{30}ClN_2PPd$, 542.0870; found, 542.0883. Palladacycle **18**: ^{1}H NMR (200 MHz, $CDCl_3$) δ 7.80–7.60 (m, 6H), 7.50–7.30 (m, 9H), 3.17 (m, 1H), 3.07 [d, $^4J(^1H-^{31}P)$ = 2.5 Hz, 3H], 3.03 [d, $^4J(^1H-^{31}P)$ = 2.0 Hz, 3H], 2.24 (t, J = 7.2 Hz, 2H), 2.02 (s, 3H), 1.65–1.30 (m, 3H), 1.14 (ddd, J = 9.5, 6.5, 3.5 Hz, 1H); $^{13}C\{^1H\}$ NMR (50 MHz, $CDCl_3$; DEPT) δ 208.33 (C), 134.64 [d, $^2J(^{13}C-^{31}P)$ = 11.7 Hz, PPh_3; CH], 131.47 [d, $^1J(^{13}C-^{31}P)$ = 49.0 Hz, PPh_3; C], 130.33 [d, $^4J(^{13}C-^{31}P)$ = 2.1 Hz, PPh_3; CH], 128.13 [d, $^3J(^{13}C-^{31}P)$ = 10.6, PPh_3; CH], 61.13 (CH), 53.44 [d, $^3J(^{13}C-^{31}P)$ = 2.0 Hz, CH_3], 49.76 [d, $^3J(^{13}C-^{31}P)$ = 1.4 Hz, CH_3], 41.07 [d, $^2J(^{13}C-^{31}P)$ = 2.0 Hz, CH_2], 40.44 (CH_2), 29.89 (CH_3), 26.97 (CH_2); $^{31}P\{^1H\}$ (121.4 MHz, $CDCl_3$) δ 36.10; IR (KBr) 3050 (w), 2900 (w), 1700 (m), 1480 (m), 1435 (s), 1175 (s), 1110 (s), 1090 (s), 1000 (w), 740 (m), 715 (m), 690 (s), 535 (s), 505 (m); MS m/z 544 (<1), 542 (<1, M^+), 506 (<1), 368 (<1), 367 (<1), 262 (100), 183 (22), 108 (42).

Acknowledgment. We are grateful to the DGICYT (Projects PB91-0612-C03-02 and PB94-0163) for support of this research. D.J.C. acknowledges the receipt of a predoctoral fellowship by the Ministerio de Educación y Ciencia.

Supporting Information Available: Copies of the ^{1}H and ^{13}C NMR spectra for palladacycles **16–18** (6 pages). This material is contained in many libraries as microfiche, immediately follows this article in the microfilm version of the journal, and can be ordered form the ACS; see any current masthead page for ordering information.

OM950227G

Reaction of a *tert*-Butyl-Substituted Iron(0) Alkynyl(ethoxy)carbene Complex with Dimethylamine

Jaiwook Park* and Jinkyung Kim

Department of Chemistry and Center for Biofunctional Molecules, Pohang University of Science and Technology, San 31 Hyoja-Dong, Pohang, Kyung-Buk 790-784, Republic of Korea

Received May 4, 1995[⊗]

*Summary: The reaction of [(3,3-dimethylbutynyl)ethoxymethylene]Fe(CO)$_4$ (**1**) with dimethylamine was investigated. [(3,3-Dimethylbutynyl)(dimethylamino)methylene]-Fe(CO)$_4$ (**2**) was formed in 95% yield by substitution of the ethoxy group at −78 °C. Meanwhile, the η^3-(2-(tert-butylcarbonyl)vinyl)carbene complex (**3**) was produced at 25 °C in 96% yield through the Michael-type addition of dimethylamine and subsequent rearrangements. The alkynyl(amino)carbene complex **2** was further reacted with dimethylamine in acetonitrile at 25 °C to give the η^3-vinylcarbene complex **4** analogous to **3**. Under CO pressure **3** and **4** were converted slowly to (η^4-α-pyrone)-Fe(CO)$_3$ complexes **5** and **6**.*

Metal alkynylcarbene complexes have attracted interest due to their distinct properties and potentials in synthetic organic chemistry.[1] For group 6 metal alkynylcarbene complexes, reactions with amines have shown a variety of reactivities depending on reaction conditions.[1e,2] Substitution reaction at the carbene carbon competes with the reaction at the β-carbon of the alkynyl group to give an alkenylcarbene complex and a 3-aminoallenylidene complex.[2] The selectivity varies considerably with reaction temperature as well as participating amines and alkynylcarbene complexes.

As a part of our research on (alkynylcarbene)Fe(CO)$_4$ complexes,[3] the reaction with amines was investigated. *tert*-Butyl-substituted alkynylcarbene complex **1** and dimethylamine were chosen for convenient manipulation and easy analysis. The reaction at −78 °C proceeded in a pathway similar to those of group 6 metal alkynylcarbene complexes.[4] However, the reaction pathway changed dramatically at 25 °C. An unexpected product was obtained through a complex rearrangement in almost quantitative yield.

Results and Discussion

The reaction pathways were affected greatly by temperature (Scheme 1): At −78 °C, substitution reaction at the carbene carbon was completed in 5 min to give the alkynyl(amino)carbene complex **2** in 95% yield. However, at 25 °C, (η^3-(β-(*tert*-butylcarbonyl)vinyl)-carbene)Fe(CO)$_3$ complex **3** was obtained in 96% yield within 2 min. At 0 °C a mixture of **2** and **3** was obtained in a 1:5 ratio. The substitution product **2** underwent an addition reaction to give **4** in 91% yield, which is analogous to **3**, by treatment with another equivalent of dimethylamine in acetonitrile at 25 °C. Under moderate CO pressure (30 psi) at 25 °C, complex **3** in 1,2-dichloroethane was slowly transformed to the (η^4-α-pyrone)Fe(CO)$_3$ complexes **5** in 77% yield. The yield decreased with increasing reaction temperature as well as with decreasing CO pressure. However, the reaction of **4** with CO was so slow at 25 °C that the reaction mixture was heated to 80 °C for 19 h to give **6** in 81% yield.

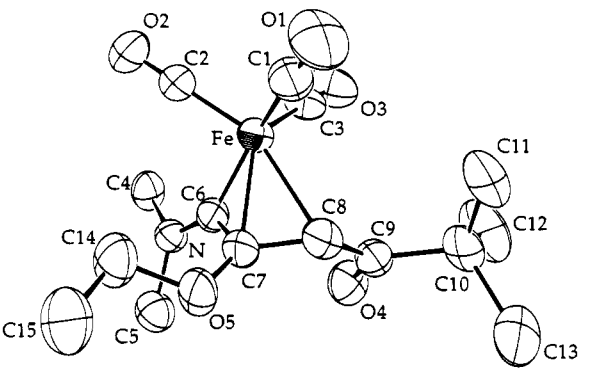

Figure 1. Structure of **3** with the atom-labeling scheme.

The spectroscopic and elemental analyses revealed that **3** is a 1:1 adduct of dimethylamine and the alkynylcarbene complex. However, the analyses were not consistent with those for a (β-aminoalkenyl)carbene complex or a 3-aminoallenylidene complex,[2] which have been observed in the reaction of group 6 metal alkynyl(alkoxy)carbene complexes with amines. Compound **3** was recrystallized from hexane, and its molecular structure was established by X-ray crystallography (Figure 1): It has the structure of an (η^3-(β-acylvinyl)-carbene)Fe(CO)$_3$ complex.[5] The structure is indicative of a CO insertion and a rearrangement involving the amino group and the carbonyl oxygen if rearrangement of the *tert*-butyl group is ruled out.

(η^3-(β-Acylvinyl)carbene)Fe(CO)$_3$ complexes analogous to **3** and **4** have been suggested as common intermediates for furans and α-pyrone complexes in reactions of metal carbene complexes with alkynes.[3a,5,6] In addition, it is well-known that a Michael-type addition of amines

[⊗] Abstract published in *Advance ACS Abstracts,* August 1, 1995.

(1) (a) Wulff, W. D. In *Comprehensive Organic Synthesis*; Trost, B. M., Fleming, I., Eds.; Pergamon Press: New York, 1990; Vol. 5. (b) Wulff, W. D. In *Advances in Metal-Organic Chemistry*; Liebeskind, L. S., Ed.; JAI Press Inc.: Greenwich, CT, 1989; Vol. 1. (c) Duetsch, M.; Vidoni, S.; Stein, F.; Funke, F.; Noltemeyer, M.; de Meijere, A. *J. Chem. Soc., Chem. Comm.*, **1994**, 1679. (d) Funke, F.; Duetsch, M.; Stein, F.; Noltemeyer, M.; de Meijere, A. *Chem. Ber.* **1994**, *127*, 911. (e) Rahm, A.; Wulff, W. D. *Organometallics* **1993**, *12*, 597. (f) Duetsch, M.; Lackmann, R.; Stein, F.; de Meijere, A. *Synlett* **1991**, 324.

(2) (a) Stein, F.; Duetsch, M.; Pohl, E.; Herbst-Irmer, R.; de Meijere, A. *Organometallics* **1993**, *12*, 2556. (b) Duetsch, M.; Stein, F.; Funke, F.; Pohl, E.; Herbst-Irmer, R.; de Meijere, A. *Chem. Ber.* **1993**, *126*, 2535.

(3) (a) Park, J.; Kang, S.; Won, C.; Whang, D.; Kim, K. *Organometallics* **1993**, *12*, 4704. (b) Park, J.; Kang, S.; Whang, D.; Kim, K. *Organometallics* **1992**, *11*, 1738. (c) Park, J.; Kang, S.; Whang, D.; Kim, K. *Organometallics* **1991**, *10*, 3413. (d) Park, J.; Kang, S.; Whang, D.; Kim, K. *Taehan Hwahakhoe Chi* **1992**, *36*, 770.

(4) Fischer, E. O.; Kalder, H. J. *J. Organomet. Chem.* **1977**, *131*, 57.

(5) For previous examples of (η^3-β-acylvinylcarbene)Fe(CO)$_3$ complexes, see: Mitsudo, T.; Watanabe, H.; Sasaki, T.; Takegami, Y.; Watanabe, Y.; Kafuku, K.; Nakatsu, K. *Organometallics* **1989**, *8*, 368 and references therein.

0276-7333/95/2314-4431$09.00/0

Scheme 1

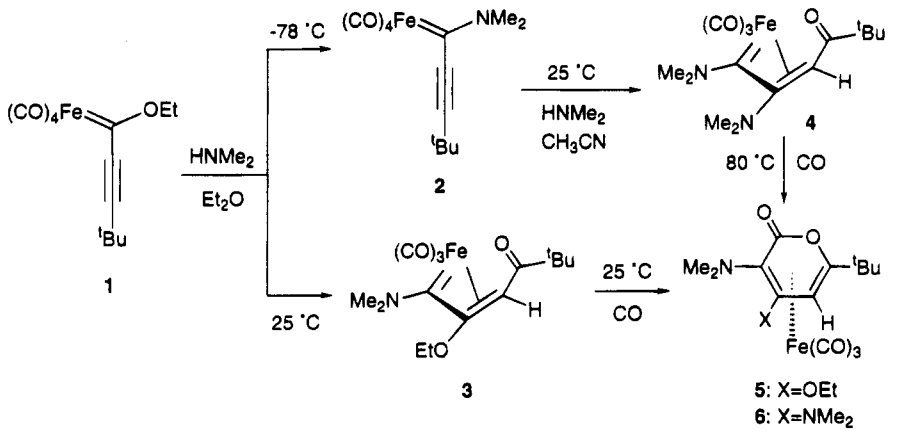

Scheme 2

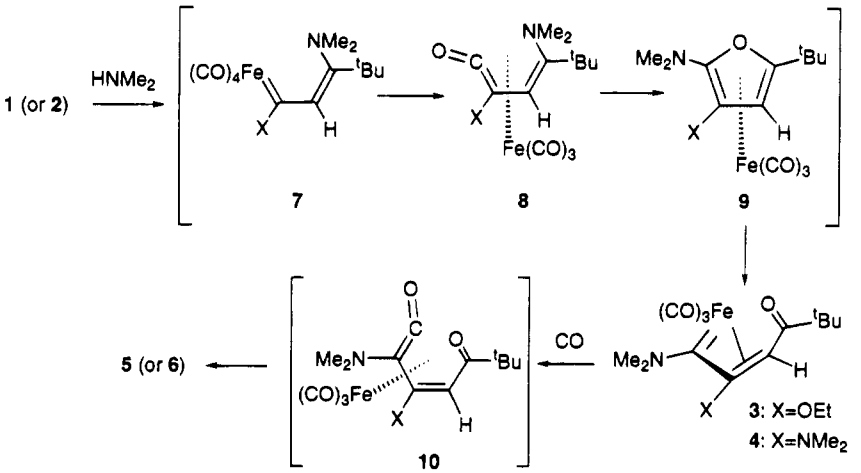

to group 6 metal alkynylcarbene complexes is predominant over substitution at the carbene carbon above room temperature.[4] Thus, a reaction pathway can be presented for the isolated products **3**–**6** as shown in Scheme 2: At first a ((β-aminovinyl)carbene)iron(0) complex (**7**) is formed by a Michael-type addition of dimethylamine to alkynylcarbene complexes **1** and **2**. Then coordination of the vinyl group to the iron and CO insertion at the carbene carbon give η^4-vinylketene complex **8**. Rearrangement of the dimethylamino unit and the ketenyl oxygen leads to ((β-acylvinyl)carbene)-$Fe(CO)_3$ complexes **3** and **4** through formation of a coordinated furan derivative (**9**) and ring opening of the furan with breaking the bond between oxygen and the carbon bearing the dimethylamino group. In the presence of CO, complexes **3** and **4** are obvious precursors of the pyrone complexes **5** and **6** which can be formed by CO insertion at the carbene carbon (to give **10**) and subsequent cyclization.[3a,6b,c]

We have observed that two types of products can be obtained selectively both in almost quantitative yields from reactions of the iron(0) *tert*-butyl-substituted alkynyl(ethoxy)carbene complex **1** with dimethylamine with varying reaction temperature. Furthermore, the X-ray crystal structure of the addition product **3** has revealed that CO insertion and rearrangement of the dimethylamino group proceed at room temperature.

(6) (a) McCallum J. S.; Kunng, F.-A.; Gilbertson, S. R.; Wulff, W. D. *Organometallics* **1988**, *7*, 2346. (b) Semmelhack, M. F.; Tamura, R.; Schnatter, W.; Springer, J. *J. Am. Chem. Soc.* **1984**, *106*, 5363. (c) Semmelhack, M. F.; Park, J. *Organometallics* **1986**, *5*, 2550.

Experimental Section

General Comments. Solvents used for reactions were all reagent grade and were further purified by standard techniques. The alkynylcarbene complex **1** was prepared by the method described previously.[3c]

All reactions and manipulations were carried out on a dual manifold providing vacuum and dry argon. For reactions involving CO pressure, a Schlenk tube equipped with high-vacuum O-ring right-angle stopcock was used. Flash column chromatography was carried out with mixtures of degassed hexane and ethyl acetate as the eluents and silica gel (Merck: silica gel 60, 40–63 μm particle size) as the stationary phase.

IR spectra were recorded on a Bomem Michelson 100 FT-IR spectrometer using a matched NaCl solution cell of 0.5-mm path length. ^1H and ^{13}C NMR spectra were recorded on a Bruker ASPECT 300 spectrometer. Chemical shifts are reported in ppm downfield from TMS but were measured relative to the residual ^1H in the solvent. Electron impact mass spectra were recorded on a Kratos 25-RAF. Melting points were measured on a Thomas Hoover capillary melting point apparatus and are uncorrected. High-resolution mass spectroscopy and elemental analyses were conducted by Korea Basic Science Center, Seoul, Korea.

Reaction of $(CO)_4Fe{=}C(OEt)C{\equiv}C\text{-}^tBu$ (1) with Dimethylamine at −78 °C. Dimethylamine was injected to a solution of **1** (10.12 mmol) in ether (30 mL) at −78 °C through a cannula with the resulting solution being stirred for 2 min until the color of the solution changed from purple to dark red. The reaction mixture was concentrated under vacuum, and the residue was chromatographed (4:1 hexane/EtOAc) to give 2.93 g (95%) of **2** as a dark red oil. High-resolution MS (EI) calcd for **2**: *m/z* 305.0346, found, 305.0351. IR (CH_2Cl_2, cm^{-1}): ν_{CC} 2194 (w), ν_{CO} 2040 (s), 1950 (s), 1937 (s). ^1H NMR

Table 1. Crystallographic Data for 3

formula	$C_{15}H_{21}NO_5Fe$
fw	351.19
space group	monoclinic, $P2_1/c$ (No. 14)
a, Å	8.834(2)
b, Å	22.484(2)
c, Å	9.380(2)
β, deg	109.626(6)
V, Å^3	1754.9(6)
Z	4
temp, °C	23
D (calcd), g cm^{-3}	1.329
crystal dimens, mm^3	0.50 × 0.40 × 0.30
radiation	Mo Kα [λ(Kα$_1$) = 0.710 73 Å]
linear abs coeff, cm^{-1}	8.76
scan mode	ω
ω-scan width, deg	0.85 + 0.35 tan θ
2θ limit, deg	48
no. of data collcd	2711
no. of unique data	2579
no. of unique data with $I > 3\sigma(I)$	1901
no. of variables	262
GOF	0.47
$R(F)^a$	0.029
$R_w(F)^b$	0.029

^{a} $R = \sum||F_o| - |F_c||/|F_o|$. ^{b} $R_w = [\sum w(|F_o| - |F_c|)^2/\sum w|F_o|^2]^{1/2}$; $w = 4F_o^2/\sigma^2(F_o^2)$; $\sigma(F_o^2) = [\sigma^2(I) + (pI)^2]^{1/2}$, $p = 0.04$.

(C_6D_6, ppm): δ 3.80 (s, 3 H, $-NCH_3$), 3.53 (s, 3 H, $-NCH_3$), 1.31 (s, 9 H, $-C(CH_3)_3$). ^{13}C NMR (C_6D_6, ppm): δ 232.0 (Fe=*C*), 216.20 (*C*O), 133.48 (−*C*≡C−), 84.98 (−C≡*C*−), 47.84 ($-NCH_3$), 45.96 ($-NCH_3$), 29.87 (−*C*Me$_3$), 29.49 ($-C(CH_3)_3$). MS (EI): m/z 305 (M$^+$, 2.0), 276 (5.0), 249 (61), 221 (86), 193 (100).

Reaction of 1 with Dimethylamine at 25 °C. Dimethylamine was injected to a solution of **1** (6.08 mmol) in ether (30 mL) at 25 °C through a cannula, with the resulting solution being stirred for 2 min. The color of the reaction mixture changed from purple to dark brown. The reaction mixture was concentrated under vacuum, and the residue was chromatographed (4:1 hexane/EtOAc) to give 2.05 g (96%) of **3** as a yellow solid. It was recrystallized from hexane to prepare single crystals for X-ray diffraction analysis. Mp: 106−107 °C. Anal. Calcd for **3**: C, 51.30; H, 6.03; N, 3.99. Found: C, 51.31; H, 6.00; N, 4.06. IR (CH_2Cl_2, cm^{-1}): ν_{CO} 2033 (s), 1956 (s), $\nu_{C=O}$ 1645 (s). ^1H NMR (C_6D_6, ppm): δ 4.29 (s, 1 H, −C=C−*H*), 3.05 (m, 1 H, $-OCH_2CH_3$), 2.90 (m, 1 H, $-OCH_2CH_3$), 2.71 (br s, 3 H, $-NCH_3$), 2.62 (br s, 3 H, $-NCH_3$), 1.28 (s, 9 H, $-C(CH_3)_3$), 0.96 (dd, J = 6.87, 8.19 Hz, 3 H, $-OCH_2CH_3$). ^{13}C NMR (C_6D_6, ppm): δ 226.04 (Fe=*C*), 213.62 (Fe−*C*O), 211.37 (−*C*=O), 107.0 (−C=*C*−H), 64.5 (−C=C−*O*CH$_2$CH$_3$), 49.4 (−C=*C*−OEt), 45.5 ($-NCH_3$), 44.6 ($-NCH_3$), 43.8 (−*C*Me$_3$), 28.0 ($-C(CH_3)_3$), 14.6 ($-OCH_2CH_3$). MS (EI) m/z 351 (M$^+$, 1.0), 323 (24), 295 (45), 267 (100).

Reaction of (CO)$_4$Fe=C(NMe$_2$)C≡C-^{t}Bu (2) with Dimethylamine. Dimethylamine was injected to a solution of **2** (424 mg, 1.39 mmol) in acetonitrile (15 mL) at 25 °C through a cannula for 5 s. After being stirred for 3 h, the reaction mixture was concentrated under vacuum and the residue was chromatographed (4:1 hexane/EtOAc) to give 442 mg (91%) of **4** as a yellow solid. Mp: 123−124 °C. Anal. Calcd for **4**: C, 51.45; H, 6.33; N, 8.00. Found: C, 51.44; H, 6.25; N, 8.12. IR (CH_2Cl_2, cm^{-1}): ν_{CO} 2020 (s), 1943 (s), $\nu_{C=O}$ 1641 (s). ^1H NMR (C_6D_6, ppm): δ 4.02 (s, 1 H, −C=C−*H*), 2.66 (br s, 6 H, $-N(CH_3)_2$), 1.72 (s, 6 H, $-N(CH_3)_2$), 1.30 (s, 9 H, $-C(CH_3)_3$). ^{13}C NMR (C_6D_6, ppm): δ 232.04 (Fe=*C*), 215.57 (Fe−*C*O), 211.33 (−*C*=O), 97.96 (−C=*C*−H), 49.46 ($-NCH_3$), 44.41 ($-NCH_3$), 43.48 ($-NCH_3$), 39.98 (−*C*Me$_3$), 28.23 ($-C(CH_3)_3$). MS (EI) m/z 350 (M$^+$, 2.0), 322 (21), 294 (40), 266 (73), 251 (100).

Reaction of 3 with CO. A Schlenk tube, containing a solution of **3** (260 mg, 0.74 mmol) in 1,2-dichloroethane (20 mL), was filled with CO gas (30 psi). After being stirred at 25 °C for 4 days, the reaction mixture was concentrated under vacuum and the residue was chromatographed (2:1 hexane/EtOAc) to give 216 mg (77%) of **5** as a yellow solid. Mp 107−109 °C. Anal. Calcd for **5**: C, 50.68; H, 5.58; N, 3.69. Found: C, 50.64; H, 5.68; N, 3.74. IR (CH_2Cl_2, cm^{-1}): ν_{CO} 2060 (s), 1994 (s), $\nu_{C=O}$ 1716 (m). ^1H NMR (C_6D_6, ppm): δ 5.30 (s, 1 H, −C=C−*H*), 3.26 (m, 2 H, $-OCH_2CH_3$), 2.56 (s, 6 H, $-N(CH_3)_2$), 1.27 (s, 9 H, $-C(CH_3)_3$), 0.95 (dd, J = 6.84, 6.84 Hz, 3 H, $-OCH_2CH_3$). ^{13}C NMR (C_6D_6, ppm): δ 209.1 (Fe−*C*O), 124.7, 74.2, 70.5, 64.3 ($-OCH_2CH_3$), 42.2 ($-N(CH_3)_2$), 34.4 (−*C*Me$_3$), 30.4 ($-C(CH_3)_3$), 14.3 ($-OCH_2CH_3$). MS (EI) m/z 379 (M$^+$, 3.0), 351 (17), 323 (63), 295 (87), 267 (100).

Reaction of 4 with CO. A Schlenk tube, containing a solution of **4** (110 mg, 0.291 mmol) in 1,2-dichloroethane (6 mL), was filled with CO gas (30 psi). After being stirred at 80 °C for 19 h, the reaction mixture was concentrated under vacuum and the residue was chromatographed (1:1 hexane/EtOAc) to give 96 mg (87%) of **6** as a yellow solid. Mp 125−

Table 2. Positional Parameters and B_{eq} Values^a for Non-Hydrogen Atoms of 3

atom	x	y	z	B_{eq}, Å^2
Fe	0.63135(5)	0.07610(2)	0.20391(5)	3.664(9)
O1	0.3832(3)	0.1248(1)	−0.0666(3)	7.53(8)
O2	0.4377(3)	−0.0204(1)	0.2569(3)	7.11(7)
O3	0.8339(3)	0.0101(1)	0.0681(3)	6.40(7)
O4	1.0153(2)	0.13373(9)	0.3532(2)	4.62(5)
O5	0.6140(2)	0.17432(9)	0.4388(2)	4.09(5)
N	0.8115(3)	0.0519(1)	0.5380(3)	3.53(5)
C1	0.4780(4)	0.1053(2)	0.0382(4)	4.89(8)
C2	0.5117(4)	0.0181(2)	0.2333(4)	4.79(8)
C3	0.7529(4)	0.0365(1)	0.1173(4)	4.39(8)
C4	0.8230(4)	−0.0129(1)	0.5465(4)	4.87(8)
C5	0.8901(4)	0.0841(2)	0.6784(4)	4.90(8)
C6	0.7493(3)	0.0798(1)	0.4101(3)	3.44(6)
C7	0.6997(3)	0.1394(1)	0.3727(3)	3.47(7)
C8	0.7431(3)	0.1612(1)	0.2506(3)	3.58(7)
C9	0.9083(3)	0.1562(1)	0.2480(3)	3.51(7)
C10	0.9464(4)	0.1828(1)	0.1129(3)	4.10(7)
C11	0.8021(4)	0.1827(2)	−0.0341(4)	5.56(9)
C12	1.0837(4)	0.1483(2)	0.0886(4)	7.0(1)
C13	0.9956(5)	0.2474(2)	0.1554(4)	6.5(1)
C14	0.4983(4)	0.1455(2)	0.4913(4)	5.33(8)
C15	0.4183(4)	0.1909(2)	0.5571(4)	6.8(1)

^{a} $B_{eq} = (4/3)\sum_i\sum_j\beta_{ij}\mathbf{a}_i\mathbf{a}_j$.

Table 3. Selected Bond Lengths (Å) and Angles (deg) for 3

		Bond Lengths	
Fe−C(1)	1.807(3)	O(4)−C(9)	1.222(3)
Fe−C(2)	1.757(4)	O(5)−C(7)	1.374(4)
Fe−C(3)	1.787(4)	N−C(4)	1.461(4)
Fe−C(6)	1.865(2)	N−C(5)	1.459(4)
Fe−C(7)	2.063(3)	N−C(6)	1.301(3)
Fe−C(8)	2.131(3)	C(6)−C(7)	1.417(4)
O(1)−C(1)	1.143(4)	C(7)−C(8)	1.412(5)
O(2)−C(2)	1.151(5)	C(8)−C(9)	1.473(4)
O(3)−C(3)	1.139(5)	C(9)−C(10)	1.538(5)
		Bond Angles	
C(1)−Fe−C(2)	95.1(1)	C(5)−N−C(6)	121.2(2)
C(1)−Fe−C(3)	100.5(2)	Fe−C(1)−O(1)	178.6(3)
C(1)−Fe−C(6)	150.6(2)	Fe−C(2)−O(2)	177.6(3)
C(1)−Fe−C(7)	110.5(1)	Fe−C(3)−O(3)	177.0(3)
C(1)−Fe−C(8)	90.6(1)	Fe−C(6)−N	148.2(2)
C(2)−Fe−C(3)	100.7(2)	Fe−C(6)−C(7)	76.5(2)
C(2)−Fe−C(6)	91.5(1)	Fe−C(7)−O(5)	132.6(2)
C(2)-Fe-C(7)	115.3(1)	Fe-C(7)-C(6)	61.5(1)
C(2)-Fe-C(8)	153.6(5)	Fe-C(7)-C(8)	73.0(2)
C(3)-Fe-C(6)	106.4(1)	Fe-C(8)-C(7)	67.7(2)
C(3)-Fe-C(7)	128.9 (1)	Fe-C(8)-C(9)	108.7 (2)
C(3)-Fe-C(8)	103.6 (1)	O(4)-C(9)-C(8)	121.4 (3)
C(6)-Fe-C(7)	41.9 (1)	O(4)-C(9)-C(10)	120.2 (3)
C(6)-Fe-C(8)	71.8 (1)	O(5)-C(7)-C(6)	126.9 (3)
C(7)-Fe-C(8)	39.3 (1)	O(5)-C(7)-C(8)	120.5 (2)
C(4)-N-C(5)	116.3 (2)	N-C(6)-C(7)	133.2 (3)
C(4)-N-C(6)	122.1 (2)	C(8)-C(9)-C(10)	118.4 (2)

127 °C. Anal. Calcd for **6**: C, 50.81; H, 5.86; N, 7.41. Found: C, 50.70; H, 6.12; N, 7.28. IR (CH_2Cl_2, cm^{-1}): ν_{CO} 2023 (s), 1945 (s), $\nu_{C=O}$ 1730 (m). ^1H NMR (C_6D_6, ppm): δ 4.79 (s, 1 H, $-C{=}C-H$), 3.12 (s, 3 H, $-N(CH_3)_2$), 2.66 (s, 6 H, $-N(CH_3)_2$), 2.21 (s, 3 H, $-N(CH_3)_2$), 1.23 (s, 9 H, $-C(CH_3)_3$), 0.95 (dd, J = 6.84, 6.84 Hz, 3 H, $-OCH_2CH_3$). ^{13}C NMR (C_6D_6, ppm): δ 215.4 (Fe–CO), 168.4 ($-C{=}O$), 162.6 ($-O-C{=}C-$), 80.2 ($-C{=}C-NMe_2$), 67.8 ($-C{=}C-NMe_2$), 64.6 ($-C{=}C-H$), 50.2 ($-NCH_3$), 48.5 ($-NCH_3$), 37.3 ($-NCH_3$), 30.7 ($-CMe_3$), 28.5 ($-C(CH_3)_3$). MS (EI): m/z 378 (M^+, 39), 322 (71), 294 (71), 266 (83), 238 (83), 210 (51), 195 (100).

X-ray Crystallography. A crystal of **3** (0.5 × 0.4 × 0.3 mm^3) sealed in a Lindemann capillary tube was mounted on an Enraf-Nonius CAD4 diffractometer using Mo Kα radiation. Cell parameters and an orientation matrix for data collection were obtained from least-squares refinement, using the setting angles of 25 reflections in the range $23.7 < 2\theta < 29.9°$. The crystallographic data and additional details of data collection are summarized in Table 1. The intensities of three standard reflections, recorded every 3 h of X-ray exposure, showed no systematic changes. All the calculations were carried out with the Enraf-Nonius MolEN package. The intensity data were corrected for Lorentz and polarization effects. Empirical absorption corrections were also applied (DIFABS). The structure was solved by a combination of Patterson and difference Fourier methods (SHELXS86).[7] All the nonhydrogen atoms were refined anisotropically by full-matrix least-squares methods. The positions of hydrogen atoms were identified on an electron density map. Each hydrogen atom was assigned an isotropic thermal parameter of 1.2 times that of attached atom. All the calculations except solving structures were carried out with the Enraf-Nonius MolEN program package.[8] The final cycle of refinement led to the R indices listed in Table 1. The atomic scattering factors were taken from ref 9 for the non-hydrogen atoms and from the ref 10 for hydrogen. The positional and equivalent isotropic thermal parameters of the non-hydrogen atoms are listed in Table 2, and selected bond lengths and bond angles for **3** are listed in Table 3.

Acknowledgment. We are grateful to the Ministry of Education (Basic Science Research Institute Program) and the Korea Science and Engineering Foundation (CBM Center) for financial support. We thank D. M. Whang and Prof. Kimoon Kim for the crystallographic analysis.

Supporting Information Available: Tables of positional parameters for hydrogen atoms, anisotropic temperature factors, bond lengths, and bond angles for **3** (3 pages). Ordering information is given on any current masthead page.

OM950321X

(7) Sheldrick, G. M. *SHELXS-86 User Guide*; Crystallography Department, University of Göttingen: Göttingen, Germany, 1986.

(8) Fair, C. K. *MolEN*; Enraf-Nonius: 2624 BD Delft, The Netherlands, 1990.

(9) Cromer, D. T.; Waber, J. T. *International Tables for X-ray Crystallography;* Kynoch Press: Birmingham, England, 1974; Vol. IV.

(10) Stewart, R. F.; Davidson, E. R.; Simpson, W. T. *J. Chem. Phys.* **1965**, *42*, 3175.

Evaluation of the Energy Barrier for Carbonyl Exchange in the Highly Fluxional $Ru_3(CO)_{12}$ System

Silvio Aime,* Walter Dastrù, Roberto Gobetto, Jochen Krause, and Luciano Milone

Dipartimento di Chimica Inorganica, Chimica Fisica e Chimica dei Materiali, Università di Torino, via Pietro Giuria 7, 10125 Torino, Italy

Received April 27, 1995[⊗]

Summary: ^{13}C spin–lattice (T_1) and spin–spin (T_2) relaxation times of carbonyl groups measured as a function of temperature in CD_2Cl_2 solution combined with the data obtained by high-resolution MAS ^{13}C NMR in the solid state have been used to evaluate the activation energy of the intramolecular exchange process in $Ru_3(CO)_{12}$. An independent evaluation of the activation energy by line shape analysis of the broadened single ^{13}C NMR resonance at very low temperature in Freon-22 solution substantially agrees with the value obtained by T_1 and T_2 measurements.

Introduction

Since the early seventies it has been well established that intramolecular CO exchange is a ubiquitous phenomenon in metal carbonyl complexes.[1] The most straightforward method to get insight into the exchange mechanism and to get an evaluation of the energy barrier associated with it consists of analyzing the spectral changes upon temperature variation. In recent years this approach is more conveniently pursued through magnetization transfer[2] and 2D-EXSY techniques.[3] There are however a number of metal carbonyl complexes which cannot be investigated by this type of approach since they are highly fluxional and their static structure cannot be "frozen out" at the lowest attainable temperature in solution. The title compound appears to be a prototype of this class of molecules as it was reported to show a single ^{13}C resonance down to 153 K at the observation frequency of 25 MHz.[4] Actually the ^{13}C NMR spectrum corresponding to its "frozen" structure has been observed in the MAS (magic angle spinning) NMR spectrum of a solid sample of $Ru_3(CO)_{12}$ even at ambient temperature.[5,6] In this paper we demonstrate that the combined use of the chemical shift information obtained from the MAS spectrum and the relaxation data obtained in solution at different temperatures provides an accurate evaluation of the energy barrier associated with the intramolecular carbonyl exchange in this type of highly fluxional molecule.

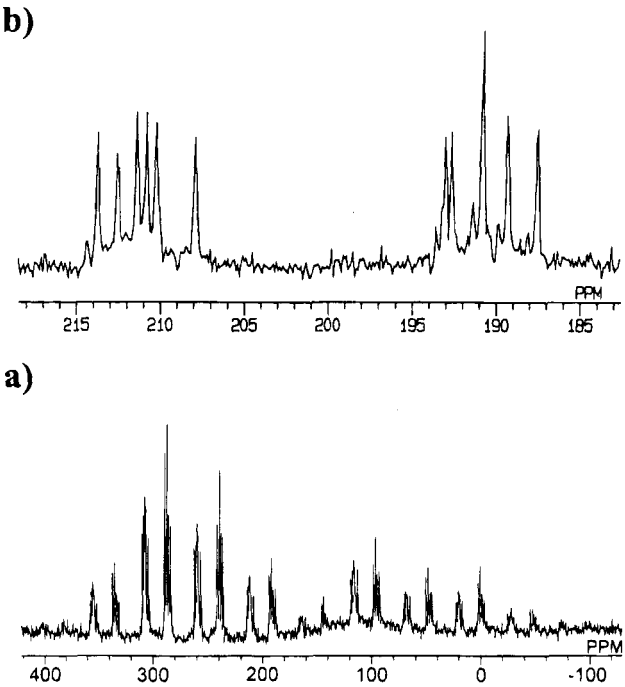

Figure 1. (a) ^{13}C MAS NMR spectra of $Ru_3(CO)_{12}$ at 298 K obtained at 125.8 MHz. (b) Expanded view of centerband region.

Experimental Section

$Ru_3(CO)_{12}$ was purchased from Strem. ^{13}CO (99% enriched) was purchased from Isotec (Miamisburg, OH) and the ^{13}C-enriched (ca. 20%) $Ru_3(CO)_{12}$ was obtained by direct exchange of ^{13}CO with $Ru_3(CO)_{12}$ in cyclohexane at 60 °C for 3 days in sealed vials.

The high-resolution ^{13}C MAS NMR spectrum was recorded on a Jeol JNM-A500 spectrometer operating at 125.8 MHz. Cylindrical 5 mm o.d. zirconia rotors with sample volume of 100 μL were employed with a spinning speed of 6400 Hz. The magic angle was carefully adjusted from the ^{79}Br MAS spectrum of KBr by minimizing the linewidth of the spinning satellite transitions. The spectrum was recorded with a 45° pulse of 1.7 μs and a delay of 150 s.

The ^{13}C solution spectra were recorded on Jeol EX400 (100.25 MHz), Jeol GX270/89 (67.8 MHz), and Jeol EX90 (22.6 MHz) spectrometers. The compound (10 mg) dissolved in 0.8 mL of CD_2Cl_2 was degassed by using a Schlenk tube apparatus and the freeze–thaw methodology.

[⊗] Abstract published in *Advance ACS Abstracts,* August 15, 1995.

(1) Band, E; Muetterties, E. L. *Chem. Rev.* **1978**, *72*, 639.

(2) (a) Forsen, S.; Hoffmann, R. A. *Prog. NMR Spectrosc.* **1966**, *1*, 173. (b) Mann, B. E. *J. Magn. Reson.* **1976**, *21*, 17. (c) Mann, B. E. *J. Chem. Soc., Chem. Commun.* **1977**, 626.

(3) (a) Ewing, P.; Farrugia, L. J.; Rycroft, D. S. *Organometallics* **1988**, *7*, 859. (b) Strawczinski, A.; Ros, R.; Roulet, R. *Helv. Chim. Acta* **1988**, *71*, 867. (c) Lindsel, W. E.; Walker, N. M.; Boyd A. S. F. *J. Chem. Soc., Dalton Trans.* **1988**, 675. (d) Johnson, B. F. G.; Lewis, J.; Pearshall, W. A.; Scott, L. G. *J. Organomet. Chem.* **1991**, *402*, C27. (e) Aime, S.; Dastrù, W.; Gobetto, R.; Arce, A. J. *Organometallics* **1994**, *13*, 3737. (f) Hawkes, G. E.; Sales, K. D. *J. Chem Soc., Dalton Trans.* **1985**, 225. (g) Hawkes, G. E.; Lian, L. Y.; Randall, E. W.; Sales, K. D. *J. Magn Reson.* **1985**, *65*, 173. (h) Beringhelli, T.; D'Alfonso, G.; Molinari, H.; Hawkes, G. E.; Sales, K. D. *J. Magn Reson.* **1988**, *80*, 45. (i) Farrugia, L. J. *Organometallics* **1989**, 9, 2410. (j) Beringhelli, T.; D'Alfonso, G.; Minoja, A. P. *Organometallics* **1991**, *10*, 394.

(4) Forester, A.; Johnson, B. F. G.; Lewis, J.; Mathenson, T. W.; Robinson, B. H.; Jackson, W. G. *J. Chem Soc., Chem. Commun.* **1974**, 1042.

(5) Aime, S.; Botta, M.; Gobetto, R.; Osella, D.; Milone, L. *Inorg. Chim. Acta* **1988**, *146*, 151.

(6) Walter, T. H.; Reven, L.; Oldfield, E. *J. Phys. Chem.* **1989**, *93*, 1320.

(7) Farrar, T. C.; Becker, E. D. *Pulse and Fourier Transform NMR-Introduction to Theory and Methods*; Academic Press: New York, 1977; p 60.

0276-7333/95/2314-4435$09.00/0

Table 1. Principal Components and Anisotropies of the Chemical Shift Tensor for the Carbonyl Resonances[a]

σ_{iso}	σ_{11}	σ_{22}	σ_{33}	$\Delta\sigma$
−213.7	−339	−324	23	355
−212.5	−336	−336	35	371
−211.3	−344	−318	29	361
−210.8	−335	−334	36	371
−210.2	−345	−325	40	376
−208.0	−346	−299	21	343
−193.2	−322	−304	46	358
−192.8	−320	−303	44	356
−190.9[b]	−311	−310	49	360
−189.3	−319	−293	44	350
−187.6	−315	−287	40	341

[a] Values are obtained from the spinning sideband manifold analysis in the ^{13}C NMR MAS spectrum of $Ru_3(CO)_{12}$ according to the Herzfeld–Berger method (see text for references). [b] This peak arises from the overlap of two carbonyl resonances.

Table 2. ^{13}C Spin–Lattice and Spin–Spin Relaxation Times of $Ru_3(CO)_{12}$ Measured at 9.4 T

T/K	T_1/s	T_2/s	T/K	T_1/s	T_2/s
193	0.43	0.17	263	2.76	1.81
213	0.85	0.38	273	3.24	2.2
233	1.53	0.78	283	3.74	2.71
243	1.92	1.12	293	4.28	3.22
253	2.31	1.35			

The spin–lattice relaxation times were measured by using the inverse recovery technique, and spin–spin relaxation times were obtained with the Carr–Purcell–Meiboom–Gill pulse sequence.[7]

The reported T_1's and T_2's are averages of several measurements, and errors are extimated to be ±2% for T_1 and ±5% for T_2.

Results and Discussion

Figure 1 shows the isotropic region of the ^{13}C MAS NMR spectrum of a ^{13}C-enriched sample of $Ru_3(CO)_{12}$ measured at 125.8 MHz. With respect to the spectra previously reported which were obtained at 67.8[5] and 90.5[6] MHz, respectively, the further increase in the field strength allows one to obtain a noticeable improvement in spectral resolution. Eleven of the twelve crystallographic independent sites are nicely resolved at 213.7-(1), 212.5(1), 211.3(1), 210.8(1), 210.2(1), 208.0(1), 193.2-(1), 192.8(1), 190.9(2), 189.3(1), and 187.6(1) ppm, respectively. These resonances are clearly split into the two sets of axial and equatorial carbonyls with a separation of 20.3 ppm between the centers of the two sets. By analogy with a large body of data from solution studies[8] we can assign the lower field set of resonances to the axial carbonyl groups. The average separation between axial and equatorial resonances in $Ru_3(CO)_{12}$ is comparable with that found in the solution spectrum of the isostructural $Os_3(CO)_{12}$.[4] The values of the principal elements of the shielding tensors (Table 1) calculated from the spinning sideband intensities according to the Herzfeld and Berger method[9] afford an average value for the chemical shift anisotropy (CSA) of 358 ppm, about 10% lower than the value of 397 ppm previously reported independently by Gleeson and Vaughan[10] and Oldfield and co-workers.[6]

As anticipated above, the evaluation of the energy barrier for carbonyl group exchange in solution is possible through the measurement of the relaxation times of the single ^{13}CO resonance. In Table 2 we report the measured values of T_1 and T_2 in the temperature range 193–293 K.

In general, the longitudinal relaxation rate is the sum of different contributions:

$$\frac{1}{T_1} = \frac{1}{T_1^{CSA}} + \frac{1}{T_1^{SC}} + \frac{1}{T_1^{SR}} + \frac{1}{T_1^{DD}} \quad (1)$$

where $1/T_1^{CSA}$ derives from CSA relaxation, $1/T_1^{SC}$ from scalar relaxation, $1/T_1^{SR}$ from spin rotation relaxation, and $1/T_1^{DD}$ from dipole–dipole relaxation.

In the case of $Ru_3(CO)_{12}$ at the magnetic field of 9.4 T used, the only relevant contribution is expected to be the one arising from the CSA. This statement has been checked by measuring the ^{13}C-T_1 of a ^{13}CO-enriched sample of $Ru_3(CO)_{12}$ at ambient temperature at three magnetic field strengths. Being that the CSA term is the only one that increases on increasing the magnetic field (eq 2), the straight line obtained on plotting $1/T_1$ vs B_0^2 indicates that the CSA relaxation mechanism is indeed operating:

$$\frac{1}{T_1^{CSA}} = {}^2/_{15}\gamma_c^2 B_0^2 \Delta\sigma^2 \tau_R \quad (2)$$

where γ_c is the gyromagnetic ratio of the ^{13}C nucleus, B_0 is the applied magnetic field, $\Delta\sigma$ is the chemical shift anisotropy defined as $\Delta\sigma = \sigma_{33} - (\sigma_{11} + \sigma_{22})/2$, and τ_R is the reorientational correlation time of the molecule.

From the slope of the line one can calculate a value for $\Delta\sigma^2\tau_R$, and therefore, using the value for $\Delta\sigma = 358$ ppm as obtained from the solid state measurements, a value of 34.7 ps is found for τ_R at 293 K that is close to those previously reported for related polynuclear derivatives.[11] Using these values for $\Delta\sigma$ and τ_R, Equation 2 gives at 9.4 T a value for $T_1^{CSA} = 4.25$ s, which is essentially the same as the experimental value of 4.28 s, proving the dominance of the CSA mechanism at this field at room temperature.[12]

In this highly fluxional system, the transverse relaxation rate ($1/T_2$) is determined by the sum of three contributions (eq 3). The $1/T_2^{CSA}$ term is easily evaluated once the term $1/T_1^{CSA}$ is known[7] (eq 4). In

$$\frac{1}{T_2} = \frac{1}{T_2^{CSA}} + \frac{1}{T_2^{SC}} + \frac{1}{T_2^{ex}} \quad (3)$$

$$T_2^{CSA} = {}^6/_7 T_1^{CSA} \quad (4)$$

$Ru_3(CO)_{12}$ the scalar interaction between ^{13}C and the NMR-active isotopes (^{99}Ru, 12.7% natural abundance; ^{101}Ru, 17.0% natural abundance) is modulated as a

(8) Mann, B. E.; Taylor, B. F. *^{13}C NMR Data for Organic Compounds*; Academic Press: New York, 1981; p 176.
(9) Herzfeld, J.; Berger, A. E. *J. Chem. Phys.* **1980**, *73*, 6021.
(10) Gleeson, J. W.; Vaughan, R. W. *J. Chem. Phys.* **1983**, *78*, 5384.
(11) Aime, S.; Botta, M.; Gobetto, R.; Osella, D. *J. Chem. Soc., Dalton Trans.* **1988**, 791. In this reference τ_R for $Ru_3(CO)_{12}$ was reported to be 24.4 ps. The difference from the herein reported value has to be ascribed to the slightly larger $\Delta\sigma$ value used in that work.
(12) Also at lower temperatures we may safely assume that only CSA relaxation is largely dominant. In fact $1/T_1^{SC}$ is still negligible in respect to $1/T_1^{CSA}$ when τ_M is increased to 10^{-6} s. The spin rotation contribution, which is negligible at ambient temperature, is even less important at lower temperatures. The $1/T_1^{DD}$ term (arising from both $^{13}C-^{13}C$ and $^{13}C-^{99/101}Ru$ dipolar interactions) is negligible at any temperature.
(13) Benn, R.; Rufinska, A.; Suss-Fink, G. Unpublished results cited in: Pregosin, P. S. *Transition Metal Nuclear Magnetic Resonance*; Elsevier: Amsterdam, 1991; p 126.

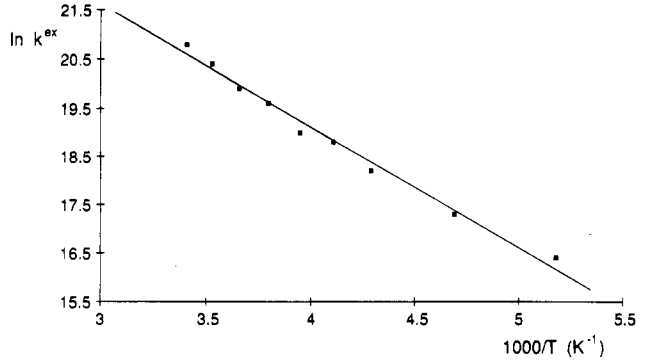

Figure 2. Arrhenius plot of ln k^{ex} vs 1000/T for $Ru_3(CO)_{12}$ obtained from the T_1 and T_2 data.

result of two contributions: (a) rapid carbonyl exchange (scalar relaxation of the first kind) and (b) relaxation of the quadrupolar nuclei (scalar relaxation of the second kind).

The $1/T_2^{SC}$ contribution can be evaluated from the equation

$$\frac{1}{T_2^{SC}} = {}^4/_3\pi^2 J^2 S(S+1)\left[\tau + \frac{\tau}{1+(\omega_c - \omega_{Ru})^2\tau^2}\right] \quad (5)$$

with

$$\tau^{-1} = \tau_M^{-1} + T_2^{99/101Ru-1} \quad (6)$$

where J is the scalar coupling of ^{13}C with ^{99}Ru or ^{101}Ru isotopes, S is the quadrupolar nuclear quantum number ($S = {}^5/_2$ for both ruthenium isotopes), τ is the time scale for the modulation of the scalar interaction, ω_C and ω_{Ru} are the carbon and ruthenium Larmor frequencies (in rad s^{-1}), respectively, τ_M is the exchange lifetime, and $T_2^{99/101Ru}$ values are the transverse relaxation rates of the NMR-active Ru isotopes.

To evaluate the scalar relaxation contribution to T_2 we should know the $^1J_{^{99/101}Ru-^{13}C}$ coupling constant and $T_2^{99/101Ru}$; unfortunately, there are no reports on the $^1J_{^{99/101}Ru-^{13}C}$ and on the linewidth of the ^{99}Ru signals (from which the T_2^{99Ru} could be found) for the $Ru_3(CO)_{12}$ molecule.

There is however a report[14] on the ^{99}Ru spectrum of $[HRu_3(CO)_{11}]^-[N(PPh_3)_2]^+$ in which a linewidth of 190 Hz (T_2^{99Ru} equal to 1.7 ms) for the $^{99}Ru(CO)_4$ fragment is given. By taking into account that the quadrupole moment is 5.78 times greater for ^{101}Ru than for ^{99}Ru, we should find a T_2 value of 51 μs for the former isotope in the same compound.

These T_2^{Ru} values are much longer than τ_M (of the order of 10^{-8} s; vide infra) in the whole range of temperature studied, so it is evident from eq 6 that τ will always be equal to τ_M.

The only reported value for a $^1J_{^{99}Ru-^{13}C}$ is 44 Hz in the case of $[Ru(CN)_6]^{4-}$;[14] by introducing such a value into eq 5, one finds that the $1/T_2^{SC}$ term will produce a negligible contribution to the transverse relaxation, so only $1/T_2^{CSA}$ and $1/T_2^{ex}$ have to be considered in eq 3. Thus we may determine at any temperature the contribution arising from $1/T_2^{ex}$ by subtracting the $1/T_2^{CSA}$ term to the observed transverse relaxation rate. As anticipated above it corresponds to the modulation of the axial–equatorial CO chemical shift separation by

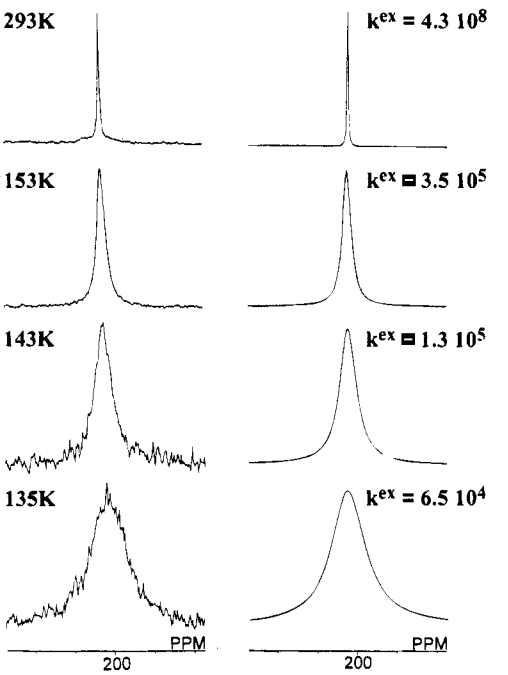

Figure 3. Calculated and observed VT ^{13}C NMR of $Ru_3(CO)_{12}$ at 100.25 MHz in CD_2Cl_2/Freon-22 solution.

the exchange lifetime τ_M[15]

$$\frac{1}{T_2^{ex}} = \sum_i p_i \delta_i^2 \tau_M \left[1 - \frac{2\tau_M}{t_{cp}} \tanh \frac{t_{cp}}{2\tau_M}\right] \quad (7)$$

where p_i is the fractional population of the ith site, δ_i the chemical shift difference in rad s^{-1} from the center of gravity of the exchanging resonances, and t_{cp} the time between the 180° pulses in the Carr–Purcell–Meiboom–Gill sequence. In our case, where $t_{cp}/2\tau_M > 5$, eq 7 simplifies[16] to

$$\frac{1}{T_2^{ex}} = \sum_i p_i \delta_i^2 \tau_M \quad (8)$$

Thus the knowledge of the chemical shifts from the solid state ^{13}C MAS spectrum and the evaluation of $1/T_2^{ex}$ allowed a straightforward determination of τ_M at each temperature. By assuming that the exchange process is first order ($k^{ex} = 1/\tau_M$), we can estimate the exchange rate from 193 to 293 K.

An Arrhenius plot of ln k^{ex} vs $1/T$ (Figure 2) affords an energy barrier for the carbonyl exchange of 4.9 ± 0.5 kcal mol^{-1}. By assuming that the average separation (20.3 ppm) between axial and equatorial carbonyls is the same in solution as the solid state, a coalescence temperature of 121 K is expected for $Ru_3(CO)_{12}$ at 100.25 MHz. Although we were not able to reach this temperature, we observed a marked increase in the linewidth of the single carbonyl resonance of $Ru_3(CO)_{12}$ in a CD_2Cl_2/Freon-22 solution as the slow-exchange regime is approached (Figure 3). Line shape analysis of VT ^{13}C NMR spectra performed using DNMR4[17] afforded the rate constants of the carbonyl exchange process. From the slope of the ln k^{ex} vs 1000/T (Figure 4) we obtained an activation energy of 4.4 ± 0.5 kcal mol^{-1} that agrees

(14) Brevard, C.; Granger, P. Inorg. Chem. **1983**, *22*, 532
(15) Luz, W.; Meiboom, S. *J. Chem. Phys.* **1963**, *29*, 366.
(16) Reference 7, p 104.
(17) Klier, D. A.; Binsch, G. *J. Magn. Reson.* **1970**, *3*, 146.

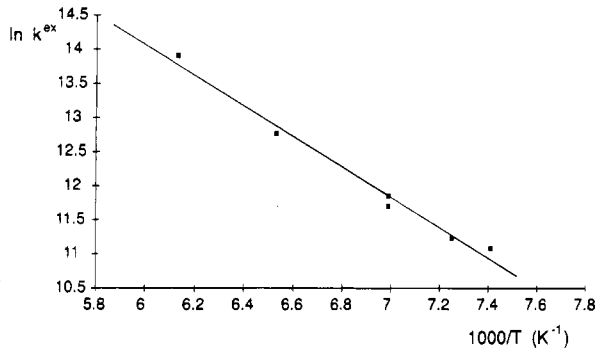

Figure 4. Arrhenius plot of ln k^{ex} vs $1000/T$ for $Ru_3(CO)_{12}$ obtained from the line shape analysis.

well with the value of 4.9 kcal mol^{-1} obtained by the procedure based on T_1 and T_2 measurements described above.

The good linearity found on plotting ln k^{ex} vs $1000/T$ points to the dominance of a single dynamic process on the transverse relaxation rate of the ^{13}CO resonance over the entire temperature range considered here. However from the available information we cannot distinguish between a metal-localized axial−equatorial exchange or a metal delocalized exchange process involving intermediates containing bridging carbonyls. Of course the occurrence of additional delocalized exchange processes involving either only axial carbonyls (i.e. through the formation of bridging intermediates above and below the Ru_3 plane) or only equatorial carbonyls (i.e. through the formation of bridging intermediates in the Ru_3 plane) could not have been detected as they occur among resonances characterized by the same chemical shifts.

Acknowledgment. We thank the Ministero dell'Università e della Ricerca Scientifica e Tecnologica (MURST) and the Consiglio Nazionale delle Ricerche (Comitato 03) for financial support. The European Community (Commission-DG XII, HCM program) is gratefully acknowledged for the postdoctoral grant provided to J.K.

OM9503050

Easy Metalation of the Substituted Dimethyl Sulfide $MeSCH_2R$ (R = C(O)OEt) by Palladium Acetate and Characterization of the Trinuclear Mixed-Sphere $[Pd_3(\mu\text{-}O_2CMe)_3(\mu\text{-}MeSCHR)_3]$ Complex

Marino Basato*

Centro di Studio sulla Stabilità e Reattività dei Composti di Coordinazione, CNR, Dipartimento di Chimica Inorganica, Metallorganica e Analitica, via Marzolo 1, I-35131 Padova, Italy

Alfonso Grassi

Dipartimento di Chimica, Università di Salerno, I-84081 Baronissi (SA), Italy

Giovanni Valle

Centro di Studio sui Biopolimeri, CNR, I-35131 Padova, Italy

Received March 31, 1995[⊗]

*Summary: Palladium acetate reacts with the weak carbon acid $MeSCH_2R$ (R = C(O)OEt) to give $[Pd_3(\mu\text{-}O_2CMe)_3(\mu\text{-}MeSCHR)_3]$ (**1**), characterized by X-ray crystallography. The $MeSCHC(O)OEt^-$ anion acts as a bidentate ligand binding two palladium atoms via a (Me)SCH(R) bridge, in which the methine carbon is chiral. Complex **1** is the first mixed-sphere palladium complex in which the solid-state nuclearity and structure of palladium acetate is retained.*

Palladium acetate is a commercially available compound widely used as a homogeneous metal catalyst in a huge number of organic syntheses.[1] This salt has a trimeric cyclic structure in the solid state,[2] whereas in benzene solution osmometric and ebullioscopic determinations indicate a trimer-monomer equilibrium, the second form being favored at higher temperatures.[3] Its basic chemistry is fairly well known. The palladium–oxygen bonds are rather labile, so that, for instance, the reaction of palladium acetate with phosphines easily produces complexes of general formula $[Pd(O_2CMe)_2(PR_3)_2]$, in which the acetato groups act as monodentate ligands. In contrast, reaction of the same compound with the bidentate β-dicarbonyls involves a complete ligand exchange process to afford the bis(carbonyl enolato) complexes $[Pd(\beta\text{-dik})_2]$.[3]

In view of our general interest in the coordination and reactivity of bidentate ligands obtained by deprotonation of acid methylene groups,[4] we aimed at extending the latter reaction to novel substrates in which active C-H bonds are present.

Here is reported the reaction of palladium acetate with ethyl (methylthio)acetate $MeSCH_2C(O)OEt$, which, combining hard and soft donor atoms, was expected to give a hemilabile S,O coordination with the metal center. Complexes which can become coordinatively unsaturated by opening of one ligand bite are likely to exhibit catalytic properties;[5] a very nice example of the use of palladium complexes with hemilabile P,O ligands in the codimerization of ethylene and styrene has been recently reported by Keim et al.[6]

The reaction proceeds in ethanol at room temperature according to eq 1;[7] the ligand exchange reaction is in this case not complete, involving only half of the acetato ligands. The deprotonation of active methylene com-

$$[Pd_3(\mu\text{-}O_2CMe)_6] + 3MeSCH_2C(O)OEt \rightarrow \underset{\mathbf{1}}{[Pd_3(\mu\text{-}O_2CMe)_3(\mu\text{-}MeSCHC(O)OEt)_3]} + 3MeCOOH \quad (1)$$

pounds *via* metal coordination has been well documented. However, most complexes involve a five-membered metallacyclic ring, where one donor atom (usually N or P) and an aromatic carbon are bonded to the same metal center.[8] Thus, the isolation of complex **1** appears of interest, because the anion of the weak acid ethyl (methylthio)acetate[9] is stabilized by coordination to two different palladium atoms.

A single-crystal X-ray analysis on the solvato complex $\mathbf{1}\cdot 0.5(CH_3)_2CO$ shows that **1** maintains the trimeric

[⊗] Abstract published in *Advance ACS Abstracts,* August 15, 1995.

(1) (a) Parshall, G. W.; Ittel, S. D. *Homogeneous Catalysis,* 2nd ed.; Wiley: New York, 1992. (b) Spencer, A. In *Comprehensive Coordination Chemistry;* Wilkinson, G., Gillard, R. D., McCleverty, J. A., Eds.; Pergamon Press: Oxford, U.K., 1987; Vol. 6, p 229.

(2) (a) Skapski, A. C.; Smart, M. L. *J. Chem. Soc., Chem. Commun.* **1970**, 658. (b) Cotton, F. A.; Han, S. *Rev. Chim. Miner.* **1983**, 496. (c) Cotton, F. A.; Han, S. *Rev. Chim. Miner.* **1985**, 277. (d) Barton, D. H. R.; Khamsi, J.; Ozbalik, N.; Ramesh, M.; Sarma, J. C. *Tetrahedron Lett.* **1989**, *30*, 4661.

(3) (a) β-dik = monoanion of a β-carbonyl compound working as an O,O′ chelating ligand. (b) Stephenson, T. A.; Morehouse, S. M.; Powell, A. R.; Heffer, J. P.; Wilkinson, G. *J. Chem. Soc.* **1965**, 3632. (c) Barnard, C. F. J.; Russell M. J. H. In *Comprehensive Coordination Chemistry;* Wilkinson, G., Gillard, R. D., McCleverty, J. A., Eds.; Pergamon Press: Oxford, U.K., 1987; Vol. 5, p 1099.

(4) Corain, B.; Basato, M.; Veronese, A. C. *J. Mol. Catal.* **1993**, *81*, 133.

(5) Bader, A.; Lindner, E. *Coord. Chem. Rev.* **1991**, *108*, 27.

(6) Britovsek, G. J. P.; Keim, W.; Mecking, S.; Sainz, D.; Wagner, T. *J. Chem. Soc., Chem. Commun.* **1993**, 1632.

(7) Palladium acetate (336 mg, 1.5 mmol) and ethyl (methylthio)-acetate (400 μL, 3.0 mmol) were dissolved in carefully deoxygenated ethanol (30 mL), under argon. The solution was stirred for 3 days to give complex **1** as a yellow greenish solid, which was filtered off, washed with ethanol (5 mL), and dried under vacuum; yield 75%. Anal. Calcd for $C_7H_{12}PdO_4S$: C, 28.15; H, 4.05; S, 10.74. Found: C, 28.29; H, 4.17; S, 10.73. IR (solid, DRIFT) (cm^{-1}): 1703 (C=O), 1558 (COO^-).

(8) (a) Newkome, G. R.; Puckett, W. E.; Gupta, V. K.; Kiefer, G. E. *Chem. Rev.* **1986**, *86*, 451. (b) Rüttimann, S.; Bernardinelli, G.; Williams, A. F. *Angew. Chem., Int. Ed. Engl.* **1993**, *32*, 392. (c) Yoneda, A.; Hakushi, T.; Newkome, G. R.; Fronczek, F. R. *Organometallics* **1994**, *13*, 4912.

(9) Estimated $pK_a = 23$ in DMSO (cf. $PhSCH_2CO_2Me$, $pK_a = 21.4$): (a) Bordwell, F. G. *Acc. Chem. Res.* **1988**, *21*, 456. (b) Bordwell, F. G.; Bares, J. E.; Bartmess, J. E.; Drucker, G. E.; Gerhold, J.; McCollum, G. J.; Van Der Puy, M.; Vanier, N. R.; Matthews, W. S. *J. Org. Chem.* **1977**, *42*, 326.

0276-7333/95/2314-4439$09.00/0

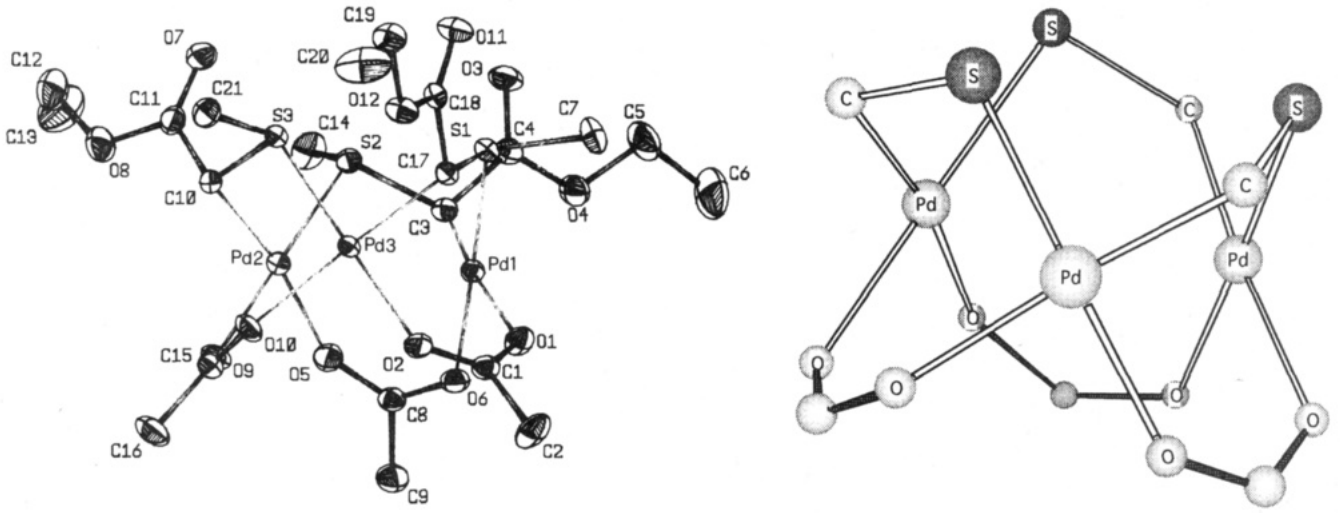

Figure 1. (a, left) ORTEP plot of the $[Pd_3(\mu\text{-}O_2CMe)_3(\mu\text{-}MeSCHC(O)OEt)_3]$ molecule (thermal ellipsoids at 30% probability level) with atom numbering. (b) Schematic view of the coordination skeleton. Selected distances [Å] and angles (deg) with standard deviations in parentheses: Pd(1)−Pd(2) = 3.2434(9), Pd(1)−Pd(3) = 3.231(2), Pd(2)−Pd(3) = 3.170(2), Pd(1)−S(1) = 2.266(1), Pd(1)−O(1) = 2.095(3), Pd(1)−O(6) = 2.066(3), Pd(1)−C(3) = 2.041(4), Pd(2)−S(2) = 2.2694(9), Pd(2)−O(5) = 2.107(3), Pd(2)−O(9) = 2.055(3), Pd(2)−C(10) = 2.044(4), Pd(3)−S(3) = 2.2695(9), Pd(3)−O(2) = 2.068(3), Pd(3)−O(10) = 2.129(2), Pd(3)−C(17) = 2.035(3); Pd(1)−Pd(3)−Pd(2) = 60.88(9), Pd(1)−Pd(2)−Pd(3) = 60.49(9), Pd(2)−Pd(1)−Pd(3) = 58.63(9), O(6)−Pd(1)−C(3) = 89.7(2), O(1)−Pd(1)−C(3) = 170.1(2), O(1)−Pd(1)−O(6) = 86.3(1), S(1)−Pd(1)−C(3) = 89.8(1), S(1)−Pd(1)−O(6) = 177.69(9), S(1)−Pd(1)−O(1) = 94.5(1), O(9)−Pd(2)−C(10) = 88.9(2), O(5)−Pd(2)−C(10) = 169.2(1), O(5)−Pd(2)−O(9) = 85.0(1), S(2)−Pd(2)−C(10) = 90.9(1), S(2)−Pd(2)−O(9) = 178.9(1), S(2)−Pd(2)−O(5) = 95.4-(1), O(10)−Pd(3)−C(17) = 170.6(2), O(2)−Pd(3)−C(17) = 89.3(1), O(2)−Pd(3)−O(10) = 85.9(1), S(3)−Pd(3)−C(17) = 89.05-(9), S(3)−Pd(3)−O(10) = 95.60(9), S(3)−Pd(3)−O(2) = 178.31(8). Additional data are given in ref 11.

bridged structure of the starting palladium acetate (Figure 1).[10,11] The three (ethoxycarbonyl)(methylthio)-methanide ligands are all on the same side with respect to the plane defined by the palladium atoms; each of these ligands bridges two metal centers *via* the sulfur and the methine carbon without any involvement of the carbonyl oxygen. The palladium is at the center of a square plane defined by a C,O,O,S set of atoms, all belonging to different ligands.

The metal−metal distances are in the range 3.2434-(9)-3.170(2) Å, and this excludes a bonding interaction between the palladium centers.[3c] These values are only slightly higher than those observed for a series of (solvato)palladium acetates (3.105(1)-3.203(1) Å),[2] thus indicating that substitution of three acetato groups by three (ethoxycarbonyl)(methylthio)methanide ligands does not alter significantly the structure, in particular the nearly equilateral triangle formed by the metal atoms.

The differences of the corresponding bond distances in the three "monomeric" units are generally small (often smaller than the esd). The distances between the metal center and the four coordination sites depend on the type of bonded atom and on the nature of the atom in the trans position. Thus, the average r(Pd−O) value is 2.063(8) Å[12] for the acetato oxygen trans to the sulfur and 2.110(19) Å for the oxygen trans to the carbon. Both values are over the range observed in the parent acetato salt (1.944−2.001 Å).[2] The means of the Pd−S and Pd−C distances are 2.268(2) and 2.040(5) Å, respectively. These values compare well with those reported for dialkyl thioethers (2.283 Å (σ = 0.030)) and alkylpalladium(II) complexes (2.083 Å (σ = 0.040)).[13] A closer insight into the type of coordination can be gained by analyzing the structural data relative to those for the mononuclear complexes $[PdCl(\eta^2\text{-}CH_2SCH_3)(PPh_3)]$[14]

(10) X-ray structure analysis of $[Pd_3(\mu\text{-}O_2CMe)_3(\mu\text{-}MeSCHC(O)OEt)_3]\cdot 0.5(CH_3)_2CO$: suitable crystals obtained as cubes (ca. 0.2 × 0.2 × 0.2 mm) by slow recrystallization (5−10 days) from an acetone solution under argon (Anal. Calcd for $C_{45}H_{78}Pd_6O_{25}S_6$: C, 29.22; H, 4.25; S, 10.40. Found: C, 29.16; H, 4.23; S, 10.58); Philips-PW 1100 four-circle diffractometer operating in the θ−2θ scan mode; Mo Kα monochomatized radiation, λ = 0.7107 Å; cell chemical composition $C_{90}H_{156}O_{50}Pd_{12}S_{12}$; M_r = 3699.71, monoclinic, $P2_1/n$; a = 12.975(2) Å, b = 14.943(2) Å, c = 17.849(3) Å, β = 101.4(1)°; V = 3392(1) Å^3, Z = 4, ϱ_{calcd} = 1.81 g cm^{-3}, μ = 16.51 cm^{-1}, $F(000)$ = 1840 e, 2θ range 4.2−56.0°; data collected at room temperature (295 K); 7447 unique reflections and 6040 assumed as observed with $F > 4\sigma(F)$; no absorption corrections; solution of the structure by direct methods (SHELXS 86) and by a few cycles of full-matrix least-squares refinement (SHELX 76) using anisotropic thermal parameters for all non-hydrogen atoms and excluding the solvent molecule; hydrogen atoms of the trimeric complex found in the difference Fourier map, refined isotropically, but not included in the final cycle; positions of the carbon and oxygen solvent atoms found, but not refined; site occupation factor for the statistically disordered solvent 0.5; acetone molecules are around the origin of the elementary cell, without close contacts with the surrounding complex molecules; final R = 0.027 and R_w = 0.031 with $w = 1/(\sigma^2(F) + 0.001459F^2)$; residual electron density 0.788 e Å^{-3}.

(11) Additional distances [Å] and angles (deg) for **1**·0.5$(CH_3)_2CO$ (standard deviations in parentheses): S(1)−C(7) = 1.803(4), S(1)−C(17) = 1.801(3), S(2)−C(3) = 1.801(3), S(2)−C(14) = 1.804(5), S(3)−C(10) = 1.797(3), S(3)−C(21) = 1.803(4), O(1)−C(1) = 1.251(5), O(2)−C(1) = 1.262(4), O(3)−C(4) = 1.199(4), O(4)−C(4) = 1.328(4), O(4)−C(5) = 1.462(6), O(5)−C(8) = 1.263(4), O(6)−C(8) = 1.264(5), O(7)−C(11) = 1.197(5), O(8)−C(11) = 1.328(5), O(8)−C(12) = 1.447(7), O(9)−C(15) = 1.266(5), O(10)−C(15) = 1.250(5), O(11)−C(18) = 1.196(4), O(12)−C(18) = 1.334(4), O(12)−C(19) = 1.478(5), C(1)−C(2) = 1.500(6), C(3)−C(4) = 1.485(5), C(5)−C(6) = 1.450(9), C(8)−C(9) = 1.501(5), C(10)−C(11) = 1.493(5), C(12)−C(13) = 1.46(1), C(15)−C(16) = 1.518(5), C(17)−C(18) = 1.494(4), C(19)−C(20) = 1.484(7); Pd(1)−S(1)−C(17) = 101.8(1), Pd(1)−S(1)−C(7) = 108.0(2), C(7)−S(1)−C(17) = 102.2(2), Pd-(2)−S(2)−C(14) = 105.8(2), Pd(2)−S(2)−C(3) = 100.9(1), C(3)−S(2)−C(14) = 102.2(3), Pd(3)−S(3)−C(21) = 106.9(2), Pd(3)−S(3)−C(10) = 100.7(1), C(10)−S(3)−C(21) = 101.5(2), Pd(1)−C(3)−C(4) = 111.9(3), Pd(1)−C(3)−S(2) = 106.1(2), S(2)−C(3)−C(4) = 112.6(2), Pd(2)−C(10)−S(3) = 106.8(2), Pd(2)−C(10)−C(11) = 111.6(4), S(3)−C(10)−C(11) = 112.4(3), Pd(3)−C(17)−S(1) = 108.3(2), Pd(3)−C(17)−C(18) = 117.3-(2), S(1)−C(17)−C(18) = 109.5(3), Pd(1)−O(1)−C(1) = 131.0(2), Pd-(3)−O(2)−C(1) = 126.2(3), O(1)−C(1)−O(2) = 127.0(4), Pd(2)−O(5)−C(8) = 133.5(3), Pd(1)−O(6)−C(8) = 124.6(2), O(5)−C(8)−O(6) = 125.6(4), Pd(2)−O(9)−C(15) = 124.4(2), Pd(3)−O(10)−C(15) = 132.9-(3), O(9)−C(15)−O(10) = 126.2(4).

(12) Values in parentheses are the greatest deviations from the unweighted mean; the same meaning holds for all average distances and angles of **1**·0.5$(CH_3)_2CO$ in the text.

(13) Orpen, A. G.; Brammer, L.; Allen, F. H.; Kennard, O.; Watson, D. G.; Taylor, R. *J. Chem. Soc., Dalton Trans.* **1989**, S1.

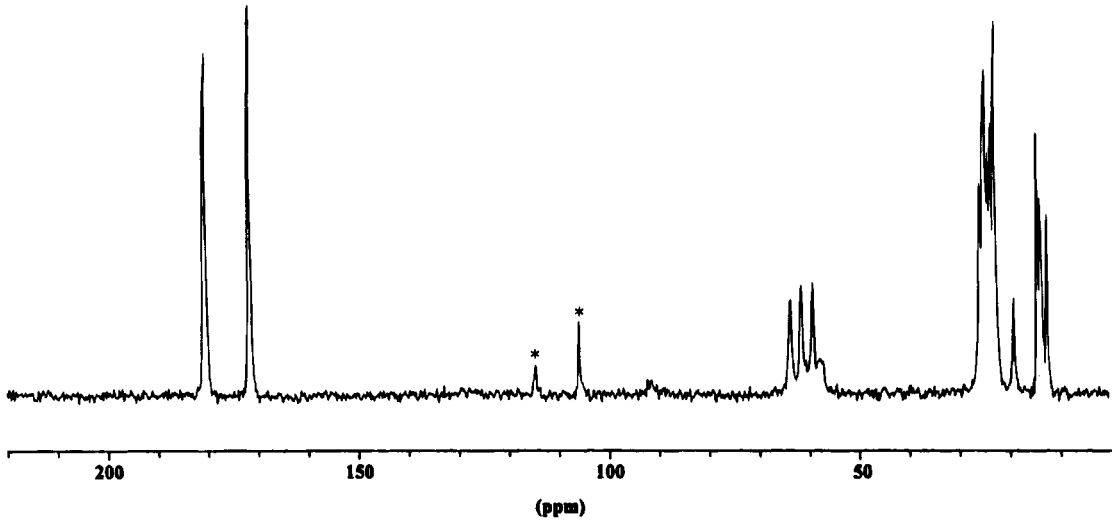

Figure 2. Solid-state ^{13}C CP/NMR spectrum of $[Pd_3(\mu\text{-}O_2CMe)_3(\mu\text{-}MeSCHC(O)OEt)_3]$ (**1**). Asterisks denote spinning sidebands.

and $[PdCl(\eta^1\text{-}CH_2SCH_3)(PPh_3)_2]$.[15] In the former case the metal forms a three-membered ring with the carbon and the sulfur atoms, whereas in the latter the SMe group is not involved in coordination. In both complexes the Pd–C bond distances are very close (2.042(6) and 2.061(3) Å) to that found in **1**, whereas r(Pd–S) in the comparable $[PdCl(\eta^2\text{-}CH_2SCH_3)(PPh_3)]$ appears somewhat greater (2.371(1) vs 2.268(2) Å). Another characteristic feature of this last complex is represented by the short S–C distance in the Pd–S–C metallacycle [r(S–CH_2) = 1.756(6) Å, vs 1.807(7) Å for r(S–CH_3)], which may be indicative of a partial double bond between the metal-coordinated carbon and sulfur atoms. In contrast, no evidence of electron delocalization results from the analysis of the structural parameters of **1**. As a matter of fact, the bond distances in the thio (r(S–CHR) = 1.803(1) Å and r(S–CH_3) = 1.800(3) Å) and ethyl acetato fragments are strictly close to those observed in nonconjugated uncharged compounds containing these groups.[16] From these structural data it may be concluded that the bridging $MeSCHC(O)OEt^-$ ligand coordinates the two metal centers *via* almost pure thioether and alkyl bonds. Bond angle values support this conclusion; in fact, the bonded carbon has a roughly tetrahedral geometry, indicative of sp^3 hybridization (C–C–S = 111.5(1.1)°), and the angles at the sulfur are characteristic of terminal SR_2 (R = C(sp^3)) groups (C–S–C = 102.0(5)°].[17] However, because of steric requirements due to the concomitant coordination of both groups, their substituents are tilted with respect to the metal–donor atom bond (Pd–C–S = 107.1(1.2)°, Pd–C–C = 113.6(3.7)°, Pd–S–Me = 106.9(1.1)°, Pd–S–CHR = 101.3(9)°). The attributions of the bridging acetato ligands in **1** do not substantially differ from those of palladium acetate.[2]

Complex **1** is stable in the solid state and in solution. It is soluble in acetone and in chlorinated solvents, from which it can be recrystallized as a solvato complex. The ^1H and ^{13}C NMR spectra at 20 °C are consistent with the structure of **1** depicted in Figure 1.[18–20] It is worth mentioning that, in the presence of the chiral methine carbon bonded to palladium, the two methylene protons of the ethoxycarbonyl group are diastereotopic. They appear in the ^1H spectrum as a complex AB system consisting of 16 lines due to geminal and vicinal coupling constants. By saturation of the methyl signal, the AB system appears as two doublets at 4.02 and 4.18 ppm with the geminal coupling constant J_{gem} = 11.0 Hz. When the temperature is increased up to 50 °C, the signal at 2.13 ppm splits into two singlets at 2.11 and 2.14 ppm, which have been attributed, respectively, to the methyl group of the acetato moiety and to the methyl group bonded to sulfur. It is also interesting to note that the $^1J_{CH}$ coupling constant observed for the chiral methine carbon bonded to palladium ($^1J_{CH}$ = 157 Hz) is larger than the corresponding coupling constant observed for the SCH_3 methyl ($^1J_{CH}$ = 142 Hz). These values suggest a small distortion for the former carbon from a pure sp^3 to an sp^2 hybridization.

The solid-state ^{13}C CP/MAS NMR spectrum of **1** (Figure 2)[21] shows single COO^- and COO(Et) carbon signals, two sets of three different signals for the methylene and methyl carbons of the ethoxy group, and at least six resonances (19.3–25.9 ppm) attributable to the methine and to the CH_3COO^- and CH_3S methyl carbons. On the whole, there is a very good correspondence with the spectrum in solution, thus sug-

(14) Miki, K.; Kai, Y.; Yasuoka, N.; Kasai, N. *J. Organomet. Chem.* **1977**, *135*, 53.
(15) Miki, K.; Kai, Y.; Yasuoka, N.; Kasai, N. *J. Organomet. Chem.* **1979**, *165*, 79.
(16) (a) Allen, F. H.; Kennard, O.; Watson, D. G.; Brammer, L.; Orpen, A. G.; Taylor, R. *J. Chem. Soc., Perkin Trans. 2* **1989**, S1. (b) Allen, F. H.; Kirby, A. J. *J. Am. Chem. Soc.* **1984**, *106*, 6197.
(17) Murray, S. G.; Hartley, F. R. *Chem. Rev.* **1981**, *81*, 365.
(18) ^1H NMR (250 MHz, $C_2D_2Cl_4$, 20 °C): δ = 1.29 (t, 3H, $COOCH_2CH_3$, $^3J_{HH}$ = 7.3 Hz), 2.13 (2s, 6H, SCH_3 and CH_3COO^-), 3.62 (s, 1H, CH_3SCH), 4.10 (AB system, m, 2H, $COOCH_2CH_3$, J_{gem} = 11.0 Hz, $^3J_{HH}$ = 7.3 Hz). ^{13}C NMR (62.89 MHz, $C_2D_2Cl_4$, 20 °C): δ 14.33 (q, $^1J_{CH}$ = 117 Hz, $COOCH_2CH_3$), 24.09 (q, $^1J_{CH}$ = 129 Hz, CH_3COO), 24.49 (q, $^1J_{CH}$ = 142 Hz, CH_3S), 25.09 (d, $^1J_{CH}$ = 157 Hz, CH_3SCH), 61.60 (t, $^1J_{CH}$ = 147 Hz, $COOCH_2CH_3$), 172.00 (s, COOEt), 181.01 (q, $^2J_{CH}$ = 3.7 Hz, CH_3COO^-). The attributions of the signals were fully confirmed by a 2D heteronuclear (C,H) shift correlation experiment.
(19) Mann, B. E.; Taylor, B. F. *^{13}C NMR Data for Organometallic Compounds*; Academic Press: London, 1981.
(20) Kalinowsky, H.-O.; Berger, S.; Braun, S. *Carbon-13 NMR Spectroscopy*; Wiley: New York, 1988.
(21) ^{13}C CP/MAS NMR (solid, 20 °C): δ 12.6, 13.9, 14.5 ($COOCH_2CH_3$), 19.3, 23.0, 23.6, 24.2, 24.9, 25.9 (CH_3S, CH_3COO, and CH_3SCH), 59.3, 61.7, 63.9 ($COOCH_2CH_3$), 171.8 (COOEt), 180.5 (CH_3COO^-). ^{13}C CP/MAS NMR measurements were performed on a Bruker AM 250 spectrometer operating at 250.19 MHz for ^1H and at 62.89 MHz for ^{13}C. The setting of the magic angle was monitored by recording the ^{79}Br NMR spectrum of KBr. The sample (ca. 250 mg) was introduced into a double-bearing zirconia rotor (7 mm o.d.) and spun at the magic angle with a frequency of 4.2 KHz. The chemical shifts were referenced to external liquid tetramethylsilane (TMS), using as secondary reference the methylene carbon signal of adamantane, 38.3 ppm downfield from TMS.

gesting the same type of coordination in the two phases.[22] The larger number of resonances observed in the solid state indicates that the sp^3 carbons external to the coordination skeleton are affected by the asymmetry of the trimeric complex **1**, so that the corresponding signals are tripled. In this view the splitting of the signals is simply due to a different packing in the elementary cell of the three monomeric units forming the complex.

The behavior of the carbon acid $MeSCH_2C(O)OEt$ toward palladium acetate shows a few interesting features. Despite its low acidity, it easily undergoes deprotonation and coordination to the palladium in an exchange reaction which liberates in solution the stronger acetic acid; this exchange process is not complete as in the case of β-dicarbonyls and involves only one acetato ligand per metal center. The coordination does not involve the ester group in the usual chelating mode to give a five-membered metallo-organic ring. To our knowledge, **1** is the first mixed-sphere palladium(II) complex which maintains the nuclearity and structure of the starting acetato salt. It is possible that its trimeric structure has favored the easy metalation of the methine carbon *via* coordination of the thioalkyl group of $MeSCHC(O)OEt^-$ on a different palladium atom. Complex **1** undergoes easy reductive elimination in dichloromethane, in the presence of tributylphosphine, to give as a final product $Pd(PBu_3)_4$.[23]

Supporting Information Available: Tables of fractional coordinates and equivalent isotropic thermal parameters, anisotropic thermal parameters, and bond distances and angles for **1**·0.5$(CH_3)_2CO$ (9 pages). Ordering information is given on any current masthead page.

OM950237H

(22) An osmometric molecular weight determination in 1,2-dichloroethane at 50 °C indicates that complex **1** is a trimer in solution (calcd for $C_{21}H_{36}Pd_3O_{12}S_3$ 896, found 905).

(23) The reduction of Pd^{II} to Pd^0 in the presence of mild reductants is an important step in many catalytic reactions; for example, mixtures of $Pd(OAc)_2/PPh_3$ generate a zerovalent palladium complex, which is a good catalyst in Heck reactions (Amatore, C.; Carrè, A.; Jutand, A.; M'Barki, M. A. *Organometallics* **1995**, *14*, 1818 and references therein).